THE JOURNAL OF

PHYSICAL

CHEMISTRY

Volume 69

SEPTEMBER—DECEMBER 1965

PAGES 2811—4466

THE JOURNAL OF
PHYSICAL CHEMISTRY

Copyright, 1965, by the American Chemical Society. Published monthly by the American Chemical Society at 20th and Northampton Sts., Easton, Pa. 18043. Second-class postage paid at Easton, Pa.

The Journal of Physical Chemistry is devoted to the publication of contributed papers in the broad field of physical chemistry. Preference for publication in *The Journal of Physical Chemistry* is given to papers dealing with fundamental concepts, atomic and molecular phenomena, and systems in which clearly defined models are applicable. Manuscripts containing extensive reviews, re-evaluations of existing data, applied chemical data, or measurements on materials of ill-defined nature are, in general, not acceptable for publication. Symposium papers may be published as a group, but only through special arrangement with the Editor.

Except as immediately following, all manuscripts should be sent to *The Journal of Physical Chemistry*, Department of Chemistry, University of California, Santa Barbara, Calif. 93106. Manuscripts originating in the British Isles, Europe, and Africa should be sent to F. C. Tompkins, The Faraday Society, 6 Gray's Inn Square, London, W. C. 1, England.

All manuscripts should be submitted in duplicate, including an original typewritten, double-spaced copy. Original drawings should accompany the manuscript. Lettering at the sides of graphs (black on white or blue) may be pencilled in and will be typeset. Figures and tables should be held to a minimum consistent with adequate presentation of information. All footnotes and references to the literature should be numbered consecutively and placed in the manuscript at the proper places. Initials of authors referred to in citations should be given. Nomenclature should conform to that used in *Chemical Abstracts*, mathematical characters should be marked for italic, Greek letters carefully made or annotated, and subscripts and superscripts clearly shown.

Articles should be written as briefly as possible consistent with clarity, avoiding historical background unnecessary for specialists. They should cover their subjects with reasonable thoroughness and completeness and should not depend for their usefulness on papers to be published later. A brief abstract, generally not exceeding 300 words, should appear at the beginning of each article. All articles are subject to critical reviews by referees.

Notes are similar to Articles, but are shorter and not accompanied by abstracts. The length of a *Note*, including tables, figures, and text, must not exceed 1.5 journal pages (1500 words or the equivalent). A *Note* treats a limited subject with reasonable completeness and should not be considered a preliminary notice. Like Articles, *Notes* are subject to critical review by referees.

Communications to the Editor are divided into two categories, *Letters* and *Comments*. The length of a *Communication*, including tables, figures, and text, must not exceed three-fourths of a page (750 words or the equivalent).

Letters should report preliminary results of immediate interest.

It is expected that the material in *Letters* may be republished in *The Journal of Physical Chemistry* at a later date in more complete form. Communications in this category will be treated expeditiously but are subject to review by the Editor and readily available experts.

Comments include significant remarks on the work of others or observations of unusual interest which the authors do not intend to pursue. In the former case, the authors of the work being discussed will, ordinarily, be allowed to reply. *Comments* are not refereed but are published at the discretion of the Editor.

Additions and Corrections are published once yearly in the December issue. See Volume 68, Number 12 for the proper form.

Extensive or unusual alterations in an article after it has been set in type are made at the author's expense, and it is understood that by entering such alterations on proofs the author agrees to defray the cost thereof.

The American Chemical Society and the Editor of *The Journal of Physical Chemistry* assume no responsibility for the statements and opinions advanced by contributors.

Correspondence regarding accepted copy, proofs, and reprints should be directed to Research Journals Production Office, American Chemical Society, 20th and Northampton Sts., Easton, Pa. 18043. Senior Production Editor: CHARLES R. BERTSCH. Assistant Senior Production Editor: MARIANNE C. BROGAN. Assistant Editors: EDWARD A. BORGER and CELIA B. McFARLAND.

Advertising Office: Reinhold Publishing Corporation, 430 Park Ave., New York, N. Y. 10022.

Business and Subscription Information

Remittances and orders for subscriptions and for single copies, notices of changes of address and new professional connections, and claims for missing numbers should be sent to the Subscription Service Department, American Chemical Society, 1155 Sixteenth St., N.W., Washington, D. C. 20036. Four weeks should be allowed for changes of address. Please include an old address label with the notification.

Claims for missing numbers will not be allowed (1) if received more than sixty days from date of issue. (2) if loss was due to failure of notice of change of address to be received before the date specified in the preceding paragraph, or (3) if the reason for the claim is "missing from files."

Subscription rates (1965): members of the American Chemical Society, $12.00 for 1 year; to nonmembers, $24.00 for 1 year. Postage to Canada and countries in the Pan-American Union, $2.00; all other countries, $3.00. Single copies for current year: $2.50. Postage, single copies: to Canada and countries in the Pan-American Union, $0.15; all other countries, $0.20. Rates for back issues are available from the Special Issues Sales Department, 1155 Sixteenth St., N.W., Washington, D. C. 20036.

ANOTHER FIRST FROM VARIAN

NEW TABLE-TOP
LOW-PRICED EPR

The E-3 is the first of its kind— an easy to operate, sensitive, reliable, low-priced spectrometer. It was specially designed to bring Electron Paramagnetic Resonance spectroscopy within the reach of *all* biologists, chemists, biochemists, and biophysicists.

Solid state construction makes the E-3 a compact, table-top spectrometer. And it's also surprisingly low-priced *(just check with us and see)*. And because it has a wide range of accessories, you can use the E-3 in many kinds of experiments. It's highly reliable and accurate, and has a sensitivity of $1\times10^{11}\triangle H$ spin/gauss.

If we sound proud of the E-3, it's because we are! To hear more about this compact little EPR system, just contact your nearest Varian Field Sales Office.
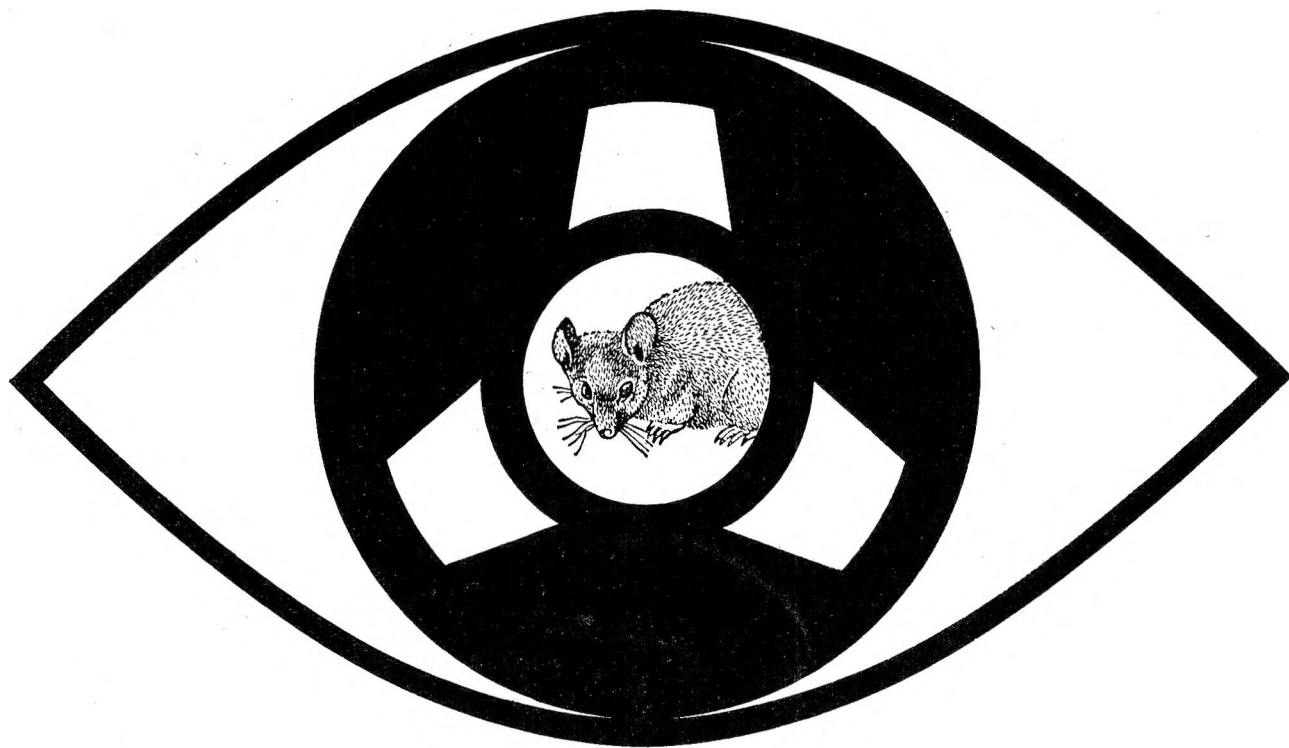
Now you can search Chemical Titles magnetic tapes by computers

Update your information dissemination program through the use of CHEMICAL TITLES Tapes or Custom Searches! These services are being offered for the first time by the Chemical Abstracts Service.

The list of uses to which you can put the tapes, compiled during the production of the printed CT, is almost endless. Indexes for the chemical journals in your company or institutional library which are covered by CT can be generated on an author, selected keyword, or title basis (or any combination of the three). Bibliographies on particular subjects that pertain to your work (reactivity of the phenanthrolines, crystal structure of ternary silicides, metabolism of porphyrins, etc.) can be compiled. Keyword indexes for any number of terms which you may suggest can be generated. Correlative machine searches can be conducted (mice that eat cheese, mice that eat cheddar cheese and Swiss cheese, white mice that eat cheddar cheese but not Swiss cheese, white mice that eat cheddar cheese or Swiss cheese, etc.) to any degree of specificity.

Answers can be in the form of bibliographies, author indexes, keyword indexes or any combination of the three. AND, all of these indexes, bibliographies, etc., can easily be duplicated and distributed to members of your staff at very low cost. No matter how you choose to use the tapes, you are screening a vast amount of unnecessary material from information which is of specific interest to you.

This tape searching service is offered in two forms —CAS will send you tapes on a biweekly basis, along with a user's manual and a searching program for an IBM 1401/1410 system, or CAS will perform the biweekly search of the tapes for you in Columbus.

The subscription price includes a $1,500-per-year base rate plus a use charge of $5 for each scientist at the subscriber's address who will use the service or who will benefit from its use. For searches performed by CAS, the rate is based on one search per set of terms per issue of CT, and an additional charge of $100 per hour for computer use time is made.

Direct inquiries to Mr. E. H. Heilman at CAS, Ohio State Univ., Columbus, Ohio 43210. and direct orders to the ACS, 1155 16th St., N.W., Washington, D.C. 20036.

COMMUNICATIONS TO THE EDITOR

AUTHOR INDEX

He graduated at the head of his class, but couldn't get a job.

The reason? Everyone thought he came from the wrong school—one for the mentally retarded—even though he was certified employable and well trained.

The employers didn't know that with proper training, the mentally retarded can become a productive part of society. Taking pride in jobs that others might not enjoy. Having better job attitudes, and often better attendance records, because they like their work.

Someday, a mentally retarded person may ask you for a job. As a general office worker, a gardener, a truck loader, a stock clerk, a messenger. Or any job that requires simple skills. Won't you give him a chance to become an asset to your company?

Here are four things you can do now to help prevent mental retardation and bring new hope to the 5½ million people whose minds are retarded:

1. Urge your community to set up workshops to train retardates who are capable of employment.
2. Select jobs in your company that the mentally retarded can fill, and hire them.
3. Accept the mentally retarded as American citizens. Give them a chance to live useful, dignified lives in your community.
4. Write for the free booklet to the President's Committee on Mental Retardation, Washington, D.C.

Dynamic Mechanical Properties of Cross-Linked Rubbers.   II.   Effects of Cross-Link Spacing and Initial Molecular Weight in Polybutadiene[1]

by Etsuji Maekawa, Ralph G. Mancke, and John D. Ferry

Department of Chemistry, University of Wisconsin, Madison, Wisconsin *(Received May 13, 1965)*

The complex shear compliances of eight samples of polybutadiene cross linked by dicumyl peroxide and four samples cross linked by sulfur have been measured over a frequency range from 0.2 to 2 c.p.s. at temperatures from −6 to 45° by a torsion pendulum. On four of the samples, measurements were extended by the Fitzgerald transducer from 45 to 600 c.p.s. at temperatures from −71 to 55°. The vulcanizates had been prepared from polymers of two different molecular weights (180,000 and 510,000) with sharp molecular weight distribution; the physical cross-link density ranged from 0.57 to 2.68 × 10^{-4} mole/cc., and the chemical cross-link density calculated following Kraus ranged from 0.22 to 1.49 × 10^{-4} mole/cc. The mechanical data were all reduced to $T_0 = 298°K$. by shift factors calculated from the equation log $a_T = -3.64(T - T_0)/(186.5 + T - T_0)$. In the transition zone of frequencies, the viscoelastic functions of the dicumyl peroxide vulcanizates were closely similar, except for a shift toward lower frequencies with increasing cross linking, corresponding to a small but unexpected increase in the monomeric friction coefficient. Cross linking by sulfur caused a somewhat larger shift toward lower frequencies at a comparable cross-link density. In the rubbery zone, the sample with least cross linking exhibited a substantial secondary loss mechanism at very low frequencies. The low-frequency losses are evident in all the samples, but their magnitude falls rapidly with increasing cross-link density as previously found for natural rubber. It also falls somewhat with increasing initial molecular weight, indicating a contribution from network strands with loose ends. The possible relation of the low-frequency losses to trapped entanglements is discussed.

Introduction

In an earlier paper,[2] we described dynamic mechanical properties of a series of natural rubber vulcanizates, cross linked by dicumyl peroxide and by sulfur, and showed that the magnitude of the anomalous losses at very low frequencies increased with the average spacing between cross links. Similar behavior was noted by Nielsen[3] in measurements on butyl and

styrene–butadiene rubbers, in which the temperature was varied at roughly constant frequency. While the origin of these losses remains uncertain, they have been tentatively attributed, at least in part, to coupling entanglements trapped between cross links.[2,4] We now report some dynamic mechanical measurements over a wide range of frequencies and temperatures on vulcanizates of polybutadiene, again cross linked by both dicumyl peroxide and sulfur. The results show a similar dependence of the low frequency losses on the cross-link spacing and also a dependence to some degree on the initial molecular weight before cross linking, reflecting the proportion of network strands with loose ends.

Experimental

Materials. The cross-linked polybutadienes were generously prepared for us by Drs. G. Kraus and C. W. Childers of the Phillips Petroleum Co. Two linear polybutadienes of sharp molecular weight distribution were employed, with the following weight-average molecular weights and microstructures as reported by Dr. Kraus: M_w 180,000, 40% *cis*, 53% *trans*, 7% vinyl; M_w 510,000, 43% *cis*, 50% *trans*, 7% vinyl. These are identified subsequently by their molecular weights. The dicumyl peroxide (DCP) vulcanizates contained amounts of peroxide ranging from 0.04 to 0.38% depending on the density of cross linking desired. The sulfur vulcanizates contained amounts of sulfur ranging from 0.42 to 1.33% and in addition 3% zinc oxide, 2% stearic acid, 3% Resin 731, 1.2% Santocure, and 1% Flexamine (all expressed as parts per 100 parts rubber). The vulcanization was always performed by heating for 45 min. at 150°. The densities, determined pycnometrically under water, were 0.897 g./cm.[3] for the dicumyl peroxide vulcanizates and 0.929 for the sulfur vulcanizates.

The density of elastically active network chains, in moles of strands per cubic centimeter, ν, was obtained by Drs. Kraus and Childers from swelling measurements in n-heptane, the necessary value of the thermodynamic parameter μ having been obtained by calibrating the swelling against elastic measurements on swollen gels.[5] The density of chemically cross-linked chains, ν^*, was calculated by the Mullins–Kraus relation[5]

$$\nu = \nu^* + a - (\nu^* + a)b/\nu^* M \qquad (1)$$

with $a = 1.5 \times 10^{-4}$ and $b = 2.73$ as determined by Kraus[5] for polybutadiene networks. These values are summarized in Table I.

The equilibrium shear compliances, J_e, were measured by torsional deformation with very small strain as previously described.[2,6] They represent minimum

Table I: Characteristics of Cross-Linked Rubbers

Agent	Sample code	M before vulcanization $\times 10^{-5}$	$\nu \times 10^4$, moles/cm.^{3}	$\nu^* \times 10^4$, moles/cm.^{3}	$-\mathrm{Log}\, J_e$
DCP	734	1.8	0.57	0.22	6.44$_5$
	735	1.8	1.42	0.51	6.74$_6$
	10H	1.8	1.8	0.76	6.88
	736	1.8	1.85	0.79	6.89$_3$
	737	1.8	2.37	1.21	. . .
	738	1.8	2.68	1.49	7.02$_7$
	10D	5.1	1.8	0.50	6.90$_3$
	740	5.1	1.99	0.66	6.96$_5$
S	10C	1.8	1.2	0.39	6.81$_4$
	739	1.8	1.79	0.75	6.81$_2$
	10B	5.1	1.2	0.19	6.88$_2$
	741	5.1	1.85	0.55	6.90$_8$

values since even after equilibration under stress for 12 hr. the slow relaxation processes may not be complete.[7] These values are also given in Table I and are plotted logarithmically against ν in Figure 1. For comparison, the prediction of the kinetic theory of rubberlike elasticity

$$J_e = 1/\nu RT \qquad (2)$$

is included as a dashed line. The observed compliances are smaller by about a factor of 0.6. Similar discrepancies have been observed recently by Thirion[7] and Nielsen,[3] in agreement with the general experience[8] that the retractive force in unswollen ("dry") rubbers includes a contribution in addition to that corresponding to eq. 2.

No account has been taken, in Table I, of several corrections to eq. 2 which have been pointed out recently: (a) a factor $\langle r_E^2 \rangle / \langle r_0^2 \rangle$, in which $\langle r_E^2 \rangle$ is the mean-square end-to-end distance of network strands and $\langle r_0^2 \rangle$ the corresponding value for free chains[9]; (b) a factor of 2 associated with the connectivity of a tetrafunctional network[10]; and (c)

(3) L. E. Nielsen, *J. Appl. Polymer Sci.*, **8**, 511 (1964).

(4) G. Kraus and G. A. Moczygemba, *J. Polymer Sci.*, **A2**, 277 (1964).

(5) G. Kraus, *J. Appl. Polymer Sci.*, **7**, 1257 (1963).

(6) R. A. Stratton and J. D. Ferry, *J. Phys. Chem.*, **67**, 2781 (1963).

(7) P. Thirion and R. Chasset, "Proceedings of the Fourth International Congress on Rheology," Interscience Publishers, New York, N. Y., Part 3, 1965, p. 525.

(8) L. Bateman, Ed., "The Chemistry and Physics of Rubber-like Substances," John Wiley and Sons, Inc., New York, N. Y., 1963, pp. 170, 175.

(9) A. V. Tobolsky, D. W. Carlson, and N. Indictor, *J. Polymer Sci.*, **54**, 175 (1961).
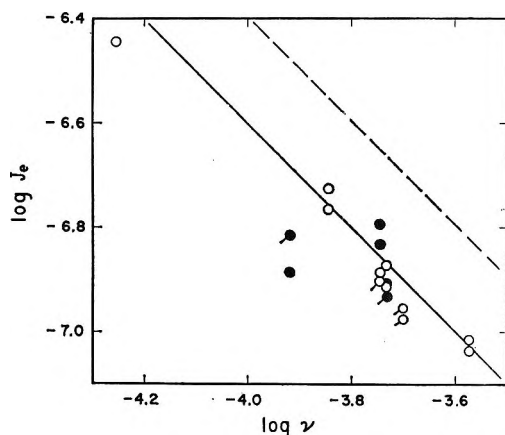
Figure 1. Equilibrium shear compliance plotted logarithmically against elastically effective network strands per cm.[3]: open circles, DCP vulcanizates; black circles, S; untagged, $M = 1.8 \times 10^5$; tagged, $M = 5.1 \times 10^5$. Some pairs of duplicate determinations are included. Dashed line is kinetic theory prediction, eq. 2.

allowance for a non-Gaussian distribution of end-to-end distances.[11] However, these corrections should affect all the values in a similar manner.

Methods. The Fitzgerald transducer[12] was used for measurements of the storage (J') and loss (J'') components of the dynamic shear compliance in the range from 45 to 600 c.p.s., and the Plazek torsion pendulum[13] from 0.2 to 2 c.p.s. The logarithmic decrement was determined from the recorder tracings of the torsion pendulum by direct matching to exponential envelopes.[14] The maximum temperature range was from −71 to 55°. The disk-shaped samples were 1.75 cm. in diameter; the thickness was about 0.19 cm. for the transducer measurements and 0.64 cm. for the torsion pendulum. Four vulcanizates (734, 736, 738, and 739) were studied with both instruments, and the others with the torsion pendulum alone.

Results

For plotting with reduced variables, the storage and loss compliances J' and J'' were reduced in magnitude by the usual factor $T\rho/T_0\rho_0$, where ρ and ρ_0 are the densities at the temperature of measurement T and the reference temperature of $T_0 = 298.2°K$.; the thermal expansion coefficient can be taken as 7.5×10^{-4} deg.$^{-1}$. The frequency shift factor a_T was calculated from the following equation[16]

$$\log a_T = -3.64(T - T_0)/(186.5 + T - T_0) \quad (3)$$

in which the numerical coefficients were obtained by preliminary empirical selection of a_T and plotting[16] $(T - T_0)/\log a_T$ against $T - T_0$. Equation 3 also fits the viscosity data of Gruver and Kraus[16] rather well

although it differs somewhat from the equations used by them. (The coefficients correspond to a free-volume thermal expansion coefficient of 6.4×10^{-4} deg.$^{-1}$, which is reasonable though somewhat high.[15])

When plotted logarithmically against the reduced frequency ωa_T, data from the transducer and torsion pendulum almost overlapped. The loss tangents tan $\delta = J''/J'$ agreed closely but the magnitudes of J'' and J' derived from the two methods differed slightly, a discrepancy attributable to uncertainty in the sample coefficient for the transducer.[6] The following small corrections were therefore applied to the transducer data for log J' and log J'' for consistency: sample 734, −0.05; sample 736, −0.06; sample 738, −0.04; sample 739, −0.07. The data for the three dicumyl peroxide vulcanizates are plotted in Figure 2; the points are omitted for sample 736 to avoid confusion. The individual temperatures and all numerical data will be recorded elsewhere[17]; tables are available upon request to the authors.

At high reduced frequencies, corresponding to the beginning of the transition zone, the shapes of the curves of J' and J'' are almost identical. There is a small shift to lower frequencies with increasing degree of cross linking. At low frequencies, the losses for the more densely cross-linked samples resemble the behavior previously reported[2,6] in persisting at a rather low level instead of vanishing with decreasing frequency as expected from molecular theories.[6] But for $\nu = 0.57 \times 10^{-4}$, the loss compliance actually passes through a large secondary maximum. This suggests that the small persistent losses seen at higher ν are residues of a secondary mechanism which is prominent only when ν is small. This mechanism is also seen in the curve for log J' which is rising at low frequencies to approach its limiting equilibrium value of about −6.4.

In Figure 3, the loss tangent again shows the large secondary loss mechanism for $\nu = 0.57 \times 10^{-4}$ and a small one for $\nu = 1.85 \times 10^{-4}$. (A minimum in the loss tangent as a function of temperature at constant frequency is also evident in the measurements of

(10) J. A. Duiser and A. J. Staverman, "Proceedings of the International Conference on Non-Crystalline Solids," North-Holland Publishing Co., Amsterdam, 1965, p. 376.

(11) W. Prins, *ibid.*, p. 360.

(12) E. R. Fitzgerald, *Phys. Rev.*, 108, 690 (1957).

(13) D. J. Plazek, M. N. Vrancken, and J. W. Berge, *Trans. Soc. Rheol.*, 2, 39 (1958).

(14) R. A. Dickie, Ph.D. Thesis, University of Wisconsin, 1965.

(15) J. D. Ferry, "Viscoelastic Properties of Polymers," John Wiley and Sons, Inc., New York, N. Y., 1961, p. 212.

(16) J. T. Gruver and G. Kraus, *J. Polymer Sci.*, 2, 797 (1964).

(17) R. G. Mancke, Ph.D. Thesis, University of Wisconsin, 1966.
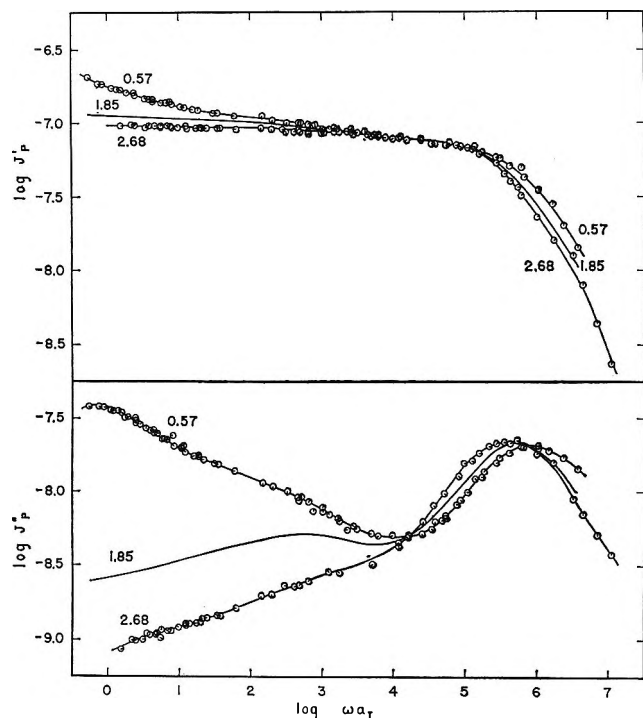
Figure 2. Storage and loss compliance reduced to 25° and plotted logarithmically against reduced radian frequency for three samples cross linked by dicumyl peroxide, identified by values of $\nu \times 10^4$. Pip directions denote different temperatures: $\nu = 0.57 \times 10^{-4}$, -64.2 to $54.7°$ in 13 steps; $\nu = 1.85 \times 10^{-4}$ (points not shown), -73 to $55.5°$ in 13 steps; $\nu = 2.68 \times 10^{-4}$, -70.8 to $55.4°$ in 13 steps. Subscript p denotes multiplication by $T\rho/T_0\rho_0$.
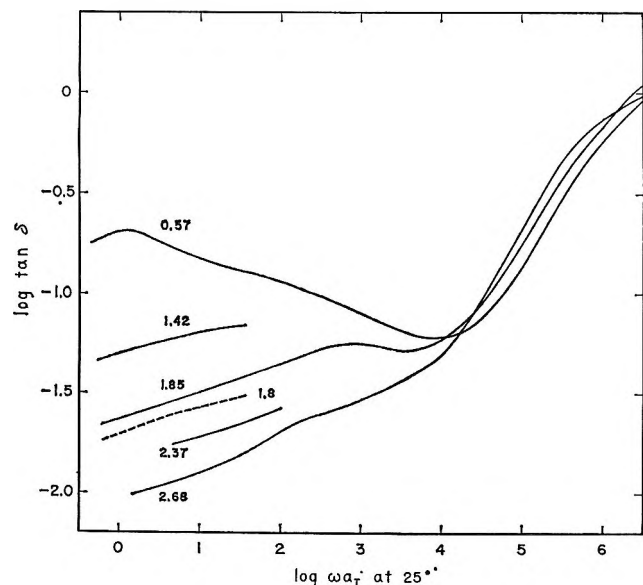
Figure 3. Loss tangents of dicumyl peroxide vulcanizates, plotted logarithmically against reduced radian frequency: numbers denote $\nu \times 10^4$; dashed line, $M = 5.1 \times 10^5$; all others, $M = 1.8 \times 10^5$.

Nielsen[3] on very lightly cross-linked rubbers.) Low frequency measurements on additional samples show a monotonic decrease in the magnitude of tan δ with increasing ν, as previously observed for vulcanizates of natural rubber. The dashed curve shows that, for approximately equal ν, a higher initial molecular weight before vulcanization gives a somewhat lower loss, so the loose ends do make a small contribution to the low frequency losses.

In Figure 4, log J' and log J'' are plotted against reduced frequency for the sulfur vulcanizate with $\nu = 1.79 \times 10^{-4}$, and the data for the dicumyl peroxide vulcanizate most nearly corresponding to it are repeated from Figure 2. At low frequencies, the storage compliances are almost identical, but the sulfur vulcanizate shows somewhat more loss. A slight secondary maximum in J'' is evident in both. At high frequencies, the dispersion of the sulfur vulcanizate is somewhat shifted to the left, corresponding to a larger local friction coefficient. The loss tangent for the sulfur vulcanizate is shown in Figure 5 together with low frequency data for three others, in the low frequency region. Here the magnitude of tan δ decreases with increasing ν and with increasing M just as for the dicumyl peroxide vulcanizates.

Discussion

Transition Zone. In Figure 3, the dispersion in the transition zone shifts to the left on the logarithmic frequency scale by 0.28 as ν is increased from 0.57 to 2.68×10^{-4}. The curve for the lowest cross linking is
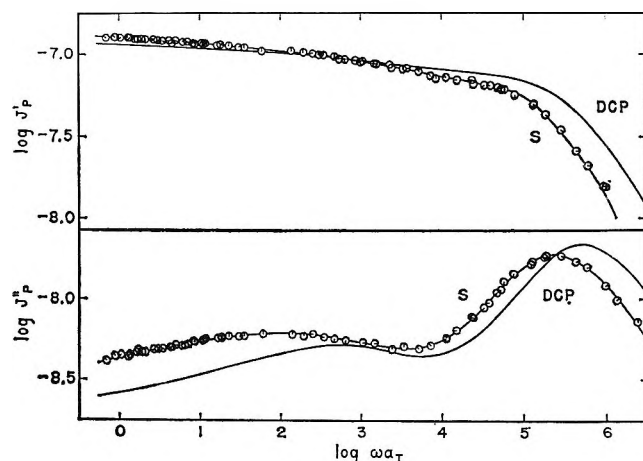
Figure 4. Storage and loss compliance reduced to 25° and plotted logarithmically against reduced radian frequency for sample cross linked by sulfur with $\nu = 1.79 \times 10^{-4}$ (curves S), compared with corresponding dicumyl peroxide vulcanizate with $\nu = 1.85 \times 10^{-4}$ from Figure 2 (curves DCP). Pip directions for S curves denote different temperatures, from -69.3 to $55.8°$ in 17 steps.
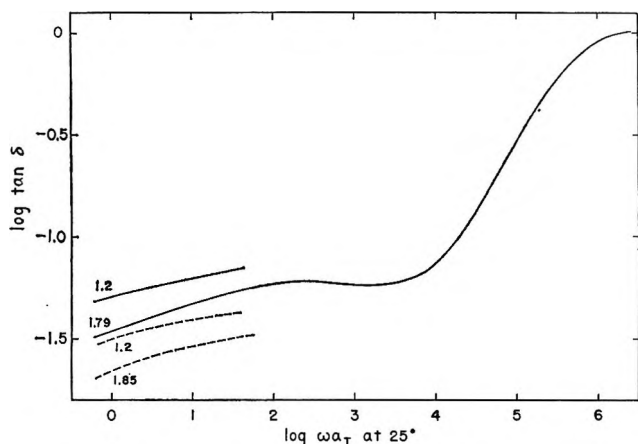
Figure 5. Loss tangents of sulfur vulcanizates, plotted logarithmically against reduced radian frequency: numbers denote $\nu \times 10^4$; dashed lines, $M = 5.1 \times 10^5$; solid lines, $M = 1.8 \times 10^5$.

very close to that for the uncross-linked polymer.[18] Plots of the relaxation spectrum H in this region show a similar spacing. The direction of shift is opposite to that which might be expected from a slight plasticization by the reaction products from the dicumyl peroxide; actually, the magnitude of the latter effect can be predicted from free-volume calculations,[19] after estimating the fractional free volume of the polymer at 25° from the parameters in eq. 3 to be $f_{25} = 0.119$. On this basis, from eq. 8 of ref. 19, with a reasonable value of the parameter β', the logarithmic shift from plasticization should not exceed about 0.02. On the other hand, if a relation is sought between ν^* and the change in local friction coefficient ζ_0 corresponding to this shift, the slope d log $\zeta_0/d\nu^*$ is found to be 0.22×10^4. This could be interpreted as a decreased free volume accompanying formation of a cross link. However, calculating $df/d\nu^* = (\text{d log } \zeta_0/d\nu^*)/(\text{d log } \zeta_0/df)$ and taking d log $\zeta_0/df = -1/2.303 f_{25}^2$, we obtain $df/d\nu^* = -71$ cc./mole of cross links, which would be surprisingly high; Mason[20] has estimated for natural rubber cross linked by dicumyl peroxide a contraction in free volume of 34 Å.^{3}/cross link or 20 cc./mole. Curiously, in our previous studies of natural rubber[2] any shift in frequency scale with dicumyl peroxide cross linking was too small to be clearly detectable. Thus, the origin of the shifts in Figure 3 is uncertain. Another difference between the logarithmic loss tangent curves for polybutadiene and natural rubber in the transition zone is in their slopes, which approximate 0.65 and 0.4, respectively. This discrepancy makes it difficult to compare their relative positions on the logarithmic frequency scale; polybutadiene lies 0.5

to 1.5 decades to the right. (If the Rouse theory applied in this region, the slope would be zero.)

In comparing the transition zone in Figure 5 and the corresponding curve in Figure 3, that for the sulfur vulcanizate lies at lower frequencies by about 0.32 on the logarithmic scale. The direction is anticipated from the chemical changes which accompany sulfur vulcanization,[2,21] but the magnitude is greater than would be expected for 1.33% of combined sulfur on the basis of experience with natural rubber.[6] We shall not attempt to interpret these differences at the present time since the primary interest of this study is in the behavior at low reduced frequencies.

Low Frequency Loss Mechanism. Since the nature of the frequency dependence, as well as the magnitude of the loss, changes markedly with the degree of cross linking in Figures 2–5, the effect of ν cannot be fully described without an analysis of the frequency dependence. As a rough measure, however, we can compare the magnitude of tan δ at a constant value of frequency (log $\omega = 1$) by plotting log tan δ against log ν in Figure 6. The loss tangent drops rapidly with increasing ν, and the dicumyl peroxide and sulfur vulcanizates fall approximately on the same curve. The values for $M = 510,000$ are somewhat below the curve drawn for $M = 180,000$.

Also included are previous data[2] for natural rubber vulcanizates with dicumyl peroxide and sulfur. This
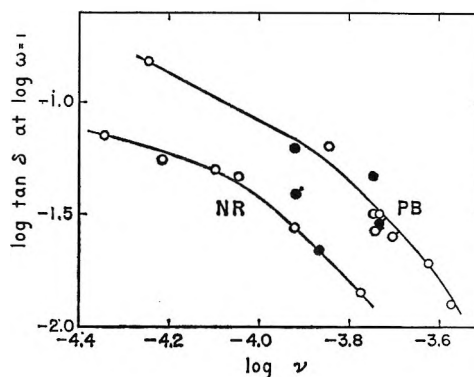
Figure 6. Log tan δ at $\omega = 10$ rads/sec. plotted against log ν for polybutadiene vulcanizates with $M = 180,000$ (PB) and natural rubber (NR) vulcanizates from ref. 2 (M probably about 500,000): open circles, cross linked with dicumyl peroxide; black circles, with sulfur; tagged circles, polybutadiene vulcanizates with $M = 510,000$.

(18) R. H. Valentine, unpublished measurements.

(19) J. D. Ferry and R. A. Stratton, *Kolloid-Z.*, 171, 107 (1960).

(20) P. Mason, *J. Chem. Phys.*, 35, 1523 (1961); *Polymer*, 5, 625 (1964).

(21) H. D. Heinze, K. Schmieder, G. Schnell, and K. A. Wolf, *Kautschuk Gummi*, 14, 208 (1961).

curve lies to the left; it is necessary to have nearly twice the density of elastically active network chains in polybutadiene as in natural rubber to achieve the same level of loss. (The difference is partly, though to a minor extent, attributable to a difference in the initial molecular weights; that for the natural rubber was not determined but was probably about 500,000. Additional experiments on natural rubbers with known initial molecular weights are in progress.)

The low-frequency loss mechanism has been tentatively attributed to coupling entanglements involving the network strands.[2,4,22] The important parameter in this concept is the average number of entanglement loci trapped in a network strand. Since the average entanglement spacing is farther apart by about a factor of 2.5 in natural rubber than in polybutadiene,[22] it appears consistent that the loss falls off at lower degrees of cross linking in the former. This comparison may be oversimplified, however, since dicumyl peroxide produces more cross links per added molecule in polybutadiene than in natural rubber,[23] and this difference may be associated with unknown differences in network topology.

In any case, it is necessary to distinguish between trapped entanglements which contribute to the equilibrium modulus as in the calculations of Mullins and Kraus[5] and the relaxing entanglements whose contribution to the modulus vanishes with decreasing frequency in the logarithmic range below 3 in Figure 2. In this figure, for example, the large maximum in J'' at low frequencies for $\nu = 0.57 \times 10^{-4}$ is associated in the usual manner of a frequency dispersion with a change in J' from 3.6×10^{-7} at equilibrium to 1.1×10^{-7} in the plateau region near $\log \omega = 3$. If the respective magnitudes of J' are inversely proportional to the number of effective network strands, then the latter value in the plateau is larger than the 0.57×10^{-4} effective at equilibrium, and it includes 1.30×10^{-4} mole of effective strands whose contribution relaxes out in the low frequency range. This quantity, ν_{rx}, is given for several other dicumyl peroxide vulcanizates in Table II and is compared with the number of nonrelaxing entanglement strands, $\nu - \nu^*$. With increasing chemical cross linking, $\nu - \nu^*$ rises, but ν_{rx} falls. One possible explanation of this apparent paradox may be outlined as follows.

It may be pointed out that the contribution of an entanglement strand at equilibrium to the modulus is probably somewhat less than that of a cross-linked strand, so $\nu - \nu^*$ can be less than the actual number of entanglement strands. In other words, an entanglement affects the entropy of strain less than does a real cross link. However, perhaps in the frequency range

near $\log \omega = 3$ the entanglement strands make their full contribution, as much as though their ends were chemically tied. Then the ratio $(\nu - \nu^*)/(\nu - \nu^* + \nu_{rx})$, also given in Table II, is a measure of the efficiency of an entanglement at equilibrium. It rises from 0.2 to unity with increasing cross-link density. It is correlated inversely with the average number of entanglements per network strand between two chemical cross links, given in the last column of the Table II as $(\nu - \nu^*)/(\nu^* - b/M)$; in fact, the product of the last two columns is roughly constant.

The concept of variable effectiveness of an entanglement in contributing to the equilibrium modulus is not consistent with the treatment of Mullins and Kraus, in which the parameter a of eq. 1 is considered to be a constant. However, the data analyzed by them refer mostly to networks in which the average number of entanglements per strand is sufficiently small that each should have at least 0.7 of its full effectiveness on the basis of the limited information in Table II. The concept of an effectiveness substantially less than unity applies only in very lightly cross-linked networks.

No attempt is made at present to account for the effect of loose ends, which is apparent in comparing different initial molecular weights. This subject will be treated in the next paper of this series. Another possible source of relaxation could be the presence of a sol fraction (molecules unattached at either end), but in the networks studied here the sol fraction should have been negligible.

The present discussion fails also to account for the topological entanglements, or interlocking structures, produced by the cross-linking process (as distinguished[22] from the entanglements in the Mullins–Kraus treatment, which are supposed to be present already in the uncross-linked polymer). The effects of such struc-

Table II: Relaxing and Nonrelaxing Effective Network Strands; $M = 180,000$, Cross Linked with DCP

Sample code	$\nu \times 10^4$	$\nu - \nu^*$ $\times 10^4$	$\nu_{rx} \times 10^4$	$\dfrac{\nu - \nu^*}{\nu - \nu^* + \nu_{rx}}$	$\dfrac{\nu - \nu^*}{\nu^* - b/M}$
734	0.57	0.34	1.30	0.21	4.3
735	1.42	0.91	0.99	0.48	2.5
736	1.85	1.06	0.46	0.70	1.6
738	2.68	1.19	0	1.00	0.9

(22) J. D. Ferry, "Proceedings of the International Conference on Non-Crystalline Solids," North-Holland Publishing Co., Amsterdam, 1965, p. 333.

(23) B. M. E. Van der Hoff, Ind. Eng. Chem., Prod. Res. Develop., 2, 273 (1963).

tures on equilibrium properties have been treated recently by Case.[24] Further experiments on other cross-linked systems are in progress.

(24) L. C. Case and R. V. Wargin, *Makromol. Chem.*, **77**, 172 (1964)

Light Scattering by Poly-γ-benzyl-L-glutamate Solutions Subjected to Electric Fields

by B. R. Jennings and H. G. Jerrard

Department of Physics, University of Southampton, Southampton, England (*Received June 8, 1964*)

The results of a study of the light scattering by solutions of poly-γ-benzyl-L-glutamate in dichloroethane are presented. The ratio of the Z-average length of the equivalent rod to the weight-average degree of polymerization was found to be 1.36 A. This would seem to agree with previous light scattering results which are consistent with the molecule having the configuration of an α-helix. The application of electric fields changes the scattered intensity if the molecules are polar or electrically anisotropic and, in particular, a.c. fields enable a distinction to be made between these two cases. The solutions were subjected to d.c. fields up to 1.9 kv. cm.$^{-1}$ and an a.c. field of 450 v. cm.$^{-1}$ at frequencies up to 10 kc./ sec. The molecule was found to possess a dipole moment of average value 3920 D. corresponding to 3.44 D. per monomer unit. It has negligible electrical anisotropy. The electric field measurements enabled a value of 3250 sec.$^{-1}$ to be found for the rotary diffusion constant D_r. The variation of D_r with molecular weight, found from the present results and those obtained by Wallach and Benoit, indicates the possibility that the molecule could be rodlike and partially flexible.

Recently, Wallach and Benoit[1] have made light-scattering studies on three samples of poly-γ-benzyl-L-glutamate (PBLG) in dichloroethane when subjected to an electric field. The results of investigations on a sample of different molecular weight are presented here.

The theory of such measurements has been summarized by Wallach and Benoit, who introduced two parameters a and R, which characterize the electrical properties of the molecule and its flexibility respectively a is obtainable from the initial gradients of the Zimm[2] plots obtained with and without the field and gives a value of the dipole moment, μ, if the anisotropy of electrical polarizability, β, is zero, and of β if μ is zero. The

(1) M. L. Wallach and H. Benoit, *J. Polymer Sci.*, **57**, 41 (1962).
(2) B. H. Zimm, *J. Chem. Phys.*, **16**, 1099 (1948).

frequency dependency of a leads to practical differentiation between whether the molecule is either predominantly polar or electrically anisotropic, and, if μ is finite, to knowledge of the rotary diffusion constant, D_r. A combination of both mechanisms is manifest by a frequency-dependent change in the scattered intensity which has a finite asymptotic value at high frequencies. R is the ratio of the intensity changes produced by the field applied in two specified directions. The directions are such that $\alpha = 0$ and $90°$, where α is the angle between the field direction and the vector $\vec{s}$ defined by $\vec{s} = \vec{i_\theta} - \vec{i_0}$, in which $\vec{i_0}$ and $\vec{i_\theta}$ are unit intensity vectors in the direction of the incident and scattered light, respectively. For rods, and all other molecules not deformed by the electric field, R should be -2: it also has this value for flexible chains which are oriented by an induced mechanism alone (β finite, $\mu = 0$), but can have a different value for molecules possessing a permanent dipole moment.

Experimental

Measurements were made both in the presence and absence of an applied field, using a modified form of the apparatus described by Jerrard and Sellen,[3] on a commercial polymer sample obtained from Mann Chemicals Ltd., New York, N. Y. (English agents: V. A. Howe and Co. Ltd., London). D.c. fields of up to 3 kv. were supplied from a stabilized supply and a.c. fields were obtained at a field strength of 450 v. cm.$^{-1}$ r.m.s., and for frequencies up to 10 kc./sec., from a high power oscillator–amplifier. The polymer sample was dissolved in reagent grade solvent to obtain a solution of approximately 3×10^{-3} g. ml.$^{-1}$. This was centrifuged in an M.S.E. nonrefrigerated preparative centrifuge for 1 hr. at 9000 r.p.m. (10,000g). The supernatant, of concentration 2.13×10^{-3} g. ml.$^{-1}$, was the most concentrated solution used for the light-scattering experiments. The incident radiation was of 4358-Å. wave length.

Results

A value of 0.105 for the refractive index increment (dn/dc) was obtained at 4358 Å. by use of a Rayleigh differential refractometer.

(a) *Electric Fields Absent.* The Zimm plot obtained when no field was applied is shown in Figure 1. K is the usual optical constant, c the concentration in grams per milliliter, θ the angle between the forward direction of the incident beam and the scattered beam, R_θ' the Rayleigh ratio corrected by the term $\sin \theta/(1 + \cos^2 \theta)$. From this plot the data given for the first five parameters of Table I were obtained. For a rigid rod, the length determined from the polar radius of gyration ρ_Z
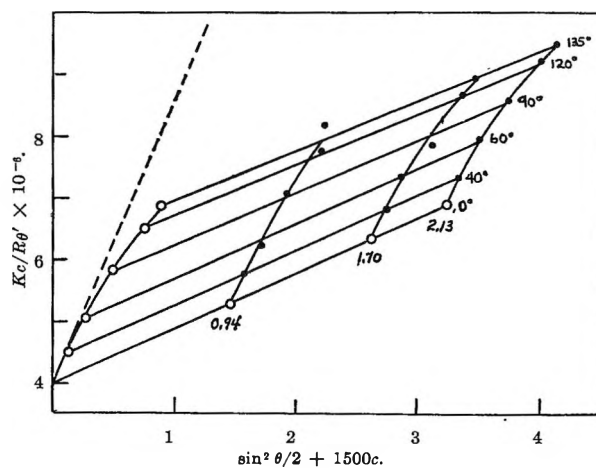
Figure 1. Zimm plot for PBLG in dichloroethane: wave length, 4358 Å.; concentrations are expressed in grams per milliliter.

Table I: Parameters Determined from Light-Scattering Data with and without Application of Electric Fields[a]

$\overline{M}_w$	$= 2.5\,(\pm 0.06) \times 10^5$
$\overline{N}_w$	$= 1.15\,(\pm 0.03) \times 10^3$
$(\langle \rho_z^2 \rangle_{av})^{1/2}$	$= 447 \pm 18$ Å.
$\overline{L}_z$	$= 1550 \pm 60$ Å.
B	$= 6.7\,(\pm 0.8) \times 10^{-4}$
$\overline{L}_w$	$= 980 \pm 50$ Å.
L_{Br}	$= 1720$ Å.
L_α	$= 1710$ Å.
μ	$= 3920 \pm 600$ D.
$\mu/\overline{N}_w$	$= 3.44 \pm 0.7$ D.
D_r	$= 3250 \pm 50$ sec.$^{-1}$
h	$= \overline{L}_z/\overline{N}_w = 1.36 \pm 0.09$ Å.
h	$= \overline{L}_w/\overline{N}_w = 0.86 \pm 0.06$ Å.

[a] L designates the lengths of the equivalent rod of the molecule. Subscripts w and z signify weight and Z average values, and Br and α the lengths calculated from the Broersma formula and for an α helix, respectively. B is the second osmotic virial coefficient.

is strictly a $[Z(Z + 1)]^{1/2}$ average but this is very close to the Z average $\overline{L}_z$. The value for $\overline{L}_w$ has been obtained from the slope of the high-angle asymptote of a graph of Kc/R_θ' against $\sin \theta/2$ by following the treatment suggested by Reichmann.[4] The depolarization ratio, ρ_u, was 0.0085 for 4358 Å.

(b) *Electric Fields Present.* Using a d.c. field of 1936 v. cm.$^{-1}$ the scattered intensity changes, ΔI, were found to be small and apparently independent of concentration. No change of the background scattering was experienced. From a graph of $(Kc/R_\theta')_E$ against $\sin^2 \theta/2$, the initial slope p_E was obtained. Using this

(3) H. G. Jerrard and D. B. Sellen, *Appl. Opt.*, 1, 243 (1962).

(4) M. E. Reichmann, *Can. J. Chem.*, 37, 489 (1959).

in conjunction with the initial slope (p_0) of Figure 1, a value of 0.13 was obtained for a from the equation $a = 5(p_0 - p_E)/p_0$.

In accord with theory, a linear dependence of $\Delta I/I$ on the square of the field strength E was found for observations at $\theta = 135°$ (Figure 2). A value for R of -1.93 was obtained.

(c) *Dispersion Measurements.* If ΔI_f is the intensity change at frequency f, then from theoretical considerations a graph of $\Delta I_{f=0}/\Delta I_f$ against the square of the angular frequency ω should be a straight line of slope $(4D^2)^{-1}$ and which gives an intercept of unity when $\omega^2 = 0$. The frequency f_c at which $\Delta I_f/\Delta I_{f=0} = {}^1/_2$ is given by $2\pi f_c = 2D_r$. The variation of the ratio $\Delta I_f/\Delta I_{f=0}$ with frequency is shown in Figure 3. The strong frequency dependency indicates a significant molecular dipole moment but as the intensity change tends to zero, the anisotropy effect must be comparatively negligible. Since all values of ΔI were positive, the moment lies predominantly along the helix axis. From Figure 3 the critical frequency f_c is 1020 c./sec. giving D_r as 3.2×10^3 sec.$^{-1}$. In Figure 4 the ratio $\Delta I_{f=0}/\Delta I_f$ is plotted against ω^2 and D_r is found to be 3.3×10^3 sec.$^{-1}$.

Discussion

The results are summarized in Table I. In addition to $\overline{L}_z$ and $\overline{L}_w$, the lengths L_{Br} and L_α are included. L_{Br} was calculated from the Broersma[5] formula taking the molecular diameter as 18 Å. and L_α was found assuming the molecule to be an α helix. The dispersion results are consistent with the presence of a moment μ and the average value of this was calculated from the value of a. The value of 3.44 D. for the moment of the monomeric unit is in excellent agreement with that found from the Kerr effect and dielectric data.[6-9] It is near the value of 3.6 D. expected from an α helix. The value of R indicates that the molecule is not deformed by the field, but it could be partially flexible.

According to Luzzati, *et al.*,[10] if h is the ratio of the length of the molecule regarded as a rod to the degree of polymerization, then h varies with the molecular weight M and approaches the value 2.0 Å. as M approaches zero. In this study $\overline{L}_z/\overline{N}_w = 1.36$ Å. and this point fits well on the graph of h against M drawn by Luzzati, *et al.*, but the seemingly more correct value of h is given by $\overline{L}_w/\overline{N}_w$ and this is 0.86 Å. The difference between these two values emphasizes the effect on h of the polydispersity of the sample and, if the samples studied by Luzzati had a similar degree of polydispersity, then their values are also too high, so that the value of 2.0 Å. could be wrong. However, whatever the correct value,
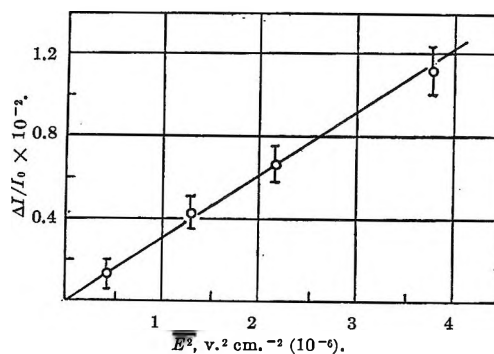
Figure 2. Relative change in scattered intensity with square of electric field: $\theta = 135°$, $\alpha = 90°$.
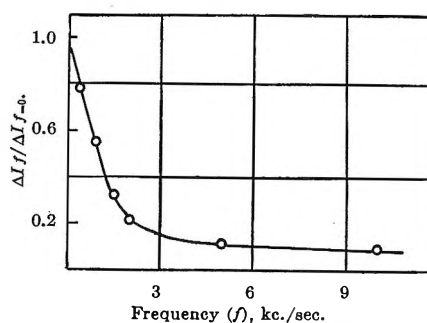
Figure 3. Intensity change dispersion curve for $\alpha = \theta = 90°$ and an electric field of 452 v. cm.$^{-1}$.
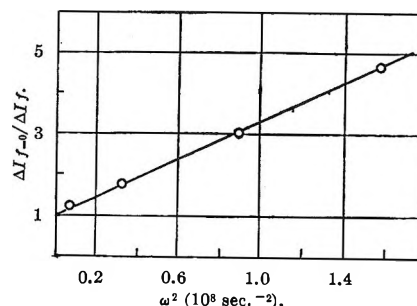
Figure 4. Intensity change variation with square of angular frequency for $\alpha = \theta = 90°$ and an electric field of 452 v. cm.$^{-1}$.

the variation of h with M would seem to indicate molecular flexibility.

The value of D_r and those obtained by Wallach and Benoit for samples of different molecular weight satisfy

(5) S. Broersma, *J. Chem. Phys.*, **32**, 1626 (1960).

(6) A. Wada, *ibid.*, **31**, 495 (1959).

(7) I. Tinocco, *J. Am. Chem. Soc.*, **79**, 4336 (1957).

(8) C. T. O'Konski, K. Yoshioka, and W. H. Ortting, *J. Phys. Chem.*, **63**, 1558 (1959).

(9) A. Mukehata, *Ann. Rept. Sci. Works, Fac. Sci., Osaka Univ.*, **11**, 1 (1963).

(10) V. Luzzati, M. Cesari, G. Spach, F. Masson, and J. M. Vincent, *J. Mol. Biol.*, **3**, 566 (1961).

a relationship of the form $\log D_r = A_1 + A_2 \log M$, where A_1 is a constant and A_2 is approximately -3. The exact value of -3 applies to rigid molecules.

The variation of h with M, the fact that A_2 may not equal -3, and the value of R all allow of the possibility, as suggested by Luzzati, *et al.*, that the form of the PBLG molecule could be a partially flexible 3.0_{10} helix, the effect of flexibility leading to results which seem to be consistent with it being an α helix. However, the authors believe that a consideration of the polydispersity of the samples is of paramount importance and that since the present results show a change of h from 1.36 to 0.86 Å., it is possible that the true value of h as m

approaches zero is nearer to the value of 1.5 Å. associated with an α-helix than the value 2.0 Å. suggested by Luzzati, *et al.* Further support for an α-conformation is givin by Parry and Elliott.[11]

(11) D. A. D. Parry and A. Elliott, *Nature*, 206, 616 (1965).

Dimerization of Anions of Long-Chain Fatty Acids in Aqueous Solutions

and the Hydrophobic Properties of the Acids

by Pasupati Mukerjee[1]

*Department of Physical Chemistry, Indian Association for the Cultivation of Science, Calcutta 32, India,
and van't Hoff Laboratory, Sterrenbos 19, Utrecht, Holland* (*Received October 14, 1964*)

The problem of the dimerization of amphipathic molecules in dilute aqueous solutions is reviewed. An extensive body of data on the distribution of fatty acids (HA) between heptane and an aqueous phosphate buffer (pH 7.45) obtained by Goodman is analyzed. The data cannot be interpreted without postulating self-association of anions, and detailed analysis shows that association involves only two anions: the formation of trimers or higher aggregates is negligible. Theoretical arguments suggest that the formation of acid soap species (or the hydrolysis of the anion dimer) is negligible at pH 7.45. The postulated equilibrium $2A^- \rightleftharpoons A_2^{2-}$ accounts for all anomalies for seven systems, and reliable values of the dimerization constant K_D are derived. K_D increases progressively with chain length to a high value for the palmitate ion, but, curiously, stearate, oleate, and linoleate all give values of the same order as palmitate. From the extrapolated values of the distribution data to infinite dilution, the free energies (ΔG) of complete transfer to the fatty acids are calculated. The change in ΔG for the addition of a CH_2 group, $\Delta G(CH_2)$, is constant between octanoic and myristic acids (-825 cal./mole) but decreases somewhat between myristic and palmitic acids. In their ΔG values, also, the three C_{18} acids appear to be similar to palmitic acid. The implications of these findings to the understanding of micellar equilibria, association of short-chain fatty acids, and some aspects of lipid biochemistry are briefly discussed. A simple, but tentative, physical explanation is suggested for the preponderance of C_{16} and C_{18} acids in many physiological systems.

Introduction

In 1958, it was shown in a series of papers[2-5] that a large number and variety of experimental results on solutions of electrolytes containing amphipathic ions are inconsistent with the commonly accepted notion that these electrolytes are unassociated below the critical micelle concentration (c.m.c.). The anomalous results could be explained qualitatively, and in several cases quantitatively, by assuming a reversible dimerization of the long-chain ions, accompanied by ion-pairing when the counterions are organic in nature. Later work has led to some conflicting results. Strong evidence of pre-c.m.c. association has been obtained in a hydrolysis study of sodium laurate[6] and in some pNa studies on sodium lauryl (NaLS) and tetradecyl sulfates[7] whereas in a series of electrolytes in which both cations and anions are organic, ion pairing, increasing

progressively with increasing organic character of the ions, has been confirmed.[8] On the other hand, a potentiometric study[9] on dodecyl sulfonates has given little evidence of dimerization, and some new conductivity data have been presented on NaLS,[10] which,

(1) Department of Chemistry, University of Southern California, Los Angeles, Calif. 90007.

(2) P. Mukerjee, K. J. Mysels, and C. I. Dulin, *J. Phys. Chem.*, **62**, 1390 (1958).

(3) P. Mukerjee, *ibid.*, **62**, 1397 (1958).

(4) P. Mukerjee and K. J. Mysels, *ibid.*, **62**, 1400 (1958).

(5) P. Mukerjee, *ibid.*, **62**, 1404 (1958).

(6) D. Eagland and F. Franks, *Nature*, **191**, 1003 (1961).

(7) L. Shedlovsky, C. W. Jakob, and M. B. Epstein, *J. Phys. Chem.*, **67**, 2075 (1963).

(8) A. Packter and M. Donbrow, *Proc. Chem. Soc.*, 220 (1962).

(9) F. van Voorst Vader, *Trans. Faraday Soc.*, **57**, 110 (1961).

(10) G. D. Parfitt and A. L. Smith, *J. Phys. Chem.*, **66**, 942 (1962).

in contrast to previous ones,[2] seem to be well accounted for by the Fuoss–Onsager extended theory[11] for nonassociated electrolytes.

The importance of any pre-c.m.c. association in any quantitative study involving amphipathic ions is very great and so are the difficulties involved in getting quantitative information about such association. At the low concentrations available for study, most equilibrium methods for studying self-association are impractical or imprecise. Some nonequilibrium methods, conductometry in particular, are capable of greater precision but involve, for every associated species, the determination of a parameter in addition to an equilibrium constant (the conductivity of the dimer in dimerization equilibria, for example). This restriction severely limits the usefulness of nonequilibrium methods.

An experimental method of great possibility for studying the self-association of amphiphatic species is the determination of partition equilibria, which can be followed by analytical means to extremely high dilutions and over large ranges of concentration. The present paper deals with the interpretation of an extensive body of data, convenient for our purposes, on the distribution of a large number of fatty acids between n-heptane and aqueous sodium phosphate buffer (ionic strength 0.16, pH 7.45, temperature 23°), published by Goodman in 1958.[12] Using C^{14}-labeled acids, Goodman measured distribution coefficients for concentrations as low as 10^{-8} M in water and over a range of several orders of magnitude. From octanoic to myristic acid, the data could be explained, over about three orders of magnitude in concentration, by a simple theoretical scheme involving three well-established equilibria, the ionization of the fatty acids (HA) in the buffer, the distribution of the undissociated monomeric HA between the phases, and the monomer–dimer equilibrium of the fatty acids in heptane. At higher concentrations the experimental data begin to show deviations from this scheme at concentrations (in water) of less than 3×10^{-3}, 2×10^{-4}, and 10^{-5} M for decanoic, lauric, and myristic acids and at much lower concentrations for the higher acids investigated—palmitic, stearic, oleic, and linoleic. The deviations are all in the direction of more fatty acid material being present in water than expected, and Goodman made the qualitative suggestion that they are due to the association of fatty acid anions. A quantitative interpretation of the distribution data is presented here. It provides good insight into the nature of the pre-c.m.c. association, reliable estimates of association constants (K_D) for monomer–dimer equilibrium $2A^- \rightleftharpoons A_2{}^{2-}$, and es-

timates of the hydrophobic characters of long-chain compounds.

The Nature of the Association

It is possible, by very general methods of dealing with equilibrium data on self-associating systems,[13] to derive information about the nature of the equilibrium species present. In Goodman's theoretical scheme, assumed to apply in the monomers in water, the partition ratio, P.R., which is the analytically determined ratio of the concentration sum of all fatty acid species in heptane and the aqueous buffer, is expressed by

$$\mathrm{P.R.} = \frac{K_p{}' + K_p{}' \sqrt{(1 + 8k_d[\mathrm{HA}]_{\mathrm{total,\,h}})}}{2} \quad (1)$$

where $K_p{}'$ is the partition ratio at infinite dilution, h stands for heptane, and k_d is the association constant of the fatty acid dimers in heptane. $K_p{}'$ equals $K_p K_a \cdot [\mathrm{H}^+]$, where K_p is the partition coefficient of HA and K_a its dissociation constant in water. In the region where the experimental P.R. is smaller than that calculated from eq. 1, the calculated P.R. gives the monomer concentration b, which may be put equal to $[\mathrm{A}^-]$ in water since $[\mathrm{HA}] \ll [\mathrm{A}^-]$. The experimental P.R. gives the total equivalent concentration of fatty acid in water, called B. Assuming an as yet undetermined but completely general scheme of self-association to $A_2{}^{2-}$, $A_3{}^{3-}$, ..., B equals $[\mathrm{A}^-] + 2[\mathrm{A}_2{}^{2-}] + 3[\mathrm{A}_3{}^{3-}] + \ldots$ If the total molar concentration of all species ($[\mathrm{A}^-] + [\mathrm{A}_2{}^{2-}] + [\mathrm{A}_3{}^{3-}] + \ldots$) be called S, then, regardless of the nature of the species present, it can be shown[13] that

$$\frac{dS}{db} = \frac{B}{b} \quad (2)$$

if the activity coefficients of the various species are assumed to be constant. In view of the constant and high ionic strength maintained, this assumption here should be excellent. S, as a function of b, can be determined by graphical integration using Kreutzer's[14] integrated form of eq. 2

$$S - S_1 = 2.303 \int_{b_1}^{b} B\,d \log b \quad (3)$$

The average number of monomers in the aggregated species, $\bar{n}$, at any concentration, is now given by[13]

(11) R. M. Fuoss and L. Onsager, *J. Phys. Chem.*, **61**, 668 (1957); **62**, 1339 (1958).

(12) D. S. Goodman, *J. Am. Chem. Soc.*, **80**, 3887 (1958).

(13) F. J. C. Rossotti and H. Rossotti, *J. Phys. Chem.*, **65**, 926 (1961).

(14) J. Kreutzer, *Z. physik. Chem.*, **53B**, 213 (1943).

$$\bar{n} = \frac{B - b}{S - b} \qquad (4)$$

If a single multimer forms, $\bar{n}$ has a constant value. For a series of multimers, $\bar{n}$ increases with concentration, its lowest value being 2 if dimers form at all.

The correctness of any model of self-association is most severely tested in our case for the C_{16} and C_{18} acids because of the wide range of concentrations over which association is evident. Figure 1 shows calculated $\bar{n}$ values for the palmitate system for two different k_d values. The lower estimate was obtained from a short extrapolation of the k_d values given by Goodman for C_8 to C_{14} acids to the C_{16} acid on a plot against the chain length. The higher estimate uses the same procedure on the revised values of k_d (see later). The K_p' values were obtained by graphical extrapolation of the P.R. data, which vary by a factor of less than 1.5. The value of $\bar{n}$ is 2 over the whole range, up to concentrations where the monomer fraction is less than 10%, and shows no trend to higher values. Thus, the associated species indicated involve two monomers only. Previous arguments[2] against the extensive formation of trimers or higher aggregates in terms of additional charge repulsions and relatively smaller reduction of the hydrocarbon–water interface are thus amply justified.

At the constant pH and a high, nearly constant, value of $[Na^+]$ employed, the formation of other binuclear species, such as HA_2^-, H_2A_2, or NaA_2^-, from the monomers and the respective counterions cannot be isolated from the dimerization equilibrium $2A^- \rightleftharpoons A_2^{2-}$ itself. However, it is argued later that these species are probably negligible in the present case.

Calculation of K_D Values

We now interpret all deviations from eq. 1 in terms of anion dimerization. Although the K_D values can be estimated in different manners,[13] the final test of their reliability is how well the experimental P.R. data can be accounted for. If P.R. (calcd.) be the value from eq. 1 (for no dimerization), then P.R. (exptl.) is given by

$$P.R.(exptl.) = \frac{P.R.(calcd.)^2}{P.R.(calcd.) + 2K_D[HA]_{total, h}} \qquad (5)$$

For fitting the data we have used Goodman's estimates for K_p' for the four lowest acids and other values derived by graphical extrapolation (Table I). Goodman's k_d values for C_{10} to C_{14} systems have been raised slightly, to obtain better fits at all concentrations, the maximum change being less than a factor of 1.5. The k_d values for the higher acids are obtained by extrapolation. The raised values are in better agreement

Table I: Partition Coefficients and Transfer Free Energies of Fatty Acids

Acid	K_p'	K_p	ΔG, kcal./mole	$\Delta G(CH_2)$, cal./mole
Octanoic	0.012	4.3	-0.86	
Decanoic	0.21	75	-2.54	-840 ± 30
Lauric	3.0	1.07×10^3	-4.10	-780 ± 30
Myristic	54	1.92×10^4	-5.80	-850 ± 30
Palmitic	580	2.06×10^5	-7.20	-700 ± 30
Stearic	760	2.70×10^6	-7.35	-75 ± 30
Oleic	570	2.28 ± 10^6	-7.25	
Linoleic	272	1.21 ± 10^6	-6.88	
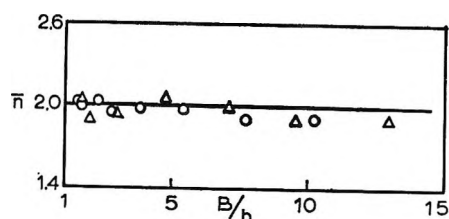
Figure 1. $\bar{n}$ calculations for the palmitate system. It is assumed that $\bar{n} = 2$ up to $B/b = 1.3$: O, $k_d = 1.0 \times 10^4$; $\triangle$, $k_d = 1.6 \times 10^4$.

with estimates of 1.4 and 2.0 ($\times 10^4$) for k_d, on a molar scale, in hexane for lauric and palmitic acids obtained from interfacial tension data.[15]

In Figure 2, the P.R. data are plotted against the total concentration in the aqueous phase, for the three smaller acids, to emphasize the higher concentrations. The expected monomer curves indicated here are linear, with an intercept of K_p' and a slope of $2k_d(K_p')^2$.[12] Figures 3 and 4 show the calculated dimer curves for the four highest fatty acids on a logarithmic scale. Figure 4 shows that, for given values of K_p' and k_d, K_D can be determined quite precisely. In view of the uncertainties in k_d and K_p', however, the over-all reliability of the estimated K_D values (Table II) is not better than 20–40%. Dimerization clearly accounts quantitatively for all anomalies in the seven systems.

When P.R. (calcd.) $\ll 2K_D[HA]_{total, h}$, i.e., for high values of K_D and $[HA]_{total, h}$, one obtains a limiting value for P.R. (exptl.)

$$P.R.(exptl.) = (K_p')^2k_d/K_D \qquad (6)$$

independent of concentration. This is, indeed, observed for the C_{16} and C_{18} acids. Equation 6, where applicable, leads to a rapid estimate of K_D.

(15) A. F. H. Ward and L. Tordai, *Rec. trav. chim.*, **71**, 482 (1952).
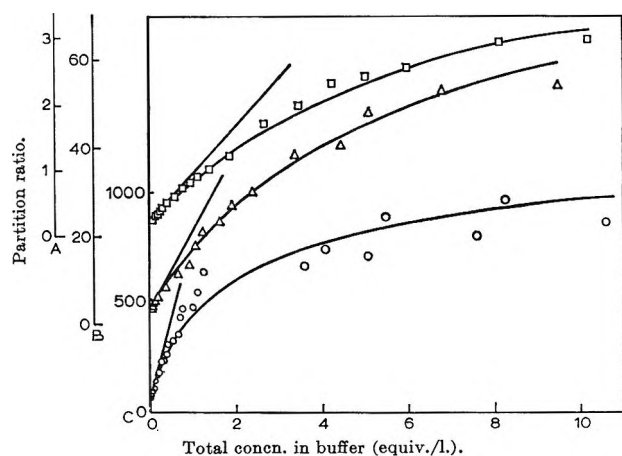
Figure 2. Partition ratios plotted against the total concentration of all species in the aqueous phase: □, decanoate system, ordinate A; △, laurate, ordinate B; O, myristate, ordinate C. Abscissas are to be multiplied by 10^{-3} for □, 10^{-4} for △, and 10^{-5} for O. Initial tangents are calculated curves for monomers only.
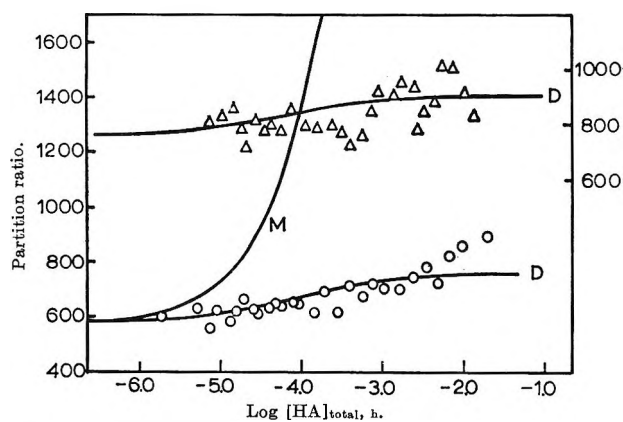
Figure 3. Partition ratios against $[HA]_{total, h}$ for palmitate (O, left-hand scale) and stearate (△, right-hand scale). Curves marked D are calculated by using K_D values of Table II. The curve marked M is the expected curve for monomers only for the palmitate system.

Table II: Dimerization Constants

Acid	$k_d \times 10^{-3}$	K_D
Octanoic	5.8	<10
Decanoic	8.2	40
Lauric	10.0	650
Myristic	13.0	2.6×10^4
Palmitic	16.0[a]	7.0×10^6
Stearic	20.0[a]	1.27×10^7
Oleic	20.0[a]	7.2×10^6
Linoleic	20.0[a]	4.0×10^6

[a] Estimated by extrapolation.
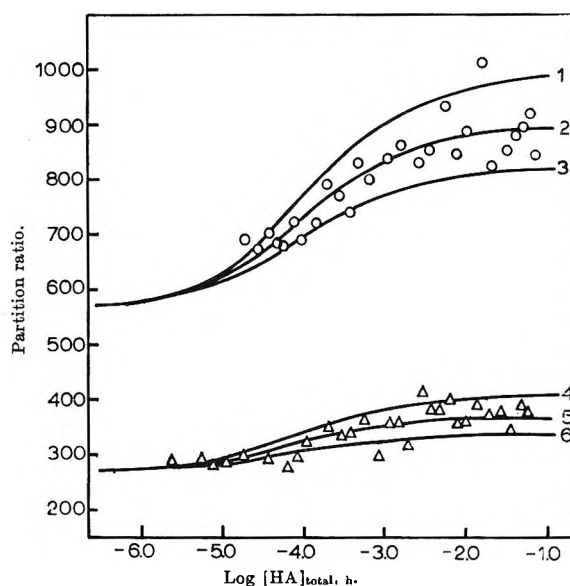
Figure 4. Partition rates for the oleate system, O, and linoleate system, △, plotted against $[HA]_{total, h}$. K_D values used are 6.5, 7.2, and 7.9 for curves 1, 2, and 3, and 3.6, 4.0, and 4.4 for curves 4, 5, and 6 (all multiplied by 10^6), respectively.

The Interpretation of K_D Values

The two most striking features of the K_D values are their great dependence on the chain length up to the C_{16} acid and the small difference between the C_{16} and C_{18} acids. This second feature is very curious and will be discussed later. From C_{10} upwards, K_D increases by progressively larger factors. This effect of chain length is consistent with the model of dimers previously advanced,[2] in which the hydrophobic chains entwine with each other, leaving the charged groups far apart. With increasing chain length and flexibility, there is more hydrocarbon–water interface to be lost while the intercoiling of the chains is facilitated. Between dimers of successive acids, there is a difference of four CH_2 groups. The complete removal of four CH_2 groups from water to a hydrocarbon environment (see later) alone can increase K_D by a factor of about 250, and an additional increase in K_D can come from the decreased charge repulsion. Thus the maximum increase in K_D observed above is not impossibly large.

The Formation of Other Species

It is expected that the formation constant K' of the acid soap species HA_2^- in the equilibrium $HA + A^- \rightleftharpoons HA_2^-$ is greater than K_D because of the absence of charge repulsion and the possibility of hydrogen bonding in HA_2. An estimate of the charge repulsion can be made for our model of A_2^{2-} (heads apart and tails intertwined). The work of repulsion ΔW, at low ionic

strengths, is given by the Kirkwood-Westheimer theory.[16]

$$\Delta W = e^2/D_e l \qquad (7)$$

e is the electronic charge, D_e the "effective" dielectric constant, and l the distance separating the charges. The value of D_e depends primarily on l, the hydrocarbon volume of the dimer, and the dielectric constant of the surrounding medium. For our systems, D_e is within a few per cent of the medium value for any reasonable geometry, including a spherical dimer. Thus, the value of ΔW is roughly $4.4/l$ kcal. mole^{-1} (l in Å. units). Considering that at our high ionic strengths, the double-layer thickness is only 7.5 Å., the charges are expected to be considerably shielded from each other[3] as the value of l is in the range of 10–25 Å. ΔW, therefore, should be below 0.4 kcal./mole for all our systems.

For hydrogen bonding to be an important factor for HA_2^-, it must have a head-to-head and tail-to-tail configuration for which the hydrophobic interactions here are expected to be less favorable. The hydrogen bonding, by itself, is not expected to be very strong in the presence of large excess of water, as evidenced by the low formation constants, K_D', of the dimers of lower fatty acids ($2HA \rightleftharpoons H_2A_2$) in aqueous media[17]: K_D' is about 0.2 for acetic acid and less than 0.1 for formic acid. Recent estimates of the enthalpy associated with K_D' for formic acid is 0 ± 1 kcal./mole[18] and for acetic acid 0.4 kcal./mole,[17] and hydrogen bonding may not be involved at all in the dimerization of HA (see later). Thus, the combined effect of the charge repulsion in A_2^{2-} and hydrogen bonding in HA_2^- should not exceed 2 kcal./mole for the extra stability of HA_2^- as compared to A_2^{2-}. This corresponds to a value of about 30 for the ratio K'/K_D and an error of 10% in the estimated K_D values since, at pH 7.45, the ratio $[A^-]/[HA]$ in water is about 300. Thus, the species HA_2^- should be negligible for the present conditions. The importance of HA_2^- should be easy to evaluate from pH-variation studies of the partition equilibria.

The extension of the above argument makes H_2A_2 of considerably lesser significance than HA_2^-. As there is little evidence of ion pairing of carboxylic acids with Na^+, it seems justified to neglect the species NaA_2^- and Na_2A_2.

Although the $\bar{n}$ calculations do not indicate the formation of trinuclear (A_3^{3-}, HA_3^{2-}, etc.) or higher species here, they may be of some importance at lower pH values and in hydrolysis studies because of the more pronounced charge effects on the acid dissociation.

Discussion of Previous Work

The previous estimates of K_D values in dilute solutions of 100–350 for NaLS[2] and a low value of the order of 10 for sodium decyl sulfate (NaDS)[19] are consistent with the present estimates for the same chain lengths, considering that the charge repulsion increases in dilute solutions. The large factors by which K_D increases with chain length provide a ready explanation of the proposed onset of "irreversible dimerization"[20] (i.e., nearly complete dimerization over certain ranges of concentration[4]) for some quaternary ammonium salts above certain chain lengths.

Regarding the negative results reported,[9,10] that of van Voorst Vader[9] was obtained with a cell with a liquid junction, which is uncertain in general and particularly for amphipathic compounds. More important, c.m.c. data obtained at 20° were used to evaluate e.m.f. data at 35°. For their analysis of equivalent conductivity data (Λ) on NaLS, Parfitt and Smith[10] used a value of 72.9 for Λ_0 (at infinite dilution at 25°). They reported only two measurements below 0.001 M. The Λ_0 value does not agree with the previous estimates of 71.7[2] and 71.4.[21] It is also too close to the Λ_0 (73.4) for NaDS.[19] The difference of 0.5 units (out of about 23) in the equivalent conductivity of the amphipathic ion for a two-carbon increment in chain length does not seem reasonable from a hydrodynamic point of view and does not agree with the difference of 1.74 obtained for the pair decyl- and dodecyltrimethylammonium ions.[22] The reliability of the experimental procedure used in the previous investigation for NaLS[2] seems to be further supported by the findings of approximately Onsager-type behavior in dilute solutions for NaDS[19] and its applicability to KCl solutions in another laboratory.[23] A value appreciably less than 72.9 for Λ_0 would not allow the conductivity data of Parfitt and Smith to be fitted by the Fuoss–Onsager extended theory and would require some association as in the case of the previous data.

The previous interpretation of the association of

(16) J. G. Kirkwood and F. H. Westheimer, J. Chem. Phys., 6, 506, 513 (1938).

(17) J. D. E. Carson and F. J. C. Rossotti in "Advances in the Chemistry of Coordination Compounds," S. Kirschner, Ed., The Macmillan Co., New York, N. Y., 1961, p. 181.

(18) E. E. Schrier, M. Pottle, and H. A. Scheraga, J. Am. Chem. Soc., 86, 3444 (1964).

(19) K. J. Mysels and P. Kapauan, J. Colloid Sci., 16, 481 (1961).

(20) E. J. Bair and C. A. Kraus, J. Am. Chem. Soc., 73, 1129 (1951); D. W. Kuhn and C. A. Kraus, ibid., 72, 3676 (1950); M. J. McDowell and C. A. Kraus, ibid., 73, 2173 (1951).

(21) B. D. Flockhart, J. Colloid Sci., 17, 305 (1962).

(22) M. J. McDowell and C. A. Kraus, J. Am. Chem. Soc., 73, 2170 (1951).

(23) R. H. Boyd, J. Phys. Chem., 65, 1834 (1961).

short-chain fatty acids in water,[17] in terms of bonding between organic parts,[2] also suggested by Kauzmann,[24] is supported by the similarity of the entropy of the first dissociation of H_2A_2 for acetic acid and that of HA.[25] An explanation in terms of hydrogen bonding requires a single hydrogen bonding in H_2A_2, instead of a cyclic structure,[17] which does not seem to be enough for stability and gives no explanation as regards why cyclization does not occur. On the other hand, hydrophobic bonding seems to give a reasonable explanation of the association.[2,18,24] If the salt effects, which are small,[18] are neglected for the K_D' values, obtained at high salt concentrations, and the charge effects for our K_D values, obtained at high ionic strengths, then both should reflect the hydrophobic bonding in dimerization for various chain lengths. Figure 5 shows that K_D values do indeed extrapolate well to K_D' values. Figure 5 should allow rough estimates of hydrophobic bonding in dimerization for intermediate chain lengths.

The Free Energies of Complete Transfer of Fatty Acids

For evaluating theories of micelle formation, a quantity of great interest is the free energy of complete transfer, $\Delta G(CH_2)$, from an aqueous to a hydrocarbon environment. The value generally used is $-1.08kT$ per CH_2 group (25°) or about -640 cal./mole.[26-29] This figure compares poorly with an estimate of about -800 cal./mole obtained from partition data but presented without details.[30] The estimated transfer free energies to air–water and hydrocarbon–water interfaces are -625[31] and -810 to -820 cal./mole,[32] respectively, so that the value of -640 cal./mole for complete transfer seems to be too low.

Reliable $\Delta G(CH_2)$ values for long-chain compounds (C_{12} or higher) are of great interest and do not seem to be available. Goodman's distribution data are suitable for this purpose.

To calculate K_p from the experimental K_p', the pK_a value for octanoic acid,[33] 4.90, is used for all the saturated fatty acids. As pK_a changes by only 0.05 units from n-valeric to octanoic acid,[33] any error should be small. Since pK_a values for both 4- and 5-hexenoic acids are reported as 4.72, intermediate values of 4.85 and 4.80 are used for the unsaturated oleic and linoleic acids. Activity coefficient corrections are neglected.

The K_p' and K_p values (molar scale), the corresponding ΔG of transfer ($\Delta G = -RT \ln K_p$), and the average values of $\Delta G(CH_2)$ are given in Table I. The estimated uncertainty in each $\Delta G(CH_2)$ corresponds to the estimated uncertainty of 10% in the ratios of K_p.

The ΔG increases linearly with chain length from octanoic to myristic acid, so that $\Delta G(CH_2)$ values are
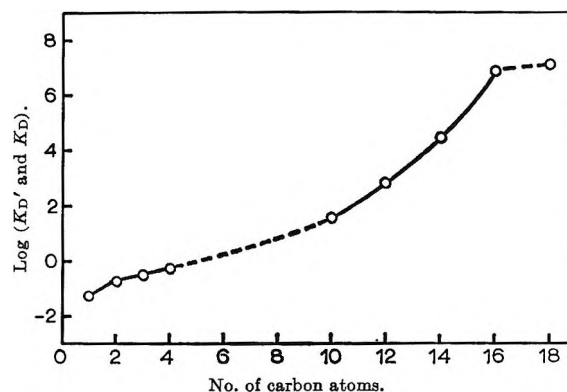
Figure 5. Logarithms of K_D' values[17] (formic to butyric acids) and K_D values (decanoate to stearate ions), present paper, plotted against the number of carbon atoms in the species.

fairly constant. Goodman has previously noted the increase in K_p' by nearly constant factors.[12] The average value of -825 ± 10 cal./mole is in good accord with previous estimates of -800 cal./mole[30] and -823 cal./mole obtained from the solubility data of medium chain alcohols.[34] The ΔG for palmitic acid is significantly lower than expected from the previous trend. The C_{18} acids are all rather similar to the C_{16} acid again, as in their K_D values (Table II).

The above $\Delta G(CH_2)$ value differs substantially from the corresponding estimate for micelles, -680 to -700 cal./mole.[29] Two possible explanations are the neglect of pre-c.m.c. association in the calculations for micelles and the inadequacy of the liquid-core model of the micelle. The chains inside a micelle are likely to be more constrained than in a liquid hydrocarbon and to have a lower entropy.

Is There a Limit to Hydrophobic Character?

The close similarity of the hydrophobic character of C_{16} and C_{18} acids is extremely curious. It is reflected both in the ΔG values (Table I) and K_D values (Table II) which are in roughly the same order. A similar

(24) W. Kauzmann, Advan. Protein Chem., 14, 1 (1959).

(25) D. L. Martin and F. J. C. Rossotti, Proc. Chem. Soc., 73 (1961).

(26) K. Shinoda, Bull. Chem. Soc. Japan, 26, 101 (1953).

(27) J. Th. G. Overbeek and D. Stigter, Rec. trav. chim., 75, 1264 (1956).

(28) R. H. Aranow and L. Witten, J. Phys. Chem., 64, 1643 (1960).

(29) P. Mukerjee, ibid., 66, 1375 (1962).

(30) D. J. Crisp, "Surface Chemistry," Butterworth and Co. Ltd., London, 1949, p. 65.

(31) I. Langmuir, J. Am. Chem. Soc., 39, 1848 (1917).

(32) J. T. Davies, Trans. Faraday Soc., 48, 1052 (1952).

(33) R. A. Robinson and R. H. Stokes, "Electrolyte Solution," Academic Press Inc., New York, N. Y., 1955.

(34) K. Kinoshita, H. Ishikawa, and K. Shinoda, Bull. Chem. Soc. Japan, 31, 1081 (1958).

sequence is observed in Goodman's study of the binding of the fatty acid anions to human serum albumin.[35] If the average number of anions bound to a protein molecule is $\bar{\nu}$ at the equilibrium anion concentration c, the extrapolated value of $\bar{\nu}/c$ at $c = 0$, $(\bar{\nu}/c)_0$, provides a good measure of the strength of binding. In the sequence laurate, myristate, palmitate, and stearate, $(\bar{\nu}/c)_0$ increase by factors of 3.8, 9.0, and 1.2, again showing the close similarity of palmitate and stearate ions. Thus, three quite different types of evidence suggest that at very high chain lengths, the hydrophobic character tends to become constant. Very large experimental errors must be involved for these findings to be entirely spurious. Some corroborative evidence for the phenomenon can also be cited. For example,[36] the c.m.c. of $C_nH_{2n+1}C_6H_4$-p-$SO_3^-Na^+$ seems to decrease by the usual factor of 4 as n increases by 2, but, as n increases from 12 to 14 and 14 to 16, the factors become 1.6 and 1.2, respectively. Similar results have been obtained for some nonionic compounds also[37,38] although, for alkyl sulfates, the C_{18} compounds does not seem to behave unusually.[39]

A possible explanation for the phenomenon can be based on the increased ease of coiling with chain length such that, for sufficiently long chains, some of the methylene groups are put effectively in an organic invironment inside the curled-up chain. Molecular models show that the explanation is plausible. Nevertheless, the changes in the trends of the ΔG, K_D, and $(\bar{\nu}/c)_0$ values between palmitic and stearic acid seems too abrupt. They raise the possibility of a sudden transition of the long chain from an extended structure to a coil at certain values of the chain length, depending, probably, upon the nature of the hydrophilic head group and temperature.

Application to Lipid Biochemistry

The pH and the ionic strength in Goodman's study correspond to those in mammalian blood plasma.[35]

The ΔG and K_p values should, therefore, be of some use in lipid biochemistry. An analysis of the binding of the anions to human serum albumin will be presented later, taking the very considerable effects of dimerization into account. A good correlation is found between K_D and $(\bar{\nu}/c)_0$ values for the saturated fatty acids, which provides some insight into the nature of this binding in terms of hydrophobic bonding.

An interesting and remarkable feature of lipid biochemistry is the preponderance of C_{16} and C_{18} acids in many physiological systems, as compared to lower and higher homologs. The differences between long-chain fatty acids lie mainly in their hydrophobic character. The present analysis suggests that this increases fairly regularly with chain length up to C_{16} but tends to level off after that. If this trend is followed, the C_{20} or higher acids may not be much more hydrophobic than the C_{18} acids. The preponderance of C_{16} and C_{18} acids may, therefore, be due to their optimum hydrophobic character. This appears to be a simple physical explanation of one of the puzzling features of lipid biochemistry, but it should be considered tentative until further experimental evidence is available.

(35) D. S. Goodman, *J. Am. Chem. Soc.*, **80**, 3892 (1958).

(36) H. Kölbel, D. Klemann, and P. Kurzendörfer, *Proc. Intern. Congr. Surface Activity, 3rd., Cologne, 1960*, **1**, 1 (1960).

(37) J. E. Carless, R. A. Challis, and B. A. Mulley, *J. Colloid Sci.*, **19**, 201 (1964).

(38) M. Donbrow and Z. A. Jan, *J. Pharm. Pharmacol.*, **15**, 825 (1963).

(39) H. C. Evans, *J. Chem. Soc.*, 579 (1956). There is a discrepancy in this paper between the c.m.c. of n-octadecyl sulfate reported from specific conductance data (1.8×10^{-4} M) and that read from a plot shown of equivalent conductance data in Figure 4 (3.0×10^{-4} M).

The Heats of Formation of Beryllium Compounds.   I.   Beryllium Hydroxides

by I. J. Bear and A. G. Turnbull

Division of Mineral Chemistry, C.S.I.R.O., Melbourne, Victoria, Australia   *(Received November 19, 1964)*

The heats of solution of ultrapure beryllium metal and of α- and β-beryllium hydroxides in aqueous HF have been measured calorimetrically to find $\Delta H_f°_{298}$ [α-Be(OH)$_2$] = -215.75 $\pm$ 0.5 kcal./mole and $\Delta H_f°_{298}$ [β-Be(OH)$_2$] = -216.5 ± 0.5 kcal./mole. From the heat of precipitation from beryllium sulfate solution has been found $\Delta H_f°_{298}$ [Be(OH)$_{2ppt.}$] = -213.1 $\pm$ 0.6 kcal./mole. Entropies and free energies of the three hydroxides have also been estimated and the free energies of several aqueous beryllium ions evaluated.

Introduction

Beryllium oxide for use in nuclear technology is usually produced by thermal decomposition of the hydroxide. The apparently simple reaction involved

$$Be(OH)_2(s) \longrightarrow BeO(s) + H_2O(g) \qquad (1)$$
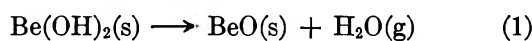
is complicated in practice by the existence of three forms of the hydroxide, amorphous, α, and β, and the initial formation of finely divided oxide with a distorted lattice and large surface energy.[1] In order to evaluate the heat and the equilibrium of this reaction, it is necessary to have precise values of heat and free energy of formation of all the possible solids involved. Although there have been several measurements of the heat of solution of the hydroxides and oxides in aqueous HF and of the heat of combustion of beryllium, many are of poor accuracy and there has been no common basis to make the data self-consistent. As discussed later, previously reported heats of formation of amorphous, α-, and β-Be(OH)$_2$ appear to be in the reverse order to that expected from chemical data. A common basis has now been provided by measuring the heat of solution of ultrapure beryllium in aqueous HF of various concentrations. The heats of solution of α-, β-, and amorphous Be(OH)$_2$ in 22.6% HF have also been measured to derive their heats of formation, and the heat of precipitation of gelatinous Be(OH)$_2$ has been studied.

Experimental

Materials. The beryllium metal used was Nuclear Metals vacuum-distilled single crystal containing 99.985% beryllium and the following impurities (in p.p.m.): Fe, 4; Ni, 2; Mn, 7; Si, 5; Al, 12; Cu, 6;

N, 8; and O, 100. Thus any corrections to the heat of solution for impurities were quite negligible (<0.01%). The metal available to previous investigators has seldom contained more than 99% beryllium, requiring appreciable corrections. The present metal dissolved in 22.6% HF in less than 15 min., leaving no detectable residue and evolving 1 mole of H$_2$/g.-atom within 0.1% as expected from the valence of two.

The beryllium hydroxides were made from Analar BeSO$_4$·4H$_2$O of >99% purity by the well-established procedures of Fricke and Wullhorst.[2] The amorphous form was precipitated by ammonia, the α-form produced by boiling the amorphous in 10% ammonia, and the β-form by hydrolysis of aqueous sodium beryllate, followed by washing with distilled water and drying in CO$_2$-free air at 60°. Analysis by ignition to the oxide gave for α, 58.2 wt. % BeO and for β, 58.4 wt. % BeO (theoret. Be(OH)$_2$, 58.14% BeO). The X-ray diffraction patterns shown in Figure 1 were recorded with Cu Kα radiation, using a Philips counter diffractometer. The 1° divergence and scatter slits and the 0.1-mm. receiving slit were used at a scan rate of 1°/min. Samples were held in thin layers on aluminum slides to reduce absorption errors, and the aluminum lines used for calibration.

The X-ray pattern of β-Be(OH)$_2$ agrees well with the powder data of Seitz, Rosler, and Schubert,[3] indicating well-crystallized orthorhombic Be(OH)$_2$ with no other

(1) R. Fricke and G. F. Huttig, "Hydroxide und Oxyhydrate," Akademie-Verlag, Leipzig, 1937.

(2) R. Fricke and B. Wullhorst, *Z. anorg. allgem. Chem.*, **205**, 127 (1932).

(3) A. Seitz, U. Rosler, and K. Schubert, *ibid.*, **261**, 94 (1960).
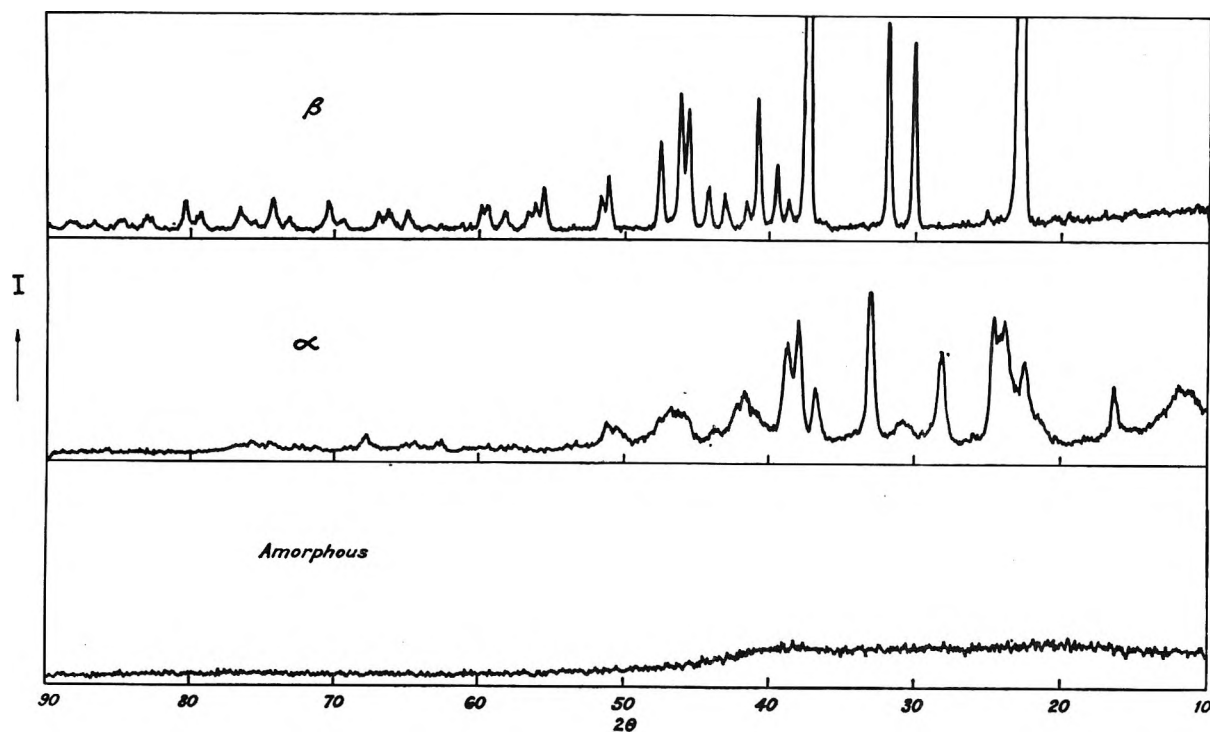
Figure 1. X-Ray diffraction patterns of $Be(OH)_2$ phases.

detectable crystalline impurities. There is good agreement between the X-ray pattern of α-$Be(OH)_2$ and the incomplete X-ray data for the original preparation given by Fricke and Humme.[4] Partial X-ray data (15–20° θ) given by Bernier,[5] for α-$Be(OH)_2$ prepared from beryllium chloride and nitrate solutions by ammonia precipitation and aging, also agree well. A tetragonal unit cell (a = 10.84, c = 7.84) has been suggested for α-$Be(OH)_2$ by Guillemat and Lecocq[6] without supporting data. On this assumption, the present data (Table I) give lattice constants a = 10.80 ± 0.10, c = 7.80 ± 0.10 with 25 $Be(OH)_2$ units per cell leading to a calculated density of 1.960 g./cc. This value bears the expected relationship to a value of 1.945 ± 0.02 g./cc. found by helium densitometry and the value of 1.920 by a pycnometric method reported by Fricke and Severin.[7]

Microscopic examination showed that the β-form consisted of 10–15-μ single crystals aggregated into grains up to 25-μ diameter. This was confirmed by the sharp X-ray peaks, which had a half-peak width of 0.17 ± 0.005° 2θ, as also found by Rau[8] for BeO crystals >1 μ using the same diffraction conditions. The α-form consisted of microcrystalline aggregates of 2–5-μ diameter formed into grains up to 25-μ diameter. A half-peak width of 0.26 ± 0.02° 2θ was observed for several α-form peaks. If the broadening is due only to small

particle size, an average size of 0.07 μ is calculated by the Scherrer method.[8]

The amorphous hydroxide when air-dried gave no discernable X-ray pattern (Figure 1) and is considered to consist of randomly oriented crystallites of <30-Å. size. It is able to absorb large amounts of water on its large surface area and could not be dried beyond the empirical composition $Be(OH)_2 \cdot 0.74H_2O$ at 60° in air. The freshly precipitated gelatinous hydroxide undoubtedly has an even larger surface to which a considerable amount of water is bound. The HF solutions were made by dilution of 40% Analar reagent and analyzed by titration with 1 N NaOH in polythene ware.

Method. Heats of solution were measured in a platinum calorimeter with isothermal jacket held at 21°, previously described.[9] The electrical calibrations were timed to ±0.001 sec. using a 1000-c.p.s. quartz crystal

(4) R. Fricke and H. Humme, *Z. anorg. allgem. Chem.*, 178, 400 (1929).

(5) M. Bernier, Commission Energie Atomique (France) Rapport CEA 2326 (1963).

(6) A. Guillemat and A. Lecocq, *Compt. rend.*, 257, 1260 (1963).

(7) R. Fricke and H. Severin, *Z. anorg. allgem. Chem.*, 205, 287 (1932).

(8) R. C. Rau, "Advances in X-ray Analysis," Vol. 5, W. M. Mueller, Ed., Plenum Press, New York, N. Y., 1962.

(9) A. G. Turnbull, *Australian J. Chem.*, 17, 1063 (1964).

Table I: X-Ray Powder Data for α-Be(OH)₂

	Sin² θ	
hkl	Calcd.	Obsd.[a]
100	0.00509	0.00511 w
001	0.00973	0.00969 m, br
200	0.0203	0.0201 m
201	0.0300	0.0334 w, sh
211	0.0351	0.0351 w, sh
002	0.0389	0.0381 m
220	0.0407	0.0419 s
102	0.0440	0.0427 s
300	0.0458	0.0452 s
202	0.0592	0.0587 s
320	0.0661	0.0701 w
400	0.0814	0.0804 vs
113	0.0978	0.0992 m
322	0.1050	0.1061 s
203	0.1079	0.1098 s
500	0.1273	0.1261 m, br
313	0.1385	0.1385 w
004	0.1556	0.1558 w, br
214	0.1810	0.1806 w
423	0.1893	0.1860 w
404	0.2370	0.2314 vw
105	0.2462	0.2458 vw
215	0.2686	0.2699 w
225	0.2839	0.2855 vw
325	0.3093	0.3103 w

[a] vw, very weak; w, weak; m, medium; s, strong; vs, very strong; br, broad; sh, shoulder.

oscillator coupled to a Dekatron counter. The temperature of 21° was chosen to enable direct comparisons with earlier work, after which final heats of formation were converted to 25° with negligible error.

The beryllium samples of about 20 mg. were weighed to 0.01% precision and enclosed in coils of platinum wire to ensure full heat exchange with the solution and saturation of the evolved hydrogen. The weight of solvent HF was used 120 ± 0.1 g. in each experiment. Electrical calibrations performed before and after each sample agreed within 0.1% and check measurements before and after the series using a similar reaction, the solution of pure magnesium in 1 *N* HCl, agreed within 0.2% with the currently accepted value −111.32 kcal./ mole.[10] The heats of solution of beryllium were corrected by −0.15 kcal./mole (40% HF) to −0.25 kcal./ mole (12% HF) for vaporization of H_2O and HF by the evolved hydrogen, using reported vapor pressures and heats of vaporization.[11]

The hydroxide samples of 80–120 mg. were lightly pelleted and dropped into the calorimeter from room temperature, (21 ± 1°), solution being complete in 10–15 min. Corrections for temperature difference between sample and solvent were negligible.

To study the precipitation of Be(OH)₂, samples of volumetric reagent grade 1 *N* NaOH were weighed into thin glass bulbs which were broken under freshly prepared BeSO₄ solutions by depressing the stirrer. A gelatinous precipitate formed and heat evolution was complete within 10 min.

Results

The corrected heats of solution of beryllium in HF of four concentrations are given in Table II. The heats of solution of α-, β-, and amorphous Be(OH)₂ in 22.6% HF are given in Table III, and the derived thermodynamic properties of the hydroxides collected in Table IV. Results are in terms of the thermochemical calorie (4.1840 joules) and based on the 1961 scale of atomic weights. Uncertainties are given as twice the standard deviations.

Table II: Heat of Solution of Be in Aqueous HF at 21°

HF concn., wt. %	−ΔH₈, kcal./mole	Av. kcal./mole
12.0	101.35, 101.2, 101.8, 101.4	101.45 ± 0.6
22.6	101.1, 100.8, 101.2, 101.1, 101.0, 101.0	101.0 ± 0.3
30.0	100.45, 100.35, 100.25, 101.0	100.5 ± 0.6
40.0	100.4, 99.8, 100.9, 100.75	100.5 ± 0.9

Table III: Heat of Solution of Be(OH)₂ in 22.6% HF at 21°

Phase	−ΔH₈, kcal./mole	Av. kcal./mole
α	22.27, 21.81, 22.31, 22.10, 22.00	22.10 ± 0.4
β	21.37, 21.01, 21.49, 21.45, 21.55	21.37 ± 0.4
Amorphous	22.25, 22.05, 22.2	22.2 ± 0.4

Table IV: Thermodynamic Properties of Be(OH)₂

Phase	$\Delta H_f°_{298}$, kcal./mole	$S°_{298}$, cal./deg. mole	$C_p°_{298}$, cal./deg. mole	$\Delta G_f°_{298}$, kcal./mole
β	−216.5 ± 0.5	12.6 ± 1[a]	15.35 ± 1[a]	−195.65 ± 0.6
α	−215.75 ± 0.5	13.4 ± 2	15.35 ± 1 (est.)	−195.15 ± 0.6
Precipitate	−213.1 ± 0.6	20 ± 4	...	−194.3 ± 0.6

[a] "JANAF Interim Thermochemical Tables," Supplement 11, Dow Chemical Co., Midland, Mich., Sept. 1963.

(10) C. H. Shomate and H. M. Huffman, *J. Am. Chem. Soc.*, 65, 1625 (1943).

(11) P. A. Munter, O. T. Aepli, and R. A. Kossatz, *Ind. Eng. Chem.*, 41, 1504 (1949).

Previously reported heats of solution of beryllium are -94.25 kcal./mole[12] and -82.2 kcal./mole[13] in 30% HF. These are 6–18 kcal./mole lower than present results due, presumably, to the large amount of oxide in beryllium of that era and the use of unreliable calorimetric methods. The heat of solution becomes slightly less negative with increasing HF concentration as is commonly found for the solution of metals in acids, the main ionic species BeF_4^{2-} and BeF_3^- being suggested by a consideration of stability constants.[14]

For β-Be(OH)$_2$, the heat of solution reported by Fricke and Wullhorst,[2] -21.64 kcal./mole in 11.6–12% HF for a similar Be:H$_2$O ratio, is consistent with present results in 22.6% HF. The trend of heat of solution with increasing HF concentration appears to be similar to that of beryllium metal when the small heat of solution of H$_2$O in HF is subtracted. This may be taken as evidence that the same final ionic state occurs in all solutions, a necessary requirement for evaluating heats of formation, but one which is difficult to check otherwise in such work.

For α-Be(OH)$_2$ also, the result of Fricke and Wullhorst,[2] -22.48 kcal./mole in 11.6–12% HF, is consistent with present results and the trend with HF concentration is again similar to that shown by beryllium.

For amorphous Be(OH)$_2$ it is necessary to assume a hydrated hydroxide, Be(OH)$_2\cdot$0.74H$_2$O, since excessive drying was avoided to keep the material as close in nature to the original precipitate as possible. This formula is supported by the infrared spectrum[15] which shows the same peaks as the crystalline hydroxides and also peaks attributable to water. This water must be strongly bound as it is not removed under conditions which give anhydrous β-Be(OH)$_2$.

Two early heats of solution of partly dried amorphous beryllium hydroxide are available, -20.47 kcal./mole in 20% HF by Mulert,[16] and -20.35 kcal./mole in 30% HF for an empirical composition BeO$\cdot$1.14H$_2$O by Matignon and Marchal.[17] Due to the probable low accuracy of measurement and lack of characterization of the solids, a comparison with the above results is not valid.

Discussion

β-Be(OH)$_2$. The heat of formation was calculated from the following summation representing average reactant ratios

$$\text{Be(c)} + 679[\text{HF, 3.80H}_2\text{O}] \longrightarrow$$
$$[\text{BeF}_2, 2580\text{H}_2\text{O}, 677\text{HF}] + \text{H}_2(\text{g}) \quad (2)$$

$$[\text{BeF}_2, 2580\text{H}_2\text{O}, 677\text{HF}] + 2\text{H}_2\text{O}(\text{l}) \longrightarrow$$
$$[\text{BeF}_2, 2582\text{H}_2\text{O}, 677\text{HF}] \quad (3)$$

$$[\text{BeF}_2, 2582\text{H}_2\text{O}, 677\text{HF}] \longrightarrow$$
$$\text{Be(OH)}_2(\text{s}) + 679[\text{HF, 3.8H}_2\text{O}] \quad (4)$$

$$\underline{2\text{H}_2(\text{g}) + \text{O}_2(\text{g}) \longrightarrow 2\text{H}_2\text{O}(\text{l}) \quad (5)}$$

$$\text{Be} + \text{H}_2(\text{g}) + \text{O}_2(\text{g}) \longrightarrow \text{Be(OH)}_2(\text{s}) \quad (6)$$
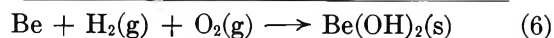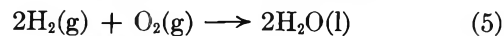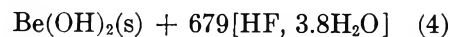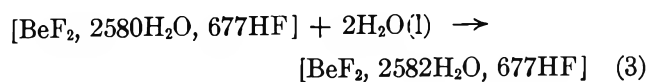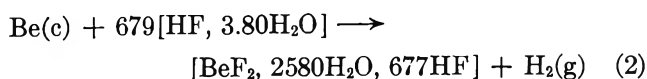
Using values of ΔH_2 and ΔH_4 from Tables II and III, ΔH_3, twice the heat of solution of H$_2$O in 22.6% HF $= -0.15$ kcal.,[18] and ΔH_5, twice the heat of formation of water at 294°K. $= -136.70$ kcal.,[18] the heat of formation of β-Be(OH)$_2$ at 294° is -216.5 ± 0.5 kcal./mole. This value may be taken as $\Delta H_f{}^\circ{}_{298}$ since ΔC_p of reaction 6 is only -2.8 cal./deg. mole.[19] A comparable value of $\Delta H_f{}^\circ{}_{298}$ [β-Be(OH)$_2$] $= -216.7$ kcal./mole may be calculated from the heat of solution in 11.6–12% HF,[2] but is less reliable since the temperature and Be: H$_2$O ratio of the work are uncertain.

An independent value of $\Delta H_f{}^\circ{}_{298}$ [β-Be(OH)$_2$] was calculated[19] from equilibrium water vapor pressures measured by Fricke and Severin[7] for the decomposition reaction 1. The value of $\Delta H_{403} = -15.5$ kcal. for this reaction was corrected to 298°K. using an estimated heat capacity for Be(OH)$_2$.[19] Then the use of $\Delta H_{f\ 298}$ [BeO] $= -143.1$ kcal./mole, found by oxygen combustion,[20] led to $\Delta H_{f\ 298}$ [β-Be(OH)$_2$] $= -216.6$ kcal./mole. This is in good agreement with the above values, but evidently arises from a fortuitous cancellation of errors, since Be(OH)$_2$ decomposes to give a finely divided, water-retaining BeO having a heat of formation some 1–2 kcal. less negative than the high-temperature form produced by oxygen combustion.[1] In addition, it has not yet been demonstrated that reaction 1 is reversible.

The entropies of beryllium hydroxides have not been measured, but for β-Be(OH)$_2$ a good estimate $S_{298}{}^\circ = 12.6 \pm 1$ e.u.[19] based on the chlorides and hydroxides of Mg, Ca, and Cd is available. Thus for β-Be(OH)$_2$ $\Delta S_f{}^\circ{}_{293} = -69.9$ e.u. and $\Delta G_f{}^\circ{}_{298} = -195.65 \pm 0.6$ kcal./mole.

α-Be(OH)$_2$. In a similar manner to β-Be(OH)$_2$, the heat of formation of α-Be(OH)$_2$ is found to be -215.75 ± 0.5 kcal./mole. The difference in $\Delta H_f{}^\circ{}_{298}$ between α and β found here, 0.73 kcal., is in good agreement with

(12) C. Matignon and M. Marchal, *Compt. rend.*, **183**, 927 (1926).

(13) H. Copaux and C. Phillips, *ibid.*, **176**, 579 (1923).

(14) K. E. Kleiner, *Zh. Obshch. Khim.*, **21**, 18 (1951).

(15) I. J. Bear, G. M. Lukaszewski, and A. G. Turnbull, *Australian J. Chem.*, **18**, 1317 (1965).

(16) O. Mulert, *Z. anorg. allgem. Chem.*, **75**, 198 (1912).

(17) C. Matignon and M. Marchal, *Compt. rend.*, **181**, 859 (1925).

(18) F. D. Rossini, *et al.*, U. S. National Bureau of Standards Circular 500, U. S. Government Printing Office, Washington, D. C., 1952.

(19) See ref. *a* in Table IV.

(20) L. A. Cosgrove and P. E. Snyder, *J. Am. Chem. Soc.*, **75**, 3102 (1953).

the values of Fricke and Wullhorst,[2] 0.84 kcal., and Wagner,[2] 0.7 kcal. This difference could arise partly from differing structures and partly from differing surface areas, since an estimated average surface energy of 1000 ergs/cm.[2] and particle size of 0.07 μ lead to a surface enthalpy of 0.4 kcal./mole for α-Be(OH)$_2$.

The value of ΔG_{298} for the change α-Be(OH)$_2 \rightarrow$ β-Be(OH)$_2$ was found to be -0.50 kcal./mole by Fricke and Humme[4] from the solubilities in concentrated alkalis. This may be combined with the above $\Delta H_f{}^\circ{}_{298}$ difference to find the change in entropy, $\Delta S_{298} = -0.8$ e.u., and thence the entropy of α-Be(OH)$_2$, $S_{298}{}^\circ = 13.4$ $\pm$ 2 e.u. This amount of entropy difference is reasonable for crystalline polymorphs, but may also be partly due to a surface or disorder effect in α-Be(OH)$_2$.

A close comparison may be made with the change β_1-Zn(OH)$_2 \rightarrow \epsilon$-Zn(OH)$_2$, the only known case where the structures probably correspond to those of Be(OH)$_2$. From a recent measurement of stability constants,[21] ΔG_{298} for this change is -0.30 ± 0.03 kcal., and from heat of solution data[22] ΔH_{298} is -0.32 ± 0.03 kcal. Thus, ΔS_{298} for this change is found to be -0.1 e.u. in fair agreement with the Be(OH)$_2$ value.

From the above data $\Delta S_f{}^\circ{}_{298}$ [α-Be(OH)$_2$] $= -69.1$ e.u. and $\Delta G_f{}^\circ{}_{298} = -195.15 \pm 0.8$ kcal./mole. It should be noted that the free energy difference of -0.50 kcal. from solubilities is in qualitative agreement with the slow, spontaneous conversion of α to β noted under water or alkaline solutions.[1,6] Also Bernier[5] has recorded d.t.a. peaks for the decomposition of Be(OH)$_2$ which are about 25° lower for α than for β, suggesting a lower stability of α toward BeO $+$ H$_2$O. In earlier evaluations the reverse order of stability has been indicated; i.e., $\Delta H_f{}^\circ{}_{298}$ [β] $= -216.1$ kcal. and $\Delta H_f{}^\circ{}_{298}$ [α] $= -216.8$ kcal.,[18] $\Delta G_f{}^\circ{}_{298}$ [β] $= -195.5$ kcal. and $\Delta G_f{}^\circ{}_{298}$ [α] $= -196.2$ kcal.[23]

Amorphous Be(OH)$_2$. The heat of formation of the hydrated amorphous hydroxide was calculated from the heat of solution (Table III)

$$\text{Be(OH)}_2, 0.74\text{H}_2\text{O(am)} + 679[\text{HF}, 3.8\text{H}_2\text{O}] \longrightarrow$$
$$[\text{BeF}_2, 2582.74\text{H}_2\text{O}, 677\text{HF}] \quad (7)$$
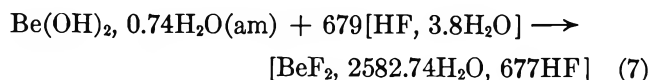
combined with the heat of solution of Be metal, eq. 2, and of the reactions

$$[\text{BeF}_2, 2580\text{H}_2\text{O}, 677\text{HF}] + 2.74\text{H}_2\text{O(l)} \longrightarrow$$
$$[\text{BeF}_2, 2582.74\text{H}_2\text{O}, 677\text{HF}] \quad (8)$$

$$2.74\text{H}_2\text{(g)} + 1.37\text{O}_2\text{(g)} \longrightarrow 2.74\text{H}_2\text{O(l)} \quad (9)$$
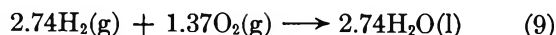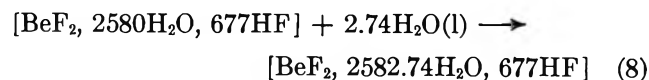
Using values of ΔH_{294} (8) $= -0.20$ kcal.[18] and ΔH_{294} (9) $= -187.27$ kcal.,[18] $\Delta H_f{}_{294}$ [Be(OH)$_2$·0.74H$_2$O] is found to be -266.25 ± 0.5 kcal./mole. The strongly ad-

sorbed 0.74 H$_2$O may be assumed to be in an icelike state for which $\Delta H_f{}_{294} = -69.8 \pm 0.5$ kcal./mole is estimated.[18] Thus $\Delta H_f{}_{294}$ of anhydrous Be(OH)$_2$(am) is found to be -214.6 ± 1 kcal./mole. This value is 1.15 kcal. more positive than that of α-Be(OH)$_2$ as expected from the greater surface area and disorder suggested by the X-ray patterns (Figure 1).

Precipitated Be(OH)$_2$. The heat of formation of a fresh, rapidly precipitated, gelatinous hydroxide was obtained from the reaction

$$[\text{BeSO}_4, 4000\text{H}_2\text{O}] + 2[\text{NaOH}, 55.6\text{H}_2\text{O}] \longrightarrow$$
$$\text{Be(OH)}_2\text{(ppt.)} + [\text{Na}_2\text{SO}_4, 4111\text{H}_2\text{O}] \quad (10)$$
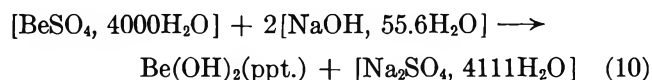
The heat of reaction 10, using a stoichiometric ratio of reactants, was measured to be -14.0, -13.9, -14.0, -13.8, -14.1, average -14.0 ± 0.2 kcal./ mole at 294°K. The heat of formation of [BeSO$_4$, 4000H$_2$O] has been redetermined,[24] from the heat of solution of BeSO$_4$·4H$_2$O(c) in 22.6% HF and in water, to be -306.7 ± 0.5 kcal./mole at 294°K. This value is based on two recent determinations of $\Delta H_f{}^\circ{}_{298}$ [H$_2$SO$_4$, 115H$_2$O], averaging -212.20 ± 0.05 kcal./mole,[25] combined with appropriate corrections for temperature and dilution.[18] On this basis, $\Delta H_f{}_{298}$ [Na$_2$SO$_4$, 4111-H$_2$O] is calculated to be -331.85 kcal./mole from the tabulated value[18] of -31.95 kcal./mole for the heat of neutralization of [H$_2$SO$_4$, 115H$_2$O] with 2[NaOH, 1998H$_2$O]. Taking $\Delta C_{p,f} = -12$ cal./deg. mole gives $\Delta H_f{}^\circ{}_{294}$ [Na$_2$SO$_4$, 4111H$_2$O] $= -331.80$ kcal./mole. For [NaOH, 55.6H$_2$O] the use of $\Delta C_{p,f} = -15$ cal./deg. mole gives $\Delta H_f{}^\circ{}_{294} = -112.10$ kcal./mole.[18] Thus, evaluation of reaction 10 leads to $\Delta H_f{}^\circ{}_{294}$ [Be(OH)$_2$-(ppt.)] $= -213.1 \pm 0.6$ kcal./mole.

The nature of Be(OH)$_2$(ppt.) will depend on the concentrations, mode of mixing, temperature, and time of aging used. The present rapid precipitation should have produced almost the maximum structural disorder and surface area for a flocculated precipitate and thus the most positive free energy and heat of formation. On stepwise titration, BeSO$_4$ is completely precipitated by 1.9NaOH, suggesting a basic sulfate 0.95Be(OH)$_2$· 0.05BeSO$_4$.[26] However, further addition of NaOH replaces SO$_4{}^{2-}$ in the precipitate by OH$^-$ giving Be-

(21) P. Schindler, H. Althaus, and W. Feitknecht, *Gazz. chim. ital.*, **93**, 168 (1963).

(22) R. Fricke and O. Meyering, *Z. anorg. allgem. Chem.*, **230**, 357 (1937).

(23) W. M. Latimer, "Oxidation States of the Elements and their Potentials in Aqueous Solutions," 2nd Ed., Prentice-Hall, Inc., Englewood Cliffs, N. J., 1952.

(24) I. J. Bear and A. G. Turnbull, to be published.

(25) M. Mansson and S. Sunner, *Acta Chem. Scand.*, **17**, 723 (1963).

(26) H. Kakihana and L. G. Sillén, *ibid.*, **10**, 985 (1956).

(OH)$_2$, which has an extremely low solubility product. The present precipitate thus will probably contain only a minor amount of adsorbed SO$_4$$^{2-}$ and an indefinite amount of water. Thus it appears reasonable that the heat of formation should be 1.5 kcal./mole more positive than that of amorphous Be(OH)$_2$ which has suffered removal of water and ion impurities and reduction in surface area.

The free energy of formation of Be(OH)$_2$(ppt.) may be found from the solubility product. Thus, for the reaction

$$Be(OH)_2(s) \rightleftharpoons Be^{2+}(aq) + 2OH^-(aq) \quad (11)$$

a value of log K_{So} = -20.8 at 298°K. has been derived[27] for ppt.-Be(OH)$_2$ from potentiometric titrations of beryllium sulfate and halide solutions.[28] However, a more recent polarographic study[29] of precipitation from BeSO$_4$ solution gave log K_{So} = -25.7 at 292°K. for Be(OH)$_2$(ppt). This value may refer to the basic sulfate known to form under these conditions. It is, moreover, inconsistent with log K_{So} = -21.1 at 298°K. for α-Be(OH)$_2$ derived from solubility in dilute acids,[30] and log K_{So} = -21.5 at 298°K. for β-Be(OH)$_2$ derived from solubilities of α and β in alkali, since the changes ppt.-Be(OH)$_2$ $\rightarrow$ α-Be(OH)$_2$ $\rightarrow$ β-Be(OH)$_2$ occur spontaneously.

Some comparable values of Δ log K_{So} for the change (initial, active precipitate) $\rightarrow$ (stable, inactive, form) are as follows[27]: Mg(OH)$_2$, -1.7; Fe(OH)$_2$, -1.1; Co(OH)$_2$, -0.9; Ni(OH)$_2$, -2.5; Cd(OH)$_2$, -0.7; Zn(OH)$_2$, -1.0. It thus appears reasonable to take Δ log K_{So} for the change ppt.-Be(OH)$_2$ $\rightarrow$ β-Be(OH)$_2$ to be -1.0, as found for ppt.-Zn(OH)$_2$ $\rightarrow$ ϵ-Zn(OH)$_2$. Thus ΔG_{298} for this change is -1.35 kcal. and $\Delta G_f°_{298}$ [ppt.-Be(OH)$_2$] = -194.3 ± 0.6 kcal. This may be combined with the calorimetric value of ΔH_{298} = -3.4 kcal. for this change to find ΔS_{298} = -6.9 e.u. and thence $S_{298}°$ [ppt.-Be(OH)$_2$] = 20 $\pm$ 4 e.u. The changes

in heat of formation and entropy from β to ppt.-Be(OH)$_2$ appear to be consistent with the large surface and disordered, polymeric structure of the gelatinous precipitate.

Ionic Species. The free energy of formation of Be$_{aq}$$^{2+}$ may be evaluated from reaction 11 using the relation $\Delta G = -RT \ln K_{So}$ and $\Delta G_f°_{298}$ (OH$^-$) = -37.6 kcal./mole.[18] The values of log K_{So} = -21.1 for α-Be(OH)$_2$ and -20.8 for ppt.-Be(OH)$_2$ give values of $\Delta G_f°_{298}$ (Be^{2+})$_{aq}$ = -91.15 and -90.7 kcal./mole, respectively. It is evident that further investigation of the solubility product is desirable.

The solubility of α-Be(OH)$_2$ in dilute acids has been explained by Schindler and Garrett[30] assuming the formation of Be^{2+} and Be$_3$(OH)$_3$$^{3+}$.

$$3\alpha\text{-Be(OH)}_2 \rightleftharpoons Be_3(OH)_3{}^{3+}(aq) + 3OH^-(aq) \quad (12)$$

Their value of log K_{S33} = -30.3 for this reaction gives $\Delta G_f°_{298}$ [Be$_3$(OH)$_3$$^{3+}$]$_{aq}$ = -431.3 kcal./mole.
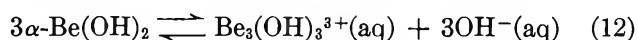
Similarly, the solubility of α-Be(OH)$_2$ in alkali[30] is explained by the reactions

$$\alpha\text{-Be(OH)}_2 + OH^- \rightleftharpoons Be(OH)_3{}^-(aq) \quad (13)$$

$$\alpha\text{-Be(OH)}_2 + 2OH^- \rightleftharpoons Be(OH)_4{}^{2-}(aq) \quad (14)$$
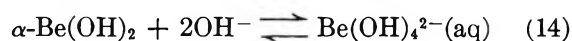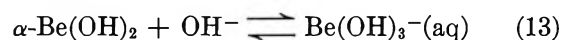
The values of log K_{S3} = -2.5 and log K_{S4} = -2.7 give $\Delta G_f°_{298}$ [Be(OH)$_3$$^-$]$_{aq}$ = -229.4 kcal./mole and $\Delta G_f°_{298}$ [Be(OH)$_4$$^{2-}$]$_{aq}$ = -266.7 kcal./mole.[31]

(27) W. Feitknecht and P. Schindler. *Pure Appl. Chem.*, 6, No. 2 (1963).

(28) M. Prytz, *Z. anorg. allgem. Chem.*, 180, 355 (1929).

(29) P. N. Kovalenko and O. I. Geiderovich, *Russ. J. Inorg. Chem.*, 4, 895 (1959).

(30) P. Schindler and A. B. Garrett, *Helv. Chim. Acta*, 43, 2176 (1960).

(31) Note Added in Proof. E. S. Funston, W. J. Kirkpatrick, and P. P. Turner present X-ray powder data and tetragonal indexing for α-Be(OH)$_2$ in substantial agreement with present work: *J. Nucl. Mater.*, 11, 310 (1964).

Dye-Sensitized Photopolymerization Processes.[1a] III. The Photoreducing

Activity of Some Dicarbonyl Compounds

by S. Chaberek,[1b] R. J. Allen, and G. Goldberg

Technical Operations Research, Burlington, Massachusetts   (*Received December 7, 1964*)

β-Diketones such as 2,4-pentanedione and dimedon were found to be photoinitiators in conjunction with thionine and methylene blue for the photopolymerization of acrylamide. Studies into the relation between photoactivity and molecular structure showed that the active compounds are those capable of undergoing keto–enol tautomerism and that the enol forms are responsible for reactivity. Photoactivity was also observed for a variety of metal chelates of 2,4-pentanedione. On the basis of limited studies on Cu(II)– and Al(III)–β-diketone chelates, it appears that the photoinitiating activity must be at least partly due to the hydrolysis of the complex to produce photoactive ligand. Studies of the Cu(II)–dimedon system have shown an accelerating effect on the photopolymerization process.

Introduction

A variety of dye-sensitized photopolymerization processes have been reported in which the polymerization-initiating free radical is produced by an oxidation–reduction reaction between the light-excited dye and a mild reducing agent.[2–9] Substances used as reducing agents include secondary and tertiary amines and amino acids, thiourea and its derivatives, ascorbic acid, and thiocyanate ion. During the course of our investigation into dye-sensitized photopolymerization processes we have found that many dicarbonyl compounds, especially β-diketones, reduced light-excited thionine (and methylene blue) in the presence of monomers and brought about polymerization. To our knowledge there has been only one report on the photoreducing action of dicarbonyl compounds in the visible light range, and none on photopolymerization. Mauzerall[10] described the photoreduction of some porphyrins in the presence of ethyl acetoacetate. This paper summarizes, then, some of our results on the photopolymerization of acrylamide initiated by free radicals formed by reaction of light-excited thionine and various dicarbonyl compounds under anaerobic conditions.

Experimental Work

Materials. A pure sample of acrylamide was obtained from the American Cyanamid Co. Preliminary screening of this sample for anaerobic thionine-sensitized polymerization showed no polymer formation in the absence of added activators and only a trace of dye bleaching over a period of 10 min.

Thionine was purified by three recrystallizations from water. The absorption coefficient was found to be 5.8×10^4 l. cm.$^{-1}$ mole^{-1} at 5980 Å.

Biacetyl, 2,5-hexanedione, 2,4-pentanedione (acetylacetone), and 5,5-dimethyl-1,3-cyclohexanedione (dimedon) were obtained from the Aldrich Chemical Co.

The metal chelates of 2,4-pentanedione were obtained from MacKenzie Chemical Works, Inc.

(1) (a) This study was performed under Contract No. AF33(657)-8754 and AF33(647)-11553, Photographic Branch, Reconnaissance Division, Air Force Avionics Laboratory, Wright-Patterson Air Force Base, Ohio; J. R. Pecqueux, project engineer; (b) to whom inquiries should be sent at Cowles Chemical Co., Skaneateles Falls, N. Y.

(2) (a) G. Oster, *Phot. Eng.*, **4**, 173 (1953); (b) G. Oster, *Nature*, **173**, 300 (1954).

(3) G. K. Oster, G. Oster, and G. Prati, *J. Am. Chem. Soc.*, **79**, 595 (1957).

(4) N. Uri, *ibid.*, **74**, 5808 (1952).

(5) G. Delzenne, W. Dewinter, S. Toppet, and G. Smets, *J. Polymer Sci.*, **2A**, 1069 (1964).

(6) A. Watanabe and M. Koizumi, *Bull. Chem. Soc. Japan*, **34**, 1086 (1961).

(7) G. Delzenne, S. Toppet, and G. Smets, *J. Polymer Sci.*, **48**, 347 (1960).

(8) S. Chaberek, A. Shepp, and R. J. Allen, *J. Phys. Chem.*, **69**, 641 (1965).

(9) S. Chaberek and R. J. Allen, *ibid.*, **69**, 647 (1965).

(10) D. Mauzerall, *J. Am. Chem. Soc.*, **82**, 1832 (1960).
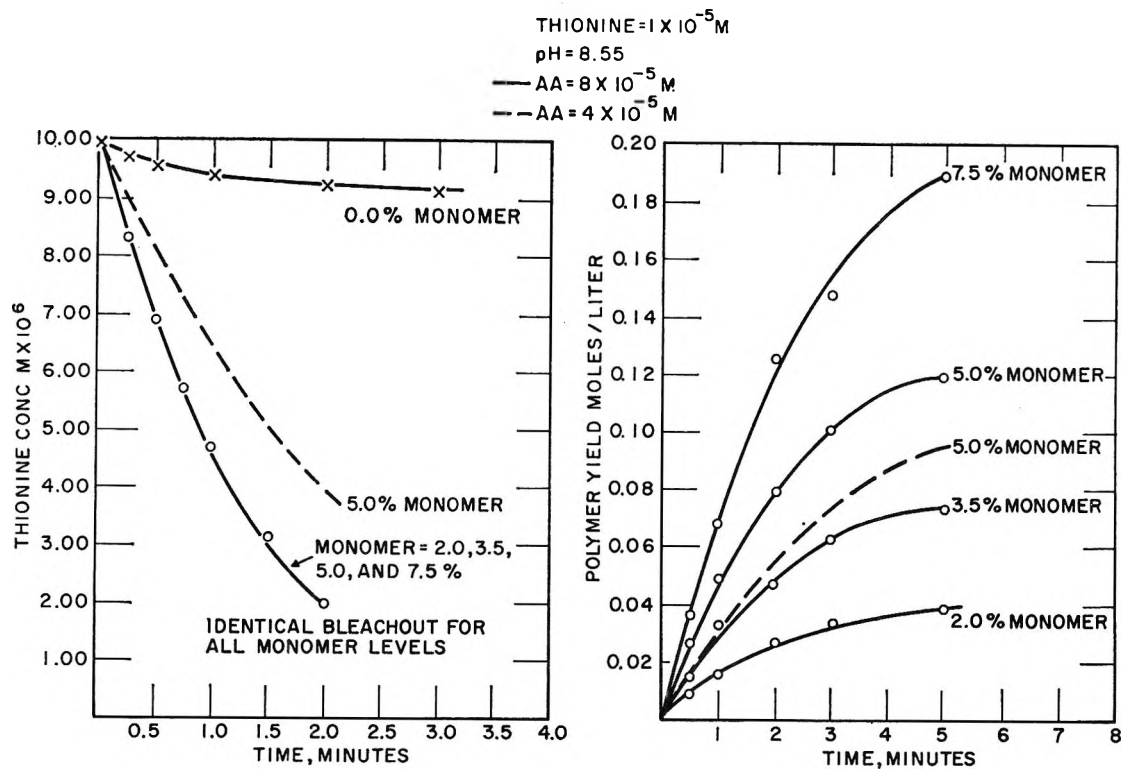
Figure 1. Effect of monomer concentration on the anaerobic thionine-AA-acrylamide system.

Triacetylmethane and the 3,3-dimethyl-, 3-iso-nitroso-, and 3-amino-2,4-pentanediones were prepared by methods described in the literature.[11-14] 3-Diethylamino-2,4-pentanedione was prepared by the reaction of 3-chloro-2,4-pentanedione and diethylamine, in the following manner. A mixture of 27 g. of 3-chloro-2,4-pentanedione and 60 ml. of diethylamine was refluxed for 17 hr. The reaction mixture was poured into 300 ml. of diethyl ether, and the precipitated diethylamine hydrochloride was filtered. The ether solution was evaporated under reduced pressure, leaving a dark oil that crystallized on standing. This crude product was recrystallized from ethyl acetate-petrol and final purification was made by vacuum sublimation. The purified product was a white solid having a melting point of 84-87°. Anal. Calcd. for $C_9H_{17}NO_2$: C, 63.1; H, 10.0; N, 8.2. Found: C, 63.2; H, 9.9; N, 8.1.

Bis(acetylacetone)ethylenediimine was prepared by the method of McCarthy, Hovey, Ueno, and Martell.[15]

Procedure. The experimental apparatus and procedures used in this study were the same as those described previously.[16] The light from a 500-w. projection lamp was passed through a Kodak Wratten 23A filter prior to illuminating the reaction cell. This filter cuts out radiation having wave lengths lower than 5600

Å., transmits 11% at 5700 Å. and 82.7% at 6000 Å. The rate of dye bleaching, R_f, was calculated directly from spectrophotometric measurements. The polymerization rate, R_p, was determined by taking aliquots of the reaction solution at several time intervals, precipitating the polyacrylamide in methanol, filtering it, and drying the residue to constant weight. Polymer molecular weights were determined viscometrically.

Results and Discussion

2,4-Pentanedione (AA). 2,4-Pentanedione was the first substance for which photoreducing activity was found. Figure 1 shows the effects of monomer and AA concentrations on the rates of photobleaching and polymerization. The solid lines show the monomer variation at an AA level of 8×10^{-5} M, while the dotted lines show the effect of a lower AA concentra-

(11) J. U. Nef, Ann., 277, 71 (1893).

(12) R. G. Pearson, E. A. Mayerle, and J. M. Mills, J. Am. Chem. Soc., 73, 927 (1951).

(13) A. Wolff, Ann., 325, 139 (1902).

(14) W. D. Cash, F. T. Semeniuk, and W. H. Hartung, J. Org. Chem., 21, 999 (1956).

(15) P. J. McCarthy, R. J. Hovey, K. Ueno, and A. E. Martell, J. Am. Chem. Soc., 77, 5820 (1955).

(16) A. Shepp, S. Chaberek, and R. MacNeil, J. Phys. Chem., 66, 2563 (1962).

tion in the presence of 5% acrylamide. These data indicate both a similarity and a difference in the behavior of this activator when compared with the amine-activated systems represented by triethanolamine (TEA).[9] As with the TEA-containing systems, both the rates of dye bleaching and polymerization increase with an increase in activator level. Also, an increase in acrylamide concentration results in an increase in the polymerization rate for AA and TEA systems.

However, the dye-bleaching rate dependences for the systems differ in two respects. First, in the absence of monomer, no significant thionine bleaching occurs in the presence of AA; in the amine systems, extensive reduction of the dye is obtained in the absence of monomer. Second, although these rates decrease with an increase in monomer level in the amine systems, Figure 1 shows that for the AA system the rate is *independent* of monomer levels between 2 and 7.5%.

In addition, both fading and polymerization rates are pH sensitive. Figure 2 shows the variation in R_f and R_p as a function of solution pH. The shapes of the curves are strikingly similar to those obtained with TEA. Both rates increase from pH 7 to maxima at 8.4 (for R_p) and 8.8 (for R_t), after which the values decrease rapidly. The strong pH dependence of this β-diketone initiator in the pH interval of 7 to the pH of maximum activity must be related to the acidic properties of the enol form of AA arising from keto–enol tautomerism. It appears that structural changes in the molecule that decrease its tendency toward tautomerism result in a loss of photoinitiating activity. Thus, biacetyl (I) and 2,5-hexanedione (II) are inactive as photopolymerization initiators. In these

$$\underset{\text{I}}{CH_3\overset{\overset{O}{\|}}{-}C\overset{\overset{O}{\|}}{-}C-CH_3} \qquad \underset{\text{II}}{CH_3\overset{\overset{O}{\|}}{-}C-CH_2CH_2\overset{\overset{O}{\|}}{-}C-CH_3}$$
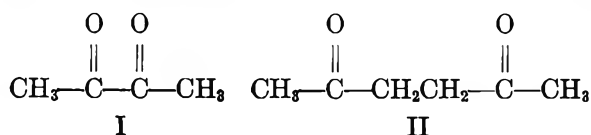
cases, both the shortening and the lengthening of the carbon chain between the carbonyl groups shifts the keto–enol equilibrium far toward the keto form. To obtain more information concerning the relation between tautomerism and photoactivity, studies were extended to dimedon (DM) and some 2-alkyl (acyl) 2,4-pentanediones.

Dimedon. Interest in this substance stemmed from its high degree of enolization. Schwarzenbach and Felder[17] showed that in dilute aqueous solutions AA exists in the enol form to the extent of about 15.5%, whereas DM is 95.3% enolized. Measurements of R_t and R_p for the thionine–DM–acrylamide combination showed this system to be similar qualitatively to the corresponding AA-containing one in that (1) R_t and R_p
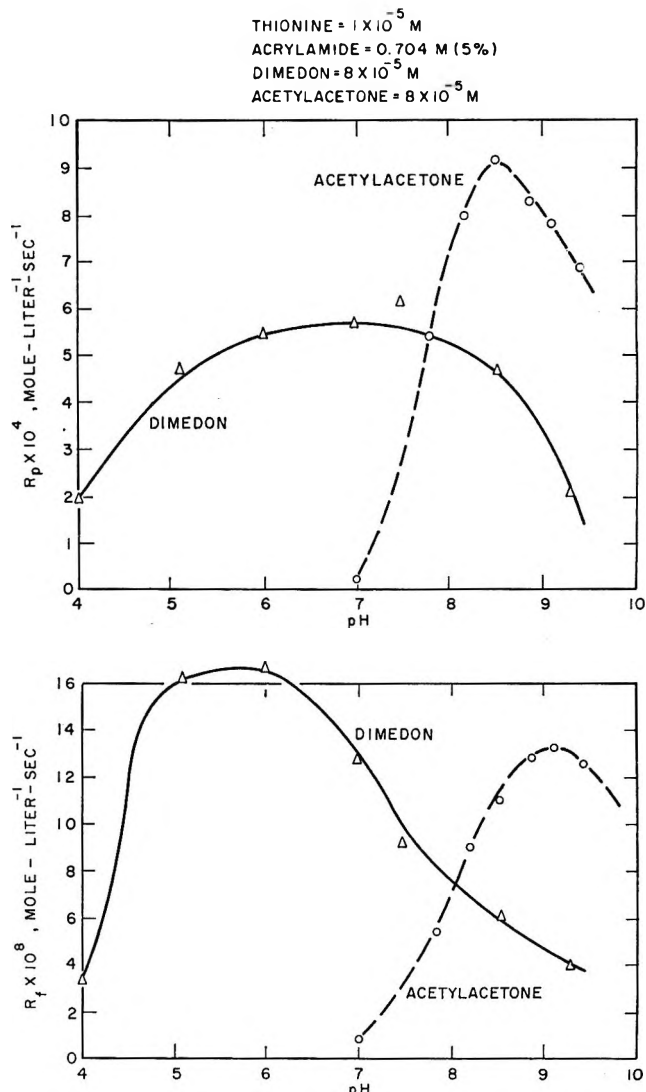
Figure 2. Effect of pH on the thionine–dimedon– and thionine–AA–acrylamide systems.

increase with an increase in the activator concentration; (2) R_f and R_p are sensitive to solution pH; (3) R_f and R_p are essentially independent of the dye concentration in the range 0.5 to 2×10^{-6} M; (4) R_f and R_p increase with an increase in monomer concentration in the range 1 to 7.5%.

The most striking aspect of the DM system, however, is its susceptibility to solution pH. A comparison of this system with the AA-containing one is shown in Figure 2. It is seen that the rates of thionine bleaching for both systems have a maximum value, but the pH at which it occurs varies markedly. For DM, it occurs at a pH of about 5.0 to 5.5; for AA, it occurs at a pH of

(17) G. Schwarzenbach and E. Felder, *Helv. Chim. Acta*, **27**, 1701 (1944).

Table I: Variation of Enolate Concentrations for Acetylacetone and Dimedon with pH

Compd.	4.0	4.5	5.0	5.5	6.0	% enolate at pH 7.0	7.5	8.0	8.5	9.0	10.0
AA	0.00	0.00	0.01	0.04	0.11	1.1	3.0	6.6	10.9	13.7	15.3
DM	5.3	15.0	35.3	62.0	81.5	93.7	94.8	95.1	95.2	95.3	95.3

about 9. The polymerization data show clearly the greater range of activity for the DM system. The rate of polymerization increases in the pH range of about 3 to 6, remains essentially constant at pH values of 6 to about 8.5, and finally decreases at higher pH values. In contrast, for AA, polymerization is restricted to a pH range starting at about 7, with maximum activity observed at a pH of about 9. In the pH range between 8 and 9, AA is a superior initiator; that is, higher polymer yields are obtained with this system. However, its efficiency rapidly falls off with increasing solution acidity, so that at pH 7.5, both systems have comparable activity, but at pH 7, AA is essentially inactive while DM shows its maximum activity.

These data on the pH dependence of the thionine–DM system indicate that the enolate ion may be the most reactive form. On the basis of this assumption, let us consider briefly the data shown in Figure 2. Schwarzenbach and Felder[17] have measured the pK_E and K_T values for AA and DM for the reactions

$$[\text{keto}] \overset{K_T}{\underset{}{\rightleftarrows}} [\text{enol}] + [\text{enolate}^-] \qquad (a)$$

$$[\text{enol}] \overset{K_E}{\underset{}{\rightleftarrows}} [\text{H}^+] + [\text{enolate}^-] \qquad (b)$$
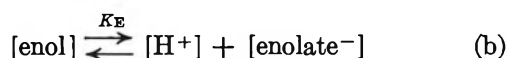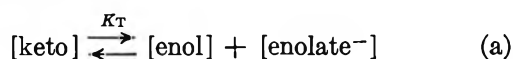
Using the following values for K_T and K_E, we have calculated the per cent enolate ion existing at various pH values for these activators.

The values of K_T and K_E for AA and DM are

	K_T	pK_E
AA	0.184	8.13
DM	20.3	5.23

These data are listed in Table I.

For AA, essentially no enolate is present at pH values lower than 7; a rapid increase in its concentration occurs in the pH interval 7 to 10. We would expect, therefore, that no photopolymerization would occur at pH values less than 7 and that an increase in pH in the 7 to 10 range would bring about increasing rates of polymer formation that would level off at values around 10. For DM, appreciable enolate ion is present at pH 4; its concentration increases in the range 4 to 8 and becomes essentially constant at values higher than 8. Thus, we would expect photopolymerization to start at pH 4, with increasing rates in the range 4 to 8,

and a constant rate at values exceeding this range. The experimental data of Figure 2 shows that these conclusions account for part of the observed results; they confirm the predicted increase in R_f and R_p in the pH range where the enolate ion concentration is increasing to its maximum value. However, the postulations do not account for the subsequent decrease in these rates at the higher pH levels where the enolate ion concentrations remain essentially constant. In the thionine–AA combination, the decrease in activity at high pH values may be correlated with changes in the light-absorbing properties of the dye. This cannot be the reason for the decrease in DM activity since it occurs at much lower pH values. Further work is required to determine the reason for this falloff.

3-Alkyl (Acyl) Substituted Acetylacetones. Table II summarizes photobleaching and photopolymerization data on systems containing 3-methyl-2,4-pentanedione (MAA), 3,3-dimethyl-2,4-pentanedione (MMAA), and triacetylmethane (TAM). Reference data for AA are included.

Table II: Anaerobic Photopolymerization of Acrylamide in the Presence of Some 3-Substituted Acetylacetones[a]

Compd.	K_T	pK_E	$R_f \times 10^1$	$R_p \times 10^4$	Enolate, $M_i \times 10^6$	Enol + enolate, $M \times 10^6$
AA	0.184	8.13	1.21	9.2	9.0	1.243
MAA	0.029	9.50	0.20	2.0	0.23	0.22
MMAA	...	...	None	None	None	None
TAM	...	...	0.76	5.4	...	...

[a] All systems contain 10^{-5} M thionine, 8×10^{-3} M activator, 0.704 M acrylamide at pH 8.55.

From the data of Table II, some interesting comparisons among the four systems can be made. First, progressive substitution of methyl groups for the hydrogen on the methylene group rapidly decreases the enolizability of the resulting β-diketone. The substitution of one CH_3 group decreases the degree of enolization by a factor of about 6, while complete substitution destroys enolization. Both the R_f and R_p values for these compounds parallel the decrease in the K_T values, the

completely substituted compound being inactive. Second, consider the relative amounts of total enol (enol + enolate) between AA and MAA. This amount is about 5.6 times greater for AA than for MAA. Therefore, if photoactivity depends upon the enol forms and all other factors are equal, we can expect the relative R_f and R_p magnitudes for AA to be 5.6 times greater than for the MAA. The experimental values of Table II show that R_f is six times greater and R_p, 4.6 times greater—an excellent agreement with the value of 5.6. Thus, these data confirm further that photoactivity resides in the enol forms and that the keto tautomer is not reactive.

Substantial activity was also observed with the triketone, TAM. Unfortunately, enolization data are unavailable for this substance, and therefore it is not possible to correlate activity with enol content. However, its appreciable efficiency indicates that substitution in the 3-position need not destroy the photoactivity of β-diketone derivatives.

Other Substituted β-Diketones. In addition to the 3-alkyl-substituted diketones, a number of 3-substituted nitrogen-containing derivatives were checked for photopolymerization activity. The screening was done qualitatively, with thionine and calcium acrylate. The criterion for activity was the onset of dye bleaching and formation of the water-insoluble calcium polyacrylate. 3-Amino-2,4-pentanedione was found to be a sufficiently strong reducing agent to bleach thionine in the dark. The corresponding 3-isonitroso derivative was inactive. However, 3-diethylamino-2,4-pentanedione showed some activity although it was inferior to AA. In addition to the above compounds, bis(acetylacetone)ethylenediimine (SB) was screened for activity. This substance has the structure
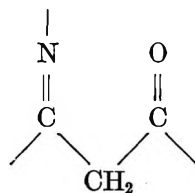
capable of undergoing keto–enol tautomerism. The polymerization rate for SB is compared with those of TEA and AA in Table III. All systems contained 10^{-5} M thionine, 2×10^{-4} M activator, and 5% acrylamide at a pH of 8.55. The activity of the diimine is seen to be substantial.

β-Diketone Initiator Systems Containing Metal Ions. One of the surprising discoveries during this research program was the photopolymerization-initiating activity of the thionine–metal acetylacetonate combinations. Although such photoactivity has been reported

Table III: R_p Values for SB, TEA, and AA

Compd.	$R_p \times 10^4$, M sec.$^{-1}$
TEA	3.05
SB	7.04
AA	10.0

for metal chelates such as ferrioxalate and uranyl oxalate upon irradiation with ultraviolet or blue light, we are not aware of any reports for a similar red-light-sensitized process for nonbiological metal chelate systems. Table IV summarizes R_p and dye bleaching data for nine metal acetylacetonate chelates.[18]

Table IV: Anaerobic Photopolymerization of Acrylamide in the Presence of Some Metal Acetylacetonate Chelates[a]

Compd.	$R_p \times 10^4$ M sec.$^{-1}$	Approx. bleaching time, min.	Compd.	$R_p \times 10^4$, M sec.$^{-1}$	Approx. bleaching time, min.
Cu(AA)$_2$	5.6	None	Al(AA)$_3$	11.0	2.5
TiO(AA)$_2$	8.9	3.5	Fe(AA)$_3$	11.0	3.5
Cr(AA)$_3$	5.4	None	Mn(AA)$_3$	10.0	3.5
Co(AA)$_3$	None	None	Ni(AA)$_2$	10.0	4.0
VO(AA)$_2$	9.4	3.5			

[a] All systems contain 10^{-5} M thionine, 10^{-4} M metal acetylacetonate, and 5% acrylamide at pH 8.6.

With the exception of the Co(III) chelate, all the remaining metal chelates showed polymerization activity. Not all activity was accompanied by bleaching of the dye, however. In the presence of the Cu(II) and Cr(III) chelates, polymerization occurred without significant dye bleaching, and the initial polymerization rates in the presence of these substances were approximately half those obtained with the other compounds. Since the polymerization rates of the remaining compounds were comparable, there appeared to be little correlation between this activity and the following: (1) stability of the metal chelates, since the magnitudes for this series vary widely; (2) visible-light absorption by the metal chelates, since some are colored and some are colorless; (3) valence state of the coordinated metal ions, since some have only one state and others have several.

To obtain a better insight into the function of these systems, we pursued a limited investigation of the be-
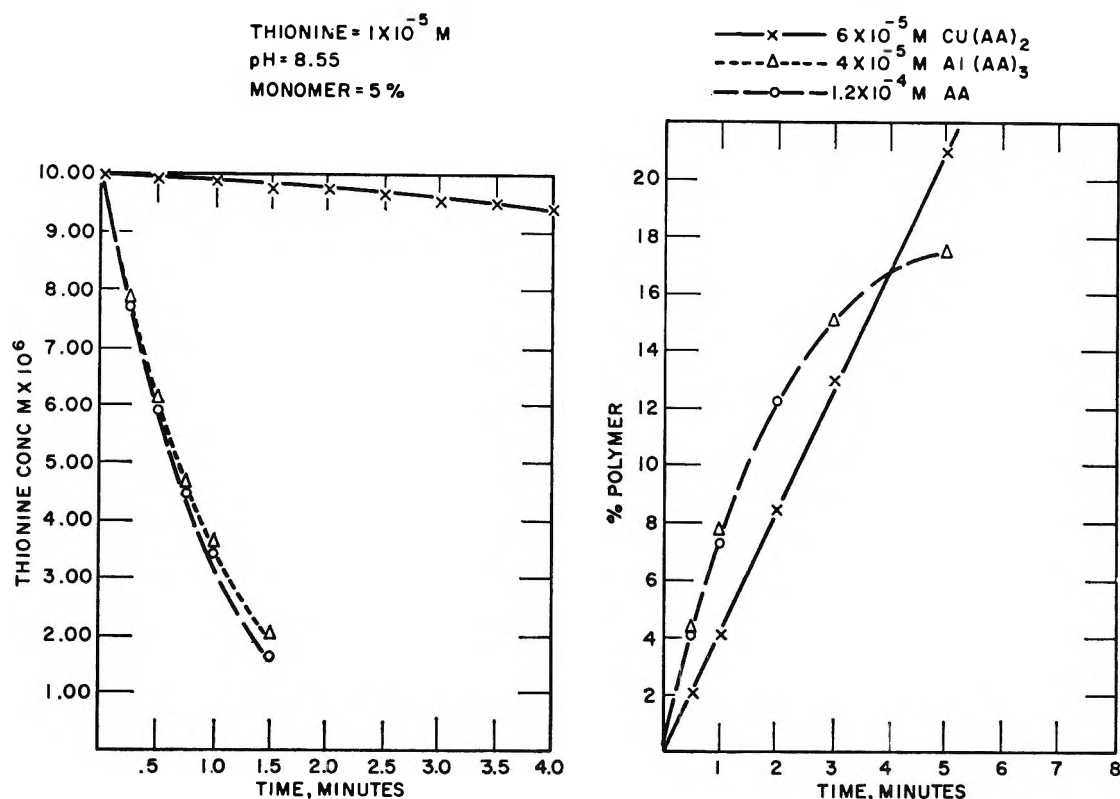
Figure 3. Comparison of acetylacetone, cupric acetylacetonate, and aluminum acetylacetonate at constant conditions.

havior of metal complexes of β-diketones as photopolymerization initiators.

The Cu(II)–AA and Al(III)–AA systems were chosen for further study because their initiating properties were substantially different. In addition, the activity of the Al(III) chelate was representative of the behavior of most of the metal chelates tested.

A comparison of the activities of Cu(II)–AA and Al(III)–AA is shown in Figure 3. All systems contain the same amount of AA. (The molar concentrations of the chelates are of course different because more than one AA molecule is bound to the metal ions.)

In the Cu(II)–AA system, the addition of Cu(II) ions to AA drastically changes the polymerization and dye-bleaching reactions. Dye bleaching is almost completely eliminated. In addition, the shapes of the polymerization rate curves for the two systems are different. Polymer formation for AA falls off at longer times, whereas in the presence of this metal chelate, polymerization begins at a rate lower than that for AA but continues at about this same initial rate for longer times.

In contrast to this behavior, the addition of Al(III) alters neither the bleaching nor the polymerization rate. In this case, and for all systems comparable in activity to Al(III)–AA, the metal chelate is probably

extensively hydrolyzed; thus, we may be observing only AA activity.

The validity of this conclusion is substantiated by the following considerations. As a rough approximation let us define the hydrolysis of the metal chelate by

$$MA_3 + 3OH^- \xrightarrow{K_x} M(OH)_3\downarrow + 3A \qquad (c)$$
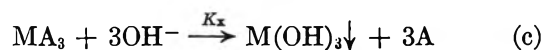
where MA_3 denotes the metal chelate and A, the displaced ligand. It follows that

$$K_x = \frac{[A]^3}{[MA_3][OH^-]^3} = \frac{1}{K_{MA}K_{So}} \qquad (1)$$

where K_{MA}, the chelate stability constant, and K_{So}, the solubility product, are defined by the equations

$$K_{MA} = \frac{[MA_3]}{[M][A]^3} \qquad (2)$$

$$K_{So} = [M][OH^-]^3 \qquad (3)$$

Let us now estimate the per cent dissociation for the aluminum(III) and iron(III) acetylacetonate chelates in solutions containing 10^{-4} M MA_3 at a solution pH of 8.55 using the following values for K_{MA}[19] and K_{So}.[20]

(19) J. Bjerrum, G. Schwarzenbach, and L. G. Sillén, "Stability Constants, Part 1, Organic Ligands," The Chemical Society, London, 1957.
(20) J. Bjerrum, "Stability Constants, Part II, Inorganic Ligands," The Chemical Society, London, 1958.

	Al(III)	Fe(III)
K_{MA}	$10^{22.3}$	$10^{26.7}$
K_{So}	$10^{-32.9}$	$10^{-37.7}$ (av.)

Using the approximation method we find that the Al(III) chelate is about 90% hydrolyzed, while the Fe(III) chelate is about 97% hydrolyzed. Insufficient K_{MA} and K_{So} data prevent our testing other metal chelates listed in Table IV in this way.

In view of the difference in the behavior of Cu(II)–AA, it was considered desirable to explore further the effect of metal chelate stability on photoinitiating activity. Two substances were chosen for this purpose: SB and DM. Since the Cu(II)–SB chelate is substantially more stable than Cu(II)–AA, its degree of hydrolysis would be less under the experimental conditions employed and consequently less free ligand would be available. In contrast, DM cannot form stable Cu(II) chelates because of steric hindrance. Consequently, in this case, solutions would contain the uncoordinated ligand and Cu(II) ions. Figure 4 summarizes bleaching and polymerization data for AA, SB, and DM in the absence and in the presence of the Cu(II) ion. Consider first the dye bleaching reaction. In the presence of Cu(II), dye bleaching is drastically

decreased compared to the systems containing the ligands alone. In fact, for SB and AA, dye fading is almost completely eliminated. Several differences are apparent between the ligand- and Cu(II)-containing plots. First, consider the shapes of the curves. In the absence of the Cu(II) ion, the plots for all three ligands start at a high rate of conversion, and this rate decreases with time, so that at times greater than about 4 min. the percentage of polymer formed remains essentially constant. In the presence of Cu(II), the polymer formation proceeds at essentially the initial rate for time intervals exceeding those at which the conversion falls off in the absence of the metal ion. Second, consider the initial polymerization rates between the corresponding ligand- and Cu(II)-containing curves. For SB and AA, the initial polymerization rates of the Cu(II)-containing systems are less than those for the ligands alone, and the difference is greater for SB. If, as it is for Al(III)–AA, photoactivity is the result of the free ligand concentration, these data show that the polymerization efficiency decreases with an increase in the stability of the Cu(II) chelates. Here, the concentration of free ligand should be substantially less in the presence of AA, and we can expect a greater decrease in the photoactivity of the Cu(II)–SB combination.
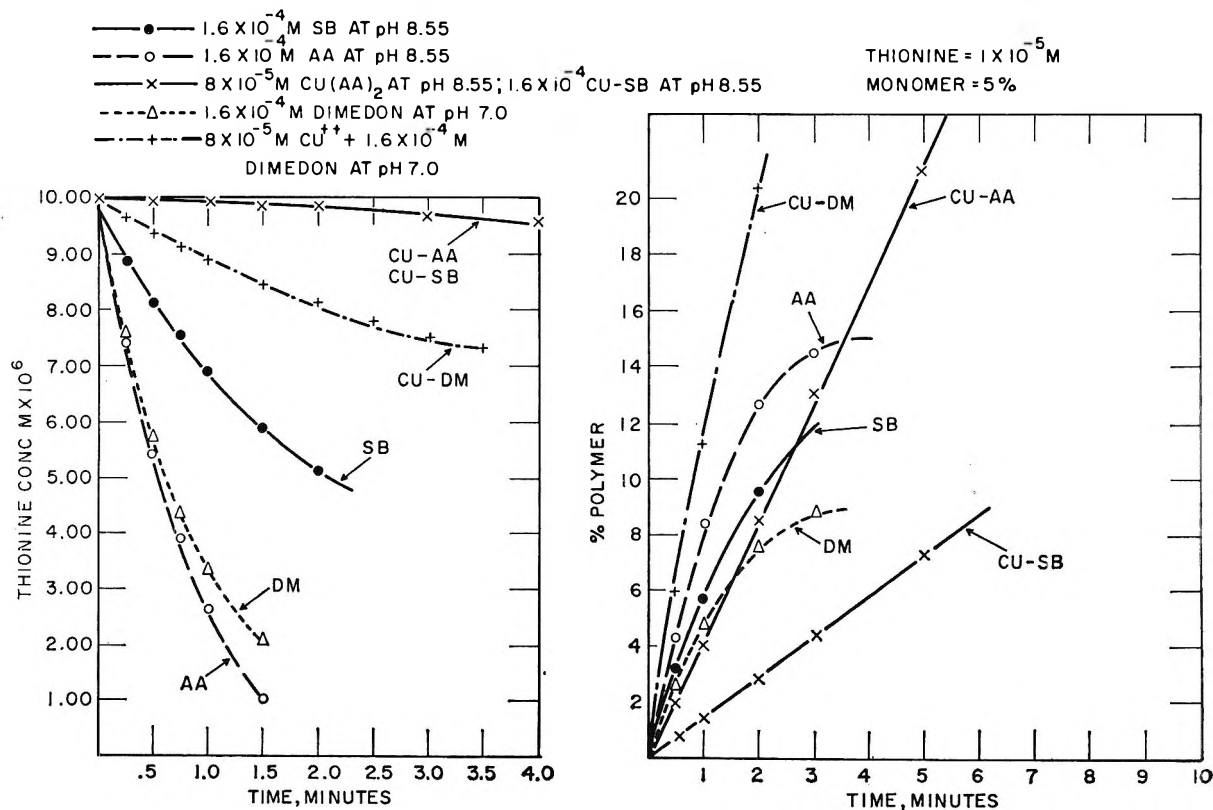
Figure 4.   Comparison of acetylacetone and dimedon and diacetylacetoneethylenediimine in the presence of Cu(II).

However, the Cu(II)–DM data of Figure 4 show conclusively that these differences cannot be ascribed solely to a reactant concentration factor. In this case Cu(II) functions as a polymerization accelerator. Contrary to its behavior with AA and SB, the metal ion *increases* the initial polymerization rate relative to DM. This increase is appreciable; in 30 sec., the Cu(II)–DM systems produce 6% polyacrylamide, compared to 4.2% for DM alone.

One may indeed inquire whether Cu(II) ions or cupric acetylacetonate are photoactive and initiate photopolymerization. Cupric ions have a weak though broad absorption band in the visible range with a maximum at about 7000 Å. However, experiments on solutions containing 8×10^{-5} M Cu(II) and 5% acrylamide at pH 8.55 show that no detectable polymer was formed during periods of 12 min. Similarly, the possibility of a thionine-sensitized reaction involving Cu(II) but no β-diketone was ruled out by similar experiments. Only a trace to 1% polymer was obtained in 10 min. This amount of polymer is obtained by irradiating anaerobic solutions containing only thionine and acrylamide, and possibly arises from the presence of trace impurities in the reagents. Finally, although copper(II) acetylacetonate has an absorption band at about 8200 Å., irradiation of solutions containing only the chelate and acrylamide gave no polymer in 18 min.

A detailed explanation of reaction mechanism for these Cu(II)-containing systems must await the results of further studies now in progress. However, even these limited data allow some speculation regarding their mode of action. We believe that the observed effects of Cu(II) are a result of its oxidizing action on the reduced forms of thionine, semithionine (ST), and leucothionine (LT) acccording to the reactions

$$LT + Cu^{2+} \longrightarrow \cdot ST + Cu^+ \qquad (d)$$

$$\cdot ST + Cu^{2+} \longrightarrow T + Cu^+ \qquad (e)$$
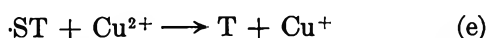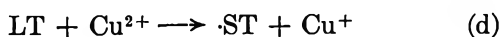
Oster and co-workers[21-23] have shown that various leuco dyes (including leucothionine and leucomethylene blue) produced by reacting the light-excited dyes with secondary and tertiary amines and amino acids are sufficiently powerful reducing agents to reduce a variety of metal ions including Cu(II).

The regeneration of thionine by reaction e accounts for the decreased rate of dye bleaching and also, at least in part, for the differences in the shapes of polymerization curves. In the absence of Cu(II), the rapid dye bleaching depletes the concentration of thionine to levels too low to sustain radical generation, and the polymerization rate consequently levels off.

In the presence of Cu(II), the dye concentration remains almost constant (at least for AA and SB), and consequently radical formation can continue as long as the solution is illuminated. However, the Cu(II)–DM data indicate that other factors must be involved. One of these probably involves a decrease in leucothionine concentration as a result of reaction f. Studies have shown that the leuco dye functions as a chain terminator—possibly through reaction with a growing polymer chain, $M_x\cdot$, according to (e).

$$LT + M_x\cdot \longrightarrow MH + \cdot ST \cdot \qquad (f)$$
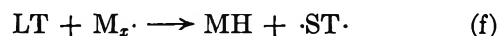
An increase in LT concentration results in lower rates of fade and of polymerization, as well as drastically reduced polymer molecular weights.

Activity of Other Carbonyl Compounds. Our studies with β-diketones described above show that keto–enol tautomerism is an important prerequisite for dye-sensitized photopolymerization activity. Hence, a variety of β-dicarbonyl compounds were screened qualitatively for photopolymerization of calcium acrylate. Substantial polymerization was obtained with the following substances: disodium malonate, malonic ester, barbituric acid, 2-acetylcyclohexananone, acetoacetanilide, and 3-ketoglutaric acid.

However, factors other than keto–enol tautomerism must be involved. Preliminary studies with 1,2-cyclohexanedione (III) and 2-hydroxy-1-methyl-1-cyclopenten-3-one (IV) showed that in presence of thionine and acrylamide, dye bleaching was obtained in the pH range of 8 to 9.5 without polymer formation.
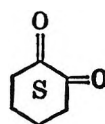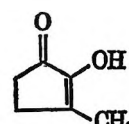
Compound III is almost completely enolized under our experimental conditions, while compound IV is a stable enol. Thus, a better understanding of the nature of these photochemical processes must await the results of detailed studies now in progress.

(21) G. Oster and N. Wotherspoon, *J. Am. Chem. Soc.*, **79**, 4836 (1957).

(22) G. Oster and G. Oster, *ibid.*, **81**, 5543 (1959).

(23) J. Joussot-Dubien and G. Oster, *Bull. soc. chim. France*, 343 (1960).

Dye-Sensitized Photopolymerization Processes.[1a] IV.   Kinetics and

Mechanism of Thionine-β-Diketone-Acrylamide Systems

by S. Chaberek,[1b] R. J. Allen, and A. Shepp

Technical Operations Research, Burlington, Massachusetts   *(Received January 4, 1965)*

A detailed study of the kinetics and reaction mechanism of thionine- (and methylene blue) sensitized photopolymerization of acrylamide in the presence of 2,4-pentanedione and dimedon has been made.   Experimental data are consistent with a mechanism involving the formation of a light-excited complex between dye and β-diketone and its subsequent reaction with monomer to give dye bleaching and polymerization.   As with amine-activated processes described in the first two papers in this series, the polymerization-initiating free radical appears to be semithionine (or semi(methylene blue)).

Introduction

β-Diketones such as 2,4-pentanedione and dimedon have recently been found to function as photoreducing agents in conjunction with thionine and methylene blue for the photopolymerization of acrylamide.[2]

Studies into the relation between photoactivity and molecular structure showed that the active compounds are those capable of undergoing keto-enol tautomerism, and that the enol forms are responsible for reactivity. Nevertheless, even the limited data reported previously showed that there are distinct differences in the photoactivity of the β-diketones compared to that of tertiary amines and amino acids. The most significant contrast is in the dye bleaching reactions. β-Diketones require the presence of monomer to bring about dye fading; the tertiary amines and amino acids photobleach the dyes in the absence of monomer. Thus, in view of the differences in the behavior of the β-diketones, a more detailed investigation into their reaction mechanism was desirable. This paper summarizes, then, our studies on the anaerobic photopolymerization of acrylamide by free radicals formed by reaction of light-excited thionine (or methylene blue) with 2,4-pentanedione (AA) and dimedon (DM).

Experimental

The acrylamide used in this investigation was a pure sample obtained from the American Cyanamid Co. Preliminary screening of this sample for anaerobic thionine-sensitized photopolymerization showed no polymer formation in the absence of added activators and only a trace of dye bleaching over periods of 10 to 15 min.

Thionine and methylene blue were purified by three recrystallizations from water. The absorption coefficients were found to be 5.8×10^4 l. cm.$^{-1}$ mole^{-1} for thionine (at 5980 Å.) and 6.4×10^4 l. cm.$^{-1}$ mole^{-1} for methylene blue (at 6620 Å.). Dimedon and 2,4-pentanedione were obtained from the Aldrich Chemical Co.

The general experimental procedures used in this study were the same as those described previously.[2,3] The rate of dye bleaching R_f was calculated directly from spectrophotometric measurements. The polymerization rate R_p was determined by taking aliquots of the reaction solution at several time intervals, precipitating the polyacrylamide in methanol, filtering it, and drying the residue to constant weight. Polymer molecular weights were determined viscometrically.

(1) (a) This study was performed under Contract No. AF 33(657)-8754 and AF 33(647)-11553, Photographic Branch, Reconnaissance Division, Air Force Avionics Laboratory, Wright-Patterson Air Force Base, Ohio, J. R. Pecqueux, Project Engineer;   (b) to whom inquiries should be sent at Cowles Chemical Co., Skaneateles Falls, N. Y.

(2) S. Chaberek, R. J. Allen, and G. Goldberg, *J. Phys. Chem.*, 69, 2834 (1965).

(3) A. Shepp, S. Chaberek, and R. MacNeil, *ibid.*, 66, 2563 (1962).

Experimental Data on Dye Bleaching and Polymerization Rates as a Function of Reaction Parameters

Activator Concentration. Table I summarizes the rates of dye bleaching and polymerization for systems containing 10^{-5} M thionine or methylene blue, 0.704 M acrylamide, and varying concentrations of AA or DM between 8.0 and 40.0 × 10^{-5} M. Solution pH values were 8.55 for thionine–AA, 8.60 for methylene blue–AA, and 7.0 for thionine–DM. The general trend for both DM and AA parallels that observed with amine-activated systems such as triethanolamine[4] (TEA) in that both R_f and R_p increase with an increase in the activator concentration. In contrast to the TEA-containing systems, however, similar R_f and R_p dependences on the AA level were found for both thionine and methylene blue. For TEA, amine concentrations had to be about five times greater in the presence of methylene blue to obtain comparable rates with thionine-containing systems. Finally, R_f values for DM are comparable with those for AA; however, R_p is 40 to 50% smaller for DM.

Table I: Effect of Acetylacetone and Dimedon Concentrations on R_f and R_p for the Anaerobic Thionine– and Methylene Blue–Acrylamide Systems[a]

AA (or DM) concn., M × 10^5	Thionine systems AA $R_f × 10^7$	Thionine systems AA $R_D × 10^2$	Thionine systems DM $R_f × 10^7$	Thionine systems DM $R_p × 10^2$	Methylene blue systems AA $R_f × 10^7$	Methylene blue systems AA $R_p × 10^2$
2.0	0.397	0.40	...	...	...	...
4.0	0.701	0.58	0.667	0.35	...	...
8.0	1.212	0.92	1.102	0.54	1.140	0.99
12.0	1.550	0.99	...	...	...	...
16.0	1.688	1.17	1.515	0.70	1.667	1.33
24.0	2.339	1.36	...	...	2.204	1.33
40.0	...	...	2.381	0.87	2.469	1.77
80.0	...	...	2.720	1.06	...	...

[a] All systems contain 10^{-5} M dye, 0.704 M acrylamide at pH 8.55 for thionine–AA, pH 7 for thionine–DM, and pH 8.60 for methylene blue–AA; $T = 24 ± 1°$; R_f and R_p are expressed as moles l.$^{-1}$ sec.$^{-1}$.

Monomer Concentration. Table II summarizes R_f and R_p data for systems containing 10^{-5} M dye and 8 × 10^{-5} M AA or DM. These data indicate both a similarity and a difference in the behavior of these substances with the amine-activated systems. The rates of polymerization are similar with both classes of activators in that they increase with an increase in the monomer concentration. However, the R_f dependences for the two classes of compounds differ

in two respects. First, in the absence of monomer, no significant dye bleaching occurs with both AA and DM; in the amine systems extensive photobleaching is obtained in the absence of monomer. Second, while R_f decreases with an increase in monomer level in the amine systems, Table II shows that the rate is *independent* of monomer concentration for AA and actually increases with an increase in monomer level for DM in the range 0.141 to 1.265 M. At lower acrylamide concentrations (1.4 × 10^{-1} to 1.4 × 10^{-3}) AA also parallels the trend with DM.

Table II: Effect of Acrylamide Concentration on R_f and R_p for the Thionine– and Methylene Blue–AA– and –DM–Acrylamide Systems[a]

Acrylamide concn., M	Thionine systems AA $R_f × 10^7$	Thionine systems AA $R_p × 10^2$	Thionine systems DM $R_f × 10^7$	Thionine systems DM $R_p × 10^2$	Methylene blue systems AA $R_f × 10^7$	Methylene blue systems AA $R_p × 10^2$
1.4 × 10^-3	0.258	...	...	...	...	...
2.8 × 10^-3	0.443	...	...	...	...	...
1.41 × 10^-2	0.874	...	...	...	...	...
1.41 × 10^-1	1.212	0.091	0.730	...	0.995	0.094
2.82 × 10^-1	1.212	0.28	...	...	...	...
3.52 × 10^-1	1.212	...	...	...	0.995	0.29
4.22 × 10^-1	...	...	1.149	0.28	...	...
4.93 × 10^-1	1.212	0.51	...	...	...	...
7.04 × 10^-1	1.212	0.85	1.299	0.56	1.042	0.65
10.56 × 10^-1	1.212	1.23	1.360	1.12	0.995	1.15
12.65 × 10^-1	...	...	1.429	1.39	...	...

[a] All systems contain 10^{-5} M dye. 8 × 10^{-5} M AA (or DM) at pH 8.55 for AA and pH 7.00 for DM; $T = 24 ± 1°$; R_f and R_p are expressed as moles l.$^{-1}$ sec.$^{-1}$.

Light Intensity. Calibrated neutral density filters were used to determine the effect of light intensity on R_f and R_p for the thionine– and methylene blue–AA–acrylamide systems. Experimental results are listed in Table III. The reaction rates for both dyes decrease with a decrease in light intensity.

Dye Concentration. Dye fading and polymerization rates were found to be independent of dye concentration over the range of 0.5 to 1.5 × 10^{-5} M, except for the dependence of the reactions on the light absorbed I_a. As the dyes fade, I_a decreases and thus the reaction rates decrease.

Solution pH. A detailed qualitative discussion of the pH effect on the thionine–DM and thionine–AA systems was given in paper III of this series.[2] However, measurements of R_f and R_p were extended to

(4) S. Chaberek and R. J. Allen, *J. Phys. Chem.*, 69, 647 (1965).

Table III: Effect of I_0 on R_f and R_p for the Thionine-
and Methylene Blue-AA-Acrylamide Systems[a]

ND filter[b]	—Thionine systems—		—Methylene blue systems—	
	$R_f \times 10^7$	$R_p \times 10^3$	$R_f \times 10^7$	$R_p \times 10^3$
None (100%)	1.294	0.80	1.170	0.79
0.28 (52.5%)	0.644	0.66	0.614	0.55
0.48 (33.1%)	0.426	0.47	0.341	0.43

[a] All systems contain 10^{-5} M dye, 8×10^{-5} M AA, 0.704 M acrylamide at pH 8.55; $T = 24 \pm 1°$; R_f and R_p are expressed as moles l.$^{-1}$ sec.$^{-1}$. [b] Value in parentheses denotes relative per cent transmission for filter.

other pH values to provide data for mathematical analysis and to include the methylene blue–AA–acrylamide system. Results are summarized in Figure 1. The most striking aspect of the DM-containing system is the shift of photoactivity to lower pH levels. This shift arises from the greater acidity of the enol form of DM. Although the data plots for thionine–DM and thionine–AA are similar in shape, maximum photobleaching is obtained at a pH of about 5.0 to 5.5 for DM and at a pH of about 9 for AA. The polymerization data show the greater range of activity for the DM system. Finally, the superiority of methylene blue–AA over thionine–AA at pH levels exceeding 9 is clearly seen. Both dyes are comparable in activity at pH levels between 7 and about 8.55, but at higher alkalinity the thionine R_f and R_p rapidly decrease, while those for methylene blue remain essentially constant.

Oxygen. As with the amine activators, oxygen affects the behavior of photopolymerization systems containing β-diketones. Representative data at an oxygen level of 2×10^{-5} M (0.64 p.p.m.) for thionine–acrylamide systems containing three concentrations of AA are shown in Figure 2.
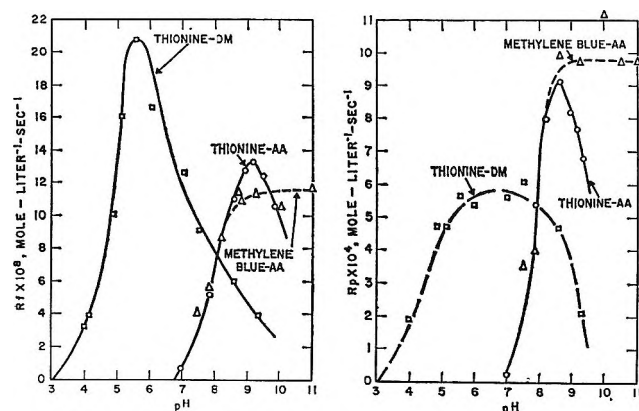
Figure 1. R_f and R_p dependence on pH.
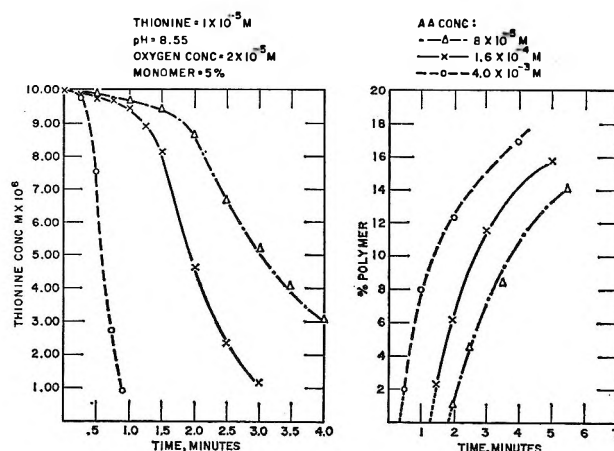
Figure 2. Effect of oxygen on the thionine–AA–acrylamide system.

The introduction of oxygen produces an induction period during which the dye is slowly bleached but no polyacrylamide is produced. At the conclusion of this period, the thionine bleachout proceeds at a rate comparable to the anaerobic control and polymer is formed. Figure 2 shows that the induction period may be decreased by increasing the activator concentration. A comparison of these data with those of other amine systems shows that AA appears to be less sensitive to oxygen. For example, at an activator concentration of 4×10^{-3} M, AA systems had a 20-sec. induction period, compared to about 45 sec. for TEA in the presence of 0.64 p.p.m. of oxygen.

Polymerization Reaction Mechanism

A reasonable reaction mechanism must account for the variations of R_f and R_p that occur with changes in the experimental parameters. We have seen above that the photoactivity of these β-diketone activators are both similar and dissimilar to that of amino derivatives such as nitrilotripropionamide and TEA for which a reaction mechanism has been postulated.[4,5] The systems are similar in that both R_f and R_p increase with an increase in activator concentration, are sensitive to solution pH, and are independent of the dye concentration in the range 0.5 to 2×10^{-6} M. They are dissimilar in that monomer must be present with AA and DM for photobleaching of the dyes, but it is not required with the amine activators. In addition, although R_p increases with an increase in monomer concentration for both classes of compounds, R_f for AA and DM increases with (or is independent of)

(5) S. Chaberek, A. Shepp, and R. J. Allen, *J. Phys. Chem.*, 69, 641 (1965).

the acrylamide level; R_f for TEA decreases with increasing monomer.

The following reaction mechanism is consistent with experimental observations on the behavior of AA and DM.

$$T \longrightarrow T^* \qquad \phi I_a \qquad (a)$$

$$T^* \longrightarrow T + \text{heat} \qquad k_c \qquad (b)$$

$$T^* + E^- \longrightarrow (TE)^* \qquad k_{E-} \qquad (c)$$

$$T^* + E \longrightarrow (TE)^* + H^+ \qquad k_E \qquad (d)$$

$$(TE)^* \longrightarrow T + E(E^-) \qquad k_1 \qquad (e)$$

$$E \rightleftharpoons E^- + H^+ \qquad K_E \qquad (f)$$

$$(TE)^* + M \longrightarrow \cdot ST + R \cdot \qquad k_2 \qquad (g)$$

$$2 \cdot ST \longrightarrow T + LT \qquad k_d \qquad (h)$$

$$\cdot ST + M \longrightarrow M \cdot \qquad k_a \qquad (i)$$

$$R \cdot + M \longrightarrow M \cdot \qquad k_{a'} \qquad (j)$$

$$M \cdot + M \longrightarrow M \cdot \qquad k_p \qquad (k)$$

$$2M \cdot \longrightarrow \text{polymer} \qquad k_t \qquad (l)$$
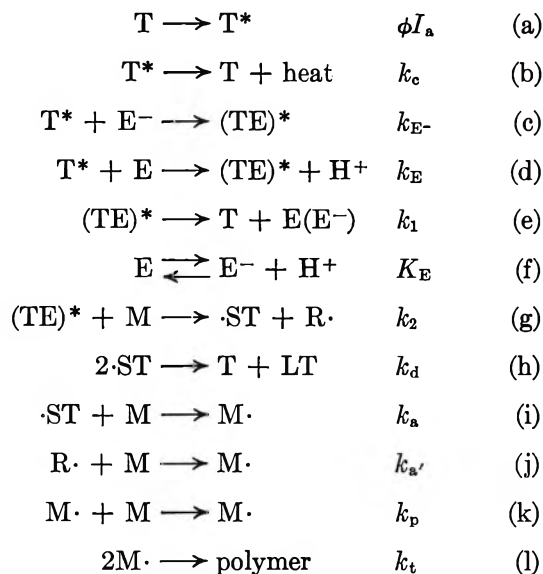
In reaction a, T^* represents the triplet state of the light-excited dye and ϕ is the efficiency of the formation of the triplet state when the dye has absorbed a quantity of light I_a. Reaction b represents the thermal deactivation of T^* to the ground state. The rate constant for this reaction has been measured by Hatchard and Parker[6] to be 5×10^4 sec.$^{-1}$ for thionine. The key step of this mechanism is the formation of an excited dye–activator complex $(TE)^*$ by interaction of the excited dye with either the enolate ion E^- (reaction c) or with enol E accompanied by the displacement of a hydrogen ion (reaction d). The activated complex can now undergo collisional deactivation and dissociation to the dye and E or E^- by reaction e, where the relative concentrations of enol and enolate ion are controlled by acidity constant K_E (reaction f). Alternately, $(TE)^*$ reacts with monomer to form semithionine (or semi(methylene blue)), $\cdot ST$, and a radical $R \cdot$ (reaction g). The structure of $R \cdot$ or its ultimate fate during the photoreaction is not known at this time.

Reaction h is the dismutation reaction that forms dye and leucodye LT; it is the only reaction in our mechanism by which LT is formed. Hatchard and Parker[6] report k_d to be 2×10^9 l. mole^{-1} sec.$^{-1}$ for thionine.

Reaction i represents the initiation of polymerization by the reaction of $\cdot ST$ with the monomer to form the initiating radical $M \cdot$. A similar possible reaction involving the photoproduct $R \cdot$ is denoted by (j).

Reactions k and l are the usual polymer propagation and polymer termination steps, respectively.

Verification of the Reaction Mechanism for R_f. The following equations form the basis of the mathematical analysis of this reaction mechanism with respect to R_f.

$$\frac{d(T^*)}{dt} = 0 = \phi I_a - k_c(T^*) - k_{E-}(T^*)(E^-) - k_E(T^*)(E) \qquad (1)$$

$$\frac{d(TE^*)}{dt} = 0 = k_{E-}(T^*)(E^-) + k_E(T^*)(E) - k_1(TE^*) - k_2(TE^*)(M) \qquad (2)$$

$$\frac{d(\cdot ST)}{dt} = 0 = k_2(TE^*)(M) - k_a(\cdot ST)(M) - 2k_d(\cdot ST)^2 \qquad (3)$$

$$R_f = k_2(TE^*)(M) - k_d(\cdot ST)^2 \qquad (4)$$

To simplify eq. 4, dye regeneration experiments were performed as described previously.[5] Approximately 60% of the faded dye was restored in all cases. Thus 60% of the fading of the dye results in the formation of leucodye and 40% results in polymer formation. We see in eq. 3 that $2k_d(\cdot ST)^2 \approx 1.2R_f$, while $k_a(\cdot ST)(M) \approx 0.4R_f$. As a first approximation, therefore, we may neglect the latter term, and eq. 3 now becomes

$$2k_d(\cdot ST)^2 \approx k_2(TE^*)(M) \qquad (5)$$

and

$$R_f = \frac{k_2(TE^*)(M)}{2} \qquad (6)$$

Finally, solving eq. 1 and 2 for T^* and TE^* and substituting in eq. 6 gives

$$R_f = \frac{\phi I_a k_2(M) \left[k_{E-} + \dfrac{k_E(H^+)}{K_E} \right](E^-)}{2[k_1 + k_2(M)] \left[k_c + \left(k_{E-} + \dfrac{k_E(H^+)}{K_E} \right)(E^-) \right]} \qquad (7)$$

For data analysis, eq. 1 is written in reciprocal forms

$$\frac{1}{R_f} = \frac{2}{\phi I_a} \left[1 + \frac{k_1}{k_2(M)} \right] \times \left[1 + \left(\frac{k_c}{k_{E-} + \dfrac{k_E(H^+)}{K_E}} \right) \frac{1}{(E^-)} \right] \qquad (7a)$$

(6) G. G. Hatchard and C. A. Parker, *Trans. Faraday Soc.*, **57**, 1093 (1961).

$$\frac{1}{R_f} = \frac{2}{\phi I_a}\left[1 + \frac{k_c}{\left(k_{E^-} + \frac{k_E(H^+)}{K_E}\right)(E^-)}\right]\left[1 + \frac{k_1}{k_2(M)}\right]$$

(7b)

Equations 7a and 7b predict a linear relationship between $1/R_f$ and $1/(E^-)$ or $1/(M)$, respectively. To test eq. 7a requires experimental values for (E^-). These values were calculated by eq. 8

$$(E^-) = \frac{C_A}{\left(1 + \frac{1}{K_T}\right)\left(\frac{(H^+)}{K_E} + 1\right)}$$

(8)

where C_A denotes the total concentration of AA or DM added, and

$$K_T = \frac{(E) + (E^-)}{(keto)}$$

(8a)

$$K_E = \frac{(H^+)(E^-)}{(E)}$$

(8b)

The following values of K_T and K_E reported by Schwarzenbach and Felder[7] were used in these calculations

	K_T	K_E
AA	0.184	$10^{-8.13}$
DM	20.3	$10^{-5.23}$

Figures 3 and 4 are plots of the data of Tables I and II using eq. 7a and 7b, respectively. These figures show that good linear relations are obtained for both β-diketones. Furthermore, eq. 7 predicts that R_f should be directly proportional to I_a, if all other reaction parameters are held constant. The experimental results in Figure 5 are in accord with prediction.

To check the pH dependence of the mechanism, the rate equation involving R_f was redefined in terms of enol (E) instead of enolate ion (E^-). Rearrangement of terms in eq. 7 gives

$$\chi = \frac{\frac{2}{\phi I_a}\left(1 + \frac{k_1}{k_2(M)}\right)}{(E)\left[\frac{1}{R_f} - \frac{2}{\phi I_a}\left(1 + \frac{k_1}{k_2(M)}\right)\right]} = k_E + \frac{k_{E^-}K_E}{(H^+)}$$

(9)

Equation 9 predicts that a plot of χ vs. $1/(H^+)$ should be a straight line whose intercept is the rate constant k_E and whose slope is related to k_{E^-}. All terms in χ are either known or may be calculated from the data plots of Figures 3 or 4. The validity of eq. 9 is obvious from the linear nature of the plots in Figure 6.
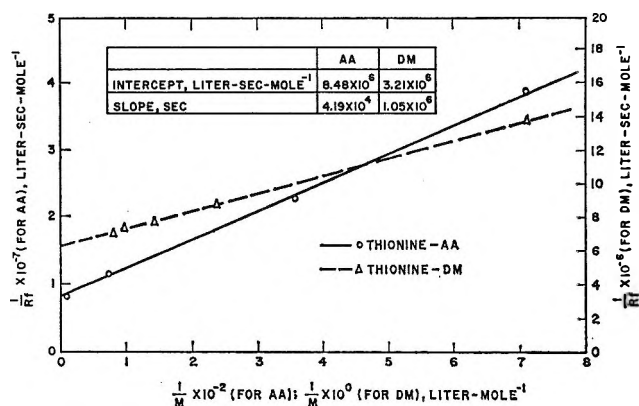
Figure 3. R_f dependence on AA and DM levels.
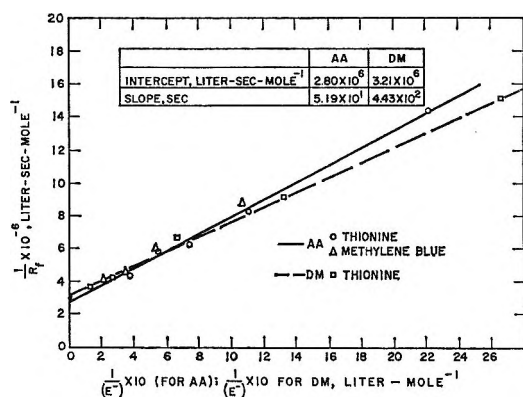
Figure 4. R_f dependence on monomer level.
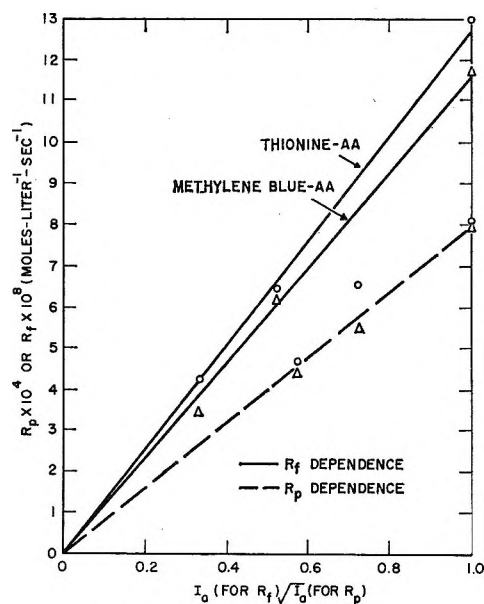
Figure 5. R_f dependence on I_a.

(7) G. Schwarzenbach and E. Felder, Helv. Chim. Acta, 27, 1701 (1944).
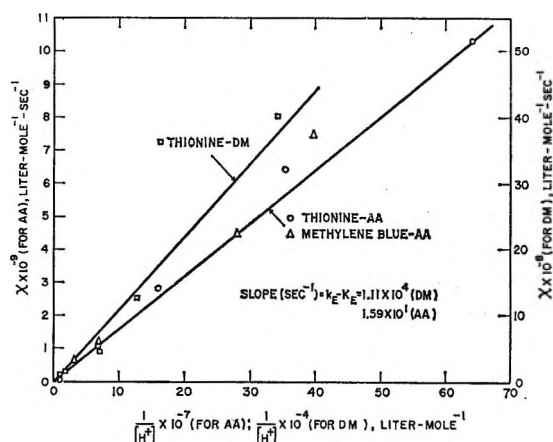
Figure 6. R_f dependence on pH.

Verification of the Reaction Mechanism with Respect to R_p. From mechanism reaction k, it follows that the rate of polymerization R_p is given by

$$R_p = k_p(M\cdot)(M) \tag{10}$$

To solve for $M\cdot$, we can set up eq. 11 for all radicals

$$-\frac{d(\text{radicals})}{dt} = 0 = 2k_2(TE^*)(M) -$$

$$2k_d(\cdot ST)^2 - 2k_t(M\cdot)^2 \tag{11}$$

Rearranging eq. 11 together with eq. 4 gives

$$k_t(M\cdot)^2 = k_2(TE^*)(M) - k_d(\cdot ST)^2 \tag{12}$$

Since the right-hand term of eq. 12 equals R_f (according to eq. 4) then combining eq. 12 with eq. 10 gives eq. 13, expressing R_p in terms of R_f and (M)

$$R_p = \frac{k_p}{k_t^{1/2}}(M)\sqrt{R_f} \tag{13}$$

For a constant concentration of enolate ion (E^-), the expression for R_f as a function of (M) is given by eq. 7b, which can be rendered to the simple form of eq. 14

$$R_f = \frac{(M)}{[a + b(M)]} \tag{14}$$

where a and b are constants defined by eq. 7b. It follows that eq. 13 for R_p can be expressed in terms of (M) for constant (E^-) by

$$R_p = \frac{k_p}{k_t^{1/2}}(M)\sqrt{\frac{(M)}{a + b(M)}} \tag{15}$$

For DM, the linear relationship between R_f and (M) given by eq. 14 is shown in Figure 4. We see that $a = 1.05 \times 10^6$ sec., while $b(M)$ varies from 0.88

$\times 10^6$ to 7.5×10^6 sec. for $(M) = 0.14$ to $1.2\ M$. There, according to eq. 15, the R_p data for DM should be

$$R_p = \text{constant } (M)^{3/2}\left[\frac{1}{a + b(M)}\right]^{1/2} \tag{16}$$

and so a plot of R_f vs. $M^{3/2}$ should be linear with a falloff of the straight line at greater (M), where $b(M) > a$. Equation 16 is confirmed in Figure 7 by a plot of the DM data for R_p vs. $(M)^{3/2}$.

The rate of fade R_f for AA is independent of monomer concentration in the range 0.14 to 1.0 M, as shown in Table II; therefore in eq. 14, $b(M)$ is much greater than a, and the equation for R_p reduces to the form

$$R_p = \frac{k_p}{(k_t b)^{1/2}(M)} \tag{17}$$

A plot of R_p vs. (M) in this concentration range for the AA system is also shown in Figure 7. Here the approximate linear relationship is again demonstrated.
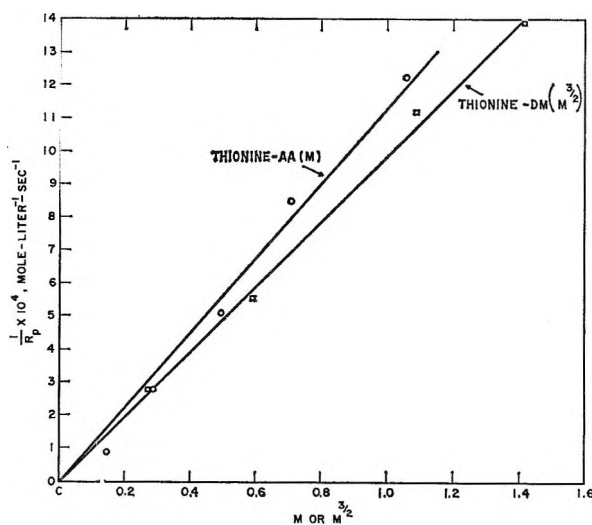
Figure 7. R_p dependence on monomer level.

Figure 4 shows that the linear relationship between R_f and (M) given by eq. 7a or 14 does hold for AA in the low monomer concentration range of 0.014 to 0.0014 M. Because R_p data could not be gathered at these low AA concentrations, we cannot check the expected $(M)^{3/2}$ dependence of R_p.

Finally, eq. 7 shows that R_f varies directly with I_a, and therefore, by eq. 13, R_p should vary with $I_a^{1/2}$. The dashed line of Figure 5 indicates that this square-root dependence holds for the thionine- and methylene blue-AA systems, and presumably should hold for thionine-DM systems.

Evaluation of Rate Constants

The data plots of Figures 3, 4, and 6, together with the following values for I_a and k_c, were used to estimate some of the rate constants

$$I_a = 8 \times 10^{-7} \text{ einstein l.}^{-1} \text{ sec.}^{-1}$$

$$k_c = 5 \times 10^4 \text{ l. mole}^{-1} \text{ sec.}^{-1}$$

The most reasonable values are summarized in Table IV. These data show that the efficiencies of formation of the light-excited dyes and the magnitudes of k_{E-} for AA and DM are comparable in magnitude.

Table IV: Rate Constants for the Thionine– and Methylene Blue–AA– and –DM–Acrylamide Systems

Parameter	AA system	DM system
ϕ	0.90	0.96
k_{E-}	2.1×10^9	1.9×10^9
k_E	$\ll 10^8$	$\ll 10^8$
k_1/k_2	5.0×10^{-3}	1.7×10^{-1}

Since the values of intercepts of the χ vs. $1/(H^+)$ plots of Figure 6 are very small, reliable values for k_E are unavailable; however, they should be consider-

ably smaller than 10^8. The only difference between AA and DM involves k_1/k_2, the ratio of the rate constants for the collisional dissociation of (TE*) and its reaction with monomer, which is approximately 300 times larger for DM than for AA.

The fact that R_f magnitudes (reaction g) are comparable for both substances indicates that the corresponding k_3 values may also be comparable. Since the rate constants for formation TE* (k_{E-}) also have similar values, the lower magnitude of k_1/k_2 for DM appears to be the result of a greater k_2 for the collisional dissociation step. The formation of a weaker T–DM complex for steric reasons could account for this trend.

The difference in the k_1/k_2 ratios also accounts for the different R_f dependencies at the higher monomer levels for AA and DM. It is obvious from eq. 7b that the $k_1/k_2(M)$ term for AA is much smaller than 1 and R_f becomes independent of (M). On the other hand, this term becomes important for DM and a monomer dependence is observed.

Interaction of Cross-Linked Polymethacrylic Acid with Polyvalent Metal Ions[1]

by Richard L. Gustafson and Joseph A. Lirio

Rohm & Haas Company, Research Division, Philadelphia 37, Pennsylvania (Received December 12, 1964)

The interactions of a polymethacrylic acid (PMA)–divinylbenzene copolymer with Fe^{3+}, Ni^{2+}, Cu^{2+}, Zn^{2+}, and Ca^{2+} ions have been measured potentiometrically at 5, 15, 25, 35, and 45° in a 1.0 M NaNO$_3$ aqueous medium. The metal complex equilibrium constants increased in the order $Ca^{2+} < Ni^{2+} < Zn^{2+} < Cu^{2+} < Fe^{3-}$. The unusual specificity for Zn^{2+} over Ni^{2+} suggests that the tetrahedral stereochemical configuration of the former ion permits binding by the PMA resin with less steric strain than is encountered in the case of the Ni^{2+} ion. This view is supported by the fact that the entropy change produced by the interaction of PMA with Zn^{2+} is greater than that for any of the other divalent ions studied. The $\Delta H°$ values of the Fe^{3+}, Ni^{2+}, and Cu^{2+} complexes are considerably less positive than those of Zn^{2+} and Ca^{2+}, suggesting that stronger chemical bonds are present in the former cases in which d orbitals are utilized. Linear plots of $-\log [H^+]$ *vs.* $\log (\alpha/(1 - \alpha))$, in accordance with the empirical modification of the Henderson–Hasselbach equation, $-\log [H^+] = pK + n \log (\alpha/(1 - \alpha))$, were obtained in the absence of and in the presence of divalent metal ions. The values of n increased in the order of decreasing degree of complexation. This suggests that the configurational entropy of the polymer chain increases because of decreasing electrostatic repulsions between neighboring charged groups as the degree of complex formation increases.

Introduction

A number of investigators[2-8] have studied the interactions of polyvalent metal ions, chiefly copper(II), with linear polyacrylic (PA) and polymethacrylic acid (PMA) polymers. More limited consideration has been given to the measurement of complex formation in cross-linked polycarboxylic acid systems. Gregor, *et al.*,[9] measured the degrees of interaction between copper(II) ions and polyacrylic and polymethacrylic acid gels and showed that, whereas coordination numbers as high as 4 were encountered in solutions of the corresponding linear polyelectrolytes, a maximum number of two carboxylate groups were bound per metal ion in the cases of the cross-linked materials. Measurements of the entropies and enthalpies of copper(II) complexation[4] for linear and cross-linked polyacrylic acid indicated that a smaller entropy loss occurred upon complex formation in the case of the more flexible linear polymer. Pennington and Williams[10] have described the binding of a number of divalent metal ions to Amberlite IRC-50, a polymethacrylic acid resin.

In the present study the interactions of Fe^{3+}, Ni^{2+}, Cu^{2+}, Zn^{2+}, and Ca^{2+} ions with a PMA gel have been measured potentiometrically at temperatures of 5.0, 15.7, 25.0, 34.9, and 43.7° in a 1.0 M NaNO$_3$ medium. Free energies, enthalpies, and entropies of complex formation have been calculated. Because of the rigidity of the PMA polymer chain, it was felt that the degree of complex formation might be influenced by

(1) Presented before the Division of Physical Chemistry at the 148th National Meeting of the American Chemical Society, Chicago, Ill., Aug. 31–Sept. 4, 1964.

(2) F. T. Wall and S. J. Gill, *J. Phys. Chem.*, 58, 1128 (1954).

(3) H. P. Gregor, L. B. Luttinger, and E. M. Loebl, *ibid.*, 59, 34 (1955).

(4) E. M. Loebl, L. B. Luttinger, and H. P. Gregor, *ibid.*, 59, 559 (1955).

(5) H. P. Gregor, L. P. Luttinger, and E. M. Loebl, *ibid.*, 59, 990 (1955).

(6) H. Morawetz, *J. Polymer Sci.*, 17, 442 (1955).

(7) A. M. Kotliar and H. Morawetz, *J. Am. Chem. Soc.*, 77, 3692 (1955).

(8) M. Mandel and J. C. Leyte, *J. Polymer Sci.*, 56, 523 (1962).

(9) H. P. Gregor, L. B. Luttinger, and E. M. Loebl, *J. Phys. Chem.*, 59, 366 (1955).

(10) L. D. Pennington and M. B. Williams, *Ind. Eng. Chem.*, 51, 759 (1959).

the stereochemical requirements of the metal ions. The choice of Ni^{2+}, Cu^{2+}, and Zn^{2+} ions was influenced by the fact that in aqueous solution the coordination numbers are normally 6, 4, and 4, respectively, and the corresponding orientations of ligand groups are octahedral (d^2sp^3), square-planar (dsp^2), and tetrahedral (sp^3), respectively.

Experimental

Reagents. A sample of PMA resin which contained 5% divinylbenzene (DVB) was characterized as described previously.[11] Solutions of reagent grade metal nitrates were standardized by titration with EDTA.[12] Reagent grade $NaNO_3$ was employed as a supporting electrolyte. Carbonate-free sodium hydroxide was prepared by dilution of a 50% stock solution and was standardized with potassium biphthalate.

Equilibrations. Samples of 9.26 mequiv. of hydrogen form resin were equilibrated for approximately 1 month with 100-ml. aliquots of 1.0 M $NaNO_3$ solution which contained either 4.63 mmoles of divalent ion or 3.09 mmoles of ferric ion and appropriate amounts of standard NaOH. A Beckman Model G pH meter, equipped with extension glass and calomel electrodes, was used to record hydrogen ion concentrations. The resins were stirred in the solutions during the pH measurements in order to eliminate slight drifts which might have otherwise occurred during measurements in the unbuffered solution phase in the absence of the resin. Purified nitrogen was bubbled through the solutions in order to maintain a carbon dioxide free atmosphere. Calibration of the electrode system was carried out with standard 0.001-0.1 M HCl solutions which were 1.0 M in $NaNO_3$. The constancy of the difference between the recorded pH and the true value was checked throughout the pH range of interest at the various temperatures employed by the use of standard phthalate, phosphate, and borate buffers.[13]

The measurements of resin volumes were carried out pycnometrically. The determinations of water content were obtained from the differences between the weights of the swollen resins and the weights of the resin matrices plus associated ions. The weights of the wet resins were determined after centrifugation as described by Gregor, *et al.*[14] The amounts of polyvalent metal ions sorbed by the resin were determined directly after displacement of the metals from the centrifuged resins with 0.5 M HCl. A small correction was made for the amount of metal ion held in the solution imbibed in the macropores of the resin. Previous measurements[11] showed that the porosity of the water-wet beads is 0.068 ml./ml. of bead.

Mathematical Treatment of Data

Zubay[15] has pointed out that calculations of equilibrium constants in polycarboxylic acid systems based on the reactions

$$M^{2+} + HA \xrightarrow{K_1} MA^+ + H^+$$

$$K_1 = \frac{[MA^+][H^+]}{[M^{2+}][HA]} \tag{1}$$

and

$$MA^+ + HA \xrightarrow{K_2} MA_2 + H^+$$

$$K_2 = \frac{[MA_2][H^+]}{[MA^+][HA]} \tag{2}$$
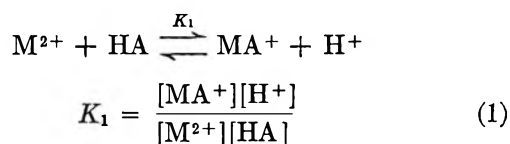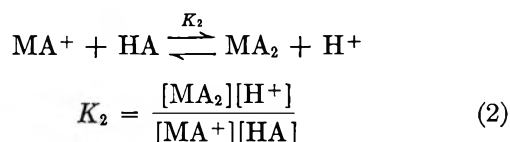
where HA represents an undissociated monomeric unit, are in error because the second step in reality merely involves dissociation of a proton from a carboxylic acid group adjacent to the metal ion bound in the complex MA^+. Reactions 1 and 2 may accordingly be redefined by the equations

$$M^{2+} + H_2A_2 \xrightleftharpoons{} MHA_2^+ + H^+$$

$$K_1' = \frac{[MHA_2^+][H^+]}{[M^{2+}][H_2A_2]} \tag{1a}$$

and

$$MHA_2^+ \xrightleftharpoons{} MA_2 + H^+$$

$$K_2' = \frac{[MA_2][H^+]}{[MHA_2^+]} \tag{2a}$$
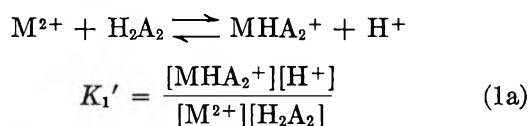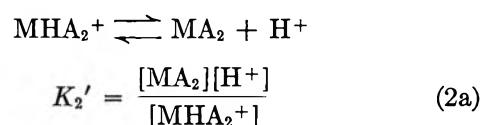
Here H_2A_2 is a chain segment consisting of two monomeric units. Since it has been shown by Gregor, *et al.*,[9] that the maximum coordination number in crosslinked polyacrylate and polymethacrylate systems is 2, only the reactions represented by (1a) and (2a) need be considered. Consideration of equilibria involving chelation by multidentate ligands such as ethylenediaminetetraacetate[16] show that, although MHA complexes are present in the case of calcium ion, measurable formation of these intermediates is apparently not detectable in the cases of the more stable Ni^{2+}, Cu^{2+}, or Zn^{2+} complexes. It would appear,

(11) R. L. Gustafson, *J. Phys. Chem.*, **67**, 2549 (1963).

(12) G. Schwarzenbach, "Complexometric Titrations," Interscience Publishers, Inc., New York, N. Y., 1957.

(13) R. G. Bates, "Electrometric pH Determinations," John Wiley and Sons, Inc., New York, N. Y., 1954.

(14) H. P. Gregor, K. M. Held, and J. Bellin, *Anal. Chem.*, **23**, 620 (1951).

(15) G. Zubay, *J. Phys. Chem.*, **61**, 377 (1957).

(16) J. Bjerrum, G. Schwarzenbach, and L. G. Sillén, "Stability Constants," Part I, The Chemical Society, London, 1957.

on the basis of entropy considerations, that the presence of MA_2 would be greatly favored over that of MHA_2^+. Hence, it is probably valid to assume that the over-all reaction

$$M^{2+} + H_2A_2 \rightleftharpoons MA_2 + 2H^+$$

$$K_3 = \frac{[MA_2][H^+]^2}{[M^{2+}][H_2A_2]} \tag{3}$$
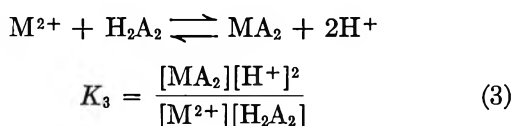
will describe the reaction adequately. Combination of eq. 3 with the material balance equations

$$\bar{n} = \frac{T_A - 2[H_2A_2] - 2[A^{2-}]}{2T_M} \tag{4}$$

and

$$2[H_2A_2] = T_A(1 - \alpha) - [H^+] \tag{5}$$

and the equation which describes the dissociation of the polymer

$$K_a = \frac{[H^+][A^{2-}]}{[H_2A_2]} \left(\frac{2[A^{2-}]}{T_A - 2[A^{2-}]}\right)^{n-1} \tag{6}$$

permits the calculation of K_3 by a method of successive approximations.

Equation 6 is equivalent to the usual expression

$$K_a = \frac{[H^+][A^-]}{[HA]} \left(\frac{[A^-]}{T_A - [A^-]}\right)^{n-1}$$

except that $2[A^{2-}]$ and $2[H_2A_2]$ have been substituted for $[A^-]$ and $[HA]$, respectively. T_A and T_M represent the total molar concentrations of carboxylic groups and metal ions, respectively, and $\bar{n}$ represents the average number of dicarboxylate groups bound per mole of metal ion. Solution of eq. 3 for K_3 yields the expression

$$K_3 = \frac{\bar{n}}{1 - \bar{n}} \frac{[H^+]^2}{[H_2A_2]} \tag{7}$$

Therefore, at $\bar{n} = 0.5$, the value of K_3 is equal to $[H^+]^2/[H_2A_2]$. The results obtained by this method will be different than those of Gregor, et al.,[3] who showed that $K = [MA_2][H^+]^2/[M^{2+}][HA]^2$ or that $K = [H^+]^2/[HA]^2$ at the point at which 50% of the metal ion is bound in cases in which eq. 1 and 2 are employed.

Values of the enthalpies of reaction, $\Delta H°$, were determined graphically from plots of log K_3 vs. $1/T$. The entropy of reaction was calculated by the relationship

$$\Delta S° = \frac{\Delta H° - \Delta F°}{T}$$

where $\Delta F° = -2.303RT \log K_3$.

Results and Discussion

Plots of $-\log [H^+]$ vs. the degree of neutralization for the various metal ion-PMA gel systems at 25° are shown in Figure 1. The relative positions of the titration curves show that the stabilities of the complexes increase in the order $Ca^{2+} < Ni^{2+} < Zn^{2+} < Cu^{2+} < Fe^{3+}$. A striking anomaly is that the degree of complexing of zinc is greater than that of nickel. Examination of a wide variety of data concerning chelation by monomeric, polydentate ligands[16] shows that, without exception, the formation constants of nickel complexes are greater than those of zinc. It may be that, in the present case, the tetrahedral steric configuration of donor atoms in Zn^{2+} complexes is more favorable than the octahedral Ni^{2+} configuration because less strain is placed on the polymer chain in the former case upon orientation around the metal ion. Further discussion of this effect will be deferred to a subsequent part of the paper.

The slopes of plots of log $(\alpha/(1 - \alpha))$ vs. $-\log [H^+]$, in accordance with the empirical equation

$$-\log [H^+] = pK + n \log \frac{\alpha}{1 - \alpha} \tag{8}$$

decreased in the order $Ca^{2+} > Ni^{2+} > Zn^{2+} > Cu^{2+}$, which is also the order of increasing degree of complexation as shown in Table I. Deviations from lin-
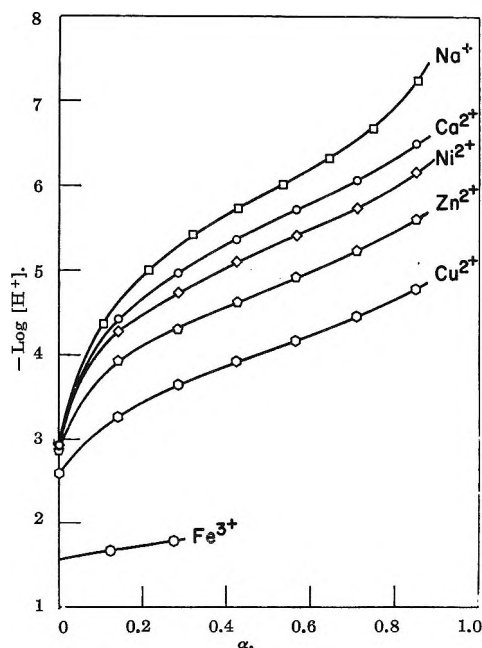
Figure 1. Plots of $-\log [H^+]$ in solution phase vs. the number of moles of hydroxide added per equivalent of PMA gel in the presence of polyvalent metal ions in a 1.0 M $NaNO_3$ medium at 25°.

earity occurred only at the highest α-values studied (0.85), and, in the case of the cupric system, the curve was linear within less than ± 0.01 pH unit over the entire range. Many workers have obtained linear plots upon the titration of polyacids with alkali metal hydroxides, but plots obtained by Gregor, et al.,[3] upon the titration of linear copper (II)–polyacrylate complexes showed pronounced curvatures under a variety of conditions. Gregor, et al.,[17] and others have suggested that the magnitude of n increases as the configurational entropy of the polymer chain decreases due to increasing electrostatic repulsions between neighboring charged groups. If electrostatic inter-

Table I: Values of Slope n and $-\mathrm{Log}\ [\mathrm{H}^+]$ at Half-Neutralization Points for Metal Ion–PMA Gel Interactions at 25° in 1.0 M NaNO$_3$

Metal ion	$-\mathrm{Log}\ [\mathrm{H}^+]\alpha = 0.5$	n
Na$^+$	5.91	1.60
Ca^{2+}	5.54	1.41
Ni^{2+}	5.26	1.26
Zn^{2+}	4.78	1.18
Cu^{2+}	4.06	1.02

actions alone were involved in the binding of Ni^{2+}, Cu^{2+}, and Zn^{2+} ions, it would be expected that, because of the nearly identical radii of these ions, the binding of PMA to these metals should be similar. The fact that the value of n decreases markedly in the order Ni^{2+} > Zn^{2+} > Cu^{2+} (which is the order of increasing PMA–M^{2+} complex formation) indicates that the degree of covalent bonding increases in that order. The fact that the value of n drops nearly to unity in the case of the Cu^{2+} complex shows that the metal ion so completely neutralizes the effects of the neighboring carboxylate groups that the remaining acidic groups undergo dissociation unhindered by the electrostatic effect which is observed upon neutralization of the polyacid in the absence of the polyvalent metal ion.

By the use of eq. 3–7, species distributions have been calculated as a function of the degree of neutralization for all of the divalent ion systems studied at 25°. The data obtained for the Cu^{2+} and Ca^{2+} systems are shown in Figures 2 and 3, respectively. The quantities of metal ions adsorbed by the resins, as determined by direct measurement, are shown for comparison. In the case of Cu^{2+}, reasonably good agreement between the calculated and measured amounts of bound metal ion are obtained. A similar result was noted previously by Gregor, et al.,[9] who measured the binding
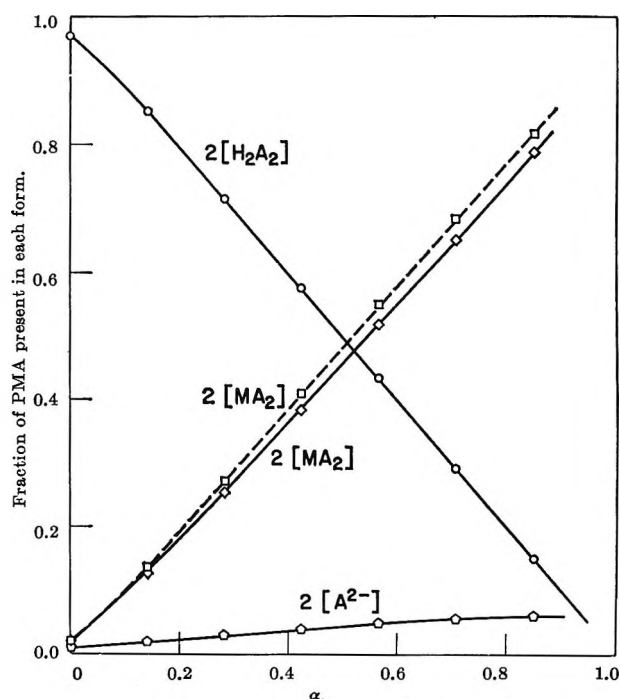
Figure 2. Distribution of Cu^{2+}–PMA species as a function of the degree of neutralization at 25°: solid lines, calculated values; dashed line, determined by direct measurement.
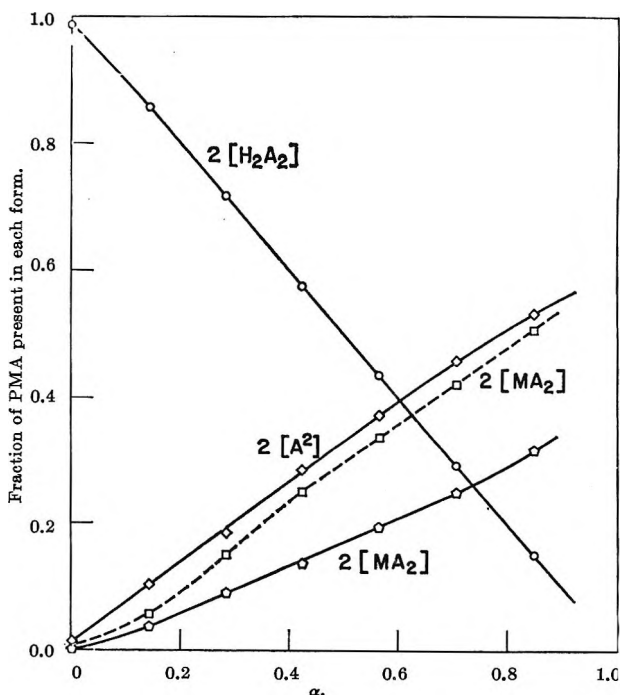
Figure 3. Distribution of Ca^{2+}–PMA species as a function of the degree of neutralization at 25°: solid lines, calculated values; dashed line, determined by direct measurement.

(17) H. P. Gregor, M. J. Hamilton, J. Becher, and F. Bernstein, $_\cup$ Phys. Chem., 59, 874 (1955).

of cupric ion by cross-linked polyacrylic and polymethacrylic acid resins. In the case of Ca^{2+} interaction (Figure 3) nearly twice as many metal ions were bound by the PMA resin as were calculated by the use of eq. 3–6. Deviations of intermediate magnitude were observed in the cases of Ni^{2+} and Zn^{2+}.

The failure of the present approach to describe adequately the binding of polyvalent metal ions is due to at least two factors. It has been tacitly assumed in the use of eq. 6 that the binding of metal ions does not affect the dissociation relation of the polyacid. Mandel and Leyte[18] have pointed out that caution should be used in the interpretation of potentiometric data because of the possible lack of validity of eq. 6 and because of the omission of activity corrections. Kunin and Fisher[19] have shown that the apparent pK values of cross-linked acrylic and methacrylic acids are markedly dependent upon the nature of the monovalent counterion. Still greater variations in the dissociation constants of polymeric acids are to be expected in the presence of polyvalent metal ions, in which case the electrostatic interactions along the polymer chain will be significantly different. In addition, the activity coefficients in the resin phases will differ appreciably as the degree of covalent binding changes, thus affecting the relationship between the hydrogen ion concentration in the resin itself and that which is measured in the external solution.

In the case of Cu–PMA, the electrostatic potential of the polymer chain is reduced nearly to zero as evidenced by the fact that $n = 1.02$ and $-\log [H^+]_{\alpha=0.5}$ is 4.06. A plot of titration data for isobutyric acid, which may be considered to be the monomer unit of isobutyric acid, would give a value of $n = 1.00$ and a pK_a value (equal to $-\log [H^+]_{\alpha=0.5}$) of 4.85 at 25° and zero ionic strength. Since, as may be shown by consideration of the Donnan membrane equilibrium, the pH inside the resin is less than that outside, a value of $-\log [H^+]_{\alpha=0.5}$ of less than 4.06 prevails in the resin phase.

In Figure 4, plots of α'/α (the fraction of ionized carboxylate groups bound to divalent metal ions) vs. α show that, after an initial rapid increase, the values of α'/α remain essentially constant above an α-value of 0.5 in the cases of Ca^{2+}, Ni^{2+}, and Zn^{2+} ions. Approximately 97% of the ionized ligands are bound throughout the entire pH range in the case of copper. Since the PMA resin is highly hydrogen bonded at low α-values, complexation in this region involves not only the formation of the metal–oxygen bond but also the breaking of the hydrogen bond. As the degree of neutralization increases, the probability for the requirement of breakage of a hydrogen bond upon
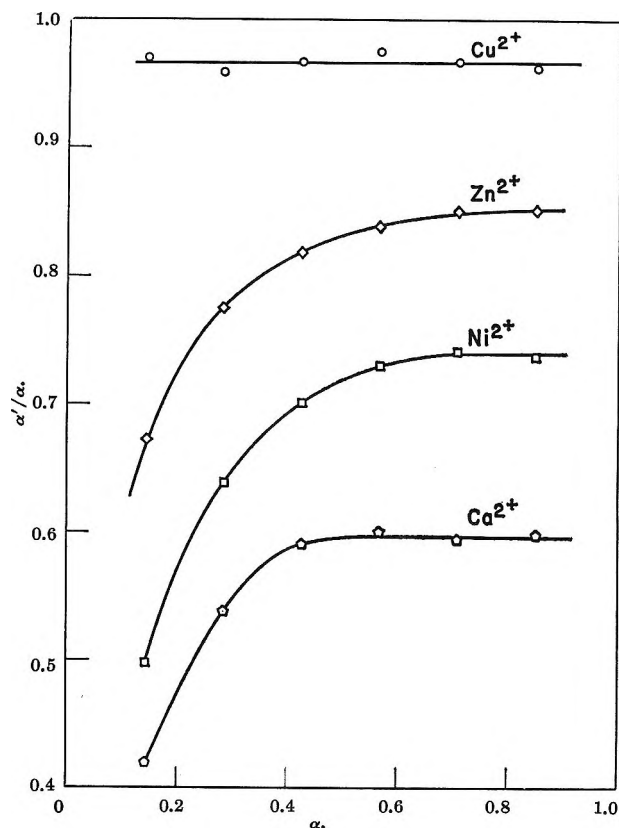
Figure 4. Plots of the fraction of bound carboxylate groups, α'/α, vs. the degree of neutralization for M^{2+}-PMA gels in 1.0 M NaNO$_3$ at 25°.

complex formation decreases. At the point at which 50% of the carboxylic acid groups have been neutralized, on the average every other group is ionized, and essentially all of the hydrogen bonds are broken. In the region $\alpha = 0.5–1.0$, complex formation proceeds without the necessity of the additional energy required to break the hydrogen bond and the ratio of bound to unbound carboxylate groups, α'/α, remains approximately constant.

Calculation of Selectivity Coefficients. On the basis of the experimentally determined species equilibria, molal selectivity coefficients have been calculated as a function of the degree of neutralization by means of the relationship

$$K_{Na^+}^{M^{2+}} = \frac{m^r_{M^{2+}}(m^s_{Na^+})^2}{m^s_{M^{2+}}(m^r_{Na^+})^2}$$

These values (Table II) show large differences in the selectivities of the PMA resin for the various ions. This is in sharp contrast to the behavior observed in

(18) M. Mandel and J. C. Leyte, *J. Polymer Sci.*, 2A, 2883 (1964).
(19) R. Kunin and S. Fisher, *J. Phys. Chem.*, 66, 2275 (1962).

Table II: Molal Selectivity Coefficients for Divalent Ion–Sodium Ion Exchange in PMA Gel at 25°

α	$K_{Na^+}^{Ca^{2+}}$	$K_{Na^+}^{Ni^{2+}}$	$K_{Na^+}^{Zn^{2+}}$	$K_{Na^+}^{Cu^{2+}}$
0.141	4.02	5.93	11.0	50.2
0.283	5.86	9.66	17.2	61.1
0.424	8.11	14.4	25.2	98.1
0.566	9.48	20.3	38.5	171
0.707	11.13	28.3	61.6	275
0.848	13.6	38.2	98.0	554

Table III: Thermodynamic Functions for the Reaction of Polyvalent Metal Ions with PMA According to the Reaction $M^{2+} + H_2A_2 \rightleftharpoons MA_2 + 2H^+$

$\bar{n}$	Ca^{2+}	Ni^{2+}	Zn^{2+}	Cu^{2+}
		$-\text{Log } K_{25}$		
0.1	9.55	8.59	7.53	...
0.2	10.37	9.07	7.69	6.17
0.3	11.06	9.44	7.94	6.36
0.4	...	9.84	8.20	6.49
0.5	...	...	8.43	6.59
0.6	...	...	8.63	6.71
0.7	...	...	...	6.83
		ΔF°_{25}, kcal./mole		
0.1	13.03	11.72	10.27	...
0.2	14.15	12.37	10.49	8.42
0.3	15.09	12.88	10.83	8.68
0.4	...	13.42	11.19	8.85
0.5	...	...	11.50	8.99
0.6	...	...	11.77	9.15
0.7	...	...	...	9.32
		ΔH°, kcal./mole		
0.1	9.9	5.3	10.4	...
0.2	11.5	7.6	11.5	7.8
0.3	...	8.3	12.4	8.4
0.4	...	10.6	14.2	8.9
0.5	...	...	15.9	9.8
0.6	...	...	16.1	10.1
0.7	...	...	...	10.4
		ΔS°, cal./mole deg.		
0.1	−10.6	−21.7	+0.4	...
0.2	−9.0	−16.0	+3.3	−2.2
0.3	...	−15.5	+5.3	−0.9
0.4	...	−9.3	+10.1	+0.1
0.5	...	...	+14.8	+2.9
0.6	...	...	+14.6	+3.0
0.7	...	...	...	+3.7

polystyrenesulfonate systems. The values of rational equilibrium constants for the exchange of divalent ions for Li^+ on sulfonic resins containing 4% DVB are 3.45, 3.29, 3.13, and 4.15 for Ni^{2+}, Cu^{2+}, Zn^{2+}, and Ca^{2+} ions, respectively,[20] showing very small differences in selectivity in cases in which no coordinate bonding occurs.

The selectivity coefficients of Table II increase in value as the degree of complexation increases. Harris and Rice[21] have shown on the basis of theoretical considerations that the selectivity for an ion should decrease as the mole fraction of that ion which is bound in the resin phase increases. However, they have also shown that the selectivity for a preferred ion increases as the concentration of functional groups increases. It is apparent in the present case that the latter effect predominates over the former such that an increase in selectivity with an increase in the degree of neutralization is observed.

Calculations of Equilibrium Constants from Potentiometric Data. Although the values of K_3 do not permit calculations of the total amounts of metal ions adsorbed by the resin, they do measure the relative tendencies of the metal ions to displace protons in complex formation. In addition, measurements of the temperature dependence of complex formation permit the calculation of contributions of the enthalpy and entropy changes to the total free energy of reaction. In Table III values of log K_3 (equal to $(\bar{n}/(1-\bar{n}))$ × $[H^+]^2/[H_2A_2])$, ΔF°, ΔH°, and ΔS° have been presented as a function of $\bar{n}$.

Gregor, *et al.*,[3] have pointed out that if the chelation reaction of a polyelectrolyte involves no net change in the charge of the system, constant equilibrium constants should be expected over a wide range of the degree of neutralization. Although the reaction $M^{2+} + H_2A_2 \rightleftharpoons MA_2 + 2H^+$ conforms to the above requirement, steadily decreasing values of K_3 with increasing α were obtained. The enthalpies of reaction are quite positive and become more so as the extent of complex formation increases. The ΔH° values of the Ni^{2+} and

Cu^{2+} complexes are considerably more negative than those of Ca^{2+} and Zn^{2+}, suggesting that stronger chemical bonds are present in the former cases in which d orbitals are utilized. Measurements of chelation by ethylenediamine[22] showed that the enthalpy of reaction of Cu^{2+} was considerably more negative than that of Zn^{2+} although the entropy change upon chelation of zinc was slightly more favorable than that of copper. The entropy change upon interaction of PMA with the Zn^{2+} ion is much greater than that for any of the other divalent metal ion systems studied. The differences of approximately 20 e.u. between the

(20) O. D. Bonner and L. L. Smith, *J. Phys. Chem.*, **61**, 326 (1957).

(21) F. E. Harris and S. A. Rice, *ibid.*, **61**, 1360 (1957).

(22) C. G. Spike and R. W. Parry, *J. Am. Chem. Soc.*, **75**, 3770 (1953).

$\Delta S°$ values for the Ni^{2+} and Zn^{2+} systems at various $\bar{n}$ values are particularly striking. This evidence indicates that the tetrahedral stereochemical configuration of the Zn^{2+} ion permits binding by the polymethacrylic acid resin with less steric strain than is encountered in the case of the Ni^{2+} ion.

In Table IV the values of log K, $\Delta F°$, $\Delta H°$, and $\Delta S°$ for the reaction $M^{2+} + A^- \rightleftharpoons MA^+$ have been tabulated. These values were calculated by means of Gregor's[3] modification of the Bjerrum method and show more dramatically the important role played by the favorable entropy change upon complex formation.

Table IV: Values of Thermodynamic Functions for the Reaction $M^{n+} + A^- \rightleftharpoons MA^{n-1}$ Calculated at $\bar{n} = 0.5$

M^{2+}	Log K	$\Delta F°$, kcal./mole	$\Delta H°$, kcal./mole	$\Delta S°$, cal./mole deg.
Ni	2.03	−2.77	2.9	19
Cu	3.45	−4.71	4.3	30
Zn	2.69	−3.67	6.1	33
Ca	1.41	−1.92	3.4	18

Comparison with Binding by Linear PMA. Mandel and Leyte[18] have calculated formation constants for the interaction of several divalent metal ions with linear polymethacrylic acid according to Gregor's modification of the Bjerrum method. The values of Table V were obtained for the reaction $M^{2+} + 2HA \rightleftharpoons MA_2 + 2H^+$ where

$$B_{av} = \left(\frac{[MA_2][H^+]^2}{[M][HA^-]^2} \right)^{1/2}$$

Table V

M^{2+}	Log B_{av} (linear)	Log B_{av} (gel)
Cu	−1.8	−2.76
Zn	−2.6	−3.62
Ni	−2.8	−4.34
Co	−2.85	...
Mg	−3.1	...

Values of the formation constants of the Ni^{2+}-, Cu^{2+}-, and Zn^{2+}-PMA gel complexes have been calculated in the same way (B_{av} is equal to log ([H$^+$]/[HA]) at $\bar{n} = 1$) and are shown for comparison. The equilibrium constants are lower in the case of the cross-linked polymer as a result of the lack of flexibility of the polymer chains. Precise comparisons of the constants cannot be made because the ionic strengths of the two systems are different. Gregor,[9] *et al.*, have

shown that the formation constants decrease slightly with increasing ionic strength in cross-linked polyacrylate and polymethacrylate systems whereas the reverse trend was observed for linear polyacrylate complexes. As is shown above, even in the case of the more flexible linear polymer, the formation of the zinc complex is more extensive than that of nickel although the difference is much less than that shown for the cross-linked polymer. Perhaps in the case of the more flexible polyacrylic acid, the nickel complex will be formed to a greater extent than that of zinc in agreement with the usual trend.

Binding of Ferric Ion. Titrations of systems which contained 3 mequiv. of PMA/mole of ferric ion produced precipitation above a pH of approximately 1.7 or an $\bar{n}$ value of 0.4 at 25°. Calculations of log K for the reaction $Fe^{3+} + H_3A_3 \overset{K}{\rightleftharpoons} FeA_3 + 3H^+$ where

$$K = \frac{\bar{n}}{1 - \bar{n}} \frac{[H^+]^3}{[H_3A_3]}$$

gave the results in Table VI at $\bar{n} = 0.30$.

Table VI

t, °C.	$-\text{Log } K$
5.0	3.88
15.7	3.58
25.0	3.45
24.9	3.24
43.7	3.02

Estimation of the slope of a log K *vs.* $1/T$ plot leads to a value of +8.7 kcal./mole for the enthalpy of the above reaction. The thermodynamic values of Table VII were obtained at 25° for the reaction $M^{n+} + mA^- \rightleftharpoons MA_m^{n-m}$ at a point at which an average of one carboxylate group is bound per metal ion. These results show that both the entropy and enthalpy changes upon complexation of Fe^{3+} are more favorable than those of the other systems studied.

Table VII

M^{n+}	Log K	$\Delta F°$, kcal./mole	$\Delta H°$, kcal./mole	$\Delta S°$, cal./mole deg.
Zn^{2+}	2.30	−3.14	6.4	32.1
Cu^{2+}	3.15	−4.30	4.7	30.0
Fe^{3+}	5.50	−7.50	2.9	34.8

Measurements of Resin Volumes. In Figure 5 the resin volumes have been presented as a function of the
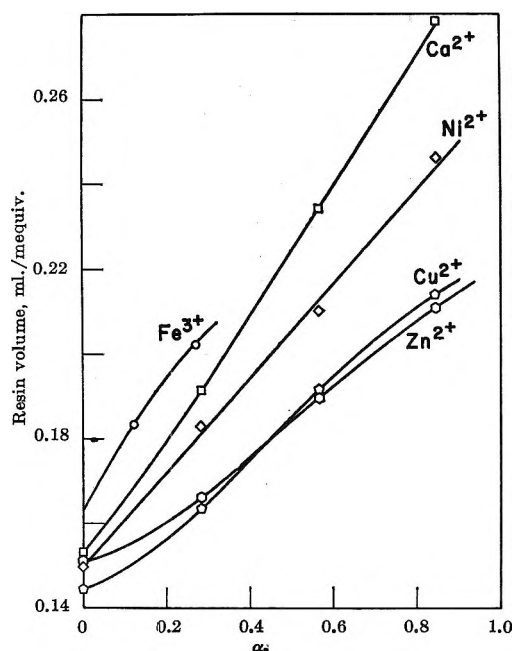
Figure 5. Resin volume as a function of the degree of neutralization for polyvalent metal ion–PMA resin interaction at 25°.

degree of neutralization. In the series of divalent metals the resin volume decreases as the complex stability increases except in the case of the zinc ion which, above an α-value of 0.5, actually has a volume which is lower than that of the cupric–PMA resin. This is particularly surprising since at a given value of α the number of carboxylate groups bound to copper is greater than that bound to zinc. Under these conditions, the mutual repulsions of ionized groups along the polymer chains would be expected to be greater in the latter case. It is probable that the stereochemical requirement of the zinc ion fits the geometry of the PMA molecule such that a considerable economy of space is realized. The volume of the ferric complex is larger than that of any of the other complexes at a given α-value because the degree of ionization of carboxylic acid groups in the former complex is enhanced by a considerable degree of spontaneous dissociation of hydrogen ions upon reaction of the resin with the ferric ion and is greater than that indicated by the α-value alone. In contrast, the total of $2[A^{2-}]$ and $2[MA_2]$ is virtually equal to αT_A in the case of the divalent metal ion complexes.

Dissociation Studies in High Dielectric Solvents. III. Conductance of

Magnesium Sulfate in Dioxane–Formamide Mixture at 25°

by P. H. Tewari[1] and Gyan P. Johari

Department of Chemistry, University of Gorakhpur, Gorakhpur, U. P., India (*Received March 1, 1965*)

The conductance of magnesium sulfate in 20–70% dioxane–formamide mixtures has been measured at 25°. The density, viscosity, and dielectric constant of each mixed solvent have also been measured at 25°. The conductance data in solvents up to 40% dioxane–formamide mixture have been analyzed by the Fuoss–Onsager equation, and reasonable Λ_0, K_A, and a_J parameters have been derived. However, the Walden product is found to vary with solvent composition, and a plot of $\log K_A$ vs. D^{-1} in the mixture range studied is found curved at lower dielectric constant values. The contact distance a_J increases with decreasing dielectric constant.

Introduction

Several 2–2 salts were reported to be much less associated in formamide than in aqueous solutions[2a] and Fuoss–Onsager[2b] theory satisfactorily explained the conductance data of the salts. However, the a_J parameter of 1.80 Å. for $MgSO_4$ was found to be too small and the theoretical crossover concentration[3] C_x did not agree with the experimental point. Further, when the data were analyzed with the equation for associated electrolytes, negative K_A was obtained, suggesting little or no association.

It was thought desirable to obtain further information by studying the conductance of the salt in a mixed solvent having a nonpolar component and to derive the results in pure formamide from Fuoss–Bjerrum theory.[4] Dioxane was selected as the nonpolar component because its mixture unlike acetone and methanol gives a more ideal solvent.

Experimental

Purification of Materials. Dioxane (B.D.H. Analar) was refluxed over pieces of sodium for 16–18 hr. After fractionating it through a 1-m. column, it was stored over sodium wire. The dioxane thus stored was distilled at least twice prior to the preparation of solvent mixtures[5] (b.p. 101.2–101.3°).

Nitrobenzene (B.D.H.) was shaken with dilute sulfuric acid, washed with saturated sodium bicarbonate solution, and finally with water. It was kept for 2 days over fused calcium chloride. The final product was obtained by distilling it twice under reduced pressure. The specific conductance of 3.2×10^{-8} mho was obtained for the pure sample.

Acetone (B.D.H. Analar) was first refluxed with $KMnO_4$ and was shaken with metallic sodium. It was then refluxed for 8 to 10 hr. with sodium and fractionated. The middle fraction with specific conductance of 3.7×10^{-7} mho was used for the experiments.

Ethanol (absolute alcohol) was kept over freshly ignited calcium oxide for 2 days. After distilling, fresh pieces of sodium metal were added to it and refluxed. The pure product (specific conductance 1.1×10^{-6} mho) was obtained by fractionating it through a 1-m. column.

Formamide was purified as reported earlier.[2a]

Magnesium sulfate used in this investigation was the same as described previously.[2a]

Measurements. Densities were determined with a 30-ml. single-stem pycnometer. The level of the liquid was adjusted with a hypodermic syringe. The pyc-

(1) Chemistry Department, University of Maryland, College Park, Md. 20742.

(2) (a) G. P. Johari and P. H. Tewari, *J. Phys. Chem.,* **69,** 696 (1965); (b) R. M. Fuoss and F. Accascina, "Electrolytic Conductance," Interscience Publishers, Inc., New York, N. Y., 1959.

(3) See ref. 2b, pp. 198, 199.

(4) R. M. Fuoss, *J. Am. Chem. Soc.,* **80,** 5059 (1958).

(5) J. E. Lind and R. M. Fuoss, *J. Phys. Chem.,* **65,** 999 (1961).

nometer was calibrated with conductivity water and nitrobenzene. At least four or five fillings were weighed with each solvent. The densities after proper vacuum correction were accurate within 0.02%.

Viscosities were measured by an Ostwald–Fenske type viscometer. The viscometer was calibrated with conductivity water ($\eta = 0.08903 \times 10^{-2}$ poise[5]), acetone ($\eta = 0.0304 \times 10^{-2}$ poise[6]), and nitrobenzene ($\eta = 1.839 \times 10^{-2}$ poise[7]). No kinetic energy correction was applied to the readings of flow time. Readings obtained from four samples of same solvent were averaged to get the viscosity. During measurements, calcium chloride guard tubes were fitted to avoid the entrance of moisture. The absolute values of viscosities obtained were better than 0.1%.

Dielectric constant measurements were based on the reasonance principle in which the measuring cell formed the condenser in the resonance circuit. A DKO3 type dekameter (W.T.W.) was used for the purpose. Two cells MFL3 and MFL3/S with brass electrodes supplied with the instrument were used. Oil from the thermostat maintained at 25.0° was circulated through the outer jacket of the brass cell. Normally it took 1–1.5 hr. for the temperature to be attained. In order to ensure that temperature was attained by the liquid in the cell, oil was also circulated through another cell jacket containing the liquid and a thermometer. For each sample of the liquid four or five readings were taken with each cell. Thus, a mean of eight to ten readings not differing by 0.05–0.1% were taken to interpolate the dielectric constant. Both the cells were calibrated with nitrobenzene[5] ($D = 34.82$), acetone[8] ($D = 20.74$), ethanol[9] ($D = 24.30$), water ($D = 78.54$), and 22.2, 43.65, and 69.9% dioxane–water mixtures. The dielectric constants for the dioxane–water mixtures were taken from Fuoss'[5] data. All measurements of dielectric constant were made at 1.8 Mc. The measurements of the dielectric constants are reproducible within 0.05% with this instrument, but the absolute values of the dielectric constants are accurate to 0.5% only.

Conductance. The apparatus for conductance measurements has been described in a previous communication as have the *modus operandi.*[2a] In the solvent mixtures having dioxane above 40%, MgSO$_4$ was difficultly soluble. Therefore, for solutions in 50, 60, and 70% dioxane–formamide mixtures, a known amount of the salt was dissolved in formamide, and subsequently weighed amounts of dioxane and formamide were added to get the required dioxane concentration. In other cases, a batch of the mixed solvent was prepared by weight, and this mixture was used for the preparation of the concentrated stock solutions and for the subsequent dilutions. Conductance of the solution

was obtained by subtracting the conductance of the solvent of the same batch determined separately in a cell at the same time.

The density of the dilute solution was taken as equal to the density of the pure solvent since the size of the correction would be of the same order as the propagated experimental error.

Results

The physical properties of the solvent mixtures obtained from measurements have been summarized in Table I, where W_2 represents weight per cent of dioxane in formamide, X_2 its mole fraction, ρ the density, η the viscosity in poise, and D the dielectric constant of the solvent mixtures. We have also derived the molar volume V_{12}, the polarizability P_{12}, and the deviation factors δ of the solvent mixtures from the data.

The deviation factor occurring during the volume additivity has been calculated by the equation

$$\delta = \frac{1}{\rho} - \frac{W_1}{100\rho_1} - \frac{W_2}{100\rho_2}$$

The molar volume V_{12} and the polarizability P_{12} were derived from the equations

$$V_{12} = (X_1 M_1 + X_2 M_2)/\rho$$

$$P_{12} = (D - 1)(2D + 1)V_{12}/9D$$

A plot of δ, the deviation factor, against the mole fraction of dioxane, X_2, shows that a contraction on the addition of dioxane to formamide occurs throughout the whole composition range, but the specific volume deviation reaches a minimum value near 70% dioxane.

A plot of the viscosity of the solvent mixture against X_2, the mole fraction of dioxane, is slightly humped upwards at the beginning, but the curve suggests that it is a monotonic function of the solvent composition. The plots of dielectric constants, molar volumes, and polarizability against X_2 show no structure complication, and they appear to be simple functions of solvent compositions.

The conductance and concentration data are presented in Table II. The data were analyzed by the Fuoss–Onsager extended equation[2b] for associated electrolytes in the form

$$\Lambda = \Lambda^0 - Sc^{1/2}\gamma^{1/2} + Ec\gamma \log c\gamma + Jc\gamma -$$
$$K_A c\gamma f^2 \Lambda \quad (1)$$

(6) M. B. Reynolds and C. A. Kraus, *J. Am. Chem. Soc.*, **70**, 1709 (1948).

(7) H. Sadek and R. M. Fuoss, *ibid.*, **76**, 5905 (1954).

(8) P. S. Albright, *ibid.*, **59**, 2098 (1937).

(9) A. A. Maryott and E. R. Smith, National Bureau of Standards Circular 514, U. S. Government Printing Office, Washington, D. C., 1951.

Table I: Properties of Dioxane–Formamide Mixtures

Serial no.	Wt. % dioxane, W_2	Mole fraction dioxane, X_2	Density, ρ, g./ml.	Dielectric constant, D	100 × viscosity, η, cp.	Molar vol., V_{12}, cm.^{3}	Polarizability, P_{12}	Dev. factor, $\delta \times 10^4$
1	0.00	0.00	1.1296	109.5	3.301	39.87	965.8	0.00
2	20	0.1133	1.1115	81.42	3.2507	44.91	807.6	−29
3	25	0.1456	1.1067	74.67	3.192	46.36	764.2	−37
4	30	0.1797	1.1019	68.17	3.133	47.90	720.0	−42
5	35	0.2159	1.0972	61.54	3.0538	49.52	673.3	−48
6	40	0.2542	1.0925	55.38	2.969	51.25	624.7	−51
7	50	0.3435	1.0826	43.17	2.695	55.27	523.9	−58
8	60	0.4344	1.0724	33.02	2.393	59.44	429.3	−59
9	70	0.5439	1.0623	21.77	2.072	64.43	304.4	−59
10	80	0.6718	1.0511	13.41	1.763	71.28	203.8	−47
11	90	0.8214	1.0379	6.850	1.431	77.47	108.0	−15
12	100	1.00	1.0269	2.209	1.196	85.80	28.27	0.00

Table II: Equivalent Conductance of MgSO$_4\cdot$7H$_2$O in Dioxane–Formamide Mixtures at 25° (C in moles per liter)

$C \times 10^4$	Λ	$C \times 10^4$	Λ
$D = 81.42$		**$D = 55.38$**	
1.8374	22.846	1.9160	17.167
2.0767	22.427	3.4054	14.897
4.0219	21.916	4.7432	13.661
4.2099	21.870	5.8313	13.007
7.9610	20.441	8.9753	11.536
14.764	18.750	9.0110	11.508
14.957	18.677	13.962	10.093
$D = 74.67$		14.740	9.9601
1.7453	22.106	17.553	9.3610
3.6732	20.900	**$D = 43.17$**	
6.3476	19.598	1.6653	10.992
11.280	17.937	2.3558	9.720
15.413	16.949	3.0917	8.853
19.583	16.080	4.3090	7.881
23.120	15.568	6.1220	6.911
$D = 68.17$		8.219	6.239
1.6717	20.702	10.535	5.618
3.2324	19.276	**$D = 33.02$**	
4.1262	18.682	1.4626	3.886
5.4370	17.935	2.7940	3.003
6.1081	17.612	4.0120	2.576
7.8946	16.773	5.1363	2.312
11.902	15.459	7.9255	1.922
12.405	15.357	11.937	1.591
16.565	14.362	14.896	1.437
$D = 61.54$		**$D = 21.77$**	
1.2254	20.867	1.7832	1.541
2.3626	19.148	2.5422	1.326
3.3965	18.064	4.6660	1.001
5.3984	16.511	6.3930	0.973
8.2493	15.095	8.721	0.897
11.928	13.796		
14.790	12.936		

on an IBM 7094 computer using a Fortran program similar to that described by Kay.[10] Since the Mg^{2+} ion is of the same order of magnitude as the solvent molecule (and even smaller), the Einstein coefficient F was taken as zero and the viscosity term $F\Lambda c$ was, therefore, neglected.[6] The higher terms in $c^{1/2}$ were also neglected.

The results of the analysis are given in Table III where Λ^0, S, E, J, etc., are the parameters as defined in the Fuoss equation,[2b] $\sigma\Lambda$ is the standard deviation in $\Delta\Lambda$-units of the data from the equation, and $\Lambda^0\eta$ is the Walden product.

The data in 50, 60, and 70% dioxane mixtures could not be analyzed with the computer owing to higher association. K_A and Λ^0 for these, therefore, have been obtained by the Fuoss and Kraus[11] method. Since K_A values are highly influenced by the errors in Λ^0, K_A values for the three systems are established only in order of magnitude and are given in Table III. This method of calculation was preferred over that of Shedlovsky to keep the same model for the calculations throughout the whole range. However, as a matter of interest, the three sets of data were treated by Shedlovsky's[12] method also, and the K_A values obtained by the two methods are quite close; for example, K_A for the 50% mixture (series number 7 in Table III) by Shedlovsky's method is 24,830 as against 24,700 by Fuoss and Kraus' method and so are the differences in the other two values.

Discussion

The contact distance a_J increases with the decrease in dielectric constant. The variation in a_J may be due

(10) R. L. Kay, J. Am. Chem. Soc., 82, 2099 (1960).

(11) R. M. Fuoss and C. A. Kraus, ibid., 55, 476 (1933); R. M. Fuoss, Chem. Rev., 17, 27 (1935).

(12) T. Shedlovsky, J. Franklin Inst., 225, 739 (1938).

Table III: Derived Parameters of Conductance Equation for $MgSO_4$ in Dioxane–Formamide Mixtures

Serial no.	Wt. % di-oxane	Dielectric const.	Λ^0	K_A	S	E	J	$\sigma\Lambda$	$\Lambda^0\eta$	a_J	$a_{Bjerrum}$
1[a]	0	109.5	28.38 ± 0.02		86.9	262	402	0.022	0.9373	1.80 ± 0.15	6.51
2	20	81.42	24.50 ± 0.03	88.4 ± 6	107.9	579	1256	0.011	0.7965	3.75 ± 0.16	4.91
3	25	74.67	24.52 ± 0.06	216 ± 22	117.7	761	1739	0.032	0.7826	3.77 ± 0.5	4.39
4	30	68.17	24.62 ± 0.08	450 ± 54	127.4	974	2583	0.033	0.7713	3.99 ± 0.8	4.39
5	35	61.54	24.68 ± 0.09	1240 ± 70	144.9	1421	4709	0.022	0.7536	5.30 ± 1.02	3.96
6	40	55.38	25.33 ± 0.18	3806 ± 300	164.8	2046	9406	0.080	0.7520	6.05 ± 1.15	3.78
7	50	43.17	26.50	2.47×10^4	227				0.7142		4.12
8	60	33.02	27.5	2.40×10^5	323				0.6581		4.35
9	70	21.77	30.0	2.64×10^6	574				0.6216		6.16

[a] Data taken from ref. 2a.

to the still missing linear terms which have been excluded by the approximations made in the theory. a_J for the data whose association constants have been calculated were plotted against $1/D^4$, and an extrapolated value of $a_J = 3.0$ Å. at infinite dielectric constant was obtained.[5] The small value of a_J in pure formamide suggests that this parameter includes short-range effects. Next to the viscosity correction which is essentially needed, slight association may also be included.

As the computer gave a negative K_A in pure formamide, an alternative procedure was tried to calculate K_A. Fuoss' equation for an electrolyte which is slightly associated may be written as ($\gamma = 1$)[13]

$$\Lambda = \Lambda^0 - Sc^{1/2} + Ec \log c + Jc - K_A cf^2\Lambda \quad (2)$$

Following Fuoss' method

$$\Lambda' - Jc = \Lambda^0 + K_A cf^2\Lambda \quad (3)$$

where

$$\Lambda' = \Lambda + Sc^{1/2} - Ec \log c \quad (4)$$

Λ' may be calculated by taking Λ^0 obtained by treating it as unassociated. A plot of $\Lambda' - Jc$ against $cf^2\Lambda$ should be a straight line with K_A as slope and Λ^0 as intercept. J was calculated by taking $a_J = 3.0$ Å. From the graph at low concentration data a K_A of 9.3 ± 0.2 was obtained. This method of calculation has little effect on the intercept, Λ^0, however.

The plot of log K_A against $1/D$ shows a curvature (Figure 1), the departure being pronounced at lower D values. However, the first five points seem to fall on a straight line, and, if the line is extrapolated to the D value of pure formamide, a K_A value of about 9.6 is obtained. This value of K_A is in good agreement with 9.3 obtained from the simplified Fuoss equation (2) for slightly associated electrolytes ($\gamma = 1$) by
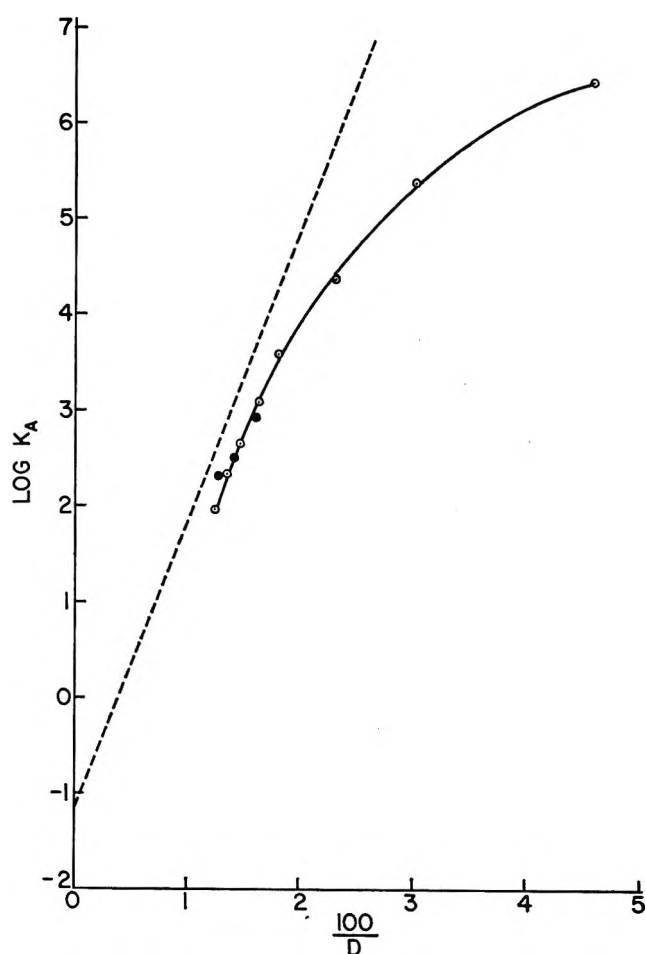
Figure 1. Dependence of the association constant on the reciprocal of the dielectric constant: dashed line, theoretical dependence for $d = 3.0$; solid circles, data of Dunsmore in dioxane–water mixture.

(13) See ref. 2b, pp. 238, 239.

putting $a_J = 3.0$ Å. This suggests that association of $MgSO_4$ in pure formamide, if at all, is very low, a result which was obtained in the earlier work.

It appears plausible that the values of K_A at the low D range are lower than the ones predicted by the Fuoss-Bjerrum[4] equation because of the accumulation of the more polar component of the solvent near ions as the average dielectric constant decreases.[14,15] Consequently, the effective size of the ion is larger on account of a selective solvation, and the microscopic dielectric constant is higher than the macroscopic value. Either or both effects may decrease the K_A from the theoretical value.

The theoretical dependence of log K_A on $1/D$ according to the Fuoss-Bjerrum equation[4] for $a = 3.0$ Å. is shown by the broken line in Figure 1. Since this equation does not take into account any ion–solvent interaction, Gilkerson's[16] equation which accounts for ion–solvent interaction energy E_s appears as a more sophisticated approach to it. The vertical displacement of the theoretical line could be related to this ion–solvent interaction.

It is interesting to note that the points of a log K_A vs. $1/D$ plot (Figure 1) for the salt in dioxane–formamide and in dioxane–water mixed solvents (solid circles represent data of Dunsmore[17] in dioxane–water) approximately lie on the same curve in the region of high dielectric constants. The a_K values computed from the slope in the D region covered by the two systems are quite close. It appears that the same model can predict the behavior of the salt in the two types of mixed solvents and that the metal–ligand type of interactions are absent in the dioxane–formamide mixture. The hydrodynamic analog of the electrostatic sphere is, however, different since the Walden product is sufficiently higher ($\Lambda^0\eta = 1.21$) in the water–dioxane system than in dioxane–formamide. A tentative explanation may be that $\Lambda^0\eta$ describes the behavior of separated ions in a continuum model while K_A depends on the short-range interactions and more specific effective solvation.

The Walden product, $\Lambda^0\eta$ (column 10, Table III), in the dioxane–formamide systems decreases with the

decrease in the dielectric constant. However, it is a monotonic function of the solvent composition in the mixture range (20–70% dioxane) studied. The inconsistency may be ascribed to an additional drag on the ions as a result of electrostatic coupling between ions and the solvent dipoles.[18-20] This ion–solvent relaxation drag decreases with an increase in the dielectric constant. Hence, this effect is more pronounced in solvent mixtures of low dielectric constants.

The hydrodynamic distance of closest approach calculated from $\lambda^0_{Mg^{2+}} = 12.34$ is considerably higher than that obtained from the electrostatic considerations (a_K) or from the curvature of the phoreogram (a_J). The Stokes radii also increase with the increase in the dioxane content of the solvent. Evidently, the hydrodynamic situation is quite complicated in dioxane-rich mixtures. The Bjerrum a values given in the last column of Table III vary widely with the dielectric constant which only reflects the nonlinearity of the log K_A vs. $1/D$ plot. However, there is no simple relationship between a_J and $a_{Bjerrum}$ values.

The functional dependence of the parameters point to the presence of specific ion–solvent interaction in these solutions. In conclusion, we can only say that $MgSO_4$ is negligibly associated in formamide and that the Fuoss–Onsager equation predicts the behavior of the salt in the mixed solvents.

We are extending the study to other 2–2 and 3–3 salts in the solvent mixtures.

(14) Y. H. Inami, H. K. Bodenseh, and J. B. Ramsey, *J. Am. Chem. Soc.*, 83, 4745 (1961).

(15) J. B. Hyne, *ibid.*, 85, 306 (1963).

(16) W. R. Gilkerson, *J. Chem. Phys.*, 25, 1199 (1956).

(17) H. S. Dunsmore and J. C. James, *J. Chem. Soc.*, 2925 (1951)

(18) R. M. Fuoss, *Proc. Natl. Acad. Sci. U. S.*, 45, 807 (1959).

(19) R. H. Boyd, *J. Chem. Phys.*, 35, 1281 (1961).

(20) R. Zwanzig, *ibid.*, 38, 1603 (1963).

Dissociation Studies in High Dielectric Solvents. IV. Conductance of

Some 3-3 Complex Salts in Formamide at 25°

by Gyan P. Johari[1a] and P. H. Tewari[1b]

Department of Chemistry, University of Gorakhpur, Gorakhpur, U. P., India   (*Received December 28, 1964*)

Equivalent conductances of $LaFe(CN)_6$, $LaCo(CN)_6$, $[Co(en)_3][Fe(CN)_6]$, $[Co(NH_3)_6]$-$[Fe(CN)_6]$, $[Co(en)_3][Co(CN)_6]$, $[Co(NH_3)_6]Cl_3$, $[Co(en)_3]Cl_3$, $K_3Co(CN)_6$, and $K_3Fe(CN)_6$ have been measured in formamide at 25°. The data have been analyzed by the Fuoss-Onsager theory. Reasonable K_A, Λ^0, and a parameters have been obtained for the 3-3 salts with the equation for associated electrolytes while for the four unsymmetrical salts Λ^0 and other parameters have been derived with the equation for unassociated electrolytes. Reasonable consistency has been found in the electrostatic and solvodynamic approaches for the ionic association for the complex 3-3 salts.

Introduction

It has been reported that several 2-2 salts[2] are much less associated in formamide than in water and the Fuoss-Onsager[3] theory explains the conductance data adequately. Although the theory has been found valid for many 1-1 salts and for several 2-2 salts in aqueous solutions,[4] little is known about its applicability to 3-3 salts.

Large spherical ions would be nearly free from solvation and therefore would closely approximate the ideal conditions of spheres moving through a homogeneous medium. The radii of such spherically symmetrical ions would permit a better prediction of the electrical and the solvodynamic properties. In order to obtain results for salts resembling the model closely, we have undertaken the study of a series of complex 3-3 salts in formamide. Complex ions such as hexacyanoferrate-(III), hexacyanocobaltate(III), hexaamminecobalt-(III), and tris(ethylenediamine)cobalt(III) have very large sizes and consequently very small charge density on their surfaces.

The present study has been carried out with a view to see how far the behavior of such salts can be predicted by the Fuoss-Onsager[3] theory.

The corresponding chlorides and potassium salts, $[Co(en)_3]Cl_3$, $[Co(NH_3)_6]Cl_3$, $K_3Co(CN)_6$, and K_3-$Fe(CN)_6$, have been studied for the evaluation of the limiting ionic conductances of the complex 3-3 salts from the law of independent ionic mobilities. Un-

fortunately, these salts are insoluble in water and hence the study could not be extended in water.

Experimental

Salts. Tris(ethylenediamine)cobalt(III)   chloride was prepared by Work's[5] method. The crystals were redissolved in water and were precipitated by addition of ethanol. This was repeated several times. The final product was dried to its constant weight at 110°. The purity of the sample was determined by the estimation of chloride.

Hexaamminecobalt(III) chloride was prepared by Bjerrum and McReynold's[6] method. After preliminary washing with ethanol, the salt was recrystallized from conductivity water and dried to constant weight at 80°.

$K_3Co(CN)_6$ was prepared by Biegelow's[7] method. The product was purified by repeated fractional precipitation with dioxane from conductivity water and

(1) (a) Grateful acknowledgments are made to the University Grants Commission, New Delhi, for granting a junior research fellowship to G. P. J.; (b) Chemistry Department, University of Maryland, College Park, Md.

(2) G. P. Johari and P. H. Tewari, *J. Phys. Chem.*, **69**, 696 (1965).

(3) R. M. Fuoss and F. Accascina, "Electrolytic Conductance," Interscience Publishers, Inc., New York, N. Y., 1959.

(4) G. Atkinson, *et al.*, *J. Am. Chem. Soc.*, **83**, 1570, 3759, 4367 (1961); *J. Phys. Chem.*, **67**, 337 (1963).

(5) J. B. Work, *Inorg. Syn.*, **2**, 221 (1946).

(6) J. Bjerrum and J. P. McReynolds, *ibid.*, **2**, 216 (1946).

(7) J. H. Biegelow, *ibid.*, **2**, 225 (1946).

Table I

Salt	Color	Solubility	Cobalt Calcd.	Cobalt Found	Nitrogen Calcd.	Nitrogen Found
[Co(en)₃] [Fe(CN)₆]	Brownish yellow	Slightly soluble	13.06	12.86	37.30	36.80
[Co(en)₃] [Co(CN)₆]	Orange	Slightly soluble	34.36	34.02	37.00	36.62
[Co(NH₃)₆] [Fe(CN)₆]	Yellow	Insoluble	15.79	15.61	45.05	44.32
[Co(NH₃)₆] [Co(CN)₆]	Orange	Insoluble	31.33	31.12	44.68	44.01

was dried *in vacuo* over P_2O_5. $K_3Fe(CN)_6$ (Judex, A.R. grade) was used after recrystallization and proper drying.

Lanthanum ferricyanide and lanthanum cobalticyanides were prepared from the pure oxide by the method of James and Willard.[8] Calculated amounts of the chloride and potassium cobalticyanide or ferricyanide were mixed in solution at 60°. The salts precipitated on cooling were washed repeatedly with conductivity water and dried over P_2O_5. Both salts attained a definite tetrahydrate form $LaX \cdot 4H_2O$. *Anal.* Calcd. for $LaFe(CN)_6$: La, 31.36. Found: La, 31.28. Calcd. for $LaCo(CN)_6$: La, 32.61. Found: La, 32.31.

The method of preparation for the 3–3 salts was based on the metathesis between complex chlorides [Co(en)₃]Cl₃, [Co(NH₃)₆]Cl₃, and $K_3Co(CN)_6$ or $K_3Fe(CN)_6$. For this, equimolar amounts of the reactants were dissolved separately in water and the two solutions were mixed with thorough stirring while the complex 3–3 salts separated out as shining crystals. As these salts were either insoluble or sparingly soluble in water, their purification was done by extensive washing with conductivity water. These were properly dried. The substances were checked for their constitution by estimating cobalt gravimetrically and nitrogen by Dumas' method. The color of the salts, their solubility, and the results of estimations are summarized in Table I.

Solvent. Formamide (Merck) was purified as reported earlier.[2] It had a specific conductance of less than 7.0×10^{-6} mho, viscosity of 0.03301 poise, density of 1.1296 g./ml., and dielectric constant of 109.50.

Measurements. The apparatus and the *modus operandi* for the conductance measurements have been described in a previous communication.[2] The conductance of the solution was obtained by subtracting the conductance of the solvent of the same batch determined separately in a cell.

Results and Discussions

The sets of equivalent conductances and concentration data for the four unsymmetrical salts [Co(en)₃]Cl₃,

[Co(NH₃)₆]Cl₃, $K_3Co(CN)_6$, and $K_3Fe(CN)_6$ are presented in Table II followed by the data for the 3–3 salts in Table III.

Table II: Equivalent Conductance, Concentration Data, and Concentration (in moles/l.)

$K_3Fe(CN)_6$ $c \times 10^4$	Λ	$K_3Co(CN)_6$ $c \times 10^4$	Λ
2.9896	31.661	1.615	32.011
4.1983	31.483	2.8926	31.778
5.4355	31.351	4.6438	31.530
7.0421	31.180	8.3237	31.192
10.026	30.959	11.912	30.841
18.716ᵃ	30.380	18.149ᵃ	30.504
25.956ᵃ	29.950	26.121ᵃ	30.003

[Co(en)₃]Cl₃ $c \times 10^4$	Λ	[Co(NH₃)₆]Cl₃ $c \times 10^4$	Λ
1.5873	31.991	2.9526	34.903
3.8425	31.442	4.3837	34.551
5.1211	31.153	6.1831	34.200
7.0373	30.775	9.3783	33.649
9.6963	30.368	14.578	33.111
12.9530	30.002	17.822	32.707
15.596	29.645	20.857ᵃ	31.898
20.037ᵃ	29.131		

ᵃ Concentrations for which $\kappa a > 0.2$ and the theory is not applicable.

The phoreograms for the four unsymmetrical salts approach the limiting law tangent from above (old criteria for unassociated salts). The data for these salts were, therefore, analyzed by the Fuoss–Onsager[3] equation in the form

$$\Lambda = \Lambda^0 - Sc^{1/2} + Ec \log c + Jc$$

The treatment is based on a Λ'–c plot. The data were analyzed by a Fortran program on IBM 7094 computer. $\lambda^0_{K^+}$ and $\lambda^0_{Cl^-}$ in formamide used in the

(8) C. James and P. C. Willard, *J. Am. Chem. Soc.*, **38**, 1497 (1916).

Table III: Equivalent Conductance, Concentration Data, and Concentration (in moles/l.)

LaFe(CN)$_6$		[Co(en)$_3$][Fe(CN)$_6$]	
$c \times 10^4$	Λ	$c \times 10^4$	Λ
1.6550	31.211	1.1417	32.113
2.2610	30.492	2.8068	29.289
3.5340	29.930	4.2228	27.782
4.0030	28.905	5.0096	27.142
4.0902	28.847	6.3122	26.234
5.3768	28.296	8.5222	24.941
5.7748	27.988	8.9135	24.738
6.2510	27.749	12.455^a	23.366
7.8161	27.125	17.573^a	21.803
8.9970	26.702		
9.7166	26.350		
10.206	26.319		
14.196^a	25.280		

[Co(NH$_3$)$_6$][Fe(CN)$_6$]		[Co(en)$_3$][Co(CN)$_6$]	
$c \times 10^4$	Λ	$c \times 10^4$	Λ
1.4892	34.260	1.0049	32.391
1.8520	33.615	1.4973	30.740
2.3681	32.898	3.1550	28.832
3.1021	31.948	3.9837	27.731
4.0790	31.011	5.2912	26.919
4.8300	30.191	7.4666	25.461
5.5655	29.411	9.2036	24.702
8.3780	27.520	13.532^a	23.214
13.7050^a	25.759	18.836^a	21.582

$c \times 10^4$	Λ
1.6696	30.702
3.9796	28.998
6.1596	27.845
8.2282	27.008
10.710	26.212
13.509^a	25.453
16.613^a	24.789

^{a} Concentrations for which $\kappa a > 0.2$ and the theory is not applicable.

analysis of the data were taken from the literature.[9] The results of the analysis are summarized in Table IV.

The phoreograms for the complex 3–3 salts approach the limiting law tangent from below thus exhibiting ion association, while in the case of lanthanum salts (Figure 1) the Λ–$c^{1/2}$ curve approaches the limiting law tangent from above, crosses it, and then approaches the limiting value from below. This behavior is similar to that of CuBDS, MnBDS, and LaNTS in water obtained by Atkinson and co-workers.[4] The data for these two salts, therefore, were analyzed by Fuoss–Onsager equation for unassociated electrolytes.[3] The equation did not give a good fit, which is not surprising.
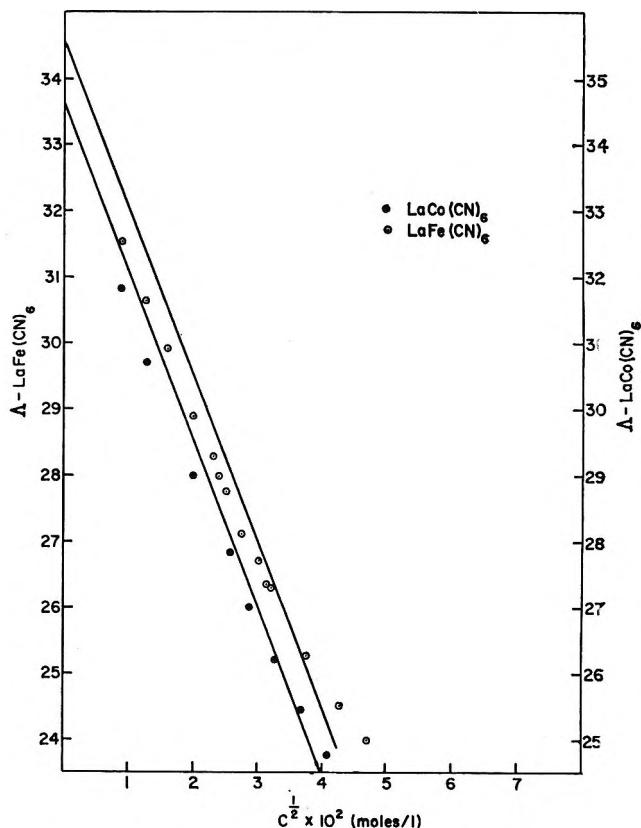
Figure 1.

These two salts are highly associated in aqueous solution[10] ($K_A = 5500$) and it may not be unreasonable to think that the salts are associated in this solvent also. The data were therefore treated as associated electrolytes by the y–x method of Fuoss using a Fortran program similar to that of Kay,[11] but the fit was poor and it gave negative K_A which is difficult to explain.

The data were further analyzed by Shedlovsky's[12] method. From a preliminary value of Λ^0 from the phoreogram final Λ^0 and K_A were obtained by the equation[13]

$$\Lambda S(Z) = \Lambda^0 - c\gamma^2 f_{\pm}^2 / \Lambda^0 K_A$$

(where K_A is the association constant, γ and $f_{\pm}$ are the same as α^2 and $y_{\pm}^2$ given in ref. 13) according to

(9) L. R. Dawson and C. Berger, *J. Am. Chem. Soc.*, **79**, 4269 (1957).

(10) C. W. Davies and J. C. James, *Proc. Roy. Soc.* (London), **A195**, 116 (1948); J. C. James, *J. Chem. Soc.*, 1094 (1950); 2925 (1951).

(11) R. L. Kay, *J. Am. Chem. Soc.*, **82**, 2099 (1960).

(12) T. Shedlovsky, *J. Franklin Inst.*, **225**, 739 (1938).

(13) H. S. Harned and B. B. Owen, "The Physical Chemistry of Electrolytic Solutions," 3rd Ed., Reinhold Publishing Corp., New York, N. Y., 1958, p. 290.

Table IV: Derived Parameters for Unsymmetrical Salts from the Fuoss–Onsager Equation

Salt	Λ^0	S	E	J	a_J	λ^0_+	λ^0_-	$\Lambda^0\eta$	$\sigma\Lambda$
$[Co(NH_3)]Cl_3$	36.56	96.9	227	803	3.5	18.90	17.66	1.207	0.003
$[Co(en)_3]Cl_3$	33.24	95.4	198	720	3.6	15.58	17.66	1.097	0.004
$K_3Co(CN)_6$	33.19	98	199	1265	7.2	12.10	21.09	1.096	0.02
$K_3Fe(CN)_6$	33.07	98	198	1300	7.3	12.10	20.97	1.092	0.02

Table V: Derived Parameters for 3–3 Salts from the Fuoss–Onsager Theory

Salt	Λ^0	K	S	E	J	$a_J \times 10^8$, Å.	$\mathring{a}_K \times 10^8$, Å. (Fuoss)	$\mathring{a}_\Lambda \times 10^8$, Å. (Stokes)	$\Lambda^0\eta$	$\sigma\Lambda$
$LaCo(CN)_6$	34.64 ± 0.11	243 ± 30	253.8	4227	15200	8.10	10.08	8.90	1.143	0.08
$LaFe(CN)_6$	34.55 ± 0.10	249 ± 27	253.5	4214	15400	8.41	9.85	8.92	1.140	0.07
$[Co(en)_3][Fe(CN)_6]$	36.47 ± 0.06	460 ± 44	261	4486	12837	6.77	7.63	8.32	1.204	0.04
$[Co(NH_3)_6][Fe(CN)_6]$	39.73 ± 0.08	426 ± 45	273	4926	14168	6.98	7.65	7.52	1.308	0.06
$[Co(en)_3][Co(CN)_6]$	36.62 ± 0.08	605 ± 66	262	4509	13914	7.93	7.05	8.33	1.209	0.06

which the slope of a $\Delta S(Z)$ vs. $c\gamma^2 f_{\pm}^2$ plot should give K_A, the association constant, and the intercept should be equal to Λ^0. In order to test if the K_A thus obtained remains unchanged, the two sets were further analyzed by the Fuoss–Onsager equation in the form

$$\Lambda_J = \Lambda + S(c\gamma)^{1/2} - Ec\gamma \log c\gamma + K_A c\gamma f_{\pm}^2\Lambda =$$
$$\Lambda^0 + Jc\gamma$$

according to which a plot of Λ_J against $c\gamma$ should be linear with J as slope and Λ^0 as intercept. K_A and γ obtained from Shedlovsky method were used to evaluate Λ_J from the above equation. The plot of Λ_J against $c\gamma$ and the Shedlovsky's plot $\Delta S(Z)$ vs. $c\gamma^2 f_{\pm}^2$ for $LaCo(CN)_6$ are given in Figure 2. The values of various parameters derived from Λ_J–$c\gamma$ plots for the two salts are given in the Table V.

The data for the other three 3–3 complex salts were analyzed by the Fuoss–Onsager[3] equation for associated electrolytes in the form

$$\Lambda = \Lambda^0 - Sc^{1/2}\gamma^{1/2} + Ec\gamma \log c\gamma + Jc\gamma - K_A c\gamma f^2\Lambda$$

on an IBM 7094 computer using a Fortran program similar to that described by Kay. K_A, the association constant, a_J derived from the J parameter of the equation, and other parameters are summarized in Table V.

As a matter of interest, the data for the three complex 3–3 salts were also analyzed by Shedlovsky's method. However, the K_A obtained for the three complex salts were 35 to 40% higher than that obtained by the Fuoss–Onsager method. It appears logically true that the K_A obtained from the Fuoss equation should be lower than that obtained from Shedlovsky's method.
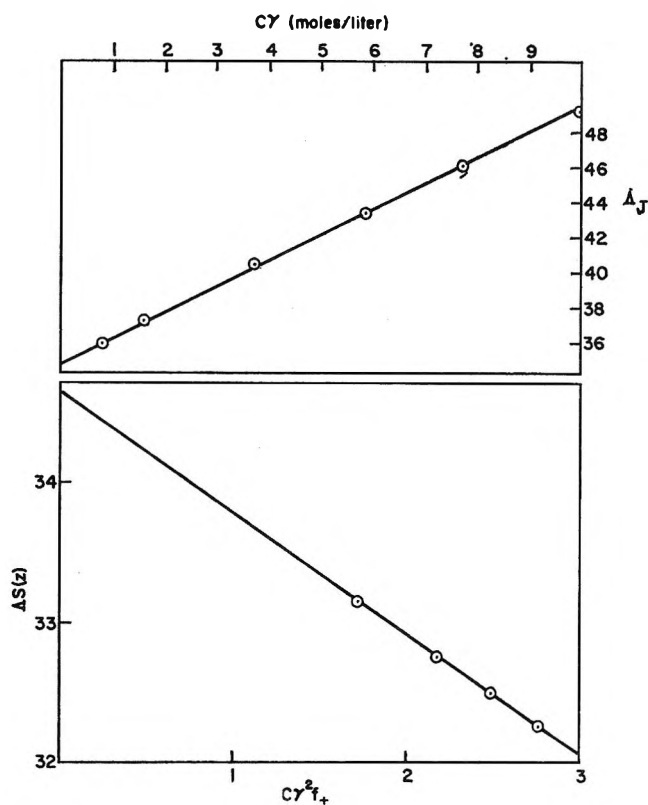
Figure 2.

$[Co(NH_3)_6][Co(CN)_6]$ could not give consistent results either by Λ_J or by the computer y–x method. This may be due to the fact that the solubility of the salt is too low for a precise conductance measurement in the solvent, and therefore the Λ–c data for this salt have been omitted.

Assuming the applicability of Stokes' law to the movement of large spherical ions of radius a and valency z acted upon an electric field xze, an ion will maintain itself at a velocity of $V = xze/6\pi\eta a$ in a continuum of viscosity η. The center-to-center ion-pair distance for a 3–3 electrolyte at 25° may be written by putting in terms of ionic mobilities as

$$\mathring{a} \text{ (Stokes } =) \frac{2.4591}{\eta}\left(\frac{1}{\lambda^0{}_+} + \frac{1}{\lambda^0{}_-}\right)$$

$\mathring{a}$ (Stokes) (a_A) for each electrolyte is summarized in Table V.

The relationship according to Fuoss[14] between K_A for an electrolyte and D of the solvent is given by

$$K_\text{A} = \frac{4\pi N}{3000} a_K{}^3 e^{z_1 z_2 e^2/a_K D k T}$$

K_A for a 3–3 electrolyte at $D = 109.50$ in this solvent were calculated from $a_K = 1$ to 25 Å. at 25° by a Fortran program. The values of K_A thus obtained were plotted against a_K and the plot was found hyperbolic in shape with the minimum at about 15 Å. (a_K). The values of a_K for the experimental K_A values were evaluated from this curve and these are given in column 8 of Table V.

Considerations of ionic mobilities show that Fe(CN)$^{-3}$ and Co(CN)$_6{}^{-3}$ ions have essentially the same sizes. Differences of ionic mobilities for Co(CN)$_6{}^{-3}$–Fe(CN)$_6{}^{-3}$ from both pairs K$_3$Co(CN)$_6$–K$_3$Fe(CN)$_6$ (Table IV) and LaCo(CN)$_6$–LaFe(CN)$_6$ (Table V) are less than 0.1 unit in each case, but the mobility for the Co(NH$_3$)$_6{}^{+3}$ ion is larger than Co(en)$_3{}^{+3}$. The difference for the mobilities of these two ions comes the same from both pairs of the salts (Table IV and Table V).

The observed mobility of La^{+3} suggests that it has greater solvodynamic dimensions than any of the [Co(NH$_3$)$_6$]$^{+3}$ or [Co(en)$_3$]$^{+3}$ ions. This is also reflected by lower K_A of its salts. K_A of the order of 5.5×10^3 in aqueous solutions[10] has been reported with an a parameter of 7.2 Å. The highly decreased value of K_A for the salts in formamide with a higher $\mathring{a}$ parameter calls for an explanation. It appears that a model in which ion–solvent interaction may be taken into consideration[15] may better account for it.

Specific interaction between ions and a definite number of solvent molecules, namely metal–ligand interaction (in which formamide acts as a ligand), may be operative. This may disturb the equilibrium between ions and ion pair in the direction of the formation of free ions resulting in decreased K_A. This speculation, however, needs the support of studies other than conductance for an adequate interpretation. We are extending the studies with these salts in mixed solvents which might also throw some light.

The Walden product $\Lambda^0\eta$ (Table V) for a 3–3 electrolyte is considerably higher than for a 2–2 or 1–1 electrolyte. This may be due to a depolymerization or reorientation of the solvent molecules in the vicinity of ions under the influence of an electric field or both. This may result in a significant variation between the macroscopic and microscopic values of the dielectric constant and the viscosity. Both of these factors effectively increase the mobility of the ions.

The reasonable agreement in the values of ion size parameters obtained from electrostatic and solvodynamic consideration ($\mathring{a}_K$, $\mathring{a}_\text{A}$) and in $\mathring{a}_J$ derived from the coefficient J of the linear long-range term suggests that the model is a good physical approximation when ion pairs are formed with large spherical ions, and Stokes' law is an adequate description for the movement of such ions. Further, the consistency of the results of $\Lambda^0 = \lambda^0{}_+ + \lambda^0{}_-$ for the complex salts also justifies the applicability of the Fuoss–Onsager equation.

Finally, we may conclude that the Fuoss–Onsager theory adequately predicts the behavior of these complex salts in formamide. We are attempting to study these salts in solvents of still higher dielectric constant and also in mixed solvents in the hope to shed more light on the problems.

(14) R. M. Fuoss, *J. Am. Chem. Soc.*, **80**, 5059 (1958).

(15) P. G. Sears, E. D. Wilhoit, and L. R. Dawson, *J. Phys. Chem.*, **59**, 374 (1955).

Radiolysis of Ethylene.   III.   Identification of Ionic Intermediates and

Formation of Excited Species by Application of Electrostatic Fields[1]

by G. G. Meisels* and T. J. Sworski

Union Carbide Corporation, Nuclear Division, Tuxedo, New York   10987   (*Received January 9, 1965*)

Formation of both methane and the methyl radical in the radiolysis of ethylene is not significantly affected by application of electrostatic fields too weak to induce secondary ionization.   This is attributed to their formation by ionic processes.   The marked enhancement in yields of molecular hydrogen, acetylene, and those products requiring hydrogen atoms and/or vinyl radicals as precursors is attributed to formation of excited species of ethylene by secondary electrons accelerated by the field.   Dissociation ensues by the processes listed below with their normalized probabilities

$$C_2H_4^* \rightarrow C_2H_2 + H_2 \qquad 0.38$$
$$C_2H_4^* \rightarrow C_2H_2 + 2H \qquad 0.46$$
$$C_2H_4^* \rightarrow C_2H_3 + H \qquad 0.16$$
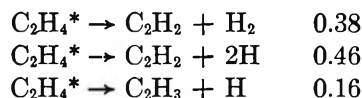
Comparison with mercury-photosensitized decomposition of ethylene indicates the role of excited states above the 4.6-e.v. triplet state.   Comparison with excitation resulting from vacuum ultraviolet and high energy radiation suggests dissociation of vibrationally excited ground state molecules formed by intersystem crossing and radiationless transitions.

Introduction

Application of electrostatic fields during radiolysis has been used by Essex and his co-workers to gain insight into the mechanism of radiation-induced reactions in the gas phase.[2]   Possible ionic and nonionic steps were inferred from reduction or limited enhancement of product yields.   Later, it was observed that yields of higher hydrocarbons from methane were increased by nearly one order of magnitude[3] at field strengths just below the onset of secondary ionization.   Since the energy of the cations is not enhanced appreciably by such small fields,[4,5] the effect must be ascribed to excitation by accelerated electrons.   Attempts to study the consequences of low energy electron impact, using the photoelectric effect for electron production,[6a] suffered from lack of sensitivity but demonstrated the validity of this interpretation.   Electric fields have been used recently to confirm the existence of ionic intermediates in propane radiolysis.[6b]

The chemical consequences of electronic excitation in ethylene have been investigated by photochemical techniques.[7-10]   Observed products could be ascribed almost exclusively to two primary processes

* Department of Chemistry, University of Houston, Houston, Texas.

(1) This paper was presented in part at the 141st National Meeting of the American Chemical Society, Washington, D. C., March 1962.

(2) (a) H. Essex, *J. Phys. Chem.*, **58**, 42 (1954);   (b) B. P. Burtt and T. Bauer, *J. Chem. Phys.*, **23**, 466 (1955);   B. P. Burtt and A. B. Zahlan, *ibid.*, **26**, 846 (1957).

(3) G. G. Meisels, W. H. Hamill, and R. R. Williams, Jr., *J. Phys. Chem.*, **61**, 1456 (1957);   P. S. Rudolph, Dissertation, Syracuse University, 1951.

(4) H. S. W. Massey and E. H. S. Burhop, "Electronic and Ionic Impact Phenomena," Oxford University Press, London, 1952.

(5) L. B. Loeb, "Basic Processes of Gaseous Electronics," University of California Press, Berkeley and Los Angeles, Calif., 1960.

(6) (a) R. R. Williams, Jr., *J. Phys. Chem.*, **63**, 776 (1959);   (b) P. Ausloos and R. Gorden, Jr., *J. Chem. Phys.*, **41**, 1278 (1964).

(7) J. R. Majer, B. Mile, and J. C. Robb, *Trans. Faraday Soc.*, **57**, 1692 (1961).

(8) M. C. Sauer, Jr., and L. M. Dorfman, *J. Chem. Phys.*, **35**, 497 (1961).

(9) H. Okabe and J. R. McNesby, *ibid.*, **36**, 601 (1962).

(10) D. W. Setser, D. W. Placzek, R. J. Cvetanović, and B. S. Rabinovitch, *Can. J. Chem.*, **40**, 2719 (1962).

$$C_2H_4 \xrightarrow{} C_2H_4^* \longrightarrow C_2H_2 + H_2 \quad \Delta H = 1.8 \text{ e.v.}$$
(1)

$$C_2H_4 \xrightarrow{} C_2H_4^* \longrightarrow C_2H_2 + 2H \quad \Delta H = 6.3 \text{ e.v.}$$
(2)
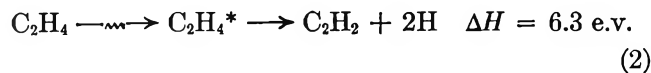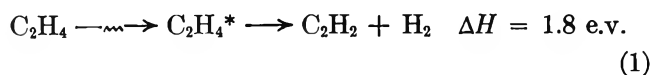
with only a very minor contribution from

$$C_2H_4 \xrightarrow{} C_2H_4^* \longrightarrow C_2H_3 + H \quad \Delta H = 4.6 \text{ e.v.}$$
(3)
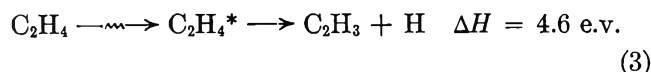
This differs from radiolytic decomposition in which the methyl radical is an important intermediate and methane is a product formed by molecular processes.[11-14] The existence of unique ion–molecule reactions for the production of CH_4 and CH_3 has been demonstrated by mass spectrometry.[15-17] This paper presents evidence that ionic processes contribute significantly to product formation in the radiolysis of ethylene and demonstrates the usefulness of applied field experiments for this purpose.

Experimental

Phillips research grade ethylene was purified by repeated distillations in a high vacuum system, the middle third being retained. Nitric oxide from the Matheson Co. was distilled from a liquid nitrogen trap. The rare gases were Matheson research grade and were used as received.

The source of radiation was a 1-Mev. Van de Graaff accelerator, High Voltage Engineering Corp. Model JN, modified for the use of electrons. Accelerator beam currents (1 to 5 μa.) were collected on a remotely controlled shutter in front of the irradiation cell, measured with an Elcor Model A-309A current indicator and integrator and periodically adjusted during radiolysis to maintain a constant rate of ionization in the irradiation cell. In a few experiments a 50-kv. X-ray source (General Electric with a Machlett AEG-50 tube) was employed as a source of ionizing radiation.

Irradiation cells were Pyrex cylinders approximately 1.9 cm. in height and 5 cm. in diameter with 0.013-cm. aluminum windows attached at the ends. High voltage was applied to the cell windows during radiolysis from a Precise Measurements Co. Model 10 kv-5MA packaged power supply controlled by an auto-transformer in its input circuit. Ionization currents in the irradiation cells were determined by measuring the potential drop across a calibrated resistor with a Leeds and Northrup Model 69950 X-Y recorder. Cells were fitted with a 2-mm. stopcock and a standard taper joint for attachment to a high vacuum system. Procedures and calibration have been described elsewhere.[18]

Gas chromatographic analyses were carried out on aliquots of the irradiated samples using a Perkin-Elmer Model 154-DG vapor fractometer. Retention volumes for the hydrocarbons were determined using authentic samples. A 2-m. column of stabilized silica gel (PE No. S) and thermal conductivity were used for detection for hydrocarbons up to n-butane, while olefins and higher hydrocarbons were separated on a 2-m. column of silver nitrate in ethylene glycol in series with a 6-m. column of bis(2-methoxyethyl) adipate and detected by flame ionization. Hydrogen was also determined by gas chromatography using a molecular sieve column and a radiofrequency detector designed and constructed by the Olefins Division of this corporation.

Results

Absolute Dosimetry. Application of an electric field during radiolysis interferes with homogeneous ion neutralization by inducing positive and negative charges to drift to the cathode and anode, respectively. The resultant observable ion current increases with increasing ratio of the electric field X to the pressure p until all ions are collected at the windows and a plateau is reached in a plot of ionization current i as a function of X/p as shown in Figure 1. Then, there is no further increase in i until the onset of secondary ionization at X/p of about 27 v. $cm.^{-1}$ $torr^{-1}$. The saturation ionization current i_s, measured at the plateau shown in Figure 1, is a measure of the rate of ionization during radiolysis. Since the energy required to produce one ion pair has been determined for ethylene ($W_{C_2H_4} = 25.9$ e.v./ion pair[19]), measurement of i_s is a method of absolute dosimetry. Dosimetry by ionization measurements can be carried out with a precision of better than 1% when using an electron accelerator as the ionizing source.[18]

Effect of Electric Fields. Application of electric fields, at X/p values just below the onset of secondary ionization, does not affect the yield of methane (Figure

(11) M. C. Sauer, Jr., and L. M. Dorfman, *J. Phys. Chem.*, 66, 322 (1962).

(12) G. G. Meisels and T. J. Sworski, *ibid.*, 69, 815 (1965).

(13) G. G. Meisels, *J. Am. Chem. Soc.*, 87, 950 (1965).

(14) G. G. Meisels, *Trans. Am. Nucl. Soc.*, 7, 308 (1964); *J. Chem. Phys.*, 42, 2328 (1965).

(15) F. H. Field, J. L. Franklin, and F. W. Lampe, *J. Am. Chem. Soc.*, 79, 2419 (1957).

(16) F. H. Field, *J. Am. Chem. Soc.*, 83, 1523 (1961); C. E. Melton and P. S. Rudolph, *J. Chem. Phys.*, 32, 1128 (1960).

(17) S. Wexler and R. Marshall, *J. Am. Chem. Soc.*, 86, 781 (1964).

(18) G. G. Meisels, *J. Chem. Phys.*, 41, 51 (1964).

(19) G. N. Whyte, *Radiation Res.*, 18, 265 (1963); J. Booz and H. G. Ebert, *Strahlentherapie*, 120, 7 (1963).
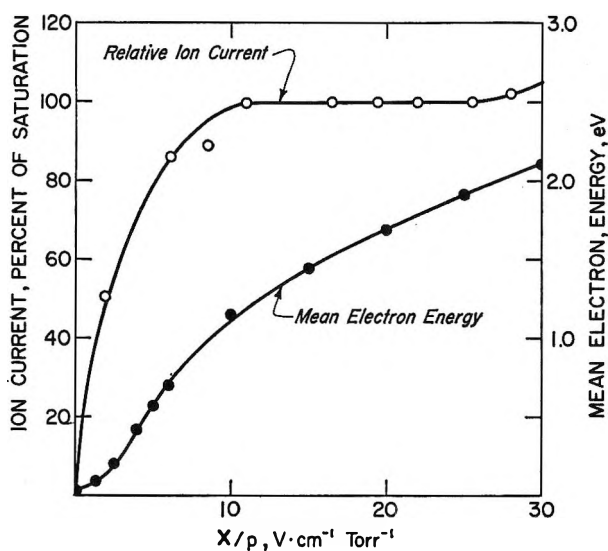
Figure 1. Dependence of relative ion current and mean electron energy[24] in ethylene on X/p.

Figure 2. Variation of methane and ethane yields with X/p.

2), causes a small increase as in the propane yield (Figure 3), but results in a marked increase in the formation of hydrogen, ethane, acetylene, n-butane, 1-butene, butadiene, n-hexane, and 1-hexene, and in ethylene disappearance (Figures 2, 4, and 5). The results for products of interest are summarized in Table I. A more complete product listing is given elsewhere.[13] M/N values (molecules of product/ion pair) are listed for experiments with and without an electric field. Values for X/p of 26.9 v. cm.$^{-1}$ torr^{-1} were selected for tabulation since the onset of secondary ionization occurs at about 27 v. cm.$^{-1}$ torr^{-1} as shown in Figure 1. The increase in M/N values attributed

Figure 3. Variation of propane yield with X/p.

to an effect of electric fields is tabulated also and is identified throughout this paper as $\Delta M/N$.

The presence of nitric oxide or oxygen during radiolysis at $X/p = 26$ (Table II) does not affect the yields of methane but eliminates the formation of ethane, n-butane, and all higher saturated hydrocarbons. The reduction of acetylene yield is probably caused by electron energy loss to the scavenger. The effect of nitric oxide on the production of butenes in the presence and absence of applied fields has already been discussed[20] and can be attributed to the simultaneous action of nitric oxide as a free-radical scavenger and charge acceptor from butene ion.

Table I: Effect of Electric Field (at X/p of 26.9 v. cm.$^{-1}$ torr^{-1}) on Product Yields in the Radiolysis of Ethylene (50 torr)

Product	M/N^a (no field)	M/N (26.9 v. cm.$^{-1}$ torr^{-1})	$\Delta M/N^b$
Hydrogen	0.34	3.64	3.3
Methane	0.067	0.067	0.00
Ethane	0.16	0.76^c	0.60
Acetylene	0.87	8.7	7.8
Propane	0.18	0.29	0.11
n-Butane	0.56	3.8	3.24
Butene-1	0.060	0.33	0.27
Butadiene	0.004	0.083	0.079
n-Hexane	0.036	0.302	0.266
Hexene-1	0.013	1.165	1.152
Ethylene	−5	−34	−29

^{a} Molecules per ion pair. ^{b} Net change due to applied field. ^{c} Interpolated.

(20) G. G. Meisels, *J. Chem. Phys.*, **42**, 3237 (1965).
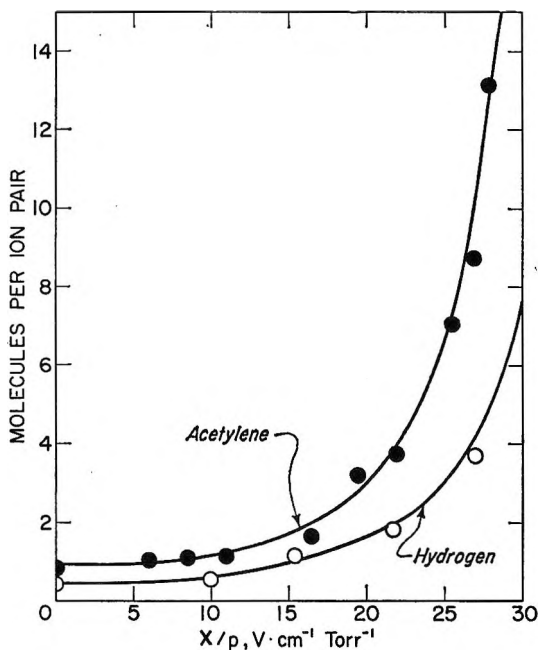
Figure 4. Variation of hydrogen and acetylene yields with X/p.

Figure 6. Effect of rare gases on enhancement of acetylene yield by applied fields: 50 torr of C_2H_4 (O), 200 torr of Ar added (◐), 200 torr of Kr added (◑), 200 torr of Xe added (●).

Figure 5. Variation of n-butane (O), butene-1 (●), and hexene-1 (◒) yields with X/p.

The addition of rare gases reduces the extent of product enhancement by the applied field (Figure 6) when X/p is expressed in volts cm.$^{-1}$ (torr of ethylene)$^{-1}$ and yields are calculated on the basis of primary ionization in ethylene alone, that is, by neglecting the presence of the rare gas and using ionization rates from ethylene samples not containing argon. The point plotted at the highest X/p for each rare gas

Table II: Effect of Scavengers and Applied Fields on the Radiolysis of Ethylene

Torr of C_2H_4	50	60	51	52
Torr of NO	10	10	...	...
Torr of O_2	..	...	5	...
X/p, v. cm.$^{-1}$ (torr of C_2H_4)$^{-1}$	..	25.7	26.2	25.7
Product	Yield, molecules/ion pair			
Methane	0.065	0.066	0.064	0.068
Ethane	...	...	...	0.70
Acetylene	0.90	5.8	7.4	7.6
Propane	...	...	...	0.27
n-Butane	...	...	...	2.6
Butene-1	0.047	0.045	0.026	0.31
cis-Butene-2	0.190	0.187	0.042	0.010
trans-Butene-2	0.149	0.151	0.026	0.015
Butadiene	0.007	...	...	0.084
n-Hexane	...	...	...	0.250
Hexene-1	...	...	...	1.03

corresponds to the onset of secondary ionization. Krypton and xenon are equally effective while argon reduces yields less efficiently. The effect of xenon pressure on butane and acetylene yields at fixed values of X/p (ethylene) was evaluated using 50-kv. X-rays as the ionizing source (Figure 7).

Discussion

Physical Interactions. The physical behavior of ions and electrons in the presence of electrostatic fields has
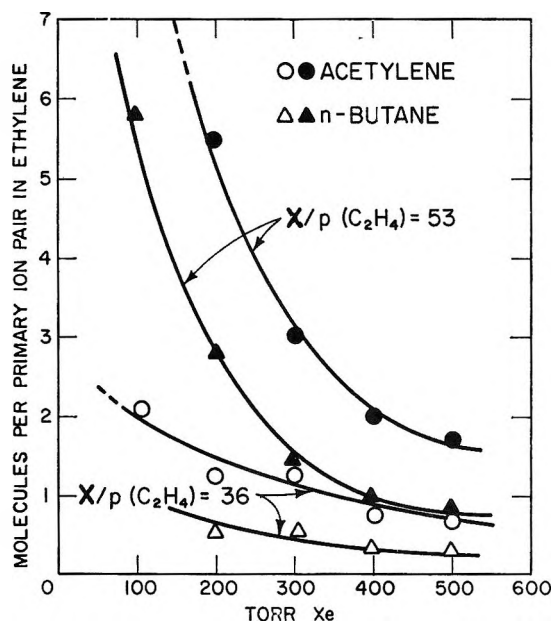
Figure 7. Dependence of product enhancement by the applied field on xenon pressure at fixed X/p (C_2H_4).

received considerable attention.[4,6] It has been established that the energy distribution of molecular ions is not shifted appreciably even when X/p exceeds the value at which secondary ionization sets in. Product enhancement by application of fields therefore cannot be ascribed to their effect on ion energy.

Collection of an ion current during irradiation is brought about by a change from ion recombination in the gas resulting from ambipolar diffusion to more rapid heterogeneous neutralization at or near the electrodes. This reduces the lifetime of the charge and the number of collision processes it experiences before neutralization. The frequency of charge–molecule interactions will also be reduced by the influence of the increased energy on the cross section for such processes.[21] Although these effects will reduce the total number of possible ion–molecule reactions a charge can undergo, primary ion fragmentation and the initial ion–molecule reactions should not be altered.

Neutralization at the electrodes may eliminate decomposition of ionic species by allowing dissipation of the recombination energy to the surface.[2a] However, field emission caused by the approaching charge is induced at a distance of several Ångstroms.[22] The ion could be neutralized more than ten vibrational lifetimes before energy equilibration with the surface becomes possible, and rapid dissociation processes may therefore be unaffected by fields. The effect of electrostatic fields on product yields resulting from intermediate ions should be minor and lead primarily

to the reduction of processes requiring a large number of collisions or homogeneous ion–electron recombination. As shown in Figures 2 to 5, product yields do not change appreciably when X/p is increased from 0 to 10 v. cm.$^{-1}$ torr^{-1} even though the fraction of neutralization processes occurring at the electrodes varies between 0 and 1. Further increases in X/p should produce no significant changes caused by ion collection, and a mechanism based on this effect cannot be held responsible for marked enhancement of yields at high X/p.

The electron energy distribution is shifted appreciable to higher values by applied fields. Experimental measurements of electron energy have generally been based on the Townsend method,[4] which assumes a Maxwellian energy distribution of the electron swarm. This assumption, although incorrect, is justified because the influence of the energy distribution on the average electron velocity calculated from the experimental data has been shown to be less than ca. 10%.[23] The mean energy of a steady-state electron swarm in ethylene is shown in Figure 1 and is ca. 2 e.v. at the onset of secondary ionization.[24] Electric fields should influence primarily the energy distribution of nearly thermal electrons, and it should be a fair approximation to apply considerations for a steady-state swarm to radiolysis conditions. Consequently, we attribute a marked increase in product yield at X/p values less than 27 to production of neutral excited states of ethylene by electrons accelerated by the field.

Products Resulting from Ionic Intermediates. The observation that the methane yield is invariant in the presence of an electric field at X/p values less than 27 is striking evidence for the participation of ionic precursors in its formation. This suggestion is further supported by its persistence in the presence of large excesses of nitric oxide or oxygen,[14] indicating that no free-radical precursors are required. Reported ion–molecule reactions[16]

$$C_2H_3^+ + C_2H_4 \longrightarrow [C_4H_7^+] \qquad (4)$$

$$[C_4H_7^+] + C_2H_4 \longrightarrow [C_6H_{11}^+] \qquad (5)$$

$$[C_6H_{11}^+] \longrightarrow CH_4 + C_5H_7^+ \qquad (6)$$
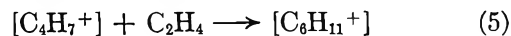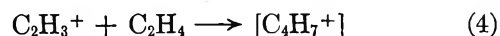
(21) (a) P. Langevin, *Ann. chim. phys.*, 5, 245 (1905); (b) G. Gioumousis and D. P. Stevenson, *J. Chem. Phys.*, 29, 294 (1958); (c) T. F. Moran and W. H. Hamill, *ibid.*, 39, 1413 (1963).

(22) S. A. Korff, "Electron and Nuclear Counters: Theory and Use," 2nd Ed., D. Van Nostrand Co., Inc., New York, N. Y., 1955.

(23) R. H. Healey and J. W. Reed, "The Behaviour of Slow Electrons in Gases," Amalgamated Wireless (Australasia) Ltd., Sydney, Australia, 1940.

(24) J. Eannon and H. L. Brose, *Phil. Mag.*, 6, 817 (1928).

adequately account for methane formation. It should be noted that reaction 4 requires a vinyl ion intermediate in contrast with the suggestion that primary ion dissociation may not occur at the pressures employed in this investigation.[25]

Propane formation is only slightly enhanced by the electric field. Its elimination by nitric oxide or oxygen indicates that free-radical precursors are required for its formation, probably methyl and ethyl radicals

$$CH_3 + C_2H_5 \longrightarrow C_3H_8 \qquad (7)$$
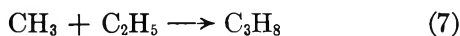
The relatively slight enhancement of the propane yield can be attributed to a decrease in the $[CH_3]/[C_2H_5]$ ratio resulting from formation of ethyl radicals by excitation. Therefore, a larger fraction of the methyl radicals yields propane instead of combining to form ethane or adding to ethylene. We conclude that methyl radicals are formed predominantly by ionic processes such as the ion–molecule reactions summarized by the over-all processes

$$C_2H_4^+ + C_2H_4 \longrightarrow C_3H_5^+ + CH_3 \qquad (8)$$

$$C_2H_4^+ + 2C_2H_4 \longrightarrow C_5H_9^+ + CH_3 \qquad (9)$$

$$C_2H_2^+ + 2C_2H_4 \longrightarrow C_5H_5^+ + CH_3 + H_2 \qquad (10)$$
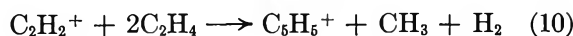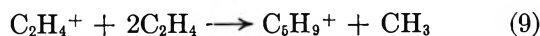
observed in the mass spectrometer.[15-17]

Products Resulting from Excited Intermediates. The oscillator strength of optically forbidden levels for interaction with electrons of a typical degradation spectrum is low.[26,27] The main contribution is ascribed to allowed levels corresponding to formation of ethylene molecules in higher excited and superexcited[27] states. This is in sharp contrast with the nonapplicability of selection rules to excitation by slow electrons. Consequently, slow electron swarms should yield principally the lowest triplet state at 4.6 e.v. and the symmetry-forbidden state at 6.5 e.v.[28] with smaller contributions from higher optically allowed and forbidden states.

Low energy electron swarms clearly produce excited states which may dissociate according to reactions 1, 2, or 3. Their relative rates are given by the hydrogen, acetylene, and vinyl radical yields. Hydrogen and acetylene formation can be measured directly, but the vinyl radical yield must be deduced from considerations of the free-radical processes. Hexene-1, butene-1, and butadiene-1,3 presumably result principally[29] from the reactions

$$C_2H_3 + C_2H_4 \longrightarrow C_4H_7 \qquad (11)$$

$$C_4H_7 + C_2H_5 \longrightarrow \begin{cases} 1\text{-}C_6H_{12} & (12a) \\ 1\text{-}C_4H_8 + C_2H_4 & (12b) \\ 1,3\text{-}C_4H_6 + C_2H_6 & (12c) \end{cases}$$
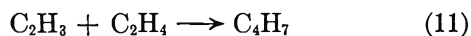
The elimination of hexene-1 by nitric oxide and oxygen indicates the absence of a molecular mechanism for its formation. The importance of these reactions in the liquid phase has been demonstrated by e.p.r.[29] and chemical techniques.[30]

Hydrogen results only from molecular detachment processes.[11,12] The relative rates of the primary processes 1 to 3 at $X/p = 26.9$ v. cm.$^{-1}$ torr^{-1} can now be obtained from Table I, column 3, setting $r_1 = \Delta(M/N)(H_2) = 3.3$ and $r_2 = \Delta(M/N)(C_2H_2) - \Delta(M/N)(H_2) = 4.5$ species/ion pair. The rate of step 3 can be estimated from the vinyl radical yield

$$r_3 = \Delta(M/N)(C_2H_3) = \Delta(M/N)(\text{hexene-1}) +$$
$$\Delta(M/N)(\text{butene-1}) + \Delta(M/N)(\text{butadiene})$$
$$= 1.5 \text{ species/ion pair}$$

Alternately, the relative contribution of the three primary steps can be estimated from the yields of acetylene, vinyl radicals, and hydrogen atoms. Under our conditions all hydrogen atoms add to ethylene,[12] and the resulting ethyl radicals undergo primarily the combination reactions ((7), (12), and (14))

$$H + C_2H_4 \longrightarrow C_2H_5 \qquad (13)$$

$$2C_2H_5 \longrightarrow n\text{-}C_4H_{10} \qquad (14a)$$

$$\longrightarrow C_2H_6 + C_2H_4 \qquad (14b)$$
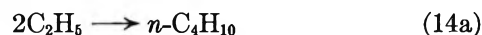
Ethyl radicals may also add to ethylene to yield *n*-butyl radicals. These will primarily lead to the formation of *n*-hexane.[13] The yield of hydrogen atoms may now be obtained from the product distribution by summing those which require ethyl radicals as precursors

$$\Delta(M/N)(H) = \Delta(M/N)(C_2H_5) =$$
$$2[\Delta(M/N)(C_2H_6) + \Delta(M/N)(C_4H_{10}) +$$
$$\Delta(M/N)(C_6H_{14})] + \Delta(M/N)(C_3H_8) +$$
$$\Delta(M/N)(\text{hexene-1}) + \Delta(M/N)(\text{butene-1}) -$$
$$\Delta(M/N)(C_4H_6) = 9.7 \text{ atoms/ion pair}$$

(25) D. P. Stevenson, *Radiation Res.*, **10**, 610 (1959).

(26) L. V. Spencer and U. Fano, *Phys. Rev.*, **93**, 1172 (1954).

(27) R. L. Platzman, *Vortex*, **23**, 372 (1962).

(28) A. Kupperman and L. M. Raff, *Discussions Faraday Soc.*, **35**, 30 (1963).

The stoichiometry of reactions 1 to 3 and the yields of hydrogen atoms, acetylene, and vinyl radical lead to the estimates $r_1 = 3.7$, $r_2 = 4.1$, and $r_3 = 1.5$. The values derived by the two methods are within experimental error of each other since small variations of the applied voltage produce large changes in yield when the enhancement is large. It may be noted that reactions of vinyl radicals with ethyl radicals cannot account for the difference

$$C_2H_3 + C_2H_5 \longrightarrow \begin{cases} C_2H_2 + C_2H_6 & \text{(15a)} \\ 2C_2H_4 & \text{(15b)} \\ 1\text{-}C_4H_8 & \text{(15c)} \end{cases}$$
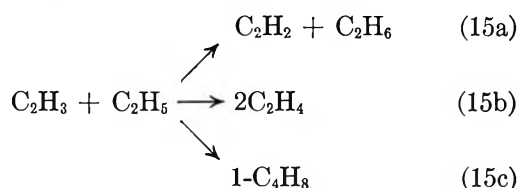
since (15a) would be counted as process 2, (15b) as complete lack of reaction, and (15c) as process 3. Moreover, the ratio $[C_2H_6]/[C_4H_{10}] = 0.19$ is lower than that observed in deuterium–ethylene mixtures under similar conditions[12] indicating the absence of reaction 15a.

Effect of Rare Gases. The presence of rare gases reduces the enhancement caused by the field at any particular field strength. This effect of rare gases is attributed to energy loss resulting from elastic scattering of the incident electron against the field. Enhanced ionization in argon containing 0.1% ethylene at X/p of the order of 0.5 v. cm.$^{-1}$ (torr of Ar)$^{-1}$ has been ascribed to excitation of argon to resonant levels and subsequent ionization of ethylene by energy transfer.[31] Such processes are not observed under our conditions since the reduction of yields is not accompanied by field-dependent secondary ionization.

Comparison with Other Methods of Excitation. The yield of hydrocarbon products accounts for only two-thirds of the consumed ethylene (Table I). This does not prevent a comparison with the results of ethylene decomposition by other methods since the importance of all three primary processes under our conditions seems well established.

The mercury-photosensitized decomposition of ethylene proceeds predominantly *via* reaction 1. It is currently interpreted on the basis of triplet ethylene formation by $Hg(^3P_1)$ with an excitation energy of 4.9 e.v.[10,32–35] The apparent primary formation of hexene and butene can probably be attributed to reactions 3 and 12 suggested here, so that the over-all reaction (3) accounts for *ca.* 8% of the primary processes. It has been suggested that this sequence is unimportant in the mercury-sensitized photolysis since it would not explain the incorporation of deuterium into the hexene-1 molecule when deuterium is

added to the system.[7] However, isotopic exchange of

$$H + D_2 \longrightarrow HD + D \tag{16}$$
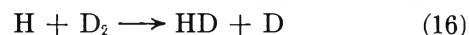
hydrogen atoms from ethylene with deuterium (reaction 16) is known to be competitive with hydrogen atom addition to ethylene since $k_{13}/k_{16} = 14 \pm 5$.[12,16] The small but apparently real contribution of step 3 may not result from the decomposition of an excited ethylene molecule but from the reaction[31,32]

$$Hg(^3P_1) + C_2H_4 \longrightarrow C_2H_3 + HgH \tag{17}$$
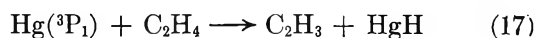
The relative extent of the apparent processes (1 and 3) may only represent the ratio of quenching to abstraction efficiencies which are known to be of this order.[32,36]

The contribution of process 3 to the mechanism of the vacuum ultraviolet photochemistry of ethylene at 1470 Å. (8.4 e.v.)[8] can be estimated on the basis of the reported yield of butene-1 as 5% of n-butane. Assuming that $[C_2H_3]/[1\text{-}C_4H_8] = 3.3$ as in the mercury-photosensitized decomposition[7] one obtains $\phi_3/\Sigma\varphi = 0.08$, while the apparent ratio of vinyl radical to butene-1 yields in this investigation leads to $\phi_3/\Sigma\varphi = 0.14$. Unfortunately, a similar analysis of the photolysis at 1236 Å. (10.0 e.v.)[9] is not possible since the radicals resulting from a small contribution of step 3 do not significantly influence the relative proportions of hydrogen, acetylene, ethane, and n-butane.

The relative extent of the three processes in the radiolysis can be approximated since it is possible to account quantitatively for the formation of hydrogen atoms by assuming that acetylene is formed only by excitation processes and that the formation of acetylene ion can be calculated from mass spectrometry.[12] Since $(M/N)(C_2H_3) = 0.025$[13] and $(M/N)(C_2H_2) = 0.87$ species/ion pair, process 3 accounts for less than 3% of the total primary excitation steps in ethylene radiolysis. The origin of the molecular hydrogen yield is uncertain. If we make the reasonable assumption that acetylene ion formation is accompanied by

(29) R. H. Schuler and R. W. Fessenden, *J. Chem. Phys.*, **39**, 2147 (1963).

(30) R. A. Holroyd and R. W. Fessenden, *J. Phys. Chem.*, **67**, 2743 (1963).

(31) M. M. Shahin and S. R. Lipski, *J. Chem. Phys.*, **41**, 2021 (1964); *Anal. Chem.*, **35**, 1562 (1963).

(32) E. W. R. Steacie, "Atomic and Free Radical Reactions," 2nd Ed., Reinhold Publishing Corp., New York, N. Y., 1954.

(33) K. J. Laidler, "The Chemical Kinetics of Excited States," Oxford University Press, London, 1955.

(34) R. J. Cvetanović and A. B. Callear, *J. Chem. Phys.*, **23**, 1182 (1955); **24**, 873 (1956).

(35) S. Arai and S. Shida, *ibid.*, **38**, 694 (1963).

(36) H. E. Gunning and O. P. Strausz, *Advan. Photochem.*, **1**, 209 (1963).

the elimination of molecular hydrogen, an upper limit of 87% may be set on the relative extent of step 2.

The normalized probabilities of the three processes obtained by the preceding considerations are summarized in Table III, using average values when necessary. The relative dissociation probabilities for ethylene at 50 torr excited by slow electrons at X/p = 26.9 differ markedly from ethylene excited by mercury sensitization to the 4.6-e.v. triplet state. This

Table III: Relative Dissociation Probabilities of Excited Ethylene Produced by Various Techniques[a]

	Mercury photo-sens.	Slow electrons (X/p = 26.9)	Vacuum ultraviolet photolysis 1470 Å.	Vacuum ultraviolet photolysis 1236 Å.	High energy radiation
Process			Relative dissociation probability		
$C_2H_2 + H_2$	0.92	0.38	0.44	<0.26	≥0.10
$C_2H_2 + 2H$	...	0.46	0.45	<0.74	≤0.87
$C_2H_3 + H$	0.08	0.16	0.11	>0.0	0.03

[a] The method of estimating these values is discussed in the text.

is not surprising since at 50 torr the decomposition of the 4.6-e.v. triplet state is largely quenched.[32,35] Dissociation by slow electrons at 50 torr must, therefore, be attributed largely to shorter-lived, higher excited states

of ethylene such as the symmetry-forbidden state at 6.5 e.v. or higher singlet states. The probability for excitation of ethylene to such higher excited states is not too low since the high energy portion of the electron swarm is not eliminated by the presence of resonance levels. Assuming a Maxwellian energy distribution for the electron swarm, it can be shown that about 25% of the electrons that are capable of exciting ethylene to the 4.6-e.v. state can excite ethylene to the 6.5-e.v. state.

Excitation to the 6.5-e.v. and higher states permits all possible dissociation processes to ensue. However, examination of Table III reveals that increasing energy of excitation favors process 2 at the expense of the other two. This may result from dissociation of vibrationally excited ground-state molecules formed by intersystem crossing and radiationless transitions, increasing energy favoring the most endothermic process. Such a mechanism has been suggested by Cundall, et al.,[37] for dissociation of the lowest triplet state.

(37) R. B. Cundall, F. J. Fletcher, and D. G. Milne, *Trans. Faraday Soc.*, **60**, 1146 (1964).

Multicomponent Diffusion Involving High Polymers. III. Ternary

Diffusion in the System Polystyrene 1-Polystyrene 2-Toluene

by E. L. Cussler, Jr.,[1] and E. N. Lightfoot

Department of Chemical Engineering, University of Wisconsin, Madison, Wisconsin 53706
(Received January 22, 1965)

Ternary diffusion coefficients for two concentrations of mixtures of two monodisperse polystyrenes of different molecular weight in toluene were measured at 25.00° with the Gouy interferometer. This system was chosen as a model of a polydisperse polymer suitable for experimental study. The results show large multicomponent effects for diffusion coefficients based on concentration gradient. The coefficients measured satisfy the Onsager reciprocal relations within experimental error. They are in qualitative agreement with those predicted from extensions of the hydrodynamic model.

The objective of the work presented here is the measurement and prediction of the diffusional behavior of solutions of polydisperse polymers. Dilute solutions of these polymers are adequately described by extensions of binary techniques,[2] but more concentrated solutions may require consideration of diffusional coupling. Since a true polydisperse system is very difficult to study, a system of mixtures of two different sharp fractions of polystyrene was chosen for experimental investigation. Deviations from binary behavior of this pseudo-polydisperse system are measured experimentally. The results are compared with calculations based on simple extensions of the hydrodynamic theory discussed below.

Theory

Model Chosen. A solution containing $n - 1$ homologs of a polymer may be idealized as a suspension of $n - 1$ species of spheres of different sizes in a viscous continuum. The diffusional behavior of this system is approximated by a modification of the hydrodynamic theory. The radii of the spheres are the "effective diameters for diffusion." Because a polymer molecule in solution is not a rigid sphere but is loosely extended through the solution, these "effective radii" are much larger than those calculated from the molecular weight and the density of the pure polymer. The idealized spheres thus contain some "trapped" solvent, which is considered as part of the polymer "spheres."

At infinite dilution, the diffusional behavior of such a system is given by the hydrodynamic theory, with the diffusion coefficient D_{ii} given by Stokes' law

$$D_{ii} = \frac{kT}{6\pi\eta a_i} \tag{1}$$

where k is Boltzmann's constant, T is the absolute temperature, a_i is the effective radius mentioned previously, and η is the solvent viscosity. However, at finite sphere concentrations, the solute species interact with one another. The diffusion of a sphere of species i affects the diffusion of spheres of all other species. At low sphere concentrations, we assume that the spheres of all species have their equilibrium distribution and that they do not collide. In this case, the interactions between spheres can be treated as perturbations of the fluid velocity. This approach was developed for the intrinsic viscosity and the frictional coefficient of binary polymer-solvent systems in excellent papers by Peterson and Fixman[3] and Pyun and Fixman.[4] Their approach is used in the development to be given.

Analysis of Model. The first step in the development is to find the sphere velocity of species i as a func-

(1) Department of Physical Chemistry, University of Adelaide, Adelaide, South Australia.

(2) (a) M. Daune and H. Benoit, *J. chim. phys.*, 51, 233 (1955); (b) E. L. Cussler, Jr., *J. Phys. Chem.*, 69, 1144 (1965).

(3) J. M. Peterson and M. Fixman, *J. Chem. Phys.*, 39, 2516 (1963).

(4) C. W. Pyun and M. Fixman, *ibid.*, 41, 937 (1964).

tion of the sphere concentrations and the sphere velocities at infinite dilution. The average velocity $\mathbf{v}_i$ of a sphere of species i may be written as a power series in the number density d_j of each species of spheres

$$\mathbf{v}_i = \mathbf{v}_i(1) + \sum_{j=1}^{n-1} d_j \int_C^{\infty} [\mathbf{v}_i(1,2) -$$
$$\mathbf{v}_i(1)] f_{ij} \, dV(\mathbf{r}) + \ldots \quad (2)$$

where $\mathbf{v}_i(1)$ is the unperturbed sphere velocity at radius $\mathbf{R}_1$ with only one sphere in the system; $\mathbf{v}_i(1,2)$ is the sphere velocity at $\mathbf{R}_1$ with a sphere of species j at $\mathbf{R}_2$; and f_{ij} is the distribution function of spheres of i and j. The differential volume $dV(\mathbf{r})$ is that located at $\mathbf{r} = \mathbf{R}_2 - \mathbf{R}_1$. If only small forces act on the particles, and if particles do not collide but interact only through their velocity fields, the distribution function may be assumed to be the equilibrium distribution function

$$f_{ij} = 1 \quad r > \sigma_{ij}$$
$$f_{ij} = 0 \quad r < \sigma_{ij} \quad (3)$$

where $\sigma_{ij} = a_i + a_j$ is the collision diameter between spheres of i and j.

The solvent velocity $\mathbf{v}_n^{\mathrm{u}}$ may be described similarly as

$$\mathbf{v}_n^{\mathrm{u}} = \mathbf{v}_n^{\mathrm{u}}(1) + \sum_{j=1}^{n-1} d_j \int_0^{\infty} [\mathbf{v}_n^{\mathrm{u}}(1,2) -$$
$$\mathbf{v}_n^{\mathrm{u}}(1)] f_{nj} \, dV(\mathbf{r}) + \ldots \quad (4)$$

where, parallel to the above, $\mathbf{v}_n^{\mathrm{u}}(1)$ is the solvent velocity at $\mathbf{R}_1$ if no spheres are present (i.e., $\mathbf{v}_n^{\mathrm{u}}(1) = 0$) and $\mathbf{v}_n^{\mathrm{u}}(1,2)$ is the solvent velocity at $\mathbf{R}_1$ with a sphere of j at $\mathbf{R}_2$. The superscript u emphasizes that the solvent velocity used here is that of the untrapped solvent. As before, the distribution function is assumed to be that at equilibrium

$$f_{nj} = 1 \quad r > a_j$$
$$f_{nj} = 0 \quad r < a_j \quad (5)$$

Combining eq. 2 and 4, we obtain an expression for the sphere velocity relative to the untrapped solvent velocity

$$\mathbf{v}_i - \mathbf{v}_n^{\mathrm{u}} = \mathbf{v}_i(1) + \sum_{j=1}^{n-1} d_j \left(-\int_{a_j}^{\sigma_{ij}} \mathbf{v}_n(1,2) \, dV(\mathbf{r}) + \right.$$
$$\left. \int_{\sigma_{ij}}^{\infty} [\mathbf{v}_i(1,2) - \mathbf{v}_i(1) - \mathbf{v}_n(1,2)] \, dV(\mathbf{r}) \right) \quad (6)$$

The integrals are evaluated in the Appendix by following the technique of Pyun and Fixman.[4] The result is

$$\mathbf{v}_i - \mathbf{v}_n^{\mathrm{u}} = \sum_{j=1}^{n-1} F_{ij} [\mathbf{v}_i(1) - \mathbf{v}_n^{\mathrm{u}}(1)] \quad (7)$$

where

$$F_{ij} = \delta_{ij} \left[1 - \sum_{k=1}^{n-1} \phi_k^{\mathrm{S}} \left[\frac{15 a_i}{4 \sigma_{ik}} \right] \left[1 - \frac{(1/5 a_k^2 + 1/3 a_i^2)}{\sigma_{ik}^2} + \frac{a_k^2 a_i^2}{5 \sigma_{ik}^4} \right] \right] - \phi_j^{\mathrm{S}} \left[\frac{3}{2} \left[\frac{\sigma_{ij}^2}{a_j^2} - 1 \right] - \frac{3}{4} \left[\frac{5 a_j a_i^5}{\sigma_{ij}^6} - \frac{5 a_j^5 a_i^3 + 8 a_j^3 a_i^5}{8 \sigma_{ij}^8} + \frac{11 a_i^5 a_j^5}{10 \sigma_{ij}^{10}} \right] \right] \quad (8)$$

where ϕ_k^{S} is the volume fraction of spheres of species k, equal to $4/3 \pi a_k^3 d_k$. The equations give the average sphere velocity as a function of the sphere velocity at infinite dilution and of the sphere radii.

We now rewrite eq. 7 as a multicomponent flux equation with the help of Stokes' law

$$\mathbf{v}_j(1) = -\frac{\nabla \mu_j}{6 \pi \eta a_j \bar{N}} \quad (9)$$

where μ_j is the chemical potential and $\bar{N}$ is Avogadro's number. By putting this expression for $\mathbf{v}_j(1)$ into eq. 7, we obtain

$$-\rho_i(\mathbf{v}_i - \mathbf{v}_n^{\mathrm{u}}) = \sum_{j=1}^{n-1} L_{ij}^{\mathrm{u}} \nabla \mu_j \quad (10)$$

where ρ_i is the mass density and

$$L_{ij}^{\mathrm{u}} = \frac{\rho_i F_{ij}}{6 \pi \eta a_j \bar{N}} \quad (11)$$

These phenomenological coefficients which are based on the average velocity of the untrapped solvent may be converted by the following transformation to the multicomponent diffusion coefficients D_{ij} relative to the volume-average velocity[5]

$$D_{ij} = \sum_{k=1}^{n-1} \sum_{l=1}^{n-1} \left(\delta_{ik} - \phi_k^{\mathrm{S}} \frac{\omega_i}{\omega_k} \right) L_{kl}^{\mathrm{u}} \left(\frac{\partial \mu_l}{\partial \rho_j} \right)_{\rho_m \neq j, n} \quad (12)$$

where the ω_i are the mass fractions. From the theory of dilute polymer solutions, we have the relation[6,7]

$$\left(\frac{\partial \mu_l}{\partial \rho_j} \right)_{\rho_m \neq j, n} = \frac{RT}{\rho_l} (\delta_{lj} + 2 M_l A_2 (\rho - \rho_n)) \quad (13)$$

where M_l is the molecular weight of species l and A_2 is the second virial coefficient of the osmotic pressure.[8] Thus, from eq. 8, 11–13, we may calculate multicomponent diffusion coefficients if we know the diffusion coefficients at infinite dilution and the solvent viscosity.

(5) S. R. de Groot and P. Mazur, "Non-Equilibrium Thermodynamics," North-Holland Publishing Co., Amsterdam, 1962, pp. 239–246.

(6) R. L. Scott, J. Chem. Phys., 17, 279 (1949).

(7) P. J. Flory and W. R. Krigbaum, ibid., 18, 1086 (1950).

(8) L. Mandelkern and P. J. Flory, ibid., 19, 984 (1951).

The $L_{ij}{}^{u}$ defined by eq. 11 do not obey the Onsager reciprocal relations. The reason for this discrepancy is not known.[8a] Because of abundant experimental support,[9] these symmetric relations are expected to hold experimentally for this system. A necessary and sufficient condition for their validity is[10]

$$a_{11}D_{12} + a_{12}D_{22} = a_{21}D_{11} + a_{22}D_{21} \qquad (14)$$

where

$$a_{ij} = \sum_{k=1}^{n-1}\left(\delta_{ij} + \frac{\rho_k \bar{V}_j}{\rho_n \bar{V}_n}\right)\left(\frac{\partial \mu_k}{\partial \rho_l}\right)_{\rho l \neq i, n} \qquad (15)$$

and $\bar{V}_j$ is the partial specific volume of species j. These equations will allow testing the Onsager reciprocal relations with the data which follow.

Experimental

Materials. The two polystyrenes used in these experiments were kindly provided by J. W. McCormick of the Dow Chemical Co. Sample S109 had a number-average molecular weight of 182,000 and a weight-average molecular weight of 193,000. Sample S111 had a number-average molecular weight of 217,000 and a weight-average molecular weight of 234,000. These weights were determined by sedimentation velocity experiments. Reagent grade toluene was used in all experiments.

Procedure. The Gouy interferometer and the procedure used in these experiments have been described previously.[11-13] The only change in experimental procedure was in the formation of the initial boundary. The boundary was first roughly formed. Diffusion was allowed to occur, and the boundary was reformed. The technique, which allows formation of the boundary with a smaller volume of solutions, is especially effective for polymers and proteins.[14] Densities were calculated from partial specific volume data in the literature.[15] The value for the second virial coefficient in toluene, a good solvent, was taken as 3.96×10^{-4} cm.[3] mole/g.[2,16]

The Gouy interferometer gives two experimental parameters, the "reduced height-area ratio" $\mathfrak{D}_A$ and the "area under the fringe deviation graph" Q. For a binary experiment, three assumptions are made: the diffusion coefficient is independent of composition, the refractive index varies linearly with composition, and the partial specific volumes are constant. In this case, $\mathfrak{D}_A$ equals the binary diffusion coefficient $D(\bar{\rho})$ at the average composition $\bar{\rho}$, and Q is zero.

However, in the binary systems studied in this work, these assumptions are not valid. To remove the concentration dependence, $\mathfrak{D}_A$ and Q must be measured at the same value of $\bar{\rho}$ but at different $\Delta\rho$. The true values are found from the extrapolations

$$\mathfrak{D}_A = D(\bar{\rho})[1 + P(\Delta\rho)^2 + \ldots] \qquad (16)$$

$$Q = S(\Delta\rho)^2 \qquad (17)$$

The first of these relations has been verified both theoretically and experimentally[13,17,18] and the second experimentally.[13] Similar relations have been verified experimentally for ternary systems[13]: the parameters $\mathfrak{D}_A$ and Q are extrapolated *vs.* $(\Delta\rho_i)^2$ at constant $\bar{\rho}_i$ to $(\Delta\rho_i)^2 = 0$. For the ternary case, however, the limiting values of $\mathfrak{D}_A$ and Q are functions of the four ternary diffusion coefficients. Thus, a minimum of four experiments is required to eliminate concentration effects.

Results

The measured parameters of the binary and ternary experiments are given in Table I. The temperature of all experiments was $25.00 \pm 0.004°$. Four ternary experiments for each ternary point were made. The ternary diffusion coefficients relative to the volume average velocity are given in Table II.

By neglecting all but terms linear in the densities, the ternary diffusion coefficients predicted for this system are

$$D_{11} = 3.766 \times 10^{-7}[1 + 2A_2 M_1(\rho - \rho_3) - 7.14\phi_1{}^{S} - 1.59\phi_2{}^{S}] \qquad (18)$$

$$D_{12} = 3.766 \times 10^{-7}(2A_2 M_1(\rho - \rho_3)) - 3.445 \times 10^{-7}\left(\frac{\rho_1}{\rho_2}\right)\left(3.99 + \frac{\rho_1}{\rho_2}\right)\phi_2{}^{S} \qquad (19)$$

$$D_{21} = -3.766 \times 10^{-7}\left(\frac{\rho_2}{\rho_1}\right)\left(5.06 + \frac{\rho_2}{\rho_1}\right)\phi_1{}^{S} + 3.445 \times 10^{-7}(2A_2 M_2(\rho - \rho_3)) \qquad (20)$$

$$D_{22} = 3.445 \times 10^{-7}[1 + 2A_2 M_2(\rho - \rho_3) - 1.71\phi_1{}^{S} - 7.14\phi_2{}^{S}] \qquad (21)$$

(8a) NOTE ADDED IN PROOF. The lack of reciprocity may be due to the model's neglect of Brownian motion.

(9) D. G. Miller, *Chem. Rev.*, **60**, 15 (1960).

(10) L. A. Woolf, D. G. Miller, and L. J. Gosting, *J. Am. Chem. Soc.*, **84**, 317 (1962).

(11) L. J. Gosting, E. M. Hanson, G. Kegeles, and M. S. Morris, *Rev. Sci. Instr.*, **20**, 209 (1949).

(12) R. P. Wendt, Ph.D. Thesis, University of Wisconsin, 1961.

(13) E. L. Cussler, Jr., and E. N. Lightfoot, *J. Phys. Chem.*, **69**, 1135 (1965).

(14) The authors are indebted to Professor L. J. Gosting for suggesting this technique.

(15) D. J. Streeter and R. F. Boyer, *Ind. Eng. Chem.*, **43**, 1790 (1951).

(16) W. R. Krigbaum and P. J. Flory, *J. Am. Chem. Soc.*, **75**, 1775 (1953).

(17) L. J. Gosting and H. Fujita, *ibid.*, **79**, 1359 (1957).

(18) H. Fujita, *ibid.*, **83**, 2862 (1961).

Table I: Experimental Results of Diffusion Experiment[a]

1 = polymer S109, 2 = polymer S111, 3 = toluene

Expt. no.[b]	ω1	ω2	10²Δρ1	10²Δρ2	α	J	10⁷𝔇A	10⁴Q
4	0.00844	...	1.523	...	...	76.311	4.705	21.3
57	0.00400	...	0.691	...	...	34.160	3.953	4.0
L[c]	0.00000	...	>0[c]	...	...	0.00	(3.766)[c]	(0.0)[c]
62	...	0.00549	...	0.949	...	47.175	3.848	17.6
58	...	0.00400	...	0.691	...	34.162	3.657	6.9
L	...	0.00000	...	>0[c]	...	0.00	(3.445)[c]	(3.1)[c]
64	0.025001	0.025007	-0.002	1.050	-0.002	51.815	8.239	36.3
61	0.024998	0.024998	-0.002	0.609	-0.003	30.150	8.268	31.4
L	0.0250	0.0250	0.000	>0[c]	0.000	0.00	(8.284)[c]	(28.8)[c]
60	0.024999	0.025005	1.051	0.000	1.000	51.801	8.663	-21.6
63	0.025003	0.024997	0.607	0.002	1.003	30.092	8.585	-26.7
L	0.0250	0.0250	>0[c]	0.000	1.000	0.00	(8.524)[c]	(-29.5)[c]
68	0.01249	0.01251	-0.022	0.863	0.002	42.464	5.921	21.2
65	0.01249	0.01250	0.000	0.606	0.000	29.523	5.834	18.1
L	0.0125	0.0125	0.000	>0[c]	0.000	0.00	(5.750)[c]	(15.7)[c]
67	0.01251	0.01250	0.866	-0.001	1.001	41.576	6.395	-11.6
66	0.01252	0.01252	0.608	0.001	0.999	29.886	6.362	-18.5
L	0.0125	0.0125	>0[c]	0.000	1.000	0.00	(6.330)[c]	(-25.0)[c]

[a] ω_i mass fraction; ρ_i mass density in units of g./cm.³; α fraction of refractive index due to component 1; J total number of fringes; $\mathfrak{D}_A$ reduced height–area ratio in units of cm.²/sec.; Q area under fringe deviation graph. [b] Experiments numbered chronologically. [c] Limits of extrapolation giving $\mathfrak{D}_A$ and Q at zero concentration difference are given in parentheses.

Table II: Multicomponent Diffusion Coefficients[a]

1 = polymer S109, 2 = polymer S111, 3 = toluene

ω1 + ω2	10⁷D11[b]	10⁷D12	10⁷D21	10⁷D22
		Exptl.		
0.0000	3.766 ± 0.011	0.00 ± 0.00	0.00 ± 0.00	3.445 ± 0.010
0.0250	4.46 ± 0.40	1.14 ± 0.38	1.73 ± 0.33	4.69 ± 0.32
0.0500	4.20 ± 0.50	4.17 ± 0.50	4.21 ± 0.48	4.23 ± 0.48
		Theoret.		
0.0000	3.77	0.00	0.00	3.45
0.0250	4.43	2.94	2.72	4.32
0.0500	5.10	5.92	5.47	5.32

[a] Based on mass concentration driving force. [b] D_{ij} in units of cm.²/sec.

Table III: Tests of the Onsager Relations

	0.0250	0.0500
Total polymer mass fraction		
(Left-hand side) × 10⁵/RT[a]	20.0	29.8
(Right-hand side) × 10⁵/RT[a]	21.8	29.9
Difference[a]	-1.8	-0.1
Expected error[b]	±5.2	±6.9

[a] In units of cm.⁵/g. sec. [b] Based on error in D_{ij} alone.

The diffusion coefficients calculated from these equations are also given in Table II.

The test of the Onsager reciprocal relations was made from eq. 13 and 14 and the coefficients in Table II. The left-hand and right-hand sides of eq. 14 are reported in Table III, which shows the Onsager relations valid within the expected error. The expected error reported is based solely on that in the diffusion coefficients.

Discussion

Before discussing the ternary results, we must first show that this system actually behaves as a ternary, that is, that each polymer behaves as a single species.

The binary results shown in Table I show that polymer S109 may be so treated, since $Q = 0$ at infinite dilution.[2b] However, polymer S111 may be treated as a single species only if an additional error in Q of ±3 × 10⁻⁴ is allowed. Thus, in our ternary experiments, we have a ternary system with an error in $\mathfrak{D}_A$ of 0.4% and in Q of ±5 × 10⁻⁴. These cause the large errors in the ternary diffusion coefficients shown in Table II.

The system polystyrene S109–polystyrene S111–toluene shows significant multicomponent effects. The refractive index gradient shown by the system deviates sharply from the Gaussian shape characteristic of a binary system.

However, if the molecular weights of the principal species are close, a polydisperse polymer may be more closely approximated as a binary than the diffusion coefficients in Table II lead one to believe. In other words, if the polymer is sufficiently monodisperse, both the coupling between species and the variation

of the main terms have a small effect. As an illustration, we consider as a polydisperse polymer a mixture of equal parts by weight of polymers S109 and S111.

The cross-term diffusion coefficients (D_{12} and D_{21}) are of the same order of magnitude as the main-term coefficients. However, these large cross terms do not represent large hydrodynamic interactions between polymer molecules. They result from the sharp activity gradients in the system. The L_{12} and L_{21} would be expected to be small relative to L_{11} and L_{22} although the poor accuracy in D_{ij} prevents accurate calculation of the L_{ij}.

A mixture of equal parts by weight of polymers S109 and S111 will behave as a binary system even if diffusion coefficients based on concentration (the D_{ij}) are used. This case corresponds to that of a polymer of slightly greater polydispersity than the samples used here. In such an experiment where $\Delta\rho_1 \doteq \Delta\rho_2$, the refractive index gradient has a nearly Gaussian shape, i.e., $Q < 4 \times 10^{-4}$. The "binary" diffusion coefficient of the mixture would actually correspond to the larger eigenvalue of the ternary diffusion coefficient matrix equal to $\frac{1}{2}(D_{11} + D_{22} + [(D_{11} - D_{22})^2 + 4D_{12} \times D_{21}]^{1/2})$.

The theoretical prediction of the ternary diffusion coefficients is only qualitatively successful. The theory does predict an increase for the diffusion coefficients with polymer concentration, with a greater increase for the cross terms than for the main terms. However, the increase predicted is about twice that observed experimentally. The theory is not adequately tested because of the large activity corrections and because of the large concentrations of spheres. Since the effective radius defined by Stokes' law is about three times the radius for a solid sphere of polymer, a system with a polymer mass fraction of 0.02 would consist of 55% "spheres." Such spheres do not interact solely through their velocity fields, but overlap and collide. The polymer molecules become entangled and move more slowly. Thus, the diffusion coefficients observed experimentally should be smaller than those predicted theoretically, as is the case.

Appendix

The evaluation of eq. 6 is exactly analogous to the corresponding development for a single species of spheres by Pyun and Fixman.[4] To save space, equations in this reference are directly referred to by following the equation number with the letter P.

By arguments paralleling eq. 23P–25P, eq. 6 may be written

$$\mathbf{v}_i - \mathbf{v}_n^u = [\mathbf{v}_i(1) - \mathbf{v}_n^u(1)] + \sum_{j=1}^{n-1} d_j \times$$

$$\left[-\int_{a_j}^{\sigma_{ij}} \mathbf{S}^{(j)}(\mathbf{r}) \cdot \mathbf{v}_j(2)\ dV(\mathbf{r}) - \int_{\sigma_{ij}}^{\infty} \mathbf{E}^{(j)}(\mathbf{r}) : [\nabla_2 \mathbf{S}^{(i)}(\mathbf{r})]^{\mathrm{sym}} \cdot \right.$$

$$\mathbf{v}_i(1)\ dV(\mathbf{r}) - \int_{\sigma_{ij}}^{\infty} \mathbf{E}^{(j)}(\mathbf{r}) : [\nabla_2 \mathbf{E}^{(i)}(\mathbf{r})]^{\mathrm{sym}} :$$

$$\left. [\nabla_2 \mathbf{S}^{(j)}(\mathbf{r})]^{\mathrm{sym}} \cdot \mathbf{v}_j(2)\ dV(\mathbf{r}) + \dots \right] \quad (22)$$

where $\mathbf{S}^{(k)}(\mathbf{r})$, $\mathbf{E}^{(k)}(\mathbf{r})$, $[\nabla_2 \mathbf{S}^{(k)}(\mathbf{r})]^{\mathrm{sym}}$, and $[\nabla_2 \mathbf{E}^{(k)}(\mathbf{r})]^{\mathrm{sym}}$ are identical with eq. 14P, 15P, 33P, and 37P if a is everywhere replaced with a_k. Higher terms, which lead to very complex algebraic ratios of the sphere radii, are small for spheres of similar size and have been neglected.

The first term may be integrated in a similar fashion to eq. 30P and 31P to yield

$$\int_{a_j}^{\sigma_{ij}} \mathbf{S}^{(j)}(\mathbf{r}) \cdot \mathbf{v}_j(2)\ dV(\mathbf{r}) = 2\pi a_j [\sigma_{ij}^2 - a_j^2] \mathbf{v}_j(2) \quad (23)$$

The second term is integrated to give (*cf.* eq. 33P–36P)

$$\int_{\sigma_{ij}}^{\infty} \mathbf{E}^{(j)}(\mathbf{r}) : [\nabla_2 \mathbf{S}^{(i)}(\mathbf{r})]^{\mathrm{sym}} \cdot \mathbf{v}_i(1)\ dV(\mathbf{r}) =$$

$$\mathbf{v}_i(1) \left[\frac{5\pi a_j^3 a_i}{\sigma_{ij}} \right] \left[1 - \frac{\frac{1}{5}a_j^2 + \frac{1}{3}a_i^2}{\sigma_{ij}^2} + \frac{a_j^2 a_i^2}{5\sigma_{ij}^4} \right] \quad (24)$$

The third term gives

$$\int_{\sigma_{ij}}^{\infty} \mathbf{E}^{(j)}(\mathbf{r}) : [\nabla_2 \mathbf{E}^{(i)}(\mathbf{r})]^{\mathrm{sym}} : [\nabla_2 \mathbf{S}^{(j)}(\mathbf{r})]^{\mathrm{sym}} \cdot \mathbf{v}_j(2)\ dV(\mathbf{r}) =$$

$$\mathbf{v}_j(2) \pi \left[\frac{5a_j^4 a_i^5}{6\sigma_{ij}^6} - \frac{5a_j^8 a_i^3 + 8a_j^6 a_i^5}{8\sigma_{ij}^8} + \frac{11a_i^5 a_j^3}{10\sigma_{ij}^{10}} \right] \quad (25)$$

The combination of eq. 23–25 with eq. 22 leads to the result given in eq. 8.

Energy-Transfer Processes in Dilute Solutions of Organometallics in Benzene.

Radiation Chemistry and Luminescence Quenching

by D. B. Peterson, T. Arakawa, D. A. G. Walmsley, and Milton Burton

Department of Chemistry and the Radiation Laboratory,[1] University of Notre Dame, Notre Dame, Indiana 46556
(Received February 8, 1965)

The perphenyl compounds of Sn, Pb, As, Sb, and Bi dissolved in benzene experience radio-sensitized decomposition when the solutions are exposed to ^{60}Co γ-radiation. The products include biphenyl, the phenylcyclohexadienes, and tetrahydroquaterphenyls. The perphenyl metals have no true effect on $G(H_2)$ or $G(C_2H_2)$ from the benzene itself. It has previously been established that these same compounds quench luminescence in benzene solutions containing such scintillators as 1,4-diphenyloxazole or p-terphenyl. The kinetics of the processes are compared, and it is shown that the state of benzene which yields H_2 or C_2H_2 is neither one which yields biphenyl *via* the metal perphenyls nor one which transfers energy to a scintillator and that the state which transfers energy to a scintillator (*i.e.*, the $^1B_{2u}$ state of benzene) is a relatively minor contributor to sensitized decomposition of the metal perphenyls. Effects of locally high concentration of free phenyl radical are revealed in the relatively large amount of biphenyl produced in the sensitized decomposition. Silicon and germanium tetraphenyls show none of the reactions exhibited by the other perphenyls; the fact is linked to longer lifetimes of their excited states.

1. Introduction

Organometallic compounds of the type $M(C_6H_5)_4$, where M is Si, Ge, Sn, or Pb, quench high-energy-induced luminescence of organic scintillators in benzene solutions.[2] For deaerated solutions the significant processes involved may be summarized as

$$S \longrightarrow\!\!\!\sim\!\!\!\longrightarrow S^* \tag{0}$$

$$S^* \longrightarrow S \tag{1}$$

$$S^* + X \longrightarrow S + X^* \tag{3}$$

$$X^* \longrightarrow X + h\nu \tag{6}$$

$$S^* + D \longrightarrow S + D \tag{7}$$

$$S^* - D \longrightarrow S + D^* \tag{8}$$

$$D^* \longrightarrow D \text{ or products} \tag{9}$$
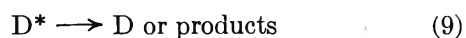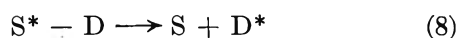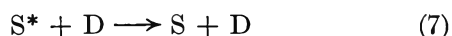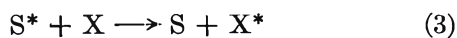
where S, X, and D here refer, respectively, to solvent,[3] scintillator, and quencher. In benzene solutions the excited state responsible for luminescence *via* processes 3 and 6 has been shown to be the first excited singlet state of benzene (*i.e.*, $^1B_{2u}$),[4] and the quenching proc-

esses of interest are those involving deactivation of this state by the quencher, *i.e.*, (7) and (8). Deactivation of excited scintillator by the quencher has been shown to be unimportant in these systems.[2]

Kropp and Burton found that $Sn(C_6H_5)$ and $Pb(C_6H_5)_4$ are very efficient quenchers of the sensitized fluorescence of scintillators such as p-terphenyl and 9,10-diphenylanthracene in benzene.[2] From a kinetic analysis of their data, they obtained $k_8/k_1(\gamma'_0$ in their terminology) equal to 1300 and 1740 M^{-1} for $Sn(C_6H_5)_4$ and $Pb(C_6H_5)_4$, respectively. $Ge(C_6H_5)_4$, on the other hand, is relatively inefficient ($\gamma'_0 = 196\ M^{-1}$), and $Si(C_6H_5)_4$ produces no measurable quenching.

(1) The Radiation Laboratory is operated by the University of Notre Dame under contract with the Atomic Energy Commission. This is A.E.C. Document No. COO-38-375.

(2) J. L. Kropp and M. Burton, *J. Chem. Phys.*, **37**, 1752 (1962).

(3) In other contexts S may refer to the solution *in toto; cf.* M. Burton, M. A. Dillon, C. R. Mullin, and R. Rein, *ibid.*, **41**, 2236 (1964).

(4) S. Lipsky and M. Burton, *ibid.*, **31**, 1221 (1959); S. Lipsky, W. P. Helman, and J. F. Merklin, "Luminescence of Organic and Inorganic Materials," John Wiley and Sons, Inc., New York, N. Y., p. 83.

This report includes the results of a study of the products formed during ^{60}Co γ-irradiation of dilute solutions of metal tetraphenyls and triphenyls in benzene and of the effect of those compounds on high-energy-induced luminescence of organic scintillators in that solvent.

2. Experimental

2.1. Chemicals. Baker Analar benzene was purified by three successive crystallizations with rejection of about one-fourth of the benzene at each freezing. Recrystallized benzene was dried with sodium. Silicon and germanium tetraphenyls (obtained from Anderson Chemical Co.) and tin and lead tetraphenyls (supplied by Metal and Thermit Co. and by K & K Laboratories, respectively) were purified by recrystallization from benzene. Arsenic and antimony and bismuth triphenyls (obtained from Eastman Organic Chemicals) were purified by recrystallization from a 4:1 mixture of ethanol and ether.

2.2. Apparatus and Procedures. Exposure cells of ca. 5-cc. volume, constructed from 30-mm. o.d. Pyrex tubing, were employed in all irradiations. Irradiations were conducted at ambient temperature either in an underground ^{60}Co source of about 800 curies or in our 10-kcurie ^{60}Co facility. Approximate dose rates for these two sources for the geometries employed were about 4×10^{17} and 2×10^{18} e.v./g. min., respectively. Prior to irradiation, solutions were thoroughly deaerated by a reflux method commonly employed in this laboratory[5] and sealed under vacuum. After irradiation, cells were attached to a vacuum line *via* break-seals, and product gases were collected and measured in conventional manner. An initial gas fraction collected at liquid N_2 temperature consisted almost exclusively of H_2. Acetylene was collected at $-80°$.

2.3. Analyses. Gas fractions were analyzed with a Consolidated 21-103A mass spectrometer.

Liquid products were analyzed by vapor phase chromatography without prior concentration of solutions and, in general, immediately after the cell was opened to the atmosphere. F & M Models 609 and 810 gas chromatographs equipped with flame-ionization detectors were used for all analyses.

Irradiated solutions of the metal perphenyls in benzene were analyzed on a 0.635 cm. × 3 m. column packed with silicone grease on firebrick and operated at 160°. This column separated biphenyl and the two isomeric phenylcyclohexadienes (the latter two were only partially resolved), which are the major products of irradiation. Qualitative analysis was based on a comparison of observed retention times with those of pure substances; phenylcyclohexa-2,5-diene was kindly made available for this purpose by M. Eberhardt.

Quantitative analysis was based on a comparison of observed peak areas with those obtained for standard solutions injected periodically during each series of analyses.

2.4. Injection-Port Temperature Effect. The biphenyl analysis was strongly dependent upon the temperature of the injection port of the gas chromatograph. This effect[6] was observed in analysis of irradiated benzene as well as in analysis of benzene solutions of the organometallics, but not with unirradiated control solutions containing biphenyl. At sufficiently high injection-port temperatures (the temperature varies with the organometallic) the metal perphenyls are themselves pyrolyzed and produce biphenyl, but the effect under consideration is observed below the pyrolysis temperature of the organometallics.

We were unable to establish the cause of this temperature effect but pyrolysis of a reaction product in the injection port with resultant production of biphenyl is a possibility. It was found that "on-column" injection eliminates this difficulty, and hence all biphenyl analyses were performed using this technique of sample introduction.

2.5. Luminescence Quenching. Apparatus and procedures used for studies of luminescence quenching are described in previous publications from this laboratory.[7,8]

3. Results

3.1. Pure Benzene. Yields of products from the radiolysis of benzene have been repeatedly determined.[9] The present investigation produced the following values: $G(H_2) = 0.040$; $G(C_2H_2) = 0.02$; $G((C_6H_5)_2) = 0.065$; $G(C_{12}H_{12})^{10} = 0.050$. No attempt was made to determine yields of other products.

3.2. Radiolysis of Benzene Solutions of the Metal Perphenyls. The relatively limited solubilities of the group IV-A metal tetraphenyls in benzene restricted the concentration range to a maximum of about 10^{-2} M. The more soluble group V-A metal triphenyls were studied over a concentration range extending to nearly 10^{-1} M. Within these concentration ranges none of the metal perphenyls had an effect on $G(H_2)$ or $G(C_2H_2)$ such as would reflect a change in the processes of benzene radiolysis.[11]

(5) L. M. Theard and M. Burton, *J. Phys. Chem.*, **67**, 59 (1963).

(6) We are indebted to S. B. Srivastava for discovery of this effect.

(7) J. L. Kropp and M. Burton, *J. Chem. Phys.*, **37**, 1742 (1962).

(8) M. Burton, P. J. Berry, and S. Lipsky, *J. chim. phys.*, **52**, 357 (1955).

(9) W. M. Patrick and M. Burton, *J. Am. Chem. Soc.*, **76**, 2626 (1954); J. P. Manion and M. Burton, *J. Phys. Chem.*, **56**, 560 (1952); S. Gordon, A. R. Van Dyken, and T. F. Doumani, *ibid.*, **62**, 20 (1958); T. Gäumann and R. Schuler, *ibid.*, **65**, 703 (1961).

(10) $G(C_6H_5)_2$ is G(biphenyl), and $G(C_{12}H_{13})$ refers to total G for the two isomeric phenylcyclohexadienes.

$Si(C_6H_5)_4$ and $Ge(C_6H_5)_4$ have no effect on either $G((C_6H_5)_2)$ or $G(C_{12}H_{12})$. However, Figures 1–5 show that the other metal perphenyls cause increases of $G((C_6H_5)_2)$ and, to a lesser extent, of $G(C_{12}H_{12})$. G values were determined from plots of yield vs. dose at low conversion.

Presumably, other products, in particular organometallic compounds, are formed during radiolysis. In the case of $Pb(C_6H_5)_4$, metallic lead was detected; at
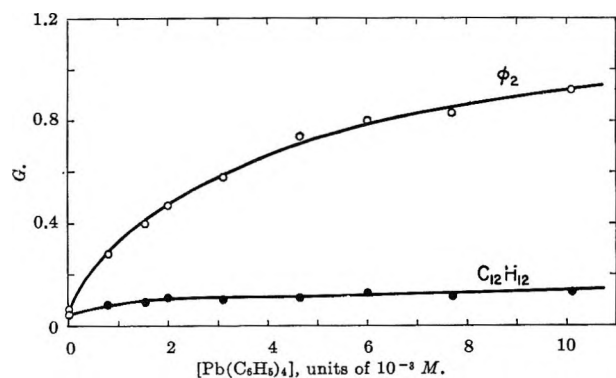
Figure 1. Product yields for ⁶⁰Co γ-radiolysis of $Pb(C_6H_5)_4$ in benzene.
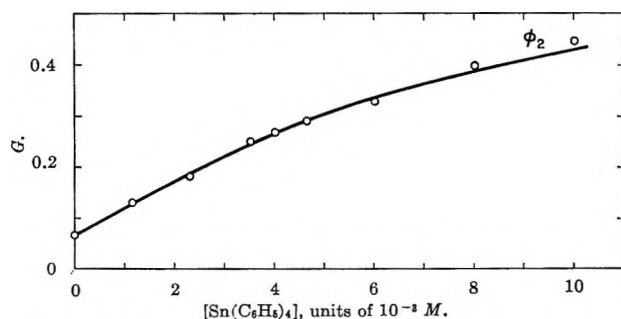
Figure 2. $G((C_6H_5)_2)$ for ⁶⁰Co γ-radiolysis of $Sn(C_6H_5)_4$ in benzene.
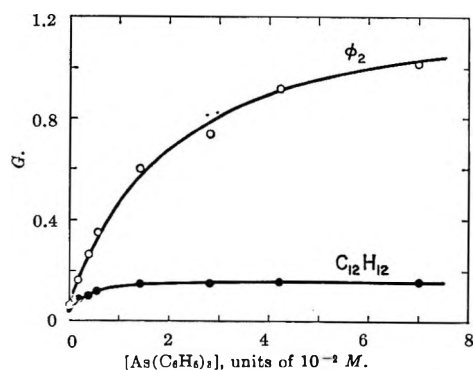
Figure 3. Product yields for ⁶⁰Co γ-radiolysis of $As(C_6H_5)_3$ in benzene.
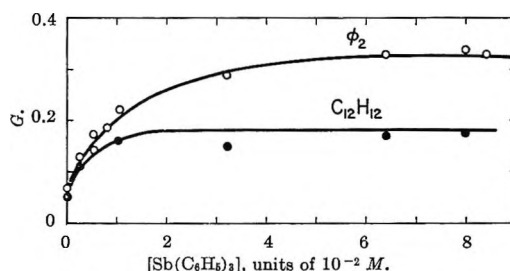
Figure 4. Product yields for ⁶⁰Co γ-radiolysis of $Sb(C_6H_5)_3$ in benzene.
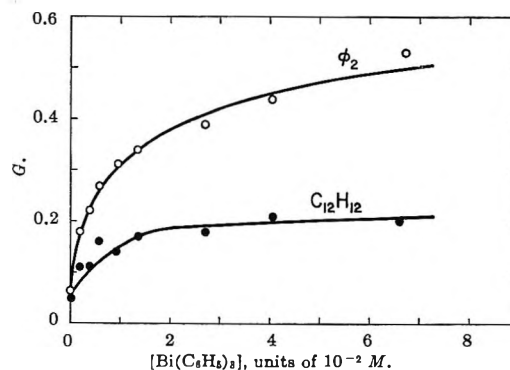
Figure 5. Product yields for ⁶⁰Co γ-radiolysis of $Bi(C_6H_5)_3$ in benzene.

high conversions, lead actually deposits on the walls of the irradiation cell. Attempts to determine the yield of lead at low dose were unsuccessful.

Solutions of the other organometallics are clear and colorless after irradiation, presumably because they are not reduced to the free metal. Irradiated solutions of $Bi(C_6H_5)_3$ turned yellow after exposure to air, and a white solid, approximately 60% by weight bismuth, precipitates from solution. No attempt was made to determine the yields of this product.

3.3. Luminescence Quenching. Values of γ'_0 for the group IV-A metals have been reported by Kropp and Burton.[2] Table I includes those values together with γ'_0 for the group V-A triphenyls obtained in this study. $Si(C_6H_5)_4$ is omitted from the table because it does not quench luminescence.

4. Discussion

4.1. Information from Luminescence Studies. The chemical consequences of ⁶⁰Co γ-irradiation of benzene solutions of the metal perphenyls are qualitatively consistent with luminescence quenching studies. Thus, the tetraphenyls of Sn and Pb, which are excellent

(11) $Sn(C_6H_5)_4$ greatly reduces both $G(C_2H_2)$ and $G(C_{12}H_{12})$, but such reductions are the result of secondary reactions with $Sn(C_6H_5)_3$, a decomposition product of $Sn(C_6H_5)_4$.

Table I: Values of γ'_0 and of i/s^a

Compd.	$\gamma'_0,{}^b$ M^{-1}	$i/s,{}^a$ M^{-1}
$Ge(C_6H_5)_4$	196^c	~ 0
$Sn(C_6H_5)_4$	1300^c	70
$Pb(C_6H_5)_4$	1740^c	237
$As(C_6H_5)_3$	300	50
$Sb(C_6H_5)_3$	440	93
$Bi(C_6H_5)_3$	500	142

^{a} Values of intercept/slope given by Figures 6 and 7. ^{b} γ'_0 determined from studies of luminescence quenching. γ'_0 is by definition k_8/k_1. ^{c} Values determined previously by Kropp and Burton.[2]

Figure 7. $\Delta G((C_6H_5)_2)^{-1}$ vs. $[M(C_6H_5)_3]^{-1}$ for ^{60}Co γ-irradiation of arsenic, antimony, and bismuth triphenyls.

Figure 6. $\Delta G((C_6H_5)_2)^{-1}$ vs. $[M(C_6H_5)_4]^{-1}$ for ^{60}Co γ-irradiation of $Sn(C_6H_5)_4$ and $Pb(C_6H_5)_4$ in benzene.

quenchers, undergo significant sensitized decomposition[12] at low concentrations. Arsenic, antimony, and bismuth triphenyls, which are somewhat less effective quenchers, also undergo sensitized decomposition. Sensitized decomposition is not observed for either $Ge(C_6H_5)_4$ or $Si(C_6H_5)_4$; the former is a relatively inefficient quencher, and the latter apparently does not quench at all. On the basis of optical spectra, $Si(C_6H_5)_4$ and $Ge(C_6H_5)_4$ would be expected to accept energy from benzene with efficiencies comparable to those of $Sn(C_6H_5)_4$ and $Pb(C_6H_5)_4$. In the interpretation of their luminescence quenching data, Kropp and Burton suggested that excited states of silicon and germanium tetraphenyls may be sufficiently long-lived to permit energy transfer to the scintillator.[2] In support of this suggestion, we find that direct excitation of silicon and germanium tetraphenyls by 2537 Å. light does not lead to measurable decomposition although tin and lead tetraphenyls dissociate with quantum yields of a few tenths.[13]

A direct quantitative comparison of luminescence yields and chemical yields is not presently possible because reliable G values for luminescence are not available. However, some estimate may be made on the basis of evidence afforded by the work of Hastings and Weber[14] on systems containing 3 g. of 2,5-diphenyloxazole (PPO) and 50 mg. of 2,2'-p-phenylbis(5-phenyloxazole) (POPOP) per liter of toluene β^- excited by hexadecane-1-^{14}C. In that case the luminescence is exclusively from the POPOP, and G(photons) ≈ 1.8. If it is assumed that G(photons) would not be increased by increase in scintillator concentration in that case, that a possible LET effect can be ignored, and that the information obtained applies to benzene systems, we can adopt the value G_{max}(photons) $= 1.8$, a number significantly higher than any of the product yields found in this work.

4.2. Chemical Processes. For initiation of discussion we represent the processes involved in a sensitized decomposition by the set of reactions

$$B \longrightarrow B_1{}^*, B_2{}^*, B_3{}^*, \ldots \tag{C}$$

$$B_1{}^* \longrightarrow B \tag{1}$$
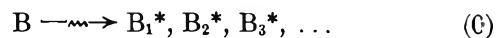
(12) Sensitized decomposition in these cases implies that energy initially *deposited* in the system is *localized* in benzene molecules before it is transmitted to $M(C_6H_5)_n$. The possibility of an important amount either of initial energy deposition in individual $M(C_6H_5)_n$ molecules or of secondary energy localization in such molecules (in preference to localization in benzene molecules) must be discounted in these cases simply because the $M(C_6H_5)_n$ is present in such small concentrations relative to the benzene.

(13) Details of the photochemistry of these systems will be published elsewhere.

(14) J. W. Hastings and G. Weber, *J. Opt. Soc. Am.*, **53**, 1410 (1963).

$$B_2{}^* \longrightarrow (C_6H_5)_2,\ C_{12}H_{12} \tag{1a}$$

$$B_3{}^* \longrightarrow H_2,\ C_2H_2 \tag{1b}$$

$$B_1{}^* + M(C_6H_5)_n \longrightarrow B + M(C_6H_5)_n{}^* \tag{8}$$

$$M(C_6H_5)_n{}^* \longrightarrow M(C_6H_5)_{n-a} + a(C_6H_5) \tag{9}$$

$$M(C_6H_5)_n{}^* \longrightarrow M(C_6H_5)_n \tag{10}$$
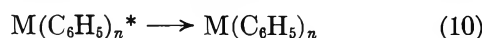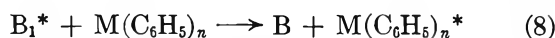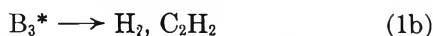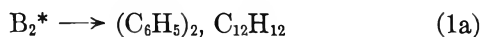
Reaction 0 (cf. section 1) indicates that energy deposited in the system is localized in various excited states of benzene which yield a number of distinguishable (but not necessarily definable) excited species.

Reaction 1b is required because reaction 8 has no effect on $G(H_2)$ or $G(C_2H_2)$. Reaction 1b may, in fact, involve more than one primary precursor ($B_3{}^*$ in our notation), and $B_3{}^*$ is not necessarily an excited benzene molecule (it may be an ion). The possibility that states $B_2{}^*$ and $B_3{}^*$ are the same cannot be ignored but it is not pertinent here.

The stoichiometric details of reaction 9 and subsequent reactions leading ultimately to biphenyl and phenylcyclohexadiene are not essential to this discussion. However, from the known chemistry of these compounds, it would be expected that a is 2 when M is Sn and 4 when M is Pb. This stoichiometry is supported by unpublished photochemical experiments in this laboratory. In the case of the group V-A triphenyls, the stoichiometry is less certain but $1 \leqq a \leqq 2$. Phenyl radicals generated by reaction 9 are expected to produce biphenyl and phenylcyclohexadiene via the sequence 11, 12a in the competitive set

$$C_6H_5 + C_6H_6 \longrightarrow C_{12}H_{11} \tag{11}$$

$$2C_{12}H_{11} \Bigg\langle \begin{array}{l} \longrightarrow (C_6H_5)_2 + C_{12}H_{12} \quad (12a) \\ \\ \longrightarrow C_{24}H_{22} \quad\quad\quad\quad\ \ (12b) \end{array}$$
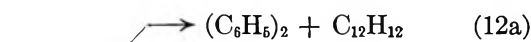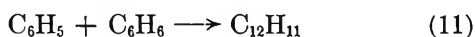
where $C_{12}H_{11}$ is phenylcyclohexadienyl radical and $C_{24}H_{22}$ is tetrahydroquaterphenyl. Considerable support for this mechanism exists in the literature,[15] and Eliel and co-workers have shown that (12a) is considerably more important than (12b).[15]

Our observation that $G((C_6H_5)_2)$ is much greater than $G(C_{12}H_{12})$ in the sensitized decomposition of $M(C_6H_5)_n$ suggests that 12a is not the only source of biphenyl. The fact that biphenyl is not a product when the various $M(C_6H_5)_n$ are dissociated by direct excitation at 2537 Å. in dilute cyclohexane solutions[13] indicates that additional biphenyl does not appear to result from a dissociative process such as

$$M(C_6H_5)_n \longrightarrow M(C_6H_5)_{n-2} + (C_6H_5)_2 \tag{13}$$
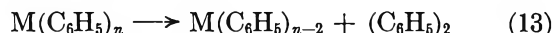
Quite possibly $G(C_6H_5)_2$ is greater than $G(C_{12}H_{12})$ because of the reaction

$$C_6H_5 + C_{12}H_{11} \longrightarrow C_6H_6 + (C_6H_5)_2 \tag{14}$$

This reaction would be particularly important in regions of high phenyl radical concentration such as are possible when $M(C_6H_5)_n$ dissociates to two or more phenyl radicals in a single step or in a sequence of fairly rapid steps.

4.3. Excited States and Specific Rates. A simple steady-state treatment of the proposed mechanism leads to the expression

$$G(-M(C_6H_5)_n) = \frac{k_8 A\,[M(C_6H_5)_n]}{k_1 + k_8[M(C_6H_5)_n]} \tag{I}$$

where

$$A = k_9 G(B_1{}^*)/(k_9 + k_{10})$$

In this notation, $G(B_1{}^*)$ is the 100-e.v. yield of excited benzene molecules capable of transferring energy to $M(C_6H_5)_n$ via reaction 8. The k's refer to specific rates of reactions indicated by subscripts; k_1 is the specific rate for the totality of processes other than (8) by which $B_1{}^*$ returns to the ground state.

In terms of biphenyl production, eq. I becomes

$$G((C_6H_5)_2) = G_B((C_6H_5)_2) + \frac{k_8\alpha[M(C_6H_5)_n]}{k_1 + k_8[M(C_6H_5)_n]} \tag{II}$$

where $G_B((C_6H_5)_2)$ is the 100-e.v. yield of biphenyl for pure benzene, $\alpha = Af$, and f is a factor expressing the stoichiometric relationship between $\Delta G((C_6H_5)_2)$ and $G(-M(C_6H_5)_n)$.

It is apparent from eq. II that, at sufficiently low concentrations of $M(C_6H_5)_n$, $G((C_6H_5)_2)$ increases linearly with $[M(C_6H_5)_n]$ and that, at high solute concentrations, $G((C_6H_5)_2)$ reaches a plateau. Equation II may be rearranged to

$$1/\Delta G((C_6H_5)_2) = \frac{1}{\alpha} + \frac{k_1}{k_8\alpha}[M(C_6H_5)_n]^{-1} \tag{III}$$

Figures 6 and 7 show plots of experimental values of $1/\Delta G((C_6H_5)_2)$ against $[M(C_6H_5)_n]^{-1}$. Values of intercept/slope, i/s, for the various metal perphenyls obtained from Figures 6 and 7 are summarized in Table I together with values of γ'_0 from studies of luminescence quenching.

The large difference between i/s obtained from chemical studies (presumably k_8/k_1 on the basis of the kinetic scheme up to this point) and γ'_0 from luminescence studies for a given organometallic indicates that transfer from the $^1B_{2u}$ state of benzene (the state responsible

(15) D. F. deTar and R. A. Long, *J. Am. Chem. Soc.*, **80**, 4742 (1958); E. L. Eliel, S. Meyerson, Z. Welvart, and S. H. Wilen, *ibid.*, **82**, 2936 (1960); E. L. Eliel, M. Eberhardt, O. Simamura, and S. Meyerson, *Tetrahedron*, **17**, 749 (1962).

or luminescence of organic scintillators) is not the only process involved in sensitized decomposition. The additional process may be excitation transfer from a state other than $^1B_{2u}$; i.e., in benzene solution the state B_1^* in reaction 1, equivalent to $^1B_{2u}$ in such case, is not the only one which enters into a reaction such as (8).

Processes such as electron capture and positive charge transfer cannot be definitely ruled out. However, such processes generally do not begin to plateau at the relatively low solute concentrations involved in this study.[16]

If a second energy-transfer process to metal perphenyl involving B_4^* is introduced, the production of such an entity must be included, and the following reactions must also be considered

$$B_4^* \longrightarrow B \qquad (15)$$

$$B_4^* + M(C_6H_5)_n \longrightarrow B + M(C_6H_5)_n^{**} \qquad (16)$$

$$M(C_6H_5)_n^{**} \longrightarrow M(C_6H_5)_{n-a} + aC_6H_5 \qquad (17)$$
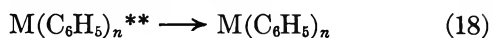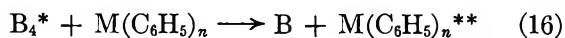
$$M(C_6H_5)_n^{**} \longrightarrow M(C_6H_5)_n \qquad (18)$$

where the possibility exists that $M(C_6H_5)_n^{**}$ may not behave precisely like $M(C_6H_5)_n^*$. The steady-state expression for $\Delta G((C_6H_5)_2)$ now becomes

$$\Delta G((C_6H_5)_2) = \frac{k_8\alpha[M(C_6H_5)_n]}{k_1 + k_8[M(C_6H_5)_n]} + \frac{k_{16}\beta[M(C_6H_5)_n]}{k_{15} + k_{16}[M(C_6H_5)_n]} \qquad (IV)$$

where β has meaning analogous to α; i.e.

$$\beta = fk_{17}G(B_4^*)/(k_{17} + k_{18}) \qquad (V)$$

Equation IV suggests that over the range of $M(C_6H_5)_n$ concentrations employed (i.e., 2×10^{-3} to 8×10^{-2} M), the value of $1/\Delta G((C_6H_5)_2)$ would not be expected to be a strictly linear function of $[M(C_6H_5)_n]^{-1}$ but the relationship could be closely linear if α and β differ in magnitude. Figures 6 and 7 unquestionably show such linear relationship. The conclusion thus is that either α or β is relatively unimportant; i.e., $G(B_4^*)$ is either significantly larger or much smaller than $G(B_1^*)$.

Studies in this laboratory[13] on photochemical processes in solutions of $Pb(C_6H_5)_4$ in benzene irradiated with 2537-Å. light, as well as certain other experimental facts, lead to the following argument and conclusions.

(1) The quantum yields, Φ, of the processes and products of interest are related by the statement $\Phi(-Pb(C_6H_5)_4) = (a/2)$, $\Phi((C_6H_5)_2)$.

(2) At $[Pb(C_6H_5)_4] \sim 10^{-2}$ M, the limiting value of $\Phi(-Pb(C_6H_5)_4)$ found was $\leq \sim 0.1$.

(3) At such a concentration of $Pb(C_6H_5)_4$, reaction 1, which represents nonproductive decay of the $^1B_{2u}$

state of benzene in the photochemical case, is practically nonoccurrent.

(4) The $^1B_{2u}$ state is the one which transmits energy to the scintillator in both ultraviolet- and γ-irradiated systems.[3]

(5) The $^1B_{2u}$ state is the state which is quenched when luminescence is quenched.[3]

(6) The $^1B_{2u}$ state is thus involved, via reactions 8 and 9, in high-energy, as well as in ultraviolet, induced processes in benzene.

(7) The limiting value $\Phi(-Pb(C_6H_5)_4) \sim 0.1$ (i.e., when $r_1 \approx 0$) in photolysis thus indicates that $k_{10} \geq \sim 9k_9$ and that, at the maximum, the number of $Pb(C_6H_5)_4$ molecules decomposed is only one-tenth the number of excited B molecules produced in the $^1B_{2u}$ state.

(8) According to section 4.1., it is possible that G(photons) in benzene containing suitable scintillator may be as high as 1.8. If the efficiency of excitation transfer from exicted benzene to scintillator ψ_t is ≈ 0.7[17] and the scintillator emission efficiency ψ_e is ≈ 0.95,[18] it follows from the presumed relationship G(photons) $= \psi_t\psi_eG(^1B_{2u})$ that $G(^1B_{2u})$ is ~ 2.7. Lipsky[19] has recently concluded on the basis of new data that a better value for $G(^1B_{2u})$ is ~ 1.7. Methods based on the assumption of efficiency of energy conversion into photons lower than the 5.25% given by Hastings and Weber[14] lead to lower values of $G(^1B_{2u})$.

(9) Thus, G(reaction 9) $\leq 0.1 \times 2.7 = 0.27$ and is probably ≤ 0.17.

(10) However, according to Figure 6, $\Delta G((C_6H_5)_2)$ in the radiation-sensitized process approaches ~ 1.2 as a limit; i.e., $G(-Pb(C_6H_5)_4) \rightarrow 0.6$ as a lower limit. Therefore, in the process of decomposition of $Pb(C_6H_5)_4$, reaction 8 (with the ensuant reaction 9) cannot be the only contributor. Indeed, it would appear that β can actually be significantly greater than α.

(11) Consequently, it is probable that in radiation chemistry the state $^1B_{2u}$ makes a minor contribution, if any, to the radiation-sensitized decomposition of the metal perphenyls. The states represented by B_4^* which make an important contribution to such a decomposition are not those which enter into reaction 1b nor, as nearly as can be judged on the basis of the

(16) W. Van Dusen, Jr., and W. H. Hamill, J. Am. Chem. Soc., 84, 3648 (1962).

(17) Estimated from data on toluene by S. G. Cohen and A. Weinreb, Proc. Phys. Soc. (London), B69, 593 (1956).

(18) From experiments by R. J. Povinelli and M. A. Dillon, of this laboratory, who compared results for solutions with the results of E. A. Andreeshchev and I. M. Rozman, Opt. Spectry., 8, 435 (1960), for p-terphenyl in plastic.

(19) S. Lipsky, private communication.

linear relationship between $1/\Delta G((C_6H_5)_2)$ and $1/[M(C_6H_5)_n]$ (*cf.* Figures 4-7), into reaction 1a.

(12) The consequence of these facts is that the kinetics of radiation-sensitized decomposition of the metal perphenyls is adequately represented by the simple Stern–Volmer relation

$$1/\Delta G((C_6H_5)_2) = \frac{1}{\beta} + \frac{k_{15}}{k_{16}\beta}[M(C_6H_5)_n]^{-1} \quad \text{(VI)}$$

The specific rate k_{15} is independent of the additive. Thus, the values of i/s in Table I represent approximate k_{16}/k_{15} values and are consequently not identifiable with γ_0' values which presumably are properly equated to k_8/k_1.

(13) The values of the intercepts in Figures 6 and 7 are themselves interesting.

$$i = (k_{17} + k_{18})/fk_{17}G(B_4^*) \quad \text{(VII)}$$

Because $G(B_4^*)$ is not known, it is not possible to establish the value of $k_{17}/(k_{17} + k_{18})$, which, in any case, must be ≤ 1. Thus, for $Pb(C_6H_5)_4$ (with f necessarily ≤ 2) because $i = 0.8$, it follows that $G(B_4^*)$ is significantly greater than 0.6. It may be inferred from the relation $k_9/(k_9 + k_{10}) = 0.1$, that $k_{17}/(k_{17} + k_{18})$ is also significantly <1. Thus, it is quite probable that $G(B_4^*)$ is significantly greater than $G(B_1^*)$.

The qualitative correlation between γ_0' and i/s is to be expected in view of the fact that both quantities reflect an excitation-transfer process. The quantitative difference is ascribable, of course, to the fact that $\gamma_0' = k_8/k_1$ and $i/s = k_{16}/k_{15}$.

Lives and Fates of Excited States. The values of γ_0' yield the specific rates of reaction VIII provided $k_1 = 1/\tau$, where τ is the decay time of the state B_1^*. Most recent results indicate that the proper τ to use is 16.0 nsec.[20] Thus, k_8 is $1.1 \times 10^{11}\ M^{-1}$ sec.$^{-1}$ for $Pb(C_6H_5)_4$. The values of k_8 so obtained pertain to the behavior of the $^1B_{2u}$ state. Doubtless, the high values are indicative of resonance transfer[21] of energy (as well as a possible effect of size of benzene domains[22]). Be-

cause benzene and the metal perphenyls can be assumed to display many similarities in their excited states, it can be reasonably assumed that B_4^* interaction with $M(C_6H_5)_n$ (reaction 16) behaves approximately like the $^1B_{2u}$ state in similar interaction (8). The decay time of B_4^* may then be estimated from the value k_{16}/k_{15} (for $Pb(C_6H_5)_4$) $= 237\ M^{-1}$ (*cf.* Table I). The relation $k_{16} \approx k_8$ gives $\tau(B_4^*) = 1/k_{15} \approx 2.1$ nsec. The interpretation of this approximate value is that the complete compendium of states corresponding to the group of excitation donor species B_4^* survives on the average about 2.1 nsec. without, to any significant degree, yielding the $^1B_{2u}$ state of benzene or any state which would normally decompose; internal conversion processes (15) responsible for the disappearance of B_4^* proceed either in cascade or in parallel or in both to the ground state almost exclusively. Such a conclusion might appear somewhat more striking than (but is consistent with) the conclusion of Braun, Kato, and Lipsky,[23] based on spectroscopic data, that higher excited states of benzene yield the $^1Bu_{2u}$ state with efficiency "significantly less than unity."

It should be emphasized that states which convert very rapidly to the $^1B_{2u}$ state are not identifiable as B_4^* states but are included in $G(^1B_{2u})$; *i.e.*, upper states which yield $^1B_{2u}$ or states decomposing very rapidly are *not* ruled out by the argument here offered.

(20) M. A. Dillon and M. Burton, *Radiation Res. Suppl.*, in press. *Cf.* T. V. Ivanova, G. A. Mokeeva, and B. Ya. Sveshnikov, *Opt. Spectry.*, 12, 325 (1962), who find τ equals either 7 or 22 nsec. (the presentation is not clear) for pure liquid benzene, using a phase-shift technique. The new result is, however, in substantial agreement with those from a number of other sources.

(21) The maximum specific rate for a collision-controlled process in benzene is $\sim 5 \times 10^{10}\ M^{-1}$ sec.$^{-1}$. *Cf.* C. R. Mullin, M. A. Dillon, and M. Burton, *J. Chem. Phys.*, 40, 3053 (1964).

(22) *Cf.* M. Burton, M. A. Dillon, and R. Rein, *ibid.*, 41, 2228 (1964).

(23) C. L. Braun, S. Kato, and S. Lipsky, *ibid.*, 39, 1645 (1963).

The Heats of Combustion, Formation, and Isomerization of

Isomeric Monoglycerides[1,2]

by Leonard S. Silbert,[3] B. F. Daubert, and Leo S. Mason

Department of Chemistry, University of Pittsburgh, Pittsburgh, Pennsylvania (*Received February 12, 1965*)

Heats of combustion for the isomeric monoglyceride series ranging from monocaprin to monostearin and for one pair of unsubstituted benzoylmonoglycerols were determined and used for calculating the heat of formation, heat of isomerization from the enthalpy difference of the isomers, and energy increment per CH_2 for their solid states. The heat of isomerization ranged from -1.99 to -3.84 kcal. mole^{-1} for the aliphatic monoglycerides and -1.08 kcal. mole^{-1} for the aromatic series in contrast to a reported value of -9.52 kcal. mole^{-1}. The kinetic equilibrium constant reported for the isomerization of 2-monoglyceride to 1-monoglyceride was compared to the equilibrium constant computed from their isomerization energies. An entropy difference for the monopalmitin pair, $\Delta S^\circ = -5.6$ cal. deg.$^{-1}$ mole^{-1}, was derived and interpreted. The energy increment per CH_2 ranged from 154.65 to 155.87 kcal. mole^{-1}, and the possible reasons for the range are briefly discussed.

Introduction

Pure aliphatic and aromatic 2-monoglycerides have been prepared and characterized,[4-8] and their rearrangement to 1-monoglycerides have been studied under acid, alkaline, and thermal conditions.[9,10] The rearrangement was recently demonstrated to be a reversible reaction, 2-monoglyceride $\rightleftarrows$ 1-monoglyceride, in which the 1-isomer is the predominant component in the equilibrium.[10]

Clarke and Stegeman[11] determined the heats of combustion for a single pair of monoglycerides, the monopalmitins, whose enthalpy difference provided the heat of isomerization evolved in the rearrangement. Their value of -9.52 kcal. mole^{-1} afforded thermodynamic evidence of the greater stability of 1-monoglycerides, but they also acknowledged this isomerization energy to be unusually large when compared to differences of 0.5–3.5 kcal. mole^{-1} normally obtained for isomeric pairs.[12] To confirm the reliability to their 1-monopalmitin heat of combustion value, they also reported preliminary heats of combustion on 1-monomyristin whose energy seemed to compare favorably with that calculated from their 1-monopalmitin value by including Rossini's[13] heat of combustion per CH_2 group.

Because the anomalously large isomerization energy was reported on only a single pair of isomeric monoglycerides, this investigation was undertaken on both

(1) This paper is based on the Ph.D. thesis of L. S. Silbert, June 1963.

(2) The authors extend their appreciation to Swift and Co. for a research grant that made this work possible.

(3) Eastern Regional Research Laboratory, Eastern Utilization Research and Development Division, Agricultural Research Service, U.S.D.A., Philadelphia, Pa. 19118.

(4) M. Bergmann and N. M. Carter, *Z. physiol. Chem.*, 191, 211 (1930).

(5) B. F. Stimmel and C. G. King, *J. Am. Chem. Soc.*, 56, 1724 (1934).

(6) B. F. Daubert, H. H. Fricke, and H. E. Longnecker, *ibid.*, 65, 1718 (1943).

(7) J. B. Martin, *ibid.*, 75, 5482 (1953).

(8) O. E. van Lohuizen and P. E. Verkade, *Rec. trav. chem.*, 78, 460 (1959).

(9) B. F. Daubert and C. G. King, *J. Am. Chem. Soc.*, 60, 3003 (1938).

(10) C. E. van Lohuizen and P. E. Verkade, *Rec. trav. chem.*, 78, 133 (1959).

(11) T. H. Clarke and G. Stegeman, *J. Am. Chem. Soc.*, 62, 1815 (1940).

(12) (a) F. D. Rossini, *J. Res. Natl. Bur. Std.*, 46, 111 (1951), butenes (2.05 kcal. mole^{-1}); (b) M. S. Kharasch, *ibid.*, 2, 339 (1929), methyl butyrates (1.4 kcal. mole^{-1}); (c) F. D. Rossini, *ibid.*, 35, 141 (1945), phenylpropanes (0.67 kcal. mole^{-1}); (d) G. S. Parks and G. E. Moore, *J. Chem. Phys.*, 1, 1066 (1939), propanols (3.35 kcal. mole^{-1}).

(13) F. D. Rossini, *Ind. Eng. Chem.*, 29, 1425 (1937).

series ranging from 10 to 18 carbon atoms per even-membered fatty acid chain in order to re-evaluate the energy difference between isomers. Reliable procedures for preparing a series of isomeric monoglycerides in high chemical and physical purity and the availability of a modern, high precision calorimeter permitted accurate heat of combustion measurements for these compounds.

Two monobenzoylglycerols were also included in this investigation to provide similar thermochemical evidence of relative stabilities for an aromatic monoglycerol pair whose physical properties are in the reverse relationship observed for the aliphatic series. The aromatic 2-monoglycerols exhibit higher melting points and lower solubilities than their 1-isomers, but like aliphatic 2-monoglycerides, they similarly rearrange to their 1-isomers in acidic or basic solution. This reversal in physical properties incurs uncertainty on establishing the relative stability of the aromatic isomers in the absence of thermodynamic information.

Experimental

Materials. Pure fatty acids used in the syntheses were derived from commercial fatty acid sources by fractional distillation and saponification of their methyl esters followed by repeated acetone crystallizations of the purified acids, excepting capric acid which crystallized from petroleum ether. The purest grade of benzoic acid was used for the monobenzoylglycerol preparations.

1-Monoglycerides. Established methods were followed for preparing 1-monoglycerides[14-18] which were crystallized from the following solvents: 1-monostearin and 1-monopalmitin from methanol-ethyl ether cosolvent, 1-monomyristin and 1-mono-laurin from ethyl ether–petroleum ether (b.p. 35–50°) cosolvent, and capric acid from petroleum ether. 1-Monobenzoylglycerol[19] was repeatedly crystallized from a 3:1 ethyl ether–petroleum ether cosolvent that was progressively cooled to −20° and seeded with a crystal of the compound at 5° to prevent oiling. The hygroscopic nature of the crystallized product necessitated storage over a drying agent.

2-Monoglycerides. The 2-acyl-1,3-benzylidene-glycerol intermediates were prepared by a slight, though critically important, modification of the Stimmel and King procedure.[5,20]

After reduction of the benzylideneglycerol intermediates, the 2-monolgycerides were isolated from solution and crystallized from the following solvents: 2-monostearin and 2-monopalmitin from methanol, 2-monomyristin from ethyl ether–petroleum ether mixture containing some methanol, and 2-monolaurin and

2-monocaprin from an ethyl ether–petroleum ether mixture. 2-Monobenzoylglycerol crystallized from ethyl ether–petroleum ether–methanol mixture (17:5:1) at −5° after seeding and the hygroscopic product stored over a drying agent.

Criteria of Purity. The purity of each monoglyceride was checked by capillary melting point, periodic acid oxidation,[21] acid number, saponification equivalent, and hydroxyl value.[22] Periodic acid oxidation of vicinal hydroxyl groups is a distinctive test to differentiate 1-monoglycerides from the 2-isomers. 1-Monoglyceride values were within 0.5% of the theoretical values. All of the aliphatic 2-monoglycerides gave slight positive values ranging from 0.15 to 0.95%, but these are considered to be spurious.[23] These results combined with acid number, saponification number, and hydroxyl value indicate a minimum chemical purity of 99.5%.

Two physical techniques were attempted.[24] Samples of 1- and 2-monostearin analyzed by infrared spectra gave spectra that were practically identical. Recent infrared studies[25] report differences between the isomers, but it is apparent from this work that the technique is

(14) E. Fischer, M. Bergmann, and E. Bärwind, *Ber.*, **53**, 1589 (1920).

(15) E. Fischer and E. Pfähler, *ibid.*, **53**, 1606 (1920).

(16) E. Fischer, *ibid.*, **53**, 1621 (1920).

(17) H. P. Averill, J. N. Roche, and C. G. King, *J. Am. Chem. Soc.*, **51**, 866 (1929).

(18) T. Malkin and M. R. E. Shurbagy, *J. Chem. Soc.*, 1628 (1936).

(19) M.p. 41.2–41.8°; van Lohuizen and Verkade[8] report 40–41°.

(20) The Stimmel and King procedure[6] using pyridine as solvent in the acylation step led to a product invariably contaminated by a palladium catalyst poison that either inhibited reduction of the 2-acyl-1,3-benzylideneglycerol compounds or induced isomerization to the 1-isomer on reducing the acylals under forcing conditions. Acylation of 1,3-benzylideneglycerol in a neutral solvent like chloroform and restriction to a slight excess in the quantity of pyridine used as acid acceptor eliminated those difficulties formerly encountered in the reduction step of the intermediates and in the isolation step of the desired 2-monoglycerides.

(21) (a) W. D. Pohle, V. C. Mehlenbacher, and J. H. Cook, *Oil & Soap*, **22**, 115 (1945); (b) E. Handschumaker and L. Lenteris, *ibid.*, **24**, 143 (1947).

(22) C. L. Ogg, W. L. Porter, and C. O. Willits, *Ind. Eng. Chem.*, *Anal. Ed.*, **17**, 394 (1945).

(23) It was observed both in this study and elsewhere[10] that the longer the aliphatic 2-monoglycerides remained in the acetic acid oxidizing solution, the more extensive was transposition to the 1-isomers. The method is more reliable for the more stable aromatic 2-monoglycerides which shift too slowly to be observed in the time interval of the analysis.

(24) Since completion of this work, additional physical techniques have been developed for the analysis of monogylcerides such as thin layer chromatography [A. F. Hofmann, *J. Lipid Res.*, **3**, 391 (1962)], countercurrent distribution [E. S. Perry and G. Y. Brokaw, *J. Am. Oil Chemists' Soc.*, **32**, 191 (1955)], and vapor phase chromatography [A. G. McInnes, N. H. Tattrie, and M. Kates, *ibid.*, **37**, 7 (1960)].

(25) (a) D. Chapman, *J. Chem. Soc.*, 55 (1956); (b) H. Susi, S. G. Morris, and W. E. Scott, *J. Am. Chem. Soc.*, **38**, 199 (1961).

unsuitable for determining traces of one isomer in the other.

The solubility method of analysis, proposed by Herriott[26] as a physical criterion to test chemical purity, was tried on the 1-monoglycerides. The technique will not be described here owing to its lack of success, the reader being referred to the thesis[1] for further details. Those solubility results obtained on the three monoglycerides submitted to the test are as follows with the solvents, temperatures, and solubility in g. of compound/100 g. of solvent (reported to two significant figures in lieu of the four figures experimentally obtained): 1-monostearin (methanol, 30°, 2.5); 1-monopalmitin (methanol, 30°, 8.0; methanol, 25°, 7.8; methyl ethyl ketone, 25°, 4.4; benzene, 25°, 0.46); 1-monolaurin (benzene, 25°, 2.6).

The most stable physical state for these monoglycerides was required for combustion. 1-Monoglycerides are known to exhibit four polymorphs, the β_L modification being the most stable form while the 2-monoglycerides appear to be monomorphic. Further elaboration of this topic is made redundant by the recent review.[27] The melting points obtained for the β_L form of the 1-monoglycerides agreed excellently with the highest reported melting values.[18,28] Melting points for the 2-isomers also agreed with their reported values.[5,28]

To supplement chemical analysis in support of the purity of monoglycerides, the following methods were used to replace the previous physical procedures. Some samples of 1-monostearin and 1-monopalmitin were solvent crystallized two or three times, followed by combustion of samples from each crystallized lot. Separate preparations of 2-monopalmitin were made from separately prepared palmitoylbenzylideneglycerol intermediates, each of which was also prepared from individually purified palmitic acid and benzylideneglycerol fractions. 1-Monocaprin, 1-monolaurin, and 1-monomyristin were obtained from their shifted 2-monoglyceride isomers, and the combustions were compared to those of the 1-monoglycerides synthesized through the isopropylidene intermediates. The remaining compounds were single preparations.

Apparatus and Method. Calorimeter. The calorimeter employed in this investigation was patterned after that of Dickinson[29] and has been described.[30] Modifications made in the instrument have been discussed by Nathan[31] and Rulon.[32] The calorimeter chamber was thermostated at 25.000 ± 0.003°. The mass of the calorimeter can and water weighed 2200.00 ± 0.05 g. using a large capacity balance with a sensitivity of ±0.01 g. The "Emerson double-valved bomb" and all connecting parts within the reaction chamber were

stainless steel, the bomb having a capacity of 545 ml. A measured volume of water (1.5 ml.) was added to the bomb prior to each combustion determination. Ignition wire used in the standardization and monoglyceride combustions was approximately 7.5 cm. in length per determination. The bomb was filled to an oxygen pressure of 450 p.s.i.g. after two flushings at this pressure.

The temperature-measuring equipment, consisting of a National Bureau of Standards platinum resistance thermometer, Mueller temperature bridge, galvanometer, and auxilliary mirror to lengthen the galvanometer-to-scale distance, was supplied by Leeds and Northrup Co. Electrical firing energy determinations taken in the absence of sample gave an average value of 6.00 ± 0.26 cal.

Preparation of Samples. Since all of the compounds submitted to study were solids, the procedures for standardization and samples were identical. Each compound was dried at 30° and 1 mm. before combustion.

(a) *Benzoic Acid Standardization.* The procedure for the standardization of the bomb was previously explained.[30,31] The benzoic acid used was National Bureau of Standards Sample 39g, with a certified heat of combustion of 26.4338 ± 0.0026 absolute joules g.$^{-1}$ (weight *in vacuo*) which calculated to 6317.83 ± 0.62 cal. g.$^{-1}$ (weight *in vacuo*) by using the conversion factor of 1 cal. equals 0.0041840 absolute kjoule and using a density of 1.320 g. cm.$^{-3}$ at 25° for benzoic acid. The bomb calorimeter was standardized with 1.5 g. of benzoic acid per calibration to give an approximate temperature rise of 3.3°.

(b) *Monoglycerides.* Sample weights were chosen to give a temperature rise comparable to the standardizations. A sample was transferred to a pill maker and compressed to a solid disk between two hard-surfaced cardboard disks. Any loose particles on the surfaces and edges were blown away by means of a gentle air jet before weighing the sample in a nickel crucible. The monobenzoylglycerols were hygroscopic compounds, but special precautions were not taken during the weighings as no significant weight changes were

(26) R. M. Herriott, *Federation Proc.*, **7**, 479 (1948).

(27) D. Chapman, *Chem. Rev.*, **62**, 433 (1962).

(28) L. J. Filer, Jr., S. S. Sidhu, B. F. Daubert, and H. E. Longenecker, *J. Am. Chem. Soc.*, **66**, 1333 (1944).

(29) H. C. Dickinson, *Bull. Bur. Std.*, **11**, 243 (1915).

(30) (a) T. H. Clarke, Thesis, University of Pittsburgh, 1939; (b) T. H. Clarke and G. Stegeman, *J. Am. Chem. Soc.*, **61**, 1726 (1939).

(31) C. C. Nathan, Thesis, University of Pittsburgh, 1948.

(32) R. H. Rulon, Thesis, University of Pittsburgh, 1951.

evident on reweighing several samples within a 15-min. period.

Combustion Product Corrections. Unburned ignition wire and loss of weight of the nickel crucible were determined, and the appropriate combustion corrections were made for each run. Traces of nitric acid produced in the combustions were not determined on every sample. An average of three nitric acid determinations per tank of oxygen consumed was sufficient for use in the combustion calculations since the contribution of the nitric acid to the combustion values was only 0.003 to 0.006% of the total energy.

Densities of Monoglycerides. Density determinations for the solid aromatic monoglycerides were obtained by a pycnometer procedure.[33] The insolubility of aromatic monoglycerides in isooctane permitted density measurements by displacement of their saturated solutions. Solubility in isooctane was obtained by evaporation of the saturated solutions.

Specific Heats. Computation of the Washburn corrections,[34] requires a knowledge of the specific heat of each compound. For this purpose the method of mixtures of an elementary design was employed using for the equipment a silvered flask, copper U-tube slug (approximately 10-ml. capacity) as sample container with a close-fitting cap easily sealed with beeswax, and Beckmann thermometer, and stirrer (*cf.* thesis for details[1]). The method, on checking against calorimetric benzoic acid as a test compound, agreed within 2% of the accepted average value for 0–25°.

Results

Units of Measurement and Auxiliary Data. All data reported are based on the 1961 atomic weights[35] (carbon, 12.01115; hydrogen, 1.00797; oxygen, 15.9994), the 1951 fundamental constants,[36] and the definitions: 0°C. = 273.15°K.; 1 cal. = 4.1840 absolute joules; R = 1.98717 cal. deg.$^{-1}$ mole^{-1}. The laboratory standard weights had been calibrated at the National Bureau of Standards. For use in reducing weights in air to *in vacuo* and in correcting to standard states, densities and specific heats of the monoglycerides are required. The densities of the solid aliphatic monoglycerides were taken from Merker's[37] studies. Density determinations for the aromatic monoglycerides, obtained at 30.00 ± 0.05° and accurate to ±0.1%, are 1.302 g. ml.$^{-1}$ for 1-monobenzoylglycerol and 1.286 g. ml.$^{-1}$ for 2-monobenzoylglycerol. The derived solubilities in g./100 g. of isooctane are 0.034 for 1-monobenzoylglycerol and 0.007 for 2-monobenzoylglycerol. Results of the specific heat measurements are listed in Table I together with values calculated from Kopp's law for comparison.

Table I: Specific Heats of Monoglycerides

| | c_p, cal. deg.$^{-1}$ g.$^{-1}$ | | |
	1-Mono-glyceride	2-Mono-glyceride	Calcd.[a]
Stearin	0.407	0.407	0.421
Palmitin	0.410	0.404	0.416
Myristin	0.411	0.400	0.412
Laurin	0.390	0.380	0.408
Caprin	0.398		0.403
Benzoylglyceride	0.291	0.288	0.314

[a] From Kopp's law.

To compute the values of the standard heat of formation of monoglycerides, the following values were used for the standard heats of formation of carbon dioxide and water, in kcal. mole^{-1}: $CO_2(g)$, −94.0517; $H_2O(l)$, −68.3149. These values are from N.B.S. Circular 500[38a] with corrections for changes in molecular weights of CO_2 and H_2O.[38b]

Determination of Temperature Rise. All calculations were identical for the standardization and monoglyceride heat runs. The method of Dickinson[39] was used for each temperature rise determination to correct for the total resistance change for heat transfer between the calorimeter and jacket.

Reduction to Standard States. The complete procedure for the "Washburn corrections" and reduction to standard conditions is given by Washburn.[34] $-\Delta E_c$ and $-\Delta E_c M^{-1}$ are the evolved heat of the bomb process in kcal. mole^{-1} and cal. g.$^{-1}$, respectively, and $-\Delta E_R°$ is the standard change in internal energy in kcal. mole^{-1}.

Calorimetric Results. An energy equivalent series of 11 calibrations gave an average value of 2859.54 ± 0.43 cal. deg.$^{-1}$ which was used in the calculations for the 12 monoglycerides studied. To ensure against any changes in energy equivalent during the combustion studies, standardizations made once every 3 or 4 days agreed excellently with the determined value.

(33) N. Bauer, "Physical Methods of Organic Chemistry," Vol. I, Part 1, A. Weissberger, Ed., Interscience Publishers, Inc., New York, N. Y., 1949, Chapter VI, pp. 253–296.

(34) E. W. Washburn, *J. Res. Natl. Bur. Std.*, **10**, 525 (1933).

(35) A. E. Cameron and E. Wichers, *J. Am. Chem. Soc.*, **84**, 4175 (1962).

(36) *Natl. Bur. Std.* (*U. S.*) *Tech. News Bull.*, **47**, 175 (1963).

(37) (a) D. R. Merker and B. F. Daubert, *J. Am. Chem. Soc.*, **80**, 516 (1958); (b) D. R. Merker, Thesis, University of Pittsburgh, 1951.

(38) (a) F. D. Rossini, D. D. Wagner, W. H. Evans, S. Levine, and I. Jaffe, National Bureau of Standards Circular 500, U. S. Government Printing Office, Washington, D. C., 1952; (b) N. K. Smith, D. W. Scott, and J. P. McCullough, *J. Phys. Chem.*, **68**, 934 (1964).

(39) H. C. Dickinson, *Bull. Bur. Std.*, **11**, 189 (1915).

The heat of combustion data obtained for 2-mono-palmitin are typical of all the experimental data. These data are shown in Table II where ΔR is the corrected resistance rise in ohms; ΔT, the corrected temperature rise in °C.; m, the *in vacuo* mass in grams; ΔE_W, the Washburn corrections; ΔE_Σ the total heat correction for the burned fuse wire, nickel crucible loss, nitric acid formation, and ignition energy; ε_{app}, the energy equivalent of the calorimeter system; and M, the molecular weight.

Table II: The Standard State Heat of Combustion of 2-Monopalmitin at 25°

Sample	ΔR, cor. rise, ohm	ΔT, cor. rise, °C.	$\varepsilon_{app}\Delta T$, cal.	ΔE_W, cal.	ΔE_Σ, cal.	m, g.	$-\Delta E_0/M$, cal. g.$^{-1}$
A-1	0.312411	3.08862	8,832.04	19.25	16.28	1.05118	8404.85
2	0.284771	2.81507	8,049.79	17.25	13.63	0.95789	8407.45
3	0.270039	2.66963	7,633.90	16.33	18.90	0.90795	8405.01
4	0.388641	3.84193	10,986.16	24.54	17.18	1.30777	8406.31
B-1	0.398507	3.94036	11,267.60	25.62	15.22	1.34146	8407.26
2	0.359066	3.55060	10,153.09	22.80	15.47	1.20885	8405.03
3	0.391025	3.86730	11,058.71	25.38	19.07	1.31606	8407.69
4	0.270703	3.66522	10,480.86	23.48	20.43	1.24712	8406.49
						Mean	8406.26

Std. dev.: $s = 1.17$; $\bar{s} = 1.33$

Results for the two series of monoglycerides are summarized in Table III. The standard deviations ranged from ±0.014% for 2-monopalmitin to ±0.045% for 2-monobenzoylglycerol and averaged ±0.027% for the combined series.

Derived Results. The standard heat of combustion, ΔH_c°, and the heat of formation, $\Delta H_f^\circ(298.15°K.)$,

Table III: Summary of Combustion Experiments

Compound	Formula	No. of samples measd.	$\Delta E_0^\circ/M \pm \bar{s}$, cal. g.$^{-1}$
2-Monoglycerides			
2-Monostearin	$C_{21}H_{42}O_4$	8	8617.85 ± 1.52
2-Monopalmitin	$C_{19}H_{38}O_4$	8	8406.26 ± 1.33
2-Monomyristin	$C_{17}H_{34}O_4$	8	8158.17 ± 1.41
2-Monolaurin	$C_{15}H_{30}O_4$	7	7863.28 ± 1.42
2-Monocaprin	$C_{13}H_{26}O_4$	6	7497.54 ± 1.69
2-Monobenzoylglycerol	$C_{10}H_{12}O_4$	7	5942.66 ± 1.31
1-Monoglycerides			
1-Monostearin	$C_{21}H_{42}O_4$	8	8607.11 ± 1.16
1-Monopalmitin	$C_{19}H_{38}O_4$	8	8397.18 ± 1.56
1-Monomyristin	$C_{17}H_{34}O_4$	10	8150.57 ± 1.15
1-Monolaurin	$C_{15}H_{30}O_4$	7	7856.16 ± 1.41
1-Monocaprin	$C_{13}H_{26}O_4$	8	7484.79 ± 1.21
1-Monobenzoylglycerol	$C_{10}H_{12}O_4$	7	5937.07 ± 1.34

in kcal. mole^{-1} for the solid state are given in Table IV with the results of ΔE_c and ΔE_R. In addition to these values, the differences in the heats of formation between 2- and 1-monoglycerides representing the heat of isomerization and the energy increment per CH_2 group, $\Delta H_{(CH_2)}$, within each of the two isomeric series are assembled in Tables V and VI, respectively.

Treatment of Data. The procedure of Rossini and Deming[40] was followed in the assignment of uncertainties. An estimate of the standard deviation for single observations of a set of n measurements is denoted by s, and the "over-all" standard deviation assigned to the average mean obtained from the combination of all of the standard deviations involved with each of the sets of observations in accordance with the law of propagation of precision indicies is denoted by $\bar{s}$. The accuracy interval $\bar{s}$ assigned to the arithmetic mean of a set of combustion determinations is determined from the uncertainty interval assigned to the thermometric value for the calorimetric standard benzoic acid, the standard deviation of the arithmetic mean of the set of calibrations, the estimate of the standard deviation of the arithmetic mean of a set of monoglyceride combustion determinations, and the uncertainty interval assigned to the Washburn corrections and firing energy, the latter two combined in an estimate of 1.0 cal./10,000 cal.

For a rejection of a few divergent measurements observed in this investigation, Chauvenet's criterion was conveniently applied.[41]

Interpretation and Significance of Data. The heats of isomerization obtained in this investigation are in the order of magnitude normally expected for isomeric pairs of compounds with values ranging from −1.99 to −3.84 kcal. mole^{-1} for the aliphatic isomers and −1.08 kcal. mole^{-1} for the aromatic isomers. These results contradict Clarke and Stegeman's isomerization value of −9.52 kcal. mole^{-1}. Their heats of combustion for 1-monopalmitin and 2-monopalmitin are 0.16 and 0.40% higher, respectively, and their isomerization energies are approximately three times our values which are internally consistent.

The decreasing progression in the heats of isomerization for the monostearin–monolaurin sequence and the relatively large increase for the monocaprin pair are of interest. The data may be reviewed by the following considerations: (1) the progression is spurious and could be represented by an average value since

(40) F. D. Rossini and W. E. Deming, *J. Wash. Acad. Sci.*, 29, 416 (1939).

(41) A. G. Worthing and J. Geffner, "Treatment of Experimental Data," John Wiley and Sons. Inc., New York, N. Y., 1943, pp. 170, 319.

Table IV: Summary of Derived Values for 25°

	$-\Delta E_0$, kcal. mole^{-1}	$-\Delta E_R{}^\circ$, kcal. mole^{-1}	$-\Delta H_0{}^\circ$, kcal. mole^{-1}	$-\Delta H_f{}^\circ(298.15°K.)$, kcal. mole^{-1}
	2-Monoglycerides			
2-Monostearin	3090.07 ± 0.55	3088.85 ± 0.55	3093.89 ± 0.55	315.81 ± 0.63
2-Monopalmitin	2778.37 ± 0.44	2777.28 ± 0.44	2781.72 ± 0.44	303.25 ± 0.52
2-Monomyristin	2467.50 ± 0.43	2466.49 ± 0.43	2470.34 ± 0.43	289.89 ± 0.49
2-Monolaurin	2157.72 ± 0.39	2156.76 ± 0.39	2160.02 ± 0.39	275.48 ± 0.45
2-Monocaprin	1847.02 ± 0.42	1846.20 ± 0.46	1848.87 ± 0.46	261.90 ± 0.50
2-Monobenzoylglycerol	1165.98 ± 0.26	1165.10 ± 0.26	1165.69 ± 0.26	184.72 ± 0.29
	1-Monoglycerides			
1-Monostearin	3086.22 ± 0.42	3085.01 ± 0.42	3090.05 ± 0.42	319.75 ± 0.52
1-Monopalmitin	2775.37 ± 0.51	2774.23 ± 0.51	2778.67 ± 0.51	306.30 ± 0.58
1-Monomyristin	2465.21 ± 0.35	2464.07 ± 0.35	2467.92 ± 0.35	292.31 ± 0.43
1-Monolaurin	2155.76 ± 0.39	2154.77 ± 0.39	2158.03 ± 0.39	277.47 ± 0.45
1-Monocaprin	1843.88 ± 0.30	1843.04 ± 0.30	1845.71 ± 0.30	265.06 ± 0.35
1-Monobenzoylglycerol	1164.88 ± 0.26	1164.02 ± 0.26	1164.61 ± 0.26	185.80 ± 0.29

Table V: Heats of Isomerization for Monoglycerides[a]

	$-[\Delta H_0{}^\circ(\text{2-MG}) - \Delta H_0{}^\circ(\text{1-MG})]$, kcal. mole^{-1}
Monostearin	3.84 ± 0.69
Monopalmitin	3.05 ± 0.67
Monomyristin	2.42 ± 0.55
Monolaurin	1.99 ± 0.55
Monocaprin	3.16 ± 0.55
Monobenzoylglycerol	1.08 ± 0.37

[a] Enthalpy difference between 2- and 1-monoglycerides.

Table VI: Energy Increment per CH_2 for Aliphatic Monoglycerides

	$\Delta H_{(CH_2)}$,[a] kcal. mole^{-1}	
	2-Monoglycerides	1-Monoglycerides
Stearin–palmitin	155.78 ± 0.35	155.39 ± 0.33
Palmitin–myristin	155.40 ± 0.30	155.08 ± 0.31
Myristin–laurin	154.82 ± 0.29	154.65 ± 0.26
Laurin–caprin	155.28 ± 0.30	155.87 ± 0.25

[a] $\Delta H_{(CH_2)}$ = one-half the enthalpy difference between successive even-carbon homologs.

a heat of isomerization is obtained by the difference between two large numbers that would result in a relatively large error; (2) the progressive decrease in the monostearin–monolaurin sequence is valid, but the monocaprin value is in error; or (3) the observed sequences from monostearins to monocaprins are real and acceptable. With reference to (1), were the average value of -2.89 kcal. mole^{-1} most probable, the extreme values of monostearin and monolaurin

would not overlap this average within their experimental precisions. However, the difference of nearly 1.9 kcal. mole^{-1} between monostearin and monolaurin exceeds the sum of their experimental precisions by 1.5 σ in partial support of the observed progression even though differences between adjacent homologous pairs are exceeded by their combined deviations. With reference to (2), if each of the observed isomerization energies is discrete, the increase exhibited by the monocaprins requires explanation, though only speculation can be made at this time. The higher isomerization energy for the monocaprins would not likely be attributed to a higher energy polymorphic form as a contaminant in the 1-isomer for this would lead to a diminished energy difference between the isomers. A higher energy polymorph for 2-monocaprin, should it exist, could account for the difference. It has been recently reported that 2-monoglycerides show the existence of another polymorphic form,[42] but this claim, based on solubility studies, must be held in reservation pending confirmation by techniques other than solubility, particularly in view of the complications encountered in our solubility test. In consideration of (3), the isomerization energies reported in this paper refer to isomer differences determined for the solid states so that the observed sequence may be a reflection of differences in their sublimation energies. With differences in sublimation energies between successive homologs amounting to about 1.5 kcal. mole^{-1} (*vide infra*), it appears unlikely that this large a difference would exist between closely structured long-chain isomers. Unfortunately, the data currently available on sublimation energies

(42) S. C. Smith, *Dissertation Abstr.*, **23**, 2326 (1963).

of fatty acid derivatives do not permit more definite conclusions.

Since the heats of isomerization show a progression, the energy increment per CH_2 for this data must similarly progress. The CH_2 energy increments of Table VI differ by 1.4 to 2.6 kcal. mole^{-1} from the CH_2 increment reported by Clarke and Stegeman, who claim agreement with Rossini's value[13] for gaseous hydrocarbons. The agreement between their CH_2 energy increment obtained for the solid state and the gaseous state CH_2 energy increment is entirely fortuitous; it is well known that the CH_2 energy increments for these different states of aggregates differ by an amount dependent upon the heat of sublimation. The most recent values for the CH_2 energy increment in $\Delta H_c(g)$ are 157.44 kcal. mole^{-1} for the normal paraffins above C_4H_{10} and 157.46 kcal. mole^{-1} for alcohols above C_4H_9OH.[43] Sublimation energy CH_2 increments of 1.5 to 1.8 kcal. mole^{-1} are reported for several classes of compounds.[44] The increments per CH_2 in $\Delta H_c(s)$ are, therefore, expected to be in the range of 155.5–156 kcal. mole^{-1} in support of the increments derived for the monoglycerides in Table VI. Consequently, Clarke and Stegeman's CH_2 energy increment must be in error by at least 1.5 kcal.

The heat of isomerization (1.08 kcal. mole^{-1}) for the aromatic monoglycerides is of the same order of magnitude as reported for the propylbenzenes (0.67 kcal. mole^{-1})[12c] but is approximately one-third of the aliphatic monoglyceride values. Although the isomerization energy is small, nevertheless, 2-monobenzoylglycerol is energetically comparable to the aliphatic 2-monoglycerides by having a heat of combustion larger than its 1-isomer. This is supporting evidence of its lower thermochemical stability which is contrary to the relative stability that would generally be deduced from the reversed relationship observed from its melting point and solubility characteristics.

Thermochemistry of the Equilibrium. In the relation $\Delta F° = \Delta H° - T\Delta S°$ the free energy change equals the enthalpy change when $\Delta S°$ is zero and is related to the equilibrium constant of the reversible reaction, 2-monoglyceride $\rightleftarrows$ 1-monoglyceride, by the equation $\Delta F° = -RT \ln (\text{1-MG}/\text{2-MG})$. (1-MG/2-MG is the per cent ratio of 1-monoglyceride to 2-monoglyceride.) The per cent of each isomer at equilibrium, calculated from the isomerization energy of -1.08 kcal. mole^{-1}, is 14% 2-monobenzoylglycerol and 86% 1-monobenzoylglycerol. This result is in excellent agreement with the position of the equilibrium for the aromatic monoglycerides determined kinetically by van Lohuizen and Verkade[10] to be 12% 2- and 88% 1-monoglyceride. (Conversely, by use of 1-MG/2-MG = 88:12, $\Delta F°$

is computed to be -1.18 kcal. mole^{-1} in comparison with our experimental value of -1.08 kcal. mole^{-1}.) The agreement between $\Delta F°$ and $\Delta H°$ confirms a negligible, if any, entropy difference of $\Delta S° = 0.3 \pm 1.0$ cal. deg.$^{-1}$ mole^{-1} between these isomers.

The equilibrium position for the monopalmitin pair has been determined by Martin[45] to be 10–8% 2-monopalmitin and 90–92% 1-monopalmitin, a result substantially confirmed (15–12% 2-isomer and 85–88% 1-isomer) by Brokaw, Perry, and Lyman.[46] Assuming a zero entropy difference and, as a first approximation, equating $\Delta F°$ to the transition energy of -3.05 kcal. mole^{-1} for the monopalmitins, the equilibrium is calculated to be 0.5% 2- and 99.5% 1-monopalmitin, a result that disagrees significantly with the reported equilibrium values. The assumption that $\Delta S°$ for the aliphatic monoglycerides is zero or negligible appears to be unjustified. Calculating for $\Delta S°$ by using the Martin range of values for 1-MG/2-MG = 90:10 and 92:8, $\Delta F° = -1.30$ and -1.44 kcal. mole^{-1}, respectively, and combining these results with $\Delta H° = -3.05 \pm 0.67$ kcal. mole^{-1}, $\Delta S°$ is calculated to -5.6 ± 2.2 cal. deg.$^{-1}$ mole^{-1}. (Similarly, Brokaw's values lead to $\Delta S° = -6.7 \pm 2.2$ cal. deg.$^{-1}$ mole^{-1}.) The negative entropy difference for the aliphatic monoglycerides[47] may be tentatively interpreted on the basis of available, though limited, physical data on the solid compounds.

Nuclear magnetic resonance of monoglycerides[48] shows that the β_L forms give rise to large second moments for 1-monostearin (19.9 $\pm$ 1.7 gauss^2), 1-monomyristin (19.7 $\pm$ 1.3 gauss^2), and 2-monopalmitin (18.2 $\pm$ 0.9 gauss^2). The smaller second moment for 2-monopalmitin shows that for this isomer the hydrocarbon chain has relatively more freedom of motion about the chain axis.

(43) J. H. S. Green, *Chem. Ind.* (London), 1215 (1960), and references contained therein.

(44) (a) A. R. Ubbelohde, *Trans. Faraday Soc.*, **34**, 282 (1938); (b) K. L. Wolf and H. Weghofer, *Z. physik. Chem.*, **339**, 194 (1938); (c) M. Davies and V. E. Malpass, *J. Chem. Soc.*, 1048 (1961); (d) H. A. Swain, Jr., L. S. Silbert, and J. G. Miller, *J. Am. Chem. Soc.*, **86**, 2562 (1964), and references contained therein.

(45) J. B. Martin, *ibid.*, **75**, 5483 (1953).

(46) G. Y. Brokaw, E. S. Perry, and W. C. Lyman, *J. Am. Oil Chemists' Soc.*, **32**, 194 (1955).

(47) A referee validly objected to the $\Delta S°$ calculation for not having allowed for activities of the components in the measured solution systems for obtaining the equilibrium constant and similarly correcting the heats of formation by heats of sublimation prior to computing the heats of isomerization. Lacking such data, it may be conjectured that the over-all effects are small as the quantitative differences between the isomers are expected to be nil. It is statistically significant that the absolute value of $\Delta S°$ is about 2.6 times the standard deviation.

(48) D. Chapman, R. E. Richards, and R. W. York, *J. Chem. Soc.*, 436 (1960).

Infrared spectroscopic examination of the OH stretching band (3200–3600-cm.$^{-1}$ region) and of the carbonyl stretching band (1700-cm.$^{-1}$ region) has been reported for monoglyceride isomers and polymorphs.[25a,49] In 1-monoglycerides, the OH and C=O stretching bands are observed to move to lower frequencies and higher frequencies, respectively, in the order liquid $\rightarrow \alpha_L \rightarrow$ sub-$\alpha_L \rightarrow \beta_L' \rightarrow \beta_L$, which is also the order of increasing stability of the polymorphic forms. Chapman[25a] interpreted this to be the order of increasing hydrogen bonding strength with preferential bonding occurring between OH groups rather than between OH and C=O groups. The 2-monoglycerides similarly prefer stronger hydrogen bonding between OH groups than between OH and C=O groups on passing from the liquid to the β_L form, its only known crystal form. A comparison of bands between the β_L forms of 1- and 2-monoglycerides indicates the former to have the stronger interaction between OH groups and the weaker OH to C=O group interaction. The comparison lends evidence of stronger interactions and lesser mobility of the chains for the 1-isomer.

The 1-monoglycerides have melting points about $10°$ higher than the 2-isomers. Malkin[50] suggests that the hydrogen bonding of 2-monoglycerides is of the head to head type and that 1-monoglycerides, because of their higher melting points, may involve lateral hydrogen bonding in addition to the normal head to head. By having lower melting points, the 2-monoglycerides

may be expected *a priori* to have larger long spacings and, inferentially, larger molar volumes; however, smaller long spacings were observed experimentally.[27,28] We calculated molar volumes from their solid densities[37,51] from which the 2-monoglycerides are larger by 0.5 to 2.9 ml. mole^{-1} for the monocaprin–monostearin sequence.[52] These physical properties, separately and *in toto*, are evidences of larger restraints in crystalline 1-monoglycerides that would also lower their entropy relative to the crystalline 2-isomers.

No supporting evidence is presently available to account for the nearly zero $\Delta S°$ for the aromatic monoglycerides whose crystal structures would not be expected to correspond to those of aliphatic structures.

(49) Bands for 1-monostearin and 1-monopalmitin are as follows: liquid state (3453 cm.$^{-1}$; 1706 cm.$^{-1}$; α_L form (3360 cm.$^{-1}$; 1720 cm.$^{-1}$); sub-α_L form (3342 cm.$^{-1}$; 1730 cm.$^{-1}$); β_L' and β_L forms are similar by having an OH split, *e.g.*, β_L' form [3342 (main component) and 3243 cm.$^{-1}$; 1736 cm.$^{-1}$] and β_L form [3243 (main component) and 3307 cm.$^{-1}$]. Analogous bands for 2-monomyristin are 3527 and 1715 cm.$^{-1}$ for the liquid state and 3347 and 1733 cm.$^{-1}$ for the β_L form.

(50) T. Malkin, *Progr. Chem. Fats Lipids*, **2**, 34 (1954).

(51) Solid densities for monoglycerides were reported for measurements at $21°$.[37a] Merker's measurements at $30°$[37b] in g./ml. are listed as follows for convenience: 2-monostearin, 1.044; 1-monostearin, 1.053; 1-monopalmitin, 1.060; 1-monomyristin, 1.068; 1-monolaurin, 1.077; 1-monocaprin, 1.088.

(52) Although solid densities of the isomers differ only by 0.002–0.009 g./ml. for the monocaprin–monostearin series and these differences may be within the experimental precision of their measurements, it is striking that the 2-isomers are uniformly less dense (with the exception of 1-monostearin at $21°$) than their corresponding 1-isomers.

Salting in by an Aqueous Polyelectrolyte Solution

by Joseph Steigman and Judah L. Lando[1]

Department of Chemistry, Polytechnic Institute of Brooklyn, Brooklyn, New York (*Received February 12, 1965*)

A study of the reaction in water at 25° between the strong polymeric acid poly(p-styrene-sulfonic acid) and the basic indicator p-nitroaniline showed that the protonation constant of the indicator (expressed in concentration units) decreased with increasing acid concentration. This was attributed to salting in of the p-nitroaniline by the polymer solutions. The acidities of mixtures of the polyacid (0.1 N) and HCl (0.05 to 0.20 M) were additive. The solubility of p-nitroaniline in water increased linearly with increasing concentrations of salts of the polyacid. The order of cation effectiveness was $Li^+ < Na^+ < K^+ < Rb^+ < Cs^+ < (CH_3)_4N^+$. Potassium chloride, which salts out the indicator, nevertheless increased the latter's solubility in potassium poly(p-styrenesulfonate) solution. These results are explained by increased organization of the water structure in the vicinity of the polyelectrolyte. Salting in is regarded as the incorporation of the solute in a cage of organized water molecules. In this connection, a brief description is given of crystalline compounds containing sodium or potassium p-toluenesulfonate, p-nitroaniline, and water. They may represent a type of clathrate since most of the solid is composed of water.

Theoretical descriptions of the distribution (and activities) of counterions in a polyelectrolyte solution have been undertaken by assuming a model for the configuration of the polymer and subsequently calculating the electrostatic potential and the small-ion concentration variation near the polyion.[2,3] The more convenient division of counterions into two limiting classes, free and bound, facilitated the interpretation of experimental data obtained from transport measurements[4] but led to difficulties when it was applied to equilibrium measurements. Metal[5] or membrane[6] electrode measurements have shown that the activity coefficients of sodium polysalts in aqueous solution are very much less than those of simple sodium salts at equivalent concentrations. It is reasonable to conclude that the bound ions do not register their presence at the electrode and that only the free ions do so. When this conclusion was applied by Mock and Marshall,[7] an unexpected relationship emerged. By means of a glass electrode they had measured the acidity of dilute aqueous solutions of a sulfonated copolymer of styrene and vinyl toluene. The observed pH was higher than that of an HCl solution at the same equivalent concentration. The classification of the hydronium counterions into free and bound resulted in a value of 0.4 for the free fraction. However, this value was independent

of polymer concentration from more dilute solutions to 0.01 equiv. of hydronium ion/l. Furthermore, the addition of HCl (to $3 \times 10^{-3} N$) to the polymeric acid (to $10^{-2} N$) lowered the pH to the same extent that would have been observed for its addition to a solution of a mineral acid whose initial pH was the same as that of the polymer solution. Hence, a mass-action constant could not be used to describe any equilibrium between bound and free counterions since this equilibrium, if it existed, was independent of the polyelectrolyte concentration and was not affected by added common ions. There was, in fact, a simple additivity in the properties of polyelectrolyte solutions containing added small electrolytes with an ion in common. The solute activity in the mixed solution

(1) From a thesis submitted by Judah L. Lando to the Graduate School of the Polytechnic Institute of Brooklyn in partial fulfillment of the requirements for the degree of Doctor of Philosophy.

(2) T. Alfrey, Jr., P. W. Berg, and H. Morawetz, *J. Polymer Sci.*, **7**, 543 (1951).

(3) S. Lifson and A. Katchalsky, *ibid.*, **13**, 43 (1954).

(4) J. R. Huizenga, P. F. Grieger, and F. T. Wall, *J. Am. Chem. Soc.*, **72**, 2336, 4228 (1950).

(5) W. Kern, *Makromol. Chem.*, **2**, 279 (1948).

(6) M. Nagasawa and I. Kagawa, *J. Polymer Sci.*, **25**, 61 (1957); *errata*, **31**, 256 (1958).

(7) R. A. Mock and C. A. Marshall, *ibid.*, **13**, 432 (1954).

was the weighted sum of the activities of polymer and added electrolyte. This additivity has also been observed by means of electrode and osmotic measurements in solutions of sodium salts of various strong polyacids.[6,8,9] Alexandrowicz[10] has found it to hold for osmotic and Donnan equilibria in solutions of sodium polyacrylate containing sodium bromide.

The relationship between polyacid acidity and the glass electrode measurements of Mock and Marshall is not clear at the present time. These measurements cannot be interpreted to mean that the polysulfonic acid is a weaker acid than HCl or even that two different species of hydronium ion are present in the polymer solution. Proton magnetic resonance studies of aqueous solutions of poly(p-styrenesulfonic acid) led to the conclusion that only one type of hydronium ion was present identical with that found in aqueous solutions of the common strong acids.[11] A similar conclusion was reached by Savo and Rice after an examination of the Raman spectra of aqueous solutions of the same polymeric acid and of p-ethylbenzenesulfonic acid.[12] Kern reported that the same polysulfonic acid was a more efficient catalyst than sulfuric acid in the inversion of sucrose.[13]

This research was initially undertaken in order to examine the acidity of poly(p-styrenesulfonic acid) by means of its reaction with a simple basic indicator at various polymer concentrations and in the presence of added HCl. The indicator was p-nitroaniline, a weak base whose pK_a is 0.99 at 25°.[14,15] It is quite convenient for the study of dilute solutions of strong acids in water. Its basic form is yellow (maximum absorption at 3800 Å.) while the conjugate acid is colorless.

Experimental

Poly(p-styrenesulfonic acid). Poly(p-styrenesulfonic acid) was prepared by the direct sulfonation of Styron PS-2 (Dow Chemical Co., Midland, Mich.). This is a linear polystyrene of molecular weight 20,000. Turbak's sulfonation procedure was followed[16] with one modification. This low molecular weight polymer after sulfonation did not precipitate out from ethanol on the addition of 1,2-dichloroethane; this complicated the separation of the sulfonic acid from excess SO₃. Accordingly, the sulfonated product was dissolved in 2 M aqueous NaOH and passed through a Dowex 21-K anion-exchange resin in the hydroxyl form in order to remove excess sulfate. After the effluent had been freed from sulfate, it was passed through a Dowex 50 W-X8 exchange resin in the hydronium form and freed from sodium. It was then

concentrated by vacuum evaporation of water at room temperature in a Buchler rotary evaporator.

The salts of the polyacid were prepared by titrating the acid with an aqueous solution of the desired hydroxide.

Salts of p-toluenesulfonic acid were prepared by titrating concentrated aqueous solutions of the purest available grade of the acid with the appropriate hydroxide and recrystallizing twice from water. The salts were then vacuum dried at 80° until their infrared spectra showed no water bands.

The p-toluenesulfonic acid was obtained from Matheson Coleman and Bell (Highest Purity) or Eastman Kodak (White Label) and recrystallized twice from chloroform.

The indicator p-nitroaniline was a Highest Purity product from Matheson Coleman and Bell. It was recrystallized repeatedly from aqueous ethanol. Aqueous solutions at 25° showed a molar absorbancy index of 13,180 ± 40 at 3800 Å. for the concentration range 4×10^{-5} to 1.3×10^{-4} M. In concentrated sodium polystyrenesulfonate the peak absorption was found at slightly higher wave lengths (up to 40 Å.) without a significant change in the index. Peak absorbance values were used for all solutions.

Rubidium and cesium hydroxides were prepared from the chlorides (products of Gallard, Schlesinger, and Co.) by means of an anion-exchange resin. The tetramethylammonium hydroxide solution was prepared in the same way from the chloride (Eastman Kodak White Label).

Spectrophotometric measurements were made on a Cary Model 14 spectrophotometer.

Measurements of pH were made with a Radiometer pH M 4 meter, using a Beckman glass electrode and a reference saturated calomel electrode.

Solubility determinations were performed at 25.0 ± 0.1° by shaking a solution with excess solid in 20.3-cm. test tubes fastened to a Burrell wrist-action shaker. At least 72 hr. was allowed for equilibration. Paul's technique[17] for taking the sample was slightly

(8) M. Nagasawa, M. Izumi, and I. Kagawa, *J. Polymer Sci.*, **A37**, 375 (1959).

(9) M. Nagasawa, A. Takshashi, M. Izumi, and I. Kagawa, *ibid.*, **A38**, 213 (1959).

(10) Z. Alexandrowicz, *ibid.*, **43**, 337 (1960).

(11) L. Kotin and M. Nagasawa, *J. Am. Chem. Soc.*, **83**, 1026 (1961).

(12) L. Savo and S. A. Rice, *ibid.*, **83**, 496 (1961).

(13) W. Kern, W. Herold, and B. Scherlag, *Makromol. Chem.*, **17**, 231 (1956).

(14) L. P. Hammett and A. J. Deyrup, *J. Am. Chem. Soc.*, **54**, 2721 (1932).

(15) M. A. Paul and F. A. Long, *Chem. Rev.*, **57**, 1 (1957).

(16) A. F. Turbak, *Polymer Preprints*, **1**, 141 (1961).

modified. The saturated solution was forced through a glass tube with a glass wool plug by cautiously applying pressure from a nitrogen tank. It was analyzed spectrophotometrically in the case of p-nitroaniline (after appropriate dilution) or by titration with standardized KOH in the case of benzoic acid.

Experimental Results and Discussion

The protonation of p-nitroaniline by the polymeric acid is described by

$$B + H^+P^- \rightleftharpoons BH^+P^- \tag{1}$$

in which B represents the basic indicator, H^+P^- stands for the polyacid, and BH^+P^- is the reaction product (whether dissociated or existing in some bound form). A similar reaction between an ordinary acid and the indicator in water could be quantitatively formulated in terms of a thermodynamic equilibrium constant since the activity coefficients of the various species would approach unity on continued dilution. This is not possible for polyelectrolyte solutions, in which, if anything, counterion activity coefficients tend to decrease as the concentration decreases.[18] Since nothing was known about the activities of the counterion species, a mass-action protonation constant, K_p, was formulated in terms of concentrations

$$K_p = \frac{[BH^+P^-]}{[B][H^+P^-]} \tag{2}$$

The polyacid concentration is expressed as equivalents of titratable acid per liter. The other quantities represent moles per liter. The extent of the reaction was determined by measuring the absorbance of the unreacted neutral indicator at 3800 Å. (since its protonated form is colorless in the visible region). If C represents the total analytical concentration of the indicator, A represents the absorbance of its solution, which contains a concentration of acid equal to $[H^+P^-]$, and 13,180 represents the molar absorptivity of the p-nitroaniline, then the protonation constant can be expressed in the form

$$K_D = \frac{\left[C - \dfrac{A}{13,180}\right]}{[H^+P^-]\left[\dfrac{A}{13,180}\right]} \tag{3}$$

The reaction was investigated at 25° in a series of polymer solutions ranging in concentration from 10^{-3} to 0.3 N. At each acid concentration the stoichiometric indicator concentration was varied over a range; for example, from 6×10^{-5} to 1.3×10^{-4} M in 5×10^{-3} N polymer and from 3×10^{-4} to 7×10^{-4} M

in 0.3 N polymer. The value of the protonation constant at each level of polymer concentration was found to be independent of the indicator concentration, pointing to a simple 1:1 stoichiometry in the reaction and showing an absence of any complicating indicator association reaction. Apart from the lowest polymer concentration (10^{-3} N) where the standard deviation was about 11% (because of the very small extent of reaction), the error was less than 1% in the values of the constant.

On the other hand, the values of K_p varied systematically with the polymer concentration, from 33.25 in 10^{-3} N acid to 14.52 in 0.3 N acid. This is explained by assuming that some fraction of the uncharged base is closely associated with the polymer, that the association increases with increasing polymer concentration, and that in this condition the activity coefficient of the molecule is decreased, so that the base is weaker. This is equivalent to salting in the indicator. For convenience, the following analysis is based on a hypothetical salting in although the polyacid solutions were not saturated with p-nitroaniline. It is assumed that the activity coefficient of the neutral base will be affected primarily by the polymer concentration and will be affected only slightly by its own concentration.

In water and in polymer solutions saturated with p-nitroaniline, the latter's activity is constant

$$f_0 S_0 = f_p S_p \tag{4}$$

Here f_0 and S_0 are the activity coefficient and the solubility of the indicator in water, and f_p and S_p are the corresponding quantities in a polymer solution. The activity coefficient in water is almost unity

$$S_p = \frac{S_0}{f_p} \tag{5}$$

Salting in by electrolytes is usually described by an approximately logarithmic relationship between solute solubility and electrolyte concentration.[19] We hypothesize that salting in by a polyelectrolyte solution is characterized by the extraction or dissolution of a constant quantity of solute by each polymer unit at fixed solute concentration. Increasing the polymer concentration should linearly increase the solubility of the solute

$$S_p = S_0 + k[H^+P^-] \tag{6}$$

(17) M. A. Paul, J. Am. Chem. Soc., 76, 3236 (1954).

(18) S. A. Rice and M. Nagasawa, "Polyelectrolyte Solutions," Academic Press Inc., New York, N. Y., 1961, p. 399.

(19) F. A. Long and W. F. McDevit, Chem. Rev., 51, 119 (1952).

Here K is a proportionality constant. Substitution and rearrangement yield

$$f_p = \frac{S_0}{S_0 + k[H^+P^-]} = \frac{1}{1 + k'[H^+P^-]} \quad (7)$$

in which k' represents k/S_0. The protonation constant takes the form

$$K_p = \frac{[BH^+P^-]}{[B][H^+P^-]f_p} \quad (8)$$

In very dilute polyacid solution there will be almost no salting in, and there will be a limiting protonation constant, K_0

$$K_0 = \frac{K_p}{f_p} = K_p(1 + k'[H^+P^-]) \quad (9)$$

Analysis of the data and a simple trial-and-error fit gave a value of 4.03 for k' and a value of 33.30 for K_0. Table I shows the experimental values of K_p at various polyacid concentrations, the calculated values of K_p, and the difference between them.

Table I: Observed and Calculated Values of K_p at 25°

Polymer concn., N	K_p(obsd.)	K_p(calcd.)	K_p(obsd.) − K_p(calcd.)
1.00×10^{-3}	33.25 ± 3.54	33.17	$+0.08$
5.00×10^{-3}	32.61 ± 0.24	32.64	-0.03
7.50×10^{-3}	32.61 ± 0.26	32.32	-0.29
1.00×10^{-2}	31.81 ± 0.26	32.01	-0.20
2.50×10^{-2}	31.35 ± 0.30	30.25	$+1.10$
5.00×10^{-2}	28.79 ± 0.27	27.72	$+1.07$
7.50×10^{-2}	26.18 ± 0.19	25.57	$+0.61$
1.00×10^{-1}	24.21 ± 0.10	23.73	$+0.48$
2.00×10^{-1}	18.35 ± 0.08	18.44	-0.09
3.00×10^{-1}	14.52 ± 0.11	15.07	-0.55

It is clear from the last column that there is some bias in the calculated results. Undoubtedly a somewhat better fit could have been made. However, even with the bias, it is evident that the agreement between the observed and calculated values is excellent since the largest difference is a little more than 3% over a large concentration range. Thus, the change in K_p with varying polymer concentration is quantitatively accounted for by a change in the activity coefficient of the neutral base. Hence, the ratio $f_{BH^+P^-}/f_{H^+P^-}$ is constant from 10^{-3} to 0.3 N acid, and the acidity of the polyacid towards the indicator is constant over the same concentration interval.

The limiting value of the indicator protonation constant for the polyacid is approximately three times greater than that obtained for the reaction between HCl and p-nitroaniline. This may be due to electrostatic binding of the anilinium ion to the polyanions, combined electrostatic and hydrophobic bonding, a higher acidity for the polyacid than for HCl, or to all of these factors. It is not possible to decide among these alternatives at the present time.

The hypothesis that the neutral indicator is salted into the polyacid solution suggested that the solubility of the indicator would increase linearly with polyelectrolyte concentration in solutions of various salts of the polyacid. The results of such solubility measurements are shown in Table II. The solubility was a linear function of concentration for each salt which was examined. From five to eight different concentrations were used for each cation. The slope for a given cation is a measure of its effectiveness in the salting-in process.

Table II: The Solubility of p-Nitroaniline in Polysalt Solutions

Cation	Concn. range, N	Slope $\times 10^2$	Intercept $\times 10^3$, M	Std. dev. of the slope, %
Water alone			4.152	
Li$^+$	0.06–0.48	2.36	4.12	1.9
Na$^+$	0.09–0.80	2.65	3.96	3.0
K$^+$	0.08–0.80	3.07	3.78	0.4
Rb$^+$	0.11–0.40	3.20	3.94	1.6
Cs$^+$	0.10–0.43	3.51	3.81	0.7
(CH$_3$)$_4$N$^+$	0.09–0.57	4.15	3.42(?)	2.6

The salting in by the polyacid is expressed by the constant k in eq. 5 and 6. From the variation of K_p with polymer concentration it is possible to calculate a value of 1.67×10^{-2} for the hydronium cation. The salting-in efficiency thus varies with cations in the order H$^+$ < Li$^+$ < Na$^+$ < K$^+$ < Rb$^+$ < Cs$^+$ < (CH$_3$)$_4$-N$^+$.

The linearity of salting in with concentration and the order of cation effectiveness are not limited to p-nitroaniline. This was shown by a similar although more limited study carried out on benzoic acid. The latter was chosen so that salting in by the polyacid would not be obscured by an acid–base reaction with the solute. The results are shown in Table III. No correction was applied for hydronium–potassium exchange in the potassium salt solution.

It should be noted that while benzoic acid is salted in more strongly than p-nitroaniline, the ratio of slopes for potassium ion to hydronium ion is virtually the same in the two cases. It is approximately 1.8.

The effect of an added strong acid on the protonation

Table III: Solubility of Benzoic Acid in Polysulfonate Solutions at 25°

Cation	Concn. range, N	Slope × 10³	Intercept, M	Relative std. dev., %
			2.753[a]	
H⁺	0.1–0.5	4.73	2.72	19.5
K⁺	0.18–0.80	8.49	2.83	1.5

[a] A. Seidell, Ed., "Solubilities of Inorganic and Organic Compounds," Supplement to the 3rd Ed., D. Van Nostrand Co., New York, N. Y., 1952, p. 680.

of p-nitroaniline by the polyacid was measured in 0.10 N polymer solution with different concentrations of hydrochloric acid. The protonation constant of HCl was first determined spectrophotometrically and is shown in Table IV.

Table IV: K_p of p-Nitroaniline with HCl

Acid concn., M	K_p
0.05	9.51 ± 0.05
0.10	10.13 ± 0.22
0.20	10.63 ± 0.04
0.40	11.66[a]
0.60	12.69 ± 0.04

[a] The protonation constant in 0.40 M HCl was calculated by least squares when it was observed that the constants for the other four concentrations fell on a straight line. The slope of the graph of K_p against molarity of acid is 5.13, the zero intercept is 9.61, and the relative standard deviation of the slope is 0.6%.

It was assumed that in mixtures of the polyacid with HCl the polymer had no effect on the indicator–HCl reaction. The extent of its reaction with the polymer was then determined by difference. These experiments were performed at a fixed concentration of the polymer (0.1 N) and with a number of different concentrations of HCl. The results appear in Table V.

Table V: K_p of p-Nitroaniline with 0.1 N Polyacid in the Presence of HCl

Added HCl concn., M	K_p of polyacid in HCl
0	24.2 ± 0.1
0.05	24.0 ± 0.4
0.10	23.1 ± 0.4
0.20	22.8 ± 1.4
0.40	17.7 ± 1.1
0.60	10.6 ± 0.5

There is very little change in the protonation constant of the polyacid until the concentration of HCl exceeds 0.2 M. This means that there is an additivity of the polymer acidity and of the HCl acidity over a much greater concentration range than that investigated by Mock and Marshall.[7] At higher mineral acid concentrations the value of K_p decreases. This could be due to a mass-action effect on the free to bound ratio of hydrions, an invasion of the polyelectrolyte volume by the HCl, or an increased salting in of the indicator because of the added HCl. It is believed that the decrease is due largely to an increased salting in of the indicator. Such increased salting in was noted in the measurement of the solubility of p-nitroaniline in solutions containing both the potassium salt of the polyacid and potassium chloride. The latter, like almost all inorganic electrolytes, usually salts out organic solutes from water. As long as the organic compound is not too soluble so that mutual interaction terms are numerically unimportant,[19] it is possible to describe the effect of added electrolyte on its solubility by means of the Setschenow equation

$$\log \frac{S_0}{S_i} = K_s C_s \tag{10}$$

Here S_0 is the solubility of the compound in water and S_i is its solubility in an electrolyte solution of concentration C_s. K_s, a constant of proportionality, is known as the Setschenow constant. If K_s is positive, the electrolyte causes salting out. Many instances have been reported of a linear relationship between the logarithm of the ratio of solubilities and the electrolyte concentration.[20,21] In the case of p-nitroaniline Paul[22] found a Setschenow constant for KCl of 0.024 at 25°. We have found substantially the same constant. This means that there is a slight decrease in indicator solubility with increasing KCl concentration. If salting out and salting in were additive properties, one would expect that the addition of KCl to a potassium poly-(p-styrenesulfonate) solution would result in a smaller solubility increase for p-nitroaniline than with the polymer alone. The results are shown in Table VI.

The data are not precise enough to show whether there is an additivity of effects in the most dilute KCl solution, particularly since the calculated intercept for the potassium salt of the polymer in Table II is a little less than the known solubility of p-nitroaniline

(20) See footnote a, Table III.

(21) F. A. Long and R. L. Bergen, Jr., *J. Phys. Chem.*, **58**, 163 (1954).

(22) M. A. Paul, *J. Am. Chem. Soc.*, **76**, 3236 (1954). The solubility in water is given as $4.20 \times 10^{-3} M$.

Table VI: Solubility of p-Nitroaniline in 0.10 N Potassium Poly(p-styrenesulfonate) with Added KCl

Concn. of added salt, M	Solubility $\times$ 10^3, M
0	6.85 (calcd.)
0.1	6.97
0.5	7.18
1.0	7.45
1.5	7.40

in water. However, there is little doubt about the effect of KCl in the higher concentration range. It produces a small but definite increase in the salting in of the indicator by the polyelectrolyte. This means that the activity coefficient of the neutral molecule is further diminished by the addition of KCl to the polymer solution. By analogy, in a polyacid solution (Table V) the salting in of the indicator would be increased by added HCl, the indicator would behave like a weaker base towards the polymer, and the value of K_p would decrease.

Potassium p-toluenesulfonate, unlike KCl, usually salts in organic solutes. Table VII shows the effect of added potassium tosylate on the solubility of p-nitroaniline in 0.1 N potassium poly(p-styrenesulfonate) solution.

Table VII: Solubility of p-Nitroaniline in 0.1 N Potassium Poly(p-styrenesulfonate) with Added Potassium Tosylate

Concn. of added salt, M	PNA solubility $\times$ 10^3, M	Calcd. PNA solubility $\times$ 10^3, M
0	7.22 (calcd.)	7.22 (calcd.)
0.2	8.59	8.53
0.4	10.74	10.35

The numbers in the third column were obtained by assuming that the polymer and the tosylate increased the PNA solubility additively. Its solubility in the polymer solution was calculated from the results in Table II; that in the tosylate solutions was calculated from data in our laboratory, using -0.60 for the Setschenow constant. Uncertainties in the slopes of the salting-in curves resulted in a large error in all the calculated results. Within that error there is a simple additivity in salting in by this electrolyte mixture, in contrast to the effect of a mixture of potassium chloride and the polymer.

These various results can be explained qualitatively in terms of the effects of ionized solutes on the structure of liquid water.[23] Electrolytes like KCl, which are

believed to disrupt the hydrogen-bonded water structure, salt out hydrophobic organic molecules. Organic electrolytes, like arylsulfonate salts or quaternary ammonium compounds salt in the same compounds.[19] Diamond[24] has advanced the idea of water structure enforced ion pairing to explain the solution properties of large hydrophobic ions. He attributed the salting in of neutral organic molecules by such ions to the ability of the water structure to force the neutral molecules into the same cavity as the structure-enforced ion pairs in order to minimize its contiguity with the hydrophobic surfaces. We believe that the water is very strongly organized in the vicinity of the polysulfonate ions and that the p-nitroaniline is salted into this organized water layer. The order of efficiency of the cations in salting in the solute is the order of ability of each polyanion–cation combination to organize the water structure. These combinations consist of a structure-destroying cation which is coupled with a structure-forming polyanion. In the alkali metal halides the larger cations disrupt the water structure to a greater extent than the smaller ones.[25] The results in Table I, however, suggest that the larger cations are responsible in some fashion for a more strongly organized water layer around the polymer than is found for the smaller ones. They may approach the sulfonate ions more closely than the smaller ions, precisely because they disrupt the water structure strongly. The resulting ion pair has a small effect on the hydrogen bonding, which is established around it. Similarly, with quaternary ammonium compounds the bromides[21] salt in benzoic acid to a much smaller extent than the corresponding iodide salts.[26] The alkali iodides disrupt the water structure more strongly than the bromides.

The tetramethylammonium salt falls into a different category. Both the cation and the anion are capable of organizing the water, and p-nitroaniline is salted in even more strongly than in the cesium salt solution.

The effects of the addition to a polyelectrolyte solution of simple electrolytes with a common ion has been examined theoretically in terms of electrical interactions.[27,28] The results reported in Tables VI and VII suggest, however, that there may be differences in effects arising from the addition of different simple

(23) See J. L. Kavanau, "Water and Solute-Water Interactions," Holden-Day, Inc., San Francisco, Calif., 1964, for general references.

(24) R. M. Diamond, *J. Phys. Chem.*, **67**, 2513 (1963).

(25) H. S. Frank and M. W. Evans, *J. Chem. Phys.*, **13**, 507 (1945).

(26) J. O'M. Bockris, J. Bowler-Reed, and J. A. Kitchener, *Trans. Faraday Soc.*, **47**, 184 (1951).

(27) Z. Alexandrowicz, *J. Polymer Sci.*, **B56**, 97 (1962).

(28) Z. Alexandrowicz and A. Katchalsky, *ibid.*, **A1**, 3231 (1963).

electrolytes. If the added salt is a structure former, like a tosylate, there may be a simple additivity in salting in. However, potassium chloride, which disrupts the solvent structure, causes an increased salting in of p-nitroaniline by the potassium polysulfonate. We interpret this as a further tightening of the water structure around the polymer as a response to the disruptive effect of the KCl. The effect is probably small at low salt concentrations because of the very high degree of organization of the water around the polymer. As the salt concentration is increased, the water around the polymer will withstand disruption through still stronger self-organization, resulting in more marked salting in of the solute. This increased self-organization may be a preliminary stage in the withdrawal of the polymer-organized water component from the solution of the KCl—that is, a coacervation or separation into two aqueous phases. In these experiments no coacervate was observed, probably because the highest KCl concentration tested was too low to cause it.[29]

Experiments were conducted to see if there was a resemblance between the salting in of p-nitroaniline by different alkali polysulfonate solutions and its adsorption from aqueous solution by ion-exchange resins with different counterions. Approximately 1 g. of Dowex 50 W-X8 resin in each form was shaken with 25-ml. aliquots of 1.96×10^{-4} M p-nitroaniline for 1 week at 25°. The following sorption values were obtained for the different resins, in per cent: K^+, 87.2; Na^+, 80.7; Li^+, 67.1. The order of adsorption of the solute by the resins is qualitatively the same as the salting-in order of the corresponding polyelectrolyte salts. Similar measurements with the anion-exchange resin Dowex 21 K with different counterions showed that the order of solute adsorption from solution was $ClO_4^- > I^- > Br^-$, which is a similar sequence for anions. Solute adsorption on ion-exchange resins is commonly ascribed to a van der Waals interaction between the solute and the organic backbone of the resin.[30] The results reported here suggest rather that the solute is salted into a highly organized water layer in the vicinity of the hydrocarbon groups of the resin. In this connection, the effect of added simple electrolytes on the sorption of neutral molecules by ion-exchange resins, which has

been called "salting-out chromatography,"[31] may be due to increased salting in because of an increase in the organization of the water in the resin phase.

Some observations on the solubility of p-nitroaniline in concentrated alkali tosylate solutions are consistent with the hypothesis of incorporation of the solute in a cavity formed by the organic salt.[24] A fuller account of these results will be reported elsewhere. The solubility of p-nitroaniline at 25° reaches a maximum in 1.7 M sodium tosylate and in 1 M potassium tosylate. There is also a change in the nature of the solid phase. If 300 mg. of the solute is heated with 10 ml. of 2.5 M sodium tosylate, it dissolves. On cooling to room temperature, almost the entire mass crystallizes. A powder diffraction diagram did not show any p-nitroaniline and was quite different from that of sodium tosylate. There are approximately 20 moles of water/mole of organic salt; the ratio is undoubtedly higher for potassium tosylate. Such a large water content is seen in the quaternary ammonium salt hydrates investigated by Jeffrey.[32] These compounds are clathrates. One reported structural unit is a $H_{40}O_{20}$ pentagonal dodecahedron.[33] The structures of alkali metal tosylate hydrates have not yet been investigated. These compounds are undoubtedly less symmetrical than the quaternary ammonium salt hydrates. It is possible that p-nitroaniline aids in the formation of a more symmetrical clathrate. It is reasonable to conclude that the solute is in a water cage in the solid and that it is probably in some kind of water cage in the tosylate solution as well.

(29) C. A. Marshall and R. A. Mock, J. Polymer Sci., 17, 591 (1955).

(30) F. Helfferich, "Ion Exchange," McGraw-Hill Book Co., Inc., New York, N. Y., 1962.

(31) W. J. Rieman, III, J. Chem. Educ., 38, 338 (1961).

(32) R. McMullan and G. A. Jeffrey, J. Chem. Phys., 31, 1231 (1959).

(33) D. Feil and G. A. Jeffrey, ibid., 35, 1863 (1961).

Comparison Standards for Solution Calorimetry[1]

by Stuart R. Gunn

Lawrence Radiation Laboratory, University of California, Livermore, California (Received February 15, 1965)

Criteria for processes to be used in checking and comparing solution calorimeters are discussed. Measurements have been made of the heats of four processes: dissolution of potassium chloride in water, dissolution of succinic acid in hydrochloric acid, reaction of sulfuric acid with excess sodium hydroxide, and reaction of tris(hydroxymethyl)aminomethane with hydrochloric acid. It is concluded that the last two are most generally satisfactory. Corrections to be applied in different types of solution calorimeters and some sources of instrumental error are discussed.

Introduction

Solution calorimetry may be broadly defined as calorimetry of all processes—dissolution, mixing, dilution, and reaction—occurring primarily in a liquid solution. This field has suffered from the lack of any generally accepted standard process for the intercomparison of calorimeters; many investigations exhibit good internal precision but are not free from suspicion of significant systematic error.

Standard substances for calorimetry may be considered to be of two kinds: first, calibrating standards, which are used to transfer the unit of energy from a standardizing laboratory for the purpose of calibrating other calorimeters, and second, comparison standards, which are used to compare the operation of various calorimeters with one another, the actual calibration of each calorimeter being, however, performed electrically or by other means. This second class should perhaps be termed "standard substances" in accordance with the nomenclature for standards proposed by McNish,[2] although this seems less descriptive of their function. The outstanding example of the first class is benzoic acid for combustion calorimetry; in the second, the most widely used are probably n-heptane, aluminum oxide, benzoic acid, diphenyl ether, and water for heat capacity calorimetry.[3]

Three important reasons for the utility of a calibrating standard in combustion calorimetry may be cited. (1) The calorimetric instrumentation is rather highly standardized. (2) The heat capacity of the reacting system—benzoic acid and oxygen—is a very small fraction of the energy equivalent of the calorim-

eter, which is hence altered only slightly in changing from the calibrating system to the experimental system. (3) The combustion reaction in the bomb is very rapid and hence the heat distribution in the calorimeter is primarily a function of its mechanical design and stirring, which also are the same for both calibrations and combustions of unknowns.

None of these conditions obtain in solution calorimetry, where the instrumentation is varied widely according to the nature of the problem under investigation, the reacting system is usually the major part of the heat capacity of the calorimetric system, and the reaction kinetics are widely variable. Electrical calibration of the calorimeter will probably always be necessary for the most accurate work. Nevertheless, it would seem to be possible and desirable to establish one or a few comparison standards of fairly broad utility for the intercomparison of solution calorimeters, the function being primarily the detection of systematic errors between calibrations and reaction heats. The following desirable characteristics of the comparison process may be suggested.

(1) The process should consist of mixing a weighed amount of a standard substance—solid or liquid—in a frangible bulb or other sample chamber with a large volume of a liquid.

(2) The liquid should be preferably pure water;

(1) Work performed under the auspices of the U. S. Atomic Energy Commission.

(2) A. G. McNish, *IRE Trans. Instr.*, I-7, 371 (1958).

(3) D. G. Ginnings and G. T. Furukawa, *J. Am. Chem. Soc.*, 75, 522 (1953).

if not, then an aqueous solution, preferably of neutral pH.

(3) The process should be rapid and complete.

(4) An exothermic process would be more desirable than an endothermic one.

(5) The temperature change should be about 1°, but the heat of the process should be known with little loss of accuracy at conditions giving considerably smaller changes.

(6) The heat should be defined at 25°, but the temperature coefficient should be small.

(7) The heat should be fairly insensitive to the ratio of standard substance to liquid, and to the concentration of solutes, if any, in the initial liquid.

(8) Exposure of the liquid to the atmosphere should have a negligible effect on the heat.

(9) The heat should be the same in closed and open calorimeters, or the difference should be readily calculable.

(10) No gases should be evolved.

(11) The change of vapor pressure of the liquid should be small.

(12) The change in volume of the liquid should be small.

(13) The volume required of the sample chamber should be no more than 5% of the liquid, and preferably less.

(14) The mass of the standard substance should be large enough for convenient and accurate weighing.

(15) The heat capacity of the standard substance should be small (this is important in isothermally jacketed calorimeters where the temperature of the standard substance isolated in the sample chamber may lag significantly behind that of the liquid during the foredrift; it is unimportant in adiabatic or isothermal calorimeters). Point 15 generally conflicts with 14.

(16) The standard substance should be available in high purity, or be readily purifiable.

(17) The standard substance should be nonhygroscopic and nonvolatile and nonreactive with the atmosphere.

(18) The standard substance should not be subject to significant energy perturbations from crystal defects or strain or surface energy effects.

The heat of solution of KCl has most often been proposed as a comparison standard. It has been measured many times, but the results are wildly discordant. Mischenko and Kaganovich[4] evaluated the literature, recommending a value of 4194 ± 3 cal. mole^{-1} for the heat of solution to give KCl·200H$_2$O. Somsen, Coops, and Tolk[5] discussed the virtues of the system as a standard; from an extensive series of

measurements at lower concentrations they give 4185 ± 2, adjusted to KCl·200H$_2$O. Parker[6] listed 70 investigations from 1872 to 1962 and recommended a "best" value of 4115 ± 10 at infinite dilution, or 4195 at KCl·200H$_2$O, but even the more modern values are scattered over a range of more than 1%. Sunner and Wadsö[7] concluded that the system is unsatisfactory. In the present work, the effect of some variations in the treatment of the KCl and in the method of temperature measurement in the calorimeter have been investigated.

The heat of neutralization of a strong acid by a strong base has sometimes been used or suggested as a standard. It appears, however, that this heat has been more uncertain than sometimes thought. Calorimetric values for the heat of ionization of water (heat of acid–base neutralization corrected to infinite dilution) scattered over a range of ca. 0.5% and furthermore differed systematically by ca. 1% from electrometric values. Recently, however, Vanderzee and Swanson[8] have published precise measurements of the heat of neutralization of sodium hydroxide and perchloric acid and Hale, Izatt, and Christensen[9] have published slightly less precise but excellently agreeing results for sodium hydroxide–perchloric acid and sodium hydroxide–hydrochloric acid. The discrepancy with respect to electrometric determinations is attributed to small systematic effects in the treatment of e.m.f. data to derive the ionization constant.[8] In the present work, the objective was to measure a neutralization heat very accurately at somewhat higher concentrations, without concern for correction to infinite dilution. Standardization of one of the reagents and introduction of an accurately known amount of it into the calorimeter present some problems compared with the more customary introduction of a weighed sample of a pure compound, but these are not insurmountable. Kunzler[10] performed an exhaustive study of the preparation of accurately known sulfuric acid solutions although the work seems to be generally ignored in acidimetry. He concluded that acid prepared by the

(4) K. P. Mischenko and Y. Kaganovich, Zh. Prikl. Khim., 22, 1078 (1949).

(5) G. Somsen, J. Coops, and M. W. Tolk, Rec. trav. chim., 82, 231 (1963).

(6) V. B. Parker, "Thermal Properties of Aqueous Uni-univalent Electrolytes," National Bureau of Standards Report NSRDS-NBS-2 (1965).

(7) S. Sunner and I. Wadsö, Acta Chem. Scand., 13, 97 (1959).

(8) C. E. Vanderzee and J. A. Swanson, J. Phys. Chem., 67, 2608 (1963).

(9) J. D. Hale, R. M. Izatt, and J. J. Christensen, ibid., 67, 2605 (1963).

(10) J. E. Kunzler, Anal. Chem., 25, 93 (1953).

constant-boiling procedure was accurate in composition to 0.01%, and better accuracy was obtainable by some other methods. The reaction of this with excess sodium hydroxide promised to give a rapid and reproducible heat and has been investigated in the present work. There appear to be no other accurate data under comparable conditions for comparison.

Succinic acid has been extensively investigated as a secondary standard for combustion calorimetry and appears to be satisfactory, although it has not been widely used. Previous work on the heat of solution is limited and apparently quite inaccurate, but the compound possesses most of the properties desired of a reference material and, at the suggestion of Wilhoit,[11] the heat of solution was further investigated. HCl (0.1 M) was chosen as the solvent instead of pure water to repress ionization at low concentrations and permit the linear extrapolation of heats of solution expected for a nonelectrolyte. The dissolution is endothermic, like that of potassium chloride; an endothermic as well as an exothermic comparison reaction may occasionally be desirable.

Wadsö and Irving[12] have recently proposed the heat of reaction of tris(hydroxymethyl)aminomethane (or 2-amino-2-hydroxymethyl-1,3-propanediol, hereinafter designated THAM) with aqueous hydrochloric acid. THAM has properties qualifying it as a primary acidimetric standard.[13] The reaction seems quite suitable as a calorimetric comparison; several other laboratories are also investigating it. In the present work, the heat has been measured over a range of THAM and acid concentrations.

Shomate and Huffman[14] determined the heat of solution of Mg in 1 M HCl. The reaction has since been used occasionally to check the operation of calorimeters, especially reaction microcalorimeters; agreement has generally been good, but none of the subsequent determinations are sufficiently precise or exhaustive to add anything to the reliability of the original determination. The particular advantages of the system are that because of the high molar heat much smaller samples can be used and concentration and dΔH/dT effects are much smaller. The evolution of hydrogen, carrying a perhaps indefinite amount of water out of constant-pressure calorimeters, is a major disadvantage. More insidious is the uncertain purity of available metal; while multiply distilled magnesium is quite low in metallic impurities and these can be adequately checked spectrographically, variable inclusions of non-metals, especially oxygen, seem to be more of a problem and these are more difficult to determine. It was originally intended to reinvestigate this system in the present work, but in view of the above difficulties it

now appears that there would be few situations where it would offer any advantage over the H_2SO_4–NaOH or THAM–HCl reactions.

Experimental

Materials. Four batches of potassium chloride were used. The first three were all taken from a single jar of Baker and Adamson reagent grade material. Batch A was oven-dried 18 hr. at 105°, batch B was heated 16 hr. at 720° in air in a muffle furnace, and batch C was fused in air in the muffle furnace and cooled slowly. Batch D was Harshaw optical quality, random-sized pieces cleaved into plates about 1 mm. thick. The salt was stored in a desiccator, then weighed into annealed Pyrex bulbs which were evacuated, filled with 5 torr of helium (to promote thermal equilibration during the foredrift of the calorimeter run), and sealed off. Weighings were corrected to *in vacuo* using a density of 1.98 g. ml.$^{-1}$. Flame photometric analysis indicated about 0.004 mole % NaCl in both the Baker and Adamson and Harshaw material. The same result was found in a sample from the jar used in previous measurements[15]; evidently the 0.028 mole % reported at that time was erroneous.

Constant-boiling sulfuric acid was prepared as described by Kunzler,[10] using a still similar to his design. A batch of reagent grade sulfuric acid was first distilled into the receiver, the still was washed out and dried, and the distilled acid was put in the pot. About half of it was then distilled over at a rate of about 5 ml. min.$^{-1}$ while dry nitrogen was flowed slowly through a tee connected to the receiver. The still was allowed to cool; then the cap of the pot was removed while the tee was temporarily blocked to give a slow flow of dry nitrogen through the still, and a joint closed by a stopper with a tube passing through it was quickly placed on the tapered joint. The tube dipped into the acid in the still and, outside, was bent to a vertical termination with constricted tip. A 1-l. Pyrex bottle was fitted with an adapter, replacing the stopper, which had a small-diameter standard taper and cap at the top. The bottle was previously flushed with dry air and weighed against a tare. The cap was then removed, the bottle quickly raised around the tube from the still, and about 100 ml. of acid forced over with nitrogen pressure. The bottle was reweighed and water was

(11) R. C. Wilhoit, private communication.

(12) I. Wadsö and R. J. Irving, *Acta Chem. Scand.*, **18**, 195 (1964).

(13) J. H. Fossum, P. C. Markunas, and J. A. Riddick, *Anal. Chem.*, **23**, 491 (1951).

(14) C. H. Shomate and E. H. Huffman, *J. Am. Chem. Soc.*, **65**, 1625 (1943).

(15) S. R. Gunn, *Rev. Sci. Instr.*, **29**, 377 (1958).

added very slowly, while the bottle was cooled in an ice bath, to the desired composition, and the bottle was again weighed. A Teflon-coated magnetic stirring bar was placed in the bottle, and the solution was thoroughly mixed by stirring and shaking. All glassware, including the calorimeter bulbs, had been kept in contact with concentrated H_2SO_4 or 6 M H_2SO_4 for 2 months before use. Three calibrated sets of weights were intercompared and used. Weighings were corrected to *in vacuo* using 1.83 g./ml. for the density of constant-boiling sulfuric acid and 1.15 for $H_2SO_4 \cdot 20H_2O$. Four batches were used; they are described in Table I. The compositions are calculated using the percentage of H_2SO_4 given by Kunzler[10] for the pressure of the distillation.

Table I: The Sulfuric Acid Solutions

Batch	Pressure of distillation, mm. (cor.)	Constant-boiling acid, g.	Solution, g.	Moles of H_2O/ moles of H_2SO_4
A	749	192.705	891.621	20.0013
B	744	213.424	982.403	20.0013
C	754	189.422	871.851	20.0000
D	744	176.765	813.717	20.0031

The calorimeter bulbs were blown on 12/30 standard taper male Pyrex joints and were annealed, cleaned, and constricted about 2.5 cm. above the shoulder. The solution was run in from a thin-tipped pipet coated with a silicone water repellent on the outside of the tip. Some of the bulbs were coated on the inside of the neck at the shoulder to prevent solution from creeping up the neck. The solution was weighed to 0.1 mg. The bulbs were capped during the weighing and showed no evaporation. After being weighed, the cap was removed, the joint greased, a compressed rubber bulb attached, the sample bulb chilled in an ice bath, and the constriction sealed off. This left about 0.9 atm. of air in the gas space, which was 20 to 30% of the total bulb volume.

The sodium hydroxide solutions for reaction with sulfuric acid were made up by weight from Hellige carbonate-free standardized concentrates.

Succinic acid batch A was J. T. Baker reagent grade, oven-dried at 120° for 17 hr., crushed and sieved to 45–80 mesh, and stored in a desiccator over $Mg(ClO_4)_2$. Batch B was the same reagent recrystallized four times from water, dried over $Mg(ClO_4)_2$ at room temperature, crushed, sieved, and further dried to constant weight over $Mg(ClO_4)_2$ at room temperature. Batches C and D were supplied by Dr. R. C. Wilhoit: batch C

was reagent grade material twice recrystallized from water and then sublimed at 0.1 mm. and 130°; batch D was this material further recrystallized from water and dried 4 hr. at 80° and 5 mm. pressure. Batches E, F, G, H, and I were all material of batch B heated in various manners: E was heated in the oven at 110° for 38 hr.; F and G were portions of unsublimed material heated under high vacuum at 115° for 4 hr. and 130 for 3 hr., respectively; H and I were sublimed under high vacuum at 130° and 140°, respectively. Weighings were corrected to *in vacuo* using a density of 1.572 g./ml.[16]

THAM batch A was Eastman 99.94% reagent, twice recrystallized from water–methanol solution as described by Irving and Wadsö[12] and Fossum, Markunas, and Riddick,[13] screened 45–80 mesh, oven-dried 22 hr. at 80°, further dried under high vacuum at room temperature for 66 hr., and stored 5 months over calcium chloride. Batch B was kindly supplied by Dr. Wadsö (his designation: sample D), and had been purified by a similar procedure and screened 50–100 mesh. It was shipped by air from Sweden in plastic-capped bottles; when stored in shallow dishes in a desiccator over calcium chloride it lost *ca.* 0.003% in weight, attaining constancy in a few days. Weighings were corrected to *in vacuo* using a density of 1.35 g./ml.[17]

Hydrochloric acid solutions for the succinic acid and THAM work were made up from Hellige standardized concentrates. The 1961 atomic weights were used throughout: KCl, 74.555; H_2SO_4, 98.078; $C_4H_6O_4$, 118.0900; $C_4H_{11}O_3N$, 121.1372; H_2O, 18.0153.

The Calorimeter. Rocking bomb calorimeter ID, similar to others previously described,[15] was used. It is fabricated of coinage gold; the bulb-breaking mechanism is of tantalum. The bomb weighs 3.6 kg. and has an internal volume of 650 ml. Temperature measurements were performed with a 2000-ohm thermistor, d.c. bridge, Liston–Becker amplifier, and recorder. A Leeds and Northrup G-2 Mueller bridge with two 100-ohm standard resistors added externally was used for the earlier work (potassium chloride, succinic acid except runs 22–25, and sulfuric acid runs except batch D); the remaining work was done with a Tinsley Type 5415 Wheatstone bridge, which proved to be more satisfactory. In each run the calorimeter was twice calibrated by electrical heating over nearly the same temperature interval as that of the reaction; the thermistor and bridge thus function as a comparison system and need not be accurately calibrated. The

(16) "Handbook of Chemistry and Physics," 45th Ed., Chemical Rubber Publishing Co., Cleveland, Ohio, 1964, p. C-548.

(17) H. A. Rose and A. V. Camp, *Anal. Chem.*, **27**, 1356 (1955).

combination was, however, calibrated against a platinum resistance thermometer and a group of mercury-in-glass thermometers to establish the reference (initial) temperature of the reaction with an accuracy of 0.01°.

Standard cells and standard resistors were calibrated at this laboratory against standards certified by the National Bureau of Standards. A calibrated Rubicon Type B potentiometer was used for the earlier work, done with the Mueller bridge; a Honeywell Model 2802 potentiometer was used for the remainder. The heating interval, usually about 3 min., was controlled by a pendulum-type standard clock; the relay lag and chatter were found oscilloscopically to introduce an error of no more than a few milliseconds. The electrical energy measurements are believed to have an over-all accuracy of 0.01%.

The difference of duplicate calibrations of the calorimeter is limited, especially at smaller temperature rises, primarily by the noise level and reproducibility of the thermistor–thermometer system. For the 12 potassium chloride runs, with a temperature rise of ca. 0.9°, the average difference was 0.005% with a maximum of 0.015%. For the earlier sulfuric acid work with similar rises, the differences were similar; for the three runs with rises ca. 0.3°, differences were 0.016, 0.007, and 0.010%. During the succinic acid work except runs 22–25 performance was somewhat poorer. The seven sulfuric acid runs with batch D, having rises ca. 0.9°, showed an average difference of 0.005% and a maximum of 0.008%. The THAM runs, with rises ca. 0.3°, showed average differences of 0.006%, with a maximum of 0.015%; performance was similar at the higher temperature rises.

Calculation of the Corrected Temperature Rise. The corrected temperature rise was obtained by the method of Dickinson[18,19] wherein a time t_x is found by graphical integration such that

$$\int_{t_i}^{t_x} (\theta - \theta_i)dt = \int_{t_x}^{t_f} (\theta_f - \theta)dt \qquad (1)$$

where t_i and t_f are the initial and final times of the main period and θ is the calorimeter temperature, and the corrected temperature rise is the difference of the foredrift and afterdrift extrapolated to t_x. The thermal leakage modulus of the calorimeter varies with the volume of solution used, but in the present runs ranged largely from 0.0008 to 0.0010 min.$^{-1}$; for the higher value, an error of 6 sec. in t_x will result in an error of 0.01% in the corrected temperature rise.

The temperature θ which should be used in evaluating the integrals of eq. 1 is the average surface temperature of the calorimeter, not a temperature measured at a single point internally. This is because the heat trans-

fer from an element of the surface of the calorimeter by radiation and residual gas conduction is proportional to the temperature difference between that surface element and the jacket, and the total heat transfer is proportional to this temperature difference integrated over all surface elements. This conclusion will be somewhat perturbed by conduction through the heater and thermometer leads and the supporting cords, and in other types of calorimeters by such components as hangers and stirrer shafts; if these components contribute a substantial part of the heat transfer, the calorimeter temperature in their vicinity must be weighted more heavily.

It is convenient to speak of a "reaction lag," the difference in time between initiating a reaction by breaking the sample bulb and t_x, and a "heating lag," the difference between the midtime of an electrical heating period at uniform power and t_x. These may be further specified as "internal" or "surface" to denote whether measured by the regular internal thermometer of the calorimeter or by a special external thermometer designed to measure the average surface thermometer. A series of experiments was performed with a no. 40 copper coil thermometer wrapped on the outside of the bomb and connected to a recording bridge. This has been shown to have negligible lag with respect to the bomb surface. The winding covered the cylindrical portion of the bomb but not the hemispherical ends, but the winding density was increased at the ends of the cylindrical portion and it is believed that the response of the winding should approximate rather closely the average surface temperature. The heating lag ranges from 25 to 45 sec., being longer when the volume of solution is greater and the stirring is evidently less efficient, but is the same within 1 or 2 sec. measured internally and on the surface. Three KCl dissolutions were performed, using material from batch 1; the internal reaction lags were 113, 115, and 118 sec.; the corresponding surface reaction lags were 53, 57, and 55 sec., respectively. For two sulfuric acid neutralizations, internal reaction lags (neglecting a small bump which occurs immediately upon breaking and is undoubtedly due to the fact that the sample bulb is mounted immediately adjacent to the thermometer well) were 47 and 58 sec.; the corresponding surface reaction lags were the same within 1 sec.

A plausible explanation of the difference in lags of KCl dissolutions can be constructed. Evidently the salt falls to the bottom of the bomb and lies there, mov-

(18) H. C. Dickinson, *Bull. Natl. Bur. Std.*, 11, 189 (1914).

(19) J. Coops, R. S. Jessup, and K. Van Ness, "Experimental Thermochemistry," F. D. Rossini, Ed., Interscience Publishers, Inc., New York, N. Y., 1956, pp. 28–35.

ing along the end somewhat as the bomb is rocked, dissolving for about 4 min. This results in a local "cold spot" much cooler than the body of the solution which is "seen" by the internal thermometer; and while most of the bomb wall would be nearly in thermal equilibrium with the body of the solution, this spot is so much colder that the average surface temperature is lower than the internally measured temperature. The surface thermometer is not used in normal operation; the internal reaction lags observed for the 12 runs were for batch A, 114, 129, and 114; bath B, 118, 115, 106; batch C, 149, 157, 156; batch D, 141, 151, and 134 sec., in order. The results were calculated using one-half of these values to determine t_x. An obvious advantage of the sulfuric acid reaction over the potassium chloride appears here: the reaction occurs in the bulk of the solution and not at a solid–liquid interface which may become located near the calorimeter wall and introduce a perturbing effect on the temperature rise correction.

A similar but smaller effect was observed for dissolution of succinic acid; the results are calculated for t_x at three-fourths of the observed internal reaction lags, which ranged from 55 to 150 sec. For THAM, the effect was still smaller; heats are calculated for a t_x 6 sec. before the observed internal reaction lags, which were mostly 40 to 50 sec.

Since this surface temperature effect might contribute an error to other investigations where in the surface temperature of the calorimeter was not examined, an apparatus was built to approximate a common type of solution calorimeter. A 1-l. spherical flask with about a 2.5-cm. neck was surrounded by an air gap and water jacket and fitted with a propellor at the center producing a downward flow. The flask was filled nearly to the neck. Internal temperature was measured with a mercury-in-glass thermometer, and the surface temperature was measured by a uniformly distributed copper resistance thermometer. Reactants were introduced in some cases by breaking a bulb and in others by pouring through a funnel. The propellor speed was varied. For four KCl dissolutions, internal and surface reaction lags were: 243, 183; 66, 46; 52, 31; and 18, 10 sec. For a sulfuric acid neutralization, the internal lag was 6 sec. and the external 13 sec. This last discrepancy is consistent with the metal bomb performance since the glass wall of the flask is quite thick, much thicker than the thermometer bulb, and it indicates that the real difference between the lags for the KCl dissolutions should be somewhat greater than here indicated. The KCl in all cases lay at the bottom of the flask; the time required for complete dissolution was highly sensitive to stirrer speed.

These observations indicate the importance of studying the surface temperature behavior of many types of calorimeters in which the thermometer is not distributed over the surface. In the present instrument, for KCl dissolutions, use of the observed internal reaction lag would have resulted in errors of 0.07 to 0.12%, but in a calorimeter with a higher thermal leakage modulus, the error would be proportionally greater.

Another serious surface–temperature effect was discovered during the course of this work: a superheating of the bomb surface in the vicinity of the heater. A cross section of the heater arrangement is shown in Figure 1. The heater well is of the same material as the bomb, coinage gold, and is welded in an off-axis hole through the hemispherical lower end of the bomb. The heater spool was copper. Use of copper was a design error, since it promotes undesirable conduction of heat to the bore and the outer end of the spool. After discovery of this local superheating, a new heater wound on a stainless steel spool was installed. The heater windings were no. 35 Formvar-insulated Manganin, and the leads were no. 26 copper. The space between the winding and the well from the inner end to the holes at point A (Figure 1) was filled with Apiezon W wax by inverting the bomb section, partially filling the well with wax, and screwing in the spool with the assembly heated to melt the wax. The copper leads had three turns around the spool immersed in the wax and were cemented to the inner surface of the spool from points B to C, and also along the outer surface of the bomb from points E to G or H. After installation of the stainless steel heater spool, the end of the heater well was covered by two layers of 0.002-in. gold foil, cemented around the rim at E except for a small notch to pass the leads.

Table II gives results of some observations of the degree of superheating at the indicated points as observed with a thermocouple taped or otherwise pressed in contact with the surface. The heater power in all cases was 11 w. Point D for the stainless steel spool refers to the center of the gold foil. Point I refers to the thermocouple attached to the heater leads, 2 cm. from the point of contact with the bomb, points G and H, respectively.

To determine the effect of this superheating upon the measurement of heats of reaction, batch D of $H_2SO_4 \cdot 20H_2O$ was prepared and eight bulbs of this were weighed on the same day. Bulbs 1, 4, and 8 were used for the first series with the copper-spool heater and bulbs 2, 3, 5, and 6 for a second series after installation of the stainless steel spool heater.

The first series gave results of 32.592, 32.591, and
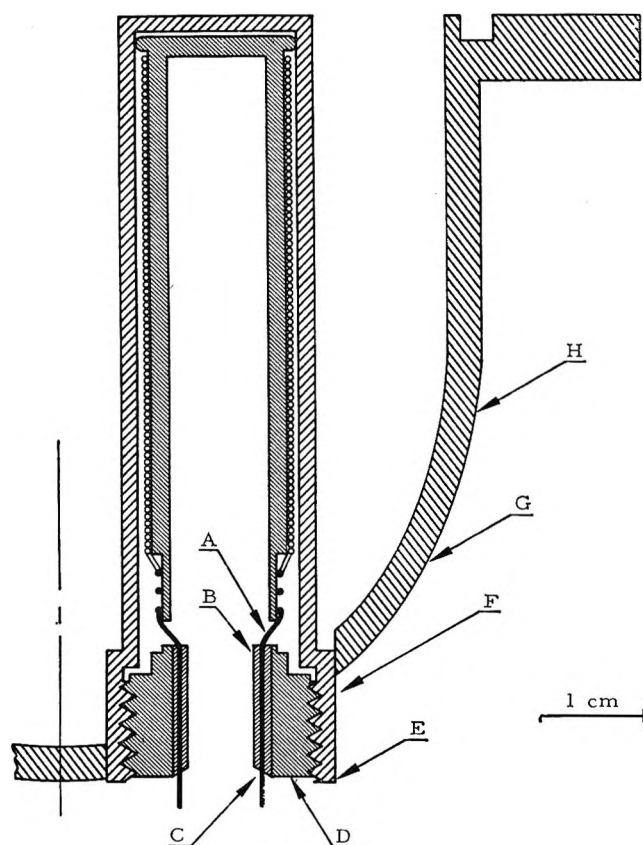
Figure 1.   Cross section of heater.

Table II: Superheating of Surface, °C.

Point	Copper spool	Stainless steel spool
B	5.6	. . .
D	2.8	0.15
F	2.2	0.2
G	0.5	<0.1
H	0.2	. . .
I	~0.7	<0.1

32.594, an average of 32.593 ± 0.002 kcal. mole^{-1} for — ΔH. The second series gave 32.556, 32.556, 32.554, and 32.556, an average of 32.556 ± 0.001. The difference between these two series is 0.111 ± 0.007%. This difference is assumed to be due solely to differences in heat loss from the heater region during the calibrations since all other variables were kept quite unchanged between the two series. Comparison of the two columns in Table II suggests that this excess heat loss for the second configuration should be well under 10% of that for the first. The copper-spool heater was waxed in the bomb without changing throughout the potassium chloride and succinic acid work, and all sul-

furic acid runs except the last four described above; the observed heats, q, for all of these have been reduced by 0.120%, and this correction should introduce little error. Data taken with the newer heater should have a negligible error from this local superheating effect. A report[20] evaluating the effect of the heater error upon other work done in this and similar calorimeters at this laboratory and previously published has been prepared.

Although this whole source of error might have been avoided in the first place by a shrewder arrangement of the heaters for these calorimeter bombs, the present work may point out two factors of importance in solution calorimetry: first, the desirability of checking the surface temperature patterns with surface resistance thermometers or thermocouples during reactions and calibrations, both averaged over the surface and at particularly suspect localities and, second, the utility of a very precise chemical reaction, such as the neutralization of dilute sulfuric acid prepared from constant-boiling sulfuric acid, for investigating variables in calorimeter performance.

A small error might occur in isothermally jacketed solution calorimeters (not adiabatic or isothermal types) due to poor heat transfer within the material in the sample bulb or chamber. Thus as the calorimeter temperature drifts upward (or downward) in the foreperiod, the temperature of the sample will lag behind and at the moment of initiation of the reaction will be lower (or higher) than the average calorimeter temperature. It is to minimize this lag that a small amount of helium is included in the sealed sample bulb. To investigate the possible magnitude of this error, a thermocouple of very fine wire was placed at the center of a bulb, about 3 cm. in diameter, nearly filled with 7.2 g. of THAM, and immersed in a stirred water bath. When the temperature of the water bath was changed, the thermocouple approached the new temperature exponentially with a half-time of about 1.5 min. From this it may be concluded that the effect of the lag would be negligible except in calorimeters having a very high thermal leakage modulus. In the present rocking calorimeter, liquid samples such as the $H_2SO_4 \cdot 20H_2O$ would be agitated inside the bulb during the foreperiod and should lag even less; this would not be the case in many static, propellor-stirred calorimeters, however.

Corrections Applied to Observed Heats. Solution calorimeters may be divided into two types: open, or constant pressure, and sealed, or constant volume. The first measures approximately ΔH and the second approximately ΔE. However, certain small correc-

(20) S. R. Gunn, University of California Radiation Laboratory Report UCRL-7992, July 1964.

Comparison Standards for Solution CalorimetryWait, I need to check header.

tions, sometimes ignored, must be made to observations in either type. It may be assumed that in open calorimeters the passages to the atmosphere are sufficiently narrow that diffusion of vapors, in the absence of a total pressure gradient, is negligible. The heat of breakage of annealed glass sample bulbs is generally negligible, but in some calorimeters the mechanical system causing breakage of the bulb may introduce a significant amount of heat; the same may be true of the opening of the sample chamber in calorimeters not using a frangible bulb.

Breaking an empty evacuated bulb in an open calorimeter causes evolution of a compressional heat, q_{comp}

$$q_{comp} = Pv_b \qquad (2)$$

where P is atmospheric pressure and v_b is the internal volume of the bulb.[21] If the bulb contains a solid sample of volume v_c, the correction is

$$q_{comp} = P(v_b - v_c) \qquad (3)$$

This corresponds to transfer of the sample from the evacuated bulb to the vapor space over the initial water or solution. If P is one standard atmosphere and v_b and v_c are in milliliters

$$q_{comp} = 0.02422(v_b - v_c) \text{ cal.} \qquad (4)$$

A volume $(v_b - v_c)$ of air will at the same time be drawn into the calorimeter, and since in general the apparent molar volume V_s of the solute in solution will be less than its molar volume V_c as a solid, an additional amount of air $(V_c - V_s)/n$ will also be drawn in, where n is the number of moles of solute. If this air has a relative humidity h (at 25°) less than that of the initial water of solution, water must vaporize to resaturate the vapor space. This vaporization heat will be termed q_{vap}. Since the heat of vaporization of water to saturate 1 ml. at 25° is 0.01340 cal.

$$q_{vap} = 0.01340h[v_b - v_c + (V_c - V_s)/n] \text{ cal.} \qquad (5)$$

If the vapor pressure p_s of the final solution is significantly less than that of the initial water or solution, p_w, heat will be evolved by condensation of water from the vapor phase; this correction, q_{cond}, is given by

$$q_{cond} = 0.01340v_v(p_w - p_s)/p_w \qquad (6)$$

The heat of reaction is given by

$$\Delta H = -q_{cor}/n \qquad (7)$$

where

$$q_{cor} = q_{obsd} - q_{comp} + q_{vap} - q_{cond} \qquad (8)$$

where q_{obsd} is the calorimetrically observed heat. It is

to be noted that although $V_c - V_s$ appears in the vaporization correction (eq. 5), it does not appear in the compression correction (eq. 4); in fact, it is $-\Delta V$, which defines the difference between the heat of reaction at constant pressure, ΔH, and the heat of reaction at constant volume, ΔE

$$\Delta H = \Delta E + P\Delta V \qquad (9)$$

In a sealed calorimeter, most of the corresponding effects occur except that there is no entering air and hence no q_{comp} term. If the water or solution is not degassed, thermal effects due to desorption of air may occur upon breaking the sample bulb[22]; these may be rather slow and irreproducible. The system is better defined if the solution is degassed and the sample bulb evacuated; this was done in the present measurements with KCl, succinic acid, and THAM, the bulbs containing only ca. 10 torr of helium to improve thermal contact. When an empty sample bulb is broken, the endothermic heat effect corresponds to the energy of vaporization rather than the heat of vaporization[23]; for water at 25° this amounts to 0.01265 cal. to saturate 1 ml. The corrections for vaporization into the increased vapor space and condensation due to the reduced vapor pressure then become

$$q'_{vap} = 0.01265(v_b - v_c) \qquad (10)$$

$$q'_{cond} = 0.01265v_v(p_w - p_s)/p_w \qquad (11)$$

It is convenient to treat the condensation correction in terms of the vapor pressure depression factor R, which is nearly independent of concentration for dilute solutions

$$R = (p_w - p_s)/cp_w \qquad (12)$$

where c is the concentration in moles per liter, or $1000 n/v_l$, v_l being the volume of the liquid phase. Then

$$q'_{cond} = 12.65Rnv_v/v_l \qquad (13)$$

$$q'_{cor} = q_{obsd} + q'_{vap} - q'_{cond} \qquad (14)$$

$$\Delta E = -q'_{cor}/n \qquad (15)$$

$$\Delta E = -[q_{obsd} + 0.01265(v_b - v_c)]/n + 12.65Rv_v/v_l \qquad (16)$$

$$\Delta E = -(q_{obsd} + 0.01265v_b)/n + 12.65Rv_v/v_l + 0.01265V_c \qquad (17)$$

Converting to the more customarily tabulated ΔH at one atmosphere pressure by addition of the term

(21) C. A. Guderjahn, D. A. Paynter, P. E. Berghausen, and R. J. Good, *J. Chem. Phys.*, 28, 520 (1953).

(22) G. C. Benson and G. W. Benson, *Rev. Sci. Instr.*, 26, 477 (1955).

(23) S. R. Gunn and L. G. Green, *J. Phys. Chem.*, 64, 1066 (1960).

$$PAV = P(V_s - V_c) \qquad (18)$$

which in calories per mole with V in milliliters is

$$PAV = 0.02422(V_s - V_c) \qquad (19)$$

$$\Delta H = -[q_{obsd} + 0.01265(v_b - v_c)]/n + 12.65Rv_v/v_1 + 0.02422(V_s - V_c) \qquad (20)$$

or

$$\Delta H = -(q_{obsd} + 0.01265v_b)/n + 12.65Rv_v/v_1 + 0.02422V_s - 0.01157V_c \qquad (21)$$

From data in the "International Critical Tables," R is 0.032 for KCl and 0.016 for succinic acid and V_s is 80 for succinic acid; from Harned and Owen,[24] V_s is 28 for KCl. Values of V_c are calculated from the previously stated densities, and v_v/v_1 was about 0.6 throughout. The sums of the second, third, and fourth terms on the right-hand side of eq. 21 are accordingly 0.54 cal. mole^{-1} for KCl and 1.10 for succinic acid. For the THAM-HCl reaction

$$\text{THAM(c)} + \text{H}^+\text{(aq)} \longrightarrow \text{THAM:H}^+\text{(aq)} \qquad (22)$$
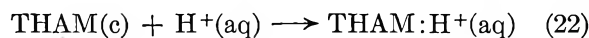
it is assumed that ΔV is zero and that the vapor pressure of the solution is unchanged since there is no change in ionic strength; the second and third terms of the right-hand side of eq. 20 are thus zero.

For the sulfuric acid–sodium hydroxide reaction neither solution was deaerated. The sample bulb was filled almost full; since the vapor pressure of water over $\text{H}_2\text{SO}_4\cdot20\text{H}_2\text{O}$ is 90% of that over pure water, vaporization effects upon breaking the bulb were negligible, and since the bulb contained air at a pressure only slightly below atmospheric, desorption effects were also negligible. The volume change of the reaction, about 30 ml. mole^{-1}, gives a heat of only 0.7 cal. mole^{-1} or 0.002% of ΔH. The effect of change of vapor pressure upon converting NaOH to Na_2SO_4 in the solution is even smaller. Thus, one of the advantages of this system is that in neither open nor sealed calorimeters need any corrections be applied to the observed heat. Also, in open calorimeters, influx of outside air is minimized.

Results

All results are given in terms of the defined thermochemical calorie, 4.1840 absolute joules. Uncertainty intervals are twice the standard deviation of the mean, $2[\Sigma d^2/n(n - 1)]^{1/2}$. The reaction temperature is 25.00° throughout unless otherwise specified.

Potassium Chloride. All samples were approximately 0.125 mole; the amount of water, about 450 ml., was in all cases within 0.2% of the amount required to give $\text{KCl}\cdot200\text{H}_2\text{O}$. Internal volumes of the sample bulbs

ranged from 13 to 18 ml. Three runs were made with each of the four batches; A gave 4196.6, 4195.4, and 4195.2 cal. mole^{-1}, an average of 4195.7 $\pm$ 0.9; B gave 4203.5, 4202.0, and 4202.9 cal. mole^{-1}, an average of 4202.8 $\pm$ 0.9; C gave 4201.3, 4199.5, and 4199.0 cal. mole^{-1}, an average of 4199.9 $\pm$ 1.4; D gave 4203.5, 4204.3, and 4203.8 cal. mole^{-1}, an average of 4203.9 $\pm$ 0.5.

Sulfuric Acid–Sodium Hydroxide. The reaction is described by the equation

$$\text{H}_2\text{SO}_4\cdot a\text{H}_2\text{O} + b(\text{NaOH}\cdot c\text{H}_2\text{O}) = $$
$$\text{Na}_2\text{SO}_4\cdot(b - 2)\text{NaOH}\cdot(a + bc + 2)\text{H}_2\text{O} \qquad (23)$$
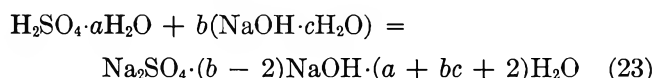
The reference conditions are $a = 20$, $b = 2.5$, and $c = 600$, which give a temperature rise of about 1°. It was expected that use of 25% excess sodium hydroxide would minimize the effect of small amounts of carbonate in it. Since the change in the apparent molar heat content of sulfuric acid is *ca.* 9 cal. mole^{-1} per 1% change in a when $a = 20$, the deviations from 20 of the mole ratio a indicated in Table I are negligible. The effects of variation in b, c, and temperature and of added CO_2 were studied.

Twenty-three runs were performed at the reference conditions; sample weights were mostly 7 to 8 g., requiring 410 to 470 ml. of NaOH solution. Six runs with batch A gave for $-\Delta H$ 32.577, 32.565, 32.556, 32.560, 32.560, and 32.559 kcal. mole^{-1}, an average of 32.560 $\pm$ 0.003; six runs with batch B gave 32.555, 32.554, 32.561, 32.562, 32.558, and 32.558 kcal. mole^{-1}, an average of 32.558 $\pm$ 0.003; four runs with batch C gave 32.564, 32.561, 32.564, and 32.561 kcal. mole^{-1}, an average of 32.562 $\pm$ 0.002; three runs with batch D gave 32.553, 32.551, and 32.555 kcal. mole^{-1}, an average of 32.553 $\pm$ 0.002; four more runs with batch D using the new stainless-steel spool heater gave 32.556, 32.556, 32.554, and 32.556 kcal. mole^{-1}, an average of 32.556 $\pm$ 0.001. The recommended best value is 32.558. For an estimate of the over-all accuracy, there may be asssumed errors of 0.01% in the composition of the constant-boiling acid, 0.01% in the dilution and sample weighing, and 0.01% in the calorimetric measurements, of an over-all uncertainty of 0.02%.

Using material of batch A, a run at $b = 2.25$, $c = 600$ gave 32.556; $b = 2.75$, $c = 600$ gave 32.560; $b = 2.25$, $c = 667$ gave 32.550; $b = 2.75$, $c = 545$ gave 32.562 kcal. mole^{-1}. These data indicate the effect of small variations in amount and concentration of the sodium hydroxide solution to be negligible. At the reference

(24) H. S. Harned and B. B. Owen, "The Physical Chemistry of Electrolytic Solutions," 3rd Ed., Reinhold Publishing Corp., New York, N. Y., 1958.

concentrations, two runs at 23.00° gave 32.595 and 32.587 kcal. mole⁻¹; two runs at 27.00° gave 32.526 and 32.525 kcal. mole⁻¹. Thus ΔC_p is 16 cal. deg.⁻¹ mole⁻¹, and $d\Delta H/\Delta H dT$ is 0.00049 deg.⁻¹.

Three runs were made at the reference concentrations but with enough CO₂ added to react with 10% of the NaOH. One with batch A gave 32.544 kcal. mole⁻¹; two with batch C gave 32.549 and 32.552 kcal. mole⁻¹. Quite elementary precautions would keep the carbonate contamination far below this level, and it should not be a significant source of error.

Some measurements and calculations were also made for the sulfuric acid-sodium hydroxide reaction at different concentrations to provide data for checking calorimeters at smaller temperature rises or using different sulfuric acid sample sizes. Three runs were made at $a = 20$, $b = 25$, $c = 2000$, giving about 0.3° temperature rise; batch C was used and results were 32.548, 32.548, and 32.553 kcal. mole⁻¹, an average of 32.550 ± 0.003 kcal. mole⁻¹. Since batch C gave a somewhat higher than average value at the reference conditions, a value of 32.547 kcal. mole⁻¹ is recommended at the present conditions. Two measurements were made of the dilution

$$H_2SO_4 \cdot 20H_2O + 180H_2O = H_2SO_4 \cdot 200H_2O \quad (24)$$
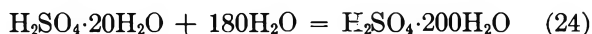
results for ΔH were -896.1 and -895.3 cal. mole⁻¹.

In principle, the heat of reaction 23 can be calculated for any values of a, b, and c if it is known at any one set a, b, c and the heats of dilution of H₂SO₄, NaOH, and the mixed Na₂SO₄–NaOH solution are known. Giauque, et al.,[25] have tabulated the enthalpy of sulfuric acid from absolute to 1 m. Their data give for the apparent molal heat content of sulfuric acid, relative to H₂SO₄· 20H₂O, 3212 cal./mole at $a = 5$, 1049 at $a = 10$, and -480 at $a = 55.506$ (1 m). For $a = 200$ (reaction 5) the NBS tables[26] give -820; we shall use our value of -896. The dilution data tabulated by Harned and Owen[24] for NaOH and Na₂SO₄ are used. Aside from possible inaccuracies in the input data, the principal uncertainty lies in the unknown heat of mixing of solutions of Na₂SO₄ and NaOH; it is assumed that the relative apparent molal heat content of both Na₂SO₄ and NaOH in a mixed solution is the same as in its own pure solution of the same ionic strength (Young's rule).[27]

Table III gives calculated values for ΔH_4 at $b = 2.5$ and various values of a and c. Using -32.558 for ΔH_4 at $a = 20$, $c = 600$, a value of -32.539 is obtained at $a = 20$, $c = 2000$, but the experimental value of -32.547 is preferred and serves as the reference for all calculations at $c > 2000$.

Constant-boiling sulfuric acid could itself be used for the reaction without dilution, but great care would be

Table III: $-\Delta H_4$ (kcal. mole⁻¹) at $b = 2.5$

a	$c = 600$	$c = 2000$	$c = 5000$	$c = 10{,}000$	$c = 40{,}000$	$c = \infty$
5	35.770	37.759	35.770	35.782	35.798	35.820
10	33.607	33.596	33.607	33.619	33.635	33.657
20	32.558	32.547	32.558	32.570	32.586	32.608
55.506	32.078	32.067	32.078	32.090	32.106	32.128
200	31.666	31.653	31.664	31.674	31.690	31.712

necessary in its handling; absorption of 0.010 wt. % water would not only reduce the amount of reaction by this percentage but would also, because of its effect on the relative apparent molal heat content of the acid, reduce the molal heat of reaction by 0.010%, or a total error of 0.020% in the heat effect. The calculated ΔH_4 for $a = 0.08409$ (98.479 wt. % H₂SO₄, the composition at 760 mm.), $b = 2.5$, $c = 600$ is -48.817. One advantage would accrue from use of more concentrated acid: the vapor pressure of water over H₂SO₄·20H₂O is about 90% that of pure water, but over H₂SO₄·7H₂O is about 50%. Weight changes during handling would be minimized if the vapor pressure were matched to the relative humidity of the room.

Succinic Acid. The reference conditions chosen for succinic acid dissolution were 0.100 N HCl and 0.160 N H₂Suc at 25.00°, but the effects of variations in the concentration of both hydrochloric acid and succinic acid and in temperature were studied, as well as variations in the sample treatment. Results are given in Table IV.

The experimental accuracy during these measurements, excepting runs 22 to 25, was less than during the other work described in this paper. For the first nine runs, the heat is linear within experimental error for the three variables and may be described as

$$\Delta H = \Delta H° - 70[(HCl) - 0.100] - 70[(H_2Suc) - \\ 0.160] + 18(T - 25) \quad (25)$$

where $\Delta H°$ is the heat of solution at the reference conditions 6823 cal. mole⁻¹. The results for recrystallized material, batch B dried at room temperature, and batch D dried at 80° agree well. Batches E, F, and G, heated to successively higher temperatures, show increasing positive deviations; batches H and I, sublimed at successively higher temperatures, show increasing

(25) W. F. Giauque, E. W. Hornung, J. E. Kunzler, and T. R. Rubin, *J. Am. Chem. Soc.*, **82**, 62 (1960).

(26) F. D. Rossini, et al., "Selected Values of Chemical Thermodynamic Properties," National Bureau of Standards Circular 500, U. S. Government Printing Office, Washington, D. C., 1952, pp. 41, 42.

(27) T. F. Young, Y. C. Wu, and A. A. Krawetz, *Discussions Faraday Soc.*, **24**, 37 (1957).

Table IV: Heat of Solution of Succinic Acid

Run	Batch	H₂Suc, mole l.⁻¹	HCl, mole l.⁻¹	T, °C.	ΔH, cal./mole
1	A	0.080	0.100	25.00	6829
2	A	0.120	0.100	25.00	6829
3	A	0.120	0.100	25.00	6828
4	A	0.160	0.100	25.00	6822
5	A	0.200	0.100	25.00	6822
6	A	0.160	0.100	23.00	6787
7	A	0.160	0.100	27.00	6859
8	A	0.160	0.050	25.00	6828
9	A	0.160	0.200	25.00	6817
10	B	0.160	0.100	25.00	6862
11	B	0.160	0.100	25.00	6866
12	B	0.160	0.100	25.00	6863
13	C	0.160	0.100	25.00	6753
14	C	0.160	0.100	25.00	6758
15	D	0.160	0.100	25.00	6868
16	D	0.160	0.100	25.00	6866
17	E	0.160	0.100	25.00	6874
18	F	0.160	0.100	25.00	6876
19	G	0.130	0.100	25.00	6886
20	H	0.130	0.100	25.00	6818
21	I	0.160	0.100	25.00	6775
22	B	0.160	0.100	25.00	6865
23	B	0.160	0.100	25.00	6863
24	B	0.160	0.100	25.00	6865
25	B	0.160	0.100	25.00	6865

negative deviations. (ΔH for runs 19 and 20, converted to 0.160 M H₂Suc, would be 6884 and 6816, respectively.) Sublimed batch C also shows a large negative deviation. Runs 22–25 were performed 2 years after the others; the succinic acid had been stored during this period in a desiccator over magnesium perchlorate.

Tests of batch C for succinic anhydride gave negative results, with a limit of detection of 0.05%. The reasons for the deviations of the heated and sublimed material are not clear, but the agreement of batches B and D suggests that recrystallized material dried at low temperature may be thermochemically reproducible. Keffler[28] found the heat of combustion to be unaffected by heating to 120°, but this measurement is much less sensitive than the heat of solution.

THAM. About 400 ml. of hydrochloric acid was used for all runs; hence sample weights were *ca.* 2.4 g. for runs at a concentration of 6 g./l., 4.8 g. for 12 g./l., and 7.2 g. for 18 g./l. Internal bulb volumes for 2.4 g. were 6 to 8 ml.; for 4.8 g., 9 to 14 ml.; and for 7.2 g., 14 to 20 ml. Thirteen runs were performed in 0.100 M HCl, 6 g. of THAM l.⁻¹: seven with batch A gave for $-\Delta H$ 7107.5, 7108.6, 7104.9, 7106.2, 7108.0, 7106.3, and 7107.4 cal. mole⁻¹, an average of 7107.0 ± 0.9,

and six with batch B gave 7107.5, 7109.0, 7107.4, 7106.4, 7106.6, and 7105.4 cal. mole⁻¹, an average of 7107.1 ± 1.0. Nine runs were performed in 0.200 M HCl with batch A: three at 6 g. of THAM l.⁻¹ gave 7118.9, 7121.1, and 7119.3 cal. mole⁻¹, an average of 7119.8 ± 1.4; three at 12 g. of THAM l.⁻¹ gave 7121.9, 7121.2, and 7121.7 cal. mole⁻¹, an average of 7121.6 ± 0.6; and three at 18 g. of THAM l.⁻¹ gave 7125.8, 7125.7, and 7125.4 cal. mole⁻¹, an average of 7125.6 ± 0.3.

Discussion

The KCl measurements previously reported[15] were performed without deaerating the water and with about 0.8 atm. of air in the sample bulbs. Under these conditions the desorption correction[22] is about 0.01 cal. and may be neglected. The values were corrected for the surface temperature curve, for evaporation due to breaking the sample bulb, and for condensation due to the decreased vapor pressure of the solution, but not for condensation due to the increased volume or for the effect of superheating near the vicinity of the heater (the heaters of calorimeters IA and IB were set in with Wood's metal; that of IA is still in existence, and from thermocouple measurements at the surface the heating error was estimated to be 0.05%; the same figure was used for IB); they also included an erroneous correction for sodium chloride (see above). The recalculated values, including the new atomic weights, are for IA, 4202, 4205, 4203 and 4204 cal. mole⁻¹; for IB, 4205, 4204, 4204, and 4205 cal. mole⁻¹. The treatment of the KCl was similar to batch B of the present work.

The present work demonstrates variations of up to 0.2% in the heat of solution of KCl according to the pretreatment and source of the salt and suggests one possible source of instrumental error, the "cold spot" surface temperature effect. It still remains difficult to understand the very large historical spread of measurements of this system. It would be interesting to have a uniform batch of KCl prepared and distributed to several laboratories capable of precise solution calorimetry, the calorimeters also being compared by means of another reaction such as one of the other three treated in the present work. For the present, however, it can only be concluded that potassium chloride is not a satisfactory substance for checking solution calorimeters and its use for that purpose should be discontinued. It might be noted in passing that papers on solution calorimetry often mention checking with KCl and quote two or three similar values from the literature to support the reliability of the measurements; with

(28) L. J. P. Keffler, *J. Phys. Chem.*, **38**, 717 (1934).

some 70 published values to choose from, such agreement is not difficult to achieve.

Compared with a salt such as KCl, the heat of solution of an organic crystal is less likely to be perturbed by lattice defects, strain energy, or surface effects. An endothermic solid–dissolution comparison reaction may occasionally be desirable; the present work on succinic acid is not wholly definitive but suggests that it may be satisfactory. THAM, dissolved in a dilute alkaline solution, might be another possibility; preliminary measurements in 0.100 M NaOH gave 4001 cal. mole^{-1} for ΔH at 0.100 M THAM and 25.00°, 4018 cal. mole^{-1} at 0.175 M THAM and 25.00°, and 4159 cal. mole^{-1} at 0.100 M THAM and 30.00°.

The present data for THAM are in excellent agreement with the value presently recommended by Wadsö,[29] 7107 ± 4 cal. mole^{-1}, for the heat of solution at 5 g./l. in 0.1 M HCl. THAM is perhaps easier to prepare, handle, and weigh than the sulfuric acid solu-

tions; it appears that the reproducibility for any one prepared batch of sulfuric acid may be somewhat better than for THAM, but that the reproducibility between batches is no better. Thus, sulfuric acid might be preferable for use within a single laboratory to compare calorimeters or the effect of structural or operational changes—as was done in the present work for two heater configurations—but THAM might be equally satisfactory for interlaboratory comparisons.

The present determination of the H$_2$SO$_4$–NaOH reaction heat could be used together with appropriate heats of dilution to calculate the heat of ionization of water for comparison with other determinations. However, the heats of dilution, especially for H$_2$SO$_4$, and the heat of unmixing of the Na$_2$SO$_4$–NaOH solution are too uncertain to make this of any value.

(29) I. Wadsö, private communication.

Cupric Ion Catalyzed Hydrolyses of Glycine Ethyl Ester,

Glycinamide, and Picolinamide[1]

by Harry L. Conley, Jr., and R. Bruce Martin

Cobb Chemical Laboratory, University of Virginia, Charlottesville, Virginia   *(Received February 16, 1965)*

Attack of hydroxide ion on protonated glycine ethyl ester at 25.00° and 0.16 ionic strength proceeds 41 times faster than the same reaction with neutral ester. Reaction of hydroxide ion with the cupric complex of glycine ethyl ester provides a further increment of 3200 over hydroxide ion attack on protonated ester, furnishing an example of super-acid catalysis due to chelation near the reactive site. A zinc–mercaptoethylamine complex catalyzes hydrolysis of glycine ethyl ester. Cupric ion also promotes the hydrolysis of glycinamide near neutral pH, but less effectively than in the case of glycine ethyl ester. Cupric ion inhibits the hydrolyses of both glycinamide and picolinamide at high pH, where ionization of amide hydrogens has taken place. Interpretations of these kinetic observations are made on the basis of equilibrium complexation of cupric ion with reactants and tetrahedral carbon addition intermediates. Results of potentiometric and spectrophotometric studies of cupric and nickel ion complexes of picolinamide are described. A 2:1 picolinamide–nickel ion complex yielding red needles in the solid state has been prepared.

Though it is generally recognized that metal ions are less effective in catalyzing amide than ester hydrolyses, direct comparisons of specific rate constants on analogous compounds of well-defined reacting species have not been possible. An early study of metal ion activated hydrolysis of amino acid esters[2] is compromised by coordination with the metal ions of the basic component of the buffer system and has been criticized on other grounds as well.[3] Further work on cupric ion promoted hydrolysis of glycine ethyl ester in the presence of glycine buffer, a product of the reaction, was performed at only one pH.[3] This latter work did establish however, that carbonyl oxygen exchange occurs in the cupric ion hydrolysis, as it does in ordinary ester hydrolysis. Since it was not possible to calculate the concentration of reacting species, only observed rate constants are given. Both of these studies followed the reaction by classical titration methods. A conductivity method has also been used to follow the hydrolysis of glycine ethyl ester in the presence of cupric and nickel ions and excess base. Formation constants were reported, but no variation in hydroxide concentration was attempted.[4] Cupric ion catalyzed hydrolysis of glycinamide has been studied as a func-

tion of pH and temperature by a spectrophotometric method in the presence of high concentrations of carbonate buffers.[5]

The work reported here aimed to determine specific rate constants for cupric ion catalyzed hydrolyses in terms of well-defined complexes of glycine ethyl ester and glycinamide. Reaction rates were followed on a pH-stat so that buffer-free solutions could be used. Hydroxide ion dependences of the rates with specific complexes are reported. Comparisons are then made among free ester and cupric ion catalyzed hydrolyses and with amide hydrolyses. Similar studies on other amino acid esters are reported elsewhere.[6]

Some of the features of glycinamide–metal ion com-

(1) This paper is abstracted from the Ph.D. thesis of H. L. Conley, Jr., 1964, from which more details may be obtained. The research was supported by grants from the National Science Foundation and the National Institutes of Health.

(2) H. Kroll, *J. Am. Chem. Soc.*, 74, 2036 (1952).

(3) M. L. Bender and B. W. Turnquest, *ibid.*, 79, 1889 (1957).

(4) J. M. White, R. A. Manning, and N. C. Li, *ibid.*, 78, 2367 (1956).

(5) L. Meriwether and F. H. Westheimer, *ibid.*, 78, 5119 (1956).

(6) H. L. Conley, Jr., and R. B. Martin, *J. Phys. Chem.* 69, 2923 (1965).

plexes appear at relatively high pH values. For this reason investigations were performed on picolinamide with a considerably lower pK_a. Picolinamide is also a derivative of an α-amino acid.

Experimental

Materials. The glycine ethyl ester hydrochloride and glycinamide hydrochloride used were the best commercial products available. Equivalent weights determined by titration were within 2% of the theoretical values. Preparation and standardization of sodium hydroxide and metal ion solutions are described elsewhere.[6]

Picolinamide was prepared by the reaction of aqueous ammonia with picolinic acid ethyl ester[7] and reprecipitated from alcohol solution by addition of benzene, m.p. 104–106°; lit.[7] 105°. *Anal.* Calcd. for $C_6H_6N_2O$: C, 59.01; H, 4.95; N, 22.94. Found: C, 59.17; H, 4.89; N, 22.97. Automatic titration of a 0.01 M solution on the pH-stat at 25.00° and 0.16 ionic strength gave $pK_a = 1.9$. This value is subject to uncertainties involved in converting hydrogen ion activities to concentrations in this low pH region, but is in agreement with a value[8] of $pK_a = 2.1$ found at the lower temperature of 20° and ionic strength 0.01.

On several occasions high pH solutions of picolinamide and cupric ion produced purple needles while nickel ion gave red needles. The red needles were prepared in larger quantity by mixing amide and nickel ion at concentrations of 0.3 and 0.1 M, respectively. Upon the raising of pH of this solution to about 11.5, red needles began to form. The red needles were collected, washed three times with water, and stored in a desiccator containing P_2O_5. Results to be presented later suggest that the red needles should be a 2:1 picolinamide–nickel ion complex with amide hydrogens ionized on both ligands. *Anal.* Calcd. for $Ni(C_6H_5N_2O)_2$: C, 47.89; H, 3.35; N, 18.62; Ni, 19.5. Found: C, 47.63; H, 3.42; N, 18.92; Ni, 19.0 and 19.4 by gravimetric dimethylglyoxime method.[9] This agreement provides strong evidence for amide hydrogen ionization because the analysis cannot accommodate the anions that would otherwise be required for charge neutralization.

Methods. Most rate runs were performed on a Radiometer pH-stat equipped with a glass jacket about the reaction vessel which permitted temperature control to ±0.02°. Experiments in this paper were performed at 25.00, 30.00, or 35.00 ± 0.02°. Other features of the experimental set up are described elsewhere.[1,6] Solutions of metal ion nitrates were used in these experiments. Ionic strength was always 0.16 controlled with KNO_3.

Some rate runs were performed spectrophotometrically on a Cary 14 spectrophotometer with metal ion chlorides and ionic strength controlled to 0.16 with KCl. The temperature was 25.0 ± 0.1°.

Whether rates were determined on the pH-stat or spectrophotometrically, pH values were read on a pH meter. Hydroxide ion activities were obtained from pH meter readings by utilizing $-\log K_w = 14.00$, 13.83, and 13.68 at 25, 30, and 35°, respectively.[10] Our second-order rate constants are obtained by dividing first-order rate constants by the activity of hydroxide ion and possess units of activity^{-1} sec.$^{-1}$. These rate constants may be converted to M^{-1} sec.$^{-1}$ by multiplying them by 0.75, the mean ion activity coefficient for both KOH in KCl and NaOH in NaCl solution at 25° and 0.16 ionic strength.[10] In this paper parentheses denote molar concentrations, and brackets denote molar activities.

The pH-stat automatically portrays on a graph the amount of a given concentration of base or acid added from a syringe buret to maintain a constant pH *vs.* time. By drawing a slope through the initial portion of the rate curve, the initial molar concentration per second, R_{stat}, of protons liberated or consumed in the reaction may be obtained, upon the appropriate manipulation of units. This initial rate of change of protons is not necessarily equivalent to the initial rate of change of molar concentration of substrate per second, the rate we wish to determine. The latter kinetically important rate can be determined from the former experimentally observed rate by a general method outlined for glycine ethyl ester. The experimentally observed rate of molar proton production, R_{stat}, is related to the molar rate of ester hydrolysis, R_E, by $R_{stat} = QR_E$. We proceed to determine the quantity Q for the substrates studied in this work.

Glycine ethyl ester may exist in protonated, EH^+, or free base form, E, and the product glycine in the dipolar ion $AH^\pm$ or anionic form A^- at pH >4. Without consideration of mechanism and merely as a material balance for protons, the hydrolysis of glycine ethyl ester may be written as

$$EH^+ + H_2O \longrightarrow AH^\pm + H^+ + C_2H_5OH$$

$$\downarrow\uparrow K_E \qquad\qquad\qquad \uparrow\downarrow K_2$$

$$H^+ \qquad\qquad\qquad\qquad H^+$$
$$+ \qquad\qquad\qquad\qquad\quad +$$
$$E \qquad\qquad\qquad\qquad\quad A^-$$
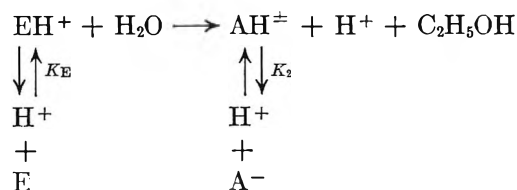
(7) R. Camps, *Arch. Pharm.*, **240**, 347 (1902).

(8) H. H. G. Jellinek and J. R. Urwin, *J. Phys. Chem.*, **58**, 548 (1954).

(9) R. Belcher and A. J. Nutten, "Quantitative Inorganic Analysis," Butterworth and Co., Ltd., London, 1955.

where K_E and K_2 are acid ionization constants. The fraction of the total glycine ethyl ester concentration in the free base form is given by $\alpha_E = K_E/([H^+] + K_E)$, and the fraction of the total concentration of glycine in the free base form is given by $\alpha_2 = K_2/([H^+] + K_2)$. For each molecule of protonated glycine ethyl ester, EH^+, that is hydrolyzed, one proton is produced for the fraction of product glycine that is $AH^\pm$, and two protons are produced for the glycine fraction that is A^-. The first fraction is given by $1 - \alpha_2$ and the second by α_2. The observed rate will be reduced by the fraction of ester that is E instead of EH^+. Totaling these results yields

$$R_{stat} = R_E[(1 - \alpha_2) + 2\alpha_2 - \alpha_E] =$$
$$R_E[1 + \alpha_2 - \alpha_E]$$

The quantity in brackets is Q for glycine ethyl ester hydrolysis. This same quantity can be derived by other arguments. Only when $\alpha_2 = \alpha_E$ is there a 1:1 correspondence between moles of ester hydrolyzed and moles of protons liberated. In order to determine R_E from R_{stat}, a value of $pK_2 = 9.66 \pm 0.04^{11,12}$ was used. By potentiometric titration we have determined $pK_E = 7.79 \pm 0.02$ at $25.0°$ and 0.16 ionic strength. A value[13] of 7.73 determined at $25°$ and 0.05 ionic strength is nearly identical when the ionic strength difference is taken into account.

For glycinamide $Q = \alpha_2 + \alpha_3 - \alpha_A$, where the successive α-values, respectively, represent the fractions of glycine, ammonia, and glycinamide in the basic forms. Since data were obtained at three temperatures, the acid ionization constants for each of the three compounds must be known at each temperature. Best values of acid ionization constants were found at 0.16 ionic strength and $25.00°$. These values were calculated for 30.00 and $35.00°$ using the integrated form of the van't Hoff equation and appropriate values for ΔH. The assumptions and results are summarized in Table I.

The ΔH value of 12 kcal./mole assumed for glycinamide is not critical for this study because runs were made in the pH range 10.7 to 11.8, where glycinamide is at least 99.7% in the free base form.

For picolinamide, the same equations apply as for glycinamide. Since all hydrolysis experiments were performed at pH >10 and $pK_a = 1.9$ for picolinamide and 1.6 and 5.4 for picolinic acid,[14] $\alpha_A = 1 = \alpha_2$.

Results

Glycine Ethyl Ester. Four reactions must be considered in the mechanisms of glycine ester hydrolysis. They involve water and hydroxide ion attack at protonated and free base ester.

$$EH^+ + H_2O \xrightarrow{k_w^+} \text{products} \tag{1}$$

$$EH^+ + OH^- \xrightarrow{k^+} \text{products} \tag{2}$$

$$E + H_2O \xrightarrow{k_w^0} \text{products} \tag{3}$$

$$E + OH^- \xrightarrow{k^0} \text{products} \tag{4}$$
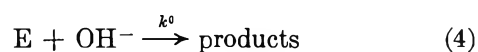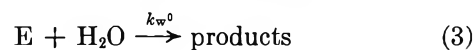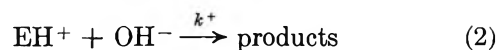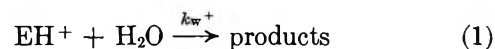
The symbols EH^+ and E represent protonated and free base ester, respectively. To the rate constants for water attack is affixed a subscript w, while the superscripts refer to the charge on the substrate ester molecule. Since all experiments were performed in dilute aqueous solutions, the constant concentration of water is included in the rate constants k_w.

Table I: Values of ΔH and pK_a for Ammonium Ionizations at 0.16 Ionic Strength

| | ΔH, kcal./mole | pK_a | | |
		$25°$	$30°$	$35°$
Glycine	10.80^a	9.66^b	9.53	9.40
Ammonia	12.40^c	9.27^d	9.12	8.97
Glycinamide	12^e	8.06^f	7.92	7.77

^{a} E. J. King, *J. Am. Chem. Soc.*, **73**, 155 (1951). ^{b} See ref. 11. ^{c} Average of three literature values: D. H. Everett and D. A. Landsman, *Trans. Faraday Soc.*, **50**, 1221 (1954); D. H. Everett and W. F. K. Wynne-Jones, *Proc. Roy. Soc.* (London), **A169**, 190 (1938); R. G. Bates and G. D. Pinching, *J. Res. Natl. Bur. Std.*, **42**, 419 (1949); *J. Am. Chem. Soc.*, **72**, 1393 (1950). ^{d} First reference in c. ^{e} Assumed. ^{f} N. C. Li and M. C. M. Chen, *J. Am. Chem. Soc.*, **80**, 5678 (1958).

The over-all rate of glycine ethyl ester hydrolysis is given by

$$R_E = k_w^+(EH^+) + k^+(EH^+)[OH^-] + k_w^0(E) +$$
$$k^0(E)[OH^-] \tag{5}$$

Dividing through eq. 5 by the total ester concentration, (E_{tot}), and letting α represent the fraction of ester in the free base form, $\alpha = K_E/[K_E + [H^+]]$, where K_E is the acid ionization constant for ester, we have

(10) H. S. Harned and B. B. Owen, "The Physical Chemistry of Electrolytic Solutions," 3rd Ed., Reinhold Publishing Corp., New York, N. Y., 1958.

(11) An average of five literature values measured at essentially the same conditions of this study: R. M. Keefer, *J. Am. Chem. Soc.*, **68**, 2339 (1946); E. J. King, *ibid.*, **73**, 155 (1951); C. Tanford and W. S. Shore, *ibid.*, **75**, 816 (1953); F. Basolo and Y. T. Chen, *ibid.*, **76**, 953 (1954); the fifth value is that of Li and Manning.[12]

(12) N. C. Li and R. A. Manning, *ibid.*, **77**, 5225 (1955).

(13) O. H. Emerson and P. L. Kirk, *J. Biol. Chem.*, **87**, 597 (1930).

(14) F. Holmes and W. R. C. Crimmin, *J. Chem. Soc.*, 1177 (1955).

$$\frac{R_E}{(E_{tot})} = k_w{}^+(1 - \alpha) + \left(k^+ + \frac{k_w{}^0 K_E}{K_w}\right) \times$$

$$(1 - \alpha)[OH^-] + k^0 \alpha[OH^-] \quad (6)$$

Three of the four rate constants of eq. 6 appear in terms of different $[OH^-]$ dependencies, but k^+ and $k_w{}^0$ cannot be separately determined experimentally.

A titration curve for glycine ethyl ester exhibits two unbuffered regions, pH 4.8 to 6.3 and pH 8.8 to 11.2. Rate runs were performed on the pH-stat in each region at ester concentrations of 0.005, 0.01, and 0.02 M. In the low pH 4.8–5.8 region, α becomes negligible compared to unity, and the last term in eq. 6 is insignificant. A straight line drawn through 12 points in a plot of $R_E/(E_{tot})$ vs. $[OH^-]$ yields $k_w{}^+ = 5 \pm 3 \times 10^{-9}$ sec.$^{-1}$ from the intercept and $k^+ + k_w{}^0 K_E/K_w = 36 \pm 2$ activity^{-1} sec.$^{-1}$ from the slope. This value of $k_w{}^+$ is in excellent agreement with one of 6×10^{-9} sec.$^{-1}$ obtained under similar conditions.[15] Since $k_w{}^+$ is surely not less than $k_w{}^0$, $k_w{}^0 K_E/K_w$ must be less than $k_w{}^+ K_E/K_w < 10^{-2}$. This last number is much less than 36, so that k^+ must equal 36; therefore, $k_w{}^0 K_E/K_w$ is negligible compared to k^+ and cannot be determined from our studies. A similar conclusion applies to other compounds in this paper.

In the high pH 8.8–11.2 region, eq. 6 reduces to

$$R_E/(E_{tot}) = [k^+(1 - \alpha) + k^0 \alpha][OH^-] \quad (7)$$

A plot of the logarithm of the left-hand side vs. pH for 19 runs yields the curve shown in Figure 1, which becomes linear above pH 10.3 where α becomes unity. From the linear region $k^0 = 0.78 \pm 0.02$ activity^{-1} sec.$^{-1}$. By utilizing this value for k^0 in eq. 7, values of k^+ were calculated for each of the 12 experimental points from $8.8 < $ pH < 10.3, yielding $k^+ = 28 \pm 3$ activity^{-1} sec.$^{-1}$. This value of k^+ agrees fairly well with that determined above in the other unbuffered region where the hydroxide ion concentration is only 10^{-4} times as great. An average value of $k^+ = 32 \pm 4$ activity^{-1} sec.$^{-1}$ is taken for this rate constant.

Experiments performed with solutions 10^{-2} M in total (Cu^{2+}) and 10^{-3} M in total ester concentration at pH 4.1 to 5.3 yield an estimate of the cupric ion catalyzed glycine ethyl ester hydrolysis. By utilizing a value of 3.87 for the logarithm of the first formation constant of cupric ion with glycine ethyl ester[4] and reasonable lesser values of the successive formation constants, it may be shown that greater than 96% of complexed cupric ion exists as 1:1 complex in this pH region.[1] One proton is liberated for each ester molecule hydrolyzed so that $R_{stat} = R_E + R_{CuE}$. In
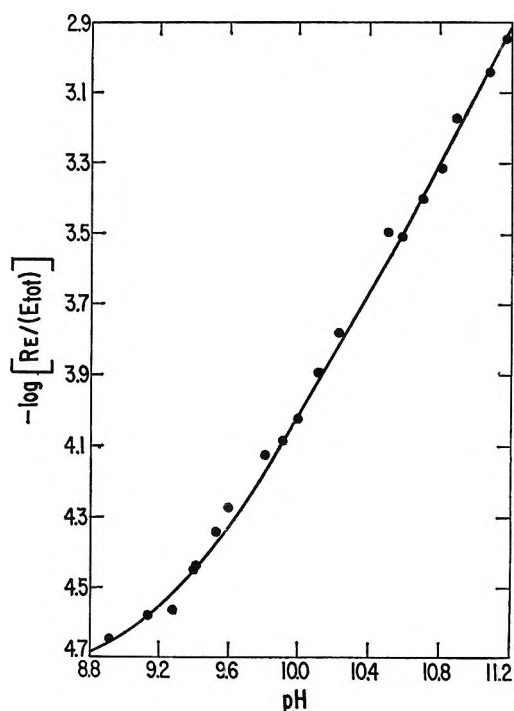
Figure 1. Hydrolysis of glycine ethyl ester. Points are experimental and smooth curve calculated from eq. 7 with $k^+ = 28$ activity^{-1} sec.$^{-1}$ and $k^0 = 0.78$ activity^{-1} sec.$^{-1}$.

this pH region eq. 2 is the most important for the free ester so that $R_E = k^+(EH^+)[OH^-]$, all quantities of which are known for a given pH. Two terms may contribute to R_{CuE} corresponding to the reactions

$$CuE^{+2} + H_2O \xrightarrow{k_{1w}{}^{2+}} products$$

$$CuE^{+2} + OH^- \xrightarrow{k_1{}^{2+}} products$$
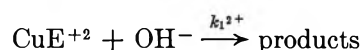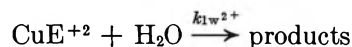
so that $R_{CuE} = k_{1w}{}^{2+}(CuE^{2+}) + k_1{}^{2+}(CuE^{2+})[OH^-]$. Rearrangement then yields

$$(R_{stat} - R_E)/(CuE^{2+}) = k_{1w}{}^{2+} + k_1{}^{2+}[OH^-] \quad (8)$$

R_E was calculated for each of six runs and was only 1–2% of R_{stat}. (CuE^{2+}) was 2 and 22% of total (Cu^{+2}) at pH 4.1 and 5.3, respectively, with intermediate percentages at intermediate pH values. A plot of the left-hand side of eq. 8 vs. $[OH^-]$ yields, as shown in Figure 2, a straight line, the intercept of which yields $k_{1w}{}^{2+} = (4.3 \pm 0.5) \times 10^{-5}$ sec.$^{-1}$ while the slope gives $k_1{}^{2+} = (1.01 \pm 0.05) \times 10^5$ activity^{-1} sec.$^{-1}$. An additional point determined with both total ester and total cupric ion concentrations equal to 0.01 M falls close to the line, lending support to the treatment of this system.

(15) V. I. Bolin, Z. anorg. allgem. Chem., 143, 201 (1925).
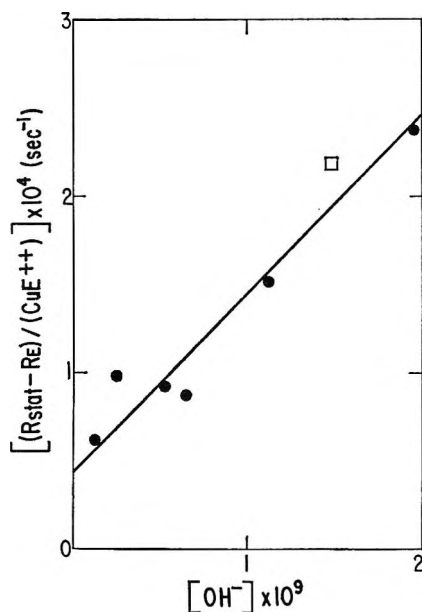
Figure 2. Hydrolysis of the 1:1 cupric ion complex of glycine ethyl ester from pH 4.1 to 5.3. Total ester concentration is 0.01 M, total cupric ion concentration is 0.001 M in circles and 0.01 M in square.

Cupric ion also catalyzes the hydrolysis of glycine ethyl ester in the pH 8.6 to 9.8 region. The distribution of ester among four cupric complexes complicates the analysis so that no quantitative treatment of the data obtained is included.[1]

Comparison of the values for water and hydroxide ion attack on glycine ethyl ester, k_w^+ and k^+, respectively, and on the 1:1 glycine ethyl ester–cupric ion complex, k_{1w}^{2+} and k_1^{2+}, indicates that at pH >5 hydroxide ion attack is the more important in both cases. Thus water should be replaced by hydroxide ion in a previous formulation[3] of cupric ion catalyzed hydrolysis of glycine ethyl ester where the experiments were performed at pH 7.3. Since hydroxide ion catalysis of hydrolysis of neutral esters extends into regions where pH <7 it is not surprising that hydrolysis of positively charged esters also does so. The ratios of the specific rate constants for hydroxide ion and water attack of greater than 2×10^9 activity^{-1} in both of the above hydrolyses are correspondingly greater than the value of a Brønsted exponent of 0.47 obtained for general base catalysis of ester hydrolysis,[16] a result suggesting that hydroxide ion functions directly as a nucleophile and not as a general base in both of the above cases.

As an approach to a model system for the enzyme carboxypeptidase, which contains zinc ion bound through sulfhydryl and amino groups,[17] the hydrolysis

of glycine ethyl ester was studied in the presence of β-mercaptoethylamine and zinc ion each at 0.05 M and from pH 6.8 to 7.8. Since log $K_f = 9.9$ for zinc ion and mercaptoethylamine,[12] this complex is fully formed in this pH region. Some estimate must be made of the binding of glycine ethyl ester to the zinc–mercaptoethylamine complex. The logarithm of this formation constant is estimated[1] to be between 2.0 and 2.3 by comparison with known values for binding of ammonia[18] and glycine ethyl ester[4] to nickel and zinc ions. The analysis that follows is not affected by the value (between 2.0 and 2.3) chosen.

Hydrolysis of unbound ester contributes less than 1% to the observed rate of hydrolysis. The main hydrolysis reaction is the zinc–mercaptoethylamine ($Zn(mea)^+$) complex catalyzed hydrolysis of glycine ethyl ester, which proceeds via hydrolysis of glycine ethyl ester in the complex $Zn(mea)(E)^+$. The rate of catalyzed ester hydrolysis R_c is due to the sum of two reactions

$$Zn(mea)(E)^+ + H_2O \xrightarrow{k_{1w}^+} \text{products}$$

$$Zn(mea)(E)^+ + OH^- \xrightarrow{k_1^+} \text{products}$$
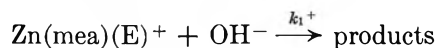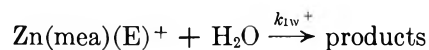
We then obtain

$$R_c/[Zn(mea)(E)^+] = k_{1w}^+ + k_1^+[OH^-]$$

A plot of the left-hand side of this equation vs. $[OH^-]$ for six points between pH 6.8 and 7.8 yields a straight line from which $k_1^+ = (2.6 \pm 0.3) \times 10^3$ activity^{-1} sec.$^{-1}$ and $k_{1w}^+ = (3.6 \pm 1.6) \times 10^{-4}$ sec.$^{-1}$.

The hydrolysis of 0.01 M glycine ethyl ester was also measured at pH 9.7–11.1 in solutions containing total concentrations of 0.01 M Ni^{+2} and 0.02 M cysteine. In these solutions cysteine and Ni^{2+} form a strong 2:1 complex,[19] which is diamagnetic[20] and presumably planar. Titration in the presence of excess cysteine reveals that only two cysteine molecules complex with a single nickel ion.[6] The rate of hydrolysis of glycine ethyl ester in the presence of the 2:1 complex is identical with the rate in absence of complex at the same pH. Thus planar, diamagnetic nickel ion complexes, which are unable to coordinate additional ligands, are not catalysts for hydrolysis reactions. A summary of the results obtained for hydroxide ion attack in glycine

(16) W. P. Jencks and J. Carriuolo, J. Am. Chem. Soc., 83, 1743 (1961).

(17) T. L. Coombs, Y. Omote, and B. L. Vallee, Biochemistry, 3, 653 (1964).

(18) J. Bjerrum, "Metal Ammine Formation in Aqueous Solution," P. Haase and Son, Copenhagen, 1957.

(19) G. R. Lenz and A. E. Martell, Biochemistry, 3, 745 (1964).

(20) R. B. Martin and R. Mathur, J. Am. Chem. Soc., 87, 1065 (1965).

Table II: Rate Constants for Hydroxide Ion Catalyzed Hydrolysis of Glycine Ethyl Ester at 25.00° and 0.16 Ionic Strength

Hydroxide ion reaction	Symbol	Activity^{-1} sec.$^{-1}$	M^{-1} sec. $^{-1a}$	Lit. M^{-1} sec. $^{-1}$
NH_2CH_2COOEt	k^0	0.78	0.58	0.73,[b] 0.60,[c] 0.83[d]
$NH_3{}^+CH_2COOEt$	k^+	32	24	20[e]
$Cu^{2+}NH_2CH_2COOEt$	$k_1{}^{2+}$	1.01×10^5	0.76×10^5	
$Zn^{2+}(NH_2CH_2CH_2S^-)$	$k_1{}^+$			
(NH_2CH_2COOEt)		2.6×10^3	2.0×10^3	

[a] Values in fourth column obtained from those in third by multiplication of latter by the mean ion activity coefficient, 0.75. [b] See ref. 4. [c] See ref. 22. [d] R. P. Bell and B. A. W. Coller, *Trans. Faraday Soc.*, **60**, 1087 (1964). [e] See ref. 16. Ionic strength 1.0.

ethyl ester hydrolysis is presented in Table II. Our results recorded as activity^{-1} sec.$^{-1}$ in the third column of Table II may be converted to the more frequently encountered units of M^{-1} sec.$^{-1}$ in the fourth column by multiplication by the mean ion activity coefficient mentioned in the Experimental section. Our rate constants expressed in units of M^{-1} sec.$^{-1}$ in the fourth column may be compared with literature values in the same units recorded in the fifth column of Table II. Agreement between our results and those in the literature varies from reasonably good to excellent.

Glycinamide. The hydrolysis of glycinamide was measured at an ionic strength of 0.16 at 25.00, 30.00, and 35.00°, at total amide concentrations of 0.01 and 0.02 M, and from pH 10.7 to 11.8. Equation 6 when applied to glycinamide hydrolysis yields

$$R_A/(\text{amide})_{tot} = k^0\alpha_A[\text{OH}^-] \qquad (9)$$

as only the glycinamide equivalent of eq. 4 is important in this high pH region. The fraction of amide in the free base form α_A is unity at these high pH values. Equation 9 may then be written in logarithmic form as

$$\log \frac{R_A}{(\text{A})} = \log k^0 + \text{pH} - \log K_w \qquad (10)$$

A plot of the left-hand side of eq. 10 *vs.* pH should yield a straight line of unit slope from which k^0 may be determined. Figure 3 shows such plots for three temperatures, 25.00, 30.00, and 35.00°. Using $-\log K_w = 14.00$, 13.83, and 13.68 at the three successive temperatures,[10] respectively, $k^0 = (2.9 \pm 0.1) \times 10^{-3}$, $(4.0 \pm 0.2) \times 10^{-3}$, and $(6.2 \pm 0.3) \times 10^{-3}$ activity^{-1} sec.$^{-1}$. The Arrhenius activation energy is 13.9 ± 0.8 kcal./mole. This value is almost the same as the activation energy of 14.3 kcal./mole reported for acetamide hydrolysis.[21] Similarly, glycine ethyl ester[22] and ethyl acetate[23] hydrolyses exhibit nearly identical activation energies of 10.9 and 11 kcal./mole, respectively. Thus an amide undergoes hydroxide ion catalyzed hydrolysis with an activation energy about 3 kcal./mole greater than that for an ester.
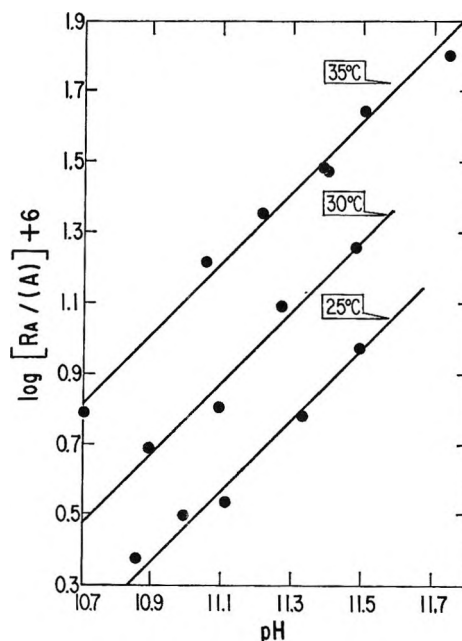
Figure 3. Hydrolysis of glycinamide at three temperatures.

A solution containing two moles of glycinamide hydrochloride per mole of cupric ion requires the addition of four equivalents of base to raise the pH to 10.[24] This result suggests that in addition to removal of protons from the substituted ammonium groups, cupric ion promotes the ionization of two amide hydrogens forming at high pH a 2:1 glycinamide–cupric ion complex with the ligands chelated through nitrogen atoms.[25,26]

(21) J. Packer, A. L. Thomson, and J. Vaughan, *J. Chem. Soc.*, 2601 (1955).

(22) C. Gustafsson, *Ann. Acad. Sci. Fennicae, Ser. AII*, 15, (1945); *Chem. Abstr.*, 41, 903h (1947).

(23) J. E. Potts, Jr., and E. S. Amis, *J. Am. Chem. Soc.*, 71, 2112 (1949).

(24) S. P. Datta and B. R. Rabin, *Trans. Faraday Soc.*, 52, 1123 (1956).

(25) B. R. Rabin, *ibid.*, 52, 1130 (1956); *Biochem. Soc. Symp.* (Cambridge, Engl.), 15, 21 (1958).

Hydrolysis experiments were attempted on solutions 0.01 M in glycinamide and 0.001 M in cupric ion from pH 6.0 to 6.7. Unlike all other hydrolysis experiments in this research performed in the pH-stat, the reaction consumed hydrogen ions so that it was necessary to have acid rather than base in the syringe buret. This result demonstrates kinetically that amide hydrogens have ionized in the pH 6.0 to 6.7 region. A net reaction illustrating hydrogen ion uptake on hydrolysis of the cupric chelate is

$$[CuNH_2CH_2CONH]^+ + H_3O^+ \longrightarrow$$
$$[CuNH_2CH_2COO]^+ + NH_4^+$$
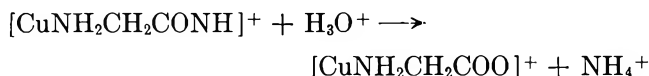
Unfortunately, a quantitative determination of reaction rates is not possible due to uncertainties in concentrations of all possible reactants and products at this halfway point in the titration curve. Since significant hydrolysis of unbound glycinamide is unlikely, cupric ion evidently promotes glycinamide hydrolysis in the pH 6.0–6.7 region. Consumption of hydrogen ions also occurs in solutions containing 0.01 M glycylglycine and 0.005 M cupric ion from pH 7.2 to 8.7. Cupric ion promotion of glycinamide hydrolysis has also been noted in the pH 9 to 10 region.[5]

The effect of cupric ion on the rate of glycinamide hydrolysis was also investigated at pH 12.0 where ionization of both amide hydrogens from the 2:1 glycinamide–cupric ion complex is complete. The reaction was followed spectrophotometrically by observing the decrease in absorption at 545 mμ where a solution 0.05 M in glycinamide and 0.005 M in cupric ion at pH 12 and 25.0° exhibits an absorption maximum. The initial molar absorption of 60 for the 2:1 glycinamide–cupric ion complex decreased to 50 after 4 days, to 43 after 11 days, and finally in 11 weeks to a constant value of 25. The final solution exhibited a visible spectrum identical with that for the corresponding glycine–cupric ion mixture at the same pH. In the absence of cupric ion, application of the above k^0 for glycinamide in eq. 9 indicates that only one part in 2 × 10^4 parts of glycinamide should remain at the end of 4 days. The only way to account for all these results at pH 12 is to postulate that cupric ion binds glycinamide more strongly than glycine, and in so doing strongly inhibits glycinamide hydrolysis.

Picolinamide. Hydrolysis experiments were conducted on solutions 0.01 to 0.03 M in picolinamide from pH 10 to 11 at 25.00° and 0.16 ionic strength. Equation 9 for glycinamide is applicable to this system. The hydrolysis rates are similar to those for glycinamide and $k^0 \simeq 2 \times 10^{-3}$ activity^{-1} sec.$^{-1}$.

The effect of the presence of cupric ion on the rate

of picolinamide hydrolysis was studied in solutions containing 6 × 10^{-3} M amide and 3 × 10^{-3} M cupric ion from pH 10.2 to 11.3. Such solutions exhibit an absorption maximum at 560 mμ with a molar extinction coefficient ϵ 53. After 20 days the spectra are superimposable on those obtained initially. A 2:1 picolinic acid–cupric ion complex exhibits maximum absorption at 650 mμ with ϵ_{650} 42 and ϵ_{560} 17. Therefore, cupric ion inhibits the hydrolysis of picolinamide at high pH values as well as that of glycinamide.

Since metal ion complexes of picolinamide had not received previous investigation, further studies were performed, particularly with regard to amide hydrogen ionizations. Automatic titrations with added NaOH at 25.0° and 0.16 ionic strength revealed no acidic groups in picolinamide from the starting pH of 4.6 up to pH 10, where the solution becomes self-buffering. The pyridinium hydrogen of picolinamide exhibits $pK_a = 1.9$, and ionization of the amide hydrogen is not expected until pH >13.[27] Titration of solutions containing 0.02 M picolinamide and either 0.01 M Zn^{2+} or Cd^{2+} precipitates the metal ion hydroxide at about pH 8, indicating a relatively weak association of these metal ions with picolinamide.

Solutions containing two moles of picolinamide per mole of either Cu^{2+} or Ni^{2+} exhibit absorptions at lower wave lengths and of greater intensity than solutions of the aqueous metal ions, indicating binding to the nitrogen containing ligand. For example, aqueous cupric ion absorbs maximally near 800 mμ with a molar extinction coefficient ϵ 13, while a 2:1 picolinamide–cupric ion solution exhibits maximum absorption at 700 mμ with ϵ 31.

Titration of solutions containing two moles of picolinamide per mole of Cu^{2+} or Ni^{2+} requires the addition of 2 equiv. of base per mole of metal ion to reach pH 10. The picolinamide–cupric ion solutions reversibly change color from blue at the beginning of the titration to violet at the end, with an absorption maximum at 560 mμ and ϵ 53. This last color does not fade on prolonged standing. Further binding to nitrogen atoms is indicated by the spectral shift to shorter wave lengths on titration. The original blue picolinamide–nickel ion solutions change to yellow-orange during the course of the titration. These color changes are typical of those found in other amides and

(26) Evidence for the view that binding occurs through the carbonyl oxygen before and the amide nitrogen after ionization of amide hydrogens has been reviewed: A. S. Brill, R. B. Martin, and R. J. P. Williams in "Electronic Aspects of Biochemistry," B. Pullman, Ed., Academic Press, New York, N. Y., 1964, p. 540.

(27) For the amide hydrogen ionization from positively charged N^L-methylnicotinamide, $pK_a = 13.2$: R. B. Martin and J. G. Hull, *J. Biol. Chem.*, **239**, 1237 (1964).

peptides where amide hydrogens are undergoing cupric[28] or nickel[29] ion promoted ionizations. Preparation of a solid, neutral nickel(picolinamide)$_2$ complex is described in the Experimental section.

The overlapping ionizations that occur when solutions 0.02 or 0.04 M in picolinamide and 0.01 or 0.02 M, respectively, in either Cu^{2+} or Ni^{2+} are titrated with base were analyzed by the projection strip method.[30] For the 2:1 cupric ion complex, $pK_1 = 5.09$ and $pK_2 = 6.51$, while for the 2:1 nickel ion complex, $pK_1 = 7.99$ and $pK_2 = 9.44$. These values may be considered reliable to ±0.05 log unit. The difference between pK_2 and pK_1 for the cupric ion complex is similar to that observed for cupric ion promoted amide hydrogen ionizations from other amides[31] and peptides.[28] The 2:1 picolinamide–nickel ion complex exhibits a difference of 1.45 log units between the two amide hydrogen ionizations. In other instances of nickel ion promoted amide hydrogen ionizations, the difference in pK_a values is 0.6 unit or less.[29] These small differences are equal to or less than those based on purely statistical grounds. The difference of about 1.45 units for the 2:1 picolinamide–nickel ion complex is larger than the statistical difference of 0.6 unit but still much less than that expected for a dibasic acid with the acidic groups so closely spaced. The cooperative nature of the transition from the blue, paramagnetic, octahedral nickel complex to the yellow, diamagnetic, planar complex upon ionization of the amide hydrogens is again indicated.

Evidence has been presented that cupric ion promotes amide hydrogen ionization in picolinamide as well as glycinamide. For both amides, hydrolysis at pH 11 to 12 is inhibited by the addition of cupric ion. On the other hand, cupric ion promotes the hydrolysis of glycinamide at pH <10.5. Evidently, cupric ion accelerates the hydrolysis of amides as well as esters at pH values where simple association or chelation through carbonyl oxygen occurs, but amide hydrolysis is markedly inhibited at pH values above which cupric ion promoted amide hydrogen ionization is complete, and chelation occurs at the amide nitrogen.

Unlike the 2:1 picolinamide–cupric ion solutions at high pH, the color of which is extraordinarily stable, the yellow of 2:1 picolinamide–nickel ion solutions fades with time. The fading is rapid at first but later slows, indicating the occurrence of at least two reactions. The speed and complexity of the kinetics preclude a definitive analysis. Fading of the yellow can be slowed by slightly increasing the ligand to metal ion ratio and by decreasing the pH. Extrapolation to zero time indicates that the absorption maximum of the yellow 2:1 picolinamide–nickel ion complex occurs

at about 400 mμ with a molar extinction coefficient of 1100–1200. This value is unusually high for this type of complex and may include some intensity from a neighboring absorption band in the ultraviolet region. The rapidity and complexity of these reactions may be features of the change in configuration about the nickel ion.

Discussion

Results for metal ion catalyzed ester hydrolysis and cupric ion promoted or inhibited amide hydrolysis may be interpreted in terms of the usual mechanism for hydroxide ion attack at the carbonyl function.

$$NH_2CH_2 \underset{\substack{\| \\ O}}{C}R + OH^- \underset{k_2}{\overset{k_1}{\rightleftharpoons}} NH_2CH_2 \underset{\substack{| \\ O^-}}{\overset{\substack{OH \\ |}}{C}}R \overset{k_3}{\longrightarrow}$$

$$NH_2CH_2COO^- + RH$$
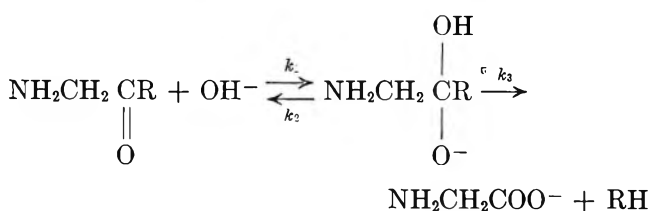
The group R represents in this study $-OC_2H_5$ and $-NH_2$. Since prototropic transfers are considered rapid compared to the other reactions, the same conclusions apply whenever any of the four equations (1) through (4) are employed in the mechanism. Assuming a steady state for the tetrahedral carbon addition intermediate in the above mechanism, the observed first-order rate constant for hydrolysis is given by

$$k_{obsd} = \frac{k_1[OH^-]}{1 + k_2/k_3} \tag{11}$$

To assess the role of metal ions on ester and amide hydrolysis, it is necessary to consider equilibria of metal ion binding to reactants, tetrahedral addition intermediates, and transition states or effects on rate constants. For ester hydrolyses, k_2/k_3 in eq. 11 is less than unity[32] and, to an approximation sufficient for our purposes, the rate-limiting step is k_1. Catalysis of phenylalanine ethyl ester hydrolysis by cupric ion also gives a similar value of k_2/k_3 less than unity,[3] so

(28) W. L. Koltun, R. H. Roth, and F. R. N. Gurd, J. Biol. Chem., 238, 124 (1963); W. L. Koltun, M. Fried, and F. R. N. Gurd, J. Am. Chem. Soc., 82, 233 (1960).

(29) R. B. Martin, M. Chamberlin, and J. T. Edsall, ibid., 82, 495 (1960); R. B. Martin and J. R. Edsall, ibid., 82, 1107 (1960). For appearance of a yellow color upon nickel ion promoted peptide ionizations in proteins, see R. B. Martin, Federation Proc., 20, No. 3, Suppl. 10, 54 (1961).

(30) F. J. C. Rossotti and H. S. Rossotti, "The Determination of Stability Constants," McGraw-Hill Book Co., Inc., New York, N. Y., 1961, pp. 99–101.

(31) S. P. Datta, R. Leberman, and B. R. Rabin, Trans. Faraday Soc., 55, 2141 (1959).

(32) M. L. Bender and R. J. Thomas, J. Am. Chem. Soc., 83, 4189 (1961); M. L. Bender, H. Matsui, R. J. Thomas, and S. W. Tobey, ibid., 83, 4193 (1961).

that the k_1 step is also rate limiting in metal ion catalyzed ester hydrolysis. Thus the catalytic effect of cupric ion on glycine ethyl ester hydrolysis is due predominantly to complexation increasing the value of the k_1 rate constant.

The rate constants $k^0 = 0.78$, $k^+ = 32$, and $k_1^{2+} = 101,000$ (all activity^{-1} sec.$^{-1}$) represent the rate of hydroxide ion attack on neutral, protonated, and cupric ion complexed glycine ethyl ester, respectively. The ratio $k^+/k^0 = 41$ is about that expected for hydroxide ion attack two carbon atoms removed from the center of positive charge and compares favorably with the ratio of acid ionization constants from the ammonium group of glycine ethyl ester and glycine, $K_E/K_2 = 74$.

Addition of another positive charge in the presence of cupric ion at the amino nitrogen yields a much larger ratio $k_1^{2+}/k^+ = 3200$ indicative of a special effect of cupric ion beyond that due to an additional positive charge. Some chelation of the carbonyl oxygen to cupric ion accounts for this large augmentation in rate and presents an example of super-acid catalysis.[33] Super-acid catalysis occurs when positive charge density, as carried by a metal ion, is placed in a molecule at a reactive position where a proton is not normally to be found at a similar pH. Even though the formation constants of metal ions with ammonia[18] and glycine ethyl ester are similar,[4] some chelation is indicated because ammonia is a 30 times stronger base. Significantly stronger metal ion binding to ammonia would be expected in the absence of chelation in glycine ethyl ester. It does not seem possible to estimate the fraction of complexed ester molecules that are also chelated, but only a small fraction is required to yield an appreciable super-acid effect with such a highly reactive chelate. Bond making and breaking between cupric ion and nitrogen or oxygen atoms of starting material or intermediates is also considered to be rapid compared to the other reactions discussed here.

For the zinc ion–mercaptoethylamine complex of glycine ethyl ester $k_1^+/k^+ = 81$. Since the substrate bears a net charge of $+1$ for both numerator and denominator rate constants, the ratio should be unity in the absence of a super-acid effect. If the last ratio is multiplied by the charge factor with no super-acid effect, $k^+/k^0 = 41$, the product 3300 is close to $k_1^{2+}/k^+ = 3200$, so that evidently the super-acid effect is about the same in the cupric and zinc ion cases. The super-acid effect is calculated as the augmentation in rate beyond that expected from electrostatic considerations of the positive charge density. Independent evidence for super-acid catalysis of glycine ethyl ester hydrolysis by cupric ion may be obtained by comparing

the ratio $k_1^{2+}/k^+ = 3200$ with much smaller or normal ratios for the effect of cupric ion on hydrolyses of histidine methyl ester with two chelating groups in addition to the ester function.[6]

In contrast to ester hydrolysis, the ratio k_2/k_3 for hydroxide ion catalysis of amides is greater than unity,[34] so that eq. 11 reduces to

$$k_{obsd} = k_3 k_1 [OH^-]/k_2$$

An equilibrium exists in the first step for amide hydrolysis, and the rate-limiting step is k_3. Cupric ion catalyzes glycinamide hydrolysis in the low pH region, but it is less effective than in ester hydrolysis. Though glycine ethyl ester and glycinamide are bases of comparable strength, the first formation constant of cupric ion is about 20 times greater for glycinamide[24] than for glycine ethyl ester.[4] Chelation is then stronger for cupric ion and glycinamide so that a greater super-acid effect is expected if the k_1 step is rate limiting. We suggest that the lesser effectiveness of cupric ion in catalyzing amide than ester hydrolyses at pH <10 is due to a greater k_2/k_3 or lesser k_3/k_2 ratio for the cupric ion catalyzed over metal free amide hydrolysis which more than compensates for the larger super-acid effect. The increased partitioning of the tetrahedral carbon addition intermediate to reactants over products in the presence of cupric ion may at least in part be due to the expected strong binding of cupric ion to the tetrahedral addition intermediate with two amino groups. Cupric ion binding to the amino and hydroxy functions of the addition intermediate for glycine ethyl ester hydrolysis is expected to be much weaker. Ethanolamine and ethylenediamine may be considered as model compounds for metal ion chelation to the tetrahedral addition intermediates of glycine ethyl ester and glycinamide, respectively. Cupric ion binds 10^7 times more strongly to ethylenediamine than to ethanolamine.[35] In the case of amide hydrolysis, the bond to be broken in the k_3 step is within the chelate ring while for ester hydrolysis it is outside.

At pH >11, cupric ion inhibits the hydrolysis of both glycinamide and picolinamide. In this pH region, where amide hydrogen ionization is complete, the 2:1 complexes are neutral and the carbonyl carbon is no longer a site of considerable positive charge density. We suggest that in this region not only is k_3/k_2 small as before but also hydroxide ion attack is very slow. This interpretation is consistent with the facile cupric

(33) F. W. Westheimer, *Trans. N. Y. Acad. Sci.*, **18**, 15 (1955).

(34) M. L. Bender, R. D. Ginger, and J. P. Unik, *J. Am. Chem. Soc.*, **80**, 1044 (1958).

(35) "Stability Constants," Special Publication No. 6, The Chemical Society, London, 1957.

ion catalyzed hydrolysis of the unsaturated dipeptide glycyldehydrophenylalanine where substantial negative charge density produced by amide hydrogen ionization may be passed to the aromatic ring.[36] Part of the complexity of the kinetics of the yellow 2:1 picolinamide–nickel ion chelate may be due to the stereochemical change from a diamagnetic, planar chelate to the nickel chelate of the tetrahedral addition intermediate, which should be paramagnetic and octahedral.

(36) B. J. Campbell, Y. Lin, and M. E. Bird, *J. Biol. Chem.*, **238**, 3632 (1963).

Transition Metal Ion Promoted Hydrolyses of Amino Acid Esters[1]

by Harry L. Conley, Jr., and R. Bruce Martin

Cobb Chemical Laboratory, University of Virginia, Charlottesville, Virginia (*Received February 16, 1965*)

Specific reaction rate constants are reported for attack of hydroxide ion on several different charged species of histidine methyl ester, cysteine ethyl ester, and aspartic acid-β-methyl ester. The diprotonated form of histidine methyl ester is hydrolyzed about 100 times faster than normal. Formation constants for association of histidine methyl ester with cupric, nickel, zinc, and cadmium ions have been determined. The effect of these divalent transition metal ions in promoting hydrolyses of the three amino acid esters has been evaluated. Though there are some exceptions, the promotional effects of the divalent transition metal ions are similar and do not differ significantly from the equivalent charge effects brought about by protons. Divalent transition metal ion promotion of hydrolyses of these amino acid esters where chelation occurs at two sites other than the labile ester bond may be accounted for primarily by electrostatic considerations. Complexes of esters and metal ions that are strongly chelated through two sites other than the reactive one are more slowly hydrolyzed than complexes of esters, such as glycine ethyl ester, and metal ions where weak chelation includes the reactive site.

Divalent metal ions of the second half of the first transition series increase the observed rates of hydrolyses of amino acid esters.[2] Precise characterization of the rate increase is difficult in solutions containing buffer components that interact with metal ions. Li and co-workers employed a conductivity method to evaluate rate constants in the presence of excess base, divalent transition metal ions, and either histidine methyl ester[3] or cysteine esters.[4,5] None of these papers reports a detailed study of the dependence of the hydrolysis rates on pH.

In this paper we report the results of detailed concentration and pH studies of cupric, nickel, zinc, or cadmium ion promoted hydrolyses of histidine methyl ester, cysteine ethyl ester, and aspartic acid-β-methyl ester. The specific reaction rate constants are calculated from measurements of the rate of proton production in buffer-free solutions on a pH-stat. In order to

(1) This paper is abstracted from the Ph.D. thesis of Harry L. Conley, Jr., 1964, from which more details may be obtained. The research was supported by grants from the National Science Foundation and the National Institutes of Health.

(2) H. Kroll, *J. Am. Chem. Soc.*, **74**, 2036 (1952).

(3) N. C. Li, B. E. Doody, and J. M. White, *ibid.*, **79**, 5859 (1957).

(4) J. M. White, R. A. Manning, and N. C. Li, *ibid.*, **78**, 2367 (1956).

(5) R. Mathur and N. C. Li, *ibid.*, **86**, 1289 (1964).

assess the effects of divalent metal ions on ester hydrolysis, detailed studies of the hydroxide ion dependence of hydrolyses rates in metal-free solutions of esters were also conducted. Formation constants of divalent transition metal ions with amino acid esters were also determined when necessary.

In order for metal ions to affect the rate of ester hydrolysis, binding must occur to reactant ester, reaction intermediates, or transition states. In the cases reported here, the rate-limiting step is considered to be hydroxide ion attack at the free or complexed ester. Chelation of the transition metal ions to the amino acid esters studied in this work occurs predominantly at two sites other than the labile ester function. A comparison of the metal ion promoted hydrolyses of these esters with that of glycine ethyl ester[6] where chelation involves the reactive ester group may then be made.

Experimental

Materials. L-Histidine methyl ester dihydrochloride, and L-cysteine ethyl ester hydrochloride were the best available commercial products. They gave equivalent weights by titration to within 2% of the theoretical values. It was necessary to recrystallize twice a commercial sample of L-aspartic acid-β-methyl ester to attain the 2% limit on equivalent weight. Stock solutions or, when necessary, dry samples of these esters were used in the rate experiments.

All solutions were prepared with triply distilled water, the second distillation from an alkaline permanganate solution. This distilled water was boiled prior to storage in Pyrex glass containers and protected from atmospheric carbon dioxide by Ascarite tubes. All samples of this water exhibited specific conductances from 3.4 to 5.0 $\times$ 10^{-7} ohm^{-1} cm.$^{-1}$. Carbonate-free sodium hydroxide solutions were prepared by dilution of filtered 50% solutions, stored in polyethylene bottles, and protected from carbon dioxide by Ascarite tubes. These dilute stock solutions were standardized by automatic potentiometric titrations against primary standard potassium acid phthalate.

Stock solutions of $Ni(NO_3)_2$, $NiCl_2$, $Cu(NO_3)_2$, $CuCl_2$, $Zn(NO_3)_2$, and $Cd(NO_3)_2$ were prepared from good quality commercial salts low in other metals and the solutions filtered where necessary. Nickel ion solutions were standardized by the gravimetric dimethylglyoxime method.[7] Cupric ion solutions were standardized by both the iodometric and thiocyanate methods[7,8]; the agreement was to within 1%. Zinc ion solutions were standardized gravimetrically[9] as $ZnNH_4PO_4$ and $ZnSO_4$ and also volumetrically by titration with potassium ferrocyanide.[10] Mean deviation of the three methods was less than 1%. The cadmium ion solution was standardized gravimetrically as $CdSO_4$.[11]

Methods. Titrations and rate runs were performed on a Radiometer TTT1 pH-stat equipped with a glass jacket about the Pyrex reaction vessel which permitted temperature control to $\pm 0.02°$ by circulation of water from an external bath. Temperature was read with a mercury-in-glass thermometer (smallest division 0.1°) calibrated against a similar thermometer calibrated by the National Bureau of Standards. All results in this study were performed at 25.00 $\pm$ 0.02°.

Solutions of metal ion nitrates were used for titration and pH-stat experiments. Ionic strength was always 0.16 M controlled with KNO_3.

A Radiometer GK2021B combined glass–calomel electrode was used with the pH-stat. Since the glass electrode portion was of the high basicity type, no sodium ion corrections were ever necessary. Beckman or other suitable buffers were used to calibrate the pH meter to ± 0.01 pH unit.

Solutions were stirred smoothly at 2000 r.p.m. Water-pumped tank nitrogen was passed through an Ascarite tube to remove carbon dioxide and through vanadous chloride scrubbers[12] to remove oxygen. Finally, just before passing over the reactant solution, the nitrogen bubbled through a 0.16 M KNO_3 solution in a gas washing bottle immersed in the same water bath mentioned above for temperature control. The nitrogen escaped from the reaction vessel through small openings about the stirrer and syringe buret delivery tube. Before mixing in the reactant vessel, all stock solutions, solution tubes, and the electrode were equilibrated in the water bath. Final reactant solution volumes were 15 ml.

Reaction rates were determined from the initial slope of the pH-stat trace of volume of base added *vs.* time.

(6) H. L. Conley, Jr., and R. B. Martin, *J. Phys. Chem.*, **69**, 2914 (1965).

(7) R. Belcher and A. J. Nutten, "Quantitative Inorganic Analysis," Butterworth and Co. Ltd., London, 1955.

(8) W. C. Pierce and E. L. Haenisch, "Quantitative Analysis," 3rd Ed., John Wiley and Sons, Inc., New York, N. Y., 1954; E. H. Swift, "Introductory Quantitative Analysis," Prentice-Hall, Inc., New York, N. Y., 1950.

(9) W. W. Scott, "Scott's Standard Methods of Chemical Analysis," Vol. 1, 5th Ed., N. H. Furman, Ed., D. Van Nostrand Co., Inc., New York, N. Y., 1939.

(10) I. M. Kolthoff and V. A. Stenger, "Volumetric Analysis, Volume II, Titration Methods," 2nd Revised Ed., Interscience Publishers, Inc., New York, N. Y., 1947.

(11) Q. Fernando and H. Freiser in "Treatise on Analytical Chemistry," Part II, Vol. 3, Cadmium Section, Interscience Publishers, Inc., New York, N. Y., 1961.

(12) L. Meites, "Polarographic Techniques," Interscience Publishers, Inc., New York, N. Y., 1955, p. 34.

The conversion of the moles of protons liberated per unit time to moles of ester reacting per unit time is described for each case in the next section. Runs on the pH-stat on solutions containing metal ions were performed in unbuffered portions of the titration curve. Limits quoted on reaction rate constants represent the maximum value permitting a reasonable fit to the data.

Hydroxide ion activities were obtained from pH meter readings by utilizing $pK_w = 14.00$. Our second-order rate constants are obtained by dividing first-order rate constants by the activity of hydroxide ion and possess units of activity^{-1} sec.$^{-1}$. These rate constants may be converted to M^{-1} sec.$^{-1}$ by multiplying them by 0.75, the mean ion activity coefficient for both KOH in KCl and NaOH in NaCl solution at 25° and 0.16 ionic strength.[13] In this paper, parentheses denote molar concentrations, and brackets denote molar activities.

In the special case of histidine methyl ester, greater precision was desired in determining acid ionization constants and formation constants with divalent transition metal ions so that a Radiometer pH Meter 4, which can be read to 0.001 pH unit, was used. Other aspects of the experimental setup, including the temperature control, are as described above, except that it was necessary to operate manually the syringe buret for NaOH delivery.

Occasionally it is necessary to compare rate or equilibrium constants obtained at 25° but at differing ionic strengths. For this purpose the negative logarithm of the activity coefficient is taken as $0.5z^2\mu^{1/2}/(1 + \mu^{1/2})$ where z is the charge and μ is the ionic strength. The extent of formation of hydroxo and other aquo complexes of the metal ions is considered unimportant under our conditions.

Results

Histidine Methyl Ester, Formation Constants. To evaluate data obtained from kinetic experiments on hydrolysis of histidine methyl ester in the absence and presence of metal ions, it is necessary to know accurately acid dissociation constants for the ester dihydrochloride and formation constants of ester–metal ion complexes.

The data obtained from automatic potentiometric titration of 0.01 M histidine methyl ester dihydrochloride at 25.00° and 0.16 ionic strength were analyzed by substitution in exact equations for the overlapping imidazolium and ammonium ionizations and by application of the projection strip method for formation constants of a 2:1 ligand–metal ion complex[14] to acid ionizations. Both methods yield $pK_{1E} = 5.35 \pm 0.02$

and $pK_{2E} = 7.30 \pm 0.03$ in activity units. These values are only 0.03 log unit less than values obtained at 0.15 ionic strength,[3] but are significantly less than values obtained at 0.12 ionic strength and the same temperature.[15] We find no evidence for a reported third ionization from histidine methyl ester with $pK_3 = 11.1$.[15] Ionization constants are difficult to determine accurately in this high pH region, and ester hydrolysis occurring during the titration liberates hydrogen ions.

Formation constants for the 2:1 complexes of divalent zinc, cupric, cadmium, and nickel ions with histidine methyl ester were evaluated by the projection strip method.[14] Most experiments were conducted at 0.01 M divalent metal ion and 0.02 to 0.08 M ester concentrations. Even at an 8:1 ratio of ester to zinc ion, no evidence for more than a 2:1 complex is obtained. In this case the formation curve of the average number of ester molecules bound to the metal ion, $\bar{n}$, vs. $-\log$ (E) where (E) is the molar concentration of the free base form of the ester, levels off at $\bar{n} = 2$. Formation curves for cupric and cadmium ion com-
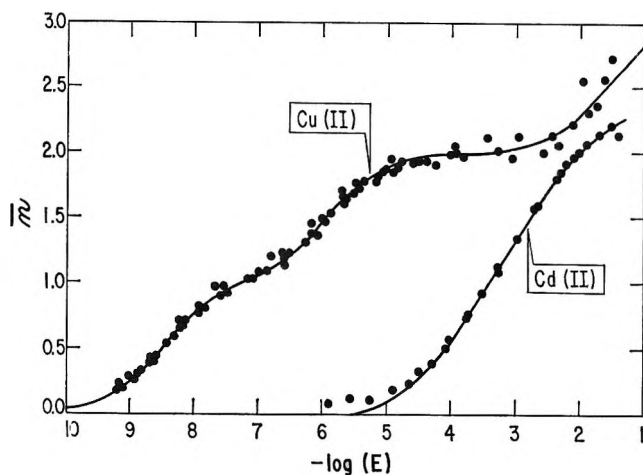
Figure 1. Formation curve of average number of histidine methyl ester molecules bound to cupric and cadmium ions vs. $-\log$ (E), where (E) is the free base ester concentration. Experimental points are from solutions containing total ester to cupric ion molar concentration ratios of (0.002)/(0.001), (0.004)/(0.001), and (0.02–0.08)/(0.01) and ester to cadmium ion concentration ratios of (0.04/(0.01) and (0.08)/(0.01). Curves are constructed from formation constants given in Table I.

(13) H. S. Harned and B. B. Owen, "The Physical Chemistry of Electrolytic Solutions," 3rd Ed., Reinhold Publishing Corp., New York, N. Y., 1958.

(14) F. J. C. Rossotti and H. S. Rossotti, "The Determination of Stability Constants," McGraw-Hill Book Co., Inc., New York, N. Y., 1961, pp. 99–101.

(15) G. Weitzel, W. Schaeg, and F. Schneider, *Ann.*, **632**, 124 (1960).

plexes shown in Figure 1 exhibit values of $\bar{n} > 2$ when the ester to metal ion concentration ratio is greater than 4. The third formation constants for these metal ions were evaluated by curve fitting at $\bar{n} > 1.5$ after evaluation of the first two formation constants from data at $\bar{n} < 1.5$ by the projection strip method. Similar calculations were performed for the third formation constant in the nickel ion complex. Results of all formation constant studies are tabulated in Table I. Our first formation constants are almost 0.6 log unit less than those previously reported.[3,15] The values recorded in Table I were used for the calculations that follow in this paper.

Table I: Logarithms of Formation Constants of Metal Ions with Histidine Methyl Ester at 25.00° and 0.16 Ionic Strength[a]

Metal ion	K_{1f}	K_{2f}	K_{3f}
Cu^{2+}	8.48 ± 0.04	5.90 ± 0.04	1.6 ± 0.2
Ni^{2+}	6.19 ± 0.04	4.91 ± 0.04	2.90 ± 0.06
Zn^{2+}	4.46 ± 0.08	4.20 ± 0.08	0.0
Cd^{2+}	3.98 ± 0.04	2.81 ± 0.04	~1

[a] For hydrogen ion, $pK_{1E} = 5.35$ and $pK_{2E} = 7.30$.

Hydrolysis of Histidine Methyl Ester. Without any committment to the mechanism of the reaction, the hydrolysis of histidine methyl ester to yield histidine and methyl alcohol may be represented by the scheme

$$EH_2{}^{2+} + H_2O \longrightarrow AH_2{}^{++-} + H^+ + CH_3OH$$

$$\left\downarrow\uparrow K_{1E} \qquad\qquad \left\downarrow\uparrow K_{2A}$$

$$EH^+ \qquad\qquad\qquad AH^{+-} \qquad\qquad (1)$$

$$\left\downarrow\uparrow K_{2E} \qquad\qquad \left\downarrow\uparrow K_{3A}$$

$$E \qquad\qquad\qquad A^-$$
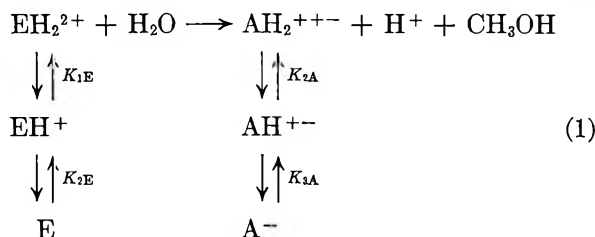
Histidine methyl ester in three stages of ionization appears on the left-hand side of eq. 1 and histidine on the right-hand side. The large K's refer to acid ionization constants. For histidine methyl ester, $pK_{1E} = 5.35$ and $pK_{2E} = 7.30$ as determined above. For histidine we take[16] $pK_{2A} = 6.10 \pm 0.07$ and $pK_{3A} = 9.17 \pm 0.04$. Since all our experiments were performed at pH >5, the carboxylic acid group of histidine is fully ionized in all experiments of this paper.

It is convenient to define terms for the fractions of the total histidine methyl ester concentration and total histidine concentration in each of the charged forms. For histidine methyl ester these are

$$\alpha_{0E} \equiv \frac{(EH_2{}^{2+})}{(E_{tot})} = \frac{[H^+]^2}{[H^+]^2 + [H^+]K_{1E} + K_{1E}K_{2E}} \quad (2)$$

$$\alpha_{1E} \equiv \frac{(EH^+)}{(E_{tot})} = \frac{[H^+]K_{1E}}{[H^+]^2 + [H^+]K_{1E} + K_{1E}K_{2E}} \quad (3)$$

$$\alpha_{2E} \equiv \frac{(E)}{(E_{tot})} = \frac{K_{1E}K_{2E}}{[H^+]^2 + [H^+]K_{1E} + K_{1E}K_{2E}} \quad (4)$$

Similar equations may be written for histidine, and we shall make use of α_{2A} and α_{3A}, which may be defined by eq. 3 and 4 where the subscript 2A replaces 1E and the subscript 3A replaces 2E, respectively. Since all constants on the right-hand sides of the α expressions are known, all α's may be evaluated at any pH >5 of interest.

The pH-stat records the number of protons liberated as a function of time, R_{stat}, as the reaction proceeds. However, we are interested in the number of ester molecules reacting per unit time, R_E. The relationship between R_{stat} and R_E may be found by reference to eq. 1 and the following argument. For each molecule of histidine methyl ester in the form $EH_2{}^{2+}$ that is hydrolyzed, one proton is produced for the fraction of product histidine that is $AH_2{}^{++-}$. This quantity is augmented by one proton for each molecule of histidine that is $AH^{\pm}$ and by two protons for A^-. The observed rate is reduced by one proton for each molecule of histidine methyl ester that is EH^+ and by two protons for each molecule that is in the free base E form. Summing these considerations yields

$$R_{stat} = R_E(1 + \alpha_{2A} + 2\alpha_{3A} - \alpha_{1E} - 2\alpha_{2E})$$

$$= R_E Q \quad (5)$$

where Q represents the terms in parentheses. For histidine methyl ester hydrolysis, Q is never unity from 4 < pH < 11. Most of our results are within this pH range.

For the mechanism of hydrolysis of histidine methyl ester in the pH 7.8 to 11.1 region, hydroxide ion attack at each of the three ester species must be considered.

$$EH_2{}^{2+} + OH^- \xrightarrow{k^{2+}} products \quad (6)$$

$$EH^+ + OH^- \xrightarrow{k^+} products \quad (7)$$

$$E + OH^- \xrightarrow{k^0} products \quad (8)$$
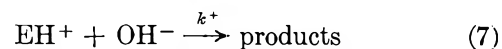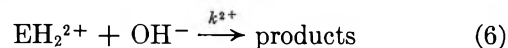
(16) Average of six literature values at 25° and adjusted to an ionic strength of 0.16 where necessary, ref. 3, 15, 17, and the following: C. L. A. Schmidt, W. K. Appleman, and P. L. Kirk, *J. Biol. Chem.*, **85**, 137 (1929); S. Kilpi, J. Vaananen, and N. E. Virkola, *Suomen Kemistilehti*, **28B**, 45 (1955); R. Leberman and B. R. Rabin, *Trans. Faraday Soc.*, **55**, 1660 (1959).

(17) N. C. Li and R. A. Manning, *J. Am. Chem. Soc.*, **77**, 5225 (1955).

Water attack on the ester species may be proved unimportant in this high pH region by arguments similar to those presented for glycine ethyl ester.[1,6] The total rate of ester hydrolyses is given by

$$R_E = [k^{2+}(EH_2^{2+}) + k^+(EH^+) + k^0(E)][OH^-]$$

Substitution of the α expressions of eq. 2 to 4 and division by the total ester concentration (E_{tot}) yields

$$R_E/(E_{tot}) = (k^{2+}\alpha_{0E} + k^+\alpha_{1E} + k^0\alpha_{2E})[OH^-]$$

In logarithmic form we obtain

$$\log [R_E/(E_{tot})] = \log (k^{2+}\alpha_{0E} + k^+\alpha_{1E} + k^0\alpha_{2E}) + \text{pH} - 14.00 \quad (9)$$

A plot of the left-hand side of eq. 9 vs. pH is shown in Figure 2. At high pH values the slope of the curve in Figure 2 approaches unity and since $\alpha_{0E} = 0 = \alpha_{1E}$ and $\alpha_{2E} \simeq 1$, the log term on the right-hand side of eq. 9 becomes log k^0. The components of all α-functions in eq. 9 are known, and the best fit for the experimental points in Figure 2 is obtained for $k^{2+} = (3.5 \pm 0.9) \times 10^4$ activity^{-1} sec.$^{-1}$, $k^+ = 75 \pm 6$ activity^{-1} sec.$^{-1}$, and $k^0 = 0.36 \pm 0.03$ activity^{-1} sec.$^{-1}$. The curve shown in Figure 2 is drawn from the values of these three rate constants substituted in eq. 9. At pH 7.8 the three terms in parentheses in eq. 9 contribute 62, 37, and 1.3%, respectively, to the total hydrolysis rate. At pH 11.0 the percentages are 0.00, 0.7, and 99.3%, respectively.

The divalent metal ion promoted hydrolysis of histidine methyl ester, E, to yield histidine, A, may proceed through three complexes with one to three molecules of histidine per metal ion. Equations of proton balance without any implications regarding mechanism are

$$ME^{2+} + H_2O \longrightarrow MA^+ + H^+ + CH_3OH \quad (10)$$

$$ME_2^{2+} + H_2O \longrightarrow MEA^+ + H^+ + CH_3OH \quad (11)$$

$$ME_3^{2+} + H_2O \longrightarrow ME_2A^+ + H^+ + CH_3OH \quad (12)$$
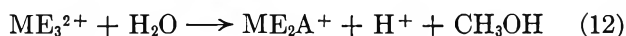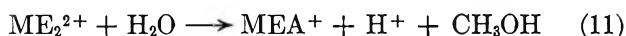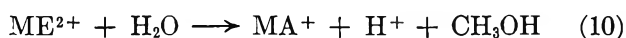
The two mixed complexes formed in eq. 11 and 12 can also undergo hydrolysis, but the contribution to overall hydrolysis may be neglected because these complexes are present in small concentrations initially and, due to their lesser charge, are probably hydrolyzed more slowly than the original complexes. If excess ester is present, eq. 10–12 may be followed by replacement of histidine by ester so that the net reaction is metal ion catalyzed hydrolysis of histidine methyl ester. In this case, the scheme of eq. 1 applies rather than eq. 10–12. Since the formation constants for divalent metal ions with histidine are about 2 log units greater
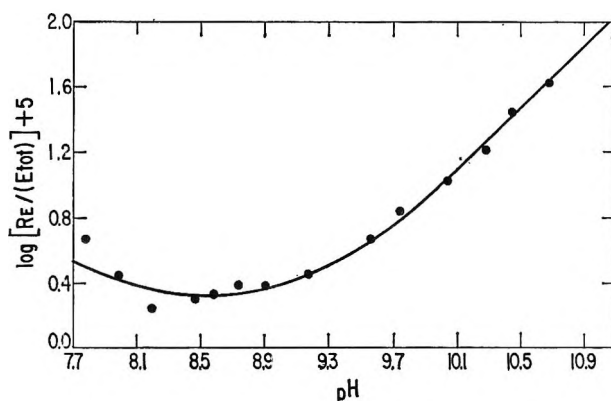
Figure 2. Hydrolysis of histidine methyl ester. Points are experimental and curve is drawn from eq. 9 and values of three rate constants in text.

than those listed in Table I for histidine methyl ester and the excess ester to acid concentration ratio is less than 100:1 for the 5–10% reaction considered in the straight line portion of the rate curve, replacement of product histidine by excess reactant ester in the coordination sphere of the divalent cation is unlikely. Nevertheless, the possibility that such replacement occurs is tested kinetically.

The total rate of production of protons in the pH-stat is the rate sum of reactions of free and complexed ester molecules. From the formation constants and rate constants already presented, the contribution of free ester to the observed total rate may be calculated for any set of initial concentrations and pH. Subtraction of this small rate contribution due to free ester from the total observed rate yields the observed rate of production of protons due to hydrolysis of ester molecules in metal ion complexes. This net rate R'_{stat} is related to the desired rate of hydrolysis of ester molecules in complexes R'_E by

$$R'_{stat} = QR'_E \quad (13)$$

If the net reactions for ester hydrolysis in the presence of metal ions are the metal ion promoted reactions 10–12, then $Q = 1$ in eq. 13. On the other hand, if the metal ion is functioning as a catalyst, the net hydrolysis reaction 1 is applicable, and Q is identical with that appearing in eq. 5, which value is never unity in these systems. The results reported below have all been tested by both possibilities and in every case only that with $Q = 1$ gave consistent results. Therefore, the ester hydrolyses are metal ion promoted and may be described by reactions 10–12 rather than the metal ion catalyzed counterpart of eq. 1. Specific examples are cited below. Under different conditions

of higher ester concentrations, metal ion promoted reactions may become metal ion catalyzed.

Since the pH is relatively high in all experiments here reported, ester hydrolysis due to water attack on metal ion complexes is negligible compared to mechanisms based on hydroxide ion attack.

$$ME^{2+} + OH^- \xrightarrow{k_1^{2+}} \text{products} \quad (14)$$

$$ME_2^{2+} + OH^- \xrightarrow{k_2^{2+}} \text{products} \quad (15)$$

$$ME_3^{2+} + OH^- \xrightarrow{k_1^{2+}} \text{products} \quad (16)$$
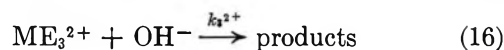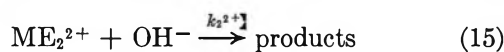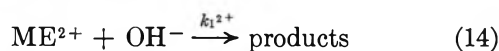
According to eq. 14–16, the rate of metal ion promoted ester disappearance is given by

$$R'_E = [k_1^{2+}(ME^{2+}) + k_2^{2+}(ME_2^{2+}) + k_3^{2+}(ME_3^{2+})][OH^-] \quad (17)$$

Combination with eq. 13 and expression of the result in logarithmic form yields

$$\log (R'_{stat}/Q) = \log [k_1^{2+}(ME^{2+}) + k_2(ME_2^{2+}) + k_3(ME_3^{2+})] + pH - 14.00 \quad (18)$$

Thus a plot of the left-hand side of eq. 18 vs. pH should yield a straight line of unit slope from which the rate constants in the bracketed term may be evaluated.

The cadmium ion promoted hydrolysis of histidine methyl ester was studied from pH 7.9 to 9.8 and with total ester to cadmium ion concentrations of (0.02)/(0.01) and (0.03)/(0.01). Under these conditions the concentration of CdE_3^{2+} is negligible so that eq. 18 reduces to

$$\log (R'_{stat}/Q) = \log [k_1^{2+}(CdE^{2+}) + k_2^{2+}(CdE_2^{2+})] + pH - 14.00 \quad (19)$$

Figure 3 shows a plot of the left-hand side of eq. 19 vs. pH at two ester concentrations for $Q = 1$ and for Q as given by eq. 5. Only the points calculated according to eq. 19 with $Q = 1$ yield a straight line of unit slope, indicating that the hydrolysis may be described by the metal ion promoted reactions 10 and 11. A striking feature of Figure 3 is that points for two different total ester to cadmium ion concentration ratios fall on the same line. The term in brackets in eq. 19 may be evaluated from the line of unit slope in Figure 3. The ratio $(CdE^{2+})/(CdE_2^{2+})$ is nearly constant over the pH range studied for one total ester to cadmium ion concentration ratio but significantly altered when the last ratio is changed. Therefore, the two cadmium ion complexes must hydrolyze at identical rates and quantitative evaluation yields $k_1^{2+} = k_2^{2+} = 66 \pm 3$ activity^{-1} sec.$^{-1}$ according to eq. 14 and 15.
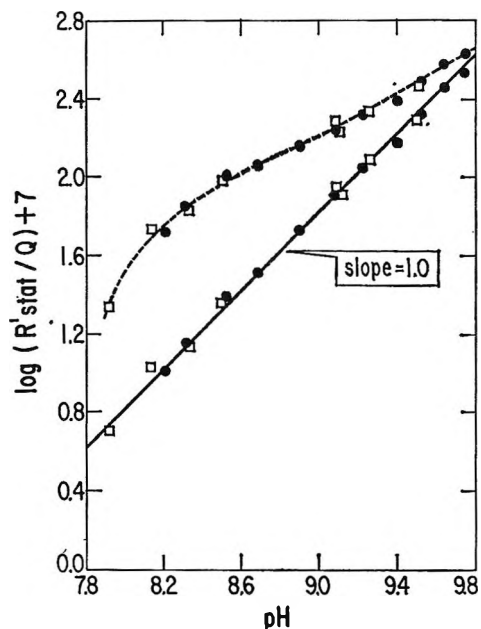
Figure 3. Histidine methyl ester hydrolysis in the presence of 0.01 M cadmium ion. Squares are for a total ester concentration of 0.02 M and circles for 0.03 M. Curved line is for Q in eq. 19 given by eq. 5 and line of unit slope for $Q = 1$.

The zinc ion promoted hydrolysis of histidine methyl ester was studied from pH 7.4 to 8.7 at total ester and zinc ion concentrations of 0.03 and 0.01 M, respectively. According to the formation constant, information provided in Table I over 99% of the zinc ion is in the ZnE_2^{2+} complex so that eq. 18 reduces to

$$\log (R'_{stat}/QC_{Zn}) = \log k_2^{2+} + pH - 14.00 \quad (20)$$

where C_{Zn} is the total molar concentration of zinc ion. In Figure 4 the left-hand side of eq. 20 is plotted against pH for the two cases of $Q = 1$ in circles and Q as given by eq. 5 in squares. Only the circles for $Q = 1$ yield a slope of unity as required by eq. 20. Therefore, the ester hydrolysis is zinc ion promoted as represented by eq. 11 and $k_2^{2-} = 120 \pm 7$ activity^{-1} sec.$^{-1}$ according to eq. 15.

Three runs were performed with histidine methyl ester and zinc ion concentrations of 0.02 and 0.01 M, respectively, at pH 7.29, 7.62, and 7.93. In this 2:1 ester to zinc ion mixture the above formation constant results indicate significant quantities of 1:1 complex are present. For this case eq. 17 and 13 may be written in logarithmic form as

$$\log \left[\frac{R'_E - k_2^{2+}(ZnE_2^{2+})[OH^-]}{(ZnE^{2+})} \right] = \log k_1^{2+} + pH - 14.00$$

From the formation constants in Table I and rate results, all quantities on the left-hand side may be calculated at each pH and plotted against pH. Only a value of $Q = 1$ yields a straight line of unit slope from which $k_1^{2+} = 340 \pm 30$ activity^{-1} sec.$^{-1}$.

The nickel ion promoted hydrolysis of histidine methyl ester was studied at total ester to metal ion concentration ratios of (0.03)/(0.01) and (0.05)/(0.01) over a pH range from 8.2 to 10.1. Under these conditions (NiE^{2+}) is negligible, and eq. 18 reduces in logarithmic form to

$$\log (R'_{\text{stat}}/Q) = \log [k_2^{2+}(NiE_2^{2+}) +$$
$$k_3^{2+}(NiE_3^{2+})] + pH - 14.00 \quad (21)$$

The left-hand side of eq. 21 with $Q = 1$ is plotted against pH in the lower line of Figure 5. Only the value of $Q = 1$ yields a straight line of unit slope, and since the points for two different total ester to nickel ion concentration ratios fall on the same line as for cadmium ion complexes, the 2:1 and 3:1 nickel ion complexes must hydrolyze at the same rate. From the lower line of Figure 5, $k_2^{2+} = k_3^{2+} = 50 \pm 2$ activity^{-1} sec.$^{-1}$.

Experiments were also performed with a total histidine methyl ester to nickel ion concentration ratio of (0.02)/(0.01) from pH 8.2 to 9.2. Under these conditions all three nickel ion–ester complexes are present in significant concentrations. Since k_2^{2+} and k_3^{2+} are already known, we write eq. 17 in the form

$$\log S \equiv \log$$
$$\left[\frac{R'_E - k_2^{2+}(NiE_2^{2+})[OH^-] - k_3^{2+}(NiE_3^{2+})[OH^-]}{(NiE^{2+})} \right]$$
$$= \log k_1^{2+} + pH - 14.00 \quad (22)$$

A plot of the left-hand side of eq. 22 vs. pH is shown in the upper part of Figure 5. Only a value of $Q = 1$ yields the line of unit slope from which $k_1^{2+} = 430 \pm 80$ activity^{-1} sec.$^{-1}$.

The cupric ion promoted hydrolysis of histidine methyl ester was studied at total ester to metal ion concentration ratios of (0.02)/(0.01) from pH 7.8 to 9.1. Under these conditions the cupric ion is 98–99% in the CuE_2^{2+} complex so that an equation similar to eq. 20 is applicable. Once again a plot of six points yields a unit slope only when $Q = 1$ from which $k_2^{2+} = 265 \pm 20$ activity^{-1} sec.$^{-1}$. Four more experiments were conducted at an ester to cupric ion concentration ratio of (0.03)/(0.01) from pH 7.6 to 8.7. In this case both 2:1 and 3:1 ester to metal ion complexes are significant, and a treatment similar to that for deriving eq. 22 enables a calculation of $k_3^{2+} = 260 \pm 40$
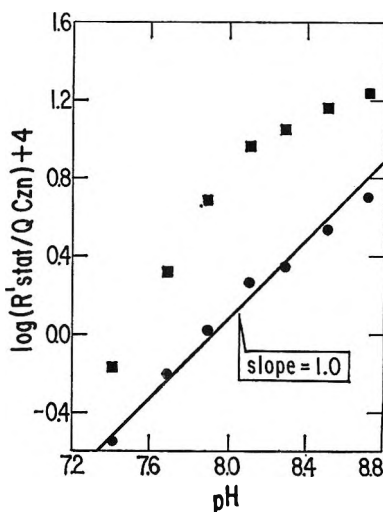
Figure 4. Hydrolysis of 0.03 M histidine methyl ester in the presence of 0.01 M zinc ion. Data are plotted according to eq. 20 with $Q = 1$ for circles and Q given by eq. 5 for squares.
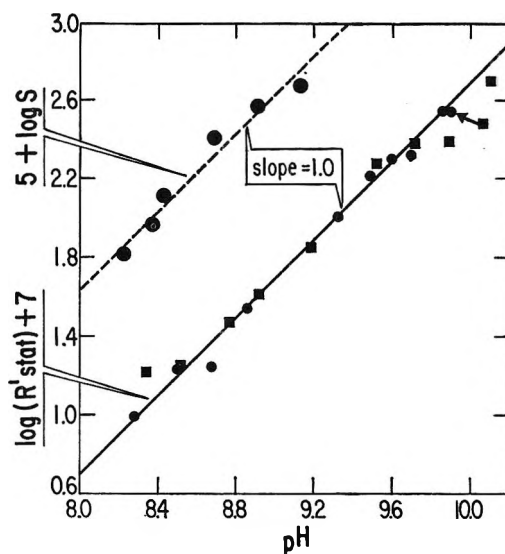
Figure 5. Histidine methyl ester hydrolysis in presence of nickel ion. Lower line of unit slope corresponds to $Q = 1$ in eq. 21 with total ester to nickel ion concentration ratios of (0.03)/(0.01) represented by squares and (0.05)/(0.01) by circles. Upper line of unit slope is a plot of eq. 22 at a concentration ratio of (0.02)/(0.01).

activity^{-1} sec.$^{-1}$ from a straight line of unit slope obtained only when $Q = 1$.

In summary, the hydrolysis of histidine methyl ester in the presence of Cd^{2+}, Zn^{2+}, Ni^{2+}, and Cu^{2+} ions is best described by the metal ion promoted eq. 10–12 rather than the metal ion catalyzed version of eq. 1. The rate constants obtained in this section according to eq. 14–16 are tabulated in Table II. Blanks in

the table are due to precipitation under conditions where the 1:1 ester–cupric ion complex concentration is significant and to weakness of binding of three ester molecules to zinc and cadmium ions.

Table II: Second-Order Rate Constants in Activity^{-1} Sec.$^{-1}$ for Hydroxide Ion Attack at Divalent Metal Ion Complexes of Histidine Methyl Ester at 25.00° and 0.16 Ionic Strength[a]

Metal ion	Rate constant		
	k_1^{2+}	k_2^{2+}	k_3^{2+}
Cu^{2+}		265	260
Ni^{2+}	430	50	50
Zn^{2+}	340	120	
Cd^{2+}	66	66	

[a] For no divalent metal ions, $k^0 = 0.86$, $k^+ = 75$, and $k^{2+} = 3.5 \times 10^4$ in the same units as above.

The values given in Table II in units of activity^{-1} sec.$^{-1}$ may be converted to units of M^{-1} sec.$^{-1}$ by multiplication by the activity coefficient 0.75 for comparison with literature values given in the latter units. A rate constant of 0.62 M^{-1} sec.$^{-1}$ determined by the conductometric method for histidine methyl ester hydrolysis in basic solutions at identical conditions of temperature and ionic strength[3] and an unspecified pH is in good agreement with our value of $k^0 = 0.64$ M^{-1} sec.$^{-1}$. These same authors[3] also report rate constants of about 2 M^{-1} sec.$^{-1}$ for cupric and nickel ion promoted histidine methyl ester hydrolyses. These values are much lower than any results in Table II.

Cysteine Ethyl Ester. In order to evaluate the α-functions at any pH necessary for the kinetic analysis of ester hydrolysis on the pH-stat, ionization constants of cysteine ethyl ester and cysteine were determined at 25.00° and 0.16 ionic strength. The ionization constants were evaluated as described above for those of histidine methyl ester. For cysteine ethyl ester we obtain $pK_{1E} = 6.65 \pm 0.03$ and $pK_{2E} = 9.06 \pm 0.05$. These values, used in this work, may be compared with those determined by a spectrophotometric method[18] and corrected to our conditions of temperature and ionic strength to yield[1] 6.69 and 9.10, respectively. For cysteine methyl ester values of 6.56 and 8.99 have been obtained under the same conditions as ours.[17]

For cysteine values of $pK_{2A} = 8.21 \pm 0.04$ and $pK_{3A} = 10.36 \pm 0.04$ were obtained at 25.00° and 0.16 ionic strength. Other values corrected to our conditions[1] are 8.28 and 10.37,[18] 8.30 and 10.39,[19] 8.19 and 10.35,[20] 8.48 and 10.54,[17] and 8.11 and 10.05.[21]

All but the last two pairs of values, which appear high and low, respectively, are averaged to obtain 8.24 and 10.37 for pK_{2A} and pK_{3A}, respectively. These average values for cysteine ionizations are used in this work.

Most features of the analysis of cysteine ethyl ester hydrolysis are similar to those for histidine methyl ester. Equations 2–6 are applicable to both systems. The most basic form of cysteine ethyl ester contains a negative charge so that for this ester we have in addition to eq. 7 and 8, the reaction mechanism

$$E^- + OH^- \xrightarrow{k^-} \text{products} \qquad (23)$$
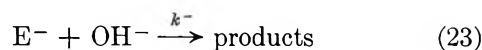
The equation analogous to eq. 9 for cysteine ethyl ester is

$$\log [R_E/(E_{tot})] = \log (k^+ \alpha_{0E} + k\alpha_{1E} + k^-\alpha_{2E}) + pH - 14.00 \qquad (24)$$

A plot of the left-hand side of eq. 24 vs. pH for 0.01, 0.02, 0.03, and 0.04 M solutions of cysteine ethyl ester is shown in Figure 6. The curve in the figure is drawn from the rate constants, $k^+ = 30 \pm 10$, $k = 2.14 \pm 0.07$, and $k^- = 0.055 \pm 0.002$, all in activity^{-1} sec.$^{-1}$. Probably due to heavy buffering, the points in the pH 9.0 to 9.5 region are slightly lower than the curve in Figure 6. The rate constant k^+ is determined from the four slow runs at low pH and is less reliable than k and k^-, evaluated from data at pH >9.5.

No superscript indicating charge of substrate species was placed on the rate constant of the middle term in parentheses in eq. 24. Neutral cysteine ethyl ester is composed of uncharged ($HSRNH_2$) and dipolar ion ($^-SRNH_3^+$) forms in a ratio of about 5:1,[18] which is not significantly altered on conversion to our conditions of temperature and ionic strength.[1] The rate constant $k = 2.14$ activity^{-1} sec.$^{-1}$ is composed of contributions from k^0 and $k^\pm$ for the uncharged and dipolar ion species, respectively, weighted according to the relative concentrations of each species. If we assign $k^0 \simeq 0.8$ activity^{-1} sec.$^{-1}$, the value for glycine ethyl ester[6] (the k^+ values are 32 and 30 activity^{-1} sec.$^{-1}$ for glycine and cysteine ethyl esters, respectively), then $k^\pm \simeq 9$ activity^{-1} sec.$^{-1}$. Though only an approximate value (the ratio $k^\pm/k^0 \simeq 10$ also appears large), the greater value of $k^\pm$ over k^0 is qualitatively consistent with the location of the positive charge center in the dipolar ion about $^1/_3$ nearer than the negative charge to the carbonyl carbon under

(18) R. E. Benesch and R. Benesch, *J. Am. Chem. Soc.*, **77**, 5877 (1955).
(19) M. A. Grafius and Neilands, *ibid.*, **77**, 3389 (1955).
(20) H. Borsook, E. L. Ellis, and H. M. Huffman, *J. Biol. Chem.*, **117**, 281 (1937).
(21) G. R. Lenz and A. E. Martell, *Biochemistry*, **3**, 745 (1964).
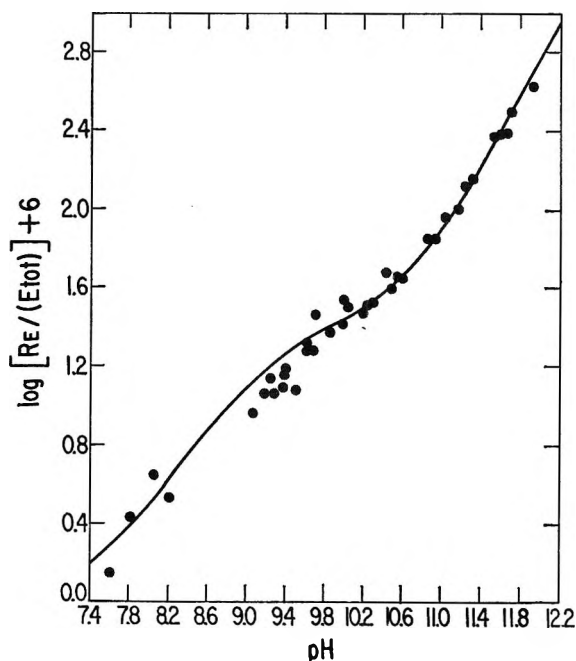
Figure 6. Cysteine ethyl ester hydrolysis at 0.01,
0.02, 0.03, and 0.04 M ester concentrations.
Points are experimental; the curve is drawn from
eq. 24 and three rate constants given in text.

attack by the negative hydroxide ion in cysteine ethyl ester.

The Ni^{2+}, Zn^{2+}, and Cd^{2+} ion promoted hydrolyses of cysteine ethyl ester were studied in solutions (0.02)/(0.01) in ester to divalent metal ion from pH 9 to 11. These metal ions are bound to cysteine derivatives[4,17] more strongly than to derivatives of histidine. In these solutions the net hydrolysis reaction is

$$ME_2 + H_2O \longrightarrow MEA^- + H^+ + C_2H_5OH$$

so that Q in eq. 13 is unity. The reaction proceeds by the mechanism

$$ME_2 + OH^- \xrightarrow{k_2^0} products$$
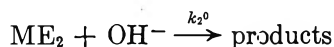
and analogous to eq. 20 the rate expression may be written as

$$\log (R'_E/C_M) = \log k_2^0 + pH - 14.00 \quad (25)$$

A plot of the left-hand side of eq. 25 vs. pH is shown in Figure 7 for the three divalent metal ions studied. From the straight lines of unit slope in Figure 7, the k_2^0 values are 3.4 ± 0.1, 2.5 ± 0.3, and 1.40 ± 0.05 activity^{-1} sec.$^{-1}$ for the Ni^{2+}, Zn^{2+}, and Cd^{2+} complexes, respectively.

Titration with base of a solution containing cysteine ethyl ester hydrochloride and nickel ion in a (0.03)/(0.01) ratio indicated that one ester ligand was free
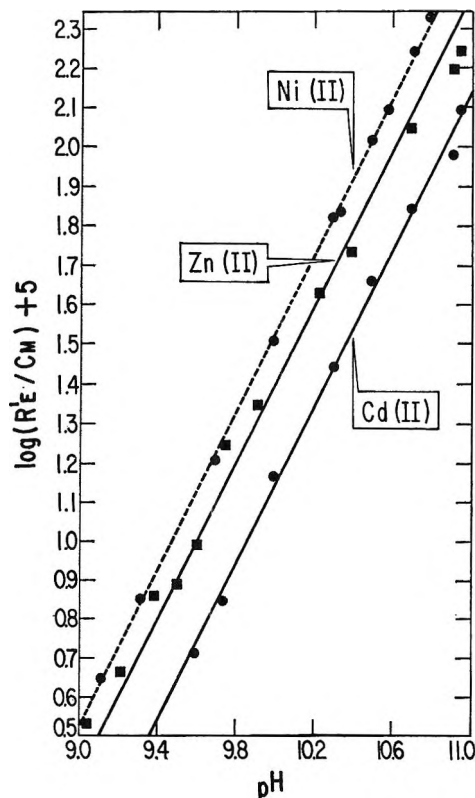
Figure 7. Cysteine ethyl ester hydrolysis in presence of divalent cations plotted according to eq. 25. Ester to metal ion concentrations are (0.02)/(0.01) except for Ni(II) points at pH 10.57 and 10.79 which are for (0.04)/(0.02).

in solution and that only two ester ligands are bound to a single nickel ion. This result is consistent with the red color of the solution at the end of the titration implying a planar complex. Since Ni^{2+} does not form a 3:1 ester to metal ion complex with cysteine ethyl ester, and because precipitation occurs at ester to metal ion ratios less than 2:1, no kinetic studies on other complexes were attempted.

Some of our rate constants summarized in Table III for cysteine ethyl ester hydrolysis in activity^{-1} sec.$^{-1}$ may be compared with those in the literature after multiplying our values by the activity coefficient 0.75 to yield units of M^{-1} sec.$^{-1}$. From a conductometric study[5] in solutions containing excess base at 25°, about 0.02 ionic strength, and an unspecified pH, a rate constant for cysteine ethyl ester hydrolysis was found to be 0.09 M^{-1} sec.$^{-1}$. We estimate the pH to be about 11.3, which is on a curved portion of the plot in Figure 6 indicating that the constant of 0.09 M^{-1} sec.$^{-1}$ is a composite constant consisting of weighted contributions from our k and k^- rate constants. Since these last two constants have values of 1.61 and 0.041 M^{-1} sec.$^{-1}$, respectively, the conductometric result is

qualitatively consistent with our rate constants. These authors[5] also added cadmium ion to the solution in several concentrations so that the total cysteine ethyl ester to cadmium ion concentration ratios varied from 1.6 to 6.5. They interpreted their rate results on the basis of a 1:1 ester to cadmium ion complex,[5] but in our view the 2:1 complex predominates in most of their cadmium ion containing solutions. Recalculating their results on this basis, we obtain from their conductometric study a value of $k_2{}^0 = 1.1\ M^{-1}\ \text{sec.}^{-1}$ identical with our value for the cadmium ion complex. A conductometric study of cysteine methyl ester hydrolysis[4] reportedly yields a rate constant for hydrolysis of free ester greater than our value for cysteine ethyl ester, while their rate constant for the nickel ion promoted reaction is less than ours.

Table III: Equilibrium and Rate Constants for Hydroxide Ion Attack in Activity^{-1} Sec.$^{-1}$ Experimentally Determined in This Work at 25.00° and 0.16 Ionic Strength

	Cysteine ethyl ester	Aspartic acid-β-methyl ester
pK_{1E}	6.65	
pK_{2E}	9.06	8.62
pK_{2A}	8.21	
pK_{3A}	10.36	
k^+	30	
k	2.14	
$k^\pm$		13
k^-	0.055	0.12
$k_2{}^0$ CuE$_2{}^0$		4.8
NiE$_2{}^0$	3.4	8.4
ZnE$_2{}^0$	2.5	
CdE$_2{}^0$	1.4	
$k_3{}^-$ NiE$_3{}^-$		1.00

Aspartic Acid-β-methyl Ester. The hydrolysis of this ester was studied from pH 9.5 to 11.6 with ester concentrations of 0.005, 0.01, and 0.02 M. The treatment of this system is similar to that of cysteine ethyl ester, and an equation analogous to eq. 24 without the k^+ term is applicable. A value of p$K_E = 8.62 \pm 0.02$ for aspartic acid-β-methyl ester was determined by potentiometric titration. For the ammonium ionization from aspartic acid a value of p$K_3 = 9.71$ was calculated from published work[22] to be used in eq. 5. A plot of the left-hand side of eq. 24 vs. pH is shown in Figure 8. From the curve are obtained values of $k^\pm = 13 \pm 2$ and $k^- = 0.12 \pm 0.01$ activity^{-1} sec.$^{-1}$.

Titration with base of solutions containing 0.02 and 0.03 M aspartic acid-β-methyl ester and 0.01 M of either cupric or nickel ions revealed strong binding
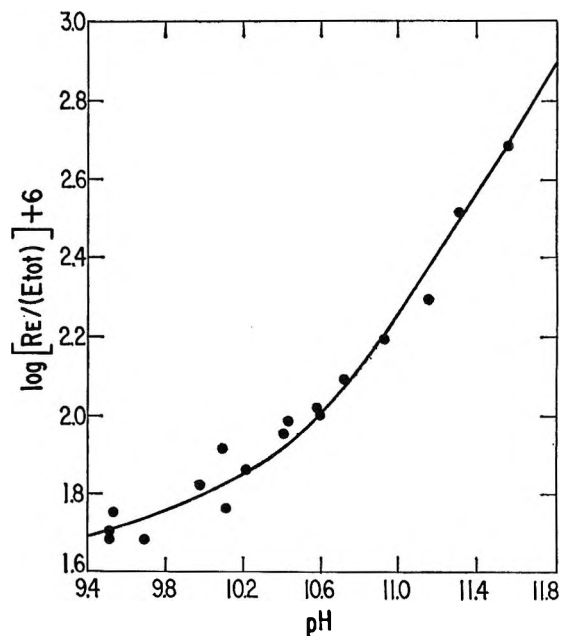
Figure 8. Hydrolysis of aspartic acid-β-methyl ester at concentrations of 0.005, 0.01, and 0.02 M. Points are experimental and curve is calculated from eq. 24 and $k^\pm = 13$ and $k^- = 0.12$ activity^{-1} sec.$^{-1}$.

of the ester to the metal ions for both 2:1 mixtures, while only nickel ion gave evidence of the formation of a 3:1 complex. Ester hydrolysis was followed in mixtures in which the total ester to cupric ion concentration ratio was (0.01)/(0.005) and (0.02)/(0.01) from pH 9.0 to 10.1. The metal ion promoted hydrolysis proceeds by hydroxide ion attack at the 2:1 ester metal ion complex. Analysis of seven runs by plotting the left-hand side of eq. 25 vs. pH yields a straight line of unit slope from which, for the cupric ion complex, $k_2{}^0 = 4.8 \pm 0.2$ activity^{-1} sec.$^{-1}$. A similar analysis of seven runs for solutions containing total ester to nickel ion concentration ratios of (0.02)/(0.01) and (0.04)/(0.02) from pH 8.4 to 8.9 yields, for the nickel ion complex, $k_2{}^0 = 8.4 \pm 0.4$ activity^{-1} sec.$^{-1}$. The pH region in the nickel ion complex is limited by incomplete complex formation below pH 8.3 and by precipitation above pH 9.2.

Kinetic experiments were also conducted with total aspartic acid-β-methyl ester to nickel ion ratios of (0.015)/(0.005) and (0.03)/(0.01) from pH 9.2 to 11.1. On the assumption that the predominant species is the 3:1 ester to nickel ion complex, analysis of seven runs by a method analogous to that described above yields $k_3{}^- = 1.00 \pm 0.04$ activity^{-1} sec.$^{-1}$.

(22) A. C. Batchelder and C. L. A. Schmidt, *J. Phys. Chem.*, **44**, 893 (1940).

Discussion

Considering first the rate constants for hydroxide ion attack in the absence of divalent metal ions, we note that the rate constants increase as the net positive charge on the ester increases. For a given ester the increase in rate of hydroxide ion attack at the protonated as compared with the neutral ester is a function of the distance of the positive charge from the reaction side. In cross comparing esters of different amino acids, care must be taken because methyl esters are known to be hydrolyzed somewhat faster than ethyl esters.

One method to compare the electrostatic effects of added charge on rate constants without specifying interaction distances and effective dielectric constants is to relate rate constant ratios to equilibrium constant ratios determined from acid ionization constants. In this fashion unusual values of rate constants appear as abnormally small or large ratios when compared to corresponding equilibrium constant ratios. The electrostatic work required to bring a hydroxide ion from an infinite distance to the carbonyl carbon is greater for neutral than for protonated glycine ethyl ester so that $k^+/k^0 = 41$. Also removal of a proton from uncharged glycine ethyl ester requires less work than its removal from dipolar ion glycine as reflected by the ratio $K_E/K_A = 74$.

These ratios are not expected to be equal because, among other reasons, the reactive center is not exactly the same distance from the charge center in the two cases. Rate and corresponding equilibrium constant ratios for all esters in this study are tabulated in Table IV. The ratios of Table IV are calculated at 0.16 ionic strength but should be evaluated at zero ionic strength. All rate and equilibrium constant ratios are about doubled at zero ionic strength but since the ratio of all rate and equilibrium constant ratios is independent of ionic strength it is more convenient

to utilize directly the 0.16 ionic strength values quoted in this paper.

Inspection of Table IV reveals that four of the six pairs of rate and equilibrium constant ratios differ by less than a factor of 3. For aspartic acid-β-methyl ester the rate constant ratio is nine times greater than the equilibrium constant ratio. Comparison of the k^0 and k^- values with those of other esters in this work indicates that the high ratio is due to an unusually large value of $k^\pm$ in aspartic acid-β-methyl ester. This enhanced rate constant may be due to a contribution from a structure with an internal hydrogen bond from the protonated ammonium group to the carbonyl oxygen resulting in a greater partial positive charge density at the carbonyl carbon. Aspartic acid-β-methyl ester is the only substrate of this study where such a six-membered ring can form. Structures involving hydrogen bonding from protonated amino groups to carbonyl oxygen atoms of esters have been proposed to account for rate enhancements of ester hydrolysis in tertiary aminoalkyl esters.[23]

By far the most unusual ratio in Table IV is the large value of $k^{2+}/k^+ = 470$ for histidine methyl ester, a ratio more than 80 times greater than the ratio of corresponding acid ionization constants. Comparison of k^+ for histidine methyl ester with the same constant for other esters reveals a larger value but little more than expected when comparing hydrolysis rates of methyl with ethyl esters. The large ratio of k^{2+}/k^- must then be due to a greatly increased value of k^{2-} obtained on adding a proton to the imidazole ring. This result is all the more remarkable because addition of a proton to the ammonium nitrogen, which is several bonds closer to the reaction center, does not yield a particularly high reaction rate as measured by k^+. We propose that the large value of k^{2+} is due to a contribution from structures like
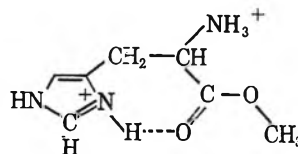
which bring the positively charged imidazolium ring to bear on the reaction center by yielding an increased partial positive charge at the carbonyl carbon, rendering it more susceptible to hydroxide ion attack. Evidently such structures, representing a kind of superacid catalysis,[6] can contribute at least a 10^2 rate en-

Table IV: Ratios of Rate Constants for Hydroxide Ion Catalyzed Ester Hydrolysis and Corresponding Ratios of Acid Ionization Constants at 0.16 Ionic Strength

	Glycine ethyl ester	Cysteine ethyl ester	Histidine methyl ester	Aspartic acid-β-methyl ester
k^{2+}/k^+			470	
K_{1E}/K_{2A}			5.6	
k^+/k^0	41	14	87	
K_E/K_A	74	39	74	
k/k^-		39		110
K_{2E}/K_{3A}		20		12

(23) B. Hansen, *Acta Chem. Scand.*, 16, 1927 (1962); J. A. Zaslowsky and E. Fisher, *J. Phys. Chem.*, 67, 959 (1963).

hancement in enzyme-catalyzed reactions at an imidazolium group.

It may be shown that a ratio of ester and acid ionization constants in Table IV is equal to the ratio of the microscopic ionization constants for carboxylic acid ionizations from microforms of the same net charges as the ester and acid, respectively.[24] If logarithms are taken, then the comparison is essentially one of log k for hydroxide ion attack on an ester species vs. pK_a for ionization of the corresponding carboxylic acid. The negative slope of such a log–log plot is a ρ-function which may also be obtained by taking the ratio of the logarithm of a rate constant ratio and the logarithm of the corresponding equilibrium constant ratio in Table IV. Since addition of a proton does not significantly alter substrate size, both steric and resonance effects are constant in the comparison, and the ρ-function comprises primarily polar contributions. Though dependent upon ionic strength, this ρ-function may be compared with ρ^* for basic hydrolysis of ethyl esters minus that for ionization of carboxylic acids,[25] $2.48 + 0.12 - 1.72 = 0.88$. This result is nearly the same obtained by dividing the log of the rate constant ratio in Table IV by the log of the equilibrium constant ratio for glycine ethyl ester (0.86), especially if zero ionic strength values are employed. Uncertainties due to competitive ionizations in cysteine ethyl ester may be bypassed by taking the logarithm of k^+/k^- and dividing by $pK_{2A} + pK_{3A} - pK_{1E} - pK_{2E}$ to obtain a ρ-value of 0.94. On the basis of a similar analysis for histidine methyl ester, it may be shown in this way also that k^{2+} is high by a factor of 100.

In passing to metal ion promoted reactions of hydroxide ion attack on ester molecules, it is apparent that, in the absence of special effects such as superacid catalysis, values of hydrolysis rate constants may be rationalized largely on the basis of charge. For histidine methyl ester where the charge on the complex is unchanged on the addition of an additional ester molecule to a divalent metal ion complex, the statistical and electrostatic factors are balanced so that all k^{2+} rate constants in Table II are divided by 2 when compared on the basis of per unit positive charge on an ester molecule in the complex. The closely similar values of k_2^{2+} and k_3^{2+} recorded in Table II for both Cu^{2+} and Ni^{2+} complexes and the identical values of k_1^{2+} and k_2^{2+} for Cd^{2+} complexes indicate that in these cases the effective charge experienced by an ester molecule under hydroxide ion attack is not affected by the number of ester molecules bound to the divalent metal ion. The relatively higher values of k_1^{2+} for the Ni^{2+} and Zn^{2+} complexes may be accounted for by a mild super-acid catalysis possible in the 1:1 ester

to metal ion complexes. In most cases, however, chelation of the ester molecule at two binding sites other than the reactive center renders unlikely superacid promotion of hydrolysis by placement of the positively charged metal ion near the region of hydroxide ion attack. The range of values of $k_2^{2+}/2$ in Table II from 25 to 130 activity^{-1} sec.$^{-1}$ per unit of positive charge on an ester molecule in the complex bracket the value of $k^+ = 75$ activity^{-1} sec.$^{-1}$ for the rate constant of monocharged ester hydrolysis in the absence of metal ions.

The trend of k_2^{2+} values in Table II is not the same as that of formation constants in Table I; values for the Ni^{2+} complex seem exceptional. Since the metal ion in the 2:1 ester to metal ion complexes is not chelated at the reactive center of histidine methyl ester but only more remotely at two nitrogen atoms in each molecule, the trend of k_2^{2+} values in Table II is evidently due to subtle effects.

For metal ion promoted cysteine ethyl ester hydrolysis, values of $k_2^0/2$ recorded in Table III range from 0.7 to 1.7 activity^{-1} sec.$^{-1}$ per ester molecule in the 2:1 complex. This range of values is less than $k = 2.14$ activity^{-1} sec.$^{-1}$ obtained in the absence of divalent metal ions. As discussed above, however, the constant k is composed of weighted contributions from k^0 and $k^{\pm}$ constants, and the range of values for metal ion promoted hydrolyses appears to bracket the value of the k^0 rate constant estimated for hydroxide ion attack on neutral, uncharged cysteine ethyl ester. Values of k_2^0 for the three metal ions studied with cysteine ethyl ester parallel values of the formation constants for association with cysteine methyl ester.[4,17]

For the cupric and nickel ion promoted hydrolyses of aspartic acid-β-methyl ester, the values of $k_2^0/2$ listed in Table III are, respectively, 2.4 and 4.2 activity^{-1} sec.$^{-1}$ per ester molecule in the 2:1 complex. These values are less than the value of $k^{\pm} = 13$ activity^{-1} sec.$^{-1}$ for the free ester of zero net charge, but we have presented evidence above that the value of the last rate constant is unusually high. For the 3:1 aspartic acid-β-methyl ester to nickel ion complex the value of $k_3^- = 1.00$ activity^{-1} sec.$^{-1}$ per unit negative charge on an ester molecule in the complex is considerably greater than $k^- = 0.12$ for the free ester. This last comparison is not really justified, however, because of the differing fractional charge distributions. As expected on electrostatic grounds

(24) R. B. Martin, "Introduction to Biophysical Chemistry," McGraw-Hill Book Co., Inc., New York, N. Y., 1964, pp. 68–70.

(25) R. W. Taft, Jr., in "Steric Effects in Organic Chemistry," M. S. Newman, Ed., John Wiley and Sons, Inc., New York, N. Y., 1956, pp. 587–607.

$k_3^-/3$ is less than $k_2^0/2$ for the nickel ion promoted hydrolyses of aspartic acid-β-methyl ester.

Perhaps the outstanding features of the results collected in Tables II and III are the relative indifference of the rate constants to the particular divalent metal ion in the complex and the lack, in the absence of super-acid catalysis, of any major difference between metal ion promoted hydrolysis and the equivalent charge effects brought about by hydrogen ions.

Amino acid esters that strongly bind transition metal ions through chelation at two sites neither of which is the reactive site are much less susceptible to metal ion promotion of hydrolysis than an amino acid ester, such as glycine ethyl ester, where chelation labilizes the re-active bond. Thus strongly chelated ester complexes are more slowly hydrolyzed than complexes of esters that undergo weak chelation through a labile ester bond. For illustration, the second-order rate constants for hydroxide ion attack at the 2:1 histidine methyl ester to cupric and cadmium ion complexes are 265 and 66, respectively; at the 2:1 cysteine ethyl ester to cadmium ion complex the rate constant is 1.4, while at the 1:1 glycine ethyl ester to cupric ion complex[6] it is 101,000 activity^{-1} sec.$^{-1}$. In the last case, where cupric ion chelates to the carbonyl oxygen, super-acid catalysis occurs and the rate constant is about 80 times larger than simple electrostatic considerations predict.[6]

Ionization and Dissociation of Diphenyl and Condensed Ring Aromatics by Electron Impact. I. Biphenyl, Diphenylacetylene, and Phenanthrene[1a]

by P. Natalis[1b] and J. L. Franklin

Department of Chemistry, Rice University, Houston, Texas (Received February 18, 1965)

Mass spectra and appearance potentials of the principal ions of benzene, biphenyl, diphenylacetylene, and phenanthrene have been determined on a Consolidated Electrodynamics Corp. Type 21-701 coincident field mass spectrometer. The mass spectra of isomeric diphenylacetylene and phenanthrene are quite similar and are characterized by a large number of doubly charged and several triply charged ions. All of the spectra have parent ions as well as fairly intense peaks corresponding to the loss of H, H_2, C_2H_2, C_3H_3, and $2C_2H_2$. In almost all cases the electron energy required to bring about a certain process (*i.e.*, loss of C_2H_2) increases with resonance stabilization in the neutral parent molecule. Except for parent ions, all ions of the same composition have similar heats of formation. It appears that all reactions studied involving energies appreciably above the ionization potential occur with ring opening.

Introduction

Several electron impact studies of aromatic compounds have been reported in the recent literature. Among them a particularly interesting investigation of benzene and its open-chain isomers has shown that electron-induced decomposition of benzene proceeds through an ionic intermediate having the structure of butadienylacetylene.[2a] Similarly a common ionic in-

termediate with a cycloheptatriene structure is considered to account for the behavior of a number of alkylbenzenes and other derivatives.[2b] Isomeric naphthalene and azulene also exhibit similar mass spectra, and it has been shown by examination of the appearance potentials of various ions that a common intermediate can explain the main features of the electron-induced dissociation of these compounds.[3]

In the present study, a similar investigation of isomeric diphenylacetylene and phenanthrene was undertaken. Mass spectra and ionization potentials of these two aromatic compounds, as well as appearance potentials of their principal fragment ions, were determined and heats of formation of various ions were calculated and compared. The mass spectrum and the ionization potential of phenanthrene have been determined before,[4] but no data on appearance potentials of fragment ions from this compound have been reported so far. Biphenyl has also been examined in this work because, although biphenyl and deuterated analogs have been studied from the point of view of isotopic effects,[5] no data on appearance potentials of fragment ions have been reported. Such determinations are of interest to provide a broader understanding of the processes by which aromatic ions decompose. Benzene and most of its fragment ions were also investigated as a means of establishing our techniques, as well as to provide data for comparison with that from the other compounds studied.

Experimental

Mass spectra and appearance potential data were obtained by means of a Consolidated Electrodynamics Corp. mass spectrometer Type 21-701. This 12-in. radius, 60° coincident field sector instrument, having the radial electric field sector immersed in the magnetic sector, has been described.[6] Some modifications were provided to this instrument to make it suitable for appearance potential study. Electron ionizing voltage was measured by a Leeds and Northrup potentiometer and controlled by a 10-turn helipot allowing increments in ionizing voltage of 0.1 v. The variable repeller voltage was replaced by a fixed potential of 1 v. provided by a battery.

The mass spectra were obtained with 50-v. electrons and an ionizing current of 4 μa., also used for appearance and ionization potential measurements. Qualitative agreement is found between mass spectra determined in this study and those reported in the literature for benzene,[7] biphenyl,[5,7] and phenanthrene.[4,8] However, the relative abundances of fragment ions, calculated as a percentage of the parent peak, appear to be higher than those found in the already published mass spectra.

It will be evident that the discrepancy becomes larger as the mass number of the fragment ions becomes smaller. We think this effect is instrumental, presumably attributable to discrimination in the electron multiplier used in the collector system. It is probably not attributable to the ionization chamber which is essentially the same as the one used in the 21-103 C.E.C. mass spectrometer. Xenon was used as a reference gas for calibration of the electron energy scale. Owing to the very high sensitivity of this instrument, the sample pressure necessary to record ionization efficiency curves could be kept very low. Usually the pressure of the xenon sample mixture was 0.5–1×10^{-7} mm. measured at the source ionization gauge. This favorable situation is a great advantage in appearance potential studies since there is no pressure effect in the tail of the ionization efficiency curves. Ionization potential data have been determined by comparison with the xenon reference curve using the semilogarithmic method[9] and taking the difference of voltage between the curves at 1% of the ion intensities measured at 50 v. Appearance potential curves have been treated in the same way except in a few cases where a long tail below the 1% intensity point was observed and for which the semilog curves were excessively divergent. In these cases the extrapolated difference method[10] was used. The potential data obtained are an average of several determinations, and ionization potential values are reproducible to ±0.05 v. The reproducibility of appearance potential values of fragment ions is usually 0.05 to 0.1 v., but the uncertainty is sometimes as much as 0.2–0.5 v. for weak ions, as indicated in tables below.

A heated Pyrex inlet system equipped with a molten gallium sintered disk valve was used for the introduction

(2) (a) J. Momigny, L. Brakier, and L. D'or, *Bull. Classe Sci. Acad. Roy. Belg.*, **48**, 1002 (1962); (b) H. M. Grubb and S. Meyerson in "Mass Spectrometry of Organic Ions," F. W. McLafferty, Ed., Academic Press Inc., New York, N. Y., 1963, Chapter 10.

(3) R. J. Van Brunt and M. E. Wacks, *J. Chem. Phys.*, **41**, 3195 (1964).

(4) M. E. Wacks and V. H. Dibeler, *ibid.*, **31**, 1557 (1959).

(5) J. G. Burr, J. M. Scarborough, and R. H. Shudde, *J. Phys. Chem.*, **64**, 1359 (1960).

(6) H. G. Voorhies, C. F. Robinson, L. G. Hall, W. M. Brubaker, and C. E. Berry, "Advances in Mass Spectrometry," Vol. I, J. D. Waldron, Ed., Pergamon Press Ltd., London, 1959, p. 44.

(7) "Catalog of Mass Spectral Data," American Petroleum Institute Research Project 44, Carnegie Institute of Technology, Pittsburgh, Pa.

(8) "Catalog of Mass Spectral Data," Manufacturing Chemists Association Research Project, Carnegie Institute of Technology, Pittsburgh, Pa.

(9) F. P. Lossing, A. W. Tickner, and W. A. Bryce, *J. Chem. Phys.*, **19**, 1254 (1951).

(10) J. W. Warren, *Nature*, **165**, 811 (1950).

of solids. The reservoir and the line going to the ionization chamber were kept at 130°, the temperature being measured by several thermocouples at different places of the system. The biphenyl and phenanthrene samples were commercial products from The Matheson Co.; diphenylacetylene was from L. Light and Co., Ltd. Mass spectra of biphenyl and diphenylacetylene showed no trace of impurities. The sample of phenanthrene was used after several recrystallizations.

General Features of the Mass Spectra

Partial mass spectra of diphenylacetylene and phenanthrene are presented in Table I. The ionization potential of benzene, biphenyl, diphenylacetylene, and phenanthrene, and the appearance potential of the main fragment ions of these compounds are given in column 4 of Tables II through V, respectively. In column 5 of these Tables are listed the calculated heats of formation of ions produced in various processes described in column 1. Experimental heats of formation of ions were computed from appearance potentials using the conversion factor 1 e.v. = 23.06 kcal./mole. Heats of formation of the various compounds studied, together with their sources, are given in Table VI. Data on heats of formation of ions are taken from Field and Franklin[11] unless otherwise noted.

Table I: Partial Mass Spectra of Diphenylacetylene (DPA) and Phenanthrene (PH)[a]

Mass no.	DPA	PH	Mass no.	DPA	PH	Mass no.	DPA	PH
50	6.8	4.9	76½	3.8	5.7	127	1.5	0.8
51	11.4	7.8	77	6.3	3.2	128	1.0	0.8
52	4.2	1.5	78	1.9	0.6			
			86	1.8	1.3	139	3.3	1.8
58⅔	0.05	0.06	87	3.8	4.8			
59	0.03	0.01	87½	0.5	2.2	149	1.7	1.2
59⅓	0.29	0.43	88	11.0	25.0	150	5.3	6.9
59⅔	0.05	0.04	88½	2.0	4.5	151	9.6	10.2
			89	30.5	39.0	152	7.5	9.5
61	0.5	0.3	89½	4.1	5.2	153	1.5	0.8
61½	0.2	0.1						
62	3.4	3.1	98	2.3	1.5	162	0.3	0.2
62½	0.4	0.3	99	1.7	1.4	163	0.8	0.6
63	13.0	14.1	100	1.2	0.8			
63½	0.6	0.9	101	0.9	0.9	174	1.0	2.1
64	1.0	0.6	102	2.7	0.8	175	1.8	2.8
65	1.4	0.8				176	18.7	19.2
			111	0.8	0.5	177	10.9	11.4
74	5.8	4.5	113	1.3	0.6	178	100.0	100.0
74½	0.2	0.3	115	1.3	0.6	179	13.9	13.7
75	8.9	13.4				180	1.1	1.0
75½	2.0	2.5	125	0.8	0.9			
76	35.3	51.2	126	5.7	2.1			

[a] Electron energy 50 v.; ion abundances in per cent of parent peak.

Table II: Data for Benzene

Process	m/e of ion	Rel. abund., % of base peak	A.P., e.v.	ΔH_f of ion, kcal./mole This study	Lit.
$C_6H_6 \rightarrow C_6H_6^+$	78	100.0	9.22 ± 0.05	233	233
$\rightarrow C_6H_5^+ + H$	77	18.0	14.44 ± 0.05	301	301
$\rightarrow C_6H_4^+ + H_2$	76	3.8	14.09 ± 0.07	345	
$\rightarrow C_4H_4^+ + C_2H_2$	52	27.0	14.95 ± 0.05	311	326
$\rightarrow C_3H_3^+ + C_3H_3$	39	30.0	15.17 ± 0.1	96[a] 87[b]	
$\rightarrow C_2H_2^+ + 2C_2H_2$	26	5.2	18.6 ± 0.3	341[c]	

[a] Calculated for neutral taking $\Delta H_f(HC\equiv C-CH_2)^+$ as 274.
[b] Calculated for neutral taking $\Delta H_f(CH_2=C=CH)^+$ as 283.
[c] Products formed with excess energy.

Table III: Data for Biphenyl

Process	m/e of ion	Rel. abund., % of base peak	A.P., e.v.	ΔH_f of ion, kcal./mole
$C_{12}H_{10} \rightarrow C_{12}H_{10}^+$	154	100.0	8.96 ± 0.05	247
$\rightarrow C_{12}H_9^+ + H$	153	38.5	14.36 ± 0.05	319
$\rightarrow C_{12}H_8^+ + H_2$	152	28.6	16.89 ± 0.08	429
$\rightarrow C_{10}H_8^+ + C_2H_2$	128	7.5	14.81 ± 0.05	328
$\rightarrow C_9H_7^+ + C_3H_3$	115	9.0	16.08 ± 0.05	321[a]
$\rightarrow C_8H_6^+ + 2C_2H_2$	102	8.9	18.10 ± 0.05	349
$\rightarrow C_7H_5^+ + ?$	89	7.4	20.85 ± 0.2	?
$\rightarrow$ (a) $C_6H_5^+ + C_6H_5$	77	14.0	18.2 ± 0.5	390
(b) $C_{12}H_{10}^{2+}$	77	42.0	21.9 ± 0.3	545
$\rightarrow$ (a) $C_6H_4^+ + C_6H_5 + H$	76	14.5	18.05 ± 0.5	334
(b) $C_{12}H_8^{2+} + H_2$	76	82.4	22.0 ± 1.0	547

[a] $\Delta H_f(C_3H_3)$ taken as 91 kcal./mole from Table II.

Table IV: Data for Phenanthrene

Process	m/e of ion	Rel. abund., % of base peak	A.P., e.v.	ΔH_f of ion, kcal./mole
$C_{14}H_{10} \rightarrow C_{14}H_{10}^+$	178	100.0	8.10 ± 0.04	235
$\rightarrow C_{14}H_9^+ + H$	177	11.3	16.25 ± 0.1	371
$\rightarrow C_{14}H_8^+ + H_2$	176	19.2	18.58 ± 0.1	476
$\rightarrow C_{12}H_8^+ + C_2H_2$	152	9.5	16.63 ± 0.05	377
$\rightarrow C_{12}H_7^+ + C_2H_2 + H$	151	10.2	19.63 ± 0.05	395
$\rightarrow C_{11}H_7^+ + C_3H_3$	139	1.9	21.1 ± 0.3	445[a]
$\rightarrow C_{10}H_6^+ + 2C_2H_2$	126	2.1	20.9 ± 0.3	422

[a] $\Delta H_f(C_3H_3)$ taken as 91 kcal./mole from Table II.

The mass spectrum of biphenyl shows a number of similarities to that of benzene. The main fragment ions observed in both compounds correspond to the

(11) F. H. Field and J. L. Franklin, "Electron Impact Phenomena," Academic Press Inc., New York, N. Y., 1957.

Table V: Data for Diphenylacetylene

Process	m/e of ion	Rel. abund., % of base peak	A.P., e.v.	ΔH_f of ion, kcal./mole	Remarks
$C_{14}H_{10} \rightarrow C_{14}H_{10}^+$	178	100	8.85 ± 0.05	303	
$\rightarrow C_{14}H_9^+ + H$	177	11.1	15.13 ± 0.1	396	
$\rightarrow C_{14}H_8^+ + H_2$	176	18.8	16.66 ± 0.05	483	ΔH_f of $C_{14}H_8^+$ = 379 if 2H as neutral
$\rightarrow C_{12}H_8^+ + C_2H_2$	152	7.5	15.58 ± 0.05	404	
$\rightarrow C_{12}H_7^+ + C_2H_2 + H$	151	9.6	17.46 ± 0.06	396	
$\rightarrow C_{11}H_7^+ + C_3H_3$	139	3.3	17.52 ± 0.1	413[a]	
$\rightarrow C_{10}H_6^+ + 2C_2H_2$	126	5.7	18.23 ± 0.1	411	
$\rightarrow C_9H_7^+ + C_5H_3(?)$	115	1.3	17.5 ± 0.1	83[b]	321 for $C_9H_7^+$ from biphenyl is used
$\rightarrow C_9H_5^+ + C_5H_5(?)$	113	1.4	21.3 ± 0.2	?	
$\rightarrow C_8H_6^+ + C_6H_4(?)$	102	2.8	17.8 ± 0.1	61[b]	349 for $C_8H_6^+$ from biphenyl is used
$\rightarrow C_{14}H_{10}^{2+}$	89	30.5	23.35 ± 0.1	538	No $C_7H_5^+$ ion
$\rightarrow C_6H_5^+ + C_8H_5(?)$	77	6.3	20.7 ± 0.1	275[b]	$\Delta H_f(C_6H_5^+)$ = 301 used
$\rightarrow C_{12}H_8^{2+}$	76	35.4	20.5 ± 0.1	572	No $C_6H_4^+$ ion

[a] $\Delta H_f(C_3H_3)$ taken as 91 kcal./mole from Table II.　　[b] Calculated for neutral.

loss of one or two H atoms or to the loss of C_2H_2, C_3H_3, and C_4H_4 groups from the molecular ions. The biphenyl mass spectrum also exhibits a number of doubly charged ions. Part of the ionic current at mass number m/e 77 is due to the doubly charged molecular ion M^{2+}, and at m/e 77$\frac{1}{2}$ to isotopic M^{2+}. Ions at m/e 76$\frac{1}{2}$ (15.3% of M^+) and 75$\frac{1}{2}$ (8.9% of M^+) correspond to $(M - H)^{2+}$ and $(M - 3H)^{2+}$, respectively, and part of the ion at m/e 76 to $(M - 2H)^{2+}$. A number of doubly charged ions of less importance (less than 5% of M^+) are to be mentioned in the 62$\frac{1}{2}$–64$\frac{1}{2}$ region corresponding to $C_{10}H_x^{2+}$ ions. A triply charged M^{3+} at m/e 51$\frac{1}{3}$ of very slight intensity, observed in this study, had been reported previously.[12]

As mentioned above, ions at m/e 76 and 77 are due to both singly and doubly charged ions. The 77$\frac{1}{2}$ peak being only the isotopic M^{2+}, it is calculated therefrom that 75% of ionic current at m/e 77 is due to $C_{12}H_{10}^{2+}$ and 25% to $C_6H_5^+$. The appearance potential of the doubly charged ion at m/e 77 is rather close to that which one would calculate for the process $(C_6H_5)_2 \rightarrow 2C_6H_5^+$. Thus it is puzzling that the major portion of this peak is the doubly charged parent ion, and the remainder, the $C_6H_5^+$, arises from a process of considerably lower appearance potential. Comparison of the relative abundances of singly to doubly charged ions of mass 154, 153, and 151 enables one to estimate that about 85% of the ionic intensity at m/e 76 is attributable to $C_{12}H_8^{2+}$ and the 15% left to $C_6H_4^+$.

The mass spectrum of diphenylacetylene, to our knowledge, had not been published previously. As shown in Table I, the mass spectrum of diphenylacetylene shows some similarity with that of isomeric phenanthrene. With both these compounds the molec-

ular ion is the most abundant ion. This observation confirms that previously reported by Hall and Elder.[13] They also have the same fragment ions, the main ones at m/e 177, 176, 152, 151, 150, 139, and 126 being present with comparable relative abundances. In addition to these fragment ions which correspond to the abstraction of one or more H atoms or to the loss of C_2H_2, C_3H_3, and C_4H_4 groups from the parent ion, both diphenylacetylene and phenanthrene exhibit a

Table VI: Thermochemical Data (kcal./mole)

Compound	ΔH_f	L_v	ΔH_{f_g}	Ref.
Benzene			19.08	a
Biphenyl	28	11.5	39.5	b, c
Diphenylacetylene			99	d
Phenanthrene	33	15[e]	48	b
Acetylene			54	a
H			51.1	a
$C_3H_3^+$			274, 283	f
C_6H_5			70	g, h

[a] F. D. Rossini, *et al.*, "Selected Values of Physical and Thermodynamic Properties of Hydrocarbons and Related Compounds," Carnegie Press, Pittsburgh, Pa., 1953.　[b] M. S. Karash, *J. Res. Natl. Bur. Std.*, **2**, 359 (1929).　[c] F. Glaser and H. Rüland, *Chem. Ingr.-Tech.*, **29**, 772 (1957).　[d] J. L. Franklin, *Ind. Eng. Chem.*, **41**, 1070 (1949); *J. Chem. Phys.*, **21**, 2029 (1953).　[e] Estimated value.　[f] See ref. 11.　[g] J. S. Roberts and H. A. Skinner, *Trans. Faraday Soc.*, **45**, 339 (1949).　[h] M. Szwarc, *Chem. Rev.*, **47**, 75 (1950).

(12) S. Meyerson and R. W. Vander Haar, *J. Chem. Phys.*, **37**, 2458 (1962).

(13) K. L. Hall and F. A. Elder, *ibid.*, **31**, 1420 (1959).

number of doubly charged ions. This is known to be a general feature of mass spectra of aromatic hydrocarbons. The most important of these ions belong to two groups: (a) the doubly charged parent ion M^{2+}, at m/e 89, and analogous ions having lost one or more H atoms and (b) a very abundant $(M - C_2H_2)^{2+}$ ion at m/e 76 with an isotopic $(M - C_2H_2)^{2+}$ at m/e $76^1/_2$ and a less important $(M - C_2H_3)^{2+}$ at m/e $75^1/_2$. It may be worthwhile to mention that a mass spectrum of diphenylacetylene recorded with high sensitivity displayed a series of doubly charged fragment ions corresponding to all main singly charged fragment ions observed between m/e 99 $(C_8H_3{}^+)$ and m/e 177 $(C_{14}H_9{}^+)$.

A triply charged molecular ion M^{3+} at m/e $59^1/_3$, together with an isotopic triply charged molecular ion at m/e $59^2/_3$, both of very low intensities (a few tenths of 1% of M^+) also appear in the mass spectra of diphenylacetylene and phenanthrene. In these two aromatic hydrocarbons, there is also another triply charged ion at m/e $58^2/_3$ corresponding to $(M - 2H)^{3+}$ (about 0.05% of M^+). The triply charged ions of phenanthrene observed in this study had been reported previously.[12]

Although the fragment ions of diphenylacetylene and phenanthrene are the same, some differences must be pointed out. Generally speaking, the abundance of most fragment ions is somewhat larger in diphenylacetylene than in phenanthrene, but the reverse is observed with doubly charged ions, especially in the case of 152^{2+} and 178^{2+} (M^{2+}) at m/e 76 and 89. Thus, phenanthrene exhibits a greater stability than does diphenylacetylene under electron bombardment.

One of the most significant differences between the mass spectra of diphenylacetylene and phenanthrene concerns the fragment ions at m/e 77 and 102, these ions being more abundant in the former than in the latter compound. This also can be expected if these ions are simply $C_6H_5{}^+$ and $(C_6H_5-C_2)^+$ which are presumably more easily produced from $C_6H_5-C\equiv C-C_6H_5$ than from the completely fused ring system of phenanthrene.

The portion of the mass spectrum recorded below m/e 77 comprises the superimposition of doubly charged fragment ions and singly charged fragment ions corresponding to parts of the phenyl ring.

Results and Discussion

Ionization Potentials. The ionization potentials of the compounds studied are listed in Table VII, along with those of azulene and naphthalene recently reported by Wacks.[3] Results of simple group orbital computations of the ionization potential of these

compounds using the simplified method of Franklin[14] based upon olefinic and acetylenic groups are also listed in Table VII. Except for biphenyl, the computed values are in fair agreement with the measured ones.

Table VII: Ionization Potential (in e.v.)

Compound	Measd.		Calcd.,
	This study	Lit.	this paper
Benzene	9.22	9.11–9.3[a]	9.2
Azulene	...	7.72[b]	7.9
Naphthalene	...	8.26[b]	8.5
Biphenyl	8.96	8.3–8.92[a]	8.2
Diphenylacetylene	8.85	...	8.7
Phenanthrene	8.10	8.03[c]	8.2

[a] R. W. Kiser, "Tables of Ionization Potential," U.S.A.E.C. Report TID 6142 (1960). [b] See ref. 3. [c] See ref. 4.

$(M - 1)^+$ *Ion.* Each of the compounds studied exhibited a modest sized peak at $(M - 1)^+$ corresponding to the loss of a hydrogen atom. The appearance potentials for $(M - 1)^+$ from these compounds and from naphthalene and azulene[3] are listed together in Table VIII. There is a general upward trend in the appearance potential of these ions with increasing resonance energy of the parent molecule. This is especially notable in the case of the condensed ring compounds for which the appearance potential increases with increasing resonance energy from 14.0 e.v. for azulene to 16.25 e.v. for phenanthrene.

The large increase in energy with increasing resonance is difficult to understand unless the loss of hydrogen atom is accompanied by the opening of one or

Table VIII: Appearance Potentials (A.P.) of $(M - 1)^+$ and $(M - 2)^+$ Ions (e.v.)

Compound	Nominal resonance energy[a]	A.P.$(M - 1)^+$	A.P.$(M - 2)^+$
Azulene	25	14.0	14.7
Benzene	41	14.44	14.09
Naphthalene	77	15.4	16.2
Biphenyl	91	14.36	16.89
Diphenylacetylene	113	15.13	16.66
Phenanthrene	130	16.25	18.58

[a] Based upon heats of combustion, taken from Wheland (G. W. Wheland, "The Theory of Resonance," John Wiley and Sons, Inc., New York, N. Y., 1947).

(14) J. L. Franklin, *J. Chem. Phys.*, 22, 1304 (1954).

more rings. In support of this view, Meyerson[2b] gives convincing evidence that $C_6H_5{}^+$ from toluene is not phenyl and concludes that $C_6H_5{}^+$ from benzene is also probably not phenyl. Momigny[2a] also produces strong evidence that $C_6H_5{}^+$ from benzene is an open chain. Lossing[15] has measured the ionization potential of the phenyl radical, and, when this is combined with the heat of formation of the phenyl radical, it gives a heat of formation of the phenyl ion of 285–288 kcal./mole. This is definitely lower than ΔH_f $(C_6H_5{}^+)$ from benzene and tends to support the view that $C_6H_5{}^+$ from benzene is not phenyl. The formation of the phenyl ion is the lower energy path to $C_6H_5{}^+$, and we do not understand why the higher-energy, ring-opening reaction seems to be preferred. Nevertheless, if such is the case, one would expect the more highly conjugated ring systems to require more energy if more than one ring is opened or if there is an activation energy for the reaction which is related to the total resonance energy of the system. The increase in appearance potential with total resonance for the condensed ring sequence azulene, benzene, naphthalene, and phenanthrene supports this interpretation.

Further, with biphenyl and diphenylacetylene there is comparatively little resonance interaction between the electron systems of the two rings, so, if the loss of H atom occurs with opening of one ring, there should be very little change in the appearance potential of the $(M - 1)^+$ ion in the sequence benzene, biphenyl, and diphenylacetylene. Our results are in good agreement with this inference and also with the conclusion derived from the work of Burr, et al.[5]

$(M - 2)^+$ Ion. Each of the hydrocarbons studied gave peaks of moderate to large intensity corresponding to the loss of two hydrogen atoms. As will be seen from Table VIII, there is a general trend toward increasing appearance potential for the $(M - 2)^+$ ion with increasing resonance energy although the value for azulene[3] falls slightly out of line. With these ions it is necessary to decide (1) whether the hydrogens are eliminated as atoms or as hydrogen molecules and (2) what is the nature of the resulting ions.

In Table IX we list the heats of formation of the various $(M - 2)^+$ ions computed on the assumption that the H_2 is lost (column 3) and that two H atoms are lost (column 4). In column 5 we also give values for ΔH_f of $C_6H_4{}^+$ formed from naphthalene and azulene[3] by loss of C_2H_2, of $C_{10}H_6{}^+$ formed from diphenylacetylene and phenanthrene by loss of two acetylene molecules, and of $C_{12}H_8{}^+$ formed from diphenylacetylene and phenanthrene by loss of C_2H_2. In all cases the heat of formation resulting from loss of one or more C_2H_2 molecules corresponds to the heat of

formation of the ion in question computed on the assumption that H_2 is the neutral fragment. Further, if we compare heats of formation of the various $(M - 1)^+$ ions with those of $(M - 2)^+$ ions we find that in all cases $\Delta H_f(M - 1)^+ > \Delta H_f(M - 2)^+$ computed on the assumption that two H atoms are ejected. It seems probable that the more hydrogen-rich ions should have the lower heats of formation, and this also points to H_2 as the probable neutral fragment. Thus, the data support the view that the appearance potentials of $(M - 2)^+$ represent the reaction $M + e \rightarrow (M - 2)^+ + H_2 + 2e$ although the conclusion is not so well established with phenanthrene and diphenylacetylene as with the other compounds.

Table IX: Heats of Formation of $(M - 2)^+$ Ions (kcal./mole)

Compound	Ion	Neutral product			Computed for linear ion
		H_2	2H	From other sources	
Benzene	$C_6H_4{}^+$	345	241	342 (azulene)[3] 343 (naphthalene)[8]	340
Azulene[8]	$C_{10}H_6{}^+$	411	307	411 ((C$_6$H$_5$)$_2$C$_2$)	405
Naphthalene[8]	$C_{10}H_6{}^+$	408	304	422 (phenanthrene)	
Biphenyl	$C_{12}H_8{}^+$	429	325	404 ((C$_6$H$_5$)$_2$C$_2$) 377 (phenanthrene)	410
(C$_6$H$_5$)$_2$C$_2$	$C_{14}H_8{}^+$	483	379	...	470
Phenanthrene	$C_{14}H_8{}^+$	476	372	...	

Lossing[16] has determined the ionization potential of benzyne to be 9.75 e.v. If we subtract this value (converted to kcal./mole) from our alternative values for $\Delta H_f(C_6H_4)^+$ we obtain values for ΔH_f(benzyne) of 120 or 16 kcal./mole, depending upon whether H_2 or 2H is the neutral product. The latter value is less than ΔH_f(benzene) and thus is unreasonable. The higher value appears to be too high by some 30 or 40 kcal./mole although we admittedly do not know the heat of formation of this compound. If, however, this is indeed too high a value, then our $\Delta H_f(C_6H_4)^+$ probably does not correspond to that of the benzyne ion. Since we concluded that the ring was ruptured when one hydrogen was lost, it seems probable that this would also occur when H_2 is lost. Momigny[2a] also concluded that $C_6H_4{}^+$ from benzene was an open-chain molecule.

The previously mentioned upward trend of A.P. $(M - 2)^+$ with resonance energy is difficult to understand unless the loss of H_2 is accompanied by ring

(15) I. P. Fisher, T. F. Palmer, and F. P. Lossing, J. Am. Chem. Soc., 86, 2741 (1964).

(16) I. P. Fisher and F. P. Lossing, ibid., 85, 1018 (1963).

Table X: Data for $(M - C_2H_2)^+$ Ions

Parent	Ion	Measd.	ΔH_f(ion), kcal./mole — Other sources	Calcd.	Assumed structure
Benzene	$C_4H_4^-$	311	294 (I.P. C_4H_4)	...	
Naphthalene[3]	$C_8H_6^-$	333 ⎫	287 (I.P. $C_6H_5C_2H$)	345	Linear
Azulene[3]	$C_8H_6^{-+}$	340 ⎭			
Biphenyl	$C_{10}H_8^+$	328	⎰ 250 (azulene)[3]	295	Phenyl plus side chain
			⎱ 225 (naphthalene)[3]	350	Linear
Diphenylacetylene	$C_{12}H_8^+$	404 ⎫	429 (biphenyl)	400	Linear
Phenanthrene	$C_{12}H_8^+$	377 ⎭		350	Phenyl plus side chain

Table XI: Data for $(M - 2C_2H_2)^+$ Ions

Parent	Ion	Measd.	ΔH_f(ion), kcal./mole — Other sources	Computed	Assumed structure
Benzene	$C_2H_2^{-+}$	341	317 (I.P. C_2H_2)		
Naphthalene[3]	$C_6H_4^{-+}$	342 ⎫	345 (benzene)	351	Linear
Azulene[3]	$C_6H_4^{-+}$	343 ⎭			
Biphenyl	$C_8H_6^{-+}$	349	⎰ 333 (naphthalene)[3] ⎱ 340 (azulene)[3]	345	Linear
Diphenylacetylene	$C_{10}H_6^+$	411 ⎫	⎰ 408 (naphthalene)[3]	400	Linear
Phenanthrene	$C_{10}H_6^+$	422 ⎭	⎱ 411 (azulene)[3]	340	Phenyl plus side chain

opening. In addition, the heat of formation of $C_{10}H_6^+$ from naphthalene and azulene agrees rather well with those from phenanthrene and diphenylacetylene although these latter were formed by processes involving profound disruption of the ring structure. A similar observation can be made of $C_{12}H_8^+$ from biphenyl for which the heat of formation is greater than that of $C_{12}H_8^+$ from phenanthrene or diphenylacetylene.

It is possible to make simple approximate calculations of the heat of formation of the $(M - 2)^+$ ions assuming their structures to involve either a single benzene ring with a side chain of acetylenic and/or olefinic groups or to involve only an open chain of acetylenic and olefinic groups. The method of group equivalents[17] combined with the group orbital method[14] is readily used for this purpose. The results are probably reliable to within about 15–20 kcal./mole. However, the differences in computed heats of formation between a linear ion and one of the same composition having a single benzene ring with side chain differ by 60–100 kcal./mole, and thus the calculations are of some value in deciding upon the probable structure of various $(M - 2)^+$ ions. In Table IX we list heats of formation thus computed for the linear structures. In all cases this agrees fairly well with the experimental heat of formation of the ion formed by loss of H_2. Thus, although we cannot provide final proof, the most reasonable and consistent interpretation of our observa-

tions is a mechanism by which $(M - 2)^+$ ions are formed along with extensive ring opening, probably to a completely linear structure.

$(M - C_2H_2)^+$ *Ion.* All of these aromatics, including naphthalene and azulene,[3] exhibited mass spectral peaks at $(M - C_2H_2)^+$ representing the loss of acetylene during decomposition. Obviously, the loss of acetylene necessitates ring opening although subsequent ring closure is not precluded. As with the loss of the H atom, there is a definite upward trend of appearance potential with delocalization energy in the condensed ring aromatics, whereas the noncondensed ring aromatics exhibit very little variation in appearance potential with loss of C_2H_2.

In Table X we list the heat of formation of $(M - C_2H_2)^+$ from the various aromatics studied and compare these values with measured heats of formation of ions of similar composition from the literature or by other processes in the present study. The present value of $\Delta H_f(C_4H_4)^+$ is in fair agreement with that obtained by direct ionization of vinylacetylene. The heat of formation of $C_8H_6^+$ is much higher than the value obtained by direct ionization of phenylacetylene and is in fair agreement with an estimated value based upon the assumption that the ion is an open chain of structure

(17) See footnote c, Table VI.

$$\underset{\displaystyle HC\equiv C-\overset{\displaystyle H}{C}=\overset{\displaystyle H}{C}-\overset{\displaystyle H}{C}=\overset{\displaystyle H}{C}-C\equiv CH}{}$$
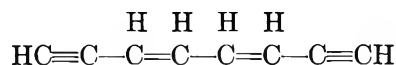
(Other structures are of course possible but would differ little in heat of formation.) Similarly, $\Delta H_f(C_{10}H_8)^+$ from biphenyl is much greater than that obtained by direct ionization of azulene or naphthalene[3] and thus must represent either a completely linear structure or one involving a benzene ring with a four-carbon side chain. Computed values of $\Delta H_f(C_{10}H_8)^+$ give results that are too high by about 25 kcal./mole for the completely linear structure and too low by about 30 kcal./mole for the phenyl group with a side chain. Although these results are not very satisfactory, they suggest that the experimental value corresponds to the latter structure formed with excess energy.

The $C_{12}H_8^+$ ions from phenanthrene and diphenylacetylene differ in heat of formation by 27 kcal./mole and thus may be of different structure. $\Delta H_f(C_{12}H_8)^+$ from diphenylacetylene agrees quite closely with the value computed for a linear structure and probably is of this or similar structure. $\Delta H_f(C_{12}H_8)^+$ from phenanthrene is much less than that computed for a linear structure and about 25 kcal./mole greater than the heat of formation computed for a phenyl ring with a linear side chain. As in the case of $C_{10}H_8^+$, we presume that the observed ion probably was formed with the latter structure and with some excess energy.

$(M - 2C_2H_2)^+$ *Ion.* All of the aromatics studied gave significant peaks at (M − 52) representing the loss of two acetylene molecules. This can occur only with very profound disruption of the molecule, and the heats of formation of the $(M - 2C_2H_2)^+$ ions all agree with values computed for linear structures and are, in general, too high to be accounted for by structures involving even one phenyl ring. Table XI compares heats of formation of $(M - 2C_2H_2)^+$ ions from this study with experimental values for the same ion from other sources and with values computed as discussed previously. Again, the data strongly support the view that all rings are opened when $2C_2H_2$ are removed.

Ionization and Dissociation of Diphenyl and Condensed Ring Aromatics by

Electron Impact. II. Diphenylcarbonyls and Ethers[1a]

by P. Natalis[1b] and J. L. Franklin

Department of Chemistry, Rice University, Houston, Texas (*Received February 18, 1965*)

The principal ions in the mass spectra of several oxygen-containing aromatic compound have been studied by electron impact methods and their appearance potentials measured. The compounds studied were benzaldehyde, acetophenone, benzophenone, benzil, phenyl ether, phenyl benzoate, and diphenyl carbonate. All of the compounds containing a carbonyl group give intense peaks for $C_6H_5CO^+$, and appearance potentials yield a heat of formation of this ion of 186 kcal./mole. This leads to a heat of formation of the phenoxy radical of 9 kcal./mole. Benzophenone shows a peak for $C_{12}H_{10}^+$ formed with considerable excess energy, which appears to decompose further by loss of one or more hydrogens. Diphenyl carbonate loses CO_2 to give an intense peak for the $C_{12}H_{10}O^+$ ion. This ion is formed with excess energy and undergoes decomposition to form several ions of the same composition as those prominent in the spectrum of diphenyl ether. Especially noteworthy is the characteristic loss of CO to form $C_{11}H_{10}^+$, apparently with little or no excess energy. The $C_6H_5^+$ ion is very intense in the spectra of all of these compounds and appears to be formed with a heat of formation of about 300 kcal./mole in benzaldehyde, acetophenone, and benzil; with all other aromatics studied $C_6H_5^+$ is formed with considerable excess energy.

Introduction

Mass spectrometry shows that many organic compounds, upon dissociation by electron impact, undergo a skeleton rearrangement. This is especially true of thiaalkanes and polythiaalkanes. For example, in thiapropane, CH_3-S-CH_3, a series of rearranged ions from C_2^+ to $C_2H_5^+$ are observed,[2] and similar $C_2H_x^+$ ions are present in mass spectra of 2,3-dithiabutane, CH_3-S-S-CH_3, and 2,3,4-trithiapentane, CH_3-S-S-S-CH_3.[2] These ions are presumably formed by rearrangement and simultaneous ejection of the central part of the molecule as neutral product(s).

Skeleton rearrangements have been found in more complex molecules such as anthraquinone, which exhibits a hydrocarbon ion of mass number 152 by successive loss of the two CO groups.[3] The mass spectra of triaryl phosphates show several ions corresponding only to hydrocarbon fragments larger than a phenyl ring.[4] Skeleton rearrangements have also been observed in other compounds such as triazine,[5a] carbon

suboxide,[5b] organometallic compounds,[2] hydrocarbons, etc., as has been reviewed recently.[6]

The present study was carried out in order to see if diphenyl compounds containing an oxygenated functional group between two phenyl rings undergo similar skeleton rearrangement by dropping a central group such as CO or CO_2 from anthraquinone or S atom from phenyl sulfide, leaving a fragment ion having the same

(1) (a) This work was supported by a grant from the Robert A. Welch Foundation; (b) Chercheur qualifié of the Belgian Fonds National de la Recherche Scientifique. On leave of absence from the University of Liége, Belgium.

(2) "Catalog of Mass Spectral Data," American Petroleum Institute Research Project 44, Carnegie Institute of Technology, Pittsburgh, Pa.

(3) J. H. Beynon and A. E. Williams, *Appl. Spectry.*, 13, 101 (1959).

(4) A. Quayle, "Advances in Mass Spectrometry," Vol. I, J. Waldron, Ed., Pergamon Press Ltd., London, 1959, p. 365.

(5) (a) C. M. Judson, R. J. Francel, and J. A. Weicksel, *J. Chem. Phys.*, 22, 1258 (1954); (b) R. Botter, "Advances in Mass Spectrometry," Vol. II, R. M. Elliot, Ed., Pergamon Press Ltd., London, 1963, p. 540.

(6) P. Natalis, *Ind. Chim. Belge*, 29, 471 (1964).

formula as biphenyl. This work will also include data on the appearance potential of normal and rearranged fragment ions in biphenyl oxygenated compounds.

The oxygenated biphenyl compounds investigated are phenyl ether, benzophenone, benzil, phenyl benzoate, and diphenyl carbonate containing, respectively, the groups -O-, -CO-, -CO-CO-, -CO-O-, and -O-CO-O- between the two phenyl rings. Benzaldehyde and acetophenone have also been examined to provide information, along with that from benzene and from biphenyl previously obtained[7] needed in the interpretation of the data obtained in this investigation.

Experimental

Mass spectral and appearance potential data were obtained by means of a Consolidated Electrodynamics Corp. mass spectrometer Type 21-701. This 12-in. radius, 60° coincident field sector instrument has been described.[8] The modifications to the ionization-emission control circuits in order to make this instrument suitable for appearance potential study have also been described previously.[7]

In the determination of appearance potential data, xenon was used as a reference gas for calibration of the electron energy scale. Ionization efficiency curves have been treated by the logarithmic method[9] to obtain the appearance potential values, taking the difference between both curves at 1% of the ion intensities recorded at 50 v. Data discussed below are an average of several determinations and are reproducible to within 0.05 to 0.15 e.v. The tables of appearance potentials give, for each value, the average deviation from the mean. This is not a measure of absolute accuracy. The xenon-sample pressure was 0.5–1 $\times$ 10^{-7} mm. The ionizing current used was 4 μa.

Relative intensities of the main ions observed in the mass spectra of these compounds have been obtained in the same conditions of sample pressure and ionizing current, with electrons of 50-v. energy. Qualitative agreement is found between mass spectra obtained in this study and those reported in the literature for phenyl ether,[2] benzaldehyde,[10,11] and acetophenone.[10] However, the higher relative abundances of fragment ions, compared with that of molecular ions, obtained in this work, are believed to be instrumental, presumably owing to discrimination by the electron multiplier used in the collection system, as already mentioned previously.[7]

The samples were introduced into the instrument through a gallium-covered porous disk connected to the all-glass heated inlet system, kept at a temperature of 130°, which can be considered as the temperature of the gas in the ionization chamber. All samples used are commercial products from Eastman Kodak Co. except benzophenone and benzil which are chemicals from The Matheson Co. Mass spectra of all these compounds showed no trace of impurities.

General Features of Mass Spectra

The relative abundances of the principal ions observed in the mass spectra of benzaldehyde and acetophenone are presented in column 3 of Table I. The appearance potentials of the principal ions are given in column 4 of the same table; column 5 shows the calculated heats of formation of the ions formed in the assumed processes described in column 1. Similar data are presented for phenyl ether, benzophenone, benzil, phenyl benzoate, and diphenyl carbonate in Tables II through VI.

Table I: Data for Benzaldehyde and Acetophenone

Process	m/e of ion	Rel. abund., % of base peak	A.P., e.v.	ΔH_f of ion, kcal./mole
$C_6H_5COH \rightarrow C_6H_5COH^+$	106	77.4	9.51 ± 0.05	209
$\rightarrow C_6H_5CO^+ + H$	105	70.8	11.35 ± 0.05	200^a
$\rightarrow C_6H_5^+ + CO + H$	77	100.0	14.54 ± 0.05	299
$C_6H_5COCH_3 \rightarrow C_6H_5COCH_3^+$	120	49.6	9.48 ± 0.05	196
$\rightarrow C_6H_5CO^+ + CH_3$	105	82.2	10.43 ± 0.05	186
$\rightarrow C_6H_5^+ + CO + CH_3$	77	100.0	14.23 ± 0.05	299

^{a} First H removed from benzaldehyde is the one of the COH group as has been shown by C$_6$H$_5$COD study: K. Biemann, "Mass Spectrometry," McGraw-Hill Book Co., Inc., New York, N. Y., 1962, p. 210.

The fragment ion $C_6H_5^+$, at mass number 77, is found to be the most abundant ion (base peak) in the 50-v. mass spectrum of benzaldehyde, C_6H_5COH, acetophenone, $C_6H_5COCH_3$, phenyl benzoate, $C_6H_5COOC_6H_5$, and diphenyl carbonate, $C_6H_5OCOOC_6H_5$, and shows up as one of the principal ions in all the other compounds. Benzophenone, $C_3H_5COC_6H_5$, and benzil, $C_6H_5COCOC_6H_5$, exhibit the base peak at m/e 105 $(C_6H_5CO)^+$ which is also one of the main fragment ions in C_6H_5COH, $C_6H_5COCH_3$, and $C_6H_5COOC_6H_5$.

Phenyl ether, $C_6H_5OC_6H_5$, appears to be the most

(7) P. Natalis and J. L. Franklin, *J. Phys. Chem.*, **69**, 2935 (1965).

(8) H. G. Voorhies, C. F. Robinson, L. G. Hall, W. M. Brubaker, and C. E. Berry, "Advances in Mass Spectrometry," Vol. I, J. Waldron, Ed., Pergamon Press, Ltd., London, 1959, p. 44.

(9) F. P. Lossing, A. W. Tickner, and W. A. Bryce, *J. Chem. Phys.*, **19**, 1254 (1951).

(10) "Catalog of Mass Spectral Data," Manufacturing Chemists Association Research Project, Carnegie Institute of Technology, Pittsburgh, Pa.

(11) T. Aczel and H. E. Lumpkin, *Anal. Chem.*, **33**, 386 (1961).

Table II: Data for Phenyl Ether

Process	m/e of ion	Rel. abund., % of base peak	A.P., e.v.	ΔH_f of ion, kcal./mole
$C_6H_5OC_6H_5 \rightarrow C_6H_5OC_6H_5^+$	170	100.0	8.82 ± 0.05	220
$\rightarrow C_{12}H_9O^+ + H$	169	17.9	12.90 ± 0.05	262
$\rightarrow$ (a) $C_{11}H_{10}^+ + CO$	142	15.4	12.56 ± 0.08	333^a
(b) $C_{10}H_6O^+ + C_2H_4$				295
$\rightarrow$ (a) $C_{11}H_9^+ + CO + H$	141	28.4	14.02 ± 0.05	314^a
(b) $C_{10}H_5O^+ + C_2H_6$				315
(c) $C_{10}H_5O^+ + C_2H_4 + H$				276
$\rightarrow$ (a) $C_9H_7^+ + C_3H_3O$ (?)	115	8.4	16.68 ± 0.15	54^b
(b) $C_3H_3O^+ + C_4H_7$ (?)				?
$\rightarrow C_6H_5OH^+ + C_6H_4$	94	6.8	13.88 ± 0.15	152^c
$\rightarrow C_6H_5^+ + C_6H_5O$	77	60.0	14.85 ± 0.05	349^d

^{a} Most probable process. ^{b} Calculated for neutral using $\Delta H_f(C_9H_7^+) = 321$ kcal./mole (?). ^{c} Calculated for neutral using ΔH_f ($C_6H_5OH^+$) = 184 kcal./mole (F. H. Field and J. L. Franklin, "Electron Impact Phenomena," Academic Press Inc., New York, N. Y., 1957). ^{d} Using $\Delta H_f(C_6H_5O) = 10$ kcal./mole.

Table III: Data for Benzophenone

Process	m/e of ion	Rel. abund., % of base peak	A.P., e.v.	H_f of ion, kcal./mole
$C_6H_5COC_6H_5 \rightarrow C_6H_5COC_6H_5^+$	182	25.4	9.46 ± 0.05	231
$\rightarrow C_{12}H_{10}^+ + CO$	154	0.8	12.24 ± 0.13	321
$\rightarrow C_{12}H_9^+ + CO + H(?)$	153	0.8	15.28 ± 0.05	339
$\rightarrow C_{12}H_8^+ + CO + H_2(?)$	152	1.6	17.48 ± 0.12	442
$\rightarrow C_6H_5CO^+ + C_6H_5$	105	100.0	12.00 ± 0.05	220
$\rightarrow C_6H_5^+ + C_6H_5 + CO(?)$	77	70.0	16.22 ± 0.07	343

Table IV: Data for Benzil

Process	m/e of ion	Rel. abund., % of base peak	A.P., e.v.	ΔH_f of ion, kcal./mole
$C_6H_5COCOC_6H_5 \rightarrow C_6H_5COCOC_6H_5^+$	210	1.9	8.78 ± 0.05	180
$\rightarrow$ (a) $C_6H_5CO^+ + C_6H_5 + CO$	105	100.0	9.70 ± 0.05	158^a
$\rightarrow$ (b) $C_6H_5CO^+ + C_6H_5CO$				16^b
$\rightarrow C_6H_5^+ + C_6H_5 + 2CO(?)$	77	76.2	15.12 ± 0.2	309^c

^{a} Improbable process. ^{b} Calculated for neutral using $\Delta H_f(C_6H_5CO^+) = 186$ kcal./mole. See Table I. ^{c} The neutral is probably either $C_6H_5CO + CO$, total $\Delta H_f = -10$ kcal./mole, or $C_6H_5 + 2CO$, total $\Delta H_f = +14$ kcal./mole. Since some excess energy is involved in any case, the greater extent of fragmentation seems the more probable.

Table V: Data for Phenyl Benzoate

Process	m/e of ion	Rel. abund., % of base peak	A.P., e.v.	ΔH_f of ion, kcal./mole
$C_6H_5COOC_6H_5 \rightarrow C_6H_5COOC_6H_5^+$	198	9.8	8.98 ± 0.05	171
$\rightarrow C_6H_5CO^+ + C_6H_5O$	105	17.6	10.01 ± 0.07	9^a
$\rightarrow$ (a) $C_6H_5^+ + C_6H_5 + CO_2$	77	100.0	15.46 ± 0.05	345
$\rightarrow$ (b) $C_6H_5 + C_6H_5O + CO$				337^b
				20^c

^{a} Calculated for neutral using $\Delta H_f(C_6H_5CO^+) = 186$ kcal./mole. from Table I. ^{b} $\Delta H_f(C_6H_5O) = 10$ is used. ^{c} Calculated for neutral products.

Table VI: Data for Diphenyl Carbonate

Process	m/e of ion	Rel. abund., % of base peak	A.P., e.v.	ΔH_f of ion, kcal./mole
$C_6H_5OCOOC_6H_5 \rightarrow C_6H_5OCOOC_6H_5{}^+$	214	19.2	9.01 ± 0.05	122
$\rightarrow C_{12}H_{10}O^+ + CO_2$	170	12.7	10.78 ± 0.05	257
$\rightarrow C_{12}H_9O^+ + CO_2 + H$	169	10.0	12.51 ± 0.05	246
$\rightarrow C_{11}H_{10}{}^+ + CO + CO_2$	142	12.9	12.41 ± 0.1	320
$\rightarrow C_{11}H_9{}^+ + CO + CO_2 + H$	141	18.4	13.90 ± 0.05	303
$\rightarrow$ (a) $C_6H_5{}^+ + C_6H_5O + CO_2$	77	100.0	12.1 ± 0.1	-14^a
(b) $C_6H_5{}^+ + C_6H_5 + CO + CO_2$				12^b

^{a} Calculated for C_6H_5O. ^{b} Calculated for C_6H_5.

stable of all these oxygenated aromatic compounds, having the molecular ion as the base peak. Several of the main fragment ions in phenyl ether are rearranged ions: at m/e 142, $C_{11}H_{10}{}^+$, formed by loss of CO from the molecular ion, or, less probably, $C_{10}H_6O^+$ formed by loss of C_2H_4. The ion at m/e 141 also appears to be a sizable rearranged ion as does $C_6H_6O^+$ at m/e 94, presumably a phenol ion $C_6H_5OH^+$.

Several interesting rearrangements are observed in the mass spectrum of benzophenone, $C_6H_5COC_6H_5$, and diphenyl carbonate, $C_6H_5OCOOC_6H_5$. Benzophenone shows a series of rearranged ions corresponding to biphenyl at m/e 154 and to fragment ions of biphenyl. The appearance potential of the 154 ion rules out the possibility of biphenyl being present as an impurity in the benzophenone sample. It thus appears that a series of decomposition processes of benzophenone under electron impact proceeds through an intermediate step involving the $C_{12}H_{10}{}^+$ ion. This ion is formed by skeleton rearrangement of the ionized benzophenone molecule, by dropping CO as a neutral, as shown in the scheme $(C_6H_5-CO-C_6H_5)^+ \rightarrow (C_{12}H_{10}{}^+) + CO$. This skeleton rearrangement of benzophenone is very similar to that observed in phenyl sulfide[2] and azobenzene.[12]

$$(C_6H_5-S-C_6H_5)^+ \longrightarrow (C_{12}H_{10}{}^+) + S$$

$$(C_6H_5-N=N-C_6H_5)^+ \longrightarrow (C_{12}H_{10}{}^+) + N_2$$
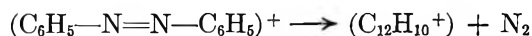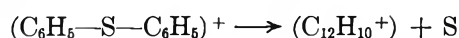
In the same way, diphenyl carbonate also undergoes a skeleton rearrangement by ejection of a CO_2 molecule from the central part of the ionized molecule. The mass spectrum of this compound exhibits an ion at m/e 170, $C_{12}H_{10}O^+$, and for the same reason as indicated in the case of benzophenone cannot be due to a phenyl ether impurity. The series of mass fragment ions observed in the mass spectrum of phenyl ether also show up as rearranged ions in the mass spectrum of diphenyl carbonate. Electron-impact-induced decomposition of diphenyl carbonate thus proceeds

through an intermediate step involving the skeleton rearrangement: $(C_6H_5-O-CO-O-C_6H_5)^+ \rightarrow C_{12}H_{10}O^+ + CO_2$.

As in most aromatic compounds mass spectra of the oxygenated aromatic compounds investigated in this study display a number of doubly charged ions. Benzaldehyde, phenyl ether, benzophenone, and diphenyl carbonate have a doubly charged molecular ion M^{2+} accompanied by an isotopic doubly charged ion. All of these compounds also have a $(M - 1)^{2+}$ ion, except diphenyl carbonate, which has neither $(M - 1)^+$ nor $(M - 1)^{2+}$. No doubly charged M^{2+} ion is observed in either the mass spectrum of acetophenone or in that of benzil in which M^{2+} (210^{2+}) would be obscured by the very abundant fragment ion $(C_6H_5CO)^+$ at m/e 105, but there is no ion at $105^1/_2$ corresponding to a doubly charged molecular ion. A doubly charged fragment ion, $(C_6H_5CO)^{2+}$, at m/e $52^1/_2$ is present in the mass spectrum of benzaldehyde and acetophenone but in none of the other compounds containing a $(C_6H_5CO)^+$ fragment ion. Benzil and benzophenone have no doubly charged ion at all. Phenyl ether shows doubly charged fragment ions corresponding to the three main singly charged fragment ions, 141, 142, and 115. It may be worthwhile to mention also that in the mass spectrum of benzophenone the doubly charged ions at m/e $75^1/_2$ and $76^1/_2$, corresponding to the rearranged biphenyl fragment ions at m/e 151^+ and 153^+, are observed. Doubly charged 152^{2+} and 154^{2+} are therefore probably present too although obscured by the singly charged 76^+ and 77^+ ions. No triply charged ion has been observed in the mass spectra of these compounds.

Apart from the doubly charged ions, the mass spectra of all these oxygenated aromatic compounds have, in the 40–77 mass number range, the same fragment ion $C_4H_3{}^+$ at m/e 51 as the principal ion. In addition,

(12) Unpublished data from this laboratory.

phenyl ether, phenyl benzoate, and diphenyl carbonate exhibit a less important fragment ion at m/e 65 which may be $C_5H_5^+$. Moreover, this 65^+ ion is observed only in the three compounds having a phenoxy group, C_6H_5O, in their molecule so that $C_5H_5^+$ may be a decomposition product of an unstable $C_6H_5O^+$ ion. A similar behavior has been shown to occur with the phenoxy radical produced by pyrolysis of anisole.[13]

Results and Discussion

The values of ionization potential of the oxygenated aromatic compounds investigated and of the appearance potential of their main fragment ions, listed in column 4 of Tables I through VI, permit the calculation of the heats of formation ΔH_f of these ions, given in column 5 of the same tables, by means of data of the heats of formation of the neutral compounds.

The values of the ΔH_f used for the gaseous neutral compounds and free radicals are given in Table VII.

Table VII: Heats of Formation ΔH_f (kcal./mole) of Neutral Oxygenated Aromatic Compounds

Compound	ΔH_f	ΔH_{vap}	ΔH_f(gas)	Ref.
Benzaldehyde	−20.3(1)	9.8	−10.5	a, b
Acetophenone	−32.8(s)	10^c	−23	a
Benzophenone			12.5	d
Benzil			−21.8	d
Phenyl benzoate	−40(s)	10^c	−30	a
Diphenyl carbonate	−96(s)	10^c	−86	e
Phenyl ether			17	f
C_6H_5			70	g
CH_3			32	h
C_2H_5			25	h
CO			−26	i
CO_2			−94	i
H			52	i
C_2H_4			12	i

a M. S. Karash, *J. Res. Natl. Bur. Std.*, **2**, 359 (1929). *b* F. Glaser and H. Rüland, *Chem. Ingr.-Tech.*, **29**, 772 (1957). *c* Estimated value. *d* H. D. Springall and T. R. White, *J. Chem. Soc.* 2764 (1954). *e* G. C. Sinke, D. L. Hindenbrand, R. A. McDonald, W. R. Kramer, and D. R. Stull, *J. Phys. Chem.*, **62**, 1461 (1958). *f* J. L. Franklin, *Ind. Eng. Chem.*, **41**, 1070 (1949). *g* J. S. Roberts and H. A. Skinner, *Trans. Faraday Soc.*, **45**, 339 (1949); M. Szwarc, *Chem. Rev.*, **47**, 75 (1950). *h* T. L. Cottrell, "The Strength of Chemical Bonds," Academic Press Inc., New York, N. Y., 1954. *i* F. D. Rossini, *et al.*, "Selected Values of Physical and Thermodynamic Properties of Hydrocarbons and Related Compounds," Carnegie Press, Pittsburgh, Pa., 1953.

(1) Benzoyl Ion $(C_6H_5CO)^+$. The benzoyl ion $(C_6H_5CO)^+$ is produced by decomposition of benzaldehyde, acetophenone, and benzophenone in the simplest

way by abstraction of an H atom, a methyl, or a phenyl radical as shown in the reactions

$$C_6H_5COH \longrightarrow (C_6H_5CO)^+ + H$$

$$C_6H_5COCH_3 \longrightarrow (C_6H_5CO)^+ + CH_3$$

$$C_6H_5COC_6H_5 \longrightarrow (C_6H_5CO)^+ + C_6H_5$$
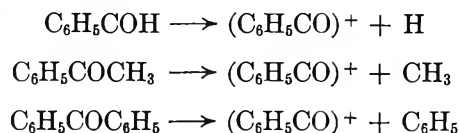
Using the values of appearance potential for $(C_6H_5CO)^+$ listed in Tables I and III combining them with ΔH_f of the neutral compounds given in Table VII, $\Delta H_f(C_6H_5CO)^+$ is found to be 200 kcal./mole in benzaldehyde, 186 in acetophenone, and 220 in benzophenone. These figures indicate some excess energy in the product of the reaction leading to the benzoyl ion from benzaldehyde and benzophenone, and the value of 186 is certainly closer to ΔH_f of the nonexcited $(C_6H_5CO)^+$ ion.

The benzoyl ion can originate from phenyl benzoate by a single cleavage involving the loss of a phenoxy radical; i.e., $C_6H_5COOC_6H_5 \rightarrow (C_6H_5CO)^+ + C_6H_5O$.

If the lowest value found for $\Delta H_f(C_6H_5CO)^+$, 186 kcal./mole, is combined with ΔH_f of neutral phenyl benzoate and the appearance potential of $(C_6H_5CO^+)$, a value of 9 kcal./mole is found for $\Delta H_f(C_6H_5O)$. Another value for ΔH_f of the phenoxy radical has been determined by other workers[14] who measured directly the ionization potential of the C_6H_5O radical, 8.84 e.v., and combined it with a value of 224 kcal./mole found for $\Delta H_f(C_6H_5O)^+$ from anisole. They obtained an upper limit of 20 kcal./mole for $\Delta H_f(C_6H_5O)$ but provided the possibility of about 10 kcal./mole of excess energy in the appearance potential of $(C_6H_5O)^+$; a better value for $\Delta H_f(C_6H_5O)$ would be, according to these authors, 10 kcal./mole, in excellent agreement with that found in the present study.

Benzil also produces a benzoyl ion by one of the two possible mechanisms

$$C_6H_5COCOC_6H_5 \longrightarrow (C_6H_5CO)^+ + C_6H_5 + CO \quad (a)$$
$$\searrow$$
$$(C_6H_5CO)^+ + C_6H_5CO \quad (b)$$
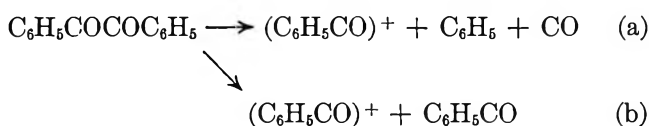
Taking $\Delta H_f(C_6H_5CO)^+$ as 186 kcal./mole one finds the heat of formation of the neutral product(s) to be 16 kcal./mole. This is much too small for the sum of $\Delta H_f(CO)$ and $\Delta H_f(C_6H_5)$. It is, however, a reasonable value for $\Delta H_f(C_6H_5CO)$ which one would estimate by the method of group equivalents to be about 12 kcal./mole after allowing some 10 kcal./mole for resonance

(13) A. G. Harrison, L. R. Honnen, H. J. Dauben, and F. P. Lossing, *J. Am. Chem. Soc.*, **82**, 5593 (1960).

(14) I. P. Fisher, T. F. Palmer, and F. P. Lossing, *ibid.*, **86**, 2741 (1964).

interaction between the unpaired electron and the
π-electron system of the benzene ring. The ionization
potential of the C_6H_5CO radical is computed from these
data to be about 7.4 e.v. which is reasonable in view of
the probable value of about 8.7 e.v. for I.P.(HCO).
Thus, the observed appearance potential is accounted
for by process b above.

(2) $C_6H_5^+$ Ion. The formation of $C_6H_5^+$ by elec-
tron-impact-induced decomposition of all oxygenated
aromatic compounds investigated in this study appears
to be an important mechanism. If the following
schemes account for the presence of this ion in benzalde-
hyde, acetophenone, and benzil

$$C_6H_5COH \longrightarrow C_6H_5^+ + CO + H$$

$$C_6H_5COCH_3 \longrightarrow C_6H_5^+ + CO + CH_3$$

$$C_6H_5COCOC_6H_5 \longrightarrow C_6H_5^+ + C_6H_5 + 2CO$$
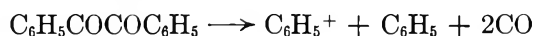
$\Delta H_f(C_6H_5)^+$ is found to be 299 kcal./mole in benzalde-
hyde, 299 in acetophenone, and 309 in benzil. All of
these figures are in close agreement with the value of
301 found from a benzene study as reported in a pre-
vious paper[7] and in the literature.[15] It should not be
assumed that $C_6H_5^+$ from any of these processes is
phenyl ion. In fact, there is considerable evidence
that the benzene ring opens and that $C_6H_5^+$ is an open-
chain molecule.[7,16]

The processes leading to $C_6H_5^+$ from the other com-
pounds studied are necessarily somewhat speculative.
Excess energy is certainly involved in the formation
of this ion from benzophenone and is probably involved
in its formation from phenyl benzoate and phenyl ether
as well. With diphenyl carbonate, however, quite the
reverse situation prevails. If, with this compound,
one assumes $\Delta H_f(C_6H_5)^+$ to be 301 kcal./mole and
CO_2 to be one of the neutral products, one computes
$\Delta H_f(C_6H_5O)$ to be -14 kcal./mole, which is un-
reasonably low. If, however, C_6H_5O is assumed to
decompose further by loss of CO, as has been observed
with anisole,[13] $\Delta H_f(C_5H_5)$ is computed to be 12 kcal./
mole. If $\Delta H_f(C_6H_6)^+$ is taken as 288 kcal./mole[17]
for phenyl ion, $\Delta H_f(C_5H_6)$ becomes 25 kcal./mole.
The ionization potential of c-C_5H_5 has been determined
as 8.72 e.v.,[13] and, if this is combined with a ΔH_f
$(C_5H_5)^+$ of 226 kcal./mole[15] from cyclopentadiene a
value of 25 kcal./mole is obtained for the heat of for-
mation of the C_5H_5 radical, which may be presumed to
be cyclopentadienyl. Since neither our value nor the
25 kcal./mole from the literature can be considered
very precise, it would be presumptuous to assert that
either is definitely the heat of formation of the cyclo-
pentadienyl radical. However, naive molecular or-
bital and valence bond calculations[18] indicate that

$\Delta H_f(c$-$C_5H_5)$ should be in the neighborhood of 30–40
kcal./mole in rough agreement with the speculative
values above. Thus, we think $C_6H_5^+$ from diphenyl
carbonate is probably phenyl ion and is probably
formed in conjunction with CO_2, CO, and the cyclo-
pentadienyl radical.

If one assumes C_5H_5 to be one of the neutral products
accompanying the formation of $C_6H_5^+$ from diphenyl
ether and phenyl benzoate, values of $\Delta H_f(C_5H_5)$ of
about 73–74 kcal./mole are obtained; thus, the
processes involve excess energy which may exhibit
itself by the formation of an open-chain C_5H_5 radical.

Among the oxygenated compounds investigated in
this study, only those which contain a phenoxy group,
i.e., phenyl ether, phenyl benzoate, and diphenyl
carbonate, have a $C_5H_5^+$ ion at m/e 65, possibly due to
a split of the phenoxy ion $C_6H_5O^+$, which does not show
up in the mass spectra of these compounds. This
would, of course, be analogous to the decomposition
of phenoxy radical discussed above. The heat of for-
mation of $C_5H_5^+$, determined from diphenyl ether,
was 353 kcal./mole, and this involved a large amount
of excess energy.

(3) Skeleton Rearrangement Process in Benzophenone
and Diphenyl Carbonate. As already mentioned in a
previous section, a series of decomposition processes
of ionized benzophenone seems to occur through an
intermediate step involving a skeleton rearrangement
of $C_6H_5COC_6H_5$ into $C_{12}H_{10}^+$. Once produced, this
intermediate decomposes to give the same principal
fragment ions as are obtained with biphenyl, namely, at
m/e 153, 152, 128, 115, 102, and 89, although those ob-
tained with benzophenone occur with very low in-
tensity. The intensity of fragment ions at m/e 154,
153, and 152, corresponding to $C_{12}H_{10}^+$, $C_{12}H_9^+$, and
$C_{12}H_8^+$, were intense enough for their ionization
efficiency curves to be recorded. Azobenzene under-
goes similar decompositions.[12] The heats of formation
of these three ions from benzophenone and azobenzene
are compared in Table VIII to those of the correspond-
ing ions from biphenyl.

Agreement is reasonably close for ΔH_f of $C_{12}H_9^+$
and $C_{12}H_8^+$, but the values found for $C_{12}H_{10}^+$ frag-
mentation indicated considerable excitation energy in
the intermediate species of azobenzene and benzo-
phenone.

(15) F. H. Field and J. L. Franklin, "Electron Impact Phenomena,"
Academic Press Inc., New York, N. Y., 1957.
(16) J. Momigny, L. Brakier, and L. D'or, Bull. Classe Sci., Acad.
Roy. Belg., 48, 1002 (1962).
(17) J. R. Majer and C. R. Patrick, "Advances in Mass Spec-
trometry," Vol. II, R. M. Elliott, Ed., Pergamon Press Ltd., 1963, p.
555.
(18) J. L. Franklin and F. H. Field, J. Am. Chem. Soc., 75, 2819
(1953).

Table VIII

	Benzo-phenone	Azo-benzene	Bi-phenyl
	ΔH_f(ion), kcal./mole		
$C_6H_5COC_6H_5 \rightarrow C_6H_5C_6H_5^+ + CO$	321	353	247
$\rightarrow C_{12}H_9^+ + CO + H$	339	319	319
$\rightarrow C_{12}H_8^+ + CO + H_2$	442	425	429

The first step in the decomposition of diphenyl carbonate appears to be the loss of CO_2 to form an ion ($C_{12}H_{10}O^+$) having the same composition as diphenyl ether. This ion then decomposes further in a manner quite like the diphenyl ether ion, giving the same principal fragment ions; i.e., m/e 169, 142, 141, and 115. The following reactions of diphenyl carbonate lead to the formation of $C_{12}H_{10}O^+$, $C_{12}H_9O^+$, $C_{11}H_{10}^+$, and $C_{11}H_9^+$. Heats of formation of these ions from diphenyl carbonate and phenyl ether are given for comparison in Table IX.

The $C_{12}H_{10}O^+$ ion in diphenyl carbonate seems to involve about 1 v. of excess energy; all of the other

Table IX

	Di-phenyl car-bonate	Phenyl ether
	ΔH_f(ion), kcal./mole	
$C_6H_5OCOOC_6H_5 \rightarrow C_{12}H_{10}O^+ + CO_2$	257	220
$\rightarrow C_{12}H_9O^+ + CO_2 + H$	246	262
$\rightarrow C_{11}H_{10}^+ + CO_2 + CO$	320	333
$\rightarrow C_{11}H_9^+ + CO_2 + CO + H$	303	314

rearrangement ions seem to be formed with somewhat less (ca. 0.5 e.v.) excess energy from diphenyl carbonate than from phenyl ether.

Proton Magnetic Resonance Studies of Hydrogen Bonding in

Amine–Acetamide–Chloroform Systems[1]

by Fujio Takahashi and Norman C. Li

Department of Chemistry, Duquesne University, Pittsburgh, Pennsylvania   (*Received February 23, 1965*)

Proton magnetic resonance studies are reported of hydrogen bonding between the amino protons of *t*-butylamine and aniline, and the electron donors, N-methylacetamide and N,N-dimethylacetamide, in chloroform medium. Carbon tetrachloride cannot be used as the solvent because of its reaction with amine. Since the proton in the solvent chloroform molecule itself participates as a hydrogen donor to the acetamide, the extent of this reaction must be taken into account in studying hydrogen bonding between the amine and the substituted acetamide. The association constants for the formation of the 1:1 acetamide-amine complexes at 36°, for the systems *t*-butylamine-N-methylacetamide, aniline-N-methylacetamide, and aniline-N,N-dimethylacetamide, are found to be 3.9, 5.8, and 6.0 M^{-1}, respectively. These values are obtained from the plots of eq. 8, after the values of K_s, the association constants for the formation of the acetamide-solvent complexes, have been determined in separate experiments.

Introduction

Quantitative hydrogen-bonding studies with the proton magnetic resonance (p.m.r.) method have generally been carried out using carbon tetrachloride as the inert solvent. However, because of solubility and other considerations, it is frequently necessary to be able to evaluate thermodynamic properties in solvents which themselves participate in hydrogen bonding. In this paper we report results of quantitative studies with *t*-butylamine and aniline as hydrogen donors, and N-methylacetamide and N,N-dimethylacetamide as electron donors, in chloroform as the solvent. Carbon tetrachloride cannot be used as the solvent because of its reaction with amine.[2] Since the proton in the solvent chloroform participates as a hydrogen donor to the N-substituted acetamide, the extent of this reaction must be taken into account in studying hydrogen bonding between the amine and the acetamide.

Mathur, *et al.*,[3] have shown that for an equilibrium between a monomeric hydrogen donor, M, and an electron donor, D, to form a 1:1 complex, MD, the following equation may be derived when $d \gg$ (MD)

$$\frac{1}{\nu - \nu_f} = \frac{1}{K(\nu_0 - \nu_f)} \frac{1}{d} + \frac{1}{(\nu_0 - \nu_f)} \tag{1}$$

In eq. 1, ν is the measured p.m.r. frequency of the hydrogen-bonding proton at a concentration d of D, ν_f and ν_c are the characteristic frequencies of M and MD, respectively, and K is the association constant for the formation of the MD complex. When chloroform is used as the solvent, eq. 1 has to be modified since the proton in chloroform also acts as a hydrogen donor to D.[4] In our present study, therefore, the interaction between the solvent and the N-substituted acetamide to form SD complex must be taken into account.

Modification of Eq. 1 for Chloroform as Solvent. Let x be the fraction of the amine concentration which is *not* hydrogen bonded to an electron donor and which is in the form of monomer,[5] and let C, d, and (S) be the total concentration of the amine, acetamide, and chloroform, respectively. If K and K_s are the as-

(1) This research was supported by P. H. S. Research Grant No. GM-10539-03 from the National Institute of General Medical Sciences, Public Health Service.

(2) R. F. Collins, *Chem. Ind.* (London), 704 (1957).

(3) R. Mathur, E. D. Becker, R. B. Bradley, and N. C. Li, *J. Phys. Chem.*, 67, 2190 (1963).

(4) C. M. Huggins, G. C. Pimentel, and J. N. Shoolery, *J. Chem. Phys.*, 23, 1244 (1955); L. W. Reeves and W. G. Schneider, *Can. J. Chem.*, 35, 251 (1957); G. Korinek and W. G. Schneider, *ibid.*, 35, 1157 (1957).

(5) F. Takahashi and N. C. Li, *J. Phys. Chem.*, 68, 2136 (1964).

sociation constants for the formation of the acetamide–amine and acetamide–solvent complexes, respectively, then when (S) $\gg$ d and $d \gg C$

$$K = \frac{\text{(MD)}}{x[C - \text{(MD)}][d - \text{(MD)} - \text{(SD)}]} \quad (2)$$

$$K_s = \frac{\text{(SD)}}{[d - \text{(MD)} - \text{(SD)}](\text{S})} \quad (3)$$

Therefore

$$\text{(SD)} = \frac{K_s(\text{S})}{1 + K_s(\text{S})}(d - \text{(MD)}) \quad (4)$$

From eq. 2 and 4, we obtain

$$K = \frac{\text{(MD)}(1 + K_s(\text{S}))}{x(C - \text{(MD)})d} \quad (5)$$

so that

$$\text{(MD)} = \frac{KCdx}{Kdx + (1 + K_s(\text{S}))} \quad (6)$$

Since hydrogen-bonding equilibria usually involve very rapid reactions, we may assume the observed frequency of the amino protons in amine to be the weighted average of ν' and ν_0, so that

$$\nu = \frac{C - \text{(MD)}}{C}\nu' + \frac{\text{(MD)}}{C}\nu_0$$

$$= \nu' + \frac{\text{(MD)}}{C}(\nu_0 - \nu') \quad (7)$$

In eq. 7, ν' is the weighted average frequency of the amine which is *not* hydrogen bonded to the N-substituted acetamide and the assumption is made that amine is not a hydrogen donor to chloroform. From eq. 6 and 7, the following equation, which is a modified form of eq. 1 for chloroform as the solvent is obtained

$$\frac{1}{\nu - \nu'} = \frac{1}{K(\nu_0 - \nu')}\frac{1 + K_s(\text{S})}{dx} + \frac{1}{(\nu_0 - \nu')} \quad (8)$$

Since the self-association of amine is very weak, in the low concentration range of amine which we use, x may be taken to be 1, and ν' becomes equal to ν_f. A plot of $1/(\nu - \nu_f)$ vs. $(1 + K_s(\text{S}))/d$ therefore should yield a straight line, from which the values of $(\nu_c - \nu_f)$ and K can be determined separately.

The value of K_s is determined in separate experiments by measuring the chemical shifts of the chloroform proton signal in carbon tetrachloride solutions containing 0.05 M CHCl$_3$ and various amounts of N-substituted acetamide.

Experimental

Materials. *t*-Butylamine and aniline were distilled twice and the fractions boiling at 44 and 184°, respectively, were collected. N-methylacetamide and N,N-dimethylacetamide were treated in the manner previously described.[5] Chloroform was purified by shaking with concentrated sulfuric acid and then distilled water, dried by calcium chloride, distilled, and the fraction boiling at 60° collected. Carbon tetrachloride was Fisher Spectroanalyzed Certified Reagent liquid.

Preparation of Samples. Samples were prepared by the same methods as described previously.[3,5]

P.m.r. Measurements. All of the p.m.r. spectra were obtained with a Varian Associates Model A-60 n.m.r. spectrometer. Chemical shifts of the CH signal in chloroform and the NH$_2$ signal in amine were measured with respect to tetramethylsilane (TMS) used as an internal standard and are quoted as c.p.s. All lines are downfield from TMS. The reported shifts are accurate to 0.3 c.p.s. for chloroform and *t*-butylamine, and 1 c.p.s. for aniline.

Results

(*A*) *Determination of* ν_f. For chloroform hydrogen bonding, the observed proton frequency of 0.05 M chloroform in CCl$_4$, in the absence of N-substituted acetamide, was taken to be ν_f. This is because the self-association of chloroform is very weak: from 36 to $-19°$, the chemical shift of the chloroform proton varied only from 434 to 435 c.p.s. for 0.05 M CHCl$_3$ in carbon tetrachloride. Neat chloroform has a proton signal at 435 c.p.s. at 36°.

The values of ν_f for *t*-butylamine and aniline were determined in the manner described by Takahashi and Li,[5] for 2-propanol. Figure 1 gives plots of ν' vs. temperature, where ν' is the amino proton frequency in *t*-butylamine and aniline in chloroform, with no N-substituted acetamide present. These curves indicate that $\nu_f = 206.5$ and 77 c.p.s. for aniline and *t*-butylamine, respectively, if we assume that for these dilute solutions at temperatures higher than 60°, the amine is a monomer.

Figure 2 gives plots of ν' vs. concentration of the amine in chloroform at 36°. If we assume that the limiting frequency at zero concentration is equal to ν_f, then the data of Figure 2 for aniline also lead to the value $\nu_f = 206.5$ c.p.s., in agreement with that found from the data of Figure 1.

It is seen from Figure 2 that in the concentration region higher than 0.6 M, the amino proton signal shifts to higher field with increasing aniline concentration in chloroform. For *t*-butylamine, the amine
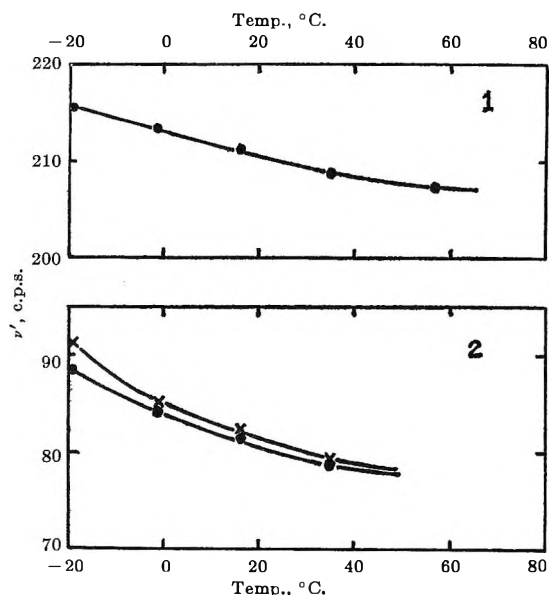
Figure 1. Determination of ν_f. Plots of ν' vs. temperature for solutions of amine in chloroform: curve 1, 0.1 M aniline; curve 2, $\times$, 0.025 M t-butylamine; $\bullet$, 0.1 M t-butylamine.
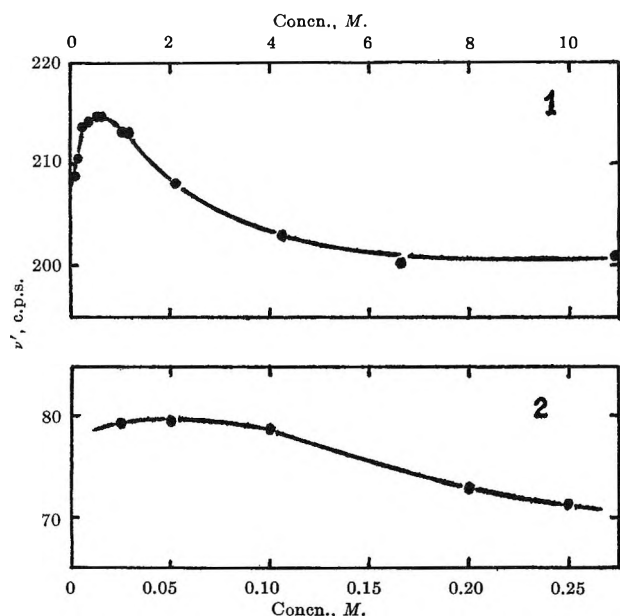
Figure 2. Determination of ν_f. Plots of ν' vs. concentration of amine in chloroform at 36°: curve 1, aniline; curve 2, t-butylamine.

proton signal overlaps with the methyl proton signal at 69 c.p.s., when the concentration is higher than 0.4 M.

(B) Chloroform Hydrogen Bonding to N-Substituted Acetamide. The chemical shifts of the chloroform proton signal in carbon tetrachloride solutions containing 0.05 M chloroform and various amounts of N-

Table I : Chloroform Bonding

To N-Methylacetamide		To N,N-Dimethylacetamide	
d, M	ν, c.p.s.	d, M	ν, c.p.s.
—36°—		—36°—	
0	434.2	0	434.2
0.481	444.1	0.421	452.1
0.511	444.3	0.472	453.7
0.574	445.1	0.588	457.1
0.708	447.0	0.684	459.0
0.946	449.9	0.802	462.3
1.148	452.1	0.976	465.7
1.664	456.7	1.590	473.1
—16°—		—16°—	
0	434.7	0	434.7
0.493	445.1	0.431	455.9
0.523	445.5	0.483	457.7
0.588	446.5	0.602	461.8
0.725	448.4	0.700	463.4
0.969	451.6	0.822	466.1
1.176	454.0	0.999	469.9
1.705	459.1	1.628	478.5
—1°—		—1°—	
0	435.1	0	435.1
0.503	446.3	0.440	459.3
0.534	446.7	0.493	460.0
0.600	447.8	0.614	465.5
0.740	449.9	0.715	467.2
0.989	453.5	0.839	471.1
1.200	456.3	1.020	474.4
1.740	461.6	1.662	481.8
—19°—		—19°—	
0	435.4	0	435.4
0.514	447.9	0.449	463.1
0.545	448.2	0.504	465.2
0.613	449.6	0.627	470.0
0.756	452.0	0.730	471.6
1.010	456.1	0.856	475.5
1.225	459.1	1.041	478.7
1.776	464.7	1.697	486.2

substituted acetamide were determined at various temperatures between —19 and 36°. Table I lists the results obtained. From the data, linear plots of 1/$(\nu - \nu_f)$ vs. 1/d (according to eq. 1) for the temperatures —19 to 36° and linear plots of log K vs. 1/T were obtained. The values of K ($=K_a$), $(\nu_c - \nu_f)$, ΔH, and ΔS for chloroform bonding to N-methylacetamide and N,N-dimethylacetamide in carbon tetrachloride are summarized in Table II.

(C) Hydrogen Bonding between Amine and N-Substituted Acetamide. The chemical shifts of the amine proton signal in chloroform solutions containing 0.05 M t-butylamine or 0.1 M aniline and various

Table II: Thermodynamic Data

	Temp., °C.	K, M^{-1}	$\nu_0 - \nu_f$, c.p.s.	ΔH, kcal./ mole	ΔS, e.u.
Chloroform bonding to	36	0.48	51		
N-methylacetamide	16	0.46	55	+0.4	−0.2
	−1	0.44	61		
	−19	0.42	69		
Chloroform bonding to	36	0.82	70		
N,N-dimethylacetamide	16	0.99	71	−1.1	−3.7
	−1	1.13	73		
	−19	1.34	74		
t-Butylamine bonding to	36	3.9	101		
N-methylacetamide	16	5.1	101	−1.8	−3.0
	−1	6.1	101		
	−19	7.5	101		
Aniline bonding to	36	5.8	48		
N-methylacetamide	16	7.3	49	−1.5	−1.2
	−1	8.3	50		
	−19	10	50		
N,N-Dimethylacetamide	36	6.0	51		
	16	9.9	51	−3.3	−6.9
	−1	14	52		
	−19	21	52		

amounts of N-substituted acetamide were determined at four different temperatures and the results are listed in Table III. From the data, linear plots of $1/(\nu - \nu_f)$ vs. $(1 + K_s(S))/d$ (according to eq. 8) for the temperatures −19 to 36° and linear plots of log K vs. $1/T$ were obtained. The values of K, $(\nu_0 - \nu_f)$, ΔH, and ΔS for t-butylamine bonding to N-methylacetamide and for aniline bonding to N-methylacetamide and N,N-dimethylacetamide, all in chloroform medium, are summarized in Table II.

The chemical shifts of the amino proton signal for t-butylamine bonding to N,N-dimethylacetamide are smaller than for t-butylamine bonding to N-methylacetamide. The errors become larger, and linear plots were not obtained. The t-butylamine–N,N-dimethylacetamide system is therefore omitted from Table II.

Discussion

Klotz and Franzen[6] and Mathur, et al.,[7] have reported on the extensive self-association of N-methylacetamide. The latter authors have given the following evidence that the self-association does not interfere with its hydrogen bonding with 0.05 M benzenethiol: the NH proton frequency of 0.4 M N-methylacetamide in CCl_4 varies by 48 c.p.s. over a temperature range of −17 to 37°, while the value of $(\nu_c - \nu_f)$ is virtually independent of temperature. Our data of Table II show that the values of $(\nu_c - \nu_f)$ for N-methylacetamide

bonding to the amines are independent of temperature, between −19 and 36°, so that we may also state with confidence that the self-association does not interfere with the hydrogen bonding between N-methylacetamide and the amines. Using the same terminology as that used by Mathur, et al.,[7] the hydrogen bonding of N-methylacetamide with the amines may be represented as

$$
\begin{array}{cc}
CH_3 & CH_3 \\
| & | \\
RNH_2 + NH\!-\!O\!=\!C & \rightleftharpoons \\
| & | \\
O\!=\!C & NH\!- \\
| & | \\
CH_3 & CH_3
\end{array}
$$

$$
\begin{array}{cc}
CH_3 & CH_3 \\
| & | \\
NH\!-\!O\!=\!C & \\
| & | \\
RNH_2\!-\!O\!=\!C & NH\!-\!\!-\quad (9) \\
| & | \\
CH_3 & CH_3
\end{array}
$$
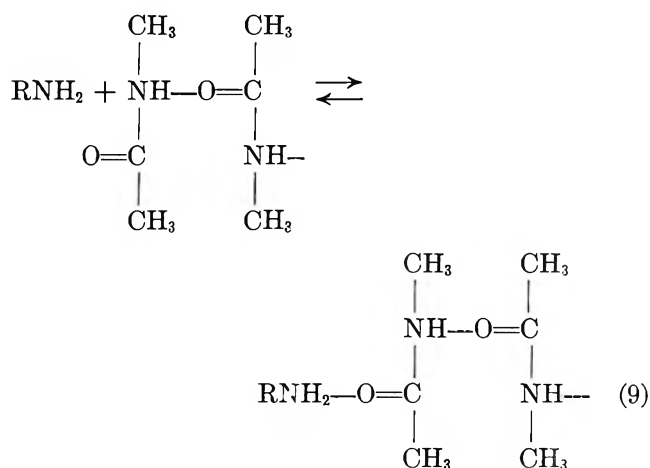
The association constant for aniline bonding to N-methylacetamide is smaller than for phenol bonding to N-methylacetamide ($K = 105$ at 30°)[8] and larger than for benzenethiol bonding to N-methylacetamide ($K = 0.13$ at 37°).[7] This order of association constants is in agreement with the order of the extent of self-association reported by Rao, et al.[9]: phenol > aniline > benzenethiol.

In Figures 1 and 2, the amino proton frequency is no doubt affected by $CHCl_3$ acting as hydrogen donor to the amines. However, since $CHCl_3$ is the solvent and is therefore in large excess, it is our opinion that this effect is constant in low concentrations of amine, so that it is canceled out in the determination of ν_f (for aniline, the lowest concentrations used in Figure 2 are 0.10, 0.14, and 0.22 M). Similarly in Table III, we may also expect that the amine proton frequency would be affected by the presence of N-methylacetamide acting as hydrogen donor to the amines. Again, since the acetamide concentration is much greater than the amine concentration, the effect on the amino proton frequency may be constant and canceled out.

(6) I. M. Klotz and J. S. Franzen, J. Am. Chem. Soc., 84, 3431 (1962).

(7) R. Mathur, S. M. Wang, and N. C. Li, J. Phys. Chem., 68, 2140 (1964).

(8) F. Takahashi and N. C. Li, ibid., 69, 1622 (1965).

(9) B. D. N. Rao, P. Venkateswarlu, A. S. Murthy, and C. N. Rao, Can. J. Chem., 40, 963 (1962).

Table III: Amino Hydrogen Bonding in Chloroform Solvent

t-Butylamine (0.05 M)–N-methyl-acetamide			Aniline (0.1 M)–N-methyl-acetamide			Aniline (0.1 M)–N,N-dimethyl-acetamide		
d, M	(S), M	ν, c.p.s.	d, M	(S), M	ν, c.p.s.	d, M	(S), M	ν, c.p.s.
——36°——			——36°——			——36°——		
0.481	11.63	100.9	0.562	11.45	223.0	0.586	11.30	220.0
0.564	11.51	102.5	0.687	11.30	224.6	0.689	11.24	221.0
0.686	11.40	106.6	0.796	11.21	226.4	0.788	11.02	222
0.958	11.18	115.0	0.916	11.11	228.1	0.964	10.91	224.8
1.382	10.78	122.7	1.125	10.88	230.3	1.157	10.54	227.5
1.761	10.49	132.2	1.816	10.26	237.0	1.577	10.15	232.0
——16°——			——16°——			——16°——		
0.493	11.94	106.2	0.577	11.75	225.8	0.601	11.59	223.6
0.579	11.81	108.5	0.705	11.59	228.0	0.707	11.53	225.2
0.704	11.70	112.6	0.816	11.50	230.6	0.808	11.31	226.5
0.983	11.48	a	0.940	11.40	232.2	0.989	11.20	229.0
1.418	11.06	129.5	1.154	11.17	233.8	1.187	10.81	231.9
1.807	10.76	139.0	1.864	10.53	240.0	1.618	10.42	236.0
——1°——			——1°——			——1°——		
0.504	12.20	110.6	0.589	12.00	228.3	0.614	11.84	226
0.591	12.08	114.5	0.720	11.84	231.4	0.722	11.78	227.8
0.719	11.95	a	0.834	11.74	233.1	0.825	11.55	230.0
1.004	11.71	a	0.960	11.64	234.6	1.010	11.43	231.8
1.448	11.30	134.5	1.179	11.40	237.3	1.212	11.04	235.1
1.845	10.99	144.7	1.903	10.75	244.2	1.652	10.64	239.7
——19°——			——19°——			——19°——		
0.515	12.45	116.1	0.602	12.26	230.1	0.627	12.09	228.8
0.604	12.31	a	0.736	12.09	233.8	0.738	12.03	230.8
0.734	12.20	a	0.852	12.00	235.7	0.843	11.80	232.9
1.026	11.96	133.8	0.981	11.89	237.6	1.032	11.68	235.0
1.480	11.52	141	1.205	11.65	239.4	1.238	11.28	238.0
1.886	11.21	151.5	1.945	10.99	246.8	1.688	10.87	245.6

a Overlap with the CH₃CO proton signal in N-methylacetamide.

From the values of K and ΔH listed in Table II, it is seen that toward chloroform and aniline, N,N-dimethylacetamide is a stronger electron donor than N-methylacetamide. This is as expected because the carbonyl group in the disubstituted acetamide is more nucleophilic than the monosubstituted acetamide.

Takahashi and Li[8] have reported that toward 2,6-di-t-butylphenol, 2-methyl-6-t-butylphenol, 2-t-butylphenol, and phenol as hydrogen donors, N,N-dimethylacetamide is in each case a stronger electron donor than N-methylacetamide.

Our experiments show that the chemical shifts of the amino proton signal for t-butylamine bonding to dimethylacetamide are smaller than for t-butylamine bonding to N-methylacetamide. Although dimethylacetamide is the stronger electron donor, the smaller shift is not surprising. Several investigators[3,10] have already commented on the observations that for a given hydrogen donor bonding to various hydrogen acceptors, the largest value of $-\Delta H$ may correlate with the smallest value of chemical shift or infrared frequency shift.

Although hydrogen bonding by amine is a very important consideration, only a few papers have been concerned with amine hydrogen-bonding studies with p.m.r. and of these,[9,11-13] no numerical value for the association constant of an amine bonding to an electron donor has been given.

It is seen from Figure 2 that for aniline in chloroform, the amino proton signal shifts upfield with decrease in concentration of aniline in the concentration region below 0.6 M and with increase in concentration of aniline above 0.6 M. The same type of concentration dependence *seems* to be exhibited by t-butylamine in Figure 2 and is reminiscent of the solvent-dilution shift of the hydroxyl proton resonance signal of acetic acid in 1,1-dichloroethane and in carbon tetrachloride.[14] Because of the limited number of p.m.r. data available for amine systems, we do not attempt to explain this feature at present.

(10) R. West, D. L. Powell, L. S. Whatley, M. K. T. Lee, and P. von R. Schleyer, J. Am. Chem. Soc., 84, 3221 (1962).

(11) J. Feeney and L. H. Sutcliffe, J. Chem. Soc., 1123 (1962).

(12) J. V. Hatton and R. E. Richards, Mol. Phys., 5, 139 (1962).

(13) J. R. Crook and K. Schug, J. Am. Chem. Soc., 86, 4271 (1964).

(14) L. W. Reeves and W. C. Schneider, Trans. Faraday Soc., 54, 314 (1958).

Anion Exchange of Metal Complexes. XVI.[1] Chloride Complexes of Zinc, Cadmium, and Mercury in Anhydrous Ethanol

by J. Penciner, I. Eliezer, and Y. Marcus

Radiochemistry Department, Soreq Nuclear Research Center, Israel Atomic Energy Commission, Yavne, Israel
(Received February 23, 1965)

Measurements have been carried out of the distribution of zinc, cadmium, and mercury tracers between Dowex 1-X8 anion exchanger and anhydrous ethanolic solutions of lithium chloride and hydrogen chloride. The invasion of the resin by electrolyte has been determined. The results can be explained in terms of uncharged complexes predominating in the resin phase and ion pairs between lithium or hydrogen cations and complex anions in the solution phase.

Introduction

The previous publications in this series have dealt with ion exchange in aqueous solutions. It is of interest to extend the original theoretical treatment[2] to nonaqueous solutions in an attempt to explain the changes in the anion-exchange behavior of metals (such as enhanced uptake and greater selectivity) with change of solvent.[3] A large body of data exists on the distribution of metal ions between anion exchangers and mixed organic–aqueous solvents.[4,5] However, little is known about the behavior in anhydrous organic solvents. This behavior should be easier to explain, because of the absence of preferential solvation effects, which are important in mixed solvents but not quantitatively known. An important factor in this behavior is the dielectric constant of the solvent. It should be easier to interpret results in mixed solvents when the effects of this factor studied in a pure nonaqueous solvent are known.

Ethanol was chosen as the solvent since it provides a drastic lowering of the dielectric constant, yet, like water, it is polar and dissolves electrolytes to some extent. Ethanol has been extensively used as a component of mixed solvents for anion-exchange studies[5] and is easily available and purified.

It was decided to study the chloride complexes of the group II-B metals because their behavior in aqueous solution is reasonably well known.[6,7] The same general methods of measuring the distribution of tracer metal ions between anion exchanger and solutions were employed.

Experimental Section

Materials. Radioactive tracers ^{65}Zn (245 days), ^{115}Cd (2.3 days), and ^{203}Hg (47 days) were obtained either from O.R.N.L, or from the Isotope Production Unit of the Soreq Nuclear Research Center.

Ethanol (Fluka Puriss grade 99.8%) was dried by distillation from magnesium ethanolate.[8] The product, checked by Karl Fischer titration, contained from 0.01 to 0.06 wt. % water.

Lithium chloride was Baker Analyzed reagent and was used without further purification, because it was sufficiently dry and its ethanolic solutions did not contain more than 0.06 wt. % water.

Hydrogen chloride gas (Matheson) was passed through concentrated sulfuric acid to ensure removal of water.

The anion-exchange resin was Dowex 1-X8 (Biorad

(1) Previous papers in series: XIV. Y. Marcus and M. Givon, *J. Phys. Chem.*, **68**, 2230 (1964); XV. Y. Marcus, *J. Inorg. Nucl. Chem.*, in press. Presented in part at 1st and 2nd Meetings of the Israel Chemical Society, Beersheva, 1963, and Jerusalem, 1964.

(2) Y. Marcus and C. D. Coryell, *Bull. Res. Council Israel*, **A8**, 1 (1959).

(3) F. Helfferich, "Ion Exchange," McGraw-Hill Book Co., Inc., New York, N. Y., 1962, Chapter 10.

(4) (a) J. Korkisch and G. E. Janauer, *Talanta*, **9**, 957 (1962); (b) D. J. Pietrzyk, Ph.D. Thesis, Iowa State University, 1960; J. S. Fritz and D. J. Pietrzyk, *Talanta*, **8**, 143 (1961).

(5) L. W. Marple, *J. Inorg. Nucl. Chem.*, **26**, 635, 643 (1964).

(6) Y. Marcus and D. Maydan, *J. Phys. Chem.*, **67**, 979 (1963).

(7) Y. Marcus and I. Eliezer, *J. Inorg. Nucl. Chem.*, **25**, 867 (1963).

(8) A. I. Vogel, "Textbook of Practical Organic Chemistry," 3rd Ed., Longmans, Green and Co., London, 1956, p. 167.

AG) 100–200 mesh in the chloride form. It was conditioned by having passed through it alternately solutions of 3 M NaOH and 3 M HCl in three cycles and finally by being washed with distilled water and ethanol and dried by drawing air through it. The water content of this air-dried resin was 0.10–0.15 g. of water/g. of resin.

Procedure

A batch technique was used, and care was taken to keep conditions as anhydrous as possible.

Distribution Measurements. a. LiCl. Samples of resin (0.1 g.), salt, and dry ethanol (20–30 g.) containing ca. 10^{-5} M tracer metal were weighed into 100-ml. glass-stoppered conical flasks. These were shaken for 2 days at 25–27°. This period has previously been found adequate for equilibrium to be reached in ethanol solutions.[9] The solutions were then quickly filtered through glass wool, and samples were taken for counting[6,7] and for determination of the equilibrium concentration of the electrolyte in the solution. The lithium chloride concentrations in the solutions were determined by Mohr titration.

b. HCl. Dried hydrogen chloride was bubbled through Dry Ice cooled ethanol. In order to obtain a concentrated solution (8–9 m), it was necessary to continue the bubbling for 15–20 hr. Two delivery flasks were used, one containing dry ethanol and the other a solution of HCl in ethanol. To each of these was added a portion of the tracer metal, and the volumes were adjusted so that the concentrations of the metal in the flasks were equal to within 1%, as checked by counting samples. Resin samples (0.1 g.) were weighed into the 100-ml. glass-stoppered flasks and then varying amounts of the two alcoholic solutions were added to a total solution weight of about 30 g. Equilibration and separation were carried out as in the LiCl experiments. The electrolyte concentration in the solutions was determined by titration with standard base.

Invasion Measurements. Since electrolyte invasion of the resin is known[2] to affect the metal distribution, invasion measurements were performed.

Equilibrations were carried out as in the experiments described above, except that no radioactive tracers were present. Upon attainment of equilibrium, the contents of the flasks were filtered through glass wool in weighed centrifuge tubes. The tubes were centrifuged according to a standard procedure which was found to yield a constant weight and were weighed to determine the amount of resin in each. In one series of measurements, all the chloride in the resin was eluted with 50 ml. of 3 M NaNO₃. In other series, only the invading excess electrolyte was eluted by washing with distilled

water. The results from both series were in agreement. The chloride from the resin and that in an aliquot of the equilibrium solution were determined by Mohr titration.

Calculations. The distribution coefficients D were calculated from the relation

$$D = \frac{A_0 - A}{A} \times \frac{\text{grams of solvent}}{\text{grams of air-dried resin}} \quad (1)$$

where A is the measured count rate of a particular sample and A_0 is the count rate of a sample from a solution without resin. No correction of A_0 for resin swelling was necessary, because of the large ratios of grams of solvent/grams of resin.

From the invasion data the effective ligand activity in the resin $\bar{a}$ can be found by the equation

$$\log \bar{a} = \log a + \frac{1}{2} \log \frac{(\text{Cl})_{\text{tot}}}{(\text{Cl})_{\text{inv}}} \quad (2)$$

where a is the mean ionic activity of the bulk electrolyte in solution, $a = m\gamma_{\pm}$, $(\text{Cl})_{\text{tot}}$ = total chloride molality in the resin phase, and $(\text{Cl})_{\text{inv}}$ = molality of excess electrolyte in the resin phase. Activity coefficients $\gamma_{\pm}$ for HCl in ethanol were obtained from Conway.[10]

Results

a. HCl. The invasion data for hydrogen chloride are shown in Figure 1, as log $\bar{a}$ vs. log a, calculated from eq. 2. It was expected[11] that $\bar{a}$ would reach a constant limit as a tends to low values. However, as in aqueous solutions, $\bar{a}$ is seen to decrease continuously. This behavior has been discussed by Freeman.[11]

In Figure 2 are plotted the distribution data for zinc, cadmium, and mercury in hydrogen chloride solutions. The figure shows the distribution coefficients for cadmium to be about an order of magnitude lower than those for zinc and mercury which are similar. In aqueous solutions, on the other hand, the order is $D_{\text{Hg}} > D_{\text{Cd}} > D_{\text{Zn}}$ at least up to 5 M HCl.[7,12] It is also seen from Figure 2 that at low hydrogen chloride concentration there is an extended region where the distribution coefficients do not vary appreciably with a, contrary to their behavior in aqueous solutions.[7,12]

b. LiCl. In Figure 3 are given distribution data for zinc, cadmium, and mercury in lithium chloride solutions. The values are plotted against log m rather than against log a because no activity coefficients

(9) D. Maydan, Ph.D. Thesis, Hebrew University, Jerusalem, 1962.

(10) B. E. Conway, "Electrochemical Data," Elsevier Publishing Co., Amsterdam, 1952.

(11) D. H. Freeman, *J. Phys. Chem.*, **64**, 1048 (1960).

(12) K. A. Kraus and F. Nelson, *Proc. Intern. Conf. Peaceful Uses At. Energy, Geneva, 1955*, **7**, 113 (1956).
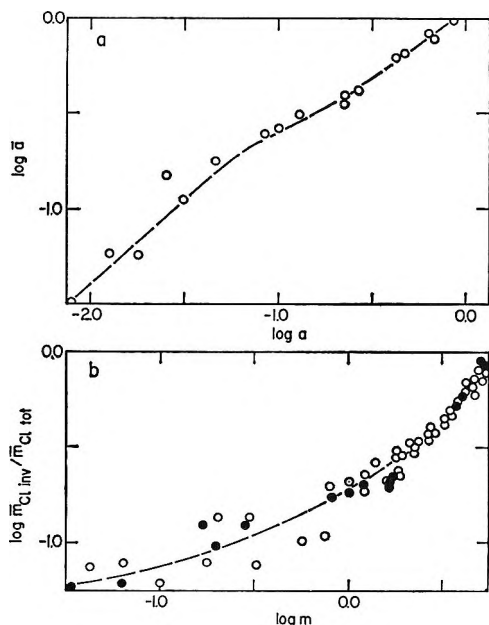
Figure 1. Resin invasion from ethanol. a: log $\bar{a}$ against log a for HCl. b: log $(m_{Cl,inv}/m_{Cl,tot})$ against log m for HCl (●) and LiCl (○).
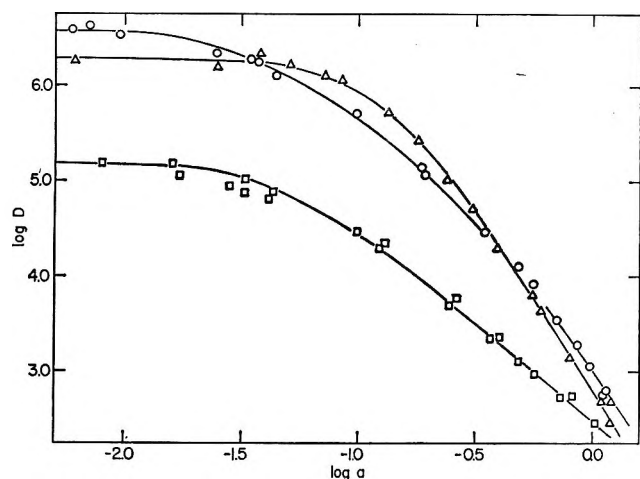
Figure 2. Anion-exchange distribution of group II-B metals from ethanolic HCl solutions: log D against log a, for Zn (○), Cd (□), and Hg (△). Curves are calculated from eq. 10a, 10b, and 10c, respectively.

for lithium chloride in ethanol are available. The trends shown in the figure are qualitatively similar to those obtained in hydrogen chloride solutions (shown by the dashed lines). Invasion data for lithium chloride are shown in Figure 1b.

Discussion

The present anion-exchange distribution system involves a solvent of a dielectric constant (ϵ 24), much lower than that of water (ϵ 78). In such a solvent,
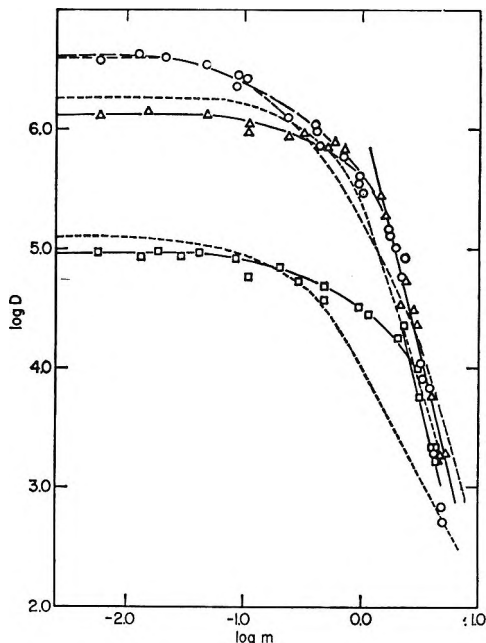
Figure 3. Anion-exchange distribution curves, log D against log m, for ethanolic HCl solutions (– – – –) and LiCl solutions [Zn (○), Cd (□), and Hg (△)]. The straight lines represent the final slope of -4.0.

ions would not exist separately, but rather as ion pairs. Neutral complex species, such as MCl_2 in the present case, would be favored over charged complexes. Hence, the species that ought to be considered in the ethanolic hydrogen chloride solution are H^+Cl^-, MCl_2, $H^+MCl_3^-$, $H^+{}_2MCl_4{}^{2-}$, ..., and the same species could also occur in the resin phase, where they will be designated with a bar over the symbols.

The following reactions will occur in the solution phase

$$MCl_2 + iH^+Cl^- \rightleftharpoons H^+{}_iMCl_{2+i}{}^{i-} \qquad (3)$$
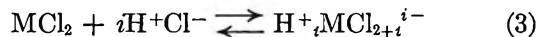
with an equilibrium constant β_i defined by

$$(H^+{}_iMCl_{2+i}{}^{i-}) = \beta_i a_{MCl_2} a^{2i} \gamma_{\pm i}{}^{-(1+i)} \qquad (4)$$

where parentheses designate the molal concentration of the enclosed species, $\gamma_{\pm i} = \gamma_{\pm H^+{}_iMCl_{4+i}{}^{i-}}$, and $a = m_{HCl}\gamma_{\pm HCl}$ as before. Similar reactions could occur in the resin phase. The distribution coefficient of tracer metal will then be given by

$$D = \frac{\overline{(MCl_2)} + \overline{(H^+MCl_3^-)} + \cdots}{(MCl_2) + (H^+MCl_3^-) + \cdots} =$$

$$\frac{\bar{a}_{MCl_2} \sum_{i=0} \bar{\beta}_i \bar{\gamma}_{\pm i}{}^{-1} \bar{a}^{2i}}{a_{MCl_2} \sum_{i=0} \beta_i \gamma_{\pm i}{}^{-1} a^{2i}} \qquad (5)$$

If the same standard states are used for both phases, $\bar{a}_{MCl_2} = a_{MCl_2}$, so that

$$D = \sum_{i=0} \bar{\beta}_i \gamma_{\pm i}^{-1} \bar{a}^{2i} / \sum_{i=0} \beta_i \gamma_{\pm i}^{-1} a^{2i} \qquad (6)$$

The value of D can remain constant for an extended region of a as observed experimentally at low a values only if terms with $\bar{\beta}_i$ for $i > 0$ are zero since d log $\bar{a}$/d log a is finite (Figure 1). In this region also, terms with $\beta_i a^{2i}$ in the solution phase are negligible compared with unity. Therefore, all the terms in eq. 6 with $i > 0$ become zero at low a, while for $i = 0$ the numerator reduces to $\bar{\gamma}_0^{-1}$ and the denominator to γ_0^{-1}, so that D becomes

$$D = \gamma_0 / \bar{\gamma}_0 = K_0 \qquad (7)$$

Thus, as in liquid–liquid partition systems, a constant Nernst distribution function is observed, equal to the inverse ratio of the activity coefficients of the partitioning species.[13]

It should be emphasized that, contrary to the behavior in aqueous solutions, where the exchange of anions is the important feature, in the present case the distribution of an uncharged species between two phases without further interactions is considered the main reaction. That such a distribution reaction is of importance in equilibria involving ion exchangers and organic solvents has been noted by other authors.[14] It is considered to be the main distinction between anion exchange in aqueous and nonaqueous media, and also the explanation of phenomena such as abnormal loading.[4a]

At higher hydrogen chloride concentrations, the following two possibilities can be considered: (1) $\overline{MCl_2}$ remains the predominating resin species, as at low concentrations; (2) some other species, $\overline{H^+_p\text{-}MCl_{2+p}{}^{p^-}}$, predominates. According to the first possibility, $\bar{\beta}_i = 0$ for $i > 0$. Therefore log D may be written as

$$\log D = \log K_0 - \log \sum_{i=0} \beta_i^* a^{2i} \qquad (8)$$

where $\beta_i^* = \beta_i \gamma_{\pm i}^{-1}$. Assuming $\gamma_{\pm i}$ not to vary appreciably with a over the region where species $H^+_{i}\text{-}MCl_{2+i}{}^{i^-}$ is important and K_0 to remain constant, as was done for aqueous systems,[2] the slope of the distribution curve is given by

$$\text{d log } D/\text{d log } a = 2\bar{i} \qquad (9)$$

where $\bar{i}$ is the average value of i in a given region of a values. The slopes of the experimental curves as a reaches high values tend to approximately -4 for mercury and zinc, and -2 for cadmium. The data

may be fitted (Figure 2) to curves calculated from the expressions

$$\log D_{Zn} = 6.60 \pm 0.10 - \log (1 + 10^{2.92\pm0.05} a^2 + 10^{6.40\pm0.10} a^4) \qquad (10a)$$

$$\log D_{Cd} = 5.20 \pm 0.10 - \log (1 + 10^{2.69\pm0.04} a^2) \qquad (10b)$$

$$\log D_{Hg} = 6.30 \pm 0.10 - \log (1 + 10^{2.00\pm0.05} a^2 + 10^{5.50\pm0.06} a^4) \qquad (10c)$$

The species predominating in the resin phase is therefore $\overline{MCl_2}$ for all three metals, while in the solution phase there is a transition from MCl_2 at low hydrogen chloride concentration to $H^+MCl_3^-$ at moderate concentrations and up to $H^+_2MCl_4{}^{2-}$ in the cases of zinc and mercury at high concentrations.

According to the other possibility, namely, that $\overline{H^+_p\text{-}MCl_{2+p}{}^{p^-}}$ predominates in the resin, log D will be written, by analogy with the treatment of aqueous systems,[2] as

$$\log D = \log K_0^* + 2p \log \bar{a} - \log \sum_{i=0} \beta_i^* a^{2i} \qquad (11)$$

where $K_0^* = K_0 \bar{\beta}_p \bar{\gamma}_{\pm p}^{-1}$ is assumed to be a constant. Differentiation of eq. 11 leads to the slopes

$$\text{d log } D/\text{d log } a = 2p \text{ d log } \bar{a}/\text{d log } a - 2\bar{i} \qquad (12)$$

At high a values d log $\bar{a}$/d log $a \simeq 0.8$ while d log D/d log $a \simeq -4$ (for Zn and Hg) or -2 (for Cd), that is $\bar{i} \simeq 4 + 1.6p$ (for Zn and Hg) or $2 + 1.6p$ (for Cd). For zinc and mercury it is seen that nonzero values of p lead to unreasonably high values of the degree of complexation (i.e., species such as $H^+_3MCl_5{}^{3-}$ for $p = 1$). Therefore, for these two elements possibility 1 considered above with $p = 0$, i.e., $\overline{MCl_2}$ predominating, is favored. For cadmium, however, the possibility of a species $H^+CdCl_3^-$ being important cannot be excluded. In this case, the species $H^+_2CdCl_4{}^{2-}$ becomes important in the solution when a reaches high values. The experimental data do not permit a decision between the two possibilities.

The discussion of the distribution data for lithium chloride solutions (Figure 3) is hampered by the lack of activity data for lithium chloride in ethanol. To circumvent this difficulty, it was attempted to employ Harned's second rule,[15] according to which, in mixed solvents

(13) W. Nernst, Z. physik. Chem., 8, 110 (1891); B. Milicevic, Helv. Chim. Acta, 46, 1466 (1963).

(14) For example: L. I. Katzin and E. Gebert, J. Am. Chem. Soc., 75, 801 (1953); M. Lederer and F. Rallo, J. Chromatog., 7, 552 (1962).

(15) H. S. Harned, J. Phys. Chem., 66, 589 (1962).

$$\gamma_{\pm LiCl(solvent)} = \gamma_{\pm HCl(solvent)}\gamma_{\pm LiCl(water)}/\gamma_{\pm HCl(water)}$$

$$(13)$$

and which was verified up to 20% methanol in water. Values of a for lithium chloride in ethanol were calculated from eq. 13 and used in plots of log D vs. log a. The slopes at high a values, however, had unreasonably high negative values, about -6. Even with $p = 0$, i.e., $\overline{MCl_2}$ predominating, such slopes correspond to unlikely species (e.g., $H^+{}_3MCl_5{}^{3-}$) in solution.

Since the use of Harned's second rule leads to difficulties, another approach was sought. It is observed that in hydrogen chloride solutions a is approximately proportional to m above 1.5 m. It is assumed as an approximation that the same holds for lithium chloride solutions. Hence, the slopes of the curves in Figure 3 at high m, which are ca. -4, may be interpreted as the analogous slopes in Figure 2, namely, indicating the presence of species $Li^+{}_2MCl_4{}^{2-}$ in solution. This seems reasonable since no difference in the ion-pairing properties of the solvated lithium and hydrogen cations with the complex anions is expected.

Examination of Figure 3 shows the behavior of lithium and hydrogen chloride to be fairly similar, contrary to what is found in aqueous solutions.[6,7] The difference in behavior in aqueous solutions has been ascribed to a number of causes. Strong arguments have been put forward attributing the difference to the much more extensive ion pairing in the resin of hydrogen chloride as compared with lithium chloride.[16,17] The very low dielectric constant obtaining in the resin saturated with ethanol would lead to as complete ion pairing of the latter electrolyte as of the former. Therefore, no difference in behavior should be expected. This point has already been discussed by Horne[16] for mixed aqueous–ethanol solutions.

For both lithium and hydrogen chloride solutions, a salient feature is the considerably higher distribution coefficients of zinc and mercury as compared with cadmium. A possible explanation for this can be sought in the less covalent nature of the cadmium chloride.[18] This would lead to its having a lower distribution coefficient because of its preferring the more polar solution phase to that of the resin, which has a lower dielectric constant, as discussed above and also by other authors.[9,16] The lower tendency to covalency of the cadmium halides is also in line with the assumption of the existence of $H^+CdCl_3{}^-$ in the resin and the non-existence of such species for mercury and zinc.

Acknowledgment. The technical help of Mrs. N. Bauman and of Miss N. Abel in carrying out the experiments is gratefully acknowledged.

(16) R. A. Horne, *J. Phys. Chem.*, **61**, 1651 (1957); R. A. Horne, R. H. Holm, and M. D. Myers, *ibid.*, **61**, 1656 (1957).

(17) B. Chu and R. M. Diamond, *ibid.*, **63**, 2021 (1959).

(18) W. Huckel, "Structural Chemistry of Inorganic Compounds," Elsevier Publishing Co., Amsterdam, 1951, pp. 335, 527, 611, 925.

Thermodynamic Data from Fluorescence Spectra. I.

The System Phenol–Acetate[1]

by A. Young Moon, Douglas C. Poland, and Harold A. Scheraga

Department of Chemistry, Cornell University, Ithaca, New York *(Received February 26, 1965)*

This paper demonstrates how fluorescence measurements may be used to determine association constants, K_{assoc}, for weak complexes, involving hydrogen and/or hydrophobic bonds. If one member of the complex fluoresces, when free, and the other member quenches the fluorescence, upon formation of the complex, then the technique of concentration quenching of fluorescence will provide a value of K_{assoc} from a quantitative measurement of the deviations from ideal or Stern–Volmer quenching behavior. Data are given for the system phenol–acetate, with the results that K_{assoc} is approximately $0.5 \ M^{-1}$ and its variation with temperature over the range 10 to 40° gives a temperature-independent enthalpy of association, ΔH, of about -400 ± 400 cal./mole. Independent measurement of K_{assoc} using the technique of ultraviolet difference spectra gives essentially the same results. From a consideration of ΔH, it is suggested that it is composed of two compensating contributions, a negative one from the intermolecular hydrogen bond and a positive one from an intermolecular hydrophobic bond in the formation of the complex. Further interpretation must await the results of experiments on the quenching of phenol fluorescence by the other members of the series of carboxylic acids. The magnitude of K_{assoc} suggests that analogous tyrosyl–carboxylate ion interactions (together with hydrophobic bonding) are potentially important in stabilizing protein structure. Discussion and quantitative interpretation are given of literature data on analogous studies of polyamino acid copolymers.

Introduction

Noncovalent bonds play an important role in maintaining the three-dimensional folding of a protein molecule. Nevertheless, even for model systems, it has been difficult to obtain reliable thermodynamic parameters for these noncovalent interactions over a range of temperatures. Schellman[2] interpreted data on the osmotic pressure and heat of dilution of aqueous urea solutions (assuming that the departure from ideality could be attributed to intermolecular hydrogen bonding), obtaining a value for ΔH, the heat of formation of the urea–urea hydrogen bond, of -1.5 kcal./mole at 25°. These calculations were recently extended to several temperatures,[3] with the result that ΔH varies very little, becoming slightly more positive with increasing temperature. Klotz and Franzen,[4] using the technique of near-infrared spectrophotometry, obtained a value close to zero for the heat of formation of the N-methylacetamide dimer; however, this value

may be the resultant of both hydrogen and hydrophobic bonding.[5] Based on titration data for formic acid in aqueous 3 M NaCl, Schrier, *et al.*,[6] computed a value of 0 ± 1 kcal./mole for the heat of formation of the formic acid dimer; these workers used this value, together with literature data for dimer formation in higher homologs, to obtain values of the free energy of formation of hydrophobic bonds between the nonpolar

(1) This work was supported by a research grant (HE-01662) from the National Heart Institute, National Institutes of Health, Public Health Service, and by a research grant (GB-2238) from the National Science Foundation.

(2) J. A. Schellman, *Compt. rend. trav. lab. Carlsberg*, 29, 223 (1955).

(3) G. C. Kresheck and H. A. Scheraga, *J. Phys. Chem.*, 69, 1704 (1965).

(4) I. M. Klotz and J. S. Franzen, *J. Am. Chem. Soc.*, 84, 3461 (1962).

(5) G. Némethy and H. A. Scheraga, *J. Phys. Chem.*, 66, 1773 (1962).

(6) E. E. Schrier, M. Pottle, and H. A. Scheraga, *J. Am. Chem. Soc.*, 86, 3444 (1964).

portions of these dimers, with good agreement with theoretical values.[5] Derivation of thermodynamic data for water from a statistical mechanical theory led to the value of -1.32 kcal./mole for the heat of formation of the water–water hydrogen bond in the liquid.[7] An even higher value was obtained for the internal hydrogen bond in salicylic acid based on ultraviolet difference spectra data.[8]

The above examples illustrate the divergence in values reported for the heat of formation of the hydrogen bond. These differences between various systems may be real. On the other hand, they may arise because of the following difficulties inherent in the methods used to determine ΔH. (1) Since hydrogen and hydrophobic bonds are relatively weak (ΔH being of the order of 1 kcal./mole) and association is accompanied by a large loss of translational entropy, high concentrations (of the order of 2 M) are required to produce a measurable degree of association; at such high concentrations the assumption that activity coefficients are unity is a very poor one. (2) Since the hydrogen bond is weak, it produces only a small perturbation in the system; e.g., it leads to only a very small change in the absorption coefficient of the bonded chromophore or in the infrared stretching frequency. Thus, in obtaining thermodynamic data for hydrogen bond formation from ultraviolet absorption, infrared absorption, or titration curves, one is utilizing these techniques close to the limit of their accuracy.

This paper will describe a method for obtaining equilibrium constants for association as a function of temperature in the phenol–acetate system; it is based on the measurement of the intensity of fluorescence. While not overcoming all the difficulties mentioned above, this method appears able to provide results which approach the precision necessary for testing the validity of presently employed concepts of protein structure.

Fluorescence of Associating Systems

Suppose a chromophore has an intensity of fluorescence I_0, in the absence of added quencher. Then, if the quenching action is by collisional processes, the intensity of fluorescence, I, in the presence of quencher concentration [Q], is given by the Stern–Volmer[9] relation

$$\frac{I_0}{I} - 1 = k_q[Q] \tag{1}$$

where k_q is the quenching constant and is equal to the product of the mean radiative lifetime of the excited state in the absence of the particular quenching process and the bimolecular rate constant for collisional quenching.

In an extensive study of the fluorescence of the aromatic amino acids that occur in proteins and of the simple analogs of these chromophores, White[10] found that the fluorescence of phenol (an analog of tyrosine) is quenched by various small molecules; in particular, carboxylate ion is a very strong quencher. White reported that the fluorescence of the phenol–carboxylate ion system obeyed eq. 1; i.e., the decrease in the intensity of phenol fluorescence upon an increase in the concentration of carboxylate ion was adequately explained by collisional quenching.

However, many systems do not obey the Stern–Volmer relation. Boaz and Rollefson[11] were able to explain deviations from the Stern–Volmer equation for inorganic systems by postulating either the association of quencher with chromophore or the self-association of the quenchers. If current concepts of noncovalent bonds are correct, there should be an association of the carboxylate ion with phenol but no self-association of carboxylate ions or phenol since, in the first case, both monomers are negatively charged and, in the second case, the concentration is very small. Using an argument completely analogous to that of Boaz and Rollefson, we can obtain a modified Stern–Volmer relation and thus have a basis for testing quantitatively the aforementioned prediction.

If the chromophore and quencher do associate by the reaction

$$F + Q \rightleftharpoons F \cdots Q \tag{2}$$
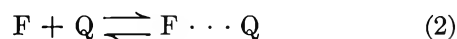
then the appropriate association constant would be

$$K_{assoc} = \frac{[F \cdots Q]}{[F][Q]} \tag{3}$$

In eq. 3, we have used concentrations to replace activities for the following reasons. (1) The concentration of F is very small, of the order of 10^{-4} M. (2) The concentration of Q is less than 0.4 M. If Q is charged, then F$\cdots$Q will also be charged, and the electrostatic part of the activity coefficients will largely cancel. (3) The only source of nonideality is thus attributable to association, which we are considering here explicitly.

If F and Q are associated, then the F molecules in the complex are always in a position to be quenched

(7) G. Némethy and H. A. Scheraga, J. Chem. Phys., 36, 3382 (1962).

(8) J. Hermans, Jr., S. J. Leach, and H. A. Scheraga, J. Am. Chem. Soc., 85, 1390 (1963).

(9) O. Stern and M. Volmer, Physik. Z., 20, 183 (1919).

(10) A. White, Biochem. J., 71, 217 (1959); Ph.D. Thesis, University of Sheffield, 1960.

(11) H. Boaz and G. K. Rollefson, J. Am. Chem. Soc., 72, 3435 (1950).

immediately. Hence, the association constant corresponds to the association of quencher and ground-state chromophore. Using eq. 3, we may express the fraction of chromophore that is free by

$$\frac{[F]}{[F] + [F \cdots Q]} = \frac{1}{1 + K_{assoc}[Q]} = \binom{\text{probability of a}}{\text{chromophore being free}} \quad (4)$$

In the absence of association, the intensity of fluorescence, I, is given by eq. 1 in the following form (involving only collisional quenching)

$$I = I_0 \frac{1}{1 + k_q[Q]} = I_0 \begin{pmatrix} \text{probability of a free} \\ \text{chromophore not being} \\ \text{quenched by collision} \end{pmatrix} \quad (5)$$

When both association and collision are possible, then the intensity of fluorescence is

$$I = I_0 \binom{\text{probability of a}}{\text{chromophore being free}} \times \begin{pmatrix} \text{probability of a free} \\ \text{chromophore not being} \\ \text{quenched by collision} \end{pmatrix} \quad (6)$$

which, upon substitution of the expressions in eq. 4 and 5, gives

$$I = I_0 \left(\frac{1}{1 + k_q[Q]}\right)\left(\frac{1}{1 + K_{assoc}[Q]}\right) \quad (7)$$

Upon rearrangement, eq. 7 becomes

$$\frac{\frac{I_0}{I} - 1}{[Q]} = (k_q + K_{assoc}) + (k_q K_{assoc})[Q] \quad (8)$$

The [Q] in eq. 8 represents the concentration of free quencher. If $[Q] \gg [F]$, as is the case in the experiments to be reported here, then [Q] may be identified with the total concentration of quencher.

Hence, if one measures the fluorescence of a chromophore (e.g., phenol) as a function of the concentration of quencher (e.g., carboxylate ion) and plots the data according to eq. 8, one should obtain a straight line with a slope of $k_q K_{assoc}$ and an intercept of $(k_q + K_{assoc})$, thereby determining both k_q and K_{assoc}. A plot according to eq. 8 is a more sensitive test of deviations from the Stern–Volmer relation than is one according to eq. 1. If the experiments are carried out at several temperatures, it is possible to evaluate the enthalpy of association and obtain all the thermodynamic parameters for the association process as well as the activation energy for collisional quenching.

Experimental work was carried out to test the validity of eq. 8, which is based on hydrogen bond formation between compounds such as phenol and acetate, the analog of the tyrosyl–carboxyl hydrogen bond which may be involved in protein molecules. For comparison purposes, ultraviolet difference spectra measurements were made on the same system, in order to verify that the fluorescence method does indeed lead to a correct association constant.

Experimental

Material and Solutions. All materials used were Mallinckrodt reagent grade. Anhydrous sodium acetate was dried at 110° overnight in an oven before use, and its purity was found to be 99.6% by potentiometric titration of a 0.02 M solution from pH 1.7 to 11.0.

Stock solutions of phenol and sodium acetate were prepared by weighing out crystalline phenol into a 1000-ml. volumetric flask for fluorescence measurements and into a 100-ml. volumetric flask for ultraviolet difference spectra measurements, and anhydrous sodium acetate into a 100-ml. volumetric flask, and by dissolving them with deionized water to volume to give concentrations of 8×10^{-4} M, 6.4×10^{-3} M, and 2.0 M, respectively.

For the fluorescence experiments the phenol concentration was 2×10^{-4} M, which lies within the range in which there is a linear dependence of fluorescence intensity on the concentration. The sample solution was prepared by pipetting 25 ml. of the 8×10^{-4} M phenol stock solution into a 100-ml. volumetric flask, adding the desired amount of quencher with a pipette, and bringing the solution to volume with deionized water. The reference solution was prepared similarly, but without quencher. The solutions were kept approximately neutral by previous adjustment of the pH of the stock solution of acetate to pH 7.0 with 1 N HCl, using a Beckman pH meter, and the ionic strength at 0.4 M by addition of the appropriate amount of sodium chloride. The prepared solutions were thermally equilibrated to the desired temperature before each run.

For ultraviolet difference spectra measurements the sample solution was prepared by pipetting 1 ml. of the 6.4×10^{-3} M phenol stock solution into a 10-ml. volumetric flask, adding the desired amount of sodium acetate solution, previously adjusted to pH 7.0 with 1 N HCl, using a Beckman pH meter, and bringing the solution to volume with deionized water. In order to avoid discrepancies in concentration, the same pipet and volumetric flask were used in the preparation of all of the solutions.

Fluorescence Measurements. The measurements of fluorescence intensity were made with an Aminco-Keir (Model No. 4-8201) spectrofluorimeter, having two grating monochromators which permitted the selection of excitation and emission wave lengths; spectra were recorded by means of an XY recorder (Model No. 1011-518). Since we are interested in the relative fluorescence intensities from solutions of phenol and phenol-plus-quencher, there was no need to determine an absolute value of the quantum yield; hence, the fluorescence intensity was read from the transistorized photometer (Catalog No. Al-63165) directly in terms of per cent transmittance. Since the instrument is a single-beam one, the fluorescence intensity from the phenol solution was measured before and after each measurement on the solution containing phenol-plus-quencher, in order to minimize errors arising from possible fluctuations in the light intensity. The maximum excitation and emission wave lengths (270 and 310 mμ, respectively[12]) were used in all experiments. The cell compartment was encased in a copper block, through which water from a constant-temperature bath was circulated, to control the temperature within $\pm0.1°$. Below room temperature, the cell compartment was flushed with nitrogen gas to prevent fogging of the windows.

Ultraviolet Difference Spectra Measurements. The measurements of difference spectra were made with a Cary Model 14 spectrophotometer, using an expanded scale. Here, too, the cell compartment was thermostated, and nitrogen gas was used for flushing at low temperature. Tandem cells (described by Herskovits and Laskowski[13]) were used for the measurements. The sample cell contained phenol, sodium acetate, and sodium chloride in the front compartment and water in the rear; the reference cell contained phenol plus sodium chloride in the front compartment and sodium acetate solution in the rear.

Results

Fluorescence Measurements. There is no shift in wave length of the fluorescence spectrum of phenol upon addition of quencher, as shown in Figure 1. Hence, all measurements were made at 310 mμ, the maximum of the fluorescence curve. Positive deviations from the Stern–Volmer equation were obtained when $(I_0/I - 1)/[\text{Ac}^-]$ was plotted against $[\text{Ac}^-]$, as suggested by eq. 8, where $[\text{Ac}^-]$ is the total concentration of acetate. An example of such a plot is shown in Figure 2. Since a plot according to eq. 8 is more sensitive to deviations from the Stern–Volmer relation than is one according to eq. 1, this may explain why White[10] did not observe the association
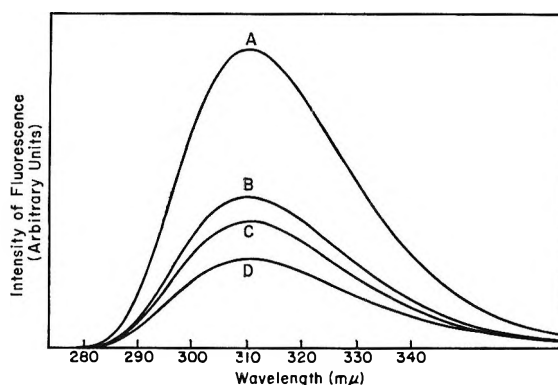
Figure 1. Fluorescence spectra of $4 \times 10^{-4} M$ phenol with various concentrations of sodium acetate: A, 0; B, 0.15; C, 0.2; D, 0.35 M.
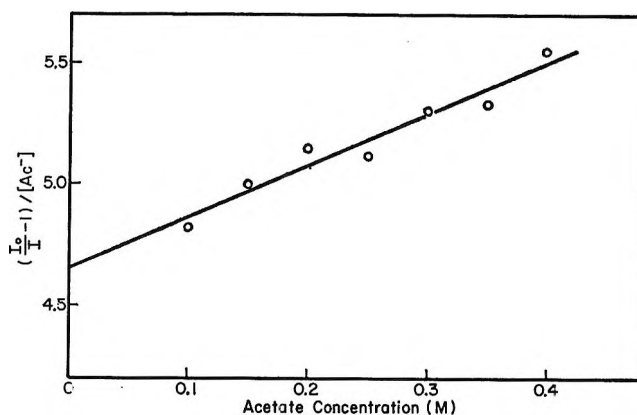
Figure 2. Plot of fluorescence data according to eq. 8. Temperature 10°; pH ~7.0; ionic strength 0.4 M; phenol concentration $2 \times 10^{-4} M$.

phenomenon in the phenol–carboxylate system. As indicated in eq. 8, the association and the quenching constants at a given temperature may be calculated from the slope and intercept of a straight line of the type shown in Figure 2. Table I shows the association and the quenching constants obtained at various temperatures. In the temperature range studied, the plot of $(1 + \log K_{assoc})$ vs. $1/T$ (Figure 3) indicates that the enthalpy of association is -400 ± 400 cal./mole, independent of temperature. This value is in good agreement with the value of -100 ± 100 cal./mole, obtained by Kresheck in this laboratory, using a calorimetric method at 25°, together with the assumption that $K_{assoc} = 0.47$ at this temperature. The

(12) The wave length scale of the instrument was calibrated with these values given in Luminescence Data Sheet No. 2392-4, Aminco Instrument Co., Inc., 8030 Georgia Ave., Silver Spring, Md.

(13) T. T. Herskovits and M. Laskowski, Jr., *J. Biol. Chem.*, **235**, PC 56 (1960); **237**, 2481 (1962).

value of k_q = 5.36 ± 0.21 at 25° is in good agreement with the value of k_q = 6.4 ± 3% obtained by Feitelson[14] for the tyrosine–acetate system. A plot of log k_q vs. $1/T$ gives an activation energy of 2.71 ± 0.12 kcal./mole. This value falls in the range characteristic of diffusion-controlled processes.[15] Additional evidence that the collisional quenching is a diffusion-controlled process is obtained from the magnitude of the quenching rate constant (8.5 × 10^8 M^{-1} sec.$^{-1}$) in the tyrosine–acetate system.[14] Since the k_q values of the phenol–acetate and tyrosine–acetate systems are similar, we may take the values of $k_{bimolec}$ as similar, by assuming comparable values of τ_s, the mean radiative lifetime of the excited state.

Table I: Temperature Dependence of the Association and Quenching Constants from Fluorescence Intensity

t, °C.	K_{assoc}, M^{-1}	k_q, M^{-1}
10	0.52 ± 0.02	4.08 ± 0.02
15	0.51 ± 0.05	4.37 ± 0.15
18	0.47 ± 0.00	4.79 ± 0.03
25	0.47 ± 0.03	5.36 ± 0.21
35	0.48 ± 0.04	6.00 ± 0.12
40	0.47 ± 0.03	6.22 ± 0.16

Ultraviolet Difference Spectra Measurements. In order to obtain an independent measurement of the association constants and thereby establish that the interpretation of the fluorescence data according to eq. 8 is correct, ultraviolet difference spectra were used to study the same association. Wetlaufer[16] and Laskowski[17] previously observed that the maxima in the absorption spectra of phenol and N-acetyltyrosine ethyl ester are shifted to longer wave lengths when sodium acetate is added. These shifts were attributed to phenol–carboxylate ion and tyrosine–carboxylate ion hydrogen bonds, respectively, from considerations of analogous shifts in proteins such as insulin[18] and ribonuclease.[19] Neither of these workers reported association constants in these particular studies; the impossibility of distinguishing complex formation from what may be a medium effect was mentioned by Wetlaufer. Wetlaufer, however, found K_{assoc} for the phenol–acetate system to be no greater than 0.10 from studies on phenol solubilities upon addition of acetate.[16]

Joesten and Drago[20] have used the method of difference spectra to study complexes of phenol and various compounds in CCl_4; our use of the method of difference spectra is similar to theirs.

Figure 4 shows two examples of the difference
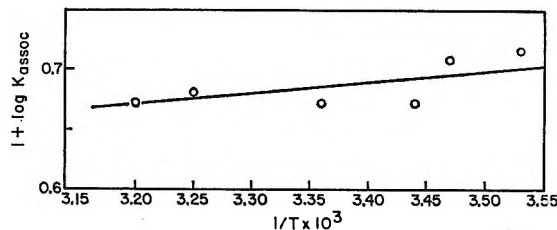
Figure 3. Temperature dependence of log K_{assoc}.
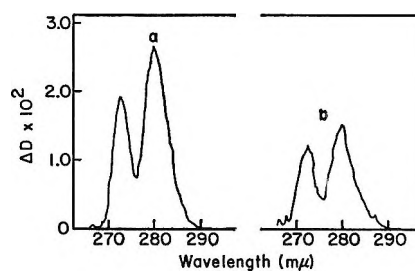
Figure 4. Ultraviolet difference spectra of 6.4 × 10^{-4} M phenol at pH ~7.0, 10°, ionic strength 1 M; a, 1 M sodium acetate; b, 0.5 M sodium acetate.

spectra with peaks at 272 and 280 mμ. Assuming that the difference spectra arise from the production of a complex, according to the equilibrium of eq. 2, then it can be shown[20] that

$$\frac{1}{\Delta D} = \frac{1}{\Delta D_{max}} + \frac{1}{K_{assoc}\Delta D_{max}}\frac{1}{[Q]} \tag{9}$$

where concentrations are equated to activities for reasons cited in connection with eq. 3 and where ΔD is the observed difference in optical density. ΔD_{max} is the value of ΔD when all the phenol is in the form of the complex. In the experiments reported here, $\Delta D/\Delta D_{max}$ is of the order of 0.25 (at 10° in 1.0 M sodium acetate), [Q] is in the range of 0.4 to 1.0 M, and [F] is 6.4 × 10^{-4} M. Hence, [Q] >> [F]$\Delta D/\Delta D_{max}$; this relation has been used in obtaining eq. 9.

A plot of $1/\Delta D$ vs. $1/[Ac^-]$ yields a straight line, as in Figure 5, and the slope and intercept give both K_{assoc} and ΔD_{max} which are shown in Table II.

(14) J. Feitelson, *J. Phys. Chem.*, **68**, 391 (1964).

(15) M. Eigen and L. De Maeyer in "Technique of Organic Chemistry," Vol. VIII, Part II, S. L. Friess, E. S. Lewis, and A. Weissberger, Ed., Interscience Publishers, Inc., New York, N. Y., 1963, p. 1033.

(16) D. B. Wetlaufer, *Compt. rend. trav. lab. Carlsberg*, **30**, 135 (1956).

(17) M. Laskowski, Jr., Abstracts, 131st National Meeting of the American Chemical Society, Miami, Fla., April 1957, p. 47C.

(18) M. Laskowski, Jr., J. M. Widom, M. L. McFadden, and H. A. Scheraga, *Biochim. Biophys. Acta*, **19**, 581 (1956).

(19) H. A. Scheraga, *ibid.*, **23**, 196 (1957).

(20) M. D. Joesten and R. S. Drago, *J. Am. Chem. Soc.*, **84**, 2037, 2696, 3817 (1962).
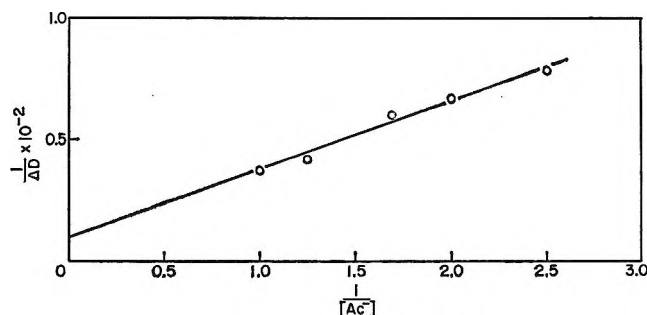
Figure 5. Plot of $1/\Delta D$ vs. $1/[\text{Ac}^-]$, according to eq. 9, at 10°, pH ~7.0, ionic strength 1.0 M, phenol concentration $6.4 \times 10^{-4}\,M$.

Table II: Temperature Dependence of the Association Constants from Ultraviolet Difference Spectra[a]

t, °C.	K_{assoc}, M^{-1}	ΔD_{max}
10	0.36 ± 0.12	0.10 ± 0.03
18	0.32 ± 0.10	0.10 ± 0.03
25	0.35 ± 0.11	0.10 ± 0.03
35	0.32 ± 0.18	0.10 ± 0.05

[a] It is possible to improve the precision in the values of K_{assoc} and ΔD_{max}. However, the precision obtained here is good enough to demonstrate that the same values of K_{assoc} are obtained by both the absorption and fluorescence techniques.

Discussion

We have shown that it is possible to measure association constants for weakly associating systems with some degree of precision using the technique of concentration quenching of fluorescence. The numerical values of K_{assoc} thus obtained are in fair agreement with those obtained from ultraviolet difference spectra. It should be noted that the data from fluorescence are more precise and the experiments employ lower concentrations (e.g., a maximum of 0.4 M Ac^- as compared with the 1 M Ac^- for ultraviolet difference spectra). The results for the phenol–acetate system may be summarized as follows in the temperature range of 0 to 40° (see Table I)

$$K_{assoc} \sim 0.5 \pm 10\%\ M^{-1}$$

$$\Delta H_{assoc} \sim -400 \pm 400\ \text{cal./mole}$$

Since the association of two small molecules in aqueous solution would be expected to involve a large loss of translational entropy, without much of an accompanying decrease in enthalpy upon formation of the hydrogen bond, we would expect K_{assoc} to be much less than 0.5. In order to account for the large experimental value of K_{assoc}, we must postulate the

existence of a large negative contribution to the free energy of association. If the corresponding groups (i.e., tyrosine, instead of phenol, and glutamic acid, instead of acetate) were attached to a macromolecule, then there would be no loss of translational entropy upon association; there would be some loss of entropy of internal rotation of the associating groups in the macromolecule, but this entropy loss would probably be smaller than that arising when independent particles associate. Hence, the postulated negative contribution to the free energy of association (to give as large a value as 0.5 to K_{assoc}) would make the tyrosyl-glutamate interaction a strong one in proteins.

Since ΔH_{assoc} is very small (-400 cal./mole) and since it is reasonable to expect a contribution of approximately -1000 cal./mole from the hydrogen bond, there is most probably a partially compensating positive enthalpy contribution from some other process. To offset the loss of translational entropy there must be a corresponding entropy gain from this other process. These two conditions, a gain in enthalpy and in entropy, are characteristic of the formation of hydrophobic bonds. We thus suggest that, in addition to the formation of the intermolecular hydrogen bond, a hydrophobic bond is formed between the methyl group of the acetate and the benzene ring of the phenol. Courtauld's space-filling molecular models indicate that this is possible. When the thermodynamics of association are known for the system phenol–formate, then the contribution of the hydrogen bond may be subtracted from the values for acetate and higher homologs to ascertain the contribution of hydrophobic bonds to the thermodynamics of such associations. Such experiments are now in progress; when they are completed, a more detailed discussion of these results will be possible. Experiments on the association of neutral carboxylic acids and amides (both of which we find do quench phenol fluorescence) are also possible. In these cases, one must consider the association of quencher with quencher as well as quencher with fluorescer.

Application of These Concepts to Polyamino Acids

We have shown that eq. 8 gives a possible interpretation of the fluorescence of the system phenol–acetate. It is of interest that this relation also can linearize the data on the fluorescence of a copolymer of glutamic acid (analog of carboxylate) and tyrosine (analog of phenol). Specifically, Fasman, et al.[21,22]

(21) G. D. Fasman, K. Norland, and A. Pesce, Biopolymers. Symp., 1, 325 (1964).

(22) A. Pesce, G. Bodenheimer, K. Norland, and G. D. Fasman, J. Am. Chem. Soc., 86, 5669 (1964).

(where references to earlier work can be found), have recently published data on the fluorescence as a function of per cent ionization for the copolymer L-Glu: L-Tyr (95:5), obtaining a sigmoidal curve. If we assume that the "concentration" of quenchers in the copolymer is proportional to the per cent ionization

$$[Q] = \alpha[\% \text{ ionization}] \quad (10)$$

then eq. 8 becomes

$$\frac{\frac{I_0}{I} - 1}{[\% \text{ ionization}]} = \alpha(k_q + K_{assoc}) + \alpha^2(k_q K_{assoc})[\% \text{ ionization}] \quad (11)$$

Figure 6 (curve A) is a plot of the data of Fasman, *et al.*, according to eq. 11. Fasman, *et al.*, have argued that their data do not imply any tyrosine–carboxylate association since "then the quenching of fluorescence should fall off sharply at the beginning (during the first 20% ionization), especially in the DL–L polymer where the tyrosines are easily accessible to carboxylate ions, however it does not." If there were no association, curve B (*i.e.*, $K_{assoc} = 0$) would result. In fact, just the opposite difficulty ensues; *i.e.*, the intensity of fluorescence falls off *too rapidly* with per cent ionization and, as a result, K_{assoc} of eq. 11 can be shown to be imaginary, independent of α. It should not be expected that tyrosine–carboxylate interactions would be very probable in the random coil form.[23] However, this does *not* argue that the same interactions are unlikely in a globular protein.

Since an equation of the form of eq. 11 can linearize the sigmoidal curve found by Fasman, *et al.*, it is of interest to see how this equation could arise without involving association. We assume that ionized carboxyl groups are present only in the random-coil form, or rather that ionization forces those portions of the molecule (in which the ionized carboxyl groups are situated) to be in a random coil form. At low pH (*i.e.*, low degrees of ionization) these random-coil portions will be small, and few in number, but will increase as the pH increases. Thus, the accessibility of carboxyl groups to tyrosyl groups will increase as the pH increases, owing to the increased flexibility of the chain; in other words, each carboxylate ion group becomes a better quencher as the pH increases. This effect would be manifested by an increase in the quenching constant with pH. Assuming that this increase in k_q is linear in [% ionization], we may write

$$k_q = k_q(0) + \beta[\% \text{ ionization}] \quad (12)$$

where $k_q(0)$ is the value of k_q when [% ionization] =
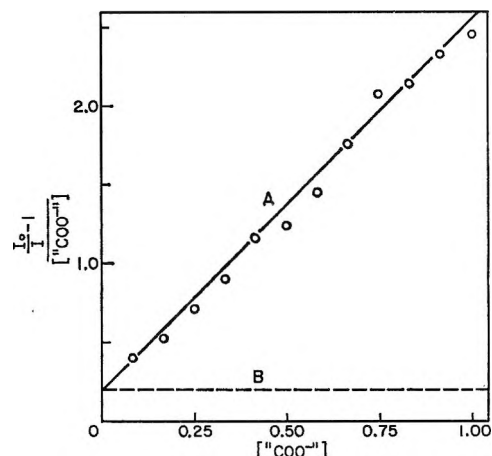
Figure 6. Re-plot of data of Fasman, *et al.*,[21] according to eq. 11. Curve A: experimental data; curve B: expected behavior if only collisional quenching is operative, *i.e.*, if no tyrosine–glutamate hydrogen bonds form.

0, and β is a constant equal to

$$\beta = \frac{\partial k_q}{\partial [\% \text{ ionization}]} \quad (13)$$

Thus, eq. 1 becomes

$$\frac{\frac{I_0}{I} - 1}{[\% \text{ ionization}]} = \alpha k_q(0) + \alpha\beta[\% \text{ ionization}] \quad (14)$$

which has the same form as eq. 11 and fits the data equally well, with a slope $\alpha\beta$ and an intercept $\alpha k_q(0)$. Although none of the parameters can be evaluated, for the slope and intercept offer only two equations with three unknowns, this mechanism of increased flexibility provides a quantitative explanation of the data of Fasman, *et al.*, on the L copolymer. One difficulty with this interpretation is that the DL copolymer, which is a random coil even at low pH, should have a quenching constant at zero concentration of quencher (zero per cent ionization) very much larger than that of the L copolymer. However, Fasman, *et al.*, report, but do not show, that the dependence of fluorescence on pH in both systems is nearly identical.

One further note is that Fasman, *et al.*, attribute the higher intensity found in the L (helical) over the DL (random-coil) copolymer to be due to environmental effects of being in a helix; since carboxylic acids (uncharged) also quench phenol fluorescence, the abovementioned collisional interaction in the DL random coil is a "first-order-effect" explanation of the lower fluorescence in that system.

(23) D. C. Poland and H. A. Scheraga, *Biopolymers*, **3**, 283 (1965).

Thermal Depolymerization of Polymethyl Methacrylate and

Poly-α-methylstyrene in Solution in Various Solvents[1,2]

by S. Bywater and P. E. Black

Division of Applied Chemistry, National Research Council, Ottawa, Canada   (Received February 26, 1965)

The thermal depolymerization of polymethyl methacrylate and poly-α-methylstyrene was investigated previously with diphenyl ether as solvent. Further experiments have now been carried out using 1,2,4-trichlorobenzene and α-methylnaphthalene. The experiments with polymethyl methacrylate show that the mechanism suggested earlier, which involves initiation at the chain ends, depropagation, and chain breaking by solvent transfer, holds for all the solvents studied. Chain transfer becomes increasingly effective in the series trichlorobenzene < diphenyl ether < α-methylnaphthalene. The rate of chain initiation is almost the same in all solvents. With poly-α-methylstyrene, the rate of depolymerization increases linearly with sample molecular weight for molecular weights below 300,000. Above this, the rate is lower than expected, which indicates that some chain termination occurs at higher molecular weights. The experiments suggest that polymer molecules once initiated degrade completely if their molecular weight is not too high. Any variation in rate with solvent should thus be due to variations in k_i. In diphenyl ether, decalin, and α-methylnaphthalene, the rates are closely similar and are consistent with almost identical chain initiation rates.

Introduction

Thermal depolymerization studies on polymers are usually carried out on bulk samples, a procedure which, from the kinetic point of view, has several disadvantages. Unless very thin films of polymer are used, the evolution of volatiles may be diffusion-controlled. For this reason, rather large area samples are required in good thermal contact with a metal base of high heat capacity. In most cases an appreciable time is required to reach the operating temperature, under these conditions, and depolymerization has proceeded to an appreciable extent in many cases before the rate can be measured. If the reaction is carried out in solution in a high-boiling solvent, these difficulties do not arise. The sample can be small and can be enclosed in a small glass bulb of low heat capacity, so that the sample temperature attains that of the thermostat bath quite rapidly. Initial rates can be measured, therefore, and in addition the rates can be measured as a function of polymer concentration, which is a valuable diagnostic tool in mechanism studies. The choice of a polymer which degrades essentially to

monomer alone enables a sensitive gas chromatographic method of analysis to be used in the determination of extent of reaction. Polymer concentrations about $^1/_{100}$ of the bulk concentration can be used and together with low rates which are measurable, this ensures that a low polymer radical concentration is formed in the systems and radical recombination reactions become less important. The kinetic chain length is, in general, increased.[3] We have previously studied the depolymerization mechanism of polymethyl methacrylate in diphenyl ether solution[4] and that of poly-α-methylstyrene in decalin and diphenyl ether.[5] This work has now been extended to include the solvents α-methylnaphthalene and 1,2,4-trichlorobenzene to assess the generality of the mechanism suggested.

(1) Issued as N.R.C. No. 8621.

(2) Presented at the Symposium on Mechanisms of Polymer Degradation, Division of Polymer Chemistry, 148th National Meeting of the American Chemical Society, Chicago, Ill., Sept. 1964.

(3) J. M. G. Cowie and S. Bywater, *J. Polymer Sci.*, 54, 221 (1961).

(4) D. H. Grant and S. Bywater, *Trans. Faraday Soc.*, 59, 2105 (1963).

(5) D. H. Grant, E. Vance, and S. Bywater, *ibid.*, 56, 1697 (1960).

Experimental

The experimental procedures used were essentially as described in earlier references.[4,5] One-per cent (w./v.) solutions of the polymer in the appropriate solvent were used throughout, enclosed in glass bulbs of small volume. All experiments were carried out at 236.5°. The depolymerization was followed by gas chromatographic estimation of the monomer concentration in solution. The samples used were the same as in the previous investigations.[4,5] The polymethyl methacrylates were whole polymers produced by A.I.B.N. initiation to low conversions at 50°. The poly-α-methylstyrenes were samples of narrow molecular weight distribution prepared by anionic initiation.

Results

(1) *Polymethyl Methacrylate.* Figure 1 illustrates typical conversion-time curves for one of the polymer samples (no. 3, $\bar{M}_v = 320{,}000$). Both initial rates and ultimate conversions increase in the series α-methylnaphthalene, diphenyl ether, and trichlorobenzene. This suggests that the effect of changing solvent is to change the kinetic chain length of the depolymerization process.

With trichlorobenzene solutions, with all samples, a very rapid generation of monomer (or some substance of the same retention time) occurred equivalent to 5.2 ± 0.1% conversion. The polymer molecular weight as measured viscometrically was unchanged during this short time interval. Attempts at further purification of the solvent by methods other than the fractionation in a 100-plate column, normally used, failed to eliminate this step. It has been assumed that this process or its products does not influence the normal (and much slower) depolymerization process and so 5.2% has been subtracted from the conversions in this solvent.

It is generally agreed that at the temperature used, depolymerization is initiated at chain ends containing double bonds, produced by disproportionation termination in the formation of the polymer samples.[6] The results obtained previously in diphenyl ether were explained by a mechanism which involves end initiation, depropagation (reverse polymerization) with a chain-breaking step consisting of transfer to solvent. It was necessary to assume that macroradicals did not undergo mutual termination either between themselves or with the smaller radicals present in the system.

Such a scheme leads to the following expression for the rate of monomer evolution[4]

$$d[M]/dt = f k_i k_p [P]/(k_p + \bar{N}_n k_{tr}[S]) \qquad (1)$$

where the rate constants have their conventional
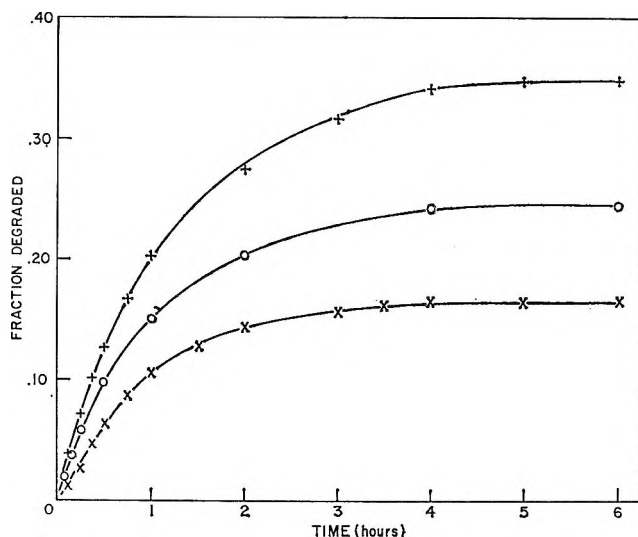
Figure 1. Conversion-time curves for polymethyl methacrylate no. 3 in: ×, α-methylnaphthalene; ○, diphenyl ether; +, trichlorobenzene.

significance; [P] is the base molar polymer concentration and [S] that of the solvent; f is the fraction of polymer molecules having thermally labile end groups. Integration of (1) yields

$$\ln(1 - C/C_\infty) = -k_i t \qquad (2a)$$

$$C_\infty = f_0/(1 + \beta \bar{N}_n) \qquad (2b)$$

where f_0 is the original fraction of polymer containing reactive end groups and is therefore a measure of the importance of disproportionation under the conditions that the polymers are prepared. C_∞ is the final conversion attained, $\bar{N}_n$ is the number average degree of polymerization, and $\beta = k_{tr}[S]/k_p$. Relationships (1) and (2) can be derived easily by use of the methods suggested by Gordon[7] which depend on the assumption that $d\bar{N}_n/dt = 0$. This will be true in an end-initiated depolymerization if the molecular weight distribution is of the exponential type.[7] The results can be confirmed more elaborately for the particular mechanism suggested in this paper by summing the steady-state concentrations of each radical species (see Appendix).

The data in Figure 1 and those obtained with the other polymers conform to eq. 2a and show that k_i (diphenyl ether) = 0.90 hr.$^{-1}$, k_i (α-methylnaphthalene) = 1.01 hr.$^{-1}$, and k_i (trichlorobenzene) = 0.91 hr.$^{-1}$. Figure 2 shows that the data for all solvents conform to eq. 1 and from the slopes, the chain transfer

(6) N. Grassie, "Chemistry of High Polymer Degradation Processes," Butterworth and Co., Ltd., London, 1956.

(7) M. Gordon, *Trans. Faraday Soc.,* **53,** 1662 (1957).
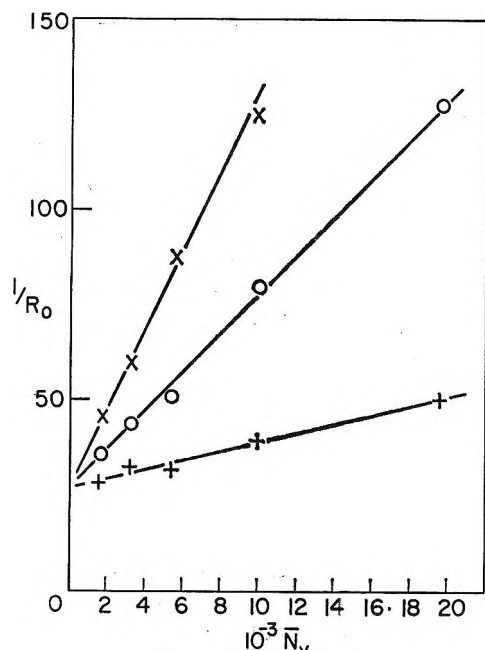
Figure 2. Reciprocal initial rate of depolymerization of polymethyl methacrylate (moles l.$^{-1}$ hr.$^{-1}$) as a function of polymer chain length. Symbols are as in Figure 1.

Figure 3. Variation of the initial rate of depolymerization of poly-α-methylstyrene with sample molecular weight. Symbols are as in Figure 1.

coefficient (β) is 4.3×10^{-4} for α-methylnaphthalene and 0.64×10^{-4} for trichlorobenzene compared with 2.0×10^{-4} previously obtained with diphenyl ether. These values are uncorrected for the difference between $\bar{N}_n$ and $\bar{N}_v$ and should be multiplied by 2.08 as indicated previously.[4] Knowing β and C_∞, it is possible to find f_0 for each sample in each solvent. All of the data are consistent with a value 0.42 ± 0.02. The present experiments confirm the mechanism suggested for f_0 is a constant dependent only on sample preparation. The k_i values obtained would be expected to be closely similar in magnitude in different solvents of the same general type and also confirm the mechanism suggested. The differences in depolymerization rate in different solvents are only dependent on varying chain-transfer coefficients.

(2) *Poly-α-methylstyrene.* Unlike polymethyl methacrylate in this temperature range, poly-α-methylstyrene degradation is initiated by random breaking of bonds in the polymer chain.[6,8] The previous experiments in diphenyl ether and decalin solution[5] showed that the rate of depolymerization was linearly dependent on the polymer chain length as expected for a randomly initiated depolymerization of very long kinetic chain length. Under these conditions the rate of monomer formation is given by

$$d[M]/dt = 2k_iN[P] \tag{3}$$

The equivalence of rates in decalin and diphenyl ether

suggested that k_i was identical in the two solvents and chain transfer to solvent was not important. The experiments in diphenyl ether have been repeated and extended to α-methylnaphthalene and trichlorobenzene as solvents (Figure 3). It will be seen that the rate increases linearly with polymer molecular weight up to a molecular weight of about 300,000. Above this point the rate is lower than expected from the linear relationship. This also occurs for diphenyl ether; the small deviation from linearity was masked by experimental scatter in the work reported earlier. Some chain termination does occur, therefore, with the higher molecular weight samples. This explains the small drop in average molecular weight observed previously with the sample of highest molecular weight.[5] For samples of molecular weight below about 300,000, chain transfer or termination is negligible and eq. 3 holds. The k_i values derived from the data are 0.19×10^{-4} hr.$^{-1}$ in α-methylnaphthalene, 0.24×10^{-4} hr.$^{-1}$ in diphenyl ether, and 0.66×10^{-4} hr.$^{-1}$ in trichlorobenzene. In decalin, k_i is almost equal to that in diphenyl ether.[5] The variation in k_i between different solvents is small; only in trichlorobenzene is the initiation rate moderately higher. This difference is, however, within the limits observed for unimolecular decompositions in a series of solvents and it would be premature to conclude that there is directly or indirectly induced initiation in trichlorobenzene.

It is tempting to assume that the chain breaking process in the depolymerization of poly-α-methyl-

(8) D. W. Brown and L. A. Wall, *J. Phys. Chem.*, 62, 848 (1958).

styrene is again chain transfer to solvent. The initial rate of depolymerization for a randomly initiated reaction can be derived in the same manner as for the end-initiated case and is

$$\frac{1}{R_0} = \frac{\beta}{\alpha} + \frac{2}{\alpha \bar{N}_n} \qquad (4)$$

where $\alpha = 4k_i[P]$. Unfortunately, the expression is only rigorously exact for a polymer having an exponential distribution of molecular weights, whereas the polymers used were almost monodisperse, and for the case where $d\bar{N}/dt = 0$. Neither assumption is true in the present case. However, a monodisperse distribution will probably not cause a large error and it is known that $d\bar{N}/dt$ is small if we confine ourselves to low conversions, even for the sample of highest molecular weight used and will be smaller for the other samples. Plots of eq. 4 do indeed give reasonable straight lines, as shown in Figure 4, which suggests that the approximations have not invalidated the treatment and that the assumption is reasonable. The intercepts are too small for accurate measurement but suggest transfer coefficients in the 10^{-4} to 10^{-5} range which is again reasonable.

Appendix

For the mechanism considered above, the stationary-state principle gives

$$(R_{\dot{n}}) = \frac{k_i}{k_p}\left[\frac{(P^*_{n+1})}{(1 + \beta)} + \frac{(P^*_{n+2})}{(1 + \beta)^2}\cdots\right] \qquad (I)$$

where the asterisk denotes only active polymer (i.e., that produced in disproportionation termination in the polymer preparation). Now $(P^*_n) = (P^*_n)_0$ exp-$(-k_i t)$ for any value of n. Therefore

$$(R_{\dot{n}}) = \frac{k_i}{k_p}\left[\frac{(P^*_{n+1})_0}{(1 + \beta)} + \frac{(P^*_{n+2})_0}{(1 + \beta)^2}\cdots\right]\exp(-k_i t) \qquad (II)$$

The molecular weight distribution of the polymer will be of the form

$$(P^*_n)_0 = (1 - a)a^{n-1}\,\Sigma(P^*_n)_0 \qquad (III)$$
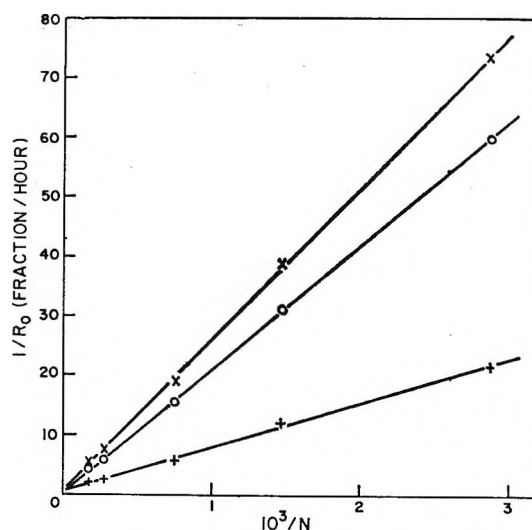
Figure 4. Reciprocal initial rate of depolymerization of poly-α-methylstyrene as a function of reciprocal degree of polymerization. Symbols are as in Figure 1.

where $a = 1 - 1/\bar{N}_n$. Therefore

$$(R_{\dot{n}}) = \frac{k_i}{k_p}\frac{(1 - a)a^n}{(1 + \beta - a)}\Sigma(P^*_n)_0\exp(-k_i t)$$

$$= \frac{k_i}{k_p}\frac{(1 - a)a^n}{(1 + \beta - a)}\Sigma(P^*_n) \qquad (IV)$$

$$\sum_2^\infty(R_{\dot{n}}) = \frac{k_i a^2}{k_p(1 + \beta - a)}\Sigma(P^*_n) \qquad (V)$$

$$d(M)/(dt) = k_p\sum_2^\infty(R_{\cdot n}) = k_i\frac{\bar{N}_n\Sigma(P^*_n)}{1 + \beta\bar{N}_n} \qquad (VI)$$

if $\bar{N}_n$ is large. $\bar{N}_n$ is the original number-average degree of polymerization of active chains. It is clear from (II) that this will not change with time. It can be shown from (IV) that the number-average degree of polymerization of the inactive polymer formed by transfer to solvent is identical with that of the active polymer.

Lattice Energy of Some Cubic Oxides

by Rinoud Hanna

State University of New York College of Ceramics at Alfred University, Alfred, New York
(Received March 1, 1965)

The bulk modulus of magnesium oxide was determined by a dynamic resonance method and equaled 23.07×10^{11} dynes/cm.^{2}. The bulk modulus calculated from Szigeti's equation was lower than that obtained experimentally. Compatible values of the lattice energy of cubic oxides could be obtained from the bulk moduli of their polycrystalline form. The sum of the first and second ionization potentials of elemental magnesium was 22.21 e.v., and the sums of the first four ionization potentials of elemental thorium and uranium were 57.27 and 52.70 e.v., respectively.

According to the classical theory of ionic crystals of Madelung and Born, the main interaction between the oppositely charged ions is the attractive (Coulomb) forces.[1] It is assumed that the neighboring ions penetrate to some extent into each other and the electrostatic field exerted in the overlapping regions is very different from its value at the ionic centers. The repulsive forces, derived from this overlapping, balance the attractive forces.

Sherman[2] was able to verify Born's theory by comparing the crystal energy calculated from the Born equation with that obtained experimentally. The latter was evaluated from the electron affinity and thermochemical data by the use of the Born–Haber cycle.

The repulsive energy depends on the relative sizes and valencies of the ions, and it is represented in the Born equation by the term Br^{-n} where B and n are constants. Several methods have been proposed to determine the overlap potential. The constant n could be calculated from the experimental values of the compressibility. Lennard-Jones[3] assigned to each inert gas a value of n when the repulsive forces between the gas atoms are represented by the same law (br^{-n}). These laws of force are also true for ions of the same electronic structure. Pauling[4] used values obtained by rules that he derived from theoretical treatment of the interaction of closed-shell electronic configurations. Born's theory was subsequently refined. For example, an exponential form, $B'e^{-r/\rho}$, was introduced instead of the inverse power form of the overlap energy;

also, the dipole–dipole and the quadrupole–dipole interactions were included.[1]

During the infrared polarization, the interaction of the atomic and electronic displacements is separated into short-range and long-range effects.[5] The former should vanish in an ideal heteropolar crystal with cubic lattice, but experimental data indicate their presence, even in alkali halides, where they act mainly in the overlap regions. Szigeti calculated the interaction of the electronic distortions with the repulsive forces. A quantitative relation between the absorption frequency and the compressibility of ionic crystals was deduced since both are determined to a large degree by these repulsive forces.

In the present work, the overlap potential in the MgO lattice was determined from the bulk modulus which is the ratio of the pressure applied to a body to the fractional decrease in its volume. The bulk modulus was calculated from the elastic moduli of polycrystalline MgO obtained from resonance frequency measurements.

(1) M. Born and J. E. Mayer, *Z. Physik*, **75**, 1 (1932); M. Born and K. Huang, "Dynamical Theory of Crystal Lattices," Oxford University Press, London, 1956, Chapter I.

(2) J. Sherman, *Chem. Rev.*, **11**, 93 (1932).

(3) J. E. Lennard-Jones, *Proc. Roy. Soc.* (London), **A109**, 584 (1925); J. E. Lennard-Jones and B. M. Dent, *ibid.*, **A112**, 230 (1926).

(4) L. Pauling, *ibid.*, **A114**, 181 (1927); *J. Am. Chem. Soc.*, **49**, 765 (1927).

(5) B. Szigeti, *Trans. Faraday Soc.*, **45**, 155 (1949); *Proc. Roy. Soc.* (London), **A204**, 51 (1950).

Experimental

Polycrystalline magnesium oxide was prepared by hot compaction. Two rectangular-shaped bars were used to determine the elastic moduli. The density of the bars was determined from their volume, which was measured by means of a mercury volumeter, and their weight. A Forster-type apparatus[6] was used to obtain the flexural (flatwise) and the torsional resonance frequencies of the two bars.

Results

The mean value of the determined density of the polycrystalline MgO was 3.586 g./cm.[3] with ±0.5% experimental error. The theoretical density[7] of MgO (calculated from the atomic weights and the X-ray determination of the lattice constant of the crystal) is 3.581 g./cm.[3].

From the flexural and torsional resonance frequencies, the average values of Young's modulus, E, and the shear modulus, G, were calculated to be 30.25×10^{11} and 11.8×10^{11} dynes/cm.[2], respectively. The bulk modulus, K, was determined from the known equation

$$K = E/3(3 - E/G)$$

and equaled 23.07×10^{11} dynes/cm.[2]. Although this value is greater than that previously reported,[8] yet its reciprocal $(0.43 \times 10^{-12}$ cm.[2]/dyne) is higher than the compressibility value $(0.25 \times 10^{-12}$ cm.[2]/dyne) calculated by Lennard-Jones and Taylor.[9]

The relation between the compressibility and the exponent n in the repulsive term of Born's equation is given by

$$n = 1 + \frac{9\alpha r^4 K}{z^2 e_+ e_- M_r}$$

where α is a constant characteristic of the type of lattice, r is the interionic distance, K is the bulk modulus, M_r is the Madelung constant, and e is electronic charge; z^2 is introduced to permit the application of the equation to crystals containing multivalent ions ($z = 2$ for $Mg^{2+}O^{2-}$ and $Th^{4+}O_2^{2-}$).

The interionic distance of magnesium oxide is 2.105 Å. and by using the experimental value of K above, n equals 6.06, which is lower than the value 7 for MgO.[10] The lattice energy per mole (including the Coulomb and repulsive interactions) is 3.85×10^{13} ergs/cm. or 919.5 kcal. (Table I). Sherman[2] obtained, from thermochemical equations, a value of 940.1 kcal./mole for the lattice energy of MgO.

In calculating the lattice energy we have neglected the van der Waals attractive forces as well as the dipole quadrupole interaction. This does not affect

Table I: Calculated Data of Polycrystalline Cubic Oxides

	Crystal structure	K, 10^{11} dynes/cm.[2]	Interionic distance, Å.	n	Lattice energy, kcal./mole	Overlap potential, kcal./mole	Ionization potential, e.v.
MgO	NaCl	23.07	2.105	6.06	919.5	181.7	22.21
ThO$_2$	CaF$_2$	21.43	2.425	5.42	2246	508	57.27
		19.30[a]	2.425	4.98	2203	553	55.42
UO$_2$	CaF$_2$	17.10	2.366	4.20	2152	673	52.70

[a] Calculated from elastic moduli of single crystal ThO$_2$.

the result appreciably since the changes in the attractive potential are compensated by changes in the overlap potential.

Discussion

Fairly accurate values of the crystal energy could be obtained from the Born equation in its simplified form provided, of course, that the values of interionic distance and compressibility are accurate. Since the bulk modulus obtained above gave compatible results, it is possible to conclude that the elastic moduli of polycrystalline form could be used to determine the overlap potential and hence the lattice energy could be calculated. This is especially useful if the compound is unobtainable in the single crystal form.

Szigeti[5] constructed a model which takes into account the interaction of the electronic distortions with the repulsive forces. This model allows deviations from spherical charge distribution but it leads to the Cauchy relation and also to the relation between the compressibility and the resonance optical frequency. His equation is

$$K = \frac{r^2 \epsilon_0 + 2}{3u \epsilon_\infty + 2} m \omega_t^2$$

where u is the volume occupied by an ion pair and m is the reduced mass defined as $1/m = 1/m_{(cation)} + 1/m_{(anion)}$. For MgO, ϵ_∞ = high-frequency dielectric constant = 2.95; ϵ_0 = low-frequency dielectric con-

(6) J. B. Wachtman, Jr., and W. E. Tafft, *Rev. Sci. Instr.*, **29**, 517 (1958).

(7) H. E. Swanson and E. Tatge, National Bureau of Standards Circular 539, U. S. Government Printing Office, Washington, D. C., 1953, p. 1.

(8) H. Scheetz, Quarterly Progress Report, PI-1273-M-11, Cornell Aeronautical Laboratory, Nov. 1961.

(9) J. E. Lennard-Jones and P. A. Taylor, *Proc. Roy. Soc.* (London), **A109**, 476 (1925).

(10) F. Seitz, "The Modern Theory of Solids," McGraw-Hill Book Co., Inc., New York, N. Y., 1940.

stant = 9.65; and ω_t = the transverse vibrational frequency[11] = 8.075 × 10^{13} rads/sec.

By substituting these values in the equation, the bulk modulus, K (reciprocal of compressibility), is 19.2 × 10^{11} dynes/cm.^{2}. The ratio between this calculated compressibility and the experimental one, obtained above, is 1.21. Szigeti found this ratio to be 0.47 and he attributed this to the presence of directed forces which result from sharing of the valency electrons between neighboring ions. In other words, although this model could represent the alkali halides it is not applicable to MgO since the Cauchy relation does not hold for the latter.

The lattice energies of thorium dioxide and uranium dioxide were also calculated. These oxides are cubic with the calcium fluorite structure, and as in the case of MgO, they contain four molecules per unit cell.[12] The bulk modulus[13] of polycrystalline thorium dioxide was calculated from the Young's and shear moduli at the theoretical density of ThO_2 and equaled 21.43 × 10^{11} dynes/cm.^{2}. Recently, however, the bulk modulus of single crystal[14] ThO_2 was computed from sound velocity determinations to be equal 19.3 × 10^{11} dynes/cm.^{2}. For uranium dioxide the bulk modulus of the polycrystalline form[8] is 17.1 × 10^{11} dynes/cm.^{2}. Table I summarizes the values of n, the crystal energy, and the overlap energy of the three cubic oxides.

The ionization potentials (Table I) were calculated from the observed lattice energies of the three oxides using the Born–Haber cycle. For the case of magnesium oxide, Q (the heat of formation of MgO(c) from the Mg(c) and $^1/_2O_2$(g)) = 144.09,[15] S (the heat of sublimation of Mg metal) = 36.3,[10] and D (the heat of dissociation of the oxygen molecule) = 118.4 kcal./mole. The electron affinity of oxygen atom is −168 kcal./mole, which is an average of values assumed, for alkaline earth oxides, by Sherman if the calculated

and experimental results of the crystal energy are to agree.^{2} For thorium and uranium dioxides, the heats of formation are 294.35 and 262.88 kcal./mole[15] and the heats of sublimation of the metal are 177 and 220 kcal./mole,[10] respectively. The ionization potential obtained for the magnesium element is the sum of the first and second ionization potentials, while it is the sum of the first four ionization potentials for the thorium and uranium elements. The value 22.2 e.v. of the magnesium element is in good agreement with the sum of the first (7.65 e.v.) and the second (15.02 e.v.) ionization potentials determined spectroscopically.[16]

The bulk modulus could be computed from the elastic coefficients or moduli if compressibility measurements are not available. There may be several values of the Young's modulus depending on its methods of determination whether, for example, they are made in tension, compression, or flexure. Accordingly, the bulk modulus would have more than one value. The effect of such difference between the values of bulk modulus on the calculated constants in Table I is illustrated in the case of thorium dioxide. While n and the overlap potential changed by nearly 9%, there was only a slight change, approximately 2%, in the lattice energy and the ionization potential.

(11) R. Hanna, *J. Am. Ceram. Soc.*, in press.

(12) R. W. G. Wyckoff, "Crystal Structures," Vol. I, Interscience Publishers, Inc., New York, N. Y., 1948, p. 61.

(13) S. Spinner, F. P. Knudsen, and L. Stone, *J. Res. Natl. Bur. Std.*, 67C, 39 (1963).

(14) P. M. Macedo, W. Capps, and J. B. Wachtman, Jr., *J. Am. Ceram. Soc.*, 47, 651 (1964).

(15) "Handbook of Chemistry and Physics," 43rd Ed., Chemical Rubber Publishing Co., Cleveland, Ohio, 1961–1962, p. 1832.

(16) L. Pauling, "The Nature of the Chemical Bond," Cornell University Press, Ithaca, N. Y., 1960, p. 57.

Heats of Mixing of Aqueous Electrolytes.   I.   Concentration

Dependence of 1-1 Electrolytes

by R. H. Wood and R. W. Smith

Department of Chemistry, University of Delaware, Newark, Delaware   *(Received March 1, 1965)*

The heats of mixing of a variety of aqueous alkali metal halide and nitrate solutions of the same ionic strength have been measured at 25° in the concentration range 0.1–0.5 *m*. The heat of mixing is very nearly a quadratic function of the mole fraction.   The concentration dependence of the heats of mixing indicates that like-charged ion pairs are important contributors to the heat of mixing and, therefore, that Brønsted's theory of specific ion interaction is not correct.   The results are in good agreement with Friedman's application of Mayer's ionic solution theory to mixed electrolytes.   Both the cross-square rule and the division of the ions into groups which were developed by Young and co-workers hold nearly within experimental error at all concentrations.

Introduction

Compared to solutions of a single electrolyte, solutions of several electrolytes have received very little study. However, many systems of economic importance and scientific interest contain mixtures of electrolytes, e.g., sea water, biological fluids, and metal ion complexes in solution. The present series of papers will be concerned with the heats of interaction of mixed electrolyte solutions.

The measurement of the heats of mixing of electrolyte solutions is an excellent way to study the interactions of ions in aqueous solution. If the measurements are made at constant ionic strength, effects of the ionic atmosphere are canceled. If the measurements are made with a common ion, the effects of oppositely charged ion pairs cancel. Thus, the pair-wise and triplet interactions of like-charged ions can be conveniently studied.

Brønsted's theory of "specific ion interaction"[1] assumes that like-charged ions do not have specific interactions. The equations of Guggenheim[2] and of Scatchard and Prentiss[3] extend Brønsted's theory while keeping the assumption that like-charged ions have no specific interactions. Recently, Friedman,[4] using Mayer's ionic solution theory, predicted that like-charged ions should have specific interactions and that these interactions should be more important than trip-

let interactions for many systems. The most sensitive free energy measurements have not shown deviations from Brønsted's principle if triplet interactions are included.[5] Since calorimetric measurements are capable of measuring a smaller energy of interaction in the 0.1 to 1.0 *M* region, the present test of Brønsted's principle was undertaken.

The heats of mixing of a wide variety of 1–1 electrolytes at 1.0 *m* and 25° have been measured by Young and co-workers.[6-8] In addition, Stern and Passchier[9] and Stern and Anderson[10] have extended measurements to several temperatures and the concentration range above 0.5 *m*. These experiments did not extend to a low enough concentration to test Brønsted's principle

(1) J. N. Brønsted, *J. Am. Chem. Soc.*, **44**, 877, 938 (1922); **45**, 2898 (1923).

(2) E. A. Guggenheim, *Phil. Mag.*, **19**, 588 (1935).

(3) G. Scatchard and S. S. Prentiss, *J. Am. Chem. Soc.*, **56**, 2315, 2320 (1934).

(4) H. L. Friedman, *J. Chem. Phys.*, **32**, 1134 (1960).

(5) G. Scatchard, *J. Am. Chem. Soc.*, **83**, 2636 (1961).

(6) T. F. Young and M. B. Smith, *J. Phys. Chem.*, **58**, 716 (1954).

(7) T. F. Young, Y. C. Wu, and A. A. Krawetz, *Discussions Faraday Soc.*, **24**, 27, 77, 80 (1957).

(8) Y. C. Wu, M. B. Smith, and T. F. Young, *J. Phys. Chem.*, **69**, 1868, 1873 (1965).

(9) J. H. Stern and A. A. Passchier, *ibid.*, **67**, 2420 (1963).

(10) J. H. Stern and C. W. Anderson, *ibid.*, **68**, 2528 (1964).

of specific ion interaction. They cannot distinguish between the effects of like-charged pairs and the effects of triplets.

The present paper reports the results of a series of measurements of the heats of mixing of 1–1 electrolytes from 0.5 to 0.1 m. The results show that like-charged ions do have specific interactions even at low concentrations. The evidence indicates that these interactions are generally larger than triplet interactions although smaller than oppositely charged-pair interactions.

Experimental

1. Analysis and Standardization. All salts used in this study were of analytical reagent or ACS reagent grade except NaBr, which was reagent grade, and LiCl, which was technical grade (typical analysis: 99.6% LiCl, 0.3% H_2O). The salts were dissolved in deionized water (distilled water passed through a demineralizer column) to prepare 2–5 m stock solutions and stored in polyethylene containers.

The chloride and bromide stock solutions were standardized by gravimetric analysis of their silver salts. The potassium nitrate solution was standardized by precipitation as potassium tetraphenylborate as described by Reilley.[11] The sodium nitrate solution was standardized by conversion to $NaClO_4$ with concentrated $HClO_4$, followed by evaporation to constant weight at 250°, as recommended by Duval.[12] Triplicate analyses for each salt yielded a standard deviation from the mean of less than 0.1% for each salt.

The heat of mixing anions containing a common cation is small, as shown by Young, Wu, and Krawetz[7]; therefore, small anion impurities have no significant effect on the heat of mixing. Heats of mixing cations are much larger, and therefore, the amounts of Na^+, K^+, Li^+, and Ca^{2+} impurities in each salt were determined at their wave length of maximum emission on a Beckman DU spectrophotometer Model 2400 with oxygen–acetylene flame attachment by use of the standard addition method, correcting for background.[13] The only cation impurity present in greater than 0.1 mole % was the K in NaBr (background wave lengths = 775 and 750 mμ) where it was found to be 0.64 mole %. The heats of mixing at 0.5 m involving NaBr were corrected for the presence of this impurity. The maximum correction was only 0.006 cal. The pH of the stock solutions varied from 7.80 to 5.05.

2. Calorimeter. The isothermal, differential calorimeter used in this study has been described previously by Jongenburger[14] except for a few modifications. These changes[15] included new calorimeter lids and support system, a new bearing system for the stir-

rers, new heaters (resistance wire sealed in glass tubing), removal of cooling coils, and insertion of plastic pipes around the stirrers in the vessels. In addition, new plungers utilizing a rubber O-ring seal at the top and bottom were made for the glass pipets. In all bur the largest heat experiments, two pipets in the same vessel were opened at the same time. A correction for the heat of opening the pipets was necessary. The average heat of opening double pipets for 21 experiments was 0.008 cal. with $\sigma_{single} = \pm 0.005$ and $\sigma_{mean} = \pm 0.001$ for pipets L13, R24, and R13. For L24, seven experiments yielded an average heat of opening of -0.005 cal. with $\sigma_{single} = \pm 0.009$ and $\sigma_{mean} = \pm 0.003$. The heats of opening were checked periodically in the course of this research. On the basis of the uncertainties in heats of opening, the pipets L24 were assigned a weight $^1/_4$ that of the other double pipets.

The calorimeter was calibrated electrically to $\pm 0.1\%$. In addition, the heat of neutralization of NaOH with HCl at infinite dilution was found to be 13.33 kcal./mole with $\sigma_{single} = \pm 0.09$ kcal./mole. This agrees with the value of 13.34 kcal./mole obtained by Hale, Izatt, and Christensen.[16]

3. Experimental Procedure. All experiments were performed at constant molality and 25.03 $\pm$ 0.02°. The mole fraction of salt from the pipets after opening all four pipets in a vessel was approximately 0.11. By loading the vessels for subsequent runs with a portion of the vessel solution from the previous experiment, any mole fraction desired could be obtained. All experiments were performed in duplicate.

4. Treatment of Data. The experimental data were fit by the method of least squares to the equation

$$\Delta H_m(\text{cal./kg. of solvent}) = X(1 - X)I^2[RTh_0 + RTh_1(1 - 2X)] \quad (1)$$

where ΔH_m is the heat of mixing in calories per kilogram of solvent, X is the mole fraction of the salt of larger formula weight, I is the ionic strength ($^1/_2 \Sigma mZ^2$), RTh_0 is a measure of the magnitude of the interaction, and RTh_1 is a measure of asymmetry. This

(11) C. N. Reilley, "Advances in Analytical Chemistry and Instrumentation," Vol. I, Interscience Publishers, Inc., New York, N. Y., 1960, p. 23.

(12) C. Duval, "Inorganic Thermogravimetric Analysis," 2nd and Revised Ed., Elsevier Publishing Co., New York, N. Y., 1963, pp. 195, 197.

(13) "Reagent Chemicals," American Chemical Society Specifications, 1960, Applied Publications, American Chemical Society, Washington, D. C., 1961.

(14) H. S. Jongenburger, Ph.D. Thesis, University of Delaware, 1963.

(15) H. L. Anderson, Ph.D. Thesis, University of Delaware, 1965.

(16) J. D. Hale, R. M. Izatt, and J. J. Christensen, Proc. Chem. Soc., 24D (1963).

Table I: Heats of Mixing at 25.0° of Various Electrolytes at 1.0, 0.5, 0.2 and 0.1 m

	$m = 1.0$ $RTh_0{}^a$	$m = 0.5$ RTh_0	$RTh_1{}^b$	$m = 0.2$ RTh_0	$RTh_1{}^b$	$m = 0.1$ RTh_0
Common anion						
LiCl–NaCl	84.6[c]	85.6[c]		79 ± 5[8]		67 ± 15[15]
	83.6[d]	86.4[d]				
		87.1 ± 0.8[15]	2.7 ± 1.2			
LiCl–KCl	−64.2[c]	−54.1 ± 0.9[15]	−1.9 ± 1.3	−50 ± 4[7]		−39 ± 8[16]
NaCl–KCl	−38.3[c]	−37.0 ± 0.5[22]		−39 ± 5[16]		−38 ± 10[14]
	−38.5[d]	−39.4[d]				
	−38.1 ± 0.2[19]					
NaBr–KBr	−37.7[c]	−38.7 ± 0.5[16]		−38 ± 3[8]		−47 ± 11[9]
NaNO$_3$–KNO$_3$	−50.3[c]	−57.8 ± 1.4[8]		−56 ± 5[8]	7 ± 7	−54 ± 11[11]
Common cation						
NaCl–NaBr	3.2[c]	2.8 ± 0.4[8]	−0.6 ± 0.6			
NaCl–NaNO$_3$	12.4[c]	16.7 ± 0.9[8]		20 ± 2[7]		
No common ions						
NaCl–KBr	4.8[c]	8.5 ± 0.9[8]		19 ± 3[8]		
NaCl–KNO$_3$	316.7[c]	393.7 ± 1[16]	18 ± 1	503 ± 6[16]		556 ± 14[e16]
NaBr–KCl	−74.8[c]	−80.7 ± 0.7[20]	−2 ± 1	−93 ± 4[15]		−96 ± 19[7]
NaNO$_3$–KCl	−400.7[c]	−475 ± 2[20]	5 ± 3	−585 ± 8[8]		−694 ± 31[f8]

[a] The number of experiments is given as an exponent. Both sides of the curve were investigated. The results are in calories per kilogram of solvent per molal[2] (see eq. 1). [b] A blank under RTh_1 means that h_1 was not significant at the 95% confidence level. [c] Data of Young and co-workers, ref. 6–8. [d] Data of Stern and Anderson, ref. 10. [e] Measurements at 0.05 m gave 617 ± 54.[16] [f] Measurements at 0.05 m gave −888 ± 105.[18]

equation is due to Friedman[17] and has the advantage that h_1 is purely a measure of skew since $X(1 - X)$ is orthogonal to $X(1 - X)(1 - 2X)$.

The calculations were performed by an IBM 1620II computer using a Fortran program.[15,18] The uncertainty of the constants in eq. 1 was calculated at the 95% confidence level. An F test (95% confidence level) was used to determine if h_1 was significant. When h_1 was not significant, the data were fit to eq. 1 with h_1 set equal to zero.

5. Errors. All dilutions were performed by weight and were accurate to 0.1%. Errors due to heats of concentration, dilution, and neutralization upon mixing any two solutions were negligible in all experiments.

Results and Discussion

The results of the measurements are given in Table I together with some results of other workers. Several duplicates of the measurements of Young and co-workers[7,8] and of Stern and Anderson[10] were made. The agreement, as shown in Table I, is satisfactory.

In most cases the skew (RTh_1) was zero within experimental error (95% confidence). The values of RTh_0 show no general trend with concentration; some values decrease while others increase. In the case of mixings with a common ion, this result is contrary to Brønsted's principle of specific ion interaction.[1] Brønsted's theory of specific ion interaction states that like-charged ions are uniformly influenced by each other. This means that replacing one ion by another should not produce specific effects so that the heat and excess free energy of mixing should be zero.

Scatchard and Prentiss[3,5] derived equations for mixed electrolytes which extend Brønsted's principle and include both oppositely charged pair and triplet interactions. Their equation predicts that both g_0 and h_0 have the form

$$g_0 = AI + BI^{1/2} + \cdots \qquad (2)$$

where ΔG_m (cal./kg.) $= X(1 - X)I^2RTg_0$ and ΔG_m is the excess free energy of mixing and the A's and B's are functions of the triple-ion interactions. Scatchard and Prentiss found that the first two terms of eq. 2 are enough to represent the free energies of the Li$^+$, K$^+$, Cl$^-$, NO$_3^-$ reciprocal salt pair up to 1 M. The first two terms of this equation cannot represent the present data for any of the salts within two to five times the estimated experimental error. The errors are always in the direction to be expected if h_0 is finite at zero concentration. As an illustration of this, Figure 1 shows a plot of RTh_0/m vs. $m^{1/2}$ for two series of measurements. The points cannot be represented by a straight line as required by the first two terms of eq. 2.

(17) H. L. Friedman, *J. Chem. Phys.*, **32**, 1351 (1960).

(18) The authors thank the computing center of the University of Delaware for the use of its facilities.
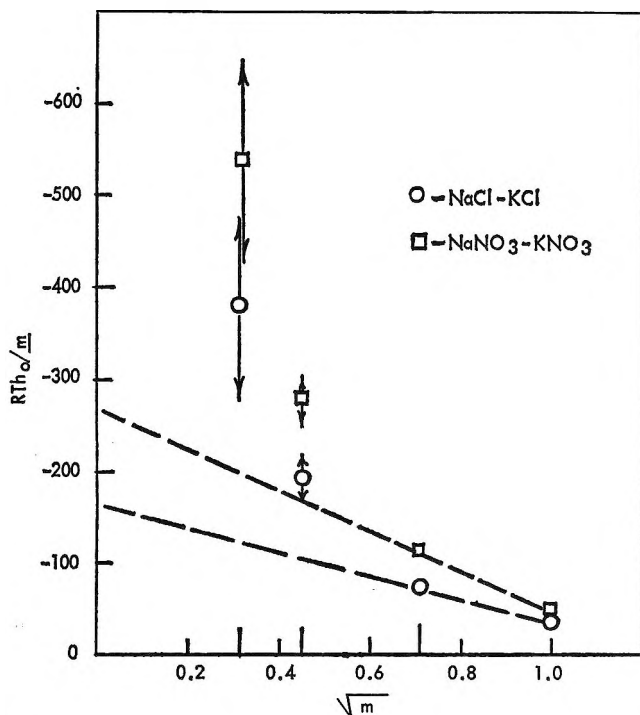
Figure 1.

They can be represented by a single like-charged pair interaction with, in some cases, a triplet contribution. The only other possibility is that the interactions are due to triplets and quadruplets which for all of the salts in this study just cancel each other in such a way that the concentration dependence of the triplets (h_0 is approximately proportional to m) just cancels the concentration dependence of the quadruplets (h_0 is approximately proportional to m^2) to give an interaction (h_0) which is nearly independent of concentration.

Guggenheim's equations for mixed electrolytes[2] include only oppositely charged ion pair interactions and have been shown to be quite accurate below 0.1 m.[19,20] This theory predicts that for common ion mixings RTg_0 is zero and thus RTh_0 is also zero.

Friedman,[4,17,21] using Mayer's ionic cluster expansion method, has derived equations for the heat and excess free energy of mixing electrolyte solutions. The equations are based on a primitive model consisting of hard spheres in a continuous dielectric and predict that RTg_0, and in general RTh_0, are finite for common ion mixtures even at infinite dilution. His equations also predict that like-charged pairs and triplets are the most important contributors to RTg_0. The present results represent experimental confirmation of Friedman's equations. It should be noted, however, that the specific effects are small at 0.1 m (less than 7 cal./mole).

This is probably why previous experiments have tended to verify Brønsted's principle.

The fact that RTh_0 usually varies slowly with molality indicates that like-charged ion pair interactions are usually more important than triplet interactions. Young, Wu, and Krawetz have shown that for many systems the heat of mixing is independent of the common ion.[7] Friedman[22] has noted that this fact indicates that like-charged ion pairs are responsible for the effect.

Young, Wu, and Krawetz[7] have noticed that for common anion mixtures the cations can be divided into two groups and that mixings of two ions in the same group give positive values for RTh_0 and mixings of two ions in different groups give negative RTh_0 values. Division into these same groups holds for all of the cations used in this investigation down to 0.1 m. Since RTh_0 is usually slowly varying, the division into groups should be independent of concentration below 1.0 m for most salts.

If one considers the number of mixings it is possible to make with four single electrolyte solutions whose component ions are limited to two different cations and two anions, one finds there are six possible mixings as represented by the sides and diagonals of the square

$$\text{MX} \boxtimes \text{NX}$$
$$\text{MY} \qquad \text{NY}$$

Krawetz[23] has shown that for the set LiCl, LiBr, KCl, KBr, the sum of the experimental heats of mixing represented by the sides of the square equals the sum of the heats of mixing represented by the diagonals. He calls this empirical relationship the cross-square rule ($\Sigma\square = \Sigma\times$). Bottcher[24] has shown that this rule will hold if the heats of mixing of the cations in the presence of each anion singly are nearly equal and the heat of mixing of the cations in the presence of an equal molal mixture of both anions has an intermediate value. Wu, Smith, and Young[8] have shown for several other sets of salts they studied at 1.0 m that the cross-square rule holds within the limits of their experimental uncertainty.

(19) H. S. Harned and B. B. Owen, "The Physical Chemistry of Electrolyte Solutions," 3rd Ed., Reinhold Publishing Corp., New York, N. Y., 1958.

(20) G. N. Lewis and M. Randall, "Thermodynamics," 2nd Ed., Revised by K. S. Pitzer and L. Brewer, McGraw-Hill Book Co., Inc., New York, N. Y., 1961.

(21) H. L. Friedman, "Ionic Solution Theory," Interscience Publishers, Inc., New York, N. Y., 1962.

(22) H. L. Friedman, Discussions Faraday Soc., 24, 74 (1957).

(23) A. A. Krawetz, ibid., 24, 77 (1957).

(24) C. J. F. Bottcher, ibid., 24, 78 (1957).

Table II: Concentration Dependence of Cross-Square Rule for the Sets NaCl, NaBr, KCl, KBr, and NaCl, NaNO$_3$, KCl, KNO$_3$ at 25°

Salt pair mixed	1.0 m^a	0.5 m	ΔH_m (cal./kg.) at $X = 0.5$ 0.2 m	0.1 m
NaCl–NaBr	0.79	0.18	0.03^c	0.01^c
KCl–KBr	0.80	0.18^b	0.03^c	0.01^c
NaCl–KCl	−9.58	−2.31	−0.40	−0.10
NaBr–KBr	−9.43	−2.42	−0.38	−0.12
NaCl–KBr	1.21	0.53	0.19	0.05^c
NaBr–KCl	−18.71	−5.04	−0.92	−0.24
Σ□	−17.42	−4.37 ± 0.06	−0.72 ± 0.07	−0.20 ± 0.04
Σ×	−17.50	−4.51 ± 0.07	−0.73 ± 0.04	−0.19 ± 0.05
NaCl–NaNO$_3$	3.10	1.04	0.20	0.05^c
KCl–KNO$_3$	0.34	0.09^c	0.02^c	0.01^c
NaCl–KCl	−9.58	−2.31	−0.39	−0.09
NaNO$_3$–KNO$_3$	−12.57	−3.61	−0.56	−0.13
NaCl–KNO$_3$	79.2	24.61	5.03	1.39
NaNO$_3$–KCl	−100.2	−29.69	−5.85	−1.74
Σ□	−18.7	−4.79 ± 0.10	−0.73 ± 0.08	−0.16 ± 0.07
Σ×	−21.0	−5.08 ± 0.11	−0.82 ± 0.10	−0.35 ± 0.09

^{a} All results at 1.0 m from Young and co-workers.[6-8] ^{b} Heat of mixing of Cl and Br in the presence of K assumed to be the same as in presence of Na ion as shown by Young, $et\ al.$, at 1.0 m. ^{c} Result calculated from measurements at higher concentration assuming an m^2 concentration dependence (h_0 constant).

The present studies allow an examination of the concentration dependence of the cross-square rule below 1.0 m. The results for the set NaCl, NaBr, KCl, KBr and the set NaCl, NaNO$_3$, KNO$_3$, KCl are given in Table II. The heat of mixing of NaCl with KBr at 0.1 m and several of the small heats of mixing of anions in the presence of a common cation were estimated from data at higher concentrations. The heat of mixing the chloride and bromide ions was assumed to be the same in the presence of either sodium or potassium as common cation. Young, Wu, and Krawetz[7] have shown this to be true at 1.0 m.

For both sets of data the sum of the cross mixings (Σ×) is nearly equal to the sum of the common ion mixing (Σ□), so that large deviations from the cross-square rule are not present. For the NaCl, NaNO$_3$, KCl, KNO$_3$ set, the sum of the common ion mixings is more positive than the sum of the cross mixings at every concentration and the difference is greater than our estimate of the experimental error in two cases. Because of this, and the fact that the measurements at 1.0 m are from a different laboratory,[8] the difference may be real. It is interesting to note that this test of the cross-square rule is the only one which contains an ion-paired salt, potassium nitrate.[25,26]

Wu[27] has shown how the individual heats of cross mixing (without a common ion) can be calculated from the cross-square rule and the relative apparent molal heat content (ϕ_L) of the four salts of a set. Wu's equations can be arranged to give

$$\Delta H_m(NX - MY) = m/4[\phi_L(NY) +$$
$$\phi_L(MX) - \phi_L(NX) - \phi_L(MY)] + \frac{1}{2}\Sigma\square \quad (3)$$

where ΔH_m and Σ□ are in calories per kilogram of solvent.

The most accurate ϕ_L data are needed to show the accuracy of this method of calculating cross mixings since the resultant heats of mixing for many salt pairs are the small differences between large ϕ_L values. The ϕ_L values used are accurate to about ±1 cal./mole at 0.1 m and ±10 cal./mole at 1.0 m for the alkali metal halides, but those for the nitrates are much more uncertain.

A comparison of the experimental heats of mixing for the four uncommon ion mixtures studied and the heats calculated from ϕ_L and common ion mixings by Wu's technique are given in Table III. The ϕ_L values used are listed in Table IV. Most of these values are from Harned and Owen,[19] but several were calculated by extrapolation to zero concentration of original heat of dilution data using a new equation[28] for ϕ_L.

The agreement between experimental and calculated heats of mixing for the salt pairs NaCl–KNO$_3$ and NaNO$_3$–KCl is excellent as shown in Table III. For the salt pairs NaBr–KCl and NaCl–KBr the agree-

(25) C. W. Davies, $Trans.\ Faraday\ Soc.$, 23, 354 (1927).

(26) R. A. Robinson and C. W. Davies, $J.\ Chem.\ Soc.$, 574 (1937).

(27) Y. C. Wu, Ph.D. Thesis, University of Chicago, 1957.

(28) R. H. Wood, R. W. Smith, and H. S. Jongenburger, unpublished results.

Table III: Comparison of Experimental ΔH_m and ΔH_m Calculated from ϕ_L and Common Ion Mixings at Various Concentrations and 25°

Salt pair	m	ΔH_m (exptl.), cal./kg.	ΔH_m (calcd.), cal./kg.
NaBr + KCl	1.0	−18.71	−24.7
	0.5	−5.08 ± 0.04	−4.95
	0.2	−0.92 ± 0.04	−0.01
	0.1	−0.24 ± 0.05	−0.12
NaCl + KBr	1.0	1.21	7.3
	0.5	0.53 ± 0.06	0.55
	0.2	0.19 ± 0.02	−0.71
	0.1	0.05 ± 0.02	−0.08
NaCl + KNO₃	1.0	79.2	77.2
	0.5	24.61 ± 0.06	26.75
	0.2	5.03 ± 0.06	5.18
	0.1	1.39 ± 0.04	1.44
NaNO₃ + KCl	1.0	−100.2	−95.9
	0.5	−29.70 ± 0.09	−31.55
	0.2	−5.85 ± 0.08	−5.92
	0.1	−1.74 ± 0.08	−1.60

[a] ΔH_m at 1.0 m due to Young, et al.[7,8]

Table IV: Relative Apparent Molal Heat Contents[a] (cal./mole) at 25°

Salt	1.0 m	0.5 m	0.2 m	0.1 m
NaCl	−23	58	90	86[d]
NaBr	−37	41	72	73
KCl	−26	48	81	78
KBr	−104	9	70	64
NaNO₃	−359[b,c]	−160[b,c]	−23[b,c]	32[b]
KNO₃	−708[b,c]	−403[b,c]	−143[b,c]	−37[e]

[a] See Harned and Owen, ref. 19. [b] Obtained by extrapolation of data of E. Lange and A. L. Robinson, *Z. physik. Chem.*, **148A**, 97 (1930). [c] Obtained by interpolation of data of F. R. Pratt, "International Critical Tables," Vol. V, McGraw-Hill Book Co., Inc., New York, N. Y., 1929, p. 160. [d] Obtained by extrapolation of data of E. A. Gulbransen and A. L. Robinson, *J. Am. Chem. Soc.*, **56**, 2637 (1934). [e] Obtained by extrapolation of data of E. Lange and J. Momheim, *Z. physik. Chem.*, **150A**, 349 (1930).

ment is not as good, although the heats do agree within the estimated uncertainty except for NaCl–KBr at 0.2 m. The agreement of the data at 0.1 m indicates that the extrapolations of ϕ_L values of all the salts in

Table IV are consistent to nearly ±0.5 cal./mole at 0.1 m. Since very accurate heat of dilution data for most of these salts are not available above 0.1 m, the agreement of the experimental and calculated results are as good as could be expected.

Hydration of Acetone in 1,2-Dichloroethane

by T. F. Lin, Sherril D. Christian, and Harold E. Affsprung

Department of Chemistry, The University of Oklahoma, Norman, Oklahoma   (*Received March 5, 1965*)

Proton magnetic resonance, water solubility, and partition measurements support the hypothesis that acetone monomer and monomer monohydrate are the major solute species present in 1,2-dichloroethane solvent. Studies were made at formal concentrations of acetone less than 0.6 M at a variety of water activities in the temperature range 25 to 45°.

Introduction

Recently, we have reported the heteroassociation of water with a number of hydrogen bonding compounds, including carboxylic acids, amides, phenols, and amines, in dilute solution in organic solvents and in the vapor phase.[1-4] In most of the systems studied, elucidation of the nature of the hydrates formed is complicated by two factors. First of all, the polar molecule being hydrated may be capable of functioning as both a proton donor and a proton acceptor. Secondly, the compound may self-associate significantly, even in dilute solution; thus, it is necessary to determine accurate values of the self-association constants for the solute before attempting to infer hydration constants from spectral or phase equilibrium data.

We thought it desirable to study the hydration of a ketone, inasmuch as the carbonyl group in ketones might reasonably be expected to interact with the proton of the water molecule but not with the oxygen. Further, ketones do not appear to self-associate in dilute solution. We report here an investigation of the heteroassociation between water and acetone in dilute solution in 1,2-dichloroethane, using equilibration techniques developed in this laboratory[5,6] and proton magnetic resonance measurements.

Experimental

Reagent grade 1,2-dichloroethane and acetone were fractionally distilled using a 30-plate Oldershaw column. Solutions of water in 1,2-dichloroethane, required for the proton magnetic resonance experiments, were determined with the Beckman KF-3 Aquameter. The Aquameter was used also in determining water in 1,2-dichloroethane solutions containing both acetone and water; however, to avoid end point drift in samples containing the ketone, it was necessary to use a modified

Karl Fischer reagent.[7] Acetone concentrations in 1,2-dichloroethane solutions were determined by measuring the absorbance at 272 mμ with a Beckman DU spectrometer, using a slit width of 0.1 mm. Beer's law was obeyed throughout the concentration range 0 to 0.12 M; the experimental absorptivity was 15.6 (mole/l.)$^{-1}$ cm.$^{-1}$.

Using the equilibration method described previously,[5,6] the solubility of water in 1,2-dichloroethane was determined at water activities ranging from 0.276 to 1.00 and acetone concentrations varying from 0 to 0.6 M. Since the activity of acetone in the system was relatively low, the transfer of acetone into the constant humidity solution (sulfuric acid) did not significantly change the water activity in the equilibrator.

Proton magnetic resonance data for solutions of water and acetone in 1,2-dichloroethane were obtained with the Varian A-60 n.m.r. spectrometer. The chemical shift of the water proton was measured relative to cyclohexane contained in a sealed capillary tube inserted in the sample tube. Formal water concentrations varied from 0.046 to 0.143 M and formal acetone concentrations ranged from 0 to 0.14 M. The water proton chemical shift was measured for a series of solu-

(1) S. D. Christian, H. E. Affsprung, and S. A. Taylor, *J. Phys. Chem.*, **67**, 187 (1963).

(2) S. D. Christian, H. E. Affsprung, and C. Ling, *J. Chem. Soc.*, in press.

(3) S. D. Christian, H. E. Affsprung, and J. R. Johnson, *ibid.*, 1 (1965).

(4) C. Ling, Ph.D. Dissertation, University of Oklahoma, 1964; J. D. Worley, Ph.D. Dissertation, University of Oklahoma, 1964.

(5) S. D. Christian, H. E. Affsprung, and J. R. Johnson, *J. Chem. Soc.*, 1896 (1963).

(6) S. D. Christian, H. E. Affsprung, J. R. Johnson, and J. D. Worley, *J. Chem. Educ.*, **40**, 421 (1963).

(7) J. Mitchell and E. M. Smith, "Aquametry," Interscience Publishers, Inc., New York, N. Y., 1958, p. 147.

tions of water in 1,2-dichloroethane varying in concentration from 0 to 0.126 M; these data indicated that water partially self-associates in 1,2-dichloroethane, in agreement with results of a previous study performed in this laboratory.[8]

Results and Discussion

Equilibration data and n.m.r. data for solutions of water and acetone in 1,2-dichloroethane are presented in Table I and Figures 1–3. Formal concentrations of water and acetone are represented by f_W and f_A, respectively; a_W is the water activity and δ is the water proton chemical shift, relative to the cyclohexane proton chemical shift at a field frequency of 60 Mc./sec.

Figure 1. Chemical shift of water protons in 1,2-dichloroethane at 30°.

Table I: The Increase of Water Solubility in 1,2-Dichloroethane in the Presence of Acetone at Various Water Activities

f_A	f_W	Δf_W	Δf_W^{calcd}	f_A	f_W	Δf_W	Δf_W^{calcd}
$a_W = 1.00$ at 25°				$a_W = 0.436$ at 25°			
0.000	0.1252	0.0000	0.0000	0.000	0.0500	0.0000	0.0000
0.015	0.1273	0.0021	0.0012	0.051	0.0526	0.0026	0.0020
0.037	0.1281	0.0029	0.0031	0.115	0.0540	0.0040	0.0046
0.074	0.1312	0.0060	0.0062	0.175	0.0573	0.0073	0.0067
0.126	0.1362	0.0110	0.0105	0.275	0.0602	0.0102	0.0105
0.133	0.1360	0.0108	0.0111	0.358	0.0625	0.0125	0.0137
0.165	0.1400	0.0148	0.0137	0.382	0.0633	0.0133	0.0146
0.182	0.1400	0.0148	0.0151	0.408	0.0648	0.0148	0.0157
0.199	0.1421	0.0169	0.0165				
0.236	0.1468	0.0216	0.0196	$a_W = 1.00$ at 35°			
0.260	0.1482	0.0230	0.0216	0.000	0.1570	0.0000	0.0000
0.306	0.1522	0.0270	0.0254	0.079	0.1645	0.0075	0.0067
0.408	0.1601	0.0351	0.0339	0.142	0.1700	0.0130	0.0126
0.410	0.1620	0.0368	0.0340	0.211	0.1780	0.0210	0.0187
				0.281	0.1830	0.0260	0.0249
$a_W = 0.890$ at 25°				0.352	0.1910	0.0340	0.0312
0.000	0.1115	0.0000	0.0000	0.409	0.1955	0.0385	0.0362
0.060	0.1150	0.0035	0.0045	0.464	0.1980	0.0410	0.0411
0.069	0.1170	0.0055	0.0052				
0.096	0.1200	0.0085	0.0072	$a_W = 0.443$ at 35°			
0.098	0.1175	0.0060	0.0075	0.000	0.0655	0.0000	0.0000
0.170	0.1260	0.0145	0.0128	0.059	0.0667	0.0012	0.0024
0.271	0.1320	0.0205	0.0204	0.105	0.0676	0.0021	0.0043
0.276	0.1350	0.0235	0.0208	0.163	0.0715	0.0060	0.0067
0.388	0.1420	0.0305	0.0292	0.226	0.0736	0.0081	0.0093
0.388	0.1400	0.0285	0.0292	0.272	0.0757	0.0102	0.0113
				0.337	p.0786	0.0131	0.0139
$a_W = 0.616$ at 25°				0.366	0.0810	0.0155	0.0151
0.000	0.0722	0.0000	0.0000				
0.025	0.0750	0.0028	0.0013	$a_W = 0.276$ at 35°			
0.108	0.0780	0.0058	0.0058	0.000	0.0395	0.0000	0.0000
0.171	0.0810	0.0088	0.0092	0.092	0.0407	0.0012	0.0024
0.240	0.0849	0.0127	0.0128	0.141	0.0426	0.0031	0.0037
0.296	0.0872	0.0150	0.0158	0.252	0.0460	0.0065	0.0066
0.362	0.0894	0.0172	0.0193	0.351	0.0478	0.0083	0.0092
0.422	0.0941	0.0219	0.0226	0.468	0.0512	0.0117	0.0122
				0.522	0.0546	0.0151	0.0144
				0.628	0.0569	0.0174	0.0164

Figure 2. Chemical shift of water protons in the system water–acetone–1,2-dichloroethane at 30°: A, $f_w = 0.058\ M$; B, $f_w = 0.078\ M$; C, $f_w = 0.100\ M$; D, $f_w = 0.126\ M$.

Both the equilibration data in Table I and the n.m.r. data in Figure 1 indicate that water aggregates are present in 1,2-dichloroethane at the higher water activities. Johnson, *et al.*,[8] have concluded that water

tends to form polymers in 1,2-dichloroethane solution. Their data on the solubility of water in this solvent are consistent with the assumption that either monomer–trimer or monomer–tetramer equilibrium occurs in solution; however, least-squares analysis of the results indicates that dimers are not present in significant concentration. They reported a water trimerization constant, K_3, of $20 \pm 3\ \text{l.}^2\ \text{mole}^{-2}$ at 10° and $4.6 \pm 0.3\ \text{l.}^2\ \text{mole}^{-2}$ at 25°. A value $K_3 = 2.0 \pm 0.2\ \text{l.}^2\ \text{mole}^{-2}$ at 35° has been calculated from the present data.

The cyclic water trimer has also been proposed by

(8) J. R. Johnson, S. D. Christian, and H. E. Affsprung, in preparation.
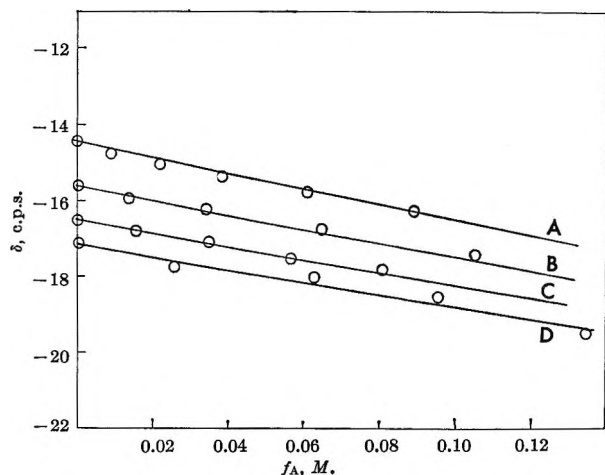
Figure 3. Chemical shift of water protons in the system water–acetone–1,2-dichloroethane at 45°: A, $f_w = 0.046\ M$; B, $f_w = 0.084\ M$; C, $f_w = 0.123\ M$; D, $f_w = 0.143\ M$.

Holmes, Kivelson, and Drinkard[9] as being one of the possible kinetic intermediates in proton exchange mechanisms in a variety of solvents. Various workers have proposed the existence of trimers and tetramers to explain n.m.r. data for dilute solutions of alcohols and phenols in organic solvents.[10,11]

Data in Figure 1 may be shown to be consistent with the trimer assumption by postulating that the associated species has the cyclic structure
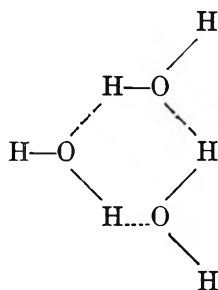
and that the hydrogen bonded protons have a chemical shift, δ_3, distinct from that of the nonbonded protons, δ_0. If it is further assumed that δ_0 is equal to the chemical shift of the protons in the water monomer, the observed chemical shift may be expressed as

$$\delta = \delta_0\left(\frac{2c_W + 3c_{W_3}}{2f_W}\right) + \delta_3\left(\frac{3c_{W_3}}{2f_W}\right) \quad (1)$$

where c_W and c_{W_3} represent the concentrations of water monomer and trimer, respectively. Using the relation $K_3 = c_{W_3}/c_W{}^3$, eq. 1 may be rewritten

$$\delta\left(\frac{2 + 6K_3c_W{}^2}{2 + 3K_3c_W{}^2}\right) = \delta_0 + \left(\frac{3K_3c_W{}^2}{2 + 3K_3c_W{}^2}\right)\delta_3 \quad (2)$$

It is possible to calculate c_W, corresponding to each value of δ in Figure 1, from the known f_W and the value of K_3 at 30° (3.1 l.[2] mole^{-2}, obtained by interpolation) by solving the cubic equation $f_W = c_W + 3K_3c_W{}^3$. If the data in the figure are replotted in the form

$$\delta\left(\frac{2 + 6K_3c_W{}^2}{2 + 3K_3c_W{}^2}\right)\ vs.\ \left(\frac{3K_3c_W{}^2}{2 + 3K_3c_W{}^2}\right)$$

a straight line is obtained, having the least-squares parameters $\delta_0 = -16.5 \pm 0.1$ c.p.s. and $\delta_3 = -98 \pm 4$ c.p.s. The solid curve in Figure 1, calculated using these parameters, agrees well with the experimental chemical shift values.

If it is assumed that the water trimer (W_3) is the only self-associated species present and that the acetone monohydrate (AW) is the sole heteroassociated species, the data in Table I may be explained. The formal concentrations of the solutes may be written

$$f_W = c_W + 3c_{W_3} + c_{AW} = c_W + 3K_3c_W{}^3 + K_{11}c_Ac_W$$

and

$$f_A = c_A + c_{AW} = c_A + K_{11}c_Ac_W \quad (3)$$

where c_A and c_W are the concentrations of monomeric acetone and water, respectively, and K_{11} is the equilibrium constant for formation of AW from the monomers, A and W. Equations 3 may be rearranged to yield

$$\Delta f_W = K_{11}(f_A - \Delta f_W)c_W = K_{11}(f_A - \Delta f_W)a_Wc_W{}^0$$

or

$$\Delta f_W/a_W = K_{11}(f_A - \Delta f_W)c_W{}^0 \quad (4)$$

in which Δf_W represents the measured difference between f_W and the value of f_W corresponding to $f_A = 0$ at the given water activity. In deriving eq. 4, c_W has been replaced by $a_Wc_W{}^0$, where $c_W{}^0$ is the concentration of water monomer at $a_W = 1$. Values of $c_W{}^0$ obtained from the water solubility data are 0.108 mole/l. at 25° and 0.143 mole/l. at 35°. Data at each temperature were treated by least squares in the linear form of eq. 4 to obtain values of K_{11}; no systematic variation of K_{11} with a_W at a given temperature was detected. Thus it is improbable that hydrates other than AW are present in significant concentrations. The equilibrium constant of acetone monohydrate, K_{11}, was calculated to be 0.85 ± 0.05 l. mole^{-1} at 25° and 0.68 ± 0.04 l. mole^{-1} at 35°. Using these values, the theoretical

(9) J. R. Holmes, D. Kivelson, and W. C. Drinkard, *J. Am. Chem. Soc.*, **84**, 4677 (1962).

(10) M. Saunders and J. B. Hyne, *J. Chem. Phys.*, **29**, 1319 (1958).

(11) A. D. Cohen and C. Reid, *ibid.*, **25**, 790 (1956).

values of Δf_W presented in Table I were calculated by the equation

$$\Delta f_W{}^{calcd} = K_{11}c_W{}^0 a_W f_A / (1 + K_{11}c_W{}^0 a_W)$$

The experimental values, Δf_W, and theoretical values, $\Delta f_W{}^{calcd}$, agree to within the expected errors in the determined values of the water solubility.

In treating the n.m.r. data in Figures 2 and 3 it is possible to relate δ to f_A and f_W through the equations

$$f_W(\delta - \delta_0) - {}^3/_2(\delta_3 - \delta_0)K_3c_W{}^3 =$$
$$K_{11}c_W \left(\frac{f_A}{1 + K_{11}c_W} \right)\left(\frac{\delta_1 - \delta_0}{2} \right) \quad (5)$$

and

$$f_W = c_W + 3K_3c_W{}^3 + \frac{K_{11}c_W f_A}{1 + K_{11}c_W} \quad (6)$$

where δ_1 is the chemical shift of a water proton bonded to the acetone carbonyl group. In deriving eq. 5 it is assumed that the complex AW has a single hydrogen-bonded proton and that the nonbonded proton has the same chemical shift as that of a proton in the water monomer (δ_0). Values of c_W may be computed numerically from eq. 6, using extrapolated and interpolated values of K_{11} and K_3 and the measured values of f_A and f_W. With c_W known, δ_1 may be calculated directly using eq. 5. However, to obtain an unbiased least-squares value of δ_1, data were plotted in the form

$$Y = f_W[(\delta - \delta') + (\delta' - \delta_0)] -$$
$${}^3/_2(\delta_3 - \delta_0)K_3c_W{}^3 \ vs. \ X = \frac{K_{11}c_W f_A}{1 + K_{11}c_W}$$

in which δ' represents the chemical shift a solution would have at a given value of f_W if f_A were zero. In other words, from the data in Figures 2 and 3, $\delta - \delta'$ has been obtained as the difference between δ at f_A and at $f_A = 0$ for each sample in a set of solutions at constant f_W. Values of $\delta' - \delta_0$ were computed from the known δ_3, K_3, K_{11}, and f_W, rather than taken as the experimental difference between the initial point on each δ vs. f_A curve and δ_0. In this way it was possible to avoid the systematic error (analogous to a base-line error) which would otherwise be introduced into a sequence of computed Y values by an error in δ for the initial sample in the series. Extrapolated and interpolated values of the equilibrium constants used in computing X and Y were: at 30°, $K_3 = 3.1 \ 1.^2$ mole^{-2}, $K_{11} = 0.76$ l. mole^{-1}; at 45°, $K_3 = 0.9 \ 1.^2$ mole^{-2}, $K_{11} = 0.55$ l. mole^{-1}. The results were analyzed by plotting Y vs. X for all n.m.r. data obtained at 30 and 45°;

both sets of data appeared to follow the same straight line passing through the origin. From the slope of the least-squares straight line the value $\delta_1 = -100 \pm 7$ c.p.s. was obtained. The curves in Figures 2 and 3 have been calculated using this value of δ_1 and the experimental values of δ'. Hence all the n.m.r. data, as well as the water solubility data at various water activities, are adequately explained by assuming the existence of a single heteroaggregate, the acetone monohydrate.

It should be noted that although available data do not make it possible to decide with certainty whether primarily water trimers, tetramers, or some combination of polymers are present, the form assumed for the water aggregates does not significantly affect the derived value of K_{11}. The computed value of $c_W{}^0$ changes by less than 3% as various combinations of species (e.g., monomer-trimer, monomer-tetramer, monomer-trimer-tetramer) are assumed in fitting water solubility data. Hence, in treating data by eq. 4, the same percentage uncertainty will be introduced into the calculated value of K_{11}.

The reported chemical shifts of the water monomer proton, the bonded proton in W_3 and the bonded proton in AW are -16.5, -98, and -100 c.p.s., respectively. These values suggest that the hydrogen bonds in W_3 and AW are approximately equal in strength—an observation supported by the fact that the enthalpy of hydrogen bond formation in both of these species is estimated to be about -5 kcal./mole of bonds from the temperature dependence of K_3 and K_{11} (over the limited range of temperatures for which the constants have been determined).

Because of the large number of unknown parameters involved, n.m.r. data by themselves are often of limited use in calculating accurate values of equilibrium constants for hydrogen bonding reactions occurring in dilute solutions. However, when it is possible to employ the n.m.r. method in conjunction with other physical techniques, the n.m.r. data may provide valuable confirmatory evidence that the postulated equilibria and calculated constants are reasonable. In the present system, a consistent explanation of all the data is provided by the assumption that in dilute solutions in 1,2-dichloroethane the associated species W_3 and AW exist in addition to the water and acetone monomers.

Assignment of Limiting Equivalent Conductances for Single Ions to 400°[1]

by Arvin S. Quist and William L. Marshall

Reactor Chemistry Division, Oak Ridge National Laboratory, Oak Ridge, Tennessee   (*Received March 8, 1965*)

Limiting equivalent conductances of the hydrogen, lithium, potassium, sodium, ammonium, hydroxide, chloride, bisulfate, and sulfate ions in water have been calculated at 100, 200, and 300° at densities of 0.958, 0.865, and 0.712 g. cm.$^{-3}$, respectively (corresponding to liquid–vapor equilibrium pressures of 1.01, 15.6, and 85.9 bars, respectively). The limiting equivalent conductances of the potassium, sodium, hydrogen, chloride, bisulfate, and sulfate ions are also given at 400° for a density of 0.8 g. cm.$^{-3}$ (corresponding to a pressure of approximately 2130 bars). Equations are given that permit the extrapolation of these limiting ionic conductances to solution densities of 1.0 g. cm.$^{-3}$ at 100, 200, 300, and 400°.

In an evaluation of the electrical conductances of aqueous electrolyte solutions at high temperatures and pressures, the limiting equivalent conductances of single ions to 400° and 4000 bars were needed. Limiting ionic conductances have been reported to 100°,[2] but we could not find values or estimates at higher temperatures.

Limiting equivalent conductances for several electrolytes at temperatures to 300°, reported in the literature and used herein for calculating limiting ionic conductances, are summarized in Table I. The equivalent conductance of K_2SO_4 at 100°, 1 atm., included in Table I, was obtained by combining the data of Noyes, *et al.*,[3] with those of Quist, *et al.*[4] (extrapolated to values for liquid in equilibrium with vapor) and using the Owen method[5] to evaluate this combined set of data. At 200°, by extrapolating the Walden product ($\Lambda_0\eta_0$) for K_2SO_4 at 0.9 and 1.0 g. cm.$^{-3}$ [4] to 0.865 g. cm.$^{-3}$ (density of water at saturation vapor pressure at 200°), a $\Lambda_0(K_2SO_4)$ of 890 was obtained ($\Lambda_0(K_2SO_4)$ at 200°, 0.9 g. cm.$^{-3}$, in Table V of ref. 4 should be 833 instead of 844). At higher temperatures, hydrolysis of the sulfate ion causes large uncertainties in the estimation of $\Lambda_0(K_2SO_4)$ by extrapolation of experimental equivalent conductances to zero concentration,[4] and therefore $\Lambda_0(K_2SO_4)$ at 300° was not included in Table I.

To calculate limiting ionic conductances from the limiting equivalent conductances of a series of electrolytes having one or more ions in common, it is necessary to know the transference numbers at in-

Table I: Limiting Equivalent Conductances to 300° at Saturation Vapor Pressure[a]

Temp., °C.	NaCl	KCl	HCl	NaOH	LiOH	NH₄OH	K₂SO₄
100	362.2	406.0 / 405[b]	845.4	589.2	603	653	441[c]
200	695	755 / 763[b]	1215 / 1214[b]	1005	1030	1095	890[c]
300	1018 / 1023 ± 2[d]	1065	1455 / 1455 ± 5[d]	1280	1383	1400	...

[a] Except where noted, the values for NaCl, KCl, HCl, and NaOH were interpolated from the re-evaluation of the data of Noyes[3] by J. M. Wright, W. T. Lindsay, Jr., and T. R. Druga, "The Behavior of Electrolytic Solutions at Elevated Temperatures as Derived from Conductance Measurements," WAPD-TM-204, Bettis Atomic Power Laboratory, Westinghouse Electric Corp., Pittsburgh, Pa., June 1961. The values for LiOH and NH₄OH were interpolated from the measurements of Wright, *et al.*, preceding source. [b] A. J. Ellis, *J. Chem. Soc.*, 545 (1963). [c] See text. [d] D. Pearson, C. S. Copeland, and S. W. Benson, *J. Am. Chem. Soc.*, 85, 1044, 1047 (1963).

finite dilution for the ions of at least one of the electrolytes. Smith and Dismukes[6] have measured cation

(1) Research sponsored by the U. S. Atomic Energy Commission under contract with the Union Carbide Corp.

(2) R. A. Robinson and R. H. Stokes,"Electrolyte Solutions," 2nd Ed., Butterworths Scientific Publications, London, 1959, p. 465.

(3) A. A. Noyes, *et al.*, "The Electrical Conductivity of Aqueous Solutions," Publication No. 63, Carnegie Institution of Washington, Washington, D. C., 1907.

(4) A. S. Quist, E. U. Franck, H. R. Jolley, and W. L. Marshall, *J. Phys. Chem.*, 67, 2453 (1963).

(5) B. B. Owen, *J. Am. Chem. Soc.*, 61, 1393 (1939).

Table II: Estimated Limiting Equivalent Conductances for Several Ions at Temperatures to 400°

	H^+	Li^+	Na^+	K^+	NH_4^+	OH^-	Cl^-	HSO_4^-	SO_4^{2-}
0°, 1 atm.[a]	225	19.4	26.5	40.7	40.2	105	41.0	...	41
18°, 1 atm.[a]	315	32.8	42.8	63.9	63.9	171	66.0	43.6[b]	68.4
25°, 1 atm.[a]	349.8	38.7	50.1	73.5	73.6	198.3	76.4	51.2[b]	80.0
100°, 1 atm.	634	156	151	195	206	447	211	140	246[c]
200°, 0.865 g. cm.$^{-3}$ (15.6 bars)	824	329	304	364	394	701	391	290	525
300°, 0.712 g. cm.$^{-3}$ (85.9 bars)	894	562	459	504	579	821	561	440	800
400°, 0.8 g. cm.$^{-3}$ (2130 bars)	960	...	430	470	...	...	510	400	770

[a] See ref. 2.   [b] M. Kerker, *J. Am. Chem. Soc.*, **79**, 3664 (1957).   [c] Robinson and Stokes[2] report 260, which was probably based on $\Lambda_0(K_2SO_4) = 455$.[3] Since the value of 455 was obtained by a semiempirical extrapolation [Λ^{-1} vs. $(c\Lambda)^n$], whereas the value of 441 in Table I is based on using the theoretical Fuoss–Onsager equation (included in the Owen method) with the combined data of Noyes, *et al.*,[3] and Quist, *et al.*,[4] the later value is considered the more reliable.

transference numbers (t) in 0.1 N KCl and NaCl solutions at temperatures to 125°. They also estimate the transference numbers at infinite dilution at 100°. Earlier cation transference measurements with KCl[7] and NaCl[8] covered the temperature range 15–45°. Smith and Dismukes[6] observed a linear relationship when log t_{Cl^-}/t_{Na^+} (or log t_{Cl^-}/t_{K^+}) was plotted against $1/T(°K.)$ from 15 to 125° for the 0.1 N solutions. We have assumed that this relationship is linear to temperatures of 400° and have obtained values of t_{Cl^-} in 0.1 N NaCl from this extrapolation. Although this is a long extrapolation, the change in transference number with temperature is small. The uncertainty in the extrapolation probably amounts to less than 1%. Transference numbers of the chloride ion at infinite dilution estimated from these values using the procedure of Smith and Dismukes[6] were 0.581,[6] 0.563, 0.550, and 0.541 at 100, 200, 300, and 400°, respectively. NaCl was chosen for this evaluation in preference to KCl because the estimation of the transference numbers at infinite dilution from those in the 0.1 N solution is somewhat simpler,[6] and because NaCl shows a "normal" variation of transference number with temperature[8] (cation and anion transference numbers approach equality with increasing temperature) while KCl departs from this usual behavior.[6]

By using these estimates of transference numbers and the limiting equivalent conductances in Table I, the limiting ionic conductances of Na^+, H^+, K^+, NH_4^+, Li^+, Cl^-, and OH^- at 100, 200, and 300° were calculated. These values are included in Table II.

Calculation of $\lambda_0(HSO_4^-)$ and $\lambda_0(SO_4^{2-})$

At temperatures of 300° and below, bisulfate ion partially dissociates to hydrogen and sulfate ions, and therefore it is difficult to obtain $\lambda_0(HSO_4^-)$ from experimental measurements. However, above 300° at

solution densities of 0.8 g. cm.$^{-3}$ and below, the dissociation constant of the bisulfate ion becomes sufficiently small that conductance of sulfate and hydrogen ions can be neglected.[9] Therefore, salts such as $KHSO_4$ or H_2SO_4 can be considered uni-univalent electrolytes under these conditions.

Limiting equivalent conductances of $KHSO_4$ and H_2SO_4 at temperatures to 800° and pressures to 4000 bars are reported elsewhere.[9] From the results above 300°, $\lambda_0(HSO_4^-)$ was obtained indirectly at 300° by applying the equation

$$\log \Lambda_0 = A - E_v/RT \qquad (1)$$

used previously by Brummer and Hills[10] to obtain E_v, the energy of activation at constant specific volume, where both A and E_v are assumed to be constants. At low temperatures, a linear plot of log Λ_0 against $1/T(°K.)$ is not observed for electrolytes in aqueous solution, undoubtedly due to the high degree of hydrogen bonding in the solvent. However, as the temperature increases, the structure of water is gradually destroyed, and at temperatures from 400 to 700° we have obtained straight lines for these plots. Examples are shown in Figure 1 where some results for $KHSO_4$ at solution densities of 0.70 and 0.75 g. cm.$^{-3}$ are plotted. By extrapolating these straight lines (Figure 1) down to 300° for solution densities of 0.7 and 0.8 g. cm.$^{-3}$, log $\Lambda_0(KHSO_4)$ at the saturation vapor pressure of H_2O (density = 0.712 g. cm.$^{-3}$) was obtained by interpola-

(6) J. E. Smith, Jr., and E. B. Dismukes, *J. Phys. Chem.*, **67**, 1160 (1963); **68**, 1603 (1964).

(7) R. W. Allgood, D. J. LeRoy, and A. R. Gordon, *J. Chem. Phys.*, **8**, 418 (1940).

(8) R. W. Allgood and A. R. Gordon, *ibid.*, **10**, 124 (1942).

(9) A. S. Quist and W. L. Marshall, *J. Phys. Chem.*, **69**, 2726, 3165 (1965).

(10) S. B. Brummer and G. J. Hills, *Trans. Faraday Soc.*, **57**, 1817, 1823 (1961).
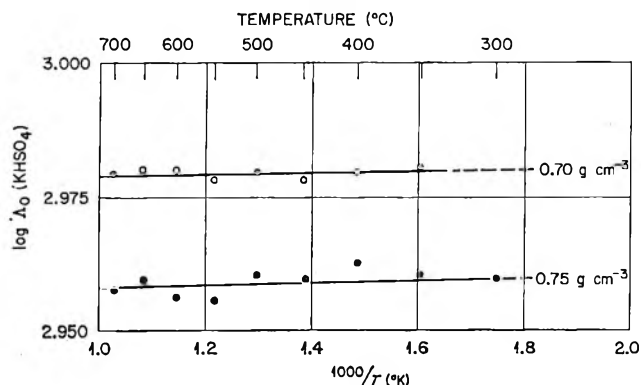
Figure 1. Log $\Lambda_0(KHSO_4)$ as a function of $1/T$ at densities of 0.70 and 0.75 g. cm.$^{-3}$.

tion, giving 944 (at 300°) for $\Lambda_0(KHSO_4)$. The same method was used for obtaining $\Lambda_0(H_2SO_4)$ at 300°, but by extrapolating only Λ_0 values at 400 and 500°. Above 500°, determined $\Lambda_0(H_2SO_4)$ values were considered to be unreliable because of the extensive association of H^+ and HSO_4^- ions. The extrapolation procedure gave a value for $\Lambda_0(HHSO_4)$ of 1335 at 300°, 0.712 g. cm.$^{-3}$. The calculated $\lambda_0(HSO_4^-)$ values at this temperature and density were 440 from both the $KHSO_4$ and H_2SO_4 data. This exact agreement was unexpected, in view of the uncertainties involved, and is considered fortuitous.

Figure 2 shows limiting ionic conductances to 300° of several ions in water at saturation vapor pressure as a function of temperature. For the HSO_4^- ion a smooth curve, similar to that for the sodium ion, was drawn between the values at 50 and 300°. Values for $\lambda_0(HSO_4^-)$ at 100 and 200° given in Table II were interpolated from this curve. A λ_0 for SO_4^{2-} at 300° (in Table II) was obtained by extrapolating to 300° a smooth curve through conductances for SO_4^{2-} (to 200°). The limiting equivalent conductance of an ion is directly proportional to the electrical charge on the ion.[11] For singly and doubly charged ions of the same size, for the ideal case the limiting equivalent conductance of the doubly charged ion would be twice that of the singly charged ion. Comparison of the estimated limiting equivalent conductances of the HSO_4^- and SO_4^{2-} ions (which might be expected to be of nearly the same size if each is hydrated to the same extent) at 100° and above, where water is less ordered than at 25°, shows the conductance of the sulfate ion to be nearly twice that of the bisulfate ion. This behavior agrees with the predictions.

Calculation of λ_0 at 400°

At 400° and above, to our knowledge the only Λ_0 values for a uni-univalent electrolyte that have ap-
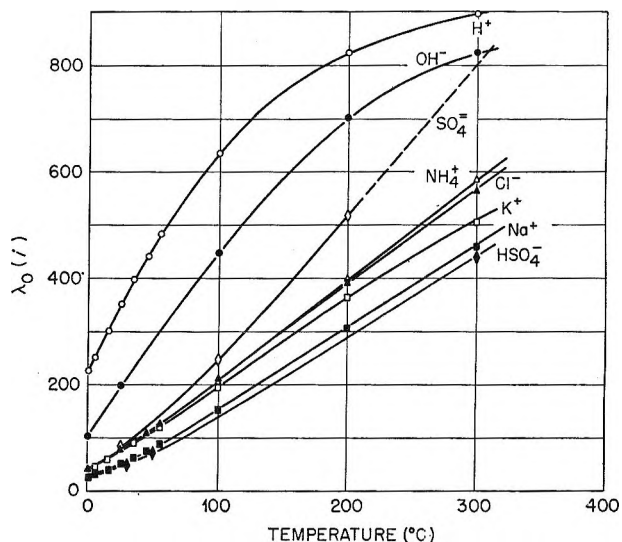
Figure 2. Limiting equivalent conductances of several ions in water as a function of temperature at saturation vapor pressure.

peared in the literature are those of Franck[12a] for KCl. Pearson, et al.,[12b] give Λ_0 values for NaCl and HCl at densities from 0.399 to 0.591 g. cm.$^{-3}$ at temperatures from 345 to 383°. From this limited amount of literature information and from some recent unpublished results on NaCl obtained in this laboratory, it appears that uni-univalent salts still behave as strong electrolytes at a density of 0.8 g. cm.$^{-3}$ at 400°. It further appears that at this temperature and density the bisulfate ion has such a small dissociation constant that H_2SO_4 and $KHSO_4$ can be considered also as uni-univalent electrolytes. From our recent measurements, we have obtained limiting equivalent conductances at 400°, 0.8 g. cm.$^{-3}$, for the several electrolytes given in Table III. Franck[12a] reported $\Lambda_0(KCl)$ to be 980 at 400°, 0.8 g. cm.$^{-3}$. From these values, and from the transference number of the chloride ion at 400° as estimated in this paper, limiting ionic conductances for Na^+, K^+, H^+, Cl^-, and HSO_4^- ions were calculated and included in Table II. A rough estimate of $\lambda_0(SO_4^{2-})$ at 400°, 0.8 g. cm.$^{-3}$, was obtained by extrapolating the curves for SO_4^{2-} and Na^+ in Figure 2 to 400°. By assuming that the ratio, $\lambda_0(SO_4^{2-})/\lambda_0(Na^+)$, was independent of density at 400°, this ratio obtained by the extrapolation was combined with the value of $\lambda_0(Na^+)$ at 0.8 g. cm.$^{-3}$ given in Table II to give an estimate of $\lambda_0(SO_4^{2-}) = 780$ at 400°, 0.8 g. cm.$^{-3}$.

(11) See, for example, S. Glasstone, "An Introduction to Electrochemistry," D. Van Nostrand Co., Inc., Princeton, N. J., 1942, p. 58 ff., 88 ff.

(12) (a) E. U. Franck, Z. physik. Chem. (Frankfurt), 8, 107 (1956); (b) see footnote d, Table I.

Table III: Limiting Equivalent Conductances at 400° (0.8 g. cm.$^{-3}$) as Obtained at Oak Ridge National Laboratory

NaCl	H$_2$SO$_4$ (1:1)^a	KHSO$_4$ (1:1)^a
940	1360	870

^{a} As a uni-univalent electrolyte.

Calculation of λ_0 at Various Densities

Limiting ionic conductances are given herein at only one density at a given temperature (0.8 g. cm.$^{-3}$ at 400°; liquid–vapor equilibrium densities at lower temperatures). Limiting ionic conductances at other densities may be calculated from these results by assuming the independency of transference numbers with pressure (density)[13] at constant temperature and by assuming that the change in the Walden product, $\lambda_0 \eta_0$, with pressure (density) at constant temperature is the same for all ions. [These assumptions may not be valid for ions such as H$^+$ and OH$^-$ that have "abnormal mobility" because this "abnormal mobility" depends to a great extent on the structure of water which in turn probably is affected by pressure (density) changes. However, in the absence of quantitative information on the change in transference numbers of H$^+$ and OH$^-$ with pressure at temperatures above 25°, the above assumptions will be used for all ions.] With these assumptions, this change in Walden product with density would be the same for ions as for electrolytes. Walden products for K$_2$SO$_4$ have been given previously.[4] At this laboratory we are completing measurements on NaCl solutions to 800° and 4000 bars. At temperatures at least to 400° and at high densities (above about 0.4 g. cm.$^{-3}$), the Walden product for NaCl was found to vary linearly with density, at constant temperature. The slopes of the lines of Walden prod-

uct *vs.* density, at constant temperature, at temperatures of 100, 200, 300, and 400° were nearly the same for NaCl as those previously observed for K$_2$SO$_4$. The linear change in Walden product with density observed for NaCl and K$_2$SO$_4$ can be expressed by the equation

$$\Lambda_0\eta_0 = (\Lambda_0\eta_0)^0 + k(d - d^0) \qquad (2)$$

where $\Lambda_0\eta_0$ is the Walden product at density d, $(\Lambda_0\eta_0)^0$ is for a reference density d^0, and k is a constant for a particular temperature. By using the limiting equivalent conductances of NaCl as obtained in this laboratory along with the viscosities of water given by Franck,[12a] values for k were calculated to be -30, -35, -35, and $+12$ at 100, 200, 300, and 400°, respectively. With the assumptions mentioned above, with eq. 2, and with the values for k, limiting ionic conductances may be calculated at other densities from the Λ_0 values at the "reference density" and from Franck's viscosity values by substituting λ_0 for Λ_0 in eq. 2. The viscosity of water at saturation vapor pressure was taken to be 0.283, 0.136, and 0.095 cp. at 100, 200, and 300°, respectively,[14] to be consistent with the viscosities estimated by Franck for higher pressures.

(13) To our knowledge, the only experimental determinations of the effect of pressure upon transference numbers are those reported by Wall and Gill (F. T. Wall and S. J. Gill, *J. Phys. Chem.*, **59**, 278 (1955)) for 0.1 *N* NaCl, KCl, and HCl solutions at 25°. On increasing the pressure from atmospheric pressure to 1000 bars, they observed a 0.5% increase in t_{H^+} and decreases of 2 and 3% in t_{K^+} and t_{Na^+}, respectively. Pressures necessary to obtain densities of 1.0 g. cm.$^{-3}$ for water are approximately 1000, 2780, 4300, and 7500 bars at temperatures of 100, 200, 300, and 400°, respectively. By assuming that pressure has no effect on transference numbers, the extrapolations to a density of 1.0 g. cm.$^{-3}$ would cause a maximum uncertainty probably less than 10% at temperatures of 300° and below. Even at 400° the maximum uncertainty caused by extrapolation to 1.0 g. cm.$^{-3}$, based on the values at 0.8 g. cm.$^{-3}$, would probably be no greater than 15%.

(14) K. Sigwart, *Forschungsarb. Gebeite Ingenieursw.*, **7**, 125 (1936).

Ionic Association in Solutions of Thionine. II. Fluorescence

and Solvent Effects

by G. Haugen and R. Hardwick

*Contribution No. 1692 from the Department of Chemistry, University of California at Los Angeles,
Los Angeles, California   (Received March 8, 1965)*

By means of fluorescence intensity measurements, the tendency of ions of the dye, thionine, to associate into dimers and higher polymers has been studied as a function of solvent composition in water–alcohol solutions. At concentrations $\sim 10^{-3}$ M the dye is highly associated in water solutions, but the degree of association is decreased by small amounts of added methanol. By the time the methanol content of the solutions reaches mole fraction $\geqslant 0.3$, the dye polymers have essentially all dissociated. In its associated state, thionine is not fluorescent, but the monomer fluoresces with maximum emission at about 620 mμ. Interpretation of these data is made through the condensation model.

I. Introduction

In a previous paper (hereafter referred to as I) we have discussed the polymerization of the dye, thionine, in water solutions.[1] The present report describes a study of the fluorescence efficiency of solutions of thionine and an investigation of the associative tendencies of the dye as they are affected by the nature of the solvent.

Of the various species of thionine in solution, only the monomer is fluorescent; thus, the fluorescence efficiency, Q, of thionine solutions decreases as the degree of association is raised by increasing concentration. Rabinowitch and Epstein[2] have noted this effect and have attempted to interpret it in terms of formation only of the thionine dimer. Because their fluorescence data did not fit the dimerization model, however, these authors were forced to attribute some of the fluorescence decline to collisional self-quenching.

Our data indicate that collisional self-quenching is negligible in thionine solutions and that the observed dependence of Q on concentration may be accounted for satisfactorily by the condensation model discussed in paper I.

The thionine polymer is stable in water but is destroyed by the presence of alcohol.[2] We have taken quantitative data on this effect and have interpreted them on the condensation model.

II. Experimental

A. Thionine Purification. The preparation of pure samples of thionine is discussed at length in I. In the present experiments, we have essentially followed our earlier methods of repeated recrystallization from 1:1 water–ethanol solutions at about 35°. This procedure was necessary to remove detectable amounts of the impurity thionol, whose excitation and fluorescence spectra are shown with those of thionine in Figures 1 and 2.

B. Spectra. All absorption spectra were taken on a Cary 14 spectrophotometer. Fluorescence spectra were taken at 25° on an Aminco spectrofluorimeter which had been extensively modified for double-beam work.[3] The curves (*e.g.*, Figures 1 and 2) are shown uncorrected for phototube cathode and monochromator transmission wave length dependence.

C. Fluorescence Efficiency. Measurement of fluorescence efficiencies over large concentration ranges is complicated by the fact that the exciting beam penetrates the cell deeply when dilute solutions are used but hardly gets beyond the surface of concentrated solu-

(1) See paper I: G. R. Haugen and E. R. Hardwick, *J. Phys. Chem.*, **67**, 725 (1963).

(2) E. Rabinowitch and L. F. Epstein, *J. Am. Chem. Soc.*, **63**, 69 (1941).

(3) W. H. Melhuish and R. Murashige, *Rev. Sci. Instr.*, **33**, 1213 (1962).
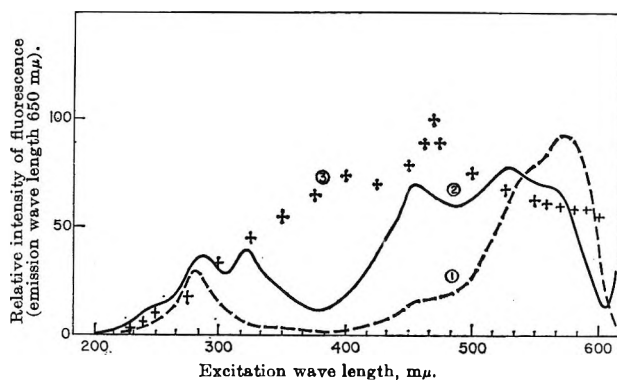
Figure 1. Excitation spectra of dye and impurity fluorescence: - - - -, dilute thionine solution; ———, dilute thionol solution (impurity); + + + +, spectral distribution from high-pressure xenon lamp and excitation monochromator.
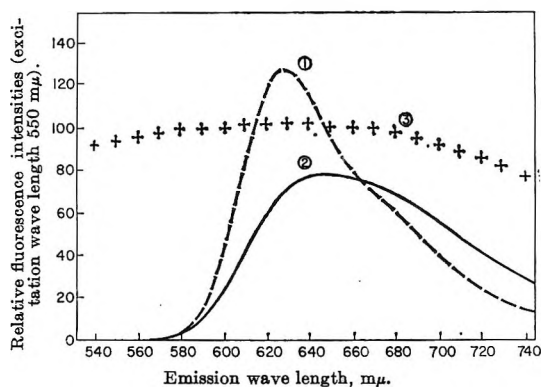
Figure 2. Emission spectra of dilute solutions of dye and impurity: - - - -, uncorrected fluorescence spectra of thionine; ———, uncorrected fluorescence spectra of thionol (impurity); + + + +, spectral response of emission monochromator and Dumont 6911 photomultiplier.

tions. This has the effect of causing the origin of fluorescence emission to shift with concentration; thus, great care must be taken to make proper correction.[4a] Because of experimental necessity, we have used both front and side scanning of the fluorescence cell. Solutions having dye concentrations greater than 5 × 10^{-5} M were observed from the front surface of the cell while those of lesser concentrations were observed from the side. In both cases, correction was made for self-absorption of fluorescence, using the method of Melhuish.[4b]

So that the fluorescence efficiency data from concentrated and dilute solutions may be compared, it is necessary to report results as a photon number ratio of the corrected fluorescence intensity to the intensity of exciting radiation. For concentrated solutions, this is trivially easy since $F = QI_0$, where F is the intensity of fluorescence produced, Q is the quantum efficiency, and

I_0 is the intensity of incident radiation, all of which is absorbed. For dilute solutions, however, $F = QI_{absorbed}$, where $I_{absorbed}$ depends on cell length and concentration. To simplify interpretation, we report all results in terms of infinite cell length, where the observed results for dilute solutions are corrected such that $f = QI_0$ (f being the corrected fluorescence intensity) for both concentrated and dilute solutions.

Finally, the relation between intensity and number of photons must be considered. Our results are reported in terms of the number of incident photons as measured by a quantum counter[5] vs. fluorescence intensity as measured by phototube current. At any given fluorescence wave length, these units are compatible since phototube output current is proportional to the number of incident quanta. All our fluorescence intensity comparisons are made from measurements taken at the fluorescence peak of thionine, ~615-620 mμ (Figure 2, curve 3); thus, correction for phototube wave length dependence was not made. We have not made absolute quantum yield measurements since our comparisons are all relative. Table I shows a sample of typical correction factors and calculated quantum efficiencies.

III. Results

A. Absorption Measurements. 1. Dilute Solutions. In extremely dilute solutions, the thionine molar extinction coefficient, E, at 600 mμ is slightly more than twice as great in methanol solutions as in water solutions; i.e., for solutions which are 5 × 10^{-7} M in thionine, $E_{600} = 8.7 × 10^4$ in CH_3OH, while $E_{600} = 3.6 × 10^4$ in H_2O.[6] Between these values, the extinction coefficient changes linearly with the mole fraction of methanol in CH_3OH-H_2O solutions.

The value of E_{560} is also a function of solvent and, like E_{600}, is linear in the mole fraction of methanol in mixed solvent solutions. We shall find it convenient to assess the changes in the relative intensities of the 560- and 600-mμ absorption peaks by plotting the ratio of the extinction coefficients E_{600}/E_{560}; Figure 3 displays curves of this ratio plotted against methanol mole fraction in the solvent. The curve for dilute solutions is linear with fairly small slope.

2. Nondilute Solutions. In solutions of higher dye concentrations, the effect of solvent composition on the relative heights of absorption peaks is much more pro-

(4) (a) Th. Förster, "Fluoreszenz Organischer Verbindungen," Vandenhoeck & Ruprecht, Göttingen, 1951, p. 35; (b) W. H. Melhuish, J. Phys. Chem., 65, 229 (1961).

(5) W. H. Melhuish, J. Opt. Soc. Am., 52, 1256 (1962).

(6) The value 3.6 × 10^4 is a calculated one which is smaller than the extrapolated 5.7 × 10^4 as reported in paper I. The difference arises from the fact that thionine dissociates slightly in highly diluted aqueous solutions; see paper I, p. 730, for discussion.

Table I: Intensity Corrections and Calculated Quantum Efficiencies

Thionine concn., M	Mole fraction of CH$_3$OH	Correction factor[a]		Calcd. relative quantum efficiencies[b]	
		590 mμ	560 mμ	580 mμ	560 mμ
Front view					
7.6×10^{-6}	1.0	0.78	0.52	0.90	0.80
1.3×10^{-5}	1.0	0.92	0.72	1.0	1.0
3.2×10^{-5}	1.0	0.99	0.95	1.1	1.1
7.6×10^{-5}	1.0	1.0	1.0	1.1	1.1
1.3×10^{-4}	1.0	1.0	1.0	1.1	1.1
3.2×10^{-4}	1.0	1.0	1.0	1.1	1.1
7.6×10^{-4}	1.0	1.0	1.0	1.0	1.0
1.0×10^{-3}	1.0	1.0	1.0	1.0	1.0
1.3×10^{-3}	1.0	1.0	1.0	0.90	1.0
3.2×10^{-3}	1.0	1.0	1.0	0.80	0.70
3.4×10^{-3}	1.0	1.0	1.0	1.1	1.0
Side view					
1.3×10^{-6}	1.0	0.91		1.0	
1.3×10^{-6}	0.92	0.89		0.85	
1.3×10^{-6}	0.80	0.91		0.99	
1.3×10^{-6}	0.60	0.92		0.79	
1.3×10^{-6}	0.21	0.91		0.67	

[a] Allows for reabsorption of emitted light and incomplete absorption of excitation light. [b] Note that for the methanol solutions the relative fluorescence efficiency is roughly constant to within the experimental error of about 0.2, even though the correction factor is fairly small at times. In the side view data, we have shown the decrease in efficiency as the solution goes from CH$_3$OH to H$_2$O.

nounced and is nonlinear. At $T_0 = 10^{-3}\,M$ the ratio E_{600}/E_{560} is 0.9 in pure water solutions but rises to about 2.0 when the mole fraction of methanol reaches only 0.3. At this point, the curve undergoes a sharp break and behaves like a dilute solution curve as further methanol is added; see Figure 3.

The difference in solvent dependence of concentrated and dilute solution curves is more easily seen if the dilute solution dependence is subtracted out; thus Figure 4 is a plot of $[(E_{600}/E_{560})_{T_0=5\times10^{-7}}] - [(E_{600}/E_{560})_{T_0=10^{-3}}]$ against mole fraction of methanol. Section IV.B.1. gives interpretations of this curve and those of Figure 3. Where comparison is possible, these data may be shown to agree roughly with points taken from some of the ethanol–water solution spectra taken by Rabinowitch.[2]

B. Fluorescence Measurements. 1. Spectra. In the absorption spectra of thionine the relative peak heights at different wave lengths show large variations which are brought about by the change of solvent from water to methanol and by changes in concentration. The fluorescence spectra, however, are independent of such changes, the peak position remaining at 615–620
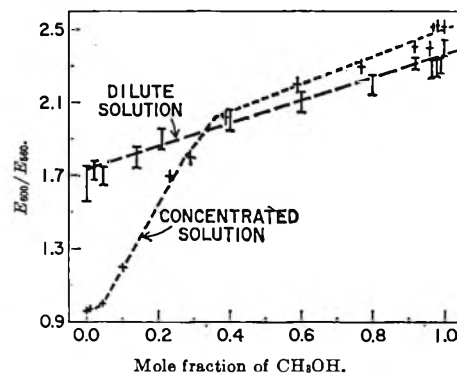
Figure 3. Variation of E_{600}/E_{560} with mole fraction of CH$_3$OH. Concentrations of dilute and concentrated solutions are 5×10^{-7} and $10^{-3}\,M$, respectively.
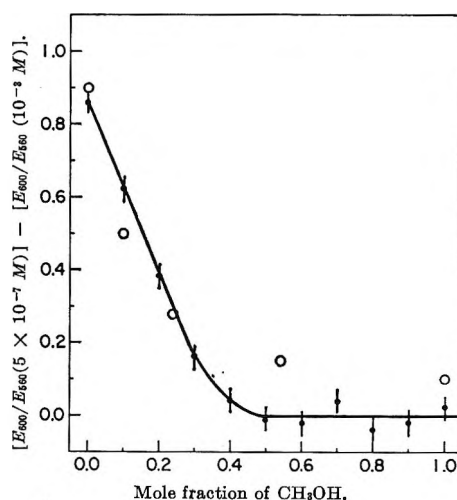
Figure 4. Effect of solvent on intensity of absorption at 560 mμ: ♦, our results with CH$_3$OH–H$_2$O solvent; O, Rabinowitch's (ref. 2) results with CH$_3$CH$_2$OH–H$_2$O.

mμ in both water and alcohol, at concentrations up to $10^{-3}\,M$ (in concentrated solutions there is a slight skewing of the peak because of self-absorption, but correction is easily made for this effect).

2. Concentration Dependence. In dilute solutions, the thionine quantum yield for fluorescence, Q, is nearly independent of solvent as demonstrated by Figure 5, curve 1, which gives Q as a function of the mole fraction of CH$_3$OH for solutions $5 \times 10^{-7}\,M$ in thionine.

In methanol solutions, Q is also independent of concentration at all wave lengths, (Figure 6, curve 1). In aqueous solutions, however, the quantum yield is independent of concentration only when excitation occurs at the extreme, long wave length of the absorption spectrum; thus, with ordinary excitation of water solutions, Q falls off rapidly with increasing concentration (Figure 6, curves 2, 3). As a result, the fluorescence efficiency

of all but the most dilute solutions depends strongly on solvent makeup unless excitation occurs in the 600–610-mμ region. Figure 5, curve 2, gives the Q of a concentrated solution (10^{-3} in thionine) as a function of the mole fraction of CH_3OH in the solvent (excitation, 590 mμ). It may be seen that the curve rises steeply for small amounts of added CH_3OH but that the change is more gradual after the solvent becomes about one-third methanol, beyond which the curves for concentrated and dilute solutions are parallel.

3. Dependence on Excitation Wave Length. In pure CH_3OH solutions the quantum efficiency is independent of the wave length of the exciting light; however, the Q of water solutions strongly depends on excitation wave length except at extreme dilution. Figure 7 shows the dependence of Q on excitation wave length for three solutions which contain 10^{-3} M thionine dissolved in alcohol, in water, and in 2:5, 1:3, and 1:5 water–alcohol mixtures. For more concentrated dye solutions in H_2O, Q drops almost to zero at 540 mμ.

IV. Discussion

Rabinowitch and Epstein have proposed that thionine dimerizes in water solutions but does not dimerize in alcoholic solutions. By means of fluorescence intensity measurements, they have concluded that the dimer is not fluorescent and that the observed concentration dependence of fluorescence quantum yield in water solutions (sometimes called self-quenching) is primarily a result of dimerization. In their quantitative measurements, however, they were unable to fit the data to a dimerization model.
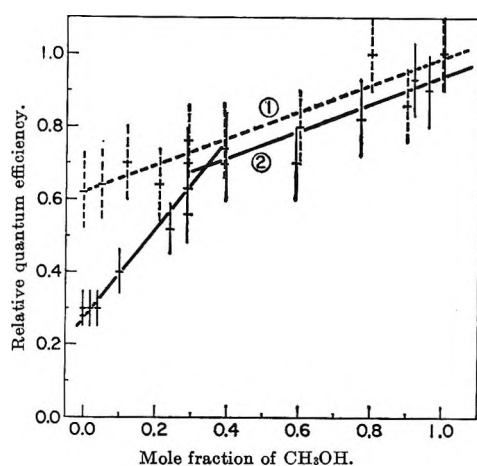
Figure 5. Variation of relative quantum efficiency with mole fraction of CH_3OH. Excitation wave length 590 mμ: curve 1, relative quantum efficiency of fluorescence of dilute ($512 \times 10^{-7} M$) thionine solutions in mixtures of CH_3OH-H_2O; curve 2, relative quantum efficiency of fluorescence of concentrated ($1.3 \times 10^{-3} M$) thionine solutions in mixtures of CH_3OH-H_2O.
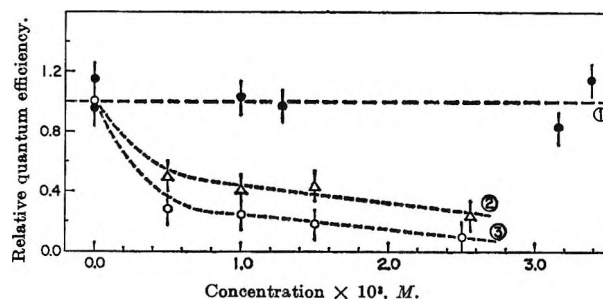
Figure 6. Relative quantum efficiency of fluorescence of thionine solutions in pure CH_3OH and pure H_2O: curve 1, solvent pure CH_3OH, excitation wave length 590 and 560 mμ; curve 2, solvent pure H_2O, excitation wave length 590 mμ; curve 3, solvent pure H_2O, excitation wave length 560 mμ.
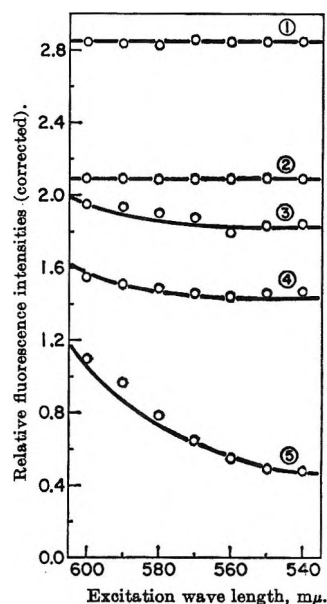
Figure 7. Variation of fluorescence efficiency with excitation wave length (mμ): curve 1, pure CH_3OH solvent; curve 2, CH_3OH-H_2O solvent, 0.39 mole fraction CH_3OH; curve 3, CH_3OH-H_2O solvent, 0.29 mole fraction CH_3OH; curve 4, CH_3OH solvent, 0.24 mole fraction CH_3OH; curve 5, pure H_2O solvent. Dye concentration $10^{-3} M$; maximum error in intensities $\pm 10\%$.

We have taken additional quantitative absorption and fluorescence data in water and in methanol solutions, including intensity and spectral measurements. Where overlap occurs, our data agree with those of Rabinowitch and Epstein; however, we have been able to explain the experimental observations on the basis of a condensation model rather than by simple dimerization. The conclusion that thionine condenses into micelles at higher concentrations in aqueous solution agrees with the discussions of paper I and with earlier work on conductivity, osmotic pressure, etc. (see I for details). The arguments are developed below.

A. Monomeric Solutions. The experimental results that the Beer law is obeyed and that the fluorescence peak position is unchanged in thionine–methanol solutions over a range of concentrations up to 10^{-3} M may be taken with the further observation that the thionine quantum efficiency in methanol is independent of concentration and of exciting wave length to indicate that the dye is unassociated over a wide range of concentrations in methanol.

It is also reasonably evident that thionine does not associate in extremely dilute aqueous solutions (see paper I).

B. Solutions of Associated Ions. 1. Absorption Measurements. Thionine does not obey Beer's law in aqueous solutions nor are the spectral curves independent of concentration (as thionine concentration increases in aqueous solutions, the short wave length spectral peak increases sharply in intensity relative to the intensity of the long wave length peak). It was concluded in paper I that this was a manifestation of association, the associated species (which, for convenience, we will call the polymer) absorbing strongly at short wave lengths (540–560 mμ) but hardly at all at the longer wave lengths >600 mμ, the position of monomer absorption. These conclusions agree with Rabinowitch's work.

Since solutions of thionine in methanol obey Beer's law, the difference in behavior in methanol and in water may easily be seen by studying the absorption at 600 and at 560 mμ. We have already seen that a plot of the ratio of the apparent extinction coefficient at 600 mμ to the apparent extinction coefficient at 560 mμ for very dilute dye solutions changes linearly as the mole fraction of methanol in the solvent is changed slightly from zero, while the behavior at higher dye concentrations gives an abrupt change with the addition of small amounts of methanol (Figures 3, 4). The latter shows not only that the presence of a small amount of alcohol destroys the associative tendency of thionine but also that, above about 0.3 mole fraction of methanol, even concentrated solutions behave spectrally as though they were highly dilute. Evidently the polymeric thionine ions are so sensitive to methanol that complete dissociation into individual thionine ions occurs by the time the solvent becomes roughly one-third methanol.

2. Fluorescence Measurements. We have seen that the fluorescence peak position of thionine does not depend on the nature of the solvent but falls at about 615–625 mμ for all proportions of water and methanol and at all dye concentrations. Although association between the dye ions must be occurring in solutions which are more than two-thirds water (unless the dye is extremely dilute), this is not manifested in the fluores-

cence spectrum. One cause for this could be, of course, that the associated form of the dye is not fluorescent. Such an assumption is reinforced by the great dependence of Q on dye concentration in aqueous solutions and the constancy of Q in the monomeric CH$_3$OH solutions. The fact that excitation of the 540-mμ peak produces no measurable fluorescence in aqueous solutions also indicates a nonfluorescent associated form since 540 mμ lies in the absorption band of the polymeric form. In view of these data, we join Rabinowitch in concluding that only the monomeric form of the dye is fluorescent.

C. Degree of Polymerization. 1. Background. Paper I contained a comparison between aqueous solution data and a model which proposed the condensation of thionine ions into polymeric form rather than merely dimerization. Although we suspected that this micelle formation did indeed occur, some uncertainty continued to exist because many of our data could still be fitted to a dimer scheme. The behavior of the water–alcohol solutions both in absorption and fluorescence, however, indicates more strongly that the association pattern in aqueous solutions is toward higher polymers.

Qualitatively, this may be seen in the sudden changes which take place as micelle-destroying alcohol is added to associated aqueous solutions of thionine. As we have seen, small amounts of CH$_3$OH produce rapid increases in quantum efficiency, until, at a CH$_3$OH mole fraction of 0.3, the curve breaks sharply (see Figure 5) and thereafter shows only the smaller solvent dependence characteristic of monomeric thionine and seen in dilute solutions. A second case of abrupt behavior is seen in the plot of the corrected extinction coefficient ratio, E_{600}/E_{560}, Figure 4, for a concentrated dye solution. The curve drops precipitously until the CH$_3$OH mole fraction is somewhat greater than 0.3; thereafter, the concentrated solution behaves as a dilute solution.

It is possible to find further support for the condensation model through quantitative interpretation of the concentration dependence of fluorescence intensity in solutions which encourage association. Such an interpretation and its various shortcomings are discussed in the following subsections.

2. Concentration Dependence of Fluorescence. The concentration dependence of the fluorescence of thionine is similar to that found for many other dyes in water. Table II gives the various processes which may follow excitation in a dye system which contains associated species.

Assuming a steady-state concentration of T*, we have

$$[\text{T}^*] = \frac{I_0(E_\text{m}/E)\alpha}{k_1 + k_2 + k_4[\text{T}] + k_5[\text{T}_\text{p}]} \tag{I}$$

The quantum efficiency, then, may be written as

$$Q = \frac{f}{I_0} = \frac{k_1[T^*]}{I_0} = \frac{(E_m/E)\alpha}{1 + \dfrac{k_2}{k_1} + \dfrac{k_4}{k_1}[T] + \dfrac{k_5}{k_1}[T_p]} \quad (II)$$

Equation II rearranges to

$$Q =$$

$$\frac{(E_m/E)\alpha}{\left\{1 + \dfrac{k_2}{k_1}\right\}\left\{1 + \left[\dfrac{k_4\alpha}{k_1 + k_2} + \dfrac{k_5}{k_1 + k_2}\left(\dfrac{1-\alpha}{P}\right)\right][T_0]\right\}} \quad (III)$$

where Q symbolizes the quantum efficiency of fluorescence; see section II. C. We may now define Q_0 as the value of this quantity extrapolated to zero concentration; i.e., $Q_0 = 1/(1 + k_2/k_1)$.

Table II[a]

Process	Rate
Absorption	
$T + h\nu \xrightarrow{\text{exc.}} T^*$	$I_0(E_m/E)\alpha$[b]
$T_p + h\nu \xrightarrow{\text{exc.}} T_p^*$	$I_0(E_p/E)(1-\alpha)/P$
Emission	
$T^* \rightarrow h\nu_F + T$	$k_1[T^*]$
Nonradiative first-order	
$T^* \rightarrow T + \text{heat}$	$k_2[T^*]$
$T_p^* \rightarrow T_p + \text{heat}$	$k_3[T_p^*]$
Second-order diffusion	
$T^* + T \rightarrow T + T$	$k_4[T^*][T]$
$T^* + T_p \rightarrow T + T_p$	$k_5[T^*][T_p]$
$T_p^* + T \rightarrow T_p + T$	$k_6[T_p^*][T]$
$T_p^* + T_p \rightarrow T_p + T_p$	$k_7[T_p^*][T_p]$

[a] $[T_0]$ denotes the total formal concentration of dye (M), [T] and $[T_p]$ the concentrations of monomer and polymer, P the average number of monomer units in a polymer unit (thus, $[T_0] = [T_m] + P[T_p]$), α the fraction of dye which is monomeric (i.e., $\alpha = [T]/[T_0]$), I_0 the intensity of exciting light, E the overall extinction coefficient of the solution, E_m the extinction coefficient of the monomer, and E_p that of the polymer (in terms of polymer units) [b] The total number of photons absorbed by the system is given by $I_0(1 - 10^{-E[T_0]l})$ while the number of photons absorbed by the monomer is represented by $I_0(1 - 10^{-E_m[T]l})$, where l is cell length. If the ratio of the number of photons absorbed by the monomer to the total number absorbed by the system is expanded in a power series the first few terms are

$$\frac{1 - 10^{-E_m[T]l}}{1 - 10^{-E[T_0]l}} = \frac{E_m[T]}{E[T_0]}\left\{\frac{1 + \dfrac{E_m[T]l}{2!}\ln 10 + \cdots}{1 + \dfrac{E[T_0]l}{2!}\ln 10 + \cdots}\right\} \approx (E_m/E)\alpha$$

The incident light flux is totally absorbed in these experiments (cf., II. C. above); hence, the flux of photons absorbed by the monomer is $I_0(E_m/E)\alpha$.

The relative magnitudes of the rate constants and the effects of environment on their values may be estimated from discussion of the fluorescence observations given in sections III. B. and IV. B.

(1) The ratio k_2/k_1 is nearly independent of the solvent composition; witness the fact that the limit of the quantum efficiency as $[T_0] \rightarrow 0$ (i.e., Q_0) decreases as little as 30% when solvent constitution is changed from pure CH_3OH to pure H_2O.

(2) The absence of "self-quenching" (i.e., concentration independence of Q) in pure CH_3OH suggests that the ratio $k_4/(k_1 + k_2)$ is very small in CH_3OH (note that the term $k_5(1 - \alpha)/(k_1 + k_2)P$ must vanish in pure methanol since $\alpha = 1$).

(3) The quantum efficiency of a concentrated solution of dye in CH_3OH does not deviate from the quantum efficiency of a dilute solution on addition of water up to a CH_3OH mole fraction of 0.3. This prompts the conjecture that the ratio $k_4/(k_1 + k_2)$ is independent of solvent composition as such and thus is small in H_2O as well as in CH_3OH.

(4) The negligibility of $k_4/(k_1 + k_2)$ and $k_5/(k_1 + k_2)$ for water systems is suggested by application of the Debye equation which relates the rate of diffusion to the viscosity of the solvent; i.e., $k_{\text{diffusion}} = 8RT/3000\eta$. Although this equation predicts a significant change in the rate of diffusion-controlled reactions with change in viscosity, we have found that there is no effect on Q when a 40% reduction in the diffusion rate is made experimentally by changing the solvent from CH_3OH to H_2O in the mole fraction range 0.3 to 1.0 in CH_3OH. (The elimination of k_5 on diffusional grounds may stand on its own merits so far as a collisional transfer is concerned, but must be re-examined from the view of nonradiative long-range energy transfer. Although such a process can be extremely efficient in certain systems, e.g., anthracene–anthracene or anthracene–naphthacene, it occurs only when there is overlap between the fluorescence wave length of the donor and the absorption wave lengths of the receiver. For transfer from one molecule to another of the same species, the overlap need not be large, but, for a transfer between species, the excited states of the receiver must be at lower energies than the corresponding states of the donor. Upstream transfers do not occur. On this ground, we discount noncollisional transfer from monomer to polymer since the polymer absorption peak lies some 40–60 Å. higher than that of the monomer.)

For these reasons, we simplify (III) by dropping the diffusional terms

$$\frac{k_4\alpha}{k_1 + k_2} \quad \text{and} \quad \frac{k_5}{k_1 + k_2}\left(\frac{1-\alpha}{P}\right)$$

$$Q = \frac{(E_m/E)\alpha}{1 + \dfrac{k_2}{k_1}} \qquad \text{(IV)}$$

Upon dividing by Q_0, we have

$$\frac{Q}{Q_0} = (E_m/E)\alpha \qquad \text{(V)}$$

At this point, let us notice that, although the fluorescence efficiency of aqueous solutions diminishes with increasing concentrations, the classical "self-quenching" mechanism has been excised from eq. V through the removal of the terms in k_4 and k_5. A mechanism which remains to explain the observed concentration dependence, however, is that light is increasingly absorbed by polymeric structures at higher concentrations and thereby is lost since these molecules do not fluoresce. We will refer to this process as "excitation dilution."

3. Discussion of the Condensation Model[7] as Interpreted by Eq. V. (a) *Quantum Yield Dependence on Solvent Composition.* (1) Equation V predicts an invariant quantum efficiency for CH_3OH solutions simply because the dye does not polymerize in this solvent; *i.e.*, $\alpha = 1$ throughout the concentration range. Moreover, as we have seen, the substitution of alcohol by water in fairly concentrated solutions of dye in CH_3OH does not occasion a variation in the quantum efficiency until the mole fraction of CH_3OH is reduced to about 0.3 (Figure 5), after which a further change produces sharp decrease of the quantum efficiency. This abrupt diminution in quantum efficiency with solvent composition occurs at the same CH_3OH concentration at which the light absorption studies suggest that polymerization appears.

(2) By invoking eq. V and reminding ourselves that Q_0 is nearly solvent independent, we may write down the ratio of the quantum efficiencies for solutions of dye dissolved in various alcohol–water solutions which have methanol mole fractions $X = X_1$ and $X = X_2$; *viz.*

$$Q_{X_1}/Q_{X_2} = [(E_m/E)_{X_1}\alpha_{X_1}]/[(E_m/E)_{X_2}\alpha_{X_2}] \qquad \text{(VI)}$$

For $X_2 \geqslant 0.4$, we remember that the dye is entirely monomeric; thus, in this range $(E_m/E)_{X_2}\alpha_{X_2} \approx 1$), and

$$\alpha_{X_1} = \frac{Q_{X_1}}{Q_{X_2}}(E/E_m)_{X_1} \qquad \text{(VII)}$$

The quantity Q_{X_2} for $X_2 \geqslant 0.4$ may be measured, and experimental values may also be determined for the other factors of the right-hand side of eq. VII at various $X_1 < 0.4$, thus giving a means of estimating α for solutions up to 0.4 mole fraction of CH_3OH. The values given below were determined in this manner for solutions of $[T_0] = 10^{-3}$.

Table III

Mole fraction of CH₃OH	α
0	0.2
0.1	0.4
0.2	0.7
0.3	0.8
>0.4	~1.0

We may compare the value of α in pure H_2O (first in the list above) with one calculated from the data of paper I; *viz.*

$$\alpha_{H_2O} = \frac{\text{optical density due to monomer}}{\text{optical density of entire solution}} =$$

$$\frac{13.0 \text{ (as estimated in paper I)}}{(5.6 \times 10^4)(10^{-3})} = 0.23$$

finding agreement well within experimental error.

(b) *Quantum Yield Dependence of Dye Concentration ("Self-Quenching").* Another test of the condensation model is offered by calculating various ratios Q_C/Q_0 for two excitation wave lengths, then comparing the calculations with experiment. Q_C designates the quantum yield for fluorescence at dye concentration $[T_0]$. The calculation may be made by means of eq. V as

$$\frac{Q_C}{Q_0} = \frac{(E_m/E)_C\alpha_C}{(E_m/E)_0\alpha_0} = \frac{(E_m/E)_C\alpha_C}{1} = (E_m/E)_C\frac{[T]}{[T_0]}$$

From paper I, we have $[T] \approx 2.3 \times 10^{-4}$ when $[T_0] \geqslant 10^{-3}$, $E_m = 5.6 \times 10^4$ at 590 mμ, and $E_m/E = 1$ at 560 mμ,[8] giving

$$(Q_C/Q_0)_{590} = (5.6 \times 10^4/E_{590})_C(2.3 \times 10^{-4}/T_0)$$

and

$$(Q_C/Q_0)_{560} = 1 \times (2.3 \times 10^{-4}/[T_0])$$

In Table IV are shown values for Q_C/Q_0 at various concentrations as determined by experiment for excitation wave lengths 560 and 590 mμ. These are compared with values calculated by means of the equations above.

Since eq. V contains no diffusional quenching constants, the agreement between measured and calculated values shown in Table IV lends support to the condensation model on the basis of which eq. V was derived.

(7) The condensation model is described completely in paper I; briefly, the monomer concentration reaches a constant value above a certain critical concentration of the total dye.

(8) Figure 3 of paper I demonstrates the essential independence of E on T_0 at 560 mμ; *i.e.*, the value of E at infinite dilution represents E_m but does not change as concentration increases; thus $(E_m/E)_{560} \approx 1$.

Table IV

[T$_0$], M	Exptl. $Q(C)/Q_0$		Calcd. $Q(C)/Q_0$	
	590 mμ	560 mμ	590 mμ	560 mμ
0	1	1	1	1
1 $\times$ 10^{-3}	0.40 $\pm$ 0.05	0.25 $\pm$ 0.05	0.43	0.23
1.5 $\times$ 10^{-3}	0.38 $\pm$ 0.05	0.18 $\pm$ 0.05	0.36	0.15
2.5 $\times$ 10^{-3}	0.27 $\pm$ 0.05	0.10 $\pm$ 0.03	0.25	0.09

4. Excitation Spectra. It remains to explain the form of the excitation spectrum curves, Figure 7, for CH$_3$OH–H$_2$O dye solutions of different solvent proportions. Using eq. VI in the case where $X_1 = 0$ and $X_2 = 1$, we have

$$Q_{X=0}/Q_{X=1} = (E_m/E)_{X=0}\alpha_{X=0}$$

a quantity, which as we have seen, depends on excitation wave length. The wave length independent term, $\alpha_{X=0}$ may be eliminated by taking relative values of the quantum efficiency ratios at different excitation wave lengths, thus

$$\frac{(Q_{X=0}/Q_{X=1})_\lambda}{(Q_{X=0}/Q_{X=1})_{600}} = \left(\frac{E_{m\lambda}}{E_{m600}}\right)_{X=0}\left(\frac{E_{600}}{E_\lambda}\right)_{X=0} \quad \text{(VIII)}$$

where the subscript λ refers to the excitation wave length of any particular experiment.

The quantity $(E_{m\lambda}/E_{m600})_{X=0}$ may be determined experimentally from absorption spectra of dilute dye solutions in H$_2$O, while $(E_{600}/E_\lambda)_{X=0}$ is just the ratio of the over-all extinction coefficients in a concentrated (*e.g.*, 10^{-3} M) solution.

Figure 7 shows plots of the excitation wave length dependence of fluorescence efficiency, Q_λ, *vs.* excitation wave length for several solutions of different $X_{\text{CH}_3\text{OH}}$. In particular, we note that for pure methanol solutions, Q_λ is independent of λ.

Taking this result, we may simplify eq. VIII to

$$\frac{(Q_{X=0})_\lambda}{(Q_{X=0})_{600}} = \left(\frac{E_{m\lambda}}{E_{m600}}\right)_{X=0}\left(\frac{E_{600}}{E_\lambda}\right)_{X=0} \quad \text{(IX)}$$

Now, using curve 5 of Figure 7, we replot, taking $(Q_{X=0})_{604}$ as unity. Simultaneously, we also take measured values of the right-hand side of (IX) from absorption experiments. It may be seen, Figure 8, that the absorption measurements agree with the measured relative fluorescence efficiencies, thus giving yet another independent verification of the assumptions leading to eq. IV.

5. Formation of Excited Dimers by Reaction of an Excited Monomer and an Unexcited Monomer. There apparently exist systems in which the excitation lifetime
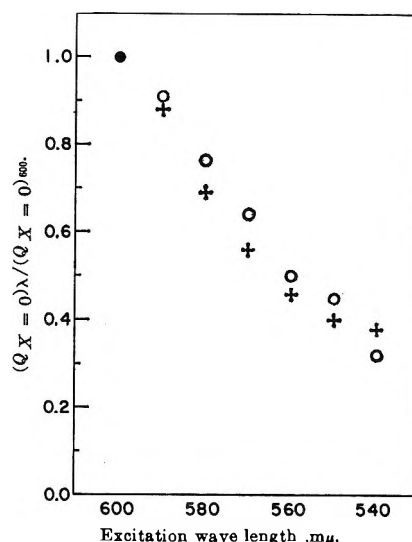
Figure 8. Test of eq. IX. Curve O: the function $(E_{m\lambda}/E_\lambda)(E_{600}/E_{m600})$. Curve +: experimental values: fluorescence of pure H$_2$O solution of a 10^{-3} M thionine solution (see Figure 7, curve 5) normalized at 600 mμ (point ●).

is long enough to allow diffusion together of an excited molecule with an unexcited one, giving formation of an excited dimer which subsequently decays nonradiatively.[9] In the thionine case, the arguments which permit dropping k_4 also rule out this mechanism; moreover, the measured lifetime of thionine is so very short $(\tau = \tau_0 Q_0 = (7 \times 10^{-9})(0.024) \cong 2 \times 10^{-10}$ sec.$)$[10] that the diffusional process is very unlikely.

IV. Summary

In paper I, we have supported the condensation model for thionine systems on the basis of absorption measurements. In the present report, we support that contention through fluorescence measurements. These latter arguments mainly fall into two categories.

(1) Explanation of "Self-Quenching." The dimer model cannot explain the observed concentration dependence of fluorescence efficiency without recourse to a diffusional or a radiationless transfer quenching of excited molecules by unexcited ones. Because of the very short lifetime of excited thionine singlets, diffusional quenching is not likely to be efficient, and this surmise is supported by experiment. Radiationless transfer is probably not responsible because (a) transfer from excited monomer to dimer or polymer is uphill and suffers from poor overlap and (b) quenching transfers between excited monomers and unexcited monomers do

(9) G. R. Haugen and W. H. Melhuish, *Trans. Faraday Soc.*, **60**, 383 (1964).

(10) C. A. Parker, *ibid.*, **57**, 1093 (1961).

not occur even slightly in solutions which contain much methanol and thus probably do not occur in water solutions since this kind of process is not likely to be critically sensitive to the differences between solutions of CH_3OH mole fractions of 0.3 and, say, 0.1. Condensation, with its concomitant excitation dilution, however, explains the "self-quenching" without recourse either to rapid diffusion processes or radiationless transfer.

(2) Experimental Support of Equations Based on Condensation Model. Equation IV and its progeny all depend on the model of condensation and excitation dilution for their genesis. In addition to the "self-quenching," two further independent types of tests verify this series of expressions; *viz.*, the quantum efficiency dependence on solvent composition and the quantum efficiency dependence on excitation wave length. Even with the aid of self-quenching, the dimer model fails to make these two correlations.

The Photochemistry of Aqueous Sulfate Ion

by Jack Barrett, M. F. Fox, and A. L. Mansell

Department of Chemistry and Biology, Hatfield College of Technology, Hatfield, Hertfordshire, England
(Received March 9, 1965)

The effects of 1849-Å. radiation upon aqueous solutions of sulfate ion have been investigated, methanol being used as a radical and electron scavenger. The irradiations were carried out *in vacuo*, the solutions used varying in pH from 7 to 14. The reactions observed are interpreted in terms of a charge-transfer-to-solvent mechanism for both sulfate and hydroxide ions.

Introduction

Many inorganic anions in aqueous solution absorb radiation in the ultraviolet region.[1] Certain of these absorptions, particularly those occurring in the far-ultraviolet, have been characterized as electron-transfer spectra.[2] Recently, the spectra of univalent and divalent ions have been investigated[3] and the initial act designated as charge-transfer-to-solvent (c.t.t.s.). A large blue shift (400–800 cm.$^{-1}$) in the absorption of anions when water as solvent is replaced by deuterium oxide has been proposed as being diagnostic for a c.t.t.s. mechanism by Halmann and Platzner.[4] This work has shown that the absorption in the far-ultraviolet by sulfate ion can be classified as c.t.t.s. Ions which show either a small blue shift or a red shift upon this change of solvent are regarded

as undergoing internal excitation in the initial act of absorption. The flash photolysis of aqueous solutions of some of these ions[5] indicates the production of hydrated electrons and is conclusive evidence for a c.t.t.s. mechanism.

In the case of sulfate ion, the initial act following the absorption of a quantum of radiation would be expected to be

(1) L. E. Orgel, *Quart. Rev.* (London), **8**, 422 (1954).

(2) E. Rabinowitch, *Rev. Mod. Phys.*, **14**, 112 (1942).

(3) (a) M. Smith and M. C. R. Symons, *Trans. Faraday Soc.*, **54**, 338, 346 (1958); (b) G. Stein and A. Treinin, *ibid.*, **55**, 1086, 1091 (1959); (c) A. Treinin, *J. Phys. Chem.*, **68**, 893 (1964); (d) R. Sperling and A. Treinin, *ibid.*, **68**, 897 (1964).

(4) M. Halmann and I. Platzner, *Proc. Chem. Soc.*, 261 (1964).

(5) M. S. Matheson, W. A. Mulac, and J. Rabani, *J. Phys. Chem.*, **67**, 2613 (1963).

$$SO_4{}^{2-}{}_{aq} \xrightarrow{h\nu} (SO_4{}^- + e^-)_{aq} \qquad (1)$$
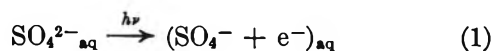
the purpose of the work reported here being to investigate the chemical consequences of the irradiation of aqueous sulfate ion and to offer an interpretation in terms of this initial photoact. A preliminary account of the work has been published.[6]

Experimental

All water used was triply distilled, made approximately 10^{-4} M in hydrogen peroxide, and irradiated until the peroxide had been completely photolyzed. High purity, stabilizer-free hydrogen peroxide was given by Laporte Industries Ltd. Analar grade methanol was further purified by a previously reported method.[7] All other chemicals were of Analar grade used without further purification. The experimental procedure for the photolyses has been described elsewhere.[8] The actinometer used for 1849-Å. radiation was an aqueous solution of 5 M ethanol which was reported by Farkas and Hirschberg[9] to have a quantum yield for hydrogen production of 0.8. Dainton and Fowles[10] have shown that inaccuracies existed in the determination of this quantum yield and have developed the use of N_2O in aqueous solution as an actinometer at 1849 Å. This has a quantum yield of unity for nitrogen production, and on the basis of this value our results indicate that the quantum yield for hydrogen production from 5 M ethanol is 0.4. All quantum yields quoted in this paper were based on this value.

Hydrogen was identified and measured with an Associated Electrical Industries MS 10 mass spectrometer. Formaldehyde was determined by the chromatropic acid method,[11] and ethylene glycol by its reaction with periodate ion.[12] Hydrogen peroxide was determined by reaction with iodide ion.[13] All ultraviolet absorption spectra were measured on a Hilger and Watts Uvispek with nitrogen flushing for wave lengths below 2000 Å.[14] Suprasil 1-mm. cells were used, Suprasil plates 0.9 mm. thick being inserted into these cells when the spectra of strongly absorbing species were being determined.

Results

An aqueous solution of 1.0×10^{-2} M sodium sulfate in the presence of 1.0×10^{-1} M methanol has been shown to evolve hydrogen when exposed to the radiation from a low-pressure mercury discharge lamp.[6] That the photochemical action was due to the 1849-Å. radiation emitted by the lamp was shown by the fact that 2 cm. of distilled water, when placed between the lamp and the reaction vessel, was sufficient to prevent

any reaction from taking place. Using the published value for the absorption coefficient of water at 1849 Å.,[14] it was calculated that 2 cm. of water would have a transmittance of only 0.1% at this wave length. Since the 1849-Å. line is the only radiation emitted by a low-pressure mercury discharge lamp that is absorbed appreciably by water, it was concluded that the photoactive wave length was 1849 Å.

Absorption Spectra of Solutions. In order to explain the photochemical results in a quantitative manner it was necessary to determine the absorption spectra of all solutions used. The spectrum of sulfate ion was found to be dependent upon the concentration of methanol present in the solution, at methanol concentrations greater than 1.0 M. The absorption data are given in Table I where ϵ is the molar absorption coefficient. The values of ϵ(methanol) are in agreement with those reported by Weeks, *et al.*[15]

Table I: Molar Absorption Coefficients for Aqueous Methanol Solutions and for Sulfate Ion in Such Solutions at 1849 Å.

Methanol concn., M	ϵ(methanol) in aqueous soln., M^{-1} cm.$^{-1}$	ϵ(sulfate) in aqueous methanol, M^{-1} cm.$^{-1}$
0.5	6.0	200
1.0	6.2	188
2.0	6.1	181
4.0	5.4	156
6.25	4.9	146

Quantum Yields for Hydrogen Production. The quantum yields for hydrogen production, ϕ_{H_2}, were determined over a range of methanol concentrations, and these are plotted against the fraction of radiation absorbed by the sulfate ion as shown in Figure 1. Extrapolation of the straight portion of this plot gives the quantum yields for the photolysis of sulfate ion and

(6) J. Barrett, M. F. Fox, and A. L. Mansell, *Nature*, **200**, 257 (1963).

(7) G. E. Adams and J. H. Baxendale, *J. Am. Chem. Soc.*, **80**, 4215 (1958).

(8) J. Barrett and J. H. Baxendale, *Trans. Faraday Soc.*, **56**, 37 (1960).

(9) L. Farkas and Y. Hirschberg, *J. Am. Chem. Soc.*, **59**, 2450 (1937).

(10) F. S. Dainton and P. Fowles, *Proc. Roy. Soc.* (London), in press.

(11) C. E. Bricker and H. R. Johnson, *Ind. Eng. Chem., Anal. Ed.*, **17**, 400 (1945).

(12) G. O. Aspinall and R. J. Ferrier, *Chem. Ind.*, 1216 (1957).

(13) C. J. Hochanadel, *J. Phys. Colloid Chem.*, **56**, 587 (1952).

(14) J. Barrett and A. L. Mansell, *Nature*, **187**, 138 (1960).

(15) J. L. Weeks, G. Meaburn, and S. Gordon, *Radiation Res.*, **19**, 559 (1963).
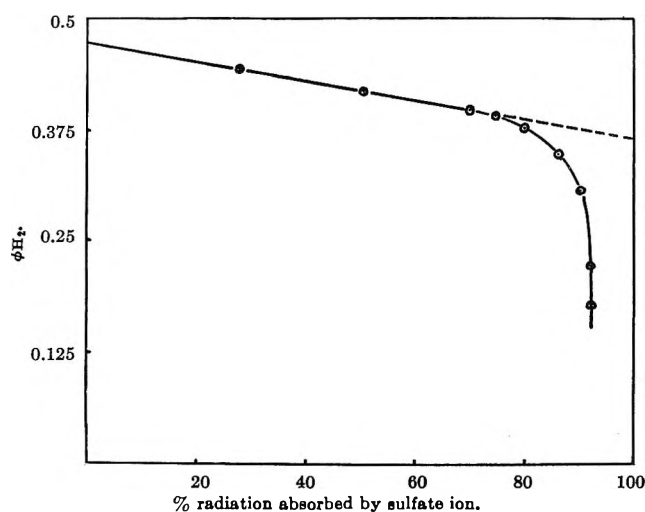
Figure 1. Quantum yield of hydrogen vs. per cent radiation absorbed by sulfate ion.

methanol in terms of hydrogen production as $\phi_{SO_4^{2-}}$ = 0.37 and ϕ_{CH_3OH} = 0.47, respectively. This latter figure is in good agreement with the previously reported value[8] of 0.98, which becomes 0.49 on the basis of the actinometry of Dainton and Fowles.

If in the irradiation of sulfate ion methanol is replaced by ethanol or 2-propanol as scavenger, we have observed that a decrease in the quantum yield for hydrogen production occurs at concentrations of those alcohols corresponding to the region of complete scavenging by methanol. For alcohol concentrations of 1.0 M the quantum yields for hydrogen production in the irradiation of 1.0 × 10^{-1} M sulfate ion are 0.39 0.23, and 0.18 for methanol, ethanol, and 2-propanol, respectively. Increases in the concentrations of ethanol and 2-propanol lead to increases in the quantum yields for hydrogen production, and we conclude that the scavenging efficiencies of the alcohols are in the order methanol > ethanol > 2-propanol.

The quantum yield for hydrogen production in the region of complete scavenging by methanol can be expressed by the equation

$$\phi_{H_2} = \phi_{SO_4^{2-}}\alpha_{SO_4^{2-}} + \phi_{CH_3OH}\alpha_{CH_3OH} + \phi_{H_2O}\alpha_{H_2O} \quad (2)$$

where the ϕ's are quantum yields and the α's are fractions of 1849-Å. radiation absorbed by the respective species present in the solutions. The values of the quantum yields are $\phi_{SO_4^{2-}}$ = 0.37, ϕ_{CH_3OH} = 0.47, and ϕ_{H_2O} = 0.3.[8] In all solutions irradiated there was complete absorption of 1849-Å. radiation so that the sum of the α values in eq. 2 is unity.

In the preliminary report of this work[6] it was stated that $\phi_{SO_4^{2-}}$ apparently varied with methanol concentration. This apparent variation was correctly attrib-

uted to changes in the absorption characteristics of the solution. The currently quoted value of $\phi_{SO_4^{2-}}$ = 0.37 is independent of methanol concentration, the data of Table I having been taken into account in its determination.

Solution Products. The products observed in the irradiated solutions were ethylene glycol and formaldehyde, the quantum yields being such that an oxidation–reduction balance occurred according to the stoichiometry

$$\phi_{H_2} = \phi_{CH_2O} + \phi_{(CH_2OH)_2} \quad (3)$$

as can be seen from the data in Table II.

Table II : Product Balance in the Irradiation of Aqueous Sulfate Ion–Methanol Solutions

Methanol concn., M	ϕ_{H_2}	ϕ_{CH_2O}	$\phi_{(CH_2OH)_2}$	ϕ_{CH_2O} + $\phi_{(CH_2OH)_2}$
5 × 10^{-1}	0.36	0.025	0.33	0.355
2.0	0.41	0.045	0.36	0.405
5.0	0.43	0.080	0.35	0.43

pH Variation. Photolyses have been carried out using solutions containing 1.0 × 10^{-1} M sodium sulfate, 1.0 M methanol, and varying amounts of sodium hydroxide in order to vary the pH from 7 to 14. The quantum yield for hydrogen production is plotted against pH in Figure 2, curve A, and, as can be seen, ϕ_{H_2} is markedly pH dependent.

The value of the quantum yield for hydroxide ion photolysis is found to be 0.11 as shown by the limiting yield of hydrogen at high pH in Figure 2, curve A. That this value is independent of the presence of sulfate ion is shown by Figure 2, curve B, which shows the effect of pH variation on the photolysis of an aqueous solution of methanol. The same value of the hydrogen yield is again observed at high pH while the upper limit of curve B corresponds to the quantum yield for hydrogen production from pure methanol, *i.e.*, 0.47. The total hydrogen yields over the pH range studied can be expressed by the equation

$$\phi_{H_2} = \phi_{OH^-}\alpha_{OH^-} + \phi_{SO_4^{2-}}\alpha_{SO_4^{2-}} +$$
$$\phi_{CH_3OH}\alpha_{CH_3OH} + \phi_{H_2O}\alpha_{H_2O} \quad (4)$$

in the presence of sulfate ion, and as

$$\phi_{H_2} = \phi_{OH^-}\alpha_{OH^-} + \phi_{CH_3OH}\alpha_{CH_3OH} + \phi_{H_2O}\alpha_{H_2O} \quad (5)$$

in the absence of sulfate ion where ϕ_{OH^-} = 0.11, ϕ_{CH_3OH} = 0.47, $\phi_{SO_4^{2-}}$ = 0.37, and ϕ_{H_2O} = 0.3. These two equations are analogous to eq. 2.
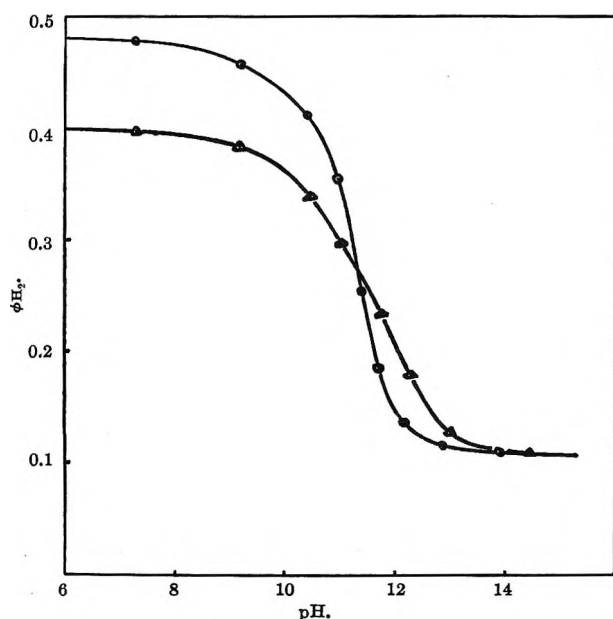
Figure 2. Quantum yield vs. pH: $\bigcirc$, curve A,
$1.0 \times 10^{-1}\,M\,SO_4{}^{2-}$, $1\,M$ MeOH; $\triangle$, curve B, $1\,M$ MeOH.

Discussion

Following the initial photoact in the irradiation of aqueous sulfate ion, as expressed by eq. 1, the following processes can occur in the presence of methanol

$$(SO_4{}^- + e^-)_{aq} \longrightarrow SO_4{}^{2-} \qquad (6)$$

$$SO_4{}^- + H_2O \longrightarrow HSO_4{}^- + OH \qquad (7)$$

$$SO_4{}^- + CH_3OH \longrightarrow HSO_4{}^- + CH_2OH \qquad (8)$$

$$e_{aq}{}^- + H_2O \longrightarrow H + OH^- \qquad (9)$$

$$e_{aq}{}^- + CH_3OH \longrightarrow H_2 + CH_2OH + OH^- \qquad (10)$$
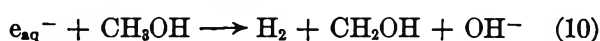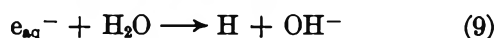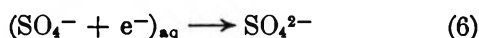
Evidence that reaction 6 occurs comes from the fact that the quantum yield for reaction 1 is less than unity, namely, 0.37. If reactions 7 and 9 occur, they would be followed by

$$OH + CH_3OH \longrightarrow H_2O + CH_2OH \qquad (11)$$

$$H + CH_3OH \longrightarrow H_2 + CH_2OH \qquad (12)$$
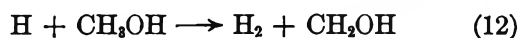
Whether the species $SO_4{}^-$ and $e_{aq}{}^-$ react with water molecules or whether they are scavenged directly by methanol can be decided on the basis of (a) bond dissociation energy data and (b) kinetic data involving absolute rate constants. Reactions 7 and 9 involve the fission of the H–OH bond in the water molecule which requires a dissociation energy of 118 kcal. mole^{-1},[16] whereas in reactions 8 and 10, energy required for the fission of the C–H bond is of the order of 85 kcal. mole^{-1}. These data would favor the occurrence of reactions 8 and 10. The latest value for the absolute rate constant for

reaction 9 is $10^2\,M^{-1}$ sec.$^{-1}$,[17] and that for reaction 10 is $5 \times 10^6\,M^{-1}$ sec.$^{-1}$.[18] For a $1.0\,M$ methanol solution the ratio of the rates of reactions 10 and 9 would, from the quoted values of these rate constants, be 900 which again would favor reaction 10 and exclude reaction 9.

Support for the argument that methanol scavenges the species $SO_4{}^-$ and $e_{aq}{}^-$ directly comes from the observation that for complete scavenging a methanol concentration of $7.5 \times 10^{-1}\,M$ is required.

In the photolysis of liquid water[3] where the primary act is

$$H_2O \xrightarrow{h\nu} H + OH \qquad (13)$$

the scavenging of the hydrogen atoms and hydroxyl free radicals is complete with a methanol concentration of $5.0 \times 10^{-3}\,M$. This much lower scavenger concentration is consistent with the greater reactivity of the hydroxyl free radical with methanol for which $k(OH + CH_3OH) = 1.0 \times 10^9$.[18]

The observation that the scavenging efficiencies of methanol, ethanol, and 2-propanol are in the reverse order to the rates of their reactions with hydrogen atoms[19] for which

$$k(H + CH_3OH) = 8.5 \times 10^4\,M^{-1}\,sec.^{-1}$$

$$k(H + C_2H_5OH) = 8.8 \times 10^5\,M^{-1}\,sec.^{-1}$$

$$k(H + i\text{-}C_3H_7OH) = 2.6 \times 10^6\,M^{-1}\,sec.^{-1}$$

is evidence for the participation of a reaction other than reaction 12. These observations, taken in conjunction with the relative rate data given earlier, suggest that reaction 9 does not occur in the systems studied.

The hydroxyl free radical is also known to react more rapidly with ethanol than with methanol[18]; hence, by an argument analagous to that employed for H atom scavenging, reaction 11 is unlikely to occur. We would therefore expect the mechanism of sulfate ion photolysis to include reactions 1, 6, 8, and 10.

The CH_2OH free radicals can produce formaldehyde and ethylene glycol by

$$CH_2OH + CH_2OH \longrightarrow CH_2O + CH_3OH \qquad (14)$$

and

$$CH_2OH + CH_2OH \longrightarrow (CH_2OH)_2 \qquad (15)$$
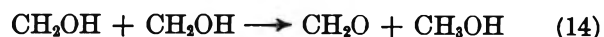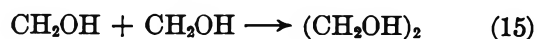
(16) T. L. Cottrell, "The Strengths of Chemical Bonds," Butterworth and Co. Ltd., London, 1958.

(17) F. S. Dainton, private communication.

(18) E. J. Hart, J. K. Thomas, and S. Gordon, Radiation Res. Suppl., 4, 74 (1964).

(19) J. Rabani, J. Phys. Chem., 66, 361 (1962).

with reaction 15 being the most probable one.

The reaction

$$SO_4^- + CH_2OH \longrightarrow HSO_4^- + CH_2O \qquad (16)$$
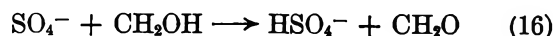
is much less likely to be responsible for the production of formaldehyde than reaction 14 because of the competition for SO_4^- by methanol molecules, which will be in vast excess of the CH_2OH radical concentration.

As can be seen from the data in Table II, formaldehyde is the minor product over the range of methanol concentrations studied and the increase in the proportion of formaldehyde produced with increasing methanol concentration is probably due to the direct photolysis of methanol

$$CH_3OH \xrightarrow{h\nu} H_2 + CH_2O \qquad (17)$$
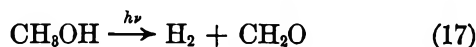
by analogy with the gas phase observations of Patat and Hoch.[20]

The decrease of ϕ_{H_2} with increasing pH we consider to be due to the increasing fraction of radiation absorbed by the hydroxide ion. The absorption spectrum which we have determined for aqueous hydroxide ion is in agreement with that reported by Ley and Arends,[21] and the value of ϵ at 1849 Å. is 3500 M^{-1} cm.$^{-1}$. At pH values greater than 12 the hydroxide ion is responsible for almost complete absorption of the radiation, and hence any hydrogen produced from such solutions must arise from the direct photolysis of the aqueous hydroxide ion. We consider the mechanism to be

analogous to that proposed for sulfate ion, the primary photoact being

$$OH_{aq}^- \xrightarrow{h\nu} (OH + e^-)_{aq} \qquad (18)$$
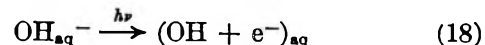
The hydrated electron can either undergo a back reaction in the solvent cage

$$(OH + e^-) \longrightarrow OH^- \qquad (19)$$

which would explain the low yield of 0.11 or be scavenged by methanol as in reaction 10, and the hydroxyl free radical would react with methanol by reaction 11. The fates of the CH_2OH free radical would then be represented by reactions 14 and 15.

We are currently investigating the effects of pH variation on the sulfate ion system in the range pH 1–7, a region in which the ion HSO_4^- is responsible for many of our observed reactions. The results of this work will be published at a later date.

(20) F. Patat and H. Hoch, *Z. Elektrochem.*, **41**, 434 (1935).

(21) H. Ley and B. Arends, *Z. physik. Chem.*, **B6**, 240 (1929).

The Heat of Formation of Aluminum(I) Chloride(g) and the

Entropy of Aluminum(III) Chloride(g)

by Margaret A. Frisch, Michael A. Greenbaum, and Milton Farber

Maremont Corporation, Rocket Power, Inc., Research Laboratories, Pasadena, California
(Received March 12, 1965)

A second-law value for the $\Delta H_f{}^\circ{}_{298}$ of AlCl(g) of -13.3 ± 0.4 kcal./mole has been obtained from a molecular flow effusion study of the reaction $2Al(l) + AlCl_3(g) \rightarrow 3AlCl(g)$ over the temperature range 930–1034°K. The first one-step determination of the $S^\circ{}_{982}$ of $AlCl_3(g)$ has also been derived from this study. This value was found to be 104.6 ± 2.1 cal./deg. mole.

Introduction

Various values ranging from -11 to -20 kcal./mole have been reported in the literature for the $\Delta H_f{}^\circ{}_{298}$ of AlCl(g). Gross, *et al.*,[1] compared the equilibrium vapor pressure of mixtures of molten aluminum with solid KCl and both liquid and solid NaCl with the vapor pressures of the pure salts. From these measurements they derived an average third-law value for the $\Delta H_f{}^\circ{}_{298}$ of -11.58 kcal./mole. They also studied the equilibrium

$$2Al(l) + AlCl_3(g) = 3AlCl(g) \qquad (1)$$
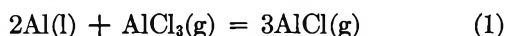
at a temperature of 1250°K. and reported a value for $\Delta H_f{}^\circ{}_{298}$ of AlCl(g) of -10.92 kcal./mole.

Russell, *et al.*,[2] measured the equilibrium constant for reaction (eq. 1) at 1400°K. and obtained a third-law value for $\Delta H_f{}^\circ{}_{298}$ of -12.18 kcal./mole. Semenkovich's[3] measurements on the reaction from 950 to 1200° gave a second-law heat of reaction at 298°K. of 77.98 kcal./mole which led to a $\Delta H_f{}^\circ{}_{298}$ for AlCl(g) of -19.20 kcal./mole. Gaydon[4] selected for D_0 of AlCl(g) the value of 5.1 ± 0.2 e.v. which resulted in a heat of formation of -11.62 kcal./mole.

The $\Delta H_f{}^\circ{}_{298}$ of $AlCl_3(g)$ was measured by several investigators[5-7] based on studies of the dimerization reaction of $AlCl_3(g)$, and their second-law values obtained for the heat of reaction agree with each other within ± 0.5 kcal./mole. The corresponding $S^\circ{}_{298}$ $AlCl_3(g)$ was derived[5] using one experimental vibrational frequency of Klemperer[8] and three estimated frequencies so that the second- and third-law values

for the heat of reaction were in agreement. This resulting entropy for $AlCl_3(g)$ (74.6 cal./deg. mole) should be considered somewhat unreliable since its value is based on the estimated entropy of $Al_2Cl_6(g)$.[5] The $S^\circ{}_{298}$ $Al_2Cl_6(g)$ was calculated using eleven observed vibrational frequencies and seven estimated ones such that the experimental[5,6,9-11] heat of sublimation of $AlCl_3(c)$ was in reasonable agreement with the third-law calculation.

In view of the uncertainty in the reported thermodynamic values for AlCl(g) and $AlCl_3(g)$, the present study was undertaken to obtain a value for both $\Delta H_f{}^\circ{}_{298}$ of AlCl(g) and $S^\circ{}_{298}$ of $AlCl_3(g)$ by a second-law measurement.

(1) P. Gross, C. S. Campbell, P. J. C. Kent, and D. L. Levi, *Discussions Faraday Soc.*, **4**, 206 (1948).

(2) A. S. Russell, K. E. Martin, and C. N. Cochran, *J. Am. Chem. Soc.*, **73**, 1466 (1951).

(3) S. A. Semenkovich, *Zh. Prikl. Khim.*, **33**, 1281 (1960); *Chem. Abstr.*, **54**, 19252d (1960).

(4) A. G. Gaydon, "Dissociation Energies and Spectra of Diatomic Molecules," Chapman and Hall Ltd., London, 1953.

(5) "Janaf Thermochemical Tables," USAF Contract No. AF 33(616)-6149, Advanced Research Projects Agency, Washington, D. C. AlCl(g), June 30, 1961; $AlCl_3$(g), March 31, 1965; Al(l) Dec. 31, 1960; Al_2Cl_6(g), March 31, 1964.

(6) A. Smits and J. L. Meijering, *Z. physik. Chem.*, **B41**, 98 (1938).

(7) W. Fischer, O. Rahlfs, and B. Benze, *Z. anorg. allgem. Chem.*, **205**, 1 (1932).

(8) W. Klemperer, *J. Chem. Phys.*, **24**, 353 (1956).

(9) C. G. Maier, U. S. Bureau of Mines, Technical Paper 360, U. S. Government Printing Office, Washington, D. C., 1929.

(10) W. D. Treadwell and L. Terebesi, *Helv. Chim. Acta*, **15**, 1053 (1932).

(11) T. G. Dunne and N. W. Gregory, *J. Am. Chem. Soc.*, **80**, 1526 (1958).

Experimental

Method. The heat of formation of AlCl(g) was determined by a molecular flow effusion[12] study of the reaction as given by eq. 1 over the temperature range 930–1034°K. This procedure consists of passing gaseous AlCl₃ at temperature T and pressure P over the surface of molten Al at the same temperature and allowing the resulting vapor species to escape through an effusion orifice into a high vacuum. The fraction of AlCl₃ molecules which leaves the surface of Al as gaseous AlCl is determined by the equilibrium constant K_p.

$$K_p = P_{AlCl}{}^3/P_{AlCl_3} \tag{2}$$

For molecular flow conditions to exist, the mean free path of the vapor must be of the order of the inside diameter of the Knudsen cell (0.6 cm. for the present system, which is equivalent to a pressure of 2×10^{-4} atm.).

The pressures of AlCl and AlCl₃ were calculated from the weight losses of Al and AlCl₃ using the Knudsen equation.

$$P_x = Z_x(M_xT)^{1/2}/(44.33AW_0) \tag{3}$$

where P_x is the pressure in atmospheres; Z_x is the effusion rate of the species in moles sec.$^{-1}$; M_x is the molecular weight of the species; T is the temperature of reaction in degrees Kelvin; A is the orifice area in cm.²; and W_0 is the Clausing factor. The cell used in these investigations had an orifice area of 2.20×10^{-2} cm.² and a Clausing factor W_0 of 0.52.

A blank run was made during which AlCl₃(g) was passed through the apparatus at 1034°K. at a high flow rate in the absence of any Al. No weight changes occurred in either the flow tube or effusion cell, thus indicating no reaction between AlCl₃ and the materials of construction.

The moles of AlCl formed and the unreacted moles of AlCl₃ were calculated according to eq. 4 and 5, respectively.

$$Z_{AlCl} = {}^3/_2(\Delta W_{Al} - \Delta W_{tube})/26.98 \tag{4}$$

$$Z_{AlCl_3} = \Delta W_{AlCl_3}/133.34 - Z_{AlCl}/3 \tag{5}$$

The flow of AlCl was corrected for back diffusion by subtracting the weight increase of the flow tube from the mass of Al lost from the cell, as indicated in eq. 4.

Procedure. A 0.25-g. sample of 99.5% Al wire was placed in a cell constructed of 99+% aluminum oxide (0.38 in. o.d. × 0.25 in. i.d. × 0.75 in. long) which was closed at one end. An effusion hole was drilled 1.64 mm. in diameter, approximately 0.13 in. off center in the closed end of the tube. The cell was press-fitted into a graphite cylinder (2 in. long × 0.94 in. o.d.)

so that the front of the cell was recessed by 0.5 in. A hole (0.25 in. diameter × 0.75 in. long) was drilled in the other end of the graphite cylinder into which an alumina flow tube (9 in. long × 0.13 in. i.d.) was inserted. The cell assembly was brought to the desired temperature using a tungsten resistance furnace with a heating zone of 3.25 in. which has been described in detail previously.[13] In Figures 1 and 2 diagrams of the furnace and AlCl₃ generator are shown. The temperature of the graphite cylinder was monitored by a calibrated chromel–alumel thermocouple. The thermocouple voltage was measured on a Rubicon potentiometer which was preset to the desired po-
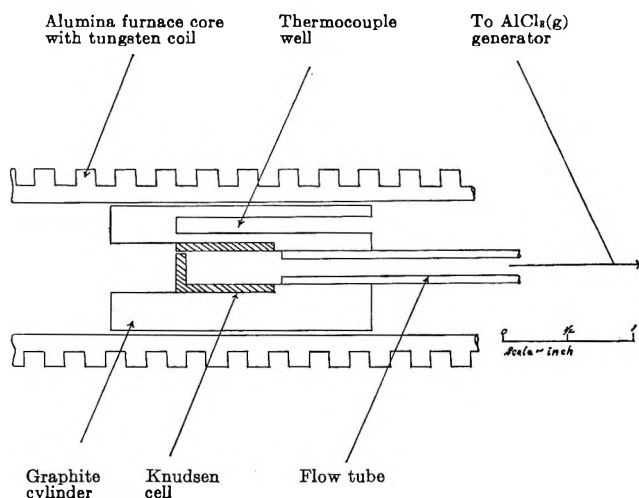
Figure 1. Knudsen cell in a tungsten resistance furnace.
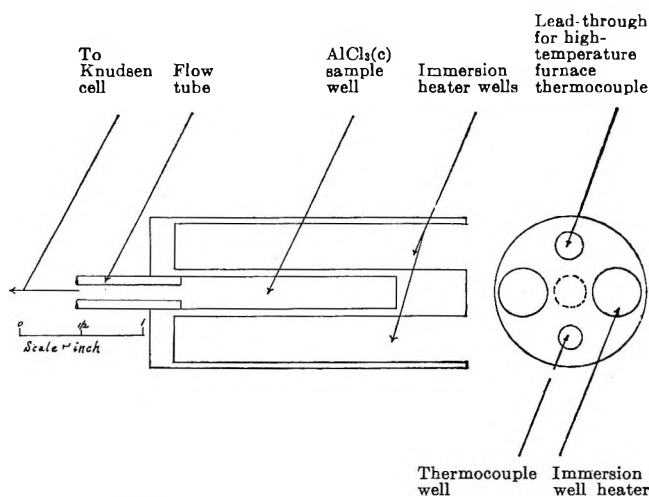
Figure 2. AlCl₃(g) generator: cross section and rear view.

(12) M. Farber and J. Blauer, *Trans. Faraday Soc.*, **58**, 2090 (1962).
(13) M. A. Greenbaum, R. E. Yates, M. L. Arin, M. Arshadi, J. Weiher, and M. Farber, *J. Phys. Chem.*, **67**, 703 (1963).

tential and the imbalance plotted on a Leeds and Northrup 5-0-5 mv. recorder. The temperature was maintained constant to ±0.3° by a Leeds and Northrup Series 60 control unit regulating the output of a Fincor saturable core reactor.

The AlCl$_3$ generator was constructed of high density graphite (1.22 in. o.d. × 2.56 in. long with a cavity 0.25 in. i.d. × 2 in. long). A 1-g. sample of 99+% purity AlCl$_3$ was placed in the cell and the other end of the alumina flow tube press fitted in the 0.25-in. opening, effecting a gas-tight seal. The AlCl$_3$(c) was handled entirely in a drybox which was maintained under a constant pressure of dry nitrogen.

Weighing of the AlCl$_3$ in the closed cell was the only operation not carried out in the drybox. Opportunity of moisture pickup must be considered negligible. The graphite cell was heated directly using two General Electric G2 immersion heaters (0.38 in. o.d. × 2.38 in. long, resistance 13.5 ohms each) in intimate contact with the graphite. The temperature of the AlCl$_3$ generator was measured by a chromel–alumel thermocouple and continuously plotted on a 0–5-mv. recorder. A Leeds and Northrup Series 60 control unit, operating a Fincor SCR power supply, automatically controlled the temperature to ±0.2°.

Both the high-temperature furnace and the AlCl$_3$ generator were mounted in a high vacuum system (3 × 10^{-6} mm.). The AlCl$_3$ generator protruded from the vacuum system through a brass tube (1.25 in. diameter × 3 in. long). The reaction furnace was brought to temperature and allowed to equilibrate for 1 hr. during which time the outgassing of the furnace diminished to give a constant pressure of approximately 2 × 10^{-5} mm. The experimental run was commenced by rapidly heating the AlCl$_3$ generator to 90° and maintaining it at that temperature for a time sufficient to lose at least 10 mg. of Al. Termination of the run was effected by cooling the brass tube with ice and in this manner the on–off time was accurate to within 2 min.

The mass loss of Al was determined from the mass difference of the Knudsen cell before and after the run and the AlCl$_3$ mass transfer was determined in a similar manner. The flow tube was also weighed to determine the extent of possible back diffusion of the AlCl. These weighings were repeated until a reproducibility of 0.1 mg. was obtained.

Results and Discussion

The reaction was studied at nine different temperatures and the data are presented in Tables IA and IB. A plot of log K_p vs. $1/T$ is shown in Figure 3. The
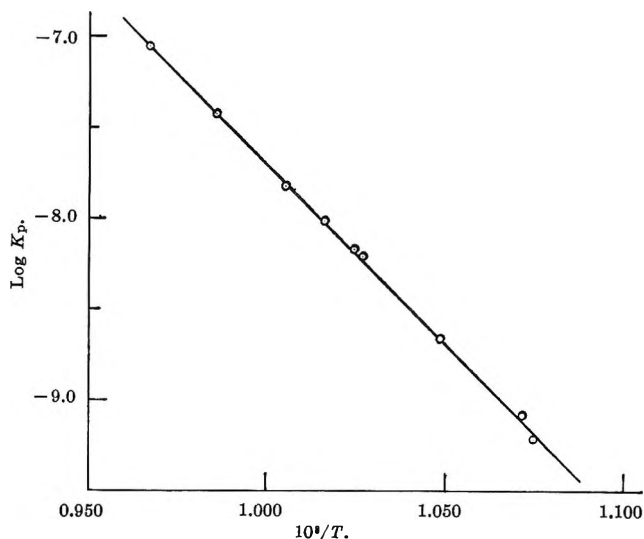
Figure 3. Equilibrium constants for reaction 1 plotted as a function of temperature.

least-squares line based on these data is given by the equation

$$\log K_p = -19{,}742/T + 12.036 \qquad (6)$$

The present work and all previous experimental data for eq. 1 are plotted in Figure 4. An extrapolation of eq. 6 as indicated in Figure 4 yields an equilibrium constant which agrees with the one obtained by Gross,
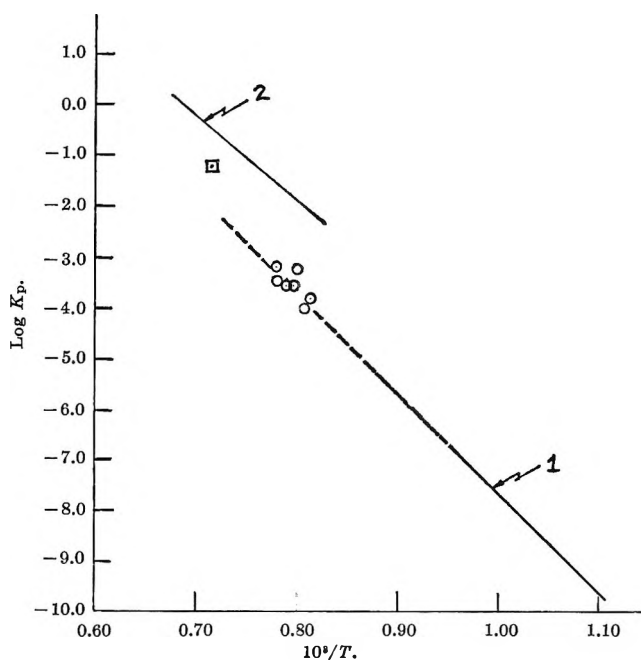
Figure 4. Summary of equilibrium data for reaction 1 plotted as a function of temperature: 1, this work; 2, Semenkovich[3]; O, Gross, et al.[1]; □, Russell, et al.[2]

Table IA: Experimental Data for the Reaction
$2Al(l) + AlCl_3(g) = 3AlCl(g)$

T, °K.	t, min.	ΔW_{AlCl_3}, g.	ΔW_{Al}, g.	ΔW_{tube}, g.	P_{AlCl}, atm. $\times 10^{-4}$	P_{AlCl_3}, atm. $\times 10^{-4}$	K_P, atm.^{2}
930.8	210	0.1599	0.01685	0.0019	0.314	0.508	6.09×10^{-10}
933.3	240	0.2801	0.02295	0.0009	0.406	0.816	8.20×10^{-10}
953.7	120	0.0934	0.0138	0.0013	0.465	0.457	2.20×10^{-9}
974.0	100	0.1302	0.0186	0.0013	0.781	0.776	6.14×10^{-9}
976.0	120	0.0529	0.0134	0.00075	0.476	0.160	6.74×10^{-9}
984.1	160	0.1379	0.0279	0.0020	0.734	0.412	9.60×10^{-9}
994.8	60	0.0513	0.0115	0.0007	0.820	0.369	1.49×10^{-8}
1014.4	60	0.0523	0.0143	0.0009	1.028	0.290	3.75×10^{-8}
1034.0	60	0.0670	0.01835	0.0000	1.421	0.329	8.72×10^{-8}

Table IB: Thermodynamic Properties for the Reaction
$2Al(l) + AlCl_3(g) = 3AlCl(g)$

T, °K.	$\log K_p$	$10^3/T$, °K.	ΔF, kcal./mole	ΔS, cal./ deg. mole	ΔH_{3rd}, kcal./mole
930.8	−9.215	1.0743	39.25	63.28	98.15
933.3	−9.086	1.0715	38.80	63.27	97.85
953.7	−8.658	1.0485	37.78	63.14	98.00
974.0	−8.212	1.0267	36.60	63.01	97.97
976.0	−8.171	1.0246	36.49	63.00	97.98
984.1	−8.018	1.0162	36.10	62.95	98.05
994.8	−7.826	1.0052	35.62	62.88	98.18
1014.4	−7.426	0.9858	34.47	62.75	98.13
1034.0	−7.060	0.9671	33.40	62.64	98.16

et al.,[1] at 1250°K. within the experimental uncertainty of the data. Furthermore, the reaction investigated was checked for any significant variation from unity of the accommodation coefficient by reducing the hole size area by a factor of 10 and observing no change in the K_p within the experimental error. Since the plot of the data is linear to a high degree of precision, the presence of a competing reaction is extremely improbable. In addition, a greater than fivefold variation in pressure of $AlCl_3(g)$ at 975°K. (*cf.* Table IA) produces a negligible effect on the K, further indicating that only $AlCl(g)$ is being produced in the reaction of $AlCl_3(g)$ with $Al(l)$. It is realized that a variation of even 10 in orifice area is probably not sufficient to eliminate the possibility of an accommodation coefficient in the range of 0.1 to 1.0. However, assuming the accommodation coefficient as small as 0.1, it would not alter significantly the reported value (within experimental error). It is felt, however, that the accommodation coefficient in the present case is essentially unity. A detailed discussion of the validity of such an assumption has been presented previously.[14,15]

Employing the second law of thermodynamics, the constants from eq. 6 lead to a value of 90.3 ± 1.1

kcal./mole for the heat of reaction and 55.1 ± 1.1 cal./deg. mole for the corresponding entropy change at the average temperature of 982°K. (The uncertainities assigned to these numbers are the normal statistical standard deviations of the slope and intercept, respectively.)

Heat of Formation of AlCl(g). Using this second-law heat of reaction at 982°K. and $\Delta H_f°_{982}$ for $AlCl_3(g)$ of -142.9 ± 0.5 kcal./mole[5] ($\Delta H_f°_{982}$ for $Al(l)$ = 0 by definition), -17.5 ± 0.4 kcal./mole is obtained for $\Delta H_f°_{982}$ for $AlCl(g)$. The uncertainty assigned to this quantity is the square root of the sum of the squares of the weighted uncertainties of $\Delta H_f°_{982}$ $AlCl_3(g)$ and $\Delta H_f°_{982}$. Employing the available heat content data for $AlCl(g)$, $Al(l)$ and $AlCl_3(g)$,[5] the $\Delta H_f°_{298}$ for $AlCl(g)$ is found to be -13.3 ± 0.4 kcal./ mole. This heat of formation is in good agreement with -11.6 ± 1.0 kcal./mole, the average of several previous third-law experiments.[1-5] The experimental and derived thermodynamic data can be found in Table II.

Entropy of AlCl_3(g). Since the entropies of $Al(l)$ and $AlCl(g)$ are known to a high degree of accuracy, the entropy of $AlCl_3(g)$ at 982°K. can be calculated

Table II: Experimental and Derived Thermodynamic Data for $AlCl(g)$ and $AlCl_3(g)$

$\Delta H_r°_{982}$	90.3 ± 1.1 kcal./mole
$\Delta S_r°_{982}$	55.1 ± 1.1 cal./deg. mole
$\Delta H_f°_{982}$ $AlCl(g)$	-17.5 ± 0.4 kcal./mole
$S°_{982}$ $AlCl_3(g)$	104.6 ± 2.1 cal./deg. mole
$\Delta H_f°_{298}$ $AlCl(g)$	-13.3 ± 0.4 kcal./mole
$S°_{298}$ $AlCl_3(g)$	76–78 cal./deg. mole

(14) M. A. Greenbaum, R. E. Yates, and M. Farber, *J. Phys. Chem.*, **67**, 1802 (1963).

(15) H. C. Ko, M. A. Greenbaum, and M. Farber, *ibid.*, **69**, 2311 (1965).

Table III: Equilibrium Data for the Reaction $2AlCl_3(c) = Al_2Cl_6(g)$

Ref.	Temp. range, °K.	T_{av}, °K.	log P (Al₂Cl₆), atm.	$\Delta H_r°$, kcal./mole	$\Delta S_r°$, cal./deg. mole	$\Delta S_r°$,[5] cal./deg. mole
6	420.8–464.6	442.7	$13.234 - 6.00 \times 10^3/T$	27.45	60.55	58.40
7	395.0–450.2	422.6	$13.192 - 5.976 \times 10^3/T^a$	27.34 ± 0.18	60.36 ± 0.43	58.74
7	392.6–428.1	410.1	$13.002 - 5.898 \times 10^3/T^a$	26.99 ± 0.46	59.48 ± 1.12	58.96
10	388.6–466.4	427.3	$13.324 - 6.025 \times 10^3/T^a$	27.57 ± 0.19	60.97 ± 0.44	58.67
11	294.2–322.2	308.0	$14.89 - 6.536 \times 10^3/T$	29.91	68.13	60.69

a Authors did not report line. Their data were fitted with a straight line by method of least squares.

Table IV: Equilibrium Data for the Reaction $Al_2Cl_6(g) = 2AlCl_3(g)$

Ref	Temp. range, °K.	T_{av}, °K.	log K_p, atm.	$\Delta H_r°$, kcal./mole	$\Delta S_r°$, cal./deg. mole	$\Delta S_r°$,[5] cal./deg. mole
6	669–816	742	$7.15 - 61.5 \times 10^3/T$	28.14	32.72	31.85
7	605–944	775	$7.692 - 6.541 \times 10^3/T^a$	29.93 ± 0.82	35.20 ± 1.12	31.67

a Authors did not report line. Their data were fitted with a straight line by method of least squares.

from the entropy of reaction obtained in this study. The $S°_{982}$ AlCl(g) of 64.84 ± 0.5 cal./deg. mole was derived from statistical mechanics using measured molecular constants,[16] while the $S°_{982}$Al(l) of 17.42 ± 0.5 cal./deg. mole is based on measurements on the solid[17-25] and the heat of fusion.[20,21,26,27] The uncertainties assigned to these entropies were estimated by the present authors. Thus, 104.6 ± 2.1 cal./deg. mole is obtained for the entropy of AlCl(g) at 982°K.

The entropy at 982°K. for AlCl₃(g) of 96.8 cal./deg. mole,[5] computed from statistical mechanics, is 7.8 entropy units smaller than the experimental value reported here. Four entropy units of this difference can be attributed to the two assigned uncertainties. The tabulated entropy at 298°K. (74.6 cal./deg. mole)[5] is uncertain by at least 2 cal./deg. mole, since this quantity is based entirely on estimated molecular parameters except for one experimental vibrational frequency using a rigid harmonic oscillator as the model. Since these frequencies [150(2), 245(1), 400(1) and 610(2)][5] are small, a sizable anharmonicity correction to the calculated entropy is certain to exist at 982°K. Furthermore, the vibrational contribution to the entropy was approximated using the equation

$$S_v = \frac{Rx}{e^x - 1} - R \ln (1 - e^{-x})$$

where $x = hc\omega_i/kT = 1.438\omega_i/T$. This approximation is valid only when x is small, which is hardly satisfied

for AlCl₃(g) even at 298°K. On this basis, it is reasonable that these statistical calculations may have an accumulated error of 3 to 4 cal./deg. mole at 982°K.

Some experimental evidence supporting the higher value is indicated by the equilibrium data presented in Tables III and IV. In each of these studies the experimental entropy of reaction is greater by 2 or more entropy units than that predicted from statistical entropies.[5]

Reduction of $S°$ at 982°K. to 298°K. is difficult because of the aforementioned corrections. The most probable value for the entropy of AlCl₃ from these experiments is in the range 76–78 cal./deg. mole.

(16) G. Herzberg, "Molecular Spectra and Molecular Structure. I. Spectra of Diatomic Molecules," D. Van Nostrand Co., Inc., New York, N. Y., 1950.

(17) N. E. Philips, *Phys. Rev.*, 114, 676 (1959).

(18) J. A. Kok and W. H. Keesom, *Physica*, 4, 835 (1937).

(19) W. F. Giauque and P. F. Meads, *J. Am. Chem. Soc.*, 63, 1897 (1941).

(20) K. K. Kelley, U. S. Bureau of Mines Bulletin 476, U. S. Government Printing Office, Washington, D. C., 1949.

(21) O. Kubaschewski, *Z. Elektrochem.*, 54, 275 (1950).

(22) J. H. Awberry and E. Griffiths, *Proc. Phys. Soc.* (London), 38, 378 (1926).

(23) E. D. Eastman, A. M. Williams, and T. F. Young, *J. Am. Chem. Soc.*, 46, 1178 (1924).

(24) H. Seekamp, *Z. anorg. allgem. Chem.*, 195, 345 (1931).

(25) P. Schubel, *ibid.*, 87, 81 (1914).

(26) W. Oelsen, O. Oelsen, and D. Thiel, *Z. Metallk.*, 46, 555 (1955).

(27) F. E. Wittig, *ibid.*, 43, 158 (1952).

Shock Tube Studies on the Condensation of Various Vapors

by Richard J. Miller and Jerome Daen

Department of Chemistry, Lehigh University, Bethlehem, Pennsylvania   (*Received March 15, 1965*)

Shock wave induced condensation of 2-butanol, ethanol, methanol, chloroform, carbon tetrachloride, hexane, pyridine, and water was followed on a microsecond time scale using light transmission measurements. In all instances, deposition began as a film; "rupture" of the film into droplets or a lenticular structure was inferred from a decrease in transmitted light at later times. Values of the condensation coefficient were computed for a steady-state model of the process and a discussion of several aspects of the rupture was made.

Introduction

Kinetic processes in phase changes have been of considerable interest. Though much attention has been paid to the vapor–liquid condensation transformation,[1-3] it appears that only one investigation has been made of early events, this being the shock tube study of water vapor condensation by Goldstein.[4] The present study was initiated to investigate the significance of various parameters in the condensation and film growth in a variety of materials.

Condensation is induced in the shock tube by utilizing the pressure increase across the shock wave. The bulk of the gas behind the shock wave is compressed adiabatically and heated very rapidly. However, the gas in the thermal boundary layer along the wall, essentially, will suffer an isothermal compression. Thus, if a gas is shocked and its resultant pressure is greater than the equilibrium vapor pressure at the wall temperature, the material in the thermal boundary layer will become supersaturated and condensation on the wall will ensue.

In this study, weak shock waves were passed through various vapors at or near their saturation vapor pressures. The resulting condensation was monitored by recording the intensity of a transmitted beam of monochromatic light passing through the shocked gas since a thin coating of condensed material influences the light reflective properties of the system.

Experimental

The shock tube was constructed of two pieces of 1.5-in. i.d. Pyrex pipe, the driver section being 3 ft. long and the channel 10 ft. long. Seals between the various sections of the tube were of Teflon gaskets. Prior to

a condensation experiment, the tube pressure was reduced to 1 μ and a leak rate of 0.3 μ/min. was maintained. Shock velocity measurements were made with two photomultiplier light screens whose signals were recorded photographically from a Tektronix Type 585 oscilloscope.

The optical system used to follow the condensation on the tube walls was composed of an Osram Model HBO 100 W/2 high-pressure mercury arc lamp, the light from which after collimation was passed through a Bausch and Lomb interference filter and then through the shock tube. The incident slit width was 0.125 in. The transmitted light impinged on a Dumont No. 6292 photomultiplier tube and was read out on a Tektronix Type 515 oscilloscope. The mercury arc lamp was powered by a d.c. supply having a ripple of less than 1%. Observations were made 8.83 ft. below the diaphragm.

Modifications were made to measure the condensation rate simultaneously at two different wavelengths, *i.e.*, at 5460 and 4000 Å. Upon emerging from the shock tube, white light from the lamp fell onto a 4000-Å. filter which was inclined at 45°. This acted as a beam splitter by transmitting the 4000-Å. radiation into the photomultiplier and reflecting all other radiation upward onto a 5460-Å. filter and then into a second photomultiplier tube. The absorption spectrum of the inclined filter showed negligible changes in its trans-

(1) W. M. Nagle and T. B. Drew, *Trans. Am. Inst. Chem. Engrs.*, **31**, 605 (1934).

(2) N. Fatica and D. L. Katz, *Chem. Eng. Progr.*, **45**, 661 (1949).

(3) J. F. Welch, *Dissertation Abstr.*, **21**, 3393 (1961).

(4) R. Goldstein, *J. Chem. Phys.*, **40**, 2793 (1964).

mission characteristics. Outputs from the two photo-multiplier tubes were read out photographically on a Type 585 oscilloscope using a Type 82 dual trace plug-in unit for simultaneous display of both signals.

Materials studied were 2-butanol from Eastman Organic Chemicals (Eastman grade), methanol, CCl_4, $CHCl_3$, and pyridine from the J. T. Baker Co., hexane from Matheson Coleman and Bell (reagent grade), and absolute ethanol from United States Industrial Chemicals. All were used without further purification. Singly distilled water was studied in all water experiments.
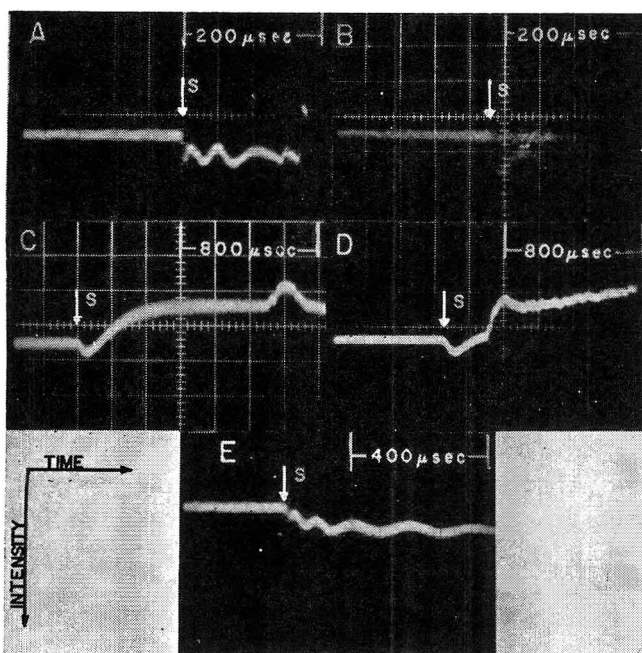
Figure 1. Typical time–transmission records for various materials: A, 2-butanol: T_2, 440°K., P_2 = 260 mm., P_2/P_8 = 13; B, ethanol: T_2, 490°K., P_2 = 250 mm., P_2/P_8 = 5.37; C, ethanol; T_2, 350°K., P_2 = 87 mm., P_2/P_8 = 1.50; D, water: T_2, 640°K., P_2 = 165 mm., P_2/P_8 = 7.40; E, chloroform: T_2, 300°K., P_2 = 530 mm., P_2/P_8 = 2.40.

The tube wall was cleaned between series of runs but not between individual runs in a series on a compound. The test area was swabbed with methanolic KOH and rinsed three times with pure methanol. Vapors were evaporated into the evacuated shock tube from a glass bulb; initial pressures were measured on a Dubrovin gauge.

Helium, oil-pumped nitrogen, and Freon-12 were the driver gases. Aluminum foils, 1.0- and 0.8-mil in thickness, were used as diaphragms; these broke at pressure differences of about 1.5 and 1 atm., respectively.

Results

2-Butanol. Experiments were carried out with 2-butanol as the condensate, using helium gas as a driver and a diaphragm of 1.0-mil foil. A typical oscilloscope trace is shown in Figure 1. When this alcohol, at its saturation vapor pressure, was shocked it was observed that the intensity of light transmitted through the tube increased by 2-5% within 5 μsec. after the passage of the shock. This initial increase was followed by oscillations in the intensity which lasted for approximately 200 μsec. At this point a large decrease in intensity occurred which marked the end of the useful portion of the record. At no time during the oscillations did the intensity return to its original level.

That the behavior apparent in the trace in Figure 1 is indicative of the formation of a thin film of condensate on the tube wall may be seen from the following argument. Suppose a film of refractive index n_1 exists between two media of refractive index n_0 and n_2, respectively; here n_0 refers to the refractive index of the vapor and n_2 to that of the wall material. If unit light intensity is incident upon this film, then the transmitted light intensity can be shown to be[5]

$$I = \frac{\left[1 - \left(\frac{n_0 - n_1}{n_0 + n_1}\right)^2\right]\left[1 - \left(\frac{n_1 - n_2}{n_1 + n_2}\right)^2\right]}{1 + \left[\frac{n_0 - n_1}{n_0 + n_1}\frac{n_1 - n_2}{n_1 + n_2}\right]^2 + 2\left[\frac{n_0 - n_1}{n_0 + n_1}\frac{n_1 - n_2}{n_1 + n_2}\right]\cos x}$$

(1)

where $x = 4\pi n_1\theta/\lambda$. Here θ is the thickness of the film and λ is the wave length of the incident light. If $n_1 < n_2$, the film formed is an antireflection film; the amount of light reflected at the surface is reduced and hence the transmitted intensity increases. As the film thickness increases, eq. 1 describes an oscillatory behavior whose minima are equal to the original intensity. Such behavior is as observed in Figure 1, with the difference that the observed intensity never returns to its original level. It is inferred that filling of surface irregularities with liquid and the subsequent removal of scattering centers from the glass surface is responsible for this increase.

It is seen from eq. 1 that maxima and minima in intensity occur at integral multiples of $x = \pi$. Presented in Table I are time–thickness data calculated for several runs for 2-butanol and other materials. In these calculations, the refractive index of the D-line of sodium was used for that at 5460 Å. The un-

(5) A. Vasicek, "Optics of Thin Films," Interscience Publishers, Inc., New York. N. Y., 1960, p. 112.

Table I : Typical Time-Thickness Data

| Material | Time (μsec.) for thickness of (cm. × 10⁵) | | | | | | | P_1,[a] mm. | P_2,[b] mm. | T_2, °K. | P_2/P_s[c] |
	1	2	3	4	5	6	7				
2-Butanol	5	20	55	90	135	200	300	19.0	140	380	7.0
2-Butanol	5	15	30	55	75	110		18.8	260	460	13.0
2-Butanol	5	12	30	50	75	110	145	19.7	284	440	10.4
2-Butanol	5	15	50	80	110			15.0	252	450	15.9
Ethanol	15	45	120	200				19.6	247	490	5.37
Methanol	45	250						19.8	158	500	1.44
Chloroform	15	30	60	100	140	225	320	219	527	300	2.40
Carbon tetrachloride	10	25	50	80	110	150		138	304	337	2.20
Hexane	10	30	80	140				21.8	270	370	1.80

[a] Subscript 1 refers to conditions ahead of the shock. [b] Subscript 2 refers to conditions behind the shock. [c] P_1/P_s is the supersaturation ratio relative to the vapor pressure of the liquid at wall temperature.

certainty in θ introduced by this approximation was estimated to be less than 0.5% based on dispersion data for several liquids. Gas properties behind the shock were calculated using the method of Bethe and Teller[6] with the required enthalpies being obtained from various sources.[7] To substantiate further that the condensation of a film on the tube wall was being observed, simultaneous measurements were made of the intensity behavior using radiation of two different wave lengths. The interference peaks in the intensity should occur earlier for the shorter wave length, but the calculated thickness at any time should agree for the two wave lengths. Curves for both wave lengths are seen to coincide on the thickness-time graph for 2-butanol given in Figure 2.

All photographs showed the characteristic large decrease in intensity which occurred at 160–200 μsec. after the shock arrival and which marked the end of the oscillatory portion of the trace. Calculations demonstrated that this decrease could not be assigned to the arrival of the cold front into the viewing area. Consequently, this decrease is ascribed to the formation of a lenticular structure such as would accompany the rupture of the film to lenses or droplets which scatter light and thus lead to a diminution in transmitted light.

Ethanol and Methanol. In general, the results for ethanol qualitatively resembled those of 2-butanol, the difference being that the condensation rate was lower for ethanol. Typical traces are shown in Figure 1. Supersaturations (P_2/P_s) ranged from 5 to approximately 1.2. Down to a supersaturation of 2, there was a gradual decrease in observed condensation rate. From supersaturations of 1.2 and 1.5 a rather different type of trace was obtained. In these instances, there was an increase in intensity as usual which was quickly
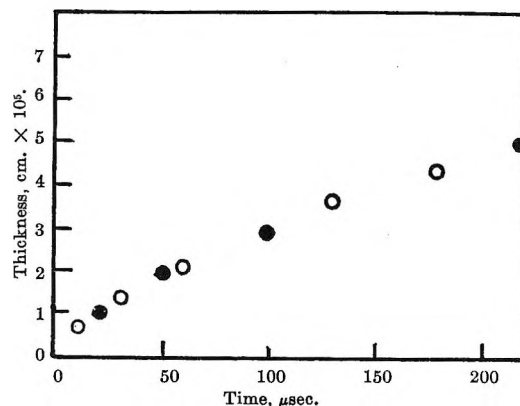
Figure 2. Simultaneous thickness-time measurements for 2-butanol: O, 5460 Å.; ●, 4000 Å.

followed by a large decrease, below the original intensity, which is ascribed to the rupture of the film.

The condensation of methanol appears to be less extensive than that of either 2-butanol or ethanol, generally affording only one maximum and one minimum in intensity before film growth ceased.

Hexane. In view of its nonpolar nature and lack of association in the vapor phase, the behavior of hexane was compared with that of the alcohols. At super-saturations of about 2, behavior similar to that of

(6) H. A. Bethe and E. Teller, Ballistics Research Laboratories, Aberdeen Proving Ground, Md., Report X-117 (1945).

(7) N. S. Berman and J. J. McKetta, *J. Phys. Chem.*, **66**, 1444 (1962) (2-butanol); K. S. Pitzer, J. C. M. Li, and E. V. Ivash, *J. Chem. Phys.*, **23**, 1814 (1955 (methanol); J. H. S. Green, *J. Appl. Chem.*, **11**, 397 (1961) (ethanol); F. D. Rossini, *et al.*, "Selected Properties of Physical and Thermodynamic Properties of Hydrocarbons and Related Compounds," Carnegie Press, Pittsburgh, Pa., 1953 (hexane); K. Li, *J. Phys. Chem.*, **61**, 782 (1957) (pyridine); E. Gelles and K. S. Pitzer, *J. Am. Chem. Soc.*, **75**, 5259 (1959) (carbon tetrachloride and chloroform); A. S. Friedman and L. Haar, *J. Chem. Phys.*, **22**, 2051 (1954) (water).

ethanol was observed. At a supersaturation of about 1.3, the behavior resembled that of methanol.

Water. Initial experiments on water, with supersaturations ranging from 7 to 9, resulted in traces which were quite different from those of hexane and the alcohols and also different from those obtained by Goldstein. An example is shown in Figure 1. At these higher supersaturations a film is observed to grow for a relatively long time, 100 to 200 μsec., although the growth rate was quite small. What occurs after this period is not entirely clear, but it involves the rupture of the film as indicated by the large decrease in intensity at about 200 μsec. The effect of lowering supersaturation and collision rate with the wall was seen to be an earlier rupture as with certain ethanol films. The difference in appearance between traces for water and the other materials previously studied is believed to be due to the relatively large surface tension of water which results in a less stable film. At supersaturation ratios of about 5, the water traces resembled Goldstein's more closely. In experiments discussed in this work, the films were stable for a larger period of time; reduced turbulence in the present shock tube is probably responsible for the difference.

Carbon Tetrachloride and Chloroform. Since CCl_4 is symmetrical and nonpolar, and $CHCl_3$ has low polarity, a comparison of their behavior with that of the rest of the materials was of interest. Typical results for $CHCl_3$ are shown in Figure 1. The traces qualitatively resemble those of the alcohols and hexane, with one difference. For the previously studied materials, the envelope of the oscillatory portion was a horizontal straight line. Here it is a straight line with a slope toward greater intensities.

Pyridine. To investigate the effect of surface tension, experiments were performed on pyridine, which has a surface tension of 38 dynes/cm., intermediate to that of water and the other materials. Pyridine exhibited a decrease in intensity as condensation was initiated, as predicted by eq. 1 for a material of refractive index slightly higher than Pyrex. This observation, of course, is additional evidence for the production of a film on the wall, as a "reflection coating" is formed. Since the refractive indices of liquid and glass were so close the oscillations in intensity were of small amplitude.

Curves of thickness *vs.* time for typical runs with various materials are displayed in Figure 3.

Discussion

A point which should be discussed is the thermal stability of the various compounds at the temperatures that exist behind the shock. In experiments
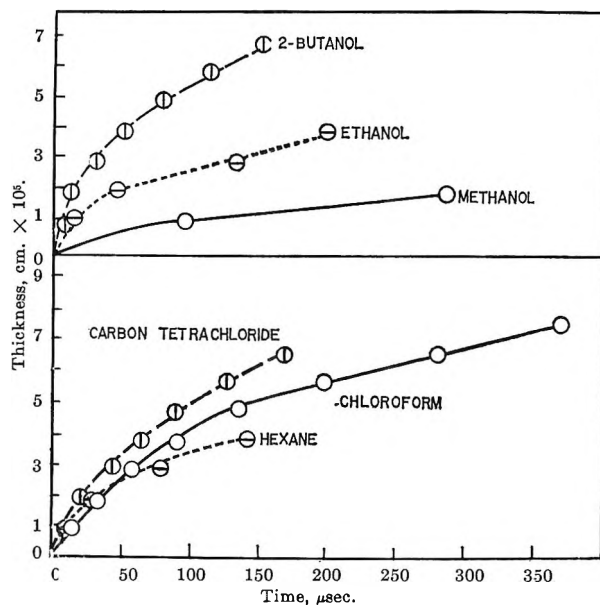
Figure 3. Deposition rates for various materials.

with CCl_4, $CHCl_3$, and hexane, temperature rises of only 50 to 100° were obtained; decomposition would be negligible here. Pyrolysis in 2-butanol, methanol, and pyridine has been observed at temperatures above 550°,[8-10] considerably higher than those obtained in these experiments. It is thus clear that pyrolysis of the gases behind the shock wave in these experiments cannot be responsible for the observations on light intensity.

The compounds do not absorb light in the visible region, their absorption peaks being far into the ultraviolet. Any decomposition, however small, which might occur here could not give products with drastically different spectral characteristics from the original material, so that absorption of the 5460-Å. light would be negligible for any species present. In other words, there could be no enhanced transmission resulting from chemical breakdown.

Close inspection of the transmission records, as in Figure 4A, reveals that for 2-butanol a very sharp decrease (of about 1 μsec.) occurs immediately after the arrival of the shock front. To investigate this more closely, photographs were obtained at higher sweep speeds. Interestingly enough, under these conditions it is possible to resolve the initial spike into two parts: a decrease followed by a less obvious abrupt increase. The decrease can be interpreted in terms of the known

(8) F. Someno, *Bull. Phys. Res.* (Tokyo), **21**, 277 (1942).

(9) E. Kuss, *Angew. Chem.*, **49**, 483 (1936).

(10) C. D. Hurd and J. L. Simon, *J. Am. Chem. Soc.*, **84**, 4519 (1962).
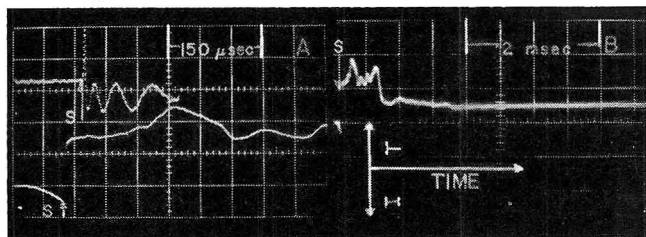
Figure 4. Simultaneous intensity–heat gauge records for
2-butanol: $P_1 = 11$ mm.; $T_1 = 298°K.$; $M_1 = 3.13$;
$P_2/P_1 = 10.0$; distance between light source and heat
gauge is 1.98 cm.; distance from diaphragm to heat
gauge is 14.3 ft. The initial rising spike in A has
been inked over to improve reproduction quality.

small though measurable reflectivity of the shock and a
slight tilt with respect to the wall; the shock passage
time over the slits is quite comparable to the width
detected. However, the second (increasing intensity)
spike is associated with the condition of the wall
surface. If the wall was cleaned with methanolic
potassium hydroxide and rinsed with methanol, the
second spike disappeared and the first intensity maxi-
mum broadened very slightly. After six consecutive
runs without recleaning in the manner described, the
second spike reappeared. What is the responsible
factor is not clear. However, it might be noted that
this behavior is observed with less polar materials
such as 2-butanol, chloroform, and carbon tetra-
chloride rather than with polar molecules such as water,
ethanol, and methanol.

Some plots of thickness vs. time have been displayed
in Figure 3. In each case there seem to be two general
regions to the curve, a region of decreasing growth rate
from the onset of condensation continuing for 50 to
100 μsec. followed by one of relatively constant growth
rate.

One factor in the change of growth rate with time in
the very early stages of the deposition and especially at
times considerably less than those corresponding to the
first datum point would lie in the changing nature of the
surface as the condensation proceeds. As the film thick-
ness increases, the condensation process changes from one
of vapor condensing on a glass surface to one of vapor
condensing on monolayer through multilayer and termi-
nating on bulk liquid. It would be unexpected to find
that the probability of a molecule condensing on the
liquid is the same as for all of the earlier stages involved.
As the growth continues, the rate approaches a con-
stant value as condensation takes place on bulk liquid.
Such effects would be expected to be most significant
at very short times, although work by Shereshefsky[11]
on evaporation of liquids from capillaries suggests that

the wall might have an effect on evaporation–conden-
sation processes at distances up to 1000 Å. from the
wall.

Beyond this "substrate influenced region" phenom-
enon, one would expect that some time would be re-
quired to reach a steady state in flow. During this
time, transient effects in heat transfer, mass flow, etc.
would be smoothed. Following this transient period,
in the steady state, condensation would proceed
on an underlaying layer of molecules of liquid, with
heat transfer taking place through the bulk. At
present, the importance of these transient effects is
not completely understood. Heat flux measurements
which are in progress[12] will be useful in clarifying the
situation.

To summarize, oscilloscope traces for the longer
lasting films showed two regions in the condensation
process, first the region of rapidly decreasing growth
rate followed by a region of relatively constant growth
rate. Calculations based on the latter were made
since any errors in choosing the slope will be small.

A condensation coefficient is defined as the fraction
of gas molecules striking a cold surface which actually
stick and, according to Mortensen and Eyring,[13] is
given by the ratio of partition functions for the mole-
cules on the surface to those in the vapor phase.
Because the vibrational degrees of freedom are the
same for these two states, these do not have to be
considered. However, the molecules in the surface
experience restricted rotation and have a smaller
rotational partition function. Therefore, the con-
densation coefficient is given by the ratio of these ro-
tational partition functions. Experimentally deter-
mined values of the condensation coefficient generally
agree with the calculated ones.[13]

In the past, rather than the condensation coefficient
itself, the quantity measured has been the evapora-
tion coefficient, the analog of the condensation coef-
ficient for the evaporation process. The two coef-
ficients are equal at a state of equilibrium between
liquid and vapor.

It will first prove helpful to have at hand an estimate
of the temperature rise in the film that would be ex-
pected under steady-state conditions. An approxi-
mate calculation of the temperature rise can be ob-
tained from a heat balance. The heat q given off in
the condensation of vapor on unit area is

(11) M. Folman and J. L. Shereshefsky, J. Phys. Chem., 59, 607
(1955).

(12) W. R. Smith and P. Kicska, private communication.

(13) E. M. Mortensen and H. Eyring, J. Phys. Chem., 64, 846
(1960).

$$q = h\dot{\theta}\rho dt$$

where h is the heat of vaporization per gram of liquid formed, $\dot{\theta}$ is the growth rate of the film, and ρ is the density of the liquid. This, of course, is equal to the sum of the heat which flows into the wall (here assuming constant wall temperature) and that which causes the temperature rise in the film; i.e.

$$h\dot{\theta}\rho dt = K(dT/d\theta)dt + \theta C_p\rho dTdt$$

where K is the coefficient of thermal conductivity, $dT/d\theta$ is the temperature gradient across the film, θ is the film thickness, and C_p is the heat capacity per gram. Values of $\dot{\theta}$ were taken directly from curves of thickness vs. time, and heat transfer between the film and gas and boundary layer effects were neglected. Temperature rises calculated by this method for 2-butanol, ethanol, methanol, hexane, CCl_4, and $CHCl_3$ are of the order of 6, 2, 0.5, 1.5, 3, and 3°, respectively. In the calculation of the condensation coefficient, these temperature rises were included.

If the following computation of the condensation coefficient is to be applicable, the rate of flow from the vapor to the film must be small in comparison to the sound speed in the vapor. Under typical conditions with 2-butanol, the deposition rate in the later stages of the process is about 3.3×10^{-2} mole/sec./cm. of wall. If all of the molecules deposited come from near the wall (maximum depletion) and the density of the gas behind the shock is 0.01 mole/l. (at conditions of the typical run quoted above), then the deposition rate is 3.3 l. of gas/sec. Consequently, there must be a velocity directed toward the wall of magnitude equal to 280 cm./sec., which is considerably less than the sound velocity. In a typical run with 2-butanol, the film reached a thickness of about 7×10^{-5} cm. before the useful portion of the trace ended, this corresponding to a maximum removal of only about 7% of the gas in the tube. One may then, for simplicity, take the conditions at the center of the tube to be essentially the same as if there were no wall-directed transport; i.e., a steady state is assumed.

The net deposition onto the wall is given by

$$\Delta = \frac{1}{4}\beta(\rho_wC_w - \rho_LC_w) \qquad (2)$$

where the first term in the parentheses accounts for the number of wall collisions from the vapor and the second gives the number evaporating from the liquid film at the temperature of the wall. The subscript w refers to the wall and ρ_L is the density of the saturated vapor at the temperature of the wall. As is usual, the evaporation and condensation coefficients have been taken to be equal and are represented by β.

Using the experimentally determined values of Δ, the estimated wall temperature rise, and the condition of the shocked gas, the values of β summarized in Table II were obtained.

Table II: Measured Condensation Coefficients

Material	β	Wall temp., °K.
2-Butanol	0.032 ± 0.005	312
Ethanol	0.026 ± 0.005	297
Hexane	0.04 ± 0.01	298
Carbon tetrachloride	0.05 ± 0.01	307
Chloroform	0.017 ± 0.004	305
Water[14]	0.036	283
Water[15]	0.35 to 1.0	
Water[16]	0.243	
Water[17]	0.042	
Carbon tetrachloride[13]	1	273
Chloroform[13]	0.16	275
Methanol[13]	0.045	273
Hexane[13]	0.70 (calcd.)	
Water[13]	0.036	273

Comparison of the condensation coefficients in Table II with those given by Mortensen and Eyring shows reasonable agreement for ethanol. For 2-butanol, β is of the same magnitude as their value for propanol, as might be expected. However, a value of β of 0.05 was obtained here for CCl_4, much less than the previously reported value of unity.[13] The other values of β are similarly lower than the previously obtained values.

Discrepancies similar to these exist between values of β of other materials obtained by various methods. Alty and McKay[14] measured β for H_2O by an evaporation method, obtaining a value of 0.036. In a recent study, Nabavian and Bromley[15] obtained a value of β ranging from 0.35 to 1.0 from a measurement of the heat transfer coefficient of a H_2O film on a copper tube. In still another study, Hickman,[16] observing the evaporation from a jet flowing under vacuum, obtained a value of 0.243 for β, which may reach unity if surface cooling is considered. This paper was discussed by Delaney, Housten, and Eagleton,[17] who themselves found β to be only 0.027. They suggested that the rate of vaporization from a rapidly renewed surface,

(14) T. Alty and C. A. McKay, Proc. Roy. Soc. (London), A149, 104 (1935).

(15) K. Nabavian and L. A. Bromley, Chem. Eng. Sci., 18, 651 (1963).

(16) K. C. D. Hickman, Ind. Eng. Chem., 46, 1442 (1954).

(17) L. R. Delaney, R. W. Housten, and L. C. Eagleton, Chem. Eng. Sci., 19, 105 (1964).

such as Hickman's, is much higher than it is from a stagnant surface.

Littlewood and Rideal[18] have discussed the dependence of the condensation coefficient on the experimental method used. These authors feel that the heat and mass transfer fluxes of evaporation experiments could have some effect on interfacial equilibrium. In other words, lack of knowledge of the surface temperature is a large contributor to the uncertainty and the value of the experimentally measured condensation coefficient is dependent on the supply of heat to the surface (when the evaporation coefficient is being measured). When heat transfer to the surface is sufficient, β will always be unity. They attributed much of Hickman's success to the fact that surface cooling is almost eliminated in the jet.

Another aspect of the deposition process merits some attention here. All films observed in these experiments, as mentioned earlier, exhibited an abrupt turbidity increase that preceded the arrival of the contact surface as calculated from idealized shock tube theory. Though it has been shown that the actual arrival of the cold front can under certain conditions occur earlier than predicted,[19] the diminished transmission intensity herein noted is assigned to a rupture of the film. In Figure 4 are displayed simultaneous light transmission and platinum thin film heat gauge measurements on a 2-butanol film; the time scale in Figure 4A is 50 μsec./cm. while in Figure 4B it is 500 μsec./cm. In Figure 4A, it is evident that the heat gauges and the intensity data correlate. That is, both indicate the shock arrival. Moreover, the optically observed growth is accompanied by a concurrent increase in temperature. When the turbidity abruptly increases, about 150 μsec. after the shock arrival, the temperature begins to drop. Displayed in Figure 4B is the same heat gauge record simultaneously recorded at a slower sweep speed. The first maximum corresponding to the ascribed rupture is apparent. This is followed by an oscillatory profile which terminates in a sharp drop about 600 μsec. after the entry of the shock into the observation station, this being ascribed to the contact surface. Idealized shock tube calculations for this experiment show that the latter should arrive 1.09 msec. after the shock front. Rupture of the film into a lenticular structure would result in enhanced light scattering as observed. Except for a few cases of early breakup, the final breakup of the film appears to be the result of a flow-enhanced instability based on observations of the time-to-rupture. For the large range of conditions achieved in experiments on 2-butanol, it is evident that the film stability decreases with increasing particle velocity
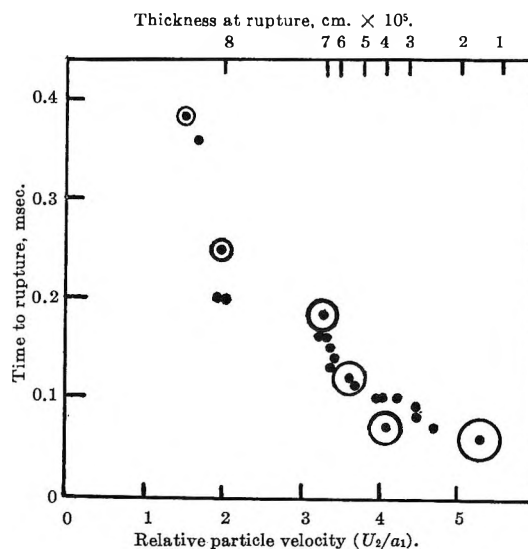
Figure 5. Time-to-rupture behavior of 2-butanol vs. particle velocity.

behind the shock front. This behavior is displayed in Figure 5 where the time between the onset of condensation and the rupture of the film is plotted against the particle velocity Mach number. Concomitant with the decrease of the time-to-breakup is a decrease in thickness at breakup as shown in Figure 5. Since breakup occurs at no particular thickness, the downward trend in stability with increasing particle velocity leads to the conclusion that the stability is dynamic in nature in the experiments summarized. Experiments are included here in which the supersaturation ratio was varied while the flow speed was held constant. All of the observations appear to fall on a common curve.

To summarize very briefly, all materials first deposited as a continuous film which later broke up. Time-to-rupture data indicate that increasing particle velocity above the deposited film can be correlated with the rate of rupture. That is, films above which a high-velocity gas is flowing break up sooner than those in a low-velocity environment. Condensation coefficients computed from these shock tube studies, though probably low, are in fair agreement with those determined by other techniques. The major source of error in this method appears to be the determination of the film temperature.

(18) R. Littlewood and E. Rideal, *Trans. Faraday Soc.*, 52, 1598 (1956).

(19) R. E. Duff, *Phys. Fluids*, 2, 207 (1959).

A Study of the Pyrolysis of Methyl Ethyl and Diethyl Carbonates in the Gas Phase

by Alvin S. Gordon and William P. Norris

Chemistry Division, Research Department, U. S. Naval Ordnance Test Station, China Lake, California 93557
(*Received May 15, 1965*)

A number of carbonates—dimethyl, methyl ethyl, and diethyl—have been pyrolyzed in quartz reaction vessels with different surface–volume ratios. Unlike some recent reports, we find dimethyl carbonate to be extremely stable to pyrolysis and photolysis to at least 350°. On the other hand, both methyl ethyl carbonate (MEC) and diethyl carbonate (DEC) pyrolyze with homogeneous, unimolecular kinetics in a temperature range where DMC is stable. The specific rate constants are: $k_{MEC} = 10^{13.7}10^{-46,000/2.303RT}$; $k_{DEC} = 10^{13.9}10^{-46,000/2.303RT}$ (sec.$^{-1}$). These kinetic factors suggest that the slow step in the reaction sequence is the same as that in esters with a β-H atom in the alkyl group, $i.e.$, the transfer of the β-H atom to the carbonyl oxygen with the concurrent breaking of the C–O bond to form the α-olefin and a carboxylic acid. The mechanism is analogous to the mechanism for xanthate pyrolysis. Our results show no evidence that alkyl radicals attack either the carbonyl oxygen or the ether oxygen of a carbonate in a radical displacement reaction.

Introduction

Wijnen[1] and Thynne and Gray[2] have studied the pyrolysis of dimethyl carbonate and report that it is a heterogeneous process on a quartz surface. Wijnen[3] has also reported that dimethyl carbonate photolyzes with the radiation from a medium pressure mercury arc. We have not been able to reproduce these results, indicating that the surface of our reaction vessel and our light source differed from those of the previous investigations.

In a quartz vessel of 45-cc. capacity, with a surface to volume ratio (s/v) of 1.55 cm.$^{-1}$, we find dimethyl carbonate to be stable at 350° for 1200 sec. at 10-mm. pressure. A significant percentage of both diethyl carbonate and methyl ethyl carbonate decomposes in 600 sec. at this temperature. Dimethyl carbonate has been photolyzed with full intensity of a Hanovia medium pressure mercury arc at various temperatures up to 350° for 1200 sec. at 10-mm. pressure with only traces of CO, CH$_4$, and CO$_2$ as photodecomposition products. Dimethyl carbonate vapor, at 25°, shows no absorption from 2000 Å. to the visible within the experimental accuracy of our apparatus.[4]

The mechanism for ester decomposition has been quite firmly established. For carbonates, the gas phase[5] decompositions of phenyl and benzyl ethyl carbonates have been shown to be first order and homogeneous in a "conditioned" stainless steel reactor.

(1) M. E. J. Wijnen, *J. Chem. Phys.*, **34**, 1465 (1961).

(2) S. C. S. Thynne and P. Gray, *Trans. Faraday Soc.*, **58**, 2403 (1962).

(3) M. E. J. Wijnen, *J. Chem. Phys.*, **35**, 2105 (1961).

(4) We wish to thank Dr. R. H. Knipe for obtaining the absorption spectrum of dimethyl carbonate.

(5) (a) G. G. Smith, D. A. R. Jones, and R. Taylor, *J. Org. Chem.*, **28**, 3547 (1963); (b) P. D. Ritchie, *J. Chem. Soc.*, 1054 (1935).

All the work was done at one temperature, and the pressure was monitored as a function of time to obtain the order and the corresponding specific rate constant. Since no variation with temperature was attempted, no energy of activation or pre-exponential factor was elucidated.

For xanthates, the effect of isotopes on the kinetics has established that the decomposition path is analogous to that of esters, the thionyl sulfur accepting the β-hydrogen atom with concurrent elimination of an olefin. The intermediate compound OC(SH)SR is unstable and in a fast reaction forms COS and RSH. The organic carbonates pyrolyze to analogous compounds, olefin, CO_2, and alcohol, and are presumed to follow the same path.

In the present work, the pyrolysis of two simple carbonates has been studied in the gas phase at low pressure, over a temperature range in a quartz reaction vessel. The effect of the surface–volume ratio has been determined, and the effect of any "falloff" in the decomposition at low pressure has been evaluated by studying the effect of inert gas on the rate.

The reaction of an alkyl free radical to displace the alkyl or an alkoxy group from a carbonate was also studied.

Materials and Apparatus

All of the carbonate esters used in the research were purified by gas chromatography.

The reaction cell was a quartz cylinder of 45-cc. capacity and $s/v = 1.55$ cm.$^{-1}$. A similar vessel was packed with quartz shell tubing, all of their axes parallel to the axis of the reaction vessel, with a resultant s/v of 7.64 cm.$^{-1}$. The reaction vessel was set into a furnace with a quartz window so that the contents of the reaction vessel could be exposed to the radiation from a medium pressure quartz mercury arc when desired. The reacted material was removed from a reaction vessel to a sample flask by a Toepler pump and then introduced onto a gas chromatographic unit (squalane on Pelletex) for analysis. The gas chromatographic apparatus had provision to trap any desired constituent for identification with the mass spectrometer.

Results

A mix of diethyl carbonate and acetone was photolyzed to see if the methyl radical from acetone photolysis could displace a radical from diethyl carbonate. Both of the reactions

$$CH_3\cdot + C_2H_5OCOC_2H_5 \rightleftarrows C_2H_5OCOC_2H_5 \longrightarrow$$

(with O double bond becoming O· radical and CH₃ substituent)

$$C_2H_5OCCH_3 + C_2H_5O\cdot \quad (1)$$

and

$$CH_3\cdot + C_2H_5OCOC_2H_5 \longrightarrow$$

$$C_2H_5OCOCH_3 + C_2H_5\cdot \quad (2)$$
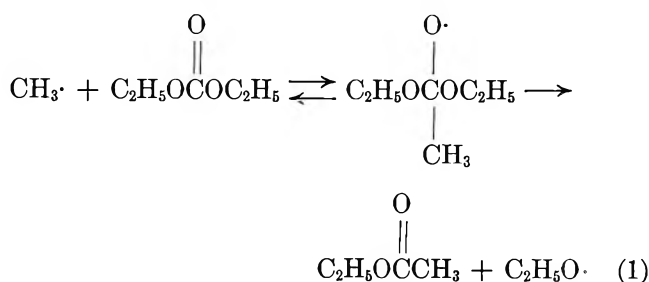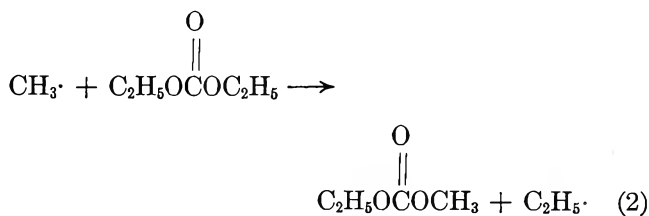
involve small heats of reaction, but no evidence of the products of either of the reactions could be found in the temperature range from 150 to 350°. Even though diethyl carbonate pyrolyzes fairly rapidly at 350°, the products of the reaction do not conceal the products of reactions 1 and 2 on the gas chromatogram.

The pyrolysis of methyl ethyl carbonate and diethyl carbonate can be studied in the temperature range 300–375°. Without heating all the tubing in the system, the highest pressure is restricted to about 20 mm. The low pressure range emphasizes any surface effects. As previously noted, two s/v ratios were employed to check for surface effects. Within the precision of our results the reaction was seen to be homogeneous. Carbon dioxide was added as an inert gas to diethyl carbonate (75:1) without any effect on the rate, showing that the rate constant was in the pressure-independent region and reinforcing the previous observations that surface plays a minor role. The products of the reaction of diethyl carbonate were ethanol, ethylene, and carbon dioxide and for methyl ethyl carbonate were methanol, ethylene, and carbon dioxide, in agreement with previous work[5] on pyrolysis of other carbonates. The products were separated on a gas chromatograph and the various fractions trapped and identified. Since CO_2 and ethylene do not separate well on the column, they were trapped together and analyzed on the mass spectrometer, which showed them to be present in equal amounts, again substantiating previous work. Once the one-to-one relationship was established, the CO_2 in the products always was removed by KOH prior to the gas chromatographic analysis. Experiments at two pressure levels showed the reaction to be first order. As will be discussed in the next section, the reaction is both intramolecular

and unimolecular. Since the concentrations of reactants were so low they changed enough during the time of reaction to make it necessary to solve for the rate constant from the integrated form of the unimolecular equation

$$\ln \frac{I_0}{I} = kt$$

where I_0 and I are the amounts of reactant at times 0 and t sec., respectively. The moles of ethylene are equal to the moles of reactant consumed.

The rate constants are plotted in an Arrhenius graph in Figure 1. The points of MEC are numerous enough to be analyzed by a least-squares treatment and result in $k_{MEC} = 10^{13.7}10^{-46,000/2.303RT}$ with a standard deviation of 2 kcal./mole in the energy of activation. The intercept is precise within a factor of about 5. Within experimental error, the energies of activation of the two carbonates are seen to be equal, and the pre-exponential factor for the diethyl carbonate is about $10^{0.2} = 1.6$ times that for the methyl ethyl carbonate over the temperature range studied. The error in the slope results in A factors for the two carbonates which are indistinguishable when projected as the intercept at T_∞.

Discussion

Methyl Radical Displacement of Ethyl Radical from Diethyl Carbonate. The lack of evidence for reactions 1 or 2 indicates that these rates are less than 5% (ability to resolve products on a chromatography unit) of the rate of abstraction of H from diethyl carbonate by a methyl radical. The energy of activation for abstraction from dimethyl carbonate is 8.9 kcal./mole[2]; the energy of activation for abstraction from diethyl carbonate is about 1.5 kcal./mole lower since β-H atoms are more easily abstracted.

The relatively unfavorable rate for reactions 1 and 2 relative to methyl radical abstraction could be the result of relatively unfavorable pre-exponential factors for k_1 and k_2. However, as noted just below, some analogous displacement reactions by alkyl radicals are seen to dominate the competitive abstraction reaction. It is likely that the rates of the competitive reactions are controlled by the energies of activation, and reactions 1 and 2 must have a *minimum* E_{act} of 11 kcal. mole.

No evidence exists for alkyl radical displacement in ketones

$$R\cdot + R_1\overset{\overset{\displaystyle O}{\|}}{\underset{\underset{\displaystyle R}{|}}{C}}R_2 \xrightarrow{\,/\!\!\!\!\rightarrow\,} R_1\overset{\overset{\displaystyle O\cdot}{|}}{\underset{\underset{\displaystyle R}{|}}{C}}R_2 \xrightarrow{\,/\!\!\!\!\rightarrow\,} R\overset{\overset{\displaystyle O}{\|}}{C}R_2 + R_1\cdot \qquad (3)$$
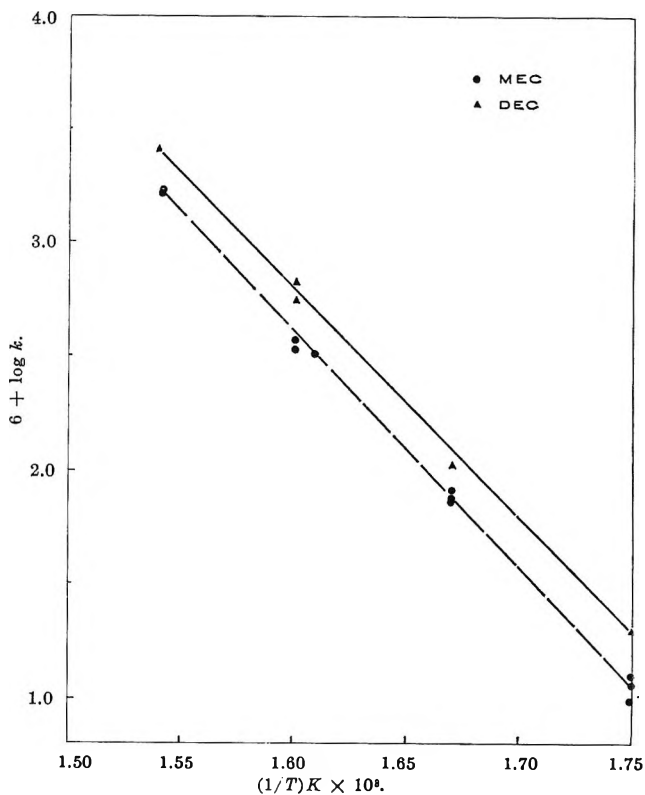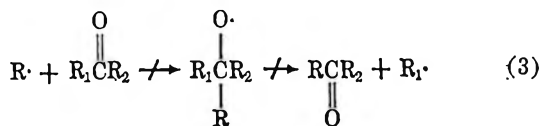
Figure 1. Arrhenius plot for decomposition of methyl ethyl carbonate (MEC) and diethyl carbonate (DEC).

although radical addition to the carbonyl carbon is almost certainly an exothermic reaction. On the other hand, it has been shown that methyl radical or ethyl radical easily displaces a perfluoroalkyl radical from perfluoroacetone[6-8] with an E_{act} of less than 7 kcal./ mole. (These unpublished results indicate that the figure may be less than 4 kcal./mole.)

$$R\cdot + CF_3\overset{\overset{\displaystyle O}{\|}}{C}CF_3 \longrightarrow R\overset{\overset{\displaystyle O}{\|}}{C}CF_3 + CF_3\cdot \qquad (4)$$
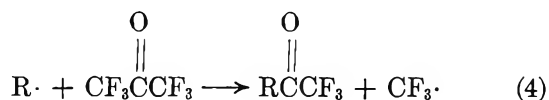
A perfluoroalkyl radical does not displace a perfluoroalkyl radical from a perfluoro ketone; only perfluoroalkyl radical addition reactions are noted in the products.[8]

Urry[9] has noted that the alkyl groups in vicinal triones equilibrate.

(6) G. O. Pritchard and E. W. R. Steacie, *Can. J. Chem.*, **35**, 1216 (1957).

(7) S. J. W. Price and K. O. Kutschke, *ibid.*, **38**, 2128 (1960).

(8) A. S. Gordon, unreported work.

(9) W. H. Urry, M. H. Pai, and C. Y. Chen, *J. Am. Chem. Soc.*, **86**, 5342 (1964).

$$2R_1CCCR_2 \rightleftharpoons R_1CCCR_1 + R_2CCCR_2 \quad (5)$$

He proposes that the reaction path is *via* acyl radical exchange

$$R_1CO\cdot + RCCCR \longrightarrow RCO\cdot + R_1CCCR \quad (6)$$
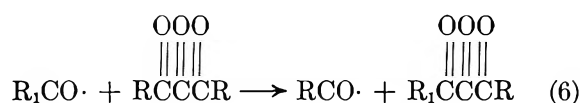
The single thread that seems to run through all the reactions is that the reaction barrier is lowered when the carbonyl carbon and the attacking radical have widely differing electronegativities. Only in reactions 4 and 6 is this condition met.

It should be mentioned that Price and Kutschke[7] report that an H atom does not displace a perfluoroalkyl group from perfluoropentanone-2, in disagreement with the above hypothesis.

Unimolecular Decomposition of Diethyl Carbonate and Methyl Ethyl Carbonate. The pyrolysis of diethyl carbonate and methyl ethyl carbonate appears to be completely intramolecular because the products are only C_2H_4 and CO_2, in a ratio equal to 1, and ethanol or methanol, respectively. If the reaction occurred *via* a radical path to any extent, then for diethyl carbonate we would expect to find $CH_3CH_2O\cdot$ as the radical carrier. Besides abstracting an H atom from the parent compound to form ethanol, $CH_3CH_2O\cdot$ would pyrolyze in this temperature range[10] to give

$$CH_3CH_2O\cdot \longrightarrow CH_3\cdot + CH_2O \quad (7)$$

and

$$CH_3CH_2O\cdot \longrightarrow CH_3CHO + H\cdot \quad (8)$$
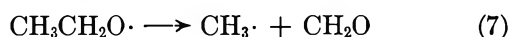
The methyl radical and hydrogen atom would abstract and appear as methane and hydrogen in the products.

In addition the radical resulting from the abstractions would decompose and the ethyl radical would appear

$$CH_3\overset{O}{\overset{\|}{C}}HOCOC_2H_5 \longrightarrow CH_3CHO + CO_2 + C_2H_5\cdot \quad (9)$$
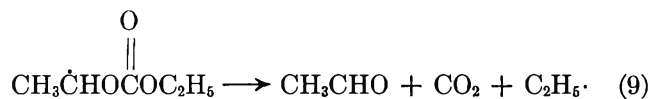
in the products, after abstraction, as ethane. Since neither methane, hydrogen, nor ethane appears in the products, the radical reaction path for diethyl carbonate decomposition is of no significance in this temperature range. The reaction to produce radicals for a chain reaction involves the breaking of the OC–O, O–C, or the C–C bond in DEC or MEC. All of these bonds are about 85 kcal./mole. Owing to this high

barrier, even long-chain reactions would be expected to have a very low rate in the temperature range of this work.

The lack of evidence for the decomposition of dimethyl carbonate also indicates that the intramolecular reaction involving a five-membered complex does not compete with the six-membered complex involving the β-H atom in the alkyl group. The reaction involving the five-membered complex is some 60 kcal./mole more endothermic than the reaction involving the six-membered complex because no olefinic bond is formed.

The products in this work suggest two possible mechanisms. Mechanism I is

$$CH_3CH_2O\overset{O}{\overset{\|}{C}}OR \longrightarrow C_2H_4 + HO\overset{O}{\overset{\|}{C}}OR \quad (10)$$
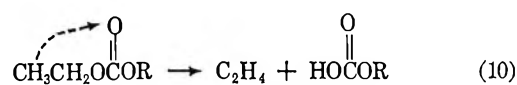
followed by a rearrangement

$$HO\overset{O}{\overset{\|}{C}}OR \longrightarrow CO_2 + ROH \quad (11)$$

and mechanism II is

$$CH_3CH_2O\overset{O}{\overset{\|}{C}}OR \longrightarrow C_2H_4 + CO_2 + ROH \quad (12)$$
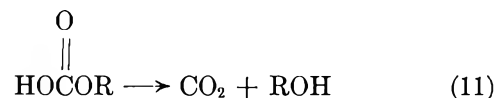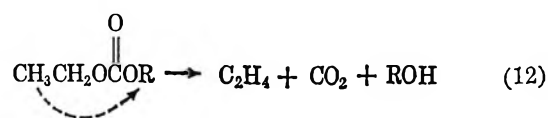
The first step in mechanism I is the generally accepted path for ester pyrolysis.[11] For ethyl acetate pyrolysis the rate constant is $5 \times 10^{12} \, 10^{-48,000/2.303RT}$, very close to the kinetic factors in this work, suggesting that the slow step in both systems is the same. Xanthates decompose to the mercaptan, olefin, and COS, quite analogously to the carbonates. Bader and Bourns[12] used marked sulfur as well as marked carbon in the xanthates to differentiate the analogous mechanisms I and II by isotope effects on the rate and concluded that their data support mechanism I.

Mechanism I is probably the correct path for the pyrolysis of the carbonates. There is one question which may be raised: why is the first step of mechanism I always followed by rearrangement to the alcohol and CO_2? No evidence for the competitive reaction

(10) P. Gray, *Chem. Rev.*, **59**, 239 (1959).

(11) C. H. DePuy and R. W. King, *ibid.*, **60**, 431 (1960).

(12) R. F. W. Bader and A. N. Bourns, *Can. J. Chem.*, **38**, 348 (1961).

$$\underset{\substack{\| \\ O}}{CH_3CH_2OCOH} \longrightarrow C_2H_4 + \underset{\substack{\| \\ O}}{HOCOH} \qquad (13)$$

$$\downarrow$$

$$H_2O + CO_2$$
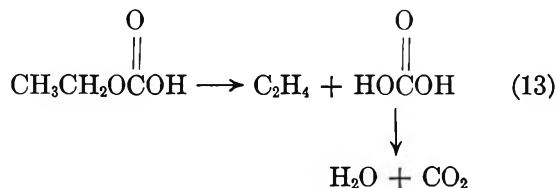
is found in the product distribution when the s/v ratio is increased fivefold or when an inert gas, CO_2, is in the reaction vessel at 75-fold the pressure of the carbonate. These data suggest that the rearrangement reaction (11) is much faster than reaction 13. The activated complex for reaction 11 contains four atoms in a ring
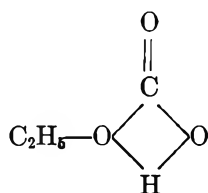
The OCO angle in carbonates is about 120°, and the OHO angle in hydrogen bonding is close to 180°. Since the C–O bond is 1.32 Å. in carbonates,[13] the OHO distance is calculated to be 2.30 Å. In hydrogen bonding in organic acids, the distance is 2.70 Å.,[13] so that the H atom in the reaction complex associated

with reaction 11 can easily span the distance between the two oxygen atoms and is in an excellent position to be transferred. If the pre-exponential factors for reactions 11 and 13 are about the same, as small a difference in E_{act} as 6 kcal./mole in favor of reaction 11 would determine its rate to be 100 times the rate of reaction 13 at 375°.

The ratio in pre-exponential factors between diethyl carbonate and methyl ethyl carbonate could be as large as 2 if the time when an H atom was close by the oxygen atom of the carbonyl was a small fraction of the total time. The larger this fraction of time, the smaller the ratio of pre-exponential factors since the carbonyl would be shielded from the other ethyl group. The ratio would become 1 if the H atom were always near the carbonyl oxygen. Our result of 1.6 is not precise enough to make any quantitative statement but suggests that some shielding may occur.

(13) L. Pauling, "The Nature of the Chemical Bond," 3rd Ed., Cornell University Press, Ithaca, N. Y., 1960.

Influence of Adsorbed Positively Charged Polyelectrolytes on Polarographic

Currents of Cationic Depolarizers.   II

by Y. F. Frei and I. R. Miller

Polymer Department, The Weizmann Institute of Science, Rehovoth, Israel   *(Received March 18, 1965)*

The effect of adsorbed polyelectrolytes on diffusion currents and on current *vs.* time curves, during the lifetime of a single mercury droplet, was measured at selected constant potentials.   Cationic depolarizers such as Cd^{2+} and Cu^{2+} and basic polyelectrolytes, for example, polyvinylpyridine and bovine serum albumin in acid solutions, were employed in these experiments.   Positively charged polymers adsorbed on the mercury surface form a barrier against the transport of charges carried by cationic depolarizers and thus impede the diffusion current.   The obstruction effect of the polymeric barrier can be suppressed by reducing, or even more by inverting, the charge of either the polyelectrolyte or the depolarizer. The polyelectrolyte charge was altered by varying the pH of the solution and the charge of the depolarizers by complexing anions.   The impeding effect of the polymer charge in the surface was also controlled by screening with the aid of different concentrations of supporting electrolyte.   The salt concentration affects the distribution coefficient of the depolarizer between the aqueous solution and the surface phase.

Introduction

The influence of adsorbed surface-active materials on polarographic waves and currents has been investigated by many authors.[1-3]   Some investigators have concentrated on the influence of the adsorbed materials on the current–voltage curves, considering the suppression of the diffusion currents, the changes in the wave shapes, and the shift in the half-wave potentials. Others have studied the effect of the kinetics of adsorption on the polarographic currents, by measuring the variation in current with time on single drops and at fixed potentials.[4]   The problem has also been treated theoretically by solving the differential equations for the simultaneous diffusion of the surface-active materials and the depolarizers.[5,6]   The structure of the adsorbed layer and its free energy of adsorption have a pronounced effect on the diffusion current through it; thus, a great deal can be learned from the diffusion current about the structure of the layer and the interacting forces.

One of the principal aims of the present study is the elucidation of the structure and conformation of adsorbed polyelectrolytes.   It is considered that valuable information can be obtained by the use of polaro-graphic techniques, especially the measurement of current–time curves, which offer detailed information on the structure of partly saturated as well as fully saturated adsorbed monolayers of polyelectrolytes.

Experimental

The experiments were performed using a Shimadzu polarograph (Type RP-2).   The surface of the mercury drop was polarized against a mercury pool, but the potentials were recorded relative to a saturated calomel electrode.   The capillary was of marine barometer type, supplied with the instrument.   A small pressure head was used in order to get long drop times, of the order of 10 to 15 sec.   The curves were recorded without damping.   Since the polarograms were taken with long drop times and at high chart

(1) C. Tanford, *J. Am. Chem. Soc.*, **74**, 211 (1952).

(2) C. N. Reilly and W. Stumm, *Progr. Polarc.*, **1**, 81 (1962).

(3) E. Yacobsen and G. Kalland, *Anal. Chim. Acta*, **30**, 240 (1964).

(4) J. Kuta and I. Smoler, *Progr. Polaro.*, **1**, 43 (1962).

(5) J. Weber, J. Koutecky, and J. Koryta, *Z. Elektrochem.*, **63**, 583 (1959).

(6) P. Delahay and I. Trachtenberg, *J. Am. Chem. Soc.*, **79**, 2355 (1957); **80**, 2095 (1958).

speed, they also have the characteristics of current–time curves. Indeed, since the voltage change was very small (between 20 and 30 mv.) and the voltage dependence of the transfer constant also quite small, the curves are essentially similar to those obtained by Schmid and Reilly[7] and Kuta and Smoler,[8] who measured true current–time (i–t) curves, and they are so designated later. They are indistinguishable from the (i–t) curves measured at constant potential. The (i–t) curves were recorded via a suitable amplifier on a Tektronix 5B 1A oscilloscope. In the type of capillary used, the mercury drops are formed in an environment which allows concentration polarization. However, in the presence of surfactants the concentration polarization is usually repressed, so that the difference between curves for first and subsequent drops disappears.

All materials used were of analytical grade. Polymers were prepared as previously reported.[9,10] Doubly distilled water was used for preparing the solutions for polarography. The concentration of the depolarizers was about 10^{-3} M, while that of the supporting electrolyte varied betweeen 0.05 and 1 N. The concentrations of polyelectrolytes were chosen so that a fully saturated monolayer was obtained within 1–10 sec.

Crystalline bovine serum albumin was employed (Armour Lot T68204).

Results

Poly-2-vinylpyridine (2PVP). 2PVP at a monomer concentration of 10^{-3} M was added to 10^{-3} M Cd-$(NO_3)_2$ solution in 0.2 M KNO_3 and 0.1 M HNO_3. At drop times of 10 to 14 sec., a splitting of the current diagram for a single drop was observed (Figure 1). The discontinuities indicate the start and termination of the drop. An initial rise in current can be seen, followed by a fall and a subsequent rise once more. The ratio of the heights of the first and second rise depends on the voltage. The whole polarographic wave is depressed in comparison with the blank containing depolarizer and supporting electrolyte only. The time taken for the current to reach its minimum value is independent of voltage. At a concentration of 2×10^{-4} N 2PVP and drop times of less than 15 sec., the polymer has no influence on the polarogram. At a polymer concentration of 5×10^{-4} N a slight flattening of the current–time wave is just discernible. Above this value and up to about 2×10^{-3} N the split illustrated in Figure 1 occurs. At still higher concentrations only the current rise through the surface fully covered by PVP is observed.

Above these concentrations there is an over-all suppression of the diffusion current which is independent
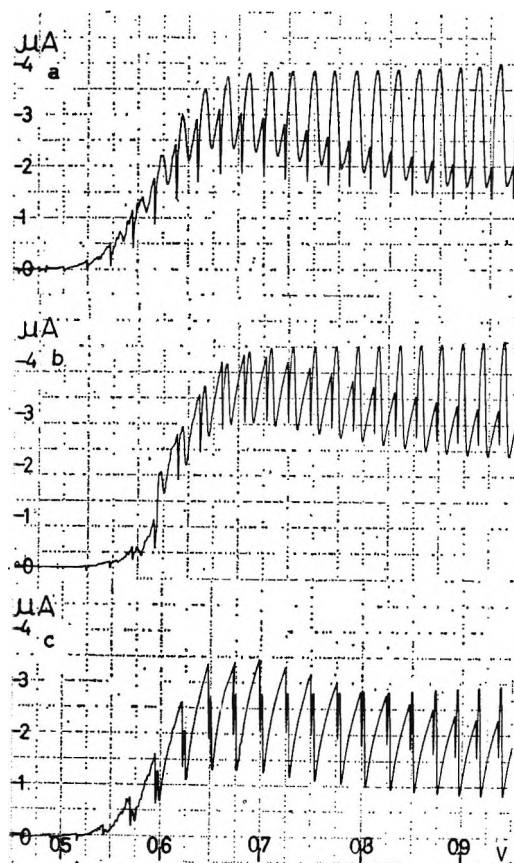
Figure 1. Polarograms of Cd^{2+} in the presence of 2PVP: (a) 2PVP, 8×10^{-4} N; HNO_3, 0.055 N; KNO_3, 0.3 N; Cd^{2+}, 10^{-3} M. (b) 2PVP, 10^{-3} N; HNO_3, 0.06 N; KNO_3, 0.3 N; Cd^{2+}, 10^{-3} M. (c) 2PVP, 1.5×10^{-3} N; HNO_3, 0.065 N; KNO_3, 0.3 N; Cd^{2+}, 10^{-3} M.

of the polymer concentration. The split-wave character of the current–time curves does not depend on the Cd^{2+} concentration. The addition of the polymer caused no shift in the half-wave potential. If the adsorption is diffusion controlled, it obeys the relation $Ct^{1/2} = $ constant, where C is the concentration of the surfactant and t the time from the beginning of growth of the drop till the current reaches its minimum. Table I shows that this relation holds true within the experimental error of the measurements.

These phenomena were not observed in $CdCl_2$ solutions as Cd^{2+} gives with Cl^- neutral and negative complexes.[1] $CuSO_4$ in 0.2 N KNO_3 and 0.1 N HNO_3 as supporting electrolyte gave results similar to those obtained with $Cd(NO_3)_2$. In the voltage range 0 to

(7) R. W. Schmid and C. N. Reilly, *J. Am. Chem. Soc.* **80**, 2087 (1958).

(8) J. Kuta and I. Smoler, *Z. Elektrochem.*, **64**, 285 (1960).

(9) I. R. Miller and D. C. Grahame, *J. Colloid Sci.*, **16**, 23 (1961).

(10) I. R. Miller and A. Katchalsky, *Proc. Intern. Congr. Surface Activity, 2nd, London, 1957,* 159 (1957).

Table I: Concentration-Time Relations at
Saturation Point

C, N	t, sec.	$Ct^{1/2} \times 10^2$
2×10^{-3}	1.5	2.45
1.2×10^{-3}	3.75	2.32
0.9×10^{-3}	8.25	2.58

−0.5 v., the first current rise is discernible only as a shoulder, and the current minimum is barely seen (see Figure 2a), indicating that in this voltage region the adsorbed 2PVP molecules do not constitute a very strong barrier to the approach of the Cu^{2+} to the mercury surface. This finding is in keeping with the only relatively small lowering of surface tension by the adsorbed 2PVP at potentials more positive than −0.3 v. with respect to s.c.e., shown in electrocapillary curves obtained in the presence of 2PVP.[9]

The polarographic waves of $Pb(NO_3)_2$ and $Fe(NO_3)_3$ were not influenced by the presence of the polymer.

Poly-4-vinylpyridine (4PVP). The phenomenon of the double-peaked current–time polarogram was also observed with 4PVP. In this case, at $10^{-3} M$ monomer concentration, the second peak was the dominant one. The ratio between the two peaks was much less dependent on voltage than in the case of 2PVP (Figure 3). From the differential capacity curves measured by Miller and Grahame[9] for 4PVP, it is seen that, while this substance is adsorbed at a more positive potential than 2PVP, the adsorption is weaker because of its more polar character. This is in keeping with the greater flexibility of 4PVP, which can be oriented on the positively polarized mercury surface with the polar groups toward the water and the hydrophobic groups toward the mercury. At negative polarization, the orientation of the polar groups can be reversed.

In aqueous solutions, 4PVP serves as a smaller barrier to the depolarization of cations than 2PVP, probably because of the larger average distances between the positive polymeric charges. Cu^{2+} as depolarizer gave at identical potentials the same results as did Cd^{2+} (Figure 2b).

Copolymers. A copolymer consisting of 40% 4-VP (4-vinylpyridine) and 60% MA (methacrylic acid) was also investigated. The influence of the copolymer on the polarograms of Cd^{2+} in nitrate solution was measured at high and low pH. At pH 1 and $10^{-3} N$ copolymer concentration, the same slight differentiation of the current–time curves into two peaks as obtained with 4PVP was observed. There was also a diffusion current depression. At a slightly higher pH (pH 2) the differentiation into two peaks became less distinct.
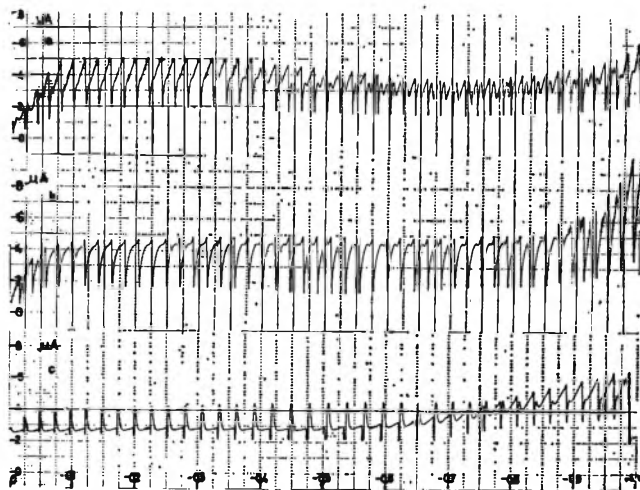
Figure 2. Polarograms of Cu^{2+} in the presence of 2PVP, 4PVP, and BSA: (a) 2PVP, $10^{-3} N$; HNO_3, 0.1 N; KNO_3, 0.2 N; Cu^{2+}, $9 \times 10^{-4} M$. (b) 4PVP, $5 \times 10^{-4} N$; HNO_3, 0.1 N; KNO_3, 0.2 N; Cu^{2+}, $10^{-3} M$. (c) BSA, 0.015%; HNO_3, 0.1 N; KNO_3, 0.2 N; Cu^{2+}, $9 \times 10^{-4} M$.
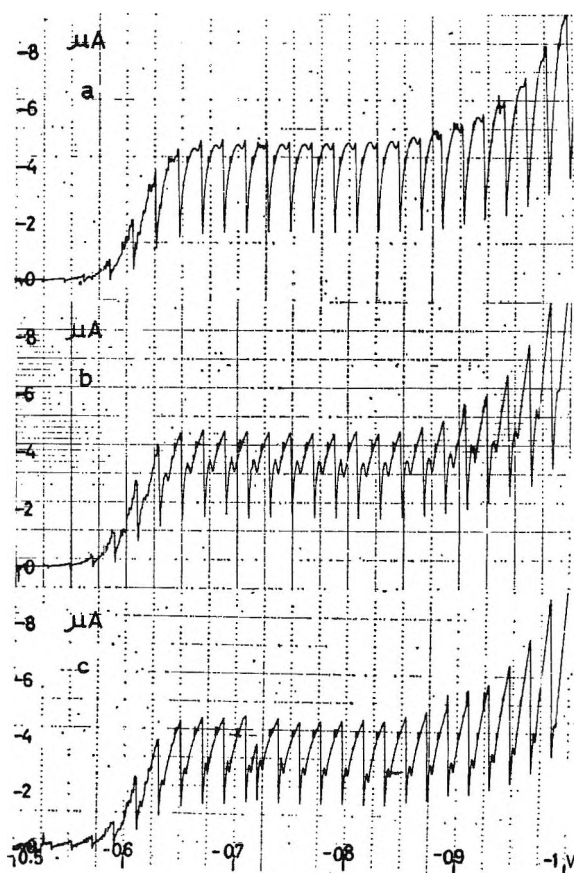
Figure 3. Polarograms of Cd^{2+} in the presence of 4PVP, 0.1 N HNO_3 and 0.2 N KNO_3 as supporting electrolyte: (a) 4PVP, $5 \times 10^{-4} N$; Cd^{2+}, $9.5 \times 10^{-4} M$. (b) 4PVP, $7.5 \times 10^{-4} N$; Cd^{2+}, $9.2 \times 10^{-4} M$. (c) 4PVP, $1.10^{-3} N$; Cd^{2+}, $9 \times 10^{-4} M$.

No influence of the negatively charged copolymer on the current–time curves in the presence of Cu^{2+} or Cd^{2+} could be observed at pH 7.

Effect of Salt Concentration. The results indicate quite clearly that it is the positive charge of the adsorbed polyelectrolytes rather than the steric hindrance which is responsible for barring the approach of the positively charged depolarizer to the surface. The results of the experiments carried out in the presence of different concentrations of supporting electrolye further support this conclusion. As shown previously[11] and as is also evident from results not yet published, increase in salt concentration enhances the adsorbability of polyelectrolyte on the polarized mercury surface. If the steric hindrance were responsible for the barrier to the charge transfer across the interface, increase in salt concentration would cause the diffusion current to fall. If, however, access of the positively charged depolarizer were barred by the screen of positive polymeric charges, increase in salt concentration would have the opposite effect. It can be seen from Figures 4 and 5 that the second alternative is the prime factor in the effect of the salt concentration on the diffusion current.

In this respect 2PVP (i–t curve Figure 4) and 4PVP (i–t curve Figure 5) behave similarly although there is a quantitative difference in their efficacy as a barrier to charge transfer.

Bovine Serum Albumin. Tanford[1] investigated the influence of adsorbed acid bovine serum albumin (BSA) on the polarograms of Cu^{2+}, Pb^{2+}, and Cd^{2+}. He used a BSA concentration of 1.23%. The curves obtained with Cu^{2+} in NO_3^- were irreversible. In KCl, no influence of BSA was observed on the waves of Cd^{2+} and Pb^{2+} because of complex formation. It was therefore interesting to investigate the influence of acid BSA at lower concentrations. With a 0.015% solution of BSA in 10^{-3} M Cu^{2+}, 0.2 M KNO_3, and 0.1 M HNO_3, a general depression of the diffusion current was observed. The current–time curve showed that up to -0.6 v. relative to s.c.e., there was only a slight rise in current after full coverage of the surface by BSA (Figure 2c). At this potential (0.6 v.) the slope of the current–time curve section, corresponding to the fully covered surface, begins to increase with increasing potential, indicating a rising tendency of the BSA to desorb. In a 0.15% BSA solution, practically complete suppression of the diffusion current was observed between 0 and -0.7 v.; the current begins to rise after -0.7 v. Only one peak was observed in the current–time curve.

With $Cd(NO_3)_2$ as depolarizer the depression of the diffusion current and of the second peak in the current–
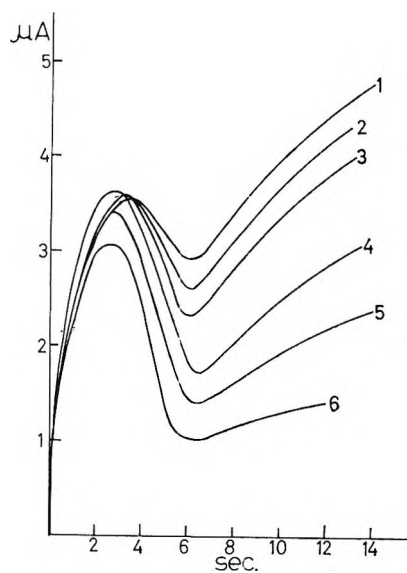
Figure 4. Current–time curves of 2PVP at various salt concentrations (at -0.75 v.): 2PVP, 10^{-3} N; Cd^{2+}, 10^{-3} M; HNO_3, 0.1 N; (1) KNO_3, 0.8 N; (2) KNO_3, 0.6 N; (3) KNO_3, 0.4 N; (4) KNO_3, 0.2 N; (5) KNO_3, 0.1 N; (6) KNO_3, 0.
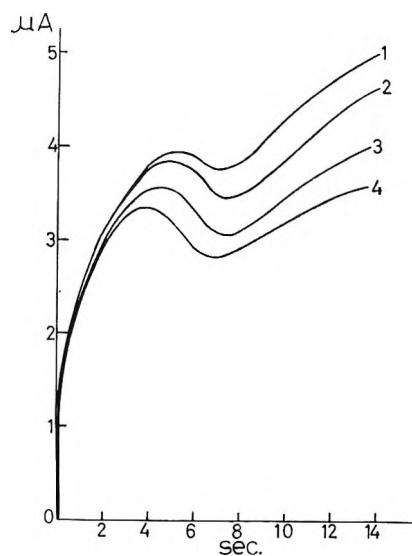
Figure 5. Current–time curves of 4 PVP at various salt concentrations (at -0.75 v.): 4PVP, 7×10^{-4} N; HNO_3, 0.105 N; Cd^{2+}, 10^{-3} M; (1) KNO_3, 0.6 N; (2) KNO_3, 0.2 N; (3) KNO_3, 0.1 N; (4) KNO_3, 0.

time curve was greater than in the case of Cu^{2+} (-0.6 to -1 v.). Also in this case, at lower acid concentrations, there is a potential dependence of the current across the covered surface. No polarographic

(11) I. R. Miller and A. Katchalsky, *Proc. Intern. Congr. Surface Activity, 4th, Bruxelles, 1964,* in press.

wave could be observed in a 0.15% BSA solution. BSA did not influence the polarographic wave of $Pb(NO_3)_2$.

Discussion

It is known from independent measurements (unpublished results) that about 10–14% of the surface area "fully saturated" by 4PVP and a slightly lower fraction of the area covered by 2PVP consists of loopholes, which are accessible to low molecular inert substances or reacting depolarizers. As these loopholes are randomly distributed on the surface, any depolarizer in the near vicinity of the surface may encounter a reaction site. The low concentration of positively charged depolarizers in the layer of positively charged polymeric chains protruding from the surface seems, therefore, to be responsible for the impedance of the surface reaction. This subsurface layer may be of the order of thickness of 50 Å. The diffusion current is assumed to be controlled by the concentration gradient of the depolarizer in this layer, which is low at the moment when surface saturation is just reached, as the outer boundary of the layer is in Donnan equilibrium with a very low local concentration of depolarizer. However, in a very short time, depending on the thickness of the subsurface layer and on the Donnan distribution of the depolarizer on the two sides of the layer boundary, the gradient rises again.

An approximate quantitative treatment of the i–t curve as a function of the surface concentration of the polyelectrolytes was published in part I of this series. It involves the solution of the Fick differential equation, taking into account the variation with time of the diffusion and distribution coefficients of the depolarizer in the polyelectrolyte surface layer.

For a saturated polyelectrolyte surface layer, a solution of the differential equation can be readily obtained, and the current is given by the approximate expression

$$i_t = 7.08 \times 10^4 nm^{2/3} t^{1/6} D_I^{1/2} C^0 / [1 + (\xi/\kappa D_{II}) \sqrt{D_I/\pi t}] \tag{1}$$

In this equation n is the number of charges taking part in the electrode process; m is the rate of flow of mercury in g. sec.$^{-1}$; C^0 is the concentration of the depolarizer in the bulk of the solution; D_I and D_{II} are the diffusion constants of the depolarizer in the aqueous solution and in the polymeric surface phase, respectively; κ is the distribution coefficient of the depolarizer between the two respective phases, and ξ is the thickness of the surface phase. Here $\kappa = \kappa_{sat}$ and D_{II}
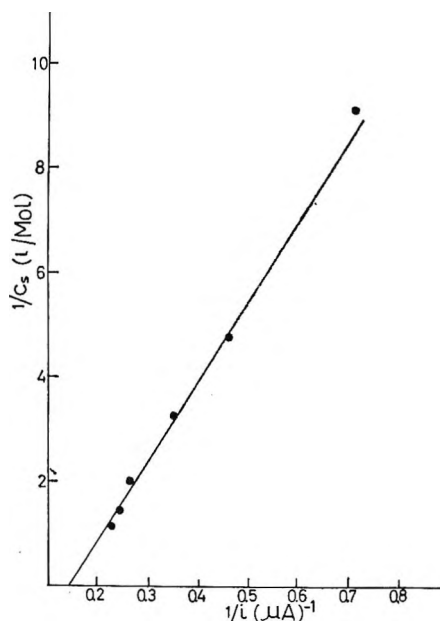
Figure 6   Plot of the reciprocal of the salt concentrations (acid ÷ salt) against the reciprocal of the current (drop age 12 sec.) (values taken from Figure 4):   2PVP, 10^{-3} N; Cd^{2+}, 10^{-3} N.

$= D_{sat}$ of part I of this series. Equation 1 is correct only when $\xi \ll \sqrt{D_I t}$.

The product $(\xi/\kappa D_{II})$ can be determined from an analysis of the i–t curves in the region where the surface reached saturation with regard to the polymer molecules. The time when this saturation point is reached depends again, as pointed out previously,[11] on the polymer concentration and on the diffusion coefficient of the polyelectrolyte.

The distribution coefficient κ can be obtained from the Donnan equilibrium. For the ordinary case when the supporting electrolyte $C_s \gg C^0$ and when the polyelectrolyte charge concentration in the surface $\nu \Gamma_p/\xi$ is very high, it is given by

$$\kappa = (C_s/\phi)^z [(\xi/\nu\Gamma_p) - v]^z [1 - (\nu\Gamma_p v/\xi)] \tag{2}$$

where Γ_p is the polymer surface excess; ν is the charge per polymer molecule; ϕ is the osmotic factor of its counterions; v is the volume per residue of a polymeric molecule bearing one charge, and z is the valency of the depolarizers.

Equations 1 and 2 can be condensed into the form

$$1/i = 1/i_0 + (A/i_0)(1/C_s)^z \tag{3}$$

where

$$i_0 = 7.08 \times 10^4 nm^{2/3} t^{1/6} D_I^{1/2} C^0$$

and

$$A = \xi\phi^z(D_I/\pi t)^{1/2}/[(\xi/\nu\Gamma_p) - v]^2[1 - (\nu\Gamma_p v/\xi)]D_{II}$$

log $(1/i)$ can be plotted against log $(1/C_s)$ whence z can be evaluated. In the case of $Cd(NO_3)_2$ the valency of the diffusing ionic form of the depolarizer was found to be 1. In Figure 6, $1/i$ is plotted against $1/C_s$ for the case of depolarization of Cd^{2+} in the presence of 2PVP with nitrate as supporting electrolyte. The results indicate that Cd^{2+} has a tendency to complex formation even with nitrate and that cadmium here is chiefly in the form $Cd(NO_3)^+$.

A Study of the Radiolysis and Luminescence Behavior of

Dioxane–Benzene Mixtures

by Enrique A. Rojo[1a] and Robert R. Hentz

Department of Chemistry and Radiation Laboratory,[1b] University of Notre Dame, Notre Dame, Indiana 46556
(Received March 22, 1965)

G values for gas products in γ-irradiation of pure, liquid dioxane were constant over the dose range $(0.46-4.6) \times 10^{19}$ e.v. g.$^{-1}$. These G values for a dose rate of 1.9×10^{18} e.v. g.$^{-1}$ min.$^{-1}$ are as follows: H_2, 2.1; C_2H_4, 0.50; C_2H_6, 0.051; CO, 0.23; CH_4, 0.035. Study of the polymer product indicated that dioxane dimers constitute the initial polymer product. G(monomer $\rightarrow$ dimer) $\approx$ 3.9. Hydrogen, biphenyl, polymer, and relative luminescence G values (p-terphenyl as scintillator) were measured for benzene–dioxane mixtures. The parallel behavior of hydrogen and polymer G value curves suggests that a common dioxane precursor of hydrogen and polymer is protected from reaction by some kind of interaction with benzene. Kinetic analysis of the G(H_2) results gives $\alpha = 0.21$ M^{-1} as the ratio of specific rate of excitation transfer to that of decay for the excited dioxane species that yields hydrogen. This analysis also indicates that thermal H atoms make a negligible contribution to the hydrogen yield from dioxane. A similar treatment of relative luminescence G values leads to an estimate of 65 M^{-1} as the corresponding ratio for the excited dioxane species that gives rise to luminescence. It is concluded that the latter species makes a negligible contribution to the yield of decomposition products and that the excited species that yields decomposition products is of very short lifetime. For protection to compete with decomposition it may be necessary that a molecule of benzene be a nearest neighbor to the labile excited dioxane species at the time of its formation.

Introduction

Numerous studies of decomposition, luminescence of added scintillators, and decay times in irradiated benzene, cyclohexane, and their mixtures have established significant differences in the radiation-induced behavior characteristic of these two substances.[2] Among the many interesting questions raised by these studies are the following. What relationship exists between the phenomena of and the excited states involved in protection and luminescence or the quenching of luminescence? To what characteristics of the system is the essentially different mechanism of sensitized luminescence and quenching in cyclohexane attributable as compared to that in benzene? What is the nature of the excited states involved in the various processes in the different systems—excited molecules, ions, collective excitations of the system? What is the nature of the energy deposition and localization process, and how does

it depend on characteristics of the system? To contribute to our understanding of some of these problems, the radiolysis and luminescence (with added p-terphenyl) of benzene–dioxane mixtures has been investigated, and the results are reported here. Dioxane was chosen because in most respects it is similar to cyclohexane while in one very important respect it is similar to benzene: namely, in dioxane, as in benzene, the existence of a lowest electronic transition with considerable vibrational structure has been established.[3]

(1) (a) International Atomic Energy Agency, Fellow, 1963–1964, on leave from the Atomic Energy Commission of Argentina. (b) The Radiation Laboratory of the University of Notre Dame is operated under contract with the U. S. Atomic Energy Commission. This is A.E.C. Document No. COO-38-404.

(2) Reference to all the papers devoted to these subjects would require an extensive bibliography; instead, reference is made throughout this paper to pertinent recent publications which serve as an introduction to the entire field.

(3) G. J. Hernandez and A. B. F. Duncan, *J. Chem. Phys.*, **36**, 1504 (1962).

Experimental

Chemicals. The 1,4-dioxane, Fisher Certified reagent, was first purified by the method of Tunnicliff.[4] In this procedure, the dioxane is refluxed during and subsequent to addition of an aqueous $KMnO_4$–NaOH solution for a total of 30 min.; the dioxane is then salted out with NaOH and, after separation, is distilled in the presence of solid NaOH. A Nester–Faust spinning-band column was used, and the fraction boiling at 101–101.5° was collected. Dioxane purified in this manner was passed through a column of activated alumina to remove peroxides and then was recrystallized twice, rejecting one-fourth each time. No impurities were detectable by gas–liquid chromatography (a flame ionization detector was used with β,β'-oxydipropionitrile at 80° and Apiezon-L at 80–150°) or ultraviolet spectrophotometry. No peroxides were detectable with acid KI solution.

Benzene, Fisher Certified reagent, was recrystallized twice and distilled. No impurities were detectable by gas–liquid chromatography. Eastman scintillation grade *p*-terphenyl was used without further purification.

Procedures. Two-milliliter samples were degassed on a vacuum line by repeated cycles of freeze (−77°), pump, and thaw with several bulb-to-bulb distillations. The degassed samples then were sublimed into 13-mm. o.d. Pyrex ampoules fitted with break-seals, and the ampoules were sealed off. Samples were irradiated in a 10-kc. ^{60}Co source under conditions giving a dose rate of 1.87×10^{18} e.v. g.$^{-1}$ min.$^{-1}$ to a Fricke dosimeter solution using $G(Fe^{3+}) = 15.6$. Dose to a particular solution was determined by correction for the electron density of the solution relative to that of the dosimeter. All irradiations were carried out at room temperature.

Gas products were recovered by a reflux technique that has been described.[5] Fractions were collected at −77 and −196° and measured in a modified Saunders–Taylor apparatus. Gases were analyzed by mass spectrometry.

For study of the polymer product it was necessary to irradiate separate samples to considerably higher doses than were used for study of gas products. An aliquot of irradiated sample, of a size dependent on dose, was transferred to a weighed bulb which was attached to the vacuum line. Benzene, dioxane, and volatile products were slowly sublimed from the solidified sample into a bulb at −196° until a residue remained that appeared to be free of volatile material. This process ordinarily required 1–2 hr. Transfer then was allowed to proceed for several more minutes. For determination of polymer yield the residue was weighed and dissolved in a measured volume of hexane. This solution was analyzed by gas–liquid chromatography (Apiezon-L at

80–150° and silicone grease at 80–200°), and the weight of polymer was obtained by correction of the weight of residue for the amounts of benzene and dioxane found. The sublimate also was analyzed chromatographically for peaks characteristic of the polymer. Only those peaks characteristic of the most volatile polymer components were present in measurable amount and corresponded to less than 2 or 3% of the corresponding peaks in the polymer fraction. Thus, a negligible fraction of total polymer was present in the sublimate, and no correction was made. Reproducibility of polymer determinations was about 5%. Special care was taken to minimize exposure to air although no increase in weight of polymer was observed after standing in air for about 24 hr. The molecular weight of polymer was determined by the Rast method using a known weight of polymer obtained from another aliquot of irradiated sample by the method described. Biphenyl yields were determined in separate irradiations by chromatographic analysis of the liquid.

An apparatus and procedure described in a previous publication[6] was used to measure relative luminescence intensities from 25 ml. of degassed, γ-irradiated solutions of benzene and dioxane containing 2.17×10^{-3} *M* *p*-terphenyl.

Results

G values (100-e.v. yields) for gas products in irradiation of pure, liquid dioxane were constant over the dose range $(0.46–4.6) \times 10^{19}$ e.v. g.$^{-1}$. Thus zero-dose *G* values are indicated. These *G* values are as follows (with *G* values of Llabador and Adloff,[7] for doses in excess of 10^{21} e.v. g.$^{-1}$, in parentheses): H_2, 2.1 (2.1); C_2H_4, 0.50 (0.56); C_2H_6, 0.051 (0.055); CO, 0.23 (0.30); CH_4, 0.035 (0.046). At the high doses used by Llabador and Adloff, it was found necessary to protect initially formed C_2H_4 and CO from subsequent decomposition by addition of I_2 in order to obtain the dose-independent *G* values given in parentheses for these compounds. The addition of I_2 was found by these authors to suppress $G(CH_4)$ and $G(C_2H_6)$ by 60 and 40%, respectively, with no effect on $G(H_2)$. The results of these authors also indicate an induction period for CH_4 and C_2H_6 formation which suggests that these are secondary products. Our results, to the contrary, show no induction period and give *G* values for CH_4 and C_2H_6 comparable to those of Llabador and Adloff although the latter were

(4) D. D. Tunnicliff, *Talanta*, 2, 341 (1959).

(5) W. Van Dusen, Jr., and W. H. Hamill, *J. Am. Chem. Soc.*, 84, 3648 (1962).

(6) M. Burton, P. J. Berry, and S. Lipsky, *J. chim. phys.*, 52, 657 (1955).

(7) Y. Llabador and J. P. Adloff, *ibid.*, 61, 681 (1964).

calculated for a dose three orders of magnitude greater than the dose used in our work. Ethanol and acetaldehyde were identified among the liquid products, but quantitative determinations were not made.

The polymer product from pure dioxane is a pale yellow, viscous liquid. Both the color and viscosity increase with increase in dose. Chromatographic analysis of the polymer formed at 1.21×10^{21} e.v. g.$^{-1}$ showed at least 15 peaks. Comparison of the total peak area to the weight of polymer suggests that an appreciable fraction of the polymer of high molecular weight escaped detection. In samples irradiated at low doses, small white crystals become visible in the polymer after standing several hours. On gentle heating, even at atmospheric pressure, the white crystals can be sublimed out of the polymer and collected in an adjacent trap. The crystals do not reappear in the polymer. The isolated white crystals dissolved in hexane give two peaks in chromatography that correspond to the two principal peaks obtained in chromatographic analysis of the entire polymer product at low dose. These two products were separated by crystallization from methanol. Melting points of 130 and 156° and a molecular weight of 168, for both products, were obtained. These values are consistent with identification of the products as the *meso* and racemic forms of dioxanyldioxane.[8]

G(polymer)[9] and molecular weight of polymer are given in Figure 1 as a function of dose in pure, liquid dioxane. Rough extrapolations to zero dose give G(polymer) ≈ 3.9 and molecular weight ≈ 174. The zero-dose molecular weight indicates that dioxane dimers are the initial polymer products and higher molecular weight polymers are secondary products. Llabador and Adloff[7] obtained G(polymer) = 3.65. In pure, liquid benzene, G(polymer) = 0.97 was obtained at a dose of 1.20×10^{21} e.v. g.$^{-1}$. This value is in good agreement with other reported values for ^{60}Co radiation.[10]

Hydrogen, biphenyl, polymer, and relative luminescence yields are given for benzene–dioxane solutions in Figures 2 and 3.

Discussion

Effects in Pure Dioxane. The zero-dose polymer appears to be essentially pure dimer. Consequently, the relationship

$$G(H_2) - (1/2)G_0(\text{polymer}) = 2.1 - 3.9/2 = 0.15 \quad (1)$$

suggests that the major *over-all* reaction in radiolysis of pure liquid dioxane is

$$C_4H_8O_2 \longrightarrow{} \quad {}^{1}/_{2}(C_4H_7O_2)_2 + {}^{1}/_{2}H_2 \quad (I)$$
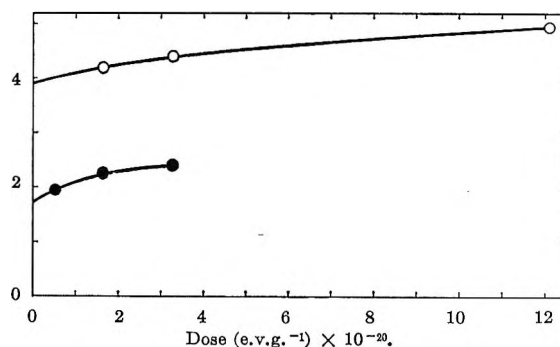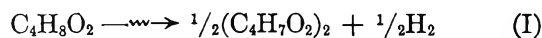
Figure 1. Molecular weight and G value of polymer as a function of dose in γ-irradiation of dioxane: O, G(polymer); ●, molecular weight $\times 10^{-2}$.
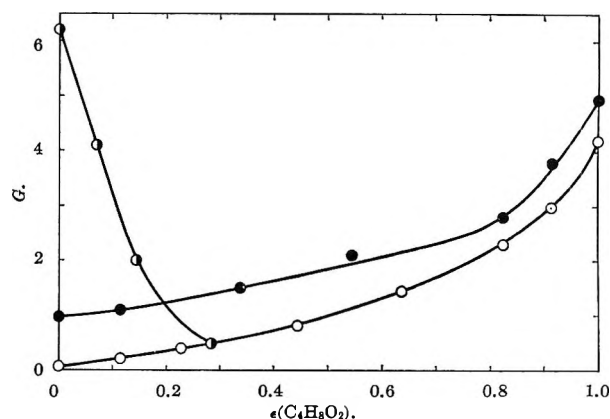
Figure 2. Yields of hydrogen, biphenyl, and polymer in γ-irradiation of benzene–dioxane mixtures: O, $G(H_2) \times 2$, dose = 9.2×10^{18} e.v. g.$^{-1}$; ◑, $G(C_{12}H_{10}) \times 10^2$, dose = 1.09×10^{20} e.v. g.$^{-1}$; ●, G(polymer), dose = 1.20×10^{21} e.v. g.$^{-1}$.

with $G \approx 3.9$. Because 3.9 is an imprecise, extrapolated value, no precise significance can be attached to the 0.15 excess of $G(H_2)$ in eq. 1. However, small yields of hydrogen-deficient products (*e.g.*, $G(CO) = 0.23$) do require hydrogen in stoichiometric excess over polymer. In radiolysis of dioxane, in contrast to cyclohexane,[11] ring fragmentation plays a significant role even in the liquid state; notably, $G(C_2H_4) = 0.50$ in dioxane as

(8) K. Pfordte, *Ann. Chem.*, **625**, 30 (1959).

(9) G(polymer) is calculated on the basis of monomer units in the polymer. In the mixtures the extent to which each monomer is incorporated in the polymer is uncertain. For calculation of G(polymer) in the mixtures, the average molecular weight of the mixture was used. Since the molecular weights of benzene and dioxane differ by only 12%, little uncertainty is caused by this procedure.

(10) S. Gordon, A. R. Van Dyken, and T. F. Doumani, *J. Phys. Chem.*, **62**, 20 (1958); W. G. Burns and C. R. V. Reed, *Trans. Faraday Soc.*, **59**, 101 (1963); T. Gaumann, *Helv. Chim. Acta*, **44**, 1337 (1961); T. Gaumann, *ibid.*, **46**, 2873 (1963); J. Lamborn and A. J. Swallow, *J. Phys. Chem.*, **65**, 920 (1961).

(11) S. K. Ho and G. R. Freeman, *ibid.*, **68**, 2189 (1964).
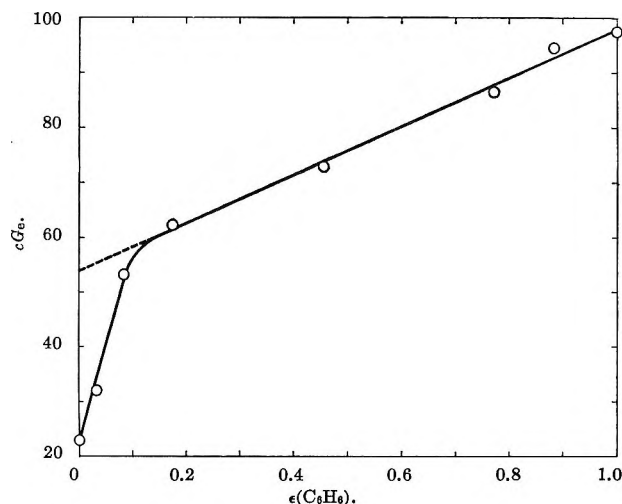
Figure 3. Relative luminescence yields in γ-irradiation of air-free mixtures of benzene and dioxane with $2.17 \times 10^{-3} M$ p-terphenyl.

compared to $G(C_2H_4) = 0.12$ in cyclohexane.[12] Mass 28 is the major peak in the 70-v. mass spectrum of dioxane, exceeding in magnitude that of the parent ion by a factor of about 3.3.[13] Minor fragmentation processes (e.g., that which gives a mass-15 peak 17% of the mass-28 peak in the 70-v. mass spectrum) can account for formation of small yields of methane and ethane as initial, rather than as secondary, products. The observed increases in molecular weight and yield of polymer with increase in dose suggest the addition of radicals, which otherwise would dimerize or disproportionate, to initially formed unsaturated products which are converted thereby into polymer of higher molecular weight than the dimer.

Benzene–Dioxane Mixtures; Hydrogen Yields. The hydrogen yield curve of Figure 2 suggests a protective effect of benzene[14] on dioxane. Such an effect is consistent with lower values of ionization potential and energy of the first electronic transition for benzene[15] as compared to dioxane.[3] It is instructive to treat the hydrogen yields in the manner of Merklin and Lipsky.[16] In the reaction sequence and associated table of rates

$$D \xrightarrow{\hspace{0.8cm}} D^* \qquad \epsilon_D R_0 G_D{}^*/N_0$$

$$B \xrightarrow{\hspace{0.8cm}} B^* \qquad \epsilon_B R_0 G_B{}^*/N_0$$

$$D^* \longrightarrow H_2 \qquad k_1[D^*]$$

$$D^* \longrightarrow \text{no } H_2 \qquad k_2[D^*]$$

$$B^* \longrightarrow H_2 \qquad k_3[B^*]$$

$$B^* \longrightarrow \text{no } H_2 \qquad k_4[B^*]$$

$$D^* + B \longrightarrow D + B^* \qquad k_5[D^*][B]$$
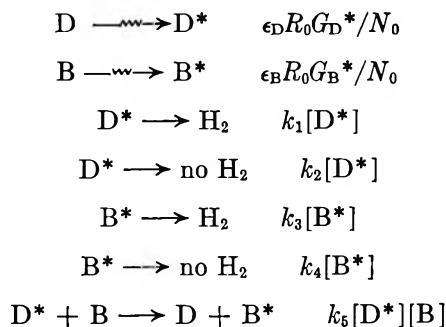
D and B refer respectively to dioxane and benzene, ϵ_D and ϵ_B to their electron fractions, R_0 to the dose rate in units of 100 e.v. $1.^{-1}$ sec.$^{-1}$, and $G_D{}^*$ and $G_B{}^*$ to 100-e.v. yields of D^* and B^*. The steady-state treatment, based on the assumption that absorbed energy is partitioned in proportion to electron fraction, yields a Merklin–Lipsky equation

$$\eta \equiv \frac{\epsilon_D(G_D - G_B)}{(G - G_B)} = \frac{1 + \alpha[B]}{1 + \gamma[B]} \qquad (2)$$

where G, G_D, and G_B refer to 100-e.v. hydrogen yields from the mixture, pure dioxane, and pure benzene, respectively; $\alpha = k_5/(k_1 + k_2)$ and $\gamma = \alpha G_B(G_D{}^*/G_B{}^* - 1)/(G_D - G_B)$.

A plot of η as a function of $[B]$[17] is shown in Figure 4 with the least-square line based on all points except that for the highest benzene concentration (90 mole %). Thus, $\gamma[B]$ would appear to be $\ll 1$ over the whole
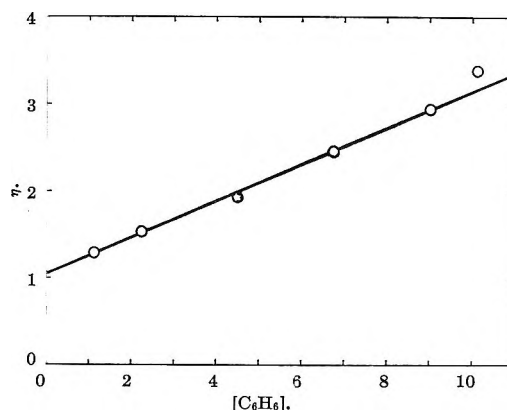
Figure 4. Dependence of η on molarity of benzene in γ-irradiation of benzene–dioxane mixtures; dose $= 9.2 \times 10^{18}$ e.v. g.$^{-1}$.

(12) S. Sato, K. Kikuchi, and S. Shida, *J. Chem. Phys.*, **41**, 2216 (1964).

(13) American Petroleum Institute Research Project 44, National Bureau of Standards, Catalog of Mass Spectral Data, Serial No. 450, contributed by the Humble Oil and Refining Co., Baytown, Texas.

(14) *Cf.* J. P. Manion and M. Burton, *J. Phys. Chem.*, **56**, 560 (1952); M. Burton, S. Gordon, and R. R. Hentz, *J. chim. phys.*, **48**, 190 (1951).

(15) K. Watanabe, *J. Chem. Phys.*, **26**, 542 (1957).

(16) J. F. Merklin and S. Lipsky, *J. Phys. Chem.*, **68**, 3297 (1964).

(17) No special significance with respect to mechanism is implied in use of molarity as the benzene concentration unit. This unit is employed by Merklin and Lipsky; it also permits a direct comparison with the luminescence behavior of this system. In view of the high benzene concentrations required for significant protection, it is clear that the rate of the excitation-transfer process involved cannot be determined by simple second-order kinetics. On the contrary, it is possible that this rate is related to the probability that a benzene molecule is a nearest neighbor to an excited dioxane molecule at the time of its formation. In this case, mole fraction would be the appropriate concentration unit. Since the ratio of molarity to mole fraction varies by less than 4% over the concentration range used in this work, the analysis is not affected significantly by the choice of concentration unit.

range of [B]. From the slope of the least-square line a value of $\alpha = 0.21\ M^{-1}$ is obtained. In accordance with the interpretations of Merklin and Lipsky, the intercept, $\eta = 1.04$, indicates that essentially all of the hydrogen yield from dioxane conforms to the postulated mechanism and can be suppressed by energy transfer to benzene. The results are thus consistent with the assumption of the mechanism that thermal H atoms (if produced) make negligible contribution to the hydrogen yield from dioxane. Such a conclusion is consistent with the observation of a negligible effect of added iodine on $G(H_2)$ from dioxane.[7] In this view, formation of hydrogen in γ-irradiation of pure, liquid dioxane must occur *via* the elimination of molecular hydrogen or the formation of "hot" H atoms or both. However, the major hydrogen formation processes should conform to the stoichiometry of reaction I, consistent with the near equality of hydrogen and dimer yields shown in eq. 1. Elimination of molecular hydrogen from a single molecule would not conform to the necessary stoichiometry unless both H atoms come from the same carbon atom which then inserts into a C–H bond of another dioxane molecule; nor would any reaction giving rise to dioxanyl radicals conform to the necessary stoichiometry, *e.g.*, formation of "hot" H atoms, unless the ratio of disproportionation to combination is negligible. Dioxene was not sought in this work; however, it was not reported by Llabador and Adloff,[7] who determined the liquid products.

Polymer and Biphenyl Yields in Mixtures. If the assumption is valid that absorbed energy is partitioned in proportion to electron fraction, then the polymer yield curve of Figure 2 constitutes rather conclusive evidence, in support of the analysis of hydrogen yield data, that dioxane is protected by energy transfer to benzene. At the very least, in the absence of any interaction, the polymer yield curve should be a straight line joining the extreme values of G(polymer) for the pure components. However, benzene appears to react rapidly with free radicals such as phenyl[18] and cyclohexyl.[19] Thus, if dioxanyl radicals are intermediates in formation of dioxane dimer, then addition of these radicals to benzene molecules, with increasing concentration of the latter, would result in conversion of more solvent monomer units to polymer than if the dioxanyl radicals simply recombined as in pure dioxane; under these circumstances, the polymer yield curve would lie above the straight line expected for no interaction. Because of the large doses necessitated in the polymer study and because of a lack of precise knowledge concerning all the elementary reactions involved in polymer formation in the mixtures, kinetic analysis of the polymer yield curve is not warranted. Very definitely, the

parallel behavior of the curves in Figure 2 for G(polymer) and $G(H_2)$ suggests that a common dioxane precursor of polymer and hydrogen is protected from reaction by some kind of interaction with benzene.

Work in this laboratory by Cramer[20] has shown that the mechanism of biphenyl formation in radiolysis of benzene appears to involve addition of phenyl radicals to benzene followed by disproportionation and combination reactions of the radical $C_6H_5C_6H_6$.[18] With addition of dioxane, particularly because G(radical) is probably larger for dioxane than for benzene, the probability of disproportionation of $C_6H_5C_6H_6$ to biphenyl will change as a result of change in the nature of the radicals most frequently encountered by $C_6H_5C_6H_6$. Further, the reaction

$$C_6H_5 + C_4H_8O_2 \longrightarrow C_6H_6 + C_4H_7O_2 \qquad (II)$$

may compete with addition of C_6H_5 to benzene. Again, in the absence of precise knowledge concerning all the elementary reactions involved, a kinetic analysis of the biphenyl yield data is not warranted. However, the rather sharp suppression of biphenyl yields on addition of dioxane to benzene (*cf.* Figure 2) seems more consistent with an appreciable role of reaction II than with a large change in the probability of disproportionation of $C_6H_5C_6H_6$ to biphenyl.

Relative Luminescence Yields. The relative luminescence yields may be analyzed in terms of a set of reactions and by a method analogous to those used in analysis of the hydrogen yields, but with some very significant differences.

$$D \longrightarrow D^{\ddagger} \qquad \epsilon_D R_0 G_D{}^{\ddagger}/N_0$$

$$B \longrightarrow B^{\ddagger} \qquad \epsilon_B R_0 G_B{}^{\ddagger}/N_0$$

$$D^{\ddagger} \longrightarrow D \text{ or product} \quad k_D[D^{\ddagger}]$$

$$D^{\ddagger} + X \longrightarrow D + X^* \quad k_{DX}[D^{\ddagger}][X]$$

$$D^{\ddagger} + B \longrightarrow D + B^{\ddagger} \quad k_{DB}[D^{\ddagger}][B]$$

$$B^{\ddagger} \longrightarrow B \text{ or product} \quad k_B[B^{\ddagger}]$$

$$B^{\ddagger} + X \longrightarrow B + X^* \quad k_{BX}[B^{\ddagger}][X]$$

$$X^* \longrightarrow X \quad k_X[X^*]$$

$$X^* \longrightarrow X + h\nu \quad k_e[X^*]$$
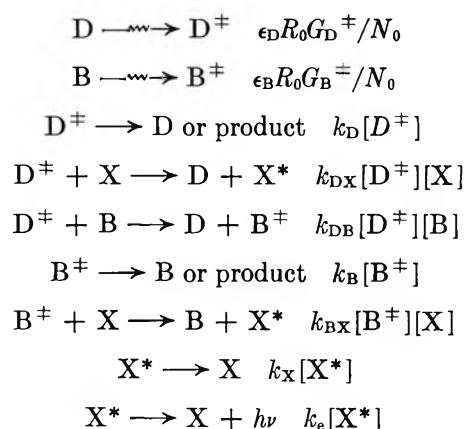
All previously used symbols have the same signifi-

(18) C. A. Barson and J. C. Bevington, *Trans. Faraday Soc.*, 55, 1266 (1959); E. L. Eliel, S. Meyerson, Z. Welvart, and S. H. Wilen, *J. Am. Chem. Soc.*, 82, 2936 (1960).

(19) T. Gaumann, *Helv. Chim. Acta*, 44, 1337 (1961).

(20) W. A. Cramer, Thesis, University of Amsterdam, 1961. *Cf.* E. A. Cherniak, E. Collinson, and F. S. Dainton, *Trans. Faraday Soc.*, 60, 1408 (1964).

cance, except that the possibility of different excited states, $D^{\pm}$ and $B^{\pm}$, being involved is specifically noted by a change in superscript. In addition, X denotes p-terphenyl and k_D, k_B, and k_X are summed rate constants for all reactions of $D^{\pm}$, $B^{\pm}$, and X^*, respectively, other than the excitation-transfer and emission processes specifically written for these species. The steady-state treatment gives

$$\frac{\epsilon_D(\rho_D G_D^{\pm} - \rho_B G_B^{\pm})}{G_e/f - \rho_B G_B^{\pm}} = \frac{1 + \alpha'[B]}{1 + \gamma'[B]} \quad (3)$$

where

$$\rho_D = k_{DX}[X]/(k_D + k_{DX}[X]) \quad (4)$$

$$\rho_B = k_{BX}[X]/(k_B + k_{BX}[X]) \quad (5)$$

$$\alpha' = k_{DB}/(k_D + k_{DX}[X]) = \rho_D k_{DB}/k_{DX}[X] \quad (6)$$

$$\gamma' = \alpha' \rho_B G_B^{\pm}(G_D^{\pm}/G_B^{\pm} - 1)/(\rho_D G_D^{\pm} - \rho_B G_B^{\pm}) \quad (7)$$

$$f = k_e/(k_e + k_X) \quad (8)$$

and G_e is the 100-e.v. yield of luminescence photons.

The results of Burton, et al.,[21] suggest that for p-terphenyl in degassed dioxane, a reasonable value of $Q_D' = k_D/k_{DX}$ would be about $4 \times 10^{-3} M$ ($Q' = 2.8 \times 10^{-3} M$ was reported for cyclohexane). If the assumption is made that $k_{DX} = 3k_{DB}$, then $k_D/k_{DB} = 12 \times 10^{-3} M$ and about 90% of $D^{\pm}$ transfer their excitation to benzene at $[B] = 0.1 M$, which corresponds to about 1 vol. % of benzene. However, in a variety of systems ("common" solvent + benzene + scintillator) Q and Q' values show a significant change as benzene concentration increases above 1 vol. % and do not become characteristic of pure benzene until a concentration near 20 vol. % is reached.[21]

In Figure 3, the relative luminescence yield, cG_e (relative luminescence intensity divided by dose rate), is plotted against ϵ_B. It is evident that some process approaches completion near 20 vol. % of benzene.[22] If $\alpha'[B]$ is large compared to both unity and $(\rho_D G_D^{\pm} - \rho_B G_B^{\pm})/(\rho_B G_D^{\pm} - \rho_B G_B^{\pm})$, then 1 can be dropped in both numerator and denominator on the right-hand side of eq. 3, and eq. 3 can be transformed into eq. 9 where c is

$$cG_e = cf[\rho_B G_D^{\pm} + (G_B^{\pm} - G_D^{\pm})\rho_B \epsilon_B] \quad (9)$$

a constant which relates G_e to the measured relative luminescence yield. For values of $\epsilon_B \geq 0.175$ the plot of cG_e against ϵ_B in Figure 3 conforms very well to the least-square line

$$cG_e = 53.9 + 44.0\epsilon_B \quad (10)$$

From the values obtained for $cG_e = cf\rho_B G_D^{\pm}$ and

$cf\rho_B G_B^{\pm}$ at $\epsilon_B = 0$ and 1, respectively, in eq. 10 and from the experimental value of $cG_e = cf\rho_D G_D^{\pm}$ at $\epsilon_B = 0$, the following ratios are obtained.

$$G_D^{\pm}/G_B^{\pm} = 0.55 \quad (11)$$

$$\rho_B/\rho_D = 2.3 \quad (12)$$

For p-terphenyl in pure, degassed benzene, Burton, et al.,[21] report $Q_B' = 10^{-3} M$. Use of this value and eq. 12 gives $Q_D' = 5.1 \times 10^{-3} M$. Thus, $\alpha' = 46 M^{-1}$ (assuming $k_{DX} = 3k_{DB}$) and at $\epsilon_B = 0.175$, $\alpha'[B] = 104$ which is indeed large compared to both unity and to the value of $(\rho_D G_D^{\pm} - \rho_B G_B^{\pm})/(\rho_B G_D^{\pm} - \rho_B G_B^{\pm}) = 1.7$.

Some Conclusions and Speculation. From the value of $\alpha' = 46 M^{-1}$, a value of $\alpha^{\pm}$ (for $D^{\pm}$ which results in luminescence) $= \alpha'(1 + [X]/Q_D') = 65 M^{-1}$ is obtained. This result may be compared with $\alpha = 0.21 M^{-1}$ for D^* which gives rise to hydrogen. It is evident that $D^{\pm}$ and D^* are different and, therefore, that $D^{\pm}$ makes a negligible contribution to the yield of chemical decomposition. Either $G_D^{\pm}$ is small compared to $G(H_2) = 2.1$, equivalent to $k_1 G_D^*/(k_1 + k_2)$, or a small fraction of the molecules $D^{\pm}$ decomposes.

Since the first electronic transition in dioxane shows considerable vibrational structure,[3] the corresponding excited state should have a lifetime of the order of 10^{-8} sec. Consequently, it is tempting to identify $D^{\pm}$ with this lowest electronic transition, as has been done in the case of benzene.[23] However, a positive identification must await measurement of the decay time of $D^{\pm}$ and measurement of Q_D' for ultraviolet excitation. It is of interest to note that the value of $Q_D' = 5.1 \times 10^{-3} M$, in contrast with the Q' values for benzene and cyclohexane,[21] is compatible with a diffusion-controlled, energy-transfer reaction for reasonable values of all parameters (sum of diffusion coefficients $\approx 4 \times 10^{-5}$ cm.²/sec., sum of the van der Waals radii ≈ 5 Å., decay time of $D^{\pm} \approx 1.2 \times 10^{-8}$ sec.).[24] One might say that the behavior of dioxane is "normal" in that it may not be necessary to invoke any special attributes to interpret luminescence and quenching parameters, contrary to the situation in benzene and cyclohexane.[21,23,24]

The value of $\alpha = 0.21 M^{-1}$ suggests that the states represented by D^*, which yield decomposition products, have a very short lifetime. Thus, the fraction of D^*

(21) M. Burton, M. A. Dillon, C. R. Mullin, and R. Rein, *J. Chem. Phys.*, 41, 2236 (1964).

(22) The value of $\epsilon_B = 0.175$ corresponds to 20 vol. % and 2.25 M.

(23) S. Lipsky and M. Burton, *J. Chem. Phys.*, 31, 1221 (1959); J. L. Kropp and M. Burton, *ibid.*, 37, 1742 (1962).

(24) C. R. Mullin, M. A. Dillon, and M. Burton, *ibid.*, 40, 3053 (1964).

protected from decomposition in essentially pure benzene, 11.27 M, is only 0.71. For protection to compete with decomposition it may be necessary that a molecule of protective agent be a nearest neighbor to an excited or ionized molecule at the time of its formation. Protection by charge or excitation transfer may be in competition with such processes of short lifetime as decomposition of an ion before neutralization, geminate recombination of an ion and its electron, or decomposition of highly excited molecules formed either directly or on ion neutralization. Whatever the process being prevented, it is responsible for essentially

the total yield of chemical decomposition. These conclusions would also appear to apply to benzene[25] and to cyclohexane (compare α = 0.84 M^{-1} for benzene in cyclohexane[16] and $1/Q'$ = 360 for p-terphenyl in cyclohexane[21]).

(25) H. F. Barzynski, R. R. Hentz, and M. Burton, to be published; D. B. Peterson, T. Arakawa, D. A. G. Walmsley, and M. Burton, to be published.

1-Pentanethiol: Heat of Vaporization and Heat Capacity of the Vapor[1]

by Herman L. Finke, Isham A. Hossenlopp, and William T. Berg

The heat of vaporization of 1-pentanethiol between 356 and 400°K. is represented by the equation ΔHv = 12,784 − 6.243T − 0.01221T^2 cal. mole^{-1}. The vapor heat capacity measured at five temperatures between 385 and 500°K. is given by the equation $C_p° $ = 3.927 + 0.11195T − 4.2289 × 10$^{-5}T^2$ cal. deg.$^{-1}$ mole^{-1}. The equation, B = −73.5 − 110.78 exp(1000/T) cc. mole^{-1}, was derived for the second virial coefficient from calorimetric data.

Introduction

As a part of the continuing research program on organic sulfur compounds of the Bureau of Mines, a study was made of the heat of vaporization and heat capacity of the vapor of 1-pentanethiol. The program is designed to obtain information concerning the variance of thermodynamic properties of carefully chosen members of families of compounds to enable calculation, by incremental methods, of tables of data for entire homologous series of sulfur compounds. As an example, the data presented here were utilized to this end, together with data for other 1-thiols in a recent publication from this laboratory[2] to calculate tables of thermodynamic properties for 1-thiols through 1-eicosanethiol.

Experimental

Materials. The sample of 1-pentanethiol was part of the Standard Sample of Organic Sulfur Compound API-USBM (PC-48-66), prepared at the Laramie, Wyo., Petroleum Research Center of the Bureau of Mines. The purity determined by a time–temperature study of the lowering of the freezing point was 99.94 mole %.

(1) This investigation was part of the American Petroleum Institute Research Project 48A on the "Production, Isolation, and Purification of Sulfur Compounds and Measurement of Their Properties," which the Bureau of Mines conducts at Bartlesville, Okla., and Laramie, Wyo.

(2) D. W. Scott and J. P. McCullough, U. S. Bureau of Mines Bulletin 595, U. S. Government Printing Office, Washington, D. C., 1961.

Apparatus and Physical Constants. Measurements were made in the vapor-flow calorimeter described by Waddington, *et al.*[3] Briefly, for heat capacity determinations, the method consists of passing a measured constant (steady-state) flow of vapor, generated by electrical evaporation in a cycling vaporizer, through a calorimeter in which the vapor is heated electrically by a measured and constant power input. For heat of vaporization determinations, the method is similar except that the vapor is not heated, and a measured amount of material is collected in a measured amount of time. The reported values are based on a molecular weight of 104.212 g./mole (1951[4a] International Atomic Weights[4b]), the 1951 values of the fundamental physical constants,[5] and the relations: $0° = 273.15°K.$ and 1 cal. $= 4.184$ joules (exactly).

Results

The experimental values of the heat of vaporization and vapor heat capacity are given in Tables I and II. The estimated accuracy uncertainty of the values of ΔHv and $C_p°$ are 0.1 and 0.2%, respectively. The heat of vaporization may be represented by the empirical equation

$$\Delta Hv = 12,784 - 6.243T - 1.221 \times 10^{-2}T^2$$

cal. mole^{-1} (356–400°K.)   (1)

Equation 1 is claimed reliable only within the range of experimental observations. An estimate of the uncertainties involved by extrapolation may be obtained by comparing the values at 298.15°K. calcu-

Table I: The Molal Heat of Vaporization, Second Virial Coefficient, and Gas Density of 1-Pentanethiol

T, °K.	P, atm.	ΔHv, cal.	$-B$, cc. Obsd.	$-B$, cc. Calcd.[a]	V, cc. Obsd.[b]	V, cc. Calcd.[c]
356.08	0.250	9014 ± 2[d]	1910	1910	114,940	114,934
376.43	0.500	8705 ± 2	1670	1652	60,061	60,078
399.80	1.000	8337 ± 3	1406	1425	31,335	31,314

[a] Calculated from eq. 2.   [b] Calculated from virial equation and Clapeyron equation.   [c] Calculated from virial equation and eq. 2.   [d] Average deviation from the mean of three observations.

lated from eq. 1 with those of Finke, *et al.*,[6] calculated from the Clapeyron equation together with the value of dp/dT determined from the Cox equation fitted to values of observed vapor pressures. These two heat of vaporization values are 9838 ± 20 and 9825 ± 50 cal. mole^{-1}, respectively.

Table II: The Molal Vapor Heat Capacity of 1-Pentanethiol (in cal. deg.$^{-1}$)

	—————————— T, °K. ——————————				
	385.22	410.23	436.24	467.21	500.20
C_p (1.000 atm.)		43.638	45.387	47.463	49.660
C_p (0.500 atm.)	41.332	43.127			
C_p (0.250 atm.)	41.051	42.944	44.872	47.126	49.418
$C_p°$	40.786	42.731	45.711	47.019	49.341
$-T(d^2B/dT^2)$, obsd.[a]	1.03	0.84	0.63	0.42	0.30
$-T(d^2B/dT^2)$, calcd.[b]	1.11	0.80	0.60	0.43	0.32

[a] Units: cal. deg.$^{-1}$ mole^{-1} atm.$^{-1}$.   [b] Calculated from eq. 2.

The effects of gas imperfection were correlated by the procedure described in an earlier paper.[7] The vapor pressure equations given by Finke, *et al.*,[6] were used. The empirical equation for B, the second virial coefficient in the equation of state, $PV = RT(1 + B/V)$, is

$$B = -73.5 - 110.78 \exp(1000/T) \text{ cc. mole}^{-1}$$

(385–500°K.)   (2)

Observed values of B and $-T(d^2B/dT^2) = \lim_{p \to 0} (\partial C_p/\partial P)_T$ and the ones calculated from eq. 2 are compared in Tables I and II.

From the values of $C_p°$ and T given in Table II, the following empirical equation was derived for the heat capacity of 1-pentanethiol vapor

$$C_p° = 3.927 + 0.11195T - 4.2289 \times 10^{-5}T^2$$

cal. deg.$^{-1}$ mole^{-1} (384–500°K.)   (3)

(3) (a) G. Waddington, S. S. Todd, and H. M. Huffman, *J. Am. Chem. Soc.*, **69**, 22 (1947); (b) J. P. McCullough, D. W. Scott, R. E. Pennington, I. A. Hossenlopp, and G. Waddington, *ibid.*, **76**, 4791 (1954); (c) G. Waddington, J. C. Smith, K. D. Williamson, and D. W. Scott, *J. Phys. Chem.*, **66**, 1074 (1962).

(4) (a) This study was originally part of a larger program in which a number of the results already have been reported using the 1951 physical constants. Use of the table of latest recommended atomic weights and fundamental physical constants [*cf.* E. R. Cohen and J. W. M. DuMond, Report to the American Physical Society, Washington, D. C., April 1962] would produce less than 0.01% difference in the final results. (b) E. Wicher, *J. Am. Chem. Soc.*, **74**, 2447 (1952).

(5) F. D. Rossini, F. T. Gucker, Jr., H. L. Johnston, L. Pauling, and G. W. Vinal, *ibid.*, **74**, 2699 (1952).

(6) H. L. Finke, D. W. Scott, M. E. Gross, G. Waddington, and H. M. Huffman, *ibid.*, **74**, 2804 (1952).

(7) J. P. McCullough, H. L. Finke, J. F. Messerly, R. E. Pennington, I. A. Hossenlopp, and G. Waddington, *ibid.*, **77**, 6119 (1955).

Studies of the Sedimentation Velocity of Ovalbumin in

Concentrated Salt Solutions[1]

by Julie Hill and David J. Cox

*Clayton Foundation Biochemical Institute and the Department of Chemistry, The University of Texas,
Austin, Texas 78712*   (*Received March 25, 1965*)

Sedimentation coefficients of ovalbumin have been measured in water at several concentrations of each of the following salts: sodium chloride, potassium chloride, cesium chloride, magnesium chloride, and ammonium sulfate. Measurements have also been made in solvents consisting of deuterium oxide and various amounts of sodium chloride, potassium chloride, and cesium chloride. When the sedimentation coefficients obtained in the several experiments in a given salt are corrected to a reference viscosity and plotted against the densities of the respective solvents, straight lines result in every case. Apparent isodensity points have been calculated by extrapolation to the density axis from the experimental data for each set of solvents. The observed density intercept in a given salt is independent of the protein concentration used in the sedimentation experiments; the intercepts are in all cases below the reciprocal of the partial specific volume of ovalbumin, but they vary from one salt to another. The density intercepts in the various salts fall in the same order in water and deuterium oxide.

Introduction

It has often been useful to observe the sedimentation behavior of macromolecular species in aqueous solvents containing high concentrations of low molecular weight second solutes. Frequently, the purpose of experiments of this kind has been to demonstrate the effect of the particular second solute on the molecular weight or on the shape of the macromolecular particles. For example, some proteins are soluble only in concentrated salt solutions and not in the dilute buffers normally used for ultracentrifugation[2,3]; the determination of the molecular weight of such proteins in the ultracentrifuge requires that their sedimentation be observed in the presence of large amounts of salt. Sedimentation in sucrose density gradients is a technique in general use for both preparative and analytical purposes. A number of proteins composed of subunits appear to disaggregate in mixed solvents: bovine procarboxypeptidase-A in concentrated urea,[4] myosin in concentrated urea[5] or guanidinium chloride,[6] and hemoglobin in concentrated sodium chloride or magnesium chloride.[7]

It is well known that the sedimentation behavior of

a macromolecule is considerably more difficult to interpret in a three-component system than it is in the classical two-component case.[8-10] In a system of one macromolecular solute in one solvent, the sedimentation coefficient, at infinite dilution of the solute, is determined by the molecular weight, partial specific volume, and shape of the solute particles. When a second solute is present, the sedimentation velocity of

(1) This work was supported by Grant GM-11749 from the United States Public Health Service.

(2) M. L. Anson, *J. Gen. Physiol.*, **20**, 663 (1937).

(3) J. A. Rupley and H. Neurath, *J. Biol. Chem.*, **235**, 609 (1960).

(4) J. R. Brown, D. J. Cox, R. N. Greenshields, K. A. Walsh, M. Yamasaki, and H. Neurath, *Proc. Natl. Acad. Sci., U. S.*, **47**, 1554 (1961).

(5) D. B. Wetlaufer and J. T. Edsall, *Biochim. Biophys. Acta*, **43**, 132 (1960).

(6) E. F. Woods, S. Himmelfarb, and W. F. Harrington, *J. Biol. Chem.*, **238**, 2374 (1963).

(7) A. G. Kirshner and C. Tanford, *Biochemistry*, **3**, 291 (1964).

(8) J. W. Williams, K. E. Van Holde, R. L. Baldwin, and H. Fujita, *Chem. Rev.*, **58**, 715 (1958).

(9) G. Scatchard, *J. Am. Chem. Soc.*, **68**, 2315 (1946).

(10) E. F. Casassa and H. Eisenberg, *J. Phys. Chem.*, **64**, 753 (1960); **65**, 427 (1961)

the macromolecules is affected, in addition, by interactions between the two solutes. The behavior of three-component systems in the ultracentrifuge has been explored theoretically by the methods of irreversible thermodynamics[11,12]; in these treatments, interaction between the solutes is described in terms of cross-diffusion coefficients, effects of each solute on the chemical potential of the other, or preferential interaction of the macromolecule either with the solvent or with the second solute. The practical usefulness of the thermodynamic treatment has thus far been limited by the fact that these interaction parameters are generally not experimentally accessible. It is not presently possible to predict how a given protein of known properties will behave in a given three-component system; nor is it possible to reason rigorously from observed sedimentation behavior to the molecular weight or other properties of the macromolecular component.

For these reasons, it seems worthwhile to proceed on an empirical basis to examine the sedimentation behavior of some well-characterized proteins in the presence of a number of second solutes. A consistent pattern may emerge from such a comparative study which will allow predictions to be made of the importance of interaction effects in other, less well-characterized systems.

This report describes the measurement of the sedimentation velocity of ovalbumin in the presence of large amounts of several common salts, both in water and in deuterium oxide. The experimental procedure is that originally used by Schachman and Lauffer.[13] Sedimentation coefficients are measured for the protein in aqueous solutions containing different amounts of a given second solute. The sedimentation coefficients are corrected to a reference viscosity, and the resulting viscosity-corrected sedimentation coefficients are plotted against the densities of the respective solvents. In the absence of interaction among the components, the viscosity-corrected sedimentation coefficient[14] should be given by

$$S\eta = \frac{M(1 - \bar{v}\rho)}{N6\pi rf/f_0} \qquad (1)$$

In eq. 1, S is the sedimentation coefficient; η is the viscosity of the solvent; N is Avogadro's number; M, $\bar{v}$, and f/f_0 are the molecular weight, partial specific volume, and frictional ratio of the protein; r is the radius of a sphere whose volume is $M\bar{v}/N$; and ρ is the density of the solvent. Dividing both sides of eq. 1 by the viscosity of water, η_0, gives

$$S\eta_{rel} = \frac{M(1 - \bar{v}\rho)}{N6\pi\eta_0 rf/f_0} \qquad (1a)$$

where η_{rel} is the viscosity of the solvent relative to that of water. Equation 1a predicts that a plot of $S\eta_{rel}$ vs. ρ will be a straight line which crosses the density axis at $1/\bar{v}$, if interaction effects are absent and if M, $\bar{v}$, and f/f_0 do not vary with salt concentration. Conversely, the degree to which the results fail to obey eq. 1 will provide an empirical index of the combined effect of solute–solute interaction and of variation in the parameters describing the macromolecules.

Experimental

Protein. Twice-crystallized ovalbumin, lot No. OA-510, was purchased from the Worthington Biochemical Corp. The sedimenting boundaries observed with this preparation were symmetrical in all solvents used. A sedimentation equilibrium experiment was carried out on a sample of this lot of ovalbumin at a mean protein concentration of 3 mg./ml. in 0.1 M potassium chloride and 0.01 M potassium phosphate buffer, pH 6.8. Rayleigh interference optics were used, and the data were handled in the usual way.[15] Plots of the logarithm of protein concentration at equilibrium against the square of the distance from the axis of rotation were linear along the entire length of the solution column; the molecular weight calculated from the slope of the plot, using a value of 0.749 for $\bar{v}$,[16] was 44,670, in agreement with data in the literature.[17] The mean deviation among the calculations from six photographs was ±100, and the maximum deviation was 200.

Solvents. All solvents were prepared in 0.01 M potassium phosphate buffer, pH 6.8. Reagent grade salts and glass-distilled water were used in all cases. Deuterium oxide (99.6%) was purchased from Biorad Laboratories. Buffers were prepared in deuterium oxide by the addition of the appropriate weighed amounts of solid monobasic and dibasic potassium phosphate. The amount of protium introduced with the buffer salts was a negligibly small proportion of the total hydrogen in the resulting solutions. When ex-

(11) R. L. Baldwin, *J. Am. Chem. Soc.*, **80**, 496 (1958).

(12) L. Peller, *J. Chem. Phys.*, **29**, 415 (1958).

(13) H. K. Schachman and M. A. Lauffer, *J. Am. Chem. Soc.*, **71**, 538 (1949).

(14) H. K. Schachman, "Ultracentrifugation in Biochemistry," Academic Press, New York, N. Y., 1959.

(15) H. K. Schachman in "Methods in Enzymology," Vol. IV, Academic Press, New York, N. Y., 1957, pp. 32–103.

(16) M. O. Dayhoff, G. E. Perlmann, and D. A. MacInnes, *J. Am. Chem. Soc.*, **74**, 2515 (1952).

(17) H. Gutfreund, *Nature*, **153**, 406 (1949).

periments were done in deuterium oxide, the protein solutions were allowed to stand at room temperature for 1 to 1.5 hr. before the beginning of the centrifuge run, to allow for essentially complete hydrogen exchange between the protein and the solvent. A longer delay between the preparation of the solutions and the beginning of the experiment had no detectable effect on the observed sedimentation coefficients.

Viscosity Measurements. Solvent viscosities were measured in standard capillary viscometers with outflow times for water of 200–300 sec. at 20°. The instruments used were calibrated with standard solutions of sucrose and of potassium chloride at several concentrations. The observed viscosities of the standards agreed well with values in the literature[18]; it was concluded that no kinetic energy or end effect corrections were required.[19] The accuracy of the measurements is estimated to be within ±0.5%; making due allowance for the presence of small amounts of potassium phosphate in each of the solvents, the measured viscosities agreed with literature data where these were available.[18,20] Solvent densities were measured in triplicate in 1-ml. vented-cap pycnometers; the mean values were reproducible within ±0.001 g./cm.³.

Sedimentation Velocity Measurements. Sedimentation velocity measurements were carried out at 20° in a Spinco Model E ultracentrifuge operated at 59,780 r.p.m. The movement of the boundaries was observed with schlieren optics at bar angles of 70 to 80°. Sedimentation coefficients were calculated from the rate of movement of the maxima of the boundaries; the photographs from each run were measured several times. In a few cases, second-moment calculations[14] were also done; the results were not different from those obtained by the maximum gradient method. Calculation according to Baldwin[21] of the error introduced by the use of the peak position also indicated that the effect should be negligible. A valve-type synthetic boundary cell was used for all of the measurements. The relative amounts of solvent and solution introduced into the cup and the centerpiece were so chosen as to allow the formation of the boundary near the center of the solution column. Thus, the redistribution of the salts and the consequent rise of the base line at the ends of the column did not distort the observed gradient curve or shift its maximum during the course of the run.

In the case of cesium chloride, some solvents with densities higher than the apparent density of ovalbumin were used. In these cases, the solvent was placed in the centerpiece and the solution in the cup of the synthetic boundary cell; negative sedimentation coefficients were observed and, at bar angles below 90°, the rising protein

boundary was observed as a trough rather than as a peak. It was found convenient in these cases to set the bar angle above 90°, thus inverting the photographic record and converting the boundary to a peak similar to those found in the less dense solvents. It was found that such records could be read more reproducibly than those obtained at bar angles below 90°. Moreover, this technique eliminated the necessity for the use of a positive wedge window in some of the experiments.

The measured sedimentation coefficients were in general reproducible to ±0.03 svedberg unit or less. The error in a given viscosity-corrected sedimentation coefficient, of course, varied in proportion to the viscosity of the solvent. The most viscous solvents used were the most concentrated sucrose and sodium chloride solutions. In these cases, the probable error in $S\eta_{rel}$ reached ±0.06 svedberg unit; in most of the solvents, the error was considerably less than this.

For each second solute, five to eight sedimentation coefficients were measured, each at a different second-solute concentration and thus at a different density. In several solvents, the entire series was repeated at each of three or four protein concentrations. The values of $S\eta_{rel}$ were plotted against density and fitted to the best straight line by the criterion of least squares; the intercept on the density axis was then calculated. The least-squares calculation was repeated, dropping one point at a time. The scatter of the density intercepts so obtained was taken as an index of the precision of the original result. Moreover, inspection of the intercepts calculated omitting each point in turn for a trend in the values served to alert us to the presence of any slight curvature in the plots. The labor required for these calculations and for the handling of the sedimentation equilibrium results mentioned above was greatly reduced by the use of a Control Data 1604 digital computer.

Results

Viscosity-corrected sedimentation coefficients of ovalbumin were measured in aqueous solutions at various concentrations of sodium, potassium, magnesium, and cesium chlorides, and of ammonium sulfate. The results were plotted as solvent density vs. $S\eta_{rel}$ (Figures 1–5). In each of the experiments shown, the protein concentration was 5 mg./ml. In each figure, the

(18) "International Critical Tables," Vol. 5, McGraw-Hill Book Co., Inc., New York, N. Y. 1926, p. 33.

(19) J. T. Yang, *Advan. Protein Chem.*, **16**, 323 (1961).

(20) S. Lengyel, J. Tamas, J. Giver, and J. Hololerith, *Magy. Kem. Folyoirat*, **70**, 66 (1964).

(21) R. L. Baldwin, *Biochem. J.*, **65**, 503 (1957).

Table I: Density Intercepts of Plots of ρ vs. $S\eta_{rel}$ in Water[a]

Ovalbumin concn., mg./ml.	KCl, g./ml.	NaCl, g./ml.	CsCl, g./ml.	MgCl₂, g./ml.	(NH₄)₂SO₄, g./ml.
3	1.274 ± 0.003 (0.005)	1.273 ± 0.004 (0.010)	1.302 ± 0.001 (0.003)		
4	1.276 ± 0.005 (0.008)				
5	1.273 ± 0.003 (0.005)	1.275 ± 0.006 (0.014)	1.298 ± 0.001 (0.003)	1.242 ± 0.002 (0.005)	1.292 ± 0.005 (0.012)
6	1.265 ± 0.001 (0.004)				
7		1.282 ± 0.003 (0.008)	1.293 ± 0.001 (0.001)		
9					
Mean value	1.272 ± 0.003	1.276 ± 0.003	1.297 ± 0.003	1.242	1.292

[a] Density intercepts were obtained by the method of least squares. The least-squares calculations for each plot were repeated omitting one experimental point at a time. The standard deviation among these latter calculations is given in italics; the number in parentheses is the largest deviation from the mean value.
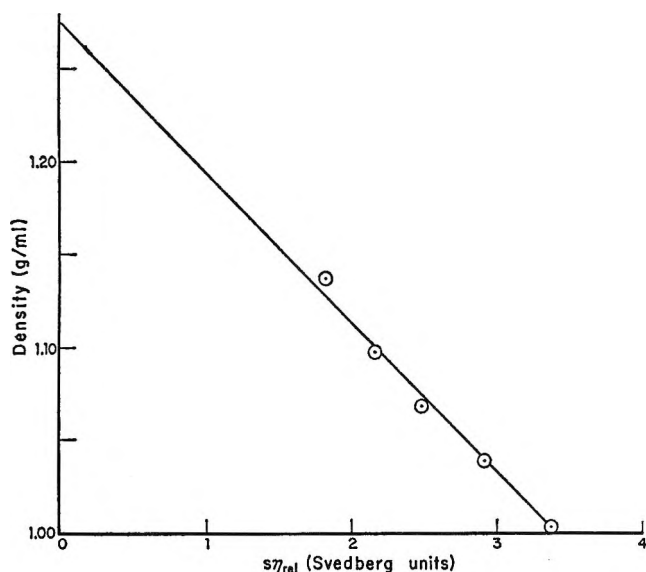
Figure 1. Plot of solvent densities (ρ) against viscosity-corrected sedimentation coefficients $(S\eta_{rel})$ for ovalbumin in sodium chloride–water. Viscosities are relative to water at 20°. Protein concentration 5 mg./ml.
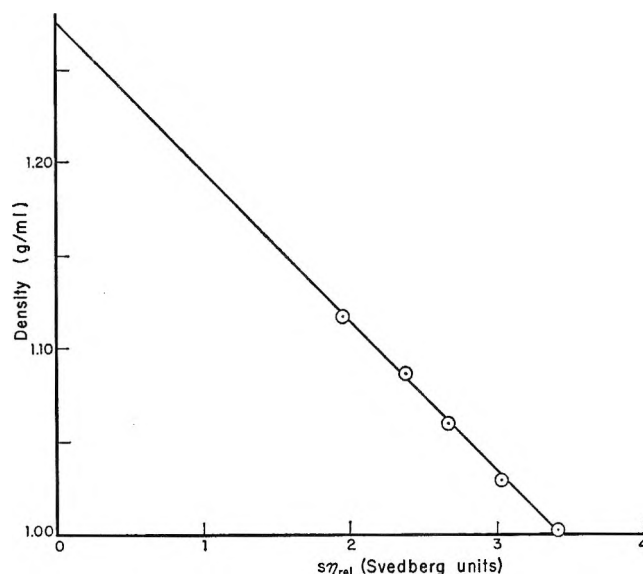
Figure 2. Plot of ρ vs. $S\eta_{rel}$ for ovalbumin at 5 mg./ml. in potassium chloride–water.

straight line is shown which gives the closest fit to the experimental points by the criterion of least squares. Inspection of the results indicates that the points follow linear plots reasonably well; the scatter of the points may be evaluated by noting that the radius of the points as drawn in Figures 1–4 corresponds to 0.04 svedberg unit along the $S\eta_{rel}$ axis. The calculated points at which the five plots intersect the density axis are given in the third row of Table I.

The results in cesium chloride are of particular interest. Here, measurements were made at densities up to 1.58; at the highest densities, as expected, nega-

tive sedimentation coefficients were observed. Figure 5 shows that the viscosity-corrected sedimentation coefficients are a linear function of density over a very large range of salt concentration. The availability of points taken at densities both above and below the intersection of the least-squares line with the density axis allowed the very precise location of the intercept. It may be noted, however, that when an independent calculation was done, using only the positive sedimentation coefficients—a calculation comparable with those done for the other salts—the result agreed very closely with that obtained using both the positive and negative sedimentation coefficients.
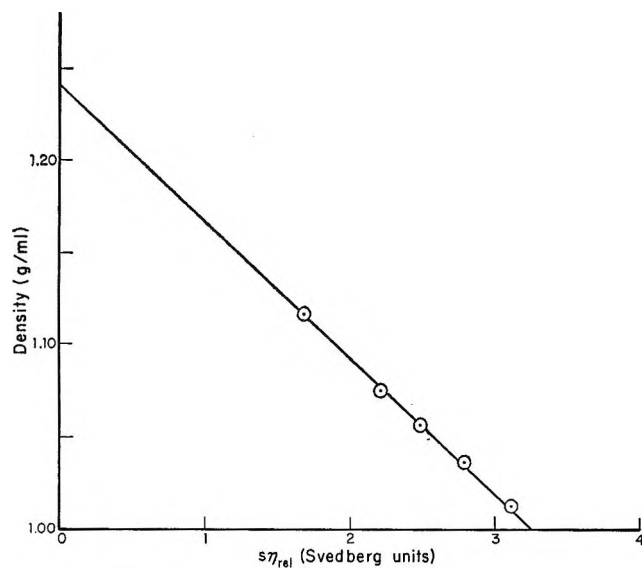
Figure 3. Plot of ρ vs. $S\eta_{rel}$ for ovalbumin at 5 mg./ml. in magnesium chloride–water.
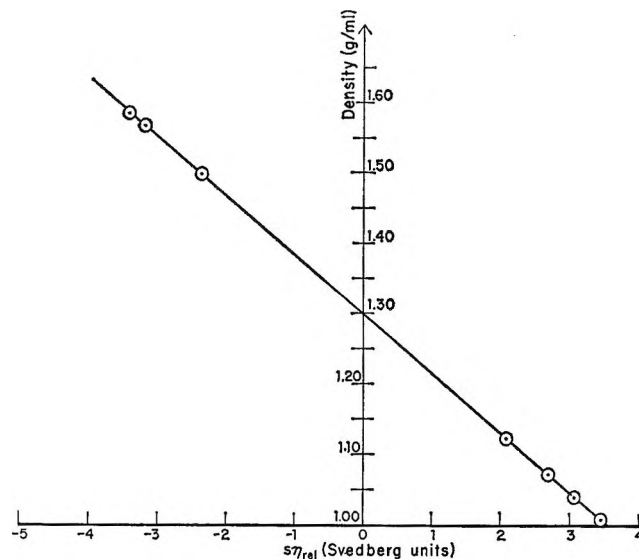
Figure 5. Plot of ρ vs. $S\eta_{rel}$ for ovalbumin at 5 mg./ml. in cesium chloride–water.
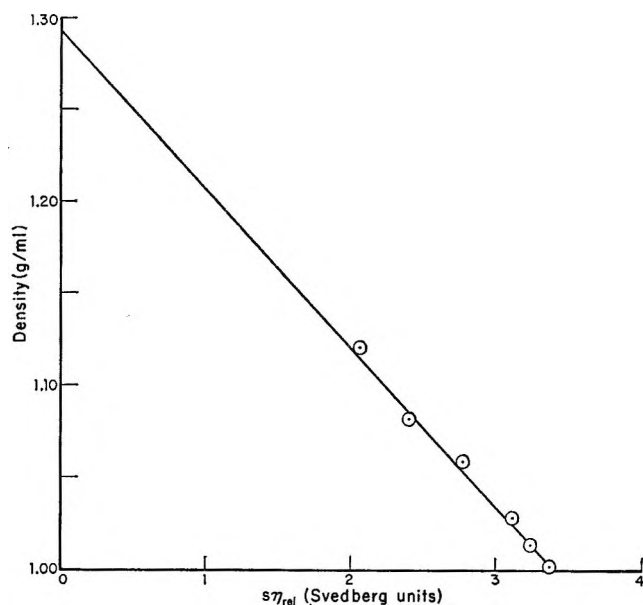
Figure 4. Plot of ρ vs. $S\eta_{rel}$ for ovalbumin at 5 mg./ml. in ammonium sulfate–water.

In addition to the experiments at 5 mg./ml., complete sets of runs in sodium chloride, potassium chloride, and cesium chloride were done at other protein concentrations. Several interesting points emerge from comparison of the results obtained in a given salt at several different protein concentrations. First, the data obtained at any given concentration, when assembled as a plot of ρ vs. $S\eta_{rel}$, gave a good fit to a straight line in every case. The 5-mg./ml. experiments shown in the figures are typical; in fact, of all the sets

of points obtained, the sodium chloride experiments of Figure 1 fit a straight line least well. The calculated density intercepts of the linear plots are presented in Table I. Second, any barely significant curvature found at one concentration was normally absent from the data at the others; thus, the possible upward curvature of Figure 1 was not apparent at 3 or 7 mg./ml. The apparent curvature in this case probably resulted from a fortuitous scatter in the data. Third, and most important, the plots derived from experiments in a given salt at several ovalbumin concentrations all converge toward the same point on the ρ-axis. The variation among the different density intercepts is of the same order as the uncertainty of the individual values. The separate values have been averaged, and the means are shown, with mean deviations, in the last row of Table I.

The density intercepts observed in the different salts may be compared by inspection of the last row of Table I. Two significant points are clear. First, in each of the five salts, the density intercept is significantly below $1/\bar{v}$; taking $\bar{v}$ for ovalbumin as 0.749, $1/\bar{v}$ is 1.335. Second, the difference between the observed density intercept and $1/\bar{v}$ varies from salt to salt. The difference is greatest in magnesium chloride, less in sodium or potassium chloride, and less still in cesium chloride or ammonium sulfate.

An analogous series of experiments was carried out in aqueous sucrose. A series of six centrifuge runs was done with ovalbumin at 5 mg./ml. in solutions of sucrose at various concentrations in water buffered at pH 6.8 with 0.01 M potassium phosphate. The resulting

ρ vs. $S\eta_{rel}$ plot appeared to show a very slight upward curvature; accordingly, six more runs were done, and the points from all the experiments were assembled as shown in Figure 6. A relatively large error in $S\eta_{rel}$ was to be expected, since the viscosities of the solvents were quite high. Within the limits of this experimental error, the points (circles in Figure 6) defined a reasonably good straight line. When experiments were done at three other protein concentrations, the results depicted by the other points in Figure 6 were obtained. Linear extrapolation toward higher densities from the experimental points would give a series of lines that cross at relatively low density and intersect the density axis at very different points. Behavior of this kind would indicate that the dependence of the sedimentation coefficient changes from inverse to direct at some intermediate sucrose concentration. A more likely alternative would be that the plots are curved at the higher densities. Further experiments in these solvents were not done, because it was noticed that the results were also unusual in that the observed dependence of the sedimentation coefficient on protein concentration was extraordinarily high. It seemed likely that the peculiarities of the data might be due to the fact that the buffer salt present was insufficient to eliminate the primary charge effect. When the experiments were repeated at an ionic strength of 0.15 M, the extreme concentration dependence did in fact disappear, but in this case the ρ vs $.S\eta_{rel}$ plots curved upward at *all* protein concentrations. Evidently, the linearity of the first series of points resulted from the fortuitous compensation of unknown concentration-dependent effects that would individually have caused the plot to curve in opposite directions.

For comparison with the results already described for aqueous salt solutions, analogous data were assembled for ovalbumin in solutions of sodium, potassium, and cesium chlorides in buffered deuterium oxide. Experiments in ammonium sulfate were not done because hydrogen exchange between the ammonium ion and D_2O would have produced a solvent containing a mixture of light and heavy water. Similarly, no deuterium oxide experiments were done in magnesium chloride because this salt is obtained as a hydrate from which water cannot be removed; according to the literature,[22] it loses HCl on drying before it loses water. A complete series of experiments was done in the three solvents at each of three protein concentrations.

The results of the experiments at an ovalbumin concentration of 5 mg./ml. are shown in Figures 7–9. The results were in every way analogous to those in the corresponding aqueous solvents. Each individual ρ vs. $S\eta_{rel}$ plot—in a given salt and at a particular
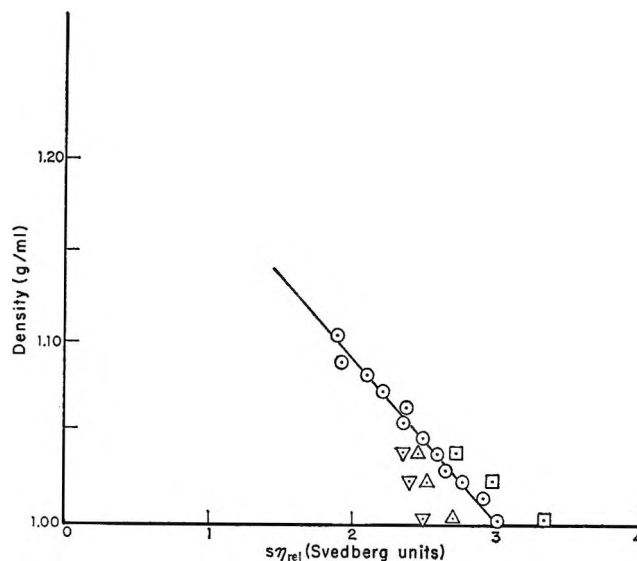
Figure 6. Plot of ρ vs. $S\eta_{rel}$ for ovalbumin in sucrose–water at several protein concentrations: $\triangledown$, 9 mg./ml.; $\triangle$, 7 mg./ml.; $\odot$, 5 mg./ml.; $\square$, 3 mg./ml. Solid line is a linear least-squares plot of the 5-mg./ml. points.
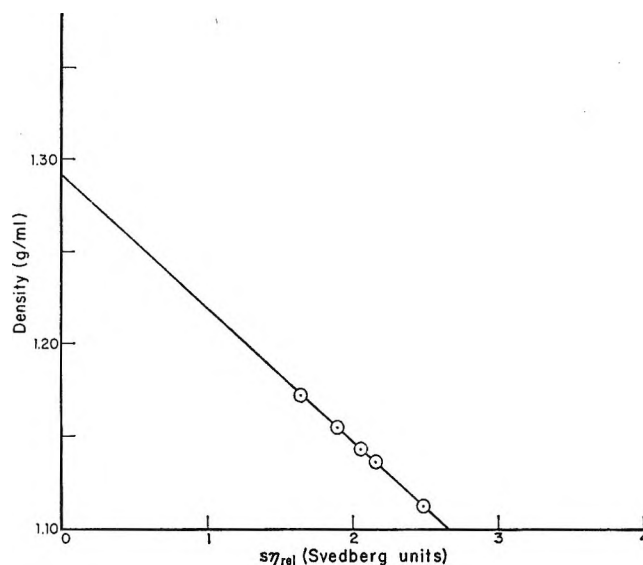
Figure 7. Plot of ρ vs. $S\eta_{rel}$ for ovalbumin at 5 mg./ml. in sodium chloride–deuterium oxide.

protein concentration—was linear within experimental error. In a given salt, the plots constructed from experiments at different protein concentration converged to the same point on the density axis. The observed density intercepts are assembled in Table II. The partial specific volume of ovalbumin should be lower in deuterium oxide than in water, since the protein undergoes hydrogen exchange with the solvent.

(22) "The Merck Index," 6th Ed., Merck and Co., Inc., Rahway, N. J., 1952, p. 590.
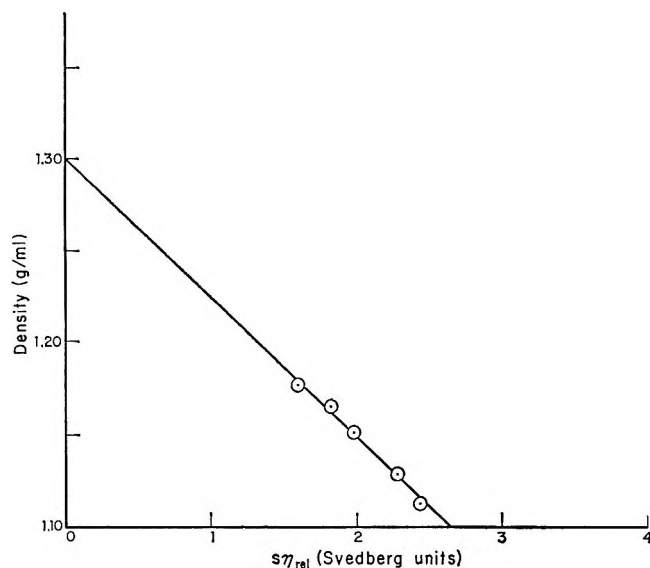
Figure 8. Plot of ρ vs. $S\eta_{rel}$ for ovalbumin at
5 mg./ml. in potassium chloride–deuterium oxide.
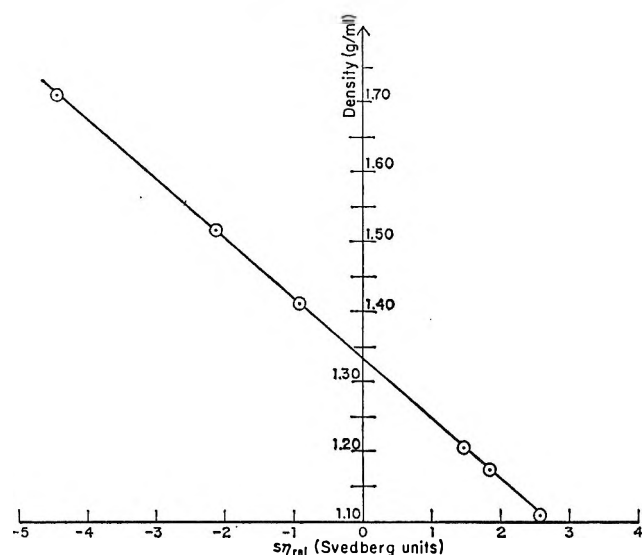
Figure 9. Plot of ρ vs. $S\eta_{rel}$ for ovalbumin at
5 mg./ml. in cesium chloride–deuterium oxide.

On the basis of the reported amino acid composition of ovalbumin,[23] 658 exchangeable hydrogens would be expected per molecule. If the partial molar volume of the protein is not affected by the exchange of hydrogen for deuterium, its partial specific volume would decrease from 0.749 to 0.738 after complete exchange. All of the density intercepts in Table II were below $1/\bar{v}$ (1.355) as was the case in water. It may also be noted that the density intercepts in the different salts fall in the same order in water and in deuterium oxide: in both cases, the intercepts in sodium and potassium

chlorides are close together and the intercept in cesium chloride is significantly higher.

Table II: Density Intercepts of Plots of ρ vs. $S\eta_{rel}$ in Deuterium Oxide[a]

Ovalbumin concn., mg./ml.	KCl, g./ml.	NaCl, g./ml.	CsCl, g./ml.
3	1.303 ± 0.003 (0.009)	1.298 ± 0.004 (0.010)	1.329 ± 0.001 (0.001)
5	1.299 ± 0.002 (0.006)	1.291 ± 0.003 (0.008)	1.332 ± 0.001 (0.001)
7	1.307 ± 0.006 (0.013)	1.311 ± 0.001 (0.003)	1.327 ± 0.001 (0.001)
9	1.305 ± 0.003 (0.006)		
Mean value	1.303 ± 0.002	1.300 ± 0.007	1.329 ± 0.001

[a] Deviations defined as in Table I.

Discussion

The sedimentation behavior of ovalbumin in concentrated salt solutions follows a reasonably consistent pattern. The viscosity-corrected sedimentation coefficients are linearly dependent on solvent density in the presence of each salt, the density intercept is depressed below $1/\bar{v}$ in each case, and the depression of the density intercept varies from one salt to another. Qualitatively similar results have been found with other systems described in the literature: influenza virus in concentrated serum albumin,[24,25] tobacco mosaic virus in serum albumin and in sucrose,[13] ribonuclease in several salts,[26] and ovalbumin in urea.[27] Curved $S\eta_{rel}$ vs. ρ plots have been observed for influenza[25,28] and vaccinia[29] virus in sucrose, bovine serum albumin in a variety of solvents,[26] and ovalbumin in sucrose as seen here. No cases have been reported in which eq. 1a is obeyed in detail, excepting those in which the second "solute" was deuterium oxide.

(23) J. C. Lewis, N. S. Snell, D. J. Hirschmann, and H. Fraenkel-Conrat, *J. Biol. Chem.*, **186**, 23 (1950).

(24) D. G. Sharp, A. R. Taylor, I. W. McLean, Jr., D. Beard, and J. W. Beard, *Science*, **100**, 151 (1944).

(25) D. G. Sharp, A. R. Taylor, I. W. McLean, Jr., D. Beard, and J. W. Beard, *J. Biol. Chem.*, **159**, 29 (1945).

(26) D. J. Cox and V. N. Schumaker, *J. Am. Chem. Soc.*, **83**, 2433 (1961).

(27) W. L. Gagen and J. Holme, *J. Phys. Chem.*, **68**, 723 (1964).

(28) M. A. Lauffer and W. M. Stanley, *J. Exptl. Med.*, **80**, 531 (1944).

(29) J. E. Smadel, E. G. Pickels, and T. Shedlovsky, *ibid.*, **68**, 607 (1938).

Even if only those cases yielding linear plots of $S\eta_{rel}$ vs. ρ are considered, there is no lack of possible rationalizations for the failure of most systems to obey eq. 1a. Such behavior could be accounted for by variation with density of the molecular weight, partial specific volume, or frictional ratio of the protein, or by solute–solute interaction. The form of the $S\eta_{rel}$ vs. ρ plots for ovalbumin in the various salt solutions probably does not result from a variation in molecular weight. If the molecular weight of ovalbumin were a slowly varying function of salt concentration, linear plots would not have been obtained. Even if a slight curvature had been missed, the plots constructed from runs at different protein concentrations would not have converged to the same density intercept. Finally, skewed boundaries would have been observed at intermediate salt concentrations. For these reasons, it seems unlikely that variation of the molecular weight of the protein with salt concentration is a serious factor in this particular case. Variation of the partial specific volume cannot be so readily dismissed, since the appropriate measurements have not been done for ovalbumin in these solvents. The little information that is available indicates that the partial specific volumes of proteins are not noticeably affected by the presence of large amounts of neutral salts.[7,26] In the lack of specific information bearing on the point, however, the possible dependence of $\bar{v}$ on salt concentration can be ignored only with explicit reservations.

The effect of solute–solute interactions on sedimentation in three-component systems is almost certainly one important cause of the failure of such systems to obey eq. 1a. It was pointed out some time ago that if the particles representing the two components of a solvent were of different sizes, a protein would be expected to behave as if it bound the smaller particles in preference to the larger, simply because the larger particles cannot approach the surface of the macromolecule as closely as the smaller.[13,30,31] In the solvents used here, ovalbumin would appear to bind water in preference to hydrated salt ions, and the effective density of the hydrodynamic unit would be decreased by the binding of the less dense component of the solvent. The steric exclusion idea is particularly attractive in the present case for several reasons. First, it leads directly to the prediction that, if M, $\bar{v}$, and f/f_0 do not vary with salt concentration, then an $S\eta_{rel}$ vs. ρ plot should be linear and should intersect the density axis below $1/\bar{v}$, as was observed here.[13,26,29] Second, the degree to which the density intercept is depressed below $1/\bar{v}$ in a particular salt should be correlated with the effective size of the hydrated ions involved, and such a correlation is observed here, at least

qualitatively. Third, the density intercepts in the presence of a series of salts should fall in the same order in water and in deuterium oxide, since the degree of hydration of the salt ions and thus their effective size should do so. Finally, the depression of the density intercept for different proteins in the same salt should be proportional to the surface area per unit weight of the protein and thus, for objects of the same shape, inversely proportional to molecular weight. Comparison of the present data for ovalbumin with those previously obtained for ribonuclease[26] reveals that such a relationship does exist between these two proteins.

It is unlikely, however, that the alteration of the effective density, which results from preferential steric exclusion of one component of the solvent from the surface of a macromolecule, accounts entirely for the behavior of a protein in a two-component solvent. Even if M and $\bar{v}$ do not vary with salt concentration, the possibility of variation in the frictional ratio remains to be considered. A change in the shape of the macromolecule as the salt concentration varies would provide the most obvious occasion for f/f_0 to vary with density. In a two-component solvent, however, there are other possible sources of variation in f/f_0. The derivation of Stokes' law assumes, for example, that the solvent has a uniform viscosity which has the same value at the surface of the moving particle as it does in the rest of the solvent. If it is accepted that the composition of a two-component solvent may vary with distance from the surface of the macromolecule— as the steric exclusion hypothesis requires—then the possibility must be considered that the effective viscosity of the solvent sheared by the passage of the sedimenting particle may be different from that of the solvent as a whole.[13] The magnitude of an error of this kind would be expected to vary with the composition of the two-component solvent. Moreover, it is possible that the hydrodynamic volume of the protein might be different in different solvents. Either a shape change or an alteration of the local viscosity of the solvent or of the effective volume of the protein molecule would be formally expressed as a variation of the frictional ratio. The results given here could be accounted for either by continuous variation of f/f_0 with salt concentration or by an alteration of the effective density of the protein molecule resulting from preferential interaction with one component of the solvent. Which effect is of greater quantitative im-

(30) S. Katz and H. K. Schachman, *Biochim. Biophys. Acta*, **18**, 28 (1955).

(31) V. N. Schumaker and D. J. Cox, *J. Am. Chem. Soc.*, **83**, 2445 (1961).

portance cannot be determined on the basis of sedimentation velocity data alone.

Considering the available information from a strictly empirical standpoint, at least one important conclusion may be drawn. The degree to which the behavior of a particular protein deviates from that predicted by eq. 1a in a given salt can be measured. It cannot be assumed, however, that the same protein in another salt or another protein in the same salt will be abnormal to the same degree. The density correction required to extract, for example, the molecular weight of a given protein from sedimentation data obtained in a con-

centrated solution of a particular salt will, in general, be unique for that combination of protein and salt. In view of the increasingly common use of two-component solvents for studies of proteins, a search for a pattern in the behavior of known systems would clearly be in order. In the meantime, the interpretation of experiments of this kind must be approached with some caution.

Kinetics and Thermodynamics of the Reaction between Iodine and Methane

and the Heat of Formation of Methyl Iodide

by C. A. Goy and H. O. Pritchard

Chemistry Department, University of Manchester, Manchester 13, England   (*Received March 23, 1965*)

The equilibrium $CH_4 + I_2 \rightleftharpoons CH_3I + HI$ has been studied in the gas phase over the temperature range 585–748°K. The heat of this reaction is calculated to be $\Delta H°_{298} = 12.67 \pm 0.05$ kcal./mole, leading to a heat of formation of gaseous methyl iodide $\Delta H_f°_{298} = 3.40$ kcal./mole. The equilibrium is established *via* the reaction $I + CH_4 \rightarrow HI + CH_3$, which has a rate constant $k = 10^{15.0} \exp[(-35.0 \pm 1.1)10^3 RT]$ cc. mole^{-1} sec.$^{-1}$ over the temperature range 548–618°K.

The reaction between HI and CH_3I has been studied by Flowers and Benson[1] over the range of temperature 533–589°K. They propose a kinetic scheme involving the reactions

$$I_2 \rightleftharpoons I + I \quad \text{equilibrium constant} = K_p$$

$$I + CH_3I \underset{k_2}{\overset{k_1}{\rightleftharpoons}} I_2 + CH_3$$

$$CH_3 + HI \underset{k_4}{\overset{k_3}{\rightleftharpoons}} CH_4 + I$$
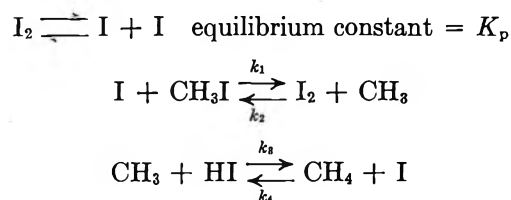
We have found that it is possible to establish this equi-

librium at somewhat higher temperatures over periods ranging from 3 days to a few hours (depending on temperature) by heating together I_2 and CH_4. Also, over a restricted temperature range, we have been able to determine the Arrhenius parameters of the rate-determining step k_4.

Experimental

All experiments were carried out by sealing up known quantities of CH_4 and I_2 in a 300-ml. Pyrex flask. The

(1) M. C. Flowers and S. W. Benson, *J. Chem. Phys.*, 38, 882 (1963).

whole flask, up to and including the break-seal, was heated in an electric furnace. The temperature, which was constant to ±1° over the volume of the vessel, was determined using a thermocouple calibrated at the melting point of lead (600.5°K.). Each experiment was terminated by breaking the seal and pumping the hot gases into a liquid nitrogen trap containing solid ICN. (This converts the HI quantitatively[2] into HCN, which is less likely to be lost by reaction with tap grease or metal parts of the gas chromatograph, and which, incidentally, is easier to resolve from CH_3I with simple column packings.) The fraction containing the CH_3I and the HCN was collected from this trap and analyzed using a gas chromatograph with thermistor detectors. Almost any column packing is satisfactory.

In the kinetic runs, reaction was never taken more than 10% of the way toward equilibrium, and, to minimize the error in timing due to heating up the flask, the following modified procedure was adopted. The flask containing the reactants was brought to temperature equilibrium in a subsidiary furnace at 550°K. and then moved into the reaction furnace. The reaction was terminated in the normal way. Experiments using a dummy flask containing unshielded thermocouples suggest that the uncertainty in the reaction time is about ±2 min., which is negligible compared with the reaction times used (3–55 hr.).

Equilibrium Measurements. Two series of experiments were performed. The first series (A) of 10 runs was carried out at or about 630°K. using wide variations in I_2 and CH_4 concentrations (over a factor of 20 in each case), in order to establish that the equilibrium really was of the form

$$CH_4 + I_2 \rightleftharpoons CH_3I + HI$$

The concentrations of both CH_3I and HI (*i.e.*, HCN) produced were checked, but the calculated equilibrium constants are based on CH_3I formation as being the more reliable. A second series (B) of 9 runs was then carried out over the range of temperature 585–748°K., a typical run having initially about 2.5 cm. pressure of CH_4 and about 0.25 g. of I_2. The results of these experiments are tabulated in Table I, and a least-squares plot of log K_T vs. $1/RT$ has a slope of 12.67 ± 0.20 kcal./mole, with an intercept of 0.759.

The Heat of Formation of Methyl Iodide

Earlier thermochemical determinations of the heat of formation of CH_3I have been discussed in detail by Hartley, Pritchard, and Skinner[3] and by Carson, Carter, and Pedley,[4] but it has so far not proved possible to select a very precise value for this quantity.

Table I: The Equilibrium $CH_4 + I_2 \rightleftharpoons CH_3I + HI$

T, °K.	Log K_T	$\Delta[-(F°_T - H°_{298})/T]$, cal. mole^{-1} deg.$^{-1}$	$\Delta H°_{298}$, cal. mole^{-1}
748	−2.9455	3.480	12,685
732	−3.0267	3.468	12,677
717	−3.0871	3.457	12,607
708	−3.1588	3.451	12,677
688	−3.2595	3.436	12,626
620	−3.7300	3.387	12,682
616	−3.7110	3.385	12,545
607	−3.8063	3.378	12,623
585	−3.9688	3.364	12,592
		Av.	12,635

The free energy function $-(F°_T - H°_{298})/T$ is tabulated in the "JANAF Tables"[5] for the molecules CH_4, I_2, and HI. The free energy function for CH_3I was calculated according to the same formulas, using the vibration frequencies given by Herzberg[6] and the internuclear separations given in ref. 7. It was found that the change in free energy function in the reaction was precisely linear over the temperature range 600–800°K., making interpolation of $\Delta[-(F°_T - H°_{298})/T]$ at the experimental temperatures a trivial matter. Table I lists the interpolated values for each run, together with the derived value of

$$\Delta H°_{298} = -RT \ln K_T + T\Delta[-(F°_T - H°_{298})/T]$$

for the reaction. The result is that $\Delta H°_{298} = 12.64 \pm 0.05$ kcal./mole, where the limits quoted include eight of the nine results. (The results of all 19 determinations, *i.e.*, series A and B, taken together also give 12.64 kcal./mole but with a somewhat larger spread.)

In the "JANAF Tables," thermodynamic functions for diatomics are calculated including vibrational anharmonicity, but for polyatomic molecules it is neglected. Comparing the molecules CH_4 and CH_3I, the neglect of anharmonicity is unlikely to cancel, and the calculations shown in Table I were repeated assuming that the two lowest frequencies ν_3 and ν_6

(2) C. A. Goy, D. H. Shaw, and H. O. Pritchard, *J. Phys. Chem.*, **69**, 1504 (1965).

(3) K. Hartley, H. O. Pritchard, and H. A. Skinner, *Trans. Faraday Soc.*, **46**, 1019 (1950).

(4) A. S. Carson, W. Carter, and J. B. Pedley, *Proc. Roy. Soc.* (London), **A260**, 550 (1961).

(5) "JANAF Interim Thermochemical Tables," Dow Chemical Co., Midland, Mich.

(6) G. Herzberg, "Infrared and Raman Spectra," D. Van Nostrand Co., Inc., New York, N. Y., 1945.

(7) S. L. Miller, L. C. Aamodt, G. Dousmanis, and C. H. Townes, *J. Chem. Phys.*, **20**, 1112 (1952).
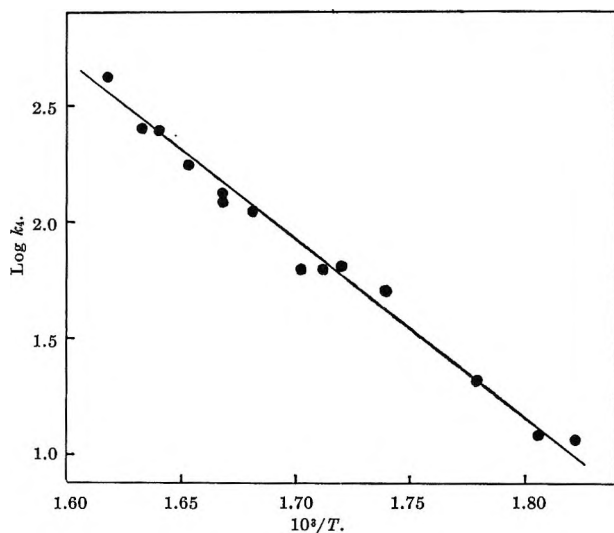
Figure 1.   Arrhenius plot for the
reaction I + CH$_4$ → HI + CH$_3$.

in CH$_3$I had values of $\omega_e x_e$ = 5 cm.$^{-1}$. This is likely
to be an overestimate, but the resulting correction
is only 30 cal./mole, giving ΔH°_{298} = 12.67 ± 0.05
kcal./mole.[8] We therefore obtain the heat of forma-
tion of gaseous CH$_3$I as $\Delta H_f^\circ_{298}$ = 3.40 ± (0.05 + x)
kcal./mole, where ±x is the uncertainty in the heats
of formation of CH$_4$, I$_2$(g), and HI, as given in the
"JANAF Tables."

Kinetic Measurements

The rate of formation of CH$_3$I in the temperature
range 548–618°K. was found to be half order in I$_2$
and first order in CH$_4$, consistent with the mechanism

$$I_2 \rightleftharpoons I + I$$

$$I + CH_4 \longrightarrow HI + CH_3 \quad (4)$$

$$CH_3 + I_2 \longrightarrow CH_3I + I \quad (2)$$
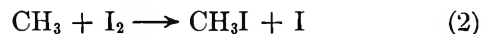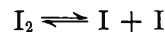
using the same numbering as Flowers and Benson.
The over-all activation energy for the formation of
CH$_3$I is 53.2 ± 1.1 kcal./mole, and, making use of
interpolated values of log K_p for the dissociation I$_2$ $\rightleftharpoons$
2I from the "JANAF Tables," one gets the rate con-
stant for reaction 4, the rate-determining step. The
values of k_4 obtained in 14 experiments are plotted in
Arrhenius form in Figure 1, and a least-squares fit to
these points gives log A = 14.95 (cc. mole^{-1} sec.$^{-1}$
units) and E = 35.04 ± 1.1 kcal/mole.

Flowers and Benson determined Arrhenius param-
eters for k_1 and k_3/k_2 in their kinetic experiments.
According to their reaction scheme, the K_T which we
have determined is related to their rate constants by
the expression K_T = k_4k_2/k_3k_1, giving k_4 = 10$^{14.7}$ exp
[(−34.1 ± 1.5)10^3/RT] cc. mole^{-1} sec.$^{-1}$, in good
agreement with our direct value. We therefore con-
firm their conclusion that the frequency factor A_4 for
this reaction is higher than the conventional collision
number.

Acknowledgment. We wish to thank Dr. G. Pilcher
for several very helpful discussions.

(8) The agreement between this value and the slope of the van't
Hoff plot is fortuitous since correction to T = 298°K. via the ap-
propriate values of H°_T − H°_{298} leads to a resultant slope of 12.37
kcal./mole.

Electron Diffraction Study of the Structure and Conformational Behavior of

Cyclopropyl Methyl Ketone and Cyclopropanecarboxylic Acid Chloride[1a]

by L. S. Bartell,[1b] J. P. Guillory, and Andrea T. Parks

Institute for Atomic Research and Department of Chemistry, Iowa State University, Ames, Iowa
(Received March 26, 1965)

The $-COCH_3$ and $-COCl$ derivatives of cyclopropane were found to exist in conformations similar to those previously reported for C_3H_5-CHO. *cis* and *trans* rotational isomers were observed rather than the *trans* and *gauche* isomers characteristic of noncyclic carbonyl derivatives. The dominance of the twofold over the threefold contribution to the barrier potential seems most easily interpreted in terms of a π-electron conjugative effect. Steric interactions in $C_3H_5COCH_3$ and C_3H_5COCl made the *trans* isomers relatively less stable than in C_3H_5CHO. Bond lengths, bond angles, and amplitudes of molecular vibration were also determined for the molecules.

Introduction

In a recent electron diffraction investigation of cyclopropylcarboxaldehyde it was discovered that the molecule exhibits a novel conformational behavior.[2] Unlike unstrained alkyl carboxaldehydes in which the rotation of the CHO group is governed by a (nominally) threefold barrier to internal rotation,[3-5] the cyclopropyl derivative is characterized by a twofold barrier. The theory of restricted rotation about single bonds is, as yet, unsettled but the simplest model which accounts for the *cis–trans* isomerization observed in the cyclic aldehyde is Walsh's π-electron model.[6] Cyclopropylcarboxaldehyde, viewed in this light, is an analog of butadiene or acrolein. It seemed desirable to study further examples of molecules with the formula of C_3H_5COX to determine whether the behavior of the aldehyde was representative. The present paper reports the results of an investigation of the methyl ketone (X = CH_3) and the acid chloride (X = Cl).

Experimental Procedure

Samples of cyclopropyl methyl ketone and cyclopropanecarboxylic acid chloride obtained from the Aldrich Chemical Co. were further purified by fractional distillation. The level of impurities detected by gas phase chromatography was less than 1.5%.

Electron diffraction photographs were taken at room temperature with the diffraction unit at Iowa State University employing an r^3 sector and an accelerating voltage of 40 kv. Specimen pressures of 30 and 14 torr were used for the ketone and acid chloride, respectively. The corresponding exposure times for a beam of 0.6 μa. were 5.5 and 2.7 sec. for the 21-cm. camera distances and 14.0 and 9.5 sec. for the 11-cm. camera distances. Diffraction patterns were recorded on 4 × 5 in. Kodak process plates.

Intensities of the patterns were determined by measuring the absorbancies of four selected plates for each camera distance. Measurements were made with a considerably modified Sinclair Smith microphotometer equipped to give a digital output.

Structure Analyses

The data were processed and analyzed using an IBM 7074 digital computer and a method fully described elsewhere.[7] Leveled experimental intensity and background curves for the molecules are shown in Figures

(1) (a) Contribution No. 1671. Work was performed in the Ames Laboratory of the U. S. Atomic Energy Commission; (b) to whom correspondence concerning reprints should be addressed: Department of Chemistry, University of Michigan, Ann Arbor, Mich.

(2) L. S. Bartell and J. P. Guillory, *J. Chem. Phys.*, **43**, 647 (1965).

(3) J. P. Guillory and L. S. Bartell, *ibid.*, **43**, 654 (1965).

(4) R. W. Kilb, C. C. Lin, and E. B. Wilson, Jr., *ibid.*, **26**, 1695 (1957).

(5) C. C. Lin and J. D. Swalen, *Rev. Mod. Phys.*, **31**, 841 (1959).

(6) A. D. Walsh, *Nature*, **159**, 167, 712 (1947); *Trans. Faraday Soc.*, **45**, 179 (1949).

1 and 2. Indices of resolution were unity to within experimental error.

Experimental radial distribution functions, $f(r)$, were calculated using a theoretical intensity function from $q = 0$ to $q = 14$ and experimental intensity data from $q = 15$ to $q = 120$. In all comparisons of experimental and synthetic $f(r)$ curves, the theoretical contribution to $f(r)_{expt1}$ is consistent with the synthetic function.

Conformational analyses were made by comparing the experimental radial distribution curves with synthetic curves constructed for various distributions of rotational isomers. For both molecules the presumably continuous isomeric distribution in the angle θ of internal rotation (reckoned from the cis configuration) was represented by a small set of discrete conformers.
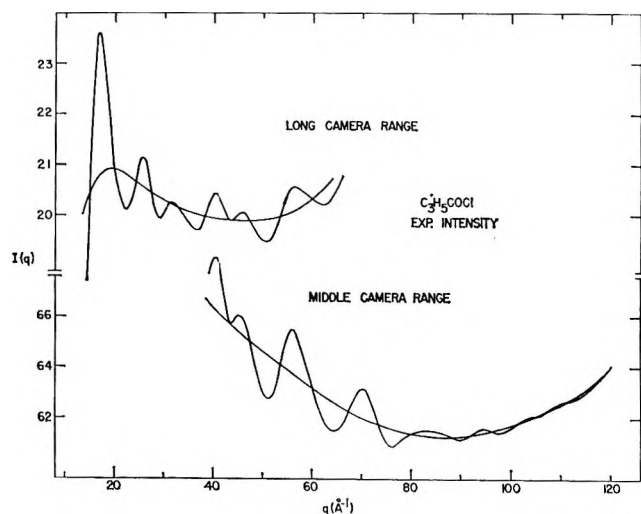
Figure 1. Experimental intensity and background curves for cyclopropyl methyl ketone.
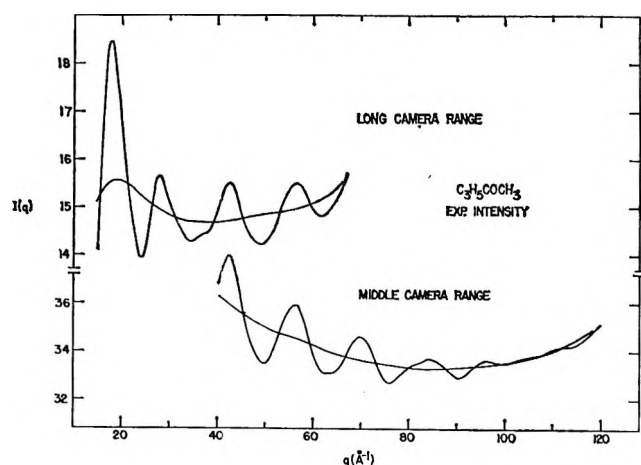
Figure 2. Experimental intensity and background curves for cyclopropanecarboxylic acid chloride.

In addition, simplifying assumptions about the ring parameters and the dependency of bond lengths and angles on θ were made as described in ref. 1 to facilitate the analyses. These assumptions are believed to influence the reported parameters and conformational characteristics by less than the reported uncertainties.

Cyclopropyl Methyl Ketone. The set of isomers chosen to represent the equilibrium distribution of the methyl ketone included s-cis ($\theta = 0°$), both "rigid" and "distorted" trans ($\theta = 180°$), two gauche-like models ($\theta = \pm 33°$ and $\pm 60°$), and an antigauche or twisted trans model ($\theta - 180° = \pm 30°$). These conformers are pictured in Figure 3.

The experimental radial distribution curve for C_3H_5-$COCH_3$ is shown in Figure 4. Bond distances, bond angles, and amplitudes of vibration determined from a least-squares analysis of this curve are reported in Table I.
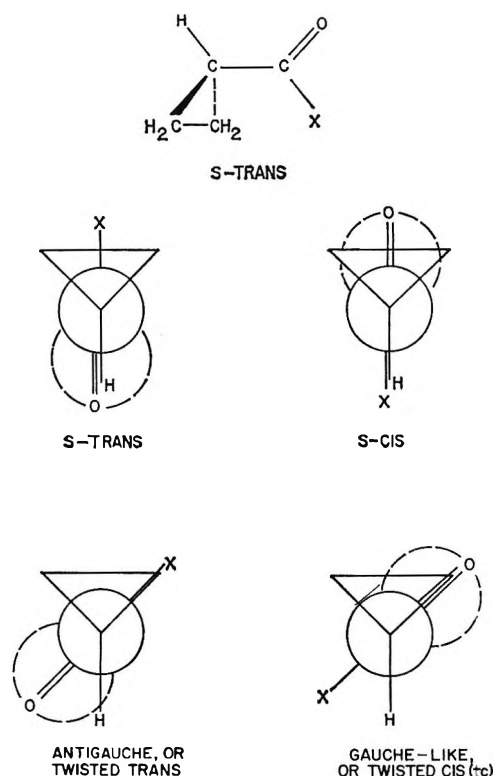
Figure 3. Molecular configurations investigated for cyclopropane deviatives. X represents a methyl group or a chlorine atom. The dashed lines in the Newman diagrams indicate the projections of double bonds to the oxygen atoms if they are regarded as two bent single bonds (cf. Pauling, ref. 11). Bonds are staggered in trans and gauche conformations, eclipsed in cis and antigauche.

(7) L. S. Bartell, L. O. Brockway, and R. Schwendeman, *J. Chem. Phys.*, 23, 1854 (1955); R. A. Bonham and L. S. Bartell, *ibid.*, 31, 702 (1959); *J. Am. Chem. Soc.*, 81, 3491 (1959).
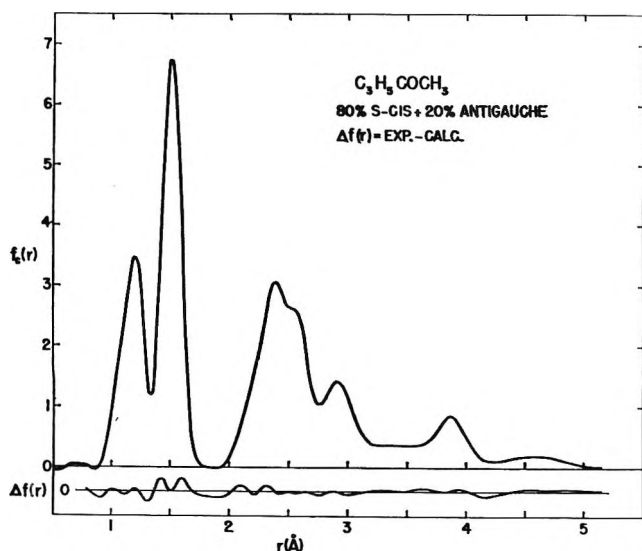
Figure 4. Experimental radial distribution curve for $C_3H_5COCH_3$. The lower curve is a plot of the difference between the experimental and calculated f(r) curves.

Table I: Structural Parameters and Approximate Standard Errors Derived from Radial Distribution Analyses (in Å. Units)

Molecule	Distance	r_g	$\sigma(r)$	$l_g{}^a$	$\sigma(l)$
$C_3H_5COCH_3$	CH	1.126	0.050[b]	0.074[c]	0.050[b]
	CC_{av}	1.510	0.003	0.048	0.003
	CO	1.225	0.020[b]	0.049	0.020[b]
	$C\cdots C_{av}$	2.556	0.020	0.048	0.030

$\angle CCO_{av}{}^d = 121.8 \pm 2°$, $\angle CCH_{av}{}^d = 117.2 \pm 3°$
% cis-like $= 80 \pm 15$; % trans-like $= 20 \pm 15$

Molecule	Distance	r_g	$\sigma(r)$	$l_g{}^a$	$\sigma(l)$
C_3H_5COCl	CH	1.105	0.060[b]	0.080[c]	0.060[b]
	CC_{av}	1.506	0.002	0.049	0.002
	CO	1.197	0.025[b]	0.039	0.025[b]
	CCl	1.797	0.009	0.064[c]	0.009

$\angle CCO^d = 127.6 \pm 3°$, $\angle CCH_{av}{}^d = 120.7 \pm 4°$
$\angle CCCl^d = 111° \pm 2.5°$, $\angle OCCl^d = 122.4 \pm 2°$
% cis-like $= 85 \pm 15$; % trans-like $= 15 \pm 15$

[a] Amplitude of vibration as reckoned from r_g. [b] Standard errors for these poorly resolved peaks calculated using the method discussed by L. S. Bartell and B. L. Carroll, J. Chem. Phys., 42, 1135 (1965). [c] Amplitudes corrected for failure of Born approximation. [d] Angles correspond essentially to s-cis isomers. Not corrected for shrinkage effect.

At an early stage of the analysis it was apparent that the molecules were predominantly in the s-cis configuration. Preliminary $f(r)_{exptl}$ curves displayed peaks at 2.90 and 3.85 Å., the positions and areas of which corresponded closely to those expected for a pure s-cis model. These peaks can be ascribed to cis $O\cdots C_R$ and $C_M\cdots C_R$ distances (where the subscripts R and M

refer to the ring and methyl group atoms, respectively). The longest $O\cdots C_R$ and shortest $C_M\cdots C_R$ distances would be expected to be approximately 3.4 Å. for a gauche conformer. The absence of a distinct peak in the 3.4-Å. region of the f(r) curve indicated that few gauche isomers were present.

Many different isomeric combinations were used in computing synthetic radial distribution curves. Five of the more significant combinations are shown in Figure 5 for the $r = 2.6$ to 5.2-Å. region. A comparison of experimental and calculated curves for the s-trans model indicates that this isomer cannot be present in large concentrations.

A problem arose in treating the s-trans isomer. For the sake of discussion, let us denote as "rigid" the trans model constructed by adopting the bond lengths and angles determined from an analysis of the (preponderantly cis) experimental f(r). This "rigid" trans model has perfectly normal bond lengths and angles but it is found to place its ring and methyl hydrogen atoms 0.4 Å. closer together than the normal 2.4-Å. van der Waals diameter.[8] In view of the likelihood that the trans configuration would spontaneously deform its bond angles to reduce this steric stress, an alternative trans model was constructed. In this "distorted" trans conformer, the $C_R-C_O-C_M$ and $C_R-C_R-C_O$ angles are opened to increase the $H_R\cdots H_M$ distance to 2.3 Å.

Standard deviations between the synthetic and the corresponding experimental f(r) curves were calculated for a variety of concentrations of s-cis, "rigid" trans, "distorted" trans, gauche, and antigauche isomers. Graphical methods yielded a composition of 80% s-cis and 20% antigauche for the minimum standard deviation. A slightly poorer fit was obtained for the 80% s-cis, 10% "distorted" trans, and 10% antigauche combination. The standard deviation associated with an 80% s-cis and 20% "distorted" trans model was at the outer limit of acceptibility. It may be concluded, therefore, that the equilibrium composition of C_3H_5-COCH₃ consists of approximately 80% s-cis conformers and 20% of forms in the general vicinity of the trans isomer. There is very weak evidence that the isomeric distribution in θ about the nominally trans form is broader for the ketone than it is in the case of the corresponding aldehyde. The standard error in concentrations is appreciable, being, perhaps, $\pm 15\%$.

Cyclopropanecarboxylic Acid Chloride. The experimental radial distribution curve for C_3H_5COCl is plotted in Figure 6. From the prominence of the 4.0-Å. peak, it is evident that a majority of the molecules

(8) L. Pauling, "The Nature of the Chemical Bond," 3rd Ed., Cornell University Press, Ithaca, N. Y., 1960, p. 260.
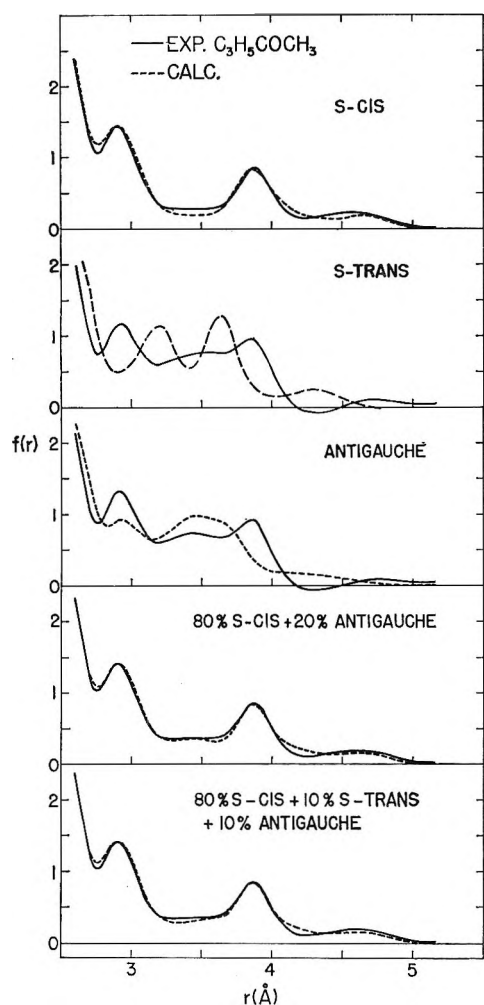
Figure 5. Experimental and calculated radial distribution
curves for various assumed isomeric concentrations
of cyclopropyl methyl ketone.

Figure 6. Experimental radial distribution curve for
C_3H_5COCl. The lower curve is a plot of the difference
between the experimental and calculated $f(r)$ curves.

exist in *s-cis* or *cis*-like forms. The isomeric set chosen
for analyses included the models *s-cis* ($\theta = 0°$), twisted-
cis, *tc*($\theta = \pm 15°$), *tc*($\theta = \pm 33°$), *tc*($\theta = \pm 60°$), and
s-trans ($\theta = 180°$). The *s-trans* form adopted repre-
sented a "distorted" configuration in the same sense
(and for the same reason) as the "distorted" *trans*
isomer of the methyl ketone. The C_R-C_O-Cl, and C_R-
C_R-C_O angles were increased from 110 and 118° to
114 and 121.5°, respectively, in order to increase to
2.73 Å. the otherwise unduly short $H_R \cdots Cl$ nonbonded
distance.

The $f(r)$ curve of Figure 6 was used to determine
mean bond lengths, angles, and amplitudes of vibration.
Least-squares results for the skeletal parameters cor-
responding essentially to *s-cis* isomers are reported in
Table I.

The C_R-C_O-Cl angle pertaining to the *cis*-like isomers

cannot be established independently of the distribution
in θ of the isomers. Accidental similarities between
the radial distribution for 33° *tc* isomers and (with
somewhat shifted peaks) for the average of *cis* and *trans*
isomers introduce into the diffraction analysis a de-
cided correlation between the C-C-Cl angle and the
distribution in θ. In an attempt to resolve this prob-
lem, the optimum distribution in θ was sought for each
of three models which differed in *s-cis* and *tc* C-C-Cl
bond angles. Bond angles of 110, 113, and 115° were
investigated since this range is representative of angles
in carbonyl compounds. In acetyl chloride, the closest
model available for comparison, the angle has been
reported to be 110° by electron diffraction[9] and 112°
by microwave spectroscopy.[10]

For each of the isomeric sets identified by its CCCl
angle, synthetic radial distribution curves with various
assumed concentrations of isomers were calculated for
comparison with $f(r)_{exptl}$. Examples of these curves are
shown in Figure 7 ($\angle CCCl = 110°$) and Figure 8
($\angle CCCl = 113°$) illustrating the region from 2.6 to 5.2 Å.
which is sensitive to conformational behavior. Re-
sults of minimizing the standard deviations between
observed and calculated $f(r)$ curves with respect to
isomeric concentrations are given in Table II. The
best fit corresponds to a value of 111° for $\angle CCCl$.
A rough idea of the breadth of the distribution in θ is
also derivable from the table.

(9) Y. Morino, K. Kuchitsu, M. Iwasaki, K. Arakawa, and A. Takahashi, *J. Chem. Soc. Japan*, 75, 647 (1954).
(10) K. M. Sinnott, *J. Chem. Phys.*, 34, 851 (1961).
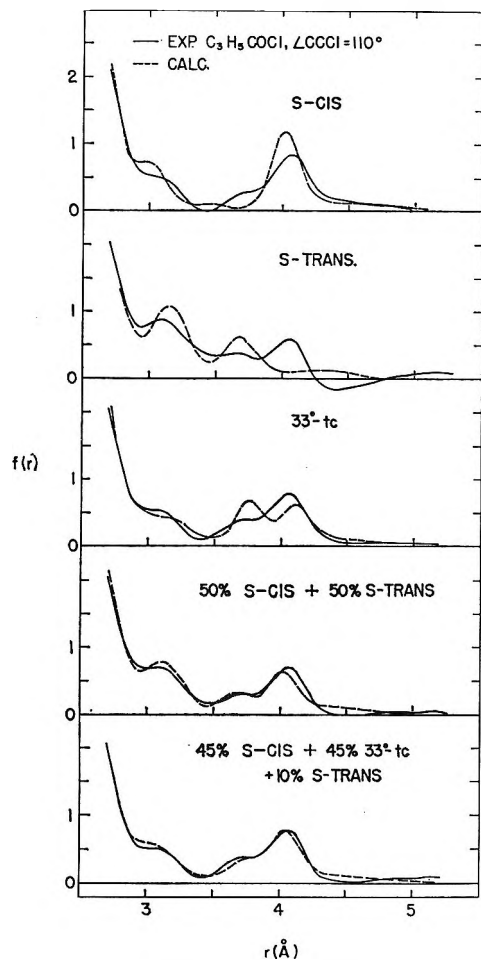
Figure 7.   Experimental and calculated radial
distribution curves for various assumed isomeric
concentrations of cyclopropanecarboxylic acid chloride;
∠CCCl taken to be 110°;   *tc* represents twisted *cis*.
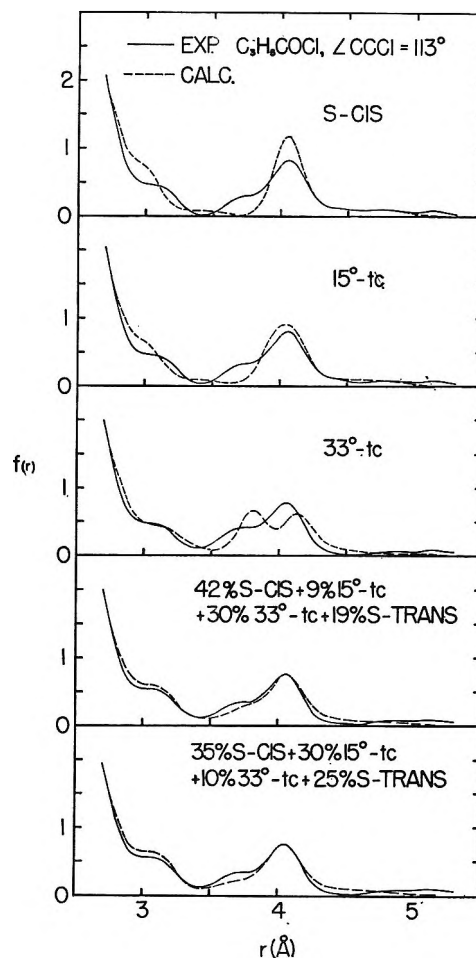
Figure 8.   Experimental and calculated radial distribution
curves for various assumed isomeric concentrations of
cyclopropanecarboxylic acid chloride;   ∠CCCl taken to be 113°.

Table II: Distribution in Angle of Internal Rotation for
C₃H₅COCl.   Results of Minimizing, with Respect to Isomeric
Concentrations, the Standard Deviation between Observed and
Calculated Radial Distribution Curves

θ for isomer	Isomeric concentrations for assumed ∠CCCl				
	110°ᵃ	110°ᵇ	113°ᵇ	113°ᶜ	115°ᵇ
0°	45%	35%	42%	35%	3%
±15°	. . .	15%	9%	15%	47%
±33°	45%	40%	30%	10%	16%
±60°	. . .	5%	0%	0%	6%
180°	10%	5%	19%	25%	27%
σ(f)ᵈ	. . .	0.050	0.060	0.063	0.098

ᵃ Analytical minimization of σ(f) for set of three discrete iso-
mers.   ᵇ Analytical minimization of σ(f) for set of five discrete
isomers.   ᶜ Distribution giving nearly as small σ(f) as the opti-
mum distribution.   ᵈ Root-mean-square deviation between ob-
served and calculated radial distribution curves from 2.6 to
5.2 Å.

Discussion

The principal conclusion derived from this research
is that the -COCH₃ and -COCl derivatives of cyclo-
propane exhibit *s-cis* isomerization just as did the
carboxaldehyde reported earlier. The barrier to in-
ternal rotation cannot be understood on the basis of the
interpretation advanced by Pauling for R-CHO and
related compounds.[11]   Molecules following Pauling's
scheme preferentially *stagger* their bent bonds at oppo-
site ends of the central C-C bond.   In the present
molecules, the bonds for *s-cis* are *eclipsed*.   A π-
electron picture in which a conjugative interaction
stabilizes *cis* and *trans* isomers provides perhaps the
simplest rationalization of the observed behavior.[6]
It also accounts for effects found in ultraviolet spectra
of related molecules.[12]   It would seem, however,

(11) L. Pauling, ref. 8, pp. 140-142.

that a conjugative interaction is not needed to account for the length of the central C–C bond,[13] as discussed in ref. 2.

Although the conformational behavior of the methyl ketone and acid chloride resembles that encountered in the aldehyde, there are pronounced differences. For the aldehyde, nearly equal concentrations of s-cis and s-trans isomers were observed. By contrast, quite low concentrations of trans isomers were found for the methyl ketone and acid chloride derivatives which have bulkier groups to be accommodated. The reason for the difference is undoubtedly steric. As discussed in the foregoing, the methyl and chloride groups have insufficient clearances unless several bond angles are strained open. The clearances in the trans-methyl ketone resemble those in gauche n-alkanes,[14] and the conformational free energy difference reported for the alkanes is quite sufficient to account for the present observations.

For cyclopropylcarboxaldehyde, a barrier to rotation in excess of 2.5 kcal./mole was found. A barrier of this magnitude implies a root-mean-square amplitude of oscillation of the cis form of 20° or less from the $\theta = 0°$ configuration. The methyl ketone data are consistent with such an amplitude. In the case of the acid chloride, however, a rather insidious pitfall was encountered which nearly led to a (probably) false conclusion. Since the example provides a good illustration of the danger in relying upon automated programs of analysis, it is perhaps worth discussing briefly.

In initial analyses of the acid chloride distribution in θ, a value of 110° for $\angle$ CCCl was adopted, corresponding to the angle reported in an electron diffraction study of CH_3COCl.[9] The resulting distribution, listed in Table II, appears to be materially broader and flatter than the corresponding distributions in the aldehyde and ketone. As discussed in the preceding section, this seems to be an artifact of a correlation between assumed values for the C–C–Cl angle and the distribution. At first glance the broadening toward gauche-like forms appears like a physically plausible result stemming

from the $H_R \cdots Cl$ cis nonbonded distance. The $H_R \cdots Cl$ distance associated with a value of 110° for $\angle$ CCCl is abnormally short and would lead to warping of the molecule out of cis planarity. When the $\angle$ CCCl is opened, however, the derived distribution approaches that of the aldehyde—and, simultaneously, the "physical" basis for a broad, flat distribution vanishes because the implied $H_R \cdots Cl$ distance increases. It seems more pleasing, subjectively, to accept the latter analysis with the larger C–C–Cl angle and narrower distribution in θ similar to that for the aldehyde and ketone, though the diffraction data do not firmly discriminate between the alternatives. The deceptive aspect is the fortuitous self-consistency of the physical and analytical implications of both alternatives.

Finally, it is interesting to note that Hoffmann has made calculations, based on his extended Hückel MO scheme, of the potential energy for internal rotation of the methyl ketone.[15] He correctly predicted, before the electron diffraction results were made known, that the barrier function has minima in the vicinity of cis and trans rather than trans and gauche, and that the cis isomer is more stable than the trans. The predicted energy difference between cis and trans, which was uncorrected for molecular deformation to relieve steric stresses, was roughly within a factor of 2 of that crudely determined by electron diffraction. The above agreement, together with Hoffmann's earlier qualitative success in the case of cyclopropyl carboxaldehyde,[2] is quite pleasing. It suggests that the Hückel model captures, in a simple manner, a significant portion of the molecular physics involved.

(12) E. M. Kosower, Proc. Chem. Soc., 25 (1962); N. H. Cromwell and G. V. Hudson, J. Am. Chem. Soc., 75, 872 (1953).

(13) It can be calculated that this bond is about 1.49 Å. in length if the ring bonds in the derivatives are assumed to have the same length as in cyclopropane itself.

(14) L. S. Bartell and D. A. Kohl, J. Chem. Phys., 39, 3097 (1963).

(15) R. Hoffmann, private communication, 1964.

Electrode Potentials in Acetonitrile.   Estimation of the Liquid Junction Potential

between Acetonitrile Solutions and the Aqueous Saturated Calomel Electrode[1]

by I. M. Kolthoff and F. G. Thomas

School of Chemistry, University of Minnesota, Minneapolis, Minnesota, 55455   *(Received March 26, 1965)*

Standard potentials in acetonitrile (AN) have been determined of the systems ferrocene–ferricinium picrate and tris(o-phenanthroline)iron(II)–(III) perchlorates, using a platinum indicator electrode and silver–0.01 M silver nitrate in AN as reference electrode.   Also, the standard hydrogen potential has been estimated from hydrogen electrode potentials in sulfuric acid–tetraethylammonium bisulfate mixtures in AN vs. the above reference electrode. Conductance measurements of various salts are reported.   Assuming that the tris(o-phenanthroline)iron(II)–(III) system has the same potential in water as in AN, we have derived the following values of standard potentials in AN vs. the standard hydrogen electrode in water $(E°_H)_{aq}$: tris(o-phenanthroline)iron(II)–(III) perchlorate, 1.120 v.; ferrocene–ferrocinium, 0.348 v.; $^1/_2H_2/H^+$, 0.30 v.; Ag/Ag^+, 0.40 v.   The liquid junction potential between a dilute solution in AN and the s.c.e. in water is of the order of 0.25 v. The solubility of ferrocene in water is 1.7×10^{-5} M.

Introduction

In polarographic studies in acetonitrile (AN) as solvent, the aqueous saturated calomel electrode (s.c.e.) has been used extensively as a reference electrode.[2-5] Although the use of the s.c.e. as a reference electrode in voltammetric studies in AN gives reproducible results, it nevertheless has the disadvantage of introducing an unknown liquid junction potential (E_{1j}) into the measurements.   An exact comparison of electrode potentials in various solvents forever will be impossible because of the unknown liquid junction potential.   By application of extra-thermodynamic considerations, efforts have been made in the literature to find a system the electrode potential of which is the same in various solvents, at the same activities of the constituents of the system, relative to the normal hydrogen electrode in water.   The e.m.f. of such a system in two different solvents would be equal to E_{1j}.   Pleskov[6,7] proposed the standard potential of the Rb–Rb$^+$ electrode, $(E°_{Rb})_s$ vs. $(E°_H)_{aq}$, as an absolute constant in all solvents since the rubidium ion is large with a charge of one and is only slightly polarizable.   Thus the electrostatic interaction between the rubidium ion and the solvent would be expected to be very similar in a variety of solvents and so the differences in the solva-

tion energies (and the differences in $(E°_{Rb})_s$) are expected to be negligible.   Strehlow[8,9] improved on the assumption of Pleskov[6,7] by calculating the solvation energies of the rubidium ion in various solvents from the concentrations of the saturated solutions of the alkali halides in the various solvents, making use of the method of Latimer, et al.[10]   Thus he was able to calculate the standard potential of the Rb–Rb$^+$ electrode in other solvents and relate the electrode

(1) Acknowledgment is made to the donors of the Petroleum Research Fund, administered by the American Chemical Society, for support of this research.

(2) I. M. Kolthoff and J. F. Coetzee, *J. Am. Chem. Soc.*, **79**, 870, 1852, 6110 (1957).

(3) J. F. Coetzee and G. R. Padmanabhan, *J. Phys. Chem.*, **66**, 1708 (1962).

(4) J. F. Coetzee, D. K. McGuire, and J. L. Hedrick, *ibid.*, **67**, 1814 (1963).

(5) I. M. Kolthoff and F. G. Thomas, *J. Electrochem. Soc.*, **111**, 1064 (1964).

(6) V. A. Pleskov, *Usp. Khim.*, **16**, 254 (1947).

(7) V. A. Pleskov, *Zh. Fiz. Khim.*, **22**, 351 (1948).

(8) H. Strehlow, *Z. Elektrochem.*, **56**, 827 (1952).

(9) H. M. Koepp, H. Wendt, and H. Strehlow, *ibid.*, **64**, 483 (1960).

(10) W. M. Latimer, K. S. Pitzer, and C. M. Slanski, *J. Chem. Phys.*, **7**, 108 (1939).

potential scales in these solvents to the standard hydrogen electrode in water, $(E°_H)_{aq}$.

Strehlow[9] further suggested that an oxidation–reduction system involving a metal complex, in which the multivalent metal ion is symmetrically surrounded by one or more large organic ligands, would be more suitable for interrelating the standard potentials in different solvents since the electric field at the periphery of such ions is much weaker than that of simple ions. Thus the differences in electrostatic interaction with the various solvents are minimized and the potentials at given activities of the constituents become less dependent on the solvent. Strehlow emphasized that the charges on the complex ions should be small and one of the species of the oxidation–reduction couple should preferably have zero charge. The couples suggested (ferrocene–ferricinium and cobaltocene–cobalticinium), however, were found to be influenced by the solvent and the difference in the standard electrode potentials for these couples in water and AN was calculated to be 0.06 v.,[8,9] the potential being more negative in AN than in water.

Ward[11] measured the potential of several cells of the type

$$Pt|MA_3^{2+}, Ma_3^{3+}||0.01 \ M \ AgNO_3|Ag$$
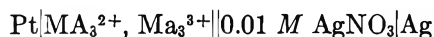
in AN, with M being iron or osmium and A being bipyridine, terpyridine, or o-phenanthroline. Assuming these oxidation–reduction couples have the same standard potentials in water and AN (relative to $(E°_H)_{aq}$), Ward calculated the potential of the silver–0.01 M silver nitrate reference electrode in AN to be 0.291 v. relative to $(E°_H)_{aq}$. Ward also measured the potentials of the cells

$$Pt|Os(Bipy)_3^{2+}, Os(Bipy)_3^{3+}||Os(Bipy)_3^{2+},$$
$$Os(Bipy)_3^{3+}|Pt$$

and

$$Ag|AgNO_3(0.01 \ M)(AN)||AgNO_3(0.01 \ M)(water)|Ag$$
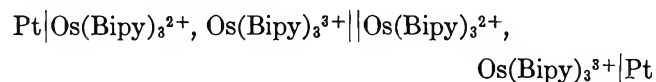
and was able to estimate the liquid junction potentials between these aqueous and AN solutions. These were found to be 0.225 and 0.269 v., respectively.

In the present work, the effect of ionic strength on the potentials of two of the oxidation–reduction couples studied by Ward,[11] ferrocene–ferricinium and tris(o-phenanthroline)iron(II)–tris(o-phenanthroline)iron(III), has been determined and the conductivity of solutions of the salts of the metal complexes has been measured in AN. The standard potential of the hydrogen electrode in AN, $(E°_H)_{AN}$, has also been estimated relative to $(E°_H)_{aq}$ using a platinum–hydrogen electrode in bisulfate–sulfuric acid buffer solutions in

AN. The potentials of all the electrodes studied in AN were also measured against the s.c.e. in order to estimate E_{1j}.

Experimental

Materials. Acetonitrile was purified by the method of Coetzee, *et al.*,[12] the final distillation being from phosphorus pentoxide under a nitrogen atmosphere (b.p. 80.9–81.0° at 746 mm.; specific conductivity 1.64 to 2.18 × 10⁻⁷ ohm⁻¹ cm.⁻¹ at 25°).

Tetraethylammonium perchlorate was prepared as described[2]; tetraethylammonium bisulfate and anhydrous sulfuric acid were obtained from Dr. M. K. Chantooni, Jr.[13]

Silver Nitrate. Analytical reagent grade material was dried at 120° under vacuum and stored over anhydrous magnesium perchlorate. Biscyclopentadienyliron(II)–ferrocene was Matheson Coleman and Bell commercial grade recrystallized from petroleum ether B, m.p. 174°. Biscyclopentadienyliron(III) picrate–ferricinium picrate was prepared by dissolving ferrocene (1 g.) and picric acid (1. 3 g.) in benzene (100 ml.) and adding benzoquinone (0.29 g.) dissolved in 75:25 benzene–ethyl alcohol mixture (50 ml.).[14] The resulting mixture was cooled in ice, the olive green solid filtered, and recrystallized from aqueous alcohol. An aqueous solution of the resulting orange-olive solid was analyzed spectrophotometrically and it was found that $[Fe(C_5H_5)_2^+] = [C_6H_2N_3O_7^-]$ within 2% with a total purity of 98 ± 2%. The product was used as such and stored over anhydrous calcium chloride. Tris(o-phenanthroline)iron(II) perchlorate was prepared as described,[15] recrystallized from acetone, and dried under vacuum at 150° to give the anhydrous salt[11] which was stored over anhydrous calcium chloride. Tris(o-phenanthroline)iron(III) perchlorate was prepared as described,[15] dried under vacuum at 150° to give the dihydrate,[11] and stored over anhydrous calcium chloride.

Hydrogen (Airco High Purity) was passed through a commercial Deoxo Catalytic Purifier, dried by passing through concentrated sulfuric acid and then through potassium hydroxide pellets, and finally saturated with

(11) W. Ward, Ph.D. Thesis, University of Iowa, 1958; W. E. Bennett and W. Ward, Abstracts of the 133rd National Meeting of the American Chemical Society, San Francisco, Calif., April 1958, p. 40L.

(12) J. F. Coetzee, G. P. Cunningham, D. K. McGuire, and G. R. Padmanabhan, *Anal. Chem.*, **34**, 1139 (1962).

(13) I. M. Kolthoff, S. Bruckenstein, and M. K. Chantooni, Jr., *J. Am. Chem. Soc.*, **83**, 3927 (1961).

(14) P. L. Pauson, *Quart. Rev.* (London), **9**, 391 (1955).

(15) F. P. Dwyer and H. A. McKenzie, *J. Proc. Roy. Soc. N.S.W.*, **81**, 93 (1947).
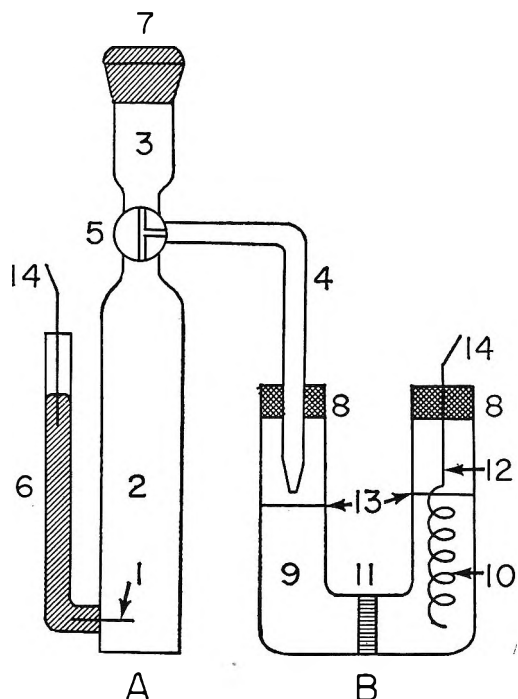
Figure 1. Half-cells used for potentiometric studies: A, reference half-cell; B, oxidation–reduction half-cell. Notes: 1. silver-plated platinum wire; 2. electrode compartment; 3. reservoir; 4. side arm; 5. three-way stopcock; 6. mercury contact; 7. ground-glass stopper; 8. polyethylene plugs; 9. intermediate compartment; 10. electrode compartment; 11. sinter disk; 12. platinum spiral electrode; 13. liquid level (slightly lower in the intermediate compartment); 14. connected to potentiometer.

AN vapor before bubbling over the platinized platinum electrode in the buffer solutions.

Cells. The reference cell (Figure 1) contained a platinum wire, electroplated with silver, sealed into the reference electrode compartment (2 in Figure 1) which was connected to a reservoir and side arm *via* a three-way stopcock. The three sections (2, 3, and 4) were filled with 0.1 M silver nitrate in AN. The reference electrode was protected from the atmosphere by ground-glass stoppers. Electrical connection to the silver electrode was made by means of a mercury contact. The oxidation–reduction half-cell consisted of an electrode and an intermediate compartment separated by a glass sinter. The solution under study was placed in both compartments. A bright platinum spiral electrode was placed in the electrode compartment through a polyethylene plug used to seal the compartment from the atmosphere. Electrical connection between the two half-cells was made by inserting the side arm of the reference half-cell into the solution in the intermediate compartment through a polyethylene plug.

The half-cell for the hydrogen electrode was similar to the oxidation–reduction half-cell with the following modifications: hydrogen, saturated with AN, was admitted to the electrode compartment *via* a glass sinter in the base; three heavily coated platinized platinum electrodes, prepared by the usual electrodeposition technique from hexachloroplatinic acid solution,[16] were used instead of the bright platinum spiral. The s.c.e. was prepared in the usual manner.[16] The conductivity cell had a cell constant of 0.0370 cm.$^{-1}$. The polarographic cell has been described previously.[17]

Instruments. A Leeds and Northrup Student potentiometer was used to measure all potentials to ±0.2 mv. and conductivity measurements were made with an a.c. resistance bridge to within ±1%. All current–potential curves were recorded on a Leeds and Northrup Electrochemograph Type E. The dropping mercury electrode (d.m.e.) employed had the following characteristics: $m^{2/3}t^{1/6} = 1.621$ mg.$^{2/3}$ sec.$^{-1/2}$, $t = 3.95$ sec., at zero applied voltage in 0.1 M tetraethylammonium perchlorate in AN with a mercury height of 53.7 cm. (cor.). The rotated platinum electrode (r.p.e.) consisted of a 1-cm. length of platinum wire sealed through glass and was rotated at 600 r.p.m.

Technique. All measurements were carried out at 25.00 ± 0.02°. When measuring potentials relative to the silver–0.01 M silver nitrate in AN electrode, electrical contact between the two half-cells *via* the side arm of the reference electrode was maintained only long enough for each individual potential to be measured; between measurements on a given solution, the side arm was raised above the level of the solution in the intermediate compartment. The potentials of the two oxidation–reduction couples studied were determined using approximately equimolar mixtures of the reduced and oxidized forms. The effect of ionic strength on the potentials was determined by varying the concentrations of the components of the oxidation–reduction couples and by adding an indifferent electrolyte (tetraethylammonium perchlorate). Potentials were measured at regular intervals up to 70 min. after mixing. In the case of the tris(o-phenanthroline)-iron(II)–tris(o-phenanthroline)iron(III) couple, the potential at zero time (time of mixing) was found by extrapolation.[11] In the case of the ferrocene–ferricinium couple the steady potential, attained 5 min. after standing in the cell, was recorded.

(16) D. J. G. Ives and G. J. Janz, "Reference Electrodes," Academic Press, New York, N. Y., 1961.

(17) L. A. Knecht and I. M. Kolthoff, *Inorg. Chem.*, 1, 195 (1962).

The potential of the hydrogen electrode in bisulfate–sulfuric acid mixtures in AN, with hydrogen passing through the solution, was found to reach a steady value within 3 min. at each of the three electrodes used and to remain constant for at least 25 min. before some drifting occurred. Potential measurements with the s.c.e. as reference electrode were carried out in a similar manner to those with the silver–0.01 M silver nitrate in AN reference electrode.

The current–potential curves of aqueous solutions of ferricinium picrate and of AN solutions of ferrocene were determined at the d.m.e. and the current–potential curves of aqueous solutions of these compounds were measured at the r.p.e.

Results

Conductivity Measurements. Tris(o-phenanthroline)-iron(II) Perchlorate. The conductivities of solutions of the anhydrous salt in AN in the concentration range 4.67×10^{-6} to 1.14×10^{-3} M were measured and plotted against the square root of the concentration, $C^{1/2}$, in Figure 2, curve A. The results are expressed by the relation $\Lambda_c = \Lambda_0 - 1410C^{1/2}$ and give a value of 191.9 ohm^{-1} cm.^{2} for Λ_0. Thus λ_0 for the tris(o-phenanthroline)iron(II) cation is 87.4 ohm^{-1} cm.^{2} $((\lambda_0)_{\text{ClO}_4^-} = 104.5$ ohm^{-1} cm.^{2} [18]$)$.

Tris(o-phenanthroline)iron(III) Perchlorate. Conductivities of solutions of the dihydrate in AN in the concentration range 8.09×10^{-6} to 1.26×10^{-3} M are plotted against $C^{1/2}$ in Figure 2, curve B. Two series of results were obtained. In series 1, transference of solutions from volumetric flasks to the conductance cell was done in the atmosphere, and with the more dilute solutions a color change from blue to reddish purple was observed, indicating that moisture from the atmosphere was causing decomposition of the tris(o-phenanthroline)iron(III) cation. When the measurements were repeated, series 2, using fresh solutions and doing all operations in a glove box filled with dry nitrogen, no color change was noticed with the dilute solutions for several hours and the plot of Λ_c vs. $C^{1/2}$ was found to remain linear down to the lowest concentrations studied. These results show that at concentrations greater than 10^{-4} M the small amount of moisture from the atmosphere has no appreciable effect on the conductivities of these solutions. However, on standing for several days, 1.0 mM solutions of tris(o-phenanthroline)iron(III) perchlorate became purplish in color, even when sealed from the atmosphere, indicating that the tris(o-phenanthroline)iron(III) cation is slowly decomposed in AN solutions. Because of this, all solutions of this ion were freshly prepared prior to any measurements (potentiometric
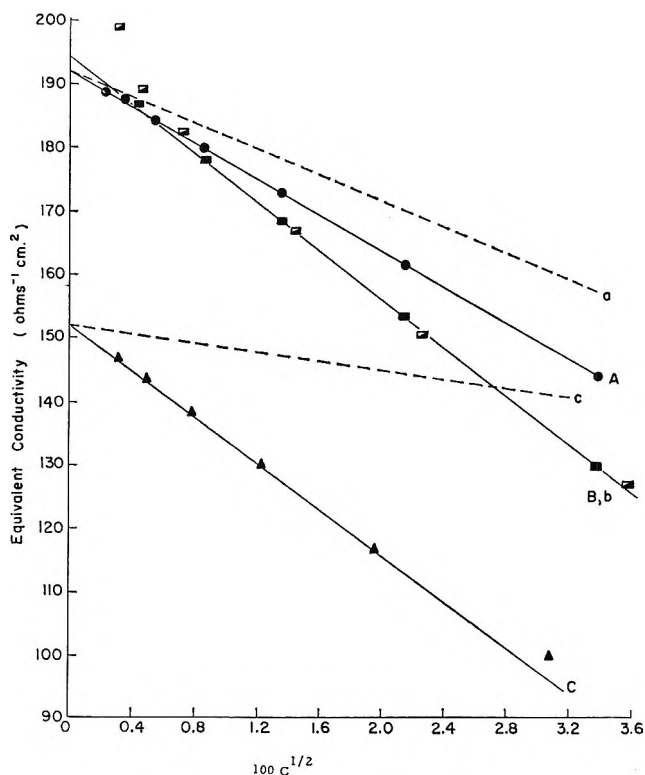
Figure 2. Conductivities in acetonitrile: A, tris(o-phenanthroline)iron(II) perchlorate, ●; B, tris(o-phenanthroline)iron(III) perchlorate dihydrate, ◪, series 1; ■, series 2; C, ferricinium picrate, ▲; a, b, and c, Onsager plots for A, B, and C, respectively.

or conductometric) being made. The results obey the relation $\Lambda_c = \Lambda_0 - 1920 C^{1/2}$ and give a value of 194.2 ohm^{-1} cm.^{2} for Λ_0; *i.e.*, λ_0 for the tris(o-phenanthroline)-iron(III) cation is 89.7 ohm^{-1} cm.^{2}.

Ferricinium Picrate. The conductivities of AN solutions of this salt are plotted against $C^{1/2}$ in Figure 2, curve C. The results are described by the relation $\Lambda_c = \Lambda_0 - 1820C^{1/2}$ and give a value of 152.1 ohm^{-1} cm.^{2} for Λ_0; *i.e.*, λ_0 for the ferricinium ion is 74.4 ohm^{-1} cm.^{2} $((\lambda_0)_{\text{C}_6\text{H}_2\text{N}_3\text{O}_7^-} = 77.7$ ohm^{-1} cm.^{2} [18]$)$.

Potential Measurements. (a) Using the Silver–0.01 M Silver Nitrate (in AN) Reference Electrode. Tris(o-phenanthroline)iron(II)–Tris(o-phenanthroline) iron-(III) Couple. The potentials developed by this couple at a bright platinum electrode, relative to that of the reference electrode $(E^{0.01}_{\text{Ag}})_{\text{AN}}$, at various ionic strengths were measured and used to calculate values of E' from the equation

$$E' = E_{\text{cell}} - 0.0591 \log [\text{Fe(phen)}_3{}^{3+}]/$$

$$[\text{Fe(phen)}_3{}^{2+}] \quad (1)$$

(18) P. Walden and E. J. Birr, *Z. physik. Chem.*, **144A**, 269 (1929).

i.e., E' is the standard potential of this couple at the given ionic strength, $I = \frac{1}{2}\Sigma C_i Z_i^2$ relative to $(E^{0.01}_{Ag})_{AN}$. E' is plotted as a function of the square root of the ionic strength, $I^{1/2}$, in Figure 3, curves A1 and A2, in the absence and presence, respectively, of tetraethylammonium perchlorate. Extrapolation of these plots to zero ionic strength gives a value of 0.8459 v. for the standard potential of this couple in AN (relative to $(E^{0.01}_{Ag})_{AN}$.

The Ferrocene–Ferricinium Couple. The potentials developed by this couple (at a bright platinum electrode) with respect to the silver–silver nitrate reference electrode were measured and used to calculate values of E'' at various ionic strengths from the relation

$$E'' = E_{cell} + 0.0591 \log a_{ferrocene}/a_{ferricinium^+} \quad (2)$$

E'' is plotted against the square root of the ionic strength in Figure 3, curves B1 and B2 (absence and presence of tetraethylammonium perchlorate, respectively). The extrapolation of curves B1 and B2 to zero ionic strength gives values of 0.0740 and 0.0738 v. for the standard potential of this couple *vs.* $(E^{0.01}_{Ag})_{AN}$, respectively.

The potentials of the hydrogen electrode in various nonaged bisulfate–sulfuric acid buffers *vs.* $(E^{0.01}_{Ag})_{AN}$ are listed in Table I together with the calculated values of the hydrogen ion concentration and mean ionic activities for the various solutions. The values of E''' for the five buffer solutions studied were calculated from the equation

$$E''' = E_{cell} - 0.0591 \log a_{H^+}/\{p_{H_2 \text{ (in atm.)}}\}^{1/2} \quad (3)$$

where p_{H_2} is the pressure of hydrogen at the platinized platinum electrode. The measured pressure was corrected for the vapor pressure of the solvent and the

Table I: E.m.f. of the Hydrogen Electrode in Bisulfate–Sulfuric Acid Buffers in AN *vs.* Silver–0.01 M Silver Nitrate Reference Electrode in AN

[(C₂H₅)₄- NHSO₄] added, mM	[H₂SO₄] added, mM	[H⁺], M × 10⁶	$f_\pm$	Ionic strength, I × 10⁴	p_{H_2}, mm.	E_{cell}, v.	E''', v.
0.204	5.1	0.848	0.948	0.208	662.8	−0.2600	0.0315
1.02	20.0	2.562	0.897	1.018	662.8	−0.2270	0.0385
2.04	20.0	1.323	0.865	1.954	646.0	−0.2365	0.0418
2.04	50.0	8.33	0.860	2.084	662.8	−0.1917	0.0437
2.04	84.2	22.65	0.856	2.238	662.8	−0.1645	0.0453

height of the solution above the electrode. Extrapolation to zero ionic strength gives a value of 0.030 v. for the standard potential of the hydrogen electrode in AN $(E^{0.01}_{Ag})_{AN}$. All the hydrogen potentials were

Figure 3. Effect of ionic strength on electrode potentials in acetonitrile: A1, Fe(phen)₃²⁺–Fe(phen)₃³⁺; A2, Fe(phen)₃²⁺–Fe(phen)₃³⁺ + Et₄NClO₄; B1, ferrocene–ferricinium; B2, ferrocene–ferricinium + Et₄NClO₄ using [ferricinium]; B3, as B2 using $a_{ferricinium}$.

measured at three different electrodes. Two of the electrodes, a and b, gave identical steady values for E_{cell} (recorded in Table I) while the third gave values between 0.5 and 1.0 mv. higher. It was noted that E_{cell} for the second buffer solution listed in Table I increased by 12 mv. on standing for 18 hr. This indicates that the proton activity slowly decreases on aging in agreement with previous observations on AN solutions which contain appreciable concentrations of solvated protons.[13] Because of this, all buffer solutions were prepared immediately before the potential measurements were made.

(b) *Using the S.c.e. as Reference Electrode.* The four half-cells used above were connected to an aqueous s.c.e. *via* a potassium nitrate–agar salt bridge and the potentials of the resulting cells are recorded in Table II.

Polarographic Studies. (a) *AN Solutions.* Ferrocene in AN gives well defined anodic waves at the d.m.e. in the concentration range 0.200 mM to 1.00 mM using 0.1 M tetraethylammonium perchlorate as supporting electrolyte. The plots of log $i/(i_d - i)$ *vs.* $E_{d.m.e.}$ (corrected for iR drop) for the five curves studied in this concentration range have a mean slope of 0.0585 ± 0.0006 v. which compares favorably with the theoretical slope of 0.0591 for a reversible, one-

Table II: Potential Measurements Using the S.c.e. as Reference Electrode

Half-cell (AN solutions)	E vs. s.c.e., v.
$Pt\|Fe(phen)_3{}^{2+}$ (1.881 × 10⁻⁴ M), $Fe(phen)_3{}^{3+}$ (1.882 × 10⁻⁴ M)	1.1155
$Pt\|Fe(phen)_3{}^{2+}$ (1.881 × 10⁻⁴ M), $Fe(phen)_3{}^{3+}$ (1.882 × 10⁻⁴ M), $(C_2H_5)_4NClO_4$ (0.1 M)	1.0350
$Pt\|Fe(C_5H_5)_2$ (1.871 × 10⁻⁴ M), $Fe(C_5H_5)_2{}^+$ (1.734 × 10⁻⁴ M)	0.3442
$Pt\|Fe(C_5H_5)_2$ (1.871 × 10⁻⁴ M), $Fe(C_5H_5)_2{}^+$ (1.734 × 10⁻⁴ M), $(C_2H_5)_4NClO_4$ (0.1 M)	0.3260
H_2 (646 mm.), $Pt\|(C_2H_5)_4NHSO_4$, H_2SO_4, H^+ (1.323 × 10⁻⁵ M)	0.0248
H_2 (646 mm.), $Pt\|(C_2H_5)_4NHSO_4$, H_2SO_4, H^+ (7.10 × 10⁻⁵ M), $(C_2H_5)_4NClO_4$ (0.0993 M)	0.0145
$Ag\|AgNO_3$ (0.01 M)	0.2725
$Ag\|AgNO_3$ (0.01 M), $(C_2H_5)_4NClO_4$ (0.10 M)	0.2588

Figure 4. Current–potential curves of ferrocene and ferricinium ion in water using the r.p.e.: A, 1.114 × 10⁻⁴ M ferricinium ion, 0.1 M tetraethylammonium perchlorate supporting electrolyte; B, saturated ferrocene solution, 0.083 M tetraethylammonium perchlorate supporting electrolyte; C, saturated ferrocene solution, 0.0204 M tetraethylammonium perchlorate supporting electrolyte.

electron oxidation. The mean value of the diffusion current constant, I_D, for these curves at 0.55 v. vs. s.c.e. is 3.99 ± 0.05 μa. mmole⁻¹ sec.$^{1/2}$ mg.$^{2/3}$ and $E_{1/2}$ is 0.379 ± 0.001 v. vs. s.c.e.

(b) *Aqueous Solutions*. The current–potential curve of an aqueous ferricinium solution (2 × 10⁻⁴ M) using the d.m.e. and 0.1 M tetraethylammonium perchlorate supporting electrolyte is well developed with $E_{1/2} = 0.147$ v. vs. s.c.e. However, the top portion of the wave is drawn out and a plot of $E_{d.m.e.}$ vs. log $(i_d - i)/i$ is only linear (slope 0.053) between $E_{d.m.e.}$ = 0.20 to 0.12 v. At more negative voltages the slope continuously increases to a value of 0.88 at 0.02 v. This indicates that at the foot of the wave a reversible one-electron reduction may_ occur but at potentials more negative than $E_{1/2}$ the reduction becomes irreversible. At higher concentrations of $Fe(C_5H_5)_2{}^+$ only the foot of the wave is observed, the current–potential curve passes through a maximum, and the current drops to a value smaller than the expected limiting current. This indicates that a film of the very slightly soluble ferrocene is formed on the drop which interferes with the reduction process. This is further indicated by the unusual shape of the instantaneous current–time curves for the individual drops at voltages more negative than that at which the maximum is observed on the current–potential curve.

Current–potential curves determined at the r.p.e. are shown in Figure 4 for: (a) 1.114 × 10⁻⁴ M $Fe(C_5H_5)_2{}^+$ in aqueous 0.1 M tetraethylammonium perchlorate solution (curve A); (b) saturated aqueous solutions of ferrocene with 0.083 M (curve B) and 0.0204 M (curve C) tetraethylammonium perchlorate as supporting electrolyte. The characteristics of these waves are

given in Table III. The slopes of the plots of log $(i_d - i)/i$ vs. $E_{r.p.e.}$ indicate that both the oxidation and reduction are reversible and involve a one-electron process with $E_{1/2}$ of 0.146 v. This is further supported by the observation that mixtures of these two species (ferrocene and ferricinium) yield composite current–potential curves at the r.p.e. which have $E_{1/2}$ values for the total wave of 0.145 to 0.146 v. in 0.1 M tetraethylammonium perchlorate supporting electrolyte. If it is assumed that in aqueous media the limiting currents at the r.p.e. of equimolar solutions of ferrocene and ferricinium are the same in the same supporting electrolyte, then it is possible to estimate the concentration of ferrocene in its saturated solution in aqueous 0.1 M tetraethylammonium perchlorate. From the data of Table III this is found to be (0.715/4.60) × 1.114 × 10⁻⁴ M = 1.7 × 10⁻⁵ M.

Discussion

The plots of $C^{1/2}$ vs. Λ_c for AN solutions of tris(o-phenanthroline)iron(II) perchlorate and tris(o-phenanthroline)iron(III) perchlorate (Figure 2, curves A and B) show these salts to be strong electrolytes which are highly dissociated at the concentrations used in the potentiometric studies. The Onsager relationships[19] for these salts were calculated to be:

(19) R. A. Robinson and R. H. Stokes, "Electrolyte Solutions," 2nd Ed., Butterworth and Co. Ltd., London, 1959.

Table III: Characteristics of Current–Potential Curves of Ferrocene and Ferricinium Ion in Water at the R.p.e. (Supporting Electrolyte Tetraethylammonium Perchlorate)

System	Supporting electrolyte concn., M	Electrode process	Limiting current, $\mu a.$	Slope of $E_{\text{r.p.e.}}$ $vs.$ log $(i_1 - i)/i$ plot	$E^1/_2$ (v. $vs.$ s.c.e.)
Ferricinium, $1.114 \times 10^{-4} M$	0.1	$Fe(C_5H_5)_2^+ + e \rightarrow Fe(C_2H_5)_2$	4.60	0.0615	0.145
Ferrocene (saturated)	0.083	$Fe(C_5H_5)_2 \rightarrow Fe(C_5H_5)_2^+ + e$	0.715	-0.0575	0.144
Ferrocene (saturated)	0.0204	$Fe(C_5H_5)_2 \rightarrow Fe(C_5H_5)_2^+ + e$	0.705	-0.058	0.148

$\Lambda_c = \Lambda_0 - 1020C^{1/2}$ for $Fe(phen)_3(ClO_4)_2$ and $\Lambda_c = \Lambda_0 - 1912C^{1/2}$ for $Fe(phen)_3(ClO_4)_3$ and are plotted in Figure 2, curves a and b, respectively. The latter is almost identical with the experimental plot (Figure 2, curve B). This agreement is rather fortuitous, especially at the higher concentrations, because of the limitations of the Onsager equation, particularly when applied to 3:1 electrolytes in solvents of only moderate dielectric strength (dielectric constant of AN $= 36.7$).[19] The conductivity results indicate that very little error will be introduced into the value of $E°$ for the tris(o-phenanthroline)iron(II)–tris(o-phenanthroline)iron(III) couple calculated on the basis of complete dissociation of the salts. Thus the values of E' (Figure 3, curve A1) give a reliable value of $E°$ (0.8459 v.) for this couple $vs.$ $(E^{0.01}_{Ag})_{AN}$, when extrapolated to zero ionic strength. Ward[11] gives a value of 0.831 v. for this cell at 30° and an ionic strength of 5.4×10^{-3}, in good agreement with our results. Regarding the effect of added tetraethylammonium perchlorate on the potential of this couple, the neutral salt added suppresses the dissociation of the iron(III) salt more than that of the iron(II) salt. Therefore, the potential of the system should become less positive (as is found). Also, there is the ionic strength effect which manifests itself in the same way as the salt effect on the dissociation.

On the other hand, ferricinium picrate appears to be only a moderately strong electrolyte in AN since the experimental results deviate appreciably from the Onsager plot (Figure 2, curve c for which $\Lambda_c = \Lambda_0 - 338\ C^{1/2}$), indicating that significant ion pair formation occurs. In order to allow for this in the calculation of the standard oxidation–reduction potential of the ferrocene–ferricinium couple, the activity of the ferricinium was calculated by multiplying the concentration of the salt by Λ_c/Λ_0. Values of Λ_c were interpolated from Figure 2, curve C for the concentrations of ferricinium picrate used in the potential measurements. Since the values of E'' calculated for this couple using these assumptions were practically constant for the three experiments in which no tetraethylammonium perchlorate was added (Figure 3,

curve B1), it is considered that the simple conductance ratio gives a reasonable value for the activity coefficient of the ferricinium ion and that the average of these three values of E'' (0.0740 v.) is a reliable value for $E°$ for this couple $vs.$ $(E^{0.01}_{Ag})_{AN}$. Ward[11] gives a value of 0.0716 v. for this couple at 30°. This is the average of several experiments in which the concentration of ferricinium picrate was 2.17 to 8.65 $\times 10^{-4} M$ and that of ferrocene was 5.0 to 6.71 $\times 10^{-4} M$. No corrections were made for the activity coefficients of the ferricinium ion in his work.

The concentrations of the solvated proton $[H^+]$ and the activity coefficients of the ions in the buffer solutions used to determine the standard potential of the hydrogen electrode in AN were calculated from the stoichiometry of the system and the relationships

$$K_{AHA^-} = \frac{[H_2SO_4HSO_4^-]}{[H_2SO_4][HSO_4^-]} = 1.03 \times 10^3 \quad (4)^{20}$$

$$K_{2(HA)} = \frac{[H^+][H_2SO_4HSO_4^-]f^2}{[H_2SO_4]^2} = 5.5 \times 10^{-5} \quad (5)^{13}$$

$$K_{d_1} = \frac{[(C_2H_5)_4N^+][HSO_4^-]f^2}{[(C_2H_5)_4NHSO_4]} = 1.4 \times 10^{-3} \quad (6)^{13}$$

and the Debye–Hückel expression

$$\log f = -\frac{1.594I^{1/2}}{1 + 0.48aI^{1/2}} \quad (7)$$

where I is the ionic strength and a is "the distance of closest approach" of the ions which has been taken as 5 Å. for all ions in this system. The activity coefficients of uncharged species and ion pairs were taken to be unity.

The standard potential E''' in Table I should be a constant. The deviation from constancy may be due in part to incorrectly approximated values of activity coefficients, in part to liquid junction potentials, and finally to abnormalities of the hydrogen electrode in solutions containing relatively high concentrations of sulfuric acid. With decreasing ionic strength the

(20) I. M. Kolthoff and M. K. Chantooni, Jr., *J. Phys. Chem.*, **66**, 1675 (1962).

liquid junction potential should become negligible because at a smaller ionic strength the ions present have about the same mobility. A value of $E''' = 0.030$ v. vs. $(E^{0.01}_{Ag})_{AN}$ is extrapolated.

The standard potentials of the three electrodes studied relative to $(E^{0.01}_{Ag})_{AN}$ are listed in Table IV, column 2 and relative to $(E^°_{Ag})_{AN}$ in column 3. The potentials of these electrode systems relative to the standard potential of the silver electrode in AN,

Table IV: Standard Electrode Potentials in AN at 25°

Electrode	$E^°$, v.			
	vs. $(E^{0.01}_{Ag})_{AN}$		vs. $(E^°_{Ag})_{AN}$	vs. $(E^°_H)_{aq}$
	This work	Ward's data[a]		
Pt|Fe(phen)$_3$²⁺, Fe(phen)$_3$³⁺	0.845$_9$	0.831	0.715$_8$	1.120
Pt|Fe(C₅H₅)$_2$, Fe(C₅H₅)$_2$⁺	0.074$_0$	0.0716	−0.056$_1$	0.348
Pt|H$_2$, H⁺	0.030	. . .	−0.100	0.304
Ag|Ag⁺	0.130$_1$[b]	0.1203[c]	0	0.404

[a] From ref. 11, at 30°; not corrected for ionic strength effects, activity coefficients all taken to be unity. [b] Calculated from the Nernst equation (see text). [c] Calculated from the Nernst equation, assuming $a_{Ag^+} = 0.01$ M.

$(E^°_{Ag})_{AN}$, were calculated from the potentials relative to $(E^{0.01}_{Ag})_{AN}$ and the Nernst equation assuming that the activity coefficient of the silver ion in 0.01 M silver nitrate in AN is given by the conductivity ratio $(\Lambda_{0.01}/\Lambda_0)_{AgNO_3}$ in AN. This assumption was made because the experimental plot of Λ_c vs. $C^{1/2}$ (from the data of Walden and Birr[18]) has a slope approximately twice that of the theoretical Onsager plot, indicating that silver nitrate is only a moderately strong electrolyte in AN (similar to ferricinium picrate). The value of $\Lambda_{0.01}/\Lambda_0$ for 0.01 M silver nitrate in AN is estimated to be 0.63 from the results of Walden and Birr.[18] The use of the conductivity ratio to obtain the silver ion activity, a_{Ag^+}, is considered to result in a better value for $(E^°_{Ag})_{AN}$ than that obtained using the concentration of silver, uncorrected for ionic strength and ion-pair effects, and the value 0.130 v. vs. $(E^{0.01}_{Ag})_{AN}$ (Table IV) obtained using a_{Ag^+} should not be in error by more than 1 or 2 mv.

The potentials listed in Table IV ignore the liquid junction potentials between the silver-silver nitrate reference electrode and the half-cell under study. Ward[11] has shown that in 0.01 M silver nitrate solutions in AN, the transference number of the silver ion is 0.499, and since the mobilities of the main current-carrying ions in each of the three electrode systems are similar, the liquid junction potentials involved are

expected to be quite small (in the case of the hydrogen electrode this is true only in very dilute solutions), probably no more than 2 or 3 mv.

Assuming that the standard potential of the tris(o-phenanthroline)iron(II)–tris(o-phenanthroline)iron(III) couple is the same in AN as it is in water (1.120 v. vs. $(E^°_H)_{aq}$),[15] the values of the standard potentials of the four electrode systems studied, relative to $(E^°_H)_{aq}$, were calculated and are listed in the final column of Table IV. The potential of the silver–0.01 M silver nitrate in AN reference electrode is 0.274 v. on this scale. The value for $(E^°_{Ag})_{AN}$ vs. $(E^°_H)_{aq}$ of 0.404 v. is in good agreement with that quoted by Ward[11] (0.41 v.) but is 0.034 v. more positive than Strehlow's[8,9] value of 0.37 v., based on the rubidium scale, corrected for solvent effects. In view of the assumptions made regarding activity coefficients and liquid junction potentials, these values are considered to be in error by no more than 5 mv.

Strehlow[8,9] gives a value of 0.14 v. for $(E^°_H)_{AN}$ vs. $(E^°_H)_{aq}$. This is considerably in error. It is based on the measurement of Hammett's acidity function[21] of dilute solutions of sulfuric acid in AN with o-nitroaniline as indicator and Pleskov's data on the measured pH of hydrochloric acid solutions in AN. Strehlow erroneously assumed that sulfuric acid is completely dissociated in AN. In solutions which are not too dilute, sulfuric acid dissociates mainly according to the equation

$$2H_2SO_4 \rightleftharpoons H^+_{AN} + H_2SO_4HSO_4^- \quad (8)$$
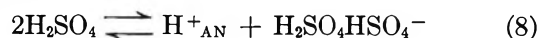
with a dissociation constant given by eq. 5.[13] Considering the change of the acidity function as an approximate indicator of the change of the standard hydrogen potential, a shift of 0.258 v. instead of 0.113 v. is calculated from Strehlow's data. From our own measurements of the acidity function[13] and the data of Coetzee[22] for the constant

$$K'_{BH^+} = [BH^+]/[B][(H^+)_{AN}]$$

B representing a variety of bases, it can be concluded that $(E^°_H)_{AN}$ must be close to 0.30 v., which agrees with our experimentally determined value. Pleskov[7] measured the potential of the hydrogen electrode in AN solutions of hydrochloric acid, and assuming $(E^°_{Rb})_{AN} = (E^°_{Rb})_{aq}$, obtained a value of 0.25 v. for $(E^°_H)_{AN}$ vs. $(E^°_H)_{aq}$. Pleskov also assumed that hydrochloric acid is completely dissociated in AN, whereas it is in fact a weak electrolyte.[13] Although Pleskov allowed

(21) L. P. Hammett and A. J. Deyrup, J. Am. Chem. Soc., 54, 272 (1932); L. P. Hammett and M. A. Paul, ibid., 56, 827 (1934).

(22) J. F. Coetzee and D. K. McGuire, J. Phys. Chem., 67, 1810 (1963).

for the volatility of hydrochloric acid from its solutions in AN, he was unaware of the decrease in both the hydrogen ion activity and the volatility of hydrochloric acid on aging the solutions.[13] Strehlow,[8,9] using Pleskov's[7] value of 0.25 v. for $(E^\circ_H)_{AN}$ (based on $(E^\circ_{Rb})_{AN} = (E^\circ_{Rb})_{aq} = -2.92$ v.) arrived at his value of 0.14 v. for $(E^\circ_H)_{AN}$ on the basis of his corrected value of -3.03 v. for $(E^\circ_{Rb})_{AN}$. Similarly, Strehlow's value of 0.37 v. for $(E^\circ_{Ag})_{AN}$ is also based on Pleskov's value measured relative to $(E^\circ_{Rb})_{AN}$. Since our value for $(E^\circ_{Ag})_{AN}$ is 0.034 v. more positive than Strehlow's, it would appear that his calculated value for $(E^\circ_{Rb})_{AN}$ of -0.11 v. relative to $(E^\circ_{Rb})_{aq}$ is in error by about 0.03 v. and that $(E^\circ_{Rb})_{AN}$ is close to -3.00 v., relative to $(E^\circ_H)_{aq}$. The uncertainty in his calculations is apparently due to his use of concentrations instead of activities of the saturated alkali halide solutions in AN and water to determine their solvation energies in AN.

Using a similar procedure to that used for the rubidium case, Strehlow[8,9] calculated the difference between $(E^\circ_{ferrocene})_{AN}$ and $(E^\circ_{ferrocene})_{aq}$ and so obtained a value of 0.34 v. for $(E^\circ_{ferrocene})_{AN}$ vs. $(E^\circ_H)_{aq}$. This compares favorably with our value of 0.348 v. and indicates that the assumption used in this work that $(E^\circ_{Fe(phen)_3{}^{2+}})_{AN}$ vs. $(E^\circ_H)_{aq}$ equals $(E^\circ_{Fe(phen)_3{}^{2+}})_{aq}$ is a good one.

The effect of added electrolyte (tetraethylammonium perchlorate) on the potentials of the iron phenanthroline and ferrocene half-cells is shown in Figure 3, curves A2, B2, and B3. In calculating the ionic strength of these solutions, allowance was made for the ion-pair formation of tetraethylammonium perchlorate using the relationship

$$K_{d_2} = \frac{[(C_2H_5)_4N^+][ClO_4^-]f^2}{[(C_2H_5)_4NClO_4]} = 5.6 \times 10^{-2} \quad (9)^5$$

In curves A2 and B2, concentrations were used to calculate the potentials from the Nernst equation and, as expected, increasing ionic strength has the greatest effect on the potential of the iron–phenanthroline system (curve A2) because of the charges on the ions involved (2+ and 3+). In curve B3, the activity of the ferricinium ion was used to calculate values of E'' (eq. 2). The deviation of E'' from a constant value is quite small, indicating that the Debye–Hückel relationship (eq. 7) gives reasonable values for the activity coefficients in this system provided the liquid junction potential between the two half-cells does not vary in the range of ionic strengths studied.

Assuming that a plot of $E_{1/2}$ for the oxidation of ferrocene in water at the r.p.e. vs. $I^{1/2}$ is linear, then a value of 0.152 v. (vs. s.c.e.) is estimated for $E_{1/2}$ for

ferrocene in water at zero ionic strength from the values of $E_{1/2}$ for this oxidation in 0.083 and 0.0204 M aqueous tetraethylammonium perchlorate solutions (Table III). Since the oxidation at the r.p.e. is reversible, $E_{1/2}$ may be identified with E° for this system and hence $(E^\circ_{ferrocene})_{aq}$ is estimated to be 0.394 v. $(E^\circ_{s.c.e.} = 0.242$ v.[23]) in good agreement with Strehlow's value of $+0.40$ v.[8,9] Thus, in this case, $E_{1/2}$ can be identified with E° for the system; however, in AN solution, in the presence of 0.1 M tetraethylammonium perchlorate E'' is 0.332 v. vs. s.c.e. (from Table II and eq. 2), whereas $E_{1/2}$ for the oxidation of ferrocene at the d.m.e. is 0.379 v. vs. s.c.e. Thus, the oxidation of ferrocene appears to be retarded at a mercury electrode, cf. a platinum electrode, indicating that, although the oxidation is reversible, some interaction between the mercury and the ferrocene or ferricinium occurs which inhibits the oxidation process.

Liquid Junction Potential between AN Solutions and the S.c.e. The potentials of the cells of Table II without added tetraethylammonium perchlorate were corrected for the effects of ionic strength using the plots of Figure 3 (curves A1 and B1). Using these potentials vs. s.c.e., corrected for ionic strength (Table V, column 2), the liquid junction potentials between the s.c.e. and AN solutions at zero ionic strength, $(E_{1j})_0$, were calculated using the data of Table IV and are given in Table V, column 3. In addition, the liquid junction potentials of these cells when 0.1 M tetraethylammonium perchlorate is present in the AN solutions $(E_{1j})_{0.1}$ were also estimated from the data in Tables II and IV and are given in column 4 of Table V. Quite good agreement for the values of $(E_{1j})_0$ is obtained with the four electrode systems studied in this work. The variation in the values of $(E_{1j})_{0.1}$ for these four electrodes is undoubtedly due to the different effects of ionic strength on the potentials of the four electrodes, this effect being most pronounced on the tris-(o-phenanthroline)iron(II)–tris(o - phenanthroline)iron-(III) electrode as expected. The results of other workers are also listed in Table V for comparison. By directly comparing a given electrode system in water with the same electrode system in AN, Ward[11] obtains values of E_{1j} which are in good agreement with our measurements using the s.c.e. From the difference between $E_{1/2}$ of the alkali ions in water and AN in 0.1 M tetraethylammonium perchlorate and the difference in the standard potentials of the alkali metals in both solvents, E_{1j} can be found from the measurements of Coetzee, et al.[4] Also from Coetzee's meas-

(23) "Handbook of Chemistry and Physics," 42nd Ed., Chemical Rubber Publishing Co., Cleveland, Ohio, 1960–1961.

Table V: Liquid Junction Potentials between Aqueous and AN Systems

Cell	$E_{(l-o)}$ [a], v.	$(E_{lj})_0$,[b] v.	$(E_{lj})_{0.01}$,[b] v.	Ref.
Pt | Fe(phen)$_3^{2+}$, Fe(phen)$_3^{3+}$ || s.c.e.	1.127	0.249	0.157	This work
Pt | Fe(C$_5$H$_5$)$_2$, Fe(C$_5$H$_5$)$_2^+$ || s.c.e.	0.351	0.245	0.220	This work
Pt | H$_2$, H$^+$ || s.c.e.	0.306	0.248	...	This work
Ag | Ag$^+$ (0.01 M) || s.c.e.	0.409	0.247	0.227	This work
Ag | Ag$^+$ (0.01 M) || s.c.e. ᵃ		0.26		3
Pt | Os(bipy)$_3^{2+}$, Os(bipy)$_3^{3+}$ || AN solution				
Os(bipy)$_3^{2+}$ Os(bipy)$_3^{3+}$ | Pt aqueous solution	0.225[c]	0.232[d]		11
Ag | Ag$^+$ 0.01 M (AN) || Ag$^+$ 0.01 M (aq.) | Ag	−0.119[c]	0.286[e]		11
$E_{1/2}$ of alkali ions in 0.1 M (C$_2$H$_5$)$_4$NClO$_4$ in AN vs. s.c.e.			0.23 to 0.26[f]	5

[a] E_{cell} (Table IV) corrected for ionic strength effects and activity coefficients in AN solutions. [b] Based on $(E°_{Ag})_{AN} = 0.404$ v.; $(E^{0.01}_{Ag})_{AN} = 0.274$ v. (vs. $(E°_H)_{aq}$). [c] E_{cell}. [d] Uncorrected for ionic strength effects. [e] Corrected for activity coefficients $(f_{Ag^+})_{AN} = 0.632$ (see text), $(f_{Ag^+})_{aq} = 0.900$ (ref. 19). [f] Assuming $(E°_{Rb})_{AN}$ vs. $(E°_H)_{aq} = 3.00$ v. (see text).

urements, it appears that E_{1j} is of the same order of magnitude in propionitrile, isobutyronitrile, benzonitrile, phenylacetonitrile, and acetone as it is in AN. From the data of Table V it can be concluded that after correcting for ionic strength effects in the AN solutions, E_{1j} of solutions in AN vs. the s.c.e. is of the order of 0.25 v.; i.e., 0.25 v. must be subtracted from the measured potential vs. s.c.e.

This value is completely at variance with the values of E_{1j} (vs. s.c.e.) estimated by Nelson and Iwamoto.[24] They determined the half-wave potentials at the r.p.e. vs. s.c.e. of the reversible anodic waves of tris(4,7-dimethyl-o-phenanthroline)iron(II), bis(2,9-dimethyl-o-phenanthroline)copper(I), ferrocene, and benzyl ferrocene in solutions in a variety of organic solvents which contained 0.1 M lithium perchlorate as supporting electrolyte. Correction was made for the iR drop. We will only consider their results in water and AN for the two systems (ferrocene and 4,7-dimethyl(o-phenanthroline)iron(II)) which they studied in both solvents. With the 4,7-dimethyl(o-phenanthroline)-iron system they report a value of $E_{1/2}$ in AN of 0.860 v. and an "extrapolated value" of $E_{1/2}$ in water of 0.830 v. vs. s.c.e. This would indicate that E_{1j} is only 0.030 v. However, Brandt and Smith[25] report a

value of 0.88 v. (vs. $(E°_H)_{aq}$) for the oxidation potential of this compound in 0.1 M aqueous sulfuric acid, i.e., 0.64 v. vs. s.c.e. This indicates that Nelson and Iwamoto's "extrapolation" technique for determining the oxidation–reduction potentials in water is questionable. Using Brandt and Smith's value of the oxidation potential in water and assuming that the corrections for ionic strength effects are the same for this system in the two solvents as they are for the tris(o-phenanthroline)iron(II) system, we calculate that the liquid junction potential is 0.28 v., in fair agreement with our results. The data obtained by Nelson and Iwamoto[24] with ferrocene do not differ much from our results (the small difference probably being due to the different types of junctions used between the solutions and the s.c.e.; they used a flowing type whereas we used an agar-saturated potassium nitrate bridge) and after allowing for ionic strength effects we derive a value of 0.26 v. for E_{1j} from their results. Thus, the conclusion drawn by Nelson and Iwamoto regarding the small value of E_{1j} in a host of organic solvents is not acceptable.

(24) I. V. Nelson and R. T. Iwamoto, *Anal. Chem.*, **33**, 1795 (1961); **35**, 867 (1963).

(25) W. W. Brandt and G. F. Smith, *ibid.*, **21**, 1313 (1949).

The Solution Thermochemistry of Polyvalent Electrolytes.   IV.

Sodium Carbonate, Sodium Bicarbonate, and Trona[1a]

by J. Paul Rupert,

Department of Chemistry, University of Pittsburgh, Pittsburgh, Pennsylvania 15213

Harry P. Hopkins, Jr., and Claus A. Wulff[b]

Department of Chemistry, Carnegie Institute of Technology, Pittsburgh, Pennsylvania 15213
(Received March 26, 1965)

The standard enthalpies of solution of sodium carbonate, sodium bicarbonate, and trona have been determined calorimetrically as -6.36, 4.46, and 5.67 kcal./mole, respectively, after correction for the heat effects arising from hydrolysis.   Three solution thermochemical paths, leading to the enthalpy of formation of trona, agree well at -641.0 kcal./mole.   Our data, when combined with those from other sources, also permit calculation of the standard entropies of trona as 72.6 cal./(mole °K.) and of the aqueous bicarbonate ion as 23 cal./(mole °K.).

This study was undertaken as a continuation of our investigation of polyvalent electrolytes.   In addition to the commercial importance of the sodium carbonate–bicarbonate system, it is of interest because of the subsidiary processes concomitant with dissolution.   Analyses of the observed enthalpies of solution of a carbonate or bicarbonate are complicated by the heat effects due to such secondary phenomena—in this case, hydrolysis.   In a closed calorimetric system, with minimal vapor space, these secondary equilibria may be derived from the changes in state represented by eq. 1–3

$$H_2CO_3(aq) = H^+(aq) + HCO_3^-(aq) \qquad (1)$$

$$HCO_3^-(aq) = H^+(aq) + CO_3^{-2}(aq) \qquad (2)$$

$$H_2O(l) \rightleftharpoons H^+(aq) + OH^-(aq) \qquad (3)$$
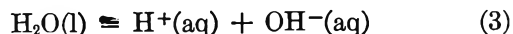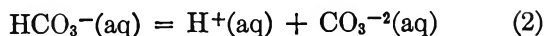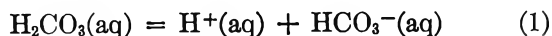
Values for the equilibrium constants governing these ionizations have been taken from literature data as follows: $K_1 = 4.45 \ (\pm 0.05) \times 10^{-7}$ (ref. 2–5), $K_2 = 5.68 \ (\pm 0.07) \times 10^{-11}$ (ref. 6, 7), and $K_3 = 1.01 \times 10^{-14}$ (ref. 8).   Pitzer[9] has determined the standard enthalpy increments (calorimetrically) to be $\Delta H_1^\circ = 1.84$, $\Delta H_2^\circ = 3.60$, and $\Delta H_3^\circ = 13.36$ kcal./mole.   Other values for ΔH_1, derived from the temperature dependence of equilibrium constants, are reviewed by

Wissbrun, *et al.*[10]   For our purposes, as will be shown later, uncertainties in this quantity of even 1 kcal./mole are negligible.   For ΔH_2° a value of 3.82 kcal./mole has been reported[5] from the temperature de-

(1) (a) Presented at the 149th National Meeting of the American Chemical Society, Detroit, Mich., April 1965; (b) to whom correspondence should be addressed.

(2) (a) S. Aybar, *Commun. Fac. Sci. Univ. Ankara*, **B10**, 44 (1962); *Chem. Abstr.*, **59**, 13397 (1963); (b) S. Aybar, *Commun. Fac. Sci. Ankara*, **B5**, 22 (1954).

(3) R. Nasanen, P. Merilainen, and K. Leppanenen, *Acta Chem. Scand.*, **15**, 913 (1961).

(4) H. S. Harned and R. Davis, Jr., *J. Am. Chem. Soc.*, **65**, 2030 (1943).

(5) Y. Kauko and H. Elo, *Z. physik. Chem.*, **A184**, 211 (1939).

(6) Y. Kauko and A. K. Airola, *Suomen Kemistilehti*, **B10**, 7 (1937).

(7) V. Y. Eremenko, *Gidrokhim. Materialy*, **28**, 233 (1959); *Chem. Abstr.*, **55**, 7014 (1961).

(8) H. S. Harned and B. B. Owen, "Physical Chemistry of Electrolytic Solutions," Reinhold Publishing Corp., New York, N. Y., 1958.

(9) K. S. Pitzer, *J. Am. Chem. Soc.*, **59**, 2365 (1937).   The enthalpy of ionization of water, ΔH_3°, has been determined by J. D. Hale, R. M. Izatt, and J. J. Christensen, *J. Phys. Chem.*, **67**, 2605 (1963), and by C. E. Vanderzee and J. A. Swanson, *ibid.*, **67**, 2608 (1963), as 13.336 ± 0.018 kcal./mole.   Since our primary interest is in the quantity $\Delta H_f^\circ - \Delta H_2^\circ$, we have used the older value of Pitzer in conjunction with his value for ΔH_2°.   The difference between these values for ΔH_3° is insignificant in our work.

(10) K. F. Wissbrun, D. M. French, and A. Patterson, Jr., *ibid.*, **58**, 693 (1954).

pendence of K_2, and a value of 4.2 kcal./mole (presumably at 18°) is due to Thomsen.[11]

Experimental

Fisher sodium bicarbonate ($NaHCO_3$), certified to have a purity of 99.98% or better, was used without further purification. The sodium carbonate (Na_2CO_3) employed was Fisher Certified reagent grade, listed as 99.9% Na_2CO_3 (minimum). Before use the sodium carbonate was dried in an oven for at least 2 days at 120°. Through the courtesy of Mr. R. E. Clagett, an analyzed sample (minimum 99%) of trona ($Na_2CO_3 \cdot NaHCO_3 \cdot 2H_2O$) was supplied by the Allied Chemical Corp. Owing to its incongruent solubility, this last sample was used without further purification. Its heat of solution was the same as that of a synthetic sample, prepared previously by Professor Clark C. Stephenson and one of the present authors (C. A. W.). All samples were dissolved into 950 ml. of distilled water at 25.0 ± 0.1°. Enthalpies of solution were calculated from the measured heats using gram formula masses of 84.01, 105.995, and 226.05 for sodium carbonate, sodium bicarbonate, and trona, respectively. The solution calorimeter, which has been described previously,[12] has as its temperature-sensing device a laboratory-wound resistance thermometer. The Mueller bridge circuitry and adjuvant electrical standards have also been described.

Discussion

Na_2CO_3. In solutions of sodium carbonate, the predominant secondary equilibrium can be characterized by the change in state

$$CO_3^{-2}(aq) + H_2O(l) = HCO_3^-(aq) + OH^-(aq) \quad (4)$$

the equilibrium constant for which is given by $K_4 = K_3/K_2 = 1.8 \times 10^{-4}$. For any molal concentrations, m, of carbonate originally dissolved, the extent of reaction 4 is described by the degree of hydrolysis $\alpha = (HCO_3^-)/m$. Assuming the activity of the water to be unity (minimum mole fraction of 0.995 in our solutions) and the common form of the Debye–Hückel relation for ionic activity coefficients (presumed valid for the dilute solutions considered in this study), α can be related to K_4 and the ionic strength, I, by

$$\log K_4 = \log \alpha^2/(1 - \alpha) + \log m + 1.018 I^{1/2}/(1 + I^{1/2}) \quad (5)$$

and

$$I = m(3 - \alpha) \quad (6)$$

Equations 5 and 6 have been solved simultaneously, by an iterative process, for α in the range 0.007 to 0.090 m.

These values accord well with older experimental degrees of hydrolysis reviewed in Mellor.[13] From Pitzer's data we obtain $\Delta H_4° = 9.8$ kcal./mole. Representative values of α and $\alpha\Delta H_4°$ are included in Table I. Sixteen determinations of the enthalpy of solution of sodium carbonate to give final concentrations in the range 0.007 to 0.085 m are also listed in Table I.

Table I: Enthalpies of Solution and Hydrolysis for Na_2CO_3[a]

m	α	$\alpha\Delta H_4°$	$-\Delta H_{obsd}$
0.00702	0.126	1.234	5.039
0.00848			5.121
0.00921			5.152
0.01025			5.184
0.01138	0.098	0.960	5.274
0.01356			5.369
0.01664			5.356
0.02171			5.443
0.02547			5.530
0.03219	0.060	0.588	5.561
0.03998			5.610
0.04885			5.727
0.05735			5.722
0.06670			5.736
0.06833	0.033	0.323	5.782
0.07531			5.730

[a] Units: kcal./mole.

The integral enthalpy of solution, $\Delta H(m)_{obsd}$, may be written as

$$\Delta H(m)_{obsd} = \Delta H_8° + \phi_L(m) + \alpha\Delta H_4° \quad (7)$$

where $\phi_L(m)$ is the apparent molal heat content of the solution at concentration m and $\Delta H_8°$ is the standard enthalpy of solution of Na_2CO_3

$$Na_2CO_3(c) = 2Na^+(aq) + CO_3^{-2}(aq) \quad (8)$$
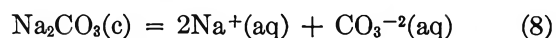
A least-squares analysis of $\Delta H_{obsd} - \phi_L(m)$ vs. α [assuming the $\phi_L(m)$ of sodium carbonate to be similar to those for the alkali sulfates[8]] gives the straight line $\Delta H_{obsd} - \phi_L(m) = -6.31 + 9.04\alpha$ kcal./mole, with an average deviation of 0.02 kcal./mole. From this analysis the extrapolated standard enthalpy of solu-

(11) J. Thomsen, "Thermochemische Untersuchungen," Johann Ambrosius Barth Verlag, Leipzig, 1883.

(12) W. F. O'Hara, C. H. Wu, and L. G. Hepler, J. Chem. Educ., 38, 519 (1961).

(13) Supplement to "Mellor's Comprehensive Treatise on Inorganic and Theoretical Chemistry," Vol. II, Suppl. II, Part 1, John Wiley and Sons, Inc., New York, N. Y., 1962.

tion is determined as $\Delta H_8° = -6.31 \pm 0.05$ kcal./mole, and $\Delta H_4° = 9.0$ kcal./mole in accord with Pitzer's data.[9] A better value of $\Delta H_8°$ may be obtained from an analysis $\Delta H_{obsd} - \alpha\Delta H_4°$ vs. $m^{1/2}$ [the usual concentration dependence of $\phi_L(m)$]. Known ϕ_L values for unhydrolyzed 2–1 electrolytes, such as the alkali sulfates,[8] show that the linearity of ϕ_L with $m^{1/2}$ holds best below $m = 0.03$. A least-squares straight line for $\Delta H_{obsd} - \alpha\Delta H_4° = \Delta H_8° + Am^{1/2}$ in the region 0.007 to 0.032 m is $\Delta H_{obsd} - \alpha\Delta H_4° = -6.37 + 1.24m^{1/2} \pm 0.03$ kcal./mole (where the uncertainty is the root-mean-square deviation). From this $\Delta H_8° = -6.37$ kcal./mole, and the concentration dependence is similar to $\phi_L(m)$ for other 2–1 electrolytes. We have selected $\Delta H_8° = -6.36 \pm 0.08$ kcal./mole.

Trona. Here again the major secondary equilibrium is represented by eq. 4. We define the extent of the hydrolysis by $\alpha = (OH^-)/m$, which, making the same assumptions as before, is related to K_4 by

$$\log K_4 = \log \alpha(1 + \alpha)/(1 - \alpha) + \log m + 1.018I^{1/2}/(1 + I^{1/2}) \quad (9)$$

and

$$I = m(4 - \alpha) \quad (10)$$

Table II contains representative values of α and $\alpha\Delta H_4°$ along with 11 determinations of the heat of solution to give final concentrations between 0.0045 and 0.0550 m. The observed enthalpy of solution, ΔH_{obsd}, can be represented by

$$\Delta H_{obsd} = \Delta H_{11}° + \phi_L (m) + \alpha\Delta H_4°$$

where $\Delta H_{11}°$ is the standard enthalpy of solution for trona (eq. 11).

$$Na_2CO_3 \cdot NaHCO_3 \cdot 2H_2O(c) = 3Na^+(aq) + CO_3^{-2}(aq) + HCO_3^-(aq) + 2H_2O(l) \quad (11)$$
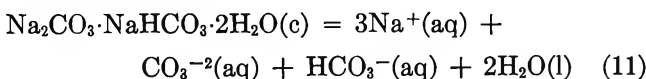
Considering the nature of the solute, an *a priori* estimate of $\phi_L(m)$ is difficult to make, and a reduction of the data was made by plotting $\Delta H_{obsd} - \alpha\Delta H_4°$ vs. $m^{1/2}$. A least-squares analysis gives the straight line $\Delta H_{obsd} - \alpha\Delta H_4° = 5.65 \pm 1.90 \; m^{1/2} \pm 0.04$ kcal./mole, which leads to an extrapolated value of $\Delta H_{11}° = 5.65 \pm 0.05$ kcal./mole. The slope of this straight line compares remarkably well with the sum of ϕ_L values for a 1–1 and a 2–1 electrolyte. The relative partial molal heat content of water in the solution was assumed negligible within the estimated uncertainty.

NaHCO₃. In solutions of sodium bicarbonate, the most important secondary reaction is

$$2HCO_3^-(aq) = H_2CO_3(aq) + CO_3^{-2}(aq) \quad (12)$$
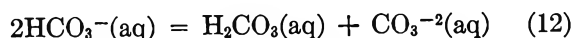
Table II: Enthalpies of Solution and Hydrolysis for Trona[a]

m	α	$\alpha\Delta H_4°$	ΔH_{obsd}
0.00429	0.026	0.256	5.991
0.00442			5.997
0.00893			5.911
0.00904	0.011	0.108	5.947
0.01381			6.041
0.01452			5.972
0.02159			6.033
0.05264	0.0017	0.017	6.077
0.05264			6.033
0.05264			6.020

[a] Units: kcal./mole.

The extent of eq. 12, defined as $\alpha = (CO_3^{-2})/m$ (where m is the molal concentration of the sodium bicarbonate originally dissolved), can be calculated from the equilibrium constant $K_{12} = K_2/K_1 = 1.2 \times 10^{-4}$ by

$$K_{12} = \alpha^2/(1 - 2\alpha)^2 \gamma_{CO_3}\text{-}_2\gamma_{H_2CO_3}/\gamma^2_{HCO_3^-} \quad (13)$$

Equation 13 may be reduced to $\alpha = 0.01$ (independent of m) without loss of precision because $\alpha\Delta H_{12}°$—the quantity of interest—is only 20 cal./mole, which is less than the experimental uncertainty. The observed enthalpies of solution have been fitted to a straight line, by the method of least squares, in the region 0.011 to 0.090 m, and are given by $\Delta H_{obsd} = 4.49 + 0.38m^{1/2} \pm 0.02$ kcal./mole. Several determinations below $m = 0.01$, where the heat effects approached the lower limit of the calorimeter's sensitivity, were not included in the least-squares analysis. For the change in state represented by

$$NaHCO_3(c) = Na^+(aq) + HCO_3^-(aq) \quad (14)$$
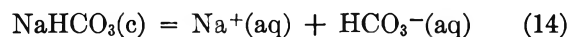
the standard enthalpy increment is then $4480 - 20$ cal. $= 4.46 \pm 0.05$ kcal./mole.

The standard Gibbs free energy for eq. 14 is calculated from the solubility, given in Mellor[13] as 1.22 m, a tabulated mean activity coefficient[14] $\gamma_\pm = 0.503$, and the relation $\Delta G_{14}° = -RT \ln 4m^2\gamma_\pm^2$, as $\Delta G_{14}° = 0.58$ kcal./mole.

From the above data $\Delta S_{14}° = (4.46 - 0.58)/0.298 = 13$ cal./(mole °K.). Utilizing the standard entropy values for NaHCO₃[15] and Na⁺(aq),[15] we calculate $\bar{S}°_{HCO_3}$

(14) S. T. Han and L. J. Bernardin, *Tappi*, **41**, 540 (1958).

(15) F. D. Rossini, D. D. Wagman, W. H. Evans, S. Levine, and I. Jaffe, "Selected Values of Chemical Thermodynamic Properties," National Bureau of Standards Circular 500, U. S. Government Printing Office, Washington, D. C., 1952.

= 23 ± 1 cal./(mole °K.). This value agrees with that tabulated by Latimer, Pitzer, and Smith[16] based solely on eq. 1.

From the standard enthalpies of solution of Na_2CO_3 (−6.36 kcal./mole), trona (5.65 kcal./mole), and $NaHCO_3$ (4.45 kcal./mole) we can compute $\Delta H_{15}°$ = −6.36 + 4.46 − 5.67 = −7.6 ± 0.2 kcal./mole, for

$$Na_2CO_3(c) + NaHCO_3(c) + 2H_2O(l) =$$
$$Na_2CO_3 \cdot NaHCO_3 \cdot 2H_2O(c) \quad (15)$$
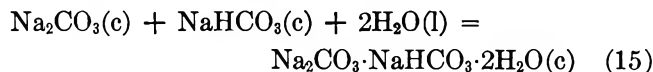
In view of the assumptions made concerning these solutions, independent routes to evaluating $\Delta H_{15}°$ would be desiderata in checking our extrapolation procedures. To this end we have measured the following heat effects. Each value is the average of several determinations (in cal./mole): (a) $Na_2CO_3(c)$ into water to give a 0.055 m solution, ΔH = −5739 ± 20; (b) $NaHCO_3(c)$ into (a) to give 0.05 m CO_3^{-2} and HCO_3^-, ΔH = 4220 ± 20; (c) $NaHCO_3$ into water to give a 0.055 m solution, ΔH = 4585 ± 10; (d) Na_2CO_3 into (c) to give 0.055 m CO_3^{-2} and HCO_3^-, ΔH = −6128 ± 10; (e) trona into water to give a 0.055 m solution, ΔH = 6056 ± 20. The enthalpy increment $\Delta H_{15}°$ can be obtained from the sum $\Delta H_a + \Delta H_b − \Delta H_e$ = −7.67 ± 0.06 kcal./mole and from the sum $\Delta H_c + \Delta H_d − \Delta H_e$ = −7.60 ± 0.04 kcal./mole. The excellent accord among the three values for $\Delta H_{15}°$ gives a posteriori support for the extrapolation methods used to account for hydrolysis effects.

Torgeson[17] by a closely related procedure obtained $\Delta H_{15}°$ = −7.76 ± 0.02 kcal./mole, in reasonable agreement with our average value of −7.64 ± 0.10 kcal./mole. For eq. 15, $\Delta G_{15}°$ = −2.47 kcal./mole[18] and $\Delta S_{15}°$ = (−7.64 + 2.47)/0.298 = −17.2 cal./(mole °K.). The above values and tabulated data[16] for Na_2CO_3, $NaHCO_3$, and $H_2O(l)$ lead to $\Delta H_f°$ = −641.0, $\Delta G_f°$ = −569 kcal./mole, and $S°$ = 72.1 ± 1.0 cal./(mole °K.) for trona. An estimate for the entropy from Latimer's[19] rules is 73.9 cal./(mole °K.).

(16) W. M. Latimer, K. S. Pitzer, and W. V. Smith, *J. Am. Chem. Soc.*, **60**, 1829 (1938).

(17) D. R. Torgeson, *Ind. Eng. Chem.*, **40**, 1152 (1948).

(18) Personal communication, C. C. Stephensen, Massachusetts Institute of Technology.

(19) W. M. Latimer, "Oxidation Potentials," Prentice-Hall, Englewood Cliffs, N. J., 1952, p. 359.

The Behavior of Some Carbonaceous Materials at Very High

Pressures and High Temperatures

by R. H. Wentorf, Jr.

General Electric Research Laboratory, Schenectady, New York   *(Received March 26, 1965)*

Several different forms of elemental carbon and a number of organic compounds were exposed to pressures in the range 95–150 kbars and temperatures in the range 1300–3000° for periods of 0.2 to 50 min. The amount and kind of diamond formed were found to depend strongly on the kind of carbonaceous starting material used. Sometimes graphite formed. It appears that structural factors are involved and that the actual transformation to diamond may follow a number of complex paths.

I. Introduction

Bundy[1] has shown that the triple point of carbon among graphite, diamond, and liquid lies at about 125 kbars and 4300°K. He also found that graphite transforms directly to diamond in times of a few milliseconds or less at pressures exceeding about 120 kbars and temperatures exceeding about 3300°K. Alder and Christian[2] have found evidence that graphite, compressed and heated by a strong shock wave to about 350 kbars and 1000°K., transformed to diamond in a few microseconds. DeCarli and Jamieson[3] actually recovered particles of diamond which were formed from graphite which had been exposed to strong shock compression. In all the foregoing experiments the rates of transformation to diamond were so rapid and the local temperatures of the specimens were changing so rapidly that no measurements of the variation of reaction rate with temperature were reported.

This paper describes the results of some experiments in which various nondiamond carbons and compounds containing carbon were exposed to pressures in the range 95–150 kbars and temperatures in the range 1300–3000°. Under these conditions most of these materials turn partially to diamond in periods of time of 0.2 to 55 min. In this way some estimates could be made of the variation of diamond formation rate with temperature. It turned out that, in spite of only one chemical element being involved in the reaction, diamond formation under these conditions was not a simple chemical reaction; instead the rate depended

strongly on the kind of carbonaceous material used and did not seem to follow any simple rate expression.

II. Experiments with Relatively Pure Carbon

In this set of experiments various kinds of relatively pure carbon, such as various graphites and carbon blacks, were compressed to pressures in the range 95 to 150 kbars and then heated by 60-cycle a.c. for periods of 0.2 to 55 min. at temperatures ranging between about 1300 and 3000°.

A. Experimental Procedure. The carbons were contained in small titanium tubes in a composite cylindrical sample arrangement as shown in Figure 1. The composite cylinders were then placed in a high-compression "Belt" apparatus as described by Bundy[1] and exposed to the desired pressures and temperatures. The heating current passed from one punch face through the molybdenum wire, through the titanium and carbon, and then out the other molybdenum wire to the other punch face. The titanium tubes were sealed, though not perfectly, by pinching their ends together after filling them; they were then flattened to 0.0508-cm. thickness.

The carbons were contained in relatively pure titanium for several reasons. The titanium isolated the carbon from contact with the pyrophyllite stone, which is known to contain small amounts of iron which

(1) F. P. Bundy, *J. Chem. Phys.*, **38**, 631 (1963).
(2) B. J. Alder and R. H. Christian, *Phys. Rev. Letters*, **7**, 307 (1961).
(3) P. S. DeCarli and J. C. Jamieson, *Science*, **133**, 1821 (1961).
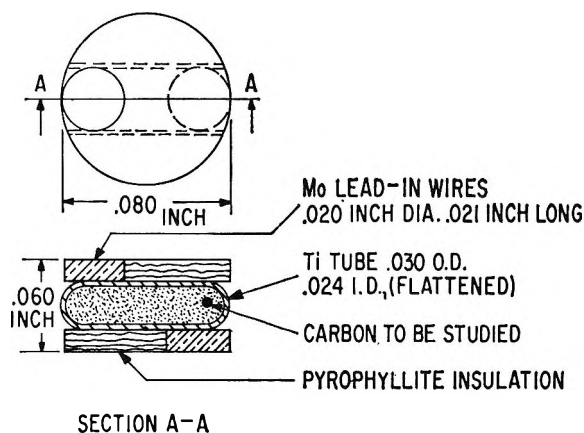
Figure 1. High-pressure sample.

is known to act as a catalyst for diamond formation. Titanium so far has not been found to be effective as a diamond-forming catalyst. The titanium tubes usually did not melt nor react very much with the carbon in these experiments, probably because of the formation of relatively refractory titanium carbides and/or the increase of melting point of titanium with pressure. Also, the high-pressure form of titanium[4] does not seem as reactive as the ordinary form. Finally, the titanium carried most of the heating current and thereby helped to maintain the carbon at a more uniform temperature. (Because diamond has a relatively high electrical resistivity, the local formation of diamond increases the local I^2R heat production and hence the local temperature. The rate of diamond formation increases rapidly with temperature so that a regenerative process begins which accentuates temperature gradients in the carbon, unless the carbon carries only a small share of the heating current.)

The pressures in the apparatus used to compress the samples were estimated by reference to the resistance changes[5] in bismuth (25, 88 kbars), barium (58, 140 kbars), iron (131 kbars), and lead (160 kbars) at 25°. The increase of resistance associated with the change in titanium[4] at about 90 kbars could often be observed during the compression of the sample.

It is likely that the local pressure fell during the heating period as a result of the density increases in the sample due to diamond formation and the formation of stishovite and kyanite from the pyrophyllite. It is not possible to estimate the magnitude of this pressure decrease precisely, but it is not likely that an original pressure of 160–170 kbars ever fell below about 130 kbars because in the hottest experiment of this series relatively large amounts of both diamond and stishovite were formed, while similar amounts of diamond and no stishovite were formed in flash-

heating experiments by Bundy[1] at 130 kbars. In view of the uncertainties regarding estimation of the pressure, the pressures listed for the various experiments are to be regarded as approximate, with possible errors of ±20 kbars relative to the reference pressures for resistance changes in Ba, Fe, Pb, etc.

Uncertainties also reduce the accuracy of the temperature reported for these experiments. The central parts of the reaction tubes were hotter than the ends because heat could flow more easily via the molybdenum wires. The central temperatures were estimated from the heating power input, using as references the powers required to melt nickel, titanium, and the titanium–carbon eutectic, and extrapolating for the probable effects of pressure on these melting points,[6] while bearing in mind the probable dimensions and thermal conductivities of the various portions of the sample. The small size of the sample magnifies small variations in the size and placement of the components. Thus, the temperatures reported here may be in absolute error by as much as 10% and in relative error by about 3%.

B. *Experimental Observations.* The findings in the high-pressure carbon heating experiments are listed in Tables I–III.

Table I: Experiments with SP-1 Graphite

Estd. temp., °C.	Time, min.	Product density, g./cc.	Estd. vol. % diamond	Remarks
		150 kbars		
25	50	2.25	0	
1300	50	2.47	17	
1300	50	ca. 2.6	25	
1300	50	ca. 2.6	40	12% B₄C added
1700	0.5	2.86	30	a
1700	2.5	2.84	30	b
1700	8.5	2.78	30	b
1700	35	2.97–3.2	70	b
2000	4	2.9–3.3	60	a
2100	0.1	3.0	50	b
2100	10	3.02	70	b
2400	2.5	2.97–3.2	70	
2800	0.2	...	70+	
		115 kbars		
1700	55	ca. 2.6		
		95 kbars		
1700	60	2.25	0	

a 3.1- and 2.19-Å. lines of δ-carbon present but not strong.
b δ-Carbon lines about as strong as diamond or graphite lines.

(4) J. C. Jamieson, *Science*, **140**, 72 (1963).

(5) R. H. Wentorf, Jr., Ed., "Modern Very High Pressure Techniques," Butterworth Inc., Washington, D. C., 1962, p. 229.

(6) See ref. 5, pp. 113–116; see also H. M. Strong, *Acta Met.*, **12**, 1411 (1964).

Table II: Experiments with Spectroscopic Carbon (150 kbars)

Estd. temp., °C.	Time, min.	Product density, g./cc.	Estd. vol. % diamond	Remarks
1700	50	ca. 2.31	5	
1700	55	ca. 2.48	18	10% B₄C added
2000	15	2.39	10	a
2000	50	2.34	8.5	
2400	5	2.39	10	
2400	15	2.42	13	
2400	15	2.43	13	

a 3.1- and 2.1-Å. lines of δ-carbon present but not strong.

Table III: Experiments with Carbon Blacks (150 kbars, 2000°, 15 min.)

Carbon	Product density, g./cc.	Estd. vol. % diamond
Kosmos 40	2.4–2.6	55
Kosmos 40		50
Statex	2.97–3.2	70
Micronex std.	2.39	15
Micronex std.	2.25	0 (1700°)

Three main types of carbon were examined: (1) SP-1 graphite, a highly refined natural graphite, easily packed to density 2.0, made by the National Carbon Co.; (2) regular spectroscopic grade carbon, in the form of powder salvaged from the turning of rods; (3) carbon blacks for reinforcing rubber.

X-Ray diffraction tests were made on most of the products. Often the relative strengths of the diamond and graphite diffraction lines could be used to estimate the fraction of diamond present in the product. It was difficult to estimate the fraction of diamond in the product by simply measuring its density on account of the frequent presence of another phase of carbon, tentatively called δ-carbon.

This new form of carbon appeared to be relatively abundant in certain of the products and was detected by its X-ray diffraction pattern, which features a strong line at 3.1 Å., a medium line at 2.19 Å., and a weaker line at 1.55 Å. δ-Carbon was also found by Bundy in some flash-heated graphites which have been largely converted to diamond.[1] So far, δ-carbon has not been prepared in a pure form, and its density and structure are unknown.

Most of the carbon products obtained in the above experiments were black, friable polycrystalline lumps. The diamond crystallites in them were too small to be seen as separate crystals under a microscope. The

X-ray diffraction patterns of the products also indicated a small diamond crystallite size, of the order of 1 μ or less.

The new crystalline phase of carbon reported by Aust and Drickamer[7] was never observed in any of the products of these experiments. Aust and Drickamer obtained this phase in best yield from single-crystal graphite exposed to pressures above 150 kbars at room temperature; the yield from other less perfectly crystalline graphite was reported to be small.

C. Comments. One notes that the effect of reducing the initial pressure from 150 to 115 kbars is to reduce the amount of diamond formed, but when the initial pressure was 95 kbars, no diamond formed even though diamond was the stable phase during the experiment.

A comparison of Tables I–III shows that there are marked differences in the abilities of the various carbons to form diamond. SP-1 graphite forms diamond most easily, but a carbon black known as Statex is next best, and the other carbon blacks are all better diamond formers than is spectroscopic carbon. One could not ascribe this difference in behavior to differences in operating pressure produced by differences in initial density because, while SP-1 may be packed most densely with ordinary hand tools, the carbon blacks are notable for their low densities when packed, and spectroscopic carbon lies between. Besides, nearly as much diamond is produced from SP-1 at 115 as at 150 kbars. It appears that the differing behavior of these carbons in forming diamond is a consequence of their "molecular" structure. However, "giant molecules" such as these carbons represent are difficult to characterize in simple ways with our present knowledge; we lack the tools to examine them as one would examine, for example, various steels. Bundy[1] has shown in flash-heating experiments that at high temperatures, 3000°K. and above, the differences in the rate of diamond formation out of various carbons are very slight. Presumably at these high temperatures the structural differences would be very slight.

There are other interesting items. One is that significant amounts of diamond may form from graphite at temperatures as low as 1300°, i.e., about as low as are found to be effective using metal alloy catalysts at pressures of 50 kbars or so. A second item is that boron carbide may act as a promoter of diamond formation, doubling or tripling the rate. At a pressure of 67 kbars boron carbide and graphite mixtures do not form any detectable amounts of diamond at about 1700°. (However, boron or boron carbide is known to accelerate diamond formation in the presence of metal

(7) R. B. Aust and H. G. Drickamer, *Science*, **140**, 817 (1963).

catalysts such as Fe, Ni, etc.) Boron carbide is known to be an effective graphitizing agent in the manufacture of graphite from coke, etc. Evidently boron atoms make carbon atoms more mobile even though no molten phases are known to form, and boron is outstanding for its relatively rapid diffusion into diamond at high pressures and temperatures.[8]

After a few of the above experiments had been performed, the hope sprang up that the rate of formation of diamond might follow a simple rule, e.g., a first-order reaction rate law. One might then determine the "activation energy" for the slowest step with the usual plot of logarithm of the rate vs. reciprocal temperature. However, an inspection of the results of the experiments in Table I or II shows that at any particular pressure and temperature the rate is extremely rapid at first, so that most of the diamond that is to be formed is formed in the first few minutes or less of heating; after this the rate becomes considerably slower. The reaction rate does not appear to follow a simple first-order law, but instead there seem to be strong nucleation effects from pre-existing nuclei which are rapidly consumed at first to leave a more resistant carbon (sometimes containing δ-carbon) in which nucleation and growth proceed more slowly. Probably many different kinds of atomic arrangements may act as diamond nuclei, and each kind of arrangement would be expected to have its own energy barrier value for diamond growth. The ones with the lowest barriers would be used most rapidly and would convert their immediate carbon environments into diamond. Further growth of diamond might require the surmounting of activation energy barriers of increasing height. Some of these higher barriers would have been present in the original mass; others would have been created as a result of the partial local transformation to diamond, etc. Evidently, the conversion to diamond can never be complete until the product consists of a single crystal, an unlikely event for those who lack patience.

In a gas or a liquid a single value of activation energy may adequately describe a rate process because most of the reacting species have the same environment. However, in a refractory, nonuniform solid such as carbon, the reacting species are not necessarily similar, and the final product may be reached by a variety of paths. An over-all description of such a process might involve several values of activation energy.

One can arbitrarily select a certain fractional conversion to diamond, say 10, 30, or 70%, and define an average rate as the inverse of the time taken to reach this diamond concentration. A plot of the logarithm of this average rate vs. reciprocal temperature would

then yield an average activation energy for the formation of diamond by all the processes operative up to the time the diamond concentration reached the arbitrary level. Such arbitrary average activation energies could be obtained for various diamond concentration levels for which data are available.

If one proceeds on this basis, with an interpolation or two from nearby diamond concentration levels and if one also estimates that the conversion to 70% diamond took place in about 3.3 msec. in the flash-heating experiments at 3600°K. of Bundy,[1] one may prepare Tables IV and V of average rate vs. reciprocal temperature for SP-1 graphite and Table VI for spectroscopic carbon.

A plot of these calculations is shown in Figure 2. The probable range of error is indicated by the vertical

Table IV: Data for 30% Conversion of SP-1 Graphite

Temp., °C.	$10^4/°K.$	Time, sec.	Rate, sec.$^{-1}$	Log (rate)
1300	6.35	5000(estd.)	2×10^{-4}	−3.7
1300	6.35	3600	2.8×10^{-4}	−3.55
1700	5.07	60	1.7×10^{-2}	−1.77
2000	4.4	6(estd.)	1.7×10^{-1}	−0.77
2100	4.2	3(estd.)	0.33×10^{-1}	−0.5

Table V: Data for 70% Conversion of SP-1 Graphite

Temp., °C.	$10^4/°K.$	Time, sec.	Rate, sec.$^{-1}$	Log (rate)
1700	5.07	2000	5×10^{-4}	−3.3
2100	4.2	12(estd.)	8×10^{-2}	−1.1
2000	4.4	300(estd.)	3.3×10^{-3}	−2.4
2100	4.2	600	1.7×10^{-3}	−2.77
2400	3.75	150	7×10^{-3}	−2.15
2800	3.25	10	1×10^{-1}	−1
3300	2.77	0.003^a	330^a	2.5^a

^{a} Estimated from flash-heat data of Bundy.[1]

Table VI: Data for 10% Conversion of Spectroscopic Carbon

Temp., °C.	$10^4/°K.$	Time, sec.	Rate, sec.$^{-1}$	Log (rate)
1700	5.07	6000(estd.)	1.7×10^{-4}	−3.8
2000	4.4	900	1.1×10^{-3}	−2.95
2400	3.75	300	3.3×10^{-3}	−2.5

(8) R. H. Wentorf, Jr., and H. P. Bovenkerk, J. Chem. Phys., 36, 1987 (1962).

extent of each estimated point. Some of the estimated rates may be on the low side because the amount of diamond formed may have remained nearly constant for the latter portion of an experiment, as mentioned earlier.
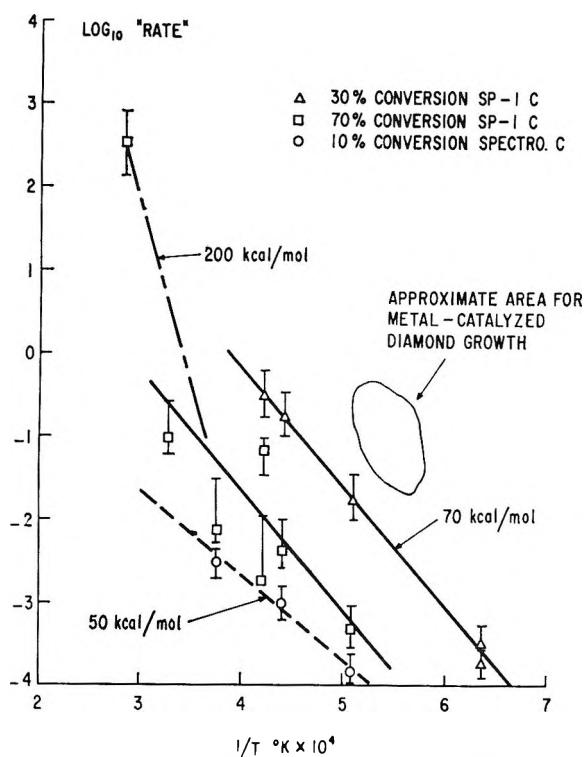
Figure 2. Plot of log (rate) vs. reciprocal temperature for fractional conversions of carbons to diamond.

Also shown for comparison in Figure 2 is an area corresponding to the conversion of graphite to diamond with a metal catalyst at say 67 kbars at 2000°K. Here the "reaction rate" would be about 0.1 sec.$^{-1}$ for "70% conversion" although with the catalyst the conversion is essentially zero on one side of a moving metal film and essentially 100% on the other side, so that the comparison is not exact.

One notes in Figure 2 that the slopes of the lines for experiments in the range 1300–2800° correspond to activation energies of 50–80 kcal./mole. This energy includes the $p\Delta V$ term. Such an energy is about that required to break two carbon–carbon bonds. However, the lines which would connect the high temperature point estimated from Bundy's experiments[1] with the points obtained at lower temperatures would have slopes corresponding to activation energies of about 200 kcal./mole. Despite the experimental uncertainties in the data, it seems that processes involving higher activation energies come into play at higher tempera-

tures. Higher activation energies would be expected for larger aggregations of atoms.

Figure 2 also indicates that the activation energy for diamond formation is about the same for SP-1 graphite and spectroscopic carbon although the rates differ by about a factor of 100. If this difference in rate were ascribed to the difference in the entropy change upon going to the activated state, the difference would be about 10 cal. °K.$^{-1}$ mole^{-1}. Thus, the activated states would be regarded as having more degrees of freedom relative to SP-1 graphite than relative to spectroscopic carbon. This is reasonable up to a point because SP-1 is the more perfectly crystalline material. However, 10 e.u. seems a large difference because the entropy of fusion of most metals is only about 2, and the two kinds of starting carbon could not differ in entropy by much more than this.

It seems more likely that the differences in reaction rates are due to differences in the probabilities that the activated complexes will drop into the final (diamond) states. Many configurations of activated states may not be suitable for diamond formation, and the configuration of an activated state during its lifetime is connected with the local structure of the solid. The ready formation of δ-carbon from some carbons and not others is also consistent with this view.

III. Experiments with Organic Compounds

It seemed evident from a study of the diamond-forming behavior of various carbons, as described above, that what might be called structural factors played an important part in the formation of diamond. In order to explore these effects further, a number of different organic compounds were heated to about 2000° for about 15 min. at a pressure of about 150 kbars. Most of the compounds yielded diamond, but a few yielded graphite.

A. Experimental Procedure. The compounds tested were packed into small titanium tubes and exposed to high pressures and temperature just as were the carbons in the experiments described above. After cooling and release of pressure, the pyrolysis products were examined by various methods, including X-ray diffraction.

B. Experimental Findings. The behavior of the various materials tested in these experiments is summarized in Table VII. The densities and estimated diamond contents of the products are given, along with other remarks about them. (For example, density 2.86–3.3 means that the density of the sample was somewhere between 2.86 and 3.3 g./cc.)

It was noticed that when graphite was the product of an experiment, the average resistance of the sample

Table VII: Pyrolysis Experiments (150 kbars, 2000°, and 15 min., except as noted)

Charge	Product density	Estd. % diamond	Remarks
Anthracene	2.2	0	Black, soft; excellent graphite by X-ray pattern
Anthracene	2.2	0	5 min., 2300°. Product was graphite
Anthracene	2.8–3.2	30	2300°. Hotter parts white, soft diamond; cooler parts black, soft graphite
Camphene	2.8–3.3	70	White, no scratch glass; X-ray shows strong diamond
Camphene	. . .	. .	1.5 min., 2300°. No free C left; TiC instead
Anthracene:camphene, 1:1		50	Hotter parts white; cooler, black; scratch glass
Anthracene:camphene, 9:1		30	Hotter parts white; cooler, black; scratch glass
Anthracene:iron, 9:1		90	9 min. Extensive formation of diamond
Naphthalene	2.2	0	Black, soft; excellent graphite by X-ray pattern
Chrysene	2.2	0	Soft, black, no scratch glass
Fluorene	>2.86	60	Hottest parts white diamond; cooler parts black graphite
Pyrene		50	Same as for fluorene
Pentaphenylcyclopentadiene	<3.3	50	Same as for fluorene
Sucrose	2.5	40	Hottest parts white, soft diamond; cooler parts black, friable carbon. Ti attacked severely in hot parts
Polyphenyl	2.86–3.3	60	Brownish red, brittle, glassy; strong diamond X-ray pattern
Camphor		60	Product nearly all white diamond
Polyethylene	2.8–3.3	60	White, insoluble; X-ray shows only crystalline phase is diamond
Adamantane	2.9–3.3	60	Same as for polyethylene.
Paraffin wax	2.8–3.3	60	Same as for polyethylene
Paraffin wax	1.83	?	1300°. Soft, white, X-ray shows broad, weak diamond lines
Hexamethylenetetramine		0	X-ray shows graphite only
Diphenylamine	<2.25	0	Soft, black; no scratch glass.
Octadecylamine	2.8–2.96	60	Scratchy, gray and black product.
Copper phthalocyanine		0	7 min. Black, brittle product; X-ray shows Cu and graphite
Raw peanut		60	5 min. Same remarks as for fluorene
Silicone rubber		0	X-Ray shows stishovite, graphite, perhaps SiC

usually decreased monotonously by about 5% during a 15-min. heating period. However, when some diamond was produced, the average resistance usually did not fall by quite as much and sometimes even increased by 1 or 2% for a few minutes early in the heating period. These resistance changes were not reproducible nor large enough to serve as reliable indicators of the course of the pyrolysis reactions.

The white diamondiferous products obtained in the above experiments were active in an adsorptive or a chemical sense, for they changed color when brought in contact with iodine in the following way. The diiodomethane used to test the density of the products contained some dissolved iodine as the result of age, exposure to light, air, etc. When a fragment of the pyrolysis product was floated on a drop of the diiodomethane, the liquid became nearly colorless in about a minute while the originally snow-white product became blue, green, yellow, and finally brown. Often, the white pyrolysis products would be similarly colored by traces of dissolved bromine in some of the other liquids used to estimate density.

C. *Comments.* Two unexpected results appeared in these experiments.

(1) Graphite of excellent crystallinity often was found as the sole product even though diamond was thermodynamically favored and even though, under the same conditions of pressure, time, and temperature, a pure carbon such as spectroscopic graphite or carbon black was found to change at least partly to diamond. Evidently compounds such as naphthalene, anthracene, or chrysene, which contain fused benzene rings, pyrolyze to graphites which are unusually reluctant to form diamond. Most of the compounds which contain relatively large amounts of nitrogen also favor the formation of graphite to the exclusion of diamond. One might ascribe this effect of nitrogen to its tendency to form three covalent bonds; four covalent bonds are required to make a diamond structure.

The experiments with anthracene mixed with camphene or iron show that the formation of diamond from anthracene is not impossible but instead requires some sort of seeding agent (camphene) or catalyst (iron). The camphor and peanut experiments illustrate that oxygen is not very effective as a blocker of diamond formation under these conditions and is not so effective as nitrogen. (Small amounts of nitrogen or oxygen

could be removed by combination with the titanium tube wall; the inside surface of the tube would usually be golden in color from TiN after nitrogeniferous compounds had been pyrolyzed. It is also likely that oxygen and hydrogen diffused rather rapidly in either direction through the hot tube wall.)

(2) The second unexpected result was that usually the diamond formed by pyrolysis of organic compounds was snow-white, often resembling paraffin wax or chalk in appearance and mechanical properties. By contrast, when carbons are transformed to diamond at temperatures of 2000°K. and higher, the product diamond is usually black.[1,3] Only rarely was the white product capable of scratching glass. Yet X-ray diffraction analyses of these white products showed that the only crystalline constituent was diamond though, of course, the diffraction lines were broad and indicated a small crystal size.

Because the ends of the titanium tube were much cooler than the midlength, as a result of the greater heat loss through the molybdenum lead-in wires, the response of the pyrolyzed material to different pyrolysis temperatures could be estimated. Paraffin and camphene, for example, gave white products at both high and low temperatures (note also experiment with paraffin at 1300°). On the other hand, substances containing some aromatic rings, such as pyrene or pentaphenylcyclopentadiene, evidently first pyrolyze to a kind of "graphite" which then becomes white diamond at higher temperatures. The pyrolysis of most carbonaceous materials is a complicated chemical process, and it appears that even at 2000° the effects of the initial molecular structure are detectable. Evidently, very slight changes in structure are sufficient to alter the outcome of the reaction. For examples, compare chrysene and pyrene, or fluorene and anthracene.

As an indication that sometimes not all of the initial molecular structure is destroyed under these rather severe conditions, one may note that polyphenyl yielded a brittle, reddish brown product of rather high density. There is a family of red organic compounds known as rubrenes which might be described as highly branched chain polyphenyls of low molecular weight, and it is very likely that the reddish diamond contains regions having rubrene structures derived from the polyphenyl starting material.

IV. Concluding Remarks

Aust, Bentley, and Drickamer[9] have found that several kinds of large organic molecules, e.g., pentacene, hexacene, or violanthrene, appear to react with each other in a sort of cross-linking fashion at high pressures (200–500 kbars) and surprisingly low temperatures, 190–300°K. Definite changes in the spectra and electrical behavior were thereby produced in these materials. They observed that the changes were more pronounced in single crystals than in polycrystalline material, which could be said to illustrate in another way the importance of structural factors in reactions involving carbon at high pressures.

It is likely that some of the unusual chemical behavior noted in the experiments described in this paper is not unique to carbonaceous materials but could probably be observed in other reactions carried out at high pressures and moderate temperatures. The elucidation of this behavior will probably not be easy, however, on account of the large numbers of complex large molecules which are likely to form.

(9) R. B. Aust, W. H. Bentley, and H. G. Drickamer, *J. Chem. Phys.*, 41, 1856 (1964).

Exchange of Deuterium with the Hydroxyl Groups of Alumina

by J. L. Carter, P. J. Lucchesi, P. Corneil, D. J. C. Yates, and J. H. Sinfelt

Process Research Division, Esso Research and Engineering Company, Linden, New Jersey
(Received March 29, 1965)

The kinetics of the exchange of deuterium with the surface hydroxyl groups of alumina have been studied by infrared spectroscopy. It was observed that the reactivity of the different hydroxyl groups with deuterium varied. Of the three hydroxyl groups present (at 3785, 3740, and 3710 cm.$^{-1}$), the high-frequency one was found to be the most reactive. The kinetics of the exchange obey a logarithmic rate law similar to that observed frequently for chemisorption processes. The kinetics may be a consequence of surface heterogeneity. It was observed that the presence of platinum on the surface of the alumina increased the rate of exchange. However, the effect depended on the method of impregnation of the platinum, probably due to the presence or absence of halogen in the platinum salt used for the impregnation. A study of the effect of platinum concentration for samples prepared by impregnation with chloroplatinic acid yielded complex results which may largely be a consequence of the presence of chlorine in the samples. Some evidence was obtained for a direct reaction (other than exchange) of deuterium with alumina at certain conditions.

The existence of hydroxyl groups on the surface of alumina has been shown by infrared spectroscopy.[1,2] Estimates of the concentration of such hydroxyl groups have been made by Hall and Lutinski[3] using a technique based on the exchange of the hydroxyl hydrogen with deuterium as the temperature is slowly and continuously increased. The method was shown to be useful for distinguishing forms of hydrogen which have markedly different reactivities with deuterium. The results of these workers indicated the presence of at least three different forms of hydrogen on alumina. This agrees with the infrared studies of Peri and Hannan[2] and of workers in this laboratory,[4] which have identified three different hydroxyl groups on alumina.

In the work of Hall and Lutinski,[3] the exchange of deuterium with surface hydrogen was also studied with samples of alumina containing approximately 0.7% platinum. These samples were prepared by impregnation of alumina with chloroplatinic acid. It was observed that the presence of platinum did not materially lower the concentration of surface hydroxyl groups on the alumina. Furthermore, it was concluded that the presence of platinum on alumina did not enhance the rate of exchange of deuterium with hydroxyl groups. However, it was also observed that the presence of

halogen (fluorine) on alumina markedly decreased the reactivity of the hydroxyl groups with deuterium. The platinum on alumina catalysts contained halogen by virtue of impregnation with chloroplatinic acid, and the authors pointed out that the presence of halogen very likely has a bearing on the comparison of the deuterium-exchange activity of their alumina and platinum on alumina samples.

While the work of Hall and Lutinski has given a clear indication of the ease of exchange of deuterium with the hydroxyl groups of alumina and certain platinum on alumina catalysts, the kinetics of the exchange were not investigated extensively. In the work discussed in the present paper, the kinetics of the exchange of deuterium with the hydroxyl groups of alumina were studied in some detail. Additional information on the effect of platinum on the exchange was also obtained. The exchange reaction was followed by observing the change in the infrared spectrum (disappearance of OH and appearance of OD groups) as a

(1) D. G. Rea and R. H. Lindquist, 136th National Meeting of the American Chemical Society, Atlantic City, N. J., Sept. 1959.

(2) J. B. Peri and R. B. Hannan, *J. Phys. Chem.*, **64**, 1526 (1960).

(3) W. K. Hall and F. E. Lutinski, *J. Catalysis*, **2**, 518 (1963).

(4) R. O. Steiner, J. L. Carter, and D. J. C. Yates, unpublished results, Esso Research and Engineering Co., Linden, N. J., 1959.

function of the time of exposure to deuterium. This was found to be a convenient way to follow the kinetics. There is also the additional interest that the study gives information on the exchange by another method, different from that employed by Hall and Lutinski. The infrared method is an especially good way to study the reactivity of a particular hydroxyl group on the surface, as distinct from simply measuring the over-all rate of exchange of deuterium with surface hydroxyl groups.

Experimental

Materials. The preparation of the Al_2O_3 and Pt on Al_2O_3 samples used in the present work has been described previously.[5,6] The Al_2O_3, designated (A) Al_2O_3 in the previous publications, was prepared by heating β-alumina trihydrate for 4 hr. at 600°. The B.E.T. surface area of the final material was 295 m.²/g. The Pt on Al_2O_3 catalysts were prepared by impregnation of the alumina with aqueous chloroplatinic acid, followed by drying at 120° and subsequent calcination in air for 1 hr. at 500°. Several Pt–Al_2O_3 catalysts were prepared using an aqueous solution of $Pt(NH_3)_2$-$(NO_2)_2$ for the impregnation.

Most of the experiments on the exchange of deuterium with the OH groups on alumina were made with a sample of (A) Al_2O_3 which was wetted with distilled water in an amount equivalent to the quantity of impregnating solution used in the preparation of the platinum catalysts and then recalcined for 1 hr. at 500°. This was done to ensure that the Al_2O_3 and Pt–Al_2O_3 catalysts were treated as nearly as possible in the same manner prior to the deuterium-exchange experiments, so that the effect of the platinum on the exchange could be more clearly defined. The sample of (A) Al_2O_3, wetted and subsequently recalcined in the manner described, is identified as (H) Al_2O_3 in this paper.

The deuterium used in the exchange studies was supplied by the Matheson Co. and had a stated purity of 99.5%. The hydrogen was obtained from the Linde Co. Both gases were dried by passing them through a liquid nitrogen trap prior to use.

Apparatus. A detailed description of the apparatus has previously been reported[5] in a study of the chemisorption of ethylene on alumina. The samples used were flakes 2 × 0.7 cm. in size with a "thickness" of about 20 mg./cm.². The flakes were prepared by pressing the powder at 15,000 p.s.i.

Procedure. The experiments reported in this paper were performed as follows. The samples were slowly heated to 600° while they were being evacuated. When the pressure reached 5 × 10⁻⁶ mm., the heating
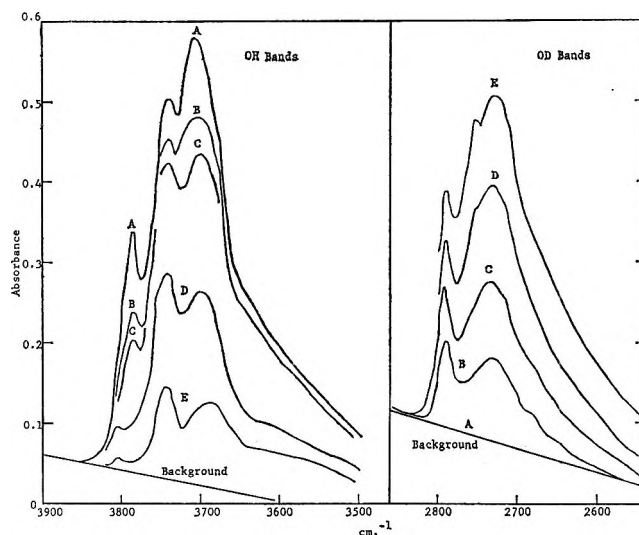
Figure 1. Typical infrared spectra of (H) Al_2O_3 as a function of time of treatment with D_2 at 250°: A, 0; B, 1; C, 10; D, 100; E, 1130 min.

was discontinued, and the sample was cooled to room temperature under vacuum. Some samples were reduced in hydrogen at 500° prior to a final outgassing to 5 × 10⁻⁶ mm. and were then cooled to room temperature under vacuum. After cooling to room temperature, the infrared spectrum was recorded. Following this, the sample was heated to the temperature to be used for the exchange experiment, and deuterium was admitted to the sample cell at a pressure of 15 cm. After the desired time had elapsed, the gas was evacuated from the cell. The sample was then cooled to room temperature and the spectrum again recorded. The amount of deuterium present during exchange corresponded to a large excess, over 10 times the amount required to exchange all the surface hydroxyl groups.

Results

The bulk of the data on deuterium exchange with the OH groups of alumina were obtained on the sample designated as (H) Al_2O_3. Typical infrared spectra obtained at room temperature, before and after exposure to deuterium for varying periods of time, are shown in Figure 1. In the original spectrum, before exposure to deuterium, three different bands due to surface OH groups were observed. These bands occurred at wave numbers of 3785, 3740, and 3710 cm.⁻¹. After exposure to deuterium, additional bands due to OD groups were observed at 2790, 2755, and

(5) P. J. Lucchesi, J. L. Carter, and D. J. C. Yates, *J. Phys. Chem.*, **66**, 1451 (1962).

(6) P. J. Lucchesi, J. L. Carter, and J. H. Sinfelt, *J. Am. Chem. Soc.*, **86**, 1494 (1964).

2730 cm.$^{-1}$. The high-frequency OH group (3785 cm.$^{-1}$) exchanged more readily with deuterium than did the other OH groups. After exposure to deuterium for 10 min. at 150°, the 3785-cm.$^{-1}$ band showed 30% exchange compared to 9% for the 3740- and 3710-cm.$^{-1}$ bands. However, the difference in exchange activity appeared to decrease with increasing temperature. The remainder of the paper, including the data shown in Figures 2 through 5, is concerned with the high-frequency OH and OD groups.

Since the absorbance scale used in recording the infrared spectra is a linear function of the amount of OH or OD present, the progress of the exchange reaction can be followed readily. Data showing the % exchange of the high-frequency OH group as a function of time over the (H) Al$_2$O$_3$ at three different temperatures are given in Figure 2. The data show a good linear relationship between the per cent exchange and the logarithm of the time. Such a relation is frequently observed in chemisorption.[7]

In the experiments on (H) Al$_2$O$_3$, the ratio of OD appearance (2790-cm.$^{-1}$ band) to OH disappearance (3785-cm.$^{-1}$ band) was essentially unity (Figure 3). The ratio was calculated simply as the ratio of the increase in absorbance of the OD to the decrease in absorbance of the OH, assuming the extinction coefficients to be equal. The reaction with deuterium

Figure 4. Effect of Pt on the exchange of D$_2$ with the hydroxyl groups of Al$_2$O$_3$ at 150°. Pt impregnated on Al$_2$O$_3$ with chloroplatinic acid solution: □, (H) Al$_2$O$_3$; ◥, 0.001% Pt on Al$_2$O$_3$; ◢, 0.1% Pt on Al$_2$O$_3$; ■, 0.6% Pt on Al$_2$O$_3$.
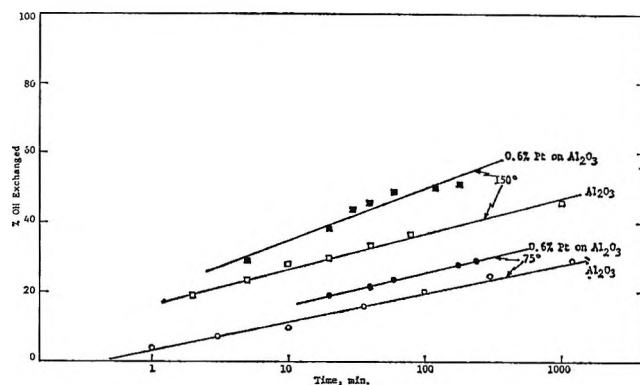
Figure 5. Effect of Pt on the exchange of D$_2$ with the hydroxyl groups of Al$_2$O$_3$. Pt impregnated on Al$_2$O$_3$ with Pt(NH$_3$)$_2$(NO$_2$)$_2$ solution: O, (H) Al$_2$O$_3$ at 75°; □, (H) Al$_2$O$_3$ at 150°; ●, 0.6% Pt on Al$_2$O$_3$ at 75°; ■, 0.6% Pt on Al$_2$O$_3$ at 150°.

on the (H) Al$_2$O$_3$ therefore appears to be limited to the exchange, there being no evidence for the additional formation of OD groups beyond that due to exchange. However, the situation does not appear to be the same for the (A) Al$_2$O$_3$, which is different from the (H) Al$_2$O$_3$ in that it was not wetted and recalcined. In the case of the (A) Al$_2$O$_3$ there was evidence for a net formation of OD groups over and above that due to exchange. A comparison of the ratios of OD appearance (2790-cm.$^{-1}$ band) to OH disappearance (3785-cm.$^{-1}$ band), as well as the extents of OH exchange, for the (A) Al$_2$O$_3$ and (H) Al$_2$O$_3$ at 150° is given in the tabulation

Figure 2. Exchange of D$_2$ with the hydroxyl groups of (H) Al$_2$O$_3$: O, 75°; □, 150°; △, 250°.

Figure 3. Ratio of OD appearance to OH disappearance on (H) Al$_2$O$_3$: O, 75°; □, 150°; △, 250°.

Time on D$_2$, min.	—% OH exchanged—		—OD/(100 − OH)—	
	(A) Al$_2$O$_3$	(H) Al$_2$O$_3$	(A) Al$_2$O$_3$	(H) Al$_2$O$_3$
2	21	19	1.3	0.95
10	29	29	1.4	1.0

(7) B. M. W. Trapnell, "Chemisorption," Butterworth and Co. Ltd., London, 1955, p. 106.

Thus, while the extent of OH exchanged is the same for (A) Al_2O_3 and (H) Al_2O_3, there is an additional reaction of deuterium with the surface in the case of (A) Al_2O_3.

Impregnation of alumina with platinum was found to increase the rate of exchange of deuterium with the surface OH groups, as shown in Figures 4 and 5 for the high-frequency OH group (3785 cm.$^{-1}$). In the data presented in Figure 4 the platinum was impregnated from an aqueous chloroplatinic acid solution. An interesting dependence of the exchange on platinum concentration was found. On addition of 0.001% platinum, the exchange increased. However, further increase in the platinum concentration resulted in a decrease in the rate of exchange, until at 0.6% platinum the rate was not significantly higher than that observed with the alumina alone. In the data presented in Figure 5 the platinum was impregnated from an aqueous solution of $Pt(NH_3)_2(NO_2)_2$. Here the data indicate that the presence of platinum significantly increases the rate of exchange even at the 0.6% platinum level, whereas in the samples prepared from chloroplatinic acid the effect was significant only at much lower platinum levels.

The results presented to this point are all for samples which were simply heated to 600° and outgassed prior to the exchange measurements. Data obtained on samples of $Pt–Al_2O_3$ prepared from $Pt(NH_3)_2(NO_2)_2$, in which the platinum was reduced in H_2 for 1 hr. at 500° prior to the final outgassing, showed little effect of the reduction on the subsequent rate of exchange of deuterium with the OH groups. Data on the extents of exchange after 1 hr. at 150° are shown below for a $Pt–Al_2O_3$ sample containing 2 wt. % platinum, and for a (H) Al_2O_3 sample for comparison

	Pt–Al₂O₃		(H) Al₂O₃
	Reduced	Not reduced	
% OH Exchanged	45	46	34

The difference shown between the reduced and non-reduced samples is probably within experimental error and not significant. Note that the extent of exchange of the 2% Pt sample is about the same as was observed on the 0.6% Pt sample (Figure 5) after 1 hr. at 150°. Thus, increasing the platinum content above 0.6% appears to have little effect.

Discussion

The present work has demonstrated the use of the method of infrared spectroscopy for studying the kinetics of a surface process involving the reaction of deuterium molecules from the gas phase with surface hydroxyl groups on alumina. Thus, infrared data are useful for characterizing reactivity as well as the structure of adsorbed species.[5,6,8]

The observation of the present work that the high-frequency OH group exchanged faster than the lower-frequency groups appears to differ from the results of Peri and Hannan[2] on alumina. These investigators reported that the lowest-frequency group frequently exchanged faster than the others. However, they used a γ-alumina, whereas the present work was conducted with η-alumina, a crystallographically different form. The detailed surface environment of the OH groups on these aluminas could be quite different and could play an important role in determining the exchange activity of the OH groups. Furthermore, the exchange data reported by Peri and Hannan were obtained in a higher temperature range, 250–500°, compared to the range 75–250° used in the present work. The results of the present study indicate that the differences in the rates of exchange of the various groups decrease with increasing temperature, and it is possible that the order of exchange activity might change at a sufficiently high temperature.

The reaction of deuterium with the surface hydroxyl groups of alumina is characterized by a strong deceleration of the rate as the reaction proceeds. The kinetics are best described by an exponential rate law, which is typical of many chemisorption processes.[7] In the present case, if we let x equal the fraction of OH groups exchanged after exposure to deuterium for a time t, the rate law is

$$r = \frac{dx}{dt} = b \exp(-\alpha x) \tag{1}$$

where b and α are parameters which are functions of temperature. These parameters can be evaluated from a plot of $\ln (dx/dt)$ vs. x, which is a straight line with slope equal to $-\alpha$ and intercept equal to $\ln b$. The values of dx/dt for various values of x can conveniently be evaluated by noting that $dx/dt = 1/t\cdot(dx/d \ln t)$. The quantity $(dx/d \ln t)$ is the slope of a plot of x vs. $\ln t$, which in the case of the (H) Al_2O_3 can be obtained from Figure 2. The values of the parameters b and α as a function of temperature are summarized in Table I. From the temperature de-

Table I: Effect of Temperature on the Parameters b and α

Temp., °C.	b, sec.$^{-1}$	α
75	2.8×10^{-5}	28.6
150	6.1×10^{-4}	23.1
250	2.9×10^{-3}	12.9

(8) J. L. Carter, P. J. Lucchesi, J. H. Sinfelt, and D. J. C. Yates, *Actes Congr. Intern. Catalyse, 3ᵉ, Amsterdam, 1964*, 644 (1965).

pendence of b the apparent activation energy E_0 at the beginning of the exchange (*i.e.*, at $x = 0$) can be calculated. When this is done, it is found that E_0 varies somewhat with temperature. In the range 75 to 150°, E_0 is 12 kcal./mole, decreasing to 7 kcal./mole in the range 150 to 250°. The parameter α characterizes the decrease in the exchange activity as the reaction proceeds and can be related to an increase in activation energy during the course of the exchange. This, in turn, may be a consequence of surface heterogeneity. With regard to the detailed mechanism of the exchange, the information available is not sufficient to establish this with any certainty. Exchange reactions of the type discussed here may be more complex than is initially apparent. For example, as Peri points out,[9] the exchange of deuterium with surface hydroxyl groups does not require substitution of deuterium on the same site from which the hydrogen was removed. It is conceivable that a surface OD group could form by interaction of deuterium with an oxide ion with subsequent removal of hydrogen from an adjacent hydroxyl site. Finally, surface migration processes could be involved; *e.g.*, deuterium could dissociate at selected sites on the surface and then migrate to hydroxyl groups to exchange, similar to the mechanism of Porter and Tompkins[10] for hydrogen chemisorption on metals.

Turning now to the observed effect of platinum on the exchange, it should be noted that most of the data were obtained with nonreduced $Pt-Al_2O_3$ samples. The promotional effect of platinum on the exchange with such samples is similar to the results of Hall and Lutinski.[3] These authors point out that reaction of deuterium with the oxygen on the platinum leads to formation of D_2O, thus providing another mechanism of exchange in the system. They also indicated that the exchange was not enhanced if the platinum was reduced but was actually decreased. However, they obtained data showing that the presence of halogen markedly decreased the exchange activity. Since their $Pt-Al_2O_3$ samples all contained chlorine, the true

effect of the platinum was obscured, as the authors pointed out. In the present work, the effect of reducing the platinum was investigated using $Pt-Al_2O_3$ samples prepared from a nonhalogen containing platinum salt to avoid the complications due to the halogen. While extensive data were not obtained on reduced samples, the available results indicate that the rate of exchange on a reduced platinum-containing sample is higher than that on alumina. Thus, when the alumina is impregnated with a nonhalogen-containing platinum salt, the rate of exchange is increased regardless of whether the platinum is reduced or not. These results are therefore taken as evidence of a cooperative effect of platinum in the exchange of deuterium with the hydroxyl groups of alumina. It may be that the effect involves transport of active species between platinum sites and sites on the alumina surface. It seems possible that deuterium would dissociate on platinum sites and subsequently migrate to hydroxyl groups on the alumina to exchange. The platinum sites would thus serve as a source of reactive deuterium atoms.

The interfering effect of the halogen observed in the work of Hall and Lutinski may account for the unusual dependence of the rate of exchange on the platinum concentration in the chloroplatinic acid preparations used in the present study. The decrease in the rate of exchange with increasing platinum concentration above the 0.001% platinum level may be related to the increasing halogen content. It seems possible that halogen displaces some of the more reactive OH groups from the surface, with the remaining OH groups exhibiting a lower over-all reactivity than is observed with the original OH groups on alumina. Alternatively, the halogen may serve as a trap for reactive species (deuterium atoms) migrating between platinum sites and hydroxyl groups on the alumina.

(9) J. B. Peri, *J. Phys. Chem.*, **69**, 220 (1965).

(10) A. S. Porter and F. C. Tompkins, *Proc. Roy. Soc.* (London), **A217**, 529 (1953).

Proton Magnetic Resonance and Infrared Studies of Hydrogen Bonding

in Tri-n-octylammonium Salt Solutions[1a]

by W. E. Keder and L. L. Burger

Chemical Laboratory, Battelle Northwest,[1b] Richland, Washington   *(Received March 30, 1965)*

Cation–anion hydrogen bonding in tri-n-octylammonium salt solutions has been studied by measuring nuclear magnetic resonance and infrared absorption spectra. Solutions of tri-n-octylammonium salts were prepared by equilibration of tri-n-octylamine (TOA) in CCl_4 with aqueous acids. A linear relationship between chemical shift of the N–H proton and stretching frequency of the N–H (or N–D) group was found to exist although deviations were found for some salts containing larger anions. Relative strengths of the tri-n-octylammonium–anion hydrogen bonds are discussed.

Introduction

The partition of acids and of metal ions between aqueous acid solutions and organic solutions of long-chain alkylamines has been the subject of considerable recent interest.[2] In the process of this extraction, alkylammonium salts are formed in which the anions either are those of the acid present or are complex metal anions. Many salts of this type are very soluble in low dielectric constant solvents, and the low conductivities of their solutions indicate that they are in the form of nondissociated ion pairs.[3] Formation of larger aggregates has also been found in some alkylammonium salt solutions.[4] Hydrogen bonding would be expected to contribute to the interionic association in these solutions and perhaps to the formation of the larger aggregates. In the present work an attempt has been made to study the strength of cation–anion hydrogen bonding in solutions of tri-n-octylammonium salts by measurement of infrared and nuclear magnetic resonance spectra. Some preliminary measurements have already been reported.[5]

Both n.m.r. and infrared techniques have been used extensively in the past to study hydrogen bonding.[6] Sandorfy and co-workers have studied cation–anion hydrogen bonding in alkylammonium salts previously but mainly in the solid phase.[7] Hydrogen bonding to anionic proton acceptors in other systems has also been studied recently by several workers.[8] Reeves, et al., have studied intramolecular hydrogen bonding which, like the interionic bonding in the alkylammonium salts,

remains intact at all measurable concentrations in nonparticipating solvents.[9] Fraenkel has measured n.m.r. spectra of some anilinium salts in solution and discussed cation–anion interaction.[10]

(1) (a) Work performed under Contract No. AT(45-1)-1350 between the Atomic Energy Commission and the General Electric Co. Presented at the 18th Northwest Regional Meeting of the American Chemical Society, Bellingham, Wash., June 18, 1963; (b) formerly Hanford Laboratories, General Electric Co.

(2) See, for example, Y. Marcus, *Chem. Rev.*, **63**, 139 (1963); G. H. Morrison and H. Freiser, *Anal. Chem.*, **36**, 93R (1964).

(3) J. M. P. J. Verstegen, *Trans. Faraday Soc.*, **58**, 1878 (1962); G. Duyckaerts, J. Fuger, and W. Müller, "L'Extraction Liquide–Liquide par de Chlorhydrate de Trilaurylamine," EURATOM Report No. EUR 426. f, Brussels, Belgium, 1963,

(4) E. Högfeldt, *Svensk Kem. Tidskr.*, **76**, 4 (1964).

(5) W. E. Keder and A. S. Wilson, *Nucl. Sci. Eng.*, **17**, 287 (1963); W. E. Keder, A. S. Wilson, and L. L. Burger, "Amine Systems in Solvent Extraction," presented at the Symposium on Aqueous Reprocessing Chemistry for Irradiated Fuels, OECD European Nuclear Energy Agency, Brussels, April 1963.

(6) O. C. Pimentel and A. L. McClellan, "The Hydrogen Bond," W. M. Freeman, San Francisco, Calif., 1960; D. Hadzi, Ed., "Hydrogen Bonding," Pergamon Press, Inc., New York, N. Y., 1959.

(7) B. Chenon and C. Sandorfy, *Can. J. Chem.*, **36**, 1181 (1958); C. Brissette and C. Sandorfy, *ibid.*, **38**, 34 (1959); P. Sauvageau and C. Sandorfy, *ibid.*, **38**, 1901 (1960).

(8) H. Lund, *Acta Chem. Scand.*, **12**, 298 (1958); J. Bufalini and K. H. Stern, *J. Am. Chem. Soc.*, **83**, 4362 (1961); J. B. Hyne and R. M. Levy, *Can. J. Chem.*, **40**, 692 (1962); J. B. Hyne, *J. Am. Chem. Soc.*, **85**, 304 (1963); A. Allerhand and P. von R. Schleyer, *ibid.*, **85**, 1233 (1963); G. Kotowycz, T. Schaefer, and E. Bock, *Can. J. Chem.*, **42**, 2541 (1964).

(9) L. W. Reeves, *ibid.*, **38**, 748 (1960); L. W. Reeves, E. A. Allan, and K. O. Strømme, *ibid.*, **38**, 1249 (1960); E. A. Allan and L. W. Reeves, *J. Phys. Chem.*, **66**, 613 (1962); **67**, 591 (1963); J. R. Merrill, *ibid.*, **65**, 2023 (1961).

(10) G. Fraenkel, *J. Chem. Phys.*, **39**, 1614 (1963).

Experimental

The tri-n-octylamine (TOA) used was obtained from the Eastman Kodak Co. in the form of the solid hydrochloride. This material had been purified by the method of Wilson and Wogman,[11] and it was found to be stable over a period of several years at room temperature. The free amine form was prepared by repeated washing of the hydrochloride with aqueous ammonia and water. It was a nearly colorless, viscous liquid when first prepared, but it gradually became yellow, and a small amount of white solid precipitated over a period of several months. Carbon tetrachloride solutions of the free amine were found to be still less stable than the pure TOA, and evidence of decomposition was noted within 24 hr. after preparation of such solutions. As a consequence, all TOA solutions were prepared immediately before use. Other chemicals used were reagent grade.

Infrared spectra were measured with a Perkin-Elmer Model 521 spectrophotometer, using CaF_2 or Irtran II cells. Proton magnetic resonance spectra were obtained with a Varian DP-60 instrument and the audio side-band technique was used to measure chemical shifts. The probe temperature (33 ± 2°) was controlled only by room air conditioning.

Each salt solution was formed by stirring a quantity of amine solution vigorously for 5-10 min. with an equal volume of the appropriate aqueous acid or metal salt-acid solution. Infrared and n.m.r. spectral measurements were made on the solutions thus prepared. The infrared spectrum was also measured of a corresponding solution in each case which was prepared by extraction from acid which was as nearly deuterated as it is possible to make with 99.8% D_2O and a minimum amount of nondeuterated, concentrated acid. The latter measurements proved convenient since there was no overlap of C-H stretching and N-D stretching frequencies in any of the salts studied.

Results and Discussion

Hydrogen bonding has been, perhaps, most widely studied by infrared spectroscopy.[6] In general, the effect of hydrogen bond formation upon the stretching mode in which the proton is involved is particularly marked. The frequency is shifted to lower values, the absorption peak is very much broadened, and the peak intensity is greatly increased. In many solutions which are only partially hydrogen bonded two stretching frequencies can be observed, and equilibria have been studied by relative intensity changes with dilution and temperature variations. Complete hydrogen bonding would be expected in the substituted ammonium salt solutions, however, since conductivity measurements indicate that these solutions are not dissociated.[3] In this case the value of the N-H stretching frequency may be used as an indication of the hydrogen bond strength.[12]

Proton magnetic resonance measurements have also been widely applied to the study of hydrogen bonding. Large downfield chemical shifts δ are normally obtained for the protons involved, making this technique potentially more precise than infrared.[6,13] Correlations between chemical shift and stretching frequency and between chemical shift and the enthalpy of hydrogen bond formation have been made and have been shown to be linear in certain cases.[9,14] Reeves has emphasized that it is important to determine δ-values for complete hydrogen bond formation when making such correlations. For incompletely bonded systems only a single resonance peak with a weighted average δ is usually observed because of rapid exchange of protons between bonded and unbonded sites.

In this work the infrared and n.m.r. spectra of CCl_4 solutions of tri-n-octylammonium salts containing a wide variety of anions were measured. All solutions were measured at 0.22 M concentration, and the chloride, nitrate, and perchlorate solutions were measured over the concentration range from 0.01 to 0.5 M. As an example of the results obtained, Figure 1 shows the infrared spectrum of 0.22 M TOA in CCl_4 (a) as prepared, (b) after contacting with 1 N HCl, and (c) after contacting with partially deuterated 1 N HCl. The N-H and N-D stretching absorption peaks are seen to be very broad and intense, and they occur in this case at 2420 and 1890 cm.$^{-1}$, respectively, frequency values which indicate strong hydrogen bonding. For the other salts studied ν_{N-H}-values range upward to about 3100 and ν_{N-D} to 2270 cm.$^{-1}$, indicating significantly weaker hydrogen bonding. Dilution of the chloride, nitrate, and perchlorate salts causes either no change in ν_{N-H} or a shift to lower frequency. This effect will be discussed below.

It is of interest to note in passing that the stretching frequency spectrum of water dissolved in these solutions is significantly different from that dissolved in CCl_4 alone. For the tri-n-octylammonium chloride solution the frequencies are 3380 and 3760 cm.$^{-1}$ compared to 3615 and 3705 cm.$^{-1}$, and the lower frequency peak is

(11) A. S. Wilson and N. A. Wogman, *J. Phys. Chem.*, 66, 1552 (1962).

(12) See, for example, G. Aksnes and T. Gramstad, *Acta Chem. Scand.*, 14, 1485 (1960); T. Gramstad, *ibid.*, 15, 1337 (1961).

(13) J. A. Pople, W. G. Schneider, and H. J. Bernstein, "High-resolution Nuclear Magnetic Resonance," McGraw-Hill Book Co., Inc., New York, N. Y., 1959, Chapter 15.

(14) J. D. Ferraro and D. F. Peppard, *J. Phys. Chem.*, 67, 2639 (1963).
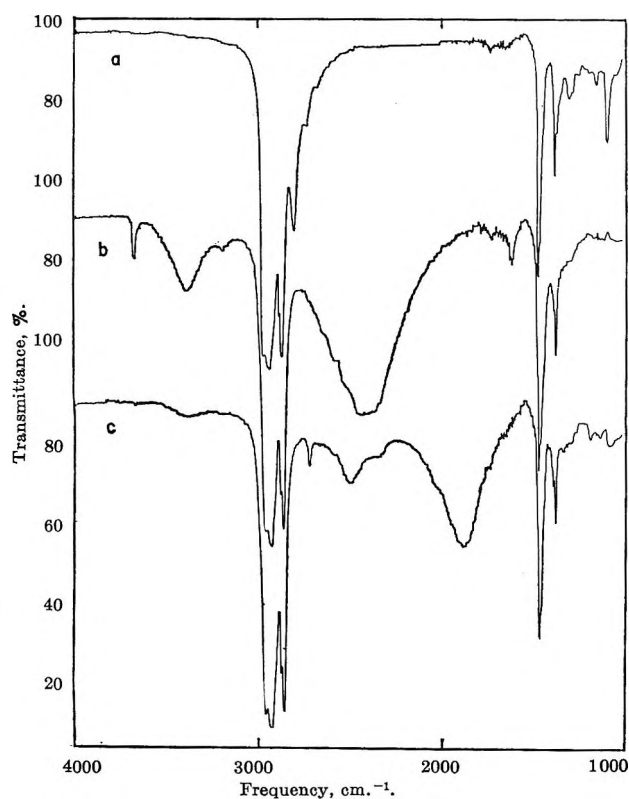
Figure 1. Infrared spectra of (a) 0.22 M TOA in CCl_4, (b) 0.22 M tri-*n*-octylammonium chloride in CCl_4, and (c) the same prepared from partially deuterated hydrochloric acid.
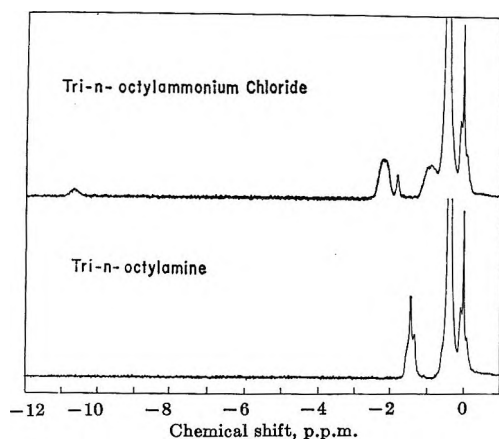
Figure 2. Proton magnetic resonance spectra of (a) 0.22 M TOA in CCl_4 and (b) 0.22 M tri-n-octylammonium chloride, showing chemical shifts relative to the methyl resonances.

relatively much broader and more intense. This spectral change and the fact that the solubility of water is much greater than in CCl_4 alone suggest specific bonding between the water and the salt.[5]

In Figure 2 the n.m.r. spectrum of 0.22 M TOA in CCl_4 is shown (a) before and (b) after equilibration

with 1 N HCl. Formation of tri-*n*-octylammonium chlorides by extraction of HCl introduces the N–H resonance at 10.7 p.p.m. downfield from CH_3 and (in this case) a resonance just upfield from α-methylene. The latter resonance has been shown previously to be due to a combination of dissolved water and acid in excess of the stoichiometric amount.[5] This spectrum shows that for tri-*n*-octylammonium chloride solutions dissolved water protons exchange rapidly (in $<10^{-3}$ sec.) with the excess acid present but that neither exchanges rapidly with the proton on the nitrogen. The latter slow exchange rate makes it possible to determine a chemical shift value which is a property of the N–H proton alone. In certain other TOA salt solutions rapid exchange of N–H protons does take place, making it impossible to obtain δ_{N-H}-values. Infrared results for some of these salts are listed in Table I.

Table I: Stretching Frequencies for Tri-*n*-octylammonium Salts

Anion	ν_{N-D}	ν_{N-H}
HF_2^-	1925	
N_3^-	(1950)	2530
$FeCl_4^-$	2300	3050
$H_2PO_4^-$	1875	2450
$PtCl_6^{2-}$	2600	
IO_3^-	2100	
HSO_3^-	2030	2620
$CoCl_4^{2-}$		2620

To support the argument that tri-*n*-octylammonium salts do not dissociate at the concentrations of interest here, n.m.r. spectra of some representative examples were measured over the range 0.01 to 0.5 M in CCl_4. If ion pair dissociation occurred upon dilution of these salts it should cause a large shift of the N–H resonances in an upfield direction. A downfield shift was actually observed, however, when the chloride, nitrate, and perchlorate salts were diluted, as is shown in Figure 3. A detailed investigation of this dilution behavior has not yet been made, but since the δ-values are nearly independent of concentrations above 0.1 M, a concentration of 0.2 M was chosen as acceptable for comparison of the N–H chemical shifts for the salts of interest here.

While a shift of the N–H resonances to lower magnetic fields upon dilution of these solutions had not been predicted, it is perhaps not unreasonable to suggest that this is the result of the breakup of dimers (polymers) of the salts involved. It seems reasonable that a diminution in the dipole–dipole interaction between such ion pairs would result in the reinforcement of the
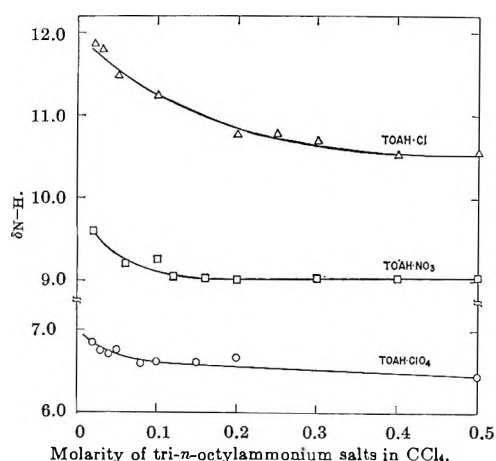
Figure 3. Chemical shift of N–H protons of tri-*n*-octylammonium salts *vs.* concentration in CCl₄.

Figure 4. Chemical shifts of N–H protons in tri-*n*-octylammonium salt solutions plotted against N–D stretching frequencies of corresponding salts prepared with deuterated acids.

ion–ion interaction and hence in an increase in hydrogen bond strength, thus causing an increased downfield shift within the rather poor limit of accuracy at the lower concentrations. The δ-values for the nitrate and chloride salts form a straight line when plotted against the square root of total salt concentration. This may be taken as an indication that dimer formation alone is involved at these concentrations. No extensive studies on degree of aggregation of these salts in CCl₄ have yet been made. The few boiling point measurements of Fomin and Potapova[15] show complete dimer formation, however, at a concentration of 0.1–0.2 *M* tri-*n*-octylammonium nitrate in CCl₄. Similar salts in hydrocarbon solvents have shown aggregation of about this magnitude.[4]

Infrared spectra would be expected to show separate N–H stretching frequencies for the independent ion pairs and for their dimers. The great width of these bands has made this observation difficult. Significant shifts toward lower frequencies upon dilution were found and are in general agreement with the n.m.r. results.

In Figure 4 chemical shifts δ_{N-H} for a number of TOA salts with univalent anions are plotted against stretching frequencies ν_{N-D} obtained for corresponding salts prepared with deuterated acids. The chemical shift values are measured from the TOA methyl resonance which is 0.91 p.p.m. downfield from internal tetramethylsilane. The points fall on a straight line within the estimated errors of the measurements which are ± 0.2 p.p.m. in δ and ± 30 cm.$^{-1}$ in ν.

The chemical shift value for tri-*n*-octylammonium cyanide was obtained with a salt prepared by metathesizing dry tri-*n*-octylammonium chloride in CCl₄ with solid AgCN. Exclusion of water was necessary
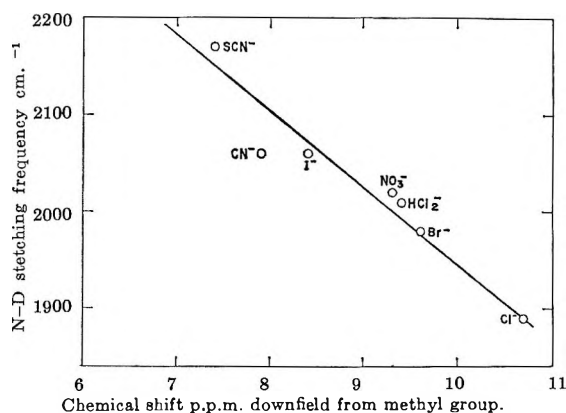
because of the rapid exchange of protons between it and the N–H site. In the process of this experiment it was shown that the δ_{N-H}-value for tri-*n*-octylammonium chloride is the same for dry CCl₄ solution as for a solution in equilibrium with 1 *N* HCl though, of course, in the former the water proton resonance is missing. This is a good indication that the varying amounts of water which extract into the different salt solutions studied do not interfere with the N–H chemical shifts obtained if an independent N–H resonance is in fact available.

The HCl₂⁻ salt was prepared by equilibration of the TOA-CCl₄ with 10 *N* HCl. Earlier experience had shown that such a solution contains 2 moles of HCl/mole of TOA and that the N–H resonance is separate from that of the water–hydrogen bichloride combination.[5] Attempts to obtain δ_{N-H}-values for F⁻ and HF₂⁻ salts were unsuccessful even when anhydrous HF was used. Infrared spectra indicated that only the HF₂⁻ salt is formed, even when the TOA/HF ratio is much greater than 1.[16] Rapid exchange between the N–H and the HF₂⁻ protons apparently prevents one from obtaining a δ_{N-H}-value for the hydrogen bifluoride salt.

The fact that a linear relationship between δ and ν is obtained suggests that both properties have the same functional relationship to hydrogen bond strength. It seems reasonable that both properties may be linear in enthalpy of bond formation since this would be the most simple case. Although many examples to the contrary are known,[6] such a linear relationship with

(15) V. V. Fomin and V. T. Potapova, *Russ. J. Inorg. Chem.*, **8**, 509 (1963).

(16) T. C. Waddington, *J. Chem. Soc.*, 1708 (1958).
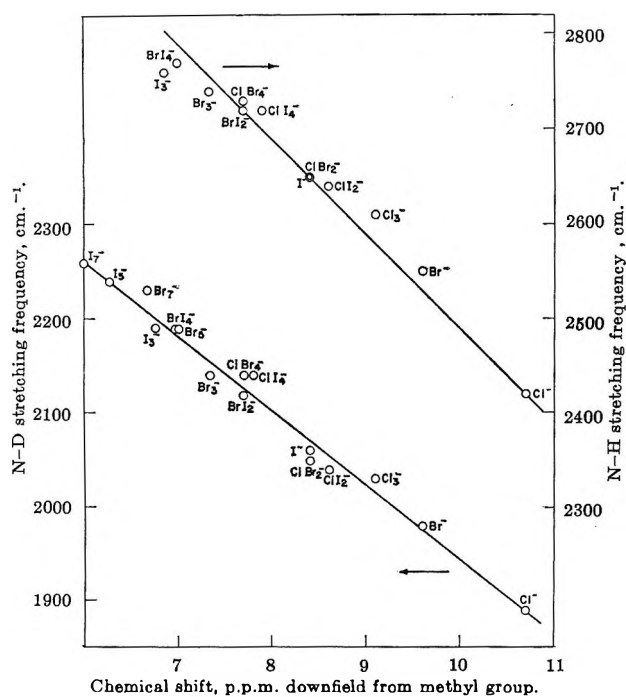
Figure 5. Chemical shifts of N–H protons in CCl₄ solutions of TOA halides and polyhalides plotted against N–H and N–D stretching frequencies of the same or corresponding deuterated salts (line transferred from Figure 4).

hydrogen bond strength has been observed in the past.[14] This relationship is likely confined to cases in which neither the proton acceptors nor the donors are very different. The present measurements cannot decide this point. If it is assumed that the chemical shift vs. enthalpy relationship for these tri-*n*-octylammonium salts is the same as that found for the group of compounds studied by Ferraro and Peppard, the hydrogen bond contribution to the ion pair formation in these salts is in the range of 4.0 to 5.4 kcal./mole.[14]

In Figure 5, δ_{N-H}-values, which were obtained for 16 tri-*n*-octylammonium halides and polyhalides, are plotted against N–H and N–D stretching frequencies measured for the same, or corresponding deuterated, solutions. The polyhalides were prepared according to the indicated stoichiometry by introduction of the proper amounts of elemental halogens into the TOA solutions during the process of equilibration with the aqueous acids. Only the polyhalide ions shown are available by this technique since introduction of a halogen into a solution of a halide lower in the periodic table would result in reduction of the halogen by halide ion from the aqueous phase during the process of extraction. The exact ionic constitution of the solutions measured is not known and may be a mixture of polyhalide anions averaging the designated stoichiometry.
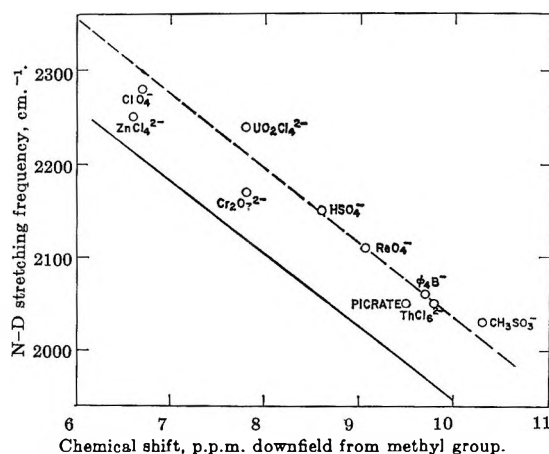
Figure 6. δ_{N-H} vs. ν_{N-D} for 0.22 *M* tri-*n*-octylammonium salts of more complex anions (solid line transferred from Figure 4).

The single (but very broad) infrared absorptions indicated, however, that only one anionic species was present in each case.

The points for the polyhalides also lie on a straight line within experimental error. The line through the N–D stretching data is the same as that shown in Figure 4. The values of both ν_{N-D} and δ_{N-H} indicate that, of the ions studied, chloride forms the strongest hydrogen bonds. As would be expected, the strength of bonding decreases with increasing anion size. An interesting order of hydrogen bond strength emerges from these polyhalide data. The bond strength is dependent upon the identity of the halide ion and upon the number of halogen atoms attached to it but appears to be nearly independent of the identity of the latter halogen atoms.

In Figure 6 we have plotted ν_{N-D} vs. δ_{N-H} for tri-*n*-octylammonium salts of some more complex anions. In this case the points lie well above the solid line, which again has been transferred from Figure 4, and they appear to form a line parallel to it. The position of these points corresponds to a greater chemical shift for a given N–D stretching frequency. The reason for this "extra" chemical shift may be connected with the symmetry of the electron density along the H anion line. As Pople, *et al.*,[17] have pointed out, loss of axial symmetry would be expected to produce a downfield chemical shift.

The relative strength of anion–cation hydrogen bonding in the tri-*n*-octylammonium salts studied is in the expected order of electrostatic interaction. It is of interest to note that the most weakly hydrogen-bonded salts are those whose anions extract most strongly.[2,11]

(17) See ref. 13, p. 408.

This indicates that the anion–cation bonding in the organic phase is of little importance in determination of the relative anion extractability. Rather, it appears that those anions which are the best proton acceptors extract most poorly because of their greater solvation in the aqueous phase. Diamond, *et al.*,[18] have suggested this explanation in their discussion of the selectivity of anion-exchange resin.

(18) B. Chu, D. C. Whitney, and R. M. Diamond, *J. Inorg. Nucl. Chem.*, **24**, 1405 (1962).

Studies of the Hydrogen Held by Solids. VII. The Exchange of the Hydroxyl Groups of Alumina and Silica–Alumina Catalysts with Deuterated Methane

by John G. Larson and W. Keith Hall

Mellon Institute, Pittsburgh, Pennsylvania (*Received March 31, 1965*)

The exchange of CD_4 (CH_4) with the OH (OD) groups of silica–alumina and alumina catalysts was studied and the mixing of isotopes between CH_4 and CD_4 was investigated. Over alumina, mixing took place at a readily measurable rate at room temperature with an activation energy of 5.7 kcal./mole. It was found that the reaction was catalyzed by a small number ($\sim 5 \times 10^{12}/cm.^2$) of active sites and involved exchange with only about 1% of the catalyst hydroxyl groups. The surface density of active sites was measured by selective poisoning with CO_2, NO, H_2O, C_2H_4, and C_3H_6. A primary isotope effect was found for the exchange of CH_4 with D_2 compared with CD_4 with H_2, indicating that the rate-determining step involved the dissociation of a CH or a CD bond. The rate of the mixing reaction was limited by the slowest step, *i.e.*, the rupture of a CD bond. Over silica–alumina, the activation energy for mixing was 33.4 kcal./mole; the reaction did not take place at a measurable rate below about 450°. As the surface hydroxyl groups are mobile at this temperature, all of the catalyst hydrogen was available for exchange. Therefore, the catalyst hydrogen content could be measured by exchange with CD_4. Such results were in good agreement with those resulting from other methods. It was shown that isotopic mixing between CD_4 and CH_4 was a stepwise process, proceeding through exchange with catalyst hydroxyl groups, and that there was a primary isotope effect between exchange of CH_4 with OD and CD_4 with OH.

Introduction

In 1948, Parravano, Hammel, and Taylor[1] reported that CD_4 and CH_4 could be equilibrated over a silica–alumina cracking catalyst. They cited the disappearance of CD_4 as evidence that the C–D bond was ruptured during chemisorption and suggested that this step is a necessary prerequisite to catalytic cracking. A thorough study was not made; the data were suf-

(1) G. Parravano, E. Hammel, and H. S. Taylor, *J. Am. Chem. Soc.*, **70**, 2269 (1948).

ficient to outline only the gross aspects of the kinetics. It was not possible to decide, for example, whether the equilibration of a CD_4–CH_4 mixture involved a bimolecular interaction or an exchange with the catalyst hydroxyl groups. While exchange between deuterated catalysts and a number of hydrocarbons has been examined, it appears that no further studies have been made with CH_4. It was deemed worthwhile, therefore, to extend our studies of the interactions between paraffin hydrocarbons and acidic surfaces to include this molecule.

Experiments were made in which CD_4 (CH_4) was circulated over the catalyst; the exchange reaction with catalyst OH (OD) groups was continually monitored via a capillary leak into a mass spectrometer. The mixing of isotopes between CH_4 and CD_4 was also studied.

Experimental

Catalysts. The silica–alumina catalyst was from a batch of Houdry M-46 used previously[2] in related studies with isobutane. It contained about 12.5% Al_2O_3 and was found to have a surface area of 270 m.^{2}/g. The high purity silica gel sample had a surface area of 565 m.^{2}/g.; spark spectral analysis indicated a total metallic impurity of less than 10 p.p.m. The alumina sample was prepared from the neutral hydrolysis of aluminum isopropoxide. Its surface area was 158 m.^{2}/g. and its total metallic impurity level was less than 50 p.p.m. Further information concerning its properties is detailed elsewhere.[3]

Catalyst Pretreatment. Oxygen at 100 torr was circulated over the catalyst at 515° for 16 hr. A liquid nitrogen cooled trap in the circulating loop collected any H_2O or CO_2 formed. When a deuterated catalyst was required, the catalyst was then repeatedly exchanged with D_2 gas at 515° until the catalyst hydrogen approached the deuterium content of "pure" D_2 (99 atom % D or better), as indicated by the mass spectral analysis.[4] The catalyst was again treated with oxygen, after the hydrogen exchange, and finally was subjected to a 16-hr. evacuation at 515°.

Gases. A center cut of Phillips research grade methane was taken during vacuum transfer. Methane-d_4, methane-d_3, methane-d_2, and methane-d_1 were from Merck Sharp and Dohme of Canada, Ltd. These were further purified by the same method. The propylene and ethylene were both Phillips research grade and were used without further purification except for "degassing" by repeated cycles of freezing, pumping, and thawing. Carbon dioxide was obtained from the Matheson Co. After degassing, mass spectral analysis showed no detectable impurities. Matheson nitric

oxide was purified by passage through a silica gel column, followed by fractional distillation. Deuterium was obtained from General Dynamics Corp. Its isotopic purity was specified to be 99.5 atom % D. Matheson hydrogen was electrolytic grade. Both hydrogen and deuterium were given a final purification by diffusion through separate heated palladium thimbles.

Equipment and Procedures. The exchange experiments were conducted under conditions of a differential reactor. The gas phase was circulated in a loop over the catalyst by a small all-glass pump.[5] The reaction was monitored by allowing the gas phase to leak continuously into a modified CEC 21-611 mass spectrometer. The capillary leak was constructed from a 6-in. length of copper tubing with an i.d. of 0.008 in. It was constricted at one point to give the proper flow rate. The end of the capillary was located in the center of the flow tube to ensure representative sampling. The calculated time delay through the capillary was of the order of a few seconds. The rate of circulation was rate limiting only when reaction half-times became less than a few minutes. The catalyst was thermostated to ±0.5° by an automatically controlled electric furnace above 100° and by liquid baths below this temperature. Specific quantities of gases or mixtures of gases could be transferred quantitatively from a calibrated gas buret attached to the circulating loop. In poisoning experiments, the quantity of the poison added to or removed from the catalyst was determined by measurement in the buret system, which was also used for the preparation of mixtures.

Treatment of Data. The methane exchange was followed by scanning m/e peaks 14 to 20. In cases where the composition was changing rapidly, m/e values were plotted against time and smooth curves were constructed to get the relative peak heights at the same instant of time. The isotopic composition was then calculated using cracking patterns determined for each of the isotopic methanes. Relative sensitivities for the isotopic methanes were determined from binary mixtures. Corrections to the observed spectra for background were made (primarily H_2O at m/e 18 and 17). The good agreement between a statistically calculated methane equilibrium distribu-

(2) J. G. Larson and W. K. Hall, *J. Am. Chem. Soc.*, 85, 3570 (1963).

(3) W. K. Hall and F. E. Lutinski, *J. Catalysis*, 2, 518 (1963); W. K. Hall, F. E. Lutinski, and H. R. Gerberich, *ibid.*, 3, 512 (1964).

(4) W. K. Hall, H. P. Leftin, F. J. Cheselske, and D. E. O'Reilly, *ibid.*, 2, 506 (1963).

(5) W. K. Hall, W. E. Wallace, and F. J. Cheselske, *J. Phys. Chem.*, 63, 505 (1959); 65, 128 (1961).

tion with that determined experimentally (see Table II) is evidence that the method was satisfactory.

Results

Silica-Alumina Catalysts. The results of an experiment in which 1.56 cc. (NTP) of methane-d_4 was circulated over 4.47 g. of catalyst at 496° are presented in Figure 1. Considering that 1.5×10^{14} OH/cm.[2] were initially present,[4] the available H amounted to about 75 cc. (NTP). During the reaction (after 140 min.), only 1.6 cc. had appeared in the gas phase so that only about 2% of the catalyst hydrogen was exchanged. The initial product was CD_3H; CD_2H_2, CDH_3, and CH_4 were formed through subsequent secondary reaction. (The partial pressure of CD_3H does not extrapolate quite to zero because of the initial 2% CD_3H impurity.)

Figure 2 shows that the disappearance of CD_4 follows first-order kinetics very closely; the data can be accurately described by a first-order rate constant. Evidently, back reaction can be neglected because of the small fraction of the total hydrogen exchanged. Therefore, the first-order rate constant is identical with that relating the rate to the distance from equilibrium[5] for this special case.

The results of a related experiment, in which 1.4 cc. (NTP) of CH_4 was circulated over 4.07 g. of a deuterated catalyst at 490°, are shown in Figure 3. The points are the experimental data; the lines were drawn on the basis of the theory described below. A comparison of the first-order rate constant for the disappearance of CH_4 (18.8×10^{-3} min.$^{-1}$) to that for the disappearance of CD_4 (9.05×10^{-3} min.$^{-1}$) indicated a primary isotope effect. When the rate of appearance of D into the gas phase was plotted for this experiment, a linear curve resulted (Figure 4). The lack of deviation from linearity indicates that a large fraction of the total deuterium in the catalyst was equally available for exchange. At the experimental temperature, hydrogen is mobile on the catalyst surface.[4] Hence, methane may be activated at a number of sites which is small compared with the total hydrogen present, provided that the mixing of hydrogen on the surface is fast compared with the rate at which it is removed from the surface.

When a 2.12-cc. (NTP) mixture of CD_4 (42.5%) and CH_4 (57.5%) was circulated over an undeuterated catalyst, Figure 5 resulted. These data show that there is no direct exchange between CD_4 and CH_4 molecules. The experiment of Parravano, *et al.*,[1] was similar to this, except that they only analyzed for CD_4 and CD_3H. These data were insufficient to distinguish between possible exchange paths.
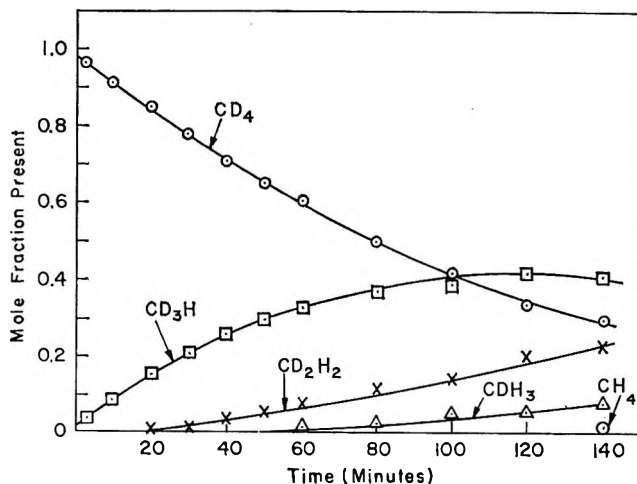
Figure 1. Distribution of products during exchange of CD_4 with hydroxyl groups of silica–alumina.
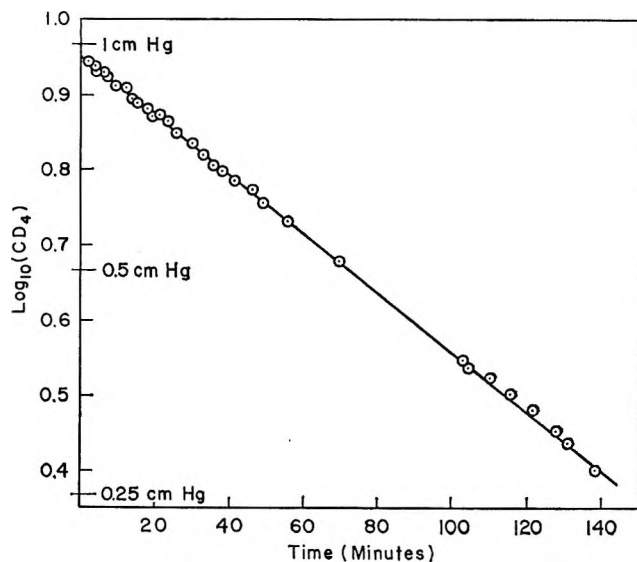
Figure 2. First-order dependence of exchange rate.

A model was derived to describe our results. Assuming that only one hydrogen (deuterium) atom is exchanged per interaction with the catalyst, and that the available OD is large compared with methane, the following reactions may be written

$$CH_4 + -OD \xrightarrow{k_1} CH_3D + -OH \qquad (1)$$

$$CH_3D + -OD \xrightarrow{k_2} CH_2D_2 + -OH \qquad (2)$$

$$CH_2D_2 + -OD \xrightarrow{k_3} CHD_3 + -OH \qquad (3)$$

$$CHD_3 + -OD \xrightarrow{k_4} CD_4 + -OH \qquad (4)$$

These reactions lead to the rate equations

$$d(CH_4)/dt = -k_1(CH_4) \tag{5}$$

$$d(CH_3D)/dt = k_1(CH_4) - k_2(CH_3D) \tag{6}$$

$$d(CD_2H_2)/dt = k_2(CH_3D) - k_3(CD_2H_2) \tag{7}$$

$$d(CHD_3)/dt = k_3(CD_2H_2) - k_4(CD_3H) \tag{8}$$

$$d(CD_4)/dt = k_4(CD_3H) \tag{9}$$

Equation 6 predicts a maximum at $d(CH_3D)/dt = 0$ when $(CH_4)/(CH_3D) = k_2/k_1$. While the preceding equations may be solved exactly without further as-
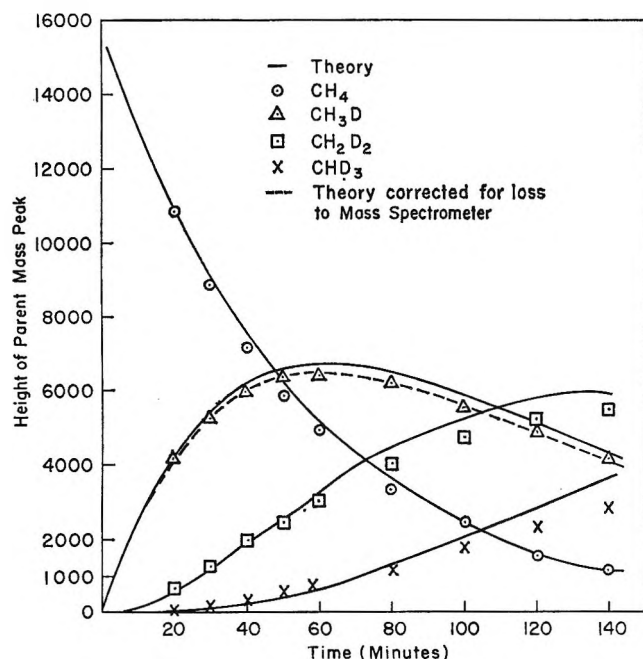
Figure 3. Distribution of products during exchange of CH_4 with deuterated silica–alumina.
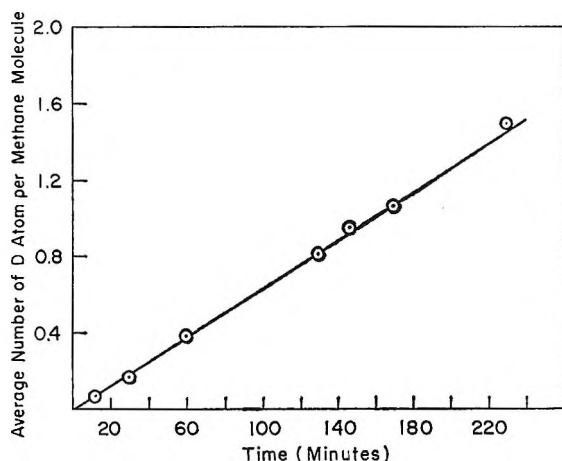
Figure 4. Integrated rate of appearance of deuterium in methanes.
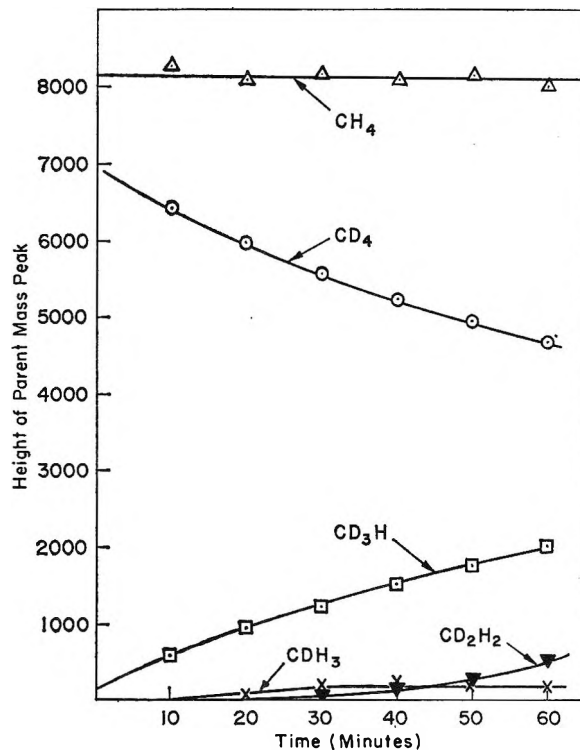
Figure 5. Exchange of CH_4–CD_4 mixture over silica–alumina.

sumptions, four rate constants are involved and only two of these (k_1 and k_2) are experimentally determined. Therefore, the model was further restricted by the assumption that the rate constant for exchange per hydrogen atom is $k_1/4$ regardless of the molecule reacting; i.e., that $k_2 = (^3/_4)k_1$, $k_3 = (^1/_2)k_1$, and $k_4 = (^1/_4)k_1$. This is equivalent to assuming that secondary isotope effects are negligible, i.e., that a hydrogen atom of CD_2H_2 has the same probability of reacting as a hydrogen atom of CH_4. The integrated forms of eq. 5–9 now reduce to two parameters: k_1 and the initial pressure of CH_4. The lines drawn in Figure 3 were calculated using this theory, taking k_1 from the first-order plot for the disappearance of CH_4. The approximation to the experimental data was remarkably good, but could be improved further by taking into account the decrease in total gas pressure due to the leak into the mass spectrometer. This is indicated by the dotted line for CH_3D.

An activation energy associated with the first-order rate constant for the disappearance of CD_4 was determined to be 33.4 kcal./mole over the range 460 to 540°. The hydrogen held by silica gel did not exchange with methane below 600°. When the data for silica–alumina were extrapolated to this temperature, it was determined that the exchange process over silica gel is only $^1/_{1000}$ as fast as that over silica–alumina.

Alumina Catalysts. The hydroxyl groups of alumina rapidly equilibrated with D_2 at 500°[4]; the catalyst hydrogen content could be measured readily from the isotope dilution which occurred. When CD_4 was circulated over the catalyst at 525°, it equilibrated with the OH groups of the catalyst as rapidly as it flowed over the catalyst. This behavior was in marked contrast to that with silica–alumina under the same conditions where the exchange proceeded at a modest but readily measurable rate. The catalyst hydrogen content could be measured from the analysis of the deuterated methanes. A comparison of the results from the two gases is made in Table I. Table II demonstrates that the equilibrium distribution of methane was obtained.

Table I: Measurement of Hydroxyl Content of the Alumina Catalyst

Method	OH/cm.$^2 \times 10^{-14a}$
D_2 exchange (before CD_4 exchange)	2.5
CD_4 exchange	2.6
D_2 exchange (after CD_4 exchange)	2.9

^{a} Values of 2.5 and 3.1 $\times 10^{14}$/cm.^{2} were found for the same catalyst using the DHA method; see ref. 3.

Table II: Methane Equilibration over Alumina

Compound	Mole % Measd.	Calcd.^{a}
CD_4	6.33	6.39
CD_3H	25.45	25.2
CD_2H_2	37.5	37.6
CDH_3	24.45	24.8
CH_4	6.31	6.13

^{a} Equilibrium calculation for D/H = 1.011.

When CD_4 was circulated over the same catalyst at 135°, there was an initial rapid exchange followed by a slower process (Figure 6). The extent of exchange is indicated by the fraction of molecules which have picked up one hydrogen atom (for this extent of exchange, essentially no CD_2H_2 was present). These results demonstrated the heterogeneous character of the catalyst hydrogen; the fraction of the hydrogen which exchanged rapidly at this temperature amounted to only a few per cent of the total. Nevertheless, as the extent of exchange increased, it became evident that the hydrogen removed from the catalyst was equilibrated among the methanes. Hence, the equilibration reaction is fast compared with the surface reaction
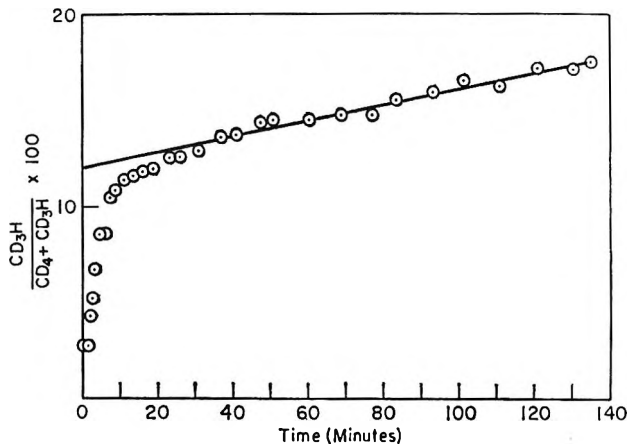
Figure 6. Rate of exchange of alumina hydroxyl groups with CD_4 at 135°.

(exchange of the hydroxyl groups). The surface density of hydroxyl groups corresponding to the initial rapid process (zero time intercept of Figure 6) amounted to about 7×10^{12} OH/cm.^{2}.

CH_4 and CD_4 equilibrated rapidly at room temperature. This was quite interesting because carbon–hydrogen bonds must be broken in order for this to occur and methane is not easily dissociated. The results presented in Figure 7 indicate that isotopic mixing occurred through the exchange of only one hydrogen (deuterium) atom per interaction with the surface. Methane-d_3 and methane-d_1 were formed at approximately the same rate; methane-d_2 was formed as secondary product. It is of particular interest that CH_4 and CD_4 disappeared at the same rate (Figure 8) whereas there was a strong isotope effect when they reacted separately.

When a mixture of CD_4 and H_2 (61.5% CD_4) was circulated over the catalyst, isotopic mixing occurred at about the same rate found for the CD_4–CH_4 equilibration. From this and the fact that the H_2–D_2 equilibration was much faster (virtually instantaneous at −78°), it was inferred that the rate-controlling step was probably the rupture of a C–D bond in the CD_4. Since the mixing of CH_4 with D_2 proceeds about 1.8 times faster than the reaction of CD_4 with H_2 (Table III), it follows that the rate of mixing of CH_4 with CD_4 is limited by the rate of breaking of the C–D bond, *viz.*, the slowest step.

In another experiment, CD_4 was exchanged with the catalyst hydrogen at 138° and the number of D atoms transferred to the catalyst was calculated from the analysis of the gas phase at the end of the experiment; this amount (3×10^{12}/cm.^{2}) was only about 1% of the total catalyst hydrogen. When the catalyst was
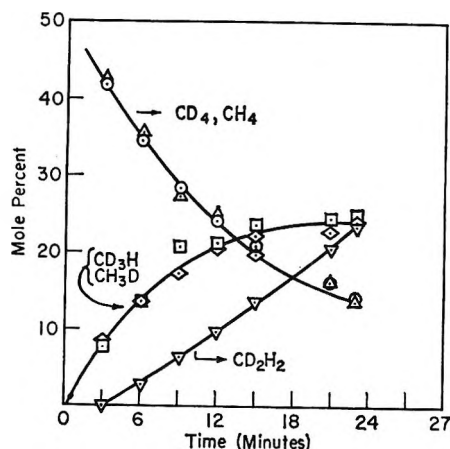
Figure 7. Distribution of methanes during exchange of equimolar CD_4 and CH_4 over alumina at 26°.
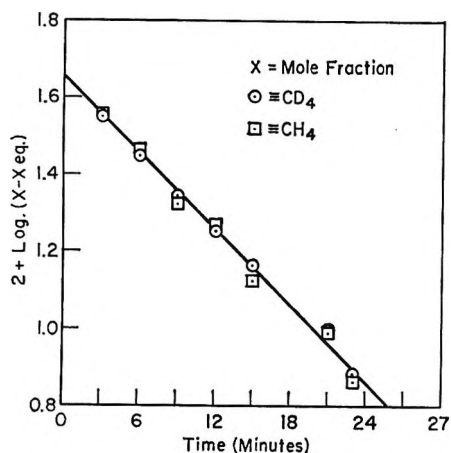
Figure 8. Proof that CD_4 and CH_4 exchange at the same rate.

Table III: Evidence that Rupture of the C–D Bond is the Rate-Determining Step of the Methane Equilibration Reaction

Mixture used	Vol. reacted, cc. (NTP)	$k,^a$ min.$^{-1} \times 10^2$
$CH_4 + D_2$	8.4	6.01
$CD_4 + H_2$	8.8	3.38
$CD_4 + H_2$	8.9	3.02
$CH_4 + D_2$	8.9	5.65
$CH_4 + CD_4$	5.9^b	3.46

^{a} $k = 1/t \log [(1 - x_{eq})/(x - x_{eq})]$ where x = mole fraction of CH_4 (CD_4). ^{b} Equivalent to 8.9 cc. (NTP) of $CD_4 + 2H_2$.

then exchanged with CH_4, virtually all of the D atoms, which had been transferred to the catalyst in the first step, now reappeared in the gas phase. This experiment proved conclusively that the exchanging hydrogen is located on specific sites; it does not mix with the

bulk of the catalyst hydrogen. It may be supposed therefore, that the diffusion of hydrogen across the surface of the catalyst is slow at this temperature. The reacting hydrogen may be held as OH, adjacent to the catalytically active sites.

A series of experiments was conducted to determine the activation energy associated with the equilibration of CD_4 and CH_4 over alumina. A good Arrhenius plot, the slope of which corresponded to 5.7 kcal./mole, was formed from rate constants determined in the range 0 to 62°. This was very much lower than the value for silica–alumina (33.4 kcal./mole).

The exchange between CD_4 and CH_4 could be completely poisoned by the adsorption of a small amount of CO_2. Peri[6] found that CO_2 was adsorbed on sites essential for the isomerization and polymerization of butene-1. These processes were not poisoned by CO_2, however, because it was displaced by the olefin. This does not happen with methane below 300°.

A series of experiments was made to determine the number of sites required for the methane equilibration reaction. The catalyst was exposed to excess CO_2 (so that some remained in the gas phase) at room temperature. After 5 min. of contact, the gas phase was condensed into a liquid nitrogen trap from which it was regenerated and measured. By difference, it was found that 2.81 cc. (NTP) of CO_2 had been retained by 1.61 g. of alumina. This corresponded to a coverage of 2.7×10^{13} CO_2/cm.^{2}. No observable exchange occurred when a mixture of CD_4 and CH_4 was circulated over the catalyst for 34 min. Moreover, no CO_2 appeared in the gas phase (less than 1×10^{12} CO_2/cm.^{2} would have been detected). The mixture was removed and the catalyst was raised in temperature to effect desorption of a portion of the chemisorbed CO_2. The CO_2 removed was measured and the catalyst was cooled to room temperature for another equilibration reaction. These alternate processes were repeated using increasing desorption temperatures until the CO_2 material balance was obtained (0.03 cc. (NTP) of CO_2 not recovered at 500°). Figure 9 is a plot of the amount of CO_2 left on the catalyst as a function of the temperature at which it was removed. The catalyst first became active for the equilibration reaction after evacuation to about 300°, where the slope changes abruptly. In agreement with Peri,[6] this finding may be taken as evidence that there are several different kinds of chemisorbed CO_2 present on

(6) J. B. Peri, Abstracts of Papers, Division of Colloid and Surface Chemistry, 145th National Meeting of the American Chemical Society, New York, N. Y., Sept. 1963; Proceedings of the 3rd International Congress on Catalysis, Amsterdam, July 1964, Preprint No. I, p. 72.
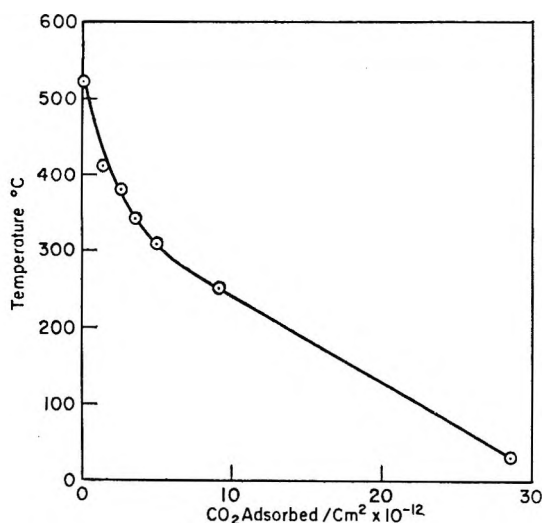
Figure 9. Retention of CO_2 by alumina; vacuum isobar.
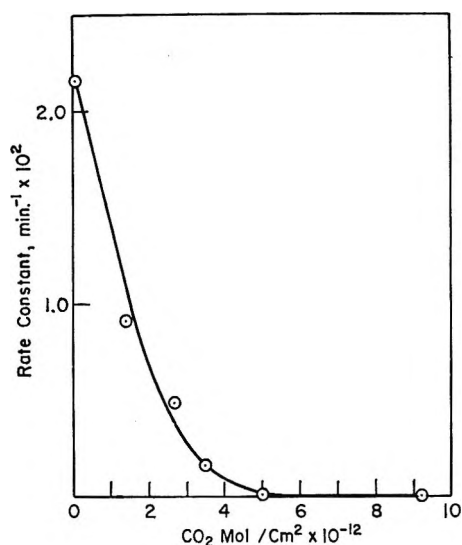
Figure 10. Poisoning plot for CO_2.

Figure 11. Poisoning plot for NO.

alumina; the portion poisoning the equilibration reaction was the more strongly adsorbed form.

The first-order rate constant for the equilibration reaction is plotted as a function of the CO_2 remaining on the catalyst in Figure 10. The approximately linear relationship between the rate constant and the number of sites covered by strongly chemisorbed CO_2 suggests that these sites are homogeneous. Little reliable information is available on this subject although one frequently reads reports referring to the distribution of acid sites (weak, medium, and strong) on these materials. Work on the isobutane exchange system[2] indicated that about 80% of the isobutane was adsorbed on silica–alumina catalysts in a homogeneous manner.

The curvature at the slower rates (Figure 10) was probably caused by the removal of two types of CO_2 in this region, only one of which was acting as a poison for the reaction. Correcting for this, the number of sites active for methane equilibration amounted to $3-4 \times 10^{12}/cm.^2$.

Several simple compounds were found which adsorbed selectively on the sites required for methane equilibration. Small measured increments of the poison were circulated over the catalyst with a diluent gas (methane). The disappearance of the poison from the gas phase was followed via the leak to the mass spectrometer. The results obtained with nitric oxide are shown in Figure 11; they demonstrate the linear relationship between the rate constant for the methane equilibration reaction and the number of sites covered by poison. Similar poisoning plots were made for other gases, viz., C_2H_4, C_3H_6, and H_2O ($H_2 + O_2$); the values of the number of active sites, as obtained

by linear extrapolation to the adsorption axis, are summarized in Table IV. All of these data lead to the conclusion that there are between 2 and 4 $\times 10^{12}$ sites/cm.^{2}. The result for H_2O requires special comment. Water is a nonselective poison and, if added directly, much larger amounts would be required to poison the reaction. The sites can be selectively poisoned, however, by forming the H_2O directly on the active sites by the reaction of hydrogen with oxygen. This also serves to identify the sites active for methane equilibration with those required for water formation.

In a similar vein, CO_2 was found to poison the equilibration of C_2D_4 with C_2H_4 and of H_2 with D_2. Since linear poisoning plots (similar to Figures 10 and 11) were obtained in all cases, it was concluded that the sites are all energetically equivalent.

Table IV: Number of Active Sites on Alumina as Determined by Poisoning the CD_4-CH_4 Equilibration Reaction

Poison	Method used	Sites/cm.^{2} $\times$ 10^{-12}
CO_2	Selective desorption	2–4
H_2 and O_2	Reaction on site	2 or 4
Ethylene	Selective desorption	2
Propylene	Selective desorption	4
NO	Selective desorption	4

Discussion

The isotopic mixing of CD_4 and CH_4 over alumina involved exchange with several per cent of the catalyst hydrogen. Moreover, this hydrogen resided at very definite sites on the alumina surface. This was shown by the fact that the deuterons introduced by exchange with CD_4 could be quantitatively recovered by a subsequent exchange with CH_4; had the few OD groups introduced mixed with the much larger amount of OH, this would not have been possible under the conditions of the experiment. The small amount of hydrogen which exchanged between room temperature and 135° is believed to be located at sites where methane is dissociatively adsorbed.

It is instructive to consider a recent model of the alumina surface. Peri[7] pictured the creation of active sites by the process of dehydroxylation; as water is removed, aluminum ions are exposed and adjacent surface O^{2-} ions are formed. In this way, dual acid–base sites are created which tend to rehydrate readily. The driving force for this is so high that analogous processes occur with other molecules, e.g., with ammonia which is cleaved to form adjacent NH_2 and OH groups. Peri classified the residual hydrogen into five categories, depending upon whether a residual hydroxyl group had 0, 1, 2, 3, or 4 immediately adjacent O^{2-} ions; he found infrared bands in the OH stretching region corresponding to each. The C site, which has the lowest frequency (3700 cm.$^{-1}$), corresponds to isolated OH groups whose *nearest* neighbor sites are all vacant, *i.e.*, sites where aluminum ions are exposed. Such OH groups have no *immediately* adjacent O^{2-} ions, but nevertheless exchanged with D_2 most readily.[8] Since the nearest neighbors are not O^{2-}, the next nearest neighbors generally are. This is exactly the situation required to afford a simple interpretation of our results.

Since methane is readily deuterated over alumina, it may be supposed that the molecule is cleaved as it is chemisorbed. If it reacted with the dual acid–base surface sites in a manner analogous to NH_3 and H_2O, then Al-CH_3 and adjacent OH groups would be formed. In some cases, the resulting aluminum alkyl would be simultaneously adjacent to an OH and an OD group so that on desorption it could equally well combine with either. Presumably, this could occur with any of the types of residual OH (OD) groups considered by Peri except one, *viz.*, the A site where the hydroxyl group is surrounded by four O^{2-} ions so that there are no adjacent vacant sites, but the situation at the C type would be most favorable. The exchange process can be expressed very simply as

$$CD_4 + O \diagdown \diagup OH \rightleftharpoons DO \diagdown \diagup CH_3 OH \qquad (10)$$
$$Al \qquad\qquad Al$$
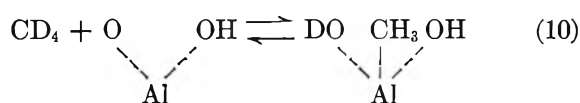
The experimental data indicate that there are 3 × 10^{12}/cm.^{2} active sites. A completely hydroxylated alumina surface would contain (Peri's model) 1.3 × 10^{15}/cm.^{2} of OH. When 90% dehydroxylated, 5 × 10^{14}/cm.^{2} of aluminum ions would be exposed and an equal number of O^{2-} ions formed; the residual hydroxyl content would be 1.3 × 10^{14}/cm.^{2}. It follows, therefore, that a large fraction of the residual OH groups would have adjacent exposed aluminum ions with an O^{2-} nearest neighbor. The surface density of such configurations is, however, at least an order of magnitude higher than the density of active sites derived from the poisoning experiments. Hence, it must be concluded that all such configurations are not catalytically active. It is probable that only the high energy sites, which are created at the domain boundaries,[7] are strong enough to dissociate methane. Nevertheless, for each active site (3 × 10^{12}/cm.^{2}) there will be one readily exchangeable OH group (3 to 4 × 10^{12}/cm.^{2} found). It seems pertinent that the strong sites which dissociate CH_4 are the ones which also strongly chemisorb CO_2, NO, etc.

Figure 6 shows that a slower exchange process occurred in addition to the rapid exchange identified with hydroxyl groups adjacent to active sites. It seems reasonable to ascribe this slower process to the diffusion of hydrogen from distant locations, to positions adjacent to the active sites. This allows one to reconcile the marked differences in behavior of silica–alumina and alumina. With the former, there was no evidence of heterogeneity of catalyst hydrogen; the

(7) J. B. Peri, *J. Phys. Chem.*, **69**, 211, 220, 231 (1965).

(8) J. B. Peri and R. B. Hannan, *ibid.*, **64**, 1526 (1960).

activation energy for exchange was much higher and reaction did not occur at measurable rates below 400°. Evidently, on silica–alumina, the sites are not the same as on alumina; they appear to be weaker. Consequently, much higher temperatures are required to activate the methane molecule. At these temperatures (above 400°), the surface migration of hydrogen is rapid; hence, all of the catalyst hydrogen appears to be equivalent. In the case of CD_4 exchange, the D left at the catalytic site by the adsorption of CD_4 is rapidly equilibrated with the total catalyst hydrogen and is not available for subsequent exchange with a CH_4 molecule (Figure 5). This may be contrasted with the result from alumina where the exchanged hydrogen maintains its identity at the active site. While the exchange of methane over silica–alumina catalysts possibly does not follow the same mechanism as with alumina, the above arguments show that there is no inconsistency in a uniform picture for both.

The manner in which *hydrogen* is activated by alumina and silica–alumina surfaces is not at all understood. By analogy with the present methane results, hydrogen may be cleaved on the alumina surface to form an Al–H and an adjacent OH. Infrared data support the view that the analogous reaction occurs on the surface of ZnO.[9] In both cases, the driving force seems to be the screening of (restoration of coordination around) the exposed cation. With silica–alumina, the situation is even less clear and anything that is written must necessarily be classified as speculation. Studies of the exchange between the hydrogen held by isobutane and deuterated cracking catalysts have been interpreted[2] in terms of abstraction of the tertiary hydride ion by the catalyst to form the isobutyl carbonium ion; the nine hydrogens remaining on the carbonium ion then exchange freely with available catalyst hydroxyl groups. The identity of the tertiary ion is conserved either by hydride transfer from incoming molecules or by recombination with the carbonium ion on desorption. A model for the active sites on silica–alumina catalysts may be drawn from the developing understanding of the acidity of the X- and Y-type zeolites,[10] with which they may be presumed to be related. When a zeolite is decationated, sites which function as Brønsted acids first form. These may be described by

(11)
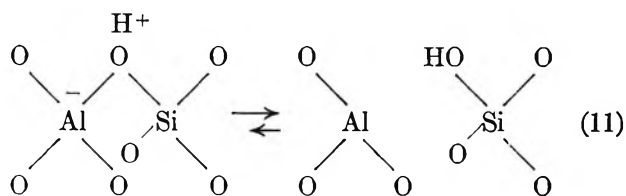
On degassing above 500°, these sites are dehydroxylated and in the process pairs of defect sites are created. One of the pairs contains an anion vacancy and the other a cation vacancy. This pair may function to form carbonium ions from paraffins by hydride ion abstraction, *i.e.*

anion vacancy + cation vacancy

(12)
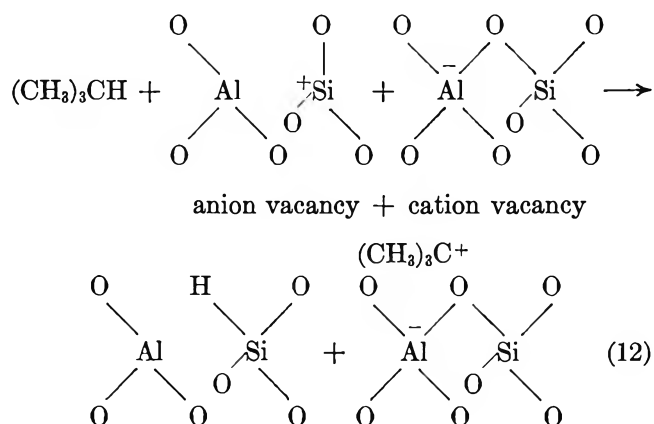
It seems doubtful whether these ideas should be extended to methane, as the existence of a methyl carbonium ion seems very unlikely. It is, of course, possible that the over-all result is given by

(13)
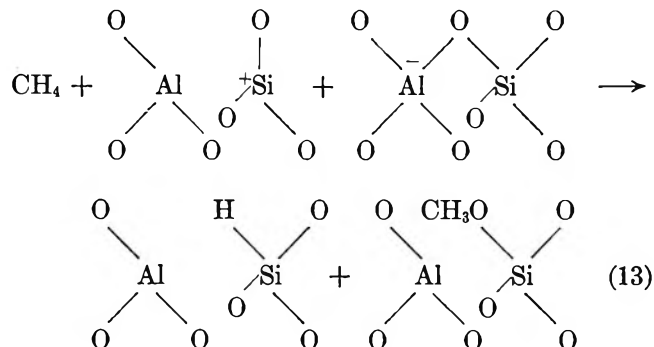
These equations indicate ways in which hydrocarbons may dissociate and adsorb, but they offer no insight into the mechanism of hydrogen exchange with catalyst deuteroxyl groups. They do, however, emphasize the important point that the ideas which have been developed concerning the intermediates involved in exchange processes over silica–alumina do not fit well with the simple type of intermediate suggested by our data for alumina. In fact, with alumina, the methyl group is thought to be held by the aluminum ion with concomitant formation of a hydroxyl group, whereas extension of current thoughts concerning silica–

(9) R. P. Eischens, W. A. Pliskin, and M. J. D. Low, *J. Catalysis*, 1, 180 (1962).

(10) J. B. Uytterhoeven, L. G. Christner, and W. K. Hall, *J. Phys. Chem.*, 69, 2117 (1965).

alumina would suggest that the methyl group be attached to oxygen and hydrogen to the cation. While this chemistry is plausible, it is highly speculative and should be so considered.

Hydrogen Bonding. II. Phenol Interactions with Substituted Pyridines[1a]

by Jerome Rubin[1b] and Gilbert S. Panson

Chemistry Department, Rutgers, The State University, Newark, New Jersey　　*(Received April 5, 1965)*

The hydrogen-bonding equilibrium constants of some substituted pyridines to phenol in carbon tetrachloride at 20 and 40° are reported. The constants are correlated with Hammett's and Tafts' substituent constants, the equation of the line having been calculated by the method of least squares. Thermodynamic data for the reaction are given. A steric effect caused by di-*o-t*-butyl groups is demonstrated, as well as a solvent effect which shows that the equilibrium constant value is dependent upon the solvent.

The hydrogen-bond formation of phenol to proton acceptors is well known and has been studied extensively.[2] Investigations have been made from merely the molecular association of phenol alone,[3] to such electron-pair donors as carbonyls,[4] ethers,[5] amides,[6] and alkyl halides.[7] However, as indicated by the authors,[2] comprehensive and complete studies are seriously lacking. The work of Gramstad is a noteworthy exception as can be seen by his contributions in this particular area. He has investigated the interaction of phenol and/or pentachlorophenol with organophosphorus compounds,[8,9] amides,[10] nitrogen compounds,[11] carbonyls and ethers,[12] and sulfoxides and nitroso compounds.[13] However, a complete and thorough study of the hydrogen bonding between phenols and pyridines had not been done. It was with this intention that the project was undertaken.

The previous communication had reported the equilibrium constants of some substituted phenols with pyridine in carbon tetrachloride.[14] It is shown that a linear correlation exists for the logarithm of the association values *vs.* Hammett's substituent constants. Continuing this investigation, the equilibrium constants of phenol with substituted pyridines are now

reported. A steric effect is studied as well as the effect on the value of the equilibrium constant by changing the solvent.

Experimental

The technique used for evaluating the equilibrium constants is the same as that reported previously.[14]

(1) (a) Parts I and II are excerpts of the thesis submitted to the Graduate School of Rutgers, The State University, by J. Rubin in partial fulfillment of the requirements for the Degree of Doctor of Philosophy. (b) E. I. du Pont de Nemours and Co., Richmond, Va.

(2) G. C. Pimentel and A. L. McClellan, "The Hydrogen Bond," W. A. Freeman and Co., San Francisco, Calif., 1960.

(3) (a) M. Iro, *J. Mol. Spectry.*, 4, 125 (1960); (b) M. M. Maguire and R. West, *Spectrochim. Acta*, 17, 369 (1961).

(4) G. Aksnes, *Acta Chem. Scand.*, 14, 1475 (1960).

(5) R. West, *et al.*, *J. Am. Chem. Soc.*, 86, 3227 (1964).

(6) N. D. Joesten and R. S. Drago, *ibid.*, 84, 2696 (1962).

(7) R. West, *et al.*, *ibid.*, 84, 3221 (1962).

(8) G. Aksnes and T. Gramstad, *Acta Chem. Scand.*, 14, 1485 (1960).

(9) T. Gramstad, *ibid.*, 15, 1337 (1961).

(10) T. Gramstad and W. J. Freglevik, *ibid.*, 16, 1369 (1962).

(11) T. Gramstad, *Spectrochim. Acta*, 16, 807 (1962).

(12) T. Gramstad, *ibid.*, 19, 497 (1963).

(13) T. Gramstad, *ibid.*, 19, 829 (1963).

(14) J. Rubin, *et al.*, *J. Phys. Chem.*, 68, 1601 (1964).

The concentration of phenol was 0.025 M as it was shown that no significant amount of self-bonding occurred at this dilution. The concentrations of the substituted pyridine ranged from 0.01 to 0.10 M. A minimum of six determinations, each with a different amount of pyridine, was made, the average value being taken as the equilibrium constant.

The solvents were either spectroscopic grade or Fisher Certified. The chloroform was passed through a column of alumina before use. The compounds were obtained commercially, and all were purified by distillation *in vacuo* and/or recrystallization prior to use. The cells were matched fused silica, 10 cm. in length.

The measurements at 40° ± 1 were obtained by preheating the cell with the solution in a constant temperature bath. The thermodynamic parameters were obtained by solving the equation $-RT \ln K = \Delta H° - T\Delta S°$ for two temperatures.

Results and Discussion

A compilation of the results of the reaction of phenol with substituted pyridines is shown in Table I. Where previous work existed such as that of Halleux[15] and Gramstad[11] and comparisons could be made, the agreement is quite good.

Figure 1. Log k vs. Hammett's σ-values. Points are:
(1) 4-t-butyl, (2) 4-methyl, (3) 4-ethyl, (4) 3-methyl,
(5) hydrogen, (6) 3-bromo, (7) 3-cyano, (8) 4-cyano.

Table I: Thermodynamic Data for Some Substituted Pyridines with Phenol in Carbon Tetrachloride

Sub-stituent	K, l./mole, 20°	K, l./mole, 40°	$\Delta F°$, kcal.	$\Delta H°$, kcal.	$\Delta S°$, cal.
H	59	29	−2.4	−6.5	−14.0
4-Methyl	82	41	−2.6	−6.4	−13.0
3-Methyl	65	31	−2.4	−6.7	−14.5
4-Ethyl	77	40	−2.5	−5.9	−11.5
4-t-Butyl	84	45	−2.6	−7.1	−12.0
4-Cyano	12	8.4	−1.5	−3.2	− 6.0
3-Cyano	14	8.3	−1.6	−4.9	−11.5
3-Bromo	15	9.2	−1.6	−4.5	−10.0

Some relationships between the equilibrium constants and other chemical or physical parameters have already been reported. Halleux had shown qualitatively and Gramstad quantitatively that there is a relationship between the log of the association constants and the pK of the proton donors. It was also reported that a linear correlation for the ionization constants of some substituted phenols with Hammett's σ-values had been found.[16] It thus seemed reasonable to expect a linear relationship between the logarithm of the association constants and the Hammett substituent constants for the system substituted phenols with pyridines and/or phenol with substituted pyridines.

Figure 2. Log k vs. Taft's σ^0-values. Points are:
(1) 4-t-butyl, (2) 4-methyl, (3) 4-ethyl, (4) 3-methyl,
(5) hydrogen, (6) 3-bromo, (7) 3-cyano, (8) 4-cyano.

(15) A. Halleux, *Bull. soc. chim. Belges*, **68**, 381 (1959).

(16) A. I. Biggs and R. A. Robinson, *J. Chem. Soc.*, 388 (1961).

As mentioned previously, the initial phase of this study experimentally verified the former half of the assumption. Plots were then made to determine the linearity of the relationship for the substituted pyridine series. The results are shown in Figures 1 and 2. Although the agreement is good for both, the correlation is slightly better with Taft's values. This was also found to be so for the plots of phenols with pyridine.

The regression line was calculated by the method of least squares and found to be $y = -1.013x + 2.235$ for the σ-values and $y = -1.063x + 2.261$ for the σ^0-values. The ρ-constants here of -1.01 and -1.06 are slightly less than the ρ-values of 1.14 and 1.21 for the substituted phenol series, the reason for the sign difference being obvious.

Steric Effect. It was then decided to study the effect of large groups in the *ortho* positions of phenol. The equilibrium constant of *o-t*-butylphenol was determined first and found to be 31. This is quite similar to the value of 39 for *p-t*-butylphenol. The smaller value may be due to the greater inductive effect of the substituent in the *ortho* position as compared to the further removed *para* position.

The equilibrium constant of 2,6-di-*t*-butyl-4-methylphenol was found to be 0.65, which is considerably less than the value of 42 for 4-methylphenol. Thus, it can be safely said that, while a single large group in an *ortho* position does not inhibit the reaction, two large substituents surrounding the hydroxyl group of phenol definitely do. This result concurs with that of Coggeshall,[17] who studied simply the molecular association of substituted phenols.

Solvent Effect. As the hydrogen bond is considered principally an electrostatic attraction,[18] it was thought that the value of the equilibrium constant for the reaction should be related to the dielectric constant of the solvent. The association of merely phenol to pyridine was then determined in other nonaqueous solvents to test this hypothesis. The choice of solvents was unfortunately restricted because of strong absorption in the near-infrared region. Table II shows how the equilibrium constant varies with the particular solvent.

Table II: The Equilibrium Constant of Phenol–Pyridine

Solvent	K, l./mole, 20°	U, D.	ϵ
Carbon disulfide	73	0	2.64
Carbon tetrachloride	59	0	2.24
Chloroform	17	1.02	4.81
Methylene chloride	17	1.54	9.08

It is obvious from this limited study that a linear relationship between the dielectric constant of the solvent and the equilibrium constant does not exist. More investigation must be made though, before it may be stated conclusively. Qualitatively, however, it may be said that the greater the dielectric constant, the smaller the value of the equilibrium constant. This, also, is as expected.

(17) N. D. Coggeshall, *J. Am. Chem. Soc.*, **69**, 1620 (1947).

(18) C. A. Coulson, *Research* (London), **10**, 149 (1957).

Kinetics of Processes Occurring on the Catalyst Surface during the

Oxidation of o-Methylbenzyl Alcohol over Vanadia

by T. Vrbaški

Sinclair Research, Inc., Harvey, Illinois 60426   *(Received April 5, 1965)*

Rates of oxidation (disappearance) of o-methylbenzyl alcohol were measured in the temperature range from 300 to 350° using a fused vanadium pentoxide catalyst. The Hinshelwood treatment suggests that the steady-state conditions are established on the catalyst surface. That the specific rate constant for the adsorption of oxygen agrees within one order of magnitude with those reported in the literature for the oxidation of other organic compounds over the same catalyst supports this conclusion. In this treatment it is supposed that only oxygen is chemisorbed on the catalyst surface; the rate of adsorption of oxygen and the rate of the chemical reaction are of the same order of magnitude; all the processes are first order in the concentration of each reactant, and the rate of desorption of oxygen from the catalyst is negligible. Application of the Hughes–Adams expression implies that the o-methylbenzyl alcohol is first chemisorbed on the catalyst and then reacts with the oxygen of the catalyst; the oxidation products desorb, and finally the catalyst is very rapidly reoxidized. The chemisorption of the o-methylbenzyl alcohol is probably a reversible process.

Introduction

A study of the vapor phase oxidation of o-methylbenzyl alcohol over vanadium oxide as catalyst was recently carried out in this laboratory.[1] This study clarified the reaction mechanism and provided, in addition to kinetic data, clues for the interpretation of processes which occur on the catalyst surface.

o-Tolualdehyde was found to be the main product in the temperature range between 280 and 350°. Carbon oxides along with o-toluic acid and small quantities of per-o-toluic acid and phthalide were also formed. No correlation was made, however, of the rate data of disappearance of o-methylbenzyl alcohol in terms of kinetic expressions which were previously found by others to be useful in describing catalytic oxidation processes.

Kinetic studies of naphthalene, toluene, and benzene in the presence of vanadium oxide as catalyst were made by Shelstad, et al.,[2] Downie, et al.,[3] and Hayashi, et al.[4] The rate equation based upon a reaction scheme proposed by Hinshelwood[5] provided good characterization of the oxidation rates of individual compounds. Alternatively, Hughes and Adams[6] developed an

expression for unimolecular surface reactions which proved useful in the interpretation of data obtained in their study on the vanadia-catalyzed vapor phase oxidation of phthalic anhydride. Using this expression they determined the heats of activation for both the irreversible adsorption of phthalic anhydride and the desorption of the oxidation products. In addition, they were able to calculate the heat of the reversible adsorption for phthalic anhydride, along with the entropy change for the reversible process.

In view of the potentially useful information which comparative studies may provide, it was of interest to attempt to apply both treatments to the oxidation of o-methylbenzyl alcohol. In the present communica-

(1) T. Vrbaški and K. W. Mathews, *J. Phys. Chem.*, **69**, 457 (1965).

(2) K. A. Shelstad, J. Downie, and W. F. Graydon, *Can. J. Chem. Eng.*, **38**, 102 (1960).

(3) J. Downie, K. A. Shelstad, and W. F. Graydon, *ibid.*, **39**, 201 (1961).

(4) R. Hayashi, R. R. Hudgins, and W. F. Graydon, *ibid.*, **41**, 220 (1963).

(5) C. N. Hinshelwood, "The Kinetics of Chemical Change," The Clarendon Press, Oxford, 1940, p. 207.

(6) M. F. Hughes and R. T. Adams, *J. Phys. Chem.*, **64**, 781 (1960).

tion the corresponding rate constants for the oxidation of o-methylbenzyl alcohol in both the Hinshelwood and the Hughes–Adams expressions were determined. These data were correlated with available literature values for naphthalene, toluene, benzene, and phthalic anhydride, and the nature of the reactions occurring on the catalyst surface was discussed.

Experimental

The reaction system, the method of analysis, and the general experimental procedure used in this study were described in a previous communication.[1]

Results

In the simplest steady-state treatment by Hinshelwood it is assumed that only oxygen is adsorbed on the catalyst surface, that its rate of adsorption and the rate of the chemical reaction are of the same order of magnitude, that the rate of desorption of the oxygen from the catalyst surface is negligible, and that all the processes are first order in the concentration of each reactant. According to this interpretation, the rate constant for the adsorption of oxygen should be independent of the organic compound employed at a given temperature and in the presence of the same catalyst. The rate of adsorption of oxygen should, therefore, be the common step for all reactions. If N is the number of moles of oxygen consumed per mole of o-methylbenzyl alcohol converted, then at the steady state the rate of adsorption of oxygen is equal to the rate of chemical reaction multiplied by the factor N. Thus

$$k_a C_0 (1 - \theta_1) = N k_r C_r \theta_1 \quad (1)$$

$$r_r = k_r C_r \theta_1 \quad (2)$$

Alternatively, at a steady-state situation, the rate of reaction of oxygen is also equal to the rate of oxidation of the organic species multiplied by the factor N

$$k_0 C_r \theta_1 = N k_r C_r \theta_1 \quad (3)$$

Solving (1) for θ_1 and substituting it into (2) the rate of o-methylbenzyl alcohol oxidation is

$$r_r = \frac{k_a k_r C_r C_0}{k_a C_0 + N k_r C_r} \quad (4)$$

Inverting and also keeping the oxygen concentration constant, eq. 4 becomes

$$\frac{1}{r_r} = \frac{1}{k_r} \frac{1}{C_r} + K_1 \quad (5)$$

where K_1 is equal to $N/k_a C_0$.

The values of the rate constants in eq. 5 were calculated from experimental points given in Figure 7 of

ref. 1, by the general method of regression analysis. The results are listed in Table I. The solid lines in Figure 7 of ref. 1 were calculated from eq. 4 by using the values for the rate constants listed in Table I. The scatter of experimental points at 340 and 350° is probably due to the slightly higher temperature gradient in the catalyst bed under these conditions. The ratio N is the average of individual values determined from the product distribution data in each series of experiments at constant temperature. The logarithms of k_a and k_r are linear functions of the reciprocal absolute temperature. The calculated Arrhenius temperature coefficient of k_a is 28.0 kcal./mole, and that of k_r is 9.4 kcal./mole.

Table I: Constants of Eq. 4 and 5[a]

Temp., °C.	$1/k_r$, g. sec./l.	$K_1 \times 10^{-6}$, g. sec./mole	$k_a \times 10^6$, l./g. sec.	$k_r \times 10^4$, l./g. sec.
300	2993.9	109.8	0.44	3.34
310	3005.5	72.6	0.67	3.33
320	2792.5	49.3	0.99	3.58
330	2264.9	34.7	1.40	4.42
340	2037.9	23.2	2.10	4.91
350	1675.0	14.8	3.29	5.97

[a] Average $C_0 = 9.3 \times 10^{-5} M$. Average $N = 4.53$.

In the Hinshelwood expression a first-order dependence of the rate on the concentrations of both the oxygen and the organic reactant is assumed. Experimental data,[1–4,7] however, show that the reaction orders vary from 0.5 to unity depending on the compound employed. In fact, only the concentration dependence for xylene in the oxidation of o-xylene and that for oxygen in the oxidation of naphthalene were found to be first order.[7,2] The adoption of an arbitrary first-order rate dependence, as proposed by Hinshelwood, was found useful by various authors in correlating the results obtained in different systems.[2–4] It is therefore believed that the adoption of the same first-order rate dependence in this study was permissible although not absolutely correct in view of the experimental results in ref. 1. The k_a values of o-methylbenzyl alcohol determined from a modified Hinshelwood expression in which the dissociative adsorption of the oxygen is taken into account ($K_1 = N/k_a C_0^{1/2}$

(7) H. Clark, G. C. Serreze, G. L. Simard, and D. J. Berets, unpublished results of the American Cyanamid Co. presented at the Gordon Research Conference on Catalysis, June 1956. See J. K. Dixon and J. E. Longfield, "Hydrocarbon Oxidation in Catalysis," Vol. VII, P. H. Emmett, Ed., Reinhold Publishing Corp., New York, N. Y., 1960, p. 183.

in eq. 5) were found to be about one-tenth of those listed in Tables I and II. The E_a values, however, remained unaffected.

Table II: Constants from o-Methylbenzyl Alcohol, Benzene, Toluene, and Naphthalene Oxidations over Vanadium Pentoxide Catalyst at 350°

Reactant	N	$k_a \times 10^5$, l./g. sec.	$k_r \times 10^8$, l./g. sec.	E_a, kcal./ mole	E_r, kcal./ mole
o-Methylbenzyl alcohol	4.53	3.3	59.7	28.0	9.4
Benzene[a,b]	3.07	3.3	0.9	7.7	27.2
Benzene[c]	3.07	4.4	12.8	8.7	28.1
Toluene[a,d]	1.35	13.9	23.8	29.4	26.4
Naphthalene[e]	~2.7	9.3	1700[f]	28.1	24.6

[a] Downie[3] and Hayashi[4] observed an appreciable initial catalyst deactivation in the oxidation of toluene and benzene, respectively. Therefore, their data were based on a catalyst activity at an age of 20 hr. [b] See ref. 4. [c] See ref. 9. [d] See ref. 3. [e] See ref. 2. [f] The k_r value for naphthalene differs from that reported for toluene by a factor of 70 (ref. 3).

No attempt was made to interpret the dependence of the rate upon the oxygen pressure at constant concentration of o-methylbenzyl alcohol (Figure 10 of ref. 1) with the Hinshelwood treatment because a very limited number of experimental results and no data on the product distributions from which the N values are determined were available.

The rate data were also correlated by the expression proposed by Hughes and Adams for surface reactions in which the rate-controlling step is either the adsorption of the organic reactant or the desorption of the oxidation products. The assumed reaction mechanism in their study of phthalic anhydride oxidation involves adsorption of phthalic anhydride followed by reaction with the oxygen of the catalyst, desorption of the oxidation products, and very rapid reoxidation of the catalyst. In this treatment two limiting cases are considered: (i) irreversible adsorption when $k_{-1} = 0$ and (ii) equilibrium adsorption when $k_{-1} \gg k_2$. The integrated rate equation is

$$2.3031 \log (1 - x) - Bp_o x = -At \tag{6}$$

in which the conversion is given in terms of the initial partial pressure of organic reactant (p_o), the contact time (t), and the rate constants A and B.

Four isotherms were obtained from experimental data and plotted in Figure 1 as conversion of o-methylbenzyl alcohol against initial pressure of o-methylbenzyl alcohol in the gas mixture at a constant oxygen concentration and 0.6-sec. contact time. The values for
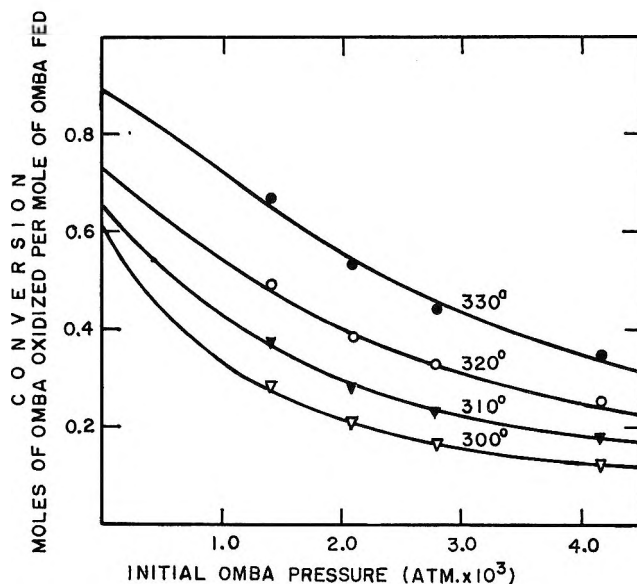
Figure 1. Conversion of o-methylbenzyl alcohol (OMBA) as a function of the initial partial pressure of the OMBA in the gas mixture. Average oxygen concentration $9.3 \times 10^{-3} M$ and contact time 0.6 sec.

constants A and B in eq. 6 of the most probable curves, shown by solid lines in Figure 1, were calculated from experimental points by the method of regression analysis. The results are summarized in Table III.

Table III: Constants of Eq. 6[a]

Temp., °C.	A, sec.$^{-1}$	B, atm.$^{-1}$	A/B, atm. sec.$^{-1} \times 10^4$
300	1.6	1580	9.9
310	1.8	1169	15.1
320	2.2	983	22.2
330	3.6	1227	29.4

[a] Contact time 0.6 sec.

The same authors showed that the constants A and B in eq. 6 were equal to $k_1 k_2 k'/(k_{-1} + k_2)$ and $k_1/(k_{-1} + k_2)$, respectively, in a rate expression derived by applying a steady-state treatment to reactions occurring on the catalyst surface. The constants k_1, k_{-1}, and k_2 are specific rate constants of adsorption and desorption of organic reactant and desorption of oxidized reactant, respectively. The conversion factor k' changes the fraction of the surface occupied by the organic reactant to its true surface concentration. The ratio A/B consequently equals $k_2 k'$ and is independent of the nature of the adsorption step.

The Arrhenius plots of constants A, B, and A/B

listed in Table III are straight lines. The slope of the line for A/B gives the heat of activation for the desorption of oxidized *o*-methylbenzyl alcohol $\Delta H_2^* = 31$ kcal./mole. In the case of irreversible adsorption of *o*-methylbenzyl alcohol, the constant k_{-1} is zero and $A = k_1 k'$. The temperature coefficient of A gives the heat of activation of the irreversible adsorption of *o*-methylbenzyl alcohol $\Delta H_1^* = 15$ kcal./mole. In the case of equilibrium adsorption and assuming a slow desorption of oxidation products from the catalyst (k_2 is small) $B = k_1/k_{-1}$, which is the adsorption equilibrium constant K. The slope of the line for B in the Arrhenius plot represents the heat of adsorption of *o*-methylbenzyl alcohol $\Delta H_1 = -16$ kcal./mole. Finally, by using the conventional thermodynamic equation which combines the equilibrium constant K with ΔF, ΔH, and ΔS, the entropy change ΔS_1 for the reversible adsorption of *o*-methylbenzyl alcohol was found to be -13 cal./(mole deg.).

It is not possible to interpret the dependence of the rate upon oxygen pressure with the Hughes–Adams expression in its present form. This could possibly be done by developing a modified equation in which the above relationship would be included. However, more experimental data than those presently available (Figure 10 of ref. 1) would be required.

Discussion

The Hinshelwood Treatment. In the Hinshelwood rate equations (4 and 5) it is assumed that in heterogeneous catalytic reactions where the temperature is relatively low the rate of adsorption of the reactant is of the same order of magnitude or even smaller than the rate of the chemical reaction ($r_a \lessgtr r_r$). It is noted that Taylor[8] reported a slow adsorption on the catalyst surface under these conditions. Consequently, the values for k_a should be in this case independent of the organic compound employed if the same catalyst is used.

The Langmuir approach, in which the concentrations in the gas phase are related to the surface concentrations (adsorption equilibrium), proved to be most successful only for high-temperature reactions in which red-hot metal wire catalysts were employed. In this treatment a necessary requirement is that r_a and $r_{a'}$ be much greater than r_r.

In Table II a summary of data obtained from the present study and those reported by other authors[2–4] or calculated from kinetic results found in the literature[9] is presented. Although the k_a values for toluene and naphthalene at 350° differ only by 30%, Hayashi's value for benzene[4] is about one-fourth that for toluene. Further information was obtained by

using data reported by Ioffe and Lyubarski[9] in their study on the vanadia–molybdena-catalyzed oxidation of benzene. Both the rate constants k_a and k_r at 350° and activation energies E_a and E_r were calculated. These results compare well with those reported by Hayashi except for the k_r value. The reasons for this discrepancy are not fully clear although the difference in the catalyst and potential difficulties inherent in comparing results of such complex reactions can, at least in part, account for it. The observed difference, however, appears to be of little significance, for it does not affect the consistency of the k_a values.

The k_a value for the oxidation of *o*-methylbenzyl alcohol obtained in the present study compares with the corresponding data reported for other aromatic compounds although there are some differences between values obtained by various workers for benzene, toluene, and naphthalene. According to the assumptions made above, k_a should be independent of the organic compound employed at a given temperature and in the presence of the same catalyst. The adsorption of oxygen should be the common step for all reactions. It is not possible to say at present how meaningful these differences are until information on the rate constant k_a of a greater number of organic compounds becomes available. However, it appears that the k_a values for the organic species vary within a relatively reasonable range and yet are within the same order of magnitude.

On the other hand, data in Figure 7 of ref. 1 show that the rate of disappearance of *o*-methylbenzyl alcohol is dependent upon the alcohol concentration in the carrier gas at low values of the alcohol concentration and at the higher temperatures. At higher concentrations and at lower temperatures the rate tends to become independent of the concentration of the alcohol. The order of reaction was found to be 0.48, and the activation energy for the disappearance of alcohol, 20.0 kcal./mole. The most logical explanation of this result is that the *o*-methylbenzyl alcohol undergoes oxidation predominantly in the adsorbed state, and its rate of adsorption on the catalyst surface tends to control under given conditions the over-all oxidation rate. If this is so, the Hinshelwood assumption that only oxygen is adsorbed on the catalyst surface does not appear to be completely correct. However, even with the organic compound adsorbed, the steady-state approach will remain valid if $r_{a'} \lessgtr r_r$. This modification seems to be permissible, for it is inherent to the

(8) H. S. Taylor, *J. Am. Chem. Soc.*, 53, 578 (1931).

(9) I. I. Ioffe and A. G. Lyubarski, *Kinetics Catalysis* (USSR), 3, 223 (1962).

steady-state concept as outlined above. Furthermore, it was found that $k_{a'} > k_a$. However, under steady-state conditions and also depending upon the actual concentrations of the components in the gas mixture, r_a may become greater than $r_{a'}$. This may well explain why a large excess of oxygen is always required in the reaction mixture during the oxidation process.

Data on the isotope exchange of O^{18} with CO on oxidic catalysts[10] indicate that the lattice oxygens of the catalyst do not participate to a larger extent in the process of oxidation of hydrocarbons at low temperatures. Under these conditions, when the stepwise oxidation of o-methylbenzyl alcohol is taking place, the reaction probably occurs mainly on account of the loosely chemisorbed oxygens on the surface. At higher temperatures when the direct oxidation process is taking place, the top layers of the catalyst were shown to participate in the reaction.[1,11] This result and the evidence on the adsorption of o-methyl benzyl alcohol make it questionable that the Hinshelwood treatment is applicable to the conditions of the direct oxidation process.

Inspection of the activation energy data in Table II shows that the E_a value for o-methylbenzyl alcohol compares with those reported for toluene and naphthalene, whereas the value for benzene is consistently three to four times lower. The reasons for this discrepancy are not fully clear. A tentative explanation, however, is that the catalytic sites which participate in the oxidation of benzene are different from those in the oxidation of other compounds studied. Hayashi[4] came to a similar conclusion in his study of the catalytic deactivation in the oxidation of benzene and toluene. Further experimental work will be necessary to clarify this point.

Experimental data reported by Hughes and Adams[6] in their study on the vanadia-catalyzed oxidation of phthalic anhydride between 472 and 575° were used to calculate the activation energies $E_a = 36.4$ and $E_r = 22.6$ kcal./mole. Furthermore, the value $E_r = 24.6$ kcal./mole for naphthalene was determined by using the available data from Shelstad's work[2] and approximating the k_r value at 350° as 17.0×10^{-5} (ref. 3). The results agree well with those reported for the majority of the other compounds studied and are presented in Table II.

The low activation energy $E_r = 9.4$ kcal./mole for o-methylbenzyl alcohol, compared with the average value of 26.0 kcal./mole for other compounds, appears to be in good agreement with the much higher susceptibility of alcohols toward oxidation.

The Hughes–Adams Treatment. In Table IV a summary of the thermodynamic quantities ΔH_1^*,

ΔH_2^*, ΔH_1, $\Delta H_2^{\ddagger}$, ΔS_1, and ΔF_1 obtained from the present study and those reported for phthalic anhydride is presented. Although the values for o-methylbenzyl alcohol agree in their main outlines with those found for phthalic anhydride, there are some significant differences. No conclusion, however, can be drawn upon the exact nature of the initial adsorption step. This is because the thermodynamic values appear reasonable for both the assumed irreversible and the equilibrium adsorption of o-methylbenzyl alcohol.

Table IV: Thermodynamic Quantities Derived from the Experimental Rate Constants A and B

Reactant	Irreversible adsorption ΔH_1^*, kcal./mole	ΔH_2^*, kcal./mole	Equilibrium adsorption ΔH_1, kcal./mole	$\Delta H_2, \ddagger$ kcal./mole	ΔS_1, cal./ (mole deg.)	ΔF_1, cal./mole
o-Methylbenzyl alcohol	15	31	−16	31	−13	−8100 at 320°
Phthalic anhydride	11	44	−33	44	−29	−9240 at 542°

(a) *Irreversible Adsorption.* The heat of activation for the irreversible adsorption of o-methylbenzyl alcohol ($\Delta H_1^* = 15$ kcal./mole) compares reasonably well with the value reported for phthalic anhydride ($\Delta H_1^* = 11$ kcal./mole). The Arrhenius activation energy for the formation of o-tolualdehyde from o-methylbenzyl alcohol, calculated from the specific rates, was found to be 30.4 kcal./mole.[1] The comparison of this value with $\Delta H_2^* = 31$ kcal./mole for o-methylbenzyl alcohol appears to be permissible since o-tolualdehyde was found to be the principal oxidation product in the temperature range from 300 to 350°. The observed Arrhenius activation energy therefore represents either the heat of activation for the desorption of o-tolualdehyde, ΔH_2^*, or that for the adsorption of o-methylbenzyl alcohol, ΔH_1^*, whichever is higher, unless the reaction is solely controlled by the adsorption of oxygen.

In an attempt to obtain information on the extent to which the presence of by-products such as carbon oxides, maleic and phthalic anhydrides, and o-toluic acid in the oxidation product affects the ΔH_2^* value for o-methylbenzyl alcohol, plots of the rate of formation of individual products against the initial alcohol

(10) L. Ya. Margolis and S. Z. Roginskiǐ, *Probl. Kinetiki i Kataliza, Akad. Nauk SSSR*, 9, 107 (1957).

(11) T. Vrbaški and K. W. Mathews, Symposium on Heterogeneous Catalysis, 150th National Meeting of the American Chemical Society, Atlantic City, N. J., Sept. 1965.

concentration in the carrier gas were constructed from experimental data reported in ref. 1. The rate isotherms for the formation of o-tolualdehyde and carbon oxides were found to exhibit the same trends as observed for the disappearance of o-methylbenzyl alcohol (Figure 7 of ref. 1), whereas the isotherms for both the maleic and phthalic anhydrides were straight lines. However, the rates of formation of o-toluic acid showed an inverse linear dependence upon the alcohol concentration, suggesting a superimposed mass-transfer effect. This phenomenon, however, appears to be of little significance in the over-all desorption process due to the small concentration of the acid formed under conditions employed in this study. It was therefore concluded that the desorption of the by-products from the catalyst surface proceeds in a fashion similar to that observed in the case of o-tolualdehyde, presumably with a heat of activation comparable to that found for the desorption of o-tolualdehyde.

(b) *Equilibrium Adsorption.* The results indicate that the ΔH_1, $\Delta H_2^{\ddagger}$, and ΔS_1 values for o-methylbenzyl alcohol are consistently about one-half those reported for phthalic anhydride. The reasons for this difference are not fully understood. Values of the same constant in similar systems should be comparable and relatively small since they characterize the transition from the activated complex on the catalyst surface to the adsorbed molecule. The values for the free energy change ΔF_1, calculated from the equilibrium constant K at selected temperatures within the extremes, are comparable and quite negative.

Although no conclusion could be made from thermodynamic data on the nature of the initial adsorption step, other evidence obtained in the course of the work tends to support the reversible process. First, the products of oxidation such as o-tolualdehyde, o-toluic acid, phthalide, and phthalic anhydride were shown to desorb readily from the catalyst surface under conditions at which o-methylbenzyl alcohol is being adsorbed. Second, these compounds also appear to adsorb on the catalyst surface under the same conditions since they undergo oxidation, when used singly, in a manner similar to that observed in the case of o-methylbenzyl alcohol.[1,6,12,13] Therefore, the equilibrium, rather than the irreversible adsorption of o-methylbenzyl alcohol, is the more probable process. It appears, however, when data are treated by the Hinshelwood model, that the equilibrium is not established on the catalyst surface during the actual oxidation process.

From average experimental data as treated by an expression derived by Hughes and Adams from the absolute rate theory,[6] about 1/30,000 of the surface oxygen sites of the vanadium oxide were found to be covered with o-methylbenzyl alcohol molecules in the actual oxidation process.[14] This suggests that the surface was very sparingly populated with molecules of o-methylbenzyl alcohol during the oxidation process. Since a portion of the alcohol always remained unreacted and therefore probably unabsorbed on the catalyst surface under conditions employed in this study, it was concluded that the rate of adsorption of o-methylbenzyl alcohol was relatively small. This result is in good agreement with the steady-state concept as outlined above.

To summarize the conclusions, the Hinshelwood treatment appears to be applicable to the oxidation of o-methylbenzyl alcohol over vanadia under conditions of partial conversion when the stepwise oxidation is taking place if it is supposed that the o-methylbenzyl alcohol is also adsorbed on the catalyst surface. The assumption that steady-state conditions are established on the catalyst surface is confirmed. Supporting evidence for this is that the specific rate constant for the adsorption of oxygen agrees within one order of magnitude with those reported in the literature for the oxidation of organic compounds over the same catalyst. It is, however, questionable that the Hinshelwood mechanism is adequate under the conditions of the direct oxidation process at the higher temperatures. The Hughes–Adams treatment suggests that, even with the milder conditions used in this study, the chemisorbed organic species reacts with the lattice oxygens of the catalyst; the oxidation products then desorb, and very rapid reoxidation of the catalyst follows. The adsorption of o-methylbenzyl alcohol is probably a reversible process.

Nomenclature

k_a — Specific rate constant of oxygen adsorption, l. g.$^{-1}$ sec.$^{-1}$

k_a' — Specific rate constant of adsorption of o-methylbenzyl alcohol, l. g.$^{-1}$ sec.$^{-1}$

k_r — Specific rate constant of reaction of organic reactant, l. g.$^{-1}$ sec.$^{-1}$

k_0 — Specific rate constant of reaction of adsorbed oxygen, l. g.$^{-1}$ sec.$^{-1}$

C_r — Concentration of organic reactant in carrier gas, M

C_0 — Concentration of oxygen in carrier gas, M

θ_1 — Fraction of the catalyst surface covered with oxygen

(12) C. E. Morrell and L. K. Beach, U. S. Patent 2,443,832 (1948).

(13) W. R. Edwards and R. D. Wesselhoft, U. S. Patent 3,128,284 (1964).

(14) $r_r = \kappa(kT/h)k'\theta_2 e^{-\Delta H_2^{\ddagger}/RT} e^{\Delta S_2^{\ddagger}/R}$. $r_r = 1.23 \times 10^{-8}$ mole/ g. sec., $\Delta H_2^{\ddagger} = 31$ kcal./mole, $\theta_2 = 0.6$ and 593°K. Assuming that κ has a value of unity and $\Delta S_2^{\ddagger}$ is zero, k' was found to be 3×10^{14} molecules of o-methylbenzyl alcohol/g. of catalyst. If the oxygen ions in the lattice are all 3.0 Å. apart and the vanadium oxide has an area of about 1 m.^{2}/g., then about 10^{19} oxygen sites exist in 1 g. of catalyst.

θ_2 Fraction of the catalyst occupied by o-methylbenzyl alcohol

r_a Specific rate of adsorption of oxygen, moles g.$^{-1}$ sec.$^{-1}$

$r_{a'}$ Specific rate of adsorption of organic reactant, moles g.$^{-1}$ sec.$^{-1}$

r_r Specific rate of reaction of organic reactant, moles g.$^{-1}$ sec.$^{-1}$

E_a Activation energy for the adsorption of oxygen, kcal./mole

E_r Activation energy for the reaction of organic reactant, kcal./mole

$K_1 = N/k_aC_0$, g. sec. mole^{-1}

A Experimental rate constant, sec.$^{-1}$

B Experimental rate constant = equilibrium constant K, atm.$^{-1}$

p_0 Partial pressure of organic reactant, atm.

x Conversion of organic reactant, moles/mole

t Contact time, sec.

ΔH_1^* Heat of activation for the irreversible adsorption of organic reactant, kcal./mole

ΔH_2^* Heat of activation for the irreversible desorption of products, kcal./mole

ΔH_1 Heat of reversible adsorption of organic reactant, kcal./mole

$\Delta H_2^{\ddagger}$ Heat of activation for the reversible desorption of products, kcal./mole

ΔS_1 Entropy change for the reversible adsorption of organic reactant, cal./(mole deg.)

$\Delta S_2^{\ddagger}$ Entropy of activation for the desorption of oxidized products, cal./(mole deg.)

k' Conversion factor for changing the fraction of the surface covered to true surface concentration, moles/g.

κ Transmission coefficient

k Bolztmann's constant, 3.295×10^{-24} cal./deg.

h Planck's constant, 1.563×10^{-34} cal. sec.

Nuclear Spin Relaxation in Solid n-Alkanes

by J. E. Anderson and W. P. Slichter

Bell Telephone Laboratories, Incorporated, Murray Hill, New Jersey (*Received April 5, 1965*)

A study has been made of the role of specific molecular motions in effecting nuclear spin relaxation in normal alkanes in the solid state. Steady-state measurements of n.m.r. absorption exhibited the onset of premelting motion in certain members of a series of n-alkanes ranging between C_6H_{14} and $C_{40}H_{82}$, notably in the odd-numbered members studied in the series and in even-numbered members of sufficiently high molecular weight. The contribution of the rotation of methyl groups to the n.m.r. spin-lattice relaxation time T_1 has also been determined in these compounds and in various solid solutions of C_8H_{18} and C_8D_{18} to assess the intermolecular contribution to the spin-lattice relaxation. All of these studies were carried out between 100°K. and the respective melting points. In the studies of spin-lattice relaxation, T_1 minima were seen in all the compounds at 150 ± 5°K., when measured at a radiofrequency of 50 Mc./sec., and the temperature dependence of T_1 corresponded to an activation energy of 2.6 ± 0.2 kcal./mole for all the compounds. These T_1 minima are ascribed to the threefold reorientation of the methyl groups. The magnitude of T_1 at the minimum depends upon the relative abundance of methyl protons. It is concluded from steady-state measurements that the methylene protons are essentially immobile at these temperatures. The spin-lattice relaxation of the methylene protons is ascribed to spin diffusion to the methyl protons. A kinetic model for this process has been developed and is found to account satisfactorily for the observed dependence of the minimum T_1 value on the CH_3/CH_2 ratio.

Introduction

The n.m.r. spin-lattice relaxation time, T_1, has been widely used to characterize molecular motions in both solids and liquids. T_1 measurements are commonly analyzed in terms of the simple expression developed[1–5] for relaxation among pairs of magnetic dipoles

$$\frac{1}{T_1} = K\left(\frac{\gamma^4\hbar^2}{\omega_0}\right)I(I+1)\sum_j r_{ij}^{-6} \times \left\{\frac{\omega_0\tau_c}{1+(\omega_0\tau_c)^2} + \frac{4\omega_0\tau_c}{1+(2\omega_0\tau_c)^2}\right\} \quad (1)$$

In eq. 1, γ is the magnetogyric ratio of the nuclear spin I, ω_0 is the angular frequency of the applied radiofrequency field, r_{ij} represents the distance between magnetic nuclei, K is a constant that depends on the process of molecular reorientation, and τ_c is the correlation time for this motion. Differentiation of (1) with respect to $\omega_0\tau_c$ shows the existence of a maximum when $\omega_0\tau_c = 0.62$. It is commonly assumed that τ_c depends on temperature according to the relation $\tau_c =$

$\tau_c^0 \exp(\Delta E/RT)$, where ΔE is the activation energy o the relaxation process and τ_c^0 is a constant of the sys tem having the dimensions of time.

The derivation of eq. 1 is based on a model of non-interacting relaxing units. This model is unsatisfactory for solids wherein spin exchange between the relaxing units is rapid. The use of eq. 1 to analyze relaxation data for solids therefore often predicts T_1 values that are much smaller than those experimentally observed. In this paper we shall explore the consequences of spin diffusion in a system in which a fraction of the nuclei couple strongly to the lattice, while the remainder experience weak coupling. We shall demonstrate by

(1) N. Bloembergen, E. M. Purcell, and R. V. Pound, *Phys. Rev.*, **73**, 679 (1948).

(2) R. Kubo and K. Tomita, *J. Phys. Soc. Japan*, **9**, 888 (1954).

(3) I. Solomon, *Phys. Rev.*, **99**, 559 (1955).

(4) E. O. Stejskal and H. S. Gutowsky, *J. Chem. Phys.*, **28**, 388 (1958).

(5) E. O. Stejskal, D. E. Woessner, T. C. Farrar, and H. S. Gutowsky, *ibid.*, **31**, 55 (1959).

means of a kinetic argument how the magnitude of T_1 is affected by the extent of this coupling to the lattice.

Experimental

All of the protonated n-alkanes studied were reagent chemicals obtained from commercial sources. Per-deuterio-n-octane with an isotopic purity of 90% H^2 and a 98% chemical purity was obtained from Merck Sharpe and Dohme of Canada, Ltd. The samples were used without subsequent purification and were sealed under vacuum. The n.m.r. spin-lattice relaxation times were determined by the 180–90° pulse technique of Carr and Purcell,[6] using the null method. Pulse lengths were of the order of 1–4 μsec. The recovery time of the system was about 10 μsec. Further details of the pulse equipment may be found elsewhere.[7] The steady-state measurements were carried out on a Varian dual-purpose spectrometer operating under wide-line conditions. Values of the spin-spin relaxation time T_2 were obtained from the line width, δH, using the expression $T_2 = 1/\gamma(\delta H)$.[1]

Species of Motion in the Solid

The n.m.r. second moment, M_2, provides a quantitative description of certain kinds of molecular motion in solids. Values of M_2 for immobile nuclei can be calculated,[8] as well as M_2 values for nuclei undergoing reorientations about specific molecular axes.[9] Experimental second moments are then compared with the calculated quantities. Using the X-ray data of Müller,[10] Andrew[11] has shown that the second moment of a completely rigid n-alkane C_nH_{2n+2} may be expressed as $M_2 = 26.3 + 19.1/(n + 1)$ gauss². Below their rotational phase transitions, experimental M_2 values for $C_{28}H_{58}$ and $C_{32}H_{66}$ agreed closely with the calculated values, and it was concluded by Andrew that these molecules were essentially motionless. However, Andrew found the second moment for $C_{18}H_{38}$ at low temperatures to be much smaller than the value calculated for immobile molecules. Similarly, the second moments for $C_{13}H_{28}$ and $C_{16}H_{34}$ at low temperatures were found[12] to be smaller than those calculated from Andrew's expression for rigid n-alkanes. Moreover, as is seen from Table I, which includes both the foregoing results and additional results from the present study, the M_2 values are found to increase with chain length, contrary to Andrew's equation for rigid n-alkanes. The disparity in the case of $C_{18}H_{38}$ was ascribed by Andrew to the presence of some effective motion even at the lowest temperatures used.

In the present investigations by steady-state n.m.r., two peaks were seen in the derivative curves for the lower alkanes at 125°K., the lowest temperature

Table I: Wide-Line Data at 148°K.

Alkane	M_2, gauss²	T_2 (wide), μsec.	T_2 (narrow) μsec.
C_6H_{14}	17.1	3.2	24
C_7H_{16}		3.2	22
C_8H_{18}	19.7	3.0	18
$C_{10}H_{22}$	20.7	3.1	30
$C_{11}H_{24}$		3.1	29
$C_{12}H_{26}$	19.5	3.1	31
$C_{13}H_{28}$	21.5^a	3.1	26
$C_{14}H_{30}$	21.6	3.1	
$C_{16}H_{34}$	23.5^a	3.0	
$C_{18}H_{38}$	23.9^b	2.9	
$C_{28}H_{58}$	25.7	2.8	
$C_{32}H_{66}$	26.9	2.8	
$C_{40}H_{82}$	24.9	2.7	

^{a} See ref. 12. ^{b} See ref. 11.

studied. The derivative curve for C_7H_{16}, taken at 150°K., is illustrated in Figure 1. The narrow component decreases in intensity with increasing chain length and cannot be clearly identified in alkanes higher than $C_{14}H_{30}$. With the exception of $C_{11}H_{24}$ and $C_{13}H_{28}$, to be discussed subsequently, these derivative curves were essentially independent of temperature over the temperature range studied, up to the temperature of the rotational transition (see below). Experimental
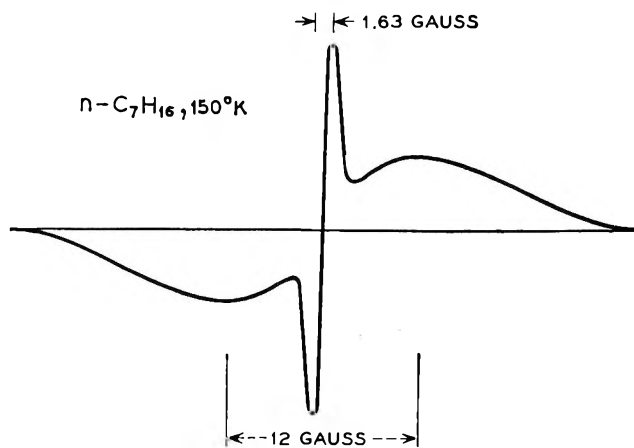
Figure 1. The derivative curve for n-C_7H_{16} measured at 150°K.

(6) H. Y. Carr and E. M. Purcell, *Phys. Rev.*, **94**, 630 (1954).

(7) W. P. Slichter and D. D. Davis, *J. Appl. Phys.*, **35**, 10 (1964).

(8) J. H. Van Vleck, *Phys. Rev.*, **74**, 1168 (1948).

(9) H. S. Gutowsky and G. E. Pake, *J. Chem. Phys.*, **18**, 162 (1950).

(10) A. Müller, *Proc. Roy. Soc.* (London), **A120**, 437 (1928).

(11) E. R. Andrew, *J. Chem. Phys.*, **18**, 607 (1950).

(12) D. F. R. Gilson and C. A. McDowell, *Mol. Phys.*, **4**, 125 (1961).

M_2 values, obtained at 150 ± 5°K., increased with chain length and appeared to approach an asymptotic value of 25–27 gauss². These data suggest the existence of a low temperature crystal structure wherein the methylene protons are held rigidly on the molecular backbone, while the methyl protons appear to be freely reorienting on the time scale of the steady-state experiment. If this is the case, the intramolecular contribution to M_2 is calculated to be $M_2 = 18.5 - 46.3/(n + 1)$ gauss². Assuming that the intermolecular contribution has the same dependence on methyl concentration, the total theoretical M_2 is $26.3 - 65.7/(n + 1)$ gauss². The measured M_2 values agree with this expression within experimental uncertainty.

It is well known[13–15] that the odd-numbered n-alkanes and their even-numbered homologs above $C_{18}H_{38}$ undergo a phase transition below their melting points, which marks the onset of considerable motion in the solid. In the present work, this transition was manifest in $C_{11}H_{24}$, $C_{13}H_{28}$, $C_{28}H_{58}$, $C_{32}H_{66}$, and $C_{40}H_{82}$ by narrow absorption lines that were first observable somewhat below the Curie temperature. These lines grew more intense as the temperature was raised. There was a sharp decrease in T_1 in the same temperature interval. The T_1 data for $C_{13}H_{28}$ are shown in Figure 2. Curves for the other four compounds are similar. All of the samples melted before T_1 minima were reached. Similar behavior has also been observed in $C_{94}H_{190}$ by McCall and Douglass.[16] In the course of such a phase transition, a wide distribution of frequencies of molecular motion will occur, causing simultaneous changes in T_1 and T'_2.

Each of the thirteen alkanes studied gave a plot of log T_1 vs. reciprocal temperature similar to those illustrated in Figure 3. Every member of the series exhibited a T_1 minimum at 148 ± 5°K. The activation energy for the correlation time τ_c, mentioned above, was determined to be 2.6 ± 0.2 kcal./mole in all samples. The M_2 studies have shown the methyl protons to be the only mobile nuclei at this temperature. We therefore assign these minima to the threefold reorienta-
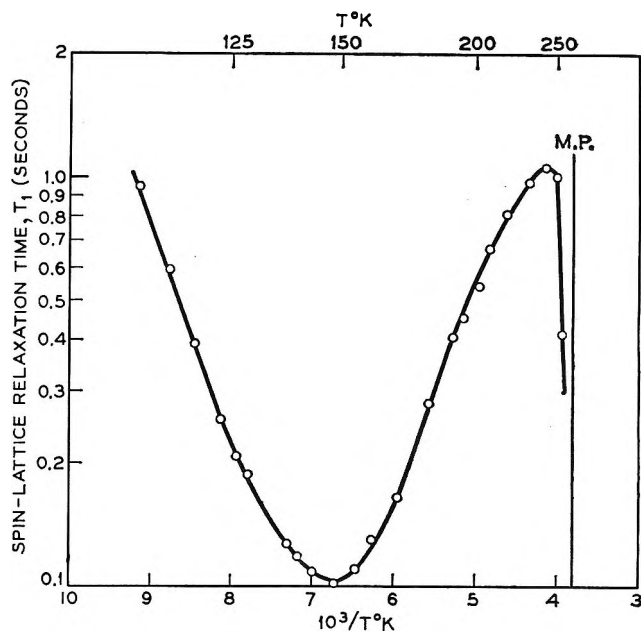
Figure 2. Temperature dependence of the spin-lattice relaxation time in n-$C_{13}H_{28}$.
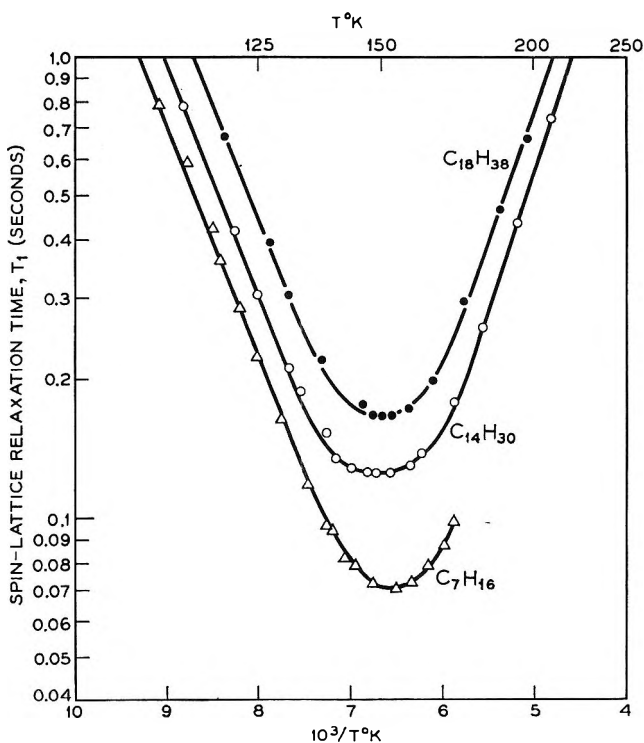
Figure 3. Temperature dependence of the spin-lattice relaxation time in n-C_7H_{16}, n-$C_{14}H_{30}$, and n-$C_{18}H_{38}$.

(13) A. R. Ubbelonde, *Trans. Faraday Soc.*, **34**, 282 (1938).

(14) W. F. Seyer, R. B. Bennett, and F. C. Williams, *J. Am. Chem. Soc.*, **66**, 179 (1944).

(15) H. L. Finke, *et al.*, *ibid.*, **76**, 333 (1954).

(16) D. W. McCall and D. C. Douglass, *Polymer*, **4**, 433 (1963).

Table II: Values of the 148°K. T_1 Minimum in n-Alkanes

Alkane	T_1 (min.), msec.	Alkane	T_1 (min.), msec.
C_6H_{14}	58 ± 2	$C_{14}H_{30}$	106 ± 2
C_7H_{16}	61 ± 2	$C_{16}H_{34}$	130 ± 5
C_8H_{18}	66 ± 2	$C_{18}H_{38}$	140 ± 5
$C_{10}H_{22}$	77 ± 2	$C_{28}H_{58}$	214 ± 7
$C_{11}H_{24}$	87 ± 2	$C_{32}H_{66}$	238 ± 15
$C_{12}H_{26}$	92 ± 2	$C_{40}H_{82}$	300 ± 15
$C_{13}H_{28}$	99 ± 2		

tion of the terminal CH_3 groups. The magnitude of T_1 at the minimum increases with chain length as indicated in Table II.

Terms corresponding to those within the sum shown in eq. 1 are generated by both *inter*molecular and *intra*molecular local fields. For reasons that will be discussed subsequently, it is of interest to discriminate between *intra*molecular and *inter*molecular contributions to T_1. One method of singling out these contributions is to reduce the *inter*molecular effects by isotopic substitution. If attention is confined to linear terms in composition, T_1 can be represented by

$$\frac{1}{T_1} = A + Bx \qquad (2)$$

In eq. 2, A and B refer to the total *intra*- and *inter*molecular proton–proton interactions, and x represents the mole fraction of the protonated molecules. The *inter*molecular relaxation caused by the deuterium nuclei is smaller than the corresponding proton relaxation by $(\gamma_D/\gamma_H)^2 = 0.0236$ and can be ignored over the concentration range studied. A plot of $(1/T_1)_{max}$ vs. mole fraction of C_8H_{18} in C_8D_{18} is shown in Figure 4. The extrapolated value of A is 12.6 sec.$^{-1}$, and B is found to be 2.55 sec.$^{-1}$. From the ratio $B/(A + B)$, we find that intermolecular local fields are responsible for 17% of the spin–lattice relaxation in pure C_8H_{18}.

Discussion of T_1 Results

Perhaps the most interesting feature of the spin-lattice relaxation data is the variation of the methyl T_1 minimum with chain length. Equation 1, which was derived for a system of noninteracting pairs of nuclei, implicitly presumes that all the nuclei are equivalent in their capability for spin-lattice relaxation. This situation does not occur in the n-alkanes. The steady-state experiments cited above show that the second moments of all members of the series are large at $\sim$150°K., the temperature of the T_1 minimum. The conclusion is that the methylene groups are effectively motionless and therefore should be inefficient in direct transfer of spin energy to the lattice. The methyl groups, however, are comparatively efficient in spin-lattice relaxation, owing to their rotation at appropriate frequencies in this temperature range. It appears that the mechanism for the dissipation of the spin energy of the methylene protons, following irradiation by the radiofrequency magnetic field, is that described by McCall and Douglass[16] in n.m.r. studies of polyethylenes. If $T_2 \ll T_1$, as it is in the n-alkanes, energy can diffuse within the spin system before being dissipated by the thermal motion of the lattice. Through this process of *spin diffusion*,[16–18] the energy of the methylenic
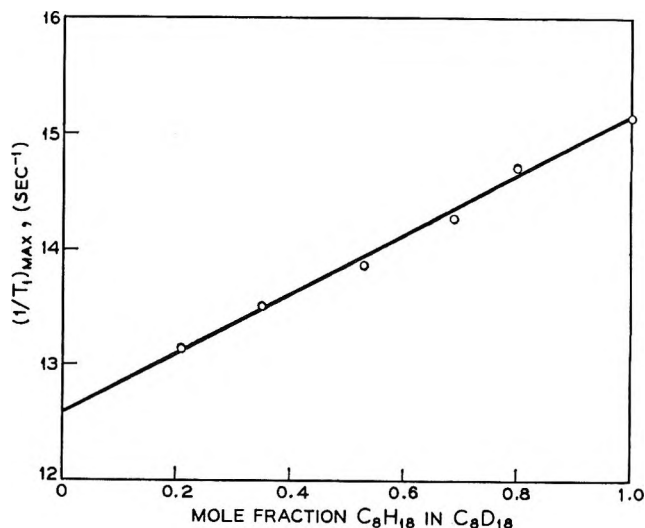
Figure 4. $(1/T_1)_{max}$ plotted as a function of mole fraction C_8H_{18} in C_8D_{18}.

spin system is conveyed to the methyl sites, where the dissipation to the lattice is comparatively effective.

Since the CH_3/CH_2 ratio is known in the n-alkane series, this over-all process of spin relaxation, which was described qualitatively for paraffinic polymers,[16] can be examined quantitatively. We use the following kinetic model. Let us divide a system composed of N_P protons into two groups. N_A will represent all those protons contained within methyl sites, and N_B, the remaining methylene protons. The populations of the upper and lower spin states will be designated A^+, A^-, B^+, and B^-. At equilibrium in a magnetic field these quantities assume the values A_0^+, A_0^-, B_0^+, and B_0^-. Relaxation in this system may be described by the expressions

$$A^+ \underset{k_{-1}}{\overset{k_1}{\rightleftarrows}} A^- \qquad (3)$$

$$B^+ \underset{k_{-2}}{\overset{k_2}{\rightleftarrows}} B^- \qquad (4)$$

$$A^+ + B^- \underset{k_{-3}}{\overset{k_3}{\rightleftarrows}} A^- + B^+ \qquad (5)$$
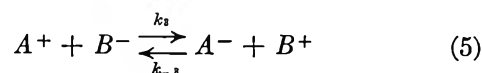
Equation 3 reflects the direct exchange of spin energy between the methyl sites and the lattice. Equation 4 represents the direct coupling between the remaining methylene protons and the lattice. Equation 5 describes the exchange of spin energy between the two groups of protons.[19] The rate constants k_{-1}, k_{-2}, and

(17) N. Bloembergen, *Physics*, **15**, 386 (1949).

(18) A. Abragam, "The Principles of Nuclear Magnetism," Oxford University Press, London, 1961, p. 382.

(19) The use of eq. 5 assumes implicitly that $k_3 \gg k_1, k_2$.

k_{-3} may be evaluated in terms of the equilibrium populations: at equilibrium $k_1(A_0{}^+) = k_{-1}(A_0{}^-)$, etc. Since $(A_0{}^+/A_0{}^-) = (B_0{}^+/B_0{}^-)$, we find $k_3 = k_{-3}$. By straightforward but lengthy algebra, the rate expressions for the two-component system can be expressed as

$$\frac{d}{dt}(\alpha - \alpha_0) = -2k_1(\alpha - \alpha_0) -$$
$$k_3 N_B[(\alpha - \alpha_0) - (\beta - \beta_0)] \quad (6)$$

$$\frac{d}{dt}(\beta - \beta_0) = -2k_2(\beta - \beta_0) -$$
$$k_3 N_A[(\beta - \beta_0) - (\alpha - \alpha_0)] \quad (7)$$

where

$$\alpha = \frac{A^+ - A^-}{A^+ + A^-}; \quad \beta = \frac{\beta^+ - \beta^-}{\beta^+ + \beta^-}; \quad \text{etc.}$$

The quantities α and β are proportional to the magnetizations and therefore to the observed signals. Equations 6 and 7 have a general solution

$$(\alpha - \alpha_0) = C_+e^{-\Phi_+ t} + C_-e^{-\Phi_- t} \quad (8a)$$
$$(\beta - \beta_0) = C'_+e^{-\Phi_+ t} + C'_-e^{-\Phi_- t} \quad (8b)$$

where $\Phi_\pm$ are the roots of the equation

$$\Phi_\pm{}^2 - [2(k_1 + k_2) + k_3 N_P]\Phi_\pm +$$
$$2k_3(k_2 N_B + k_1 N_A) + 4k_1 k_2 = 0$$

and

$$C'_\pm = \frac{2k_1 + k_3 N_B - \Phi_\pm}{k_3 N_B} C_\pm = \frac{k_3 N_A}{2k_2 + k_3 N_A - \Phi_\pm}C_\pm$$

The absolute values of C_+ and C_- are established by the boundary conditions.

The experimental significance of k_1 and k_2 may now be seen by considering systems composed entirely of methyl sites or isolated methylene protons. The relaxation process is then described by $\exp(-2k_1t)$ or $\exp(-2k_2t)$, and we can associate $1/(2k_1)$ and $1/(2k_2)$ with the T_1 values of the isolated methyl and methylene protons, respectively. The term k_3 represents spin-lattice relaxation caused by spin flipping between the methylene and methyl sites. The relaxation process envisaged here is formally similar to the relaxation of the nuclear spin system by paramagnetic impurities, which was treated by Bloembergen.[17] In his kinetic model, k_3 can be approximated

$$k_3 \cong \frac{1}{[15 + 7(n - 2)]T_2} \quad (9)$$

where n is the number of carbon atoms in the alkane. Taking his model to be an adequate basis for compari-

son in the present case, and considering the range of values of n that occur here, we can estimate that k_3 is comparable to $1/T_2$ within two orders of magnitude. On the basis of the T_2 data in Table I, it then follows that $k_3 \gg k_1, k_2$ in all the alkanes at 150°K. In this case, the system effectively relaxes by the expression[20]

$$[(\alpha + \beta) - (\alpha_0 + \beta_0)] = [(\alpha + \beta) -$$
$$(\alpha_0 + \beta_0)]_{\text{initial}}e^{-t/T_1} \quad (10)$$

where

$$\frac{1}{T_1} = 2\left[\left(\frac{N_A}{N_P}\right)k_1 + \left(\frac{N_B}{N_P}\right)k_2\right] \quad (11)$$

Equation 10 can be seen to revert to (1) whenever $k_1 = k_2$. If $k_1 \gg k_2$, as is the case for the n-alkanes, this treatment predicts that the minimum values of T_1 ought to vary linearly with the relative abundance of methyl sites. On the other hand, it shows that the position of the T_1 minimum along the temperature axis and the activation energy of the relaxation process are independent of the number of methyl sites. We have already mentioned the close agreement among the activation energies of the various alkanes and among
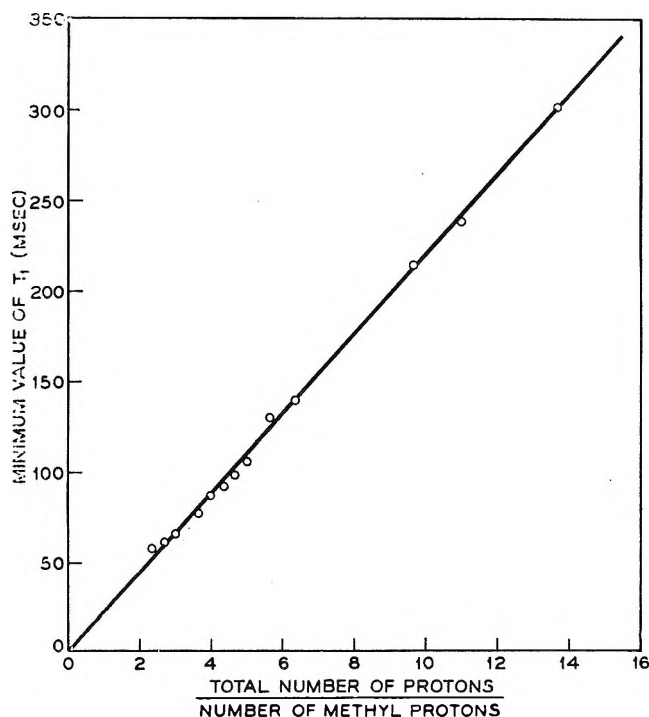
Figure 5. The methyl T_1 minimum value in the n-alkanes as a function of the relative number of methyl protons.

(20) Equations 10 and 11 may be obtained from eq. 6 and 7 directly by imposing the condition that a common spin temperature is maintained throughout the system at all times.

the temperatures at which T_1 minima occur. Figure 5 shows the linear relationship between the experimental T_1 minimum values and the N_P/N_A ratio. The agreement between theory and experiment is excellent. The T_1 minimum for a system composed entirely of methyl sites can be determined from the slope of the line in Figure 5. A value of 22 msec. is obtained by this method. We extended the work of Gutowsky, et al.,[5] to obtain a 24 ± 1 msec. T_1 minimum in $C(CH_3)_4$ at 114 ± 2°K., which can be attributed to CH_3 rotation.

We now examine the separation of the intra- and intermolecular contributions to T_1. Using eq. 2, the T_1 study of the C_8H_{18}–C_8D_{18} system indicated that a protonated n-octane molecule completely surrounded by its deuterated analogs would give a T_1 minimum of 79 msec. at 50 Mc. Application of eq. 11 eliminates the effect of methylene relaxation through the methyl "sink" and yields a value of 26 msec. for the intramolecular contribution to methyl relaxation. Hubbard[21] has calculated the time variation of the nuclear magnetization of three equidistant, identical nuclei, using a semiclassical density-matrix theory of relaxation, and has found that the relaxation consists of the sum of two terms that decay exponentially with different time constants. Practically speaking, however, the decay of the magnetization is adequately represented[22] by a single exponential of the form appropriate to relaxation in the absence of correlation between relative motions of pairs of spins.[1-3] As calculated for a radiofrequency of 50 Mc./sec., the magnitude of the T_1 minimum for relaxation via the rotation of methyl groups about the threefold axis, in a polycrystalline sample, is 28 msec. This calculation involves only pairwise interactions,[1-3] with no cross terms, and is in close agreement with our experimental results. Using an essentially classical calculation, Stejskal and Gutowsky[4] have developed an expression that predicts a T_1 minimum for methyl rotation of 57 msec., at a resonant frequency of 50 Mc./sec. It seems that the latter calculation of the cooperative influence of the two neighbors that relax the third methyl proton is fundamentally an overestimate. Thus, it appears that the agreement between the 57-msec. value and some of our earlier experimental results on relaxation in camphor[23] was fortuitous. The methyl T_1 minimum in camphor is 50

msec. at a radiofrequency of 50 Mc. However, the seven protons in the camphor molecule that are immobile at low temperatures were not adequately accounted for in calculating the magnitude of the T_1 minimum: properly, their presence would raise the magnitude of the T_1 minimum to be expected in camphor.

The ratio of 22 msec., the experimental value for the T_1 minimum, to 28 msec., the calculated value arising from interactions within a CH_3 group, shows that about 79% of the methyl spin-lattice relaxation in the n-alkanes is generated within the CH_3 group. The relative magnitudes of these intra- and extra-group contributions should not differ greatly for any hydrocarbon. This suggests that the methyl T_1 minimum, when obtainable, could provide a qualitative measure of the number of reorienting CH_3 groups present in a solid sample. In principle, this figure can be measured quantitatively by the n.m.r. second moment. As illustrated in the M_2 study of the n-alkanes, this method becomes increasingly insensitive as the relative concentration of methyl protons decreases. In contrast, the T_1 minimum is probably more sensitive to the number of reorienting CH_3 groups as their concentration diminishes; e.g., a sample with a 10% concentration of mobile CH_3 protons will have a much larger minimum than a sample with a 15% concentration. Using the slope of Figure 5, we have obtained satisfactory determinations of mobile CH_3 content in a number of polyolefins[7] and ethylene–propylene copolymers.[24] Of course, the treatment set forth here for mobile CH_3 groups is applicable to any mobile unit, once its intrinsic relaxation time is known.

(21) P. S. Hubbard, Phys. Rev., 109, 1153 (1958).
(22) A. Abragam, ref. 18, p. 293 ff.
(23) J. E. Anderson and W. P. Slichter, J. Chem. Phys., 41, 1922 (1964).
(24) E. G. Kontos and W. P. Slichter, J. Polymer Sci., 61, 61 (1 62)

A Relationship between the Carbon-13 Carbonyl Chemical Shifts and n → π*

Transition Energies in Cyclic and Bicyclic Ketones

by George B. Savitsky, Keishi Namikawa, and George Zweifel

Department of Chemistry, University of California, Davis, California   (*Received April 6, 1965*)

A considerable low-field shift in C^{13} carbonyl spectra is usually observed in simple five-membered ring compounds. The same low-field shift of the sp^2 carbon is observed in cyclo-pentanone oxime, but it is much less pronounced in methylenecyclopentane when com-pared to its four- and six-membered analogs. It also appears that the low-field carbonyl shift no longer characterizes a five-membered ring when it is fused with another ring in bicyclic ketones. It is suggested that unusually low or high carbonyl chemical shifts in homologous compounds may be explained in terms of their electronic excitation energies. A good linear correlation between the carbonyl shifts in some cyclic and bicyclic ketones and the n → π* transition energies has been established.

Introduction

As an extension of a general program undertaken in our laboratory to study stereochemical effects on C^{13} chemical shifts we have investigated the carbonyl shifts in some cyclic and bicyclic ketones and related compounds. This paper represents an attempt to rationalize the magnitude and direction of these shifts in terms of current theories of chemical shifts.

Experimental

The C^{13} spectra were measured under experimental conditions previously described.[1] All shifts were measured with respect to an external aqueous sodium acetate-1-C^{13} reference but subsequently referred to benzene. The liquid compounds were measured neat, and the solids were measured as concentrated solu-tions in CCl_4. Succinic and glutaric anhydrides were measured in dimethyl carbonate, being not sufficiently soluble in other solvents to result in measurable signals. All compounds except the two listed below were commercial reagents of high purity. Bicyclo-[2.2.1]hept-2-en-7-one and bicyclo[2.2.1]heptan-7-one were prepared from hexachlorocyclopentadiene by a series of steps described by Gassman and Pape.[2]

Results and Discussion

Although proton n.m.r. spectra of small- and medium-sized ring ketones have been reported by several authors,[3] the analysis and interpretation of the spectra

have not been made because of their complexity. C^{13} shifts of the carbonyl carbon for cyclopentanone and cyclohexanone were first reported by Lauterbur.[4] The considerable downfield carbonyl shift of cyclo-pentanone with respect to cyclohexanone was at that time attributed to the "strain" effect in the five-membered ring. More recent extension of this study to cyclic ketones of various sizes by Stothers and Lauterbur[5] has indicated, however, that this low-field shift is not exhibited by the supposedly more strained cyclobutanone. Thus, the carbonyl shift in the five-membered cyclic ketone is significantly lower than either one of its four- and six-membered homologs (about 10 p.p.m. lower than in cyclobutanone and about 8 p.p.m. lower than in cyclohexanone). The same authors found other instances of low-field car-bonyl shifts in five-membered rings, that in thujone being about the same as in cyclopentanone, that in 2-cyclopentenone being 11 p.p.m. lower than in 2-

(1) G. B. Savitsky and K. Namikawa, *J. Phys. Chem.*, **67**, 2430 (1963).

(2) P. G. Gassman and P. G. Pape, *J. Org. Chem.*, **29**, 160 (1964).

(3) H. Primas, K. Frei, and Hs. H. Günthard, *Helv. Chim. Acta*, **41**, 35 (1958); K. B. Wiberg and B. J. Nist, *J. Am. Chem. Soc.*, **83**, 1226 (1961); F. A. L. Anet, *Can. J. Chem.*, **39**, 2316 (1961).

(4) P. C. Lauterbur, "Determination of Organic Structures by Physi-cal Methods," Vol. 2, Academic Press Inc., New York, N. Y., 1962.

(5) J. B. Stothers and P. C. Lauterbur, *Can. J. Chem.*, **42**, 1563 (1964).

cyclohexenone. In five-membered γ-butyrolactone the carbonyl shift is 7 p.p.m. lower than in four-membered β-propiolactone. Our recent value on the carbonyl shift of the six-membered δ-valerolactone (−43.6 p.p.m. with respect to benzene) shows that the five-membered cyclic lactone is also about 6 p.p.m. lower than its six-membered analog, the situation being again similar to the corresponding cyclic ketones.

In Table I we have listed some additional information obtained in our laboratory on the C^{13} shifts of sp^2 ring carbons in four-, five-, and six-membered rings, together with some literature results for comparison.

Table I: C^{13} Chemical Shifts (in p.p.m.) with Respect to Benzene on sp^2 Carbons in Some Simple Four-, Five-, and Six-Membered Ring Compounds

Compound	Ring size	sp^2 ring carbon chemical shift
2-Methylcyclopentanone	5	−91.6
2-Methylcyclohexanone	6	−83.6
3-Methylcyclopentanone	5	−88.2
3-Methylcyclohexanone	6	−80.9
Succinic anhydride	5	−47.3
Glutaric anhydride	6	−38.7
Cyclopentanone oxime	5	−37.7
Cyclohexanone oxime	6	−28.3
Methylenecyclobutane	4	−21.5
Methylenecyclopentane	5	−22.9
Methylenecyclohexane	6	−20.2
Cyclobutanone	4	−79.0[a]
Cyclopentanone	5	−89.3[a]
Cyclohexanone	6	−81.0[a]
β-Propiolactone	4	−42.4[a]
γ-Butyrolactone	5	−49.4[a]
δ-Valerolactone	6	−43.6

[a] See ref. 5.

These results indicate that the low-field shifts of the sp^2 carbons in five-membered rings are common to all carbonyl carbons. It can be seen that, in spite of the 2-methyl and 3-methyl substituents, the low-field shift of the five-membered with respect to the six-membered ring is still apparent. Also, since the carbonyl shift in 3-methylcyclohexanone is practically the same as in cyclohexanone, it appears that the carbonyl shift is insensitive to the so-called "3-alkyl effect."[6]

In case of the sp^2 carbon bonded to the nitrogen in the cyclic oximes, the same pronounced low-field shift in the five-membered compound is observed. On the

other hand, in the methylene series, although the same inversion in trend is observed on the ring sp^2 carbon, it is much less pronounced, amounting to less than a 2-p.p.m. downfield shift in methylenecyclopentane as compared to its four- and six-membered analogs. It appears, therefore, that the pronounced low-field shift is not simply characteristic of the five-membered ring but depends on the type of group attached to the ring sp^2 carbon.

No other physical properties seem to point to similar inversion in trend on the five-membered ring in the first few members of cyclic ketones. Thus, for example, the dipole moments of cyclic ketones increase monotonically with the increase in ring size from the four-membered to the six-membered ring, attaining a maximum value for cyclohexanone and then decreasing slowly up to the eight-membered compound, the values being, respectively, 2.76, 2.86, 3.08, 3.04, and 2.93 D., in this order.[7]

It appears that this inversion in trend can be explained in terms of the theory developed by Pople and Karplus[8] which assumes the dominance of paramagnetic shielding in C^{13} chemical shifts. This theory which is based on the approximate LCAO molecular orbital treatment of diamagnetism formulates the chemical shift as a function of total electronic charge on the atom in question, the bond orders of bonds around it, and the average electronic excitation energy ΔE. All other factors being equal or relatively unimportant, the effect of ΔE to which the negative value of paramagnetic contribution is inversely proportional is as follows. The low excitation energy will lead to a low-field shift and *vice versa*. Interestingly enough, the results obtained from ultraviolet measurements on some cyclic ketones[9] in an inert solvent (isooctane) show that cyclopentanone has the lowest n → π* transition energy among four- to ten-membered cyclanones. Recently, Closson and Haug[10] reported that the n → π* transition energy of the five-membered butyrolactone (λ_{max} 214.0 mμ) is also significantly lower than that of the four-membered propiolactone (λ_{max} 207.2 mμ). If these particular transitions are roughly indicative of the average excitation

(6) E. L. Eliel, "Stereochemistry of Carbon Compounds," McGraw-Hill Book Co., Inc., New York, N. Y., 1962, p. 240.

(7) Hs. H. Günthard and T. Gäumann, *Helv. Chim. Acta*, **34**, 39 (1951); R. Arndt, Hs. H. Günthard, and T. Gäumann, *ibid.*, **41**, 2213 (1958).
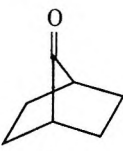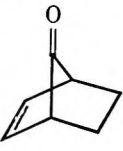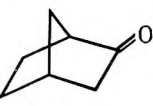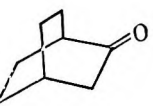
(8) J. A. Pople, *J. Chem. Phys.*, **37**, 53, 60 (1962); M. Karplus and J. A. Pople, *ibid.*, **38**, 2803 (1963); J. A. Pople, *Mol. Phys.*, **7**, 301 (1964).

(9) E. M. Kosower and G. S. Wu, *J. Am. Chem. Soc.*, **83**, 3142 (1961).

(10) W. D. Closson and P. Haug, *ibid.*, **86**, 2384 (1964).

energies ΔE, the low-field shifts in cyclopentanone and butyrolactone may be understood if one assumes that other factors are relatively less important in homologous compounds of this type or follow essentially the same trend as ΔE.

Table II: Carbonyl Carbon Chemical Shifts and n → π* λ_{max} of Some Bicyclic Compounds

Compound	Carbonyl shift	n → π* λ_{max}
I	−86.5	293[a]
II	−76.5	274[a]
III	−87.4	293[b]
IV	−85.0	298[b]

[a] See ref. 2; in isooctane. [b] Determined by us, in cyclohexane, using the Cary recording spectrometer.

Listed in Table II are the carbonyl carbon chemical shifts of four bicyclic compounds measured by us which are interesting from the following points of view.

In spite of the different positions of the carbonyl group and ring sizes in I, III, and IV the carbonyl chemical shifts are very close in value. Therefore, the low-field shift can no longer be used for the characterization of five-membered rings when they are fused with other rings.

Compound II is of interest because of the pronounced effect of the double bond (10 p.p.m. upfield shift in comparison with I) which is not conjugated with the carbonyl. This is probably due to the strained geometry of the molecule. The carbonyl shift in $C_6H_5CH_2$-COOCH< in which the π-system of the benzene ring is two bonds away from the carbonyl group was found to be −44.7 p.p.m., which compares with the −42.0-p.p.m. shift of the carbonyl in CH_3COOCH_3. Thus, the effect on the carbonyl shift of the π-system two bonds away from the carbonyl group is normally at

best very small and in the opposite direction of the effect which is exemplified by compound II.

It can be noted again that, in comparison with the three remaining bicyclic ketones, the low chemical shift of II is associated with the high n → π* transition energy which is again in qualitative agreement with theory.

If one assumes that ΔE plays a dominant role in the carbonyl chemical shifts of cyclic and bicyclic ketones and that n → π* transition energies are approximately proportional to ΔE, one would expect to find a linear correlation of the type

$$\delta_{CO} = a\lambda_{max}^{n \to \pi^*} + b$$

A plot of the carbonyl chemical shifts vs. n → π* λ_{max} for the 12 cyclic and bicyclic ketones (listed in Tables II and III) is shown in Figure 1. The least-square linear fit yields the following regression coefficients: $a = -0.474$ and $b = 53.5$ p.p.m. The coefficient of correlation is 0.873, and the root mean square of deviations is 1.95 p.p.m.

Table III: Carbonyl Chemical Shifts and n → π* λ_{max} of Some Cyclic Ketones

Compound	Carbonyl shift[a]	n → π* λ_{max}[b]
Cyclobutanone	−79.0	281.5
Cyclopentanone	−89.3	300.1
Cyclohexanone	−81.0	291.4
Cycloheptanone	−83.7	291.8
Cyclooctanone	−86.7	290.5
Cyclononanone	−86.6	292.6
Cyclodecanone	−83.8	288.3
Cyclopentadecanone	−81.0	285.9

[a] Data taken from ref. 5 for cyclic ketones. [b] Data taken from ref. 9 for cyclic ketones; isooctane solvent.

A similar plot for the 10 acyclic ketones (listed in Table IV) is shown in Figure 2. Again, the trend is in the same direction, but the least-square linear fit results in a different correlation line with the regression coefficients $a = -0.861$ and $b = 161.7$ p.p.m., the coefficient of correlation being 0.912 and the root mean square of deviations 1.78 p.p.m. It may be noted, however, that only three points deviate significantly from the correlation line established for the cyclic ketones. These points correspond to the ketones in which the carbonyl group is bonded to two bulky groups simultaneously.

Such linear correlations cannot be extended to carbonyl compounds in general or even to ketones whose carbonyl group is conjugated to a double bond and
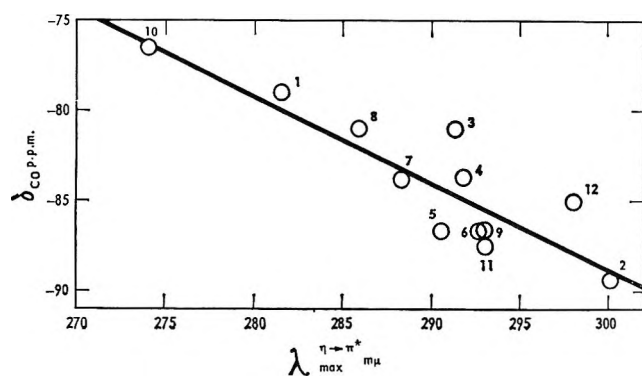
Figure 1. The plot of carbonyl carbon chemical shifts vs. λ_{max} of n → π^* transitions of some cyclic and bicyclic ketones: (1) cyclobutanone, (2) cyclopentanone, (3) cyclohexanone, (4) cycloheptanone, (5) cyclooctanone, (6) cyclononanone, (7) cyclodecanone, (8) cyclopentadecanone, (9) compound I, (10) compound II, (11) compound III, (12) compound IV.
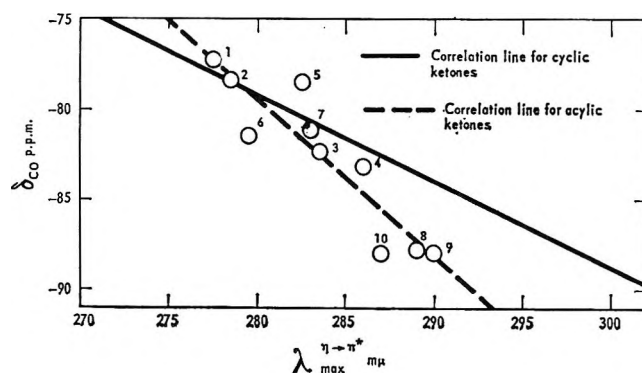
Figure 2. The plot of carbonyl carbon chemical shifts vs. λ_{max} of n → π^* transitions of some acyclic ketones, RCOR':
(1) CH_3, CH_3; (2) CH_3, C_2H_5; (3) CH_3, i-C_3H_7; (4) CH_3, t-C_4H_9; (5) CH_3, i-C_4H_9; (6) C_2H_5, C_2H_5; (7) C_3H_7, C_3H_7; (8) i-C_3H_7, i-C_3H_7; (9) t-C_4H_9, t-C_4H_9; (10) i-C_4H_9, i-C_4H_9.

Table IV: Carbonyl Chemical Shifts and n → π^* λ_{max} of Some Acyclic Ketones RCOR'

R	R'	Carbonyl shift[b]	n → π^* λ_{max}[a]
CH_3	CH_3	−77.2	277.5
CH_3	C_2H_5	−78.4	278.5
CH_3	i-C_3H_7	−82.3	283.5
CH_3	t-C_4H_9	−83.1	286
CH_3	i-C_4H_9	−78.4	282.5
C_2H_5	C_2H_5	−81.4	279.5
C_3H_7	C_3H_7	−81.1	283
i-C_3H_7	i-C_3H_7	−87.7	289
t-C_4H_9	t-C_4H_9	−87.9	290
i-C_4H_9	i-C_4H_9	−87.9	287

[a] P. Maroni, Ann. Chim. (Paris), 2, 757 (1957); hexane solvent. [b] All chemical shifts taken from ref. 5 except for dipropyl ketone which was measured by us.

whose charge densities and bond orders must be strongly affected by resonance interaction. Furthermore, even in the series of saturated ketones, the trend is evidently modulated by variation in electronic structure. Thus, according to the numerical formulation of the Pople–Karplus theory, a variation of 10% in ΔE should result in about a 40-p.p.m. variation in the carbonyl chemical shifts if all other factors would remain constant. This amounts to about a 1.3-p.p.m. variation per 1-mμ shift in n → π^* λ_{max}. The slope of the correlation line for the cyclic ketones indicates only about a 0.5-p.p.m. variation per mμ. The correlation established for the acyclic ketones is about 0.9 p.p.m. per 1-mμ shift and is thus closer to the theoretically predicted value.

The magnitudes of the n → π^* transition energies considered in this work are in themselves of great theoretical interest. In particular, the relatively high n → π^* transition energy of compound II, as compared with its saturated analog, I, merits some discussion. The increase in the n → π^* ΔE cannot be ascribed to the interaction of the π-system of the carbon–carbon double bond with the unshared pair of electrons in the p orbital of oxygen because, as it was pointed out by Cookson and Hudec,[11] this orbital is orthogonal to the π-system. For the overlap integral with the oxygen p orbital to have a nonzero value it must be nonparallel to the carbon–carbon double bond. This condition is satisfied in dehydronorcamphor, V, and the interaction

V
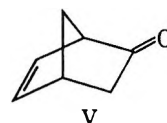
results in a significant intensification of the n → π^* transition[11] [λ_{max} 304 mμ (ϵ 290)]. We have recently measured the C^{13} n.m.r. spectra of dehydronorcamphor, V, and found the carbonyl shift to be −87.7 p.p.m. This is about 3 p.p.m. higher than the value predicted from the correlation established for the cyclic ketones. This small deviation may not be indicative of the effect of the double bond–carbonyl interaction discussed by Cookson and Hudec. However, the shifts of the two nonequivalent double-bond carbons (−7.2 and −13.6 p.p.m.) in dehydronorcamphor, as compared to the shift of the two equivalent double-bond carbons in compound II (−5.5 p.p.m.), indicate that there is a considerable deshielding and polarization of the carbon–carbon double bond in the former.

It is possible that the highly strained geometry of compound II is responsible for its rather short n →

(11) R. C. Cookson and J. Hudec, J. Chem. Soc., 429 (1962).

π^* wave length. This is compatible with the explanation of the abnormally short wave length of the four-membered propiolactone in terms of bond angle strain advanced by Closson and Haug.[10] According to their interpretation, reduction of the internal angles leads to an increase in the s-character in the σ-bond of the carbonyl group, which in turn leads to the shortening of both the σ- and π-bonds and thus raises the π^*-level.

This explanation is also compatible with the high energy of the n $\rightarrow$ π^* transition observed in cyclobutanone in comparison with the other members of the series. However, this theory fails to explain the lowest n $\rightarrow$ π^* transition energy in cyclopentanone. Also, compounds I and III would be expected to differ significantly, in the degree of strain, yet their n $\rightarrow$

π^* transition energies are experimentally indistinguishable. At the same time, compound IV should be less strained than either I or III and does show a lower n $\rightarrow$ π^* transition energy, which is in qualitative agreement with the strain theory.

In spite of the preliminary and tentative nature of the correlations presented in this work, they point to the importance of considering excitation energies in the discussion of C^{13} chemical shifts.

Intrinsic Viscosity of Linear Polyethylene in a Θ-Solvent

by Carl J. Stacy and Raymond L. Arnett

Research Division, Phillips Petroleum Company, Bartlesville, Oklahoma 74004   (*Received April 8, 1965*)

An investigation of critical precipitation temperatures has established the Θ-temperature for the system, linear polyethylene–dodecanol-1, at 138° and has estimated Θ-temperatures for other solvents with the same polymer. The intrinsic viscosity–molecular weight relationship for linear polyethylene in dodecanol-1 at 138° is found to be $[\eta]_\Theta = 3.16 \times 10^{-3} \times M_\Theta^{1/2}$, where $M_\Theta \ (= (M^{1/2})_w{}^2)$ is that viscosity-average molecular weight appropriate for Θ-conditions. The mean-square molecular radius obtained from these measurements is compared with recent theoretical estimates.

I. Introduction

Unbranched polyethylene as the simplest hydrocarbon polymer is of unique importance to conformation concepts.[1-3] Much attention has been given recently to its ratio of mean-square radius to molecular weight, as unperturbed by long-range segment–segment interaction,[3-7] including estimates from both theory[4,5] and experiment.[3,6] However, the experimental values have not included results from intrinsic viscosities measured under Θ-conditions. It is the purpose of this paper to report such measurements.

II. Experimental

Polymers. The linear polyethylenes used in this investigation are whole polymers. Those numbered

(1) M. V. Volkenstein, "Configurational Statistics of Polymeric Chains," Interscience Publishers, Inc., New York, N. Y., 1963.

(2) P. J. Flory, "Principles of Polymer Chemistry," Cornell University Press, Ithaca, N. Y., 1953.

(3) M. Kurata and W. H. Stockmayer, *Fortschr. Hochpolymer-Forsch.*, **3**, 196 (1963).

(4) C. A. J. Hoeve, *J. Chem. Phys.*, **35**, 1266 (1961).

(5) K. Nagai and T. Ishikawa, *ibid.*, **37**, 496 (1962).

1 through 9 in Table I have previously been characterized[8,9] as to molecular weight. Although they have a relatively broad molecular weight distribution, M_w/M_n = 11.3, the distribution function (logarithmic normal by number of molecules) is sufficiently well known to allow calculation of the appropriate viscosity-average molecular weights. Polymer 11 is a relatively narrow distribution linear polyethylene[10] having the ratio M_w/M_n = 1.6.

Table I: Intrinsic Viscosity of Linear Polyethylenes in Docecanol-1 at 138°

Polymer	$[\eta]\theta$	$M_w \times 10^{-3}$	$M\theta \times 10^{-3}$
2	0.673	82	44.7
1	0.679	92	50.2
3	0.726	101	55.2
6	0.817	118	64.4
7	0.875	122	66.6
8	0.827	133	72.6
9	1.072	165	90.0
11	1.58	317	282.0

θ-Conditions. A problem in this investigation was finding a solvent for linear polyethylene with an experimentally accessible θ-temperature. Obvious criteria (boiling points, chemical stability, etc.) were used to select a list of possible solvents which included those previously suggested as θ-solvents for branched polyethylene (nitrobenzene,[11] amyl acetate,[11] 2-ethylhexyl adipate[12]). The list was narrowed by preliminary observation of the precipitation temperature of a single polymer sample from a 0.5% solution. θ-Temperatures were estimated for several solvents by measuring precipitation temperatures over a concentration range for several molecular weights.[13] Shultz and Flory[14] suggest that, when whole polymers are used in these experiments, the temperature, θ, is found by correlating the critical precipitation temperatures with an average molecular weight that lies between M_w and M_z. We used M_w measurements, which in view of a constant M_z/M_w ratio for the logarithmic normal distribution will correctly give θ at $M_w^{-1/2}$ = 0.

Results of phase equilibria measurements on a single sample are summarized in Figure 1. The required amorphous phase separation is confirmed by the well-established maxima in the curves. For contrast, a few points for *p*-xylene are included. This solvent shows only the increasing precipitation temperature with polymer concentration characteristic of crystallization from good solvents.[2,15]
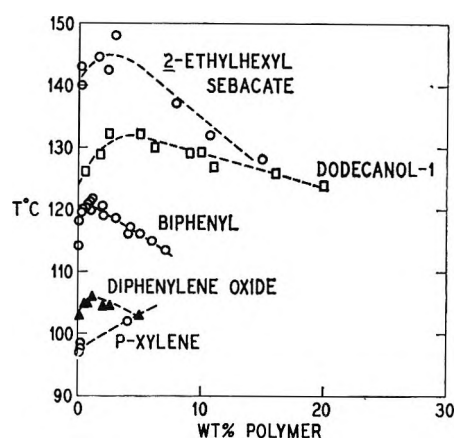
Figure 1. Summary of phase equilibria data.

The θ-conditions found by this work are listed in Table II. The most promising solvents for polymer work, from the standpoint of chemical stability of both solvent and polymer, are biphenyl and dodecanol-1. The viscosity measurements reported here were made using dodecanol-1 at 138°.

Table II: θ-Conditions for Linear Polyethylene

Solvent	θ, °C.
Diphenylene oxide	~118
Biphenyl	~125
Dodecanol-1	138
2-Ethylhexyl sebacate	150
2-Ethylhexyl adipate	170
Nitrobenzene	>200
Dibutyl phthalate	>200

Viscometry. Polymer solutions were prepared in the same manner as for measurements of scattered

(6) P. J. Flory, A. Ciferri, and R. Chiang, *J. Am. Chem. Soc.*, 83, 1023 (1961).

(7) C. A. J. Hoeve and M. K. O'Brien, *J. Polymer Sci.*, A1, 1947 (1963).

(8) R. L. Arnett, M. E. Smith, and B. O. Buell, *ibid.*, A1, 2573 (1963).

(9) C. J. Stacy and R. L. Arnett, *ibid.*, A2, 167 (1964).

(10) Sample kindly supplied by Joseph J. Smith, Plastics Division, Union Carbide Corp. See W. L. Carrick, R. W. Kluiber, E. F. Bonner, L. H. Wartman, F. M. Rugg, and J. J. Smith, *J. Am. Chem. Soc.*, 82, 3883 (1960).

(11) See ref. 2, p. 574.

(12) L. D. Moore, Jr., *J. Polymer Sci.*, 36, 155 (1959).

(13) See ref. 2, p. 547.

(14) A. R. Shultz and P. J. Flory, *J. Am. Chem. Soc.*, 74, 4760 (1952).

(15) L. Mandelkern, "Crystallization of Polymers" McGraw-Hill Book Co., Inc., New York, N. Y., 1964.

light.[9] Solution concentration was varied by making dilutions of stock solutions in the viscometer. The viscometer is similar to others described in the literature. Provisions were made for dilution, for inert atmosphere, and for two shear rates.

The viscometers were rigidly mounted in a stirred silicone oil bath regulated to ±0.01° near 138°. They were cleaned with a filtered solvent and flushed dry with filtered nitrogen. The hot filtered solution was added and manipulated by means of valves so as to be lifted and timed as it flowed between fiduciary marks. Flow times for the solvent were about 100 and 200 sec. for the upper and lower bulbs, respectively. The shear rate dependence of the observed viscosities was quite negligible for the polymers reported here.

Relative viscosities (corrected for kinetic energy) were calculated from the measured flow times, t, by means of the expression

$$\eta_r = \frac{t(\text{solution}) + C/t(\text{solution})}{t(\text{solvent}) + C/t(\text{solvent})}$$

The constant C was determined for each bulb in each viscometer.

III. Results and Discussion

Treatment of Observations. The quantity, $(\ln \eta_r)/c$, was fitted by the method of least squares to the equation[2]

$$(\ln \eta_r)/c = [\eta] + k''[\eta]^2 c \tag{1}$$

with the polymer concentration, c, in grams per deciliter. Values of k'' so determined appeared to scatter in a random fashion, and, since there is no reason apparent for k'' to differ among the polymers in this series, we computed a mean k'' weighting each value according to the goodness of fit of the data giving that value. The weighted mean for k'' is 0.20 with an estimated standard deviation of 0.05. This numerical value was put back in eq. 1 and $[\eta]$ was redetermined by the method of least squares for each polymer. These final values of $[\eta]$ are listed in Table I together with appropriate molecular weight data. It is estimated from prior measurements carried out in the same way that the standard error in determination of our intrinsic viscosities is 0.016. Figure 2 displays the fit of $(\ln \eta_r)$ vs. c with k'' constant. There appears to be no significant departure from linearity.

Molecular Weight Dependence. The Flory-Fox relation for Θ-conditions and polydisperse polymer can be written

$$[\eta]_\Theta = K M_\Theta^{1/2}; \quad K = \Phi(6s_0^2/M)^{1/2} \tag{2}$$

where M_Θ is the symbol we give for that particular viscosity-average molecular weight appropriate under Θ-conditions and s_0 is the root-mean-square molecular radius. Since M_Θ is the square of the weight average of $M^{1/2}$ and since the relation between M_Θ and M_w for our polymers (except polymer 11) is the same as that given by Chiang,[16] we have $M_w/M_\Theta = (M_w/M_n)^{1/4}$ or $M_\Theta = M_w/(11.3)^{1/4}$ for polymers 1-9. The values for M_Θ so calculated are listed in Table I. The distribution of polymer 11 is narrow enough to estimate M_w/M_Θ with little error regardless of its distribution form. We assumed the logarithmic normal form and calculated $M_\Theta = M_w/(1.6)^{1/4}$ to include in Table I.

The second column of Table I was correlated with the fourth by the method of least squares allowing the exponent of M_Θ to be an adjustable parameter. In the fitting each pair of variables was given a statistical weight in accord with the reliability of the determi-
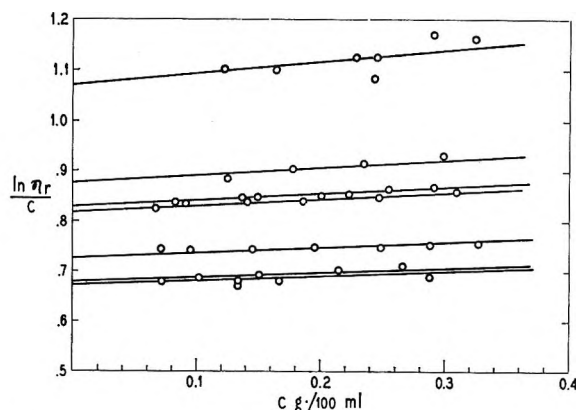
Figure 2. Determinations of intrinsic viscosity.
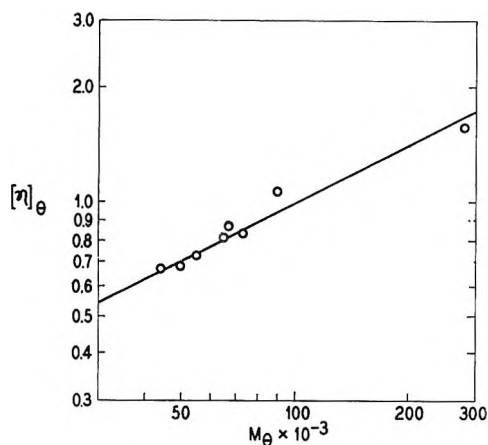
Figure 3. Molecular weight dependence of intrinsic viscosity of linear polyethylene in dodecanol-1 at 138°.

(16) R. Chiang, *J. Polymer Sci.*, **36**, 91 (1959).

nations of $[\eta]_\Theta$ and M_Θ.[9] The value for the exponent found by this procedure was 0.46 with a standard error of estimate of 0.03. We conclude the exponent does not differ significantly from $^1/_2$. With the exponent set at $^1/_2$ a second least-squares fitting gave the value $K = 3.16 \times 10^{-3}$ with a standard error of estimate of 0.07×10^{-3}. The data and the second fitted line are shown in Figure 3.

Molecular Radius. In order to calculate a molecular dimension from the experimentally determined value of K by means of (2), it is necessary to have a value for the constant, Φ. Numerical values of Φ calculated from theory are 2.86×10^{21} and 2.84×10^{21} as quoted by Volkenstein[2] for the Kirkwood–Riseman theory and Zimm theory, respectively. An experimentally determined value of $\Phi = 2.5 \times 10^{21}$ is quoted by McIntyre, *et al.*[17] Each of these values is judged to be that appropriate for Θ-conditions, and each is the value for $[\eta]_\Theta$ expressed in deciliters per gram, s_0 in centimeters, and M in grams per mole. Solving (2) for $6s_0^2/M$ $(=(K/\Phi)^{2/3})$ we find 1.07×10^{-16} cm.^{2} mole/g. when the theoretical value of Φ is used and 1.17×10^{-16} from the experimental value. The estimated standard deviation (occasioned by the uncertainty in K) for each of these values is 0.02×10^{-16}.

Hoeve[4] has made a direct calculation of $6s_0^2/M$ for polymethylene taking into account the possibility of additional steric hindrance from certain conformations of adjacent *gauche* states. His result is given in terms of an undetermined parameter having the meaning of the frequency of occurrence of these adjacent states. The parameter can be fixed by forcing agreement between calculation and experiment for the temperature coefficient $\mathrm{d} \ln s_0^2/\mathrm{d} \ln T$. When this is done using the weighted mean of the observations of Ciferri, Hoeve, and Flory[18] ($\mathrm{d} \ln s_0^2/\mathrm{d} \ln T = -0.433$), the calculated value for $6s_0^2/M$ becomes 1.133×10^{-16} cm.^{2} mole/g. at $160°$.[19] On using this same temperature coefficient, the calculated value becomes 1.159×10^{-16} at $138°$. Thus, this work coupled with the works of Hoeve and Ciferri, *et al.*, supports the value 2.5×10^{21} for Φ.

(17) D. McIntyre, A. Wims, L. C. Williams, and L. Mandelkern, *J. Phys. Chem.*, 66, 1932 (1962).

(18) A. Ciferri, C. A. J. Hoeve, and P. J. Flory, *J. Am. Chem. Soc.*, 83, 1015 (1961).

(19) Hoeve[4] chose the value $\mathrm{d} \ln s_0^2/\mathrm{d} \ln T = -0.44$ and so obtained $6s_0^2/M = 1.128 \times 10^{-16}$ at $160°$.

Radiolysis of Cyclohexane-d_{12}-Cyclopentane Mixtures

by John Y. Yang and Inge Marcus

North American Aviation Science Center, Thousand Oaks, California (Received April 9, 1965)

The yields of dimers and olefins in irradiations of C_6D_{12}–C_5H_{10} solutions have been determined and these values are compared with the corresponding yields from radiolysis of C_6H_{12}–C_5H_{10} solutions. In C_6D_{12}–C_5H_{10} solutions, cyclopentene and bicyclopentyl yields are much higher and, in contrast to C_6H_{12}–C_5H_{10} solutions, the cyclohexene-d_{10} yields are somewhat less than those corrected for energy absorption in the cyclohexane component alone. The nature of the solvent–solute interaction between cyclohexane and cyclopentane is accounted for by hydrogen abstraction reactions. The nonideal behavior of the cyclohexene and cyclopentene yields in the radiolysis of C_6H_{12}–C_5H_{10} solutions is attributed to disproportionation processes, $C_6H_{11}\cdot + C_5H_9\cdot \xrightarrow{k_9} C_6H_{10} + C_5H_{10}$ and $C_6H_{11}\cdot + C_5H_9\cdot \xrightarrow{k_{10}} C_6H_{12} + C_5H_8$, in which the rate constant k_9 is greater than k_{10}.

Introduction

In the radiolysis of saturated hydrocarbon pairs, there is a reasonable expectation that chemical as well as physical effects on each of the components might be proportional to its concentration. Such ideal behavior has been observed by Muccini and Schuler[1] in irradiations of cyclohexane–cyclopentane solutions by high energy electrons. However, in irradiations by Co^{60} γ-rays, at much lower dose rates, departures from statistically expected product yields have been reported. The bicyclohexyl[1] yields are found to be depressed, but the cyclohexene[2] yields are shown to be increased by the presence of cyclopentane in cyclohexane. Since cyclohexene and bicyclohexyl yields are related (at least to some extent) by radical combination and disproportionation processes,[3] the above observations appear somewhat puzzling. Therefore, we have carried out Co^{60} γ-irradiations of cyclohexane-d_{12}–cyclopentane solutions in order to study further the nature of such solvent–solute interactions.

Experimental Results

Experimental procedures have been described elsewhere.[4] Cyclohexane-d_{12} was purified by gas chromatography, but it still contained two unidentified contaminants each amounting to less than 0.05%.

The yields of dimers and olefins in irradiations of cyclohexane-d_{12}–cyclopentane solutions are summarized in Tables I and II. Due partly to the presence of im-

purities in cyclohexane-d_{12}, the cyclopentene yields at low cyclopentane contents could not be measured accurately and these are not reported. In Table II, the differences in cyclohexene-d_{10} yields from those expected according to proportionality to cyclohexane-

Table I: Dimer Yields from Cyclohexane-d_{12}-Cyclopentane Solutions[a]

Electron fraction of C_6D_{12}, ϵ	G(bicyclopentyl)	G(cyclopentyl-cyclohexane)	G(bicyclohexyl)
1	...	...	0.85
0.995	...	0.16	0.79
0.99	0.04	0.34	0.70
0.95	0.20	0.53	0.40
0.89	0.25	0.42	0.22
0.69	0.50	0.41	0.13
0.50	0.81	0.35	0.06
0.31	0.94	0.24	0.03
0.12	1.15	0.10	...
0	1.25	...	...

[a] Total dose = 2 × 10^{20} e.v./g. of sample.

(1) G. A. Muccini and R. H. Schuler, *J. Phys. Chem.*, **64**, 1436 (1960).

(2) S. Z. Toma and W. H. Hamill, *J. Am. Chem. Soc.*, **86**, 4761 (1964).

(3) C. E. Klots and R. H. Johnsen, *Can. J. Chem.*, **41**, 2702 (1963).

(4) (a) J. Y. Yang and I. Marcus, *J. Chem. Phys.*, **42**, 3315 (1965); (b) J. Y. Yang and I. Marcus, to be published.

d_{12} contents are calculated and given as $\Delta G(C_6D_{10})$ values. Because of small uncertainties in cyclopentene measurements, cyclopentene yields in excess of those expected from proportionality to the cyclopentane content are not tabulated. In the radiolysis of cyclohexane-d_{12} alone, hexene-2 was not detected and hexene-1 was found only as a minor product with G(hexene-1) being about 0.1.

Table II: Olefin Yields from Cyclohexane-d_{12}–Cyclopentane Solutions[a]

Electron fraction of C_5D_{12}, ϵ	$G(C_5H_8)$	$G(C_6D_{10})$	$\epsilon \times G_0(C_6D_{10})$	$\Delta G(C_6D_{10})$
1	...	0.98	0.98	...
0.995	...	0.90	0.97	−0.07
0.99	...	0.88	0.97	−0.09
0.95	...	0.82	0.93	−0.11
0.89	...	0.67	0.87	−0.20
0.69	1.5	0.56	0.68	−0.12
0.50	1.7	0.42	0.49	−0.07
0.31	2.3	0.24	0.30	−0.06
0.12	2.8	0.14	0.12	+0.02
0	3.0	...	...	...

[a] Total dose = 2×10^{20} e.v./g. of sample.

Discussion

In the radiolysis of cyclohexane-d_{12}–cyclopentane solutions, the bias in favor of cyclopentyl dimer yields is even higher than that reported by Muccini and Schuler[1] for irradiations of cyclohexane–cyclopentane solutions. In contrast to the cyclohexane–cyclopentane system,[2] the cyclopentene yields are higher and cyclohexene-d_{10} yields are somewhat less than those expected from proportionality to each of the components. Muccini and Schuler[1] have shown that the initial radiation-induced formation of cyclohexyl and cyclopentyl radicals follows an ideal behavior and they accounted for the lower cyclohexyl dimer yields by proposing the abstraction reactions

$$C_6H_{11}\cdot + C_5H_{10} \xrightarrow{k_1} C_6H_{12} + C_5H_9\cdot \quad (1)$$

$$C_5H_9\cdot + C_6H_{12} \xrightarrow{k_2} C_5H_{10} + C_6H_{11}\cdot \quad (2)$$
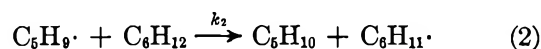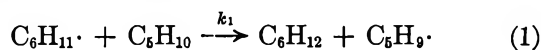
in which the rate constant k_1 is greater than k_2. They further proposed dimer formations by radical recombinations

$$C_6H_{11}\cdot + C_6H_{11}\cdot \xrightarrow{k_3} C_{12}H_{22} \quad (3)$$

$$C_6H_{11}\cdot + C_5H_9\cdot \xrightarrow{k_4} C_{11}H_{20} \quad (4)$$

$$C_5H_9\cdot + C_5H_9\cdot \xrightarrow{k_5} C_{10}H_{18} \quad (5)$$
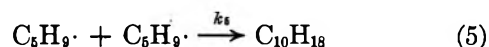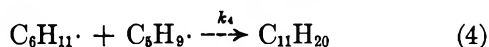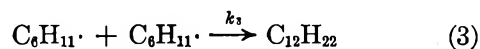
for which the rate constants k_3, k_4, and k_5 are shown to be virtually identical. In the C_6D_{12}–C_5H_{10} system, hydrogen abstraction from cyclohexane would be inhibited owing to the deuterium isotope effect. The observed high bicyclopentyl yields together with the low values of bicyclohexyl serve to confirm the importance of such hydrogen abstraction reactions.

The observed nonideal behavior in cyclohexene and cyclopentene formations is not as easily explained. Toma and Hamill[2] attributed the higher cyclohexene yields to charge transfer from cyclopentane ions to cyclohexane, resulting in proportionally greater reactions by cyclohexane. This mechanism, however, is not consistent with our olefin yield data. Most probably, olefin formation may arise both by radical disproportionation and by molecular dissociation as in reaction 6.

$$C_6H_{12}^+ + e \longrightarrow C_6H_{12}^* \longrightarrow C_6H_{10} + 2H \quad (6)$$
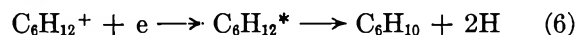
In the radiolysis of cyclohexane-d_{12}, disproportionation by the $C_6D_{11}\cdot$ radical would be inhibited by an expected deuterium isotope effect and the observed G(cyclohexene-d_{10}) may be attributed largely to molecular dissociation. In cyclohexane-d_{12}–cyclopentane solutions, the observed cyclopentene yield is higher at the expense of the cyclohexene-d_{10} yield. Apparently, charge transfer from cyclopentane to cyclohexane-d_{12} does not take place. Since the ionization potential of a hydrocarbon is scarcely affected by deuterium substitution,[5] we expect charge-transfer processes in cyclohexane–cyclopentane solutions, likewise, to be not appreciable.

It is further observed that cyclohexene-d_{10} yields are only slightly smaller than those expected from proportionality to the cyclohexane-d_{12} content. This shows that contribution to cyclohexene-d_{10} formation by radical disproportionation must be small, since large isotope effects in both hydrogen abstraction and radical disproportionation reactions are expected to give rise to C_6H_8 formation at the expense of C_6D_{10}. The cyclohexene yield from cyclohexane is about three times that from cyclohexane-d_{12}, and the difference may be attributed largely to disproportionation of the cyclohexyl radical. For cyclohexane and cyclohexane-d_{12} samples each irradiated to a dose of about 2×10^{20} e.v./g., the difference in $G(C_6H_{10})$ and $G(C_6D_{10})$ values is about 2.0 and G(bicyclohexyl) from cyclohexane radiolysis is 1.45. The ratio 2.0/1.45 is in close agreement with the $C_6H_{11}\cdot$ radical disproportionation to recombination rate constant ratio of 1.31 as reported

(5) F. H. Field and J. L. Franklin, "Electron Impact Phenomena," Academic Press, Inc., New York, N. Y., 1957.

by Klots and Johnsen,[3] showing that our assumption is justified.

In the radiolysis of cyclohexane–cyclopentane mixtures, disproportionation of cyclohexyl and cyclopentyl radicals may proceed by four different paths as

$$C_6H_{11}\cdot + C_6H_{11}\cdot \xrightarrow{k_7} C_6H_{10} + C_6H_{12} \qquad (7)$$

$$C_5H_9\cdot + C_5H_9\cdot \xrightarrow{k_8} C_5H_8 + C_5H_{10} \qquad (8)$$

$$C_5H_9\cdot + C_6H_{11}\cdot \xrightarrow{k_9} C_5H_{10} + C_6H_{10} \qquad (9)$$

$$C_5H_9\cdot + C_6H_{11}\cdot \xrightarrow{k_{10}} C_5H_8 + C_6H_{12} \qquad (10)$$
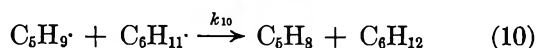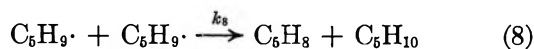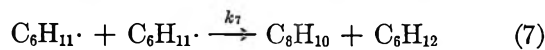
The rate constants for recombination of cyclohexyl and cyclopentyl radicals are shown to be nearly identical.[1] Since, in the absence of hydrogen abstraction reactions 1 and 2, each of the radical yields and its corresponding dimer yields are found to be statistical, the disproportionation rate constants k_7 and k_8 must also be nearly the same. If we discount appreciable energy or charge transfer from cyclopentane to cyclohexane, the observed nonideal behavior of the cyclohexene and cyclopentene yields can be accounted for only by a difference between the rate constants k_9 and k_{10}.

We now examine probable activated complexes

I   II

respectively, for reactions 9 and 10 and compare these with similar activated complexes

III   IV

for the abstraction reactions 1 and 2. Since it has been demonstrated that $k_1 > k_2$, we may suggest that the driving force facilitating hydrogen abstraction from cyclopentane is due to a smaller free energy difference between the cyclopentyl radical and cyclopentane as compared to that between the cyclohexyl radical and cyclohexane. Such a suggestion is consistent with the known strain (6 kcal.) in cyclopentane resulting from repulsion between eclipsed hydrogen atoms.[6] The

heats of formation[7,8] at room temperature for liquid cyclohexane, cyclopentane, cyclohexene, and cyclopentene are, respectively, -36.7, -25.3, -9.7, and 1.2 kcal./mole. Thus, the free energy difference between the cyclopentyl radical and cyclopentene is likewise smaller than that between the cyclohexyl radical and cyclohexene. In reactions proceeding from the activated complexes I and II, the rate-determining processes are, respectively, the scission of the C–H bond in the $C_6H_{11}\cdot$ radical to give cyclohexene and that in the $C_5H_9\cdot$ radical to give cyclopentene. Therefore, we may expect $k_9 > k_{10}$ at least to the same degree as $k_1 > k_2$.

It is interesting to note that interactions in the radiolysis of cyclohexane and cyclopentane may be accounted for by chemical processes alone. Certainly, possible effects due to energy or charge transfer[2,9] appear to be small, yet the photoionization potentials for cyclohexane (9.88 e.v.) and cyclopentane (10.51 e.v.) are highly different.[10] For example, the difference is comparable to that between cyclohexane (9.88 e.v.) and cyclopentene (9.01 e.v.) and even more than some other paraffin–olefin pairs. Charge transfer between a large number of saturated hydrocarbon pairs has been investigated by Hardwick,[11] and the extent of such processes is found to be relatively small, at least at low acceptor concentrations. On the other hand, very large contributions to paraffin–olefin interactions by energy or charge transfer are well demonstrated.[2,4] We may conclude, therefore, that the difference in ionization potentials cannot be the sole factor controlling the rate of charge transfer. Charge exchange must compete with ion neutralization. The cross sections for such processes apparently depend greatly on the availability of π-electrons in the acceptor.

(6) J. D. Cox, *Tetrahedron,* 19, 1175 (1963).

(7) N. A. Lange, "Handbook of Chemistry," McGraw-Hill Book Co., Inc., New York, N. Y., 1961, p. 1634.

(8) (a) M. B. Epstein, K. S. Pitzer, and F. D. Rossini, *J. Res. Natl. Bur. Std.,* 42, 379 (1949); (b) A. Labbauf and F. D. Rossini, *J. Phys. Chem.,* 65, 476 (1961).

(9) J. A. Stone, *Can. J. Chem.,* 42, 2872 (1964).

(10) W. C. Price, R. Bralsford, P. V. Harris, and R. G. Ridley, *Spectrochim. Acta,* 14, 45 (1959).

(11) T. J. Hardwick, *J. Phys. Chem.,* 66, 2132 (1962).

The Intradiffusion[1,2] and Derived Frictional Coefficients for Benzene and

Cyclohexane in Their Mixtures at 25°

by Reginald Mills

*Diffusion Research Unit, Research School of Physical Sciences, Australian National University,
Canberra, A.C.T., Australia* *(Received April 12, 1965)*

The intradiffusion coefficients of both benzene and cyclohexane in mixtures of these two
components have been measured over the whole mole fraction range at 25°. The limiting
values of these intradiffusion coefficients agree well with the corresponding limiting mutual-
diffusion coefficients. Calculations have been made of certain of the frictional coefficients,
R_{ik}, which relate to the interaction of isotopic species.

Introduction

In recent years, the view has been advanced that
data from diffusion studies might be most informative
from a fundamental standpoint if expressed in the form
of frictional coefficients. One type of system of con-
siderable interest in this respect is the ternary one in
which two of the components are chemically identical
and differ only in isotopic composition. Frictional
coefficients which are related to the interaction
between the isotopic species can be obtained from ex-
perimental data and their variation with a changing
environment studied. In order to calculate this par-
ticular type of frictional coefficient, intradiffusion and
mutual-diffusion coefficients must be available together
with activity coefficient data for any given system.
At the present time there are very few suitable sets of
intradiffusion data that can be used for this purpose be-
cause to be meaningful such measurements must be de-
termined with precision of the order of a few tenths of
1%.

Recent studies in this laboratory on the benzene–
diphenyl[3] and urea–water[2] systems[4] have shown that
precision of this order can be obtained. Both of these
systems are, however, limited in the range of concen-
tration that can be studied owing to solubility con-
siderations. The benzene–cyclohexane system was
therefore selected for study as the liquid components
are completely miscible over the entire composition
range at 25°. Mutual-diffusion coefficients for the sys-
tem obtained by the accurate Gouy method have been
reported by Harned,[5] and activity coefficients can be

calculated from the relations given by Scatchard
Wood, and Mochel.[6] Some measurements of the intra-
diffusion coefficients of benzene in the system have
been made by Collins and Watts[7] but at three concen-
trations only and designed to test empirical viscosity
relations.

(1) The meaning of the term "intradiffusion" is presented as follows.
In a section of a homogeneous multicomponent system at uniform
temperature, let a portion of one of the components present be re-
placed by an isotopically labeled form of the same component and
hence by a new component whose concentration may be separately
measured. Further, let the chemical differences between the new
and original components be negligible with regard to diffusion in the
system. Then equivalent and opposite concentration gradients will
be established between these two components which will result in
equivalent and opposite flows relative to the volume-fixed frame of
reference. (Of course, under the specified conditions, this frame of
reference will coincide with the solvent-fixed and number-fixed frames
of reference). It is this mutual diffusion between the two chemically
equivalent components which we define to be intradiffusion. The
"intradiffusion coefficient" for these components is obtained by
treating the system as a two-component system and applying Fick's
laws. In the text, the intradiffusion coefficient is represented by the
symbol, $D\dagger$. The relation of this intradiffusion coefficient to other
diffusion coefficients, as well as the reasons for introducing it, is dis-
cussed in a recent paper by Albright and Mills.[2]

(2) J. G. Albright and R. Mills, *J. Phys. Chem.*, 69, 3120 (1965).

(3) R. Mills, *ibid.*, 67, 600 (1963).

(4) For convenience we refer to the benzene–diphenyl or benzene–
cyclohexane systems. It should be understood however that, when
considered in relation to intradiffusion and frictional coefficients, these
systems are ternary ones consisting of the two components referred
to above together with a labeled but chemically identical species of
either one of them.

(5) H. S. Harned, *Discussions Faraday Soc.*, 24, 7 (1947).

(6) G. Scatchard, S. E. Wood, and J. M. Mochel, *J. Phys. Chem.*, 43,
119 (1939).

(7) D. A. Collins and H. Watts, *Australian J. Chem.*, 17, 516 (1964).

Experimental

Materials. Analar grade benzene was found by gas chromatographic analysis in the previous study[3] to be sufficiently pure for diffusion studies. Cyclohexane purified for spectroscopic use was kept over sodium wire for several days and then distilled, the middle fraction being collected. Its density was 0.7732 g./ml. compared to the value of 0.7738 g./ml. reported by Timmermans.[8] Benzene and cyclohexane both labeled with C^{14} were used as the tracer species and obtained from the Radiochemical Centre, Amersham, England.

Mixtures of benzene and cyclohexane were made up approximately by weight and their densities determined later by using a set of three matched pycnometers. The data and equations given by Wood and Austin[9] were then used to compute the mole fractions accurately from these measured densities.

Apparatus and Procedure. The diaphragm cell technique used in this study has been described in the first paper of this series.[3] One small modification was the use of Teflon stoppers to seal both bottom and top compartments. Rotation of plugs within the stoppers allowed complete sealing of the compartments for the intradiffusion measurements. The design also allowed a negligible amount of the contents of the compartments to be retained in the stoppers. In previous designs a small systematic error may be caused by retention of small amounts of the cell contents within the capillaries and their subsequent release into the cell when it is opened for sampling.

Calibration and counting procedures were the same as in ref. 3.

Results

The intradiffusion coefficients measured in this work are given in Table I. The average error in the coefficients was estimated to be $\pm 0.3\%$, and this was verified by replicate measurements at the same concentration. In this table and in the Discussion which follows, subscripts for the components of the system under study are assigned in this manner: labeled benzene, 1; benzene, 2; labeled cyclohexane, 3; cyclohexane, 4. The subscript v indicating the volume-fixed frame of reference is used on the intradiffusion coefficients to be consistent with the mutual-diffusion data.

Discussion

In order to examine broad relations among the mutual-diffusion, intradiffusion, and viscosity coefficients, the relevant data are plotted together in Figure 1. Excellent agreement is obtained between the limiting mutual-diffusion coefficient for cyclohexane in benzene

Table I: Intradiffusion Coefficients of Benzene and Cyclohexane in Benzene–Cyclohexane Mixtures at 25°

Mole % cyclohexane	$(D^{\dagger}_{1,2})_v \times 10^5$, cm.^{2}/sec.	$(D^{\dagger}_{3,4})_v \times 10^5$, cm.^{2}/sec.
0	2.247	2.104
9.99	2.308	2.124
19.21		2.142
20.12	2.362	
24.85	2.369	2.132
38.89	2.352	
40.80		2.073
60.31	2.264	
67.21		1.872
78.92		1.733
81.23	2.118	
100.00	1.895	1.475

as reported by Harned[4] and the intradiffusion coefficient from this work, the respective values being 2.101 and 2.104 $\times 10^{-5}$ cm.^{2}/sec. For benzene in cyclohexane, the measured value of the intradiffusion coefficient is 1.890 $\times 10^{-5}$ cm.^{2}/sec., whereas a value of 1.876 $\times 10^{-5}$ obtained by extrapolation of mutual-diffusion values is given by Harned.[4] However, it will be observed from Figure 1 that it would not be unreasonable to extrapolate the latter values to the limiting intradiffusion figure and for the sake of consistency in later calculations, this has been done.

It is noteworthy also that the maxima in both intradiffusion coefficient curves coincide almost exactly with the minimum in the viscosity curve at about 76 mole % benzene. The curve for the "activity-corrected"[10,11] mutual coefficients D_v' also has a maximum but at about 60 mole % benzene. In the system under study essentially three frictional coefficients can be considered to be involved in the process of viscous flow. One coefficient relates to the interaction between unlike molecules and the other two to interaction between like molecules for each of the two chemical components. Since intradiffusion involves two of these, the better correlation with the viscosity data as compared to mutual diffusion where only one interaction is involved is not unexpected. In fact, if the viscosity and diffusion coefficients can be related, it should be possible

(8) J. Timmermans, "Physico-Chemical Constants of Pure Organic Compounds," Elsevier Publishing Co., Amsterdam, 1950.

(9) S. E. Wood and A. E. Austin, *J. Am. Chem. Soc.*, **67**, 480 (1945).

(10) $D_v' = D_v/(\partial \ln a_2/\partial \ln x_2)$ where D_v is the observed mutual diffusion coefficient and a_i and x_i are the thermodynamic activity and mole fraction, respectively, of component i.[11]

(11) In ref. 3, the mole fraction of species i was represented by N_i. However, since the use of x_i to represent mole fraction is in more general use, it is adopted here.
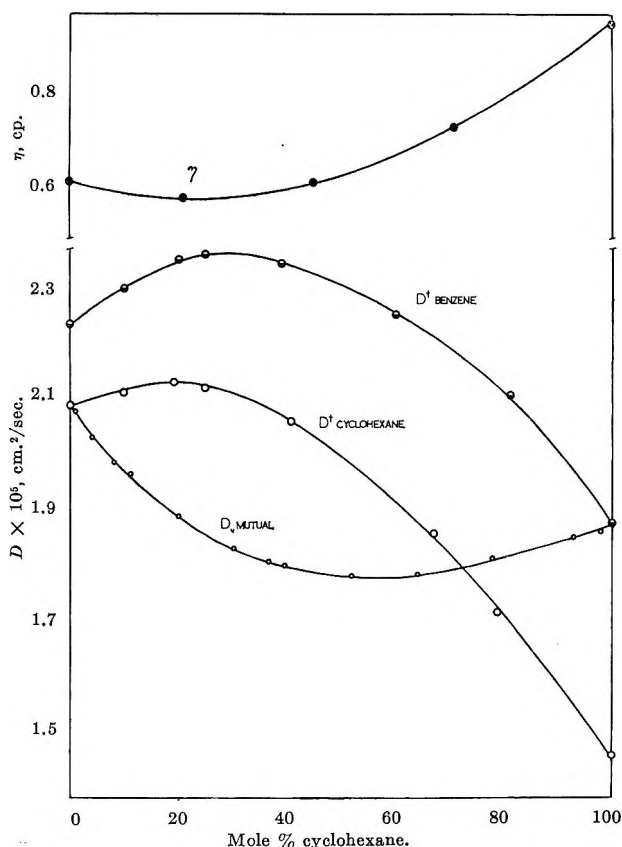
Figure 1. Comparison of viscosity, mutual-diffusion, and intradiffusion coefficients in benzene–cyclohexane mixtures at 25°.

to do so by using some combination of the two intradiffusion coefficients without recourse to the mutual coefficients.

For the reasons outlined in a previous paper,[3] there seems little point in using the diffusion data from this study to test equations of the Hartley–Crank type. Such equations are applicable only to regular solutions, and the present system does not come under this category.

We propose, however, to examine this system by calculating frictional coefficients and studying their variation with composition. This should be of considerable interest as the system is the first in which the isotopic frictional coefficients, in particular, can be calculated over the whole composition range with sufficient accuracy to be meaningful. The R_{ik} formalism which was first introduced by Onsager[12] will be used. The isotopic coefficients, R_{ik}, can be calculated from an equation given by Albright and Mills[2]

$$R_{ik} = RT\left[\frac{\bar{V}_0 c_0 (\partial \ln a_s / \partial c_s)}{1000 D_v} - \frac{1}{(D^\dagger)_v c_s} + \frac{\delta_{ik}}{c_i (D^\dagger)_v}\right]$$

(1)
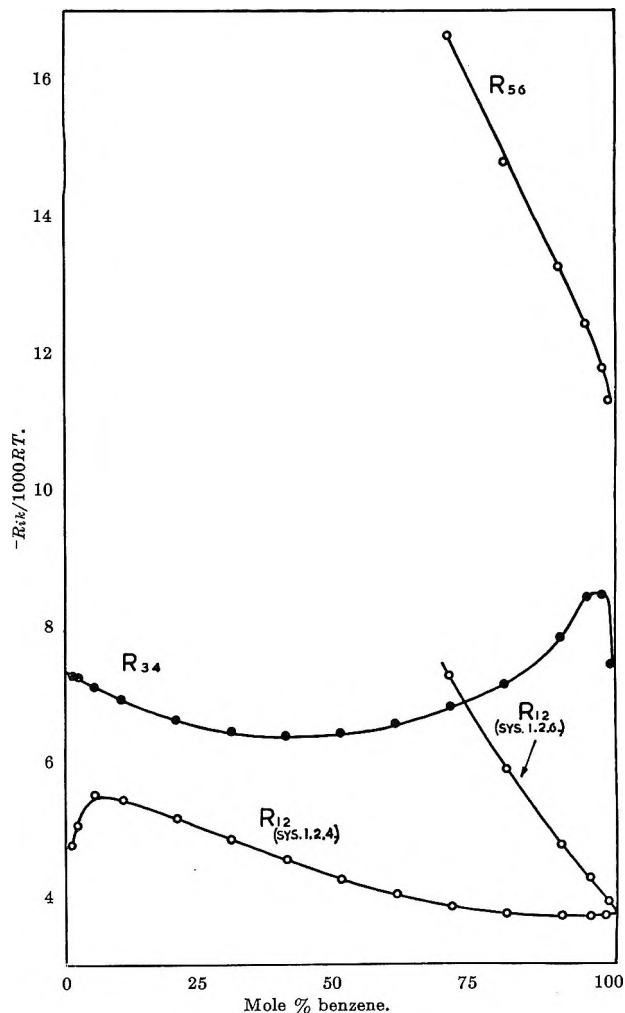
Figure 2. Graph of $R_{ik}/1000RT$ for benzene–cyclohexane and benzene–diphenyl mixtures in which components are separately labeled to give ternary systems.

where the subscripts i and k each refer to either of the two isotopic forms of the same chemical species, and 0 refers to the other component, s refers to the sum of the concentrations of these two forms, R is the gas constant, T the absolute temperature, $\bar{V}_i$ the partial molal volume in milliliters per mole, c_i the concentration in moles per liter, and δ is the Kronecker delta. The coefficients, R_{i0} for interaction between differing chemical species may also be simply determined from the equation

$$R_{i0} = \frac{RT \bar{V}_0 c_s (\partial \ln a_s / \partial c_s)}{1000 D_v}$$

(2)

In Table II are listed the R_{ik} and R_{i0} coefficients for the benzene–cyclohexane and benzene–diphenyl[3] systems.

(12) L. Onsager, Ann. N. Y. Acad. Sci., 46, 241 (1945).

Table II: Frictional Coefficients for the Systems Benzene–Cyclohexane and Benzene–Diphenyl at 25°[a]

| Mole % benzene | Benzene–cyclohexane | | | Benzene–diphenyl | | |
	$\dfrac{R_{12}}{1000RT}$	$\dfrac{R_{34}}{1000RT}$	$\dfrac{R_{14}}{1000RT}$	$\dfrac{R_{12}}{1000RT}$	$\dfrac{R_{56}}{1000RT}$	$\dfrac{R_{16}}{1000RT}$
1	−4.91	−7.35	−5.739			
2	−5.22	−7.30	−5.687			
5	−5.65	−7.17	−5.515			
10	−5.55	−6.99	−5.263			
20	−5.30	−6.72	−4.833			
30	−4.99	−6.55	−4.574			
40	−4.71	−6.49	−4.339			
50	−4.44	−6.52	−4.166			
60	−4.22	−6.64	−4.056			
70	−4.05	−6.85	−4.016	−7.34	−16.45	−9.569
80	−3.97	−7.23	−4.020	−6.00	−14.64	−8.117
90	−3.95	−7.88	−4.104	−4.94	−13.17	−6.831
95	−3.96	−8.40	−4.167	−4.45	−12.33	−6.269
98	−3.97	−8.47	−4.222	−4.17	−11.72	−5.943
99	−3.97	−7.54	−4.225	−4.08	−11.23	−5.833

[a] Labeled benzene, 1; benzene, 2; labeled cyclohexane, 3; cyclohexane, 4; labeled diphenyl, 5; diphenyl, 6.

The frictional coefficients derived from the intra-diffusion measurements are plotted in Figure 2.

The first feature of interest is that R_{56}, the coefficient for diphenyl–diphenyl friction is much greater than any of the other coefficients. In fact, it is about 2.5 times as great as the R_{12} benzene–benzene interaction in the same system, thus giving a rough correlation with size. The rapid increase of R_{56} with increasing diphenyl concentration is probably connected with the fact that the component is approaching its saturated solution value. The marked effect of environment on

the benzene–benzene interaction is also evident in the values of R_{12} for the two systems, the system with diphenyl having an effect increasing rapidly with the concentration of diphenyl.

A second feature observable in the Figure 2 is the behavior of the two curves in the benzene–cyclohexane system. It will be seen that at compositions where each component is at low concentration, in a large excess of the nonisotopic one, the corresponding frictional coefficients R_{12} and R_{34} rise to a maximum value and then drop sharply. It is not clear at this stage whether this effect is real or is an artefact. It is apparently not observed in R_{56} interaction for diphenyl nor for urea in water.[2] Also as Tyrrell[13] has pointed out, the expected error in this type of frictional coefficient increases rapidly as the concentration of the components becomes very small. From the form of the curves, if the effect is due to error, it is evidently not from a random but from a systematic one.

Finally, it is noteworthy that the behavior of the two systems is quite different with regard to relations between the frictional coefficient R_{i0} which is derived from the mutual-diffusion coefficient and the isotopic coefficients R_{ik}. In the benzene–diphenyl system it is evident from Table II that the coefficients are linearly related and in fact can be expressed by an equation of the form

$$R_{16} = 0.24R_{56} + 0.76R_{12} \qquad (3)$$

which is accurate to about 1%. However, no functional relation of this kind is applicable to the benzene–cyclohexane system, but it is observed that the R_{14} coefficients are very close to the R_{12} ones.

(13) H. J. V. Tyrrell, *J. Chem. Soc.*, 1599 (1963).

A Study of Diffusion in the Ternary System, Labeled Urea–Urea–Water, at 25°

by Measurements of the Intradiffusion Coefficients[1] of Urea[2]

by J. G. Albright[3] and R. Mills

Diffusion Research Unit, Research School of Physical Sciences, Australian National University, Canberra,
Australia   (*Received May 10, 1965*)

The term "intradiffusion" has been defined to facilitate the description of diffusion in certain multicomponent systems. The relations between the "intradiffusion coefficient" and the other diffusion and transport coefficients in ternary systems containing two forms of the same chemical species have been formulated. Intradiffusion coefficients measured at 25° for the system labeled urea–urea–H_2O up to total solute concentrations of 4 moles/l. are reported. The coefficients, R_{12}, for the interaction between the two forms of urea, obtained from these data, are shown to be linear with concentration over the above range.

Introduction

Recent work[4] in binary mixtures of organic liquids has shown that accurate tracer-diffusion coefficients of organic components labeled with C^{14} can be obtained with the diaphragm cell method. There are, however, no data of comparable accuracy for organic molecules in aqueous solution. In the study now reported, the techniques used in the above work have been applied to the measurement of intradiffusion coefficients of urea labeled with C^{14} in the system labeled urea–urea–H_2O. This system was chosen for study because accurate mutual-diffusion and activity coefficients for the system urea–H_2O are available in the literature[5] which when combined with intradiffusion data allow computation of frictional coefficients. It was thought also that data of this kind for a compound which is important in biological systems would be of considerable interest.

Because the experimental system in which intradiffusion coefficients were measured is a ternary system, a formulation is derived in which the four diffusion coefficients that describe a ternary system are expressed in terms of the intradiffusion and mutual-diffusion coefficients for the solute. These coefficients when combined with the relevant thermodynamic activity data are used to obtain the transport coefficients which appear in the linear equations that relate the flow of the components to the gradients of chemical potential.

Theory

In the description of diffusion processes in liquids, it is convenient to employ two types of flow equations. Following Gosting,[6] we can term these *experimental*

---

(1) The meaning of the term "intradiffusion" is presented as follows. In a section of a homogeneous multicomponent system at uniform temperature, let a portion of one of the components present be replaced by an isotopically-labeled form of the same component and hence by a new component whose concentration may be separately measured. Further, let the chemical differences between the new and original components be negligible with regard to diffusion in the system. Then equivalent and opposite concentration gradients will be established between these two components which will result in equivalent and opposite flows relative to the volume-fixed frame of reference. (Of course, under the specified conditions, this frame of reference will coincide with the solvent-fixed and number-fixed frames of reference.) It is this mutual diffusion between the two chemically equivalent components which we define to be intradiffusion. The "intradiffusion coefficient" for these components is obtained by treating the system as a two-component system and applying Fick's laws. In the text, the intradiffusion coefficient is represented by the symbol, $D^\dagger$.

We have introduced the term intradiffusion because of the inadequacy and ambiguity of the terms tracer diffusion and self-diffusion which are commonly used to describe the type of system considered in this definition. The intradiffusion coefficient will be numerically equal to the tracer-diffusion coefficient in this case. However, it should be emphasized that the meanings of the two terms differ significantly. In the process associated with the latter, attention is focused on a diffusing component which may or may not have a chemically equivalent component in the system and which is in very low concentration in an essentially homogeneous environment. With the former, it is clear from the chemical identity of the two isotopic components that the intradiffusion coefficient is independent of the ratio of the concentrations of the two components and depends only on the sum of their concentrations and the concentrations of the other components of the system. The term intradiffusion is also related to the term self-diffusion; self-diffusion is the special case of intradiffusion for systems that contain no other components than two isotopic forms of a chemical species.

flow equations and *theoretical flow equations.* Experimental flow equations, which are based on Fick's laws, employ diffusion coefficients to describe the relations between flows and concentration gradients. Theoretical flow equations have their basis in the thermodynamics of irreversible processes and employ transport coefficients to describe the relations between flows and thermodynamic forces.

Experimental Flow Equations. Isothermal diffusion in one dimension for the ternary system, labeled urea–urea–H$_2$O, can be completely described in terms of the flows, J_i, the diffusion coefficients, D_{ik}, and the concentration gradients, $\partial c_i/\partial x$, by the equations

$$- (J_1)_v = (D_{11})_v \frac{\partial c_1}{\partial x} + (D_{12})_v \frac{\partial c_2}{\partial x} \qquad (1)$$

$$- (J_2)_v = (D_{21})_v \frac{\partial c_1}{\partial x} + (D_{22})_v \frac{\partial c_2}{\partial x} \qquad (2)$$

where 1 and 2 denote labeled urea and urea, respectively; the subscript 0 is reserved for the solvent, water. The subscript v denotes the volume-fixed frame of reference which is defined by the equation

$$\sum_{i=0}^{2} (J_i)_v \bar{V}_i = 0 \qquad (3)$$

in which $\bar{V}_i$ is the partial molal volume of component i in milliliters per mole. If length and time are measured in centimeters and seconds, respectively, then the diffusion coefficients have the dimensions of square centimeters per second. For this development, concentration is to be measured in moles per liter. From the following considerations it is shown that the four diffusion coefficients in eq. 1 and 2 are directly related to the intradiffusion coefficient and mutual-diffusion coefficient for the system.

In a system undergoing intradiffusion, the sum of the concentrations of the two solute forms is initially constant and remains constant with time throughout the system within experimental error.[7] Thus we may write the equation

$$\partial c_1/\partial x = -\partial c_2/\partial x \qquad (4)$$

Equations 1 and 2 may now be written

$$- (J_i)_v = (-1)^i [(D_{i2})_v - (D_{i1})_v] \frac{\partial c_i}{\partial x} =$$

$$(D^\dagger)_v \frac{\partial c_i}{\partial x} \quad (i = 1, 2) \qquad (5)$$

and thus

$$(D^\dagger)_v = (D_{11})_v - (D_{12})_v = (D_{22})_v - (D_{21})_v \qquad (6)$$

The values of the coefficients D_{ik}, defined by eq. 1 and 2 may be related also to the mutual-diffusion coefficients for the system urea–H$_2$O. In a system undergoing mutual diffusion, a homogeneous mixture of the isotopic forms of each of the two components is interdiffusing and no distinction is made for any differences attributable to isotopic effects; *i.e.*, we assume that the ratios of the isotopic forms are constant throughout the system. If in such an experiment observations are made from which an isotopic form of the solute is distinguished from the rest of the solutes, then the system, although otherwise unaltered, may be formally treated as a ternary system. Equations 1 and 2 may then be applied to the system with the added restraint that c_1/c_2 is a constant independent of x or time. We may write

$$(J_i)_v = \frac{c_i}{c_s} (J_s)_v = -D_v \frac{c_i}{c_s} \frac{\partial c_s}{\partial x} \quad (i = 1, 2) \qquad (7)$$

where

$$c_1 + c_2 = c_s \qquad (8)$$

$$(J_1)_v + (J_2)_v = (J_s)_v \qquad (9)$$

Here, D_v is the mutual-diffusion coefficient that would be obtained for either form of the solute at concentration c_s. By noting that

$$\frac{\partial c_i}{\partial x} = \frac{c_i}{c_s} \frac{\partial c_s}{\partial x} \quad (i = 1, 2) \qquad (10)$$

we may now write with the use of eq. 1 and 2, the equations

$$- (J_i)_v = (D_{i1})_v \frac{c_1}{c_s} \frac{\partial c_s}{\partial x} + (D_{i2})_v \frac{c_2}{c_s} \frac{\partial c_s}{\partial x} \quad (i = 1, 2) \qquad (11)$$

Hence

$$- \frac{c_i}{c_s} (J_s)_v = \left(\frac{c_1}{c_s} (D_{i1})_v + \frac{c_2}{c_s} (D_{i2})_v \right) \frac{\partial c_s}{\partial x} \quad (i = 1, 2) \qquad (12)$$

from which it follows that

(2) Portions of this paper were presented at the ANZAAS meeting in Canberra, Australia, Jan. 20–25, 1964.

(3) Visiting N.I.H. Fellow.

(4) R. Mills, *J. Phys. Chem.*, **67**, 600 (1963).

(5) L. J. Gosting and D. F. Akeley, *J. Am. Chem. Soc.*, **74**, 2058 (1952).

(6) L. J. Gosting, "Advances in Protein Chemistry," Vol. XI, Academic Press, Inc., New York, N. Y., 1956, p. 429.

(7) Experimental evidence indicates that this assumption for intradiffusion is reasonable for most systems where the isotopic masses of the diffusing components differ by less than about 5%. For greater mass differences, the possibility of isotope effects cannot be excluded.

$$D_\mathrm{v} = (D_{11})_\mathrm{v} + \frac{c_2}{c_1}(D_{12})_\mathrm{v} = (D_{22})_\mathrm{v} + \frac{c_1}{c_2}(D_{21})_\mathrm{v} \quad (13)$$

Equation 13 may now be combined with eq. 6 to yield the general result

$$(D_{ik})_\mathrm{v} = \frac{c_i}{c_\mathrm{s}}(D_\mathrm{v} - (D^\dagger)_\mathrm{v}) + \delta_{ik}(D^\dagger)_\mathrm{v} \quad (i = 1, 2)$$
$$(k = 1, 2) \quad (14)$$

where δ_{ik} is the Kronecker δ.

It may be noted that eq. 14 will apply for the solvent-fixed and number-fixed frames of reference with the appropriate change of the subscript v. For a discussion of frames of reference, the reader is referred to Kirkwood, et al.,[8] and Woolf, Miller, and Gosting.[9]

Theoretical Flow Equations. According to the theory of the thermodynamics of irreversible processes, flows and thermodynamic forces for isothermal diffusion are related to the rate of entropy production, σ, by the equation

$$T\sigma = \sum_{i=0}^{n} J_i X_i \quad (15)$$

Here T is the absolute temperature, J_i is the flow of component i, X_i, the thermodynamic force, is the negative gradient of the chemical potential of component i, $-\nabla\mu_i$, and n is the number of solutes. A further postulate of the theory is that linear relations exist between flows and forces. This condition may be written in the form

$$-(J_i)_\mathrm{S} = \sum_{k=0}^{2} (L_{ik})_\mathrm{S} \nabla\mu_k \quad (i = 0, 1, 2) \quad (16)$$

where S denotes a class of frames of reference which includes the solvent-fixed and volume-fixed frames of reference.[9] The coefficients, L_{ik}, are transport coefficients. By beginning with eq. 16 and writing equations in which the forces and flows are independent, Woolf, Miller, and Gosting[9] give relations for the solvent-fixed and volume-fixed frames of reference in one-dimensional systems. They write for a ternary system the equations

$$-(J_i)_0 = \sum_{k=1}^{2} (L_{ik})_0 \frac{\partial\mu_k}{\partial x} \quad (i = 1, 2) \quad (17)$$

where here the subscript 0 denotes the solvent-fixed frame of reference. For the volume-fixed frame of reference they write

$$-(J_i)_\mathrm{v} = \sum_{k=1}^{2} (L_{ik})_\mathrm{v} Y_k \quad (i = 1, 2) \quad (18)$$

where

$$Y_k = \sum_{j=1}^{2} (\delta_{kj} + c_j \bar{V}_k/c_0 \bar{V}_0) \frac{\partial\mu_j}{\partial x} \quad (19)$$

For these cases the Onsager reciprocal relations, another postulate of the theory of the thermodynamics of irreversible processes, may be written

$$(L_{ik})_0 = (L_{ki})_0; \quad (L_{ik})_\mathrm{v} = (L_{ki})_\mathrm{v} \quad (20)$$

If the flows for a particular frame of reference in the theoretical and experimental sets of equations are equated, the coefficients, L_{ik}, may then be expressed in terms of the coefficients, D_{ik}. Dunlop and Gosting[10] and Woolf, Miller, and Gosting[9] have developed equations relating the two sets of coefficients for the solvent-fixed and volume-fixed frames of reference, respectively.

At this point several further simplifications may be made which again arise from the chemical equivalence of solutes 1 and 2. These concern the partial molal volumes, $\bar{V}_i$, and the activity coefficients, y_i. In a solution of total solute concentration c_s, it is clear that $\bar{V}_1 = \bar{V}_2 = \bar{V}_\mathrm{s}$ and, similarly, $y_1 = y_2 = y_\mathrm{s}$, where again the subscript s signifies that the two isotopic forms of the solute are not to be distinguished, but are to be considered as a single solute. It may be seen also that

$$\frac{\partial \ln a_i}{\partial c_k} = \frac{1}{y_\mathrm{s}} \frac{\partial y_\mathrm{s}}{\partial c_\mathrm{s}} + \frac{\delta_{ik}}{c_k} \quad \begin{array}{l}(i = 1, 2) \\ (k = 1, 2)\end{array} \quad (21)$$

where a_i is the activity of component i. By introducing these conditions together with eq. 14 into expressions given in ref. 9 and 10, the general equations

$$(L_{ik})_0 = (RT)^{-1} \left[\frac{1000 c_i c_k D_\mathrm{v}}{c_0 \bar{V}_0 c_\mathrm{s}^2 (\mathrm{d} \ln a_\mathrm{s}/\mathrm{d} c_\mathrm{s})} + \right.$$
$$\left. (-1)^{i+k} \frac{c_1 c_2 (D^\dagger)_\mathrm{v}}{c_\mathrm{s}} \right] \quad \begin{array}{l}(i = 1, 2) \\ (k = 1, 2)\end{array} \quad (22)$$

and

$$(L_{ik})_\mathrm{v} = (RT)^{-1} \left[\frac{c_0 \bar{V}_0 c_i c_k D_\mathrm{v}}{1000 c_\mathrm{s}^2 (\mathrm{d} \ln a_\mathrm{s}/\mathrm{d} c_\mathrm{s})} + \right.$$
$$\left. (-1)^{i+k} \frac{c_1 c_2 (D^\dagger)_\mathrm{v}}{c_\mathrm{s}} \right] \quad \begin{array}{l}(i = 1, 2) \\ (k = 1, 2)\end{array} \quad (23)$$

may be derived.

An alternative representation of the theoretical flow equations is obtained by expressing the forces as being

(8) J. G. Kirkwood, R. L. Baldwin, P. J. Dunlop, L. J. Gosting, and G. Kegeles, *J. Chem. Phys.*, **33**, 1505 (1960).

(9) L. A. Woolf, D. G. Miller, and L. J. Gosting, *J. Am. Chem. Soc.*, **84**, 317 (1962).

(10) P. J. Dunlop and L. J. Gosting, *J. Phys. Chem.*, **63**, 86 (1959).

proportional to the flows. The original equations for this representation were given by Onsager,[11] and for our system may be written as

$$-\frac{\partial \mu_i}{\partial x} = \sum_{k=0}^{2} R_{ik} J_k \quad (i = 0, 1, 2) \tag{24}$$

where the Onsager reciprocal relations

$$R_{ik} = R_{ki} \quad (i \neq k) \tag{25}$$

apply. Onsager includes the restrictions

$$\sum_{k=0}^{2} R_{ik} c_k = 0 \quad (i = 0, 1, 2) \tag{26}$$

from which it may be shown that the coefficients, $R_{i,k}$ are independent of the frame of reference of the flows.

From eq. 17 and 24–26, a relation among the coefficients, R_{ik} and $(L_{ik})_0$ (for $i = 1, 2$, and $k = 1, 2$), is obtained which with the application of eq. 22 yields the result

$$R_{ik} = RT \left[\frac{\bar{V}_0 c_0 \, (d \ln a_s/dc_s)}{1000 D_v} - \frac{1}{(D^\dagger)_v c_s} + \frac{\delta_{ik}}{c_i (D^\dagger)_v} \right] \quad \begin{array}{l} (i = 1, 2) \\ (k = 1, 2) \end{array} \tag{27}$$

It may also be noted from eq. 26 and 27 that

$$R_{10} = R_{20} = R_{01} = R_{02} = -\frac{c_0}{c_s} R_{00} =$$

$$\frac{RT \bar{V}_0 c_s \, (d \ln a_s/dc_s)}{1000 D_v} \tag{28}$$

Experimental

Materials. Analar reagent grade urea was purified by one recrystallization from water with the mother liquor removed by centrifugal drainage. In this process, care was taken to avoid heating the urea above 65°. Conductivity measurements on aqueous solutions of the recrystallized urea showed that ionic impurities were negligible. It is known that a major impurity in urea is biuret which results from its thermal decomposition. Tests on concentrated solutions showed that the purified urea contained less than 0.02% biuret by weight. The urea labeled with C^{14} was obtained from the Radiochemical Centre, Amersham, England. Purified nonradioactive urea was added to the labeled urea to give a total weight of 0.5 g. and the combined sample was recrystallized once from water with centrifugal drainage. The Analar KCl which was used for the calibrations of the diaphragm cell was recrystallized once from water followed by centrifugal drainage. Naphthalene for the scintillator solution was recrystallized once from methanol.
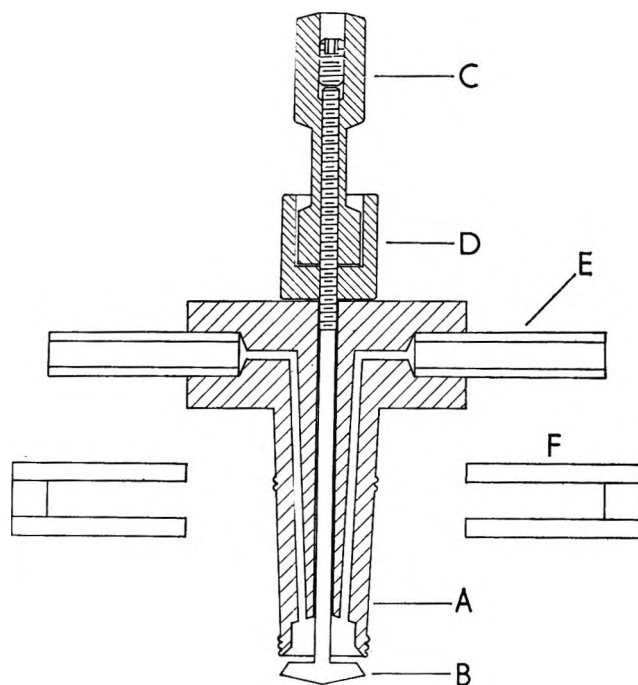
Figure 1. Sectional view of the assembly of the bottom plug: A, Teflon body; B, stainless steel valve; C and D, brass knobs; E, glass tubes; F, rubber sleeves.

Apparatus. Diaphragm cells with magnetic stirring of the type designed by Stokes[12] were used. The glass sinters in these cells were Pyrex brand of porosity No. 4 (5–10 μ). A special bottom plug for the cells was developed and is shown in Figure 1. This plug is inserted with valve B open to ensure complete filling. B is then closed by holding knob C and rotating knob D. The internal chamber in the Teflon body A is then dried by drawing in turn water, acetone, and air through the side tubes E. The tubes E are sealed with caps F before inserting the cell into the thermostat. At the end of an experiment and after the top compartment has been emptied, the cell may be inverted and diffusion from the diaphragm into the bottom section quickly and simply quenched by removing one of the caps, opening B, and forcing a little of the solution through the diaphragm by air pressure. The cells, after initial alignment, were permanently strapped to a brass rod with a slotted base which in turn fitted into a mount in the thermostat. This allowed the cells to be located reproducibly in a fixed position relative to the magnets with the diaphragm within 1° of being horizontal. The stirring rods were normally rotated at 60 r.p.m. although in some experiments the speed reached 90 r.p.m. The water

(11) L. Onsager, *Ann. N. Y. Acad. Sci.*, **46**, 241 (1945).

(12) R. H. Stokes, *J. Am. Chem. Soc.*, **72**, 763 (1950).

thermostat was maintained at 25.00° to within ±0.01°. The temperature was measured by a calorimeter thermometer which had been calibrated against a platinum resistance thermometer. The conductivity bridge used for measuring the concentrations of solutions of KCl and the apparatus for counting have been described previously.[4]

Experimental Procedure. All solutions were prepared gravimetrically. The cells were calibrated in the usual manner by allowing an aqueous solution containing 0.5 mole/l. of KCl to diffuse into pure water. The scintillator solution was essentially that previously used in this laboratory except that the concentration of naphthalene was reduced to 20 g./l. for the more concentrated solutions to avoid precipitation. Counting procedures were similar to those described in previous papers.[4]

Results

The intradiffusion coefficients measured in this work[13] are recorded in Table I. The experimental error in these measurements was estimated to be ±0.3%.

Table I: Intradiffusion Coefficients between Urea and Urea Labeled with C^{14} in Aqueous Solutions at 25°

c_s, mole/l.	$(D^\dagger)_v$, × 10^5, cm.²/sec.	c_s, moles/l.	$(D^\dagger)_v$, × 10^5, cm.²/sec.
0.1	1.374	2.0	1.234
0.25	1.370	3.0	1.163
0.5	1.344	4.0	1.107
1.0	1.305		

Discussion

In Figure 2, diffusion coefficients, D_v, measured by Gosting and Akeley[5] for the binary system urea–H_2O are compared with the values of $(D^\dagger)_v$ reported in this work which were measured over the same range of concentration. It is apparent that at infinite dilution, the two curves converge approximately to the same limiting value. This convergence for nonelectrolytes is predicted by theory[14] and has previously been found to be true experimentally (see for example ref. 4).

An analytical expression for the coefficient, $(D^\dagger)_v$, has been derived in the following manner. In the first instance, the curve was fitted to a cubic equation by the method of least squares which gave an intercept at zero concentration for $(D^\dagger)_v$ of 1.386 × 10^{-5}. Since the extrapolation of the data obtained from experiments performed with the Gouy method is probably the more accurate, we have adjusted the
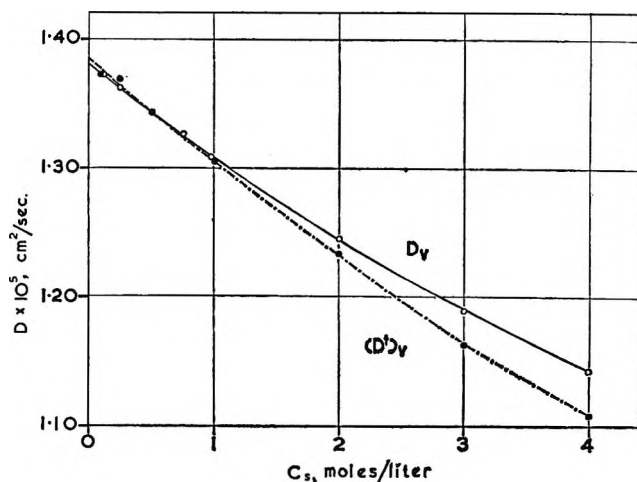
Figure 2. Comparison of values of D_v measured by Gosting and Akeley[6] for the system urea–H_2O with the values of $(D^\dagger)_v$ measured in this work.

value of the constant in the analytical equation to be 1.381$_7$ × 10^{-5}. In so doing, we allow for the possibility of small systematic errors in the diaphragm cell method which may arise from such effects as convection in the diaphragm due to stirring. The modified analytical expression becomes

$$(D^\dagger)_v \times 10^5 = 1.381_7 - 0.0840c +$$
$$0.0035c^2 \qquad c \leqslant 4 \qquad (29)$$

Analytical expressions for the values of D_v and ln y for aqueous solutions of urea given by Gosting and Akeley[5] are

$$D_v \times 10^5 = 1.381_7 - 0.0783_0c + 0.004646c^2$$
$$c \leqslant 4 \qquad (30)$$

and

$$\ln y = -0.0373_0c + 0.003684c^2 \quad c \leqslant 4 \qquad (31)$$

From data listed by Gucker, Gage, and Moser,[15] we have also derived an expression for $\bar{V}_s$ (in milliliters per mole) for the urea solution, which is

$$\bar{V}_s = 44.221 + 0.275c - 0.01207c^2 \quad c \leqslant 4 \qquad (32)$$

By substitution of eq. 29–32 into each of the eq. 22,

(13) It should be emphasized here that, within the error of measurement, the urea labeled with C^{14} is assumed to be chemically equivalent to the unlabeled urea. If it were believed that such an assumption was not legitimate, then the measured diffusion coefficients should be termed tracer-diffusion coefficients.

(14) See, for example, eq. 5c and 8 of R. J. Bearman, *J. Phys. Chem.*, 65, 1961 (1961).

(15) F. T. Gucker, Jr., F. W. Gage, and C. E. Moser, *J. Am. Chem. Soc.*, 60, 2582 (1938).

23, and 27, we have calculated normalized values of $(L_{12})_0$, $(L_{12})_v$, and R_{12}, respectively, at a series of concentrations. These data are listed in Table II. Values of R_{10} which were obtained from data reported by Ellerton, et al.,[16] have also been included in Table II (it should be noted that these authors use the opposite sign for R_{ik} from that used in this article).

Table II: Transport Coefficients for the System, Labeled Urea–Urea–H$_2$O at 25°

c_s, moles/l.	$\dfrac{(L_{12})_0 RT c_s^2}{c_1 c_2} \times 10^{-5}$	$\dfrac{(L_{12})_v RT c_s^2}{c_1 c_2} \times 10^{-5}$	$\dfrac{R_{12}}{1000RT}$	$\dfrac{R_{10}}{1000RT}$
0.25	0.007	−0.0004	−6.15	−1.314
0.50	0.029	−0.0021	−6.10	−1.322
0.75	0.063	−0.0060	−6.04	−1.336
1.00	0.110	−0.0128	−5.99	−1.340
1.25	0.168	−0.0233	−5.94	−1.350
1.50	0.238	−0.0381	−5.88	−1.362
1.75	0.317	−0.0580	−5.83	−1.372
2.00	0.405	−0.0835	−5.77	−1.384
2.25	0.502	−0.1151	−5.72	−1.397
2.50	0.606	−0.1533	−5.66	−1.413
2.75	0.718	−0.1985	−5.60	−1.430
3.00	0.835	−0.2511	−5.55	−1.448
3.25	0.957	−0.3113	−5.49	−1.465
3.50	1.085	−0.3794	−5.44	−1.471
3.75	1.216	−0.4554	−5.38	−1.507
4.00	1.352	−0.5395	−5.33	−1.528

In Figure 3, we plotted the values of R_{12} as a function of concentration and included for comparison the values of R_{10}. It is evident from this figure that the values of R_{12} are linear with respect to concentration up to concentrations of 4 moles/l. These points have therefore been fitted to a straight line by the method of least squares to obtain the relation

$$R_{12}/1000RT = -6.21 + 0.220c_s \quad c \leqslant 4 \quad (33)$$

It will be observed that the values of R_{10} are not linear with respect to concentration; however, for both cases the coefficients have only a small variation with concentration. This is consistent with the fact that the activity coefficients (see eq. 31) only change slightly over the same range. The significance of the linearity with concentration of the coefficients, R_{12}, cannot be evaluated at this stage and must await further studies on comparable systems. We now propose to measure the intradiffusion coefficients of other organic molecules in aqueous solutions with a view to making such intercomparisons and to studying the relation of dipole moment and other molecular properties to the values of R_{10} and R_{12}.
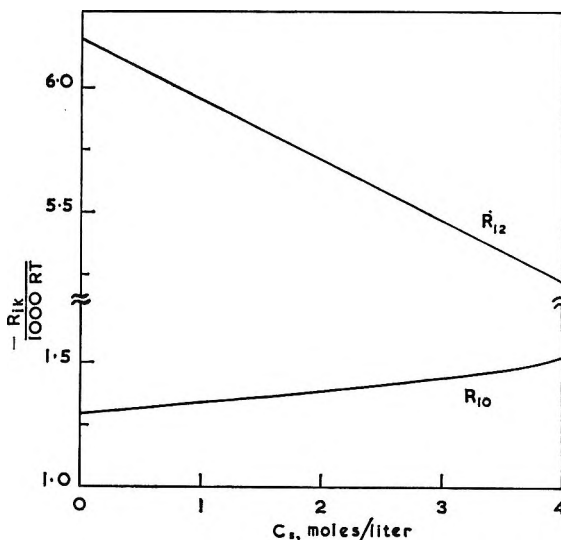
Figure 3. Graph of values of $-R_{12}/1000RT$ and $-R_{10}/1000\ RT$ as a function of the concentration c_s.

The expressions derived in this paper together with the results in Table II give some indication of the relative merit of the different formulations which have been used to express the linear laws for the case of isothermal diffusion. All three representations given by eq. 22, 23, and 27 have the merit that the Onsager reciprocal relations apply in a simple manner. However, the relation given by eq. 27 has the following advantages.

(1) As has been noted by other authors,[17,18] the values of the coefficients, R_{ik}, are independent of the frame of reference for the flows.

(2) The expression for the coefficients, R_{12}, presented in eq. 27 depends only on c_s and not on the individual values of c_1 and c_2, whereas the expressions for $(L_{12})_0$ and $(L_{12})_v$ involve the product $c_1 c_2$. In this connection, it can be shown that if one considered a case of not 2 but n equivalent isotopic forms of the solute, the values of the coefficients, R_{ik}, with $i \neq k$ for the interaction between any two of the solutes, would be equal to the expression presented in eq. 27 with c_s as the sum of the concentrations of all the isotopic solutes.

(3) The results in Table II indicate that for a nonelectrolyte the values of R_{12} do not vary greatly with concentration and extrapolate to a finite value at zero concentration while the values of $(L_{12})_0$ and $(L_{12})_v$ vary greatly with concentration and become zero

(16) H. D. Ellerton, G. Reinfelds, D. E. Mulcahy, and P. J. Dunlop, *J. Phys. Chem.*, **68**, 403 (1964).

(17) R. W. Laity, *ibid.*, **63**, 80 (1959).

(18) P. J. Dunlop, *ibid.*, **68**, 26 (1964).

at zero concentration. Although the values of R_{12} in Table II are for the interaction between two isotopic solutes, it is reasonable to suppose that this relative variation would apply to nonisotopic forms of organic solutes also.

These considerations tend to reinforce the view that Onsager's[11] presentation of the linear laws in terms of the coefficients, R_{ik}, is the more fundamental formulation and the more useful one.

The Heat Capacity and Entropy of Hexamethylbenzene from 13 to 340°K.

An Estimate of the Internal Rotation Barrier

by M. Frankosky and J. G. Aston

Contribution No. 126 from the Cryogenic Laboratory of the College of Science of the Pennsylvania State University, University Park, Pennsylvania (Received April 15, 1965)

The heat capacities of hexamethylbenzene were measured from 13 to 340°K. Assignment of the normal coordinates permitted calculation of an entropy which was compared with that calculated from heat capacity and vapor pressure measurements. A value for the barrier hindering internal rotation is deduced.

Introduction

An inspection of a Hirschfelder model of hexamethylbenzene reveals considerable repulsion between methyl groups. Spectroscopic evidence has been presented to show that the molecule has S_6 symmetry in the crystal at room temperature.[1]

There is a transition in the crystal at 116.48°K., and spectroscopic studies above and below this transition have been interpreted as indicating that it is associated with the molecule becoming nonplanar.[2]

Recently a normal coordinate treatment of the molecule which included all modes except those of internal rotation has been made on the basis of C_{6h} symmetry.[3] This permits a calculation of the standard entropy for the molecule in the vapor at any temperature if the barriers hindering internal rotation are assumed. Since the frequencies will be altered little by symmetry, the spectroscopic entropy can be calculated for the symmetry S_6 ($\sigma = 6$) as well as C_{6h} ($\sigma = 12$).

The results can be compared with a third-law entropy. For this purpose we have measured the heat capacities from 13 to 340°K., along with the heat of transition at 116.48°K., on a pure sample of hexamethylbenzene. These values along with the vapor pressures and heats of sublimation derived from the data of Seki and Chihara[4] allow the evaluation of the standard entropy at 323.15 and 343.15°K. Heat capacity and heat of transition data are available, but these only extend down to 85°K. and have an accuracy of only a few per cent.[5-7]

(1) O. Schnepp and D. S. McClure, *J. Chem. Phys.*, **26**, 83 (1957).

(2) O. Schnepp, *ibid.*, **30**, 48 (1959).

(3) M. A. Kovner and A. M. Bogomolov, *Fiz. Sb. L'vovsk. Gos. Univ.*, **3**, 84 (1957).

(4) S. Seki and H. Chihara, *Collected Papers Fac. Sci. Osaka Univ., Ser. C, Chem.*, **11**, 1 (1950).

(5) H. M. Huffman, G. S. Parks, and A. C. Daniels, *J. Am. Chem. Soc.*, **52**, 1547 (1930).

Experimental

The sample consisted of 37.112 g. (*in vacuo*) of hexamethylbenzene which was purified in this laboratory by zone melting and was subsequently found to contain less than 0.1 mole % impurity. The purification by zone melting and determination of the melting point and purity from the freezing point of this substance is described elsewhere.[8] The melting point of the sample was 165.66°, and the theoretical melting point of the pure substance has been calculated to be 165.75°.

Apparatus. The hexamethylbenzene sample was placed inside a gold-plated, copper calorimeter which replaced the gold calorimeter in the adiabatic assembly designated as J(I).[9-11] The present assembly, designated as J(II), is fitted with a gold-plated, stainless steel O-ring to facilitate loading of the sample into a vessel which could be made vacuum-tight without subjecting the sample to excess heat as with soldering methods. The O-rings were found to be vacuum-tight throughout two cycles between room temperature and the λ-point of helium.

A strain-free platinum resistance thermometer designated Pt-G-5 was used for all temperature measurements. The calibration has been described previously.[12] Just prior to this series of measurements the thermometer was checked at the oxygen point against its original calibration.[13] During this series the ice-point resistance was measured and found to be unchanged.

The calorimetric assembly was operated adiabatically in all measurements.

Results

Heat Capacities. The heat capacity of hexamethylbenzene was obtained by subtracting the heat capacity of the calorimeter from the heat capacity of the calorimeter and sample. The results of the measurements are presented on a molar basis in Figure 1, which is a graph of the deviation from the rounded values in Table I. In Table I, column 1 gives the temperature while column 2 gives the molar heat capacities. The approximate rises were: 14–50°K., $\Delta T \approx 2.2°$; 50–100°K., $\Delta T \approx 4.4°$; 130–200°K., $\Delta T \approx 4.7°$; 200–333°K., $\Delta T \approx 11.3°$. The transition region is omitted since this is dealt with in Figure 2. It was found near room temperature that sufficiently adiabatic conditions could be maintained only within 10° of the bath temperature. The heat capacity curves were then drawn through these points in preference to values obtained at the end of a continuous range. The points at temperatures above those at which adiabaticity could be maintained tended to be higher although relatively smooth indicating a systematic error.
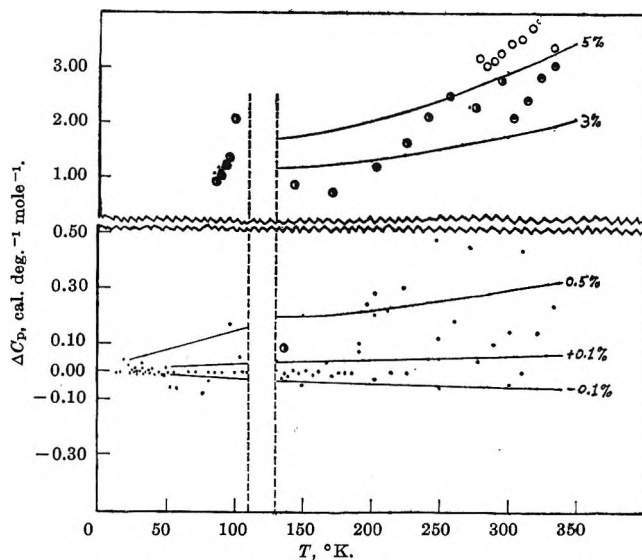
Figure 1. Deviation of the experimental heat capacities: ·, this research; ◑, Huffman, Parkes, and Daniels; ◓, Parkes, Thomas, and Spaght; O, Momotani, Suga, Seki, and Nitta.

Other values obtained from the literature are also plotted as designated in Figure 1.

Huffman and co-workers reported rounded values obtained from points within ±2% from a smooth curve and with an estimated reliability of ±3%. The present results approximate the −3% line of their data.[5,6] The data of Momotani, *et al.*, was taken in an apparatus similar to Huffman's,[7] and it is expected that the long equilibrium times will effect the apparent heat capacities determined by a nonadiabatic method.

Transition. In the present measurements the second-order transition in the heat capacities was observed at a substantially higher temperature than observed previously.[5] This can be attributed to the higher purity of the sample in the present work and perhaps to a difference in the crystal dependent on its purity and history. Parks purified his hexamethylbenzene by recrystallization from ethanol.

Some difficulty was found in reproducing heat capacity points in the region of the solid–solid transition. The results are displayed in Figure 2. In

(6) G. S. Parks, S. B. Thomas, and M. E. Spaght, *J. Phys. Chem.*, 36, 882 (1932).

(7) M. Momotani, H. Suga, S. Seki, and I. Nitta, *Proc. Natl. Acad. Sci. India*, A25, 74 (1956).

(8) J. E. Overberger and J. G. Aston, *Anal. Chem.*, 37, 1167 (1965).

(9) J. G. Aston and G. J. Szasz, *J. Am. Chem. Soc.*, 69, 3108 (1947).

(10) J. A. Morrison and G. J. Szasz, *J. Chem. Phys.*, 16, 280 (1948).

(11) J. G. Aston, H. L. Fink, G. J. Janz, and K. E. Russell, *J. Am. Chem. Soc.*, 73, 1939 (1951).

(12) D. M. Nace and J. G. Aston, *ibid.*, 79, 3627 (1957).

(13) P. Mitacek, Jr., and J. G. Aston, *ibid.*, 85, 137 (1963).

Table I: Molar Heat Capacities at Rounded T^a

T	C_p, cal.	T	C_p, cal.
14	1.712	125	38.73
15	1.872	130	39.47
16	2.044	135	39.96
18	2.489	140	40.30
20	3.035	145	40.63
25	4.595	150	40.92
30	6.267	160	41.37
35	7.949	170	41.92
40	9.696	180	42.65
45	11.48	190	43.55
50	13.27	200	44.58
55	15.06	210	45.73
60	16.77	220	46.95
65	18.38	230	48.23
70	19.88	240	49.56
75	21.36	250	50.99
80	22.76	260	52.51
85	24.18	270	54.06
90	25.67	280	55.67
95	27.19	290	57.32
100	28.78	300	59.03
105	30.45	310	60.80
110	32.21	320	62.64
115	34.18	330	64.53
116.48	(transition)	335	65.46
		340	66.42

^{a} Rounded gram molecular heat capacities of hexamethylbenzene. 0°C. = 273.15°K.; 1 cal. = 4.1833 international joules; molecular weight = 162.276.

Figure 2. Molar heat capacity of hexamethylbenzene in the transition region.

Series I the sample was slowly cooled to liquid nitrogen temperatures while maintaining a dynamic vacuum of 10^{-6} mm. in the cryostat can. Before the measurements of Series I were taken, the sample was slowly heated with the calorimeter heater to a temperature just below the transition temperature. The times required to reach equilibrium were approximately 1 hr. just before the transition, approximately 2.5 hr. within the transition, and approximately 1 hr. just after the transition. The necessity of adhering to a slow cooling through the transition became apparent when reproduction of the data was attempted. In Series II an attempt was made to resume heat-capacity determinations at some point above the transition. In cooling, the transition region was passed. The sample was heated immediately to a temperature above the transition, and then drift-free heat capacities were observed. After completion of Series II, the sample was maintained at approximately 129°K. for 10 hr. It was then slowly cooled to 118°K. The points then observed in Series III showed that supercooling was possible and that this probably accounted for the

spurious results near the transition temperature. Above the transition, times to reach equilibrium increased and at the highest temperatures were over 3 hr. for each heat capacity point.

Table II gives the heats of transition observed for 0.22896 mole of hexamethylbenzene. Numbers 1, 2, 4, and 5 were observed after slow cooling through the transition. Number 3 was observed after rapid cooling following number 2. Since the heat capacity curve changes slope rather drastically after the transition, equations for the heat capacities in the region immediately before (C') and after (C'') the transition were required for extrapolation into the transition region. These are given in footnote b of Table II.

C' was integrated between the initial temperature and the midpoint of the transition and C'' was integrated between the midpoint and the final temperature for each heat of transition determination, and the sum of the two integrations was subtracted from the total heat input to obtain a value of ΔH due to causes other than normal heat capacity. The standard deviation is rather large for a measurement of this type and is probably due largely to the same effects which made normal heat capacity measurements difficult to reproduce in this area of the curve.

Table II: Heat of Transition at 116.48°K.[a]

Temp. interval, °K.	Heat input, cal.	$\int_{T_1}^{116.48} C' dT +$ $\int_{116.48}^{T_2} C'' dT$[b]	ΔH, cal./ 0.22896 mole
(1) 104.555–127.068	628.016	567.789	60.221
(2) 108.503–129.989	618.702	555.740	62.962
(3) 105.341–127.900	617.230	572.380	45.850[c]
(4) 112.989–128.661	473.523	411.017	62.506
(5) 107.443–127.073	561.234	500.862	60.372
			Av. 61.515

$$\Delta H(\text{trans.}) = 268.7 \pm 5.4 \text{ cal./mole}$$

[a] 0°C. = 273.15°K.; molecular weight = 162.76. [b] Includes calorimeter: $C' = 0.24800T - 0.27247 \times 10^{-3}T^2$; $C'' = 0.29922T - 0.66910 \times 10^{-3}T^2$. [c] Not included in average.

The value of ΔH thus deduced represents the heat of transition. If all the transition were to occur at 116.48°K., it corresponds to an entropy of transition of 268.7/116.48 = 2.307 e.u. The entropy which the compound gains during the real transition is obtained as the difference between the area under the curves of C_p vs. ln T extrapolated from above and below 116.48 and the area under the heat capacity curve C_p vs. ln T corresponding to the solid line in Figure 2. The two highest points were taken consecutively. The value thus obtained is 2.410 e.u. The calculation can readily be performed by short extrapolations of the data in Table I and the data in Figure 2 together with the upper three heat capacity values at 116.31, 116.67, and 117.01°K. which are 252.0, 245.5, and 93.77 cal./mole and not given to sufficient accuracy in Figure 2. The fact that the entropy calculated by the latter (proper method) is higher merely indicates that the hypothetical isothermal transition is unstable with respect to the real transition. The latter method of calculation must be used for entropy calculations of the solid.

Huffman and co-workers observed a bump in the heat capacity curve at 151°K. No deviation from a smooth curve was observed in the present results. While their results may have been due to impurity, it is doubtful that the 0.1% impurity in our sample could markedly affect the calorimetric behavior.

Derived Heat of Vaporization and Vapor Pressure. To evaluate the entropy, values of the heat of sublimation and vapor pressures are required. Vapor pressure data have been obtained from 306.45 to 343.15°K. by Seki and Chihara by an effusion method.[4] It is possible to test the consistency of these data making use of heat capacity equations for the solid and for the

gas in this region. The necessary equation for the solid was derived from our experimental data by least squares using the IBM 7074. It is, for T between 270 and 350°K.

$$C_s = 41.651 + 0.35954 \times 10^{-3}T + 0.19977 \times 10^{-6}T^2 + 0.63493 \times 10^{-6}T^3 \quad (1)$$

The average barrier for internal rotation of the six methyl groups in the gas was taken as 9000 cal. as a preliminary value although this is 1130 cal. higher than the highest value later estimated. Other uncertainties did not justify recalculation. Then, using these values, the heat capacities of the ideal gas were calculated at integral temperature increments over the same temperature range. An equation for these was derived by least squares. It is

$$C_g = 43.155 + 0.62615 \times 10^{-3}T + 0.29257 \times 10^{-6}T^2 + 0.45104 \times 10^{-6}T^3 \quad (2)$$

Equations 1 and 2 combined with the Clausius–Clapeyron equation yield the following equation for the vapor pressure

$$\log P(\text{mm.}) = 8.262196 - \frac{3882.51}{T} + 0.756855 \log T + 0.0291336 \times 10^{-3}T + 0.00338022 \times 10^{-6}T^2 - 0.003349077 \times 10^{-6}T^3 \quad (3)$$

The heat of sublimation is given by

$$\Delta H_T = 17,765 + 1.504T + 0.133305 \times 10^{-3}T^2 + 0.03093 \times 10^{-6}T^3 - 0.04597 \times 10^{-6}T^4 \quad (4)$$

In deriving eq. 3 and 4 the following expression, referred to as Σ, was plotted against $1/T$ using the vapor pressure data of Seki and Chihara.

$$\Sigma = 4.575638 \log P(\text{mm.}) - 3.46395 \log T - 0.133305 \times 10^{-3}T - 0.01546667 \times 10^{-6}T^2 + 0.01532417 \times 10^{-6}T^3 = -\frac{\Delta H_0}{T} + I \quad (5)$$

The best straight line was drawn through the five points at higher T with the slope of the upper three. This choice was made because the upper three values were completely consistent with the equations while the lower ones showed a trend indicating development of a systematic error. The value of ΔH is thus based on the upper three points alone.

Table III compares the experimental values of the vapor pressure with those calculated using eq. 3.

The Derived Calorimetric Entropy. Table IVA summarizes the calculation of the entropy of the crystal

Table III: Comparison of Calculated and Experimental Vapor Pressures

T	$P_{obsd} \times 10^3$ mm.	$P_{calcd} \times 10^3$ mm.	P_{obsd}/P_{calcd}
306.45	1.8815	2.4415	0.771
313.15	4.1562	4.5664	0.910
317.45	6.6436	6.7273	0.988
328.25	17.885	16.992	1.053
338.25	40.23	37.927	1.061
343.15	57.943	55.211	1.049

at 323.15 and 343.15°K., respectively. The values of the integrals above 15°K. were obtained by tabular integration from Table I. Corrections for curvature are negligible. Estimates of uncertainties can readily be made from Figure 1. The value of ΔS for the transition has already been discussed. In view of the obviously complicated nature of any Debye treatment for the solid, use was made of the relation valid at low temperatures.

$$S_T = \left(\frac{C_V}{3}\right)_T \approx \left(\frac{C_p}{3}\right)_T \tag{6}$$

Part B of Table IV summarizes the calculation of the entropy of the hypothetical ideal gas at 1 atm. at the same two temperatures.

Spectroscopic Assignment. The frequencies used in the calculation of the standard entropy of the gas were taken from the work of Kovner and Bogomolov.[3] These are listed in Table V where ω' refers to frequencies peculiar to the ring alone, ω'' refers to those of the ring and the methyl groups (considered as point masses) together, ν refers to hydrogen stretch, δ to hydrogen bend, γ to methyl rocking in and out of plane, and Γ to hindered rotation. Assuming S_6 symmetry, all modes are either infrared or Raman active. Actually, of the 17 different frequencies below 1000 cm.$^{-1}$, *i.e.*, those contributing appreciably to the entropy, seven have been observed in the infrared and Raman. For thermodynamic calculations, the observed frequencies were used in preference to calculated values, which for the most part were slightly lower than those observed for frequencies below 1000 cm.$^{-1}$. Since the low-lying frequencies are more important for thermodynamic calculations, it is reasonable that their contribution to the standard entropy will be too high because calculated values had, of necessity, to be used for the unobserved frequencies. In order to estimate the extremes of the internal contribution to the entropy, the Einstein functions were summed using only calculated frequencies and again using as many observed frequencies as possible. At 343.15°K.

Table IV[a]

A. The experimental molar entropy of solid hexamethylbenzene at 323.15 and 343.15°K.

	323.15°K.	343.15°K.
0–15.00°K., $C_{15}/3$	0.624	0.624
15.00–115.72°K., graphical $\int C_p$ d ln T	25.742	25.742
115.72–116.48°K., graphical $\int C_p$	0.804	0.804
Transition, graphical as discussed	2.410	2.410
126.48–124.95°K., graphical $\int C_p$ d ln T	2.347	2.347
114.95–323.15°K., graphical $\int C_p$ d ln T	44.644	44.644
$S_{323.15} - S_0$	76.571 e.u.	
323.15–343.15°K., graphical $\int C_p$ d ln T		3.907
$S_{343.15} - S_0$		80.478 e.u.

B. The experimental molar entropy of hexamethylbenzene vapor at 323.15 and 343.15°K.

	323.15°K.	343.15°K.
$S_{T°K} - S_{0°K}$ (solid)	76.571	80.478
$\Delta H_T/T$ (sublimation)	54.974	51.467
$-R \ln 760/p$ (compression)	−22.086	−18.842
$S_{T°K} - S_{0°K}$ (gas)	109.459 e.u.	113.103 e.u

$p = 11.322 \times 10^{-3}$ at 323.15°K., $p = 57.943 \times 10^{-3}$ at 343.15°K.

C. The molar entropy of hexamethylbenzene vapor from spectroscopic and molecular data at 323.15 and 343.15°K. ($ABC = 0.11579 \times 10^{-110}$ g.^{3} cm.^{6})

	323.15°K.	343.15°K.
$S_{rot} + S_{trans}$ ($\sigma = 6$)	69.066	69.543
S_{vib}	32.960	35.532
$S_{int\ rot}$ ($V_0 = 7870$ cal. mole^{-1})	7.444	8.028
	109.470	113.103

[a] Molecular weight = 162.276; 1 cal. = 4.1833 international joules; 0°C. = 273.15°K.

the contribution to the entropy from the internal modes amounted to 43.56 e.u. for the former and 43.02 e.u. for the latter, or a difference of 0.54 e.u. Since most of this difference is due to the seven observed frequencies below 1000 cm.$^{-1}$, it is reasonable that the spectroscopic entropies as given in Table IV could be as much as 1 e.u. lower, but not higher.

Barrier. The frequency for the hindered rotation was taken as 362 cm.$^{-1}$ as calculated from the relationship

$$\nu_0 = \frac{n}{2\pi}\sqrt{\frac{V_0}{2I_{red}}} \tag{7}$$

Table V: Frequency Assignment for Hexamethylbenzene on the Basis of S_6 Symmetry[a]

	A_g p ia	B_u v M_s	E_g dp ia	E_u v M ⊥
ω'	(508)	167, 552, 1542	(229), 1454	124, (792)
ω''	171, (550), (1298)	187, 707, 1333	(343), (450), (1385)	241, 538, (1050)
ν	(2918), 2976, (2985)	2900, 2976, (2985)	(2918), (2985), (2985)	2900, 2976, 2976
γ	(992), 1037	959, 1042	961, 1011, 1095	1028
δ	(1365), (1465), 1464	(1373), (1430), 1470	1470, (1583)	(1373), (1430), (1456), 1480
Γ	362, 362		362	362

[a] Values in parentheses are observed frequencies.

n was taken as 3,[14] V_0 as 7870 cal., and I_{red} as 5.29 × 10^{-40} g. cm.^{2} as calculated from the following bond lengths: $(C-C)_{ar}$ = 1.40 Å., $C_{ar}-C_{al}$ = 1.53 Å., and C-H = 1.09 Å.[15] Atomic weights of 12.011 and 1.008 for carbon and hydrogen, respectively, give a molecular weight of 162.276.

For 1,2,3-trimethylbenzene two barriers of 2100 cal. and one of 750 were assigned[16a]; however, the measured third-law entropy[16b] indicates a considerably higher average value. Pitzer and Scott[17] assign a barrier of 2000 cal. hindering rotation in o-xylene,[14] which has since been raised to 2100 cal.[16a]

It is reasonable then to assume that in hexamethylbenzene with each methyl group doubly hindered and not having the freedom in the plane of the ring that the partially substituted polymethylbenzenes have, that the barrier will be much higher than 2.1 kcal.

Discussion. The values for the entropy of the ideal gas at 1 atm. calculated from the experimental data in Table IVB at 323.15 and 343.15°K. are based on the three vapor pressure points at the higher temperatures. Table IVC summarizes the calculation of the entropy of the ideal gas at the same two temperatures assuming a symmetry number of 6 and an average barrier of 7870 cal. mole^{-1} for the internal rotation of the six methyl groups, chosen to obtain a reasonable agreement with the experimental values.

In order to estimate the possible error in the experimental entropies of the ideal gas introduced by our interpretation of the vapor pressure data, a recalculation was made considering all the vapor pressure points.

Table VI summarizes a calculation of the entropy at 303.15, 313.15, 323.15, and 343.15°K. using equations for log P and ΔH obtained by giving equal weight to all of the vapor pressure data of Seki and Chiara.

The differences in the entropy, at 323.15 and 343.15°K., between the two tables probably indicate the maximum error possible in Table IV.

Assuming a symmetry number of 6, the average

Table VI: Entropy Comparison Using Heats of Sublimation and Pressures Derived from a Least-Squares Analysis of All Vapor Pressure Points[a]

T	S (solid)	Sublimation	Compression	S_{exptl}	S_{calcd}
303.15	72.647	64.889	−26.619	110.917	110.753
313.15	74.613	62.695	−24.548	112.760	112.639
323.15	76.571	60.622	−22.609	114.584	114.513
343.15	80.478	56.783	−19.086	118.175	118.225

[a] Units: °K., cal., mole.

barrier to obtain satisfactory agreement with experiment is then 2985 cal./mole for the six internal rotational modes.

It is evident that the vapor pressure data are such that only the upper and lower limits of 7870 and 2985 cal./mole^{-1} can be placed on the estimated barrier. Any possible errors in the solid heat capacities are negligible compared to the uncertainty in the vapor pressure equation.

A series of vapor pressure measurements by the transpiration method are being carried out in this laboratory which, it is hoped, will largely remove this uncertainty in the limits of the barrier thus estimated.

(14) K. S. Pitzer and D. W. Scott, *J. Am. Chem. Soc.*, **65**, 803 (1943).

(15) "Tables of Interatomic Distances and Configuration of Molecules and Ions," Special Publication No. 11, The Chemical Society, London, 1958.

(16) (a) W. J. Taylor, D. C. Wagman, M. G. Williams, K. S. Pitzer, and F. D. Rossini, National Bureau of Standards, Research Paper RP-1732, No. 37, Aug. 1946, p. 95; (b) R. D. Taylor, B. H. Johnson, and J. E. Kilpatrick, *J. Chem. Phys.*, **23**, 1225 (1955).

(17) K. S. Pitzer and D. W. Scott, *J. Am. Chem. Soc.*, **65**, 803 (1943).

refrigerants and maintenance of facilities as well as Mr. J. E. Overberger for the preparation of the pure

sample of hexamethylbenzene and Mr. William James for the several computer programs employed.

The Effect of D_2O on the Thermal Stability of Proteins. Thermodynamic

Parameters for the Transfer of Model Compounds from H_2O to D_2O[1,2]

by Gordon C. Kresheck,[3] Henry Schneider, and Harold A. Scheraga

Department of Chemistry, Cornell University, Ithaca, New York (*Received April 19, 1965*)

Solubility data have been obtained for propane, butane, and several amino acids in H_2O and D_2O. The solubility of the hydrocarbons was measured as a function of temperature in order to determine enthalpies and entropies of transfer from H_2O to D_2O, whereas enthalpies of transfer were obtained calorimetrically at 25° for the amino acids and also for several alcohols. Thermodynamic parameters for the transfer of the nonpolar portions of the amino acids and alcohols were computed on the basis of the assumption that the contributions of the polar and nonpolar portions are additive. The enthalpy of transfer was negative for the hydrocarbons as well as for the hydrocarbon portions of the amino acids and alcohols; the entropy of transfer was negative for the two former classes of compounds. The free energy of transfer was negative (but became less negative with increasing temperature) for hydrocarbons and positive for the nonpolar portions of the amino acids at 25°. Assuming that the behavior of the amino acids most closely reflects the situation which exists in proteins even though the free amino acids contain charged α-amino and α-carboxyl groups, it is predicted that hydrophobic bonds between protiated amino acid side chains will be stronger in D_2O than in H_2O. This prediction was confirmed by experiments on detergent micelles, in which it was found that the critical micelle concentration is lower in D_2O than in H_2O.

Introduction

The substitution of D_2O for H_2O has been found to affect the thermal transition curves of poly-γ-benzyl-L-glutamate,[4] ribonuclease,[5] phycocyanin,[6] and gelatin,[7] but not that of DNA,[8] and to alter the rate of modification of ovalbumin by urea,[9] and of the thermal inactivation of catalase.[10] It is not possible to state, on an *a priori* basis, whether the effects observed with these macromolecules are due to a difference in hydrogen bond strength, when deuterium is substituted for hydrogen, or to a possible difference in hydrophobic bond strength when protiated nonpolar groups having

nonexchangeable hydrogens are placed in D_2O, on the one hand, and in H_2O on the other. It appears that

the O–D⋯O bond is stronger than the O–H⋯O bond in D_2O and H_2O, respectively[11]; further work on the relative strengths of such bonds is in progress in our laboratory. However, since there is no information available on the effect of D–H substitution on hydrophobic bond strength, this study was carried out in order to obtain thermodynamic parameters for the transfer, from H_2O to D_2O, of nonpolar model compounds and of polar compounds bearing nonpolar groups. Specifically, the solubilities, in H_2O and in D_2O, of hydrogen-containing propane and butane (at several temperatures) and of various amino acids at 25° were determined. In addition, enthalpies of transfer of amino acids and alcohols from H_2O to D_2O were measured in a calorimeter. Also, the critical micelle concentration (c.m.c.) of a detergent was measured in the same two solvents. The resulting data provide information about the relative strengths of hydrophobic bonds between protiated nonpolar groups in H_2O and D_2O, respectively.

A theoretical treatment of the relative strengths of hydrophobic bonds in H_2O and D_2O is in progress.[12] The theoretical work is based on previous treatments of the structure of liquid[13] H_2O, liquid[11] D_2O, solutions of protiated hydrocarbons[14] in H_2O, and hydrophobic bond strengths between protiated nonpolar groups[15] in H_2O.

Experimental

A. *Materials.* Propane and butane were purchased from The Matheson Company, East Rutherford, N. J., and were 99.92 and 99.94 mole %, respectively, by the manufacturer's analysis. The amino acids used were a chromatographically pure grade (Mann Research Laboratories). Carefully dried and distilled methanol[16] and ethanol[16] containing less than 0.1% water were provided by Mr. M. E. Friedman[17] of this laboratory. All other alcohols were either reagent or spectral grade. Laboratory distilled water was deionized prior to use and 99.7% D_2O (acquired from the U. S. Atomic Energy Commission, Chemical Processes Branch, Savannah River Branch, Aiken, S. C.) was bottled by the Cornell University Department of Chemistry.

Dodecylpyridinium bromide (DPB) was obtained from K & K Laboratories, Inc., Plainview, N. Y.; it was used to prepare dodecylpyridinium iodide (DPI) by crystallization twice from saturated aqueous KI solutions and twice from distilled water.

B. *Solubility of the Hydrocarbons.* To determine the solubility of propane and butane a known quantity of the hydrocarbon gas was introduced from a gas buret into a calibrated volume which contained a

weighed quantity of water and then stirred until equilibrium was attained (3 to 4 hr.). The amount of hydrocarbon in solution was taken to be equal to the difference between the amount introduced into the reaction vessel and the amount remaining in the vapor phase. The amount in the vapor phase at equilibrium was determined from the partial pressure of the hydrocarbon and the volume of the vapor space in the reaction vessel, this latter quantity being computed from the volume of the liquid used in the experiment and that of the reaction vessel when empty. The density of 99.7% D_2O at the various temperatures employed was computed with the formula given by Kirshenbaum,[18] using the density data of Steckel and Szapiro[19] for 100% D_2O, and literature values[20] for that of H_2O. In computing the number of moles of gas introduced into the apparatus and that in the vapor phase at equilibrium, small deviations from ideality (less than 3%) were accounted for using the compressibility factor data of Silberberg, et al.[21] Application of this correction consists of computing the number of moles in the volume of interest using the ideal gas law and then dividing this quantity by the compressibility factor for the appropriate temperature and pressure.

The procedure usually followed was to measure first the solubility at the lowest temperature of interest and then at increasingly higher temperatures using the material already in the apparatus. At 4° the partial pressures employed were about 0.5 and 0.7 atm. and at 50°, 1.2 and 1.6 atm. for propane and butane, re-

(6) D. S. Berns, *Biochemistry*, **2**, 1377 (1963).

(7) W. F. Harrington and P. H. von Hippel, *Arch. Biochem. Biophys.*, **92**, 100 (1961).

(8) H. L. Crespi and J. J. Katz, *J. Mol. Biol.*, **4**, 65 (1962).

(9) R. H. Maybury and J. J. Katz, *Nature*, **177**, 629 (1956).

(10) W. R. Guild and R. P. van Tubergen, *Science*, **125**, 939 (1957).

(11) G. Némethy and H. A. Scheraga, *J. Chem. Phys.*, **41**, 680 (1964).

(12) G. Némethy and H. A. Scheraga, work in progress.

(13) G. Némethy and H. A. Scheraga, *J. Chem. Phys.*, **36**, 3382 (1962).

(14) G. Némethy and H. A. Scheraga, *ibid.*, **36**, 3401 (1962).

(15) G. Némethy and H. A. Scheraga, *J. Phys. Chem.*, **66**, 1773 (1962); **67**, 2888 (1963).

(16) A. I. Vogel, "Practical Organic Chemistry," Longmans, Green and Co., New York, N. Y., 1951, Method I, p. 166.

(17) See M. E. Friedman and H. A. Scheraga, *J. Phys. Chem.*, to be published, for details of purification.

(18) I. Kirshenbaum, "Physical Properties and Analysis of Heavy Water," National Nuclear Energy Series, Manhattan Project Technical Section, Division III-Volume 4A, McGraw-Hill Book Co., Inc., New York, N. Y., 1951.

(19) F. Steckel and S. Szapiro, *Trans. Faraday Soc.*, **59**, 331 (1963).

(20) "Handbook of Chemistry and Physics," 42nd Ed., The Chemical Rubber Company, Cleveland, Ohio, 1960–1961.

(21) I. H. Silberberg, P. K. Kuo, and J. J. McKetta, Jr., *Petrol. Engr.*, **24**, C9 (1954).

spectively. All solubility data are reported normalized to a partial pressure of hydrocarbon of 1 atm. The deviation from the mean of the solubility values obtained in duplicate experiments was less than ±0.5% in most instances.

The apparatus employed for the solubility measurements was designed for this purpose and also to study the adsorption of hydrocarbon gases at a water-polystyrene interface. One of its features was that all joints and stopcocks associated with the vessel in which the gas and liquid were equilibrated were grease-free. Details concerning its construction are provided elsewhere.[22]

C. Solubility of the Amino Acids. The solubility of the amino acids was determined gravimetrically. The procedure employed consisted of shaking an excess of the solid amino acid with solvent at 25 ± 0.1° in sealed test tubes for a minimum of 24 hr., filtering, and then weighing a 4-ml. aliquot of solution, removing the solvent, and finally weighing the residue. The solvent was removed in two steps; in the first, the major portion was removed by evaporation at 70° and in the second, the samples were heated to constant weight at 110°.

D. Calorimetry. Enthalpies of transfer of the amino acids and alcohols were determined with the aid of an adiabatic solution calorimeter modeled after the one recently described by Benjamin.[23] They were evaluated either from the difference in the integral heats of solution of solid solute in H_2O and in D_2O in the dilute solution range or from the difference in the heat of dilution of a small quantity of a dilute H_2O solution of solute with relatively large amounts of H_2O or D_2O (about 3 ml. of a 0.8% solution diluted with 40 ml. of water).

The heat changes in all processes measured calorimetrically were determined from the measured temperature change, the known heat capacity of the calorimeter vessel, the heat capacity of the solvent, and the heat associated with opening the sample cell. The effect of the solutes on the total heat capacity of the solutions was estimated since such low concentrations were used that the resulting errors are outside the limits of our experimental precision, ±0.1%, which is comparable to that found by Benjamin.[23] Measurements were not corrected for small deviations from 25.00°, normally ±0.05°, and are expressed in terms of the defined calorie (4.184 absolute joules). Solid samples were dried *in vacuo* over P_2O_5 for a minimum of 24 hr. prior to use, and liquid samples were stored in sealed bottles in a desiccator over $CaCl_2$. Weights were corrected to vacuum.

The integral heat of solution, ΔH_s, and the enthalpy

of transfer, ΔH_t, measured by the direct solution technique, were calculated from the measured heat change upon solution, q, the weight of solute, g, and the molecular weight, M, of the solute, with the aid of the equations

$$\Delta H_s = \frac{qM}{g} \quad (1)$$

and

$$\Delta H_t = (\Delta H_s)_{D_2O} - (\Delta H_s)_{H_2O} \quad (2)$$

The ΔH_t values, obtained from the dilution experiments were calculated by means of the equation

$$\Delta H_t = \frac{q_t M}{g} \quad (3)$$

where q_t is the heat change accompanying the transfer of solute from H_2O to D_2O and is represented by

$$q_t = q_{mix} - q_{H_2O} - q_{dil} \quad (4)$$

The term q_{mix} represents the heat of dilution of the H_2O solution of solute with D_2O, q_{H_2O} is the heat associated with the mixing of an equal amount of solute-free H_2O with D_2O, and q_{dil} is the heat of dilution of the H_2O–solute solution with H_2O. Since the weights of H_2O and D_2O used in the experiments with solutes were not always the same as when H_2O was added to D_2O, q_{H_2O} was corrected for this difference[24] on the basis of the results of Narten.[25]

Enthalpies of transfer, evaluated by the dilution procedure, correspond to the process in which solute molecules in a dilute solution in H_2O are transferred to a more dilute 94% D_2O solution. The values and precision obtained with this procedure were essentially the same as those obtained by the direct solution technique and required fewer determinations for their evaluation. Most measurements were made using the dilution procedure for this reason, and also because it was found to be less sensitive to small amounts of H_2O present in experiments with D_2O, and because it is not subject to difficulties arising from the slow rate of solution of solid samples.

It is considered that the integral heats of transfer, ΔH_t, measured by the two procedures, correspond, to a

(22) H. Schneider, G. C. Kresheck, and H. A. Scheraga, *J. Phys. Chem.*, **69**, 1310 (1965).

(23) L. Benjamin, *Can. J. Chem.*, **41**, 2210 (1963).

(24) In essence, this correction depends on the linearity of the plot of the excess enthalpy of mixing against the mole fraction of D_2O, X_{D_2O}, in the region 0.94 to 1.0 for X_{D_2O}. The ratio of q_{mix} to the weight of H_2O was equal to 1.620 ± 0.003 cal./g., on the basis of the four determinations listed at the bottom of Table VII.

(25) A. Narten, *J. Chem. Phys.*, **41**, 1318 (1964).

good first approximation, to those which would be measured at infinite dilution. Thus, if the properties of the solute in the standard state are taken to be those of the solute in an infinitely dilute solution, ΔH_t may be identified with the corresponding change in the standard partial molal quantity, $\Delta \bar{H}_t^\circ$. The precision of the final values of $\Delta \bar{H}_t^\circ$ is estimated from duplicate determinations to be ±50 cal./mole or less.

E. Detergent Micelles. The detergent DPI was used because a spectral change occurs above the c.m.c. when micelles are formed[26,27]; this provides a simple and sensitive determination of the c.m.c. Mukerjee and Ray[27] have obtained an ultraviolet difference spectrum in the range 280–380 mμ and assumed that the difference spectrum arises from micelle formation. Using this method, we have determined the c.m.c. from the concentration dependence of the absorbance of DPI at 287 mμ in both H_2O and D_2O at 22°. Both 1-cm. and 2-mm. quartz cells were used to cover a wide concentration range. The cells were maintained at constant temperature in a Beckman DU spectrophotometer.

The c.m.c. was also determined by a conductivity method,[28] using an Industrial Instruments, Inc., conductivity bridge, Model RC16B2, and a Fisher low-conductivity type conductivity cell immersed in a water bath at 25°. Measurements were made at 1000 c.p.s.

Results

A. Hydrocarbons. The solubility data obtained in the present study for propane and butane in H_2O (Figure 1) agree favorably with those of Claussen and Polglase[29] and Wishnia[30] but are somewhat higher than those of Morrison and Billet[31] at temperatures below 30° in the case of propane and over the entire temperature interval investigated in the case of butane. The values of Wetlaufer, *et al.*,[32] agree closely with those of Morrison and Billet and are not plotted. The values of McAuliffe[33] are lower than those of all other workers.

The variation of the logarithm of the solubility of the hydrocarbons in H_2O and D_2O as a function of the reciprocal of the absolute temperature is compared in Figure 2. These curves show that the solubility, on a mole fraction basis, is greater in D_2O than in H_2O at low temperature, and that the difference becomes smaller as the temperature increases. At the highest temperatures (45–55°) the values become equal within experimental error.

As indicated in Table I, the solubilities on a molar basis at the lower temperatures are higher in D_2O than in H_2O, and this behavior is analogous to that found when concentrations are expressed in terms of
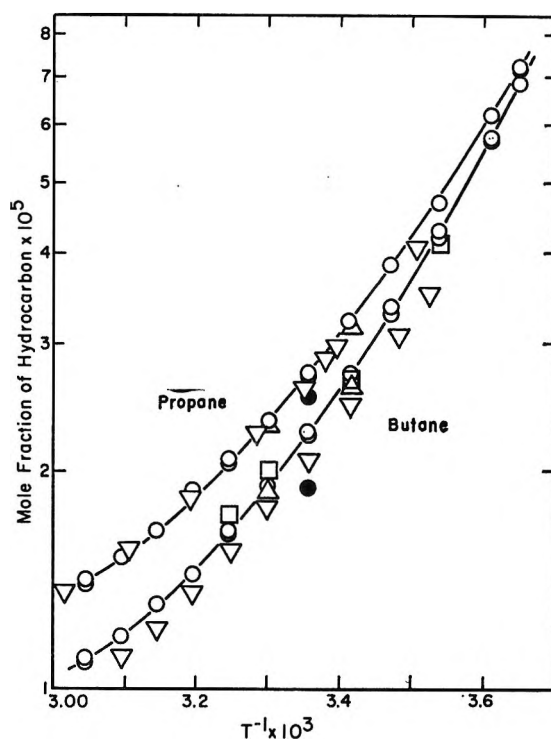
Figure 1. The solubility of propane and butane in H_2O as a function of temperature: O, present study; □, Wishnia[30]; Δ, Claussen and Polglase[29]; ▽, Morrison and Billet[31]; ●, McAuliffe.[33]

mole fractions. However, when concentrations are expressed in terms of molality, the solubility is greater in H_2O than in D_2O. The relationships observed when the concentrations are expressed in mole fraction and molar terms arise because the molar volumes of the two solvents are similar, as indicated in ref. 11. The trends observed on a molality basis result from the ∼10% difference in the molecular weight of D_2O and H_2O.

It is evident that, because the solubilities depend on concentration unit used, the relationships involving the free energy and entropy of transfer will also vary with the particular units employed in computing them.

(26) W. D. Harkins, H. Krizek, and M. L. Corrin, *J. Colloid Sci.*, **6**, 576 (1951).

(27) P. Mukerjee and A. Ray, *J. Phys. Chem.*, **67**, 190 (1963).

(28) J. E. Adderson and H. Taylor, *J. Colloid Sci.*, **19**, 495 (1964).

(29) W. F. Claussen and M. F. Polglase, *J. Am. Chem. Soc.*, **74**, 4817 (1952).

(30) A. Wishnia, *J. Phys. Chem.*, **67**, 2079 (1963). Thanks are due to Dr. Wishnia for sending us the exact values for the butane data shown in this paper.

(31) T. J. Morrison and F. Billet, *J. Chem. Soc.*, 3819 (1952).

(32) D. B. Wetlaufer, S. K. Malik, L. Stoller, and R. L. Coffin, *J. Am. Chem. Soc.*, **86**, 508 (1964).

(33) C. McAuliffe, *Nature*, **200**, 1092 (1963).

Table I: Variation of Solubility Relationships with Concentration Units

Hydro-carbon	Temp., °C.	Mole fraction $\times 10^5$		$M \times 10^3$		$m \times 10^3$	
		H₂O	D₂O	H₂O	D₂O	H₂O	D₂O
Propane	4	6.24 ± 0.02	6.68 ± 0.07	3.46 ± 0.01	3.68 ± 0.03	3.46 ± 0.01	3.33 ± 0.03
	25	2.74 ± 0.01	2.83 ± 0.01	1.53 ± 0.01	1.56 ± 0.01	1.53 ± 0.01	1.41 ± 0.01
	50	1.53 ± 0.01	1.54 ± 0.01	0.84 ± 0.01	0.84 ± 0.00	0.85 ± 0.01	0.76 ± 0.00
Butane	4	5.79 ± 0.01	6.25 ± 0.03	3.21 ± 0.01	3.44 ± 0.02	3.21 ± 0.01	3.12 ± 0.02
	25	2.27 ± 0.01	2.35 ± 0.02	1.26 ± 0.01	1.29 ± 0.01	1.26 ± 0.01	1.17 ± 0.01
	50	1.19 ± 0.01	1.21 ± 0.01	0.66 ± 0.01	0.66 ± 0.01	0.66 ± 0.01	0.63 ± 0.01
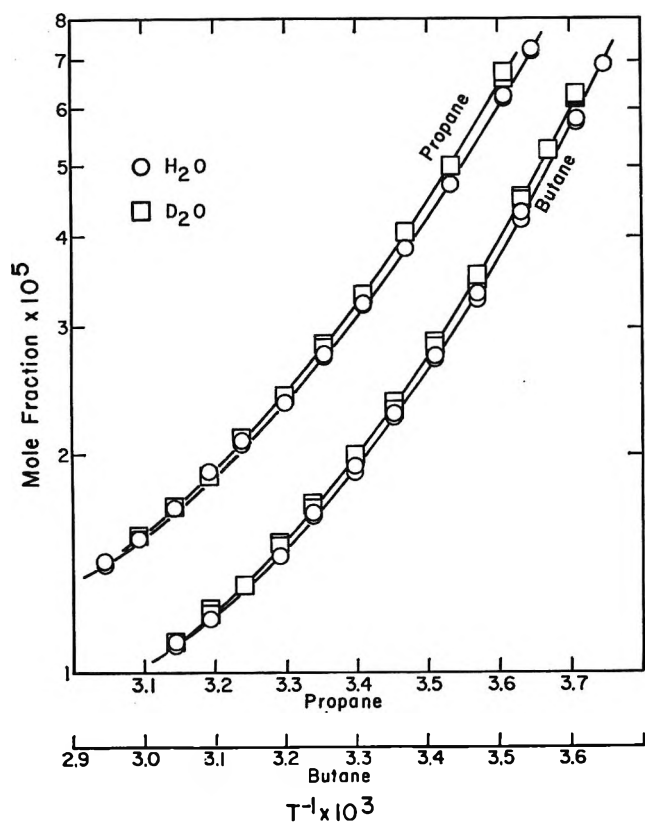
Figure 2. The solubility of propane and butane as a function of temperature in H₂O and in D₂O.

Hence, the thermodynamic parameters for mixing will differ, and this difference will be included in the transfer parameters. Difficulties arising in this way can be eliminated if mole fraction units are employed.[34] Accordingly, the standard free energy of solution was computed using the relation

$$\Delta F^\circ = -RT \ln X_2 \qquad (5)$$

where X_2 represents the mole fraction of dissolved hydrocarbon, choosing the standard state for this species to be mole fraction unity and for the hydrocarbon gas, 1 atm. It can easily be shown that the

free energy change obtained using these units is essentially equal to the unitary free energy change,[35] ΔF_u°, that is, the free energy change resulting only from the interactions of solute and solvent.

The variation in ΔF_u° with temperature could be expressed by the polynomial

$$\Delta F_u^\circ = A + BT + CT^2 + DT^3 \qquad (6)$$

obtained by a least-squares procedure, with a standard error of estimate[36] equal to or less than 0.006 kcal./mole. The values of the coefficients for the various systems are summarized in Table II. The standard enthalpy of solution, the standard unitary entropy of solution, and the corresponding change in the excess partial molal heat capacities may be deduced from eq. 6 as

$$\Delta H^\circ = A - CT^2 - 2DT^3 \qquad (7)$$

$$\Delta S_u^\circ = -B - 2CT - 3DT^2 \qquad (8)$$

$$\Delta C_p = -2CT - 6DT^2 \qquad (9)$$

and their confidence limits may be estimated from the variance and covariance of the coefficients.[36,37] The values of ΔH° and ΔS_u° computed from eq. 7 and 8, together with the 90% confidence limits for several temperatures, are represented in Figures 3 and 4 for propane and butane, respectively. It is evident from these figures that the difference in ΔH° and ΔS_u° for solution in the two solvents is significant only over a limited temperature interval. In the case of propane, the differences are significant at low temperatures but lose their significance somewhere between 25 and

(34) Of course, if concentrations are expressed in units other than mole fractions, conversion of ΔF° to the unitary[35] ΔF_u° corresponds to a conversion from the units used to mole fractions.

(35) W. Kauzmann, Advan. Protein Chem., 14, 1 (1959).

(36) G. W. Snedecor, "Statistical Methods," 4th Ed., Iowa State College Press, Ames, Iowa, 1946, p. 347.

(37) We are indebted to Dr. S. R. Searle, Biometrics Unit, Cornell University, for advice and assistance in the statistical treatment of the solubility data.

Table II: Coefficients of Polynomials of Eq. 6

System	A	B	C	D
Propane–H₂O	−13.84232	8.12266 × 10⁻²	0	−1.56749 × 10⁻⁷
Propane–D₂O	−25.01314	1.87925 × 10⁻¹	−3.41536 × 10⁻⁴	2.09408 × 10⁻⁷
Butane–H₂O	−16.39287	9.32092 × 10⁻²	0	−1.91123 × 10⁻⁷
Butane–D₂O	−38.33623	3.08356 × 10⁻¹	−7.04660 × 10⁻⁴	5.79321 × 10⁻⁷
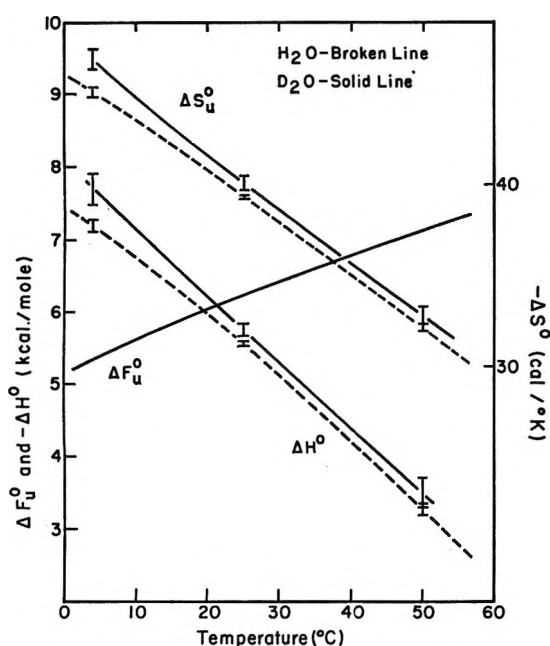
Figure 3. Thermodynamic parameters for the solution of propane in H_2O and in D_2O. The difference between the standard free energy of solution in the two solvents is indistinguishable on the scale employed. The vertical lines represent the 90% confidence limits for the standard enthalpy and entropy of solution. The corresponding limits for the free energy change are less than 10 cal./mole.
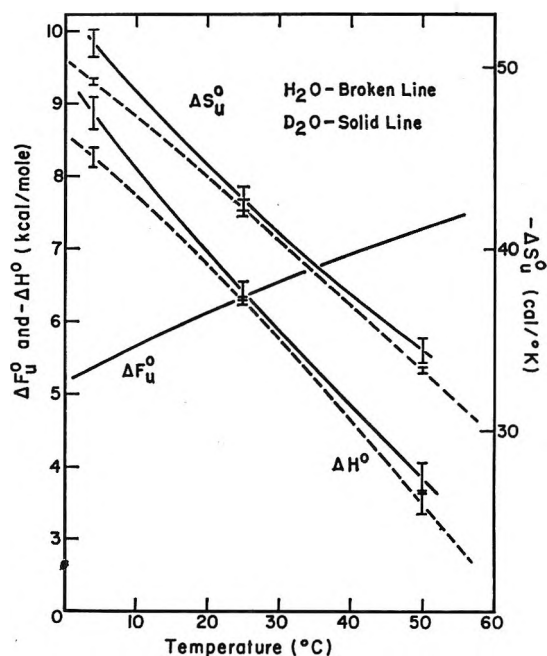
Figure 4. Thermodynamic parameters for the solution of butane in H_2O and in D_2O. The difference between the standard free energy of solution in the two solvents is indistinguishable on the scale employed. The vertical lines represent the 90% confidence limits for the standard enthalpy and entropy of solution. The corresponding limits for the free energy change are less than 10 cal./mole.

50°; in the case of butane the differences are significant only at low temperature.

The ΔC_p data and their 60% confidence limits are shown in Figure 5, and numerical values together with their 90% confidence limits are shown for several temperatures in Table III. In the H_2O systems ΔC_p increases with temperature and also with chain length, and, except for propane at 25° and butane at 4°, the values at 4, 25, and 50° agree with those computed by Némethy and Scheraga,[14,38] which are shown in Table III. In the D_2O system, ΔC_p seems to decrease with temperature but, except for the low temperature region in the case of butane, the differences in ΔC_p for the H_2O and D_2O systems are not significant at the 90% confidence level (Table III). However, the differences are significant over an appreciable temperature range at the 60% confidence level as shown in Figure 5.

The differences between ΔF_u° in the two solvents are small and cannot be seen on the scale employed in Figures 3 and 4, but may be visualized readily from the plot of the free energy of transfer of the hydrocarbons from H_2O to D_2O, ΔF_t°, where

$$\Delta F_t^\circ = (\Delta F_u^\circ)_{D_2O} - (\Delta F_u^\circ)_{H_2O} \qquad (10)$$

Such a plot is shown in Figure 6. The salient feature of these curves is that the transfer process seems to become less favorable as the temperature is raised. Because of experimental error, it is not possible to determine at what temperature, if at all, ΔF_t° becomes equal to zero or positive in sign. Numerical values

(38) The theoretical values for 4° were kindly supplied by Dr. G. Némethy.
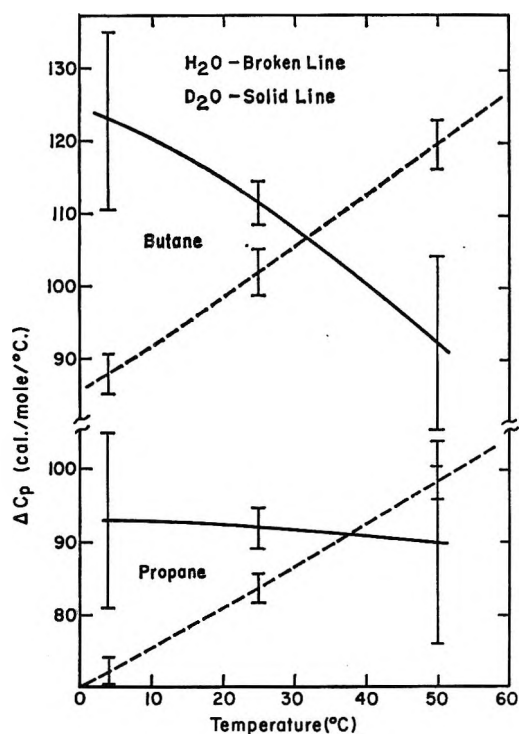
Figure 5. The partial molal excess heat capacity
of propane and butane in H_2O and D_2O. The vertical
lines represent the 60% confidence limits.

Figure 6. Standard free energy of transfer from H_2O to D_2O
of propane and butane. The 90% confidence limits are shown
for butane only; those for propane are comparable in size, and
their numerical values are given in Table IV.

Table III: ΔC_p and Its 90% Confidence Limits as a
Function of Temperature

System	Temp., °C.	ΔC_p, cal./mole deg. Exptl.	Theoret.[14,38]
Propane–H_2O	4	72.3 ± 3.1	70
	25	83.6 ± 3.6	90
	50	98.3 ± 4.2	102
Propane–D_2O	4	92.8 ± 21.4	
	25	91.9 ± 4.7	
	50	89.5 ± 25.1	
Butane–H_2O	4	88.0 ± 4.7	77
	25	101.9 ± 5.4	99
	50	119.7 ± 6.4	115
Butane–D_2O	4	123.6 ± 20.5	
	25	112.2 ± 5.4	
	50	92.4 ± 21.7	

Table IV: Thermodynamic Parameters and Their 90%
Confidence Limits for the Transfer of Propane and Butane
from H_2O to D_2O

Hydro-carbon	Temp., °C.	$-\Delta F_t°$, cal./mole	$-\Delta H_t°$, cal./mole	$-\Delta S_t°$, e.u.
Propane	4	38.4 ± 9.8	531 ± 188	1.78 ± 0.57
	25	14.4 ± 3.2	222 ± 88	0.70 ± 0.33
	50	2.4 ± 10.2	225 ± 194	0.69 ± 0.61
Butane	4	40.2 ± 11.4	619 ± 279	2.09 ± 1.63
	25	17.4 ± 4.4	142 ± 142	0.42 ± 1.65
	50	4.5 ± 11.3	355 ± 238	1.08 ± 1.56

for $\Delta F_t°$ for several temperatures are shown in Table
IV.

Curves representing the variation with temperature
of the enthalpy of transfer, $\Delta H_t°$, are shown in Figure 7.
These have a minimum between 30 and 40° but veri-
fication of its existence is not possible with the present
data because the confidence limits are rather wide.

In any event, it can be seen from Figure 7 and the data
in Table IV that the values of $\Delta H_t°$ at 4° are signifi-
cantly greater at the 90% confidence level than those
at 25 and 50° in the propane system and from the value
at 25° in the butane system.

Curves of $\Delta S_t°$ as a function of temperature can be
shown to have minima similar to those found with
$\Delta H_t°$ but, again, the wide confidence limits preclude
verification of their existence. Values of $\Delta S_t°$ at several
temperatures are given in Table IV.

The fact that both $\Delta H_t°$ and $\Delta S_t°$ are negative sug-
gests that the structural order of the solvent in the hy-
drocarbon solutions is greater in D_2O than in H_2O.
Furthermore, the larger negative values for $\Delta H_t°$ at *lower*
temperatures suggest that the structural order increases
with a decrease in temperature, faster in D_2O than in

Table V : Solubility Data[a] Used for Calculating the Free Energy of Transfer of the Amino Acids from H_2O to D_2O at 25°

Compound	Side chain	X_{H_2O}	X_{D_2O}	$(\Delta F_t°)_u$, cal./mole	$(\Delta F_t°)_{aa} - (\Delta F_t°)_{gly}$, cal./mole
Glycine	H	5.578×10^{-2}	5.889×10^{-2}		
		5.646×10^{-2}	5.881×10^{-2}	-28 ± 4	...
DL-Alanine	CH_3	3.209×10^{-2}	3.360×10^{-2}		
		3.167×10^{-2}	3.289×10^{-2}	-24 ± 3	4 ± 3
DL-α-Aminobutyric acid	CH_2CH_3	3.490×10^{-2}	3.502×10^{-2}		
		3.486×10^{-2}	3.512×10^{-2}	-3 ± 1	25 ± 3
DL-Norvaline	$CH_2CH_2CH_3$	1.292×10^{-2}	1.263×10^{-2}		
		1.289×10^{-2}	1.272×10^{-2}	13 ± 0	41 ± 3
DL-Norleucine	$CH_2CH_2CH_2CH_3$	1.495×10^{-3}	1.463×10^{-3}		
		1.459×10^{-3}	1.428×10^{-3}	13 ± 0	41 ± 3
L-Norleucine	$CH_2CH_2CH_2CH_3$	2.235×10^{-3}	2.195×10^{-3}		
		2.273×10^{-3}	2.220×10^{-3}	13 ± 0	41 ± 3
L-Phenylalanine	$CH_2C_6H_5$	2.873×10^{-3}	2.491×10^{-3}		
		3.000×10^{-3}	2.527×10^{-3}	127 ± 1	155 ± 2

[a] The double entries in the X_{H_2O} and X_{D_2O} columns represent duplicate independent determinations.
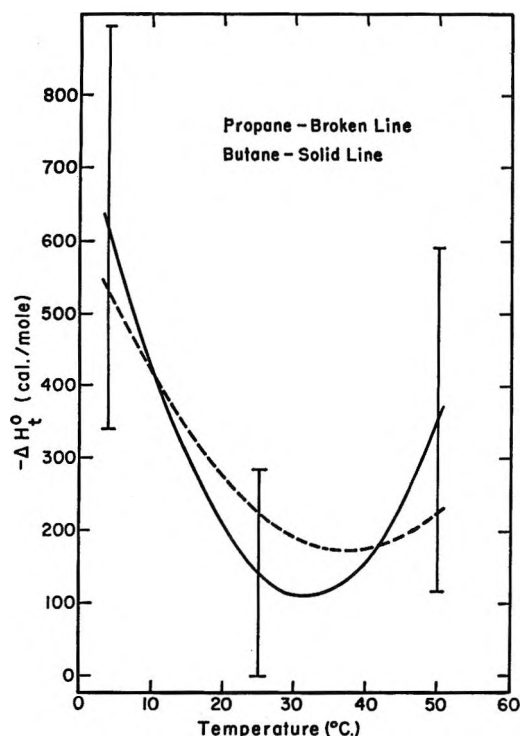
Figure 7. Standard enthalpy of transfer from H_2O to D_2O of propane and butane. The 90% confidence limits are shown for butane only; those for propane are given in Table IV.

H_2O. In this connection, it is of interest to note that the calculated fraction of unbroken hydrogen bonds increases faster,[11] with decreasing temperature, in pure D_2O than in pure H_2O.

B. Amino Acids and Alcohols. The values of the mole fraction, X, of the amino acids at saturation in H_2O and in D_2O at 25° are shown in Table V. Our values for solubility in H_2O agree within a few per cent with those of other workers,[39] with the exception of the data for norvaline for which data are not available for comparison.

The standard free energy of transfer from H_2O to D_2O, $\Delta F_t°$, was computed in terms of the standard unitary free energy of solution. The standard state employed for the solute was a hypothetical solution in which the concentration of solute is mole fraction unity, but in which it has the properties it would possess in an infinitely dilute solution, so that $\gamma_2/X_2 \to 1$ as $X_2 \to 0$, where γ_2 is the activity coefficient of the solute. The chemical potential of the solute in the saturated solution, μ_2, is related to X_2 and the chemical potential of the solid solute, $\mu_2{}^s$, by means of the equation

$$\mu_2{}^s = \mu_2 = \mu_2{}° + RT \ln X_2\gamma_2 \qquad (11)$$

where $\mu_2{}°$ is the chemical potential of the solute in the standard state. The standard unitary free energy of solution, $\Delta F_u{}°$, is given by the expression

$$\Delta F_u{}° = \mu_2{}° - \mu_2{}^s = -RT \ln X_2\gamma_2 \qquad (12)$$

Consequently, for the transfer from H_2O to D_2O

(39) E. J. Cohn and J. T. Edsall, "Proteins, Amino Acids, and Peptides," Reinhold Publishing Corp., New York, N. Y., 1943, p. 199.

Table VI: Integral Heats of Solution for Several Amino Acids and the Related Transfer Values Calculated from the Solution and Dilution Data

Compound	Solvent	Wt. of solute, mg.	Wt. of solvent, g.	q, cal.	ΔH_s, cal./mole	$\Delta \bar{H}_t°$, cal./mole Soln.	Dil.	Average
Glycine	H$_2$O	39.2	40.9529	1.701	3259	-195 ± 74	-184 ± 34	$-190 + 27$
		27.1	40.9788	1.273	3528			
		50.9	39.9336	2.357	3478			
		43.2	40.6130	1.928	3352			
		43.5	40.8231	1.982	3422			
		49.6	41.5999	2.313	3502			
		27.2	41.1264	1.215	3355			
		27.8	40.9100	1.277	3450			
		54.5	40.9155	2.449	3375			
					3413 ± 83^a			
	D$_2$O	34.1	44.8910	1.463	3222			
		50.7	44.3351	2.174	3220			
		43.9	44.8046	1.847	3160			
		52.7	46.8011	2.294	3269			
		43.9	44.9118	1.804	3086			
		42.7	45.0747	1.895	3332			
		33.6	44.9036	1.428	3192			
		39.8	45.7795	1.728	3261			
	94% D$_2$O	46.1	43.3836	1.961	3195			
		38.5	42.9323	1.662	3242			
					3218 ± 65^a			
DL-Alanine	H$_2$O	72.0	39.8013	1.778	2200	-322	-334 ± 19	-328 ± 17
	D$_2$O	70.5	43.9862	1.486	1878			
DL-α-Aminobutyric acid	H$_2$O	54.1	38.9496	0.802	1528	-353	-395 ± 12	-374 ± 21
	D$_2$O	53.0	42.7439	0.604	1175			
L-Norvaline	H$_2$O	49.4	39.8959	-0.231	-548	-406	$-452 + 5$	-429 ± 23
	D$_2$O	56.2	44.0529	-0.458	-954			

^{a} Average value of ΔH_s with standard deviation.

$$\Delta F°_{D_2O} - \Delta F°_{H_2O} = (\mu_2°)_{D_2O} - (\mu_2°)_{H_2O} =$$

$$-RT \ln \frac{(X_2)_{D_2O}}{(X_2)_{H_2O}} - RT \ln \frac{(\gamma_2)_{D_2O}}{(\gamma_2)_{H_2O}} = \Delta F_t° \quad (13)$$

Since the concentrations of amino acids in saturated solutions in H$_2$O and in D$_2$O on a mole fraction basis are similar, and since many of the physical properties of H$_2$O and D$_2$O are similar,[11] it is likely that deviations from ideal behavior in the two solvent systems will be almost identical. Thus, it is reasonable to assume that the activity coefficients in eq. 13 may be considered equal, so that eq. 13 may be written as

$$(\Delta F_t°)_u \approx -RT \ln \frac{(X_2)_{D_2O}}{(X_2)_{H_2O}} \quad (14)$$

Values for $(\Delta F_t°)_u$, together with their standard deviations, computed with eq. 14 are shown in Table V. The contribution of the nonpolar portion to $(\Delta F_t°)_u$ for the various amino acids was obtained by subtracting

the value observed for glycine; these results are given in the last column of Table V. It can be seen that, except possibly for alanine, $(\Delta F_t°)_u$ for the nonpolar side chains is positive. This behavior is opposite to that found with the hydrocarbons.

The results obtained by direct measurement of the integral heat of solution of several amino acids in H$_2$O and D$_2$O, ΔH_s, are presented in Table VI. The values obtained for the partial molal enthalpies of transfer from H$_2$O to D$_2$O, $\Delta \bar{H}_t°$, determined both by direct solution and by the dilution technique, are also given. Details concerning the dilution experiments with the amino acids and also those with the alcohols are presented in Table VII. The average of the $\Delta \bar{H}_t°$ values obtained by the solution and by the dilution techniques are shown in Table VI. It is evident from the data in Table VI that $\Delta \bar{H}_t°$ is negative for the transfer of glycine, and that it becomes more negative with increasing length of the nonpolar side chain. An

Table VII: Summary of the Data Related to the Dilution Experiments for the Enthalpy of Transfer of Various Amino Acids and Alcohols from Dilute H_2O to Dilute D_2O at 25°

Compound	Wt. of solute, mg.	Wt. of H_2O, g.	Wt. of D_2O, g.	q_{mix},[a] cal.	q_{H2O},[a] cal.	$-q_{dil}$,[a] cal.	$-q_t$,[a] cal.	$-\Delta \bar{H}_t°$, cal./mole	Average $-\Delta \bar{H}_t°$, cal./mole
Glycine	56.7	3.0092	44.5236	4.732	4.875	0	0.143	189	184 ± 34
	38.1	3.0038	44.3421	4.787	4.866	0	0.079	156	
	32.2	3.0002	43.9585	4.774	4.860	0	0.086	201	
	55.2	2.9709	44.2637	4.707	4.813	0	0.106	144	
	36.4	2.9968	43.9487	4.779	4.855	0	0.076	157	
	22.7	2.9686	43.1632	4.731	4.809	0	0.078	258	
DL-Alanine	54.7	3.0049	44.2776	4.674	4.868	0	0.194	316	334 ± 19
	27.5	2.9990	44.4375	4.750	4.859	0	0.109	353	
DL-α-Aminobutyric acid	32.6	2.9973	44.1102	4.734	4.855	0	0.121	383	395 ± 12
	46.5	2.9968	44.3042	4.672	4.855	0	0.183	406	
DL-Norvaline	54.2	2.9908	44.3295	4.638	4.845	0	0.207	447	452 ± 5
	26.7	3.0042	44.2970	4.763	4.867	0	0.104	456	
DL-Norleucine	22.7	2.9915	44.1041	4.756	4.846	0	0.090	520	512 ± 7
	27.3	3.0081	44.3152	4.768	4.873	0	0.105	505	
L-Phenylalanine	46.0	3.0045	44.3384	4.788	4.867	0	0.079	284	308 ± 24
	69.2	3.0052	44.2693	4.730	4.869	0	0.139	332	
Methyl alcohol	51.4	2.9960	44.3532	4.448	4.854	0.088	0.318	198	182 ± 16
	26.8	2.9925	44.2990	4.663	4.848	0.046	0.139	166	
Ethyl alcohol	42.6	3.0004	44.3447	4.561	4.861	0.014	0.286	309	311 ± 2
	45.8	3.0056	44.3334	4.543	4.869	0.015	0.311	313	
n-Propyl alcohol	65.3	3.0061	43.9105	4.427	4.870	0.025	0.418	385	383 ± 2
	23.5	3.0090	44.3709	4.717	4.875	0.009	0.149	381	
Isopropyl alcohol	46.0	3.0102	44.2853	4.550	4.877	0.020	0.307	401	405 ± 4
	23.5	3.0008	44.2408	4.691	4.861	0.010	0.160	409	
n-Butyl alcohol	38.8	2.9940	44.4197	4.583	4.850	0.030	0.237	453	469 ± 16
	53.9	3.0090	44.2560	4.480	4.875	0.042	0.353	485	
sec-Butyl alcohol	46.9	3.0094	44.3975	4.584	4.875	0.021	0.270	427	433 ± 6
	30.4	2.9956	44.3653	4.660	4.853	0.013	0.180	439	
t-Butyl alcohol	37.0	3.0024	44.3577	4.632	4.864	0.016	0.216	433	450 ± 17
	44.4	3.0038	44.3367	4.567	4.866	0.019	0.280	467	
n-Pentyl alcohol	33.3	3.0050	44.3597	4.653	4.868	0.027	0.188	498	495 ± 4
	28.2	3.0058	44.3614	4.690	4.870	0.023	0.157	491	
Benzyl alcohol	106.3	3.0062	44.3118	4.572	4.870	0	0.298	303	285 ± 18
	43.4	2.9969	44.3340	4.748	4.855	0	0.107	267	
H_2O	...	3.0005	44.5030	4.874	...	...	...	...	
	...	2.9977	43.9998	4.845	...	...	...	...	
	...	3.0110	44.3338	4.869	...	...	...	...	
	...	3.0008	44.2893	4.864	...	...	...	...	

[a] Definition of symbol given in text.

analogous trend is present in the alcohol series (Table VII). Branching has a small effect on the heat of transfer in the case of both propanol and butanol. The value of -140 cal./mole, obtained by Benjamin and Benson,[40] for the difference between the integral heat of mixing extrapolated to infinite dilution of CH_3OH–H_2O and CH_3OD–D_2O agrees favorably with our value of -182 ± 16 cal./mole (Table VII).

(40) L. Benjamin and G. C. Benson, *J. Phys. Chem.*, **67**, 858 (1963).

An interesting similarity is shown between the influence of the length and configuration of the nonpolar portions of the various alcohols on (i) the partial molal enthalpy of transfer from dilute H_2O to dilute D_2O, $\Delta \bar{H}_t°$, (ii) the heat of solution in H_2O, $\bar{H}$ − $\bar{H}°$,[41] and (iii) the enthalpy of transfer, ΔH_{vap}, from the vapor phase to dilute aqueous solution.[42] These data are compared in Figure 8. An analogous side-chain influence was noted by Lange and Möhring for the heat of dilution of the same alcohols.[43]

The thermodynamic parameters for the transfer of the nonpolar portions of amino acids and alcohols from H_2O to D_2O at 25°, computed on the assumption that the contributions of the polar and nonpolar portions are additive, are summarized in Table VIII. The validity of additivity for computing values for the thermodynamic transfer parameters for model compounds has recently been demonstrated.[22] It has also been shown that the enthalpy and partial molal heat capacity of transfer from water to 6 M urea are essentially the same for an amino acid side chain when it exists as part of an amino acid or as part of a dipeptide.[44] Data for the transfer of hydrocarbons at 25° are also included in Table VIII. It is clear from these results

Figure 8. Comparison of the experimental values obtained in this study for the enthalpy of transfer of various alcohols from H_2O to D_2O with corresponding partial molal enthalpies of solution[41] and enthalpies of vaporization from dilute aqueous solution[42] at 25°. The line is drawn through the experimental points.

Tbale VIII: Thermodynamic Parameters Obtained for the Transfer of Various Nonpolar Groups from a Dilute Solution of H_2O to a Dilute Solution of D_2O at 25°

Group	How obtained	$\Delta F_t°$, cal./mole	$-\Delta \bar{H}_t°$, cal./mole	$-\Delta \bar{S}_t°$, e.u.
Methyl	Ala–Gly	4 ± 3	138 ± 24	0.48 ± 0.06
	EtOH–MeOH		129 ± 11	
	Butane–propane	−3 ± 4	−80 ± 117	−0.28 ± 1.18
Ethyl	α-NH₂Bu–Gly	25 ± 3	184 ± 24	0.70 ± 0.06
	PrOH–MeOH		201 ± 11	
n-Propyl	Norval–Gly	41 ± 3	239 ± 25	0.94 ± 0.06
	BuOH–MeOH		287 ± 16	
	Propane	−14 ± 3	222 ± 88	0.70 ± 0.30
n-Butyl	Norleu–Gly	41 ± 3	322 ± 20	1.22 ± 0.05
	PeOH–MeOH		313 ± 11	
	Butane	−17 ± 4	142 ± 142	0.42 ± 1.65
Phenyl	Phe–Ala	151 ± 2	−20 ± 21	0.44 ± 0.06
	BzOH–MeOH		103 ± 17	

that there is a head group effect on the transfer parameters. The values of $\Delta F_t°$ for the hydrocarbons are negative (about −15 cal./mole), whereas those for the propyl and butyl groups computed from the amino acid solubility data are positive (about 40 cal./mole). It is worth noting that Wetlaufer, et al.,[32] also obtained evidence for a head group effect in a transfer process, in which nonpolar groups were transferred from H_2O to 6.96 M urea. In their experiments, $\Delta F_t°$ de-

termined from solubility data of amino acids was about 50 cal./mole more negative than that obtained from hydrocarbon solubilities. Head group effects have been observed also for the adsorption of the nonpolar portions of carboxylic acids, alcohols, and amino acids at a polystyrene–water interface.[22]

There is an apparent leveling off of the transfer parameters at the third and fourth carbon atom beyond the head group. This is, perhaps, reflected by the same value for $\Delta F_t°$ for propane and butane and for the norvaline and norleucine side chains. Also, the values of $\Delta \bar{H}_t°$ determined for the 1-butanol and 1-pentanol side chains and for propane and butane are not significantly different. On the basis of these results it would be expected that $\Delta \bar{H}_t°$ for the amino acid side chains would begin to level off beyond the butyl group.

A plot of $-\Delta \bar{H}_t°$ as a function of $-\Delta \bar{S}_t°$ for the amino acid series is shown in Figure 9. From this plot there appears to be a linear relationship between these two quantities, within the experimental error. In view of the temperature dependence of the transfer parameters for propane and butane, the slope of this line would be

(41) See ref. 39, p. 182.

(42) J. A. V. Butler, *Trans. Faraday Soc.*, **33**, 229 (1937); R. Aveyard and A. S. C. Lawrence, *ibid.*, **60**, 2265 (1964).

(43) E. Lange and K. Möhring, *Z. Elektrochem.*, **57**, 660 (1953).

(44) G. C. Kresheck and L. Benjamin, *J. Phys. Chem.*, **68**, 2476 (1964).
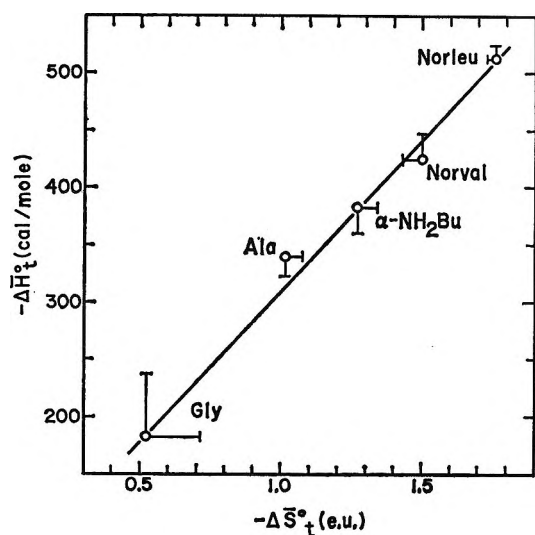
Figure 9. Plot of $-\Delta \bar{H}_t^\circ$ vs. $-\Delta \bar{S}_t^\circ$ for glycine, alanine, α-aminobutyric acid, norvaline, and norleucine at 25°.
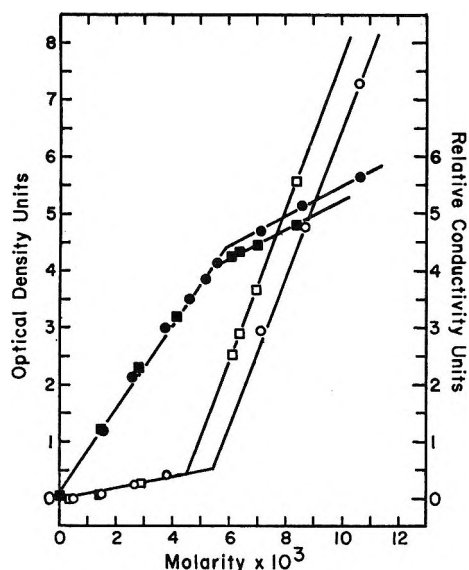
Figure 10. Concentration dependence of optical density at 287 mμ (open symbols) and relative conductivity (filled symbols) of DPI in H_2O (circles) and in D_2O (squares). The breaks in the curves occur at the c.m.c.

expected to depend on temperature. The value of this slope can easily be shown to indicate if ΔF_t° will be positive, as with the amino acids, or negative, as with the hydrocarbons. Linear relationships for other transfers involving water have been found by several groups of workers.[15,41,42,45]

C. *Detergent Micelles.* The c.m.c. of DPI was determined in H_2O and in D_2O by the spectral method at 22°, and by the conductivity method at 25°, the results being shown in Figure 10. The conductivity data

have been corrected by application of Walden's rule.[46] The values of the c.m.c. are shown in Table IX. The plots of specific conductance vs. molarity in Figure 10 were superposable up to the c.m.c. within experimental error. The c.m.c. in H_2O was distinguishably higher. Despite the fact that the values of the c.m.c. differ somewhat according to the method used to determine them, the lower value in D_2O (using a given method) seems to be a real effect. Schick[47] has also observed similar discrepancies in the c.m.c. determined by different methods.

Table IX : Values of C.m.c. for DPI

Solvent	Method	Temp., °C.	C.m.c. m	C.m.c. M
H_2O	Spectral	22	$5.4_2 \times 10^{-3}$	$5.4_0 \times 10^{-3a}$
	Conductivity	25	$6.0_0 \times 10^{-3}$	$5.9_8 \times 10^{-3}$
D_2O	Spectral	22	$4.0_9 \times 10^{-3}$	$4.5_0 \times 10^{-3}$
	Conductivity	25	$4.9_1 \times 10^{-3}$	$5.4_2 \times 10^{-3}$

^{a} This value is in good agreement with those previously reported.[26,27]

Discussion

The negative free energy of transfer of hydrocarbons from H_2O to D_2O indicates that hydrophobic bonds involving these molecules (e.g., their association in aqueous solution) will be stronger in H_2O than in D_2O. The positive free energy of transfer found for the nonpolar side chains of amino acids and for DPI indicates that hydrophobic bonds involving the side chains of these molecules will be stronger in D_2O, in contrast to those involving hydrocarbons. The contrasting behavior between hydrocarbons and the other compounds at 25° suggests that the sign of the free energy of transfer depends on whether or not a polar group is attached to the nonpolar residue. Because of the head group effect, it is difficult to make a straightforward extrapolation from the behavior observed with model compounds to that which obtains in proteins. However, it is reasonable to consider amino acids as more suitable than hydrocarbons as models for protein side chains. On this basis, it may be predicted that hydrophobic bonds involving the protiated nonpolar side chains of proteins will be *slightly* stronger in D_2O than in H_2O. Accordingly, it would be expected that, at 25°, hydrophobic bonds would make a *slightly* larger

(45) E. F. G. Herington, *J. Am. Chem. Soc.*, **73**, 5883 (1951).

(46) S. Glasstone, "An Introduction to Electrochemistry," D. Van Nostrand Co., Inc., New York, N. Y., 1942, pp. 64, 65.

(47) M. J. Schick, *J. Phys. Chem.*, **67**, 1796 (1963).

contribution in maintaining the native structure of a protein[48] in D_2O than in H_2O.

The factors determining the variation with temperature of the stability of protein structures in water have been discussed by Scheraga, *et al.*[49] They concluded that, although hydrophobic bonds become stronger with increasing temperature, proteins denature eventually because of other factors. If the free energy of transfer of nonpolar amino acid side chains were to become more positive with increasing temperature, like that for hydrocarbons, then hydrophobic bonds involving these side chains would become stronger with increasing temperature at a somewhat greater rate in D_2O than in H_2O. An immediate consequence of this would be that proteins would be more stable to thermal modification in D_2O, if all factors remained unchanged, when deuterium was substituted for hydrogen. Interestingly, such an effect has been observed for ribonuclease,[5] gelatin,[7] and catalase.[10] For ribonuclease, the free energy of unfolding was estimated[5] to be 1 kcal./mole more positive in D_2O than in H_2O. The magnitude of this difference is such that it would not take an unreasonable number of hydrophobic bonds between aromatic and the larger nonpolar side chains to account for a good part of it. It cannot be stated, however, with any degree of certainty that the observed behavior[5,7,10] is due *only* to differences in hydrophobic bond strength since intramolecular hydrogen bonds may also be subject to an isotope effect. Without doubt, the observation of Appel and Yang[50] that deuterated helices of poly-L-glutamic acid and poly-L-lysine in D_2O have the same thermal stability as protonated ones in H_2O when changes in optical rotation are plotted against degree of dissociation instead of pH or pD is pertinent.

Finally, it is interesting to cite a paper,[51] appearing at the time of submission of this article, which reported similar results for the transfer of argon from H_2O to D_2O; these results agree with ours for the hydrocarbons.

(48) The choice of amino acids instead of hydrocarbons as model compounds for evaluating *differences* in hydrophobic bond strength between protein side chains in H_2O and D_2O does not invalidate the use of hydrocarbons as model systems for the theory[14,15] of hydrophobic bonding in proteins. This is so because ΔF_t° is small compared to the free energy of formation of hydrophobic bonds; thus, the small magnitude of ΔF_t° falls within the limits of error of the theory of hydrophobic bonding in a *given* solvent (*i.e.*, H_2O or D_2O).

(49) H. A. Scheraga, G. Némethy, and I. Z. Steinberg, *J. Biol. Chem.*, **237**, 2506 (1962).

(50) P. Appel and J. T. Yang, Abstracts, Meeting of the American Society of Biological Chemists, Chicago, Ill., April 1964, p. 216.

(51) A. Ben-Naim, *J. Chem. Phys.*, **42**, 1512 (1965).

Photochemical Rearrangement Reactions of 2-n-Propylcyclopentanone

by R. Srinivasan and Sheldon E. Cremer

IBM Watson Research Center, Yorktown Heights,. New York 10598   (*Received April 19, 1965*)

Photolysis of 2-n-propylcyclopentanone in the vapor phase at about 140° with 3130-Å. radiation gave rise to carbon monoxide, ethylene, propylene, 1-pentene, a C_7 hydrocarbon, cyclopentanone, and *trans*-4-octenal. The production of carbon monoxide, along with C_2, C_5, and C_7 hydrocarbons, and the formation of *trans*-4-octenal represent well-known primary processes in cyclic ketones. However, the formation of cyclopentanone and propylene in equivalent amounts represents the first observation of the Norrish type II process in an alicyclic ketone. The quantum yield for this process has been determined to be 0.08. The reaction was essentially unaffected by adding oxygen or by carrying it out in the liquid phase. Photolysis of 2-(n-propyl-2,2-d_2)cyclopentanone showed, as in other instances, the specific nature of the hydrogen atom that underwent intramolecular transfer.

Introduction

The occurrence of an intramolecular hydrogen migration process on the irradiation of aliphatic ketones with at least one proton on the γ-carbon atom has long been recognized.[1] The mechanism of this process was postulated to involve a six-membered cyclic intermediate (i) in which the bonds break along the broken

i
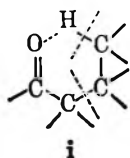
lines to give an olefin and the enol form of the ketone.[2] Indirect evidence for this mechanism has been obtained by deuterium-labeling experiments,[3] while very recently the enol form of the ketone that is obtained transiently has been directly observed by infrared spectroscopy.[4]

Although cyclic ketones with at least six carbons in the ring may possess hydrogen atoms attached to the γ-carbon atom, the analog of the type II process has not been observed. Thus this process in cyclohexanone would be expected to give 5-hexen-2-one *via* the intermediate ii. A careful search for this product in both the vapor phase and liquid phase photolysis of cyclo-

ii
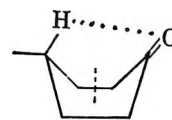
hexanone has failed to give positive results.[5] This study was undertaken to see if the type II process would occur in a cyclic ketone which had hydrogen atoms on a γ-carbon along a side chain rather than in the ring itself.

Experimental

2-n-Propylcyclopentanone (K & K Laboratories) was fractionated on a 24-plate spinning-band column. A narrow middle cut was collected and used. 2-(n-Propyl-2,2-d_2)cyclopentanone was synthesized by the condensation of propyl bromide-2,2-d_2 with 2-carbethoxycyclopentanone, followed by hydrolysis and decarboxylation of the condensate. The propyl bromide had an isotopic purity of over 98 atom % ac-

(1) For a review see, J. N. Pitts, Jr., *J. Chem. Educ.*, 34, 112 (1957).

(2) W. Davis, Jr., and W. A. Noyes, Jr., *J. Am. Chem. Soc.*, 69, 2153 (1947).

(3) R. Srinivasan, *ibid.*, 81, 5061 (1959).

(4) G. R. McMillan, J. G. Calvert, and J. N. Pitts, Jr., *ibid.*, 86, 3602 (1964).

(5) R. Srinivasan, unpublished work.

cording to the manufacturer (Merck Sharp and Dohme, Montreal). This purity could not have changed during the course of the synthesis of the 2-n-propylcyclopentanone.

Photolyses were carried out in a quartz cell 3.0 cm. long and 5.0 cm. in diameter, which was fitted with a break-seal to remove the volatile products for analysis. The light source was a Hanovia S-100 medium pressure mercury arc filtered by 2 mm. of Pyrex glass (Corning 0–53). It transmitted $\sim$5% at 2800 Å. and $\sim$36% at 3000 Å. In each experiment, a measured quantity of the ketone was introduced into the cell, which was then evacuated, degassed, and sealed. The cell was placed in a furnace, allowed to come up to temperature, and irradiated.

Analyses were conducted by a combination of vapor phase chromatography and mass spectrometry.

Results

Products. In a typical photolysis at 147°, the products that were measured and their relative amounts were: carbon monoxide, 1.70; ethylene, 1.05; propylene, 5.43; cyclopentanone, 5.3; *trans*-4-octenal, 3.2. The identity of the cyclopentanone was established by infrared analysis and by comparison with the authentic material. 1-Pentene was identified qualitatively while a C_7H_{14} product that was found was taken to be n-propylcyclobutane. The aldehyde was found to be isomeric to the starting material. Its infrared spectrum showed strong absorptions at 2720, 1735, and 975 cm.$^{-1}$. The intense absorption at 975 cm.$^{-1}$ and the lack of any strong absorption below 850 cm.$^{-1}$ was indicativ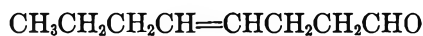e of the exclusive formation of the *trans* product.[6] The nuclear magnetic resonance spectrum showed a proton distribution of 1:2:6:5 at the τ-values 0.22, 4.55, 7.85, and 8.9. However, this in itself does not distinguish between the structures

$$CH_3CH_2CH_2CH{=}CHCH_2CH_2CHO$$

iii

$$CH_3CH_2CH{=}CHCH_2CH_2CH_2CHO$$

iv

both of which are possible. It was observed[7] that photolysis of 2-methylcyclopentanone gave only *trans*-4-hexenal (no $CH{=}CH_2$ grouping in the infrared spectrum), while 2-ethylcyclopentanone gave *trans*-4-heptenal (proton distribution of 1:2:6:3 in the τ-ranges 0–1, 4–5, 7–8.5, and 9 rather than a distribution of 1:2:7:2) exclusively. By analogy, the single compound that was formed in the present instance was taken to be *trans*-4-octenal.

The equivalence between the yields of propylene and

cyclopentanone (within experimental error) was observed in all of the experiments in the vapor phase. The stoichiometry of the reactions is given by

$$\longrightarrow CO + C_2H_4 + C_5H_{10} \qquad (1)$$

$$\longrightarrow CO + CH_2CH_2CH_2CHC_3H_7 \qquad (2)$$

$$\longrightarrow C_3H_6 + CH_2CH_2CH_2CH_2CO \qquad (3)$$

$$\longrightarrow CH_3CH_2CH_2\,CH{=}CHCH_2CH_2CHO \;(4)$$
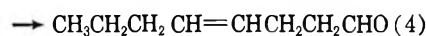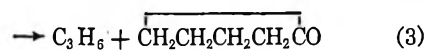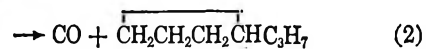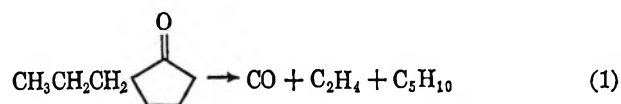
Quantum Yields. The light source was calibrated with a diethyl ketone actinometer at 120° ($\Phi_{CO} = 1$). The quantum yields for carbon monoxide, cyclopentanone, and 4-octenal were 0.03, 0.08, and 0.05, respectively. These values, which were obtained by averaging the results from at least four runs, were reproducible to ±10%. Since the yield of ethylene was 0.62 of that for CO, the quantum yields for reactions 1 and 2 are 0.02 and 0.01, respectively. In the presence of 11.2 mm. of oxygen, the quantum yield of cyclopentanone was 0.08; that of propylene was not determined although its formation was observed. In the photolysis of 2-n-propylcyclopentanone as a liquid, the quantum yields for cyclopentanone and *trans*-4-octenal were 0.19 and 0.38, respectively. These values may be uncertain by as much as ±50%, as the absorbed intensity was calculated from the geometry of the optical train. No effort was made to look for emission of radiation from 2-n-propylcyclopentanone on excitation.

Deuterium-Labeling Studies. The results of the photolysis of 2-(n-propyl-2,2-d_2)cyclopentanone
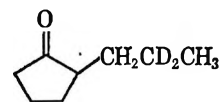
as a function of reaction conditions are given in Table I. The procedure that was used to coat the walls with deuterium oxide has been described.[3] In one experiment photolysis of the "light" ketone was carried out in a cell that had previously been coated with deuterium oxide. The isotopic composition of the cyclopentanone that was obtained in this experiment was: d_0 99.2%; d_1 0.8%. The amount of cyclopentanone-d_1 is less than the uncertainty in the analysis and is hence not significant.

(6) R. Srinivasan and S. E. Cremer, *J. Am. Chem. Soc.*, **87**, 1647 (1965).

(7) R. Srinivasan and S. E. Cremer, unpublished work.

Table I: Photolysis of 2-(n-Propyl-2,2-d_2)cyclopentanone

Conditions	Time, min.	% pro- pylene-d_1	Isotopic composition of products		
			% cyclopentanone[a]		
			d_0	d_1	d_2
"Untreated" quartz cell	150	100[b]	88.8	11.2	0.0
"Untreated" quartz cell, repeat of above	150	100[b]	90.0	9.1	0.0
Quartz cell, flamed out and then coated with D_2O	180	100[b]	92.3	7.7	0.0
Quartz cell from above, coated again with D_2O	150	100[b]	82.4	17.6	0.0
Uncoated cell, unfiltered arc	15	100[b]	93.0	7.0	0.0

[a] Not corrected for small (~2%) quantity of unlabeled ketone in starting material. [b] Refers to same isotopic content as starting material.

Discussion

The equivalence in the yields of propylene and cyclopentanone, the lack of any effect on their formation on the addition of oxygen, and the equal facility with which these products are formed, both in the vapor and liquid phases, leave no doubt that reaction 3 is an example of the Norrish type II process. This appears to be the first instance in which the reaction has been observed to involve an alicyclic ketone. The exclusive formation of propylene-d_1 in the photolysis of the deuterium-labeled ketone strongly favors a mechanism analogous to that observed in the aliphatic ketones, i.e., one that involves a six-membered intermediate

$$(5)$$
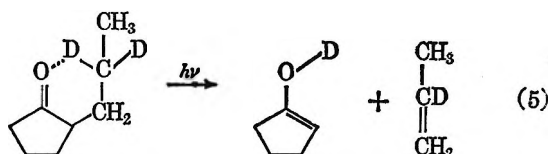
While it may seem that the formation of cyclopentanone-d_0 rather than cyclopentanone-d_1 as the major product is a point of difference between the present system and the earlier results[3] with 2-hexanone-5,5-d_2, it should be borne in mind that both the temperature and the pressures used were quite different in the two systems. The temperature was more than 100° higher,

which would tend to decrease the amount of water adsorbed on the walls. The pressures were tenfold greater, which would slow down the diffusion of active species to the walls. Under these circumstances the rearrangement of the enol form of the ketone that is formed in reaction 5 to the keto form is probably not a wall reaction but a homogenous reaction in the gas phase for the most part. Since the starting material could not be freed entirely from H_2O, the rearrangement with H_2O as the other reactant would invariably proceed with loss of labeling. The results in Table I merely point out that attempts to minimize this exchange by coating the walls with D_2O proved to be futile.

The most significant conclusion that can be drawn from the present study is the importance of the geometry of the proton which undergoes transfer with respect to the carbonyl group. Two different requirements arise, depending on the abstracting atom.[8] In
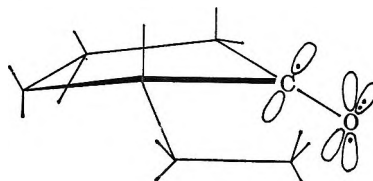
the Norrish type II process the oxygen of the carbonyl group is the abstracting atom, and its bonding orbital lies in the plane of the cyclopentanone ring. As a result it can easily abstract only a proton in the side chain and not one on the ring (there is no γ-carbon in cyclopentanone but the argument is applicable to cyclohexanone). The proton migration which leads to trans-4-octenal involves the carbon of the carbonyl group as the abstracting atom. The bonding orbital on this carbon is perpendicular to the ring so that only a proton on a carbon in the ring can successfully undergo bonding. This would readily explain why the product is exclusively 4-octenal and not 5-octenal. The selectivity in the protons that undergo transfer implies that the ring is virtually intact at the instant of the migration.

Electrokinetic Phenomena at the Thorium Oxide–Aqueous Solution Interface[1]

by H. F. Holmes, Charles S. Shoup, Jr., and C. H. Secoy

Oak Ridge National Laboratory, Oak Ridge, Tennessee   (*Received April 19, 1965*)

Electrokinetic effects of aqueous solutions in porous plugs of thorium oxide have been investigated from the standpoint of irreversible thermodynamics. A kinetic electroosmotic technique was used to determine the electrokinetic potential. This method gave results in agreement with streaming potential data except in the presence of acidic solutions. The cell constant for bulk electrical conductance was observed, in some cases, to be dependent on the nature of the electrolyte within the plugs. Despite variations in cell constants, the measured surface conductances of several plugs and capillaries of thorium oxide could be interpreted in terms of the specific surface conductivity. The specific surface conductivities were much larger than those predicted from the classical theory of surface conductance. The mechanism of surface conductivity in this system was ascribed to the conductivity of ionizable surface hydroxyl groups.

Introduction

According to the theory of irreversible thermodynamics,[2] fluxes, J_i (such as electric current, mass flow, and chemical reaction rate), can be expressed by phenomenological relations of the type

$$J_i = \sum_{k=1}^{n} L_{ik} X_k \qquad (i = 1, 2, \dots, n) \qquad (1)$$

Thus, a given irreversible flux is a linear function of the forces (here represented by X_k) present in the system, provided that the system is in a state of microscopic reversibility. If the fluxes and forces are chosen properly, the Onsager reciprocal relation[3] states that the matrix of the phenomenological coefficients must be symmetric, *i.e.*

$$L_{ik} = L_{ki} \qquad (2)$$

In the case of electrokinetic phenomena, the fluxes are electric current, I, and volume flow rate, $dV/dt = \dot{V}$, while the forces at constant temperature are the potential gradient, E, and the pressure gradient, P. Thus

$$I = L_{11}E + L_eP \qquad (3)$$

$$\dot{V} = L_eE + L_{22}P \qquad (4)$$

where L_{11} is the electrical conductance, L_{22} is the permeability, and L_e is the electrokinetic coefficient with the Onsager reciprocal relation taken into account.

Onsager's reciprocal relation has been shown to be valid for a wide variety of electrokinetic systems.[4] Electrokinetic effects can now be expressed in terms of the phenomenological coefficients; for example, the streaming potential

$$(E_s/P)_{I=0} = -L_e/L_{11} \qquad (5)$$

The study of electrokinetic effects in porous plugs is fraught with pitfalls, both experimental and theoretical. Unless otherwise noted, subsequent discussion will be based on the following assumptions which are common to this type of investigation. (1) The electrokinetic system is in a state of microscopic reversibility. (2) The ratio of the dielectric constant to the viscosity of the solution (D/η) is constant throughout the double layer. (3) Either the geometry of the plug is independent of time and the nature of the electrolyte within its pores, or changes in geometry must be recognized and their effects determined. (4) The radius of curvature of the pores is much larger than the thickness of the double layer.

For a plug of arbitrary geometry, the electroosmotic

(1) Research sponsored by the U. S. Atomic Energy Commission under contract with the Union Carbide Corp.

(2) S. R. deGroot, "Thermodynamics of Irreversible Processes," Interscience Publishers, Inc., New York, N. Y., 1951.

(3) L. Onsager, *Phys. Rev.*, **37**, 405 (1931); **38**, 2265 (1931).

(4) D. G. Miller, *Chem. Rev.*, **60**, 15 (1960).

flow rate due to an applied potential in the absence of a pressure gradient is[5]

$$\dot{V}_{P=0} = \frac{D\zeta}{4\pi\eta}\int E dA \qquad (6)$$

integrated over the total cross-sectional area, A. Thus

$$\dot{V}_{P=0} = \frac{D\zeta}{4\pi\eta}\frac{\Delta E}{k_b} \qquad (7)$$

where ΔE is the applied potential between the ends of the plug, ζ is the electrokinetic potential at the slipping plane, and k_b is the cell constant for electrolytic conductance through the bulk solution within the pores of the plug. From eq. 4 and 7

$$L_e = D\zeta l/4\pi\eta k_b \qquad (8)$$

where l is the length of the plug.

The present paper describes a series of experiments undertaken for the purpose of studying the electrokinetic properties of the thorium oxide–aqueous solution interface in porous plugs.

Experimental

The porous plugs were constructed of powdered thorium oxide which had been prepared by calcining two different batches of thorium oxalate at 650° for 4 hr. in air. Part of batch A was divided into smaller portions, which were subsequently fired for 4 hr. more at 800, 1000, 1200, and 1400°, respectively. Batch B was subsequently fired at 1600°. Most of the investigations reported here were carried out on the material from batch A.

The specific surface areas of the various samples, as determined by the B.E.T. nitrogen adsorption technique, ranged from 0.99 to 14.7 m.²/g., while the X-ray crystallite sizes varied from 200 to more than 2500 Å. As expected, the specific surface areas decreased, and the crystallite sizes increased with increasing firing temperature. The average particle sizes, which were independent of firing temperature, were 2.7 and 1.2 μ for batches A and B, respectively. Spectrographic analyses revealed that no impurities were present to an extent greater than a few parts per million.

Deionized water and reagent grade chemicals were used at all times. The experiments were carried out at room temperature (24.7 ± 0.4°), and the system was protected from the atmosphere by Ascarite.

The glass electrokinetic cell is illustrated schematically in Figure 1. The powder, in the form of a thick aqueous slurry, was introduced into the electrokinetic cell and retained by a disk of filter paper at each end of
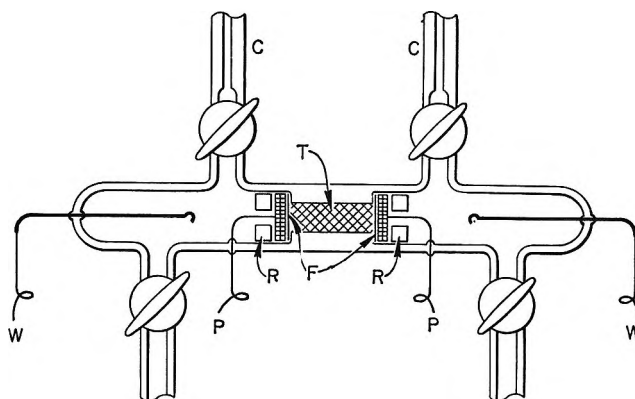
Figure 1. Porous powder electrokinetic conductance cell: C, capillaries of identical known radii; F, filter paper disks; R, polyethylene or Teflon retaining rings; P, probe electrodes; T, porous plug of ThO₂; W, working electrodes.

the plug. Probe electrodes of platinized platinum gauze were pressed against the filter paper by a tightly fitting polyethylene or Teflon ring. The plug was packed by a vacuum applied to the end opposite that which was being filled, resulting in a void space of 60 to 70%. The cell was constructed in such a way as to make each plug 1.00 cm. in length with a diameter of about 0.6 cm.

A bright platinum electrode was installed at each end of the cell, a few centimeters removed from the plug itself, the pair serving as working (current-carrying) electrodes in the electroosmotic experiments. The cell was provided with vertical identical capillaries of known radius near each end of the plug. Blank runs were carried out with the cell completely assembled except for the thorium oxide, and no electrokinetic effects were observed.

A.c. resistance measurements at 2000 c.p.s. were made with a Jones bridge coupled to an oscillator and tuned amplifier, with an oscilloscope used as the detector. Whenever the oscilloscope pattern indicated the presence of polarization, the resistance measurements at 2000, 1000, and 500 c.p.s. were extrapolated to infinite frequency and the extrapolated resistance used in all calculations. The plug resistance was measured across the probe electrodes. Previously calibrated conductivity cells were placed on both the entrance and exit sides of the electrokinetic cell in order to monitor the specific conductivity of the bulk solution, λ_b, within the system. The cell constant for the plug was determined from the product of these two values (plug resistance and λ_b) after λ_b on the exit

(5) J. Th. G. Overbeek in "Colloid Science," Vol. I, H. R. Kruyt, Ed., Elsevier Publishing Co., New York, N. Y., 1952, Chapter V.

side of the plug was found to agree within 1% of the value of λ_b on the entrance side.

Streaming potentials were determined as a function of the applied pressure by the use of a high input impedance pH meter with a millivolt scale. The potential drop across the plug was measured with and without the application of a known pressure, and the difference was taken as the streaming potential. The applied pressure seldom exceeded 50 cm. of water although a residual pressure drop of up to 100 cm. of water due to gravity was sometimes present. The residual pressure drop was the same before and after the application of the known pressure and had no effect on the streaming potential measurement itself.

The electrokinetic coefficient, L_e, can be determined from electroosmotic experiments in a number of ways. The two most common methods are: (1) determination of the electroosmotic flow rate under an applied potential by measuring the volume flow rate in a horizontal capillary of known radius and (2) determination of the electroosmotic pressure developed by an applied potential under the condition that no net flow occurs through the plug.

In the present investigation, a kinetic electroosmotic technique was used to determine L_e and L_{22} simultaneously. An electrical potential was applied across the working electrodes and adjusted to give a known potential drop across the probe electrodes. The latter was measured potentiometrically, with a Leeds and Northrup K-3 potentiometer serving as the primary potential-measuring instrument.

The height of the liquid level in one of the two capillaries at the ends of the porous plug was then monitored as a function of time. If h_0 is the equilibrium height of the liquid levels with the electrodes shorted and h_1 is the height in either capillary at time t, then from eq. 4

$$\pi r^2 \, dh/dt = L_e \Delta E + 2L_{22} gh\rho \qquad (9)$$

where r is the radius of the two identical capillaries, ρ is the density of the solution, g is the acceleration due to gravity, h is $h_1 - h_0$, and ΔE is the applied potential as measured across the probe electrodes. By following the change in height of one of the liquid levels with a cathetometer or traveling microscope as a function of time it is possible to use the linear relation

$$\Delta h/\Delta t = (Le/\pi r^2)\Delta E + (2L_{22}\rho g/\pi r^2)\bar{h} \qquad (10)$$

Here $\bar{h}$ is the average value of h during the time interval Δt, and Δh is the linear distance traveled by the same liquid level during that time interval.

Potential gradients of 1 to 7 v./cm. and time in-

tervals of 100 to 300 sec. were used to obtain plots similar to that shown in Figure 2. From the intercept and slope of these plots, L_e and L_{22}, respectively, were determined by the method of least squares. It is to be noted in Figure 2 that line A does not pass through the origin as would be expected from eq. 10 for a truly constant permeability. Small deviations (always less than 10%) in both L_e and L_{22} were characteristic of all the data obtained. Repeated experiments with the polarity of the electrodes reversed and, with the flow in first one direction and then in the other, indicated the presence of small degrees of both electrical asymmetry and hydrodynamic asymmetry. No method of either eliminating or reproducibly measuring these asymmetries was found. It was assumed that the best data were obtained by using the mean values found for L_e and L_{22} from the four combinations of electrical polarity and flow direction. In actual practice, it was only necessary to measure a few points in each of two groups well separated on the $\bar{h}$ axis and draw the best straight line through them.
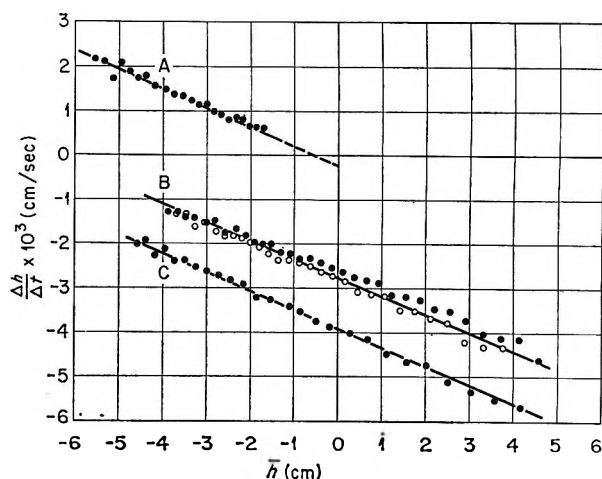
Figure 2. Typical electroosmotic data: NH_4OH (pH 10.10) on porous plug of ThO_2 ($k_b = 9.70$ cm.$^{-1}$); A, $E = 0.00$ v./cm. (probe electrodes shorted); B, $E = 3.30$ v./cm. (open and closed points represent different experimental runs); C, $E = 4.40$ v./cm.; average $\zeta = -20.7 \pm 5\%$ mv.; average $L_{22} = 4.13 \times 10^{-9} \pm 5\%$ cm.^{6} dyne^{-1} sec.$^{-1}$.

Results and Discussion

Cell Constants and Surface Conductance. Experimental measurements of the cell constant in porous plugs of ThO_2 using KCl solutions revealed that it is highly dependent on the specific conductivity of the bulk solution, λ_b, particularly at low electrolyte concentrations. The apparent cell constant, k', was observed to increase with increasing KCl concentration,

approaching a constant value with relatively concentrated solutions.

This behavior implies that one or more additional conductance mechanisms are present. In subsequent discussion the additional conductance is treated as surface conductance. With solutions of specific conductivity sufficiently high for the surface conductance to be negligible compared to the total conductance, the apparent cell constant was independent of λ_b and was therefore assumed to be equal to k_b. Although k_b for the various plugs ranged from 4.69 to 10.57 cm.$^{-1}$, the ratio k'/k_b was very nearly the same at any given specific conductivity (Figure 5).

In an attempt to determine if this phenomenon is unique with porous plugs, two ceramic ThO_2 capillaries were obtained with geometrically measured cell constants of 94.5 and 144.4 cm.$^{-1}$. The apparent cell constant of each capillary was measured with KCl solution flowing through it. Initial resistance measurements showed a strong time dependence, indicating that the solution was penetrating slowly into the porous structure of the capillary walls. (The ceramic ThO_2 was many orders of magnitude less porous than the porous plugs.) In an attempt to correlate the resistance measurements with the macroscopic capillary geometry, the solution was permitted to flow through a previously rinsed (deionized H_2O) and dried (120°) capillary and its resistance measured as a function of time. Extrapolation of the resistance readings to zero time gave reproducible results. By following this procedure, the apparent cell constants were determined as a function of KCl concentration and are illustrated in Figure 3. The extrapolated values of k_b for the two capillaries were found to be 97.3 and 145.6 cm.$^{-1}$. These values compare quite favorably with the geometrically determined cell constants. This fact lends additional support to the use of k_b values for the porous plugs as determined in concentrated solutions. The ratio k'/k_b was observed to follow a curve similar to those for the porous plugs (Figure 5).

If the electrokinetic system is represented as a pair of parallel conductance paths, the total conductance can be expressed as

$$L_{11} = \frac{1}{R} = \frac{\lambda_b}{k'} = \frac{\lambda_b}{k_b} + \frac{\lambda_s}{k_s} \qquad (11)$$

where λ_s and k_s are the specific surface conductivity and its associated cell constant. This equation can be rearranged to yield an expression for the specific surface conductivity

$$\lambda_s = \left(\frac{\lambda_b}{k'} - \frac{\lambda_b}{k_b}\right)k_s \qquad (12)$$
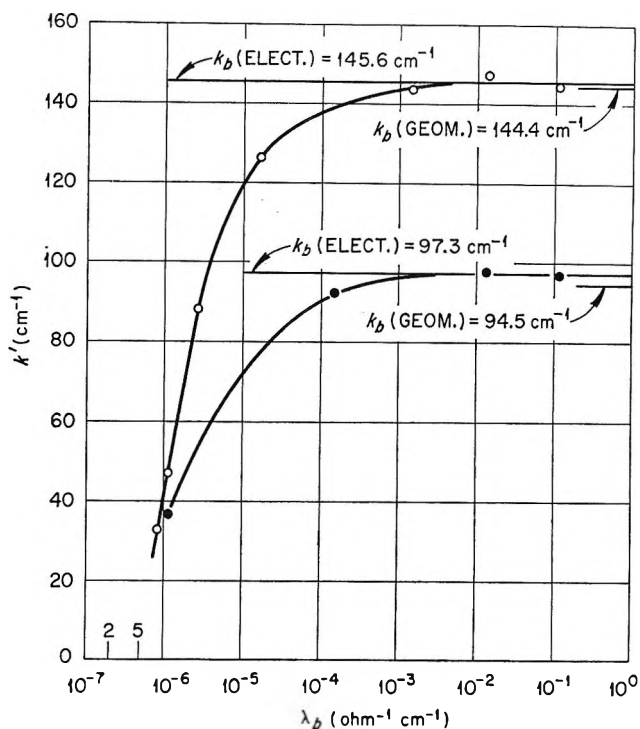
Figure 3. Cell constants for ThO_2 capillaries; KCl solutions.

For a single capillary, $k_s/k_b = a/2$, where a is the radius of the capillary. In the case of the two ThO_2 capillaries used in the present investigation, this ratio is 0.045, and thus the specific surface conductivity of the ThO_2 capillaries can be readily determined. Since λ_s is independent of geometry, it should be the same for the porous plugs as for the capillaries, thus making it possible to determine k_s for the various porous plugs whose apparent cell constants have been determined by the use of KCl solutions at different concentrations. Once k_s and k_b have been established for a particular plug, it should be possible to determine λ_s for a variety of electrolytes.

Measurements of the apparent cell constant as a function of the concentration of other electrolytes, however, revealed that the value obtained for k_b was dependent on the electrolyte used for its evaluation. In general, the variation of k' with concentration of a given electrolyte followed a smooth curve. The use of different electrolytes often resulted in displaced curves, with k' approaching a constant value characteristic of the electrolyte used at high concentration within a particular plug.

The nature of the variation of k_b with the electrolyte used for its determination was complex and not entirely reproducible. In general, however, 10^{-4} N or greater concentrations of Na_2CO_3 or acid solutions caused a downward shift in the values obtained for k' and thus a
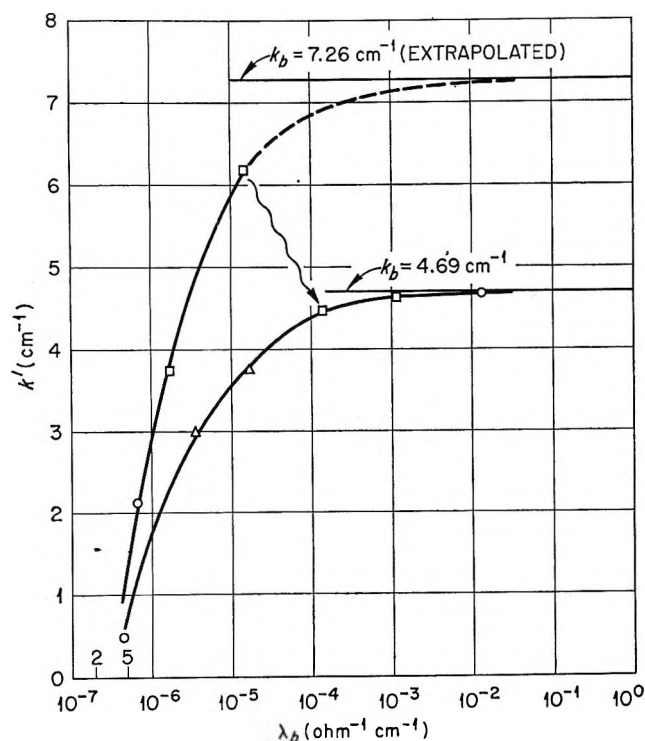
Figure 4. Apparent cell constant as a function of
electrolyte specific conductivity showing electrolyte shift.
Batch A ThO$_2$, plug No. 52: O, H$_2$O, KCl;
□, Na$_2$CO$_3$; △, H$_2$SO$_4$.
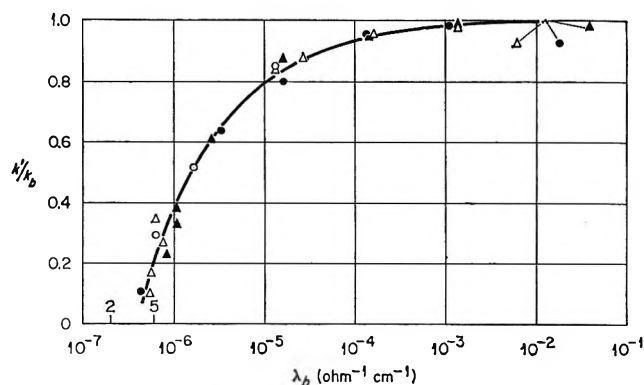
Figure 5. Normalized apparent cell constant, k'/k_b, as a
function of electrolyte specific conductivity: ●, A ThO$_2$, plug
No. 52 (after electrolyte shift); O, A ThO$_2$, plug No. 52
(before electrolyte shift); △, A ThO$_2$, plug No. 31 and No. 50,
H$_2$O, KCl; ▲, capillaries, H$_2$O, KCl.

lower value for k_b than determined previously by the
use of other solutions. Subsequent use of KCl usually
resulted in a variation of k' identical with that of the
electrolyte used immediately prior to the introduction
of the KCl solution. Some of these effects are illus-
trated in Figure 4 for a porous plug of ThO$_2$ from
batch A.

Despite the complexities involved in the electrolyte
shifts observed for the cell constants, the ratio k'/k_b
was found to be essentially independent of the history
of the sample, provided the appropriate value of k_b
is used. This independence is illustrated in Figure 5
in which the variation of k'/k_b with specific conductivity
of the solution is shown to be the same for the capil-
laries and porous plugs, even in the presence of electro-
lyte shifts.

The value of L_{22} obtained for the porous plugs varied
considerably from plug to plug, but all were of the
order of magnitude of 10^{-9} cm.^{6} dyne^{-1} sec.$^{-1}$. For a
given plug, L_{22} was reproducible to within ±10%.
In contrast to the variations of k' and k_b with the
electrolyte studied, the measured permeability of the
plugs showed no dependence on the electrolyte present
within the plug. Since permeability is more sensitive
to geometry than the cell constant is, this implies that
the cell constant variation is not necessarily due to a
gross change in the geometry of the plug but may be
due to some sort of surface effect.

Since the ratio k'/k_b was essentially the same for the
plugs and capillaries investigated, the variation in the
specific surface conductivity, λ_s, of "indifferent"
electrolytes such as KCl must be less than the experi-
mental errors involved in determining it. By use of
eq. 11 and λ_s for KCl obtained from the capillaries,
k_s was evaluated for a limited number of plugs, making
it possible to determine λ_s for electrolytes other than
KCl. The specific surface conductivity so determined
is illustrated in Figure 6 for a variety of plugs and
capillaries. No significant differences were observed
among the ThO$_2$ plugs from different batches of ThO$_2$
nor among the plugs which were prepared from ThO$_2$
calcined at different temperatures.
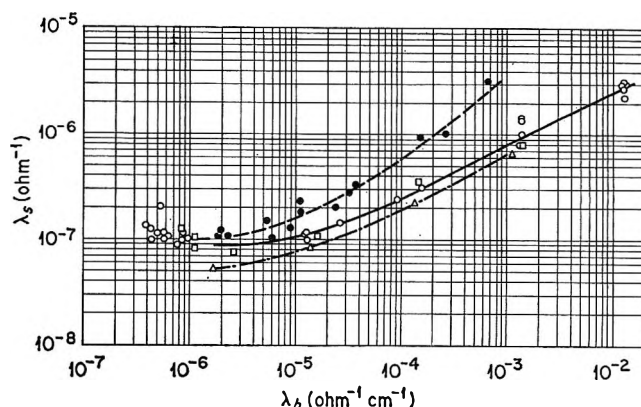
Figure 6. Specific surface conductivity as a function of
electrolyte specific conductivity: O, H$_2$O and KCl
in porous plugs; □, H$_2$O and KCl in capillaries;
●, NH$_4$OH in porous plugs; △, Na$_2$CO$_3$ in porous plugs.

An important feature of the results shown in Figure 6 is the fact that they are some two to three orders of magnitude larger than would be predicted from the classical theories of surface conductance.[5] Most of these theories attribute surface conductivity solely to an excess of ions in the diffuse part of the double layer while assuming that those ions in the Stern layer are immobile. Most of the reported surface conductivity values have been obtained from experiments with the glass–aqueous solution interface. Although highly divergent, these reported results are consistently larger than would be predicted from the classical theories. However, Urban, White, and Strassner[6a] succeeded in agreeing fairly well with the experimental results by adding to the classical theory a term involving the mobility of ions in the Stern layer. McBain and Foster[6b] also concluded that their experimental surface conductivities for glass were much too large to be attributed solely to ions in the diffuse layer. Failure of the classical theories of surface conductance is even more strikingly illustrated by considering reported results for materials other than glass. For comparison with Figure 6, theoretical values for specific surface conductivity range from about 10^{-9} to 10^{-8} ohm^{-1}, with the larger values obtained by also considering the mobility of ions in the Stern layer. This discrepancy between the experimental and theoretical values is also apparent in the reported surface conductivities for TiO_2,[7] SnO_2,[8] and Fe_2O_3[7] although the authors attributed this excess surface conductivity to the semiconducting properties of the bulk oxide.[7] Although ThO_2 has some semiconductor properties at very high temperatures, this characteristic is negligible at ordinary temperatures.

It would appear that there is an extra surface conduction mechanism which can be many times larger than those considered in the classical theory. Many workers, in interpreting electrokinetic data for oxide surfaces in aqueous media, have used an acid–base model involving ionization of surface hydroxyl groups. It seems equally probable that this same model can qualitatively explain the large surface conductivity of oxide surfaces. Several features of Figure 6 point to this mechanism. One of these is that the surface conductivity is relatively independent of the bulk conductivity (bulk ionic concentration). This fact indicates that the concentration of the surface conducting species is also relatively independent of bulk ionic concentration. Actually, one would expect that, in the absence of strong specific adsorption, the surface would be saturated with hydroxyl groups regardless of bulk ionic concentration. If the major mechanism for surface conduction is ionization of surface hydroxyl

groups, it should be dependent on pH. Evidence for this is seen in Figure 6 with the consistently high values obtained with NH_4OH. Further evidence for this may be seen in the consistently high values for the surface conductivity of glass in solutions of HCl and HNO_3.[5] In all fairness it should be pointed out that the results for the ThO_2 surface conductivity in Na_2CO_3 solutions are slightly, but consistently, lower than those in KCl solutions. According to the present hypothesis, the results for Na_2CO_3 should more closely resemble those for NH_4OH since Na_2CO_3 solutions are basic. It is quite possible that, in this case, we are dealing with strong specific adsorption. As a matter of fact, the concept of an immobile surface carbonate ion has been used to explain the adsorption of CO_2 on ThO_2.[9] It should also be pointed out that a model involving ionizable surface hydroxyl groups has been used in interpreting electrokinetic data obtained for the ThO_2 surface in aqueous solutions.[10] The relationship between surface conductance and the electrokinetic potential will be discussed in a subsequent section.

Electrokinetic Potentials. The observed streaming potential was a linear function of the applied pressure in all cases, as it should be in the absence of turbulent flow. With neutral or basic solutions the values of L_e determined from streaming potential and electroosmotic measurements under identical conditions were in good agreement. Once the plug had been exposed to acidic solutions, however, the electroosmotic experiments almost invariably gave values for L_e that were considerably smaller in absolute value than those from streaming potential measurements. According to the Onsager reciprocal relation,[3] identical values of L_e should have been obtained from the two types of experiments. Differences in the electroosmotic and streaming potential data may be related to the unexplained variation of the cell constant with the nature of the electrolyte which was discussed in the previous section. Experimentally identical values of L_e could be obtained by using cell constants calculated from electrical conductivity measurements taken with KCl as the electrolyte before and after exposure to acidic solutions for the streaming potential and electroosmotic data, respectively. However, the data were not

(6) (a) F. Urban, H. L. White, and E. A. Strassner, *J. Phys. Chem.,* **39,** 311 (1935); (b) J. W. McBain and J. F. Foster, *ibid.,* **39,** 331 (1935).

(7) D. J. O'Connor, N. Street, and A. S. Buchanan, *Australian J. Chem.,* **7,** 245 (1945).

(8) D. J. O'Connor and A. S. Buchanan, *ibid.,* **6,** 278 (1953).

(9) C. H. Pitt and M. E. Wadsworth, "Carbon Dioxide Adsorption on Thoria," Technical Report, University of Utah, Salt Lake City, Utah, Feb. 15, 1958.

(10) P. J. Anderson, *Trans. Faraday Soc.,* **54,** 130 (1958).

treated in this manner, for there seems to be no valid reason for using two different cell constants for the identical porous plug. This anomaly should not be taken as implying failure of the Onsager reciprocal relation in acidic solution as it is probably due to an inadequacy in the classical experimental definition of the phenomenological coefficients. Failure of one or more of the four basic assumptions listed in the introduction may be responsible. Resolution of this important and presently unexplained anomaly must, of necessity, await further experimental work.

Some of the pertinent electrokinetic potential data are shown in Figure 7. ThO_2 samples from batches A and B are seen to have significantly different electrokinetic potentials in KCl solutions. As a matter of fact, no positive electrokinetic potential was ever observed with ThO_2 from batch B. If one compares the electrokinetic potential of batch A in Na_2CO_3 and Na_2SO_4 solutions, one infers that there is specific adsorption of the carbonate ion. This is in line with the postulated effect of Na_2CO_3 on surface conductance.

The effect of pH on the electrokinetic potential is illustrated in Figure 8. Although the ThO_2 from batch A had an isoelectric point at a pH of approximately 9.5, no positive electrokinetic potential was observed for batch B over the pH range studied. The isoelectric point for batch A agrees quite favorably with that obtained from electrophoresis measurements on other ThO_2 samples.[11,12] However, the values of the reported electrokinetic potentials were different in all cases.

Brief investigations of ThO_2 plugs from a variety of sources, including single crystals, indicate that the electrokinetic potential is strongly influenced by the method of preparation. For example, an increase in the calcining temperature of batch A produced an increase in the electrokinetic potential of ThO_2 in pure water or very dilute KCl solutions. The effect of calcining temperature has also been noted in heat of immersion measurements[13] on ThO_2 samples from batch A. The effect of calcining temperature on the electrokinetic potential of ThO_2 has been noted briefly by Anderson.[10] Douglas and Burden[11] obtained different electrokinetic potentials for ThO_2 before and after grinding the sample to a smaller particle size. The three samples of ThO_2 studied by Sowden and Francis[12] had approximately the same isoelectric point but gave very different results for the electrokinetic potential and surface charge density.

The complex behavior of the electrical double layer is not limited to the thorium oxide–aqueous solution interface. Of the three samples of SnO_2 investigated by O'Connor and Buchanan,[8] two gave positive electro-
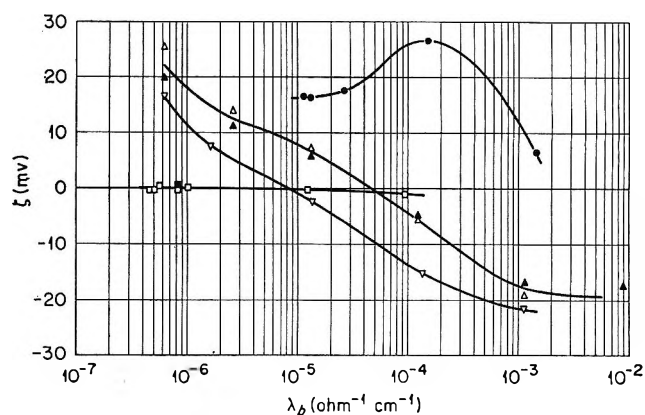
Figure 7. Electrokinetic potential as a function of electrolyte specific conductivity; open points, by streaming potential, closed points, by electroosmosis: ●, A ThO_2, plug No. 30, KCl; △▲, A ThO_2, plug No. 51, Na_2SO_4; ▽, A ThO_2, plug No. 52, Na_2CO_3; □■, B ThO_2, plug No. 60, KCl.
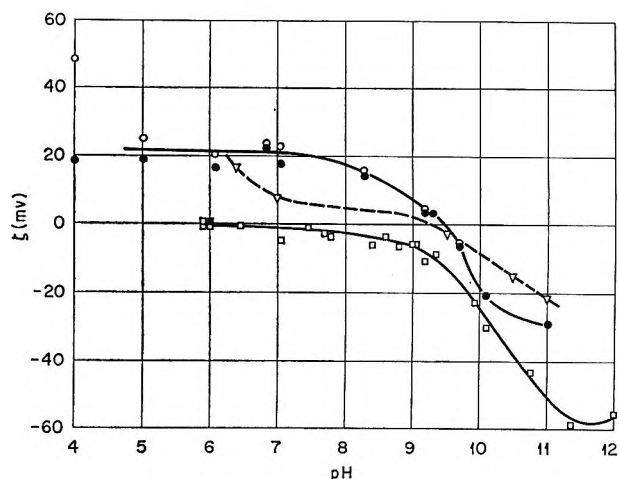
Figure 8. Electrokinetic potential as a function of pH; open points, by streaming potential; closed points, by electroosmosis: ○●, A ThO_2, plug No. 50, NH_4OH and HCl; ▽, A ThO_2, plug No. 52, Na_2CO_3; □■, B ThO_2, plug No. 60, NH_4OH and HCl.

kinetic potentials while the third was negative. The initial positive electrokinetic potential of Al_2O_3 could be changed to negative by ignition above 1000° and then back to positive by grinding lightly.[14] Morimoto and Sakamoto[15] attributed their results for the dependence of the electrokinetic potential of TiO_2 on calcining temperature to a phase transition between

(11) H. W. Douglas and J. Burden, Trans. Faraday Soc., 55, 350 (1959).
(12) R. G. Sowden and K. E. Francis, Nucl. Sci. Eng., 16, 1 (1963).
(13) H. F. Holmes and C. H. Secoy, J. Phys. Chem., 69, 151 (1965).
(14) D. J. O'Connor, P. G. Johansen, and A. S. Buchanan, Trans. Faraday Soc., 52, 229 (1956).
(15) T. Morimoto and M. Sakamoto, Bull. Chem. Soc. Japan, 37, 719 (1964).

anatase and rutile. Quantitative differences in their three samples of TiO_2 were ascribed to differences in impurities. However, ThO_2 has no solid phase transition, and samples from the same batch (identical impurity concentration) show a dependence on calcining temperature. The electrokinetic properties of the TiO_2 surface has also been shown to be dependent on the size of the particles.[16] It is interesting to compare the pH dependence of the electrokinetic potential for batch B with the results of Street[17] for synthetic sapphire. He found that while powdered specimens exhibited an isoelectric point, bulk specimens did not.

Apparently, the properties of the electrical double layer at an oxide–aqueous solution interface are complex functions of the chemical and thermal history of the sample. The behavior of amorphous surfaces such as glass is not quite so complex.[5] Until this dependence can be put on a concrete basis, electrokinetic results for such systems must be assumed to be valid only for a specific sample. This fact has also been emphasized by Anderson[10] in his work on ThO_2.

Surface Conductance and the Electrokinetic Potential. Classical theories of surface conductance treat this phenomenon as an exponential function of the electrokinetic potential.[5] An inspection of Figures 6, 7, and 8 fails to reveal any obvious relationship between surface conductivity and the electrokinetic potential. The exponential dependence in the classical theories arises from a consideration of excess ions in the double layer due to the potential difference. It seems logical that these excess ions would make a contribution to surface conductance. However, in the present system, and others as well, it is quite probable that the contribution of the excess ions in the double layer is masked by a second mechanism which is much larger in magnitude. It is equally probable that this second mechanism is the conductivity of ionizable surface hydroxyl groups. Perhaps a better test of the classical theories of surface conductance would be a system in which the solid surface is not so intricately associated with the liquid as is the case in oxide–aqueous solution systems.

(16) E. J. W. Verwey, *Rec. trav. chim.*, **60**, 625 (1941).

(17) N. Street, *Australian J. Chem.*, **17**, 828 (1964).

Galvanic Cells with Molten Bisulfate Solvents

by Ralph P. Seward and Jerome P. Miller[1]

Department of Chemistry, The Pennsylvania State University, University Park, Pennsylvania
(Received April 21, 1965)

Fused bisulfates, mainly ammonium bisulfate, have been used as solvents in galvanic cells which appear to operate reversibly with silver and mercury(I), mercury(II) platinum electrodes. The latter electrode with excess solid mercury(I) sulfate and mercury(II) sulfate present served as the reference electrode. The dependence of cell e.m.f. on mercury(II) concentration has been investigated. The silver electrode is shown to behave ideally with respect to silver ion concentration but to be dependent on the acidity or basicity of the solvent in an unexpected way.

While galvanic cells have been most fruitfully employed in evaluating the thermodynamic properties of fused salt solutions, their use has largely been confined to cells having fused nitrates or halides as solvents. The investigation reported here was undertaken with the object of finding other fused salts which would serve as solvents in reversibly operating cells. Measurements on cells with bisulfate solvents, mainly ammonium bisulfate, are described below and the results are discussed. The strongly acidic nature of fused bisulfates precludes the use of more active metals as electrodes, but silver has been found to be satisfactory and platinum inert. Solute salts have been limited to sulfates since most common anions would react with the solvent forming volatile or unstable acids.

Experimental

Materials. Mercury(I) sulfate was prepared by the reaction of aqueous mercury(I) nitrate and sulfuric acid solutions. Other salts were commercial reagent quality chemicals. Ammonium bisulfate after 2–3 hr. at 110° under about 1 mm. pressure melted at 145°. Potassium bisulfate as received melted at 212°. Sodium bisulfate, obtained as the hydrate, was dehydrated under vacuum at about 110°. It then melted at 183°. When analyzed for bisulfate hydrogen and ammonium by the method of Kolthoff and Stenger[2] the ammonium bisulfate was found to contain excess acid, in three different lots amounting to 0.42, 0.48, and 0.66 wt. % when calculated as H_2SO_4. The excess sulfuric acid content of the sodium bisulfate was 2.1%. Some maximum freezing point (100%) sulfuric acid

was prepared in order that the effect of excess sulfuric acid and of excess base (ammonium sulfate) on the cell e.m.f. values could be explored.

Electrodes. A platinum wire immersed in fused bisulfate in contact with an excess of both solid mercury(I) sulfate and solid mercury(II) sulfate served as the reference electrode. The reference electrode, a glass tube about 10 × 1.0 cm., was suspended in a larger tube (3.5 cm. diameter) where it was surrounded by a solution of variable content with which it was in electrolytic contact through an asbestos fiber junction. Dipping into the solution in the outer tube were also a thermistor probe, a thermocouple junction, a mechanical stirrer, and a second electrode. Two cells designated as A and B have been investigated. In cell A, the outer electrode was the same as the reference electrode except that the solution in contact with the platinum wire was unsaturated, and of variable concentration in mercury(II) sulfate. In cell B, the electrode in the outer chamber was a piece of silver foil.

Operation. Weighed amounts of the desired materials were placed in the larger tube, brought to 160°, and stirred continuously during measurements. Excess mercury(I) and mercury(II) sulfate was stirred in fused ammonium bisulfate and this mixture then added to the reference electrode. After 0.5 hr., the silver foil electrode was dipped into the melt and within 1

(1) From the Ph.D. Thesis of J. P. Miller, The Pennsylvania State University, June 1964; supported by the U. S. Atomic Energy Commission under Contract AT(30-1)-1881.

(2) I. M. Kolthoff and V. A. Stenger, "Volumetric Analysis," Interscience Publishers, Inc., New York, N. Y., 1947.

Table I: E.m.f. of Cell A as a Function of $HgSO_4$ Concentration at 160°

$10^3(HgSO_4)$	1.134	1.295	1.590	1.788	1.839	2.211	2.250
E, v.	0.06900	0.06626	0.06083	0.0583	0.05581	0.04950	0.0484

min. stable e.m.f. measurements could be made. The silver foil was not kept continuously in the melt but pulled out and allowed to cool except when measurements were being made. This was done to minimize the attack of the solvent on the metal. An experimental determination showed that silver immersed in ammonium bisulfate at 150–160° lost 0.17 mg./cm.² hr. Under the conditions of cell operation this is not sufficient to alter the silver content in the surrounding solution by a significant amount. Moist nitrogen was bubbled through the cell to prevent decomposition of the solvent into pyrosulfate and water.

The thermistor probe actuated a relay to control current in a furnace which surrounded the cell, maintaining the temperature at 160 ± 1°. Temperatures were obtained from a chromel–alumel thermocouple and all of the e.m.f. values were measured with a Leeds and Northrup Type K3 potentiometer, a Leeds and Northrup Type E galvanometer serving as null point detector.

Solubility Measurements. Excess solid was stirred in molten ammonium bisulfate for about 2 hr. at 160° and, after standing 0.5 hr. to permit excess solid to settle, samples of clear solution were removed by means of a preheated pipet. After cooling and weighing the samples, they were dissolved in water and mercury(I) precipitated and weighed as Hg_2Cl_2, mercury(II) as HgS, and silver as AgCl. Solubilities in moles of solute per mole of ammonium bisulfate at 160° were found as Hg_2SO_4 0.00065, $HgSO_4$ 0.0085, and Ag_2SO_4 0.0215.

Viscosities. The viscosities of certain solutions were measured, using Cannon–Fenske viscometers. A Westphal balance was employed to obtain the densities needed for calculation of the viscosity.

Results and Discussion

Cell A may be formulated as

$$Pt \begin{vmatrix} Hg_2SO_4(c), \ HgSO_4 \\ \\ NH_4HSO_4 \end{vmatrix} reference \ electrode \quad (A)$$
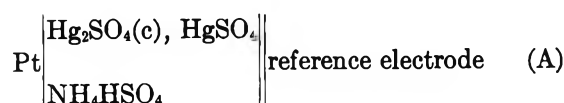
where (c) indicates the crystalline state and the reference electrode is the one described above. Hence the left-hand electrode differs from the reference electrode only in having a lower and variable concentration of $HgSO_4$. Electromotive force values for
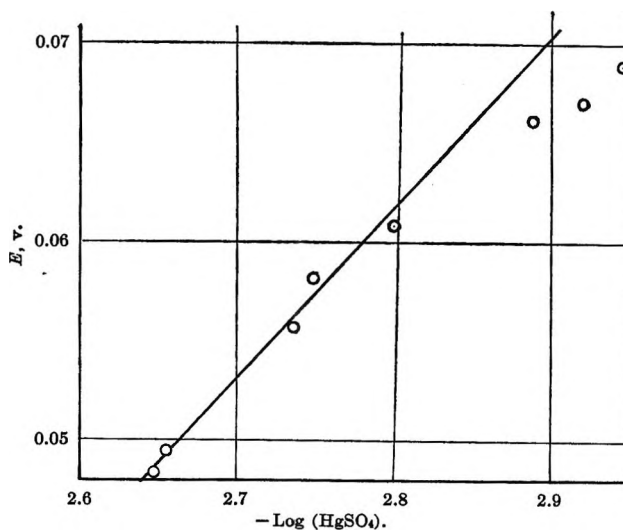
Figure 1. Dependence of e.m.f. of cell A on $HgSO_4$ concentration.

various concentrations are given in Table I and graphically in Figure 1. Concentrations throughout this paper are the ratios of the number of moles of the species whose formula appears in parentheses to the number of moles of bisulfate ion in the solution.

The effect of variation in sulfate ion concentration was studied by adding ammonium sulfate to the cell. The results are presented in Table II.

Table II: Variation of E.m.f. of Cell A with Changes in $SO_4{}^{2-}$ Concentration

$$(HgSO_4) = 2.23 \times 10^{-3}$$

$10^3(SO_4{}^{2-})$	3.41[a]	7.08	9.61	12.5	26.6
E, v.	0.0487	0.0637	0.0668	0.0694	0.0868

[a] Excess acid; the figure is that of (H_2SO_4).

It is assumed that junction potentials are a negligible factor in all of the measured e.m.f. values. Transport through the junction should be essentially all by $NH_4{}^+$ and $HSO_4{}^-$ ions and the solutions sufficiently dilute that the activities of these ions on each side of the junction should not differ by a significant amount.

If the electrode reaction is $Hg_2{}^{2+} = 2Hg^{2+} + 2e^-$, the e.m.f., for ideal solute behavior and with $2.3RT/F = 0.0861$ v. at 433°K., should be

$$E = E° + E_{ref} - \frac{0.0861}{2} \log \frac{(Hg^{2+})^2}{(Hg_2^{2+})} \quad (1)$$

In the presence of excess solid Hg_2SO_4, $(Hg_2^{2+}) = Ksp/(SO_4^{2-})$. If complete dissociation of $HgSO_4$ and no reaction of SO_4^{2-} with the slightly acidic solvent to form HSO_4^- are assumed, $(Hg^{2+}) = (HgSO_4)$. Hence

$$E = E° + E_{ref} - \frac{0.0861}{2} \log \frac{(HgSO_4)^2(SO_4^{2-})}{Ksp} \quad (2)$$

This equation is not consistent with the rise in e.m.f. with increasing (SO_4^{2-}) observed and shown in Table II.

If incomplete dissociation of $HgSO_4$ is assumed, $(Hg^{2+}) = (HgSO_4)Keq/(SO_4^{2-})$ which gives

$$E = E° + E_{ref} - \frac{0.0861}{2} \log \frac{(HgSO_4)^2 K^2eq}{(SO_4^{2-})Ksp} \quad (3)$$

The slope of a plot of E vs. log $(HgSO_4)$, if (SO_4^{2-}) is assumed constant, should be 0.0861 v. The line shown on Figure 1, drawn with this slope, is consistent with the experimental values at higher concentrations of $HgSO_4$. Equation 3 predicts qualitatively the dependence of E on (SO_4^{2-}) which was observed. The slope of E vs. log (SO_4^{2-}) is 0.031 rather than the predicted value of 0.043. This disagreement could be the result of nonideal behavior, related to that shown below for silver sulfate solutions. If the concentration of $HgSO_4$ on the left side of cell A is increased to saturation, the two electrodes become identical and the e.m.f. must become zero. If the straight line in Figure 1 is extrapolated to $E = 0$, the concentration corresponding to this point is found to be 0.0083, which agrees with the measured solubility within the experimental uncertainty of the latter.

Cell B had a silver electrode and silver sulfate in solution in the outer electrode chamber. With the same reference electrode as cell A, cell B may be formulated as

$$Ag \begin{vmatrix} Ag_2SO_4 \\ \hline NH_4HSO_4 \end{vmatrix} \begin{vmatrix} \\ \end{vmatrix} \text{reference electrode} \quad (B)$$
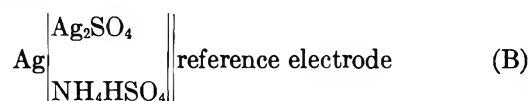
The e.m.f. of cell B was measured as a function of silver sulfate concentration including the special case of saturation, and as a function of the acidity or basicity of the solution as altered by adding varying amounts of H_2SO_4 and $(NH_4)_2SO_4$.

The measurement with excess solid Ag_2SO_4 was made with the idea that the e.m.f. might be calculated and agreement with the observed value would show that the electrodes were truly reversible. The cell reaction in this case is

$$2Ag(c) + 2HgSO_4(c) + SO_4^{2-}(anode) \longrightarrow$$
$$Hg_2SO_4(c) + Ag_2SO_4(c) + SO_4^{2-}(cathode) \quad (4)$$
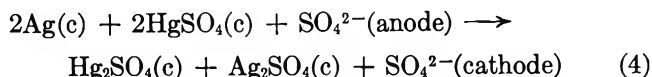
Using values of standard enthalpies of formation and entropies as given by Latimer[3] for the four solids involved, $\Delta G°_{298} = -15.6$ kcal., which corresponds to an e.m.f. of 0.338 v. The observed value was 0.3335 v., in reasonable agreement. Since the heat capacity of $HgSO_4$ has not been measured and the entropy of $HgSO_4$ was only an estimated value, a more accurate comparison, taking into account the difference in temperature and the SO_4^{2-} activities, could not be made. When ammonium sulfate was added to the solution around the silver electrode the e.m.f. did increase, as it should according to the cell reaction equation. The increase, however, was much smaller than that predicted on the assumption that SO_4^{2-} activity is proportional to SO_4^{2-} concentration. The effect of added sulfate is described further below.

Since the solvent originally contained a small excess of sulfuric acid, ammonium sulfate was added to neutralize it. As the cell e.m.f. was changed when this was done, the effect of adding sulfuric acid and ammonium sulfate was investigated extensively with solutions having several different silver sulfate concentrations. For any solution containing a definite quantity of silver sulfate, addition of sulfuric acid increased the cell e.m.f. and addition of ammonium sulfate decreased it. These changes were reversible in that the e.m.f. may be altered by adding either the acid or base and then restored to its original value by addition of an equimolar amount of the other. The silver electrode thus acts as an indicator for this titration although why it does so is not clear. This behavior is shown graphically in Figure 2, where the parallel curves become linear with a slope of -0.30 at higher sulfate concentrations and become slightly steeeper on the acid side. All sulfate concentrations have been calculated on the assumption that the reaction $H_2SO_4 + SO_4^{2-} = 2HSO_4^-$ is complete. Hence the number of moles of SO_4^{2-} is assumed to be the sum of moles of sulfate added, as ammonium sulfate and silver sulfate, less the number of moles of sulfuric acid present or added. Where the acid is in excess, the concentration is recorded as (H_2SO_4). The decrease in E with increasing sulfate concentration is opposite to what had been expected. A decrease in E corresponds to an increase in silver ion activity. Any complex ion formation with silver ion or simply the effect of the presence of doubly charged anions around the silver ions would be expected to decrease the silver ion activity.

(3) W. M. Latimer, "Oxidation Potentials," Prentice-Hall, Inc., New York, N. Y., 1952.

The dependence of the cell e.m.f. on silver ion concentration was investigated by taking values of E at three arbitrarily selected sulfate concentrations from each curve of Figure 2. When these E values were
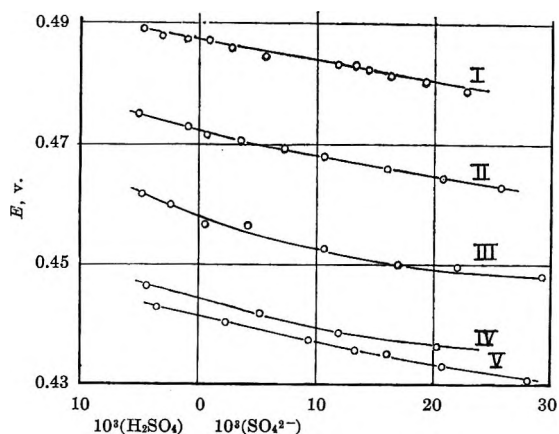
Figure 2. Dependence of e.m.f. of cell B on acid and base concentration: $10^3(Ag^+)$ for I, 0.80; II, 1.18; III, 1.68; IV, 2.58; V, 2.88.

plotted against the logarithms of the silver ion concentrations, three parallel straight lines were obtained. The slope of these lines was -0.086 ± 0.002 v., in agreement with the value predicted for ideal behavior of the silver ion. To include nonideal behavior as well, the cell e.m.f. may be described by the equation

$$E = E° + E_R - 0.086 \log (Ag^+)\gamma_{Ag^+} \qquad (5)$$

where $E°$ is a standard potential for the silver electrode, E_R the reference electrode potential, and γ an activity coefficient. If γ is assumed to be unity in those solutions for which the calculated sulfate concentrations are zero, on substitution of the measured e.m.f. and silver ion concentration, a numerical value of $E° + E_R$ may be obtained. When this was done for six solutions with silver ion concentrations varying from 0.8×10^{-3} to 2.88×10^{-3} and e.m.f. values from 0.487 to 0.441 v., values of $E° + E_R$ from 0.2200 to 0.2221 v. were obtained, the mean value being 0.2206 v.

Activity coefficients for the silver ion in solutions containing excess H_2SO_4 or SO_4^{2-} may be obtained from the curves of Figure 2. For the region of excess sulfate ion concentration where the curves are very close to straight lines, the activity coefficient is empirically

$$\log \gamma = 4.5(SO_4^{2-}) \qquad (6)$$

The utility of this relation will be illustrated by a calculation of the solubility of Ag_2SO_4 in pure ammonium bisulfate. When excess solid Ag_2SO_4 was

present and enough ammonium sulfate was added to neutralize the original excess of sulfuric acid, the cell e.m.f. was 0.3339 v. In this solution $(Ag^+) = 2(SO_4^{2-})$ and $\log \gamma = 2.25(Ag^+)$. On substituting this for $\log \gamma$ in eq. 5 and solving for the silver ion concentration, $(Ag^+) = 0.0392$, and thus $(Ag_2SO_4) = 0.0196$. This value is thought to be more nearly correct than the measured value of 0.0215. The slight excess of acid in the solvent which had been used for the solubility measurement had not been neutralized. This acid, by reaction with the sulfate ions from silver sulfate, would cause the silver ion concentration to be higher than it would have been in a neutral solvent.

As the changes in cell e.m.f. which accompanied increase in sulfate ion concentration could not be accounted for in terms of a simple silver–silver ion electrode reaction, various changes in the solution were investigated. A cell was set up identical with cell B except that the ammonium bisulfate solvent was completely replaced by an equimolar mixture of sodium bisulfate and potassium bisulfate. The titration curve here was of the same nature as that for the ammonium salt solvent, decreasing e.m.f. with increasing sulfate content. A cell having $(Ag^+) = 12.6 \times 10^{-3}$ had an e.m.f. of 0.3860 v. at the point corresponding to zero sulfate ion content. The e.m.f. for this concentration of Ag^+ when calculated by eq. 5 is 0.3841 v. It is concluded that the cell characteristics are not significantly dependent on the presence of the ammonium cation.

Other substances which might form in the cell owing to solvent decomposition are water and pyrosulfate. The effect of addition of each was investigated. Passing water vapor into the cell did not produce any detectable change, nor did addition of potassium pyrosulfate.

The viscosity of ammonium bisulfate with various additions of ammonium sulfate was measured at five different temperatures in the 160–180° range. As a bisulfate melt is a favorable situation for hydrogen bonding, the structure of the melt may well be quite different from simple random mixing. It was thought that the anomalous effect of sulfate ion on the silver–silver ion electrode might be caused by a change in the structure of the medium accompanying addition of sulfate ion. Should this be so, evidence of such a change might show up in viscosity. Experimentally, it was found that the viscosity of the melt increased on the addition of ammonium sulfate, and also on the addition of silver sulfate. The temperature coefficient of the viscosity, however, was found to be independent of sulfate concentration. To $\pm 2\%$, the observed viscosities in centipoises are given by $\eta = 0.00197 \cdot [1 + 10(SO_4^{2-})]e^{4070/T}$. Although the viscosity in-

creases caused by rather small increases in sulfate ion content do suggest a significant change in the struc-

ture of the melt, why this should increase the silver ion activity is not evident.

Thermochemistry of Interconversion of $H_2B_2O_3(g)$ and $H_3B_3O_3(g)$[1]

by Lawrence Barton, Satish K. Wason, and Richard F. Porter

Department of Chemistry, Cornell University, Ithaca, New York   *(Received April 26, 1965)*

The thermochemical stability of gaseous $H_2B_2O_3$ has been investigated. Alternate routes in the preparation of $H_2B_2O_3$ were employed to establish upper and lower limits in $\Delta H°$ for the reaction $H_3B_3O_3(g) + \frac{1}{2}O_2(g) = H_2B_2O_3(g) + \frac{1}{6}B_2H_6(g) + \frac{1}{3}B_2O_3(s)$. The methods of chemical preparation involve the reaction of boroxine with oxygen and the reaction of diborane with oxygen under electrical discharge conditions. The molecules $H_2B_2O_3$ and $H_3B_3O_3$ have been shown to be precursors to each other. Mechanisms for the interconversion reactions have been suggested from results of isotopic substitution experiments in the $H_3B_3O_3$-O_2 and $H_2B_2O_3$-B_2H_6 reactions using infrared and mass spectrometric techniques. From these observations, a mechanism for the formation of boroxine in the explosive reaction of pentaborane-9 with oxygen is proposed.

Introduction

Reactions of gaseous boranes with oxygen are frequently explosive and lead to the formation of stable boron oxide. For this reason, it has been difficult to isolate partially oxidized compounds having both B–H and B–O bonds. One interesting intermediate was observed in the reaction of B_5H_9 with oxygen by Bauer and Wiberley.[2] Later, Ditter and Shapiro[3a] identified the compound as $H_2B_2O_3$ from its mass spectrum. This compound is also observed as a product in the reaction of gaseous boroxine ($H_3B_3O_3$) and O_2.[3b] When mixtures of B_2H_6, $H_2B_2O_3$, and O_2 are heated, an explosive reaction occurs and boroxine is observed as a product.[4] The high temperature stability of boroxine was demonstrated from its preparation in a reaction of $H_2O(g)$ and elemental boron at temperature of about 1400°K.[5] Taken collectively these observations suggest that $H_2B_2O_3$ and $H_3B_3O_3$ are precursors to each other under different sets of experimental conditions. In the work described in this paper, certain aspects of the thermochemistry and reaction mechanism

of the conversion of $H_2B_2O_3$ to $H_3B_3O_3$ and $H_3B_3O_3$ to $H_2B_2O_3$ are examined. Two procedures for the preparation of $H_2B_2O_3$-B_2H_6 mixtures used in these studies are described below.

Experimental

It has been reported that $H_2B_2O_3$ is unpredictably explosive in the condensed state. Thus, although very low pressures were used in this work, caution was observed at all times.

The first method for the preparation of $H_2B_2O_3$ was

(1) Work supported by the U. S. Army Research Office (Durham) and the Advanced Research Projects Agency; presented at the 149th National Meeting of the American Chemical Society, Detroit, Mich., April 1965.

(2) W. H. Bauer and S. E. Wiberley, Abstracts of Papers, 133rd National Meeting of the American Chemical Society, San Francisco, Calif., April 1958, p. 13L.

(3) (a) J. F. Ditter and I. Shapiro, *J. Am. Chem. Soc.*, **81**, 1022 (1959); (b) S. K. Wason and R. F. Porter, *J. Phys. Chem.*, **68**, 1443 (1964).

(4) G. H. Lee, W. H. Bauer, and S. E. Wiberley, *ibid.*, **67**, 1742 (1963).

(5) W. P. Sholette and R. F. Porter, *ibid.*, **67**, 177 (1963).

the reaction of boroxine with oxygen. Solid boroxine was prepared by passing $H_2O(g)$ over a mixture of B(s) and B_2O_3(l) at a temperature of about 1400°K. and condensing the product in a bulb at liquid nitrogen temperatures. Hydrogen, which is one of the by-products of the reaction, was removed by pumping. The apparatus is illustrated in Figure 1. Solid boroxine was warmed to room temperature and diborane which is formed by partial decomposition was removed. Oxygen at 40 torr pressure was added to the bulb slowly through a 1.25-mm. Teflon needle valve and the reaction vessel was then heated to 60°. Product gases were withdrawn into a 10-cm. infrared cell and spectra were recorded on a Perkin-Elmer Model 337 grating infrared spectrophotometer. Bands due to B_2H_6 and $H_2B_2O_3$(g) were observed. No improvement in the yield of $H_2B_2O_3$(g) was observed when the reaction products were re-analyzed after 24 hr. At room temperature the yield of $H_2B_2O_3$ was very low. When the reaction between boroxine and oxygen was carried out at ~85° a slight explosion was observed. Infrared spectra of the products indicated bands due to B_2H_6(g) and $H_3B_3O_3$(g). This behavior is similar to that reported by Lee, Bauer, and Wiberley.[4] In a separate experiment,[6] $^{18}O_2$ was substituted for ordinary oxygen and the reaction with boroxine (containing ordinary oxygen) was carried out at 60° in the manner just described.

A second method of preparation of $H_2B_2O_3$ starting with diborane was developed. Oxygen was slowly added to diborane (20 torr pressure at room temperature) through a Teflon needle valve in a 300-ml. Pyrex bulb. An electric discharge was maintained near the neck of the flask with an ordinary Tesla discharge coil. The flow rate of oxygen, controlled by a pressure head of oxygen, had to be sufficiently slow to prevent "flashing" (i.e., rapid oxidation of diborane) and fast enough to cause the small intermediary concentrations of higher boranes to be oxidized rather than to polymerize further to give solid boranes. The correct oxygen flow rate was distinguished by the appearance of a white layer of boric oxide on the walls of the vessel, thickest near the point of discharge. A very slow flow rate of oxygen resulted in the formation of a yellow-white deposit which contained high molecular weight boranes. Under these conditions the yield of $H_2B_2O_3$ was extremely low. The presence of the intermediary boranes B_4H_{10}, B_5H_{11}, and B_6H_{10} in concentrations of the order 4, 1.5, and 0.5%, respectively, was shown by allowing diborane to leak slowly into a mass spectrometer in the presence of an electrical discharge. The preparation of these boranes from B_2H_6 under electrical discharge conditions has been described by Kotlensky
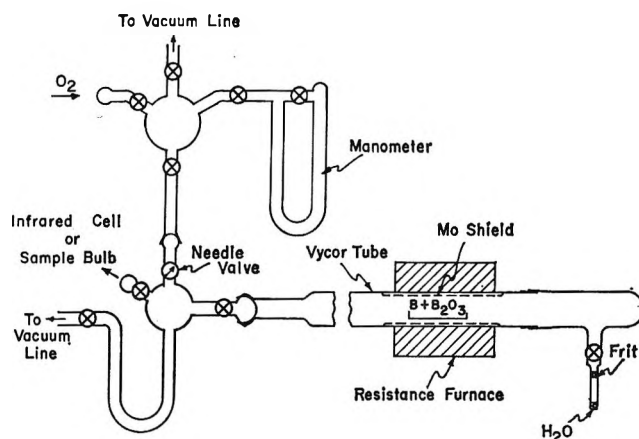
Figure 1. Apparatus for the preparation of $H_2B_2O_3$ from the reaction of oxygen with boroxine.

and Schaeffer.[7] Maximum yields of $H_2B_2O_3$ were obtained when a ratio of $B_2H_6:O_2$ of 1:1.25 was used. The whole procedure required about 30 min.

Thermodynamic Stability of $H_2B_2O_3$(g)

Reaction of gaseous boroxine with O_2 yields $H_2B_2O_3$, B_2H_6, and B_2O_3(s) as final products.[3b] The thermodynamic stability of $H_2B_2O_3$(g) was determined from measurements of $\Delta F°$ for the reaction

$$H_3B_3O_3(g) + \frac{1}{2}O_2(g) = H_2B_2O_3(g) +$$
$$\frac{1}{6}B_2H_6(g) + \frac{1}{3}B_2O_3(s) \quad (1)$$
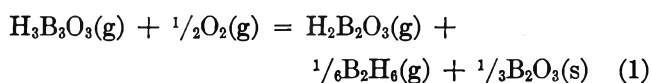
By utilizing the two procedures described above starting with either $H_3B_3O_3$ or diborane, it was possible to approach reaction 1 under different experimental conditions. In the first series of experiments, a reaction vessel (Figure 1) containing boroxine and oxygen was joined to the inlet of a mass spectrometer. The vessel was immersed in an oil bath that could be heated to about 150°. A small quantity of gas was withdrawn and ion currents at m/e 27, 32, 71, and 83 were monitored. These correspond to the major ion peaks for B_2H_6, O_2, $H_2B_2O_3$, and $H_3B_3O_3$, respectively. Immediately following the mass spectral analysis, the total pressure in the reaction vessel was measured. Diborane and oxygen were the major constituents and their partial pressures were calculated from the total pressure and the relationship $P_{B_2H_6}/P_{O_2} = 1.27(I_{27})/(I_{32})$ which was obtained by calibration with a low pressure sample of B_2H_6 and O_2 of known composition. For reaction 1 we have

(6) Sample contained 98% $^{18}O_2$ and was obtained from Yeda Research and Development Co. Ltd., Rehovoth, Israel.

(7) W. V. Kotlensky and R. Schaeffer, J. Am. Chem. Soc., 80, 4157 (1958).

Table I: Thermodynamics of the Reaction $B_3O_3H_3(g) + {}^1/_2O_2(g) \rightarrow B_2O_3H_2(g) + {}^1/_6B_2H_6(g) + {}^1/_3B_2O_3(s)$

Initial system	Sample history	Temp. of Kp deter- mination, °K.	$P_{B_2H_6}$, atm.	P_{O_2}, atm.	$\frac{I_{H_2B_2O_3}}{I_{H_3B_3O_3}}$	Kp	$-\Delta H$, kcal./mole
$B_2H_6 + O_2 + $ discharge	Immediate analysis	298	2.9×10^{-3}	1.5×10^{-5}	1.3×10^3	9.6×10^4	10.2
	Immediate analysis	298	3.9×10^{-3}	1.1×10^{-5}	3.5×10^3	4.2×10^5	11.1
	Sample maintained at 323°K. for 30 min.	298	3.8×10^{-3}	1.5×10^{-4}	1.6×10^3	5.0×10^4	9.9
	Sample maintained at 298°K. for 36 hr.	298	2.0×10^{-3}	2.3×10^{-4}	1.2×10^3	2.9×10^4	9.5
	Sample warmed to 373°K.	373	7.9×10^{-3}	1.4×10^{-3}	2.3×10^3	2.7×10^3	10.3
	Sample warmed to 373°K.	373	9.4×10^{-3}	1.4×10^{-3}	2.5×10^2	3.1×10^3	10.4
$B_3O_3H_3 + O_2$	Sample warmed to 331°K.	331	1.0×10^{-1}	1.1×10^{-2}	6.2×10^3	3.8×10^2	7.0
	Sample warmed to 331°K.	298	8.2×10^{-2}	6.1×10^{-3}	4.4×10^2	3.7×10^3	8.3
	Sample maintained at 298°K. for 6 hr.	298	6.7×10^{-2}	3.5×10^{-3}	2.2×10^2	2.7×10^3	8.1

$$K_{eq} = \frac{(P_{B_2H_6})^{1/6}}{(P_{O_2})^{1/2}}\left(\frac{P_{H_2B_2O_3}}{P_{H_3B_3O_3}}\right) \quad (2)$$

The partial pressure of $H_3B_3O_3$ was too low for measurement by conventional methods. However, a good approximation to eq. 2 is given by

$$K_{eq} = \frac{(P_{B_2H_6})^{1/6}}{(P_{O_2})^{1/2}}\left(\frac{I_{H_2B_2O_3}}{I_{H_3B_3O_3}}\right) \quad (3)$$

where the pressure ratio of $H_2B_2O_3$ to $H_3B_3O_3$ in eq. 2 has been replaced by a ratio of total ion intensities. This is equivalent to assuming that the ionization cross sections for the two molecules are nearly equal. Equation 3 may be further simplified by the relation $I_{H_2B_2O_3}/I_{H_3B_3O_3} = 1.6(I_{71})/(I_{83})$ which was obtained by analysis of complete mass spectral patterns. The high concentration of B_2H_6 in the reaction products results largely from the partial decomposition of solid boroxine. When the sample is heated, the decomposition reaction also yields an excess of $B_2O_3(s)$ in the solid coating in the reaction vessel. In another series of experiments, samples of $H_2B_2O_3$ were prepared from B_2H_6 and O_2 by the electrical discharge technique. Partial pressures of gaseous components in the products were determined mass spectrophotometrically. After correction or $H_2(g)$ which is produced in the discharge, the data were treated in the same manner as for the $H_3B_3O_3-O_2$ reaction.

Equilibrium constants for reaction 3 computed from the experimental results, are listed in Table I. The heat of the reaction was calculated from values of K_{eq} and the standard entropy change. Entropies of gaseous B_2H_6, O_2, and solid B_2O_3 were taken from the "Janaf Tables."[8] A value of $S°_{H_3B_3O_3} - S°_{H_2B_2O_3}$

was estimated to be 1.0 ± 1.0 cal./deg. mole at 300°K. This estimation was based on the D_{3h} (six-membered ring) and C_{2v} (five-membered ring) structures for $H_3B_3O_3$ and $H_2B_2O_3$, respectively. Uncertainties in the absolute entropies of $H_3B_3O_3(g)$ and $H_2B_2O_3(g)$ are in the vibrational contributions since the lowest vibration frequencies for the molecules have not been observed. However, at ordinary temperatures, the vibration terms will nearly cancel in evaluating the entropy difference for the two molecules. A somewhat similar comparison can be made for cyclohexane and cyclopentane where the entropy difference is only 1.3 e.u. at 300°K. Results of $\Delta H°$ calculations are shown in Table I.

Interconversion of $H_2B_2O_3(g)$ and $H_3B_3O_3(g)$

$H_3B_3O_3-{}^{18}O_2$ *Reaction.* In Figure 2, we compare mass spectral patterns for the highest mass groupings for $H_2B_2O_3$ prepared in the reaction of boroxine with ordinary oxygen and with ${}^{18}O_2$. The spectral pattern for $H_2B_2O_3$ having the normal boron isotope abundance is similar to that reported by Ditter and Shapiro.[3a] The mass spectrum of $H_2B_2O_3$ obtained from the reaction with ${}^{18}O_2$ shows that the isotope distribution in the product is not statistical in all three oxygen atoms but is weighted towards the species $H_2B_2{}^{18}O_2{}^{16}O$. A small quantity of $H_2B_2{}^{18}O_3$ is present but the $H_2B_2{}^{18}O_2{}^{16}O$ constitutes about 80% of the total amount of $H_2B_2O_3$. On the basis of this result, it is inferred that O_2 reacts without rupture of the O-O bond. To account for a homogeneous gas phase reaction between $H_3B_3O_3(g)$ and $O_2(g)$, we might assume that a biradical

(8) "Janaf Interim Thermochemical Tables," The Dow Chemical Co., Midland, Mich. Data for B_2H_6 were taken from the tabulation of Dec. 31, 1964; for O_2, March 31, 1961; for B_2O_3, Dec. 31, 1964.
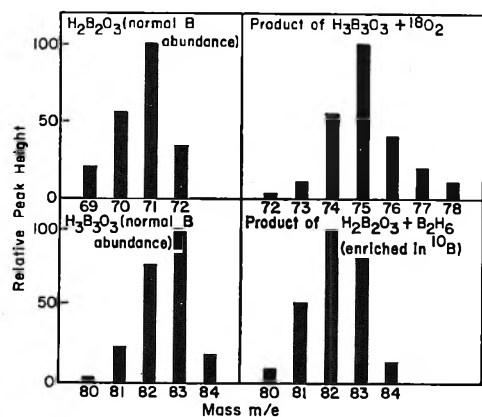
Figure 2. Mass spectral data illustrating the effect of isotopic substitution upon the reaction of $H_3B_3O_3$ with O_2 and $H_2B_2O_3$ with B_2H_6 ($^{10}B/^{11}B = 1:1.2$ in B_2H_6).

Figure 3. Curves showing the variation with time of the concentrations of the major species involved in the reaction of B_2H_6 with $H_2B_2O_3$ in an electrical discharge.

H–BO$_2$ is formed as a transient second product. This species, rather than HO–B = O(g), could be a precursor to B_2H_6 and B_2O_3, which are the stable final products. However, since B_2O_3 appears as a solid, it is possible that the reaction proceeds by a heterogeneous path.

B_2H_6–$H_2B_2O_3$ *Discharge Reaction.* At ordinary temperatures and low pressures, reaction between diborane and $H_2B_2O_3$ was not observed. Results of a mass spectrometric study of the discharge reaction are illustrated in Figure 3. A continuous discharge maintained at the reaction vessel resulted in a diminution in $H_2B_2O_3$ and an increase in $H_3B_3O_3$. When the discharge was first applied, the ion intensity of $HB_2O_3^+$ did not change noticeably. This effect was observed whenever a small amount of oxygen was present initially. After this residual O_2 had been removed by reaction with the intermediate boranes, the intensity of $HB_2O_3^+$ dropped rapidly as indicated. The effect of the discharge on the disappearance of B_2H_6 and appearance of B_4H_{10} is also noted in Figure 3.

Some information related to the mechanism of conversion of $H_2B_2O_3$ to $H_3B_3O_3$ was derived from observations on reaction mixtures prepared by adding $^{10}B_2H_6$ to B_2H_6–$H_2B_2O_3$ samples containing the natural $^{10}B/^{11}B$ isotope abundance. Mass spectral patterns obtained for these mixtures are compared with that for normal $H_3B_3O_3$ in Figure 2. Analysis of these data show that the main product, other than that with the normal isotopic spectrum is $H_3{}^{11}B_2{}^{10}BO_3$. From the observed $^{10}B/^{11}B$ composition of the diborane, it is evident that boron exchange is not a major factor and that a preferred mechanism is involved. This behavior can be interpreted on the basis of the postulated reaction
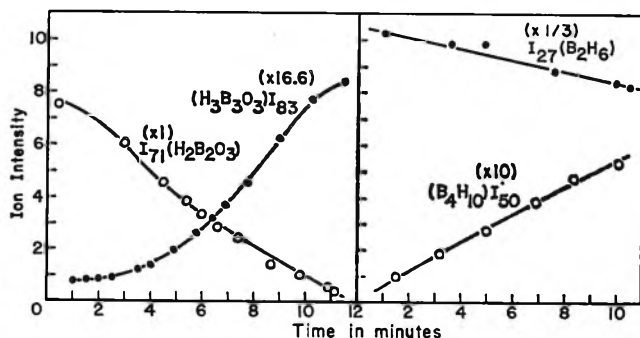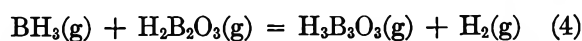
$$BH_3(g) + H_2B_2O_3(g) = H_3B_3O_3(g) + H_2(g) \quad (4)$$
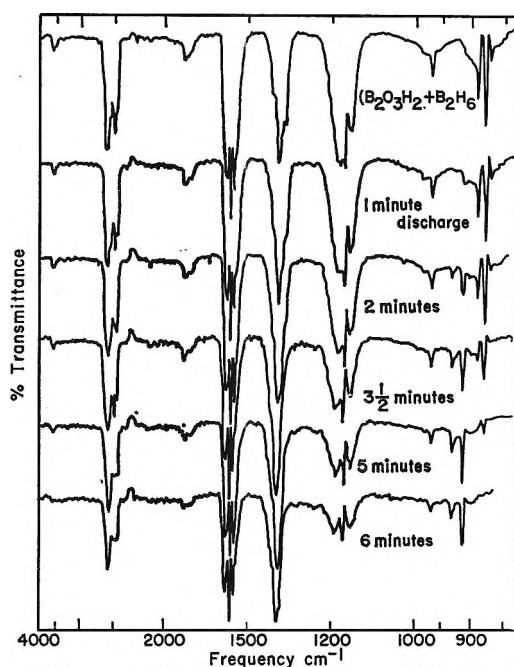
Figure 4. Infrared spectra of a mixture of B_2H_6 and $H_2B_2O_3$ taken at intervals during the course of reaction in an electrical discharge. Lower curve is for the final mixture of B_2H_6 and $H_3B_3O_3$.

The formation of higher molecular weight boranes under discharge conditions supports the supposition that BH_3 is the actual intermediate. Recently, direct evidence for BH_3 and BH_2 intermediates has been reported.[9,10]

The main features of the discharge reaction between $B_2H_6(g)$ and $H_2B_2O_3(g)$ were confirmed by observing changes in the infrared spectra of a mixture of the two compounds. The discharge was applied to a small Pyrex thimble joined to a 10-cm. infrared cell. A

(9) T. P. Fehler and W. S. Koski, *J. Am. Chem. Soc.*, 86, 2733 (1964).

(10) T. P. Fehler and W. S. Koski, *ibid.*, 87, 409 (1965).

Discussion

As we noted in Table I, variations in ΔH° values for reaction 1 are dependent on the method of sample preparation. The experimental data from B_2H_6–$H_2B_2O_3$ samples obtained by the discharge technique indicate a higher stability for $H_2B_2O_3(g)$ than the data obtained from the $H_3B_3O_3$–O_2 reaction. In the electrical discharge experiment, the chemical mechanism for formation of $H_2B_2O_3$ is assumed to involve the reaction of oxygen with the borane intermediates as in the B_5H_9–O_2 reaction.[2,3a] In this case, the main products (aside from H_2) are $B_2H_6(g)$ and $H_2B_2O_3(g)$ while $O_2(g)$ and $H_3B_3O_3(g)$ are in relatively small yield. In the $H_3B_3O_3$–O_2 reaction, $H_3B_3O_3$ is present initially in the reaction vessel and a high concentration of O_2 is arbitrarily fixed. Thus, the two sets of data tend to establish upper and lower limits on K_{eq} and on the value of ΔH°. From the results given in Table I, we obtain for the "best value" of $\Delta H^\circ_{298}'$, 9.5 ± 1.5 kcal./mole. This value was combined with the heats of formation for $B_2H_6(g)$,[8] $B_2O_3(s)$,[8] and $H_3B_3O_3(g)$[11] of 7.5, −305.3, and −291 ± 2 kcal./mole, respectively, to give a heat of formation of −200.4 ± 3.5 kcal./mole for $H_2B_2O_3(g)$ at 298°K. The stability of $H_2B_2O_3(g)$ could have been determined by a thermochemical analysis of the reaction

$$^2/_3H_3B_3O_3(g) + {}^1/_2O_2(g) = H_2B_2O_3(g) \qquad (5)$$
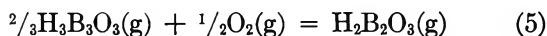
However, this would not afford an independent check on the heat of formation of $H_2B_2O_3(g)$ since the ΔH° for reaction 5 is a combination of the ΔH° for reaction 1 and ΔH° for the reaction

$$^1/_2B_2H_6(g) + B_2O_3(s) = H_3B_3O_3(g) \qquad (6)$$
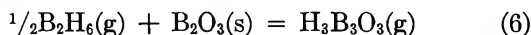
on which the heat of formation of $H_3B_3O_3(g)$ is based.[11]

The observation of Lee, Bauer, and Wiberley[4] that $H_3B_3O_3$ is a product in the explosive oxidation of B_5H_9 may be accounted for in a mechanism similar to that proposed in reaction 4. Under the conditions of their experiment, when oxygen is added to B_5H_9 in a 3:1 molar ratio, the products should contain B_2H_6, $H_2B_2O_3$, and unreacted oxygen. The explosion that occurs when this mixture is heated should result in a sudden temperature rise to shift the equilibrium

$$B_2H_6(g) = 2BH_3(g)$$
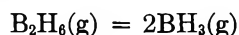
to the right, thus generating a transient concentration of BH_3. Under such conditions, reaction 4 is possible. The presence of intermediate boranes in these explosive oxidation reactions has been postulated previously.[2,12] A calculation based on the heat of formation of $H_2B_2O_3$ obtained here and published values for BH_3 (i.e., 18 kcal./mole) and $H_3B_3O_3$ indicates that reaction 4 is exothermic to the extent of 110 kcal./mole. Since gaseous boroxine is unstable with respect to B_2H_6 and B_2O_3 at ordinary temperatures, reaction 4 provides a mechanism for the ultimate decomposition of $H_2B_2O_3$ to B_2O_3 and H_2.

The chemical behavior of $H_2B_2O_3$ with respect to its formation from $H_3B_3O_3$ and its precursor relationship to $H_3B_3O_3$ is consistent with the C_{2v} structure[13]
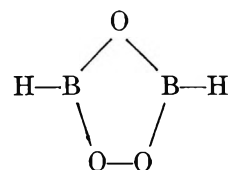
This structure enables us to visualize the reaction of $H_3B_3O_3$ and O_2 as an "addition" of O_2 to boroxine and reaction 4 as an insertion of a BH group into the $H_2B_2O_3$ ring at the O–O bond. The mass spectral patterns in Figure 2 show that $H_2B_2{}^{18}O_3$ is a minor product in the $H_3B_3O_3$–${}^{18}O_2$ reaction. The origin of this species is not entirely clear but it could be obtained from a reaction of ${}^{18}O_2$ with traces of B_4H_{10} or B_5H_9, i.e., pyrolysis products from B_2H_6. Similarly, the production of small amounts of ${}^{10}B_2{}^{11}BO_3H_3$ in the reaction of traces of oxygen with the higher boranes produced from ${}^{10}B$-enriched diborane upon electrical discharge. Interconversion reactions between H_2B_2O and $H_3B_3O_3$ also may lead to some redistribution of isotopic species.

Appearance potential measurements gave an ionization potential of 13.6 ± 0.2 v. for $H_2B_2O_3(g)$. The major ion fragments on electron impact are $HB_2O_3{}^+$, $HBO_2{}^+$, and HBO^+. Appearance potentials for these ions are 15.5 ± 0.2, 14.5 ± 0.4, and 14.5 ± 0.4 v., respectively. The ionization potential of $H_2B_2O_3$ is close to the value of 13.5 v. reported for $H_3B_3O_3(g)$.[5]

(11) R. F. Porter and S. K. Gupta, *J. Phys. Chem.*, **68**, 280 (1964).

(12) A. T. Whatley and R. N. Peace, *J. Am. Chem. Soc.*, **76**, 1996 (1954).

(13) C. C. Costain, W. V. F. Brooks, and R. F. Porter, "The Microwave Spectrum and Structure of $H_2B_2O_3$," to be published.

NOTES

Estimation of the Dielectric Constant of Water to 800°[1]

by Arvin S. Quist and William L. Marshall

Reactor Chemistry Division, Oak Ridge National Laboratory, Oak Ridge, Tennessee (*Received March 8, 1965*)

The electrical conductances of dilute aqueous solutions of K_2SO_4[2] and other salts have been measured in this laboratory at temperatures to 800° and pressures to 4000 bars. In order to use the Onsager limiting law[3] to calculate the theoretical variation of conductance with concentration, the dielectric constant of the solvent must be known. Although this constant for water has not been measured at temperatures above 393°, it has been estimated to 800° and densities of 1.0 g. cm.$^{-3}$ by Franck.[4] These estimates were based on a graphical fit of the Kirkwood equation for the dielectric constant of polar liquids[5,6] to several sets of experimental data. Since 1956 additional results on water have been published. Therefore, we have reviewed the previous and more recent data and have applied computer techniques in an attempt to obtain better estimates of this constant at high temperatures and pressures.

The experimental data used by Franck were those of Wyman[7,8] (0 to 100°, 1 atm.), Akerlöf and Oshry[9] (110 to 370° in the presence of vapor), and Fogo, Benson, and Copeland[10] (377 to 393° at densities from 0.2 to 0.5 g. cm.$^{-3}$). Other earlier measurements include those of Kyropoulos[11] (20° to pressures of 3000 kg. cm.$^{-2}$ or 2942 bars), Lees[12] (0 to 50° at pressures to 12,000 kg. cm.$^{-2}$ or 11,770 bars), Harris, Haycock, and Alder[13] (25.6° to pressures of 127 atm.), and Scaife[14] (20° at pressures to 6000 kg. cm.$^{-2}$ or 5884 bars). More recent measurements are those of Owen, *et al.*[15] (0 to 70° at pressures to 1000 bars), Vidulich and Kay[16] (0 to 40° at atmospheric pressure), and T. E. Gier and H. S. Young[17] (at 200, 250, 301, and 350° at pressures to 2000 bars).

By using a modification of Franck's approach,[4] the Kirkwood equation

$$\frac{(2\epsilon + 1)(\epsilon - 1)}{9\epsilon} = \frac{4\pi Nd}{3M}\left(\alpha + \frac{\mu^2 g}{3kT}\right) \quad (1)$$

(where ϵ is the dielectric constant, N is Avogadro's number, k is the Boltzmann constant, M is the molecular weight in grams mole^{-1}, α is the polarizability,

which is 1.58×10^{-24} cm.^{3} mole^{-1},[18] μ is the dipole moment of the water molecule, T is degrees Kelvin, and g is the Kirkwood correlation factor that accounts for orientation between neighboring molecules) was used to calculate $\mu^2 g$ from the various values of dielectric constant. Densities of water were obtained from the tabulation of Voukalovitch[19] along the liquid-vapor equilibrium curve, and from those values of Kennedy[20–24] and Sharp[25] at higher temperatures and pressures. Values of $\mu^2 g$ calculated in this manner from several sets of data are shown in Figure 1.

At low densities (and of necessity at high temperatures for water, which has a critical temperature of 374° and critical density of 0.32 g. cm.$^{-3}$), short-range interactions between molecules (*e.g.*, hydrogen bonding) should become small, and, as density approaches zero, the Kirkwood correlation factor theoretically should

(1) Research sponsored by the U. S. Atomic Energy Commission under contract with the Union Carbide Corp.

(2) A. S. Quist, E. U. Franck, H. R. Jolley, and W. L. Marshall, *J. Phys. Chem.*, **67**, 2453 (1963).

(3) L. Onsager, *Physik. Z.*, **28**, 277 (1927).

(4) E. U. Franck, *Z. physik. Chem.* (Frankfurt), **8**, 107 (1956).

(5) J. G. Kirkwood, *J. Chem. Phys.*, **7**, 911 (1939).

(6) G. Oster and J. G. Kirkwood, *ibid.*, **11**, 175 (1943).

(7) J. Wyman, Jr., *Phys. Rev.*, **35**, 623 (1930).

(8) J. Wyman, Jr., and E. N. Ingalls, *J. Am. Chem. Soc.*, **60**, 1182 (1938).

(9) G. C. Akerlöf and H. I. Oshry, *ibid.*, **72**, 2844 (1950).

(10) J. K. Fogo, S. W. Benson, and C. S. Copeland, *J. Chem. Phys.*, **22**, 209 (1954).

(11) S. Kyropoulos, *Z. Physik*, **40**, 507 (1926).

(12) W. L. Lees, Dissertation, June 1949, Department of Physics, Harvard University.

(13) F. E. Harris, E. W. Haycock, and B. J. Alder, *J. Chem. Phys.*, **21**, 1943 (1953).

(14) B. K. P. Scaife, *Proc. Phys. Soc.* (London), **B68**, 790 (1955).

(15) B. B. Owen, R. C. Miller, C. E. Milner, and H. L. Cogan, *J. Phys. Chem.*, **65**, 2065 (1961).

(16) G. A. Vidulich and R. L. Kay, *ibid.*, **66**, 383 (1962).

(17) A. W. Lawson and A. J. Hughes in "High Pressure Physics and Chemistry," Vol. I, R. S. Bradley, Ed., Academic Press Inc., New York, N. Y., 1963, Chapter 4, iv.

(18) R. M. Waxler and C. E. Weir, *J. Res. Natl. Bur. Std.*, **A67**, 163 (1963).

(19) M. P. Voukalovitch, "Thermodynamic Properties of Water and Steam," 6th Ed., Veb Verlag Technick, Berlin, 1958.

(20) G. C. Kennedy, *Am. J. Sci.*, **248**, 540 (1950).

(21) G. C. Kennedy, *ibid.*, **255**, 724 (1957).

(22) G. C. Kennedy, W. L. Knight, and W. T. Holser, *ibid.*, **256**, 590 (1958).

(23) W. T. Holser and G. C. Kennedy, *ibid.*, **256**, 744 (1958).

(24) W. T. Holser and G. C. Kennedy, *ibid.*, **257**, 71 (1959).

(25) W. E. Sharp, "The Thermodynamic Functions for Water in The Range −10 to 1000°C. and 1 to 250,000 Bars," University of California Radiation Laboratory Report UCRL-7118, 1962.
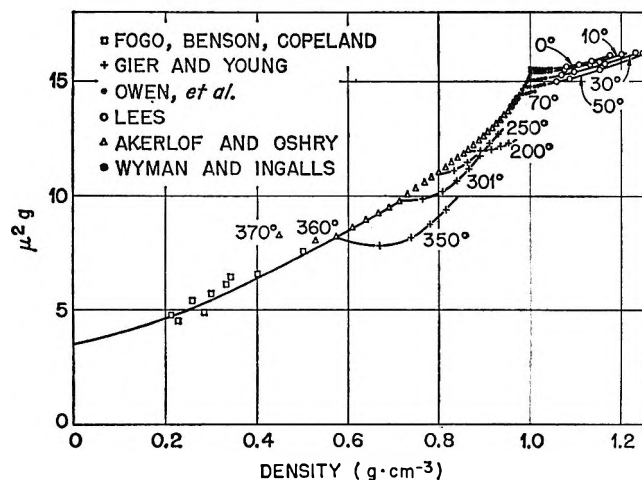
Figure 1. Calculated values of μ^2g (from the Kirkwood equation) for water.

approach a value of unity. Accordingly, the dipole moment of the water molecule would approach 1.87, the value reported for an isolated water molecule.[26] If the Kirkwood equation is correct, the term μ^2g should then approach 3.50 (1.87^2) at low densities and high temperatures. This behavior is observed in Figure 1, where it is seen that μ^2g extrapolates to approximately 3.50 at zero density. This observation based on experimental measurements substantiates the use of the Kirkwood equation.

Values of μ^2g obtained from the data of Owen, et al.,[15] and Lees[12] initially decrease as the density increases from approximately 1 g. cm.$^{-3}$ to higher values along the 0 and 10° isotherms. The viscosity of water in this low-temperature region also initially decreases with increasing density. Both μ^2g and viscosity isotherms at 20° and higher show a steady increase with increasing density.

The points at 360 and 370° in Figure 1 calculated from the constants of Akerlöf and Oshry deviate from the smooth curve. A corresponding deviation in dielectric constant was mentioned by Akerlöf and Oshry. Consequently, these two points were omitted in the determination of equations for μ^2g as a function of temperature and density. Those values of μ^2g obtained from the data of Gier and Young show some unexpected behavior. At 250, 301, and 350°, with increasing density they extrapolate to μ^2g values higher than the calculated values at 200° (compared at the same density at densities higher than approximately 0.9 g. cm.$^{-3}$). Also, when their experimental dielectric constants are plotted against density (not shown), at a density of 1.0 g. cm.$^{-3}$ the extrapolated value for the dielectric constant at 250° is somewhat greater

than the experimental value at 200°. The reverse behavior would be expected.

Several types of equations estimating μ^2g as a function of temperature and density were fitted to the data in Figure 1 (excepting those of Gier and Young) by the use of a generalized least-squares program.[27] The equation that best fitted the data had the form

$$\mu^2g = 3.50 + d(A_1 + A_2(d) + A_3(d)^2)f(T) \quad (2)$$

where A_1, A_2, and A_3 are adjustable parameters, d is the density in g. cm.$^{-3}$, and f(T) is a function of temperature (°K.) represented by either of the three equations

$$f(T) = T^{-0.5} \quad (3)$$

$$f(T) = T^{-A_4} \quad (4)$$

$$f(T) = e^{-A_4(T)} \quad (5)$$

where A_4 is another adjustable parameter. In obtaining the parameters for eq. 2 through 5, several combinations of the various sets of experimental data were tried. Those parameters considered most reliable were obtained by combining and using the data of Owen, et al.[15] (88 points, 0–70°, by 10° intervals, 1–1000 bars, by 100-bar intervals), Lees[12] (22 points), and Akerlöf and Oshry[9] to 350° (25 points, every 10° from 110 to 350°, as given in the table in their paper), and three values joining Owen's data to the Akerlöf-Oshry data (80, 90, 100°). All data were given equal weight. Each of the functions represented by the combination of eq. 2 with eq. 3, 4, or 5 fitted the experimental data equally well as judged from the standard error of each parameter and variance of fit obtained from the least-squares program. The parameters obtained for the combinations of eq. 2 with eq.

Table I: Values for Parameters in Eq. 2 and 3, 2 and 4, and 2 and 5

Eq.	A_1	A_2	A_3	A_4	ϵ, calcd. at 800° and 1.0 g. cm.$^{-3}$	ϵ, calcd. at 200° and 1.0 g. cm.$^{-3}$
(2) and (3)	175	136	−111	...	15.1	42.3
(2) and (4)	11.0	167	−94	0.35	16.9	44.1
(2) and (5)	12.2	13.7	−9.8	0.00113	12.9	42.6

(26) R. A. Robinson and R. H. Stokes, "Electrolyte Solutions," 2nd Ed., Butterworths Scientific Publications, London, 1959, p. 1.

(27) M. H. Lietzke, "A Generalized Least Squares Program for the I.B.M. 7090 Computer," USAEC Report ORNL-3259, 1962.

Table II: Dielectric Constant of Water Calculated from Eq. 1-3 Using the Parameters from Table I

Temp., °C.	Density, g. cm.$^{-3}$										
	0.0001	0.1	0.2	0.3	0.4	0.5	0.6	0.7	0.8	0.9	1.0
0										(88.4)^a	88.4
25										(78.1)^a	78.5
100										(54.6)^a	58.0
200									(34.3)^a	36.4	42.3
300								(20.0)^a	23.8	28.4	33.0
400	1.001	1.83	3.13	4.9	7.1	9.7	12.7	16.0	19.5	23.2	26.8
500	1.001	1.71	2.81	4.3	6.1	8.3	10.8	13.5	16.5	19.5	22.6
600	1.000	1.63	2.58	3.9	5.4	7.3	9.4	11.7	14.2	16.8	19.4
700	1.000	1.56	2.40	3.5	4.9	6.5	8.3	10.4	12.5	14.8	17.0
800	1.000	1.51	2.26	3.2	4.5	5.9	7.5	9.3	11.2	13.2	15.1

^{a} For liquid in equilibrium with vapor at the temperatures shown in the heading.

3, 4, or 5 are given in Table I. For comparison, calculated values are included for the dielectric constant of water at 200 and 800° at a density of 1.0 g. cm.$^{-3}$ using these parameters.

Since eq. 2 and 3 gave an intermediate value at 800°, this combination was used to calculate the dielectric constants for water at integral temperatures and densities given in Table II. The values are generally somewhat lower (10–20% at 1.0 g. cm.$^{-3}$; 3% at 0.6 g. cm.$^{-3}$; no difference at 0.2 g. cm.$^{-3}$) than those of Franck.[4] With eq. 2 and 3 the average deviation of the calculated dielectric constants from the experimental values used to obtain the parameters was 1.1%.

At densities from 0 to 1.0 g. cm.$^{-3}$ the value of $\mu^2 g$ for water might be expected to lie between the limits of 3.50 (where g is unity) and 15.55 (Figure 1, at 0° and $d = 1.0$ g. cm.$^{-3}$). By substituting these limiting values for $\mu^2 g$ into the Kirkwood equation, boundaries of 6.53 and 23.1 for the dielectric constant were obtained at 800° and a density of 1.0 g. cm.$^{-3}$. The calculated constant (15.1) given in Table II lies within these limits.

When only the data along the liquid–vapor equilibrium curve were used to obtain the parameters, it was found that a combination of eq. 2 and 4 gave the best fit, using parameters of 43.0462 (A_1), 43.3064 (A_2), −14.7365 (A_3), and 0.318561 (A_4). The average deviation of the calculated dielectric constants from the experimental values (from 0–350°) was 0.12% with the largest difference (0.39%) at 350°.

Acknowledgments. The authors wish to thank Professor J. E. Ricci, New York University, for helpful discussions on this work. The advice of Dr. M. H. Lietzke, ORNL, on the use of his computer program is gratefully acknowledged.

Dissociation Studies in High Dielectric Solvents. V. Magnesium Sulfate as an Unassociated Salt in N-Methylformamide

by Gyan P. Johari and P. H. Tewari

Chemistry Department, University of Gorakhpur, Gorakhpur, India
(Received May 19, 1965)

We have demonstrated that $MgSO_4$ behaves as a slightly associated salt in formamide, and the Fuoss–Onsager theory predicts its conductance data satisfactorily.[1] This salt has been found as completely unassociated in another amide solvent, N-methylformamide ($D = 182.4$).[2] The solvent was purified by keeping it over anhydrous $AlCl_3$, refluxing, and fractionally distilling it at least four times under reduced pressure (specific conductance 0.8–1.5 × 10^{-6} mho cm.$^{-1}$, viscosity 0.0165 poise, and density 0.99885 g./ml.; viscosity and density values are in good agreement with the literature value[3]).

The apparatus and the *modus operandi* for the conductance measurements have been described in previous communications.[1] The conductance of the solution was obtained by subtracting the conductance of the solvent of the same batch determined separately in a cell. All resistance measurements were obtained from solutions prepared from solvents which were purified less than 24 hr. before.

(1) G. P. Johari and P. H. Tewari, *J. Phys. Chem.*, **69**, 696 (1965).
(2) G. R. Leader and J. F. Gormley, *J. Am. Chem. Soc.*, **73**, 5731 (1951).
(3) C. M. French and K. H. Glover, *Trans. Faraday Soc.*, **51**, 1417 (1955).

Table I

$C \times 10^4$, M	3.068	5.599	7.960	10.701	13.821	19.471	27.032
Equiv. conductance	43.440	42.750	42.339	41.891	41.430	40.751	40.022

The equivalent conductance concentration data of $MgSO_4$ (same as used in the previous study[1]) at 25° are shown in Table I.

The data were analyzed by the Fuoss–Onsager equation[4] for unassociated electrolytes in the form

$$\Lambda = \Lambda^0 - Sc^{1/2} + Ec \log c + Jc \qquad (1)$$

on an IBM 7094 computer using a Fortran program similar to that described by Kay[5] (higher terms in $c^{1/2}$ were neglected and the Einstein correction term in the viscosity was set to zero).

The results of the analysis are given below where Λ^0 is the limiting equivalent conductance, a_J is the ion-size parameter from J terms in the equation, and $\sigma\Lambda$ is the standard deviation in $\Delta\Lambda$-units of the data from the equation.

Λ^0	S	E	J	a_J	$\sigma\Lambda$
45.31 ± 0.01	109.2	56.75	288.3	3.38 ± 0.10	0.002

Thus eq. 1 describes the conductance data very well. An ion size of 3.38 Å. is a reasonable value for $MgSO_4$. The experimental data in the phoreogram do not show any crossover at the limiting law curve.[4] This is because in this case the theoretical crossover concentration C_x is 8.32×10^{-6} M and the maximum concentration C_{max} is 4.42×10^{-6} M. Evidently these concentrations are too low to be observed in the conductance data reported.

This work adds to the small group of known high charge symmetrical salt–solvent systems, whose conductance data are adequately represented by the modern theory. It also suggests that the well-known 2–2 salt which is highly associated in water[6] is unassociated in N-methylformamide. At present we hope to extend this study to other 2–2 salts as well as to mixtures of N-methylformamide with solvents of lower dielectric constant.

Acknowledgment. The authors wish to thank Dr. R. P. Rastogi, Head of the Chemistry Department, for providing the necessary facilities and the research group of Dr. G. Atkinson of the University of Maryland

(4) R. M. Fuoss and F. Accascina, "Electrolytic Conductance," Interscience Publishers, Inc., New York, N. Y., 1959.

(5) R. L. Kay, *J. Am. Chem. Soc.*, **82**, 2099 (1960).

(6) H. S. Dunsmore and J. C. James, *J. Chem. Soc.*, **82**, 2099 (1960).

for computer processing of the data. G. P. J. is thankful to the University Grants Commission, New Delhi, for granting a fellowship.

Some Electrochemical Aspects of Germanium Dissolution. Valence States and Electrode Potential

by Walter E. Reid, Jr.

National Bureau of Standards, Washington, D. C.
(Received December 30, 1964)

Germanium has been reported to dissolve anodically in aqueous solutions with a valence of 4.[1] At high current densities and on prolonged electrolysis, the formation of a white to orange-red oxide film is usually observed on the Ge at the solution–gas interface. The formation of this film and the fact that it contains divalent germanium have been explained in various ways.[1-3] This evidence indicates that Ge dissolves with valences of both 2 and 4. Anodic dissolution efficiencies of about 103–105% have, in fact, been reported.[4] Investigation of the equilibrium potential of the Ge electrode has also indicated that Ge^{2+} is involved.[5]

In the present investigation the anodic dissolution of Ge was examined to determine if the accompanying formation of divalent Ge is governed by thermodynamic or kinetic processes or by both and to determine quantitatively the ratio of Ge^{2+}/Ge^{4+} produced. From this information an estimate could then be made of the standard electrode potential of germanium.

Experimental

Preliminary experiments showed that, for an assumed dissolution valence of 4, Ge (n and p types)

(1) F. Jirsa, *Z. anorg. allgem. Chem.*, **268**, 84 (1952).

(2) F. Beck and H. Gerischer, *Z. Elektrochem.*, **63**, 500 (1959).

(3) D. R. Turner, *J. Electrochem. Soc.*, **103**, 252 (1956).

(4) M. V. Sullivan, D. L. Klein, R. M. Finne, L. R. Pompliano, and G. A. Kolb, *ibid.*, **110**, 412 (1963).

(5) B. Lovrecek and J. O'M. Bockris, *J. Phys. Chem.*, **63**, 1368 (1959).

dissolved anodically with an efficiency of 101–105% at room temperature in both acidic and basic solutions. In no case was the formation of finely divided elemental Ge observed at the anode.

To determine quantitatively the amount of divalent Ge produced, the Ge was dissolved in acidic KI solutions and the Ge^{2+} then oxidized by iodine generated electrolytically *in situ*. Although preliminary experiments showed that solutions of KI of concentrations 5, 10, and 20 wt. % were equally effective, most of the experiments were performed in a 20% KI solution which was 1 M with respect to H_2SO_4. The high acidity was necessary to prevent precipitation of metagermanic acid as the germanium content of the solutions increased. The anode compartment was a four-neck flask containing a Teflon-encased stirring magnet, a siphon tube leading to the cathode compartment (a beaker containing the same solution used in the anode compartment), a gas inlet and exit (exit tube exhausting into a water trap of about 0.5-cm. head), an auxiliary Pt electrode for generating I_2 *in situ*, and a very small siphon which was used initially to prepare the solutions as described below. The siphons were both equipped with glass frits to minimize diffusion between the two compartments being used. A brass clamp, attached to a long copper rod which passed through a rubber stopper, was used to support the Ge rod specimen used. The anode ensemble could be placed in the anode compartment, and, after flushing the flask with N_2, the Ge specimen could be lowered into the solution.

Nitrogen was bubbled through the 1 M H_2SO_4 solution placed in the anode compartment for 1 hr. before the KI was added to ensure that most of the dissolved oxygen would be removed. This usually gave a colorless solution upon addition of the KI, but in those cases where a yellow color did appear some Ge was dissolved anodically using a removable auxiliary Ge anode and an external cathode *via* the small auxiliary siphon until the solution was colorless. Then, I_2 was generated until a very slight yellow color appeared. This was taken as the reproducible starting point for the experiment. The siphon connecting the anode and cathode compartments was filled by suction, and the Ge electrode to be used was placed in the solution.

The Ge was dissolved anodically at a fixed current for a definite time. After this, I_2 was generated *in situ* using the Pt anode at a fairly low constant current with moderate stirring until the appearance of a slight yellow color. The number of coulombs (it) required to produce the I_2 was taken as the number of coulombs required to oxidize the Ge^{2+} formed in the Ge dissolution process. The visual detection of the end point was found to be accurate to within 0.2 mg.

Although there was some heating of the solutions at the higher current densities for the experiments of 2-hr. duration, this was not considered a significant factor since the short-time experiments at similar current densities gave essentially the same results. The exposed area of the p-type Ge anode used was 8 cm.^{2}. Its resistivity was 18 ohm-cm.

Experimental Results

Ge was dissolved at various current densities to determine if the amount of Ge^{2+} produced was related to the current density. The results are given in Table I.

Table I

Current density, ma./cm.^{2}	Total coulombs for Ge dissolution	Coulombs for I_2	% coulombs for Ge^{2+}	Mole % Ge^{2+}
6	6	0.25	4.2	8.0
13	30	1.0	3.3	6.5
31	92	3.0	3.3	6.3
90	294	11.2	3.8	7.3

In other experiments performed in a similar manner for longer periods of time the results in Table II were obtained.

Table II

Current density, ma./cm.^{2}	Time, min.	Coulombs	Wt. of Ge dissolved, g.	Calcd. wt. of Ge dissolved, g., 0.18813 mg. = 1 coulomb	% anode efficiency, actual/calcd. wt. × 100
90	125	5250	1.0288	0.9877	104.2
44	120	2520	0.4893	0.4741	103.2
38	120	2160	0.4210	0.4064	103.6

Discussion

It is thus clearly established that germanium dissolves anodically with valences of Ge^{2+} and Ge^{4+} and the average amount of Ge^{2+} appearing is about 7 mole % of the total, a value which is independent of the current density within experimental error. Since the fraction of Ge^{2+} formed is independent of current density, its formation is attributed to the relative free energy of formation of the two species rather than to certain interfacial phenomena which could affect their relative rates of formation.

Previous qualitative observations of oxide formation at the Ge solution–gas interface[2] can be reconciled

with the above data as follows. For n-type and high resistivity p-type Ge the potential drop at the Ge solution interface can become large enough at very high current densities for O_2 to be evolved in H_2SO_4 solutions. As shown elsewhere,[6] the actual potential drop at the Ge solution interface is always fairly low for low resistivity p-type Ge even at high current densities. The actual potential of the bulk Ge may be very high, however. At the solution–gas interface of a Ge anode dissolving at moderate current densities, there generally exists a large potential gradient. The high charge on the Ge increases its wettability considerably,[7] and the solution tends to be drawn up onto the part of the Ge anode which is not in the solution. At these higher potentials the formation of O_2 or I_2 occurs readily, and I_2 evolution can easily be observed near the solution–gas interface at moderate to high current densities for a brief period after electrolysis is begun when acidic KI solutions are used. This behavior may have caused small errors in the values reported above. Normally, an oxide film is formed at the solution–gas interface on the polarized anode. This results because of the insolubility of the reaction products in the small amount of solution drawn up on the anode; this oxide film usually increases in thickness and area with time. The scarcity of solution above the solution–gas interface favors the formation of divalent Ge compounds such as GeO since the availability of oxidizable materials other than Ge is limited. (Qualitatively it was observed that, when the solution was stirred so that the solution occasionally wetted the oxide film, it usually became white. When the solution was not stirred, the oxide film was orange in color indicating a higher concentration of lower valent Ge ions.) In some cases the growth of the oxide films was observed to extend below the solution–gas interface, but this was attributed to the growth process of the oxide film.

The oxide film was soluble in the solutions used, but its dissolution rate was low. In one case the thin oxide film formed at the solution–gas interface after about 10 hr. at 10 ma./cm.^{2} was a transparent glass which was very hard and brittle. In this case the oxide formed almost entirely at the interface and did not extend for any appreciable distance onto the region above the solution.

Since the oxide film normally contains both Ge^{2+} and Ge^{4+} oxides, it is very likely to have semiconductor properties of its own which may be considerably different from those of Ge. For those experiments listed in Table II any oxides formed were easily washed off with water.

The possibility exists that an anodic surface compound involving I^- ions may be involved in the dissolution of Ge in KI solution.[8] This could have an effect on the Ge^{2+}/Ge^{4+} ratio. This point was examined by following the pH change of the solution as Ge dissolved in 1 M NaCl and in 10% KI in 1 M NaCl as the pH changed from 8 to 3. In 1 M NaCl the anodic reaction is

$$Ge + 3H_2O \longrightarrow H_2GeO_3 + 4H^+ + 4e^-$$

For the NaCl solutions the pH change was followed with a glass electrode. For the KI solutions a mixed indicator was used. Repeated cycling between two fixed pH values at 2 to 5 ma./cm.^{2} required, within experimental error ($\sim$4%), the same number of coulombs for the anodic and the cathodic processes, both with and without KI in the solution, showing that the anodic process does not involve I^- ions directly for these experimental conditions.

The Ge Electrode Potential

Examination of the data in Table I shows an average Ge^{4+}/Ge^{2+} mole ratio of about 13.4 for a wide range of current densities. It is assumed this ratio exists at the unpolarized Ge electrode. Using the $E°$ (vs. n.h.e.) values obtained elsewhere[6] for the couples $Ge^{2+}/Ge^0 = 0.24$ v. and $Ge^{4+}/Ge^{2+} = 0.00$ v., the value of the couple Ge^{4+}/Ge^0 is calculated to be 0.12 v. There are experimental difficulties in measuring the standard electrode potential of Ge in highly acidic solutions,[5] but the expected value in 1 M H_2SO_4 can be estimated in the following way. Making the reasonable assumption that the formation of divalent and tetravalent Ge involves two reactions and knowing the average value of the fraction (f_1) of coulombs going to form Ge^{4+} ions (from Table I), it is shown that

$$E°_{Ge} = (1 - f_1)E°_{Ge^{2+}/Ge^0} + f_1E°_{Ge^{4+}/Ge^0}$$

or

$$E°_{Ge} = 0.037(0.24) + 0.963(0.12) = 0.12_4 \text{ v.}$$

in good agreement with the expected thermodynamic value (ref. 7, p. 205) and the $E°_{Ge}$ ($\sim$0.12 v.) estimated from the experimental value of the Ge electrode potential obtained by Lovrecek and Bockris at pH 0.[5] The proof of this equation is based on general thermodynamic considerations. The path of formation of hydrated tetravalent Ge ion can be considered to involve two states

(6) W. E. Reid, Jr., *J. Phys. Chem.*, **69**, 2269 (1965).

(7) C. G. B. Garrett, "The Electrochemistry of Semiconductors," P. J. Holmes, Ed., Academic Press, Inc., New York, N. Y., 1962, p. 153.

(8) W. W. Harvey, W. J. Lafluer, and H. C. Gatos, *J. Electrochem. Soc.*, **109**, 155 (1962).

$$\text{Ge} \longrightarrow \text{Ge}^{2+} + 2e^- \qquad E^\circ{}_2 = 0.24 \text{ v.} \qquad (1)$$

$$\text{Ge}^{2+} \longrightarrow \text{Ge}^{4+} + 2e^- \qquad E^\circ{}_{2-4} = 0.00 \text{ v.} \qquad (2)$$
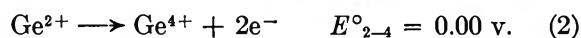
The free energy change would then be given by

$$\Delta G^\circ = -4\mathfrak{F}E^\circ{}_4 = -(2\mathfrak{F}E^\circ{}_2 + 2\mathfrak{F}E^\circ{}_{2-4})$$

which gives

$$E^\circ{}_4 = {}^2\!/_4 E^\circ{}_2 + {}^2\!/_4 E^\circ{}_{2-4} = \frac{E^\circ{}_2 + E^\circ{}_{2-4}}{2}$$

If, however, all of the ions formed in (1) are not oxidized in step 2, then the standard electrode potentials must be corrected. Assuming that the process is reversible and no other equilibria are involved, we have

$$-(4Z - 2\alpha)E_{\text{obsd}}\mathfrak{F} = -[2ZE_2\mathfrak{F} + 2(Z - \alpha)E_{2-4}\mathfrak{F}]$$

where Z is moles of Ge ions formed, α is net moles of Ge^{2+} formed, $Z - \alpha$ is moles of Ge^{4+} produced, and $4Z - 2\alpha$ is equivalents of Ge dissolved; α is not arbitrary but is determined by the experimental conditions.

Substituting into the above equations

$$E_2 = E^\circ{}_2 - RT/2\mathfrak{F} \ln a_{\text{Ge}^{2+}}/a_{\text{Ge}^0}$$

$$E_{2-4} = E^\circ{}_{2-4} - RT/2\mathfrak{F} \ln a_{\text{Ge}^{4+}}/a_{\text{Ge}^{2+}}$$

$$E_4 = E^\circ{}_4 - RT/4\mathfrak{F} \ln a_{\text{Ge}^{4+}}/a_{\text{Ge}^0}$$

$$2E^\circ{}_4 = E^\circ{}_2 + E^\circ{}_{2-4}$$

gives

$$E_{\text{obsd}} = \frac{2Z}{2Z - \alpha}E^\circ{}_4 - \frac{\alpha}{2Z - \alpha}(2E^\circ{}_4 - E^\circ{}_2) - \frac{RT}{(4Z - 2\alpha)\mathfrak{F}}[(Z - \alpha) \ln a_{\text{Ge}^{4+}} + \alpha \ln a_{\text{Ge}^{2+}}]$$

or

$$E_{\text{obsd}} = E^\circ - \frac{RT}{\mathfrak{F}}\left(\frac{Z - \alpha}{4Z - 2\alpha}\right) \ln a_{\text{Ge}^{4+}} - \frac{RT}{\mathfrak{F}}\left(\frac{\alpha}{4Z - 2\alpha}\right) \ln a_{\text{Ge}^{2+}}$$

The present state of knowledge of Ge ions in solution does not enable a precise evaluation of the last term in this equation to be made; however, the standard electrode potential of Ge can be estimated to be 0.124 v. since Z and α are constant, and only the activities are variables.

The effect of impurity type and concentration in the Ge anode and electrolyte composition on the fraction of divalent ions formed was not investigated.

The relatively large amount of Ge^{2+} formed at the Ge anode suggests much smaller differences than exist between the relative values of the respective Ge couples.

The constancy of the $\text{Ge}^{4+}/\text{Ge}^{2+}$ ratio over such a wide range of current densities indicates, however, that the extrapolation of this ratio to zero current may be valid. Reconciling these two facts requires that the activities of the Ge^{2+} and Ge^{4+} ions be fairly small or that the electrode be, at most, only slightly reversible. The data suggest that both factors may be involved. Irrespective of the validity of the assumptions made, the calculations do show that the true equilibrium value of the $\text{Ge}^{4+}/\text{Ge}^{2+}$ mole ratio will not be substantially less than that reported here, and E° for this electrode will be within a few millivolts of the potential value indicated.

Aqueous Solubilities of n-Dodecanol, n-Hexadecanol, and n-Octadecanol by a New Method

by Frank P. Krause and Willy Lange

The Procter & Gamble Company, Miami Valley Laboratories, Cincinnati, Ohio 45239 (Received February 23, 1965)

n-Hexadecanol and n-octadecanol have attracted considerable interest for retarding evaporation from lakes and reservoirs.[1] This usage and the improved drought tolerance of plant seedlings grown in soil to which long-chain fatty alcohols have been added[2] made experimental data on the water solubility of the alcohols desirable. The conventional method of solubility determination failed with these alcohols because (a) during the agitation of the crystals in water, film fragments are dispersed in the solution and are very difficult to remove and (b) saturation of the solution is lost during the removal of dispersed matter and transfer to a new vessel due to adsorption of the alcohols at the newly available air–water and glass–water interfaces.

In the present method, solution in water of the C^{14}-labeled fatty alcohols proceeds from a virtually stationary surface film that is in contact with excess alcohol in the bulk phase. Any turbulence in the solution is avoided. Film fragmentation and dispersion does not occur, and hence no processing of the solutions prior to the determination of the dissolved alcohol is needed.

(1) V. K. La Mer, Ed., "Retardation of Evaporation by Monolayers: Transport Processes," Academic Press Inc., New York, N. Y., 1962.

(2) W. Lange, *Bull. Intern. Assoc. Hydrology*, 9, 71 (1964).

Experimental

Material. The fatty alcohols were C^{14}-labeled at position 1. *n*-Dodecanol with a specific activity of 25 mcuries/g. was prepared in this laboratory ($C_{11}H_{23}Br$, Grignard addition of $C^{14}O_2$, reduction of the tagged lauric acid). *n*-Hexadecanol and *n*-octadecanol with specific activities of 6 mcuries/g. were purchased.[3] All three compounds were purified by vapor phase chromatography. In each case, 10 mg. was processed and 4–5 mg. of the major fraction collected. Dodecanol was passed through a 0.6 × 200 cm. column of 30% diglycolic acid polyethylene glycol on 60/80-mesh Chromosorb W at 180° with helium carrier at a flow rate of 50 cm.³/min., hexadecanol through a 0.5 × 75 cm. column of 10% Dow-Corning silica-free silicone (prepared from high-vacuum silicone stopcock grease by petroleum ether (b.p. 38–56°) extraction of the silicone fraction) on 60/80-mesh Chromosorb W at 162° with helium at 62 cm.³/min., and octadecanol through a 0.6 × 75 cm. column of 20% Tween 80 on 60/80-mesh HMDS–Chromosorb W at 180° with a helium flow rate of 67 cm.³/min.

The purified dodecanol was diluted with 99 parts of an inactive, 99.5% pure *n*-dodecanol. The purified hexadecanol and octadecanol were used as is. All three compounds were kept in hexane solution at concentrations of 0.1–1%. The fatty alcohols were free of comparatively water-soluble impurities, such as lower homologs; *e.g.*, two solubility determinations with dodecanol at 16°, one with 1 mg. and the other with 5 mg., gave the same results.

Apparatus. Saturated aqueous solutions of the fatty alcohols were prepared in a closed cylindrical glass container with rounded bottom. Near the bottom was a horizontal, eye dropper type outflow tip which was capped by a hollowed-out rubber stopper. The top was stoppered with a downward-curving glass vent tube containing a wad of glass wool. A Teflon-coated spherical magnet at the bottom of the vessel stirred the solution. The vessel had a cross-sectional area of 60 cm.² and a volume of about 700 ml. It was stored in a constant-temperature box.

Solution of Fatty Alcohols in Water. About 500 ml. of distilled water in the vessel was sterilized by boiling and was then cooled to or below the test temperature after closure of the vessel. (Sterilization was effected because fatty alcohols are an excellent carbon source for certain microorganisms.[4]) An aliquot of the hexane solution of the fatty alcohol was quickly transferred to the surface of the water, and the hexane was evaporated with a stream of heat-sterilized and cooled nitrogen. Care was taken that the evaporating hexane

droplets remained near the center of the water surface. When all the hexane had evaporated, the fatty alcohol crystals or droplets were held in place by the surface film. The amounts of fatty alcohols used were 1–5 mg. of dodecanol, 0.2 mg. of hexadecanol, and 0.1 mg. of octadecanol, respectively. In one test, 5 mg. of solid dodecanol was added as such to the surface of the water at 16°.

After the addition of the fatty alcohol, the water was agitated with a magnetic stirrer at such a predetermined rate that in the absence of a film the surface of the water rotated roughly at the rate of 1 r.p.m., as indicated by a marker or speck of dust on the surface. The films reduced the movement of the surface to a few revolutions per day. When the surface movement increased, the film was considered to have become defective, and the test was discarded.

Samples of the solution were periodically withdrawn from the eye dropper type tip for fatty alcohol determination by removing the rubber cap and permitting the aqueous solution to jet out of the vessel in a thin stream. The first 5–10 ml. was discarded. The following 10–25 ml. was collected in a 50-ml. graduate. Exposure of the jet stream to open air was minimized, and use of a funnel was avoided. After collection of the sample, the graduate was immediately closed with a glass stopper, and the solution was made ready for counting.

Solution of the films was allowed to proceed until the fatty alcohol concentration in the water was constant. This usually required 1–2 weeks (Figure 1). The slow approach to equilibrium may well be due to the time required for adsorption of the fatty alcohol on the glass surface of the containing vessel. Under these circumstances the analysis of samples withdrawn into a clean graduated cylinder and analyzed will not be subject to error due to adsorption of the dissolved alcohol on this fresh surface.

Determination of Fatty Alcohols in Water. Without delay, the solution samples collected for analysis were diluted with about 10 ml. of ethanol and were then extracted with 10 ml. of hexane. Five milliliters of the hexane layer was diluted with 5 ml. of a phosphor-toluene stock solution[5] and counted in a liquid scintillation spectrometer. From the sample count, the count of a similarly prepared standard of about the same concentration, and the hexane and solution volumes, the concentration of the fatty alcohol in the solution was calculated.

(3) Isotopes Specialties Co., Burbank, Calif.

(4) F. P. Krause and W. Lange, *Appl. Microbiol.*, **13**, 160 (1965).

(5) J. D. Davidson and P. Feigelson, *Intern. J. Appl. Radiation Isotopes*, **2**, 1 (1957).
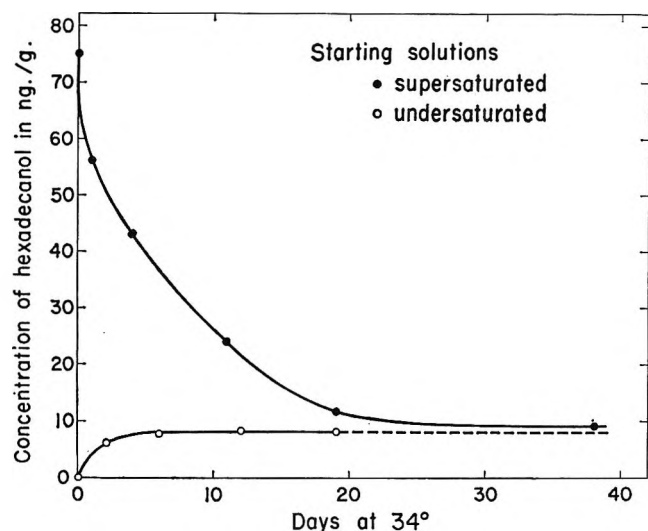
Figure 1. Determination of the solubility of hexadecanol in water at 34° with excess alcohol in the bulk phase. Approach to equilibrium concentration from undersaturated and supersaturated solutions. Supersaturation obtained by heating the water with excess hexadecanol at the interface for 1 day at 80° and cooling to 34°.

Completeness of the extractions was ascertained by separate tests in which ethanol solutions of similar but known amounts of the labeled fatty alcohols were transferred into ethanol–water systems, extracted with hexane, and the fatty alcohols then determined as described. Direct addition of the same quantities of the fatty alcohols in hexane to the phosphor solution also gave the same counts.

Validity and Accuracy of the Determinations. Saturation equilibrium at 34° with hexadecanol was approached as described and also by starting with a solution initially supersaturated at 80°. The results (Figure 1) show that, within the limits of accuracy of the tests, the same equilibrium concentrations were obtained.

Probably the largest source of error in the determination was the slight warming of the solutions above the temperature of the ambient air by the magnetic stirrer. Although allowance for the heating was made in the recorded temperatures, the corrections were uncertain by 1–2°, as determined in pilot tests. Primarily for this reason, the accuracy of the determinations is estimated at only ±10%. The solubility of octadecanol at 34° is probably even less accurate.

Results and Discussion

In Table I are listed the solubilities of dodecanol, hexadecanol, and octadecanol at 34° and at other temperatures below and above the melting point of the alcohols. Kinoshita[6] reported a formula

$$\ln c = -1.39n + 5.53 \qquad (1)$$

to relate with good accuracy the solubility c (mole/liter) of the normal primary alcohols from butanol to decanol in water at 25° to n, the number of carbon atoms in the alcohols. Data calculated by eq. 1 are included in the table. As expected, the solubilities of the fatty alcohols increase with increasing temperature, decrease with increasing chain length of the alcohols, and are exceedingly low for hexadecanol and octadecanol. The calculated solubilities agree approximately with the experimental solubilities. With allowance for the temperature difference, the agreement is quite good for dodecanol, which is liquid at 34°. The solubility of hexadecanol, however, is definitely lower than that given by eq. 1, probably because the compound is a solid at 34°. At 25° the actual solubility of hexadecanol may be only half the calculated one. The solubility of octadecanol is apparently in good agreement with eq. 1 but, being exceedingly low, merits no further consideration.

Table I: Solubilities of Fatty Alcohols in Water

Temp., °C.	Dodecanol (m.p. 25°), mole/l. × 10⁹	Hexadecanol (m.p. 49°), mole/l. × 10⁹	Octadecanol (m.p. 59°), mole/l. × 10⁹
	Exptl.		
16	9,100		
34	15,600	33	4
49	19,300		
55		127	
65			22
	Calcd. by eq. 1		
25	14,400	55	3

Polymorphism should not be a factor in the present solubility determinations since the same results (within experimental error) were obtained with bulk phase formed by evaporation of a hexane solution below the melting point and by crystallization from a melt floating on the water surface (Figure 1). The existence of fatty alcohol hydrates[7] may have only a minor bearing on these determinations.

The new method for the determination of aqueous solubilities may be applicable to a variety of synthetic and biological surface-active compounds of extremely low solubility.

(6) K. Kinoshita, et al., Bull. Chem. Soc. Japan, **31**, 1081 (1958).
(7) A. S. C. Lawrence, A. Bingham, C. B. Capper, and K. Hume, J. Phys. Chem., **68**, 3470 (1964).

Knudsen and Langmuir Measurements

of the Sublimation Pressure of

Cadmium(II) Fluoride

by G. Besenbruch, A. S. Kana'an, and
J. L. Margrave

Department of Chemistry, Rice University, Houston, Texas
(Received March 3, 1965)

Sublimation pressures for CdF_2 have been measured over wide ranges of temperature by both the Knudsen and Langmuir techniques utilizing a vacuum semimicro balance. Vaporization data for CdF_2 were reported by Ruff and LeBoucher,[1] who investigated the vapor pressure of CdF_2 over the temperature range 1689–2023°K. by a boiling point technique. Brewer, *et al.*,[2] in their review of thermodynamic properties of gaseous metal dihalides, derived the heat of sublimation, $\Delta H°_{298} = 76$ kcal. mole^{-1}.

Experimental

The vapor pressure studies were carried out with an Ainsworth RVA-AU-2 semimicro balance which recorded the weight loss of the sample as a function of time. The sample (either a single crystal or a powder contained in a Knudsen cell) was suspended by a tungsten wire and enclosed in a quartz or Vycor tube. A Kanthal wire-wound tube furnace with a Barber–Coleman controller, Model 622, was used for maintaining the sample at the desired temperature ($\pm 1°$) as measured by a calibrated Pt—Pt–10% Rh thermocouple suspended inside the Vycor tube, with the junction and sample at the same level. The Knudsen cell was machined from a spectroscopic grade graphite rod and the orifice in the lid was 2.46 mm. in diameter and 0.56 mm. deep. The CdF_2 single crystal (surface area = 1.43 $\pm$ 0.2/cm.^{2}) was obtained from Semi-Elements Inc., Saxonburg, Pa. After the Langmuir studies were completed, the crystal was powdered for the Knudsen studies.

For increased accuracy, two or more measurements of the rate of weight loss at each temperature were made and the vapor pressure was calculated from the appropriate equations[3] on the assumption that $CdF_2(g)$ is the vapor species. Mass spectrometric studies of related fluorides by Klemperer[4] and Ehlert, *et al.*,[5] showed that only the metal difluoride vapors result from heating the solids at temperatures in the range of these studies. Also, there was no evidence for a reaction between the graphite crucible and $CdF_2(g)$.

Thermodynamic calculations show that such reaction is unlikely under the conditions of these experiments. The Clausing factor used in the calculations was $W_0 =$

Table I: Sublimation Pressures of CdF_2 by the Knudsen Method

T, °K.	Press. obsd., atm.	$-\Delta(F°_T - H°_{298})/T$, cal. deg.$^{-1}$ mole^{-1}	$\Delta H°_{298.18}$, kcal. mole^{-1}
1092	2.87 × 10^{-6}	41.8	73.18
1098	4.07 × 10^{-6}	41.8	73.17
1118	6.70 × 10^{-6}	41.7	73.27
1128	8.36 × 10^{-6}	41.7	73.32
1138	1.02 × 10^{-5}	41.7	73.38
1148	1.33 × 10^{-5}	41.6	73.42
1158	1.67 × 10^{-5}	41.6	73.45
1160	1.68 × 10^{-5}	41.6	73.47
1172	2.32 × 10^{-5}	41.6	73.53
1183	2.92 × 10^{-5}	41.5	73.58
1191	3.60 × 10^{-5}	41.5	73.61
1193	3.78 × 10^{-5}	41.5	73.63
1203	4.79 × 10^{-5}	41.5	73.65
1214	6.13 × 10^{-5}	41.4	73.70
1223	7.43 × 10^{-5}	41.4	73.70
1235	9.71 × 10^{-5}	41.4	73.75
1245	1.19 × 10^{-4}	41.3	73.78
1255	1.51 × 10^{-4}	41.3	73.82
		Av.	73.52

Table II: Sublimation Pressures of CdF_2 by the Langmuir Method

T, °K.	Press. obsd., atm.	$-\Delta(F°_T - H°_{298})/T$, cal. deg.$^{-1}$ mole^{-1}	$\Delta H°_{298.1b}$, kcal. mole^{-1}
921	9.76 × 10^{-9}	42.3	72.72
941	2.08 × 10^{-8}	42.3	72.81
951	3.31 × 10^{-8}	42.2	72.87
961.5	4.25 × 10^{-8}	42.2	72.91
971	6.88 × 10^{-8}	42.2	72.97
982	8.52 × 10^{-8}	42.2	73.03
992	1.35 × 10^{-7}	42.1	73.08
1002	1.70 × 10^{-7}	42.1	73.11
1012	2.50 × 10^{-7}	42.1	73.15
1022	3.36 × 10^{-7}	42.0	73.20
1041	6.20 × 10^{-7}	42.0	73.27
		Av.	73.01

(1) O. Ruff and L. LeBoucher, *Z. anorg. allgem. Chem.*, **219**, 376 (1934).

(2) L. Brewer, G. R. Somayajulu, and E. Brackett, *Chem. Rev.*, **63**, 111 (1963).

(3) J. L. Margrave in "Physico-Chemical Measurements at High Temperatures," J. O'M. Bockris, J. L. White, and J. D. MacKenzie, Ed., Butterworth and Co., Ltd., London, 1959, Chapter 10.

(4) W. Klemperer, *J. Chem. Phys.*, **40**, 3471 (1964).

(5) T. C. Ehlert, R. A. Kent, and J. L. Margrave, *J. Am. Chem. Soc.*, **86**, 5093 (1964).

0.492 as obtained from the tabulations of Iczkowski, et al.,[6] relating the length/radius of the orifice to W_0. The surface area was assumed to decrease linearly with the weight loss and corrections for this changing area were made in the calculation of the rate of weight loss per unit area. This change was less than 35% of the original area.

Results and Discussion

The observed sublimation pressures, P_K and P_L, are given in Tables I and II. The experimental data were fitted to a log P vs. $1/T$ equation by the least-squares method using an IBM 1620 computer. The Knudsen and Langmuir data are fitted by eq. 1 and 2, respectively

$$\log P_K = 7.391 \pm 0.015 - \frac{(14.089 \pm 0.080) \times 10^3}{T} \tag{1}$$

$$\log P_L = 7.563 \pm 0.021 - \frac{(14.341 \pm 0.113) \times 10^3}{T} \tag{2}$$

and are plotted in Figure 1.

The second-law heats of sublimation obtained from Clausius–Clapeyron plots are

$$\Delta H°_{1185} = 64.47 \pm 0.36 \text{ kcal. mole}^{-1}$$

(Knudsen experiments)

and

$$\Delta H°_{990} = 65.62 \pm 0.52 \text{ kcal. mole}^{-1}$$

(Langmuir experiments)

When corrected to 298°K. assuming $\Delta C_p = -9.0$ cal. deg.$^{-1}$ mole^{-1} for the sublimation process, these heats are identical within experimental error, $\Delta H°_{298} = 72.0 \pm 3.0$ kcal. mole^{-1}. The small uncertainties are standard deviations of the experimental points from the straight line and do not include the uncertainties in the temperature, surface area, orifice cross section, and ΔC_p values; a more realistic appraisal of the results suggests ± 3 kcal. mole^{-1} as the possible error for the second-law heat of sublimation.

A combination of the vapor pressure data with the free energy functions from Brewer, et al.,[2] produces an average third-law heat of sublimation at 298°K. of 73.3 ± 3.0 kcal. mole^{-1}. Thus, $\Delta H°_{298} = 72.6 \pm 3.0$ kcal. mole^{-1} is the selected sublimation energy for CdF$_2$. P_L is always slightly lower than P_K and from the ratio, P_L/P_K, one concludes that α_L, the Langmuir coefficient, is in the range 0.9–1.0.
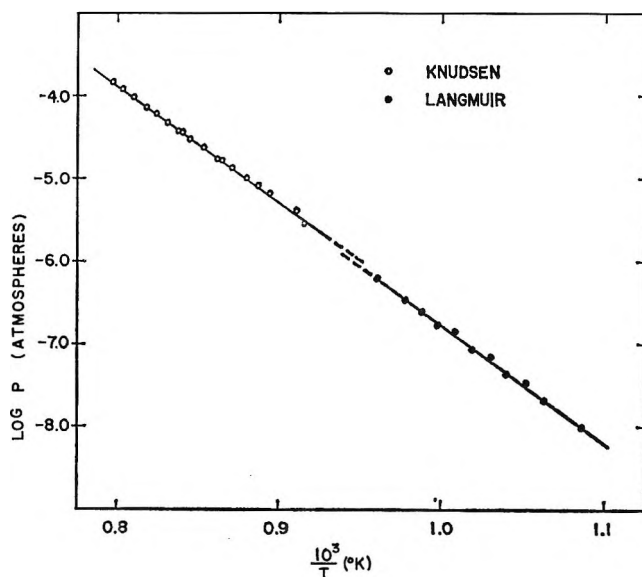
Figure 1. Sublimation pressure of cadmium fluoride.

The second-law entropies of sublimation obtained from Clausius–Clapeyron plots are

$$\Delta S°_{1185} = 33.82 \pm 0.07 \text{ e.u.} \quad \text{(Knudsen experiments)}$$

and

$$\Delta S°_{990} = 34.61 \pm 0.10 \text{ e.u.} \quad \text{(Langmuir experiments)}$$

These values are in excellent agreement with the corresponding values obtained from the data given by Brewer, et al.[2] When corrected to 298°K., the entropy of sublimation of CdF$_2$, $\Delta S°_{298} = 45.8 \pm 0.5$ e.u.

The heats and entropies of sublimation obtained by both methods are in satisfactory agreement when one considers the difficulty of maintaining isothermal conditions and of finding a nonreactive cell, along with the uncertainties in the thermodynamic functions. The results are also in reasonable agreement with the early work of Ruff and LeBoucher.[1]

The atomization energy of CdF$_2$(g) may be calculated from the heat of sublimation and other available thermochemical data.[7–9] One finds $\Delta H_a° = 158.6 \pm 3$ kcal. mole^{-1} as compared with 153.2 given by Brewer, et al.,[2] and thus an average Cd–F bond energy

(6) R. P. Iczkowski, J. L. Margrave, and S. M. Robinson, J. Phys. Chem., 67, 229 (1963).

(7) G. N. Lewis and M. Randall, "Thermodynamics," revised by K. S. Pitzer and L. Brewer, 2nd Ed., McGraw-Hill Book Co., Inc., New York, N. Y., 1961, p. 672.

(8) (a) R. P. Iczkowski and J. L. Margrave, J. Chem. Phys., 30, 403 (1959); (b) J. G. Stamper and R. F. Barrow, Trans. Faraday Soc., 54, 1592 (1958).

(9) E. Rudzitis, H. M. Feder, and W. N. Hubbard, J. Phys. Chem., 67, 2388 (1963).

of 79.3 ± 1 kcal. mole^{-1}. Herzberg[10] and Gaydon[11] found the data on CdF(g) inadequate for establishing the dissociation energy. By comparison with the ratios $D(\text{Mn–F})/\Delta H_a{}^\circ(\text{MnF}_2) = 0.46$,[12] $D(\text{Cr–F})/\Delta H_a{}^\circ(\text{CrF}_2) = 0.47$,[13] and the general conclusions from studies of group II and group IV mono- and dihalides,[14,15] one estimates $D(\text{Cd–F})/\Delta H_a{}^\circ(\text{CdF}_2) = 0.46 \pm 0.02$ and $D(\text{Cd–F}) = 73 \pm 5$ kcal. mole^{-1}.

(10) G. Herzberg, "Molecular Spectra and Molecular Structure. I. Spectra of Diatomic Molecules," D. Van Nostrand Co., Inc., New York, N. Y., 1950.

(11) A. G. Gaydon, "Dissociation Energies," Chapman and Hall, Ltd., London, 1953.

(12) R. A. Kent, T. C. Ehlert, and J. L. Margrave, *J. Am. Chem. Soc.*, **86**, 5090 (1964).

(13) R. A. Kent and J. L. Margrave, to be published.

(14) G. D. Blue, J. W. Green, T. C. Ehlert, and J. L. Margrave, *Nature*, **199**, 804 (1963).

(15) T. C. Ehlert and J. L. Margrave, *J. Chem. Phys.*, **41**, 1066 (1964).

The Relation between Electrochemical and Spectroscopic Properties of the Halide and Pseudohalide Ions in Solution

by E. Gusarsky and A. Treinin

Department of Physical Chemistry, Hebrew University, Jerusalem, Israel   (Received March 10, 1965)

The reducing power of the halide and pseudohalide ions, as measured electrochemically, increases in the following order[1]: F$^-$, NCO$^-$, Cl$^-$, N$_3{}^-$, Br$^-$, SCN$^-$, I$^-$, SeCN$^-$, TeCN$^-$. This sequence also should be reflected in the electronic spectra of the ions, especially in their charge-transfer-to-solvent (c.t.t.s.) bands which involve a kind of an oxidation–reduction process (the halide ions display only this type of excitation). Thus we expect a gradual shift of the c.t.t.s. band to longer wave lengths when proceeding along the series from F$^-$ to TeCN$^-$. This is actually the case for the halide ions.[2] The c.t.t.s. band of N$_3{}^-$ has been studied[3] and though its λ_{max} could not be exactly located it is prob-

ably close to that of Br$^-$. NCO$^-$ appears to reach its peak in the vacuum ultraviolet spectrum.[4] The spectrum of SCN$^-$ was first reported by Rabinowitch,[5] who assigned the inflection in the 220-mμ region to a c.t.t.s. band with λ_{max} 224 mμ. No evidence was given to this assignment and it was recently stated that the peak actually lies in the vacuum ultraviolet spectrum.[6] The electronic spectra of SeCN$^-$ and TeCN$^-$ have not been reported before. We wish to report here some results concerning the spectra of SCN$^-$, SeCN$^-$, and TeCN$^-$ and to show the relation between the electrochemical and spectroscopic series.

Experimental

KNCS (C.P.) was twice recrystallized from ethanol and dried over CaCl$_2$ in a vacuum desiccator. The solvents used were of Spectrograde quality and all other materials of Analar grade. Aqueous solutions of NaNCSe and NaNCTe were prepared by shaking Se and Te, respectively, in 10^{-1} M NaCN solutions. Accurately weighed quantities of Se were dissolved (*ca.* 1 mg. in 50 ml.) whereas Te dissolved only slightly after long shaking and warming, so the concentration of TeCN$^-$ could not be determined.

All of the spectra were taken with a Hilger Uvispek spectrophotomer in a thermostated cell compartment; 5-mm. silica cells were used. The sample differed from the reference solution only by containing $\sim$2 × 10^{-4} mole/l. of the solute investigated.

Results and Discussion

Figure 1 shows some of the results obtained. There is a close resemblance between the spectra of the three anions, showing a gradual shift to long wave lengths as the electronegativity of the group VI atom decreases. In water they all display a long wave length "shoulder" with a relatively high intensity, which is presumably due to the overlap of two electronic transitions. The properties of the long wave length band (A), as studied for SCN$^-$, lead to its assignment to a c.t.t.s. origin. Thus, it appears to be sensitive to environmental effects and its response is of the same type as that of a c.t.t.s. band[7]: relative to H$_2$O it is blue shifted by alcohol and red shifted by CH$_3$CN. A large red shift

(1) (a) L. Birckenbach and K. Kellermann, *Ber.*, **58**, 786 (1925); (b) G. R. Levi and A. Perotti, *Gazz. chim. ital.*, **88**, 640 (1958).

(2) For recent data see J. L. Weeks, G. M. A. C. Meaburn, and S. Gordon, *Radiation Res.*, **19**, 559 (1963).

(3) I. Burak and A. Treinin, *J. Chem. Phys.*, **39**, 189 (1963).

(4) I. Burak and A. Treinin, unpublished results.

(5) E. Rabinowitch, *Rev. Mod. Phys.*, **14**, 112 (1942).

(6) J. C. Barnes and P. Day, *J. Chem. Soc.*, 3889 (1964).

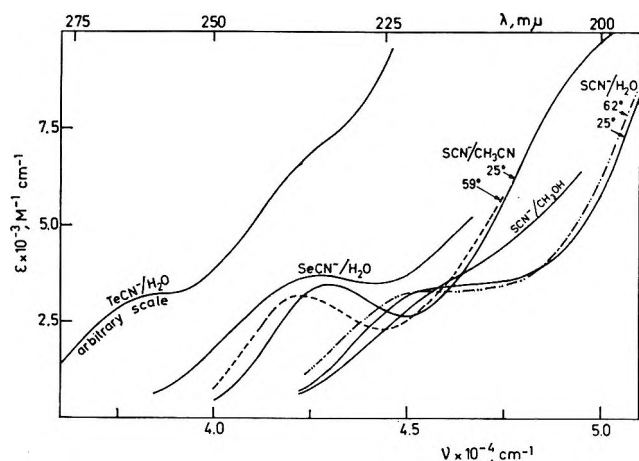(7) I. Burak and A. Treinin, *Trans. Faraday Soc.*, **59**, 1490 (1963).

Figure 1. The absorption spectra of SCN^-, $SeCN^-$, and $TeCN^-$ (unless otherwise stated, at 25°).
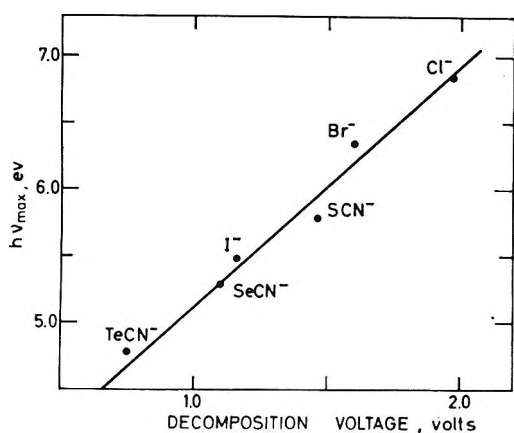
Figure 2. Correlation between $h\nu_{max}$ of X^- and the decomposition voltage of 0.1 M KX (from Figure 3, ref. 1a). For Br^- and I^- $h\nu_{max}$ refers to the low-energy band.

was also observed in liquid NH_3.[8] On the other hand, the overlapping band (on its short wave length side) appears to follow the regular blue shift with increase in polarity of the solvent. The c.t.t.s. nature of band A is also reflected in its relatively large temperature sensitivity (Figure 1). In CH_3CN $d(h\nu_{max})/dT \sim 24$ cm.$^{-1}$ deg.$^{-1}$, which is close to that displayed by I^-[9]) and in its being considerably blue shifted by adding sucrose and KF to the aqueous solution.

When water is replaced by CH_3CN, the c.t.t.s. band of I^- is red shifted by 3600 cm.$^{-1}$ and ϵ_{max} is hardly affected. Assuming[10] the same effect on SCN^- we estimate the following data for its c.t.t.s. band in aqueous solution: $h\nu_{max} = 5.75$ e.v., ϵ_{max} 3500 M^{-1} cm.$^{-1}$. The position of this band can be also estimated from the spectra of the charge-transfer complexes.[3]

The data for some thiocyanate complexes seem to be in agreement with locating its c.t.t.s. band at about 220 mμ. Moreover, there is photochemical evidence that irradiation of SCN^- at 228 mμ leads to release of electrons to the solvent.[4]

Figure 2 shows the relation between the spectroscopic and electrochemical properties[1a] of the halide and pseudohalide ions, X^- ($h\nu_{max}$ of the halides were taken from ref. 2; $h\nu_{max}$ of $SeCN^-$ and $TeCN^-$ were estimated from Figure 1). The nearly linear relation should be considered only as an empirical result since the slope of the line is larger than 1. The proper correlation should take into account the dissociation energy of X_2, the solvation energy of X, and entropy effects. The proper slope was obtained for the halides when all these terms were taken into account.[11] However, Figure 2 may be helpful for estimating the positions of the c.t.t.s. bands of other ions in this series.

From the energy of the c.t.t.s. band information can be derived about the electron affinity of the ion. The electron affinity of SCN had been determined by the magnetron technique[12]; the value obtained is 46 kcal./mole. Since the hydration energy of SCN^- is close to that of Br^- and I,$^-$[13] this value seems to be too small to account for a c.t.t.s. band in the 220-mμ region, unless the corresponding transition leads to an excited SCN radical which is unlikely for the lowest energy band. Using the theoretical expression relating $h\nu_{max}$ of a c.t.t.s. band to the radius of the ion[14] and putting $r_{SCN^-} = 1.95$ Å.,[15] we obtain $E \sim 69$ kcal., where E is the vertical ionization potential of the ion. The discrepancy between this and the magnetron value is rather large and can be only partly due to the strain of the radical produced by the vertical process. For the halides the magnetron and c.t.t.s. results agree rather well. The origin of the discrepancy for SCN^- is not clear.

(8) D. Shapira and A. Treinin, unpublished results.

(9) M. Smith and M. C. R. Symons, *Trans. Faraday Soc.*, 54, 338 (1958).

(10) In liquid NH_3 (−33°) the c.t.t.s. bands of both ions are red shifted by ∼1400 cm.$^{-1}$ with respect to their CH_3CN solutions.[8]

(11) A. Treinin, Ph.D. Thesis, Hebrew University, Jerusalem, 1958.

(12) M. Page, Advances in Chemistry Series, No. 36, American Chemical Society, Washington, D. C., 1962, p. 68.

(13) (a) D. F. G. Morris, *J. Inorg. Nucl. Chem.*, 6, 295 (1958); (b) V. P. Vasilev, *et al.*, *Zh. Fiz. Khim.*, 34, 1763 (1960).

(14) G. Stein and A. Treinin, *Trans. Faraday Soc.*, 55, 1086 (1959).

(15) K. B. Yatsimirski, *Izv. Akad. Nauk SSSR, Otd. Khim. Nauk*, 398 (1948).

Orientation in Pyridine–Iodine Complexes

by P. L. Kronick

*The Franklin Institute Research Laboratories, Chemistry Division,
Philadelphia, Pennsylvania 19103*   (*Received March 15, 1965*)

In solution, pyridine and iodine form a molecular complex with a blue-shifted iodine band and an unusually high heat of formation (−8.0 kcal.).[1] On the basis mostly of spectroscopic and thermodynamic properties, it is believed that the interaction between the donor and acceptor components in this complex involves the unpaired electrons on the nitrogen atom in pyridine. The simple 1:1 complex pyridine–iodine is believed to be not a π-complex but an n-complex.

When iodine is absorbed by solid poly(4-vinylpyridine) in fairly small amounts, an adduct is formed which resembles the pyridine–iodine solutions. Films of the adduct, for example, have the blue-shifted iodine bands. Also, the system is reversible,[2] desorbing iodine under high vacuum, but much more slowly than polystyrene–iodine. Because of similarities in chemical composition and in physical behavior between iodine–poly(4-vinylpyridine) on one hand, and iodine–pyridine and 4-picoline solutions in aliphatic hydrocarbon solvents on the other, it seems likely that both should have similar structures.

The actual configuration in this type of complex, however, has been determined directly only for the 4-picoline–bromine crystal.[3] As expected, the conformation is not the same as that in benzene–halogen complexes in which the halogen molecules interact with the π-electrons of the benzene ring.[4] In the complex with picoline, the halogen molecules interact specifically with the nitrogen atoms, forming linear arrays, the Br–Br–N directions being inclined to the planes of the rings by 13°. This angle of inclination may mean that crystal-ordering forces are operating in defining the complex in the crystal and raises the question whether the solid state configuration is at all comparable to that in amorphous phases. Some information about this question can be obtained from a measurement of the dichroism of the shifted iodine band in oriented poly-(4-vinylpyridine)–iodine films.

Experimental

Poly(4-vinylpyridine) was prepared by peroxide-initiated polymerization of 4-vinylpyridine. The polymer was dissolved in pyridine and cast as films. When peeled from the substrate and stretched, the films became negatively birefringent, the direction of
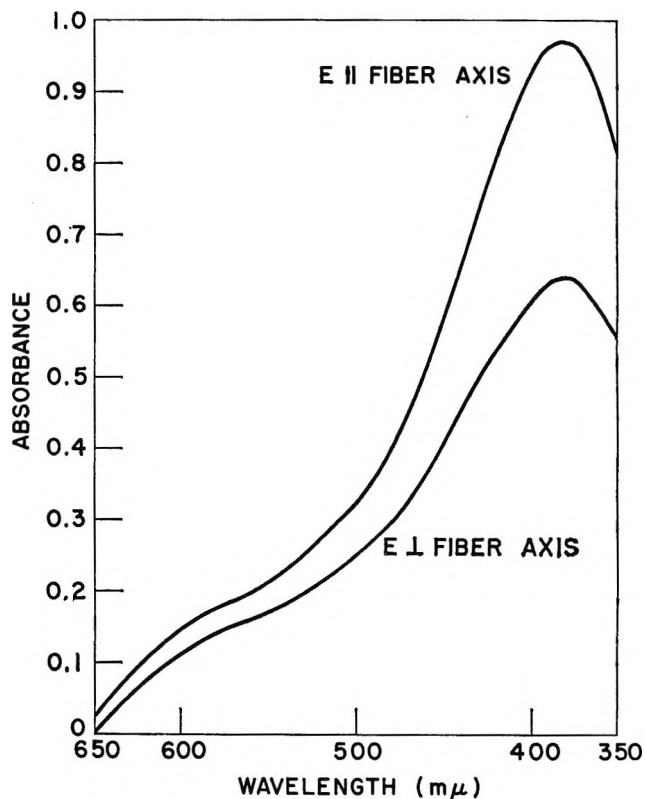
Figure 1.   Dichroism of the shifted iodine absorption band in oriented polyvinylpyridine–iodine film.

greatest molecular polarizability being perpendicular to the direction of stretch. This behavior is to be expected from the simplest model of deformation of high polymers, the aromatic ring planes assuming orientations perpendicular to the direction of stretch; the main chains, parallel.[5]

Films of polyvinylpyridine are brittle and difficult to stretch. To facilitate uniform drawing for the dichroism measurement, they were cast for support on a 5-mil polyethylene substrate, which itself showed no absorption in the near-ultraviolet region and did not absorb iodine. The thickness of the polyvinylpyridine layer was 1 to 10 μ. The double films were then oriented by stretching. The complex was formed by exposing the oriented films to iodine vapor in the presence of air.

(1) C. Reid and R. S. Mulliken, *J. Am. Chem. Soc.*, **76**, 3869 (1954).

(2) S. B. Mainthia, P. L. Kronick, and M. M. Labes, *J. Chem. Phys.*, **41**, 2206 (1964).

(3) O. Hassel, "Investigation of Molecular Structures," U. S. Department of Commerce Office of Technical Services, Publication Board Report 155,783 (1960).

(4) O. Hassel and K. O. Stromme, *Acta Chem. Scand.*, **12**, 1146 (1958); **13**, 1781 (1959).

(5) R. D. Andrews, *J. Appl. Phys.*, **25**, 1223 (1954).

The dichroism of the shifted iodine band was observed by vertically polarizing the two beams of a Bausch and Lomb 505 spectrophotometer with Glann polarizers and measuring the spectrum of the stretched film with the direction of stretch first parallel and then perpendicular to the polarization direction. The spectra are shown in Figure 1. It is seen that the absorption intensity is strongest for light polarized in the direction of the stretch. The electronic transition of the iodine is $^3\Pi_0{}^+ \leftarrow {}^1\Sigma^+$, polarized perpendicular to the molecular iodine axis.[6] Thus the dichroic ratio $E_\parallel / E_\perp$ of 1.50 indicates that the axes of the iodine molecules are preferentially oriented perpendicular to the direction of stretch. Since the pyridine rings are also perpendicular to the molecular chains, the iodine molecules are parallel to the planes of the aromatic rings.

We were unable to measure directly the degree of orientation of the chains in the polyvinylpyridine part of the film because of interference from the polyethylene substrate both in the quartz-ultraviolet absorption spectrum and in the birefringence effect. The polyethylene film itself was stretched to a birefringence of 0.005, corresponding to 0.41 for $\langle \cos^2 \phi \rangle_{av}$, the average orientation cosine, calculated from the expression $\langle \cos^2 \phi \rangle_{av} = 2(\Delta n / \Delta n_\infty) + \frac{1}{3}$ using known parameters.[7] This value in turn corresponds to a stretch ratio of 1.15, both experimentally and theoretically.[7,8] The dichroic ratio of the CH_2 rocking frequency in polyethylene with this stretch ratio[7,3] is the same as that for our shifted iodine band. Polyvinylpyridine being essentially amorphous has a different internal texture than polyethylene; yet it would seem that the polyvinylpyridine chains "follow" the orientation of the polyethylene substrate, at least at low degrees of stretch.

These observations show that the iodine molecules interact strongly with the pyridine rings, taking up fixed orientations with their long axes parallel to the planes of the rings. The stability of the complex over that of the polystyrene complex is independent evidence of interaction with the nitrogen atom. Thus the iodine molecules may lie folded over the pyridine rings but parallel to the C_4-N direction; they may lie in arrays tending toward linear C_4-N-I-I arrangements; or they may be perpendicular to C_4-N. The symmetrical perpendicular arrangement gives, to a first approximation, zero overlap, not to be expected in such a strong complex. Geometric considerations and the results for the picoline–bromine crystals[3] are more consistent with the linear model. None of these structures is consistent with the "oblique model."[1]

(6) J. Ham. *J. Am. Chem. Soc.*, **76**, 3886 (1954).

(7) R. S. Stein and F. H. Norris, *J. Polymer Sci.*, **21**, 381 (1956).

(8) B. Baule, O. Kratky, and R. Treer, *Z. physik. Chem.*, **50B**, 255 (1941).

(9) M. C. Tobin and M. J. Carrano, *J. Polymer Sci.*, **24**, 93 (1957).

The Entropy of $K_3Fe(CN)_6$ and $Fe(CN)_6{}^{3-}(aq)$. Free Energy of Formation of $Fe(CN)_6{}^{3-}(aq)$ and $Fe(CN)_6{}^{4-}(aq)$[1]

by R. H. Busey

Chemistry Division, Oak Ridge National Laboratory, Oak Ridge, Tennessee (*Received March 25, 1965*)

Hepler, *et al.*,[2] give 63.4 ± 1.0 cal. deg.$^{-1}$ mole^{-1} for the standard partial molal entropy of the ferricyanide ion, $Fe(CN)_6{}^{3-}(aq)$. This result was derived in the usual manner from their measurements of the heat of solution of $K_3Fe(CN)_6$ combined with other thermodynamic data available from the literature. For the entropy of $K_3Fe(CN)_6$ required in the calculation, they used 100.4 cal. deg.$^{-1}$ mole^{-1} and referred to heat capacity measurements of Stephenson and Morrow.[3] They apparently do not include, however, in the estimated uncertainty of ±1.0 cal. deg.$^{-1}$ mole^{-1} in the entropy of $Fe(CN)_6{}^{3-}(aq)$ the uncertainty attached by Stephenson and Morrow to their value for the entropy of $K_3Fe(CN)_6$. The latter uncertainty is concerned with what portion of the magnetic entropy (R ln 2 for the spin-paired 3d^5 complex) exists below 15°K.

More recently Watt, *et al.*,[4] determined calorimetrically the standard heat changes, $\Delta H°$, for the reactions

$$Fe^{3+}(aq) + 6CN^-(aq) = Fe(CN)_6{}^{3-}(aq) \quad (1)$$

$$Fe^{2+}(aq) + 6CN^-(aq) = Fe(CN)_6{}^{4-}(aq) \quad (2)$$
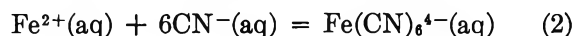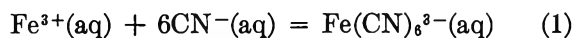
These data were combined with appropriate entropy data from the literature, which included the above value for $\bar{S}_2°(Fe(CN)_6{}^{3-}(aq))$, to obtain $\Delta F°$ for each

(2) L. G. Hepler, J. R. Sweet, and R. A. Jesser, *J. Am. Chem. Soc.*, **82**, 304 (1960).

(3) C. C. Stephenson and J. C. Morrow, *ibid.*, **78**, 275 (1956).

(4) G. D. Watt, J. J. Christensen, and R. M. Izatt, *Inorg. Chem.*, **4**, 220 (1965).

reaction. It is the purpose of this note to show that data have existed in the literature since 1961 which may be employed to remove the major portion of the uncertainty in Stephenson and Morrow's value for the entropy of $K_3Fe(CN)_6$ and to present revised values for the thermodynamic properties of $Fe(CN)_6{}^{3-}$(aq) and $Fe(CN)_6{}^{4-}$(aq).

Stephenson and Morrow observed a small anomaly near 131°K. in the low-temperature heat capacity of $K_3Fe(CN)_6$. They considered the anomaly to be magnetic in nature because none was observed in their heat capacity measurements on diamagnetic $K_3Co(CN)_6$, which is isomorphous with the iron salt. Utilizing the heat capacity of $K_3Co(CN)_6$, they estimated that the anomaly extended over a temperature range of 100° and had an entropy of 0.9 ± 0.2 cal. deg.$^{-1}$ mole^{-1} associated with the gradual transition. They give the entropy increase between 15 and 298.16°K. as 99.58 cal. deg.$^{-1}$ mole^{-1} and add a Debye extrapolation estimate of 0.81 (exclusive of any magnetic entropy) for the interval 0 to 15°K. to give 100.4 cal. deg.$^{-1}$ mole^{-1} at 298.16°K. To indicate the uncertainty they attach to this value, a direct quotation from their paper is given: "Since the Debye extrapolation ignores any magnetic contribution, an additional term may be necessary. We have suggested that this amounts to 0.5 cal. deg.$^{-1}$ mole^{-1}; its maximum could be 1.38 cal. deg.$^{-1}$ mole^{-1}." (0.5 cal. deg.$^{-1}$ mole^{-1} is the difference between the magnetic entropy and the estimated entropy associated with the anomaly: R ln 2 − 0.9 = 0.5.) Unfortunately, at least two frequently used tabulations[5,6] of thermodynamic properties list the value 100.4 with no qualifying statement.

Gregor and Fritz[7] have measured the heat capacity and magnetic susceptibility of $K_3Fe(CN)_6$ from 0.6 to 20°K. Ohtsuka[8] has also made adiabatic demagnetization measurements on $K_3Fe(CN)_6$; his measurements extend to ∼0.2°K. This latter investigation clearly demonstrates that the magnetic entropy of R ln 2 is fully developed at a temperature of a few degrees above 0°K. Using this information the revised value for the entropy of $K_3Fe(CN)_6$ at 298.15°K. is calculated to be: $S_{298.15} = 0.87 + 1.38 + 99.58 = 101.83$ cal. deg.$^{-1}$ mole^{-1}. The heat capacity data of Gregor and Fritz from 5 to 15°K. were joined smoothly to the data of Stephenson and Morrow above 15°K. and extrapolated to 0°K. using the Debye T^3 law. The resulting curve was utilized to obtain the lattice entropy at 15°K., 0.87 cal. deg.$^{-1}$ mole^{-1}, exclusive of the magnetic entropy of R ln 2 = 1.38 cal. deg.$^{-1}$ mole^{-1}. The entropy increase from 15 to 298.15°K., 99.58 cal. deg.$^{-1}$ mole^{-1}, is Stephenson and Morrow's result.[3]

There remains the question of the nature of the anomaly near 131°K. Although this is of no consequence to the thermodynamic properties under consideration, it is of interest to consider the possible origin of the anomaly. It is suggested that the anomaly is the result of a change in crystal structure due to a distortion of the octahedral anion and/or its orientation in the crystal. The absence of a corresponding transition in $K_3Co(CN)_6$ is not too surprising since, in spite of the close similarity of the room temperature crystal structures[9,10] of the two compounds, there are other significant differences in their properties; e.g., the difference in the M–C stretching frequencies[11] reflects the stronger metal to cyanide bonding in the Co complex. Such crystal structure changes are not uncommon among salts containing octahedral halide anions.[12]

The revised value for the standard partial molal entropy of $Fe(CN)_6{}^{3-}$(aq) becomes $\bar{S}_2{}^{\circ}(Fe(CN)_6{}^{3-}$(aq)) = 64.8 cal. deg.$^{-1}$ mole^{-1} using the above revised value for the entropy of $K_3Fe(CN)_6$ with the heat and free energy of solution data given by Hepler, et al.[2] For reaction 1 Watt, et al.,[4] have measured $\Delta H_1{}^{\circ}$ = −70.14 kcal. mole^{-1}. Using partial molal entropy values given by Latimer[13] and $\bar{S}_2{}^{\circ}(Fe(CN)_6{}^{3-}$(aq)) = 64.8 cal. deg.$^{-1}$ mole^{-1}, the standard entropy and free energy changes are: $\Delta S_1{}^{\circ}$ = −34.3 cal. deg.$^{-1}$ mole^{-1} and $\Delta F_1{}^{\circ}$ = −59.9 kcal. mole^{-1}. The latter value combined with values for the standard free energy of formation of Fe^{3+}(aq)[14] and CN^-(aq)[13] gives the standard free energy of formation of ferricyanide ion: $\Delta F_f{}^{\circ}(Fe(CN)_6{}^{3-}$(aq)) = 176.6 kcal. mole^{-1}.

For reaction 2 Watt, et al.,[4] measured $\Delta H_2{}^{\circ}$ =

(5) K. K. Kelley and E. G. King, U. S. Bureau of Mines Bulletin 592, U. S. Government Printing Office, Washington, D. C., 1961.

(6) Landolt-Börnstein, "Fahlenwerte und Funktionen aus Physik, Chemie, Astronomie, Geophysik und Technic," II Band, 4 Teil, Kalorische Fustandsgrossen, Springer-Verlag, Berlin, Göttingen, Heidelberg, 1961.

(7) L. V. Gregor and J. J. Fritz, J. Am. Chem. Soc., 83, 2832 (1961). Certain statements made in this paper are erroneous or misleading because the authors misquote Stephenson and Morrow's estimate of the entropy associated with the heat capacity anomaly near 131°K. as 0.09 ± 0.02 instead of 0.9 ± 0.2 cal. deg.$^{-1}$ mole^{-1}.

(8) T. Ohtsuka, J. Phys. Soc. Japan, 16, 1549 (1961).

(9) N. A. Curry and W. A. Runciman, Acta Cryst., 12, 674 (1959).

(10) V. Barkhatov and H. Zhdanov, Acta Physicochim. URSS, 16, 123 (1942).

(11) S. Mizushima and I. Nakagawa, Kagaku no Ryōiki, 10, 173 (1956).

(12) R. H. Busey, R. B. Bevan, Jr., and R. A. Gilbert, J. Phys. Chem., in press.

(13) W. M. Latimer, "Oxidation Potentials," 2nd Ed., Prentice-Hall, Inc., New York, N. Y., 1952.

(14) W. A. Patrick and W. E. Thompson, J. Am. Chem. Soc., 75, 1184 (1953), give for the Fe–Fe^{2+} couple, 0.409 v. This gives $\Delta F_f{}^{\circ}(Fe^{2+}$(aq)) = −18.86 kcal. mole^{-1}. Using −0.771 v.[13] for the Fe^{2+}–Fe^{3+} couple, $\Delta F_f{}^{\circ}(Fe^{3+}$(aq)) = −1.09 kcal. mole^{-1}.

-85.77 kcal. mole^{-1} and calculated ΔS_2° for the reaction in order to obtain a value for ΔF_2°. For the entropy calculation they employed Latimer's[13] value for $\bar{S}_2^\circ(\mathrm{CN}^-(\mathrm{aq}))$ and Hepler's values for $\bar{S}_2^\circ(\mathrm{Fe}^{2+}(\mathrm{aq}))$[15] and $\bar{S}_2^\circ(\mathrm{Fe(CN)}_6{}^{4-}(\mathrm{aq}))$.[2] The latter value is based upon the standard oxidation potential for the ferrocyanide–ferricyanide couple[16] and Hepler's[2] values for $\bar{S}_2^\circ(\mathrm{Fe(CN)}_6{}^{3-}(\mathrm{aq}))$ and the heat of oxidation of $\mathrm{Fe(CN)}_6{}^{4-}(\mathrm{aq})$ to $\mathrm{Fe(CN)}_6{}^{3-}(\mathrm{aq})$ with $\mathrm{Br}_2(\mathrm{l})$. As pointed out by Hepler, et al.,[2] this latter measurement is more uncertain than desired because of the slowness of the oxidation of $\mathrm{Fe(CN)}_6{}^{4-}(\mathrm{aq})$ by $\mathrm{Br}_2(\mathrm{l})$. Instead of calculating ΔF_2° [17] as done by Watt, et al., the observed $\Delta H_2^\circ = -85.77$ kcal. mole^{-1} may be used to calculate a value for $\bar{S}_2^\circ(\mathrm{Fe(CN)}_6{}^{4-}(\mathrm{aq}))$, giving a result which should be better than that obtained by Hepler, et al., because this heat of reaction observation is superior to that obtained for the oxidation of $\mathrm{Fe(CN)}_6{}^{4-}(\mathrm{aq})$ by $\mathrm{Br}_2(\mathrm{l})$. Using -0.356 v.[16] for the potential of the ferrocyanide–ferricyanide couple and $\Delta F_f^\circ(\mathrm{Fe(CN)}_6{}^{3-}(\mathrm{aq})) = 176.6$ kcal. mole^{-1} given above, there is obtained $\Delta F_f^\circ(\mathrm{Fe(CN)}_6{}^{4-}(\mathrm{aq})) = 168.4$ kcal. mole^{-1}. The standard free energy and entropy changes for reaction 2 then are calculated to be: $\Delta F_2^\circ = -50.3$ kcal. mole^{-1} and $\Delta S_2^\circ = -119.0$ cal. deg.$^{-1}$ mole^{-1}. From the latter the partial molal entropy of the ferrocyanide ion is calculated to be $\bar{S}_2^\circ(\mathrm{Fe(CN)}_6{}^{4-}(\mathrm{aq})) = 24.0$ cal. deg.$^{-1}$ mole^{-1}. This may be compared to the value 18.1 cal. deg.$^{-1}$ mole^{-1} computed from data given by Hepler, et al.,[2] but using 101.8 cal. deg.$^{-1}$ mole^{-1} for the entropy of $\mathrm{K}_3\mathrm{Fe(CN)}_6$. Table I summarizes the results derived.

Table I: Thermodynamic Properties of $\mathrm{K}_3\mathrm{Fe(CN)}_6$, $\mathrm{Fe(CN)}_6{}^{3-}(\mathrm{aq})$, and $\mathrm{Fe(CN)}_6{}^{4-}(\mathrm{aq})$ at $298.15^\circ\mathrm{K}$.

	ΔH_f°, kcal. mole^{-1}	ΔS_f°, cal. deg.$^{-1}$ mole^{-1}	ΔF_f°, kcal. mole^{-1}	S° or $\bar{S}_2^\circ$, cal. deg.$^{-1}$ mole^{-1}
$\mathrm{K}_3\mathrm{Fe(CN)}_6(\mathrm{c})$	0.7	-95.8	-27.9	101.8
$\mathrm{Fe(CN)}_6{}^{3-}(\mathrm{aq})$	150.6	-87.2	176.6	64.8
$\mathrm{Fe(CN)}_6{}^{4-}(\mathrm{aq})$	130.2	-128.0	168.4	24.0

Of primary importance to the above calculation of the thermodynamic properties of $\mathrm{Fe(CN)}_6{}^{4-}(\mathrm{aq})$ is the value of the potential observed by Kolthoff and Tomiscek[16] for the $\mathrm{Fe(CN)}_6{}^{4-}$–$\mathrm{Fe(CN)}_6{}^{3-}$ couple. A verification of this value has recently been obtained[18] which contradicts the suggestion by Hepler, et al.,[2] that the value of the potential may be quite uncertain. As emphasized by Hepler, et al., however, more reliable thermodynamic properties of $\mathrm{Fe(CN)}_6{}^{4-}(\mathrm{aq})$ may be

obtained by measuring the low-temperature heat capacity of $\mathrm{K}_4\mathrm{Fe(CN)}_6{\cdot}3\mathrm{H}_2\mathrm{O}$ to obtain the third-law entropy and by combining this entropy with heat and free energy of solution results to get a more reliable $\bar{S}_2^\circ(\mathrm{Fe(CN)}_6{}^{4-}(\mathrm{aq}))$.

(15) H. C. Ko and L. G. Hepler, J. Chem. Eng. Data, **8**, 59 (1963).

(16) I. M. Kolthoff and W. J. Tomiscek, J. Phys. Chem., **39**, 945 (1935).

(17) This computed ΔF_2° is not independent of the value for the potential of the $\mathrm{Fe(CN)}_6{}^{4-}$–$\mathrm{Fe(CN)}_6{}^{3-}$ couple as implied by Watt, et al. In the calculation they used $\bar{S}_2^\circ(\mathrm{Fe(CN)}_6{}^{4-}(\mathrm{aq}))$, an entropy value whose derivation[2] employed this potential.

(18) J. Jordan and G. J. Ewing, Inorg. Chem., **1**, 587 (1932).

Revised Thermodynamic Properties of

Aqueous Strontium Ion

by Richard M. Noyes

University of Oregon, Eugene, Oregon, and Max Planck Institut für physikalische Chemie, Göttingen, Germany

Dr. E. Glueckauf of the Atomic Energy Research Establishment at Harwell has called the author's attention to an anomalous entropy of hydration of aqueous strontium ion reported previously.[1] Examination has revealed that this anomaly arises from a mistake in a listed value for the free energy of formation of strontium vapor.

Both Bureau of Standards Circular No. 500[2] and Latimer[3] give 39.2 kcal./mole, 26.3 kcal./mole, and 39.325 cal./mole deg. for ΔH_f°, ΔF_f°, and S°, respectively, for strontium vapor at 1 atm. fugacity and 25°. The entropy of the crystalline standard state at the same temperature is 13.0 cal./mole deg.

These entries are not internally consistent, and further correspondence has revealed that a mistake of about 5 kcal./mole was made in calculating the free energy of formation from the entropy and enthalpy data. Dr. Leo Brewer of the University of California has pointed out that corrected free energy values of about 31.2 kcal./mole may be found in two more recent compilations.[4,5] Use of the corrected value significantly

(1) R. M. Noyes, J. Am. Chem. Soc., **84**, 513 (1962).

(2) "Selected Values of Chemical Thermodynamic Properties," National Bureau of Standards Circular 500, U. S. Government Printing Office, Washington, D. C., 1952.

(3) W. M. Latimer, "The Oxidation States of the Elements and their Potentials in Aqueous Solutions," 2nd Ed., Prentice-Hall, Inc., New York, N. Y., 1952.

affects some of the previously estimated thermodynamic properties of aqueous strontium ion.

The entropy changes in ref. 1 were computed as $(\Delta H° - \Delta F°)/T$ in order to avoid an inconsistency associated with the usual entropy convention for aqueous ions as discussed elsewhere.[6] This calculation accentuated the effect of the error and led Dr. Glueckauf to notice the anomaly. Values of $\Delta F°_{el}$ and $\Delta S°_{el}$ for the hydration of Sr^{2+} in Table I of ref. 1 should be changed to -344.8 and -50.2, respectively. Although the entropy of hydration of strontium ion still seems surprisingly closer to that of calcium than of barium, the anomaly is certainly reduced to relatively minor proportions.

Entropy calculations in a subsequent paper[7] did not use properties of strontium vapor and are not affected by this change. However, values for $\bar{F}°_{el}$ and ϵ_{eff} in Table I of ref. 7 should be changed to 241.8 and 2.430, respectively. The latter change is in the direction to make an even smoother curve when effective dielectric constant is plotted against radius for aqueous alkaline earth ions.

Acknowledgment. The author is deeply indebted to Dr. Glueckauf for calling his attention to a glaring discrepancy that should have disturbed him earlier and to Dr. Brewer for telling the author of more recent reference works that he should have checked. The work on properties of aqueous ions has been supported by a grant from the National Science Foundation. This manuscript was prepared at the Max Planck Institut für physikalische Chemie while on a National Science Foundation Senior Postdoctoral Fellowship.

(4) D. R. Stull and G. C. Sinke, "Thermodynamic Properties of the Elements," American Chemical Society, Washington, D. C., 1956.

(5) R. Hultgren, R. L. Orr, P. D. Anderson, and K. K. Kelley, "Selected Values of Thermodynamic Properties of Metals and Alloys," John Wiley and Sons, Inc., New York, N. Y., 1963.

(6) R. M. Noyes, *J. Chem. Educ.*, 40, 2, 116 (1963).

(7) R. M. Noyes, *J. Am. Chem. Soc.*, 86, 971 (1964).

Diffusion Coefficients of Iodine Atoms in Carbon Tetrachloride. A Correction

by Richard M. Noyes

University of Oregon, Eugene, Oregon, and Max Planck Institut für physikalische Chemie, Göttingen, Germany
(*Received April 12, 1965*)

Levison and Noyes[1] recently used a photochemical space intermittency technique to estimate that the diffusion coefficients of iodine atoms in carbon tetrachloride are 8.0×10^{-5} and 11.8×10^{-5} cm.^{2}/sec. at 25 and 38°, respectively.

Professor R. H. Stokes of the University of New England in Armidale, New South Wales, has expressed his concern that these values are much larger than any that have been reliably reported for any stable species in the same medium. Although diffusion coefficients of free radicals have never before been measured in liquid phase, there seems no reason to expect them to be so greatly different from those of comparable stable species. The assumptions inherent in the experimental technique have therefore been re-examined.

The technique appears to be unexceptionable provided the areas of illumination are sufficiently uniform and sufficiently sharply defined. Because of the finite size of the light source employed, the beams in the experiment lost resolution as they traversed the cell. A somewhat elaborate mathematical technique was developed to correct for this situation if the beam remained of uniform intensity as it diverged. This assumption may be fairly reasonable for small beams but certainly fails for large beams where the chief effect of divergence is a fuzzing of the boundaries without affecting the intensity in the center. Such a fuzzing would cause atom concentrations in the large-beam experiments to be larger than they would be for homogeneous beams with the same area and same total incident light.

An examination of Figures 3 and 4 of the original reference[1] indicates that the experimental points do not exactly fit the shape of the theoretical curve and that the divergence is in the direction of too high atom concentrations with large beams. The original fit of these curves to the experimental points was designed to minimize deviations throughout the entire range of observations. If the fitting is designed to emphasize the small beams only, the curves should be shifted to the left 0.14 and 0.17 log unit at 25 and 38°, respectively. Diffusion coefficients computed in this way are 4.2×10^{-5} cm.^{2}/sec. at 25° and 5.3×10^{-5} cm.^{2}/sec. at 38°.

Although these values are still somewhat larger than might have been anticipated from the behavior of stable species, they are not sufficiently out of line to cast doubt on the basic validity of the method. The difficulties encountered in this case emphasize the need to use an intense virtual point source of light if photochemical space intermittency is to become a valuable technique.

These corrected diffusion coefficients are in better

(1) S. A. Levison and R. M. Noyes, *J. Am. Chem. Soc.*, 86, 4525 (1964).

agreement with values predicted by conventional equations for diffusion-controlled reactions.[2] At least at 25°, the measured diffusion coefficient is still somewhat larger than that predicted by the equation that treats an atom as a stationary sink in an isotropic continuum; however, the discrepancy is not as large as it previously appeared to be.[2]

(2) R. M. Noyes, *J. Am. Chem. Soc.*, **86**, 4529 (1964).

On the Role of Water in Electron-Transfer Reactions. I

by I. Ruff

Institute of Inorganic and Analytical Chemistry, L. Eötvös University, Budapest, Hungary   (*Received November 16, 1964*)

The kinetic investigation of electron-transfer reactions revealed, in general, that the high rate of these reactions could not be accredited simply to collisions of the reaction partners.[1,2] Making use of the number of collisions per unit time, good agreement could be reached between calculated and experimental reaction rates by assuming relatively large ionic sizes.

Eyring and co-workers[1] and Marcus[3] explained electron transfer using a model which allowed electron transfer even when the reactants were separated from each other by a considerably larger distance than the sum of their respective ionic radii. Both theories have been based on the electrostatic properties of the more or less isolated activated complex.

In the present paper a new model is suggested to explain the velocity of electron-transfer reactions on the basis of tunnel effect, where more emphasis is laid on the properties of the solvent—particularly of water—than in the above-mentioned theories.

According to experience, the electron-transfer reactions are first-order reactions in the involved ions.

Thus, the rate of reaction can be described in general by the equation

$$v = \frac{kT}{h}\chi_e \exp\left(-\frac{E^*}{RT}\right)[\text{ox}][\text{red}] \tag{1}$$

where v is the rate of exchange, k is the Boltzmann constant, T is the absolute temperature, h is the Planck constant, χ_e gives the probability of the electron's transfer in activated state to the other ion (the transmission coefficient of the electron), E^* is the energy of activation, R is the universal gas constant, and [ox] and [red] are the concentrations of the lower and higher charged ions, respectively. Hence, to evaluate the rate constant

$$K = \frac{kT}{h}\chi_e \exp\left(-\frac{E^*}{RT}\right) \tag{2}$$

χ_e and E^* is to be determined theoretically.

If the χ_e electron transmission coefficient is supposed to be the probability of the transfer of an electron through a potential barrier lying between the ions, then for the determination of χ_e the shape of the barrier, its height, the distance of the two interacting ions, and the kinetic energy of the electron must be known. Some informations on these parameters can be gained through the following considerations.

It is well known that only those ions are stable in solution for which the bonding energy of the attached electron falls between certain limits, determined by the nature of the solvent; *e.g.*, in water an electron cannot be bonded to an ion with an energy lower than the bond strength between an electron and a hydrogen atom dissolved in water. On the other hand, however, it cannot be bonded with an energy higher than the bond strength of an electron in the H_2O molecule; otherwise, the solvent would suffer chemical decomposition. Thus, in water (at equilibrium conditions) only such ions can exist which have oxidation–reduction potential values confined to the

$$-2.4 \text{ v.} < \epsilon° < +2.10 \text{ v.} \tag{3}$$

range. The upper limit is given here by the thermodynamically calculated normal oxidation–reduction potential of the

$$H \rightleftharpoons H^+ + e \tag{I}$$

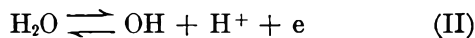process, while the lower limit is given by that of the

(1) R. J. Marcus, B. J. Zwolinski, and H. Eyring, *J. Phys. Chem.*, **58**, 432 (1954), and references therein.

(2) A. C. Wahl, *Z. Elektrochem.*, **64**, 90 (1960).

(3) R. A. Marcus, *J. Chem., Phys.* **24**, 966 (1956); **26**, 867 (1957); *Can. J. Chem.*, **37**, 155 (1959); *Discussions Faraday Soc.*, **29**, 21 (1960); *J. Phys. Chem.*, **67**, 853 (1963).

$$H_2O \rightleftharpoons OH + H^+ + e \qquad (II)$$

process. In the calculation of the potential of equilibrium II, the heat of hydratation of the OH radical was supposed to be zero[4]; thus this value was most probably too low. Using in the calculation the hydration energy of one hydrogen bridge, the mentioned oxidation–reduction potential will be about −2.4 v. (The origin of the potential scale is set by the normal potential corresponding to the

$$H_2 \rightleftharpoons 2H^+ + 2e \qquad (III)$$
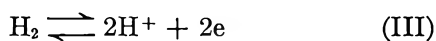
process.)

Thus, the energy of the electron bonded to the ion may cover a range of 4.5 e.v. Its position related to the relative energy levels of equilibria I and II is expressed by the normal oxidation–reduction potential.

These energy conditions are plotted schematically in Figure 1. The "donor" level represents here the state of the very electron which is attached by smallest energy to the ion with lower charge, i.e., the state of the electron which is involved in the exchange. The "acceptor" level is, on the other hand, the lowest, yet unfilled energy level of the ion with higher charge. These two states are energetically equivalent since they refer to two ions of the same element, being in different states of oxidation.

A one-direction exchange means the transfer of an electron from the donor level to the acceptor level. This can happen in one of the following ways.

(1) A hydrogen atom is formed and it "transports" the electron to the acceptor level if the energy of activation is larger than (or equal to) the difference between the donor state and the bond energy of the electron attached to the hydrogen atom, which is represented by the upper horizontal line. This electron transport may run, however, faster than determined by the diffusion velocity of the hydrogen atom since the electron can go from hydrogen atom to hydrogen atom also by tunnel effect. This is so because the exchange reactions are carried out generally in strong acidic solutions, where the mutual distance of hydrogen ions is a few Ångstrøms. Hence, in this case, the electron moves "quasi-free" up to the acceptor ion in the nearly periodic potential field of the hydrogen ions.

According to another theory,[5] the "free" electron bound to a proton may move with the Grotthus mechanism. This mechanism is supported by the experimental fact that the Fe(II)–Fe(III) exchange proceeds in ice too, and the process is not diffusion controlled.[5]

(2) If the energy of activation is smaller than E° (see Figure 1), then the kinetic energy of the electron (which is regarded approximately equal to the acti-
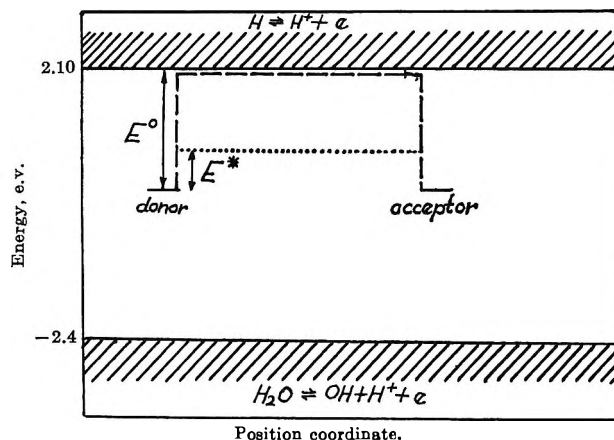
Figure 1.

vation energy) is not sufficient to overcome the barrier. In this case it can reach the acceptor ion only with the aid of the tunnel effect.

Utilizing these ideas one can determine the parameters of the potential barrier opposing the exchange reaction. The shape of the barrier is in close approximation rectangular (dotted line in the figure); its height is given by

$$E^\circ = 2.10 - E_0 \text{ e.v.} \qquad (4)$$

where E_0 is the energy corresponding to the oxidation–reduction potential. Thus, to describe the passage of an electron through the rectangular potential, we can use the Gamow equation

$$\chi_0 = \exp\left(-\frac{2}{\hbar}d\sqrt{2m(E^\circ - E^*)}\right) \qquad (5)$$

where m is the mass of the electron and d is the width of the barrier. Since the donor ion will be activated, quite independently of its distance from the other reactant, electron transfer is possible at all values of d. Therefore, in a 1 M solution (with respect to both ions) an average value for d (9.4 Å.) may be used in the calculation of the resultant reaction rate.

In order to calculate the χ_0 transmission coefficient and in consequence to determine theoretically the K rate constant defined by eq. 2, it would be necessary to calculate E^*, in addition to the above parameters.

E^* is, according to the Frank–Condon principle, the thermal energy which is necessary for the rearrangement of water molecules caused by the new charge distribution due to the electron transfer.[1] One can imagine this fact as follows: the electron can leave

(4) W. M. Latimer, "Oxidation Potentials," Prentice Hall, Inc., New York, N. Y., 1953.

(5) R. A. Horne and E. H. Axelrod, J. Chem. Phys., 40, 1518 (1964).

Table I

System	E^*, kcal./mole	E_0, v.[a]	$\Delta E \times 10^{13}$, ergs	$\log\left(\dfrac{kT}{h}\chi_e\right)$, calcd.	$\log\left(\dfrac{kT}{h}\chi_e\right)$, exptl.	Ref.
		Electron-transfer reactions				
V(II)–V(III)	13.2	0.25	20.5	8.1	7.6	b
Ce(III)–Ce(IV)	7.7	−1.61	54.0	5.1	4.1	c
		Hole-transfer reactions				
$Co(en)_3{}^{2+}$–$Co(en)_3{}^{3+}$	14.3	∼−0.1	∼27	∼7	6.4	c
V(III)–V(IV)	10.7	−0.33	26.0	7.5	7.6	c
Fe(II)–Fe(III)	9.9	−0.77	19.5	8.2	7.8	c
Np(V)–Np(VI)	8.3	−1.15	14.6	8.8	8.1	d
Tl(I)–Tl(III)	12.1	−1.25	10.4	6.0	6.0	c
$Fe(CN)_6{}^{4-}$–$Fe(CN)_6{}^{3-}$	4.7	−0.36	18.2	8.3	6.3[e]	f
Mn(VI)–Mn(VII)	10.5	−0.56	9.4	9.6	10.0[e]	f
Ce(III)–Ce(IV)	23.0	−1.61	−3.0	. . .	18.2	c
Co(II)–Co(III)	21.6	−1.81	−5.5	. . .	16.7	g

[a] See ref. 4.   [b] K. V. Krishnamurty and A. C. Wahl, *J. Am. Chem. Soc.*, **80**, 5921 (1958).   [c] See ref. 1.   [d] D. Cohen, J. C. Sullivan, and J. C. Hindman, *J. Am. Chem. Soc.*, **76**, 552 (1954).   [e] Recalculated to the pH of the kinetic measurements.   [f] See ref. 2.   [g] J. Shankar and B. C. de Souza, *J. Inorg. Nucl. Chem.*, **24**, 693 (1963).

the ion with smaller charge only if the thermal excitation had already removed the ligands from its first coordination sphere to a distance corresponding to the complex of the ion with higher charge. Thus, an excitation of the ligands producing valence vibrations is the required condition for electron transfer.

The calculation of E^* is, however, in this way very problematic because, generally, the corresponding bond energies and force constants are unknown though the applicability of the described model can be controlled by comparing the observed χ_e-values with the data calculated by the combination of (5) and the measured E^* values.

Up to this point only the upper limits of the possible donor-energy values have been considered. The electron transfer, however, can be envisaged in another way, too. This happens namely if the electron is excited from the level corresponding to process II (represented in the figure by the lower horizontal line) to the acceptor state, whereas the appropriate amount of activation energy must be yielded. An H_2O^+ molecule, an electron deficiency (a hole), is created in this process, which can move comparatively fast to the donor state in the periodic potential field of the water molecules. When arriving at the donor, the hole recombines with its electron. As in the example of electron transfer, the hole can reach the acceptor level only by tunnel effect if the excitation energy is smaller than the difference between the considered state and the energy corresponding to the process II. (From the point of view of the electron,

the acceptor level is a donor level.) The circumstances are in this case completely analogous to that of the electron tunneling with the only deviation that now

$$E^\circ = 2.4 - E_0 \text{ e.v.} \tag{6}$$

(Taking into account the hole, the energy scale is now reversed, and hence the opposite sign of the original $E_0 - 2.4$ term.)

According to the cited principles, two ways are available for every electron-transfer reaction: one by "electron transfer" and another by "hole transfer." The two ways of reaction are parallel, and therefore the rate-determining process is the faster one. One can thus admit that the electron-transfer reactions take place mainly by "hole transfer" if the ion pair has a smaller normal oxidation–reduction potential than about −0.1 v., and they occur mainly by "electron transfer" if the oxidation–reduction potential of the partners is higher than this value.

If, however, it turns out that in the different modes of reaction the smaller probability of tunneling is coupled with lower energy of activation and the larger probability with the higher one, then it may happen that the two rates of reaction are commensurable (see eq. 1) and so may be observed experimentally. This is the case, for example, in the Ce(III)–Ce(IV) exchange reaction.[1]

The pH dependence of the reactions has two reasons. (1) The change in pH of the solution may result in a change of the coordination sphere of the reactants

(e.g., hydrolysis), thus causing a deviation in the Franck–Condon restriction by the change of the force constants; this means a change of the activation energy. Thus, the reaction order in hydrogen ion is governed by coordination chemical laws. These reasons are responsible for the pH dependence of the Ce(III)–Ce(IV) reaction, proceeding by hole transfer. (2) The limits of the potential in reactions I and II are also pH dependent, and thus another "slight" pH dependence can be observed[6] (eq. 5). This later phenomenon was taken into account in calculating the $MnO_4{}^{2-}$–$MnO_4{}^-$ and $Fe(CN)_6{}^{4-}$–$Fe(CN)_6{}^{3-}$ systems. When both effects are significant, their separation is very difficult.

In Table I the log $(\chi_e kT/h)$ values calculated with the aid of (5) according to the described method are compared with the measured values of the action constant. (For the calculation of the observed action constant, the experimentally obtained values of the entropy of activation were used.) In some exchange reactions, *e.g.*, U(IV)–U(VI), the agreement between calculated and observed values seems to be poor. The explanation for it is that these ions preferably form polynuclear hydroxy complexes, and therefore the OH^- bridges existing between the reactants are involved in the electron transfer.

The Ce(III)–Ce(IV) and Co(II)–Co(III) hole-transfer reactions unfold an interesting fact. According to experience here $\chi_e > 1$. Up to Eyring's theory about the rate of reaction

$$\chi_e = \exp\frac{\Delta S^*}{R} \tag{7}$$

where ΔS^* is the entropy difference due to activation. Positive ΔS^* means that the degrees of freedom of the activated complex grow larger. According to the model suggested in the present paper, this is obvious. The activation energy belonging to the mentioned exchange reaction happening by hole transfer is namely higher than $E°$, which refers to a "free" hole. The increase in the degrees of freedom is thus reasonable.

Regarding the figures collected in the table, we have to remark that, when a reaction proceeds by two-electron transfer, the probability of the simultaneous tunneling of two electrons is given by the square of the single electron's transfer probability. The Tl(I)–Tl(III) exchange was calculated on this basis.

(6) I. Ruff, *Acta Chim. Acad. Sci. Hung.*, in press.

Electron Trapping in Rigid Ethanol–Methyl-2-tetrahydrofuran Mixtures

by L. Shields

Department of Physical Chemistry, The University of Leeds, Leeds 2, England   (*Received January 28, 1965*)

Color centers produced by ionizing radiation in rigid organic solvents have been assigned to trapped or solvated electrons[1,2] although the latter term implies the orientation of solvent molecules to an unrealizable extent. The trapped electron bands are solvent dependent having less energy in methyl-2-tetrahydrofuran (MTHF) than in alcohols[1]; in this respect they resemble the optical absorption bands of solvated halide anions which are shifted to low energies in low polarity solvents.[3] In mixed solvents the halide bands, ascribed to charge-transfer-to-solvent transitions,[4,5] move continuously, but not uniformly, with mole fraction of either solvent between the limits set by the bands in each pure solvent. These observations are interpreted in terms of a continuous interchange of solvent molecules between the solvation shell and the bulk solvent, thus allowing for the continuous variation of the solvation shell with solvent composition. The nonuniformity of the shift is attributed to preferential solvation by the more polar solvents, particularly those solvents containing hydroxyl groups. The effect of solvent composition on the trapped electron band in relation to the solvation spectra of halide ions in mixed solvents should test the application of the term "solvated" electrons to these color centers.

The nature of trapping sites in vitreous ethers and alcohols has been discussed.[1] In the former, electrons are trapped in relatively large holes, and in vitreous alcohols the electric field of the electron is sufficient to align the hydroxyl dipole of the peripheral layer of molecules and thereby further confine and stabilize the electron. Following from a simple description for the electron trapped in a spherical potential well, it can be shown that the optical band energy is governed by cavity size which is solvent dependent. The

(1) M. J. Blandamer, L. Shields, and M. C. R. Symons, *J. Chem. Soc.*, 1127 (1965).

(2) W. H. Hamill, J. P. Guarino, and M. R. Ronayne, *J. Am. Chem. Soc.*, **84**, 500 (1962); **84**, 4230 (1962); *Radiation Res.*, **17**, 379 (1962).

(3) M. J. Blandamer, T. R. Griffiths, L. Shields, and M. C. R. Symons, *Trans. Faraday Soc.*, **60**, 1524 (1964).

(4) M. Smith and M. C. R. Symons, *Discussions Faraday Soc.*, **24**, 206 (1956).

(5) T. R. Griffiths and M. C. R. Symons, *Trans. Faraday Soc.*, **56**, 1125 (1960).

electrons possess less kinetic energy, but less stability through polarization, in large cavities.

Experimental

The procedure for recording optical spectra of glasses in the region of 77°K. has been described.[6]

Color centers were produced by subjecting vitreous mixtures of MTHF and ethanol, purified by standard distillation techniques, to γ-rays from a Co^{60} source.

Electron spin resonance (e.s.r.) measurements were made at 9.4 kMc./sec.

Results and Discussion

The band at *ca.* 18,000 cm.$^{-1}$ assigned to the electron trapped in ethanol (e^-_{EtOH}) is retained in solvent mixtures containing as little as 0.15 mole fraction of ethanol. This band is observed as an absorption maximum on a rising absorption due to light scattering and the absorption of the molecular free radical[1]
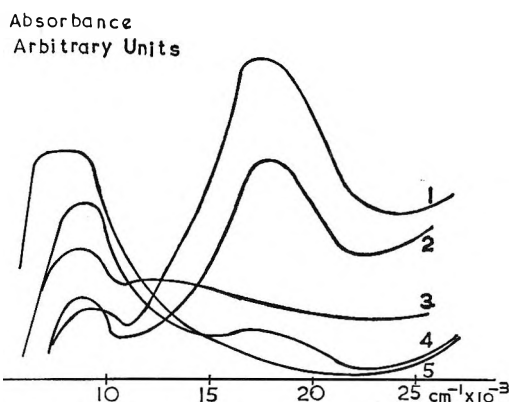
Figure 1.   Optical absorption of irradiated mixture of methyl-2-tetrahydrofuran–ethanol.   Mole fraction of ethanol: (1) 0.33, (2) 0.29, (3) 0.23, (4) 0.15, and (5) 0.09.
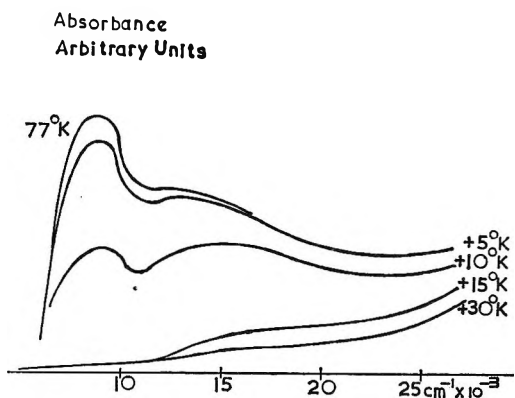
Figure 2.   Optical absorption spectra of irradiated mixture of methyl-2-tetrahydrofuran–ethanol at 77°K. and warmed to 77 + 5°K., 77 + 10°K., 77 + 15°K., and 77 + 30°K.   Mole fraction of ethanol 0.23.
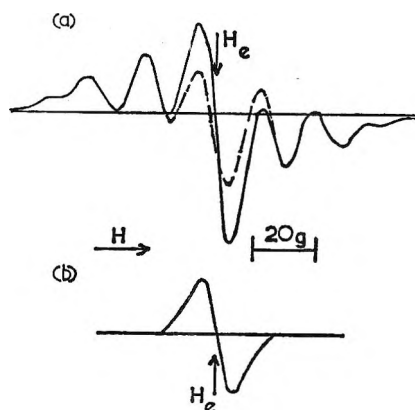
Figure 3.   E.s.r. spectra of irradiated mixture of ethanol and methyl-2-tetrahydrofuran at 77°K.   Mole fraction of ethanol 0.45: (a) ———— before bleaching and – – – – after bleaching; (b) difference spectrum. H_e is the field for which $g = 2.0023$.

(Figures 1 and 2).   The e^-_{EtOH} band is extinguished in mixtures containing less than 0.15 mole fraction of ethanol and replaced by the band (8000 cm.$^{-1}$) of the trapped electron in a methyl-2-tetrahydrofuran environment (e^-_{2MTHF}).   Within the composition range 0.15 to 0.35 mole fraction of ethanol the optical bands characteristic of electrons trapped in the pure solvents coexist (Figure 1).

Associated with the optical band at 8000 cm.$^{-1}$ is a narrow e.s.r. absorption line which is in evidence in the e.s.r. spectra of the irradiated solvent mixtures supporting both species e^-_{EtOH} and e^-_{2MTHF}.   The broad e.s.r. line of e^-_{EtOH} is less evident in these systems but preponderates in mixtures containing greater than 0.4 mole fraction of ethanol (Figure 3 and Table I).

The coexistence of the e^-_{2MTHF} and e^-_{EtOH} bands in certain solvent mixtures indicates that the two trapping sites are different in kind and not just different in the

Table I: E.s.r. Characteristics Associated with the Color Center in Vitreous Ethanol–Methyl-2-tetrahydrofuran Mixtures at 77°K.[a]

Mole fraction of ethanol	ΔH_{MS}, gauss
0.0, 0.15, 0.25, 0.29, 0.33	5 ± 1
0.37	7 ± 1
0.40	12 ± 1
0.45	10 ± 1
1.0	14 ± 1

[a] The g factor for the lines was 2.001 ± 0.001.   [b] ΔH_{MS} is the line width between positions of maximum slope.

(6) F. S. Dainton and G. A. Salmon, *Proc. Roy. Soc.* (London), **A285**, 319 (1965).

degree of confinement or dielectric properties. Unlike the solvated halide ions, the solvation shell of the trapped electron cannot interchange solvent molecules with the bulk solvent. Consequently, the band positions do not reflect the bulk solvent composition. The orientation of O–H bonds serves to differentiate in kind the electron trapped in an ethanol from a methyl-2-tetrahydrofuran environment. Although no phase separation was evident, the mixtures might separate into domains of pure ether and ethanol character, in which case no specific difference in the kind of electron traps existing in rigid ethanol and methyl-2-tetrahydrofuran could be inferred.

A mixture showing the near-infrared band, together with an intermediate absorption, showed the relative stability of the latter subject to heating (Figure 2). Electrons trapped in mixed ethanol and ether environments would be responsible for the intermediate optical (and e.s.r.) absorptions, which correspond to deeper potential traps than those provided by pure ether.

Refractive Index Dispersion in Equine

Hemoglobin Solutions[1]

by W. H. Orttung and J. Warner

Department of Chemistry, University of California, Riverside, California 92502 (*Received February 18, 1965*)

Refractive index dispersion has been measured for several globular proteins in solution,[2–4] but the available data on hemoglobin[5–7] do not include wave length dependence. The data reported here were taken to complement Kerr effect optical dispersion studies,[8] but appear to be of some intrinsic interest, not only because regions of heme absorption are spanned, but also because hemoglobin is more α-helical than most other globular proteins. The refractive indices of dilute solutions of horse met- and oxyhemoglobin were measured in the 500–700-mμ range using a Brice–Phoenix differential refractometer[9] modified by the addition of an Engis S05-01 monochromator and tungsten lamp. The contribution of the visible and near-ultraviolet spectrum to $\Delta n/c$ was calculated by the

Kramers–Kronig relation and subtracted from the data. The residual dispersion was normal, but considerably less than that of other nonheme globular proteins.

Experimental

Hemoglobin was prepared from freshly drawn horse blood run directly into iced saline citrate solution to prevent clotting. The cells were spun out, then resuspended and washed five times with 1% NaCl. The packed cells were hemolyzed with 0.5 vol. of cold water and 0.4 vol. of cold toluene. The pH was brought to 6.8 by bubbling a 4:1 mixture of CO_2 and O_2 through the slurry and then crystallization was allowed to proceed overnight. Most of the cell bodies were separated by centrifugation and one washing with cold water. Two recrystallizations were carried out by raising the pH to 7.4 with 1 M K_2HPO_4, adding a minimum amount of water to achieve solution, and centrifuging, with removal of more cell bodies. An equal volume of cold saturated $(NH_4)_2SO_4$ was then added for recrystallization. All steps were carried out at 0°. Methemoglobin was prepared from oxyhemoglobin by ferricyanide oxidation according to Benesch, *et al.*,[10] and crystallized by dialysis against 2 parts of 4 M $(NH_4)_2SO_4$ and 1 part of 2 M $(NH_4)_2$-HPO_4. Concentrated stock solutions of both oxy- and methemoglobin were prepared and dialyzed extensively against cold distilled water, the concentrations then being determined by evaporation to dryness at 110°. Dilutions of the stock solutions were made by weight with distilled water. Volume concentrations, c, in grams per milliliter, were calculated from weight fractions. The quality of the dilutions was monitored on a Cary 14 spectrophotometer.

Calibration of the refractometer at 25° was carried out in a manner similar to that described previously.[11]

(1) This investigation was supported in part by Public Health Service Research Grant GM11683-01 from the Division of General Medical Sciences.

(2) G. E. Perlmann and L. G. Longsworth. *J. Am. Chem. Soc.*, 70, 2719 (1948).

(3) M. Halwer, C. G. Nutting, and B. A. Brice, *ibid.*, 73, 2786 (1951).

(4) T. L. McMeekin, M. L. Groves, and N. J. Hipp, Advances in Chemistry Series, No. 44, American Chemical Society, Washington, D. C., 1964, p. 54.

(5) J. L. Stoddard and G. S. Adair, *J. Biol. Chem.*, 57, 437 (1923).

(6) O. Lamm and A. Poulson, *Biochem. J.*, 30, 528 (1936).

(7) A. Rossi-Fanelli, E. Antonini, and A. Caputo, *J. Biol. Chem.*, 236, 391 (1961).

(8) W. H. Orttung, *J. Am. Chem. Soc.*, 87, 924 (1965).

(9) Phoenix Precision Instrument Co., Philadelphia 40, Pa.

(10) R. Benesch, R. E. Benesch, and G. Macduff, *Science*, 144, 68 (1964).

(11) W. H. Orttung, *J. Phys. Chem.*, 67, 1102 (1963).
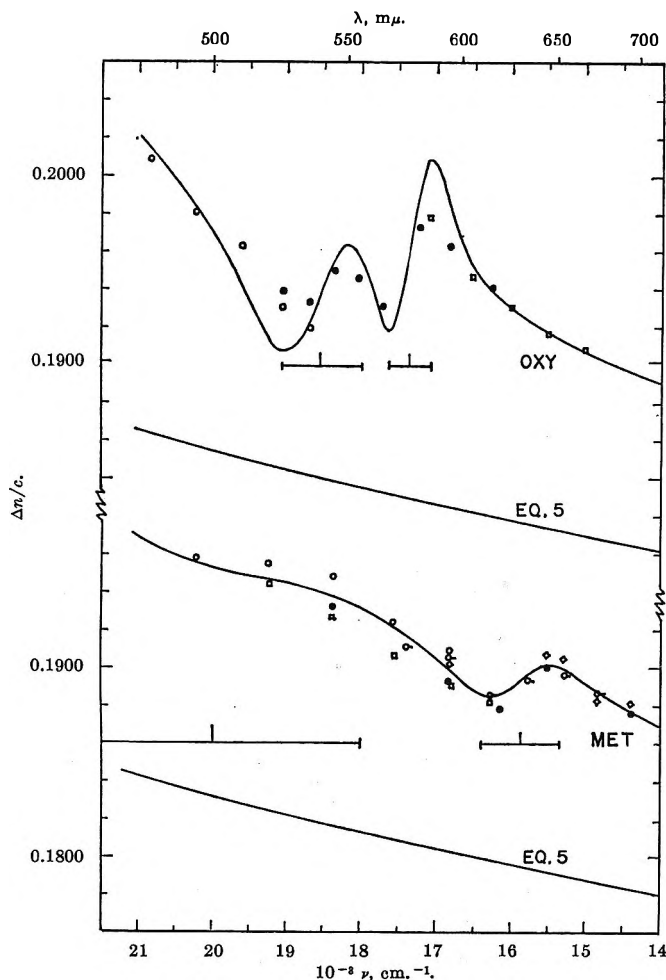
Figure 1. Refractive increments for oxyhemoglobin (top) and methemoglobin (bottom) solutions in distilled water at 15°. Absorption peaks and half-widths are indicated by the horizontal lines below each set of data. The line through each set of points is the sum of a spectral and a residual contribution, the latter being eq. 5. The concentrations, $10^3 c$, were as follows: O, -4.579, ●, -4.636, □, -10.031 for oxyhemoglobin; O, -4.537, ●, -7.159, □, -7.747, O-, -10.995, and ◇, -14.417 for methemoglobin.

The calibration did not change significantly in cooling the refractometer to 15°, the temperature at which data were taken. Values of $\Delta n/c$ at 15° are plotted vs. $\nu = 1/\lambda$ in Figure 1. ($\Delta n = n - n_0$, where n and n_0 are the refractive indices of solution and solvent.) The precision of the data is close to the limiting precision of the apparatus.[11]

Calculations

For present purposes, the Kramers–Kronig relation[12] may be put into the form

$$(\Delta n/c)_{\text{sp}} = \frac{2303}{2\pi^2 M} P \int_0^\infty \frac{\epsilon(\nu')}{\nu'^2 - \nu^2} d\nu' \quad (1)$$

where $\epsilon(\nu')$ is the molar extinction coefficient at $\nu' = 1/\lambda'$, M is the corresponding solute molecular weight, P indicates the principal value of the integral, and $(\Delta n/c)_{\text{sp}}$ is the contribution of the absorption spectrum to $\Delta n/c$ at ν. The spectra of met- and oxyhemoglobin from 250 to 700 mμ[13] were plotted vs. ν. It was assumed that ϵ corresponds to $M = 16,700$. Each spectrum could be fitted by seven gaussian functions of the type

$$\epsilon(\nu) = \epsilon_0 e^{-4 \ln 2 (\nu - \nu_0)^2/\gamma^2} \quad (2)$$

the parameters of which are given in Table I. Fitting of the spectra with gaussians is a mathematical step that simplifies the calculations; i.e., if eq. 2 is substituted in eq. 1, the following approximate result may be deduced[14]

$$(\Delta n/c)_{\text{sp}} \cong - \frac{2303 \epsilon_0}{2\pi^{3/2} M} \frac{1}{\nu_0} e^{-\beta^2 (\nu - \nu_0)^2} \int_0^{\beta(\nu - \nu_0)} e^{t^2} dt \quad (3)$$

where $\beta^2 = 4 \ln 2/\gamma^2$. For present purposes, eq. 3 is satisfactory for $|(\nu - \nu_0)/\gamma| \leqslant 2$. Far from regions of absorption, when $|(\nu - \nu_0)/\gamma| \geqslant 2$, eq. 1 and 2 become

$$(\Delta n/c)_{\text{sp}} = \frac{2303 \epsilon_0}{2\pi^{3/2} M} \frac{\gamma}{2\sqrt{\ln 2}} \frac{1}{\nu_0^2 - \nu^2} \quad (4)$$

The contributions of each of the seven gaussians to $\Delta n/c$ were then calculated from eq. 3 and 4 and summed to obtain the total contribution for the spectral region 250–700 mμ. The calculated contribution was subtracted from the data of Figure 1 and the remainder was plotted vs. ν^2. A straight line of the form

$$(\Delta n/c)_{\text{exptl}} - (\Delta n/c)_{\text{sp}} = a + b \times 10^{-8} \nu^2 \quad (5)$$

was fitted to the methemoglobin data by least squares, giving $a = 0.1731 \pm 0.0007$ and $10^4 b = 25.3 \pm 2.4$. A straight line with the same slope and $a = 0.1753$ could be drawn through the end regions of the oxyhemoglobin data. The spectral contributions were then combined with eq. 5 and plotted in Figure 1 for com-

(12) See, for example, L. D. Landau and E. M. Lifschitz, "Electrodynamics of Continuous Media," Addison-Wesley, Reading, Mass., 1960.

(13) R. Lemberg and J. W. Legge, "Hematin Compounds and Bile Pigments," Interscience Publishers, Inc., New York, N. Y., 1949, p. 749. The data reported here are for the human (oxy) and ox (met) species, but are in satisfactory agreement with our own Cary 14 measurements on horse hemoglobin in the visible region, as might be expected from the fact that the spectrum is insensitive to species difference for this molecule.

(14) G. E. Pake and E. M. Purcell, Phys. Rev., **74**, 1184 (1948).

parison with the data. The agreement is good for methemoglobin, but there are noticeable deviations for oxyhemoglobin that are undoubtedly partly explained by some monochromator slit width averaging of the peaks (2-mm. slits were used and the monochromator dispersion was 6.6 mμ/mm.).

Table I: Gaussian Fit of Spectra

λ, mμ	ν_0, cm.$^{-1}$	γ, cm.$^{-1}$	ϵ_0
	Methemoglobin		
630	15870	1060	4.2
500	20000	4000	9.5
406	24650	1400	125
388	25800	1300	30
369	27100	5400	27.0
300	33300	5100	16.0
265	37750	3200	31.5
	Oxyhemoglobin		
576	17355	550	16.0
540	18540	1100	15.0
450	22200	3200	11.0
416	24050	1400	118
394	25400	1200	17.0
349	28670	6200	28.4
275	36363	4220	35.8

Discussion

Earlier results[2,3] gave $10^4 b = 33$–36 for other nonheme globular proteins, a significantly higher range than the hemoglobin results reported here. Far-ultraviolet or infrared transitions of the heme groups would cause greater dispersion in the visible and therefore predict an opposite difference. The peptide chains must therefore be responsible for the difference observed.

Variations in amino acid composition were considered, but a rough calculation suggested that this effect would not account for the magnitude of the difference. A hypochromic effect in the 190-mμ peptide band[15,16] was also considered (hemoglobin is considerably more α-helical than the other proteins), but the predicted reduction in slope was only a fraction of the observed difference. We have therefore observed a significantly lower dispersion in the globin as compared to other proteins that have been studied, but have not established a quantitative explanation.

(15) I. Tinoco, Jr., A. Halpern, and W. T. Simpson in "Polyamino Acids, Polypeptides, and Proteins," M. A. Stahmann, Ed., University of Wisconsin Press, Madison, Wis., 1962, p. 157.

(16) K. Rosenheck and P. Doty, *Proc. Natl. Acad. Sci. U. S.*, **47**, 1775 (1961).

Volume–Energy Relations in Liquids at 0°K.

by A. A. Miller

General Electric Research Laboratory, Schenectady, New York
(Received March 15, 1965)

By a special (nonlinear) extrapolation of measured liquid densities, Doolittle[1] derived the relation, ln $v_0 = 10/M$, for the specific volumes of n-alkanes in the hypothetical liquid state at 0°K. These values were shown to agree with several earlier, independent estimates.[1,2] Additional confirmation by more recent methods will be presented later.

For ethane, which consists of only two methyl groups, $v_0 = 1.396$ cc./g. or 21.0 cc./mole of CH_3. For the infinite polymethylene chain, $v_0 = 1.00$ cc./g. or 14.0 cc./mole of CH_2. Comparison of these molar volumes shows that $v_0(H) = 7.0$ cc./mole, with no contribution by the internal carbon atom. Thus, the minimum volume at 0°K., where $(dE/dv)_T = 0$, can be attributed entirely to the attraction–repulsion of the peripheral H atoms. By comparison, the *van der Waals* volumes are $v_w(CH_3) = 13.67$, $(CH_2) = 10.23$, $(H) = 3.45$, and

$$(-\overset{|}{\underset{|}{C}}-) = 3.33 \text{ cc./mole.}[3]$$

The vaporization energy, ϵ_0, for the hypothetical liquid at 0°K. is given by the B constant of the Frost–Kalkwarf vapor pressure equation: $\epsilon_0 = -2.3RB$ cal./mole.[4,5] Thodos and co-workers have reported the F–K constants for saturated aliphatic,[6] olefinic,[7] naphthenic,[8] and aromatic[9] hydrocarbons, and miscellaneous compounds including CCl_4.[10] It was shown that B is an additive function of the chemical structure. For the n-alkanes,[6] following ethane ($B = -1070°$), the slope of the linear plot of B vs. the number of carbon atoms gives $\Delta B = -340°$/methylene unit. Hence, $\epsilon_0(CH_3) = 2.45$ and $\epsilon_0(CH_2) = 1.55$ kcal./mole, and the ratio is 1.58, which is close to the ratio of the number of H atoms in the two groups. For the cohesive energy densities, $(\epsilon/v)_0 = 117$ cal./cc. for CH_3

(1) A. K. Doolittle, *J. Appl. Phys.*, **22**, 1471 (1951).

(2) A. P. Mathews, *J. Phys. Chem.*, **20**, 554 (1916).

(3) A. Bondi, *ibid.*, **68**, 441 (1964).

(4) See E. A. Moelwyn-Hughes, "Physical Chemistry," Pergamon Press, Inc., New York, N. Y., 1961, p. 696 ff.

(5) A. A. Miller, *J. Phys. Chem.*, **68**, 3900 (1964).

(6) N. E. Sondak and G. Thodos, *A.I.Ch.E. J.*, **2**, 347 (1956).

(7) C. H. Smith and G. Thodos, *ibid.*, **6**, 569 (1960).

(8) G. J. Pasek and G. Thodos, *J. Chem. Eng. Data*, **7**, 21 (1962).

(9) D. L. Bond and G. Thodos, *ibid.*, **5**, 288 (1960).

(10) E. C. Reynes and G. Thodos, *Ind. Eng. Chem. Fundamentals*, **1**, 127 (1962).

and 110 cal./cc. for CH_2, using the Doolittle v_0 values. By linear extrapolation of vaporization energy $vs.$ liquid density plots, it was found earlier that $(\epsilon/v)_0 \simeq$ 117 cal./cc. for the C_5 to C_{12} n-alkanes.[5]

The following new relationship between ϵ_0 and v_0 and the van der Waals constants a and b is proposed

$$\epsilon_0 = ab/v_0^2 \qquad (1)$$

This originates from the equation $\epsilon_0 = a'/v_0$, for a van der Waals liquid,[11] with the argument that the a' applying at $0°K.$ and the van der Waals a applying at the critical point are related as $a' = a(b/v_0)$. It will be recalled that, in terms of the critical constants, $a = 27R^2T_c^2/64P_c$ and $b = RT_c/8P_c$. By structural additivity, Thodos has derived a and b values which give excellent agreement with the observed critical constants for olefinic, saturated aliphatic, naphthenic, and aromatic hydrocarbons.[12] By eq. 1, using the Thodos ϵ_0, a, and b values, we may compute v_0.

Table I compares several estimates of v_0 for n-alkanes. For the van der Waals rule,[2] $v_0 = z_c v_c$ where $z_c = (PV/RT)_c$, the critical constants reported by Kobe and Lynn were used.[13] Although the methods of Riedel[14] and Pitzer are similar, the latter's equation[15] with reported "acentric factors"[16] and critical densities[13] gives v_0 values which are 5% lower. After methane, the other four methods show agreement to within 2%. Above C_8H_{13}, however, $v_0 = e^{10/M}$ and eq. 1 give diverging values, and for $C_{20}H_{42}$, $v_0 = 1.036$ and 0.976 cc./g., respectively. The zero-point volumes of the crystalline solids[17] are 2 to 3% lower than the values in the first column of Table I.

Table I: Specific Volumes of n-Alkane Liquids at $0°K.$

	$e^{10/M}$	$(ab/\epsilon_0)^{1/2}$	$z_c v_c$	Riedel[14]	Pitzer[15]
CH_4	...	1.88	1.78	1.75	1.64
C_2H_6	1.396	1.40	1.40	1.335	1.28
C_3H_8	1.256	1.27	1.26	1.235	1.17
C_4H_{10}	1.189	1.19	1.20	1.180	1.12
C_5H_{12}	1.150	1.15	1.16	1.150	1.09
C_6H_{14}	1.123	1.12	1.13	1.130	...
C_7H_{16}	1.105	1.10	1.10	1.116	1.05
C_8H_{18}	1.092	1.08	1.10	1.105	...

The v_0 values, computed by eq. 1, for four compact molecules with spheroidal symmetry, are compared in Table II with "hard-core volumes," v^*, derived by Flory and Abe from thermal expansion coefficients at $25°.$[18] Based on Thodos' ϵ_0-values, the cohesive energy density at $0°K.$ is compared with the Flory p^* energy parameter.[18]

Table II: Volume–Energy Parameters for Spheriodal Molecules

	v_0, cc./g.[a]	v^*, cc./g.[b]	ϵ_0/v_0, cal./cc.	P^*, cal./cc.[b]	Ratio
C_6H_6	0.880	0.885	163	150	0.92
CCl_4	0.492	0.485	146	136	0.93
c-C_6H_{12}	0.980	1.00	133	127	0.95
$C(CH_3)_4$	1.14	1.19	102	95	0.93

[a] By eq. 1. [b] See ref. 18, at $25°.$

By the van der Waals rule, $v_0 = z_c v_c$, and eq. 1, we obtain

$$\epsilon_0(\text{cal./mole}) = (0.0527 z_c^{-4}) RT_c$$

It may be noted, in passing, that if $v_0 = z_c v_c$, $b = v_c^2/8v_0$, rather than $b = v_c/3$, a well-known discrepancy in the van der Waals equation.

Discussion

The scope of the simple relation, $\epsilon_0 = ab/v_0^2$, requires further empirical examination, particularly since its theoretical basis is not immediately apparent.

The Frost–Kalkwarf vapor pressure equation, in a reduced form, has been shown to apply to a broad range of polar and nonpolar, organic and inorganic liquids, where hydrogen bonding is absent.[10,19] For such liquids, the empirical constants of the F–K equation can be calculated from a single reduced vapor pressure point. Thus, the critical pressure and temperature and the normal boiling point, for example, are sufficient to define v_0 via eq. 1 and also v_c via the van der Waals rule: $v_c = (v_0 RT_c/P_c)^{1/2}$.

A thermochemical interpretation of the F–K equation, in terms of $\Delta H°_0$ and ΔC_p, has been discussed.[20] The present work, together with the ϵ–ρ relations reported previously,[5] may be useful for deriving an alternate interpretation, with the liquid volume as an explicit parameter.

(11) See ref. 4, pp. 378, 379.

(12) G. Thodos, *A.I.Ch.E. J.*, **1**, 165, 168 (1955); **2**, 508 (1956); **3**, 428 (1957).

(13) K. A. Kobe and R. E. Lynn. *Chem. Rev.*, **52**, 117 (1953).

(14) L. Riedel, *Chem. Ingr.-Tech.*, **26**, 257 (1954).

(15) See G. N. Lewis and M. Randall, "Thermodynamics," McGraw-Hill Book Co., Inc., New York, N. Y., 1961, p. 621.

(16) K. S. Pitzer, *et al.*, *J. Am. Chem. Soc.*, **77**, 3433 (1955).

(17) See A. Bondi, *J. Phys. Chem.*, **58**, 929 (1954), Table V, eq. 2.

(18) P. J. Flory and A. Abe, *J. Am. Chem. Soc.*, **86**, 3563 (1964).

(19) See D. G. Miller and G. Thodos, *Ind. Eng. Chem. Fundamentals*, **2**, 78, 80 (1963), for the reduced F–K equation in terms of the Riedel α_c-parameter.

(20) A. Bondi and R. B. McConaughy, *Proc. Am. Petrol. Inst.*, *Sect. III*, **42**, 40 (1962).

λ-Type Thermal Anomaly in

Tetrauranium Enneaoxide at 348°K.

by Edgar F. Westrum, Jr., Yoichi Takahashi,

Department of Chemistry, University of Michigan,
Ann Arbor, Michigan

and Fredrik Grønvold

Chemical Institute A, University of Oslo, Blindern, Oslo, Norway
(Received March 17, 1965)

The contraction in the lattice constants of U_4O_9 between 293 and 359°K. observed by Grønvold[1] and the divergence of the heat capacity[2] above 270°K. from that of the structurally closely related triuranium heptaoxides[3] led Westrum and Grønvold[3,4] to deduce the probable existence of a transition near 350°K. in this substance. Heat capacity measurements have subsequently revealed the reality of this predicted phenomenon.

Experimental

The preparation and characterization of the sample has been recorded.[2] Heat capacity measurements were made both in the Mark III cryostat[5] and, at higher temperatures, in the Mark IV[6] thermostat. In both instances the quasi-adiabatic technique was employed. The heat capacity of the 82.5-g. sample represented about 61 and 42% of the total in the cryostat and thermostat, respectively. All measurements were referred to calibrations or standardizations of the National Bureau of Standards.

The curvature corrected data obtained are presented in Table I in terms of the defined thermochemical calorie of 4.1840 joules and in chronological sequence so that the approximate temperature increments employed in the measurements may usually be deduced from the adjacent (mean) temperatures. The probable errors of the heat capacity and the derived thermodynamic functions are less than 0.1%. The data accord well with previous adiabatic heat capacity measurements on this sample made in another laboratory.[2] The enthalpy $(H°_{400} - H°_{298.15})$ and entropy $(S°_{400} - S°_{298.15})$ increments over the temperature range are 9152 cal./g.f.m. and 28.04 cal./(g.f.m. °K.) based on the formula U_4O_9.

A λ-type thermal anomaly with a peak near 348°K. is apparent in Figure 1.[7-11] If the heat capacity of the closely related α-$UO_{2.33}$ phase (i.e., $^1/_3\alpha$-U_3O_7) is used to represent the lattice (vibrational) heat capacity, the excess enthalpy of the transition in $UO_{2.25}$ (i.e.,

Table I: Heat Capacity of Tetrauranium Enneaoxide[a]

$\bar{T}$	c_p	$\bar{T}$	c_p	$\bar{T}$	c_p
Series I		198.05	55.15	342.32	84.2
		207.07	56.78	346.09	86.6
285.04	68.26	216.37	58.34		
295.26	69.64	255.09	64.21	Series IV	
300.82	70.59	261.23	65.06		
303.29	70.89	306.31	71.46	343.6	85.3
308.10	71.63	311.94	72.66	346.9	88.1
313.70	72.96	317.49	74.01	347.6	90.0
319.21	74.76	322.29	75.45	349.9	96.2
329.95	78.51			351.2	88.1
335.15	80.6	Series III		354.4	84.4
340.28	83.2			357.5	82.0
345.33	86.7	309.69	72.12	362.4	79.4
349.10	97.0	315.23	73.49	367.5	77.5
		321.38	75.14	375.7	75.4
Series II		327.44	76.91	385.0	75.1
		332.70	79.56	392.5	75.6
190.02	53.70	337.86	81.8	399.2	76.0

[a] Units: cal., g.f.m., °K.; g.f.m. of U_4O_9 = 1096.3. Series I, II, and III in Mark III cryostat; series IV in Mark IV thermostat.

$^1/_4U_4O_9)$ between 240 and 390°K. aggregates to 150 ± 2 cal./g.f.m., and the corresponding entropy increment is 0.45 ± 0.01 cal./(g.f.m. °K.).

The mechanism of the transition is presumably of structural origin in view of the well-behaved paramagnetism of the oxide above the antiferro- to paramagnetic transition at 6.4°K.[12] and up to 450°K.[7] The structure of U_4O_9 is related to the fluorite-type structure of UO_2, but with interstitial oxygen atoms.[13] The resulting unit cell is cubic with quadrupled axial

(1) F. Grønvold, *J. Inorg. Nucl. Chem.*, **1**, 357 (1955).

(2) D. W. Osborne, E. F. Westrum, Jr., and H. R. Lohr, *J. Am. Chem. Soc.*, **79**, 529 (1957).

(3) E. F. Westrum, Jr., and F. Grønvold, *J. Phys. Chem. Solids*, **23**, 39 (1962).

(4) E. F. Westrum, Jr., and F. Grønvold, "Thermodynamics of Nuclear Materials," International Atomic Energy Agency, Vienna, 1962, p. 3.

(5) E. F. Westrum, Jr., *J. Chem. Educ.*, **39**, 443 (1962).

(6) J. C. Trowbridge and E. F. Westrum, Jr., *J. Phys. Chem.*, **67**, 2381 (1963).

(7) E. F. Westrum, Jr., *et al.*, unpublished data.

(8) G. E. Moore and K. K. Kelley, *J. Am. Chem. Soc.*, **69**, 2105 (1947).

(9) E. F. Westrum, Jr., and F. Grønvold, *ibid.*, **81**, 1777 (1959).

(10) M. M. Popov, G. L. Gal'Chenko, and M. D. Senin, *Zh. Neorgan. Khim.*, **3**, 1734 (1958).

(11) W. M. Jones, J. Gordon, and E. A. Long, *J. Chem. Phys.*, **20**, 695 (1952).

(12) M. J. M. Leask, L. E. J. Roberts, A. J. Walter, and W. P. Wolf, *J. Chem. Soc.*, 4788 (1963).

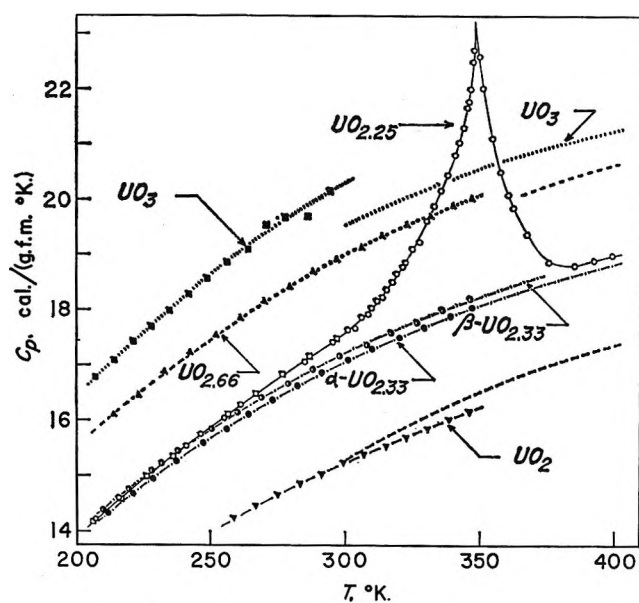(13) H. Hering and P. Perio, *Bull. soc. chim. France*, 351 (1952).

Figure 1. Heat capacity of $UO_{2.25}$ —O— compared
with data on the same sample by Osborne, et al., —□—,[2]
and with that of UO_2 – -▼- -,[7] – – – –,[8]
α-$UO_{2.33}$ · – -●- – ·,[8] β-$UO_{2.33}$ – · -◐- · -,[3] $UO_{2.66}$
– – -▲- – ·,[9] – – – –,[10] and UO_3 · · -■- · ·,[11] . . . . .[8]

dimensions compared to UO_2 according to Belbeoch, et al.,[14] and Willis,[15] while Andresen[16] indexed it as tetragonal with $A = 2a\sqrt{2}$ and $C = 2a$. Placement of the interstitial oxygen atoms in the cubic interstices with eight oxygen atoms as nearest neighbors is clearly objectionable from a chemical point of view, and the thorough neutron diffraction study of single crystals of U_4O_9 by Willis[15] has shown that incorporation of the interstitial oxygen atoms is accompanied by ejection of about 10% of the oxygen atoms from their positions in the fluorite-type structure. The interstitial and ejected oxygen atoms are located in the vicinity of the center of the cubic interstices, 60% of them 0.86 Å. away along the $\langle 110 \rangle$ directions and 40% 1.05 Å. away along the $\langle 111 \rangle$ directions. Although the detailed ordering of the interstitials has not yet been worked out, it is apparent that about half of the uranium atoms are formally present as U^{5+}. Thus, a formula $2UO_2 \cdot U_2O_5$ represents the situation better than $3UO_2 \cdot UO_3$.

At low temperatures an ordered arrangement of interstitial and displaced oxygen atoms is expected, which again results in an ordered distribution of the cations. It seems tempting to relate the λ-type thermal anomaly with an order–disorder process involving the interstitial and displaced oxygen atoms although no changes in the structure of U_4O_9 have yet been reported in this temperature region.

In the zeroth approximation, the extra oxygen atom in U_4O_9 may either be in a fixed position or randomly distributed over four positions, which, for $UO_{2.25}$, would lead to an entropy increment of $^1/_4R$ ln 4 or 0.68 cal./(g.f.m. °K.). The actual situation is apparently much more complicated, in that different possible modes of ejecting the normal oxygen atoms tending to increase the entropy may exist, while the requirement of even distribution of U^{4+} and U^{5+} will appreciably reduce the entropy. Detailed delineation of the structure is an obvious desideratum.

The thermal effect may be somewhat broadened by radiation damage to the sample accumulated over a 10-year period at room temperature. Although repetition of the measurements after conditioning the sample at high temperature would test this point, a more thorough elimination of this possibility will be achieved by heat capacity measurements to 800°K. on a new sample at the University of Oslo.

(14) B. Belbeoch, C. Piekarski, and P. Perio, *Acta Cryst.*, **14**, 837 (1961).

(15) B. T. M. Willis, *J. phys. radium*, **25**, 431 (1964).

(16) A. F. Andresen, Enlarged Symposium on Reactor Materials, Stockholm, Sweden, Oct. 1959.

Dissociation and Homoconjugation of Certain Phenols in Acetonitrile

by J. F. Coetzee[1] and G. R. Padmanabhan[2]

Department of Chemistry, University of Pittsburgh, Pittsburgh, Pennsylvania 15213 *(Received March 25, 1965)*

As compared to water, acetonitrile provides striking differentiation in the dissociation of Brønsted acids, mainly as a result of the following three factors. (1) The proton-acceptor power of acetonitrile is smaller than that of water by five powers of ten, as given by its reaction with a reference acid of type BH^+.[3] Hence, the primary reaction of Brønsted acids with the solvent, which is the first step in the over-all dissociation reaction

(1) Address all correspondence to this author.

(2) From the Ph.D. thesis of this author, University of Pittsburgh, 1963.

(3) J. F. Coetzee and D. K. McGuire, *J. Phys. Chem.*, **67**, 1810 (1963).

$$HB^{n+} + S \rightleftharpoons SH^{+}B^{(n-1)+} \rightleftharpoons SH^{+} + B^{(n-1)+} \tag{1}$$
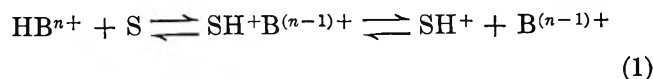
where n can be positive, negative, or zero, is less complete in acetonitrile than in water. (2) The dielectric constant of acetonitrile (36.0) is smaller than that of water (78.5). Hence, for purely electrostatic reasons, as indicated by the Born equation, the second (dissociation) step of reaction 1 will be more sensitive to variations in the effective radii of the ions in acetonitrile than in water, particularly for acids with n values other than $+1$. (3) A critical factor for acids with n values that are negative or zero is the limited capacity of acetonitrile to stabilize anions by hydrogen bonding. Consequently, subtle variations in the polarizability or other properties of the anion affect the equilibrium constant of reaction 1 much more markedly in acetonitrile than in water. In fact, certain anions derive stability by resorting to hydrogen bonding with undissociated acid, with the result that dissociation reactions such as the following occur.

$$2HB^{0} + S \rightleftharpoons SH^{+}BHB^{-} \rightleftharpoons SH^{+} + BHB^{-} \tag{2}$$
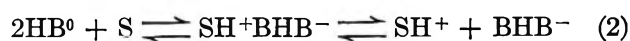
Considerable qualitative information is available on the differentiation of uncharged or anionic acids in acetonitrile, mainly from the results of empirical potentiometric titrations.[2] However, quantitative information is lacking. The main exception is provided by the results of a conductometric and spectrophotometric study by Kolthoff, Bruckenstein, and Chantooni on hydrochloric, hydrobromic, nitric, sulfuric, and picric acids.[4] In this communication we report the results of an exploratory potentiometric study of five phenols in acetonitrile. We have shown before that under properly controlled conditions the glass electrode responds reversibly to hydrogen ion activity in anhydrous acetonitrile.[5] The measurements reported here were carried out in a similar manner.

Experimental

Sohio acetonitrile was purified as described before.[6] Allied Chemical Co. C.P. phenol was used without further purification. The remaining phenols were recrystallized and then dried *in vacuo* as indicated: Eastman White Label *o*-nitrophenol (from methanol, at 25°) and *p*-nitrophenol (water, 50°); Fisher reagent grade 2,4-dinitrophenol (water, 40°); and Baker and Adamson picric acid (twice from acetone, 80°). Tetraethylammonium perchlorate and picrate were prepared as described before.[5] Tetraethylammonium *o*-nitrophenoxide and *p*-nitrophenoxide, and tetrabutylammonium phenoxide and 2,4-dinitrophenoxide, were prepared by titrating the phenol with tetraalkylammo-

nium hydroxide, using a glass electrode to detect the equivalence point. The solutions were evaporated and then cooled in ice, and finally the salts were recrystallized from ethyl acetate and dried *in vacuo* at 40–50°.

Measurements. For each phenol the potential of a Beckman General Purpose No. 1190-80 glass electrode was measured in a series of 10 to 15 buffer solutions containing a constant concentration $(5.0 \times 10^{-4} M)$ of phenoxide and varying concentrations (typically 2.5×10^{-4} to $5 \times 10^{-1} M$) of the corresponding phenol, using the instrumentation described before.[5] Absorbance measurements were made with a Beckman Model DB spectrophotometer, using a matched pair of silica cells (Beckman No. 46007). Further details are given in ref. 2.

Results and Discussion

The results obtained at 25° are presented in Tables I and II and Figure 1. Equilibrium constants were calculated as described elsewhere for amines.[7] The results in Table II lead to the following conclusions.

(1) All phenols tested, except picric acid, form relatively stable homoconjugate complexes, $BH \cdots B^{-}$. In addition, unsubstituted phenol also forms a 2:1 complex, $(BH)_2 B^{-}$. The existence of such complexes is well established, even in the solid state,[8] and their formation has been inferred from the shapes of titration

Table I: Spectrophotometric Determination of Formation Constant of Homoconjugate Complex of o-Nitrophenol in Acetonitrile

$C_{HB}{}^a$	$C_{B}{}^{-b}$	$[B^{-}]_{measd}{}^c$	$[BHB^{-}]^d$	$[HB]^e$	$K_{f,1}{}^f$
5.0×10^{-4}	2.0×10^{-5}	1.9×10^{-5}	1.2×10^{-6}	5.0×10^{-4}	130
5.0×10^{-3}	2.0×10^{-5}	1.3×10^{-5}	7.5×10^{-6}	5.0×10^{-3}	119
5.0×10^{-2}	2.0×10^{-5}	3.1×10^{-6}	1.7×10^{-5}	5.0×10^{-2}	109
5.0×10^{-2}	5.0×10^{-4}	8.0×10^{-5}	4.2×10^{-4}	5.0×10^{-2}	105

^{a} Total (analytical) molar concentration of *o*-nitrophenol. ^{b} Total molar concentration of tetraethylammonium *o*-nitrophenoxide. ^{c} Measured by absorbance at 452 mμ. BHB^{-} has absorption maximum at lower wave length. Validity of Beer's law established. ^{d} $[BHB^{-}] = C_{B^{-}} - [B^{-}]_{measd}$. ^{e} $[HB] = C_{HB} - [BHB^{-}]$. ^{f} $K_{f,1} = [BHB^{-}]/[B^{-}][HB]$, assuming that $f_{BHB^{-}}/f_{B^{-}}f_{HB} \sim 1$. Average value of 1.1×10^2 assumed.

(4) I. M. Kolthoff, S. Bruckenstein, and M. K. Chantooni, Jr., *J. Am. Chem. Soc.*, **83**, 3927 (1961).

(5) J. F. Coetzee and G. R. Padmanabhan, *J. Phys. Chem.*, **66**, 1708 (1962).

(6) J. F. Coetzee, G. P. Cunningham, D. K. McGuire, and G. R. Padmanabhan, *Anal. Chem.*, **34**, 1139 (1962).

(7) J. F. Coetzee and G. R. Padmanabhan, *J. Am. Chem. Soc.*, in press.

(8) D. Hadži, A. Novak, and J. E. Gordon, *J. Phys. Chem.*, **67**, 1118 (1963).

Table II: Formation Constants of Homoconjugate Complexes and Acid Dissociation Constants of Phenols in Acetonitrile (AN) and Water (W)

Acid	$(-pK_{f,1})_{AN}$	$(-pK_{f,2})_{AN}{}^a$	$(-pK_{f,12})_{AN}{}^b$	$(pK_a)_{AN}{}^c$	$(pK_a)_W{}^d$	$\Delta pK_a{}^e$
Phenol			5.76	26.6	10.00	16.6
o-Nitrophenol	2.00^f	None		22.0	7.23	14.8
p-Nitrophenol	3.15	1.78	4.93	20.7	7.15	13.5
2,4-Dinitrophenol	2.00	None		16.0	4.11	11.9
2,4,6-Trinitrophenol	None			11.0^g	0.71	10.3

^{a} Referring to reaction: $BHB^- + BH \rightleftharpoons (BH)_2B^-$. ^{b} Referring to over-all reaction: $B^- + 2BH \rightleftharpoons (BH)_2B^-$. ^{c} From measurements on solutions containing $1.0 \times 10^{-2} M$ Et_4NClO_4 as well, added to maintain constant junction potential Calculations as described elsewhere for amines (ref. 7). ^{d} From compilation in R. A. Robinson and R. H. Stokes, "Electrolyte Solutions," Butterworths and Co. Ltd., London, 1959. ^{e} $\Delta pK_a = (pK_a)_{AN} - (pK_a)_W$. ^{f} Value from Table I: 2.04. Estimated uncertainty in pK values: ± 0.1. ^{g} Private communication from I. M. Kolthoff and M. K. Chantooni, Jr., University of Minnesota. On this basis, autoprotolysis constant of acetonitrile (ref. 5) becomes 3×10^{-29}. Calibration of scale of acidities is discussed further in ref. 7.
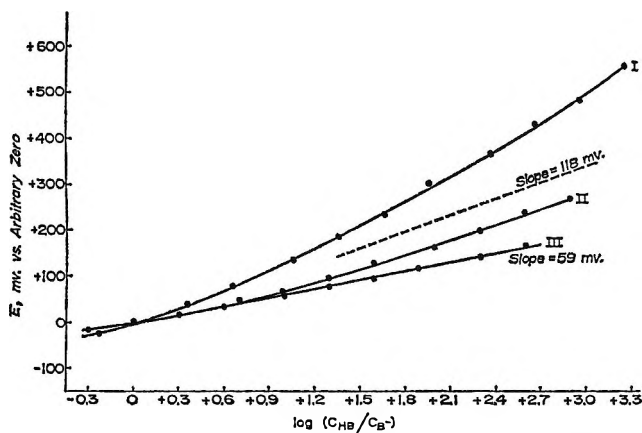

Figure 1. Response of glass electrode in phenol–phenoxide buffers in acetonitrile at a constant salt concentration of $5.0 \times 10^{-4} M$: I, phenol; II, o-nitrophenol; III, picric acid. In all cases, potentials refer to arbitrary zero at $C_{HB} = C_{B^-}$.

curves in several solvents; for a literature survey, see ref. 2.

(2) Substitution of either phenol or p-nitrophenol with a nitro group in the ortho position to the hydroxy group markedly reduces homoconjugation, and substitution of the latter phenol in both ortho positions entirely eliminates complexation. This effect is attributed mainly to stabilization of the acid form by intramolecular hydrogen bonding. That such stabilization occurs is indicated by the fact that whereas o- and p-nitrophenol have similar dissociation constants in water, the former acid is considerably weaker than the latter in acetonitrile. This conclusion is supported by the infrared data of Brooks and Morman,[9] which show that in acetonitrile some hydrogen bonding between hydroxy and nitro groups persists even in compounds such as 2-hydroxy-3-nitrobenzaldehyde, in which strong competitive hydrogen bonding to the carbonyl group

occurs. On the other hand, in aqueous solution o-nitrophenol shows little or no intramolecular hydrogen bonding,[10] undoubtedly owing to effective competition from hydration.

(3) The results show no evidence of dimerization of phenols in acetonitrile, in agreement with the behavior of other acids in this solvent.[11]

(4) In acetonitrile, differentiation in the dissociation of the phenols listed is increased by 6 pK units (8 kcal. mole^{-1}) over that observed in water. The stabilization of the acid form caused by ortho substitution must be more than offset by stabilization of the anion, undoubtedly in part as a result of the increasing polarizability.

(5) A serious limitation of acetonitrile as a medium for acid–base reactions is the unavailability of a relatively strong base for this solvent. Any attempt to generate the lyate ion, CH_2CN^-, in sufficiently high concentration (e.g., by treating acetonitrile with lithium or sodium metal) leads to polymerization of the solvent. Alkali metal hydroxides are virtually insoluble (the absolute activity of the high charge density hydroxyl ion is extremely high in a nonhydrogen-bonding solvent), and anhydrous solutions of tetraalkylammonium hydroxides are unstable. Phenoxide ion is the strongest stable base that we have encountered in acetonitrile ($pK_b = 28.6 - 26.6 = 2.0$). However, the homoconjugation undergone by this ion would detract from its usefulness as a base. It will be worthwhile to investigate the applicability of a hindered phenoxide, such as the tetraalkylammonium salt of 2,6-di-t-butylphenol.

(9) C. J. W. Brooks and J. F. Morman, *J. Chem. Soc.*, 3372 (1961).

(10) L. B. Magnusson, C. A. Craig, and C. Postmus, Jr., *J. Am. Chem. Soc.*, 86, 3958 (1964).

(11) J. F. Coetzee and R. Lok, *J. Phys. Chem.*, 69, 2690 (1965).

High Resolution Mass Spectrum

of Piperidine

by L. W. Daasch

Chemical Research and Development Laboratories, Edgewood Arsenal, Edgewood, Maryland   (Received March 26, 1965)

Budzikiewicz, Djerassi, and Williams[1] refer to their cleavage mechanisms for piperidine as tentative and in need of verification by isotope labeling or high resolution mass spectrometry. Such a spectrum[2] under a resolution of about 1 in 2500 [$\Delta h/H \cong 0.01$] is presented in Table I.[3]
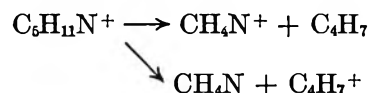
Mass determinations for the fragments which produce the single peaks at m/q 42, 43, 44, 56, 57, and 70

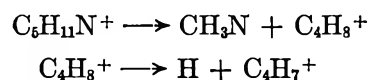Table I: Mass Spectrum of Piperidine

m/q	Empirical formula	Intensity, arbitrary units[a]
26	C_2H_2	16
27	C_2H_3	44
	CHN	3
28	C_2H_4	18
	CH_2N	80
	N_2 (background)	17
29	C_2H_5	18
	CH_3N	64
30	CH_4N	71
39	C_3H_3	37
40	C_3H_4	3
	C_2H_2N	3
41	C_3H_5	30
	C_2H_3N	10
42	C_2H_4N	68
43	C_2H_5N	58
44	C_2H_6N	84
54	C_4H_6	3
	C_3H_4N	7
55	C_4H_7	21
	C_3H_5N	4
56	C_3H_6N	100
57	C_3H_7N	100
70	C_4H_8N	26

[a] Since instrumental adjustments were necessary while these data were being obtained, the relative intensities from one group of peaks to another (as indicated by the spacings in the table) should be considered as only approximately correct.

prove that the ion formulas proposed for these fragments by B, D, and W are correct. This is equally true for the major peak contributing to m/q 28 and 29 whose structures were apparently chosen by B, D, and W on the basis of the ease with which nitrogen assumes a positive charge in ionization reactions. Note, however, that both m/q 28 and 29 have contributions from hydrocarbon fragments. The fragments $(CH_3-NHCH_2)^+$, m/q 44 and $(CH_3NH)^+$, m/q 30 require transfer of hydrogen and the moderately intense hydrogen-deficient hydrocarbon fragments C_4H_7, C_3H_5, and C_2H_3 probably result from these abstracting reactions. The hydrocarbon ions could be formed concurrently, with the corresponding nitrogen-containing ion, in competing reactions, or from an initial fragmentation without rearrangement and then subsequent loss of hydrogen.

$$C_5H_{11}N^+ \longrightarrow CH_4N^+ + C_4H_7$$
$$\searrow CH_4N + C_4H_7^+$$

or

$$C_5H_{11}N^+ \longrightarrow CH_3N + C_4H_8^+$$
$$C_4H_8^+ \longrightarrow H + C_4H_7^+$$

There is no evidence in these spectra of the hydrocarbon ion immediately above m/q 55 (or m/q 41) as might be expected from the second reaction mechanism.

Some indication of the purity of this sample of piperidine was obtained from a gas chromatographic analysis in which only 0.01% impurity was detected.[4]

(1) H. Budzikiewicz, C. Djerassi, and D. Williams, "Interpretation of Mass Spectra of Organic Compounds," Holden-Day, Inc., San Francisco, Calif., 1964, pp. 98–102.

(2) J. Beynon, "Mass Spectrometry and Its Application to Organic Chemistry," Elsevier Publishing Co., New York, N. Y., pp. 52, 53.

(3) Peaks in parent range and several very weak peaks are not included in the data. The low resolution spectrum is in agreement with that given in "Catalog of Mass Spectra," American Petroleum Institute Research Project 44, Agricultural and Mechanical College of Texas, College Station, Texas, Spectrum No. 618. Spectrometer used here is a Model 21-110 double focusing instrument, manufactured by Consolidated Electrodynamics Corp.

(4) Results obtained by Mr. Robert Grula, CRDL, are much appreciated.

The Behavior of Alkali Metal Cations in the

Pores of Silica Gel

by Russell W. Maatman

Department of Chemistry, Dordt College, Sioux Center, Iowa (Received April 1, 1965)

Tien interpreted the interaction of alkali metal cations with silica gel in terms of ion exchange, physical

sorption, and ion exclusion from small pores.[1] This conclusion was based on his experimental results along with those of Dalton, et al.,[2] and Dugger, et al.[3] It is the purpose of this note to show that there has been some misinterpretation of the results of Dalton, et al., and that there is therefore no need to postulate physical sorption and ion exclusion for these systems.

Tien found that the gel preference for cation is in the order Cs > Rb > K > Na > Li. This order, determined by a very accurate tracer method, is in agreement with the results for K, Na, and Li of Dugger, et al. (who did not work with Rb and Cs), taking into account their reported experimental error. Tien, however, bases much of his interpretation on a seemingly contradictory order deduced from pH measurements reported by Dalton, et al. There is actually no contradiction among the results reported in ref. 1-3. The pH values reported by Dalton, et al., were given to indicate that the amount of exchanged metal cation was orders of magnitude less than the amount of unexchanged metal cation in the pores. This gel and other commercial silica gels must be acid-treated before pH differences as small as those found by Dalton, et al., who did not acid-treat, can be used to deduce differences in the amount of exchange. To show that the gel which has not been acid-treated does not give the desired reproducible results, compare the equilibrium pH values obtained by Dalton, et al., with those of Daniel, et al.,[4] who used the same materials in very similar experiments and who measured pH values for the same reason. The difference between the two sets of experiments is that the former equilibrium was attained at 22° and the latter at 80°, although in both cases the measurements were made at room temperature. The pH values are, respectively: Cs, 2.7, 2.4; K, 3.1, 2.8; Na, 2.6, 2.5; Li, 2.2, 2.7. The order is thus radically different. It does not seem likely that the temperature of equilibration is the important variable. Rather, there is an impurity problem: the necessity of acid-treating such gels to eliminate such surface reaction problems has been shown.[5,6]

There then remains no experimental result indicating that some experimental conditions can alter the order Cs > Rb > K > Na > Li found by Tien. Since Dugger, et al., determined affinities by H^+ release from the surface, their results (and, by inference, those of Tien, who observed metal–metal exchange) can be interpreted in terms of ion exchange with surface H^+, without invoking physical sorption. It seems difficult to visualize H^+ release from the surface connected with physical sorption. Furthermore, while Dalton, et al., did suggest that large, hydrated ions are excluded from the smallest pores, this effect has been shown not to

exist.[7] (Reference 7 had, however, not appeared when ref. 1 was submitted.) By considering a geometric effect found at any solution–solid interface, it was shown that even hydrated Al^{3+} of radius 5–7 Å., much larger than any alkali metal ion, can enter the smallest pores in all the gels used by this group. There thus seems to be no need to postulate either physical sorption or ion exclusion from small pores in alkali metal cation–silica gel systems.

Dugger, et al., in considering the silica gel reactions of 22 very different cations, found reasonable correlation with the tendency of the cation to hydrolyze. On the other hand, with ions as similar as the alkali metal cations only small differences in reactivity are expected and found. To make a correct prediction of affinity order, one would obviously need detailed knowledge concerning several factors; an "order of hydrolysis" is not enough. Rosseinsky[8] showed that the matter is very complicated: cation hydration, the nature of the anion, and other factors must be considered.

(1) H. T. Tien, J. Phys. Chem., 69, 350 (1965).

(2) R. W. Dalton, J. L. McClanahan, and R. W. Maatman, J. Colloid Sci., 17, 207 (1962).

(3) D. L. Dugger, J. H. Stanton, B. N. Irby, B. L. McConnell, W. W. Cummings, and R. W. Maatman, J. Phys. Chem., 68, 757 (1964).

(4) J. L. Daniel, J. Netterville, and R. W. Maatman, J. Mississippi Acad. Sci., 8, 193 (1962).

(5) S. Ahrland, I. Grenthe, and B. Noren, Acta Chem. Scand., 14, 1059 (1960).

(6) J. Stanton and R. W. Maatman, J. Colloid Sci., 18, 132 (1963).

(7) B. L. McConnell, K. C. Williams, J. L. Daniel, J. H. Stanton, B. N. Irby, D. L. Dugger, and R. W. Maatman, J. Phys. Chem., 68, 2941 (1964).

(8) D. R. Rosseinsky, J. Chem. Soc., 785 (1962).

Observations Concerning Directly and Nondirectly Bonded ^{13}C–H Couplings with Respect to Symmetry Considerations

by T. Vladimiroff

Department of Chemistry and Chemical Engineering, Stevens Institute of Technology, Hoboken, New Jersey
(Received April 6, 1965)

The Fermi[1] contact contribution to n.m.r. spin–spin coupling for nuclei N and N' was first given by Ramsey[2] to be

$$\delta^F{}_{NN'} = -(2/3h)(16\pi\beta\hbar/3)^2\gamma_N\gamma_{N'}\sum_{nkj}(E_n - E_0)^{-1} \times$$

$$\langle 0|\delta(\vec{r}_{kN})\hat{S}_k|n\rangle \langle n|\delta(\vec{r}_{jN})\hat{S}_j|0\rangle \quad (1)$$

γ_N is the gyromagnetic ratio of nucleus N, $|0\rangle(|n\rangle)$ represents the ground (excited state) of the molecule with energy $E_0(E_n)$, $\delta(\vec{r}_{kN})$ is a δ-function centered on nucleus N, $\hat{S}_k$ is the electron spin operator, and all the other symbols have their usual meaning. After making the "average energy" approximation[2] some progress has been made by McConnell[3] using a molecular orbital approach and by Karplus and Anderson[4] using a valence-bond wave function. Recently Pople and Santry[5] used eq. 1 in conjunction with a molecular orbital approximation. Exact calculations, however, are difficult, and any general observations that can be made are helpful. Some preliminary results on the basis of symmetry considerations are reported here.

Consider the operator $\hat{R}$ which reflects the electronic states of ethylene in the plane of symmetry which is perpendicular to the C–C axis of the molecule. All the states of this molecule may be characterized as symmetric, $|S\rangle$, or antisymmetric, $|A\rangle$, such that $\hat{R}|S\rangle = |S\rangle$ and $\hat{R}|A\rangle = -|A\rangle$. Equation 1 may be written as a sum of contributions due to symmetric and antisymmetric states. In the light of this, the direct and indirect ^{13}C–H coupling in ethylene can be written as

$$\delta^F{}_{^{13}C_2-H_1} = K\sum_{Skj}(E_S - E_0)^{-1}\langle 0|\delta(\vec{r}_{kC_2})\hat{S}_k|S\rangle \times$$

$$\langle S|\delta(\vec{r}_{jH_1})\hat{S}_j|0\rangle + K\sum_{Akj}(E_A - E_0)^{-1} \times$$

$$\langle 0|\delta(\vec{r}_{kC_2})\hat{S}_k|A\rangle \langle A|\delta(\vec{r}_{jH_1})\hat{S}_j|0\rangle \quad (2)$$

$$\delta^F{}_{^{13}C_3-C_2-H_1} = K\sum_{Skj}(E_S - E_0)^{-1}\langle 0|\delta(\vec{r}_{kC_3})\hat{S}_k|S\rangle \times$$

$$\langle S|\delta(\vec{r}_{jH_1})\hat{S}_j|0\rangle + K\sum_{Akj}(E_A - E_0)^{-1} \times$$

$$\langle 0|\delta(\vec{r}_{kC_3})\hat{S}_k|A\rangle \langle A|\delta(\vec{r}_{jH_1})\hat{S}_j|0\rangle$$

Since the value of a matrix element is invariant under any symmetry operation, it follows that

$$\langle 0|\delta(\vec{r}_{kC_3})\hat{S}_k|S\rangle = \hat{R}\langle 0|\delta(\vec{r}_{kC_3})\hat{S}_k|S\rangle = \langle 0|\delta(\vec{r}_{kC_2})\hat{S}_k|S\rangle$$

$$\langle 0|\delta(\vec{r}_{kC_3})\hat{S}_k|A\rangle = \hat{R}\langle 0|\delta(\vec{r}_{kC_3})\hat{S}_k|A\rangle = -\langle 0|\delta(\vec{r}_{kC_2})\hat{S}_k|A\rangle$$

It becomes obvious that the terms in the expansion of $\delta^F{}_{^{13}C_2-H_1}$ and $\delta^F{}_{^{13}C_3-C_2-H_1}$ are identical in magnitude but have different signs for the antisymmetric contributions. Denoting the symmetric and antisymmetric contributions by S and A, eq. 2 may be written as

$$\delta^F{}_{^{13}C_2-H_1} = S + A$$

$$\delta^F{}_{^{13}C_3-C_2-H_1} = S - A$$

The data of Lynden-Bell and Sheppard[6] for ethylene

$(J_{^{13}C_2-H_1} = 156.4$ c.p.s. and $J_{^{13}C_3-C_2-H_1} = -2.4$ c.p.s.) imply that the symmetric and antisymmetric contributions are 77.0 and 79.4 c.p.s., respectively.

The difference in magnitude and relative sign for the directly and nondirectly bonded ^{13}C–H coupling can be interpreted as the result of approximately equal contributions from the symmetric and antisymmetric states. Molecular symmetry requires that these contributions add in the case of the former and cancel in the case of the latter. Thus, a minimum of two excited states must be considered when eq. 1 is used. This analysis also suggests that in the "average energy" approximation[7] different Δ-values should be used in the case of direct and indirect couplings because the symmetric ground state used in such calculations could not be expected to take into account the symmetry properties of all the excited states. Couplings in other molecules with a high degree of symmetry are presently being investigated in this laboratory.

(1) E. Fermi, *Z. Physik*, **60**, 320 (1930).

(2) N. F. Ramsey, *Phys. Rev.*, **91**, 303 (1953).

(3) H. M. McConnell, *J. Chem. Phys.*, **24**, 460 (1956).

(4) M. Karplus and D. H. Anderson, *ibid.*, **30**, 6 (1959).

(5) D. P. Santry and J. A. Pople, *Mol. Phys.*, **8**, 1 (1964).

(6) R. M. Lynden-Bell and N. Sheppard, *Proc. Roy. Soc.* (London), A269, 385 (1962).

(7) The "average energy" approximation has also been discussed by M. Karplus, *J. Chem. Phys.*, **33**, 941 (1960), and A. D. McLachlan, *ibid.*, **32**, 1263 (1960).

Ionization Potentials and Mass Spectra of Cyclopentadienylmolybdenum Dicarbonyl Nitrosyl and 1,3-Cyclohexadieneiron Tricarbonyl[1]

by Robert E. Winters and Robert W. Kiser

Department of Chemistry, Kansas State University, Manhattan, Kansas 66504 (Received April 12, 1965)

Recently, we reported[2] mass spectrometric studies of the ionization and dissociation in several transition metal carbonyls. From the measured ionization potentials it was suggested that the electron removed

upon ionization may be considered to have been localized on the metal atom rather than in the carbonyl groups. Unimolecular decompositions of the parent molecule ions of these carbonyls by apparent stepwise losses of CO groups were indicated. In order to study these phenomena in more complex systems, we have investigated the mass spectra and ionization potentials for two substituted transition metal carbonyls of varying composition: cyclopentadienylmolybdenum dicarbonyl nitrosyl and 1,3-cyclohexadieneiron tricarbonyl.

Experimental

The samples of cyclopentadienylmolybdenum dicarbonyl nitrosyl and 1,3-cyclohexadieneiron tricarbonyl were kindly provided by Dr. R. B. King of Mellon Institute. Low-voltage mass spectrometry indicated that no volatile impurities were present in the two compounds.

The mass spectra and ionization potentials were determined with a Bendix (Model 12-100) time-of-flight mass spectrometer. The instrumentation has been described previously.[3] Mass spectra for each of the compounds were obtained at nominal electron energies of 70 e.v.

The experimental ionization efficiency curves for the parent molecule ions were interpreted using the extrapolated voltage difference method described by Warren[4] and the method of Lossing, Tickner, and Bryce.[5] Since the compounds were not sufficiently volatile to use any of the noble gases for calibration purposes, mercury (from the diffusion pump) and oxygen (from a small air leak) backgrounds in the mass spectrometer were used to calibrate the ionizing voltage scale. Spectroscopic values for the ionization potentials of mercury (10.43 e.v.[6]) and of oxygen (12.08 e.v.[7]) were employed for this purpose.

Decomposition products were repeatedly cleaned from the ion source and the Wiley magnetic electron multiplier components throughout this study. Also, frequent replacement of tungsten filaments was necessary. The mass spectra were found to remain constant and the ionization potentials were reproducible to within the quoted error limits (one standard deviation) for independent runs.

Results and Discussion

Ionization Potentials. The ionization potentials determined for cyclopentadienylmolybdenum dicarbonyl nitrosyl and 1,3-cyclohexadieneiron tricarbonyl are 8.1 ± 0.2 and 8.0 ± 0.2 e.v., respectively. The fact that the ionization potentials are lower than those of the substituents[8] but only slightly greater than the

ionization potentials of the metals again suggests that ionization subsequent to electron impact involves the removal of an electron associated with the metal atom—possibly from a hybrid molecular orbital involving considerable contribution from the metal atomic orbital. As one would anticipate, therefore, the ionization potentials of these substituted metal carbonyls are comparable to the ionization potentials[2] of the corresponding metal carbonyls, *e.g.*, iron pentacarbonyl and molybdenum hexacarbonyl.

Mass Spectra. A partial monoisotopic mass spectrum of the important ion fragments formed when $C_5H_5Mo(CO)_2NO$ was sublimed into the ion source is shown in Table I. The isotopic abundances were found to agree, within the experimental error, with the presently accepted values.[9]

The ion of greatest mass which was observed was the parent molecule ion. No indication of association of molecules in the gas phase was detected and there was no evidence of thermal decomposition in the ion source. Fragmentation ions formed by loss of CO groups in preference to cleavage of nitrosyl or cyclopentadienyl groups were found. This is not surprising; the stronger bonds are between the metal and NO or C_5H_5 groups.[10] Also, the presence of $MoC_5H_5^+$ ions and the absence of $MoNO^+$ ions in the mass spectrum indicate that the $Mo-C_5H_5$ bond is somewhat more difficult to rupture than the $Mo-NO$ bond.

Dissociation involving loss of hydrocarbon aggregates smaller than C_5H_5 from $C_5H_5Mo(CO)_2NO$ was observed,

(1) This work was supported in part by the U. S. Atomic Energy Commission under Contract No. AT(11-1)-751 with Kansas State University; a portion of a dissertation presented by R. E. Winters to the Graduate School of Kansas State University in partial fulfillment of the requirements for the degree of Doctor of Philosophy.

(2) R. E. Winters and R. W. Kiser, *Inorg. Chem.*, 3, 699 (1964); 4, 157 (1965); *J. Phys. Chem.*, 69, 1618 (1965).

(3) E. J. Gallegos and R. W. Kiser, *J. Am. Chem. Soc.*, 83, 773 (1961); *J. Phys. Chem.*, 65, 1177 (1961).

(4) J. W. Warren, *Nature*, 165, 810 (1950).

(5) F. P. Lossing, A. W. Tickner, and W. A. Bryce, *J. Chem. Phys.*, 19, 1254 (1951).

(6) C. E. Moore, "Atomic Energy Levels," National Bureau of Standards Circular 467, U. S. Government Printing Office, Washington, D. C., 1958.

(7) G. Herzberg, "Molecular Spectra and Molecular Structure. I. Spectra of Diatomic Molecules," D. Van Nostrand Co., Inc., New York, N. Y., 1950.

(8) Y. Kaneko, *J. Phys. Soc. Japan*, 16, 1587 (1961): *I*(CO) = 14.11 e.v.; A. G. Harrison, L. R. Honnen, M. J. Dauben, Jr., and F. P. Lossing, *J. Am. Chem. Soc.*, 82, 5593 (1960): *I*(C₅H₅) = 8.69 e.v.; G. G. Cloutier and H. I. Schiff, *J. Chem. Phys.*, 31, 793 (1959): *I*(NO) = 9.25 e.v.; W. C. Price and A. D. Walsh, *Proc. Roy. Soc.* (London), A179, 201 (1941): *I*(C₆H₈) = 8.40 e.v.

(9) J. H. Beynon, "Mass Spectrometry and Its Applications to Organic Chemistry," Elsevier Publishing Co., Amsterdam, 1960, pp. 557, 559.

(10) C. T. Mortimer, "Reaction Heats and Bond Strengths," Pergamon Press, New York, N. Y., 1962, pp. 149-154.

Table I: Relative Abundances of the Principal Positive Ions from Cyclopentadienylmolybdenum Dicarbonyl Nitrosyl at 70 e.v.

m/e	Ion	Relative abundance	m/e	Ion	Relative abundance
249	$C_5H_5Mo(CO)_2NO^+$	64.6	137	$C_3H_3Mo^+$	95.0
221	$C_5H_5Mo(CO)NO^+$	46.2	110	MoC^+	47.1
193	$C_5H_5MoNO^+$	72.4	98	Mo^+	51.9
167	$C_3H_3MoNO^+$	96.3	81.5	$C_5H_5Mo^{2+}$	34.1
163	$C_5H_5Mo^+$	100.0			

e.g., the formation of $C_3H_3Mo^+$. An ion similar to this, $FeC_3H_3^+$, has been reported[11] to occur in the mass spectrum of ferrocene.

The doubly charged $MoC_5H_5^{2+}$ ion appears in significant quantity in the mass spectrum of this compound. This ion is very abundant; it is much more abundant than the commonly encountered relative abundances of approximately 0.01 to 0.1% for doubly charged ions in many hydrocarbons.[12] Similar observations of the great intensity of doubly charged ions in the mass spectra of the carbonyl compounds were reported in earlier studies of molybdenum hexacarbonyl.[2]

Hoehn, Pratt, Watterson, and Wilkinson[13] have reported a partial mass spectrum for the perfluoro derivative of 1,3-cyclohexadieneiron tricarbonyl, i.e., C_6F_8-$Fe(CO)_3$. Ions corresponding to $C_6F_8Fe(CO)_2^+$, C_6-F_8FeCO^+, and $C_6F_8Fe^+$ were noted; it was suggested that they were formed by a stepwise loss of CO from the parent molecule ion. The most abundant ions detected in the mass spectrum of the analogous C_6-$H_8Fe(CO)_3$ are shown in Table II. Ions formed by successive removal of CO groups from the parent molecule ion were detected also in the mass spectrum of this compound. However, two striking differences were noted in the fragmentation of the C_6H_8-iron tricarbonyl and the previously studied C_6F_8-iron tricarbonyl.

First, $C_6H_6FeCO^+$ was formed upon electron impact

Table II: Relative Abundances of the Principal Positive Ions from 1,3-Cyclohexadieneiron Tricarbonyl at 70 e.v.

m/e	Ion	Relative abundance	m/e	Ion	Relative abundance
220	$C_6H_8Fe(CO)_3^+$	1.0	84	$FeCO^+$	10.6
192	$C_6H_8Fe(CO)_2^+$	3.5	80	$C_6H_8^+$	1.7
164	$C_6H_8FeCO^+$	0.9	79	$C_6H_7^+$	3.2
162	$C_6H_6FeCO^+$	2.4	78	$C_6H_6^+$	2.4
134	$C_6H_8Fe^+$	57.8	56	Fe^+	100.0
112	$Fe(CO)_2^+$	0.9	39	$C_3H_3^+$	3.0

in addition to the $C_6H_8FeCO^+$ ion fragmented by simple removal of two CO groups. Also, no ion of composition $C_6H_8Fe^+$ was detected in this study; however, $C_6H_6Fe^+$ ion was observed in large abundance. The deficiency of $C_6F_6FeCO^+$ and $C_6F_6Fe^+$ in the mass spectrum of the perfluoro derivative[13] may be due to the greater strength of the C–F bonds as compared to the C–H bonds in the ionic species.

The second striking difference in the cracking patterns for these two related compounds lies in the intensities of the metal carbonyl ions of the type $Fe(CO)_x^+$. Iron dicarbonyl and iron monocarbonyl ions were found to have a low abundance in the $C_6H_8Fe(CO)_3$ mass spectrum and no $Fe(CO)_3^+$ was observed. Since the iron carbonyl ions were the most abundant ions in the cracking pattern of $C_6F_8Fe(CO)_3$, the low abundance (or absence) of similar ions in the mass spectrum of the hydrogen-containing compound indicates that the C_6H_8–Fe^+ bond is stronger than the C_6F_8–Fe^+ bond.

(11) F. W. McLafferty, *Anal. Chem.*, **28**, 306 (1956).

(12) See, for example, F. H. Field and J. L. Franklin, "Electron Impact Phenomena and the Properties of Gaseous Ions," Academic Press Inc., New York, N. Y., 1957, p. 183.

(13) H. H. Hoehn, L. Pratt, K. F. Watterson, and G. Wilkinson, *J. Chem. Soc.*, 2738 (1961).

Solubilities of Fluorocarbons in Cyclohexane and 1,4-Dioxane

by J. L. Carson, R. J. Knight, I. D. Watson, and A. G. Williamson

Department of Chemistry, University of Otago, Dunedin, New Zealand (Received April 14, 1965)

Konecny and Deal[1] have reported solubility measurements for mixtures of 1-hydroperfluoroheptane with paraffins, aromatics, and polar compounds, which they interpret as indicating that the behavior of $C_7F_{15}H$ in paraffins and alkylbenzenes is dominated by the fluorocarbon chain while in polar solvents specific interactions involving the CH group of $C_7F_{15}H$ strongly influence the solution behavior.

The solubilities of C_7F_{16} and $C_7F_{15}H$ in cyclohexane and 1,4-dioxane reported here are in qualitative agree-

(1) J. O. Konecny and C. H. Deal, *J. Phys. Chem.*, **67**, 504 (1963).

ment with this observation. However, comparison of the data for several systems suggests that the critical solution temperatures themselves may be a better indication of the interactions than is the comparison of the solubility parameters derived from the solubility measurements with those obtained from latent heats of vaporization.

Experimental

A.R. grade cyclohexane was purified by the method described by Dyke, Rowlinson, and Thacker.[2] A.R. grade 1,4-dioxane was purified by the method described by Vogel[3] followed by repeated fractional crystallization. 1-Hydropentadecafluoroheptane was prepared by the method described by La Zerte,[4] et al. The product was fractionally distilled in a 14-plate column, the middle fraction (b.p. 94.4–95°) being used for the solubility measurements. Gas chromatographic analysis[5] showed this material to consist of 70% n- isomer and 30% branched chain isomers of $C_7F_{15}H$. The nuclear magnetic resonance spectrum indicated that the isomers present were ones in which the chain branching occurred well away from the terminal hydrogen atom. Solubility data shown in Figure 1 for both the isomer mixture and for 99.7% pure n- isomer prepared by preparative scale gas–solid chromatography[6] indicate that the solubility behavior of $C_7F_{15}H$ with cyclohexane is unaffected by the presence of the branched chain isomers. Perfluoroheptane was supplied by the Birmingham University Chemistry Department and was shown by gas chromatographic analysis to consist of a mixture of isomers of C_7F_{16} of which the major component (70%) was n- isomer. In view of the results with the two samples of $C_7F_{15}H$, the C_7F_{16} was used without further purification.

Solubilities were measured by the cloud point method on mixtures prepared by weight in sealed Pyrex tubes. Temperatures were measured with laboratory calibrated thermometers accurate to 0.1° and the data shown in Figure 1 are the means of three determinations which agreed within 0.3° or better.

Results and Discussion

The liquid–liquid solubilities are shown in Figure 1 and the upper critical solution temperatures in Table I. This table also shows the values of δ_H, the solubility parameters derived from the approximate relation[7]

$$4RT_o = (V_F + V_H)(\delta_F - \delta_H)^2 \qquad (1)$$

where V_F and V_H are the molar volumes of the fluorocarbon and hydrocarbon, respectively, at 25°, δ_F is the solubility parameter of the fluorocarbon at 25°, and T_o is the upper critical solution temperature. The values
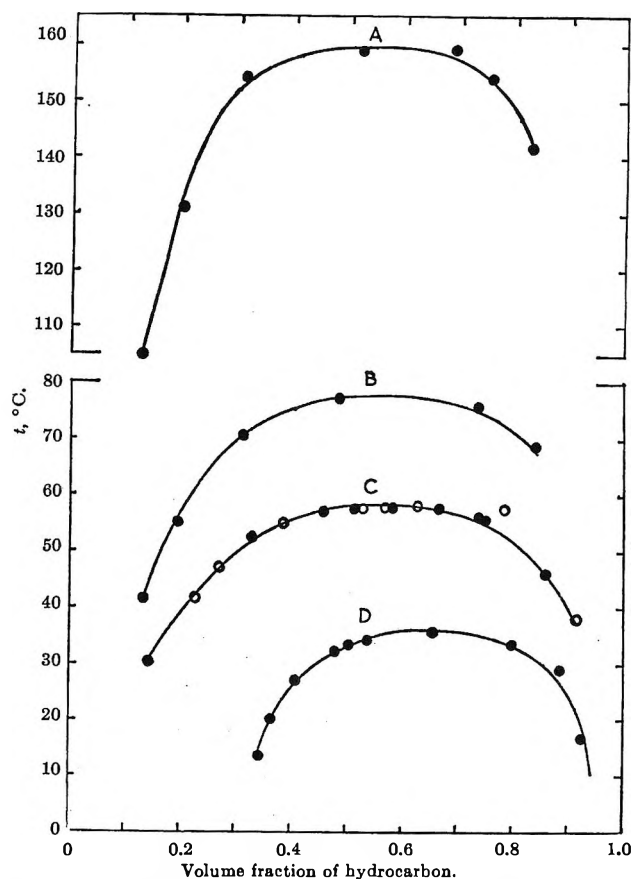
Figure 1. Solubilities of $C_7F_{15}H$ and C_7F_{16} in cyclohexane and dioxane: A, C_7F_{16}–dioxane; B, C_7F_{16}–cyclohexane; C, $C_7F_{15}H$–cyclohexane: ●, n-$C_7F_{15}H$; ○, 70% n-$C_7F_{15}H$ mixture; D, $C_7F_{15}H$–dioxane.

used for δ_F for C_7F_{16} and $C_7F_{15}H$ are 5.85 and 6.3, respectively.[8] Also shown are values of δ_H* taken from the latent heats of vaporization of the hydrocarbons.[8] The differences between δ_H and δ_H* for the mixtures of $C_7F_{15}H$ with cyclohexane and with dioxane are consistent with Konecny and Deal's[1] classification. However, we consider that comparisons of the differences in the values of $(\delta_F - \delta_H)$ for C_7F_{16} and $C_7F_{15}H$ solutions calculated from eq. 1 are a more direct indication of the interactions. Since $(\delta_1 - \delta_2)$ for a given pair of

(2) D. E. L. Dyke, J. S. Rowlinson, and R. Thacker, *Trans. Faraday Soc.*, **55**, 903 (1959).

(3) A. I. Vogel, "Practical Organic Chemistry," Longmans Green and Co., London, 1951.

(4) J. D. La Zerte, L. J. Hals, T. S. Reid, and G. H. Smit, *J. Am. Chem. Soc.*, **75**, 4525 (1953).

(5) C. G. Pope, *Anal. Chem.*, **35**, 654 (1963).

(6) R. C. Stewart, unpublished results.

(7) R. L. Scott, *J. Phys. Chem.*, **62**, 136 (1958).

(8) J. H. Hildebrand and R. L. Scott, "Regular Solutions," Prentice-Hall, Inc., Englewood Cliffs, N. J., 1962, p. 172.

compounds 1 and 2 is generally less temperature dependent than are the individual δ, the uncertainties involved in comparing data derived from different critical solution temperatures with data for 25° are minimized.

Table I: Comparison of Critical Solution Temperatures and Solubility Parameters for Solutions of C_7F_{16} and $C_7F_{15}H$

Mixture	T_c, °K.	$\delta_H - \delta_F$	δ_H	$\delta_H{}^*$	Ref.
$C_7F_{16} + C_7H_{16}$	323	2.62	8.5	7.4	a
$C_7F_{16} + C_6H_{12}$	350	2.88	8.7	8.2	This work
$C_7F_{16} + C_6H_6$	387	3.20	9.0	9.2	a
$C_7F_{16} + C_4H_8O_2$	431	3.32	9.2	10.0^b	This work
$C_7F_{15}H + C_7H_{16}$	305	2.58	8.9	7.4	1
$C_7F_{15}H + C_6H_{12}$	331	2.86	9.2	8.2	This work
$C_7F_{15}H + C_6H_6$	314	2.87	9.2	9.2	1
$C_7F_{15}H + C_4H_8O_2$	308	2.86	9.2	10.0^b	This work

^{a} J. H. Hildebrand, B. B. Fisher, and H. A. Benesi, J. Am. Chem. Soc., 72, 4348 (1950). ^{b} From solubility in nonpolar solvents.

For both C_7H_{16} and $c\text{-}C_6H_{12}$, the change in $(\delta_F - \delta_H)$ in going from C_7F_{16} to $C_7F_{15}H$ is practically negligible. For benzene, on the other hand, the value of $(\delta_F - \delta_H)$ is 0.33 unit lower in $C_7F_{15}H$ than in C_7F_{16} and for dioxane the difference is 0.46 unit. We interpret these changes as indicating that the interactions of C_7F_{16} and $C_7F_{15}H$ with heptane and cyclohexane are virtually the same but that in benzene there is a considerable contribution to the solution behavior from interactions between the CH group and the π-electrons of the benzene molecule, the indications of which are suppressed in the comparison of δ_H with $\delta_H{}^*$. In dioxane, the interaction between the oxygens and the CH group of the $C_7F_{15}H$ is sufficiently strong to show even in the comparison of δ_H and $\delta_H{}^*$. The same conclusions are suggested by the direct comparison of the T_c values. For both n-heptane and cyclohexane, T_c for $C_7F_{15}H$ mixtures is about 20° lower than for C_7F_{16} mixtures. For benzene, the difference is 73° and for dioxane it is 123°. The interactions suggested by this comparison have been revealed in n.m.r. spectroscopy in solutions of both $CHCl_3{}^9$ and $C_7F_{15}H^{10}$ in benzene. The heats of mixing[11] of $C_7F_{15}H$ with dioxane are also consistent with the formation of hydrogen bonds between dioxane and $C_7F_{15}H$.

(9) W. G. Schneider, J. Phys. Chem., 66, 2653 (1962).

(10) D. L. Anderson, R. A. Smith, S. K. Alley, A. G. Williamson, D. B. Myers, and R. L. Scott, ibid., 66, 621 (1962).

(11) R. J. Knight and A. G. Williamson, unpublished results.

Chemical Species Containing P^{32} and S^{35} Subsequent to the Neutron Irradiation of Thiourea[1]

by Cleon C. Arrington and Robert W. Kiser

Department of Chemistry, Kansas State University, Manhattan, Kansas 66504 (Received April 27, 1965)

The chemistry of recoiling atoms following bombardment with heavy nucleons has been investigated in some depth. However, a detailed understanding of the nature of the products to be expected from the neutron irradiation of a given substance and satisfactory explanations of the modes of formation of all of the products are yet to be realized. In an early study, Whitmore[2] investigated the production of phosphorus-32 from sulfur-32 in the neutron irradiation of thiourea; he reported the chemical oxidation state of the phosphorus-32 produced and discussed a possible mode for its formation. There have been no further studies of the neutron irradiation of thiourea since Whitmore's investigation and a brief report by Adams and Campbell.[3]

The purpose of this note is to present the results of an investigation of the labeled products formed upon neutron irradiation of thiourea, the nature of the species resulting from the recoil and radiation damage effects, and the relative quantities for both sulfur-35 and phosphorus-32 in these species.

Experimental

Sample Irradiation. Thiourea (Matheson Coleman and Bell, reagent grade) was recrystallized three times from ethanol and dried for 24 hr. over sulfuric acid. Two 5.0-g. samples were irradiated in air in the ORNL graphite pile. Pertinent data concerning the irradiations are: thermal neutron flux, 5×10^{11} cm.$^{-2}$ sec.$^{-1}$; irradiation time, 3 days; γ-ray flux, 7×10^6 r./hr.; sample temperature, $\sim 50°$.

Counting Procedures. Total activity measurements for P^{32}- and S^{35}-containing samples were made using a Packard Tri-Carb liquid scintillation spectrometer and PPO–POPOP–naphthalene–dioxane scintillator solutions.[4] A Geiger–Müller "dip counter" tube (window

(2) F. E. Whitmore, Nature, 164, 240 (1949).

(3) A. Adams and I. G. Campbell, Trans. Faraday Soc., 59, 2001 (1963).

thickness ~30 mg./cm.²) and a Borg-Warner scaler also were used to determine the total P^{32} activities. The counter was regularly standardized with aqueous solutions of P^{32} standard (as $H_3P^{32}O_4$).

With the Packard Tri-Carb liquid scintillation spectrometer, the S^{35} and the P^{32} activities were determined in separate counting channels. With 620 v. on the photomultiplier tubes only the P^{32} activity was counted. With 920 v. on the photomultiplier tubes, both the P^{32} and the S^{35} activities were counted. The count rates at the higher voltage were corrected appropriately to yield the S^{35} activities. The small amounts of C^{14} and P^{33} produced in the irradiation (less than 1% of the S^{35} produced) were neglected. The average of all determinations for the two samples gave 388 ± 16 μcuries of P^{32} and 77.8 ± 1.5 μcuries of S^{35} produced. The error limit represents one standard deviation.

Analytical Methods. Paper electrophoretic techniques similar to those employed by Lindner and Harbottle[5] and Grassini and Lederer[6] were used in the chemical separations of the ionic species. In the analyses 0.1 N NaOH electrolyte was used with a commercial paper electrophoresis apparatus and a constant potential gradient of 33 v./cm. With three parallel 1 × 12 in. Whatman 3 MM chromatography paper strips, currents were less than 25 ma.

Samples of 20–100 λ per strip were analyzed for 2.5 hr. The strips were dried at 25° and cut into 0.4–0.5-in. sections. Each section was placed into separate scintillation solutions and counted. No carriers were employed in these experiments.

The mobilities of species containing the P^{32} and the S^{35} activities were compared to the mobilities of authentic samples. Radiolabeled PO_4^{3-} and SO_4^{2-} standard samples were used to establish the ionic mobilities. The ionic mobility of S^{2-} was determined from a basic S^{2-} solution and development of the strip with a Pb-(OAc)₂ solution.

Electrophoretic analysis of the irradiated samples indicated that essentially all of the sulfur-35 was contained in ionic species. Theoretical considerations indicated that the parent thiourea molecule should be labeled at least in part. It was found that in basic solutions, the thiourea hydrolyzed to yield S^{2-}. Therefore the amount of labeled thiourea present was determined by reverse isotope dilution and recrystallization to constant specific activity. The values obtained by this technique compared well with values determined from 9-xanthenol derivatives.[7]

Results and Discussion

The electrophoresis of the irradiated samples indi-

cated the activity to be principally in the form of S^{2-} and SO_4^{2-} (67 and 29%, respectively). A portion of the S^{2-} activity determined was found to be due to the hydrolysis of labeled thiourea. From the reverse isotope dilution experiments, thiourea was found to contain 31% of the total sulfur-35 produced. By difference, S^{2-} contained 36% of the total sulfur-35 formed. About 4% of the S^{35} activity was found to remain at the origin of the electrophoresis strip. The lack of mobility of this labeled species leads us to the conclusion that it is probably covalent in nature. We cannot satisfactorily explain the lack of oxidation of the S^{35} produced. It is possible that the double bond to the sulfur atom makes the bond less susceptible to rupture during recoil of the S^{35} atom. This would lead to a higher percentage of the S^{35} being found in the thiourea molecule and as S^{2-}. The S^{35}-containing species, as determined, accounted for all of the S^{35} produced in the sample.

The P^{32} species found to remain on the strip accounted for only 57% of the total P^{32} produced in the sample and was found to be distributed among hypophosphate (61%) and phosphate (39%). The hypophosphate ion or its precursor was found to be oxidized to phosphate upon storage of the sample at room temperature during the analyses. This phenomenon also has been observed to occur in inorganic salts.[3,5,8] Adams and Campbell[3] have investigated the effect of oxygen in the lattice upon the final oxidation state of the recoiling P^{32} atom and concluded that in matrices in which the molecule itself does not contain oxygen and where oxygen is carefully excluded, the P^{32} can be expected to be in a +5 oxidation state. Where oxygen is present, the percentage of labeled +3 oxyanions increases significantly. Oxygen is considered to act as a scavenger, stabilizing the recoil species in a state which leads to +3 oxyanions upon dissociation of the sample. Since the samples reported in this study were irradiated in air, it is concluded that the presence of oxygen had such an effect and therefore a significant portion of the activity (43%) was incorporated in +3 oxyanions of phorphorus.

The data indicate that, in the recoil processes for both the sulfur-35 and phosphorus-32, most of the

(4) T. W. Lapp and R. W. Kiser, *J. Phys. Chem.*, **66**, 152 (1962).

(5) L. Lindner and G. Harbottle in "Chemical Effects of Nuclear Transformations," Vol. I, International Atomic Energy Agency, Vienna, Austria, 1961, p. 485.

(6) G. Grassini and M. Lederer, *J. Chromatog.*, **2**, 326 (1959).

(7) R. W. Kiser, M. D. Shetlar, and G. D. Johnson, *Anal. Chem.*, **33**, 314 (1961).

(8) R. F. C. Claridge and A. G. Maddock, *Trans. Faraday Soc.*, **59**, 935 (1963).

bonds to these atoms are broken (the recoil energy of P^{32} is of the order of 200 kev.) and that, subsequent to the thermalization of these atoms (little ionization is expected), the resulting species are either oxidized or reduced by their immediate surroundings to form matrix-stabilized precursors of the observed products.

Measurement of the Spin-Lattice Relaxation Times of Dimethyloctylamine Oxide through the Critical Micelle Concentration

by Kenneth D. Lawson and Thomas J. Flautt

The Procter & Gamble Company, Miami Valley Laboratories, Cincinnati, Ohio 45239 *(Received May 3, 1965)*

The nuclear spin-lattice relaxation times (T_1) of the various proton moieties of the nonionic surfactant dimethyloctylamine oxide [$CH_3(CH_2)_7N(O)(CH_3)_2$] (DC$_8$AO) have been determined. The measurements were made on oxygen-free solutions of DC$_8$AO in D_2O at 32°. A Varian Associates Model A-60 spectrometer was used and the T_1 values were determined by the progressive saturation method.[1] A "doped" water sample with a known relaxation time was used to calibrate the instrument. The preparation of the surfactant has been described elsewhere.[2] The experimental T_1 values are shown in Figure 1 as a function of the concentration of DC$_8$AO in moles per liter. There was no indication that there is more than one T_1 for a band of a given chemical shift. However, the method used to determine the relaxation times would indicate multiple T_1 values only if a substantial distribution were present. All of the T_1 values show an apparent maximum near the critical micelle concentration (c.m.c.) of the surfactant.[3] The magnitudes of the relaxation times are in the order $T_{1,CH_3} < T_{1,NCH_3} < T_{1,CCH_3}$ at any given concentration.

The apparent increase in the T_1 values (decrease in the relaxation rate) with increasing concentration below the c.m.c. is not fully understood. On the basis of viscosity data the opposite trend would be expected. The increase in T_1 may be a result of the physical configuration of the hydrocarbon chains of the DC$_8$AO molecules in the monomer state. Thermodynamic studies of similar systems[4] have indicated that below the c.m.c. long hydrocarbon chains may curl or fold in order to reduce the amount of contact with the solvent. If a change in the degree of curling occurs as the c.m.c. is approached, the intramolecular and
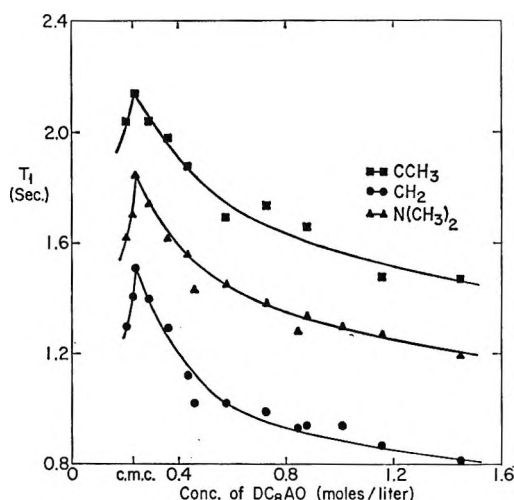

Figure 1. Spin-lattice relaxation times of DC$_8$AO as a function of concentration.

intermolecular contributions to the relaxation times would change. An unfolding of the chains would replace H–H interactions by H–D interactions and/or increase distances between interacting protons and thus increase the relaxation times. Further work is underway to investigate this possibility.

At concentrations greater than the c.m.c. the DC$_8$AO exists in two forms, as monomers and micelles. Any given surfactant molecule will be exchanging between the two environments at some relatively rapid rate. It has been shown[5] that in such a system an average spin-lattice relaxation time will be observed if $t_i \ll T_{1,i}$, and $t_j \ll T_{1,j}$, where t_i and t_j are the average lifetimes of a nucleus or molecule in states i and j and $T_{1,i}$ and $T_{1,j}$ are the spin-lattice relaxation times of the respective states. If the above conditions are fulfilled in the present system, it should be possible to express the observed relaxation times in terms of the relaxation times of the monomeric and micellar species by the equation

$$1/T_1 = (\text{c.m.c.}/c)/T_{1,\text{mon}} + [(c - \text{c.m.c.})/c]/T_{1,\text{mic}}$$

$$(1)$$

where c is the total concentration of the surfactant.

Assuming that the above equation adequately describes the system, plots of c/T_1 against (c − c.m.c.) will be straight lines with intercepts of c.m.c./$T_{1,\text{mon}}$

(1) J. A. Pople, W. G. Schneider, and H. S. Bernstein, "High Resolution Nuclear Magnetic Resonance," McGraw-Hill Book Co., Inc., New York, N. Y., 1959, pp. 82, 83.

(2) W. L. Courchene, *J. Phys. Chem.*, **68**, 1870 (1964).

(3) J. M. Corkill and K. W. Herrmann, *ibid.*, **67**, 935 (1963).

(4) L. Benjamin, *ibid.*, **68**, 3575 (1964).

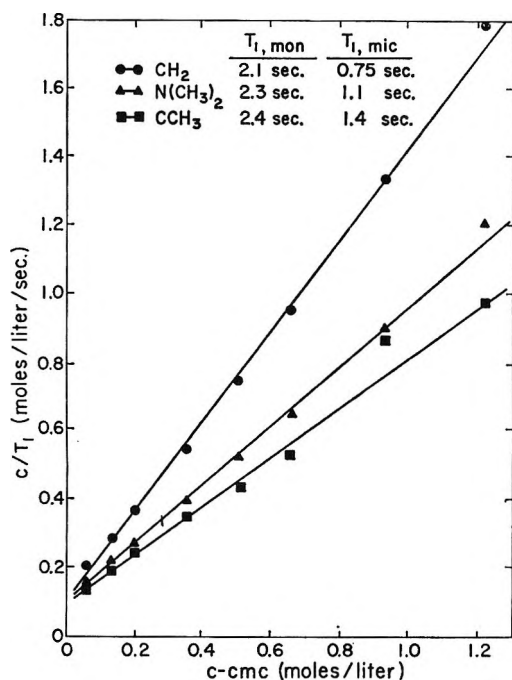(5) J. R. Zimmerman and J. A. Lasater, *ibid.*, **62**, 1157 (1958).

Figure 2. Plots of c/T_1 vs. $(c - \text{c.m.c.})$ and derived values of $T_{1,\text{mon}}$ and $T_{1,\text{mic}}$ for DC_8AO.

and slopes of $1/T_{1,\text{mic}}$. Plots of this type are shown in Figure 2 and to a good approximation straight lines are produced for all of the proton moieties.

The values of $T_{1,\text{mon}}$ and $T_{1,\text{mic}}$ extracted from the plots are tabulated in Figure 2. The order of the T_1 values remain the same in both the micellar and monomeric forms. The micellar values are about 1 sec. less than the monomeric values. The decrease in the relaxation times with micelle formation may reflect the restraint placed upon the molecules when incorporated into micelles. It is expected that internal chain motions (both translational and rotational) would be hindered in the micellar species relative to the corresponding motions in the monomeric form. Another factor which may be important is the change in environment which a molecule undergoes during micelle formation. The intermolecular interactions would be mainly between protons and deuterons for the monomer, but the same interactions would be mainly proton–proton interactions in the micelles—this would lead to a relative decrease in relaxation for the micellar form.

The relaxation time of the HOD in the solvent was also determined at several different concentrations of surfactant. The observed value decreases from 4.3 sec. in the pure solvent to about 3.9 sec. for a 1 M solution of DC_8AO. No indications of a maximum were found near the c.m.c. of the surfactant as shown by the DC_8AO relaxation times. The value of 4.3 sec. observed for the pure solvent is less than previously re-

ported values of T_1 for HOD[6] and probably represents the upper limit of T_1 which can be measured under the experimental conditions used in this investigation. The decrease in the T_1 (increase in the relaxation rate) of the HOD with increasing concentration of surfactant probably results from the increase in the amount of solvent tied up in ordered layers about the micelles as the number (and perhaps the size) of the micelles increases. Water, or HOD, molecules in hydration shells have increased reorientation times and thus increased relaxation rates as compared to pure water. The correlation times of water of hydration have been found to be anywhere from two[7] to ten[8] times as long as those in the pure liquid state. The change in the observed T_1 depends upon both the amount of water in the hydration layers and the degree of binding.

It appears that T_1 measurements may offer another method of determining critical micelle concentrations; however, the relatively low sensitivity of the n.m.r. experiment offers a serious limitation to the method. Determination of the relaxation times of the species present in a micellar solution, which can be obtained from data collected entirely above the c.m.c., appears to offer a method of obtaining information about the species not readily obtainable by other methods.

(6) W. A. Anderson and J. T. Arnold, Phys. Rev., 101, 511 (1956).

(7) H. G. Hertz and M. D. Zeidler, Ber. Bunsenges. physik. Chem., 68, 821 (1964).

(8) S. S. Danyluk and E. S. Gore, Nature, 203, 748 (1964).

Mercury-Photosensitized Isomerization of Perfluorobutene-2[1]

by Dennis Saunders and Julian Heicklen

Aerospace Corporation, El Segundo, California
(Received May 12, 1965)

The study of excited states has been reviewed recently by Hammond and Turro.[2a] Wyman's review of cis–trans isomerization[2b] provides a background to the subject. In recent years, a number of papers have appeared on the photosensitized isomerization of butene-2.[3–7] Each has discussed the role of excited states

(1) This work was supported by the U. S. Air Force under Contract No. AF 04(695)-469.

(2) (a) G. S. Hammond and N. J. Turro, Science, 142, 1541 (1963); (b) G. M. Wyman, Chem. Rev., 55, 625 (1955).

(3) R. B. Cundall and T. F. Palmer, Trans. Faraday Soc., 56, 1211 (1960).

in isomerization. The results of Heicklen, Knight, and Greene[8-11] have indicated that triplet states are produced by the mercury-sensitized photolysis of C_2F_4, C_3F_6, and C_4F_8-2. It was our purpose, then, to prove the existence of this excited species by studying the cis-trans isomerization of perfluorobutene-2.

Matheson Company perfluorobutene-2 was separated into its components chromatographically, by use of the column described by Greene and Wachi.[12] The infrared spectra of each isomer identically matched those reported by Heicklen, Wachi, and Knight.[13] Analyses were accomplished by calibration of all of the infrared bands against a Consolidated Vacuum Corp. McLeod gauge. The optical assembly and the gas-handling techniques have been described previously.[14] I_a was calculated by photolyzing mixtures of 10 mm. of C_2H_4 and 500 mm. of N_2O and measuring the noncondensables formed. The procedure was simply to introduce a sample of one isomer and to scan the infrared spectrum frequently during photolysis. With the scan rate of the instrument known, the time rate of change of both reactant and products could be followed.

Initially, 0.6 mm. of the unseparated mixture was photolyzed for 36 hr. The final equilibrium mixture contained 40% cis, corresponding to a slight gain in the cis concentration. All other runs were made with pure isomers but not quite run to equilibrium. In all cases, no products were found other than cis- and trans-C_4F_8-2. Figure 1 is a plot of the pressure of the cis compound P_{cis} divided by the initial pressure $P_{initial}$ as a function of time in four runs. Two of the runs were started with 100% cis, the others with 100% trans. Figure 2 is a complementary set of curves for the pressure of the trans compound P_{trans} in the same four runs.

It is not clear whether the above-mentioned curves come to a common asymptote. The initial linear regions of the reactions were plotted and the quantum yields calculated. The results are compiled in Table I. The Φ_{cis}(formation) is fairly constant at about 0.045, while the Φ_{trans}(formation) varies considerably, but is about 0.12. No pressure dependence is indicated. The sum of the average quantum yields is about 0.16.

Excited with 2537-Å. radiation, mercury possesses 112.7 kcal./mole of triplet energy over its ground state. When this energy is transferred to C_2F_4, dissociation occurs through a vibrationally excited molecule.[8] In C_3F_6, however, where the bond energy is 114.9 kcal./mole, dissociation does not occur significantly unless additional thermal energy is supplied.[9,10] Finally, in C_4F_8-2, where the inductive effect of the
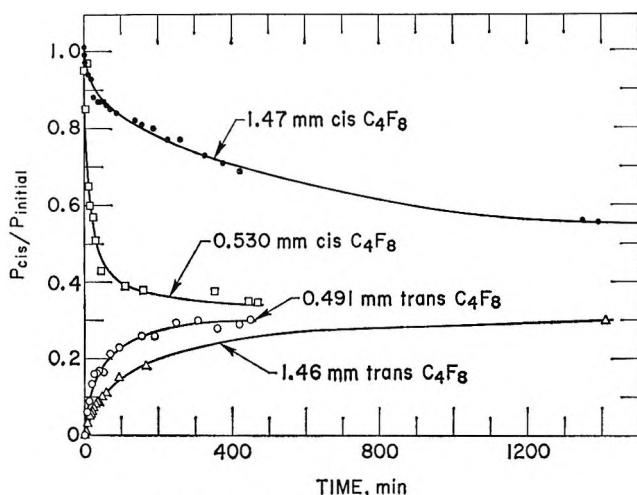
Figure 1. Fraction of cis-C_4F_8 vs. time.
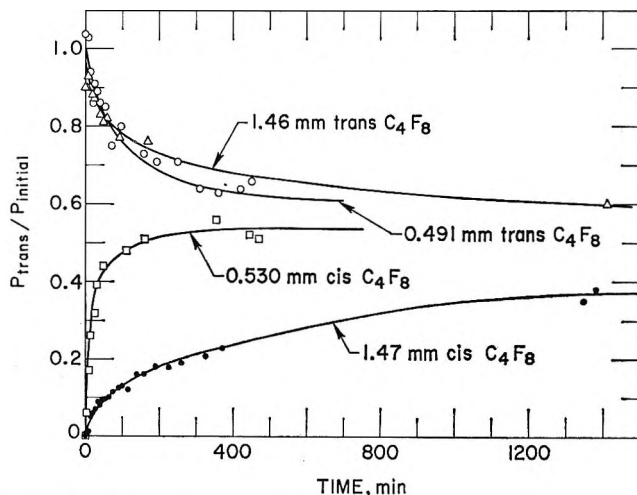
Figure 2. Fraction of trans-C_4F_8 vs. time.

fluorine substituents is further attenuated, no dissociation has been observed, even at 370°.[11] Thus, the ex-

(4) R. B. Cundall and D. G. Milne, *J. Am. Chem. Soc.*, **83**, 3902 (1961).

(5) R. B. Cundall, F. J. Fletcher, and D. G. Milne, *J. Chem. Phys.*, **39**, 3536 (1963).

(6) S. Sato, K. Kikuchi, and M. Tanaka, *ibid.*, **39**, 239 (1963).

(7) R. J. Cvetanović, H. E. Gunning, and E. W. R. Steacie, *ibid.*, **31**, 573 (1959).

(8) J. Heicklen, V. Knight, and S. A. Greene, *ibid.*, **42**, 221 (1965).

(9) J. Heicklen and V. Knight, Aerospace Corp. Rept. TDR-469-(5250-40)-5, Feb. 15, 1965; *J. Phys. Chem.*, in press.

(10) J. Heicklen and V. Knight, Aerospace Corp. Rept. TDR-469(5250-40)-7, Feb. 15, 1965; *J. Phys. Chem.*, in press.

(11) V. Knight, unpublished results of this laboratory.

(12) S. A. Greene and F. M. Wachi, *Anal. Chem.*, **35**, 928 (1963).

(13) J. Heicklen, F. Wachi, and V. Knight, Aerospace Corp. Rept. TDR-269(4240-20)-5, July 24, 1964; also *J. Phys. Chem.*, **69**, 693 (1965).

(14) D. Saunders and J. Heicklen, *J. Am. Chem. Soc.*, **87**, 2088 (1965).

Table I: Photolysis of Perfluorobutene-2

| Initial pressure, mm. | | I_a, 10^{-13} quanta/ cc. sec. | Initial Φ | |
cis	trans		Φ_{cis}	Φ_{trans}
000	0.491	5.1	0.037	
000	1.46	5.1	0.045	
000	1.73	5.1	0.067	
000	5.02	5.1	0.031	
0.530	000	6.0		0.075
0.653	000	5.4		0.086
1.47	000	6.0		0.032
1.49	000	5.4		0.158
5.26	000	5.4		0.229
5.29	000	6.0		0.148

cited molecule proposed is deactivated to the ground state. In the present study, the excited-state intermediate has been confirmed. As seen in Table I, Φ_{cis} is 0.045 and Φ_{trans} is 0.12; the sum is clearly not unity.

Some runs were conducted in the presence of O_2, and it was found that $\Phi(CF_3CFO) = 0.16$. At elevated temperatures, Knight[11] has found an additional product which is also produced in C_3F_6–O_2 photolysis.[9,10]

The small yield of CF_3CFO in the presence of oxygen, as well as the small sum of Φ_{cis} + Φ_{trans} in the absence of oxygen, suggests that both the CF_3CFO production and the isomerization occur from the same electronic state and that this state is produced with an efficiency less than one. Alternatively, the excited molecule might be produced with unit efficiency, but a barrier to internal rotation or oxidation of about 1 kcal./mole inhibits reaction.

Acknowledgment. The authors wish to thank Mrs. Barbara Peer for assistance with the manuscript.

The Ground State Electronic Configurations of

Ferricenium and Dibenzenechromous Cations[1a]

by Donald R. Scott[1b] and Ralph S. Becker

Department of Chemistry, University of Houston, Houston, Texas
(Received May 14, 1965)

The question of the relative ordering of the d orbitals in the sandwich complexes has been a matter of great interest since the discovery of these compounds. It is now generally accepted that the $e_{1g}(d_{xz},d_{yz})$ orbital is least stable, but the relative stabilities of the $a_{1g}(d_{z^2})$

and $e_{2g}(d_{xy},d_{x^2-y^2})$ orbitals is less certain. The purpose of this communication is to show that fairly definite conclusions may now be arrived at concerning the orbital order in the d^5 complexes, $Cr(bz)_2^+$ and $Fe(cp)_2^+$.

The question of the relative stabilities of the e_{2g} and a_{1g} orbitals in $Cr(bz)_2^+$ and $Fe(cp)_2^+$ was discussed by Levy and Orgel[2] in 1961. They used a ligand field model and on the basis of the experimental absorption spectrum concluded that in $Fe(cp)_2^+$ the e_{2g} level lay about 0.7 e.v. *below* the a_{1g} level. They also concluded that the e_{2g} level in $Cr(bz)_2^+$ lay about 2.9 e.v. below the a_{1g} level. However, these authors pointed out that their use of the free-ion Slater–Condon parameters, F_2 and F_4, was incorrect and would cause an overestimation of the energy separation between the e_{2g} and a_{1g} orbitals.

Let us consider the ferricenium cation. We agree with Levy and Orgel that the ground state of this complex is $^2E_{2g}[(a_{1g})^2(e_{2g})^3]$ on the basis of its magnetic susceptibility. The excitation energy to the low-lying $^2A_{1g}[(a_{1g})^1(e_{2g})^4]$ state, neglecting any configuration interaction, is given by

$$^2E_{2g} \longrightarrow {}^2A_{1g}$$
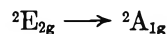
$$\text{T. E.} = \Delta E(e_{2g} - a_{1g}) + 20B(\text{complex})$$

where $B(\text{complex})$ is the Racah parameter for the complex. Since $\beta(\text{nephelauxetic parameter}) = B(\text{complex})/B(\text{free ion})$, this excitation energy may be rewritten as
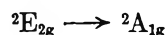
$$^2E_{2g} \longrightarrow {}^2A_{1g}$$

$$\text{T. E.} = \Delta E(e_{2g} - a_{1g}) + 20\beta B(\text{free ion})$$

Taking $B(Fe^{3+}, \text{free ion})^3 = 1090$ cm.$^{-1}$ and assigning the experimental absorption band at 16.21 kK.[4] as the $^2E_{2g} \rightarrow {}^2A_{1g}$ transition, we may readily show that the a_{1g} level lies *below* the e_{2g} level for all values of β less than 0.74. Since the value for β in ferrocene has been determined to be 0.4,[5] it is reasonable to expect that β in $Fe(cp)_2^+$ is less than 0.74. Using an estimated β-value of 0.5, we estimate that the a_{1g} orbital lies 5300 cm.$^{-1}$ below the e_{2g} level in $Fe(cp)_2^+$.

(1) (a) Supported in part by the Robert A. Welch Foundation, Houston, Texas; (b) Abstracted from the Ph.D. Dissertation of D. R. Scott, University of Houston, Houston, Texas, Jan. 1965; National Science Foundation Cooperative Predoctoral Fellow, 1962–1963.

(2) D. A. Levy and L. E. Orgel, *Mol. Phys.*, 4, 93 (1961).

(3) C. K. Jørgensen, "Absorption Spectra and Chemical Bonding in Complexes," Pergamon Press, Ltd., Oxford, 1962, p. 109.

(4) D. R. Scott, Ph.D. Dissertation, University of Houston, Jan. 1965; ferricenium tetrafluoroborate in water or dibenzenechromium iodide in water.

(5) D. R. Scott and R. S. Becker, *J. Organometal. Chem.*, in press.

In the $Cr(bz)_2^+$ complex, the ground state is assumed to be $^2A_{1g}[(a_{1g})^1(e_{2g})^4]$ on the basis of magnetic susceptibility and e.s.r. results.[2,6] Similar to the ferricenium cation, the excitation energy to the low-lying $^2E_{2g}$ state may be expressed as
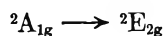
$$^2A_{1g} \longrightarrow {}^2E_{2g}$$

$$\text{T. E.} = \Delta E(a_{1g} - e_{2g}) - 20\beta B(\text{free ion})$$

Thus the a_{1g} level must lie *above* the e_{2g} level for all values of β. Assigning the absorption band at 8.50 kK.[4] to the $^2A_{1g} \rightarrow {}^2E_{2g}$ transition and taking $B(Cr^+$, free ion)[7] $= 706$ cm.$^{-1}$, we find that $\Delta E(a_{1g} - e_{2g})$ lies between 8.50 kK. $(\beta = 0)$ and 22.62 kK. $(\beta = 1)$. A reasonable estimate of $\beta = 0.6$ gives an energy separation of 17 kK.

In conclusion, we have shown that the a_{1g} level lies about 5000 cm.$^{-1}$ *below* the e_{2g} level in $Fe(cp)_2^+$ and that the e_{2g} level lies about 17,000 cm.$^{-1}$ *below* the a_{1g} level in the $Cr(bz)_2^+$ cation. The differences between these conclusions and those of Levy and Orgel are due to their use of the free-ion Slater–Condon parameters. The rather large depression of the e_{2g} level below the a_{1g} level in $Cr(bz)_2^+$ indicates a large participation of the e_{2g} ligand orbitals in the bonding of the dibenzene complexes. This is in agreement with current thoughts of the bonding in the dibenzene complexes.

The analysis of the ligand field spectra of these d^5 complexes is in progress and will be described in a later publication.

(6) R. E. Robertson and H. M. McConnell, *J. Phys. Chem.*, **64**, 70 (1960).

(7) J. Hinze and H. H. Jaffé, *J. Chem. Phys.*, **38**, 1834 (1963).

Transport Numbers in Aqueous Potassium

Chloride Solutions at 0°

by B. J. Steel[1a]

Department of Physical and Inorganic Chemistry, University of New England, Armidale, New South Wales, Australia
(Received May 20, 1965)

In view of the recent publication of a paper[1b] concerning transport numbers in aqueous potassium chloride solutions at elevated temperatures, some interest may attach to measurements made some time ago[2] of transport numbers in this system at 0°. As a test of the method used, results are presented also for 25°.

Experimental

The apparatus and procedure for determinations at 25° have been described previously.[3-5] The only change in this procedure has been made in the preparation of the electrodes. These are now formed by rolling cylinders of platinum gauze and welding them to stout platinum wires sealed through standard B. 10 Pyrex cones. Silver is deposited electrolytically onto the gauze and, in the case of the electrode to be used as the cathode, some of the silver is converted electrolytically into silver chloride.

For runs at 0°, the conductometric analyses were performed at 25°; only the electrolysis was carried out at 0°. After the initial analysis of the solutions, the apparatus was placed in a 4-gal. drum provided with drainage holes. The drum was then filled with flaked ice. After waiting for 1 hr. to ensure complete cooling of the solution, the electrolysis was commenced. As soon as the electrolysis current was switched off, the two compartments of the transport number cell were isolated by turning the tap on the apparatus. The ice was then washed out of the drum using a jet of water. The solution was reanalyzed at 25°. During the electrolysis the temperature of the ice bath was checked using a thermometer previously calibrated with ice formed from distilled water. No part of the ice bath showed a temperature differing from 0° by more than 0.01°.

Results and Discussion

In Table I, the results obtained at 25° are compared with values interpolated from data obtained using the Hittorf[6] and moving boundary[7] techniques. The agreement among the various methods is excellent.

The results obtained at 0° are shown in Table II.

The final column of Table II lists the limiting values of the transport numbers calculated using the equation

$$t^0_+(\text{calcd.}) = t_+ - [B_2 C^{1/2}(t_+ - 0.5)/\Lambda^0(1 + B\mathring{a}C^{1/2})]$$

obtained by rearranging eq. 7.40 of ref. 5. Values of the parameters B and B_2 are given in Appendix 7.1 of

(1) (a) Department of Physical and Inorganic Chemistry, University of Adelaide, South Australia; (b) J. E. Smith, Jr., and E. B. Dismukes, *J. Phys. Chem.*, **67**, 1160 (1963).

(2) B. J. Steel, Ph.D. Thesis, University of New England, N.S.W., Australia, 1960.

(3) B. J. Steel and R. H. Stokes, *J. Phys. Chem.*, **62**, 450 (1958).

(4) B. J. Steel, J. M. Stokes, and R. H. Stokes, *ibid.*, **62**, 1514 (1958).

(5) R. A. Robinson and R. H. Stokes, "Electrolyte Solutions," Butterworth and Co. Ltd., London, 1959, p. 103.

(6) D. A. MacInnes and M. Dole, *J. Am. Chem. Soc.*, **53**, 1357 (1931).

(7) L. G. Longsworth, *ibid.*, **54**, 2741 (1932).

Table I: Transport Numbers in Aqueous Potassium Chloride Solutions at 25°

Concn., g.-equiv. l.$^{-1}$	t_{K^+}, this work	t_{K^+}, ref. 6	t_{K^+}, ref. 7
0.015984	0.4906	0.4910	0.4902
0.022056	0.4899	0.4904	0.4901
0.031242	0.4898	0.4904	0.4900
0.042914	0.4900	0.4906	0.4900

Table II: Transport Numbers in Aqueous Potassium Chloride Solutions at 0°

Concn., g.-equiv. l.$^{-1}$	t_{K^+}	$t^0_{K^+}$(calcd.)
0.012235	0.4962	0.4963
0.020038	0.4943	0.4945
0.030846	0.4953	0.4955
0.041281	0.4957	0.4959
0.051719	0.4947	0.4950

Figure 1. Temperature dependence of transport numbers in aqueous potassium chloride solutions: X, this work; O, ref. 12; □, ref. 1.

ref. 5; d was taken to be 3.8 Å. Lange's[8] determination of Λ^0 for KCl at 0° = 81.7 was used. The average of t^0_+(calcd.) = 0.4954 was taken as the limiting value of the transport number of potassium ion in potassium chloride solution at 0°. This is appreciably lower than the estimate of $t^0_{K^+}$ = 0.498 made by Robinson and Stokes by extrapolation of results at higher temperatures.[9] However, the mobility of the chloride ion at 0° using the present data is $\lambda^0_{Cl^-}$ = 81.7(1 − 0.4954) = 41.2. This mobility may also be calculated from results of transport numbers[10] and conductances[10,11] of hydrochloric acid solutions at 0°. These data give $\lambda^0_{Cl^-}$ = 265.2(1 − 0.8441) = 41.3, in good agreement with the result obtained above. The results of this work are combined with those of Smith and Dismukes[1b] and of Allgood, LeRoy, and Gordon[12] in Figure 1, where log $[(1 − t^0_{K^+})/t^0_{K^+}]$ is plotted vs. the reciprocal of the absolute temperature. (The data from ref. 1 are t_{K^+} at approximately 0.1 N and not $t^0_{K^+}$. The difference would not be large in these systems.) A straight line can be drawn through all the points within the estimated experimental error. Thus the conclusion of Smith and Dismukes that the difference in the activation energies of migration for potassium and chloride ions is independent of temperature is valid down to 0°. The slope of the line in Figure 1 corresponds to an activation energy for the chloride ion that is 110 ± 10 cal./g.-ion greater than that for the potassium ion. Horne and Courant[13] have shown that the temperature coefficient of the conductance of 0.1 M potassium chloride changes markedly between 9 and 0°. They attribute this change to alterations in the water structure as the temperature is lowered. The results described in this paper indicate that the chloride and potassium ions are affected to much the same extent by these alterations. This is perhaps not surprising in view of the similar mobilities of these ions. It would be interesting to examine the temperature dependence of the mobility of other ions in water between 0 and 10°.

Acknowledgment. The author wishes to acknowledge helpful discussions with Professor R. H. Stokes during the course of this research.

(8) J. Lange, *Z. physik. Chem.*, **A188**, 384 (1941).

(9) See ref. 5, p. 127.

(10) A. K. Covington and J. E. Prue, *J. Chem. Soc.*, 1930 (1957).

(11) M. Randall and A. P. Vanselow, *J. Am. Chem. Soc.*, **46**, 2418 (1924).

(12) R. W. Allgood, J. D. LeRoy, and A. R. Gordon, *J. Chem. Phys.*, **8**, 418 (1940).

(13) R. A. Horne and R. A. Courant, *J. Phys. Chem.*, **68**, 1258 (1964).

A Simple Reduced Equation for the Estimation of Vapor Pressures[1]

by Donald G. Miller

Lawrence Radiation Laboratory, University of California, Livermore, California (*Received April 30, 1965*)

In a recent paper[2] (whose notation is adopted here), the reduced vapor pressure predictor

RPM $\log P_r = -\dfrac{G'}{T_r}\left[1 - T_r^2 + k'(1 - T_r)^3\right]$ (1)

was derived from the four-constant equation

$$\log P = A + B/T + CT + DT^2 \qquad (2)$$

using critical constants and the Riedel–Plank condition.[2-4] The constant G' correlates linearly with a, defined by

$$a = \frac{T_{rb}\ln P_c}{(1 - T_{rb})} \qquad (3)$$

This a is a characterizing parameter of liquids and will be called the *vaporization parameter* for lack of a better name.

also had the advantage of being much simpler than other predictors because a value of $\log P_r$ is obtained in a single pass on a hand calculator capable of repeated and accumulative multiplications, once G' and k' are available.

It would be more convenient, however, to have a single equation for which the "constants" are more constant over the whole liquid range. For this reason and also because it seemed that Waring's criteria[8] might better be satisfied by a higher power of T for the D term,[9] the equation

$$\log P = A + B/T + CT + DT^3 \qquad (4)$$

was considered.

Table I: Comparison of Reduced Predictors (Input Data: T_b, T_c, P_c)

	Equation	34 hydro-carbons	45 nonpolar organics	8 polar organics	All 53 organics	All 18 inorganics	All 71 compounds	66 compounds[a]	No. not within 10% (of 71)	Av. max. error, % (for 71)
		—————————————— 10³S ——————————————								
10-1500 mm.	RPME	7.2	22.8	35.5	58.3	11.4	69.7	43.6	11[b]	5.3
	RPML	7.7	20.6	37.3	58.0	12.7	70.7	40.7	11	5.2
	R	9.3	20.5	35.8	56.3	17.1	73.4	43.4	12	5.3
	FK	6.5	17.4	37.0	54.4	20.1	74.5	43.2	12	5.1

		All 24 compounds[c]	Without NO	No. not within 10% (of 24)	Av. max. error, % (for 24)
		———— 10⁴S ————			
T_b-T_c	RPME	30.4	24.7	0	1.69
	RPML	55.4	50.3	0	2.34
	RPMH	25.7	18.5	0	1.54
	R	36.6	26.0	0	1.67
	FK	29.1	21.3	0	1.54

[a] Excluding organic acids and alcohols. [b] These compounds are methanol, propanol, butanol, butyric acid, ethyl mercaptan, thiophene, dichloromethane, ethylamine, and fluorine, with methylamine and chlorine borderline. Of the 77 compounds with good data in ref. 5, all but He, H₂, acetic acid, HF, and SO₃ satisfy the 10% criterion above 60 mm. Although the liquid metal Hg was not included in the tabulations, predictions are also within 10% from 10 to 1500 mm. [c] These 24 compounds are described in ref. 5. They are mostly inorganic for lack of any uniform presentation of critically reviewed data for organics.

When values of k' and G' for a given substance were actually computed for each experimental vapor pressure point using the boiling and critical points as references, k' was found to increase on the average about 15 to 20% between the triple and critical points. As a result, vapor pressure predictions with **RPM** were best with one correlation of $G'(a)$ for the region 10–1500 mm. and another for the region T_b–T_c. The comparison of **RPM** with experiment and with other reduced predictors, given briefly in ref. 2 and extensively elsewhere,[5] showed that these **RPM** equations were as good or better than others such as Riedel's[6] (denoted by **R**) and Frost–Kalkwarf's[7] (denoted by **FK**). They

The reduced form of this equation, which is similar to eq. 1 and which also exhibits the known curvatures of $\log P_r$ *vs.* $1/T_r$ plots,[2,8] is given in eq. 5.

(1) This work was performed under the auspices of the U. S. Atomic Energy Commission.

(2) D. G. Miller, *J. Phys. Chem.*, **68**, 1399 (1964).

(3) R. Plank and L. Riedel, *Ingr.-Arch.*, **16**, 255 (1948).

(4) R. Plank and L. Riedel, *Texas J. Sci.*, **1**, 86 (1949).

(5) D. G. Miller, *Ind. Eng. Chem.*, **56**, No. 3, 46 (1964).

(6) See ref. 2, eq. 28.

(7) See ref. 2, eq. 29.

(8) W. Waring, *Ind. Eng. Chem.*, **46**, 762 (1954).

(9) *Cf.* footnote 31 of ref. 2.
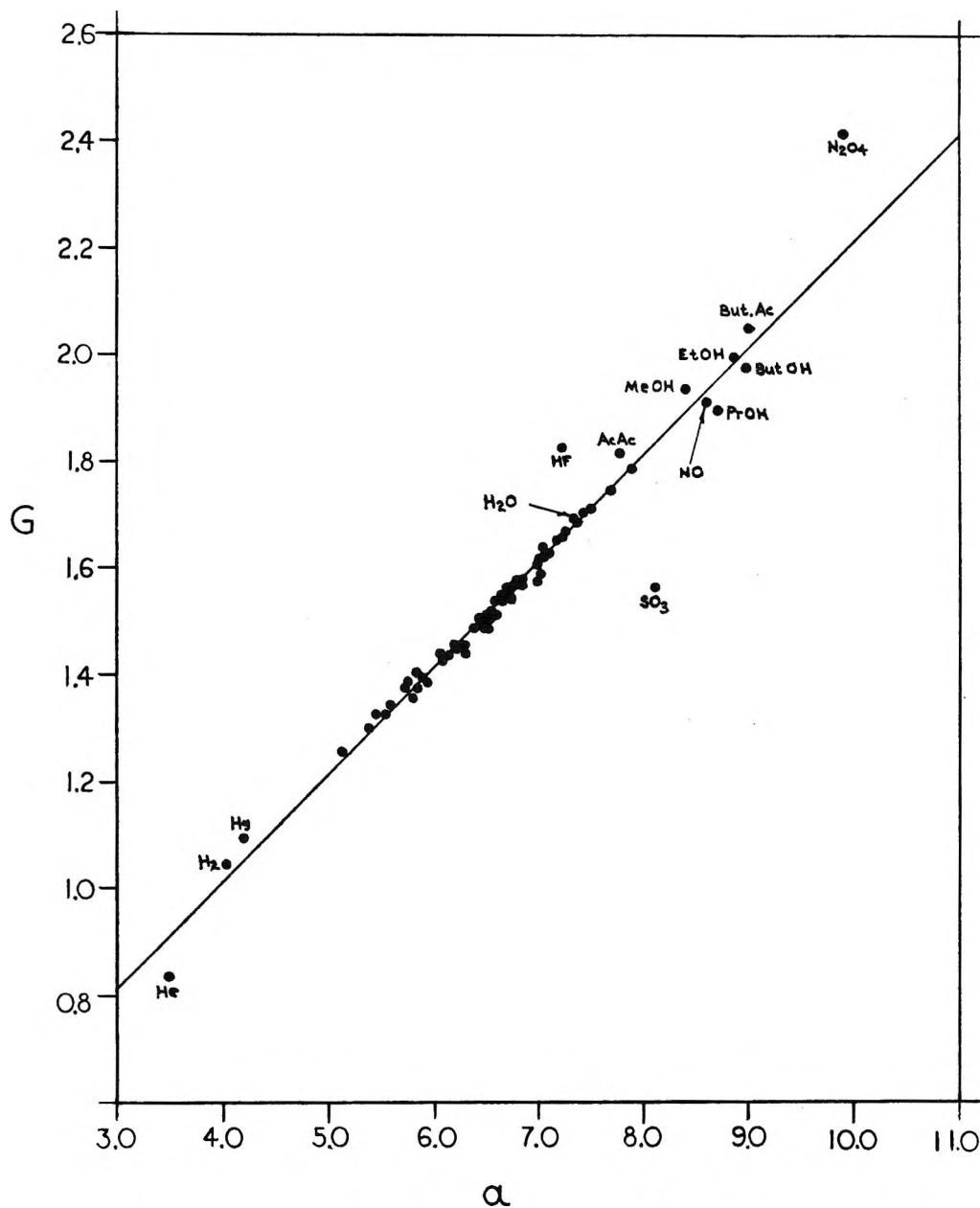
Figure 1. Plot of G vs. a for 77 compounds. Solid line is eq. 6.

RPME

$$\log P_r = -\frac{G'}{T'_r}\left[1 - T_r^2 + k(3 + T_r)(1 - T_r)^3\right] \quad (5)$$

(The designation **RPME** also includes eq. 6 below.) It is derived by means of the Riedel–Plank condition in exactly the same way as **RPM**.[2] Equation 5 is nearly as simple as eq. 1 and much simpler than **R** and **FK**.

Notice that $k(3 + T_r)$ in **RPME** replaces k' in **RPM**. Because this $(3 + T_r)$ factor has about the 20% observed increase between the triple point and T_c, G

and k should be more constant for a given substance than were G' and k'. This was verified upon comparing k and G calculated from experimental pressures using the boiling and critical points as reference points.

G also correlates well with a (see Figure 1). The best correlation for use over the whole liquid range is

$$G = 0.210 + 0.200a \quad (6)$$

which is based on the 77 widely different compounds listed in ref. 5. Solving eq. 5 at T_b yields

$$k = \frac{(a/LG) - (1 + T_{rb})}{(3 + T_{rb})(1 - T_{rb})^2} \tag{7}$$

where $L = 2.3026$. Since the terms of eq. 7 are functions of T_b, T_c, and P_c only, vapor pressures can be predicted from just these input data.

Detailed comparisons of **RPME** with experiment and with the better reduced predictors, namely, **RPML** (low pressure), **RPMH** (high pressure), **R**, and **FK**, are given in Table I, including the number of compounds whose vapor pressures are not predicted to within 10%, the average maximum % error,[10] and S for various classes of compounds[5] where

$$S = \sum_{\text{compounds}} \left(\frac{\sum\limits_{\text{points}} \delta^2}{n} \right) \tag{8}$$

Here n is the number of experimental vapor pressure points and δ is the per cent residual in P divided by 100.

Table I shows that **RPME** is equivalent or superior to all the others in the 10–1500-mm. range in terms of over-all S, average maximum per cent error, and the number within 10%. In the T_b–T_c region, it is slightly better than **R**, is only slightly poorer than **FK** or **RPMH**, and is an excellent predictor. Therefore it compares favorably over-all with the pair of **RPM** equations as well as with **R** and **FK**. Moreover, it has the important advantage of being much simpler for hand calculations than **R** or **FK**, since no log terms or iteration are required. As with **RPM**, a value of log P_r is obtained with one pass on a hand calculator once G and k are calculated.

In common with other reduced predictors, **RPME** is not too good at low pressures with pathological liquids such as alcohols, carboxylic acids, and associated or dissociating ones if G is estimated by eq. 6. However, the predictions are substantially improved if G is calculated from a low pressure point, should one be available in addition to the regular input data.

The expression for $\Delta H/\Delta Z$ derived from the Clapeyron equation is also rather simple; namely

$$\frac{\Delta H}{\Delta Z} = LRT_c G\left[(1 + T_r^2) + 3k(1 - T_r^2)^2 \right] \tag{9}$$

Unpublished calculations show that the heat of vaporization at the boiling point, ΔH_b, can be estimated with an average error of only 1.2% (1.6% if the pathological liquids are included) using eq. 6, 9, and Thomson's estimate[11] of ΔZ_b

$$\Delta Z_b = 1 - \frac{0.97}{P_c T_{rb}} \tag{10}$$

Because **RPME** is over-all as good or better a predictor than other single reduced equations and because it is substantially simpler for calculations, it is recommended for rapid estimation of vapor pressures over the whole liquid range using only the normal boiling and critical points as input data.[12–14]

(10) This quantity is the maximum per cent error for each compound averaged over all the compounds. It is a more stringent measure of good fit than the average per cent error; the latter is about half the former. Ordinarily, the maximum error occurs at the lowest temperature when below T_b, and in the middle of the range when between T_b and T_c.

(11) G. W. Thomson, *Chem. Rev.*, **38**, 1 (1946).

(12) However, if an experimental value of ΔH_b should be available as well as P_c, substantially better estimates of P in the 10–1500-mm. region are given by the semireduced predictor MRA.[2,5]

(13) Othmer and Huang have shown (private communication) that slightly better reduced predictions in the 10–1500-mm. region can be made using Othmer's reference liquid method.[14] However, the method requires an extensive table of data for the reference liquid in addition to the RPME input data.

(14) D. F. Othmer, *Ind. Eng. Chem.*, **34**, 1072 (1942).

Proton Magnetic Resonance Line Widths, Ligand Exchange, and Electronic Relaxation Times for Some Arylphosphine Complexes of Cobalt(II) and Nickel(II)[1a]

by Gerd N. La Mar[1b]

Frick Chemical Laboratory, Princeton University, Princeton, New Jersey (*Received May 21, 1965*)

The careful analysis of proton magnetic resonance (p.m.r.) line widths for paramagnetic complexes can result in a variety of useful information.[2,3] The observed line width in excess of that for the pure diamagnetic ligand can arise from two main sources— ligand exchange and paramagnetic relaxation due to the unpaired electron(s) on the metal. From a temperature study, the contribution from chemical exchange may be estimated,[3] and the remaining excess line width can then be attributed to paramagnetic relaxation effects.[2a,3] The systems of interest here are the bis(triarylphosphine) dihalides of Co(II) and Ni(II).[4]

(1) (a) This research has been supported by a grant from the National Institutes of Health; (b) Chemical Laboratory IV, H. C. Ørsted Institute, University of Copenhagen, Copenhagen, Denmark.

(2) (a) N. Bloembergen and L. O. Morgan, *J. Chem. Phys.*, **34**, 842 (1961); (b) E. A. LaLancette and D. R. Eaton, *J. Am. Chem. Soc.*, **86**, 5145 (1964).

(3) Z. Luz and S. Meiboom, *J. Chem. Phys.*, **40**, 1058, 1066 (1964).

It has been observed[2b] that for these Ni complexes, ligand exchange is quite important in determining the line widths $(\Delta H_{1/2})$. LaLancette and Eaton concluded that the rate of ligand exchange for the iodide complex was slow by the n.m.r. criterion, with the rates increasing in the order I < Br < Cl.[2b] Upon addition of excess ligand to solutions of the Co complexes, we observed the same phenomenon as for the Ni complexes[2b]: that the ligand exchange rate increases in the order I < Br < Cl, with the rate for the iodide also very slow as measured by n.m.r. The observed[4] p.m.r. lines for the ortho protons for both the pure Co and Ni complexes exhibit increasing widths, I < Br < Cl, indicating increasing contributions to the line widths due to ligand exchange. In order to determine the relative importance of ligand exchange for the various halides, we obtained $\Delta H_{1/2}$ for the two complexes, $(p\text{-tol}_3P)_2CoI_2$ and $(p\text{-tol}_3P)_2NiI_2$, in CDCl$_3$ over the temperature range -60 to $60°$, using a Varian DP-60 spectrometer in conjunction with a variable temperature probe. The results are illustrated in Figure 1.

The curves of line width vs. temperature exhibit two distinct regions[3]; at low T, $\Delta H_{1/2}$ decreases with T, and at high T, $\Delta H_{1/2}$ increases with T. The former region gives the variation of $\Delta H_{1/2}$ in the absence of ligand exchange, while the latter region indicates increasing contributions to the width from ligand exchange. The data exhibit too much scatter to make any quantitative estimates to the rate of exchange; however, two conclusions may be drawn from inspection of Figure 1. The first is that the contribution to $\Delta H_{1/2}$ due to ligand exchange appears to set in at lower temperature for the Co than for the Ni complex, indicating, at least for the iodides, that the Ni complex is more stable than the Co complex.[2b] Similar measurements on the bromides and chlorides were inconclusive since the data were quite unreproducible and there was evidence for some decomposition or precipitation of ligand. Since ligand exchange contributed significantly to the observed line widths for the bromides and chlorides to much lower temperatures than for the iodides, it could not be definitely established whether there exists significant differences in $\Delta H_{1/2}$ for the three halides in the absence of ligand exchange.

Since the order of ligand labilities for the Co and Ni[2b] complexes is identical, the explanation offered by LaLancette and Eaton[2b] appears to be applicable also to the Co systems.[4] Their reasoning[2b] is that the donation of an electron to the phosphine ligand via $d\pi$–$d\pi$ bonding is partially compensated by π-bonding with the halide, and the order of halogen π-bonding abilities is I > Br > Cl. The fact that for the iodide
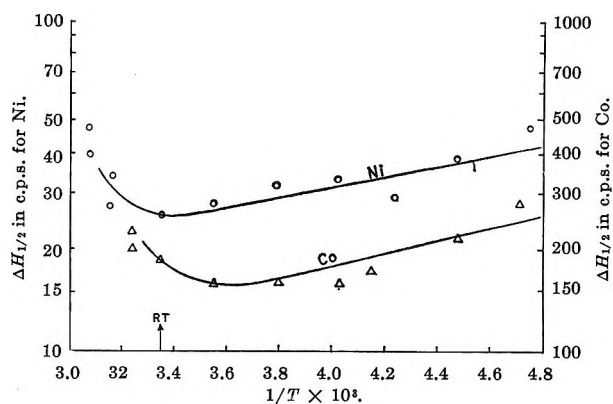

Figure 1. P.m.r. line widths as a function of temperature for the ortho protons in $(p\text{-tol}_3P)_2CoI_2$ and $(p\text{-tol}_3P)_2NiI_2$.

complexes the Ni appears to be more stable than the Co bears out this postulate[2b,5,6] that $d\pi$–$d\pi$ bonding is very significant in determining the stabilities of these complexes. From p.m.r. contact shifts, it has been established[2b,4,7] that the unpaired spin densities on the phosphine ligands for the Ni complexes are consistantly 50% greater than in the Co complexes, indicating that $d\pi$–$d\pi$ delocalization is more extensive in the Ni systems, hence their greater stabilities.

The second conclusion indicated by Figure 1 is that the contributions to the observed line widths at room temperature are essentially negligible for both the Ni and Co complexes. These $\Delta H_{1/2}$ values must thus result from paramagnetic relaxation effects since the width for the pure ligand is only $\sim$2–3 c.p.s.[4] The p.m.r. line widths due to the presence of unpaired electrons have been related to the electron correlation times by Solomon[8] and Bloembergen.[9] The combined equation[2a] can be expressed as

$$\Delta H_{1/2} = B\left[4\tau_c + \frac{3\tau_c}{1 + \omega_I^2\tau_c^2} + \frac{13\tau_c}{1 + \omega_S^2\tau_c^2}\right] + C\left[\tau_e + \frac{\tau_e}{1 + \omega_S^2\tau_e^2}\right] \quad (1)$$

Here $B = S(S + 1)\gamma_1^2 g^2\beta^2/(15r^6)$, $C = S(S + 1)A^2/3h^2$, τ_c and τ_e are the electron dipolar and exchange correlation times, respectively, ω_I and ω_S are the proton and electron Larmor frequencies, and the other symbols have their conventional meanings.[2b,3] Since the ortho

(4) G. N. La Mar, W. D. Horrocks, Jr., and L. C. Allen, J. Chem. Phys., 41, 2126 (1964).

(5) M. C. Browning, J. R. Mellor, D. J. Morgan, S. A. J. Pratt, L. E. Sutton, and L. M. Venanzi, J. Chem. Soc., 693 (1962).

(6) A. D. Allen and C. D. Cook, Can. J. Chem., 41, 1235 (1953).

(7) G. N. La Mar, J. Chem. Phys., 41, 2992 (1964).

(8) I. Solomon, Phys. Rev., 99, 559 (1955).

(9) N. Bloembergen, J. Chem. Phys., 27, 592 (1955).

proton peaks are considerably broader than the other peaks,[4] the main relaxation is *via* the dipolar part of eq. 1, rather than the term depending on the hyperfine interaction. This is due to the r^{-6} dependence of the first term in eq. 1 and the nearness of the *ortho* position to the metal. Using only the first term, with $\langle r^6 \rangle_{av} = 6.8 \times 10^{-43}$ cm.[6] (structural parameters taken from ref. 4), $g = 2.39, S = {}^3/_2$ for Co,[10] and $g = 2.32, S = 1$ for Ni,[11] an upper limit to the dipolar correlation time, τ_c, is calculated.[3] We obtain $\tau_c = 2 \times 10^{-13}$ and 6×10^{-13} sec. for the Ni and Co complexes, respectively. These τ_c values are too short to be associated with the molecular tumbling time in solution, which the Debye equation estimates to be $\sim 10^{-11}$ sec., so that τ_c may be identified[3] with the electronic relaxation time, T_1. For the related complex anions,[7] [(phen$_3$-P)CoI$_3$]$^-$ and [(phen$_3$P)NiI$_3$]$^-$, similar calculations using the observed line widths[7] yield T_1 values of about the same magnitude as for the complexes discussed above. Only very rough estimates to the *ortho* proton line widths are available for the anionic complexes, due to considerable overlapping of lines.[7] It is of interest that for these complexes $\tau > T_1$, where τ is the molecular tumbling time in solution, the opposite to what has been previously assumed in the analysis of the isotropic shifts.[4,7,12]

Acknowledgments. The author wishes to acknowledge the hospitality of the Bell Telephone Laboratories, Murray Hill, N. J., and thanks Mr. E. W. Anderson for obtaining the p.m.r. spectra. Valuable discussions with Profs. L. C. Allen and W. D. Horrocks, Jr., are gratefully acknowledged.

(10) F. A. Cotton, O. D. Faut, D. M. L. Goodgame, and R. H. Holm, *J. Am. Chem. Soc.*, 83, 1780 (1961).

(11) F. A. Cotton, O. D. Faut, and D. M. L. Goodgame, *ibid.*, 83, 344 (1961).

(12) H. M. McConnell and R. E. Robertson, *J. Chem. Phys.*, 29, 1361 (1958).

The Abnormal Relation between the
Velocity of Sound and the Temperature
in Sodium Sulfate Solution

by Tatsuya Yasunaga, Mitsuyasu Tanoura, and Masaji Miura

Department of Chemistry, Faculty of Science, Hiroshima University, Hiroshima, Japan (*Received January 25, 1965*)

Since the first report by one of the authors[1] on the abnormality in the velocity of sound in sodium sulfate

and sodium carbonate aqueous solutions near the crystal transition point of the salts, a similar abnormality has been discovered in the electric conductivity for sodium sulfate by Hirano[2] and in the viscosity of sodium carbonate by Fujita.[3] This communication is to report more detail on the abnormal relation between the temperature and the velocity of sound in sodium sulfate aqueous solution.

The velocity of sound was measured by an ultrasonic interferometer described in detail elsewhere.[4] The electrical oscillations controlled by quartz crystals having each fundamental frequency 2.5, 3.5, 4.5 Mc./sec. in a thermostat were derived to the X-cut quartz crystal having its fundamental frequency 0.5 Mc. Special circuits were added to detect precisely only the change in the interference. The frequency of oscillation was measured carefully within ±50 c.p.s. during each series of runs by a frequency meter. The vertical double glass tubes were sealed through a Teflon O ring to a holed stainless steel plate, below which was attached a gold-plated 0.5-Mc. crystal. A plane reflector made of stainless steel was connected to a micrometer and balanced for the crystal by controlling a spring. It could be moved vertically without any rotation, and its position was determined within ±0.001 mm. with the micrometer having a traveling range of 6 cm. In order to protect the sample solution from contamination during measurement, a glass tube was fixed to the shaft of the micrometer. The ultrasonic interferometer was immersed in a water bath and maintained at a constant temperature to ±0.002°.

The velocity of sound at 3.5 Mc. for various concentrations of sodium sulfate solution at different temperatures (0.1963–1.849 M) is given in Table I and shown in Figure 1. From these results, it is clearly seen that the change in the velocity of sound with temperature below 32.4° is not the same as that for greater temperatures, even for solutions as dilute as 0.1963 M. In particular, a discrepancy in the velocity of sound was observed for the concentrated solution at 32.4°. A similar measurement was also done for a 1.144 M solution at various frequencies. The results obtained in the process of increasing the temperature are shown in Table II and show no dispersion in the velocity of sound by frequency. This suggests that the abnormality is not caused by a relaxation phenom-

(1) T. Sasaki and T. Yasunaga, *Kagaku To Kogyo* (Tokyo), 7, 146 (1954).

(2) K. Hirano, *Nippon Kagaku Zasshi*, 79, 648 (1958).

(3) K. Fujita, *Bull. Chem. Soc. Japan*, 32, 1005 (1959).

(4) T. Yasunaga, M. Tanoura, and M. Miura, in preparation.

Table I: Velocity of Sound in the Aqueous Solution of Various Concentrations of Na_2SO_4 as a Function of Temperature at 3.5 Mc.[a]

Temp., °C.	H₂O *3.49948* Mc.	0.1963 *M* *3.49948* Mc.	Sound velocity, m./sec. 0.5717 *M* *3.49935* Mc.	0.9846 *M* *3.49935* Mc.	1.849 *M* *3.49926* Mc.
30.0	1509.20	1538.28 (1538.30)	1593.93 (1593.93)	1648.80 (1648.84)	1749.80 (1749.83)
31.0	1511.49	1540.38	1595.76	1650.41	1750.74
31.5	1512.63	1541.43 (1541.42)	1596.61	1651.02 (1651.01)	1751.06 (1751.06)
31.8		1542.10	1597.05	1651.29	
32.0	1513.59	1542.51	1597.25	1651.40	1751.33
32.2		1542.90	1597.42 (1597.43)	1651.52 (1651.52)	1751.42 (1751.41)
32.4		1543.45 (1543.44)	1597.98 (1597.98)	1652.19 (1652.19)	1751.93 (1751.91)
32.5	1514.58				
32.6		1543.82 (1543.83)	1598.30	1652.48	1752.01 (1752.01)
32.8		1544.20	1598.56	1652.86	1752.11 (1752.11)
33.0	1515.58	1544.47 (1544.47)	1598.88	1653.18 (1653.19)	1752.16
33.5		1545.37	1599.70	1654.26	1752.40
34.0	1517.50	1546.19	1600.57	1655.42	1752.72

[a] The quantities in parentheses are the experimental values obtained by decreasing the temperature. Italicized numerals show the frequency.
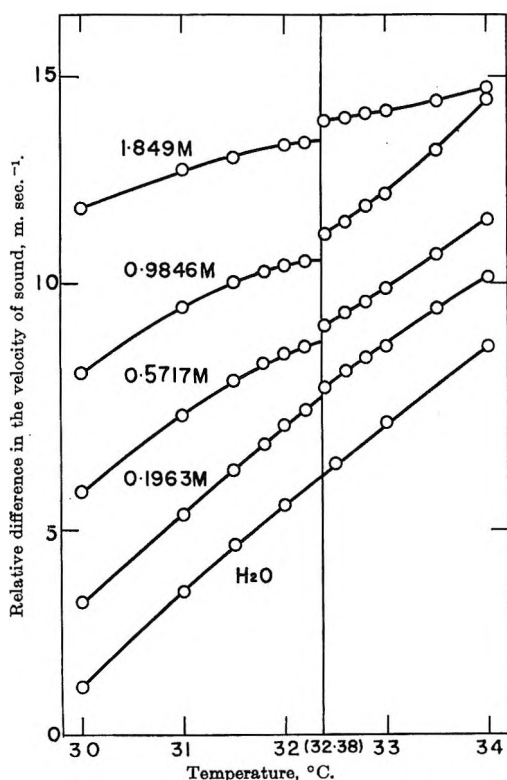

Figure 1. Variation of the velocity of sound with temperature for various concentrations of Na_2SO_4 aqueous solution at 3.5 Mc.

enon. It is remarkable that the temperature which shows the discontinuity is in excellent agreement with the transition point of the saturated sodium sulfate solution coexisting with the solid. This phenomenon, therefore, should be considered in connection with the transition phenomenon in the solid.

Table II: Velocity of Sound in the Aqueous Solution of 1.144 *M* Na_2SO_4 at Various Frequencies as a Function of Temperature[a]

Temp., °C.	2.5 Mc.	Sound velocity, m./sec. 3.5 Mc.	4.5 Mc.
30.0	1670.81 (1670.82) *2.49959* Mc.	1670.80 (1670.79) *3.49948* Mc.	1670.79 (1670.80) *4.49991* Mc.
31.0	1672.07 *2.49959*	1672.07 *3.49934*	1672.04 *4.49973*
32.0	1672.82 (1672.81) *2.49959*	1672.81 (1672.80) *3.49935*	1672.79 (1672.79) *4.49973*
32.5	1673.72 (1673.74) *2.49959*	1673.72 (1673.74) *3.49935*	1673.71 (1673.73) *4.49973*
33.0	1674.05 *2.49959*	1674.05 *3.49935*	1674.00 *4.49973*
34.0	1675.37 *2.49959*	1675.36 *3.49935*	1675.34 *4.49973*

[a] The quantities in parentheses are the experimental values obtained by decreasing the temperature. Italicized numerals show the frequency.

It is conceivable that an electrolyte dissolved in water exists as ions and embryonic aggregates, especially in the concentrated solution. The following scheme may be proposed for the embryo in the solution.

$$Na_2SO_4 \cdot 10H_2O \rightleftharpoons Na_2SO_4 + 10H_2O$$
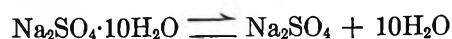
That is, the embryo at the lower temperature has the same structure as that of the hydrous sodium sulfate but turns to the anhydrous form at the higher tempera-

ture. Then the change in the structure of the embryo causes the discrepancy in the velocity of sound in solution at the transition temperature. However, it is quite difficult to explain such a change in the velocity of sound as shown in the figure by consideration of the change in the structure of the embryo since the thermodynamic properties of these structures have not yet been studied.

As a result of the above description, it should be considered that a very small amount of hydrous sodium sulfate embryo exists even in the dilute solution at the lower temperature and it changes to that of anhydrous at the transition temperature when the temperature is increased. It is worth noting that no hysteresis could be observed in this phenomenon as shown in Table I, and this phenomenon may be applied to accurately determine the transition point.

Spin-Echo Nuclear Magnetic Resonance

Studies of Chemical Exchange.

V.   Perfluorocyclohexane[1]

by H. S. Gutowsky and Fu-Ming Chen

Noyes Chemical Laboratory, University of Illinois, Urbana, Illinois
(Received April 22, 1965)

The chair–chair isomerization of perfluorocyclohexane has been investigated by Tiers,[2] who used steady-state, high-resolution n.m.r. methods for the purpose. However, neglect of internuclear coupling in determining exchange rates from high-resolution spectra tends to give systematic errors which make the apparent rates too high at lower temperatures near the slow exchange limit. This can be circumvented by using a complete line shape method which includes the effects of the coupling.[3] Another, simpler approach is afforded by spin-echo techniques,[4-6] for which it has been demonstrated recently that homonuclear coupling, J, in cycles per second, between exchanging nuclei does not affect the apparent exchange rate $1/2\tau$ provided that $1/2\tau \gtrsim 3\alpha$, where $\alpha = 2\pi|J|$.[6] The finding by Tiers[2] of a relatively large, negative entropy of activation, about -10 e.u., for the perfluorocyclohexane isomerization led us to suspect the accuracy of his results, for reasons discussed in part III.[5] Because of this, we have used perfluorocyclohexane as a further test of the spin-echo methods developed to study intramolecular exchange of a coupled AB

system, applied in part IV[6] to ^{19}F in 1,1-difluorocyclohexane.

Experimental Section

The spin-echo apparatus and experimental procedures used in this study were the same as those described previously,[4-6] as are the experimental errors. The sample of perfluorocyclohexane was obtained from Pierce Chemical Co., Rockford, Ill., with indicated b.p. 52° and m.p. 51°. It was used without further purification. The pure liquid was studied between 54 and 112°, in a sealed tube under its own vapor pressure. Also, measurements were made between 54 and 23° upon extending the liquid range by adding 30% by weight of isopentane as a diluent; this sample was degassed. A suitable solvent was not found for measurements at lower temperatures.[7]

Results and Discussion

In the methods employed,[4-6] the decay constant $1/T_2$ for the amplitudes of successive echoes in a Carr–Purcell train[8] is determined as a function of the pulse separation t_{cp}. The parameters for perfluorocyclohexane are such that we observed only region A of the $1/T_2$ vs. $1/t_{cp}$ curves,[4] in which $1/T_2$ is relatively insensitive to $1/t_{cp}$ and has for $1/t_{cp} \rightarrow 0$ the limiting value

$$(1/T_2) = (1/T_2^0) + (1/2\tau) - [(1/2\tau)^2 - \frac{1}{4}(\delta\omega)^2]^{1/2} \quad (1)$$

Thus, independent values are required for $1/T_2^0$ and for the chemical shift $\delta\omega$ in order to determine the exchange rate $1/2\tau$ from the $1/T_2$ data.

The low-temperature, high-resolution value of 18.2 p.p.m. for the axial–equatorial ^{19}F chemical shift[2] was used to calculate $\delta\omega$; and $1/T_2^0$ for each temperature was obtained by measuring the ^{19}F $1/T_1$ with the null method[8] and assuming[5,6] that $1/T_1 = 1/T_2^0$. With these values as input parameters, the computer pro-

(1) This research was supported by the U. S. Office of Naval Research and by the National Science Foundation.

(2) G. V. D. Tiers, *Proc. Chem. Soc.*, 389 (1960).

(3) J. Jonáš, A. Allerhand, and H. S. Gutowsky, *J. Chem. Phys.*, **42**, 3396 (1965).

(4) II: A. Allerhand and H. S. Gutowsky, *ibid.*, **42**, 1587 (1965). See also prior work cited therein.

(5) III: A. Allerhand, F. M. Chen, and H. S. Gutowsky, *ibid.*, **42**, 3040 (1965).

(6) IV: A. Allerhand and H. S. Gutowsky, *ibid.*, **42**, 4203 (1964).

(7) The CFCl₃ used as a solvent in the low-temperature high-resolution work interferes with the spin-echo measurements. In principle, the spin-echo method of IV[6] could give accurate values for the perfluorocyclohexane isomerization rate down to about 0°.

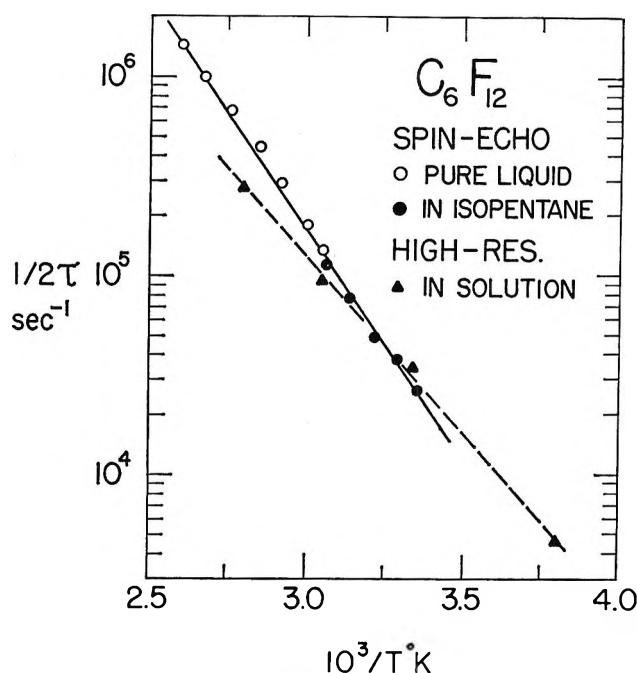(8) H. Y. Carr and E. M. Purcell, *Phys. Rev.*, **94**, 630 (1954).

Figure 1. Arrhenius plot of log $(1/2\tau)$ vs. $1/T$ for chair–chair isomerization of perfluorocyclohexane. The spin-echo data are from our [19]F n.m.r. experiments at 25.26 Mc./sec. on the pure liquid and on a 70% by weight solution in isopentane. The high-resolution data are from ref. 2 and are for 0.7 M solutions of perfluorocyclohexane in $CFCl_3$ and in benzotrifluoride.

the exchange rate is shown in Figure 1, as an Arrhenius plot, along with the results of Tiers[2] for comparison. The linear least-squares fit of our data gives a frequency factor of 1.35×10^{12} sec.$^{-1}$ and an activation energy E_a of 10.5 ± 0.2 kcal./mole.

It may be seen from the summary of activation parameters in Table II that our E_a and $\Delta H^*{}_{cc}$ are sub-

Table II: Activation Parameters for the Chair–Chair Isomerization of Perfluorocyclohexane, Obtained from the Temperature Dependence of $1/2\tau$ as Determined from [19]F N.m.r. Studies[a]

Method	E_a, kcal.	$\Delta G^*{}_{cc}$, kcal.	$\Delta H^*{}_{cc}$, kcal.	$\Delta S^*{}_{cc}$, e.u.
High resolution[b]	8.1 ± 0.3	10.9	7.5 ± 0.3	-10.2
This work	10.5 ± 0.2	11.2	9.9 ± 0.2	-4.4

[a] All parameters except E_a are given for 298°K.   [b] These data are from ref. 2.

gram FIT2X[5,6] was used to determine the best fit value[9] for $1/2\tau$ from the $1/T_2$ vs. $1/t_{cp}$ data obtained for each temperature. The results are given in Table I, which includes the $1/T_1$ measurements but not the more copius $1/T_2$ values. The temperature dependence of

stantially larger than the earlier values while our value for $\Delta S^*{}_{cc}$ is closer to zero. On the other hand, the free energy of activation $\Delta G^*{}_{cc}$ is the same within experimental error for the two studies. It was pointed out in part III[5] that comparative results of this nature occur when there are systematic errors in one set of data (or both). For the reasons mentioned in the introduction, we feel that such errors are present in the high-resolution study. The values for ΔG^* are more reliable than for the other activation parameters,[5] and it is of interest to compare them for cyclohexane,[5] 1,1-difluorocyclohexane,[6] and perfluorocyclohexane. Conversion to values appropriate for the chair–boat isomerization[5] gives $\Delta G^*{}_{cb}$ to be 10.3, 9.5, and 10.8 kcal./mole, respectively, for the three compounds. These values are surprisingly close to one another, but the differences are still large enough to be significant. The various activation parameters obtained for the isomerization of cyclohexane and of its derivatives have been discussed.[5,10]

Acknowledgment. We, particularly F. M. C., wish to thank Dr. Adam Allerhand for his help in many ways.

Table I: [19]F Spin-Echo N.m.r. Determinations of the Rate of Chair–Chair Isomerization of Perfluorocyclohexane[a]

Pure liquid			70% in isopentane		
Temp., °C.	$1/2\tau$, sec.$^{-1}$	$1/T_1$, sec.$^{-1}$	Temp., °C.	$1/2\tau$, sec.$^{-1}$	$1/T_1$, sec.$^{-1}$
54	1.37×10^5	0.204	23	2.63×10^4	0.113
60	1.78×10^5	0.198	30	3.80×10^4	0.110
70	2.92×10^5	0.193	37	4.90×10^4	0.110
78	4.40×10^5	0.185	46	7.73×10^4	0.110
90	6.75×10^5	0.169	53	1.12×10^5	0.113
102	1.02×10^6	0.161			
112	1.45×10^6	0.154			

[a] The spin-echo measurements were made at a ^{19}F frequency of 25.26 Mc./sec.; in the calculations of $1/2\tau$ from the apparent T_2, T_2^0 was taken equal to T_1 and the axial–equatorial chemical shift was taken to be 18.2 p.p.m., the low-temperature value from ref. 2.

(9) We wish to thank the Department of Computer Science for their service in processing the data.

(10) F. A. Bovey, E. W. Anderson, F. P. Hood, and R. L. Kornegay, *J. Chem. Phys.*, **40**, 3099 (1964).

Acetylene Production in the Radiolysis of Methane[1]

by R. H. Johnsen

*Department of Chemistry, Florida State University,
Tallahassee, Florida*   (*Received April 7, 1965*)

An earlier study in this laboratory of the radiolysis of methane[2] carried out at low conversion and in the presence of various radical scavengers did not reveal the production of significant amounts of acetylene although this substance was specifically sought, nor have earlier workers reported the presence of acetylene in the reaction products. On the other hand, it is well known that acetylene is one of the chief products in the electric discharge, where high local concentrations of reactive transients would be expected.

Recently, a paper has appeared in which it was reported that acetylene was produced in significant quantities when methane at a pressure of 800 torr was irradiated with electron pulses.[3] The G value reported varied from 0.25 to 0.01, depending on dose.

More recently, Hauser,[4] using a tracer method, reported that methane irradiated at 100 torr with 2.8-Mev. electrons at a dose rate of 2.6×10^{20} e.v. min.$^{-1}$ g.$^{-1}$ produced only very small amounts of acetylene, presumably detected because of the great sensitivity of the analytical method.

The most obvious difference in the experiments of Hummel and those carried out in this laboratory is the dose rate. Using a pulsed linear acceleration, the dose rate in Hummel's experiments was 9.6×10^{23} e.v. min.$^{-1}$ g.$^{-1}$ per pulse, while in this laboratory the earlier work was carried out at a mean dose rate of approximately 10^{19} e.v. min.$^{-1}$ g.$^{-1}$. Since Hummel has reported a dose rate effect for the production of ethylene over a tenfold change in dose rate, it was deemed of some interest to increase the dose rate of our experiments to the limit of the Van de Graaff accelerator (3×10^{21} e.v. min.$^{-1}$ g.$^{-1}$) as well as to explore other possibilities such as variation in temperature and in pressure, the material of the radiation cell, as well as the rigorous exclusion of oxygen in order to determine the influence of these parameters in acetylene production.

Experimental Section

Experiments were carried out in two types of radiation cells. The first series employed a stainless steel cell with aluminum windows which has been described previously.[2] For the second series, a Pyrex bulb of 300-ml. capacity was used. Methane employed in these experiments was Matheson C.P. grade which contained 0.006% ethane as the sole detectable impurity. To remove any traces of oxygen, which has been suggested as an inhibitor of acetylene formation, it was degassed by pumping under high vacuum using pumped nitrogen as a refrigerant. This methane was then vaporized and passed through a column containing a freshly deposited surface of metallic sodium directly into the reaction cell. Samples were collected in a side arm following irradiation with 2.0-Mev. electrons by freezing with liquid nitrogen. This sample was introduced into the gas chromatograph by means of an ampoule crusher. Analysis was by means of a combination silica gel–squalene on Chromosorb P column calibrated with authentic samples. Total doses varied from 3.3×10^{19} e.v. g.$^{-1}$ to 3.2×10^{21} e.v. g.$^{-1}$. The lowest dose corresponds to about 0.01% decomposition. Dosimetry was by means of the production of ethane ($G = 2.00$) from pure methane.

Results

Multiple runs were made in which oxygen was rigorously excluded, the dose rate varied by a factor of 300, the dose varied over two orders of magnitude, the temperature during irradiation varied from $+300$ to $-78°$, the pressure varied from 200 torr to 2 atm., and cell materials changed from stainless steel to Pyrex glass. Some of these variations in irradiation conditions had small effects on the over-all distribution of products. For example, at the lowest doses, ethylene was observed, in agreement with the work of Hummel, but in no case was acetylene observed as a product. That this was not due to the insensitivity of the analytical method was checked by adding acetylene to the reaction mixture. Levels of acetylene of the order of 0.005% were detectable.

When a small amount of acetylene (0.5%) was added to methane and irradiated, acetylene was consumed, producing ethane and propane in amounts proportionately larger than those formed in the absence of acetylene.

It is interesting to note that when irradiations were made with 10-Mev. protons from the Florida State University Tandem Van de Graaff accelerator, where the high LET has an effect similar to a very high local dose rate, acetylene was not observed.

There is some evidence for a dose rate effect in the production of propane. At a dose rate of 3.9×10^{20} e.v. min.$^{-1}$ g.$^{-1}$, the yield of propane was 0.36. At a dose

(1) Supported in part by U. S. Atomic Energy Commission Contract AT-(40-1)-2001.
(2) L. W. Sieck and R. H. Johnsen, *J. Phys. Chem.*, **67**, 2281 (1963).
(3) R. W. Hummel, *Discussions Faraday Soc.*, **36**, 75 (1963).
(4) W. P. Hauser, *J. Phys. Chem.*, **68**, 1576 (1964).

rate of 3×10^{21} e.v. min.$^{-1}$ g.$^{-1}$, the yield was of the order of 0.7. Hauser has reported a yield of 0.24 for a dose rate of 2.6×10^{20} e.v. min.$^{-1}$ g.$^{-1}$.

COMMUNICATIONS TO THE EDITOR

Rates of the Simultaneous Oxidation and Reduction of Diphenylpicrylhydrazyl on Titanium Dioxide and Carbon Black. The Role of F-Centers in Catalytic Activity[1]

Sir: Solutions of diphenylpicrylhydrazyl in benzene (about 1.27×10^{-2} m) in the presence of certain surfaces undergo intermolecular oxidation and reduction. The percentage yields at the completion of the reaction are essentially the same on all surfaces studied as indicated by thin layer chromatographic studies of the final solution. The main portion of the reaction proceeds according to the over-all process

Ph
\
4N—NPic + 2H$_2$O ⟶
/
Ph

Ph
\
3N—NHPic + O=⟨　⟩=O + H$_2$N—⟨　⟩—NHPic
/
Ph
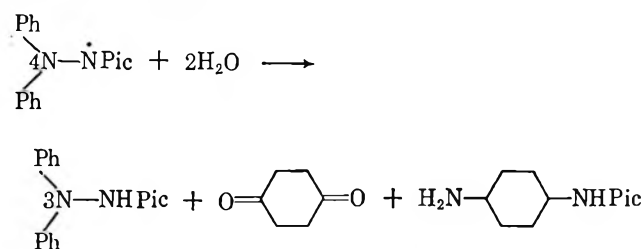
as has been demonstrated by isolating the products. Without the presence of the surface there is no appreciable reaction even on stirring the solutions with air.[2]

It is a simple matter to ascertain the order of this reaction by following the disappearance of the radical from the solution using the electron spin resonance signal as a measure of concentration. The line shape derivative traces were taken on aliquots of the solution at certain time intervals. The instrument was the low-frequency electron spin resonance apparatus manufactured by Alpha Scientific Laboratories (Model AL-340). The relative concentration of the solution was obtained by integrating the trace from zero to infinity.

In all cases 10 cc. of solution, shaken uniformly with the amounts of catalyst specified below, was used. Measurements were made at 24° with 1.25 g. of anatase (263 m.^{2}/g. B.E.T.: N$_2$) and on 1.25 g. of the same

anatase after it had been exposed to benzene solution, initially 1.27×10^{-2} m in benzene, for sufficient time for the above reaction to have become essentially complete. Neither sample was previously evacuated. The anatase initially had 7.55 wt. % of a sample of sulfuric acid adsorbed on its surface and presumably held by ester-type linkages. It was found by acid-base titration that after having catalyzed the complete reaction of a 1.27×10^{-2} m solution *none* of the sulfuric acid was removed from this anatase. Measurements were also made on a sample of 0.5 g. of carbon black (Cabot Carbolac 2, 800 m.^{2}/g.).

Figure 1 is a graph of log C vs. T for the reaction at 24° for all three samples. Clearly, the reaction is first
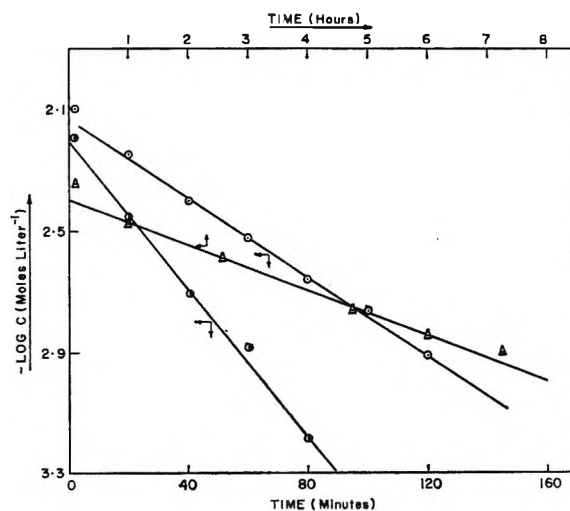

Figure 1. Rate of intermolecular reaction of diphenylpicrylhydrazyl in benzene; log C vs. time at 24°: O, anatase (263 m.^{2}/g.) 1.25 g./10 cc.; △, carbon black (800 m.^{2}/g.) 0.50 g./10 cc.; ◑, anatase treated as in text, 1.25 g./10 cc.

(1) This work was supported by a grant from the National Science Foundation.

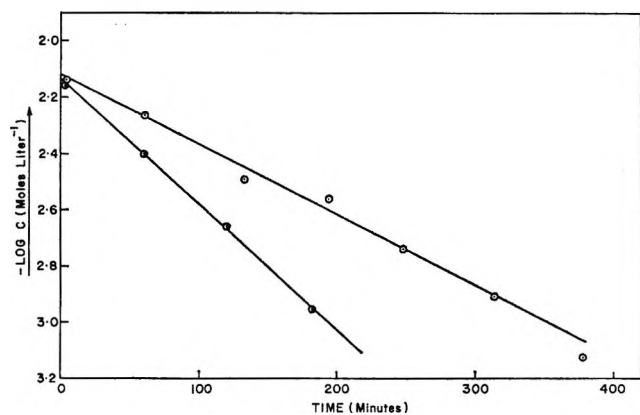(2) J. G. Aston, D. N. Misra, and K. M. Cresswell, *Nature*, in press.

Figure 2. Rates of intermolecular reaction of diphenylpicrylhydrazyl in benzene: log C (moles liter^{-1}) vs. T (min.) for 1.25 g. of anatase (263 m.^{2}/g.) for 10 cc. of solution: ●, 20°; ○, 10°.
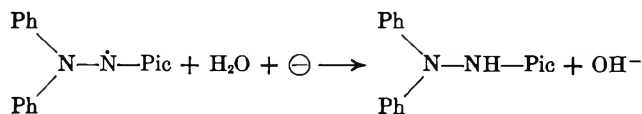
order. The more rapid rate on the used anatase is probably due to modification of the ester linkages by atmospheric moisture taken up while filtering the anatase off from the initial reaction mixture. Solutions of diphenylpicrylhydrazyl without catalyst in the presence of air and light are relatively stable.

Figure 2 shows similar graphs for 10-cc. samples of a 1.27×10^{-2} m solution in benzene shaken with 1.25 g. of a fresh sample of the same anatase at 10 and 20°.

A plot of the values of log k vs. $1/T$ for the reaction catalyzed by the fresh anatase shows that the energy of activation is approximately 10 kcal. mole^{-1}.

A first-order reaction on the surface would produce an apparent first-order reaction based on the solution concentration if the adsorption isotherm were essentially linear.

In view of the complicated nature of the oxidation products and the fact that only one reduction product, diphenylpicrylhydrazine, is found one must conclude that the rate-determining step is the surface reaction

$$
\begin{array}{c}
Ph \\ \diagdown \\ \diagup \\ Ph
\end{array}
N—\dot{N}—Pic + H_2O + \ominus \longrightarrow
\begin{array}{c}
Ph \\ \diagdown \\ \diagup \\ Ph
\end{array}
N—NH—Pic + OH^-
$$

the electron coming from a carbon radical or a Ti^{3+} F-center. It follows that the carbon radical or F-center must be regenerated elsewhere by the oxidative side of the reaction and that therefore the radical centers and the F-centers are mobile.

It cannot be the oxidation step that triggers, since this involves a complicated series of consecutive reactions. Both the anatase and the carbon black had evidently contained sufficient water for there to have been a large excess available to the surface. If there were 0.05 monolayer of water on either surface this

would correspond to approximately a 20-fold excess of that needed for the reaction.

Spackman[3] has made electron spin resonance observations on what he considers to be diphenylpicrylhydrazyl chemisorbed on carbon black. From the increased signal intensity he concludes that diphenylpicrylhydrazyl does not pair with the free electrons on carbon black. However, he records that the signal does not change with time. We have found an appreciable decrease in signal by the above reaction according to a well-defined surface unimolecular rate law. This surface reaction is now being studied exhaustively. It is probable that in Spackman's results all the diphenylpicrylhydrazyl had disappeared.

(3) J. W. C. Spackman, Chem. Ind. (London), 1532 (1961).

DEPARTMENT OF CHEMISTRY   J. G. ASTON
THE PENNSYLVANIA STATE UNIVERSITY   D. N. MISRA
UNIVERSITY PARK, PENNSYLVANIA

Relationship between Parachor and Zisman's Critical Surface Tension of Polymers

Sir: The surface free energy of a liquid, which is identical with its surface tension, is well known. An empirical relation between surface tension, γ, and molecular structure exists

$$P = \gamma^{1/4} \frac{M}{(D - d)} \tag{1}$$
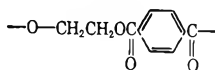
where M is the molecular weight of the liquid, D and d are the densities of the liquid and its vapor, and P, parachor, has the additive property for constituent chemical units. If $d << D$

$$P = \gamma^{1/4} V_m \tag{2}$$

where V_m is the molar volume of the liquid. Theoretical support for the molecular additivity of parachor stems from the principle of corresponding states, since from eq. 2 parachor is the molar volume of unit surface tension. This additivity of parachor is useful to estimate the surface tension of a liquid from knowledge of its chemical structure.

In contrast, very little is known of the exact magnitude of the surface free energy of solids, even for simple ionic crystals. It was of interest to establish a similar empirical relationship whereby estimates might be obtained for surface free energy of solids. However, the general surface morphology, particularly the crystal structure, often predominates over the chem-

Table I

Constituent group	γ_p, ergs/cm.^{2}	Polymer	γ_c, ergs/cm.^{2}	Ref.
$-CF_2-$	7.4	Polytetrafluoroethylene	18	a
$-CH_2-CH-$ OH	7.5	Polyvinyl alcohol	37	b
$-CF_2-CFH$	7.95	Polytrifluoroethylene	22	a
$-CF_2-CH_2-$	8.47	Polyvinylidene fluoride	25	a
$-CFH-CH_2-$	9.22	Polyvinyl fluoride	28	a
$-CH_2-C(CH_3)_2-$	10.0	Polyisobutylene	..	
$-CH_2-$	10.2	Polyethylene	31	a

$-CH_2-C-$
     CH$_3$
     COOCH$_3$
	13.0	Methyl methacrylate	39	a

$-CCIH-CH_2-$	14.2	Polyvinyl chloride	39	a
$-CH_2-CH-$ C$_6$H$_5$	15.0	Polystyrene	33–43	a
$-CH_2-C=CH-CH_2-$ Cl	15.6	Neoprene		
$-CCl_2-CH_2-$	16.9	Polyvinylidene chloride	40	a
$-O-CH_2CH_2OC\!\!\diagup\!\!\diagdown\!\!C-$ O O	17.6	Polyethylene terephthalate	43	a

^{a} W. A. Zisman, ref. 1. ^{b} B. R. Ray, J. R. Anderson, and J. J. Scholz, *J. Phys. Chem.*, **62**, 1220 (1958).

ical constitution in determining the surface free energy of most solids. Organic polymers represent possible exceptions. The surface of solids can generally be considered as an extension of the bulk structure, with an increased number of defects. Since commonly available polymers are often amorphous in the bulk, their surface is probably liquid-like. Furthermore, the constituent groups and side chains of these polymers should be able to move more freely in the surface than in the bulk. Although the surface cannot be considered truly liquid, the correlation of surface free energy with constituent groups such as additivity of parachor appears possible.

Zisman[1] established the concept of critical surface tension, γ_c, of polymers, which he defined as the surface tension of the liquid below which a liquid spreads on the solid surface. This critical surface tension, γ_c, is useful as a first approximation to surface free energy of these low energy solids. Limitations of this approximation are numerous, such as negligible vapor adsorption, additivity of interaction, and the rule of geometric mean for interaction between unlike molecules.[2,3] However, extrapolation of surface free energy of polyethylene from high temperature measurements[4] gives

a value of 35 ergs/cm.^{2}, which compares favorably to γ_c measurements of 31 ergs/cm.^{2}. Thus we may be justified in using γ_c in an empirical correlation.

Assuming the validity of eq. 2 for these low energy polymer solids and that each polymer chain consists of basically repetitive monomer units [*i.e.*, polyethylene to be essentially methylene units, $(-CH_2-)_n$, and polytetrafluoroethylene to be fluorocarbon, $(-CF_2-)_n$] the additivity of parachor becomes

$$\gamma_p{}^{1/4} = \frac{P \text{ (polymer)}}{V_m \text{ (polymer)}}$$

$$= \frac{nP \text{ (monomer)}}{nV_m \text{ (monomer)}}$$

$$= \frac{P \text{ (monomer)}}{V_m \text{ (monomer)}}$$

(1) W. A. Zisman, Advances in Chemistry Series, No. 43, American Chemical Society, Washington, D. C., 1964, p. 1.

(2) R. J. Good and L. A. Girifalco, *J. Phys. Chem.*, **64**, 561 (1960).

(3) A. W. Adamson and I. Ling, Advances in Chemistry Series, No. 43, American Chemical Society, Washington, D. C., 1964, p. 57.

(4) H. W. Starkweather, Jr., *Soc. Plastics Engrs. J.*, **5**, 5 (1965).

Parachor values of many constituent groups have been reported.[5] The molecular volumes used are those at the boiling point,[6] since molecules are thereby at the same reference state and the additivity of molar volumes of constituents can be invoked. γ_p values calculated for various constituent groups from eq. 3 are shown in Table I. Also tabulated are the critical surface tension values γ_c of various polymers which correspond to the constituent groups. Figure 1 shows the correlation of γ_c with γ_p. The generally good correlation seems to suggest amorphous or liquid-like surface structure of the polymers, at least as far as the sensitivity of the contact angle and critical surface tension measurements can determine. Figure 1 should
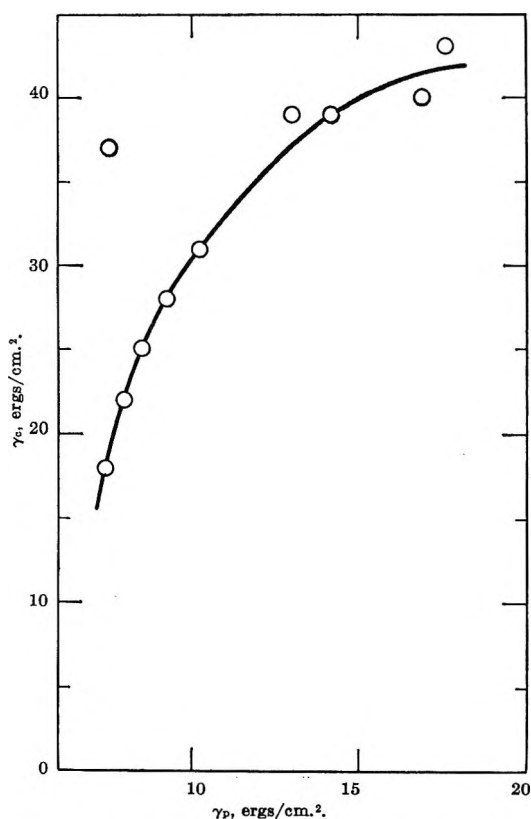

Figure 1. Correlation of γ_c with γ_p calculated from parachor.

also serve as a guide for estimating surface free energy of polymers. The apparent decrease of the slope of γ_c vs. γ_p may indicate gradual departure of the critical surface tension from the true surface free energy. The deviation of polyvinyl alcohol may be due to the polar hydroxyl groups which are prone to adsorb water from the air through hydrogen bonding.

the National Institutes of Health, National Heart Institute, under Contract PH 43-64-84.

(5) R. R. Dreisbach, Advances in Chemistry Series, No. 29, American Chemical Society, Washington, D. C., 1961, p. 9.
(6) C. W. Bunn, *J. Polymer Sci.*, **17**, 323 (1955).

POLYMER SCIENCES DEPARTMENT   IRENE J. LEE
STANFORD RESEARCH INSTITUTE   WILLIAM M. MUIR
MENLO PARK, CALIFORNIA 94023   DONALD J. LYMAN

RECEIVED JULY 6, 1965

Apparent Violations of Gibbs–Duhem Relations and the Limiting Laws of Dilute Solutions

Sir: Elliott, *et al.*,[1] have recently published their results on the activity of Cd, a_1, in liquid Cd–Ga solutions. The purpose of this communication is (1) to show that the equations used to represent a_1 as a function of composition violate the Gibbs–Duhem relations and lead to the rejection of their equation for the activity of Ga, a_2, even if an apparent violation of Raoult's law is accepted, and (2) to clarify the discussions concerning the laws of dilute solutions.[2,3]

The Gibbs–Duhem relations are based on (1) the axiom that the extensive thermodynamic properties, *e.g.*, the Gibbs free energy, G, are homogeneous functions of first degree in the number of moles, (2) the existence of $dG = VdP - SdT$ in accordance with the first and the second laws, and (3) integration of dG at constant temperature leading to the recognition of chemical potential and the definition of activity. It is therefore valid irrespective of the validity of Raoult's and Henry's laws.[4] The equation used for the activity of Cd by Elliott, *et al.*, is

$$a_1 = \gamma_1(1 - N) = 1 - gN + hN^2 \qquad (1)$$

where N is the mole fraction of Ga, γ_1 the activity coefficient of Cd, and g and h are the constants independent of N. The values of g and h for Cd representing the best data were shown to be 0.856 and 0.943, respectively.[1] Their proposed equation for Ga is

$$a_2 = \gamma_2 N = jN + kN^2 \qquad (2)$$

Substitution of these equations in the Gibbs–Duhem relation, $(1 - N) \, d \ln a_1 + N \, d \ln a_2 = 0$, and simplification yields

(1) G. R. B. Elliott, J. F. Lemons, and H. S. Swofford, *J. Phys. Chem.*, **69**, 933 (1965).
(2) S. D. Christian and N. Fogel, *ibid.*, **69**, 2135 (1965).
(3) G. R. B. Elliott and J. F. Lemons, *ibid.*, **69**, 2135 (1965).
(4) N. A. Gokcen, *ibid.*, **64**, 401 (1960).

$$(2hk - hj - kg)N^2 + (2k + 2hj - kg)N +$$

$$j(1 - g) = 0 \quad (3)$$

Since the coefficients of N and N^2 in eq. 3 are independent of N and eq. 3 is zero for all values of N, it follows that the term $j(1 - g)$ as well as the coefficients of N and N^2 must each be identically zero. Substitution of the authors' values for g and h shows that it is not possible to satisfy eq. 3 in view of the fact that j and k cannot be simultaneously zero. It is irrelevant to the present discussion to consider $j = k = 0$ but if this were so, then $a_2 = 0$, and this would simply indicate the disappearance of Ga by a strong compound formation with Cd in which case it is necessary to choose the second component as the compound rather than Ga and again use eq. 2 so that j and k cannot both be zero. The possible sets of values satisfying eq. 3 without $j = k = 0$ are (1) $g = 1, h = 0, k = 0, j > 0$; (2) $g = 1, h = 0.25, j = -2k$; (3) $g = 2, h = 1, j = 0$, $k > 0$. The last set is of questionable validity but need not concern the present discussion. It is therefore evident that for the system Cd–Ga, eq. 1 and 2 proposed by the authors[1] and the molecular reasoning supporting these equations are unacceptable. Also, the only possible value of g satisfying the set of equations $a_1 = 1 - gN$ and eq. 2, i.e., their eq. 6C and 7 (or $a_1 = 1 - gN$ and $a_2 = jN$), is $g = 1$, hence, the authors' contention that Henry's law is obeyed but Raoult's law may not be obeyed violates mathematics and the laws of thermodynamics. Further, the restrictions imposed by eq. 3 on eq. 1 and 2 make these equations useless for the representation of activity data. There are numerous satisfactory equations[5] for this purpose which satisfy the requirements of the Gibbs–Duhem relations and fit any set of data when a functional representation is desired.

The limiting laws of solutions state that $\gamma_1 \to 1$ and $\gamma_2 \to j$ as $N \to 0$ and j is a finite positive nonzero quantity in measurably miscible systems. In general the more accurate the measurements the smaller the composition range where the deviation from $\gamma_1 = 1$ is not distinguishable from the experimental errors. The deviation reported by the authors at the lowest Ga content is no larger than that in aqueous electrolytic solutions and does not constitute a violation, although it is surprising for nonelectrolytic, and in particular for metallic, solutions. The argument presented by Christian and Fogel[2] that Ga is dissolved by substantial dimerization is plausible, but it must await direct measurements on the activity of gallium. Finally, it is suggested here that direct measurements of the vapor pressure of Cd over Cd–Ga are highly desirable before the two indirect sets of data by means of isopiestic

balance[1] are accepted in order to assure that there are no unknown sources of errors.

(5) See, for example, E. Hala, *et al.*, "Vapor–Liquid Equilibrium," Pergamon Press, London, 1960, p. 60.

CHEMICAL THERMODYNAMICS SECTION,   N. A. GOKCEN
  LABORATORIES DIVISION
AEROSPACE CORPORATION
EL SEGUNDO, CALIFORNIA

Interionic Vibrational Absorption Bands of Ion Aggregates in Benzene Solution

Sir: The existence of ion pairs, triple ions, and higher aggregates in solutions of ionic salts in solvents of low dielectric constant has long been recognized and much information has accumulated.[1] Vibrational spectroscopy promises to provide additional information— the frequency of vibration, and hence the force constant, of the ion-pair bond. The purpose of this communication is to demonstrate that absorption bands which may be assigned to interionic vibrational modes of these aggregates can be observed in the low-frequency infrared spectra of solutions in benzene. These bands were observed during the course of a study of the strongly hydrogen-bonded hydrogen dihalide ions.[2]

Spectra were recorded, using a Beckman IR-II instrument with polyethylene cells, of benzene solutions of some tetra-*n*-butylammonium and tetra-*n*-pentylammonium halide and hydrogen dihalide salts. The solubilities of the lower members of the tetraalkylammonium salt series in benzene were found to be too low for this study because solvent absorption restricted the usable thickness to a maximum of a few millimeters. This latter restriction also limited the concentration range of study of the more soluble salts and this in turn, coupled with the broad nature of the absorption bands which limited the accuracy of band-center determination, prevented an adequate study of the dependence of band position upon solution concentration from being made. No band shifts were observed over the concentration range 0.05 to 0.2 *M*. Some typical spectra are illustrated in Figure 1, which also includes the spectra of the solid materials suspended in Nujol. Table I contains the wave number values of the bands assigned to the interionic modes of aggregates in benzene solution. These assignments are

(1) C. A. Kraus, *J. Phys. Chem.*, **60**, 129 (1956).

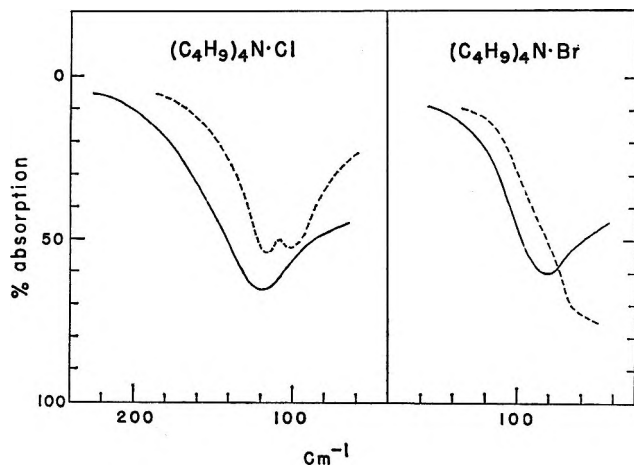(2) J. C. Evans and G. Y-S. Lo, to be published.

Figure 1. Spectra of solids (dotted lines) and of benzene solutions (full lines); tetrabutylammonium chloride (0.059 M) in 2-mm. cell; tetrabutylammonium bromide (0.066 M) in 2-mm. cell.

Table I: Bands Observed in the Far-Infrared Region for Solutions of Salts in Benzene and Assigned to Ion-Aggregate Modes[a]

Salt	cm.$^{-1}$
$(n\text{-}C_4H_9)_4N \cdot Cl$	120 ± 3
$(n\text{-}C_5H_{11})_4N \cdot Cl$	119 ± 3
$(n\text{-}C_4H_9)_4N \cdot Br$	80 ± 4
$(n\text{-}C_5H_{11})_4N \cdot Br$	80 ± 4
$(n\text{-}C_4H_9)_4N \cdot ClHCl$	102 ± 5
$(n\text{-}C_4H_9)_4N \cdot ClDCl$	102 ± 5
$(n\text{-}C_4H_9)_4N \cdot BrHBr$	73 ± 5

[a] Asymmetry of the bands on the lower wave number side suggests the presence of other unresolved bands.

based mainly upon a comparison of the spectra of the chlorides and bromides, upon the established existence of ion aggregates in these solutions, and upon the band locations; they are near to but somewhat higher in frequency than the lattice modes of the solid salts. Evidence presented recently[3] indicates the presence of shorter interionic distances in ion pairs than in the solid lattice, which implies stronger bonds and higher vibrational frequencies for the ion pairs. Comparison of the infrared spectra of chloride and bromide salts of a common cation shows that the only major difference occurs in the 100-cm.$^{-1}$ region where the chlorides and the bromides show bands near 120 and 80 cm.$^{-1}$, respectively. The ratio of frequencies, 1.5, is suggestive of interionic vibrational modes since the square root of the ratio of reduced masses of bromide and chloride ion pairs is about 1.4. The bands for the corresponding tetrapentylammonium and the tetrabutylammonium salts differ by only 1 or 2 cm.$^{-1}$, which is

again in agreement with the expectation suggested by the reduced mass ratio.

Earlier studies[1,4] support the belief that, at the concentration level presently used of about 0.05 M in benzene solution, the ion pairs are further associated to form quadrupoles and, possibly, even higher species. For our present purpose a simple model must be assumed and the best choice appears to be the quadrupolar model. This is also the model which has been successfully applied in several recent studies of alkali–metal halide dimers, M_2X_2.[5-7] A planar, rhombic structure with D_{2h} symmetry has six normal modes, three of which are infrared active. Two of these are ring stretching modes which are degenerate if the structure is a square while the third is an out-of-plane mode expected to be at lower frequency. In the present system, the cation is larger than the anion and the structure is probably not a square; the asymmetry apparent on the low-frequency sides of the observed bands may be associated with the second infrared-active stretching mode. For the simple chlorides this is estimated to be near 80 cm.$^{-1}$ and, if we follow the assumptions of White, et al.,[6] concerning the values of the several interaction force constants, we derive a value of about 70° for the acute angles of the rhombus and a value of 0.22 mdyne/Å. for the stretching force constant of the cation–anion bond. These are crude approximations only.

Additional studies using other nonpolar solvents at these concentration levels should be possible. However, attempts to use solvents of higher dielectric constant which are known to break up ionic aggregates were unsuccessful. Methylene chloride, acetonitrile, and acetonitrile–benzene mixtures were unsuitable because of the presence of very broad solvent absorption bands in the 100-cm.$^{-1}$ region. Such absorptions are generally present in the spectra of polar liquids and have been assigned to vibrational modes of the intermolecular dipole–dipole complexes present.[8]

(3) H. K. Bodenseh and J. B. Ramsey, J. Phys. Chem., 69, 543 (1965).

(4) E. D. Hughes, C. K. Ingold, S. Patai, and Y. Pocker, J. Chem. Soc., 1206 (1957).

(5) J. Berkowitz, J. Chem. Phys., 29, 1386 (1958); 32, 1519 (1960).

(6) D. White, K. S. Seshadri, D. F. Dever, D. E. Mann, and M. J. Linevsky, ibid., 39, 2463 (1963).

(7) S. Schlick and O. Schnepp, ibid., 41, 463 (1964).

(8) R. J. Jakobsen and J. W. Brasch, J. Am. Chem. Soc., 86, 3571 (1964).

CHEMICAL PHYSICS RESEARCH LABORATORY   J. C. EVANS
THE DOW CHEMICAL COMPANY   G. Y-S. LO
MIDLAND, MICHIGAN 48640